RRFM

EUROPEAN RESEARCH REACTOR CONFERENCE 2016

IGORR

Conference Proceedings

Berlin, Germany

13-17 March 2016

EUROPEAN NUCLEAR SOCIETY

ENS CONFERENCE

RRFM/IGORR 2016 Gold Sponsors

AREVA

MIRION TECHNOLOGIES

ROSATOM

Total Solution Provider
SOOSAN ENS
for Human, Nature and Future

RRFM/IGORR 2016 Silver Sponsor

HYUNDAI ENGINEERING & CONSTRUCTION

organised in collaboration with:

IAEA
International Atomic Energy Agency

European Nuclear Society
Avenue des Art 56
1000 Brussels, Belgium
Phone + 32 2 505 30 54
Fax +32 2 502 39 02
E-mail ens@euronuclear.org
Internet www.euronuclear.org

ISBN 978-92-95064-25-6

TABLE OF CONTENTS

Plenary Sessions

Fuel

RRFM2016-A0102	MULTISCALE SIMULATION OF MICROSTRUCTURAL EVOLUTION IN IRRADIATED U-MO	Liang, L. (1); Mei, Z.-G. (1); Ye, B. (1); Kim, Y. S. (1); Hofman, G. (1); Anitescu, M. (1); Yacout, A. (1) 1 - Argonne National Lab, United States
RRFM2016-A0207	PLASMA SPRAYED ZIRCONIUM DIFFUSION BARRIER DEVELOPMENT FOR MONOLITHIC U-MO METALLIC FUEL	Hollis, K. (1); Cummins, D. (1); Dombrowski, D. (1) 1 - Los Alamos National Laboratory, United States

RRFM2016-A0121	MODELING THE PORE FORMATION MECHANISM IN UMO/AL DISPERSION FUEL MEAT	Kim, Y. S. (1); Jamison, L. (1); Hofman, G. (1); Jeong, G. Y. (2) 1 - Argonne National Laboratory, United States 2 - UNIST, Korea, Republic of

RRFM2016-A0170	ECONOMY OF BR2 FUEL CYCLE WITH GADOLINIUM AS BURNABLE ABSORBER	Kalcheva, S. (1); Koonen, E. (1) 1 - SCK-CEN, Belgium

RRFM2016-A0045	THE EFFECT OF THERMAL CONDUCTIVITY UNCERTAINTIES ON THE OPERATING TEMPERATURE OF U–MO/AL DISPERSION FUEL	Sweidan, F. (1); Mistarihi, Q. (1); Ryu, H. J. (1); Yim, J. S. (2) 1 - Korea Advanced Institute of Science and Technology, Korea, Republic of 2 - Korea Atomic Energy Research Institute, Korea, Republic of
RRFM2016-A0055	PIE ANALYSES OF U-MO/AL DISPERSION FUEL WITH DIFFERENT U-MO PARTICLE SIZES	Ryu, H. J. (1); Mistarihi, Q. M. (1); Lee, K. H. (2); Jeong, Y. J. (2); Jung, Y. H. (2); Yoo, B. O. (2); Park, J. M. (2) 1 - Korea Advanced Institute of Science and Technology, Korea, Republic of 2 - Korea Atomic Energy Research Institute, Korea, Republic of
RRFM2016-A0073	PRELIMINARY EVALUATION ON THE KJRR FUEL INTEGRITY	Yim, J. (1); Kim, H. (1); Tahk, Y. (1); Oh, J. (1); Kong, E. (1) 1 - KAERI(Korea Atomic Energy Research Institute), Korea, Republic of
RRFM2016-A0215	US PROGRESS ON PROPERTY CHARACTERIZATION TO SUPPORT LEU U-10 MO MONOLITHIC FUEL DEVELOPMENT	Cole, J. (1); Rabin, B. (1); Smith, J. (1); Scott, C. (1); Benefiel, B. (1); Larsen, E. (1); Lind, P. (1); Sell, D. (1) 1 - Idaho National Laboratory, United States

RRFM2016-A0119	MCNP CALCULATION OF CORE PHYSICS PARAMETERS OF NIRR-1 LEU CORE USING MANUFACTURER'S RECOMMENDED VALUE OF 13% ENRICHED UO2 FUEL	Ibikunle, K. (1); Ibrahim, Y. (2); Jonah, S. (2) 1 - Department of Physics, Ahmadu Bello University, Zaria, Nigeria 2 - Centre for Energy Research and Training, Ahmadu Bello University, Zaria, Nigeria
RRFM2016-A0137	PVD-BASED MANUFACTURING PROCESS OF MONOLITHIC LEU FOIL TARGETS FOR 99MO PRODUCTION	Hollmer, T. (1); Baumeister, B. (1); Steyer, C. (1); Petry, W. (1) 1 - Forschungs-Neutronenquelle Heinz Maier-Leibnitz (FRM II), Germany
RRFM2016-A0181	JM-1 RESEARCH REACTOR CONVERSION DEMONSTRATED AT POLYTECHNIQUE MONTREAL	Chilian, C. (1); Muftuoglu, A. (1) 1 - Polytechnique Montreal, Canada

Utilisation

RRFM2016-A0019	PREPARING JHR INTERNATIONAL COMMUNITY THROUGH DEVELOPMENTS OF THE FIRST EXPERIMENTAL CAPACITY	Gonnier, C. (1); Bignan, G. (1); Estrade, J. (1); Santucci, C. (1); Parrat, D. (1); Le Jolu, T. (1); Gaillot, S. (1); Miklos, M. (2); Al-Mazouzi, A. (3); Kinnunen, P. (4) 1 - CEA, France 2 - UJV, Czech Republic 3 - EDF, France 4 - VTT, Finland
RRFM2016-A0046	CURRENT AND FUTURE UTILISATION OF MARIA RESEARCH REACTOR	Krzysztoszek, G. (1) 1 - National Centre for Nuclear Research, Poland
RRFM2016-A0059	DESIGN IMPROVEMENT OF CAPSULE FOR A HIGHER NEUTRON IRRADIATION FLUENCE	Choo, K. (1); Cho, M. (1); Yang, S. (1); Yang, T. (1); Kim, M. (1); Hong, S. (2) 1 - Korea Atomic Energy Research Institute, Korea, Republic of 2 - Chungnam National University, Korea, Republic of
RRFM2016-A0062	OUT-OF-PILE TESTING OF THE CALIPSO IRRADIATION DEVICE FOR THE JULES HOROWITZ REACTOR	Moulin, D. J. (1); Charvet, P. (1); Challet, F. (1); Chaumont, G. (1) 1 - CEA, DEN, Department of Nuclear Technology, Cadarache, France
RRFM2016-A0156	STATUS AND SCIENTIFIC USE OF THE TRIGA RESEARCH REACTOR AT THE UNIVERSITY OF MAINZ	Geppert, C. (1); Eberhardt, K. (1); Karpuk, S. (1) 1 - Institut für Kernchemie, Johannes Gutenberg-Universität Mainz, Germany
RRFM2016-A0161	RA-6 ONLINE + IRL: AN EFFECTIVE COLLABORATION BETWEEN CNEA AND IAEA FOR THE DEVELOPMENT OF A RESEARCH REACTOR EDUCATION REMOTE TOOL	Cantero, P. (1); Mangiarotti, D. (1); Brollo, F. (1); Sanchez, F. (1); Longhino, J. (1); Chiaraviglio, N. (1); Balumann, H. (1); Borio di Tigliole, A. (2); Vyshniauskas, J. (2) 1 - Nuclear Engineer Division – Nuclear Energy Department – National Atomic Energy Commission (CNEA), Argentina 2 - Research Reactor Section, Department of Nuclear Energy - IAEA, Austria

RRFM2016-A0184	IMPLEMENTATION OF A FISSION GAS RELEASE AND MEASUREMENT LOOP AT THE PULSTAR REACTOR	Hawari, A. (1); Liu, M. (1); Smith, M. (1); Harp, J. (2); Pastore, G. (2); Williamson, R. (2) 1 - Nuclear Reactor Program, North Carolina State University, United States 2 - Idaho National Laboratory, United States

RRFM2016-A0075	QUALIFICATION OF POWER DETERMINATION FOR F&M EXPERIMENTS IN RESEARCH REACTOR	Volkov, B. (1) 1 - OECD Halden Reactor Project, Norway
RRFM2016-A0123	LOW POWER RESEARCH REACTOR TO IMPEL CREATION OF NATIONAL INFRASTRUCTURE	Mazzi, R. (1) 1 - INVAP SE, Argentina
RRFM2016-A0128	FEASIBILITY STUDY OF INSTALLING A THERMAL TO 14 MEV NEUTRON CONVERTER INTO A RESEARCH NUCLEAR REACTOR	Snoj, L. (1); Radulović, V. (1); Trkov, A. (1); Lengar, I. (1); Žerovnik, G. (1); Jazbec, A. (1); Kolšek, A. (2); Sauvan, P. (2); Ogando, F. (2); Sanz, J. (2) 1 - Jozef Stefan Institute, Slovenia 2 - Universidad Nacional de Educacion a Distancia, Ingenieria Energetica, Spain
RRFM2016-A0145	MAXIMIZING UTILIZATION OF NEUTRONS AT A RESEARCH REACTOR BY EMPLOYING AUTOMATION OF IRRADIATION AND COUNTING PROCEDURES FOR THERMAL AND EPITHERMAL NEUTRONS, CYCLIC NAA AND COMPTON SUPPRESSION	Landsberger, S. (1); Biegalski, S. (1); Copple, B. (1); Welch, L. (1) 1 - University of Texas at Austin, Nuclear Engineering Teaching Lab, United States
RRFM2016-A0236	OPTIMIZING PALLAS REACTOR UTILIZATION TO SUPPORT A ECONOMICALLY VIABLE BUSINESS CASE	Zekveld, D. (1) 1 - Stichting Voorbereiding Pallas-reactor, Netherlands
RRFM2016-A0034	ZERO POWER REACTOR AGN-201K FOR UNIVERSITY EDUCATION	Kim, M. H. (1) 1 - Reactor Research & Education Center, Kyung Hee University, Korea, Republic of
RRFM2016-A0070	MEASUREMENT OF POSITIVE TEMPERATURE COEFFICIENTS OF REACTIVITY FOR RACK-LIKE ARRANGEMENTS OF REACTOR FUEL IN THE NEPTUNE ZERO ENERGY FACILITY	Walley, S. (1); Bean, P. (1); Sainsbury, I. (1); Gill, D. (2); Sottosanti, D. (2); Zerkle, M. (2); Kelly, D. (3) 1 - Rolls-Royce (Nuclear), United kingdom 2 - Bettis Atomic Power Laboratory, United States 3 - Knolls Atomic Power Laboratory, United States
RRFM2016-A0110	FUTURE EXPERIMENTAL PROGRAMMES IN THE CROCUS REACTOR	Lamirand, V. (1); Hursin, M. (1); Perret, G. (2); Frajtag, P. (1); Pakari, O. (2); Pautz, A. (1) 1 - Ecole Polytechnique Fédérale de Lausanne (EPFL), Switzerland 2 - Paul Scherrer Institute (PSI), Switzerland

RRFM2016-A0204	THE INTERNET REACTOR LABORATORY PROJECT: STATUS AND THE EXPERIENCE OF THE ISIS RESEARCH REACTOR	Foulon, F. (1); Borio-di-Tigiole, A. (2); Vyshniauskas-Gomez, J. (2) 1 - National Institute for Nuclear science and Technology,French Atomic Energy and Alternative Energies Commission (CEA), France 2 - Research Reactor Section, Division of Nuclear Fuel Cycle and Waste Technology, Department of Nuclear Energy, IAEA, Austria

Safety

RRFM2016-A0030	CHARACTERIZATION OF THE OPERATING STRATEGY AND SAFETY MARGIN AT NOMINAL WORKING CONDITIONS OF THE MADISON EXPERIMENTAL SYSTEM IN THE JHR RESEARCH REACTOR.	Weiss, Y. (1); Bourdon, S. (2); Jaecki, P. (2); Bonnier, C. (2); Blandin, C. (2) 1 - Rotem Industries LTD, Israel 2 - French Atomic Energy Commission (CEA) - Cadarache Centre, France, France
RRFM2016-A0050	ACCIDENT SCENARIO DEVELOPMENT OF THE NUCLEAR RESEARCH REACTOR 'HANARO' FOR A FULL SCALE NUCLEAR EMERGENCY EXERCISE	Goanyup, L. (1); Bongseok, K. (1); Haechoi, L. (1); Jongsu, K. (1) 1 - Korea Atomic Energy Research Institute, Korea, Republic of
RRFM2016-A0125	A CASE STUDY: SAFARI-1 - IMPLEMENTATION OF THE SAFETY CLASSIFICATION IN THE EXISTING FACILITIES USING A GRADED APPROACH	Malaka, S. (1) 1 - Necsa, SAFARI-1, South Africa
RRFM2016-A0175	STUDY OF THE IMPACT OF ION IRRADIATION ON THE CORROSION KINETICS AND THE OXIDE LAYER MICROSTRUCTURE OF ALFENI ALUMINIUM ALLOY	Nabhan, D. (1); Kapusta, B. (1); Colas, K. (1); Dacheux, N. (2) 1 - CEA Saclay, DEN/DANS/DMN/SEMI/LM2E, France 2 - ICSM-LIME, UMR 5257, France
RRFM2016-A0238	ACQUISITION OF A SAFE MULTI-PURPOSE REACTOR	Van der Walt, M. (1) 1 - PALLAS, Netherlands
RRFM2016-A0020	HIGHLIGHTS OF REGULATORY ASPECTS OF RESEARCH REACTORS IN THE RUSSIAN FEDERATION: FROM FUKUSHIMA TO FUTURE	Sapozhnikov, A. (1) 1 - Federal Environmental, Industrial and Nuclear Supervision Service of Russia, Russian Federation
RRFM2016-A0041	EVALUATION ON SEISMIC INTEGRITY OF HTTR CORE COMPONENTS	Ono, M. (1); Iigaki, K. (1); Shimazaki, Y. (1); Tochio, D. (1); Shimizu, A. (1); Inoi, H. (1); Hamamoto, S. (1); Takada, S. (1); Sawa, K. (1) 1 - Japan Atomic Energy Agency, Japan
RRFM2016-A0225	SOME SUGGESTED METHODOLOGIES FOR USE WHEN PERFORMING PERIODIC SAFETY REVIEWS AND SAFETY REASSESSMENTS FOR RESEARCH REACTORS	Summerfield, M. (1) 1 - Australian Nuclear Science and Technology Organisation (ANSTO), Australia
RRFM2016-A0228	DEVELOPMENT OF EVACUATION TIME ESTIMATES ON RESEARCH REACTOR 'HANARO'	Kim, B. (1); Lee, G. (1) 1 - Korea Atomic Energy Research Institute, Korea, Republic of
RRFM2016-A0085	FRENCH POST-FUKUSHIMA COMPLEMENTARY ASSESSMENTS – GENERAL APPROACH AND RESULTING SAFETY IMPROVEMENTS FOR THE HIGH FLUX REACTOR LOCATED IN GRENOBLE	Grolleau, E. (1); Jouve, A.-C. (1); Kanamori, S. (1) 1 - Institut de Radioprotection et de sûreté Nucléaire, France

RRFM2016-A0087	APPLICATION OF SAFETY REASSESSMENT IN THE LIGHT OF FUKUSHIMA DAIICHI ACCIDENT TO NEW DESIGNS: THE RA-10 REACTOR CASE	Ramirez, P. (1); Cantero, P. (1); Brollo, F. (1); Blaumann, H. (1) 1 - National Atomic Energy Commission (CNEA), Argentina
RRFM2016-A0107	SAFETY REASSESSMENT OF HANARO AND STATUS OF SAFETY IMPROVEMENT MEASURES	Lim, I.-C. (1); Lee, C.-S. (1); Shin, J.-W. (1); Yim, S.-P. (1); Doo, S.-G. (1); Wu, S.-I. (1); Ryu, J.-S. (1) 1 - Korea Atomic Energy Research Institute, Korea, Republic of
RRFM2016-A0129	STATUS OF JRR-3 AFTER GREAT EAST JAPAN EARTHQUAKE	Arai, M. (1); Wada, S. (1); Murayama, Y. (1) 1 - Japan Atomic Energy Agency, Japan

Innovative Methods

RRFM2016-A0083	COCONEUT: ENHANCING NEUTRONIC DESIGN FOR RESEARCH REACTORS	Lacombe, J.-G. (1); Bouret, C. (1); Koubbi, J. (1); Manifacier, L. (1) 1 - AREVA TA, France

RRFM2016-A0114	BEST ESTIMATE PLUS UNCERTAINTY APPROACH IN THE ANALYSIS OF TRANSIENTS IN RESEARCH REACTORS	Doval, A. (1); Lupiano Contreras, J. (1) 1 - INVAP S.E., Argentina
RRFM2016-A0132	ADVANCED SMALL AND LARGE CORE DISTORTIONS MODELING IN ZPR TO ASSESS CORE RECRITICALITY SCENARIOS OF SFR CORE DEGRADATION SEQUENCES	Margulis, M. (1); Blaise, P. (2); Gilad, E. (1) 1 - Department of Nuclear Engineering, Ben Gurion University of the Negev, Israel 2 - Experimental Physics Service, CEA Cadarache, France
RRFM2016-A0162	COMPARISON OF MEASURED AND CALCULATED NEUTRONIC AND THERMAL HYDRAULIC REACTOR PARAMETERS OF THE LEU-FUELLED JAMAICAN SLOWPOKE-2 RESEARCH REACTOR	Puig, F. (1); Dennis, H. (2) 1 - Argonne National Laboratory, United States 2 - International Centre for Environmental and Nuclear Sciences, University of the West Indies-Mona Campus, Jamaica
RRFM2016-A0189	RECENT DEVELOPMENTS IN THE TRIPOLI-4® MONTE-CARLO CODE - APPLICATIONS FOR RESEARCH REACTORS	Malouch, F. (1) 1 - CEA, Saclay center, DEN/DANS/DM2S/SERMA, France
RRFM2016-A0218	IN-CORE FUEL MANAGEMENT OPTIMISATION OF THE HOR REACTOR USING THE OSCAR-4 CODE SYSTEM	Schlünz, E. B. (1); Winkelman, A. J. M. (2); Prinsloo, R. H. (3); Bokov, P. M. (3); Van Vuuren, J. H. (4) 1 - Department of Logistics, Stellenbosch University, South Africa 2 - Reactor Institute Delft, Delft University of Technology, Netherlands 3 - Radiation and Reactor Theory, The South African Nuclear Energy Corporation SOC Ltd, South Africa 4 - Department of Industrial Engineering, Stellenbosch University, South Africa

Operation & Maintenance

RRFM2016-A0010	FRM II: NON-DESTRUCTIVE TESTING OF THE PRIMARY COOLING LOOP	Pichlmaier, A. (1); Gerstenberg, H. (1); Kastenmüller, A. (1); Krokowski, C. (1); Kreß, M. (1); Schmidt, M. (1) 1 - TU-München, ZWE FRM II, Germany
RRFM2016-A0037	NUCLIDE DETERMINATION OF TRIGA FUEL ELEMENTS BY GAMMA SPECTROSCOPY	Eichleitner, D. (1); Villa, M. (1); Cagnazzo, M. (1); Boeck, H. (1) 1 - Technical University Vienna - Atominstitut, Austria
RRFM2016-A0065	RADIATION DAMAGE INDUCED IN ZR-4 ALLOYS BY 2.6 MEV PROTON: APPLICATION FOR NUCLEAR RESEARCH REACTOR	Izerrouken, M. (1); Menchi, O. (1); Souami, N. (2); Sari, A. (3); Medjkoun, H. (1) 1 - Nuclear Research Center of Draria, Algeria 2 - Nuclear Research Center of Algiers, Algeria 3 - Nuclear Research Center of Birine, Algeria
RRFM2016-A0120	AN FACILITY INFRASTRUCTURE MANAGEMENT SYSTEM FOR THE JM-1 SLOWPOKE RESEARCH REACTOR	Preston, J. (1); Dennis, H. (1); Cushnie, R. (1) 1 - International Centre for Environmental and Nuclear Sciences, University of the West Indies Mona Campus, Jamaica
RRFM2016-A0143	THE NEW I&C SYSTEM OF THE TRIGA MARK II REACTOR VIENNA	Villa, M. (1); Bergmann, R. (1); Böck, H. (1); Kroc, M. (2); Prokš, M. (2); Valenta, V. (2); Kase, M. (3); Herrmann, J. (3); Matoušek, J. (3) 1 - Vienna University of Technology, Atominstitut, Austria 2 - ŠKODA JS a.s, Czech Republic 3 - dataPartner, Czech Republic
RRFM2016-A0060	THE THIRD REFURBISHMENT PROGRAMME OF THE BR2 REACTOR IN MOL, BELGIUM	Van Dyck, S. (1); Verpoorten, J. (1); Claes, W. (1); Leysen, P. (1) 1 - SCK CEN, Belgium
RRFM2016-A0149	IAEA ACTIVITIES IN THE OPERATION AND MAINTENANCE RESEARCH REACTORS	Kim, H. K. (1); Morris, C. R. (1) 1 - International Atomic Energy Agency, Austria
RRFM2016-A0153	EXACT POWER EVALUATION TO INTRODUCTION OF-LEU TARGETS FOR FRM II	Röhrmoser, A. (1) 1 - TU Munich, Germany
RRFM2016-A0197	TRIGA® 250 KW REACTOR I&C SYSTEM REFURBISHMENT	Růžička, P. (1) 1 - ŠKODA JS a.s., Czech Republic
RRFM2016-A0208	OPAL REACTOR CONTROL SYSTEM UPGRADE AND THE CONVERGENCE OF THE INFORMATION TECHNOLOGY AND CONTROL SYSTEM INDUSTRIES	Harrison, S. (1) 1 - Australian Nuclear Science and Technology Organisation, Australia

Security

RRFM2016-A0103	MANAGEMENT OF SAFETY AND SECURITY FOR HANARO RESEARCH REACTOR AND NUCLEAR FACILITIES	Jung, H.-S. (1); Kim, B.-H. (1); Kang, M.-J. (1); Hwang, I.-A. (1) 1 - Department of Nuclear Safety and Security, Korea Atomic Energy Research Institute , Korea, Republic of

Fuel Back-end

RRFM2016-A0069	NEW DUAL-PURPOSE CASK CASTOR® MTR 3 FOR DISPOSAL OF SPENT FUEL FROM GERMAN RESEARCH REACTORS	Bozkurt, M. (1); Becker, J. (1); Landsiedel, D. (1) 1 - GNS Gesellschaft für Nuklear-Service mbH, Germany
RRFM2016-A0144	AUSTRALIAN RESEARCH REACTORS SPENT FUEL MANAGEMENT: THE PATH TO SUSTAINABILITY	Finlay, R. (1); Domingo, X. (2); Laloy, V. (3); Dimitrovski, L. (1); Miller, R. (1); Landau, P. (2); Valery, J.-F. (2) 1 - Australian Nuclear Science and Technology Organization (ANSTO), Australia 2 - AREVA NC, France 3 - AREVA TN, France

RRFM2016-A0201	OPTIMIZING APPROACHES TO SPENT NUCLEAR FUEL TRANSPORT	Dewes, J. (1); Bolshinsky, I. (2); Tozser, S. (3) 1 - Savannah River National Laboratory, United States 2 - Idaho National Laboratory, United States 3 - International Atomic Energy Agency, Austria

CNS

RRFM2016-A0023	DEVELOPMENT OF A COLD NEUTRON SOURCE AND COLD NEUTRON BEAM FACILITIES AT THE PENN STATE BREAZEALE REACTOR.	Unlu, K. (1) 1 - Pennsylvania State University, Radiation Science and Engineering Center, United States
RRFM2016-A0052	12 YEARS OF EXPERIENCE FROM RUNNING A COLD NEUTRON SOURCE AT FRM II RESEARCH REACTOR	Päthe, D. (1); Wirtz, A. (1); Gerstenberg, H. (1); Kastenmüller, A. (1) 1 - Technische Universität München, ZWE FRM-II, Germany
RRFM2016-A0066	OPERATIONAL EXPERIENCE ON THE COLD NEUTRON SOURCE AT THE OPAL REACTOR	Sah, A. (1); Walsh, P. (1); Tobin, A. (1); Breslin, S. (1); Abraham, R. (1); Lu, W. (1) 1 - Australia Nuclear Science and Technology Organisation, Australia
RRFM2016-A0084	COLD NEUTRON SOURCES – AN INTERNATIONAL TECHNICAL MEETING IN AIX-EN-PROVENCE	Manifacier, L. (1); Koubbi, J. (1); Boyard, M. (1) 1 - AREVA TA, France
RRFM2016-A0093	THE ORNL HIGH FLUX ISOTOPE REACTOR SUPERCRITICAL HYDROGEN COLD SOURCE	Selby, D. (1); Christian, C. (2) 1 - National Resource Management, United States 2 - Oak Ridge National Laboratory, United States

RRFM2016-A0176	STATUS OF THE LIQUID DEUTERIUM COLD NEUTRON SOURCE FOR THE NIST RESEARCH REACTOR	Williams, R. (1); Middleton, M. (1); Kopetka, P. (1); Rowe, M. (1); Brand, P. (1) 1 - National Institute of Standards and Technology, United States

New Projects

RRFM2016-A0009	JULES HOROWITZ REACTOR: PREPARATION OF THE COMMISSIONING PHASE AND NORMAL OPERATION	Estrade, J. (1); Bravo, X. (1); Bignan, G. (1); Fabre, J.-L. (1); Marcille, O. (1) 1 - COMMISSARIAT A L'ENERGIE ATOMIQUE ET AUX ENERGIES ALTERNATIVES, France
RRFM2016-A0025	TREAT TRANSIENT TEST REACTOR RESTART STATUS	Bumgardner, J. (1) 1 - Idaho National Laboratory, United States
RRFM2016-A0027	MANAGING CONCURRENT DESIGNS OF NEW RESEARCH REACTORS	De Lorenzo, N. (1) 1 - INVAP S.E., Argentina

RRFM2016-A0068	PROGRESS OF KIJANG RESEARCH REACTOR PROJECT	Kwon, T.-H. (1); Lee, K. H. (1); Kim, J. Y. (1); Kim, J. (1); Kim, J.-K. (1) 1 - Korea Atomic Energy Research Institute, Korea, Republic of
RRFM2016-A0109	REVIEW OF POOL TYPE RESEARCH REACTORS DESIGN AND UTILIZATION RELATED FEATURES IN LIGHT OF UP TO DATE PRACTICES	Pascal, C. (1); Estrade, J. (2) 1 - Research Reactors & Installation Department, AREVA TA, France 2 - Nuclear Energy Directorate, French Alternative Energies and Atomic Energy Commission - Cadarache Research Centre, France
RRFM2016-A0111	CONCEPTUAL DESIGN OF A LOW-POWER HYBRID RESEARCH REACTOR FOR EDUCATION AND TRAINING	Lim, I.-C. (1); Hong, S.-T. (1) 1 - Korea Atomic Energy Research Institute, Korea, Republic of
RRFM2016-A0136	THE INVESTIGATION OF THE NEW MULTIPURPOSE RESEARCH REACTOR SUCCEEDING TO JRR-3	Takino, K. (1); Arai, M. (1); Murayama, Y. (1) 1 - Japan Atomic Energy Agency, Japan
RRFM2016-A0159	KEY TECHNICAL CHARACTERISTICS RELATED TO THE DESIGN OF THE RA-10 MULTIPURPOSE REACTOR	Cantero, P. (1); Ramirez, P. (1); Brollo, F. (1); Marinsek, G. (1); Balumann, H. (1); Zalcman, J. (2); Milberg, M. (2); Giuliodori, L. (2); Marzano, L. (2); Quesada, G. (2); Estryk, D. (2); Rios, G. (2); Alarcon, J. (2); Rodriguez, G. (2); Lee, J. (2); Garcia, D. (2); Verrastro, C. (2); Hofer, C. (2) 1 - Nuclear Engineer Division – Nuclear Energy Department – National Atomic Energy Commission , Argentina 2 - I&C Division – Nuclear Energy Department – National Atomic Energy Commission, Argentina

Decommissioning

RRFM2016-A0118	DISMANTLING OF THE SVAFO-RESEARCH REACTOR R2&R2-0 IN SWEDEN	Clement, G. (1); Arnold, H.-U. (1); Schmidt, N. (1) 1 - AREVA, France

RRFM2016-A0174	AN OPTIMIZED CASK TECHNOLOGY FOR CONDITIONING, TRANSPORTATION, STORAGE UP TO FINAL DISPOSAL OF NUCLEAR WASTE AND MATERIAL	Domingo, X. (1); Laloy, V. (2); Lefort-Mary, F. (1); Lamouroux, C. (1); Kerr, B. (2); Dumont, B. (2) 1 - AREVA NC, France 2 - AREVA TN, France
RRFM2016-A0211	PREPARATION OF OSIRIS REACTOR SHUTDOWN AND DECOMMISSIONING	Zampa, J. S. (1); Lasou, G. (2); Auclair, M. (3) 1 - OSIRIS reactor, DRSN/SEROS, CEA Centre de Saclay, France 2 - DPAD/CPSA, CEA Centre de Saclay, France 3 - DRSN/SIREN, CEA Centre de Saclay, France
RRFM2016-A0227	ANALYSIS OF THE ACTIVATION AT THE END OF OPERATION OF THE BERLIN EXPERIMENTAL REACTOR II	Lapins, J. (1); Guilliard, N. (1); Bernnat, W. (1); Welzel, S. (2); Rose, M. (2) 1 - Institut for Nuclear Technology and Energy System, University of Stuttgart, Germany 2 - Helmholtz-Zentrum Berlin GmbH, Germany

POSTER

Poster CNS

RRFM2016-A0115	A MCNPX TRIGA RC-1 EXPERIMENTAL CHANNELS MODEL FOR THE DESIGN OF A NEW NEUTRONIC DIFFRACTION FACILITY	Falconi, L. (1); Burgio, N. (1); Palomba, M. (1); Santoro, E. (1); Carta, M. (1); Ghigna, P. (2); Prata, M. (3); Salvini, A. (3); Altieri, S. (4); Bortolussi, S. (5); Reversi, L. (6) 1 - ENEA CR Casacci, Italy 2 - Dipartimento di Chimica - Università degli Studi di Pavia, Italy 3 - L.E.N.A. - Laboratorio Energia Nucleare Applicata - Università degli Studi di Pavia, Italy 4 - Dipartimento di Fisica- Università degli Studi di Pavia, Italy 5 - INFN - Istituto Nazionale di Fisica Nucleare, Italy 6 - Università degli Studi di Firenze, Italy
RRFM2016-A0180	MECHANICAL SIZING METHODOLOGY FOR A COLD NEUTRON SOURCE	Kohler, J. (1); Lecarpentier, B. (1) 1 - AREVA TA, France

Poster Safety

RRFM2016-A0022	EFFECT OF REACTOR REGULATING SYSTEM ON A FLOW BLOCKAGE EVENT OF A RESEARCH REACTOR	Yum, S.-B. (1); Park, S.-K. (1) 1 - Korea Atomic Energy Research Institute (KAERI), Korea, Republic of
RRFM2016-A0032	A SELF-CONTROLLED LOW POWER REACTOR	Boschetti, F. (1); Doval, A. (1); Hergenreder, D. (1); Lupiano contreras, J. (1); Masriera, N. (1); Sarabia, G. (1) 1 - INVAP S.E., Argentina
RRFM2016-A0043	INFLUENCE OF CRITICAL HEAT FLUX CORRELATIONS ON SAFETY ANALYSIS OF RESEARCH REACTORS WITH NARROW RECTANGULAR FUEL CHANNELS	Rawashdeh, A. (1); Albati, M. (1); Abusaleem, K. (2); Abushqair, A. (1); Omari, M. (1); Alrwashdeh, M. (1); Lee, B. (3); Chung, Y. J. (3) 1 - Jordan Atomic Energy Commission (JAEC), Jordan 2 - The University of Jordan, Jordan 3 - Korea Atomic Energy Research Institute (KAERI), Korea, Republic of

RRFM2016-A0051	A COMPARISON OF THERMO-T SYSTEM CODE WITH EXPERIMENTAL DATA FROM THE SPERT-IV D-12/15 SERIES	Margulis, M. (1); Gilad, E. (1) 1 - The Unit of Nuclear Engineering, Ben-Gurion University of the Negev, Israel
RRFM2016-A0058	DETECTION OF BOILING OCCURRENCE BY SENSING PRESSURE WAVE OF COLLAPSING BUBBLES IN SUBCOOLED WATER	Jo, D. (1); Jo, H. (1) 1 - School of Mechanical Engineering, Kyungpook National University, Korea, Republic of
RRFM2016-A0169	A REVIEW OF THE DESIGN FEATURES OF RESEARCH REACTOR AIR VENTILATION AND CLEANING SYSTEM	Kim, M. (1); Lee, C. (1) 1 - Korea Atomic Energy Research Institute, Korea, Republic of
RRFM2016-A0190	DYNAMIC ANALYSIS OF A TRIGA REACTOR	Domitry, P. (1); Ramsey, J. (2); Kohut, P. (3) 1 - PAA, National Atomic Energy Agency, Poland, Poland 2 - US Nuclear Regulatory Commission, United States 3 - Brookhaven National Laboratory, United States
RRFM2016-A0198	HYPOTHETICAL ACCIDENT ANALYSES ON THE PROPOSED SPLIT CORE AT NIST USING ANL-PARET CODE	Wu, Z. (1); Williams, R. (1); Rowe, J. M. (1) 1 - NIST Center for Neutron Research, United States

Poster New Projects

RRFM2016-A0214	DESIGN AND QUALIFICATION OF JULES HOROWITZ REACTOR CONTROL ROD DRIVE MECHANISMS	Dumanois, C. (1); Valy, R. (1); Ropke, P. (1); Donnier, F. (1); Ranc, L. (1) 1 - AREVA TA, France

Poster Decommissioning

RRFM2016-A0080	SAFETY AND REGULATORY ASPECTS OF SHUTDOWN OPERATIONS AND DECOMMISSIONING OF PHÉNIX REACTOR.	Masseau, X. (1); Massieux, S. (1) 1 - Institut de Radioprotection et de Sûreté Nucléaire (IRSN), France

Poster Innovative Methods

RRFM2016-A0054	DESIGN OF A DRY BEAM RADIATION SHIELDING PLUG FOR RESEARCH REACTORS	Meier, H. (1); Hergenreder, D. (1) 1 - INVAP S.E., Argentina
RRFM2016-A0078	CALCULATION METHODS FOR SAFETY ASSESSMENTS OF RESEARCH REACTORS	Koubbi, J. (1); Bayol, C. (1); Lacombe, J.-G. (1); Bouret, C. (1); Manifacier, L. (1); Krohn, H. (2); Welzel, S. (2) 1 - AREVA TA, France 2 - Helmholtz-Zentrum Berlin für Materialien und Energie, Germany
RRFM2016-A0081	COCONEUT: FIRST VALIDATION STEPS OF THE AREVA TA NEUTRONIC SCHEME FOR RESEARCH REACTOR DESIGN	Bouret, C. (1); Lacombe, J.-G. (1); Bayol, C. (1); Koubbi, J. (1); Manifacier, L. (1); Vidal, J.-F. (2); Gastaldi, B. (2) 1 - AREVA TA, France 2 - CEA/DEN/DER/SPRC CEA Cadarache, France

RRFM2016-A0090	HEAT TRANSFER ANALYSIS OF MICROSCALE UO2 PARTICLE-GRAPHITE SYSTEM IN TREAT FUEL	Mo, K. (1); Miao, Y. (1); Yacout, A. (1); Wright, A. (1); Connaway, H. (1) 1 - Argonne National Laboratory, United States
RRFM2016-A0113	FIRST STEPS TOWARDS A COUPLED CODE SYSTEM FOR TRANSIENT CALCULATIONS	Reiter, C. (1); Breitkreutz, H. (1); Röhrmoser, A. (1); Petry, W. (1) 1 - Forschungs-Neutronenquelle Heinz Maier-Leibnitz (FRM II), Technische Universität München, Germany
RRFM2016-A0116	IMPROVEMENTS IN NEUTRON AND GAMMA MEASUREMENTS FOR MATERIAL TESTING REACTORS	Villard, J.-F. (1); Destouches, C. (1); Barbot, L. (1); Fourmentel, D. (1) 1 - CEA, DEN, DER, Instrumentation Sensors and Dosimetry Laboratory, France
RRFM2016-A0117	FLAT REACTIVITY OPERATION COURSE WHEN CONVERTING FRM II	Röhrmoser, A. (1) 1 - TU Munich, Germany
RRFM2016-A0139	THE ANET CODE: FROM HIGH ENERGY PHYSICS TO STOCHASTIC DYNAMIC NEUTRONICS WITH THERMAL HYDRAULIC FEEDBACK	Xenofontos, T. (1); Mylonakis, A. (1); Savva, P. (1); Varvayanni, M. (1); Silva, J. (2); Maillard, J. (3); Catsaros, N. (1) 1 - Institute of Nuclear and Radiological Sciences & Technology, Energy & Safety, NCSR "DEMOKRITOS", Greece 2 - Université Pierre et Marie Curie, Campus Jussieu, France 3 - Inst. du Dévelop. et des Ressources en Inform. Scient., CNRS, France
RRFM2016-A0142	ENHANCED COMPUTATIONAL MODELS OF THE UNIVERSITY OF FLORIDA TRAINING REACTOR (UFTR)	Springfels, D. (1); Jordan, K. (1) 1 - University of Florida, United States
RRFM2016-A0163	NEUTRON SHIELDING CALCULATION FOR NEUTRON IMAGING FACILITY AT MAÂMORA TRIGA REACTOR	Ouardi, A. (1) 1 - Centre National de L'énergie des Scinces et des Techniques Nucléaires, Morocco
RRFM2016-A0177	NDT TECHNIQUE APPLIED TO DIRECT MEASURING OF THERMAL CONDUCTIVITY IN UMo FUEL MINIPLATE	Lisboa, J. (1); Marin, J. (1); Barrera, M. (1); Gutierrez, C. (1); Salinas, P. (2); Olivares, L. (1) 1 - CHILEAN COMMISSION FOR NUCLEAR ENERGY, Chile 2 - UNIVERSIDAD DE SANTIAGO DE CHILE - USACH, Chile
RRFM2016-A0188	VALIDATION OF THE NEUTRON CALCULATION TOOL ANUBIS V3 FOR THE OSIRIS MATERIAL TESTING REACTOR	Malouch, F. (1); Lopez, F. (1) 1 - CEA, Saclay Center, DEN/DANS/DM2S/SERMA, France
RRFM2016-A0191	DEVELOPMENT OF AN ADVANCED RELAP/SCDAPSIM/MOD4.0 U-AL FUEL PLATE COMPONENT MODEL FOR THE ANALYSIS OF DESIGN BASIS AND SEVERE ACCIDENTS IN RESEARCH REACTORS	Shumski, S. (1); Delbianco, D. (2); Pericas, R. (3); Allison , C. (4); Hohorst, J. (4) 1 - Warsaw University of Technology , Poland 2 - INVAP, SE, Argentina 3 - Technical University of Catalonia, Spain 4 - Innovative Systems Software, United States
RRFM2016-A0196	EXPERIMENTAL DATA ON CRITICALITY OF URANIUM-ZIRCONIUM HYDRIDE SYSTEMS WITH 21 AND 36 % ENRICHED URANIUM-235	Sikorin, S. (1); Polazau, S. (1); Hryharovich, T. (1) 1 - Joint Institute of Power and Nuclear Research-Sosny of the National Academy of Science of Belarus , Belarus
RRFM2016-A0235	THERMAL-HYDRAULIC MODELING OF A TYPICAL MULTI-PURPOSE RESEARCH REACTOR (MPRR)	Mousavian, S. K. (1); Khoshnevis, T. (1); Bahrevar, M. H. (1) 1 - Atomic Energy Organization of Iran, Iran, Islamic Republic of

Poster Utilisation

RRFM2016-A0017	JULES HOROWITZ REACTOR, FRANCE. DEVELOPMENT OF AN EXPERIMENTAL LOOPAN OPTIMIZED IRRADIATION PROCESS	Gaillot, S. (1); Dousson, T. (1); Nicolas, W. (2) 1 - CEA Cadarache, France 2 - EDF, SEPTEN, France
RRFM2016-A0029	DEVELOPMENT OF IRRADIATION TARGETS FOR 99MO PRODUCTION BY NUCLEAR FISSION	Durazzo, M. (1); Conturbia, G. (1); Souza, J. A. B. (1); Urano de Carvalho, E. F. (1); Riella, H. G. (1) 1 - Nuclear and Energy Research Institute - IPEN-CNEN/SP, Brazil
RRFM2016-A0040	EFFECTIVE UTILISATION OF THE REZ´S RESEARCH REACTOR LVR-15 IN BASIC, INTERDISCIPLINARY AND APPLIED RESEARCH	Mikula, P. (1); Strunz, P. (1) 1 - Nuclear Physics Institute ASCR, v.v.i., Czech Republic
RRFM2016-A0057	SILICON INGOT THERMAL PERFORMANCE DURING IRRADIATION AND EFFECTS ON ELECTRONIC PARAMETER	Othman, M. (1); Agamy, S. (2); Nagy, M. (2); Sultan, M. (1) 1 - Egyption Atomic Energy Authority (EAEA), Egypt 2 - Alexandria University , Egypt
RRFM2016-A0130	PERFORMANCE TEST OF SPND FOR THE DEVELOPMENT OF LLICI AT THE UCI TRIGA REACTOR	Yang, S. W. (1); Park, S. J. (1); Cho, M. S. (1); Wallick, J. (2); Miller, G. E. (2); Shin, H. C. (3); Cha, K. H. (3) 1 - Korea Atomic Energy Research Institute, Korea, Republic of 2 - The University of California, Irvine, United States 3 - Korea Hydro & Nuclear Power co., ltd, Korea, Republic of
RRFM2016-A0140	THE POWER CONTROL BASED SUBCRITICALITY MONITORING (PCSM) METHOD FOR ADS REACTORS	Burgio, N. (1); Carta, M. (1); Fabrizio, V. (1); Falconi, L. (1); Gandini, A. (2); Iorio, M. G. (1); Peluso, V. (3); Santoro, E. (1) 1 - ENEA CR Casaccia, Italy 2 - Dipartimento DIAEE - Università degli Studi di Roma 'La Sapienza', Italy 3 - ENEA C.R. BOLOGNA, Italy
RRFM2016-A0147	NEUTRON ACTIVATION ANALYSIS IN SUPPORT OF UNDEGRADUATE RESEARCH	Landsberger, S. (1); Tamalis, D. (2); Tipping, T. (1); Biegalski, S. (1) 1 - University of Texas at Austin, Nuclear Engineering Teaching Lab, United States 2 - Florida Memorial University, Department of Health and Natural Sciences, United States

Poster Operation & Maintenance

RRFM2016-A0031	GRADED APPROACH OF COMPONENT CLASSIFICATION IN NUCLEAR RESEARCH REACTORS	Ellethy, Y. (1) 1 - Egyptain Atomic Energy Authority (EAEA), Egypt
RRFM2016-A0074	Development of transportation container for the neutron startup source of High Temperature Engineering Test Reactor (HTTR)	Shimazaki, Y. (1); Sawahata, H. (1); Kawamoto, T. (1); Shinohara, M. (1); Ono, M. (1); Tochio, D. (1); Hamamoto, S. (1); Takada, S. (1) 1 - Japan Atomic Energy Agency, Japan

RRFM2016-A0108	USE OF UNICORN ANALOGUE I&C PLATFORM FOR RPS IN RESEARCH REACTOR	Lobry, C. (1) 1 - AREVA TA, France
RRFM2016-A0122	GAMMA AND NEUTRON RADIATION FIELDS ABOVE THE REACTOR POOL OF THE LVR-15 RESEARCH REACTOR	Viererbl, L. (1); Lahodová, Z. (1); Mojžíš, Z. (1); Klupák, V. (1); Voljanskij, A. (1) 1 - Research Centre Rez Ltd., Czech Republic
RRFM2016-A0182	ADVANCES IN MATERIALS SURVEILLANCE PROGRAMME FOR THE RA10 RESEARCH REACTOR	Versaci, R. (1); Bertolino, G. (1); Yawny, A. (1); Arias, G. (1); Blaumann, H. (1) 1 - Comisión Nacional de Energia Atómica , Argentina
RRFM2016-A0210	QUALITY ASSURANCE AND QUALIFICATION OF NEW DIGITAL I&C SYSTEMS AFTER REFURBISHMENT OF THE TRIGA AND LVR-15 REACTORS	Matoušek, J. (1); Herrmann, J. (1); Kochová, M. (1) 1 - dataPartner s.r.o, Czech Republic

Poster Fuel Cycle

RRFM2016-A0021	A CLADDING THICKNESS MEASUREMENT OF RESEARCH REACTOR FUEL PLATE USING NONDESTRUCTIVE TESTING METHOD.	Lee, Y.-S. (1); Joo, Y.-S. (1); So, W. (1); Park, S. (1) 1 - Korea Atomic Energy Research Institute, Korea, Republic of
RRFM2016-A0076	STATUS UPDATE ON MINIPLATE EXPERIMENTS DESIGNS PLANNED FOR IRRADIATION IN ATR	Glagolenko, I. (1); Woolstenhulme, N. (1); Lillo, M. (1); Nielsen, J. (1); Choe, D. (1); Navarro, J. (1); Jensen, C. (1); Crawford, D. (1); Jones, W. (1); Snow, S. (1); Hawkes, B. (1); Wiest, J. (1); Keiser, D. (1); Holdaway, K. (1); Schulthess, J. (1); Rabin, B. (1) 1 - Idaho National Laboratory, United States
RRFM2016-A0091	ION IRRADIATION AND SYNCHROTRON MICRODIFFRACTION ANALYSIS OF UMO-AL INTERACTION LAYER	Jamison, L. (1); Mo, K. (1); Ye, B. (1); Miao, Y. (1); Bhattacharya, S. (2); Xu, R. (1); Yacout, A. (1) 1 - Argonne National Laboratory, United States 2 - Northwestern University, United States
RRFM2016-A0096	OPTIMIZATION OF A THIN U-10MO FUEL PLATE CASTING BY MODELING AND EXPERIMENT	Aikin, R. (1); Dombrowski, D. (1) 1 - Los Alamos National Laboratory, United States

RRFM2016-A0097	CAN-LESS HIP METHOD FOR PRODUCING FUEL PLATES	Lienert, T. (1); Dvornak, M. (1); Dombrowski, D. (1) 1 - Los Alamos National Laboratory, United States
RRFM2016-A0098	ELECTROPLATING OF ZIRCONIUM ON URANIUM-MOLYBDENUM ALLOY FUEL FOR HIGH PERFORMANCE RESEARCH REACTORS.	Meinhardt, K. (1); Lavender, C. (1); Coffey, G. (1); Smirnov, A. (2); Shchetkovskiy, A. (2); O'Dell, S. (2) 1 - Pacific Northwest National Laboratory, United States 2 - Plasma Processes, United States
RRFM2016-A0135	BURNABLE ABSORBER OPTIMIZATION IN A SUPER-FLUX RESEARCH REACTOR UTILIZING PLATE-TYPE FUEL	Nguyen, X. H. (1); Venneri , P. (1); Kim, Y. (1); Beeley, P. (2) 1 - Korea Advanced Institute of Science and Technology, Korea, Republic of 2 - Khalifa University, United Arab Emirates
RRFM2016-A0138	ALL-IN-ONE CHEMICAL CLEANING AND DEOXIDATION PROCESS FOR MONOLITHIC URANIUM-MOLYBDENUM FOILS	Schwarz, C. (1); Dirks, T. (1); Baumeister, B. (1); Steyer, C. (1); Petry, W. (1) 1 - Forschungs-Neutronenquelle Heinz Maier-Leibnitz (FRM II), Germany
RRFM2016-A0183	DESIGN, FABRICATION AND CALIBRATION OF THE SLOWPOKE-2 LEU COMMISSIONING ROD ASSEMBLY	Koclas, C. (1); Muftuoglu, A. (1); Teyssedou, A. (1); Grant, C. (2); Chilian, C. (1) 1 - Polytechnique Montreal, Canada 2 - ICENS, Jamaica
RRFM2016-A0187	HOT ISOSTATIC PRESS CLADDING PROCESS OPTIMIZATION AND HIP CAN SCALE-UP FOR THE PRODUCTION OF MONOLITHIC FUEL PLATES	Clarke, K. (1); Tucker, L. (1); Aikin, B. (1); Vargas, V. (1); Dvornak, M. (1); Strandy, M. (1); Hudson, R. (1); Dombrowski, D. (1); Imhoff, S. (1); Montalvo, J. (1); Mauro, M. (1); Alexander, D. (1); Liu, C. (1); Lovato, M. (1) 1 - Los Alamos National Laboratory, United States

RRFM2016-A0233	IMPLEMENTATION OF REACTOR CORE CONVERSION PROGRAM OF GHARR-1	Odoi, H. C. (1); Nyarko , B. J. B. (1); Morman , J. (2); Aboh, I. J. K. (1) 1 - Ghana Atomic Energy Commission , Ghana 2 - Argonne National Laboratory - II, United States


RRFM
EUROPEAN RESEARCH REACTOR CONFERENCE 2016
IGORR
BERLIN
13 - 17 March 2016
GERMANY

Plenary

The CEA scientific and technical offer as a designated ICERR (International Center based on Research Reactor) by the IAEA

Gilles Bignan, Jean-Yves Blanc, Xavier Bravo, Jérôme Estrade

French Atomic and Alternative Energies Commission
Nuclear Energy Division
Cadarache and Saclay Research Centres
France
Corresponding author: gilles.bignan@cea.fr

Abstract

The IAEA Director General has approved on September 2014 a new initiative, namely the IAEA designated **International Centre based on Research Reactors (ICERR)**, which will help Member States to gain access to international research reactor infrastructures. In fact, for the agency, one of the main goals of this ICERR scheme is to help Member States, mainly without research reactors, to gain timely access to research reactor infrastructure to carry out nuclear research and development and build capacity among their scientists.
CEA has decided to be candidate to its designation as an ICERR and consequently has established a candidacy report following criteria given by the IAEA in the Terms of Reference (logistical, technical and sustainability criteria). The CEA offer is covering a broad scope of activities on the 3 following topics:

- Education & Training
- Hands-On Training
- R&D Projects.

The perimeter (facilities and associated scientific and technical skills) proposed by CEA on this ICERR is centred on JHR project (its future international Material Testing Reactor under construction in Cadarache) associated to ancillary facilities in operation such as:

- ORPHEE research reactor in Saclay, a neutron beams reactor used for science,
- ISIS, EOLE and MINERVE zero/low power reactors located in Saclay and in Cadarache, dedicated to Core Physics and Education & Training in nuclear engineering,
- LECA-STAR and LECI hot laboratories for fuel and material Post Irradiated Examinations, located in Cadarache and in Saclay.

The designation was the result of a rigorous process, including the review of the application and support documentation, an audit mission performed at the CEA sites, as well as a comprehensive evaluation and recommendation by an international selection committee made up of representatives from the global research reactor community and IAEA staff.

CEA Cadarache and Saclay centers are the first designated ICERR by the agency; this has become official during the last General Conference on the **14th September 2015**. The Director General of the agency indicated the agency motivations at a ceremony during which he awarded the designation to CEA: *"Such centers will enable researchers from IAEA Member States, especially developing states, to gain access to research reactor capabilities and develop human resources efficiently, effectively, and, probably, at a lower cost. The ICERR scheme will also contribute to enhanced utilization of existing research reactor facilities and, by fostering cooperation, to the development and deployment of innovative nuclear technologies".*

This paper presents in detail the facilities proposed by CEA in its ICERR designation for welcoming scientists on the 3 topics indicated above (Education & Training, Hands-On Training, R&D Projects).

Introduction

The "IAEA designated International Centre based on Research Reactor (ICERR)" scheme was approved by IAEA Director General on 9th September 2014 and officially presented to the IAEA Board of Governors during the meeting held on 15th September 2014.

The ICERR scheme is intended to help IAEA Member States gain timely access to relevant nuclear infrastructure based on RRs and their ancillary facilities. ICERRs will make available their RRs and ancillary facilities and resources to organizations/institutions of IAEA Member States seeking access to such nuclear infrastructure (named Affiliates). For Affiliates, ICERRs will provide an opportunity to access RR capabilities much sooner and, probably, at a lower cost.

The implementation of the ICERR scheme will also contribute to enhance the utilization of some existing RR facilities (e.g. those that, in order to meet the criteria for designation would be stimulated to enhance their utilization and to foster their accessibility to attract potential Affiliates). On the other hand, an ICERR could benefit, for example, from additional scientific and/or technical resources made available by the Affiliate (e.g. Secondees) and by the increase of its international visibility.

By fostering wider utilization in cooperative manner of RR(s) and ancillary facilities capabilities, ICERRs could also effectively contribute to the development and deployment of innovative nuclear technologies.

Brief description of CEA Facilities proposed in the ICERR

CEA has decided to be candidate to its designation as an ICERR and has prepared a candidacy report indicating its motivation and answers to the Terms of Reference criteria's as being designated an ICERR- See Terms Of Reference in [1]. This report has been sent to the Agency in January 2015 for examination.

CEA has a few decades-long experiences in operating and using research reactors for various purposes, Zero Power Reactors for Core physics, Material Testing Reactors, safety-dedicated Reactors, neutron beams reactors for science and Low Power Reactor for Education & Training.

CEA maintains a long tradition of international collaboration agreements in the field of peaceful uses of Nuclear Energy both with Member States or organizations having extensive nuclear programs, but also with new comers (potential or existing ones) or countries with no or limited nuclear power experience.

The perimeter (facilities and associated scientific and technical skills) proposed by CEA to be include in this ICERR is centered on its future international Material Testing Reactor; the Jules Horowitz Reactor under construction in Cadarache. Ancillary facilities will also be a very important part of the ICERR; they include:

- ORPHEE research reactor in Saclay, neutron beams reactor used for science, academic and industrial research, training and education to the use of neutrons scattering,

- ISIS EOLE and MINERVE zero/low power reactors located in Saclay and in Cadarache, dedicated to Core Physics and Education & Training in nuclear engineering,

- LECA-STAR and LECI hot laboratories for fuel and Material Post Irradiated Examination, located in Cadarache and in Saclay.

1] The Jules Horowitz Reactor

The Jules Horowitz Reactor (JHR) is a new Material Testing Reactor (MTR) currently under construction at CEA Cadarache research centre in the South of France. It will represent a major research infrastructure for scientific studies dealing with material and fuel behaviour under irradiation (and is consequently identified for this purpose within various European road maps and forums: ESFRI, SNETP…). The reactor will also contribute to medical isotope production.

The reactor will perform R&D programs for the optimization of the present generation of Nuclear Power Plans (NPPs), will support the development of the next generation of NPPs (mainly LWRs) and also offer irradiation capabilities for future reactor materials and fuels.

JHR is fully optimized for testing material and fuel under irradiation, in normal and off-normal conditions:

- with modern irradiation loops producing the operational condition of the different power reactor technologies,
- with major innovative embarked in-pile instrumentation and out-pile analysis to perform high-quality R&D experiments,
- with high thermal and fast flux capacity to address existing and future NPP needs.

JHR is designed, built and will be operated as an international user-facility open to international collaboration. This results in several aspects:

- a partnership with the funding organizations gathered within an international consortium,
- setting-up of an international scientific community around JHR through seminars, working groups to optimize the experimental capacity versus future R&D needs.
- preparation of the first JHR International Program potentially open to non-members of the JHR consortium.

Consequently, the JHR facility will become a major scientific hub for cutting edge research and material investigations (multilateral support to complete cost effective studies avoiding fragmentation of scientific effort, access to developing countries to such state of the art research reactor facilities, supra national approach….). Many publications [2, 3, 4] described in detail the JHR project. It will answer needs expressed by the scientific community (R&D institutes, TSO…) and the industrial companies (utilities, fuel vendors…).

To prepare the future JHR scientific community, CEA has started five years ago a “Secondee program” welcoming scientists, engineers in the CEA team to prepare the first experimental capacity. Up to now more than 20 Secondees from various countries have participated to this program. **This hosting possibility within JHR team will be enhanced using the recent ICERR designation**.

2] The ORPHEE Research Reactor

ORPHEE is a pool-type reactor specifically designed to produce thermal neutron beams primarily used by the French user community of academic and industrial researchers working on neutron scattering instruments. **ORPHEE Research Reactor has a long tradition of welcoming foreign visiting professors, scientists but also post-doctoral students and such hosting capacity is proposed here through this ICERR designation**. This reactor of 14 MW power uses light water as coolant and heavy water as reflector reaching maximum thermal flux in the reflector of 3.10^{14} $n.cm^{-2}.s^{-1}$. It has 2 CNS - Cold Neutron Sources- (20 K) and 1 hot source (1400 K), 9 horizontal channels, 20 neutron beams, 9 vertical irradiation channels and 26 experimental areas.

The various devices (neutron radiography, imaging station…) around the neutron guides of the ORPHEE reactor are used for several industrial and research applications.

3] ISIS Research Reactor

The ISIS reactor is the neutron mock-up of the OSIRIS Material Testing Reactor. Both reactors are located in the same facility on the CEA Saclay Research Centre. The ISIS reactor has a maximal rated power of 700 kW. Although OSIRIS has been shut down last December 2015, ISIS will at least continue being in operation until the end of this decade.
The reactor is now mainly used for Education and Training in the frame of academic programs. An extensive panel of experiments covering the reactor operation and related activities has been developed. They are addressed to trainees from different fields and education levels, i.e. bachelor and master students, technicians, engineers and staff from various organisations including the French regulatory body. About 50 % of the teaching is carried out in English for foreign trainees. Since 2007, ISIS is typically operated 350 hours per year for education and training and about 400 trainees attend the courses every year (Master students, engineers, ASN staff, future operators of research reactors, etc.). The typical duration of a course is 3 hours, the courses being spread over 60 operating days. Concerning Education and Training, it is worth quoting that ISIS reactor has been designated as an Internet Reactor Laboratory (IRL) by the IAEA for Europe and Africa since 2013. This project is partially funded by the IAEA and aims at providing countries with access to the ISIS practical work sessions by means of live video-conferences. Video signals and graphs, including all the parameters relevant to reactor operation, will be transmitted while ensuring the strictest conditions of safety and security.
Thus, further development of the education and training activity could easily be achieved within the ICERR.

4] EOLE & MINERVE Reactor

The EOLE critical mock-up is a very low power experimental reactor (ZPR) designed to study the neutron behaviour of moderated lattices, in particular those of pressurised water reactors (PWR) and boiling water reactors (BWR). The first studies specifically dedicated to the French PWRs and the qualification of core calculation tools were launched in the early eighties.
EOLE provides fluxes up to 10^9n.cm^{-2}.s^{-1}. Thanks to the high level of flexibility of the reactor, it is possible to implement complex experimental set-ups representing various core configurations to be studied. The physical measurements recorded during the experimental programmes are used to fully characterise the configurations (critical sizes, absorber weights, refined power distributions, spectral indices, material buckling, reactivity effects – boron and/or temperature, kinetic parameters, etc.) thanks to proven experimental techniques:

- Gamma spectrometry
- Measurements using miniature fission chambers
- Thermo-luminescent detectors (TLD)
- Neutron activation dosimeters.

MINERVE is also a ZPR designed for neutron studies mainly aiming to improve the nuclear database for fuel systems representative of various nuclear reactor technologies. The thermal neutron flux in the vessel is 10^9n.cm^{-2}.s^{-1} (maximal power of 100 Watt).
Physical measurements (spectral index, conversion rates, axial and radial fission rate distributions, neutron activation) are also performed to characterize the neutron behaviour of both the core and the samples under investigation.
MINERVE is also used to test the performance of mini fission chamber prototypes developed by CEA and its partners. It is clearly identified as a reference facility for international collaborations on various aspects of experimental physics.
MINERVE is also a key-tool for Education & Training either for Nuclear Engineering Students or for Reactor Operators. **Both these 2 Zero Power Reactors have a long tradition to host foreign scientists, PhD, Post-Doc students for E&T and R&D projects and this capacity will also be enhanced through the ICERR designation.**

5] LECA-STAR Hot Laboratory

The LECA-STAR, located on the Cadarache nuclear centre, is the CEA hot laboratory in charge of the characterization of irradiated fuel for various types of nuclear industrial and/or research reactor.

The LECA-STAR was extensively refurbished between 2001 and 2011 to extend its operation. It represents a reference hot laboratory in support to the fuel experiments performed in any MTR. That means that refabricated short fuel rods to be irradiated in JHR will be manufactured there, and that fuel materials will be sent to LECA-STAR after their irradiation in JHR.

The LECA-STAR includes about 20 hot cells (up to 9 m long), with all the equipment for a wide range of irradiated fuel rod examinations, namely: non-destructive examination (visual inspection, confocal, radionuclide distribution by gamma-spectrometry, diameter measurement, eddy current

testing for cladding integrity and zirconia thickness, X-rays), puncturing and fission gas release measurements, cutting, macro- and microscopy examinations. A special area is devoted to micro-analysis, with fully-shielded SEM/FIB, EPMA, SIMS and XRD, all these equipment being adapted to irradiated-fuel or material examination.

The LECA-STAR facility is mainly devoted to R&D development within French joint programs with industrial partners as EDF and AREVA. Nevertheless this laboratory is able to welcome foreign scientists and engineers in other scientific and technical areas, such as the development of new hot cell equipment, fundamental or academic research topics and safety tests required to perform PIE conducted within the framework of International collaboration.

6] LECI Hot Laboratory

The LECI, located on the Saclay nuclear centre, is the CEA reference hot laboratory in support to JHR for Material testing. This laboratory is in charge of the characterization of irradiated non fissile materials for:

- Water cooled reactors (PWR and Material Testing Reactors): Pressure Vessel life extension (embrittlement, mechanical properties), Internals (swelling, creep, stress corrosion cracking of 304 or 316 stainless steels), Zirconium alloys for fuel pin cladding and assembly (evolution of metallurgical and mechanical properties in incidental, accidental or in service reactor conditions, in storage or retrieving after interim storage conditions of spent fuel pins-corrosion-interaction between fuel pellets and cladding), and Aluminium alloys for Material Testing Reactors: vessel and cladding materials,
- Generation IV reactors: Characterization of materials for fuel pin cladding and assembly for sodium or gas-cooled reactors (steels, ODS, ceramics, refractory materials, graphite).

The LECI includes about 50 hot cells, with up-to-date scientific equipment: metallography & optical microscopy, micro-hardness, SEM, TEM, EPMA, XRD, density, Raman spectroscopy, thermoelectric power, H_2 measurements, Eddy currents, metrology, 4 autoclaves (360°C, 220 bar, 1 coupled to slow tensile testing), machining (conventional, ram and wire spark erosion machining) and welding (TIG and Laser).

The LECI is the hot laboratory in support to OSIRIS -CEA MTR- for structural materials investigation (guide tube, fuel cladding, pressure vessel steel…). That means that refabricated short fuel rods to be irradiated in Osiris were manufactured there or in the LECA, and that materials were and are still sent to LECI after their irradiation in Osiris. It will also be the reference non-fissile material hot laboratory for JHR.

The LECI facility is mainly devoted to R&D development within French joint programs with industrial partners as EDF and AREVA. Nevertheless this laboratory is able to welcome foreign scientists and engineers in other scientific and technical areas, such as the development of new hot cell equipment, fundamental or academic research topics and experimental devices required to perform PIE on material.

Both these 2 Hot Laboratories have a long tradition to perform R&D programs within an international framework and consequently are ready to welcome scientists for Hands-On Training, R&D projects through this ICERR designation.

Review Process by the IAEA

The ICERR designation process, as described in the approved ICERR scheme Terms of Reference [1], takes into account and is limited to the specific area(s) of research reactor(s) activities for which the designation is requested. The assessment of the ICERR candidate covers the period of five (5) years immediately preceding the date of the submission of the application. The ICERR designation lasts for a period of five (5) years starting from the date of the designation.

To review the ICERR candidate's application and to provide recommendations to the IAEA on the ICERR designation of the applicant, the IAEA appoints a Selection Committee.

The tasks of the Selection Committee include:

- Review assigned request(s), including candidate(s) self-assessment and, if necessary, ask for additional information to the ICERR candidate(s) through the IAEA;
- Plan and prepare the review mission(s) at the ICERR candidate(s) site(s); and
- Prepare the review mission(s) report(s) that includes the recommendation for decision by the IAEA.

The review of the ICERR candidate's application, including the self-assessment, against the ICERR eligibility and criteria for designation [1] is performed by the Selection Committee before the review mission at ICERR candidate site(s) takes place. The review mission at the ICERR candidate site(s) is performed by designated members of a Selection Committee and according to the IAEA rules and regulations.

The IAEA informs the ICERR candidate of the result of its decision based on the candidate's self-assessment and on the recommendation of the Selection Committee. In case of a negative outcome, the IAEA provides recommendations to the ICERR candidate to meet the criteria for designation and the time frame to implement them.

Results of the IAEA Review Process and CEA offer as an ICERR

The review mission took place from 23rd to 27th March 2015 in Saclay and Cadarache centres.

The specific objectives of the mission were:

1. To assess the ICERR candidate' self-assessment against evidences available at ICERR candidate site(s);
2. To perform a technical visit of the research reactor(s) and, eventually, of the ancillary facilities considered for the ICERR designation; and
3. To prepare a comprehensive meeting report to be considered and included in the Selection Committee's recommendations for the decision by the IAEA.

The IAEA Team reviewed the self-assessment provided by CEA in the application for the ICERR designation against the evidences provided during the mission. The IAEA Team assessed separately each facility included in CEA's application and identified the specific areas of activity that each facility contributes to the purposes of the designation requested by CEA. The analysis of the different

contributions has been carried out against the ICERR designation criteria as determined in the Terms of Reference of the ICERR scheme. In particular, the IAEA Team recognizes that the contributions of the facilities to the different areas of activity are as follows:

- **ISIS research reactor**: Education and Training, Hands-on Training
- **ORPHEE research rector**: Joint Research and Development Projects
- **LECI Hot Laboratory**: Joint Research and Development Projects, Education and Training
- **Jules Horowitz Reactor**: Hands-on Training, Joint Research and Development Projects
- **LECA-STAR Hot Laboratory**: Joint Research and Development Projects
- **EOLE research reactor**: Joint Research and Development Projects
- **MINERVE research reactor**: Joint Research and Development Projects, Education and Training

It should be emphasized that all these facilities have a long experience of welcoming foreign students or engineers either for internships, or through secondments in the frame of collaboration agreements between CEA and foreign institutes.

Therefore, based on such evaluation, the IAEA Team recommends that the Selection Committee award the ICERR designation to CEA for the following areas of activity:

- **Education and Training**
- **Hands-on Training**
- **Joint Research and Development Projects**

Following the IAEA recommendation, CEA Cadarache and Saclay centers were the first designated ICERR by the agency; this has become official during the last General Conference on the **14th September 2015.** The Director General of the agency indicated the agency motivations at a ceremony during which he awarded the designation to CEA: "Such centers will enable researchers from IAEA Member States, especially developing states, to gain access to research reactor capabilities and develop human resources efficiently, effectively, and, probably, at a lower cost. The ICERR scheme will also contribute to enhanced utilization of existing research reactor facilities and, by fostering cooperation, to the development and deployment of innovative nuclear technologies".

Applications

CEA is now ready to welcome scientists, engineers within its facilities described above in the framework of this ICERR designation.

In a practical point of view, for welcoming scientists from Member States at CEA through this ICERR designation, a bilateral agreement has to be signed between the assigning party (organisation from which the scientist belongs to) and CEA. Such agreement will indicate the scientific/technical topic of collaboration, and rights and duties of both parties including the financial issues. The IAEA is here a "facilitator" creating the network between its Member States and the CEA and having eventually the possibility to partially sponsor some part on a "case by case" basis.

References

[1] http://www.iaea.org/OurWork/ST/NE/NEFW/Technical-Areas/RRS/documents/ICERR_Concept_ToR_Final.pdf

[2] "Sustaining Material Testing Capacity in France: From OSIRIS to JHR", G. Bignan, D. Iracane, S. Loubière, C. Blandin, CEA (France) IGORR 2009 Conference (Beijing)

[3] "The Jules Horowitz Reactor: A new European MTR open to International collaboration" Gilles Bignan et al, IGORR 2010 (Knoxville TN –ORNL- September 2010)

[4] "The Jules Horowitz Reactor: A new European MTR (Material Testing Reactor) open to International collaboration: Description and Status", G. Bignan, J. Estrade – IGORR 2013 – Daejeong Korea (October 2013)

[5] "The Jules Horowitz Reactor: A new high performance MTR (Material Testing Reactor) working as an International User Facility in support to Nuclear Industry, Public Bodies and Research Institutes", X. Bravo, G. Bignan, Journal of Nuclear Energy International - December 2014

IAEA Activities on the Safety Reassessments of Research Reactors in Light of the Feedback from the Fukushima Daiichi NPP Accident

D.F. SEARS, A. M. SHOKR, W. KENNEDY, D. RAO AND A. D'ARCY

Research Reactor Safety Section, Division of Nuclear Installation Safety
International Atomic Energy Agency, Wagramerstrasse 5, PO Box 100
A-1400 Vienna, Austria

E-mail: D.Sears@iaea.org

Abstract

The IAEA conducts a broad range of activities to enhance the safety of research reactors. These activities help Member States to improve their regulatory effectiveness and to enhance the management of safety of their facilities through the application of the Code of Conduct on the Safety of Research Reactors. One of the key activities is the development of IAEA safety standards and supporting technical documents and supporting their application by Member States. These standards form the basis of the IAEA safety review services for research reactors, including Integrated Safety Assessment for Research Reactors (INSARR) missions, safety reviews and expert missions.

In response to the accident at the Fukushima Daiichi nuclear power plant, the IAEA published the Safety Reports Series No. 80 (SRS-80) to provide guidance on safety reassessments of research reactors. This document was needed to assist research reactor organizations to perform, and regulatory bodies to review, safety reassessments in light of the feedback from the accident, considering that the majority of research reactors were constructed decades ago and may not be fully in conformance with the current safety standards, that most research reactors are located near populated areas, and in many cases the characteristics of the reactor site and vicinity have changed since the construction of the facility. These issues have not been considered or reflected in the safety analysis of many of the existing research reactors.

The SRS-80provides suggestions and methods for performing safety reassessments of research reactors thus promoting harmonization of methods and approaches, and it provides information on the use of the relevant IAEA safety standards in performing the reassessment. It covers all of the steps in performing safety reassessment for research reactors and associated experimental facilities, and it addresses: regulatory aspects; reassessment of the reactor facility; reassessment of the site; reassessment of

the emergency preparedness and response; application of a graded approach; and, implementation of the identified improvements following the reassessment findings.

The IAEA has held a series of regional training workshops on safety reassessment, as well as technical meetings and workshops on the implications of the Fukushima Daiichi nuclear power plant accident on the safety of research reactors. Feedback was obtained from questionnaires that were distributed at the International Conference on Research Reactors, held in Morocco in 2011 and in Vienna in 2015. Most organizations that responded to the 2015 survey have performed reassessments following the guidance in SRS-80, or a similar national process. The feedback shows that the majority have implemented modifications to the facility, procedures and emergency plans that resulted in improvements to withstand beyond design basis accidents and enhanced safety management. However, efforts are still needed in many facilities to complete the reassessment or to implement the results.

This paper discusses the IAEA activities on safety reassessments of research reactors, recent progress and achievements for strengthening research reactor safety worldwide, and the strategy for implementing further improvements.

1. INTRODUCTION

Following the Fukushima Daiichi nuclear power plant accident, Member States of the International Atomic Energy Agency (IAEA) have conducted safety reassessments of their nuclear facilities to evaluate their ability to withstand the effects of extreme external events on the safety of the facilities. The initial focus of Member States has been the reassessments of nuclear power plants but many have extended the scope to include research reactors.

The inventory of radioactive material and hence the potential hazard associated with research reactors is typically much lower than that for nuclear power plants. However, many research reactors were designed and built decades ago and are located near populated areas, the characteristics of the site and areas in the vicinity may have changed since the facilities were constructed, and their design requirements may not be fully in conformance with current IAEA safety standards. These and other issues can complicate the management of accidents that may result in radioactive releases, and therefore safety reassessments of research reactors are warranted.

The following sections describe the observations and lessons from the Fukushima Daiichi accident that relate to research reactors, and the associated IAEA activities to support and implement safety reassessments of research reactors in light of the feedback from the accident.

2. SAFETY CONSIDERATIONS FOR RESEARCH REACTORS

Since the Fukushima Daiichi nuclear power plant accident, there have been many analyses of its causes and consequences, as well as detailed considerations of its implications for nuclear safety, by the IAEA Member States and international organizations. The IAEA report by the Director General on the Fukushima Daiichi Accident [1] and the associated technical volumes provide a

description of the accident and its causes, evolution and consequences, and it highlights the main observations and lessons. Many of the observations and lessons are relevant for reassessment of the safety of research reactors when subjected to extreme external events, including, inter alia:

- The assessment of natural hazards needs to be sufficiently conservative.
- The safety of nuclear facilities needs to be re-evaluated on a periodic basis to consider advances in knowledge, and necessary corrective actions or compensatory measures need to be implemented promptly.
- The assessment of natural hazards needs to consider the potential for their occurrence in combination, either simultaneously or sequentially, and their combined effects.
- Operating experience programmes need to include experience from both national and international sources.
- The defence in depth concept remains valid, but implementation of the concept needs to be strengthened at all levels by adequate independence, redundancy, diversity and protection against internal and external hazards.
- Instrumentation and control systems that are necessary during beyond design basis accidents need to remain operable in order to monitor essential plant safety parameters and to facilitate plant operations.
- Robust and reliable cooling systems that can function for both design basis and beyond design basis conditions need to be provided for the removal of residual heat.
- There is a need to ensure a reliable confinement function for beyond design basis accidents to prevent significant release of radioactive material to the environment.
- Accident management provisions need to be comprehensive, well designed and up to date.
- Training, exercises and drills need to include postulated severe accident conditions to ensure that operators are as well prepared as possible.
- In order to ensure effective regulatory oversight of the safety of nuclear installations, it is essential that the regulatory body is independent and possesses legal authority, technical competence and a strong safety culture.
- In order to promote and strengthen safety culture, individuals and organizations need to continuously challenge or re-examine the prevailing assumptions about nuclear safety and the implications of decisions and actions that could affect nuclear safety.
- Arrangements need to be in place to allow decisions to be made on the implementation of predetermined, urgent protective actions for the public, based on predefined plant conditions.

For details of the main observations and lessons on nuclear safety considerations, emergency preparedness and response, radiological consequences, and post-accident recovery, see the report by the Director General on the Fukushima Daiichi Accident [1].

3. IAEA ACTIVITIES ON SAFETY REASSESSMENTS FOR RESEARCH REACTORS

The experience available from the Fukushima Daiichi accident is crucial for defining and implementing measures to prevent large releases of radioactive material at nuclear installations due to accidents caused by extreme external events. The areas involved include: regulatory effectiveness, safety requirements of the design, site specific hazard assessment, total loss of

electrical power supply, hydrogen control, loss of ultimate heat sink, accident management, safety of spent fuel, emergency preparedness, communication of information, and safety culture. Most of these topics also apply to research reactors when subjected to extreme external events. In response to the Fukushima Daiichi accident, the IAEA has adapted its programmes and activities to address the observations and relevant lessons that apply to research reactors. The following section discusses some of the key IAEA activities related to safety reassessments for research reactors.

3.1 Development of IAEA Guidance on Safety Reassessments

As Member States extended the scope of their reassessments to include research reactors, it was recognized that there was a need for guidance on performing safety reassessments, to promote harmonization of methods and approaches and to provide information on the use of the relevant IAEA safety standards in performing the reassessment. Accordingly, the IAEA undertook the development of the publication *Safety Reassessment for Research Reactors in the Light of the Accident at the Fukushima Daiichi Nuclear Power Plant* (Safety Report Series No.80) [2]. The first draft was developed in a Consultants Meeting held in 2012 and was subsequently reviewed in a Technical Meeting with the participation of 40 Member States. Following a comprehensive review within the IAEA, it was published in March 2014.

The SRS-80 provides guidance to Member States, on the basis of international good practice, for performing safety reassessments that are complete and consistent with the IAEA safety standards. The SRS-80 also provides methods for performing safety reassessments of research reactors and information on the use of the relevant IAEA safety standards in performing this reassessment. It applies to all research reactor types and sizes with appropriate use of a graded approach [3] that is commensurate with the potential hazards of the facility. Although the primary focus is on operating research reactors, the information provided also applies to research reactors in the planning, design, construction and extended shutdown stages. The publication covers all of the steps in performing safety reassessment for research reactors and associated experimental facilities, including: regulatory aspects; reassessment of the reactor facility; reassessment of the site; reassessment of the emergency preparedness and response; application of a graded approach; and, implementation of the identified improvements following the reassessment findings.

The IAEA also assisted Member States in the application of the guidelines provided by SRS-80. Such assistance included expert missions and technical meetings on the safety of research reactors. One of the recent activities was a meeting on the implications of the Fukushima accident on the safety of research reactors, held in Tel Aviv, April 2015. The meeting provided an opportunity to share experience and information on the results of safety reassessment based on the guidance of SRS-80 and supported the participating organizations in the development of future actions to enhance the safety of their facilities. Additionally, the IAEA is continuing activities on development of guidelines on implementation of periodic safety review for research reactors (based on the experience acquired from a similar process for nuclear power plants) and on the application of the recently established requirements on design extension conditions.

3.2 Revision of IAEA Safety Standards on Safety of Research Reactors

The IAEA safety standards, as a key element of the global safety regime, are regularly reviewed by the IAEA, the Safety Standards Committees and the Commission on Safety Standards. The IAEA gathers information on experience in the application of the safety standards and information gained from the follow-up of events for the purpose of ensuring that the standards continue to meet users' needs. For research reactors, these sources are mainly:

- Insights from the Member States' self-assessments on application of the Code of Conduct on the Safety of Research Reactors [4, 5];
- Feedback from the IAEA safety review missions [6];
- Feedback from incidents which occurred at research reactors and other nuclear installations, including at the Fukushima Daiichi nuclear power plant [1, 2, 7, 8].

The IAEA Safety Standards Series No. NS-R-4, Safety of Research Reactors, was published in 2005. This document established requirements for all areas of research reactor safety, with particular emphasis on requirements for design and operation. However, it is recognized that technology and scientific knowledge advance, and that nuclear safety and the adequacy of protection against radiation risks need to be considered in the context of the present state of knowledge. Accordingly, the IAEA has undertaken the revision of NS-R-4, consistent with the roadmap for the long term structure of IAEA safety standards. The scope of NS-R-4 remains essentially unchanged, but sub-critical assemblies and the interfaces between safety and security are now covered. Material on regulatory supervision, siting, and management systems has been updated and text more relevant to guidance has been removed. The revision of NS-R-4 ensures coherency and consistency of the technical content with other relevant IAEA Safety Standards. It reflects feedback and experience accumulated up to 2015, including feedback from studying the accident at the Fukushima Daiichi nuclear power plant as it relates to research reactors.

The draft Safety Requirements text was submitted to Member States for comments in 2015. A revised draft was approved by the Safety Standards Committees in November and December 2015 [9]. The document will be submitted for endorsement by the Commission on Safety Standards and approval by the Board of Governors in 2016.

In addition, the IAEA will continue to conduct training activities on implementing the IAEA safety standards and assist Member States to adopt these standards in the national regulations.

3.3 International Exchange of Information and Experience

The IAEA has held several regional training workshops on safety reassessment following the Fukushima Daiichi nuclear power plant accident. These include the:

- Workshops on Regulatory Supervision of Research Reactors;
- Workshops on Regulatory Inspection Programmes for Research Reactors;
- Workshop on Considerations of Human Factors in Different Stages of Research Reactors;
- Workshop on Complimentary Safety Assessment of Research Reactors Following the Lessons Learned from the Fukushima Accident;
- Workshop on Safety Reassessment of Research Reactors in Light of the Feedback from the Fukushima Accident.

In addition, the implication of the accident on research reactor safety was a major topic in several international conferences and meetings, including:

- Technical Meeting on Implications of the Fukushima Accident on the Safety of Research Reactors, Vienna (2012);
- International Meeting on Application of the Code of Conduct on the Safety of Research Reactors, Vienna (2014);
- Meeting on the Implications of the Fukushima Accident on the Safety of Research Reactors, Tel Aviv (2015).
- Meetings of the Regional Advisory Safety Committees for Research Reactors (Europe, Africa and Asia, respectively);
- Meetings on the Safety of Research Reactors under Project and Supply Agreements (2013, 2015);
- Meetings on the Incident Reporting System for Research Reactors.

Questionnaires were distributed at the International Conference on Research Reactors, held in Morocco in 2011 and in Vienna in 2015, to obtain information on safety reassessments conducted by Member States. The feedback from these and other recent IAEA activities on the safety of research reactors [10] shows an increasing trend in the number of research reactors conducting safety reassessments, with the objective of improving their ability to withstand extreme external events.

At the International Conference on Research Reactors, held in Vienna in November 2015, many research reactor organizations reported that they have performed safety reassessments in light of the lessons learned from the accident at the Fukushima Daiichi nuclear power plant. Of the Member States contacted, over 50% responded to the survey, with 25 responses received from operating organizations and 2 from regulatory bodies.

The majority of organizations that responded to the 2015 survey have performed reassessments, following the guidance in SRS-80 or a similar national process. Almost all responses indicated reassessment of design basis accidents and consideration of additional single external or internal events, with emphasis on the loss of electrical power supply. Many reassessments included consequential events, for example, earthquake with loss of cooling accidents or loss of power supply. Some considered combined earthquake and flooding events. Many implemented seismic monitoring and automatic protective actions, including improved protection of control rod drives. The majority have implemented related modifications to the facility, procedures and emergency plans that have resulted in improvements to withstand beyond design basis accidents and enhanced safety management. However, efforts are still needed in many facilities to complete the reassessment or to implement the results.

The Conference recommended that safety reassessments be performed for all research reactors, including those that are in the design or construction phases. It was also recommended that the IAEA continue its efforts to disseminate the relevant lessons learned from the accident and to support Member States in addressing these lessons through implementation of technical meetings, workshops, peer reviews and advisory missions.

The feedback from other recent IAEA activities, including regional training workshops and technical meetings, also indicate a continuing need for the exchange of information on methods for the safety reassessments, the use of a graded approach when applying the relevant IAEA safety standards, and the implementation of improvement measures based on the findings of the safety reassessments.

4. CONCLUSIONS

The observations and lessons from the Fukushima Daiichi nuclear power plant accident apply to operating research reactors as well as those in the design, construction and shutdown stages. The IAEA activities on the safety of research reactors support Member States to address the lessons from the accident. The main activities in this regard include: the development and application of the IAEA publication *Safety Reassessment for Research Reactors in the Light of the Accident at the Fukushima Daiichi Nuclear Power Plant* (Safety Reports Series No. 80); the revision of the IAEA Safety Standard on Safety of Research Reactors to incorporate the feedback and experience accumulated up to 2015, including feedback from studying the accident at the Fukushima Daiichi nuclear power plant as it relates to research reactors; and, activities to support the international exchange of information and experience via technical meetings and workshops on safety reassessments of research reactors in light of feedback from the accident.

These IAEA activities have resulted in progress in enhancing the safety of research reactors in IAEA Member States. Feedback shows that many research reactor organizations have performed safety reassessments to improve the ability of their facilities to withstand extreme external events. However, further efforts are still needed in many facilities to complete the safety reassessment and to implement improvement measures based on the findings.

The IAEA, through its sub-programme on research reactor safety [10], will continue to provide its Member States with support to address the issues and challenges identified above.

5. REFERENCES

[1] IAEA, "The Fukushima Daiichi Accident", Report by the Director General, GC (59)/14, IAEA, Vienna, 2015.
[2] IAEA, "Safety Reassessment for Research Reactors in the Light of the Accident at the Fukushima Daiichi Nuclear Power Plant", Safety Reports Series No. 80, IAEA, Vienna, 2014.
[3] IAEA, "Use of a Graded Approach in the Application of the Safety Requirements for Research Reactors", IAEA Safety Standards Series No. SSG-22, IAEA, Vienna, 2012.
[4] IAEA, "Code of Conduct on the Safety of Research Reactors", IAEA/CODEOC/RR/2006, Vienna, 2006.
[5] SHOKR, A.M. "Insights from the Member States Self-assessments on Application of the Code of Conduct on the Safety of Research Reactors", paper presented at the International Meeting on Application of the Code of Conduct on the Safety of Research Reactors, 14-18 June 2014, IAEA, Vienna.
[6] IAEA, "Nuclear Safety Review 2016" (in preparation).
[7] IAEA Incident Reporting System for Research Reactors (IRSRR), in: http://www-ns.iaea.org/tech-areas/research-reactor-safety/irsrr-home.asp?S=2&L=10

[8] IAEA, "Operating Experience from Events Reported to the IAEA Incident Reporting System for Research Reactors", IAEA TECDOC 1762, IAEA, Vienna, 2015.
[9] IAEA, "Safety of Research Reactor", Draft Safety Standards: Revision of the NS-R-4, IAEA, Vienna (in preparation).
[10] SHOKR, A.M. "IAEA Sub-programme on Safety Enhancement of Research Reactors", paper presented at the International Conference on Research Reactors: Safety Management and Effective Utilization, 16-20 November 2015, IAEA, Vienna.

RESEARCH REACTORS FOR DEVELOPMENT OF MATERIALS AND FUELS FOR INNOVATIVE NUCLEAR ENERGY SYSTEMS - A COMPENDIUM

F. MARSHALL, A. BORIO DI TIGLIOLE
Research Reactor Section
Division of Nuclear Fuel Cycle and Waste Technology
Department of Nuclear Energy
International Atomic Energy Agency
P.O. Box 100, 1400 Vienna - AUSTRIA

M. KHOROSHEV
Nuclear Power Technology Development Section
Division of Nuclear Power
Department of Nuclear Energy
International Atomic Energy Agency
P.O. Box 100, 1400 Vienna – AUSTRIA

ABSTRACT

In 2013, International Atomic Energy Agency's (IAEA's) Research Reactor Section (RRS) initiated development of a compendium on existing and future services that can be provided by existing and planned research reactors for innovative nuclear energy system and technology R&D, specifically focusing on needs for materials and fuels development. This is to support an IAEA initiative to identify 'Research Reactor Support Needed for Innovative Nuclear Power Reactors and Fuel Cycles'. One of the objectives of this activity was to identify existing (or soon to be operational) RR facilities capable of supporting innovative nuclear development, including identification of constraints potentially limiting a facility's ability to provide support. The resulting Compendium is in the publishing process in 2016 and is expected to be published by the end of the year.

The purpose of this compendium is to give an overview of the major material test research reactors (MTR) in IAEA Member States and in this way to contribute to their application to present day and future nuclear energy systems. The compendium focuses on the contributions that these RRs and associated facilities can provide to major areas of research and development for advanced materials and fuels. However, since many MTR reactors are multipurpose facilities, this publication also includes some information related to other RR applications. This publication presents an overview of research reactor (RR) capabilities and capacities, including power level, mode of operation, current status and historical overview of their utilization. A summary of these capabilities and capacities, together with reactors availability for materials and fuel testing is also presented in tables. The main component of the Compendium consists in papers providing a technical description of the research reactors, including their specific features for materials and fuels research, as well as other applications offered by the RR facilities. These papers are collected as profiles on CD-ROM attached to this document and represent an integral part of the document. It is expected that the Compendium will serve as a supporting tool for the establishment of regional and international networking through RR coalitions and IAEA designated international centres based on RRs (ICERRs).

1. Introduction

1.1 Motivation for Project

Research reactors (RRs) are indispensable tools to support the nuclear power industry in material characterization and testing for life extension of operating plants and in the qualification of structures, systems, and components of the new generation of nuclear power plants. RRs also play an important role for research and development of fission and fusion technologies, basic research, isotope production, neutron radiography, neutron beam research, education and training and other applications. The IAEA strives to foster efforts in ensuring wide access to existing research reactors to support the missions identified above. One effort that was recommended was for IAEA to develop a compendium of material test research reactors (MTRs) whose capabilities would be beneficial in developing new nuclear energy systems.

The purpose of this compendium is to give an overview of the major MTRs in IAEA Member States to contribute to their application to present day and future nuclear energy systems. The compendium focuses on the contributions that these RRs and associated facilities can provide to major areas of research and development for advanced materials and fuels. However, since many MTR reactors are multipurpose facilities, this publication also includes some information related to other RR applications.

1.2 Historical Overview of Research Reactors for Material Investigations

When the use of commercial nuclear power commenced in the 1950s, much was unknown about the effects of radiation on materials, fuels, and core components that were to be used in nuclear reactors. In order to learn about radiation effects on materials, several MTRs were built and operated to perform applied research for commercial power reactors. The total number of operational RRs peaked in the 1970s at 400 [1] and has now decreased to less than 250. Only few of them are MTRs.

The MTRs have proved to be an essential tool for fundamental research providing representative conditions in nuclear power reactors, for example strong radiation, high temperature and pressure, resistance of fuels and structural materials, etc. Many of the powerful MTRs are still in use today, even though they started their operation in the late 1950s and 1960s. Additional reactors were added in the 1970s for power pulse reactivity insertion accident (RIA) mode of testing.

Considerable experience with fuels and materials testing has been gained during the six decades since the first MTRs commenced their services, and a wealth of knowledge on fuels and materials behaviour has been documented. Questions were addressed and answered, but new questions continue to emerge, triggered by increased demand on fuels and materials. Innovative nuclear energy systems, like Generation IV fission reactors and fusion reactors, bring *new* requirements and *new* conditions, not yet experienced in the past on industrial scale.

2. R&D Needs to Support Future Reactor Development

The innovative fission nuclear energy systems (NES) being designed and developed worldwide today pose even more challenges than did present-day light water reactors (LWR). Their operating conditions, as illustrated in Fig. 1, are much more demanding and require new materials and fuels to be developed.

The development challenges for these new fission materials and fuels, however, pale in comparison to those for fusion materials where the structural materials in the first demonstration fusion reactor will be expected to satisfactorily operate up to damage levels exceeding 100 displacements per atom (dpa). This is arguably the greatest materials development challenge in history.

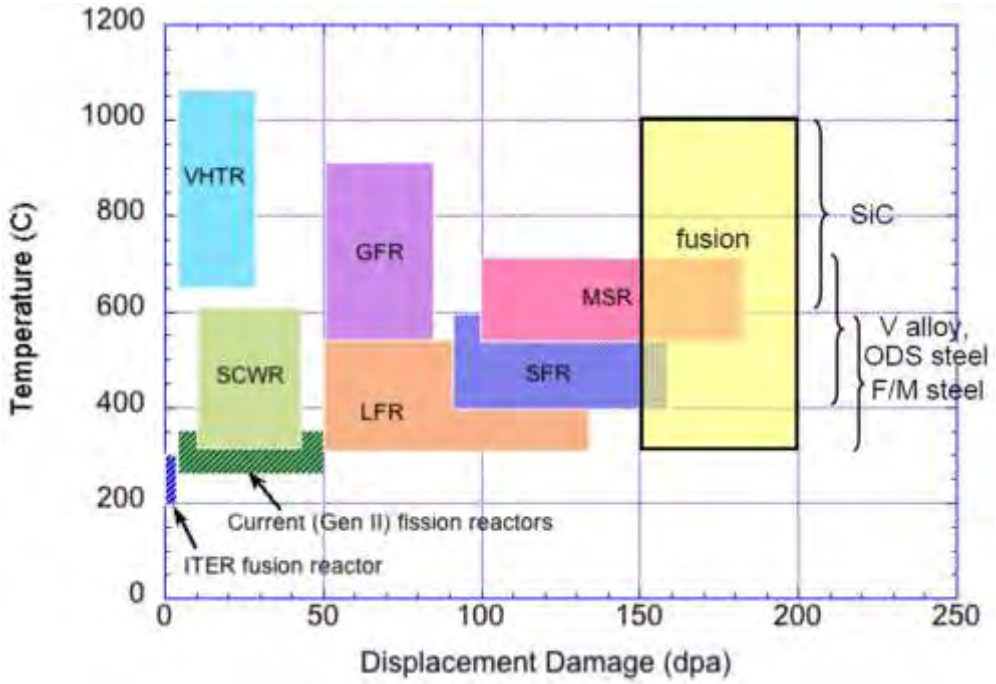

F/M steel – Ferritic/martensitic steel
GFR – Gas cooled fast reactor
ITER – International Thermonuclear Experimental Reactor
LFR – Lead cooled fast reactor
MSR – Molten salt cooled reactor
ODS steel – Oxide dispersion strengthened steel
SCWR – Supercritical water cooled reactor
SFR – Sodium cooled fast reactor
VHTR – Very high temperature reactor

FIG. 1. Requirements on materials in future nuclear energy systems [2]

It is apparent that the existing and planned MTRs are indispensable for the design and deployment of innovative nuclear energy systems and their fuel cycles. The current worldwide fleet of operating RRs includes approximately 15 reactors that are capable of supporting material testing for new nuclear energy systems and technologies. Some of these reactors have unique systems and capabilities for addressing some of the most difficult problems facing current and future materials and fuels research. Maintaining them and developing further sophisticated up-to-date experimental capabilities is crucial.

Nuclear energy system R&D is generally focused on advanced materials research which includes testing of advanced fuels and structural materials (e.g. liquid metal as coolant or molten salt as fuel, etc.), studying minor actinides and long-lived fission products burn-out as well as extension of fuel resources using thorium fuel cycle options or fusion technologies. Existing and planned RRs have or will have capacities to perform a broad spectrum of R&D aimed at developing innovative power reactors. Some of these required capabilities are flexible testing positions that can accommodate several types of test at one time, high fast and thermal fluxes, sophisticated in-situ instrumentation to allow the researchers to monitor and change test conditions during the irradiation testing, loop testing facilities that enable testing of material in actual coolant conditions, and comprehensive post irradiation examination laboratories that enable full analysis of the irradiated material.

3. Compendium Structure

In support of material testing research activities, the IAEA has developed this comprehensive compendium on existing and future services to be provided by existing and planned MTRs

for innovative nuclear energy system and technology R&D. It is intended that publication of this Compendium will foster wider access to information on existing RRs and thus facilitate material testing research. It is expected that the Compendium will serve as a supporting tool for the establishment of regional and international networking through RR coalitions and international centres based on RRs (ICERRs) [3].

The Compendium provides mainly contributions of RRs and associated facilities to major areas of research on the development of advanced materials and fuels. As many of MTRs are multipurpose RR facilities, this publication also includes some information on other RR applications. The Compendium development was supported during the meeting of the IAEA Technical Working Group on RRs in April 2013.

The main component of the Compendium consists of individual papers (profiles) providing a technical description of the research reactors, including their specific features for utilization. These profiles are collected in country alphabetical order on CD-ROM attached to the document and represent an integral part of the document. The profiles describe RRs according to the template, which was agreed among a broad group of international experts contributing to this report. Most papers were provided to the IAEA secretariat by institutions in the IAEA Member States in response to the letters requesting the inputs to the Compendium.

3.1 Reactor Facilities Included in the Compendium

Table 1 lists the reactor facilities for which a profile has been developed. Each profile contains a detailed physical description of the reactor facility, with figures to illustrate the features of the facility, and discussion of the experiment capabilities. Many include examples of specific research program that have been completed using the reactor facility and its associated research laboratories. There are some reactors not yet operating that are expected to have these capabilities, but they have been left out and are expected to be include in future revisions of this Compendium.

Country	Research Reactor	Full Facility Name	Readiness for Material Testing Research*
Argentina	RA-10	Argentinean multipurpose reactor	2
Belgium	BR-2	Belgium Reactor -2	1
China	CEFR	China Experimental Fast Reactor	1
China	CARR	China Advanced Research Reactor	1
Egypt	ETRR-2	Experimental Training Research Reactor -2	1
France	JHR	Jules Horowitz Reactor	2
Hungary	BRR	Budapest Research Reactor	3
India	DHRUVA		1
India	HFRR	High Flux Research Reactor	3
Indonesia	RSG-GAS	Reaktor Serba Guna G.A. Siwabessy	1
Japan	JMTR	Japan Materials Testing Reactor	1
Japan	JOYO	Experimental fast reactor	3
Kazakhstan	IGR	Impulse Graphite Reactor	1
Republic of Korea	HANARO	High-flux Advanced Neutron Application Reactor	1
Netherlands	HFR	High Flux Reactor	1
Norway	HBWR	The Halden Boiling Water Reactor	1

Poland	MARIA	The MARIA reactor	1
Romania	TRIGA II PITESTI SS CORE	Training, Research, Isotope General Atomics (TRIGA) Steady State research reactor	1
Russian Federation	BIGR	Fast pulse graphite reactor	1
Russian Federation	IR-8	IR-8 pool-type reactor	1
Russian Federation	IVV-2M	Water moderated, water cooled multi-purpose nuclear research reactor	3
Russian Federation	MIR.M1	The research reactor MIR.M1	1
Russian Federation	SM-3		1
Russian Federation	BOR-60	Experimental fast sodium reactor	1
Russian Federation	RBT-6	Thermal neutron pool-type reactor	1
Slovenia	TRIGA Mark II reactor	Training, Research, Isotope General Atomics, Mark II reactor	1
USA	ATR	Advanced Test Reactor	1
USA	HFIR	High Flux Isotope Reactor	1
USA	MITR	MIT research reactor	1
Italy	TRIGA RC-1	The TRIGA RC-1 nuclear research reactor	1
Italy	TAPIRO	*TA*ratura *PI*la *R*apida Potenza Zer*O*	1
Russian Federation	BFS-1 & 2	Critical stands BFS-1&2	1

*Readiness for material testing research
1 - Operational
2 - Planned
3 – Potential

Tab 1. List of MTR facilities for which a profile has been developed.

3.2 Categorization of Material in the Compendium

The information in the Compendium is presented with several different perspectives. Each one of these perspectives is intended to assist researchers in identifying which research reactor could best suit their research material testing programs. Some of the specific perspectives are summarized below.

The first category that is usually used to distinguish between different research reactors and their capabilities is power and flux. This is a key feature for the material testing research, as one of the fundamental questions about reactor materials is the ability to withstand high neutron doses, which can be simulated in research reactors. A shorter testing period is preferred so that research results can be obtained sooner, however, in some cases, particular for fuels, it is more important to perform the test at the same neutron flux that will exist in the operating reactor. It is also important to distinguish between the fast and thermal flux, or perhaps to focus on the ratio of the two flux levels, again to be able to match the experiments to the actual expected operating conditions. Somewhat contrary to the above discussion, low power reactors can also provide valuable data for preliminary studies, prior to initiating a lengthy experiment campaign in a high flux reactor. Thus, several lower power reactors that are typically not considered “MTRs” are included in this compendium.

Another key distinguishing capability is whether the reactor operates at steady state or if it can pulse for the purpose of testing transients (e.g., reactivity insertion accidents). There are not many pulsing reactors available, however, there is increasing interest in testing fuel and cladding material for what are considered “beyond design basis” accidents.

The most sophisticated reactor irradiation tests are likely to be performed in test loops that enable testing to occur in the actual coolant conditions for which the fuel and materials are being tested. Parameters such as coolant (e.g., water, liquid metal, gas), flow rate, temperature, and pressure need to be adapted to the specific fuel and material to be tested. Several MTRs have these loop testing facilities to enable the prototypical testing to occur. Along with the loop testing capability is the need for sophisticated instrumentation to enable the researcher to fully monitor the experiment in real time. This Compendium provides detailed information about the loop testing and experiment instrumentation capabilities in the facility profiles.

Most experimenters are looking for large irradiation spaces to perform several experiments simultaneously or to test actual size fuel elements or assemblies prior to final reactor design and fuel fabrication. This feature frequently competes with the high flux desirability, however, so it is important for researchers to be able to ensure their test criteria are well developed and can be accommodated by the MTR they seek to use. Several reactors have unique designs to optimise the combination of high flux and large irradiation spaces; these reactors are included in the compendium.

Finally, it is important for researchers to understand what facility capabilities are available outside the reactor. These include the ability to design and build experiments, as well as the post irradiation examination (PIE) capabilities at the facility. It is also helpful to understand what assistance the facility staff can provide to researchers in terms of developing the actual testing program, transportation of materials, the facility’s capability to reconfigure an experiment for subsequent irradiation testing. Equally important as the facility capabilities is the ability of the facility organization to provide access to researchers for the use of the facility. Information about these facility attributes is included in the Compendium.

4. Conclusions

There are many operating research reactor whose primary function is material testing. These reactors are fundamental to supporting existing and proposed nuclear power reactors and technologies. IAEA has developed a document, a “Compendium” of information about material test reactors to enable researchers to easily access information about the capabilities that could be used for their programs. It is anticipated that use of this Compendium will foster knowledge sharing between research reactor facility organizations and researchers, and could lead to more formal networking opportunities within the research reactor community. The Compendium is in the publishing process at IAEA and is expected to be published in 2016.

5. References

[1] INTERNATIONAL ATOMIC ENERGY AGENCY, Research Reactor Database (RRDB), http://nucleus.iaea.org/RRDB/

[2] ZINKLE, S.J., BUSBY, J.T., Structural materials for fission and fusion energy, Materials Today, **12** 11 (2009) 12–19

[3] INTERNATIONAL ATOMIC ENERGY AGENCY, International Centres based on Research Reactors: https://www.iaea.org/OurWork/ST/NE/NEFW/Technical-Areas/RRS/documents/ICERR_Concept_ToR_Final.pdf

IGORR: THE FIRST TWENTY-FIVE YEARS

D. L. SELBY
Oak Ridge National Laboratory
708 Andover Blvd. Knoxville, Tennessee 37934

K. F. ROSENBALM
Oak Ridge National Laboratory
PO Box 2008 MS6255 Oak Ridge, Tennessee 37831-6255

ABSTRACT

This paper will provide a history of the formation of the International Group on Research Reactors (IGORR) and its scope transition from the early days to the technical organization that it is today. This will include a discussion of some of the reasons for the formation of IGORR and its original charter for the organization. Recognition will be given to the key organizers of IGORR and the roles that they played in the formation of IGORR along with recognition of the people who have served as Chairmen of IGORR over the first 25 years. Finally, the 16 previous IGORR meetings will be addressed with summaries of locations of meetings, attendance numbers, demographics of attendees and session topics, and some important highlights from a few of the previous IGORR meetings.

1. Introduction

In 1989 the idea for IGORR was born out of the Advanced Neutron Source (ANS) project at Oak Ridge National Laboratory (ORNL) in the United States. Colin West, the Director of the ANS project, recognized that there were several countries that were engaged in the planning or implementing of new or major upgrade research reactor projects. However, there was no forum for informal discussions and sharing of information, even though we were in many cases working on the same problems. A number of organizations around the world were contacted, and essentially all agreed that the formation of a group with common goals was a good idea and IGORR was formed.

The original Charter was short and general: "*The International Group on Research Reactors was formed to facilitate the sharing of knowledge and experience among those institutions and individuals who are actively working to design, build and promote new research reactors or to make significant upgrades to existing facilities.*"

An IGORR Steering Committee was formed composed of one senior staff member from each of the major organizations that had agreed to participate. There were 17 initial members of the steering committee from 7 countries. A list of the members of the initial Steering Committee is provided in Table 1. Colin West served as the Chairman of the Steering Committee and tasked the group with the organization of the first IGORR meeting, which was hosted by the ANS project at the airport Hilton Hotel in Knoxville, Tennessee in March of 1990. The Steering Committee has lost and gained members over the 25-year history with size of the committee ranging from a low of 15 members to a high of 21 members.

It should be noted that the original focus of IGORR was the larger, higher power research reactors. This was very clear from the first meeting where all but one of the papers was tied to research reactors with power levels at 20 MW or above. This was a somewhat selfish objective inherent with the formation of the IGORR organization in that the intent was to involve those organizations that would have the most to contribute to the new large research reactor projects and those existing large reactors with planned major upgrades.

Table 1: Members of the Original IGORR Steering Committee

1. J. Ahlf, Joint Research Center – Petten (The Netherlands)
2. P. Armbruster, Institut Laue-Langevin (France)
3. J. D. Axe, Brookhaven National Laboratory (USA)
4. A. Axmann, Hahn Meitner Institute (Germany)
5. K. Boning, Technischen Universitat Munchen (Germany)
6. C. Desandre, Technicatome (France)
7. A. F. DiMeglio, Rhode Island Atomic Energy Commission (USA)
8. B. Farnoux, Laboratory Leon Brillouin (France)
9. O. K. Harling, Massachusetts Institute of Technology (USA)
10. R. F. Lidstone, Whiteshell Nuclear Research Establishment (Canada)
11. S. Matsuura, JAERI, Tokai (Japan)
12. J. C. McKibben, University of Missouri (USA)
13. H. Nishihara, Research Reactor Institute, Kyoto University (Japan)
14. Y. V. Petrov, St Petersburg Nuclear Physics Institute (Russia)
15. H. J. Roegler, Interatom (Germany)
16. J. M. Rowe National Institute for Standards and Technology (USA)
17. C. D. West, Oak Ridge National Laboratory (USA)

2. The First IGORR Conference

The authors of this paper were heavily involved in the organization of the initial IGORR meeting, and thus, are qualified to say that the first meeting was not the well-defined meeting that the present IGORR meetings have come to be. Almost all of the papers were invited papers given by the Steering Committee Members. The meeting lasted 2½ days and was attended by 52 scientists and engineers from 25 organizations in 10 counties. Speakers were asked to provide copies of their papers so that they could be provided to the attendees. The proceedings from this first meeting (as well as subsequent IGORR meetings) can be accessed from the IGORR website.

One of the features of the first few IGORR meetings that has been lost over the years was time set aside for open discussion in workshops. For the first two IGORR meetings two workshops were held: one on R&D needs of IGORR members and one on research reactor user needs. For the next four IGORR meetings only the workshop on R&D needs was included. In all workshops topics for discussion were pre-submitted to the organizing committee by IGORR members prior to the conference. Two-hour time periods were set aside for each of the workshops for open discussions of the topics. This was an important and beneficial activity that was part of these early IGORR meetings. Topics for discussion included: fuel development, aluminum oxidation, cold sources, issues with dealing with

users, and neutronics and thermal hydraulics codes and methods. The discussions from these workshops provided the opportunity for networking and collaboration efforts among the various IGORR organization members. As the purpose of the IGORR organization expanded over the years and the IGORR meetings trended more toward a more topical conference, the organizing committee recognition of the need for the workshops diminished, and they were eventually dropped from the agenda. The authors of this paper believe that this was unfortunate and somewhat diminished the recognition that there is a research reactor community with similar problems and interests.

In the Summary session for the meeting the organizing committee and other attendees agreed that the first IGORR meeting was a success and served a useful purpose. Therefore, it was decided to continue with the meetings on an 18-month interval schedule, and Bernard Farnoux offered to host the meeting in Saclay, France in fall of 1991. For various reasons it was the spring of 1992 before the second meeting was held, but in general we have held to the 18-month cycle over the 25-year history.

3. Subsequent IGORR Meetings

Over the first 25 years of the IGORR organization, there have been a total of 16 IGORR meetings held in 9 countries. Table 2 is a summary of the 16 IGORR conferences that were held over the first 25 years of the organization. It should be noted that several of these meetings (particularly over the last few years) have been held jointly with other organizations with similar interests.

There are several points of interest from studying Table 2. First of all, in general from the first meeting the attendance and number of papers presented had a general increasing trend up to IGORR 8. With several of the major research reactor projects nearing an end and the cancellation of the Advanced Neutron Source Project in the US, there appeared to be a decline in participation in the IGORR meetings, and the perception was that this trend might continue. This was a major topic of discussion by the Steering Committee at the IGORR 8 meeting, and plans were to try and find related topical meetings to partner with for joint meetings in the future. There were three main reasons for doing this: 1) It was noted that the inefficiencies of potential smaller meetings (less than 75 attendees) would lead to higher registration costs, 2) Several Steering Committee members noted that the number of conferences each year with ties to Research Reactors was becoming unmanageable, and 3) It was felt that joint meetings would expand the scope of topics for the meeting providing a wider range of interest for attendees. Although the idea of joint meetings could not be accomplished for the IGORR 9 meeting held in Australia, this became the trend starting with the IGORR 10 meeting. It should be noted that the only negative feedback to the joint meetings identified at later Steering Committee meetings was that particularly for meetings held jointly with the TRTR organization in the US, the IGORR papers represented considerably less than half of the conference papers.

The other point worth mentioning from Table 2 is the large number of countries that have been represented at IGORR meetings, which emphasizes the true international nature of this meeting. The maximum number of countries represented at a single meeting was 34 at IGORR 15 in Korea, but it should be noted that over the 25-year history, papers have been given from a total of 48 countries. This is a number never envisioned when the first IGORR

meeting was organized at which time it was felt that a representation of 10 countries was very good. This significant increase in the number of countries involved in IGORR meetings is in part due to the increase in scope of the meetings and the decrease in the emphasis on just the major research reactors around the world. It is also worth mentioning that International Atomic Energy Agency (IAEA) participation and support has contributed to the increase in the participation of attendees from many countries.

Table 2: Summary of the IGORR Meetings from the First 25 Years

	Location	Date	# of Papers	# of Attendees	# of Countries Represented	Special Notes
IGORR 1	Knoxville, Tennessee USA	March 1990	14	52	10	Included 2 workshops
IGORR 2	Saclay, France	May 1992	20	56	14	Included 2 workshops
IGORR 3	Naka, Ibaraki, Japan	September 1993	25	135	14	Included 1 workshop
IGORR 4	Gatlinburg, Tennessee USA	May 1995	29	56	13	Included 1 workshop
IGORR 5	Aix-En-Provence, France	November 1996	31	73	21	Included 1 workshop
IGORR 6	Taejon, Korea	April 1998	39	118	16	Included 1 workshop
IGORR 7	Bariloche, Argentina	October 1999	49	~100	17	
IGORR 8	Munich, Germany	April 2001	37	93	12	
IGORR 9	Sydney, Australia	March 2003	49	~100	22	
IGORR 10	Washington DC, USA	September 2005	83	137	14	Joint with TRTR
IGORR 11	Lyon, France	March 2007	98	141	26	Joint with RRFM
IGORR 12	Beijing, China	October, 2009	54	95	16	
IGORR 13	Knoxville, Tennessee USA	September 2010	94	148	14	Joint with TRTR
IGORR 14	Prague, Czech Republic	March 2012	137	~250	29	Joint with RRFM
IGORR 15	Daejeon, Korea	October 2013	108	250	34	Joint with IAEA
IGORR 16	Bariloche, Argentina	November 2014	117	150	28	Joint with IAEA

4. IGORR Chairmen

In addressing the history of the IGORR organization it is important to recognize the people who have served as a Chairman of IGORR. Without their time and efforts the IGORR organization would not have survived the first 25 years.

As previously mentioned, Colin West, who was the Director of the proposed new research reactor the Advanced Neutron Source at Oak Ridge National Laboratory, served as the original Chairman of the IGORR organization. Colin served as Chairman from 1989 until 1996 and oversaw the first five IGORR meetings.

Colin was followed by Klaus Böning, a professor at the Technical University of Munich, who was the FRM-2 Project Leader at the time. Klaus served as Chairman from 1996 until 2003 overseeing the IGORR 6 through IGORR 9 meetings.

Alain Ballagny, JHR Project leader at the time, with CEA/Cadarache in France was the third IGORR Chairman taking over in 2003. However, Alain retired a little over a year later and thus was only able to serve as Chairman for a short time. Shortly after the IGORR 10 meeting in 2005 he passed the Chairmanship to a fellow Frenchman Joël Guidez.

Joël Guidez, who at the time was with CEA/Saclay, became the fourth IGORR Chairman and oversaw the organization of the IGORR 11 and IGORR 12 meetings. However, in late 2009, due to a reassignment within CEA, Joël stepped down from the chairmanship position and passed the Chairmanship on to Gilles Bignan, JHR User Facility Interface Manager, with CEA/Cadarache.

Gilles Bignan has served as Chairman since that time overseeing IGORR 13 through the present IGORR 17 meeting.

5. Points of Interest Concerning the IGORR Organization

The following are some points of interest regarding the IGORR organization over the years:

- From the beginnings of IGORR in 1989 the primary purpose of the organization has been to facilitate communication and collaboration across the broad range of research reactors around the world, as reflected in the before mentioned IGORR Charter. The original charter was held intact until 2007 when phrasing was added to the charter to emphasize the importance of promoting safe operation in the research reactor community. In the late nineteen eighties and early nineteen nineties, following the Three Mile Island and Chernobyl accidents, the nuclear power industry recognized that no single power reactor operates outside the influence of the performance of other power reactors. As a result, the nuclear power industry throughout most of the world placed a good bit of emphasis on self-policing and the promotion of common safe operation practices. There was some delay with this message filtering throughout the research reactor community, but with the guidance of IAEA, which had taken the lead in promoting safety practices across the research reactor community, this became a major topic of discussion at the IGORR meetings

in 2005 and 2007. Thus, in 2007 the Steering Committee revised the Charter to reflect this important aspect of the scope of the IGORR organization.

- There are no longer any original IGORR Steering Committee members still active on the committee. José Lolich (INVAP-Argentina), Bob Williams (NIST- USA), and Douglas Selby (ORNL-USA) have served the longest on the IGORR Steering Committee with nearly 20 years of involvement on the committee.

- Through 2004 the IGORR Chairman distributed a newsletter on a regular basis that was comprised of short research reactor status updates supplied by the IGORR research reactor members. Although the newsletter supplied interesting reading material, it was determined that with a meeting on average every 18 months there was little need for a newsletter update on activities.

- Through the present IGORR 17 conference, the IGORR meeting has been hosted six times in Europe, four times in North America, four times in Asia, two times in South America, and once in Australia.

- In the first 10 years of the IGORR organization the majority of the papers presented were tied to new reactor projects or major upgrades to existing reactors. In the last 15 years this has shifted toward more papers being presented on R&D, Reactor Utilization, and Operations related research reactor topics.

6. Closing Remarks

Over the last 25 years there have been many dismal opinions on the future of research reactors. Many have pointed to the decline in the number of research reactors in operation around the world. However, as noted by Shojiro Matsuura (Executive Director of JAERI at the time) at the IGORR 3 meeting and Wolfgang Gläser (Former Director of ILL) at the IGORR 8 meeting, the number of requests to use the existing research reactors is on the increase. This is consistent with the experience at the High Flux Isotope Reactor at ORNL where today we have about a factor of three more requests for beam time than we can accommodate on an annual basis, and this is only expected to increase with time. Nevertheless, we must recognize that whether it is isotope production, neutron beam, or materials irradiation science, many of the top facilities are aging. Thus, part of the IGORR objectives should be to support organizations around the world in their attempt to promote and pursue new research reactor facilities and to upgrade existing facilities to increase their anticipated lifetime. This can only be done if we can continue to show that the research reactors are both safe and cost effective, which should be two more key support objectives of the IGORR organization working with IAEA.

Clearly the practice of finding related topical meetings for joint conferences with IGORR has been successful, as shown recently with the last 2 IGORR meetings organized with an embedded IAEA topical meeting (2013 in Korea and 2014 in Argentina), and should be continued. This has led to more efficient conference planning, reduced costs, and increases the chances for commercial sponsorships of the meeting. It has also increased the scope of topics presented at the IGORR meeting.

In the beginnings of IGORR the intention was that the IGORR organization be more than just a group that holds a conference every 18 months. The Steering Committee was intended to be a constant working committee with representatives from around the world serving as contact points for research reactor organizations to promote a continuous networking capability across the research reactor community. Clearly country and facility intellectual property restrictions impact what networking can be done. However, it is important that this aspect of the Steering Committee responsibilities not be forgotten, and the Steering Committee should work with IAEA to help with future networking activities.

Finally, it should be noted that it is the authors' opinions that IGORR is presently as strong as it has ever been and the scope of presentations has increased over the years while keeping the quality of the presentations at a high level. It is perceived and hoped that in another 25 years another person will present a similar paper on the second 25 years of IGORR.

DISPOSAL FACILITIES FOR COUNTRIES WITHOUT A NUCLEAR POWER PROGRAMME

J. FEINHALS
DMT GmbH & Co. KG
Gr. Bahnstr. 31, 22525 Hamburg, Germany

D. KEMP
Waste Management Services, ANSTO
Locked Bag 2001, Kirrawee DC NSW 2232, Australia

A.SAVIDOU
INRASTES, NCSR "Demokritos"
Aghia Paraskevi, 15310 Athens,Greece

ABSTRACT

Countries with a nuclear power programme are making strong efforts to guarantee the safe disposal of radioactive waste. The solutions in those countries are large disposal facilities near surface or in deep geological layers depending on the activity and half-life of the nuclides in the waste. But what will happen with the radioactive waste in countries that do not have NPPs but have only low amounts of radioactive waste from medical, industrial and research facilities as well as from research reactors?
Countries producing only low amounts of radioactive waste need convincing solutions for the safe and affordable disposal of their radioactive waste. As they do not have a fund by an operator of nuclear power plants, those countries need an appropriate and commensurate solution for the disposal of their waste. In a first overview five solutions seem to be appropriate: (i) the development of multinational disposal facilities by using the existing international knowhow; (ii) common disposal with hazardous waste; (iii) permanent storage; (iv) use of an existing mine or tunnel; (v) extension of the borehole disposal concept for all the categories of radioactive wastes.

1. The challenge

Nuclear power plants are operated worldwide in 30 countries, while 71 countries are operating research reactors [1]. Even if the spent fuel is returned to the manufacturer and the production rate of radioactive waste is much lower than at a NPP, the radioactive waste from operation and future decommissioning cannot be neglected. As there is not commercial power generation, there is also not the levy on power consumption that goes to a waste fund. There is not the money set aside for the disposal of radioactive wastes generated in these countries. Therefore these countries look for more cost effective disposal routes for the wastes that they produce. The European Commission stipulates each state needs to develop a national programme for the safe disposal of radioactive waste (Council Directive 2011/70/EURATOM) [2]. Similar requirements do exist outside the European Union, with every nation responsible for the safe management of radioactive waste, including the need to have a disposal plan. The challenge for the future is: which alternatives for the safe disposal of radioactive waste are possible for countries generating small amounts of radioactive waste?

2. Radioactive waste in countries without nuclear power programme

Countries without nuclear power plants or any nuclear fuel cycle facilities do not have high level waste (HLW), particularly when the fuel from research reactors is returned to the country of origin. In these countries, only small amounts of radioactive waste are produced. The main sources of this waste are the use of radioactive material in medicine, industry and research as well as the operation and decommissioning of nuclear research facilities like research reactors. Usually a large part of the waste can be cleared as non-radioactive waste after storage or decontamination. The amount of remaining radioactive waste that is suitable for near-surface disposal (LLW) is less than ten thousand tons while the amount that is not suitable for near-surface disposal (ILW) is less than a few hundred tons. Furthermore, in all countries there are disused sealed radioactive sources, including long-lived sources such as lightning conductors containing mainly ^{241}Am (432.2 a) or ^{226}Ra (1.6×10^{3} a), and ionization chamber smoke detector (ICSD) containing mainly ^{241}Am, ^{226}Ra and sometimes ^{239}Pu (2.41×10^{4} a) which are not suitable for near surface disposal in large quantities due to their long half life.

In countries without a nuclear programme, significant amounts of radioactive waste arise from the operation and decommissioning of research reactors [3]. The radioactive waste streams depend on the reactor type, the implemented applications and the schedule of operation. They can be activated and include contaminated materials. The most activated part of the reactor structure is the core, while the biological shield, usually made of concrete and steel reinforcements, is exposed to relatively low neutron fluxes. Contamination arises from the activation of the corrosion/erosion products as well as from the dispersion of the irradiated fuel and fission products through cladding breaches and conveyed by the coolant. Fission products in contaminated materials generally become significant in the case of failure of fuel elements. A large variety of radionuclides can be produced by neutron activation at nuclear reactors. The radionuclides which are important from the viewpoint of disposal are the long-lived radionuclides (half-lives higher than 30 a). The major long-lived nuclides are: ^{14}C (5730 a) which is significant in concretes and graphite; ^{36}Cl (3.01×10^{5} a) is present in some stainless steels and aluminum reactors components; ^{41}Ca (1.03×10^{5} a) is one of the main constituents of bioshield concrete; ^{59}Ni and ^{63}Ni (7.6×10^{4} a and 100.1 a respectively) is found in nickel alloys and stainless steel; ^{93}Mo (3500 a) is present in some stainless steels; ^{93}Zr (1.5×10^{6} a) is important in irradiated cladding and in moderator tubes; ^{108m}Ag (130 a) is significant in control rods with large amounts of silver.

Common examples of solid very low level waste (VLLW) and low level waste (LLW) are items contaminated during handling of radioactive materials such as personnel protection items, cleaning materials and tools as well as components exposed to neutron beams such as containers for production of radioisotopes or for irradiation of samples. Low and intermediate level waste (LLW and ILW) can be materials used for cleaning of water, such as ion exchange resin or materials in the ventilation systems as well as irradiated components of the reactor such as the materials at the reactor core, monitoring equipment (ionization and fission chambers, thermocouples etc.), control rods and startup neutron sources.

Liquid radioactive wastes during operation are usually coolant from the reactor pool or vessel, liquids used for decontamination and liquids produced from hot chemistry laboratories. In case the aqueous wastes cannot be discharged, they are concentrated to minimize the volume and the residues usually solidified in cement. Other liquid wastes like organic solvents are solidified in cement directly or incinerated together with other radioactive waste.

Tritium in liquid wastes is of higher importance in reactors cooled and/ or moderated with heavy water. In gaseous radioactive wastes, the main radionuclides are ^{41}Ar and ^{14}C which are produced by activation of the air present in the reactor coolant/moderator and irradiation facilities.

A significant application in research reactors is the production of radioisotopes for medicine, agriculture, industry and research. Radioisotopes are produced at research reactors by neutron capture in targets or by nuclear fission of ^{235}U [4]. In the case of radioisotope production by neutron capture, target encapsulation is an important stream of solid radioactive waste. The use of zircaloy for encapsulation yields waste with ^{93}Zr while the use of stainless steel results mainly in waste with ^{55}Fe, ^{63}Ni, ^{60}Co. The nuclear fission of ^{235}U produces the full set of fission products and some actinides.

The main decommissioning wastes are activated and contaminated metals (e.g., stainless steel, carbon steel, lead, aluminum) and concrete from the biological shield. More than 50% of materials from dismantling of research reactors are exempt waste and a small amount, less than 10%, are ILW. In research reactors some specific materials like graphite or beryllium are also used. Graphite is used as a moderator and reflector. Some research reactors have a stacking of graphite in one of their irradiation facilities, the thermal column. The long lived ^{14}C isotope can be produced by neutron activation in the graphite. The activity of this isotope determines the management/ disposal options of graphite. Beryllium is used in research reactors as a source of neutrons, moderator and reflector. The material itself is extremely toxic. The main radionuclides in beryllium are ^{3}H and the long lived ^{10}Be (1.6×10^{6} a).

2.1 Australian case

Australia is involved in diverse nuclear activities; historical nuclear weapons testing by the UK; uranium and rare earth minerals mining; oil and gas industries; minerals research (creating TENORM); three research reactors (only one still operational – OPAL); radiopharmaceutical production; particle accelerators; and industrial sources. Australia has been involved in research and mining involving radioactivity from the discovery of radioactivity. As an example Radium Hill mine in South Australia was opened in 1906. The wastes from the processing of uranium and other rare earths are still managed to this day as there is no disposal site for this material.

All mines in Australia which produce radioactive tailings have to manage those wastes at the point of generation and the wastes should be made safe from human, animal or flora interference at the closure of the mine. For most mine sites this will mean placing the tailings back into the excavated mine and closing the site like a landfill. Every company that owns a mine in Australia has to put up a bond to the government to cover the costs of remediation of the mine site.

The UK used Australian sites (Emu Flat, Monte Bello Islands and Maralinga) for the testing of nuclear weapons, and the debris was later cleaned up. The process used in the clean up was in-situ vitrification (Geomelt). The wastes were collected and put into pits in the sand, then large electrodes were used to vitrify the substances into a large block of glass. This block was then buried in the desert area and classed as a disposal site. This method is not suitable for the majority of industrial wastes in Australia.

Australia has used three research reactors since 1956: HIFAR a heavy water moderated 10 MW reactor; Moata, a 100kW Argonaut reactor; and OPAL, a light water cooled open pool 20MW reactor. HIFAR initially used HEU but was converted to LEU. OPAL uses LEU fuel, and LEU targets for radiopharmaceutical production. The HIFAR reactor has been placed in a shutdown state from 2006 after 49 years of operation, Moata has been decommissioned, and OPAL is operational since 2007. The reactors were used for research, particularly neutron beam research, irradiations of silicon and radiopharmaceutical production. Just under 50% of the volume of Australia's radioactive wastes, both low level and intermediate level, come from ANSTO. It covers around 90% of the activity of Australia's radioactive waste. [5] Spent fuel from the reactors was sent overseas; to the USA as part of the research reactor take back scheme; to France and UK to be reprocessed. The reprocessed vitrified

fission products will be stored in Australia until disposal. The majority of waste at ANSTO is not conditioned for disposal. Australia has no high level waste.

Research institutions in Australia have their own radioactive waste stores ranging from a small cabinet in a locked room to facilities the size of aircraft hangars. These facilities just store the waste and the material accounts for just under half the volume of waste to be disposed of. Disused Sealed Radioactive Sources are the responsibility of the user and should be returned to the manufacturer, however orphaned sources (no viable ownership) have been taken by local radiation protection agencies and stored pending a disposal route.

There are many radioactive wastes which require treatment before long term storage or disposal. Examples include the oil and gas scale, flammable radioactive liquids from experiments, contaminated pumps and other equipment, activated carbon/graphite, tritiated water, nuclear materials, highly caustic solids and very large, very active equipment (cyclotrons, reactor components). Liquid wastes are kept on site unless they meet the World Health Organisation radioactivity requirements for drinking water. Airborne radioactivity is captured by filters as much as possible, however there are radio-xenon releases from the radiopharmaceutical production which are difficult to fully capture. Solid wastes are kept until they meet the exemption criteria as specified by Australian laws and regulations.

Australia currently has approximately 4100 m^3 of low level radioactive waste and 465 m^3 of intermediate level waste to manage. The future projections are a generation rate of 50m^3 of low level waste per year plus another 500 m^3 of decommissioning wastes, and a generation rate of 10 m^3 of intermediate level waste per year plus another 500 m^3 of decommissioning wastes [5].

The Australian government has been searching for a disposal site for low and intermediate level wastes since 1992. The current process is a volunteer process that requires owners to nominate the land required and requires a level of community support. There is no land in Australia which is not owned or claimed by a person or group. This volunteer process is currently going through the community support assessment stage and a decision on the location will be made in the next two years. The concept design for the low level waste facility is an engineered facility above ground using concrete vaults. The waste packages will be placed into the concrete vaults and cemented into place. At the end of 100 years of operation the facility will be closed and returned to a natural looking environment, that is covered with earth and water barriers. The monitoring for the low level waste facility will be monitored for 200 years post closure. The intermediate level waste will be stored at the same site while a search is on for an intermediate level waste disposal site. This site will involve geological disposal, most likely a borehole style. The economics at present do not support geological disposal yet as Australia's quantity of ILW is small on a global scale. This central facility will hopefully replace most of the 130 radioactive waste stores in Australia. [6]

The disposal of high level waste is not being considered by the government, and the disposal of intermediate level waste is on hold until there is enough waste to justify the economics of disposal. The search for a cost-effective disposal option continues for Australia.

2.2 Greek case

Greece has an open pool type, light water moderated and cooled heterogeneous reactor with thermal power at 5 MW. The Greek reactor (GRR-1) went critical for first time in June 1961 and has been in extended shut down since July 2014. Reactor control was performed by five control rods composed of Ag-Cd-In alloy with composition 80%, 5% and 15%, respectively. An irradiation facility of the reactor is the graphite thermal column for slowing down fast neutrons to thermal energies. For neutron reflection, beryllium blocks were used. From the future reactor dismantling, it will arise about 1 ton of materials (metals and graphite) not suitable for near surface disposal [7].

Moreover, about 2000 sealed sources, which potentially might become waste, are in use in industrial, medical and research laboratories within the country. Furthermore, Greece has some radium sources from the past as well as items with ^{226}Ra like dials of gauges. Also, this country has a large inventory of lightning rods containing radioactive sources (^{226}Ra and ^{241}Am). Well over 1000 are still erected on buildings. These sources need to be removed from buildings, conditioned and stored for future disposal [8].

Greece is a touristic country and the public is very sensitive about the environment. Also all the areas of the country are inhabited. The country supports the idea that sharing of disposal facilities in the context of an agreement between the countries, taking into account the conditions specified in the European Council Directive 2011/70/Euratom is a beneficial, cost-effective and safe option. In case the idea of a multinational disposal facility does not go ahead, the establishment of a small scale and cost affordable geological disposal facility for LLW and ILW seems to be the appropriate disposal solution and most acceptable by the public.

3. Existing concepts for disposal of radioactive waste

Europe is running a very intensive research in the area of disposal facilities [9]. For coordination of all the research projects for an effective exchange of information technical platforms were established [10]. The IGD-TP (Implementing Geological Disposal – Technical Platform) was launched for the research for deep geological disposal facilities, where the concept of near surface disposal facilities is described as sufficient for low level and intermediate level waste with short half-life. Geological disposal is recommended for intermediate level and high level waste especially containing isotopes with long half-lives. All these projects for disposal facilities have one thing in common: They are very money and time consuming, because they are designed for large amounts of radioactive waste. Such solutions seem to be not adequate for the disposal of some thousand drums with radioactive waste. Nevertheless, countries with a high progress in such disposal projects shall take over a lighthouse function for those countries, which have just started planning for a disposal facility.

Existing concepts are:

- Near Surface burial – low level waste is buried within 10 m of the surface in a conventional style landfill
- Shallow burial – low level waste is packaged and buried within 100 m of the surface
- Engineered structures and concrete vaults – typically for 100,000 m^3 of waste or more
- Engineered boreholes for disused sealed radioactive sources
- Geological caverns for the disposal of intermediate level waste or high level waste

4. Alternatives

Fully aware of this challenge the following alternative solutions are also discussed.

4.1 Multinational disposal facility

A multinational disposal facility is a disposal facility, which is used by several countries (sometimes also called “regional disposal facility”). This approach investigated by WNA [11] and IAEA [12] makes sense from the technical as well as from the economical view. In EU, the European Repository Development Organization (ERDO) works for the implementation of one or more shared regional repositories for radioactive waste. The idea is compelling, but the political challenges are very difficult. The definition of the area of competence for a supervising and licensing authority might be easy, although it has to be active beyond state borders to control waste packages in other countries and to decide whether waste packages are acceptable or not. There are many challenges:

- How will the costs be shared for the participating countries if the project has a significant delay (which is very normal in those projects) or has to be abandoned?
- What will happen if acceptance of foreign waste is suddenly unenforceable due to a lack of public acceptance?
- How stable will the country, its government and borders be for the life of the control period?
- Would the site become a security risk for all the countries around it?

These challenges are only some of the reasons why politicians see only little chances for a multinational disposal facility.

Groups have nominated Australia as the site of a multi-national repository, and discussed the concept of uranium leasing; the country which mines the uranium has to take the uranium back at the end of its useful life, along with whatever other wastes were produced with it. There is no political will or public support for either idea within Australia, and there is a minority viewpoint that if we are exporting radiopharmaceuticals then Australia should be exporting that portion of the radioactive waste to the country using the radiopharmaceuticals. There is an idea for a south-east Asian repository, however the issues are still over who will have control, where it will be situated and how this will impact on the regional tensions between countries. This would be a long term goal (100 years) for the region.

4.2 Common disposal with hazardous waste

This alternative idea seems to be smart, as requirements for technical barriers at landfills for hazardous (toxic, harmful, dangerous goods) waste are comparable to near surface disposal facilities for very low level waste. Already existing capacities at landfills for toxic waste might be usable for low level waste [13]. But it has to be considered, that in case of a failure of the technical barriers of the landfill the impact on the environment will significantly increase. The health effects by incorporation of radioactive substances might be of minor importance compared to the toxic substances, but the effort for remediation will be much higher. In any case an additional safety assessment is required. This would not be suitable for intermediate level wastes. One advantage is that radiation will eventually disappear, unlike the other hazardous and toxic wastes.

For some governments, the very low level radioactive waste can be stored in hazardous waste facilities.

4.3 Permanent Storage

A different solution can be found in the Netherlands. Radioactive waste has to be stored in a central interim storage (COVRA), designed for an operation of 100 years. Actually, already conditioned waste (supercompacted and cemented) will be checked for their specific activity. Those drums below the Dutch clearance values, are opened, sorted and cleared as conventional waste. By this way COVRA could increase their capacity significantly (s. fig. 1) [14]. For some countries generating only small amounts of waste this strategy of permanent storage with subsequent clearance might be fully sufficient, especially, if the half-life of the nuclide is short. Additional individual considerations for a specific clearance might be helpful, if an enhancement of clearance values is radiological acceptable on the basis of the de minimis concept. Independent of the consideration about the amount of radioactive waste such a solution makes sense even for countries with high amount of radioactive waste, because permanent storage enables the use of the option clearance and goes easy on the resource capacity of a disposal facility. Such a strategy is under discussion for example in Switzerland.

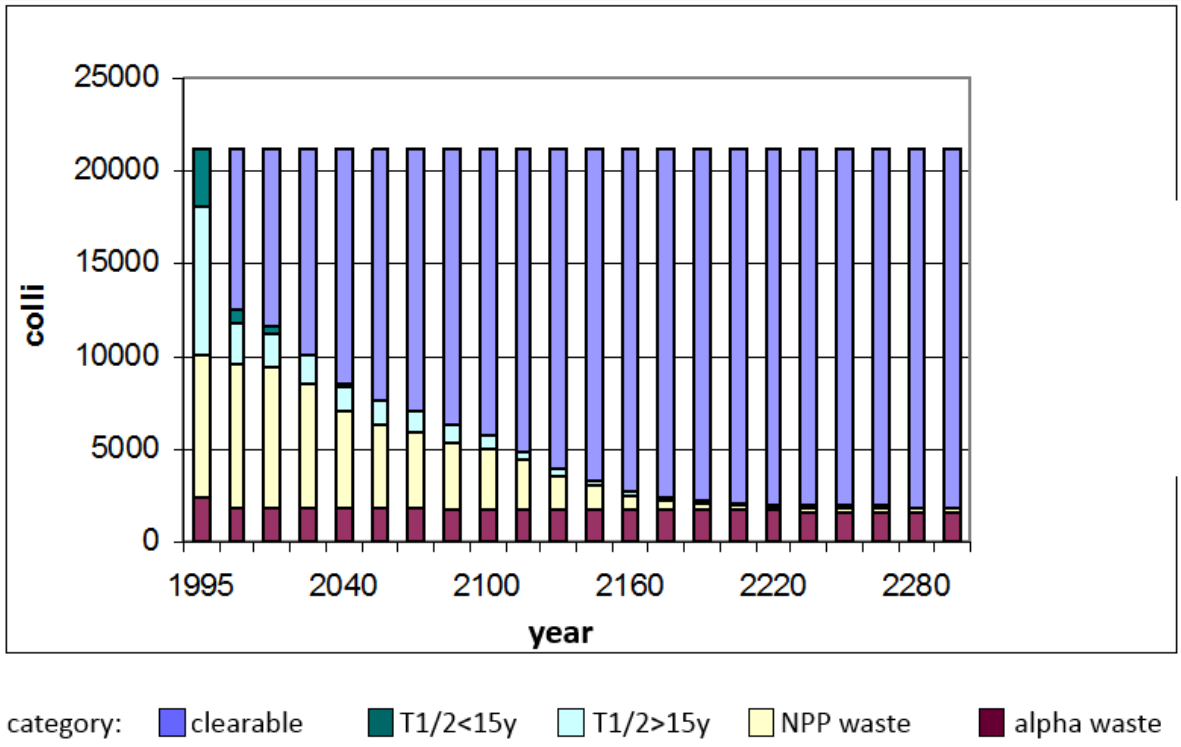

Fig. 1: Number of clearable drums in Dutch permanent storage COVRA [14]

4.4 Small scale disposal facility

If the above mentioned alternatives are not applicable or do not fulfill the radiological requirements, the following alternatives should also be investigated:

- New construction of a small scale near surface disposal facility for radioactive waste
- Use of an already existing mine or tunnel
- Development of a borehole disposal concept appropriate for more categories of wastes besides the sealed sources The already existing concept published by IAEA [15] is related only to the disposal of sealed sources

A commensurate solution is possible on the basis of a for each country individual consideration of the following parameters:

- The waste properties; like specific activity, half-life, amount, chemical waste form etc.
- The technical conditions; like an appropriate disused mine or permanent storage already existing
- The geological conditions; like site selection for a new near surface or geological disposal facility
- The legal conditions; like use of specific clearance values.

4.4.1 Use of an already existing mine

For discussion of the use of an already existing mine as a disposal facility the following aspects have to be considered:

- Geological situation, the system of natural barriers: Is a proof for long term safety possible and for which time duration is it necessary? Which additional measures are necessary to keep the safety requirements? For this case additional concrete structures for sealing the drums with radioactive waste from the host rock can be helpful. The safety parameters have to be calculated on the basis of the radioactive inventory, which might be brought into the disposal facility in future. The aim is to

prevent radioactive material from coming into contact with groundwater in which it could dissolve, as this is the principal route by which radionuclides could be transported from a disposal facility through the host rock to the near surface, where it can affect humans.

- History of the mine, rock stability: stability of caverns and pillars especially in old mines has to be checked under consideration of the planned operational life time. Additionally, two shafts, a good ventilation and ways for rescue and emergency are state of the art requirements. In general, the use of the mine for the time of operation and closure as disposal facility has to be added into the safety assessment. This can cause a significant effort for repair, reconstruction, and maintenance. Additionally, measures for backfilling of empty caverns have to be taken into account.
- Robustness against incidents and events: In old mines shafts are often not appropriate for transport of radioactive waste. A design including the drop of waste packages into the shaft as well as earthquakes is necessary. The results of calculations of the potential dose in case of such incidents and events must demonstrate that the legal requirements are not exceeded.
- Site selection: In case of selection between different sites logistical aspects for the transport to the site and the infrastructure at the site have to be considered as well as the public acceptance in the surrounding communities.

In consideration of all these points it becomes clear that a disused mine could meet all the safety requirements with a small need for reconstruction would be a very good choice.

4.4.2 Extension of the borehole disposal concept

Borehole disposal is to dispose of items in a vertical cylindrical hole underground. There are two types – shallow and geological boreholes. If the waste is below a depth of 150 m it is considered as geological disposal. The current use of a borehole is designed for the disposal of disused sealed radioactive sources generally. The extension of this concept is to make the hole diameter slightly bigger and have waste canisters placed into the hole. The borehole could be up to 5 km deep and it would be lined to prevent water from filling the borehole. The waste would be placed in the hole, fill placed around the waste, a spacer to the next waste canister and it would be filled up to an appropriate level depending on groundwater levels. The advantage of this method is that it does not rely on creating tunnels, inspection systems or ventilation systems. With the mining knowledge and capabilities a borehole down 1 or 2 km is possible now which could be used. This is a much cheaper form of geological disposal. The packages will have to be stronger as there will be tonnes of force on each package.

4.5 Other disposal concepts

Other disposal concepts are also discussed:

- Subsea burial – boreholes under the ocean as another level of protection. The boreholes could be shallower and the capping will increase over time through sedimentation. This method has very little public support, and is more complicated and costly than land based borehole disposal. This method is banned by international treaties
- Subduction zone burial – emplacement of waste in land, which is slowly moving under another tectonic plate. The idea is that eventually the waste will be in magma and dissolved in the fluid rock. This method has never been implemented as the uncertainties around earthquakes and eruptions are too high.
- Use of already contaminated areas (nuclear weapons testing sites)- Use of an area within a nuclear test site (above or below ground) for disposal of radioactive wastes, or use of contaminated tunnels for waste placed by robots. This could only be used by a small number of countries, and would have to demonstrate adequate radiation protection to all workers to be enacted. This option is used by Kazakhstan.

5. Conclusion

Countries without a nuclear power programme may produce radioactive waste, and have to responsibly deal with that waste. As there is not commercial power generation, there is also not the levy on power consumption that goes to a waste fund. There is not the money set aside for the disposal of radioactive wastes generated in these countries. Therefore these countries look for more cost effective disposal routes for the wastes that they produce.

With the wide variety of radioactive wastes which are produced, the simpler forms of conditioning and disposal are more suitable for countries with a small radioactive waste inventory. The first step is to understand the waste that the country has, and will generate. This should all be reported in the national reports to the Joint Convention on the Safety of Spent Fuel Management and on the Safety of Radioactive Waste Management as coordinated by the IAEA. The next step is to understand the options that are available to the country.

The most practical solution is a multi-national repository, where the countries pool resources to build a larger facility than any one country could do on their own. However there are many political problems which are not yet solved. The states may look to co-disposal with other hazardous wastes, or for permanent storage until a disposal option becomes viable, whether that be exemption or a radioactive waste disposal site.

If these possibilities are not feasible, the next option is to create a small scale disposal facility based on existing technologies. This could be a smaller engineered concrete vault structure, the use of an existing disused mine for geological disposal or extending the borehole concept to take in other wastes. These smaller scale structures will still cost money, but not as much as for waste facilities for nuclear power plants.

There is a chance to combine existing possibilities and to fit them individually for each country. But it has to be considered, that

- Governments in some of these countries have not realized the necessity of a final solution for the radioactive waste.
- Some countries might have proceeded in treatment of waste without knowing the final disposal solution; the problems may increase as the waste may need to be re-conditioned.
- At the moment there is no way for funding of a disposal facility.

Especially, the last item hampers small scale and affordable solutions. A support by the European Community in this direction can be useful for many countries.

6. References:

[1] IAEA http://nucleus.iaea.org/RRDB/RR/ReactorSearch.aspx?rf=1

[2] Council Directive 2011/70/Euratom of 19 July 2011 establishing a Community framework for the responsible and safe management of spent fuel and radioactive waste

[3] International Atomic Energy Agency (1998). Radiological Characterization of Shut Down Nuclear Reactors for Decommissioning Purposes. Technical Report Series No. 389, IAEA, Vienna.

[4] International Atomic Energy Agency (2003). Manual for Reactor Produced Isotopes. TECDOC-1340, IAEA, Vienna.

[5] Joint Convention on the Safety of Spent Fuel Management and on the Safety of Radioactive Waste Management; National Report of the Commonwealth of Australia 10 October 2014
http://arpansa.gov.au/pubs/regulatory/conventions/jc2014NationalReport.pdf

[6] www.radioactivewaste.gov.au

[7] Savidou et al., Inventory and Classification of the Components and Systems of the GRR-1 for Decommissioning Planning. International Nuclear Safety Journal, vol.3, issue 4, pp. 72-81, 2014.

[8] Joint Convention on the Safety of Spent Fuel Management and on the Safety of Radioactive Waste Management; National Report of Greece 10 October

[9] D. Bosbach: Research for the safe management of radioactive waste in the Helmholtz Association FS-Symposium Zwischenlager-Dauerlager-Endlager
22.-24.09.2014, Mainz

[10] www.igdtp.eu

[11] http://www.world-nuclear.org/info/Nuclear-Fuel-Cycle/Nuclear-Wastes/International-Nuclear-Waste-Disposal-Concepts/

[12] Developing multinational radioactive waste repositories: Infrastructural framework and scenarios of cooperation
IAEA TECDOC 1413, Vienna 2004

[13] M. Dützer: Very low level waste disposal in France: a key tool for the management for decommissioning wastes in France
StrahlenschutzPraxis 2/2015

[14] J. Wellbergen, E. Verhoef, R. Wiegers: Radioactive waste: from cradle to cradle TÜV NORD Symposium Provisions for Exemption and Clearance 21-23 Sept. 2009, Wiesbaden, Germany

[15] Borehole Disposal Facilities for Radioactive Waste, IAEA SSG-1, Vienna 2009

AAEA Contribution towards Optimal Research Reactors Use in Arab Countries

MAHJOUB, Abdelmajid and MOSBAH, Daw
Arab Atomic Energy Agency
7 Rue de l'assistance; cité el Khadhra
1003 Tunis, TUNISIA
Corresponding Author: aaea_org@yahoo.com

There are nine research reactors (RR) at present in the Arab world, one under construction, another one is planned and two are shutdown and decommissioned. The level of their operation and utilization differ from one country to another depending on the individual situation in a particular country. Some other Arab countries are considering or planning to build new research reactors. These RRs are mostly used in: Analysis of the structure of matter, radiation damage studies to develop better materials for nuclear and industrial applications, neutron activation analysis for accurate determination of elemental concentrations in material, production of isotopes that are used in biology, medicine, agriculture, industry, hydrology and research and training of scientists, engineers and technicians needed to support the nuclear power industry.

The Arab Atomic Energy Agency (AAEA) is a regional specialized organization working within the framework of the League of Arab States (LAS) to coordinate the scientific efforts of the Arab Countries in the field of peaceful uses of atomic energy. It contributes also to the transfer of the peaceful nuclear knowledge and technologies.

One of the most important tasks of AAEA is to coordinate between Arab states to share their laboratory facilities and develop the human resources which have the capabilities of assimilating the nuclear knowledge and its application. The use of nuclear research reactors depends heavily on the availability of qualified scientists, engineers and technicians. Many Arab countries still have insufficient training capabilities in the nuclear fields, and are experiencing problems with high staff turnover and shortage of specialized professionals in these areas.

AAEA sponsored a coordinated research project [2] put down by Arab experts according to the needs of sustainable development in Arab states and implemented within the human and technological resources available in the country and sharing of laboratory and technological capabilities with other AAEA member states.

The project is accompanied by continuous cooperation between researchers and by human resources development and expert missions for the participating researchers and technicians in order to improve their skills and performances. The ultimate objective of the coordinated research project is to define and develop the preliminary steps and methods necessary to help in establishing a sound research and utilization program of available RRs in the Arab region.

Many activities have been undertaken by AAEA related to the utilization of RRs such as: training courses, on-the-job training, training schools, scientific visits, scientific and experts

meeting. Those activities cover a wide range of subjects related to RRs. Following are some of the training subjects undertaken regularly by AAEA:

- Research reactors: Design, operation and applications.
- Neutron Activation Analysis using RRs.
- Reactor safety and security systems.
- Radiation protection, regulations and legislations.
- Emergency plans, waste management, monitoring and early warning.
- Modelling of nuclear accidents and their effects on the environment and public health.
- Workshops and fora about the applications of RRs.

The research reactor is a very versatile tool, that when used effectively, can contribute to a country's technological and scientific development. As most of the research reactor facilities are not being fully utilized, therefore AAEA regards that its technical cooperation project between Arab countries in the field of RRs utilization is of most interest on long-term sustainability of RRs utilization programmes. Therefore, countries which do not have a RR can benefit a great deal from these AAEA activities and enjoy the availability of facilities they do not have.

A need to improve the utilization and safety of research reactors are very important. Arab countries that are embarking or considering building nuclear power plants may use research reactors as a training tool for the future staff of power reactors.

Below we summarized the characteristics of the research reactors in Arab countries [1]

ANNuRMS with RR	Facility Name	Facility Type	Power (kWth)	Status	Vendor Country	Date commissioned
Algeria	NUR	Pool	1000	Operational – being upgraded to 3 MW	Argentina	1989
	Es-Salam	Heavy water	15000	Operational	China	1992
Egypt	ETRR-1	Tank WWR	2000	Operational	Russia	1961
	ETRR-2	Pool	22000	Operational	Argentina	1997
Iraq	IRT-5000	Pool, IRT	5000	Extended shut down	Russia	1968
	TAMMU	Pool	500	Extended shut	France	1980

	Z-2			down		
Jordan	JSA	Sub-critical	0	Operational	China	2014
	JRTR	Tank in pool	5000	Under construction	Korea	Imminent (2016)
Kuwait	–	–	–	Planning	TBD	–
Lebanon	–	–	–	Considering	–	–
Libya	TNRC	Critical assembly	0.1	Operational	Russia	1981
	IRT-1	Pool, IRT	10000	Operational	Russia	1981
Morocco	MA-R1	Triga Mark II	2000	Operational	USA	2006
Saudi Arabia	RR-1	Pool	30	Under construction	Argentina	–
	–	–	TBD (high power)	Planning	TBD	–
Sudan	–	–	–	Considering	–	–
Syria	SRR-1	MNSR	30	Operational	China	1996
Tunisia	–	Sub-critical	0	Planning	TBD	–

Table 1: Status of Research Reactors in Arab Countries, including critical and sub-critical facilities, [1].

Under the auspices of AAEA and with the support of IAEA, it was established the Arab Network for Nuclear Regulators (ANNuR)[3]. Among the thematic groups of ANNuR, there is one that concerns RRs and their safety and proper management. The thematic expert group of the research reactors will help to identify and share best practices for safety design, construction, operation (including ageing management), modification and decommissioning of RRs as well as to be a source of expertise in these matters. The objectives of this group are:

- To promote the implementation of the Code of Conduct on the Safety of Research reactors and the application of IAEA Safety Standards.

- To enhance the peer review process in the area of Integrated Safety Evaluation, promoting the establishment by participating Member States of self-assessment reports on the safety of research reactors, evaluating the results and providing recommendations for further improvement.

- To promote the mutual exchange of information through ANNuR and to foster the sharing of knowledge and experience on the safety of research reactors.
- To promote the mutual cooperation between participating member States in the safety operation of Research Reactors.

There is a need in many of Arab countries to improve the capabilities of regulatory bodies in the oversight of research reactor safety. In the framework of its programme on enhancing nuclear safety in the Arab region and particularly the safety of research reactors, the IAEA recently conducted expert review activities and a consultancy meeting with the participation of IAEA Staff, international experts and experts from the regulatory bodies in a number of ANNuR Member States, with the objective to review the status of regulatory supervision programmes for research reactors in these Member States, to identify areas needing improvement and possible IAEA assistance to address the identified needs. The relevant findings and recommendations are provided in a very valuable technical report with suggested actions to be taken within the next three years in the framework of the workplan activities of ANNuR [4].

References

[1] IAEA Research Reactor Database, http://nucleus.iaea.org/RRDB/
[2] Arab Strategy for Peaceful use of Atomic Energy up to 2020, AAEA 2008 (Arabic)
[3] Arab Network of Nuclear Regulators (ANNuR) Terms of References.
[4] Report on Assessment of the Needs of the ANNuR Member States on Regulatory Supervision of Research Reactors and the Actions Proposed to address those Needs, IAEA, July 2015


RRFM
EUROPEAN RESEARCH REACTOR CONFERENCE 2016
IGORR
BERLIN
13 - 17 March 2016
GERMANY

Fuel

ON THE EFFICIENCY OF DIFFUSION BARRIER COATING ON U-MO FUEL PARTICLES IN DISPERSION FUELS

B. Ye, G.L. Hofman
Argonne National Laboratory
9700 South Cass Ave, Argonne, IL 60439 USA

A. Leenaers
Nuclear Material Science Institute, SCK·CEN
Boeretang 200, 2400 Mol Belgium

ABSTRACT

The interaction layers (ILs) observed in the SELENIUM plates show irregular appearance and an abrupt growth at the regions with a fission rate $\geq 7\times10^{14}$ fissions/cm^3/s. The formation and growth mechanism of the IL in coated particles was investigated by applying the radiation enhanced diffusion model used for understanding ion beam mixing. IL thickness and volume fraction were calculated using the IL growth correlation for U-Mo/Al dispersion fuels with a pure Al matrix, which is expressed as a function of fission rate and temperature. The calculation results suggest that the IL in coated particles started to form from the beginning of the irradiation and its accelerated growth at high fission rate regions is a temperature effect.

1. Introduction

The fission enhanced interdiffusion between U-Mo fuel alloy and Al matrix in dispersion fuel has proven to be a life limiting effect for high fission rate (high power density) reactor operation. A solution for all but very high power density application was found by adding Si to the Al matrix. For these high power density applications a novel modification of the dispersion fuel system, consisting of a thin ZrN coating on the UMo fuel particles, was tested. The first test was conducted by RIAR in the MIR reactor in Dimitovgrad, Russia [1]. The test fuel reached a LEU burnup of ~ 85% without showing substantial Al-UMo interdiffusion. A second test was conducted by SCK in the Belgium BR2 reactor [2-4]. The results were also positive, however, at the highest fission rate parts of the test plate diffusion of Al through the ZrN barrier occurred. This paper examines this diffusion phenomenon, its consequences and explores mitigations.

2. Post irradiation examination (PIE) observations of SELENIUM plates

In the SELENIUM test, two full-size plates (U7MD 1221 and U7MD 1231) were irradiated in the BR2 reactor of SCK·CEN for a total of 69 EFPD. The SELENIUM plates have a fissile material loading of 8 gU/cm^3 and a uranium enrichment of 19.7% ^{235}U. The fuel meat of the plates contains coated atomized U-7wt%Mo (denoted as U7Mo) fuel particles dispersed in a pure Al matrix. The coating of fuel particles is 600 nm thick Si for plate U7MD 1221 and 1000 nm thick ZrN for plate U7MD 1231. A peak fission density (FD) of 5.3×10^{21} fissions/cm^3-UMo and a mean FD of 3.5×10^{21} fissions/cm^3-UMo were achieved in both plates. Table 1 lists the fabrication and irradiation data of the test. The irradiation conditions of the SELENIUM test were arranged to resemble the irradiation history of the E-FUTURE irradiation to allow a direct comparison [4].

Table 1. Fabrication and irradiation history of the SELENIUM fuel plates [4].

		U7MD 1221	U7MD 1231
Fabrication data			
Cladding		AG3NE	AG3NE
Matrix		Al	Al
Coating		600 nm Si	1000 nm ZrN
Loading		8 gU/cm^3	8 gU/cm^3
Enrichment		19.75 %^{235}U	19.75 %^{235}U
wt% Mo		7	7
Irradiation data			
EFPD		69	69
Fission density (f/cm^3 UMo)	Mean	3.5×10^{21}	3.5×10^{21}
	Max	5.3×10^{21}	5.3×10^{21}
Peak heat flux (W/cm^2)		466	466

2.1 Fuel swelling of the SELENIUM plates

The fuel swelling (S_F) of the SELENIUM plates plotted in Fig. 1 was converted from the measured plate thickness increase (S_P) after irradiation using the equation below [3]:

$$S_F = \frac{S_P}{V_F^0 \times t_i} \quad (1)$$

where V_F^0 is the initial volumetric fraction of U-Mo in the fuel meat and t_i is the meat thickness. The fuel swelling profiles in Fig. 1 show that the fuels underwent a low swelling rate in the low and middle FD region, attributed to fission product accumulation [5], and a sudden acceleration in fuel swelling rate at a FD of ~4-4.5×10^{21} fissions/cm^3-UMo. The enhanced swelling rate at high burnup coincides with fission induced recrystallization and accelerated fission gas bubble nucleation and growth [6-8]. Modeling studies show that annealing treatment of U-Mo particles in the high temperature gamma phase would delay recrystallization and thereby reduce the swelling rate increase [9].

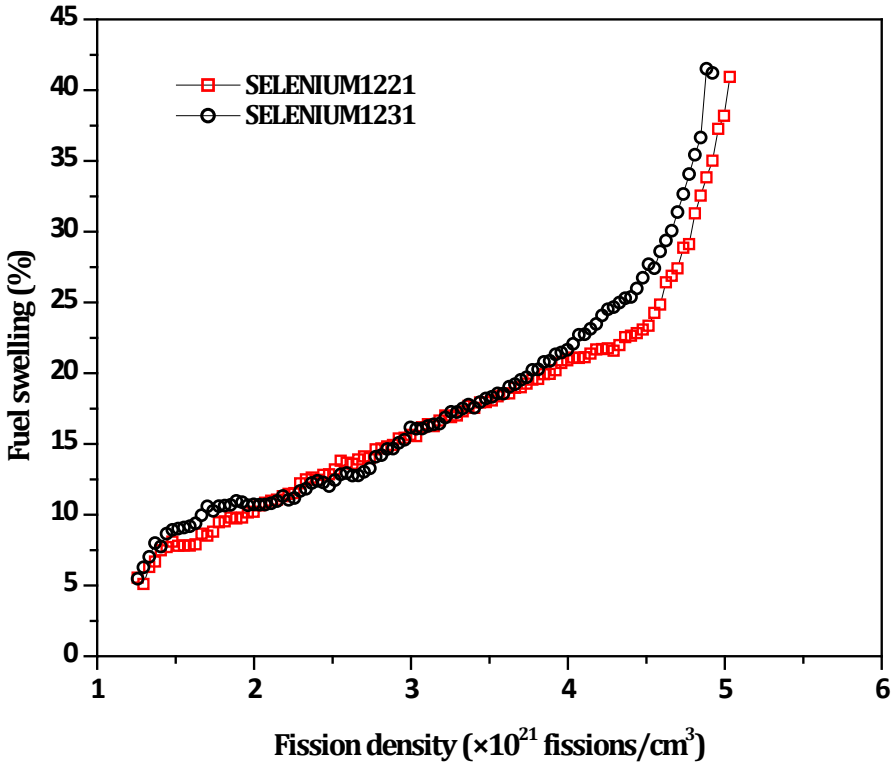

Fig. 1 Fuel swelling profile including the 1σ spread of the data points of the SELENIUM plates as function of the FD, calculated from plate thickness measurement [4].

2.2 Interaction layer (IL) appearance

Destructive examinations of the SELENIUM plates reveal that both Si and ZrN coated particles exhibit significant UMo-Al interaction at, curiously, also ~4-4.5×10^{21} fissions/cm^3-UMo [4, 7]. Fig. 2 shows the microstructures of the fuel meat in various regions in the SELENIUM plates. In the low burnup regions (<4.4×10^{21} fissions/cm^3-UMo), the fuel particles are intact; in the higher burnup regions, a growth of the coating/interaction layer is seen.

(a) SELENIUM U7MD1221 (Si)

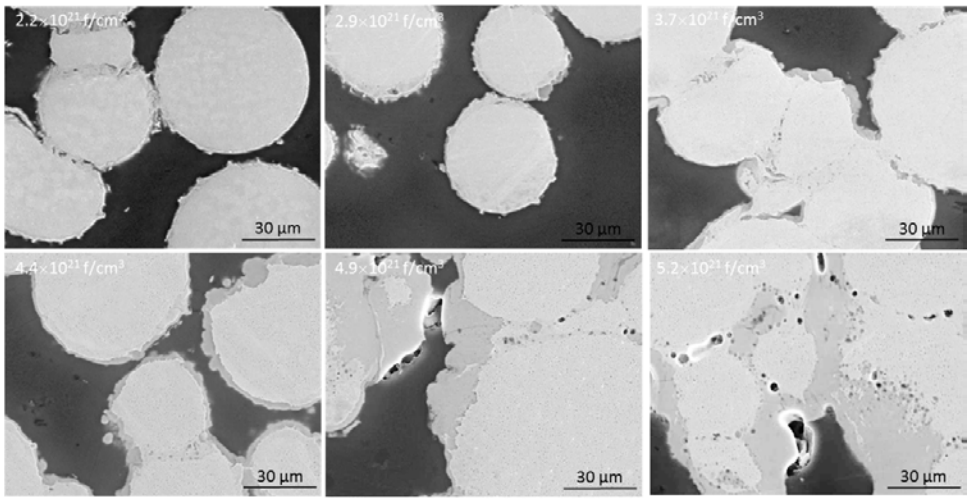

(b) SELENIUM U7MD1231 (ZrN)

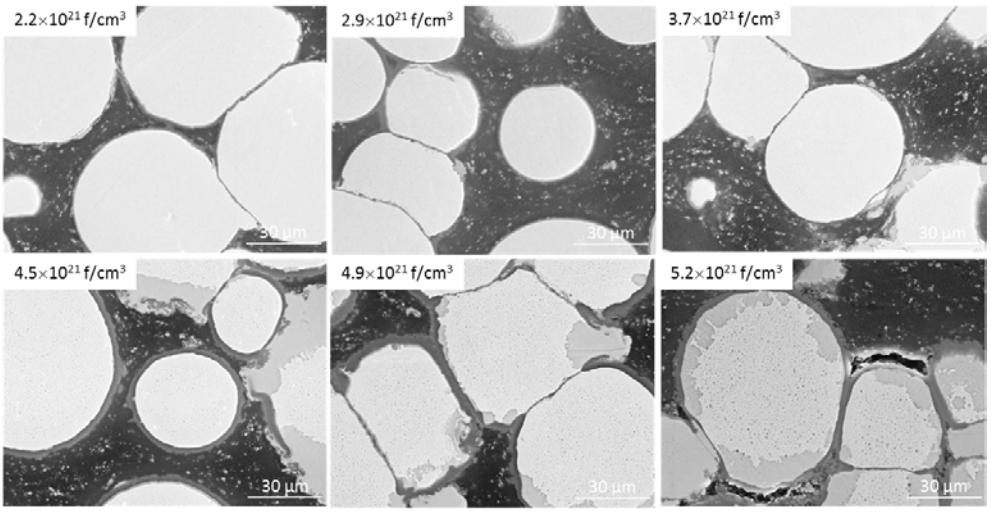

Fig. 2 The microstructures of the fuel meat at the various FDs of fuel plate (a) U7MD1221 and (b) U7MD 1231 [4].

Although the significant IL formation appears to occur at a similar FD for both Si and ZrN coated particles, their microstructural appearance is found different. In the case of Si coating, rather large porosity has begun to form at the high FD. This phenomenon resembles that was found in previous experiments with uncoated fuel particles where it resulted in fuel plate pillowing [10]. For this reason, it was decided not to continue exploring Si coating as a means of achieving high FD performance for high power density fuel.

Different types of ILs surrounding the ZrN-coated fuel particles were observed, as shown in Fig. 3. In Fig. 3 (a) is the type of double coating layer (Al-Zr-N and ZrN layers). Fig. 3 (b) shows IL ($UMoAl_x$) bursts through the coating layer, presumably via cracks in the coating. Fig. 3 (c) exhibits IL formation under an intact coating layer that might have a crack located in another plane. The IL type shown in Fig. 3 (c) appears only at highest burnup positions, and the IL is in the familiar $(UMo)Al_x$ amorphous phase [4].

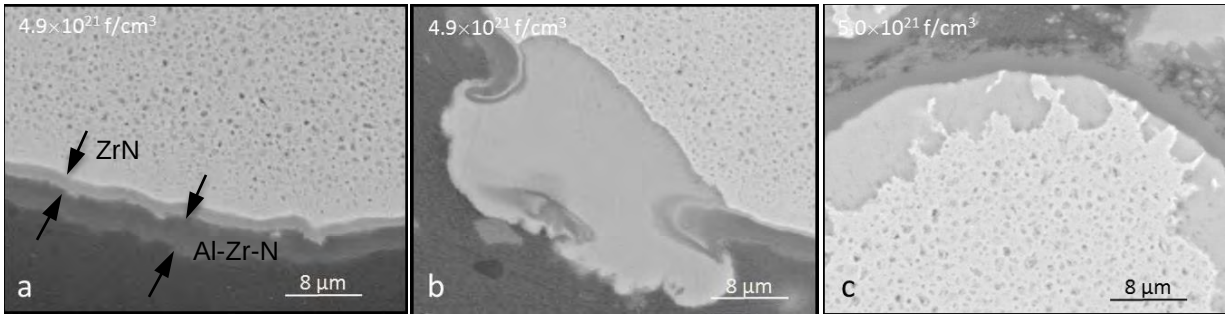

Fig. 3 Different types of ILs surrounding the fuel particles with ZrN coating: (a) double coating layer, (b) IL bursting through the coating layer, and (c) IL under an intact coating layer [4].

3. Al diffusion mechanism in coated particles

In order to determine the IL formation mechanism in coated particles, it is necessary to examine the IL growth behavior during irradiation. The measured volume fractions of the IL plotted as a function of fission density (or burnup) are shown in Fig. 4, increasing in rate at 4.5×10^{21} fissions/cm^3, for both ZrN and Si coated particles. The growth profile of IL volume fractions in Fig. 4 implies that over a fission density interval from 4.5×10^{21} to 5.0×10^{21} fissions/cm^3, approximately 7 days of the total 69 days irradiation, the IL volume fraction grows from ~5% to ~30%. This rate is not consistent with the interdiffusion correlation (Eq. (2)) developed for the U-Mo/Al dispersion fuels with a pure Al matrix based on in-pile test data [11]:

$$Y^2 = 2.6\times10^{-16}(\dot{f})^{0.5}\cdot t\cdot\exp(-\frac{7700}{R\cdot T}) \qquad (2)$$

where Y is IL thickness in μm, $\dot{f}$ is fission rate in f/cm^3/s, t is irradiation time in s, R=1.987 cal/K/mol, and T is temperature in K.

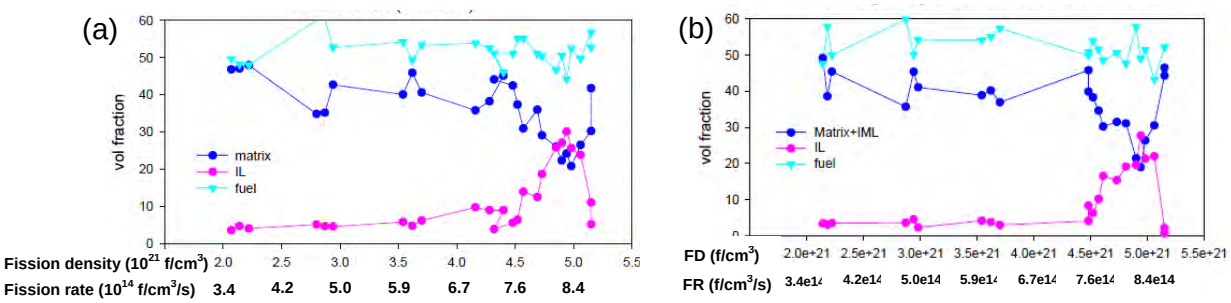

Fig. 4. Measured constituent volume fraction as a function of FD/FR in plate (a) U7MD 1221(Si) and (b) U7MD 1231(ZrN) [12].

Assuming plate U7MD 1231 has an constant average fission rate of 5.8×10^{14} f/cm^3/s and a constant fuel meat temperature of 130°C, the IL thickness can be calculated using Eq. (2). Its comparison with the measured IL thickness at the high FD areas is shown in Fig. 5. This calculation shows that the interdiffusion in ZrN-coated particles need to start at the beginning of the irradiation instead of after certain burnup in order to reach the final thickness. The same IL thickness calculation was performed for the FUTURE test that has a lower temperature (~110°C) and a shorter irradiation time (40 EFPD) [4]. The agreement between the calculation results and the measurement confirms that IL growth can be reasonably described with Eq. (2). It is noted that in single plate tests high FD is always accompanied with high $\dot{f}$. In other words, it is impossible to separate FD and $\dot{f}$ effects in single plate tests. According to Eq. (2), the increase of IL formation is a primary function of $\dot{f}$ instead of FD. Thus, it is more appropriate to use $\dot{f}$ in the study of IL growth.

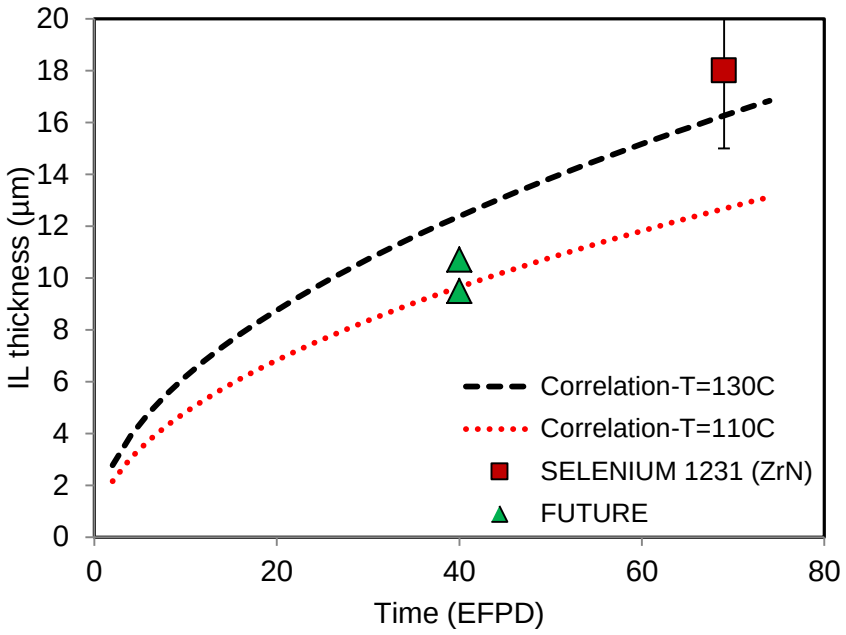

Fig. 5 Calculated and measured IL thicknesses for the SELENIUM and FUTURE tests.

It was observed that ZrN coating was consumed during irradiation by reacting with the Al matrix to form an Al-Zr-N layer as indicated in Fig. 3(a). The reaction is a diffusion process which, presumably, is an irradiation effect. The Al-Zr-N layer thickness and the corresponding ZrN layer thickness measured in various regions in plate U7MD 1231 are illustrated in Fig. 6.

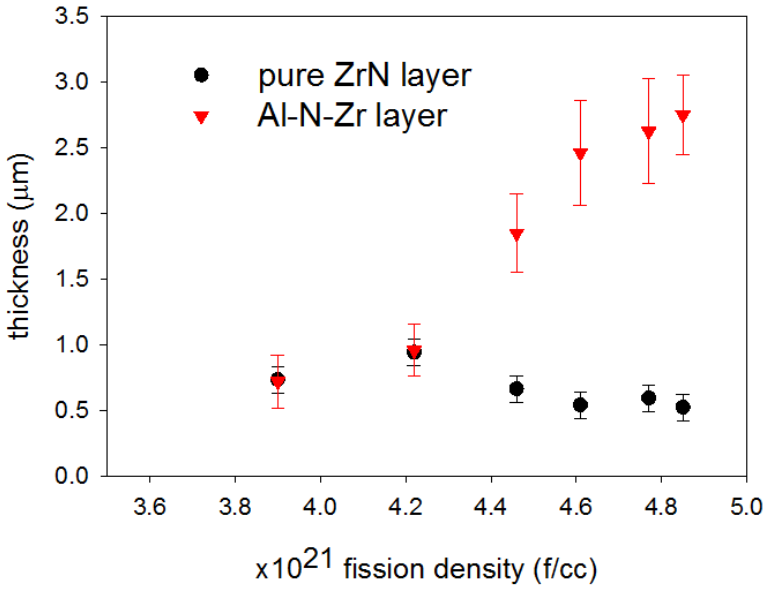

Fig. 6 Measured Al-Zr-N layer and ZrN layer thicknesses in plate U7MD 1231 (ZrN).

There are two possible ways for Al to diffuse into U-Mo. One is through the ZrN layer and the other through damaged areas in the coating. The irradiation results in Fig. 6 show that it takes a

considerable time or dose for fission-induced mixing of Al and ZrN to render the Al-Zr-N layer transparent for Al, so that Al can get access to U-Mo. If the IL formation is caused by the Al through the coating, it is contradicted by the conclusion made above on the start of the IL formation. For this reason and the fact that the appearance of the ILs is irregular, it is reasonable to infer that the Al diffusion path is through damaged area in the coating instead of through the ZrN coating.

4. IL volume fraction growth mechanism in coated particles

The IL formation is a result of the reorganization of constituent target atoms when irradiated with energetic particles generated in fission. The IL formation and growth mechanism can therefore refer to the basic work done on ion beam mixing [13,14]. When a bilayer specimen is irradiated with ions, the width of the mixed layer shows little effect of irradiation temperature or fission rate at low temperature; the temperature dependence becomes apparent at higher temperatures [13]. For example, Fig. 7 shows the temperature dependence of ion mixing in Nb-Si system. For temperatures below about 200°C the magnitude of the intermixing is observed to be temperature independent and proportional to the square root of dose, while above 200°C the reaction shows an Arrhenius increase with a small activation energy. According to the radiation enhanced diffusion (RED) theory [13], the width of the mixed layer in the Arrhenius regime depends on dose rate and temperature,

$$X \propto (\dot{\phi})^{-1/4} \exp(-\frac{H_v^m}{4kT})\phi^{1/2} \qquad (3)$$

where X is the width of the mixed layer, $\dot{\phi}$ and ϕ are the dose rate and the dose, respectively, H_v^m is the vacancy migration enthalpy, and T is the temperature.

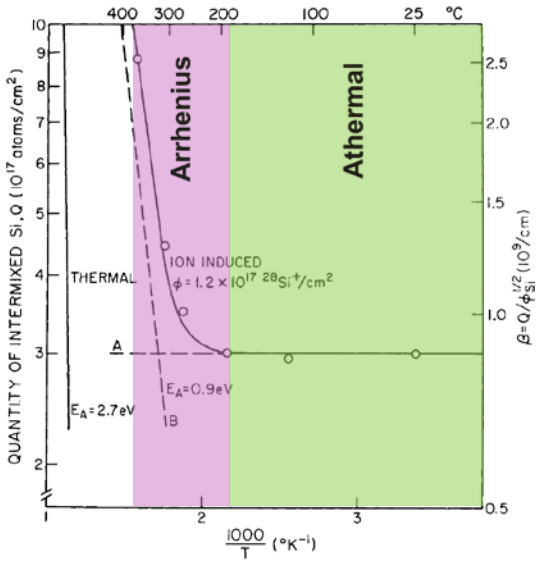

Fig. 7 Temperature dependence of ion mixing in Nb-Si system (from Ref. [14]).

Comparing to the bilayer specimens in ion beam mixing experiments, it is more reasonable to present the IL growth behavior in coated particles using measured IL volume fraction instead of thickness because of the irregular appearance of the ILs. The data in Fig. 4 was re-plotted as a function of $(\dot{f})^{0.75}$. The form of $(\dot{f})^{0.75}$ comes from Eq. (2) that shows the IL thickness is dependent on $(\dot{f})^{0.25}$. The data measured from the SELENIUM and MIR test plates is illustrated in Fig. 8 in which an almost linear correlation between the measured IL volume fraction and $(\dot{f})^{0.75}$ is evident when $\dot{f}$ > 7×10^{14} fissions/cm^3/s ($(\dot{f})^{0.75}$ > 4.3).

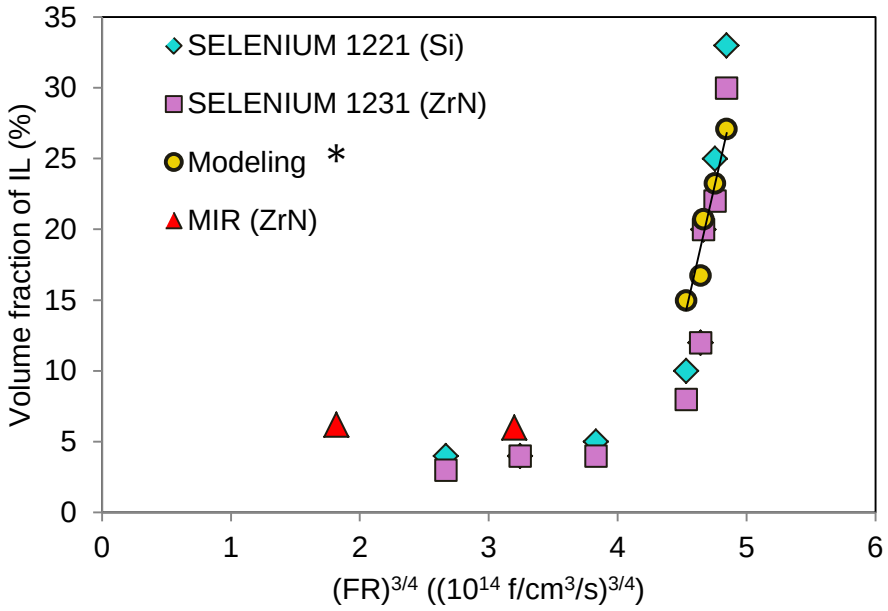

Fig. 8 Measured and calculated IL volume fraction as a function of fission rate.

Both figs. 7 and 8 show a rapid growth of reaction products within a small range of either temperature (Fig. 7) or fission rate (Fig. 8). The resemblance between Figs. 7 and 8 motivates a qualitative explanation for the abrupt increase behavior of the IL volume fraction in coated particles using the RED model. Assuming that the fuel temperature is proportional to fission rate (power production), then the IL growth profile in Fig. 8 shows that part of the fuel plate has a temperature and fission rate independent intermixing behavior changing at 7×10^{14} fissions/cm^3/s to a thermally activated behavior. According to the hypothesis, the same sudden increase in IL growth rate should also occur in uncoated particles, which is however difficult to verify with the currently available data because of the complex interrelation among FD, $\dot{f}$, and temperature in single plate tests. Therefore, a well-defined in-pile or out-of-pile irradiation experiment is needed to separate the effects of different variables and provide clear evidence.

The IL growth correlation in Eq. (2) was used to fit the IL volume fraction when $\dot{f}$ > 7×10^{14} fissions/cm^3/s. The calculation results demonstrate that the data can be fit by changing the rate coefficient in Eq. (2) from 2.6×10^{-16} to ~ 0.1×10^{-16} and assuming U-Mo and Al contact at the area

with damaged coating. This reduction of rate coefficient represents the area fraction of damaged ZrN through which Al can enter the U-Mo particle and spread through the fuel in an irregular fashion. The correspondence between the calculated results and the measured data suggests that the proposed hypothesis can qualitatively explain the IL growth behavior in coated particles.

5. Conclusion

Post-irradiation examination results have shown that Al-U-Mo interdiffusion is not prevented in either Si or ZrN coated U-Mo particles at high FD areas of the SELENIUM test plates. In the case of Si coated particles, the IL at high FD resembles that found in tests with uncoated fuel particles in appearance if not in extend. Relatively large fission gas bubbles have formed indicating a likelihood of plate pillowing at higher FD. As for ZrN coated particles, the IL occurs behind the coating layer and appears to start at damaged areas and cracks in the coating, providing a path for Al diffusion into the U-Mo.

The seemingly FD dependence of IL formation is not commensurate with the observation of IL formation in a large number of previous irradiation experiments. Fission rate ($\dot{f}$) is a more appropriate parameter - in single plate tests, *FD* and $\dot{f}$ cannot be separated as variables. In order to explain the measured rate and extend of IL formation, fuel temperature as a parameter needs to be explored in more detail. Chemical ion mixing experiment and theory can be used to qualitatively explain the observation in the SELENIUM test. This study concludes that coating damage (probably during plate fabrication) is the main cause of extensive IL formation at high $\dot{f}$. Exploring ways to reduce coating damage during fabrication may be the most efficient means of reducing IL formation if it turns out to be a limiting phenomenon to high $\dot{f}$ operation.

Acknowledgements

This work was supported by the U.S. Department of Energy, National Nuclear Security Administration (NNSA), Office of Material Management and Minimization (NA-23) Reactor Conversion Program.

This work is supported by the U.S. Department of Energy, Basic Energy Sciences, Office of Science, under contract # DE-AC02-06CH11357. The submitted manuscript has been created by UChicago Argonne, LLC, Operator of Argonne National Laboratory ("Argonne"). Argonne, a U.S. Department of Energy Office of Science laboratory, is operated under Contract No. DE-AC02-06CH11357. The U.S. Government retains for itself, and others acting on its behalf, a paid-up nonexclusive, irrevocable worldwide license in said article to reproduce, prepare derivative works, distribute copies to the public, and perform publicly and display publicly, by or on behalf of the Government.

Reference

[1] A.L. Izhutov, V.V. Alexandrov, A.E. Novoselov, V.A. Starkov, V.E. Fedoseev, V.V. Pimenov, A.V. Sheldyakov, V.Yu, Shishin, V.V. Yakovlev, I.V. Dobrikova, A.V. Vatulin, V.B. Suprun, G.V. Kulakov, *Proceedings of the 32nd International Meeting on Reduced Enrichment for Research and Test Reactors (RERTR)*, Lisbon, Portugal, October 10-14 (2010).

[2] A. Leenaers, S. Van den Berghe, C. Detavernier, "Surface engineering of low enriched uranium-molybdenum", *J. Nucl. Mater.*, 440, 220-228 (2013).

[3] S. Van den Berghe, Y. Parthoens, G. Cornelis, A. Leenaers, E. Koonen, V. Kuzminov, C. Detavernier, “Swelling of U(Mo) dispersion fuel under irradiation – Non-destructive analyses of the SELENIUM plates,” J. Nucl. Mater., 442, 60-68 (2013).
[4] A. Leenaers, “Surface-engineered low-enriched Uranium-Molybdenum fuel for research reactors,” PhD thesis 2014, University of Ghent-SCK·CEN, ISBN-9789076971223.
[5] Y.S. Kim, G.L. Hofman, “Fission product induced swelling of U-Mo alloy fuel,” *J. Nucl. Mater.*, 419, 291-301 (2011).
[6] Y.S. Kim, G.L. Hofman, J.S. Cheon, “Recrystallization and Fission-Gas-Bubble Swelling of U-Mo Fuel,” *J. Nucl. Mater.*, 436, 14 (2013).
[7] A. Leenaers, S. Van den Berghe, E. Koonen, V. Kuzminov, C. Detavernier, “Fuel swelling and interaction layer formation in the SELENIUM Si and ZrN coated U(Mo) dispersion fuel plates irradiated at high power in BR2,” *J. Nucl. Mater.*, 458, 380-393 (2015).
[8] A. Leenaers, S. Van den Berghe, D. Wachs, “Advanced PIE on the irradiated U(Mo)/ZrN coated fuel plate,” *Presentation at the 19th International Meeting on Research Reactor Fuel Management (RRFM)*, Bucharest, Romania, April 19-23 (2015).
[9] B. Ye, Y.S. Kim, G. Hofman, J.Rest, *Proceeding of the 18th International Meeting on Research Reactor Fuel Management (RRFM)*, Ljubljana, Slovnia, Mar. 30-Apr. 3 (2014).
[10] A. Leenaers, S. Van den Berghe, J. Van Eyken, E. Koonen, F. Charollais, P. Lemoine, Y. Calzavara, H. Guyon, C. Jarousse, D. Geslin, D. Wachs, D. Keiser, A. Robinson, G. Hofman, Y.S. Kim, *J. Nucl. Mater.*, 441, 439 (2013).
[11] Y.S. Kim, G.L. Hofman, H.J. Ryu, J.M. Park, A.B. Robinson, D.M. Wachs, Nucl. Eng. Technol., 45, 827 (2013).
[12] A. Leenaers, S. Van den Berghe, presented at *the 18th International Meeting on Research Reactor Fuel Management (RRFM)*, Ljubljana, Slovenia, Mar. 30-Apr. 3 (2014).
[13] R.S. Averback, Nucl. Instrum. Meth. B, 15, 675 (1986).
[14] S. Matteson, J. Rothi, M-A. Nicolet, Radiat. Eff., 42, 217 (1979).

MULTISCALE SIMULATION OF MICROSTRUCTURAL EVOLUTION IN IRRADIATED U-MO

LINYUN LIANG, ZHI-GANG MEI, BEI YE, YEON SOO KIM, GERARD HOFMAN, MIHAI ANITESCU, AND ABDELLATIF M. YACOUT
Nuclear Engineering Division, Argonne National Laboratory
9700 South Cass Avenue, Argonne, IL 60439 - USA

ABSTRACT

This paper presents a multiscale simulation of the microstructural evolution in the irradiated U-7Mo alloy fuel. Atomistic simulation methods, such as density functional theory and molecular dynamics simulations, are utilized to predict the material properties of U-7Mo alloys including the formation energies and diffusivities of defects, surface energies, and elastic constants. The obtained material properties are then incorporated into a mesoscale model to study the evolution of fission gas bubbles in the irradiated U-Mo. The predicted intragranular bubble size distribution is consistent with experimental measurement. The swelling of U-Mo due to the fission gas bubble is simulated and compared to experimental observations. Based on the dislocation density and critical recrystallization nucleation size and density predicted by the rate theory model, the fission-induced recrystallization in U-7Mo is studied using a multi-phase phase-field model. The predicted volume fraction of recrystallization agrees well with the experimental measurements. The effect of grain morphology in the initial grain structure is investigated. The grain size in the initial structure is found to have a great impact on the recrystallization kinetics. It is desirable to increase the grain size in the fuel in order to reduce the rate of recrystallization and therefore fuel swelling. We believe the current studies are useful for further improvement of the performance of U-Mo alloy fuels for future research reactors relying on low enriched uranium (LEU) fuels.

1. Introduction

Understanding the microstructural evolution in irradiated materials is of great importance for developing new nuclear fuels. Fuel performance, e.g., thermal conductivity, fission gas release, and mechanical stability, is strongly affected by the microstructural change in the materials. However, microstructure is not explicitly considered in traditional fuel performance modeling codes, instead the burnup or fission density is generally used as an index for structural damage because of the irradiation. U-Mo based fuel is the primary fuel currently being investigated as a high-density, low-enriched uranium fuel to reduce the demand of highly enriched uranium used in research reactors. The swelling of U-Mo fuel at high burnups is a major concern to its qualification for high performance research reactors. The swelling of U-Mo fuel is closely related to the irradiation-induced microstructural change, e.g., the formation of fission gas bubbles and radiation-induced recrystallization. Due to the cost and safety concern, computer simulations are playing a critical role in the fuel development.

A multi-scale simulation approach is used to study the microstructural evolution in irradiated U-Mo fuels. Density function theory based first-principles calculations are utilized to predict the material properties of U-Mo alloys, including defect formation energies, diffusivities of defects, U-Mo surface energy, and elastic constants. These obtained material properties are then incorporated into a mesoscale model to study the fission gas bubble formation and irradiation-induced recrystallization in U-Mo. By coupling the rate theory and phase-field models, we investigate the recrystallization in U-7Mo alloys due to fission. The predicted recrystallization kinetics is compared with experimental measurement. Additionally, the effect of grain morphology in the initial fuel grains on the rate of recrystallization is studied. Based on the simulation results, a scheme of optimizing the grain morphology of U-Mo fuel is proposed for the fuel fabrication community.

2. Computational methodology

2.1 First-principles calculations

To perform density functional theory (DFT) based first-principles calculations, we use the projector augmented wave method (PAW) [1] as implemented in the Vienna *ab initio* simulation package (VASP) [2, 3]. The exchange-correlation functional was described by the generalized gradient approximation (GGA) parameterized by Perdew Burke and Ernzerhof [4]. The $6s^2 6p^6 5f^2 7s^2$ and $4s^2 4p^6 4d^5 s^1$ electrons were treated as valence electrons for U and Mo, respectively. The atomic structures of U-Mo alloys were modeled by the SQS method using the Alloy Theoretic Automated Toolkit (ATAT) code [5, 6]. The standard method was used to construct the coincidence site lattice grain boundaries. The atomic structures for the STGBs were generated by GBstudio [7]. More details about the setup of DFT calculations can be found elsewhere [8]. The molecular dynamics simulations are performed by LAMMPS (Large-scale Atomic/Molecular Massively Parallel Simulator).

2.2 Phase field models

2.2.1 Grain growth

Phase field variables $\eta_i(r)$ are chosen to distinguish the different orientations of grains. The total free energy of the interested system can be represented in a Ginsburg-Landau form as [9, 10]

$$F = \int \left[f_0(\eta_1, \eta_2, \dots, \eta_q) + \frac{1}{2}\kappa \sum_i \nabla^2 \eta_i(r) \right] d^3 r, \quad (1)$$

where f_0 is the local free energy density of the system, the second term is the gradient energy term and κ is its gradient coefficient [11].

The spatial and temporal evolutions of grain parameters follow the Allen-Cahn equation [12],

$$\frac{\partial \eta_i}{\partial t} = -L \frac{\delta F}{\delta \eta_i}, \; i = 1,2,\dots,q. \quad (2)$$

where L is the kinetic coefficient of grain boundary movement.

The temperature effect can be considered in the kinetic coefficient L according to the Arrhenius formula as [13]

$$L = L_0 e^{-\frac{Q}{k_B T}}, \quad (3)$$

where L_0 is a constant, k_B the Boltzmann's constant, T temperature, and Q the activation energy of grain boundary.

In order to quantitatively simulate the U-Mo materials based on the above model, the grain boundary energy, grain boundary mobility, and activation energy have to be determined by atomic calculations or experiments. In this work, the grain boundary energy will be calculated by using DFT. Based on this value, the expansion coefficients of chemical free energy and the gradient coefficient can be determined [14]. Due to the difficulty of calculating the grain boundary mobility, it will be calibrated by the experimental measurement of grain size at different time. The activation energy of the GB diffusion measured for Mo [15], i.e., 2.73 eV, is adopted in this work. We believe this value should be close to that for U-7Mo alloy, since Mo is the element with much slower diffusivity in U-Mo alloys [16].

The phase field model was implemented in a simulation code and the semi-implicit FFTW numerical method was employed to solve the Allen-Cahn equations [17]. Periodic boundary conditions were imposed on the simulation domain. The time step for the evolution is t = 0.8, and the spacing $\Delta x = \Delta y = 1.0$ μm. A model size of 200 μm×200 μm and the U-Mo plate size of 180 μm are used in the simulations.

2.2.2 Gas bubble evolution

To consider the Xe gas bubble evolution kinetics in the U-7Mo matrix under the irradiation condition, three parameters including the compositions $c_X(r,t)$ of Xe atom, $c_V(r,t)$ of vacancy, $c_I(r,t)$ of self-interstitial atom, which represent atoms or mole fractions at position *r* and time *t*, are chosen as composition fields. The phase parameter $\eta(r,t)$ is chosen to represent the gas bubble phase with $\eta = 1$ and the matrix with $\eta = 0$. The total energy of the system can be constructed as [18-20]

$$F(c_X, c_V, c_I, \eta, \varepsilon_{ij}) = \int \left[f_{chem}(c_X, c_V, c_I, \eta, T) + \frac{\kappa_X}{2}|\nabla c_X|^2 + \frac{\kappa_V}{2}|\nabla c_V|^2 + \frac{\kappa_I}{2}|\nabla c_I|^2 + \frac{\kappa_\eta}{2}|\nabla \eta|^2 + f_{elas}(c_X, \eta, \varepsilon_{ij}) \right] dV, \quad (4)$$

where f_{chem} is the chemical free energy density describing the composition and volume fraction of the equilibrium phases, κ_X, κ_V, κ_I and κ_η are the gradient energy coefficients for Xe, vacancy, and self-interstitial atom (SIA) concentrations as well as the phase parameter, respectively, $f_{elas}(c_X, c_V, c_I, \varepsilon_{ij})$ is the elastic energy density. Detail expressions of the chemical free energy and elastic energy can be found in somewhere else [21].

The spatial and temporal evolutions of phase parameter and the Xe, vacancy and SIA compositions are controlled by the following equations as [18]

$$\frac{\partial \eta}{\partial t} = -L\frac{\delta F}{\delta \eta} + \dot{\xi}_\eta \quad (5a)$$

$$\frac{\partial c_X}{\partial t} = \nabla\left(M_X \nabla \frac{\delta F}{\delta c_X}\right) + \dot{\xi}_X + \dot{P}_X \quad (5b)$$

$$\frac{\partial c_V}{\partial t} = \nabla\left(M_V \nabla \frac{\delta F}{\delta c_V}\right) + \dot{\xi}_V + \dot{P}_V - \dot{R}_{VI} - \dot{S}_V \quad (5c)$$

$$\frac{\partial c_I}{\partial t} = \nabla\left(M_I \nabla \frac{\delta F}{\delta c_I}\right) + \dot{\xi}_I + \dot{P}_I - \dot{R}_{VI} - \dot{S}_I \quad (5d)$$

where $\dot{\xi}_i$ (*i* = η, *X*, *V*, *I*) is the thermal induced fluctuation, $\dot{P}_i$ (*i* = *X*, *V*, *I*) is the species production rate, $\dot{R}_{VI}$ is the recombination rate, $\dot{S}_i$ (*i* = *V*, *I*) is the source/sink term. The production rate of species $\dot{P}_i = \gamma_i Ran$, where γ_i is related to the *dpa* rate, and *Ran* is the random number uniformly between 0 and 1. $\dot{R}_{VI} = \nu_r c_V c_I$, where ν_r the recombination rate of vacancy and SIA. To account the faster recombination rate at the void surface, we define it as $\nu_r = \nu_b + \eta^2 \nu_s$. The nucleation/annihilation of vacancy and SIA at the dislocations or grain boundaries are neglected in this paper for simplicity, thus $\dot{S}_V$ and $\dot{S}_I$ are set as zero.

In the simulations, a model size of 89.6 nm × 89.6 nm was used. The time step used for the numerical integration is $t = 0.05$, and the grid spacing is $\Delta l = 0.35$ nm. The model was implemented in a 2D simulation code. Periodic boundary conditions were imposed on the simulation domain. Simi-implicit FFTW method were employed to solve the coupled equations (5a-d) [17].

3. Results and discussion

3.1 Material properties by atomistic simulations

In order to study the bubble evolution in U-Mo alloys, material properties—including bubble surface energy, defects formation energies, elastic constants, and defect diffusivities—are needed in the simulations. Because of the scarcity of information in the literature about these properties for U-Mo alloys, atomistic methods, such as density functional theory (DFT) and molecular dynamic (MD), were utilized to predict the parameters. Table 1 presents the values of these parameters.

Table 1. Materials properties of U-7Mo alloy used in the simulations.

Physical parameter	Symbol	Value
Surface energy	σ	1.64 J/m^2
Gradient coefficients	$\kappa_{X,V,I,\eta}$	$6.26 \times 10^{-9} J/m$

Potential height	w	$7.73 \times 10^9\ J/m^3$
Vacancy formation energy	E_V^f	1.12 eV
Interstitial formation energy	E_I^f	1.48 eV
Xe formation energy	E_X^f	6.95 eV
Xe diffusivity	D_X	4.10×10^{-13} cm^{2}s^{-1}
Interstitial diffusivity	D_I	2.05×10^{-10} cm^{2}s^{-1}
Vacancy diffusivity	D_V	3.84×10^{-13} cm^{2}s^{-1}
Elastic constant	C_{11}	173 Gpa
Elastic constant	C_{12}	138 Gpa
Elastic constant	C_{44}	50 Gpa

3.2 Evolution of intragranular fission gas bubble

At constant temperature, the formation of gas bubble is driven by the supersaturation of point defects under irradiation. The production and annihilation of defects, especially vacancies, can promote the nucleation and growth of gas bubbles. Small high-pressurized bubbles are able to grow in size by absorbing both thermal and radiation-induced vacancies. To simulate the gas bubble nucleation and growth in U-Mo, the following parameters are used: production rate of Xe is $\gamma_X = 2.0 \times 10^{-6}$ dpa/s, and SIA is $\gamma_I = 5.0 \times 10^{-6}$ dpa/s, and vacancy is $\gamma_V = 15.0 \times 10^{-6}$ dpa/s. These defect production rates were kept as constants unless the new values are mentioned. Although SIA and vacancy are equally generated during irradiation as Frenkel pairs, SIA often have higher sink rate than vacancy in metals.[22] Therefore biased generation rate for SIA and vacancy are used in the simulations.

The calculated phase parameter, gas atom, vacancy, and SIA concentrations are plotted as a function of evolution time in Fig. 1, which clearly shows the nucleation and growth processes of gas bubbles under radiation. The Xe bubbles continuously grow under the irradiation. The size of Xe gas bubbles is around 1-3 nm and with the space between them around 10 nm. The gas bubbles appear to be randomly distributed in irradiated U-7Mo. The bubble migration is not considered in this work due to the low mobility of Xe gas bubbles. Therefore, the coalescence only happens when adjacent bubbles grow to contact with each other. Bubble growth is driven by the absorption of vacancies to a void, which must be more probable than the absorption of interstitials to the void. Thus, if a void grows by the absorption of vacancies, more free volume is available for fission gas accumulation inside the void. SIA has lower concentration inside the gas bubble compared with the one in the matrix. The gas bubble pressure largely depends on the ratio of Xe atoms and vacancies inside the bubble.

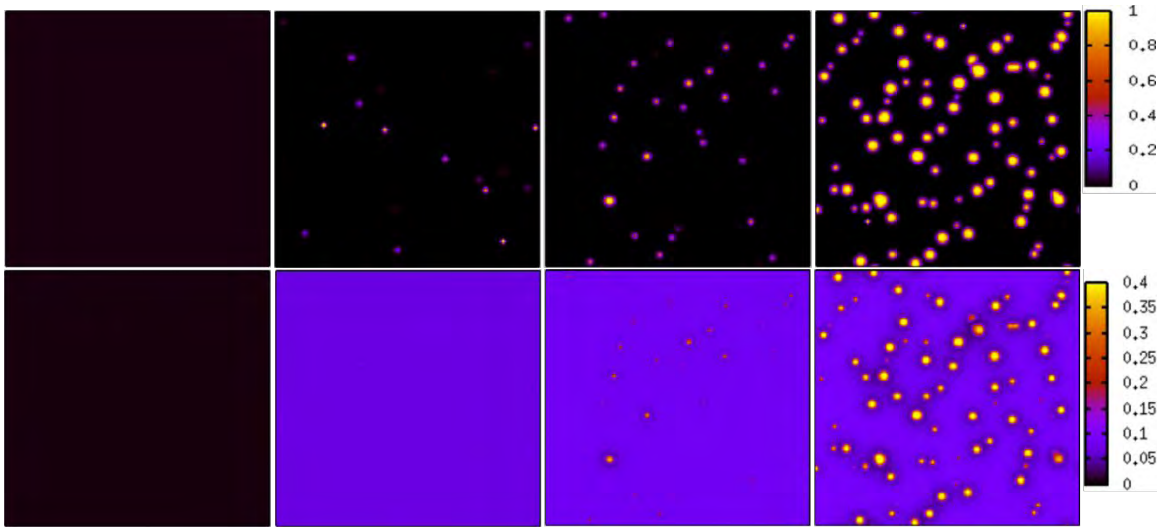

t = 0 min t = 3.36 min t = 3.78 min t = 4.08 min

Fig. 1 Temporal evolutions of (a) phase parameter and (b) Xe of concentrations in irradiated U-7Mo.

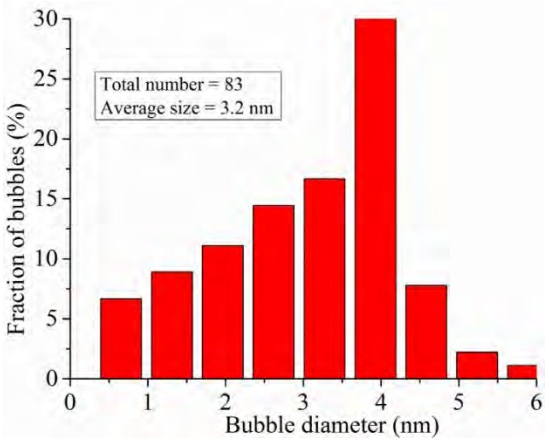

Fig. 2 Simulated size distribution of intragranular gas bubbles in U-7Mo.

The effects of vacancy production rates on the fuel swelling and the gas bubble size distribution are computed and shown in Fig. 2 at 4.08 minutes. The SIA and Xe production rates are fixed. With the higher vacancy production rate, the incubation period of swelling is shortened and the total swelling of the fuel increases. The results are consistent with the experimental observations. The measured bubble size distribution shows that the higher the irradiation rate, the larger the average bubble size. Moreover, the distribution of bubble size is broader for the higher irradiation rate. This might be explained by the fact that bubbles can grow faster by absorbing vacancies with the higher vacancy supersaturation or by bubble coalescence with a larger number of bubbles due to the higher vacancy production rate. These results are consistent with the recent experimental results performed in pure Mo [23]. The average bubble size increases from 3.2 nm to 4.0 nm when the vacancy production rate increases from 3.0×10^{-4} dpa/s to 3.4×10^{-4} dpa/s. These results show that the swelling of fuel is very sensitive to the vacancy production rate.

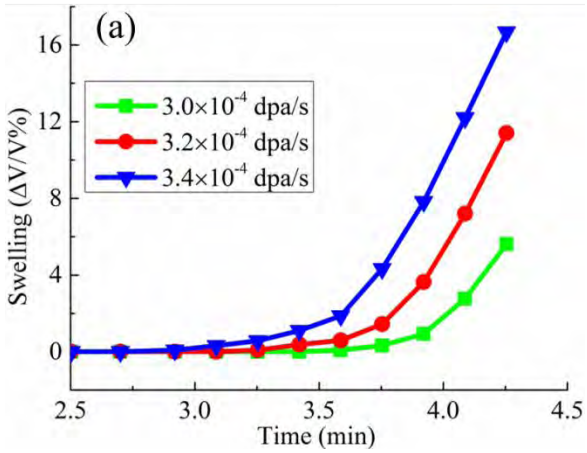

Fig. 3 Effect of fission rate on the fuel swelling of U-7Mo.

3.3 Dislocation density by rate theory model

By adopting the rate theory model, the initial dislocation densities for the onset of recrystallization can be estimated. The recrystallization starts when the fission density is above 2.40×10^{21} cm^{-3} as indicated from experiments [24]. Figure 4 shows the calculated dislocation density in irradiated U-7Mo alloys as a function of fission rate. The predicted dislocation density is in the order of 10^{15} m^{-2}, which is consistent with the dislocation density in in-pie-irradiated U-7Mo fuels measured by Miao et al. [25]. It should be pointed out that the experimental data were measured at slightly different temperatures and fission rates. Overall, the dislocation density in the U-7Mo alloy increases with the increasing fission rate and temperature. Thus, high fission rate and high temperature may expedite the recrystallization process.

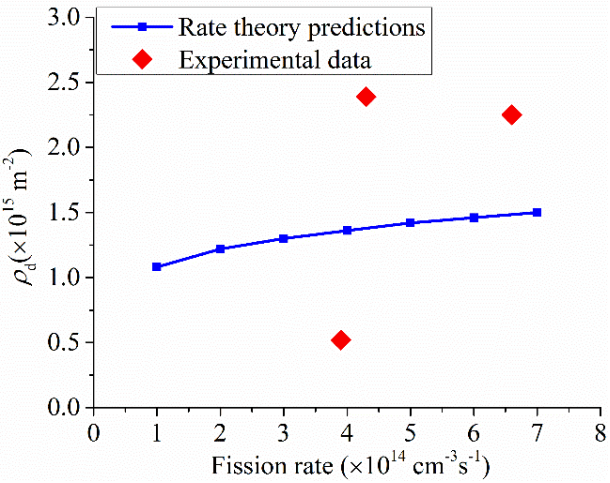

Fig. 4 Dependence of dislocation density on fission rate at 373K predicted by the rate theory models together with experimental data [26].

3.4 Fission-induced recrystallization

With the predicted dislocation density, critical nucleation size and density of recrystallized nuclei, the recrystallization kinetics of U-7Mo alloys are simulated using the multi-phase phase-field model. The simulated microstructure evolution in U-7Mo with respect to fission density is shown in Fig. 5. The total number of initial grains in the simulation is 89, and the average grain size in the initial microstructure is about 3.0 μm.

The recrystallization starts from the pre-existing grain boundaries, and then these recrystallized grains grow towards the center of the original grains due to fission. The number and size of the initial grains decrease with increased fission density. The newly formed grain boundaries become new nucleation sites for recrystallization. With increased area of grain boundaries, the number of recrystallized grains significantly increases at high fission density. The early formed recrystallized grains are larger than the latter nucleated grains simply due to the evolution. The full recrystallization of U-7Mo alloys at a fission rate of 3.0×10^{14} $cm^{-3}s^{-1}$ can be achieved at a high fission density around 5.5×10^{21} cm^{-3}. The grain size of fully recrystallized U-7Mo alloys ranges from 0.2 μm to 0.5 μm [27]. During the recrystallization process, the grain boundary energy and stored energy are the main driving forces for grain growth. The grain boundary energy drives the large grain to grow at the expense of small grains with the reduction of grain boundary energy. The stored energy in the deformed grains induces the growth of the recrystallized grains. Within the recrystallized area or after the fully recrystallization, the grain growth is only driven by the grain boundary energy.

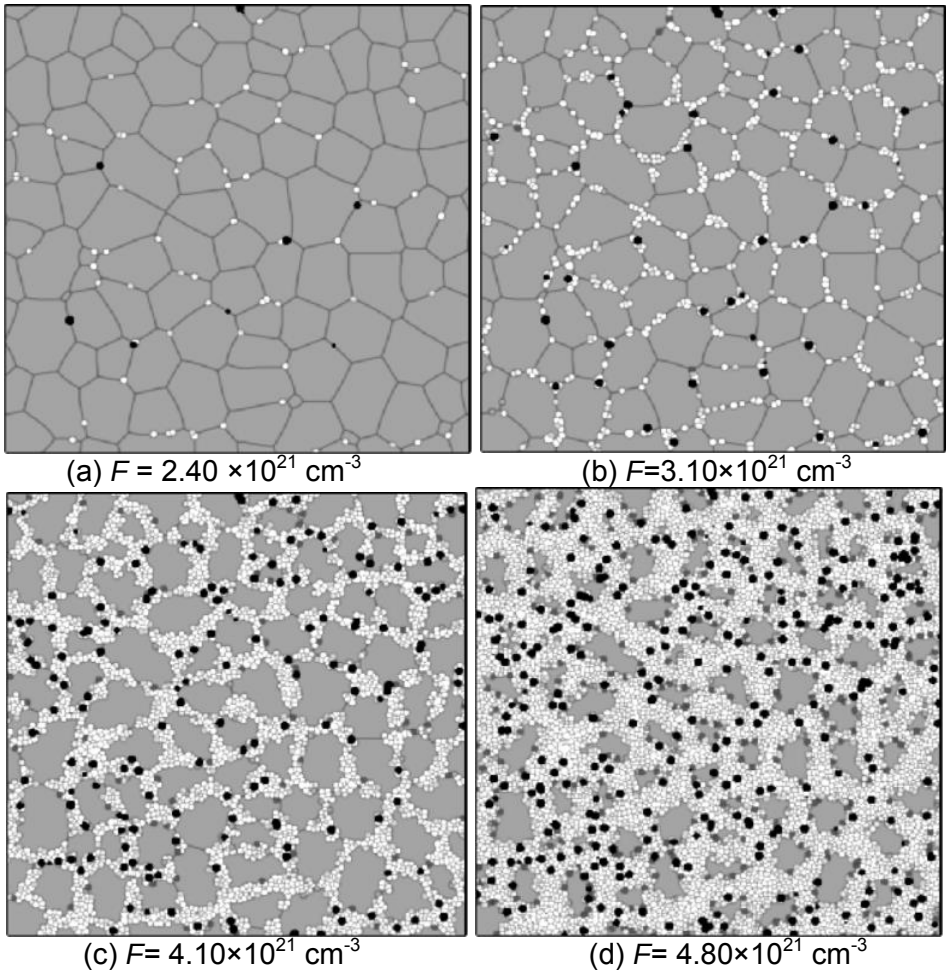

(a) $F = 2.40\times10^{21}$ cm^{-3} (b) $F=3.10\times10^{21}$ cm^{-3}

(c) $F= 4.10\times10^{21}$ cm^{-3} (d) $F= 4.80\times10^{21}$ cm^{-3}

Fig. 5 Simulated grain structures in U-7Mo at different fission densities with the fission rate of 3.0×10^{14} $cm^{-3}s^{-1}$. Grey: Original grains; White: Sub-gains; Black: Gas bubbles.

To study the recrystallization kinetics, the recrystallized volume fraction as a function of fission density is calculated with the fission rate $\dot{f}$ = 3.0×10^{14} $cm^{-3}s^{-1}$. The recrystallization volume fraction is obtained by dividing the total volume of the recrystallized grains and newly formed gas bubbles by the initial sample volume, an approach similar to the one used by Kim et al. [24]. The predicted volume fraction of recrystallized grains is shown in Fig. 6 together with experimental data compiled by Kim et al. [24]. A good agreement with experimental results is obtained in the whole range of fission density.

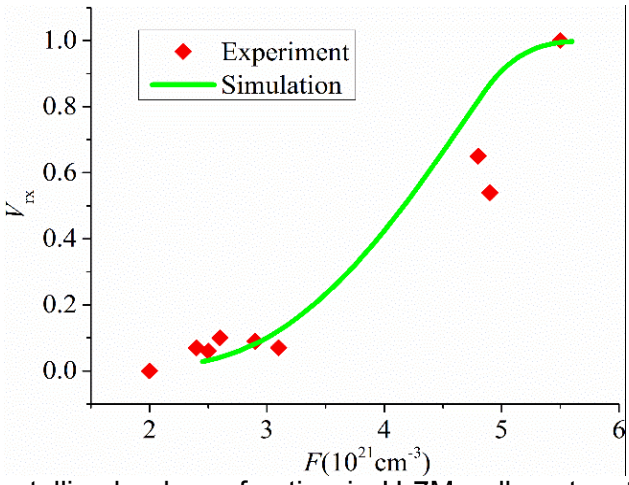

Fig. 6 Calculated recrystallized volume fraction in U-7Mo alloys together with experimental data compiled by Kim et al. [24]. The filled diamonds represent the experimental data and the line denotes the simulation results.

We also studied the effect of initial grain size on the recrystallization kinetics in U-7Mo. Figure 7 shows the simulated microstructures of three different initial grain size, i.e., 3.0 μm, 5.0 μm and 9.6 μm, at fission density of 4.1×10^{21} cm^{-3}. It can be seen that more recrystallized grains form in the case with smaller initial grain size due to its larger grain boundary length. To study the effect of the initial grain size on the rate of recrystallization, we compare the volume fraction of the recrystallized grains as a function of fission density. The case with the smallest initial grain has the largest volume fraction of recrystallized grains, and this effect becomes more prominent at high fission density. Accordingly, the full recrystallization in the microstructure with the largest grain size is achieved at the highest fission density of 6.4×10^{21} cm^{-3}, compared to the fission density of 5.5×10^{21} cm^{-3} and 5.9×10^{21} cm^{-3} needed for the other two cases with smaller initial grain size.

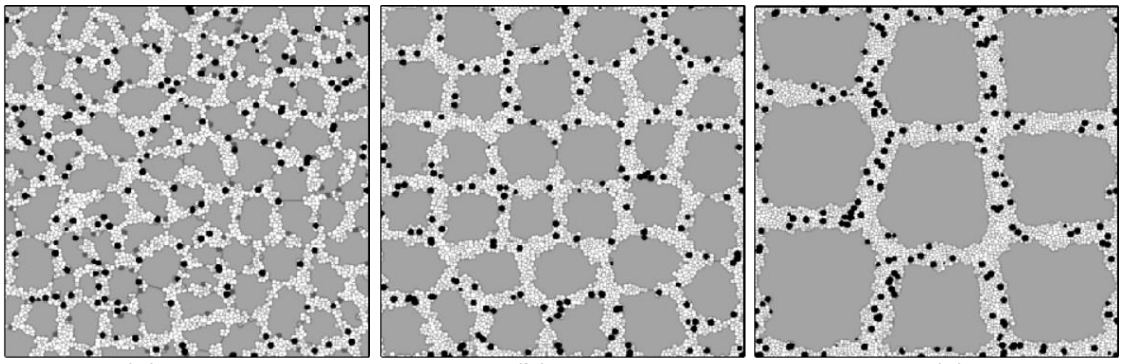

(a) (b) (c)

Fig. 7 Simulated grain microstructures of U-7Mo with different initial grain sizes (a) 3.0 μm; (b) 5.0 μm; (c) 9.6 μm at a fission density of 4.1×10^{21} cm^{-3}.

4. Summary

To summarize, we studied the microstructural evolution in irradiated U-7Mo alloy fuels using a multiscale simulation approach, including density functional theory, molecular dynamics, rate theory, and phase-field model. The material properties predicted by atomistic methods are used as parameters for phase-field models to study the formation and growth of intragranular gas bubbles in U-7Mo. The predicted bubble size distribution and bubble-induced swelling are in agreement with experimental results. Using the dislocation density and critical nucleation density and size predicted by the rate theory model, we investigated the fission-induced recrystallization in U-7Mo by the multi-phase phase-field model. The recrystallization kinetic in U-7Mo can be well captured by the current model. The volume

fraction of recrystallized grains in the irradiated U-Mo agrees will with experimental data. We also studied the effect of grain morphology in the initial grain structure on the recrystallization kinetics. It is found that the initial grain size has a profound effect on the rate of recrystallization. Therefore, it is desirable to increase the grain size in order to supress the rate of recrystallization in U-Mo fuels. More experiments on the effect of grain size on recrystallization and swelling in U-Mo fuels are required in order to verify our simulation.

Acknowledgements

This work is sponsored by the U.S. Department of Energy, National Nuclear Security Administration (NNSA), Office of Material Management and Minimization (NA-23) Reactor Conversion Program.

References

[1] P.E. Blöchl, Physical Review B 50 (1994) 17953.
[2] G. Kresse, J. Furthmüller, Phys. Rev. B 54 (1996) 11169.
[3] G. Kresse, D. Joubert, Phys. Rev. B 59 (1999) 1758.
[4] J.P. Perdew, K. Burke, M. Ernzerhof, Phys. Rev. Lett. 77 (1996) 3865.
[5] A. van de Walle, G. Ceder, Journal of Phase Equilibria 23 (2002) 348.
[6] A. van de Walle, P. Tiwary, M. de Jong, D.L. Olmsted, M. Asta, A. Dick, D. Shin, Y. Wang, L.Q. Chen, Z.K. Liu, Calphad 42 (2013) 13.
[7] H. Ogawa, MATERIALS TRANSACTIONS 47 (2006) 2706.
[8] Z.-G. Mei. 2015.
[9] D. Fan, L.Q. Chen, Acta Materialia 45 (1997) 611.
[10] D.N. Fan, C.W. Geng, L.Q. Chen, Acta Materialia 45 (1997) 1115.
[11] Z.-G. Mei, L. Liang, Y.S. Kim, W. Tom, E.O. Hare, A.M. Yacout, G. Hofman, M. Anitescu, Journal of Nuclear Materials (2015).
[12] I. Steinbach, Annual Review of Materials Research, Vol 43 43 (2013) 89.
[13] M. Wang, B.Y. Zong, G. Wang, Computational Materials Science 45 (2009) 217.
[14] N. Moelans, B. Blanpain, P. Wollants, Physical Review B 78 (2008).
[15] D.C. Blaine, J.D. Gurosik, S.J. Park, D.F. Heaney, R.M. German, Metallurgical and Materials Transactions a-Physical Metallurgy and Materials Science 37A (2006) 715.
[16] D.E. Smirnova, A.Y. Kuksin, S.V. Starikov, Journal of Nuclear Materials 458 (2015) 304.
[17] L.Q. Chen, J. Shen, Computer Physics Communications 108 (1998) 147.
[18] L.Q. Chen, Annual Review of Materials Research 32 (2002) 113.
[19] P.C. Millett, A. El-Azab, S. Rokkam, M. Tonks, D. Wolf, Computational Materials Science 50 (2011) 949.
[20] P.C. Millett, A. El-Azab, D. Wolf, Computational Materials Science 50 (2011) 960.
[21] L. Liang, Z.-G. Mei, Y.S. Kim, T. Wiencek, G. Hofman, M. Anitescu, A.M. Yacout. Intragranular Gas bubble kinetics in an irradiated U-Mo fuel using a multistate simulation approach. 2015.
[22] L. Pagano, A.T. Motta, R.C. Birtcher, Journal of Nuclear Materials 244 (1997) 295.
[23] D. Yun, M.A. Kirk, P.M. Baldo, J. Rest, A.M. Yacout, Z.Z. Insepov, Journal of Nuclear Materials 437 (2013) 240.
[24] Y.S. Kim, G.L. Hofman, J.S. Cheon, Journal of Nuclear Materials 436 (2013) 14.
[25] Y. Miao, K. Mo, B. Ye, L. Jamison, Z.-G. Mei, J. Gan, B. Miller, J. Madden, J.-S. Park, J. Almer, S. Bhattacharya, Y.S. Kim, G.L. Hofman, A.M. Yacout, Scripta Materialia 114 (2016) 146.
[26] B.D. Miller, J. Gan, D.D. Keiser, Jr., A.B. Robinson, J.F. Jue, J.W. Madden, P.G. Medvedev, Journal of Nuclear Materials 458 (2015) 115.
[27] R. Ho Jin, K. Yeon Soo, G.L. Hofman, J. Rest, P. Jong Man, K. Chang Kyu, Materials Science Forum 558-559 (2007) 319.

PLASMA SPRAYED ZIRCONIUM DIFFUSION BARRIER DEVELOPMENT FOR MONOLITHIC U-MO METALLIC FUEL

DUSTIN R. CUMMINS, KENDALL J. HOLLIS, CHENG LIU, MANUEL L. LOVATO, DAVID E. DOMBROWSKI
Materials Science and Technology, Los Alamos National Laboratory
Los Alamos, NM 87545 U.S.A

ABSTRACT

Development activities for producing a zirconium diffusion barrier between the U-Mo fuel and the 6061 aluminum cladding for monolithic metallic research reactor fuels has been ongoing at Los Alamos National Laboratory. Parameters of plasma spraying including plasma power, gas flow rates, and substrate temperature affect the coating density and bond strength. The surface composition of the U-Mo immediately prior to coating and the interfacial layer that forms between the U-Mo and the zirconium affect coating adhesion and are controllable to some extent by the processing parameters for plasma spraying. There is a clear correlation between increased substrate temperature during spraying and improved bond strength. Microscopic analysis suggests that as deposition temperature increases, thickness of a U-Mo-Zr-O interfacial layer increases; the coating bond strength seems to correlate with interlayer thickness. The information gained during this development program is being used to optimize zirconium diffusion barrier coatings for the production of test samples for the upcoming MP-1 reactor experiment.

1. Introduction

1.1 Program Background

The United States government is committed to nuclear security and nonproliferation. To meet this important mission, the US Department of Energy and National Nuclear Security Agency (NNSA) established the Office of Material Management and Minimization (M^3) Reactor Conversion Program, with the mandate to reduce and protect vulnerable nuclear and radiological materials located in civilian sites worldwide. M^3 seeks to convert research reactors and radioisotope production facilities from the use of highly enriched uranium (HEU) to a low enriched uranium (LEU) fuel, which is not at risk of being developed into a weapon. However, currently there is no suitable LEU fuel available for high performance research reactors. The M^3 Reactor Conversion Program is committed to developing a high-density LEU fuel, as well as efficient and economical fabrication capabilities for successful implementation. Los Alamos National Laboratory (LANL) has been tasked with development of a Zirconium fuel diffusion barrier *via* plasma spraying to prevent reaction between the U-Mo fuel and the aluminum cladding.

A successful diffusion barrier requires adequate Zr thickness, uniform coverage, adequate bonding at the Zr/fuel and Zr/cladding interfaces, and maintenance of the original fuel properties (*i.e.* dimensions, crystal phase concentration, alloy composition and dispersion, neutronics, *etc.*). This work outlines Zr plasma spraying techniques [1-4], parameters affecting bond strength [5-6], and characterization of the Zr diffusion barrier [7].

2. Plasma Spray Procedures

2.1 Spraying

Depleted uranium with 10 weight percent molybdenum (DU-10Mo) ingots were cast and foils rolled from the castings at LANL. The foils were coated with Zr by vacuum plasma spraying in an Ar-He plasma. Following rolling, the uranium foil has a black oxide scale, shown in Figure 1A. This oxide layer, as well as other contaminants, is removed using a sequence chemical cleaning. First, the foil is sonicated in Blue Gold ™ detergent at 60°C to remove surface organics, then soaked in a caustic 10% NaOH solution, and then finally transferred to 50% HNO_3 etchant to expose bare uranium foil (Figure 1B). The cleaned foil is rinsed with DI water and dried in a nitrogen atmosphere. For plasma spraying, the foil is mounted onto a stainless steel support, with screws to secure the edges of the foil, as shown in Figure 1C.

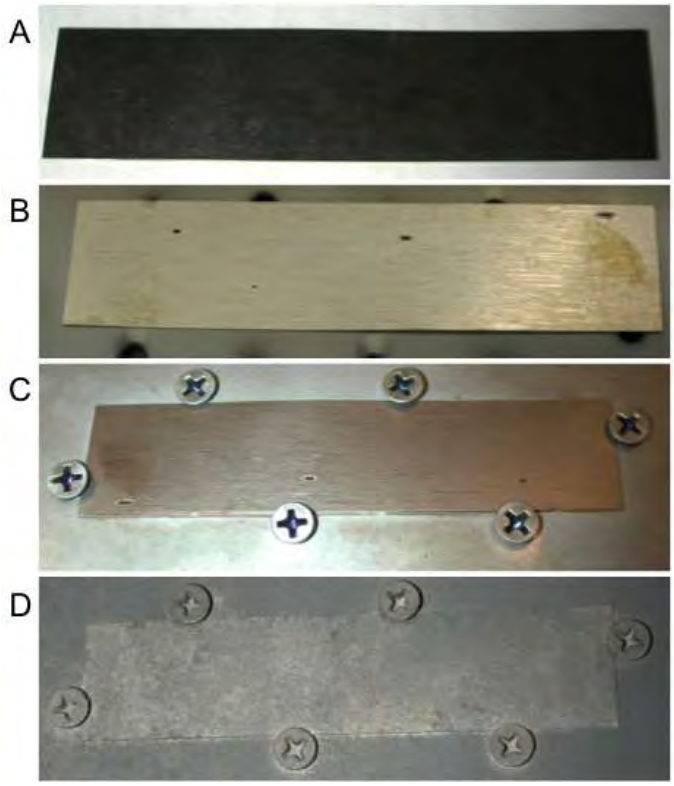

Fig. 1. A) Photograph of rolled DU-10Mo with black oxide surface. B) Bare DU-10Mo foil after chemical cleaning. C) Bare DU-10Mo foil mounted in plasma spray chamber holder. D) DU-10Mo foil following Zr plasma spray coating.

The foils were mounted onto a square tube, allowing four foils to be sprayed at one time. This holder rotates while the plasma gun (SG-100, Praxair/TAFA, Concord, NH, USA) rasters in the over the rotating tube. The vacuum chamber was evacuated, then backfilled with argon to 70 Torr, with an oxygen content of less than 100 ppm prior to spraying. 99.2% purity Zr powder (ATI Wah Chang, Albany, OR, USA) with particle size ranging from 5 – 50 microns is used to deposit a ~30 micron Zr coating. A photograph of a sprayed foil in the mount is shown in Figure 1D. To test the effects of spraying conditions on bond strength, deposition conditions were varied; these parameters are outlined in Table 1. Following the plasma spraying of one side of the foil, the foils are turned over, mounted again in a similar way, then sprayed on the second side. The maximum foil temperature (T_{MAX}) during plasma spraying was determined using an infrared camera. The bond temperature for each sample is the lower of the temperatures reached on the two sides during the two spray runs.

Sample ID	Plasma Current (Amps)	Plasma Gas (SLM)		Bond Temp (°C)
		Argon	Helium	
151007	6,574	30	25	602
151008	6,823	30	25	655
151013	9,095	30	25	726
151014	10,684	25	30	843
151015	9,738	25	30	776

Table 1. Summary of Zr Layer Plasma Spray Conditions

3. Fuel and Cladding Characterization

3.1 Bond Strength

Development of the viable low enrichment fuel requires a thin Zr layer with strong adhesion between the Zr and nuclear fuel, as well as strong adhesion between the Zr and eventual Al cladding layer. To quantitatively test the adhesion strength of the plasma sprayed Zr coating to the U-10Mo foil, room temperature, quasi-static tensile strength testing was performed. Aluminum mounts were fabricated and attached to each side of the Zr coated foil using commercial grade epoxy. A foil and the testing mounts are shown in Figure 2A. These mounts are then loaded into a tensile testing apparatus, which applies a uniaxial force on the foil mount. The mount fixtures are connected by ball joints to prevent twisting, shearing, etc. during the test (Figure 2B). The tension force is increased steadily until failure; this failure force divided by the area of the foil is determined to be the “strength” of the Zr-U-Mo bonding.

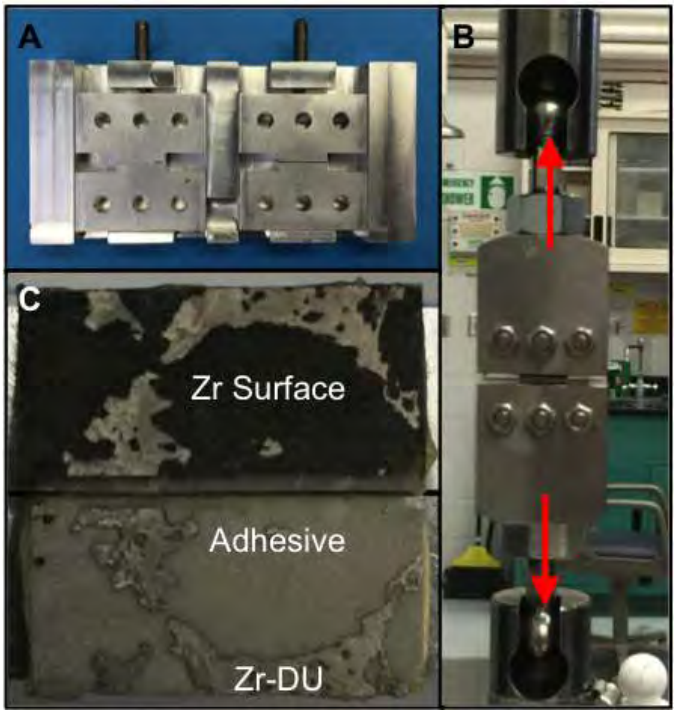

Fig. 2. A) Aluminum tensile testing mounts for determining bond strength of Zr coating on U-10Mo foils. This photo shows two testing mounts, resting side by side in a holder, to ensure proper sample orientation during epoxy curing. B) Tensile testing apparatus, with sample mount loaded and attached by ball joints. Arrows show the direction of force. C) Typical image of fractured foil surfaces, following tensile testing. In this sample, the failure can be said to have

occurred primarily in the mounting adhesive, as indicated by the overall integrity of the Zr coating on one side and adhesive on the other. In some small areas, the failure seems to have occurred in a Zr-U interface layer.

Analysis of the fractured surfaces (Figure 2C) following tensile testing helps to determine in what portion of the foil the failure occurred. The results of the tensile bond strength testing are summarized in Table 2. The weakest bond sample (ID# 151007) failed at a load of 6,574 N, which translates to a strength of 36.23 MPa. Visual inspection, together with SEM/EDS analysis, suggests that the bond failure occurred primarily in a Zr-U intermetallic layer, with significant amounts of Zr and U-10Mo remaining on both sides of the fracture surface. A representative backscattered electron SEM image of the fracture surface is shown in Figure 3A. ID# 151008 failed at a similar load as the weakest sample, with a strength of 37.60 MPa. Adjustment of plasma spray parameters lead to an increase in bond strength, with ID# 151013, 151014, and 151015 showing a tensile strengths of 50.12, 58.88, and 53.66 MPa, respectively. Visual analysis of the stronger samples suggests that the failure occurred primarily in the adhesive epoxy, with a significant amount of the Zr coating on one testing mount and adhesive on the other corresponding mount. A photograph of the two sides of the fracture surface for the strongest sample (ID# 151014) is shown in Figure 2C and a representative backscattered SEM image is shown in Figure 3B. Note that there is significantly less U-10Mo exposed in the stronger bound sample (Figure 3B) than in the weakest sample, Figure 3A. Characterization of the Zr/U10Mo interface, and how that correlates to plasma spray conditions and resulting bond strength will show which factors affect the Zr coating adhesion strength.

Sample ID	Failure Load (N)	Strength (MPa/psi)	Failure Point
151007	6,574	36.23 / 5255	Zr-U10Mo Interface
151008	6,823	37.60 / 5453	Zr-U10Mo Interface
151013	9,095	50.12 / 7269	Zr-U10Mo Interface
151014	10,684	58.88 / 8540	Adhesive
151015	9,738	53.66 / 7783	Zr-U10Mo Interface

Table 2. Summary of Bond Strength Testing

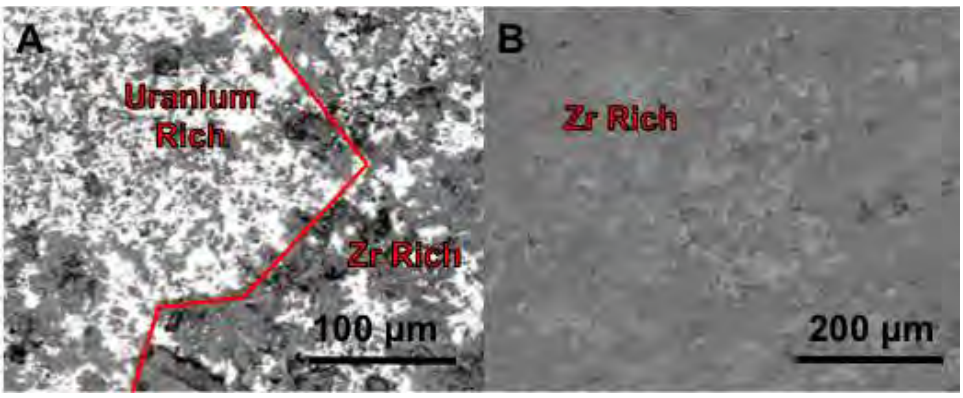

Fig. 3. A) Backscattered electron SEM image of Sample ID# 151007 fracture surface following tensile strength testing (weakest bond). B) Backscattered SEM image of Sample ID# 151014 fracture surface following tensile strength testing (strongest bond). Notice the much higher

concentration of uranium in A) fracture surface, indicative that the fracture occurred at the Zr-U10Mo interface, as compared with the more uniform Zr coating in B) where the fracture occurred in the testing epoxy.

3.2 Zr-U Interfacial Layer Characterization

To characterize the Zr coating and interfacial phenomenon, the coated DU-10Mo foil was cross-sectioned, mounted in epoxy, and polished using standard metallographic techniques. Before imaging with SEM, the mount was sputtered with a thin layer of carbon to improve conductivity.

The Zr coated DU-10Mo foil with the strongest bond strength (ID# 151014) was SEM imaged using a backscattered electron detector. Backscattered electrons result from elastic scattering of the incident beam with the sample; higher Z (atomic number) elements are more likely to produce elastic collisions and appear "brighter" in a backscattered electron image, allowing for composition analysis of a sample, compared to the topographic information provided by conventional, secondary electron SEM. Backscattered imaging of the coated foil can be seen in Figure 4, along with selected area elemental analysis (using standard-less energy dispersive spectroscopy or EDS) of the Zr coating, DU-10Mo foil, and interfacial layer. The high carbon content in the elemental analysis, and to some extent the oxygen content, result from a combination of the polymer epoxy mount and carbon surface sputtering and should be regarded as background.

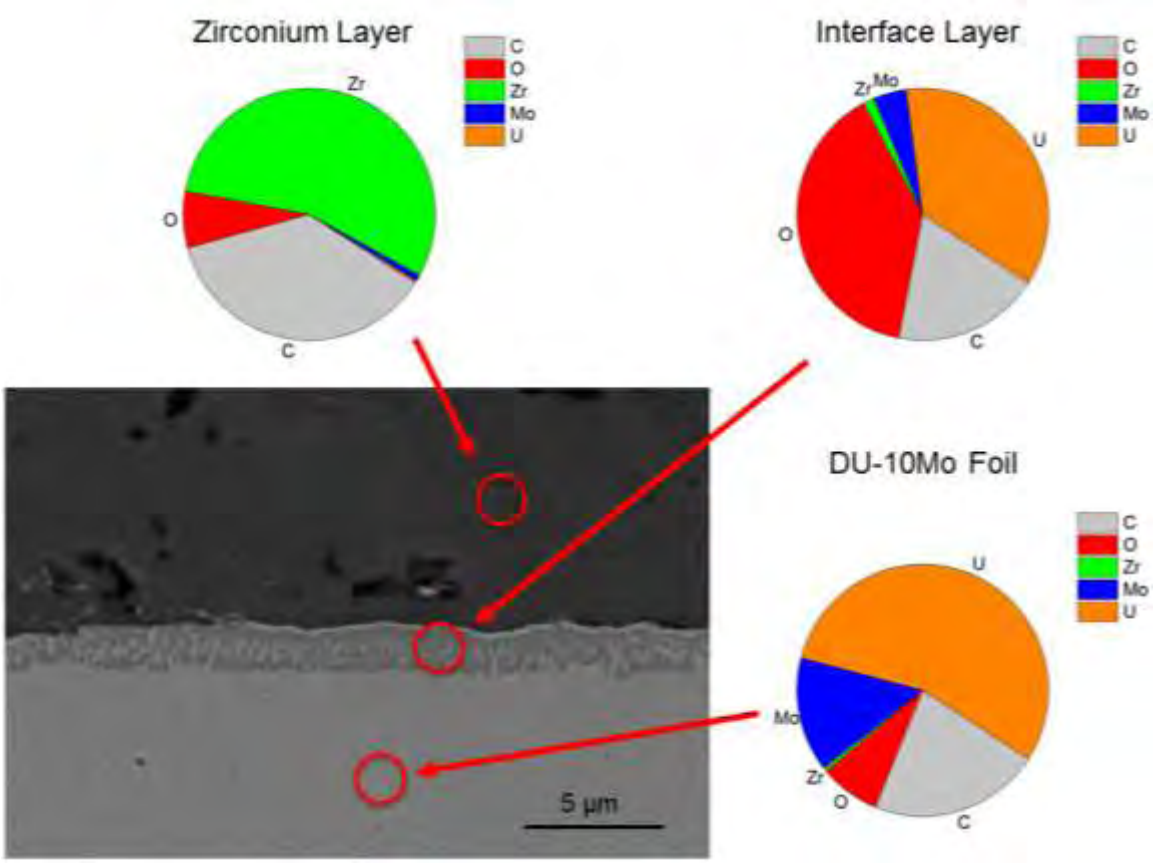

Fig 4. Backscattered SEM imaging of Zr plasma spray coated DU-10Mo foil cross section (ID# 151014), highlighting the Zr-U interface. Pie charts show result of EDS elemental analysis (at%) of the Zr coating, Zr-U interfacial layer, and bulk U foil, respectively. The high carbon content in the elemental analysis, and to some extent the oxygen content, result from a

combination of the polymer epoxy mount and carbon surface sputtering and should be regarded, for the most part, as background.

EDS Element	Zr Barrier	DU-10Mo	Interface
C K	36.52%	21.99%	0.19%
O K	7.29%	7.75%	39.15%
Zr L	55.06%	0.50%	1.44%
Mo L	0.81%	14.76%	4.21%
U M	0.32%	55.00%	36.31%

Table 3. EDS Elemental Analysis (atomic %) of Zr coated DU10Mo ID#151014

Backscattered electron imaging of the interfacial layer seems to show an interdiffusion Zr-U layer of ~ 1 micron thickness. This interfacial layer is relatively uniform across the entire length of the coated foil. Table 3 quantifies the selected area elemental analysis. As expected, the Zr coating is almost pure Zr metal, with minimal oxidation; likewise, the bulk DU-10Mo foil is predominantly U and Mo. However, spot analysis of the interfacial layer shows a strong oxidation signal, almost equimolar with uranium. There is also a trace amount of Zr, which indicates diffusion of Zr, but not as significant as qualitative analysis of the backscattered image would suggest. Further, more sensitive characterization is necessary to determine if this interfacial is an existing uranium oxide prior to spraying, or an U-Mo-Zr-O interfacial layer formed during deposition.

Comparison of the approximate interfacial layer thickness, together with plasma spray processing temperatures with the bond strength is shown in Table 4. The effect of interfacial layer thickness and plasma spray temperature on the Zr-DU10Mo bond strength is graphically compared (Figure 5). Clearly, there is a correlation between increased bonding temperature during the plasma spray process and the resulting bond strength, with the highest strength bond (ID# 151014) having the highest processing temperatures. Also, the approximate thickness of the interfacial layer increases with processing temperature, and seems to correlates with bond strength. More in depth and sophisticated characterization of the composition of this interfacial layer and its effects on bond strength must be performed. Also, post processing heat treatments of the Zr coated foils, in order to artificially increase of diffusion of the Zr-DU10Mo system and the thickness of the interfacial layer, will give a much clearer idea of the impact of processing conditions on the resulting bond strength.

Sample ID	Bond Strength (MPa)	Bond Temp (°C)	Interface Layer Thickness (μm)
151007	36.23	602	0.263
151008	37.60	655	0.648
151013	50.12	726	0.868
151014	58.88	843	1.185
151015	53.66	776	0.83

Table 4. Effects of Processing Temperature and Interface on Bond Strength

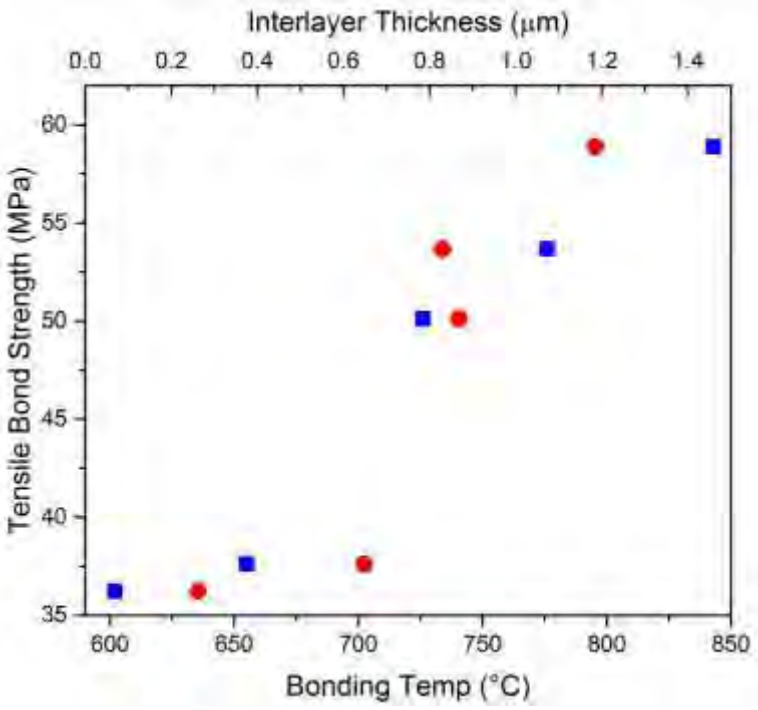

Figure 5. Effect of bonding temperature (blue square – bottom axis) and interfacial layer thickness (red circle – top axis) on the Zr-U10Mo bond strength.

4. Conclusions

In this work, the effects of substrate temperature, and corresponding interfacial layer thickness, on bond strength of plasma sprayed Zr diffusion barrier coatings on DU-10Mo are investigated. The integrity of the Zr-U bond is quantitatively measured by room temperature quasi-static tensile strength testing. There is a clear correlation between improved bond strength and higher substrate temperature during plasma spraying. There also appears to be a correlation between improved bond strength and thickness of the interfacial layer between the Zr coating and the DU-10Mo surface. Microscopic elemental analysis shows this ~1 μm interfacial layer is composed of U, Mo, Zr, and O. Further characterization will help elucidate the composition of this interface and what role it may play in coating bond strength.

5. Acknowledgments

The authors gratefully acknowledge Joel Montalvo and Pallas Papin for the metallographic preparation. The authors would like to acknowledge the financial support of the U.S. Department of Energy (DOE) National Nuclear Security Administration (NNSA) Office of Materials Management and Minimization (M3) Reactor Conversion Program. Los Alamos National Laboratory, an affirmative action equal opportunity employer, is operated by Los Alamos National Security, LLC, for the NNSA of the U.S. DOE under contract DE-AC52-06NA25396.

6. References

[1] K. J. Hollis, “Diffusion Barrier Coatings for Uranium Fuel used in Nuclear Reactors”, Advanced Materials & Processes, Vol. 168, No. 11 (2010), 57-59.

[2] K. J. Hollis, “Plasma Spraying of Diffusion Barrier Coatings for LEU Monolithic Fuel”, Proc. RERTR 2012 – 34th International Meeting on Reduced Enrichment for Research and Test Reactors, Warsaw, Poland, October, 2012.

[3] K.J. Hollis, R. Leckie, and D.E. Dombrowski, “Plasma Sprayed Zirconium for US HPRR LEU Conversion Fuel Diffusion Barrier, Proc. RERTR 2012 – 35th International Meeting on Reduced Enrichment for Research and Test Reactors, Vienna, Austria, October, 2014.

[4] K.J. Hollis, D.R. Cummins, and D.E. Dombrowski, “Optimization of Zirconium Plasma Spraying for MP-1 Fabrication”, Proc. RERTR 2015 – 36th International Meeting on Reduced Enrichment for Research and Test Reactors, Seoul, South Korea, 2015.

[5] K. Hollis, C. Liu, R. Leckie, M. Lovato, “Bulge Testing and Interface Fracture Characterization of Plasma Sprayed and HIP Bonded Zr Coatings on U-Mo”, Journal of Thermal Spray Technology, Vol. 24 Issue 1 (2015), pp. 271-279.

[6] Hollis, K., N. Mara, R. Field, T. Wynn, J. Crapps, P. Dickerson: Characterization of Plasma Sprayed Zirconium on Uranium Alloy by Microcantilever Testing. Journal of Thermal Spray Technology, 22 (March 2013), Issue 2-3, pp. 233/41.

[7] K.J. Hollis, M.E. Hawley, P.O Dickerson, “Characterization of Thermal Diffusion Related Properties in Plasma Sprayed Zirconium Coatings”, J. Therm. Spray Technol., 21(3-4), June 2012, p 409-15.

MODELING THE PORE FORMATION MECHANISM IN UMo/Al DISPERSION FUEL

YEON SOO KIM, L. JAMISON, G. HOFMAN
Nuclear Engineering Division, Argonne National Laboratory
9700 South Cass Ave, Argonne, IL 60439 – USA

G.Y. JEONG
Ulsan National Institute of Science and Technology
50 UNIST-gil, Eonyang-eup, Uljoo-gun, Ulsan 689-798 - Republic of Korea

ABSTRACT

In UMo/Al dispersion fuel meat, pores formed in the ILs or at IL-Al interfaces tend to increase in size with irradiation, potentially limiting performance of this fuel. There has been no universally accepted mechanism for the formation and growth of this type of pore. However, there is a consensus that the stress state determined by meat swelling and fission- induced creep is one of the determinants, and fission gas availability at the pore site is another. Five dispersion RERTR miniplates that have well defined irradiation conditions and PIE data were selected for examination. Meat swelling and pore volume were measured in each plate. ABAQUS finite element analysis (FEA) package was utilized to obtain the time-dependent evolution of mechanical states in the plates while matching the measured meat swelling and creep. Interpretation of these results give insights on how to model a failure function – a predictor for large pore formation – using variables such as meat swelling, interaction layer growth, stress, and creep. This model can be used for optimizing fuel design parameters to reach the desired goal: meeting high power and performance reactor demand.

1. INTRODUCTION

Several types of pores, visible through OM and SEM, have been observed in UMo/Al dispersion fuel. Small fission gas bubbles in the UMo fuel particles, larger fission gas bubbles formed on the contact surface between two UMo particles, larger fission gas bubbles at the UMo Si-added matrix interface due to U-silicide phase formation, and fission-gas-filled pores that form at the interaction layer (IL) – Al interface. Among these, the pores at the IL-Al interface pose the largest obstacle to sound fuel performance, and, hence, to the qualification of this fuel, which is discussed within this paper.

The possible causes for the formation of this pore type are: imperfect bonding or non-uniform bonding between the UMo and Al during plate fabrication, and Kirkendall void formation at the UMo-Al interface. The former is most probable in that the UMo particle surface is microscopically rough, and normally covered with a thin oxide layer. Hence, some parts of the surface are under lower pressure than the neighboring parts. IL growth is pressure-dependent, with the IL growing at a faster rate in the harder contact regions. In addition, because IL yields a net volume expansion [1], the region with a thicker IL generates a compressive stress, and the neighboring region with a thinner IL region generates a tensile stress. This stress state promotes formation of lenticular pores.

No matter the cause, the pores in their initial stage do not directly cause fuel meat swelling, which eventually leads to pillowing. In order to enhance pore growth, two prerequisites must be satisfied: One is fission gas release to the pore, and the other is a favorable stress state. The

former is inevitable. In other words, to achieve a desired burnup goal, fission gas release to the pore is more or less set. However, the latter depends on many factors.

Using ABAQUS simulation, we calculated the stress states of plates that have known in-pile test data. The pore radius is solved assuming a mechanical equilibrium between gas pressure inside the pore and surface tension plus stress as a function of burnup.

2. EXPERIMENTAL DATA

Five dispersion fuel plates irradiated in the ATR were selected for the ABAQUS simulation. Their test conditions are given in **Table 1**.

Table 1 Summary of irradiation data for five miniplates

In-pile test ID	Plate ID	U-density (gU/cm^3)	Fuel type	Matrix type	Particle size (μm)	FD at meat center (10^{21} f/cm^3)	FD 5.1 mm meat center-to-edge (10^{21} f/cm^3)
RERTR-4	V6022M	6	U-10Mo	Al	65	5.09	6.40
RERTR-5	V6019G	6	U-10Mo	Al	65	2.85	3.57
RERTR-6	R3R030	6	U-7Mo	Al-5Si	65	2.77	4.54
RERTR-7	R0R010	6	U-7Mo	Al	140	3.54	7.54
RERTR-9	R3R108	8	U-7Mo	Al-5Si	50	3.14	7.31

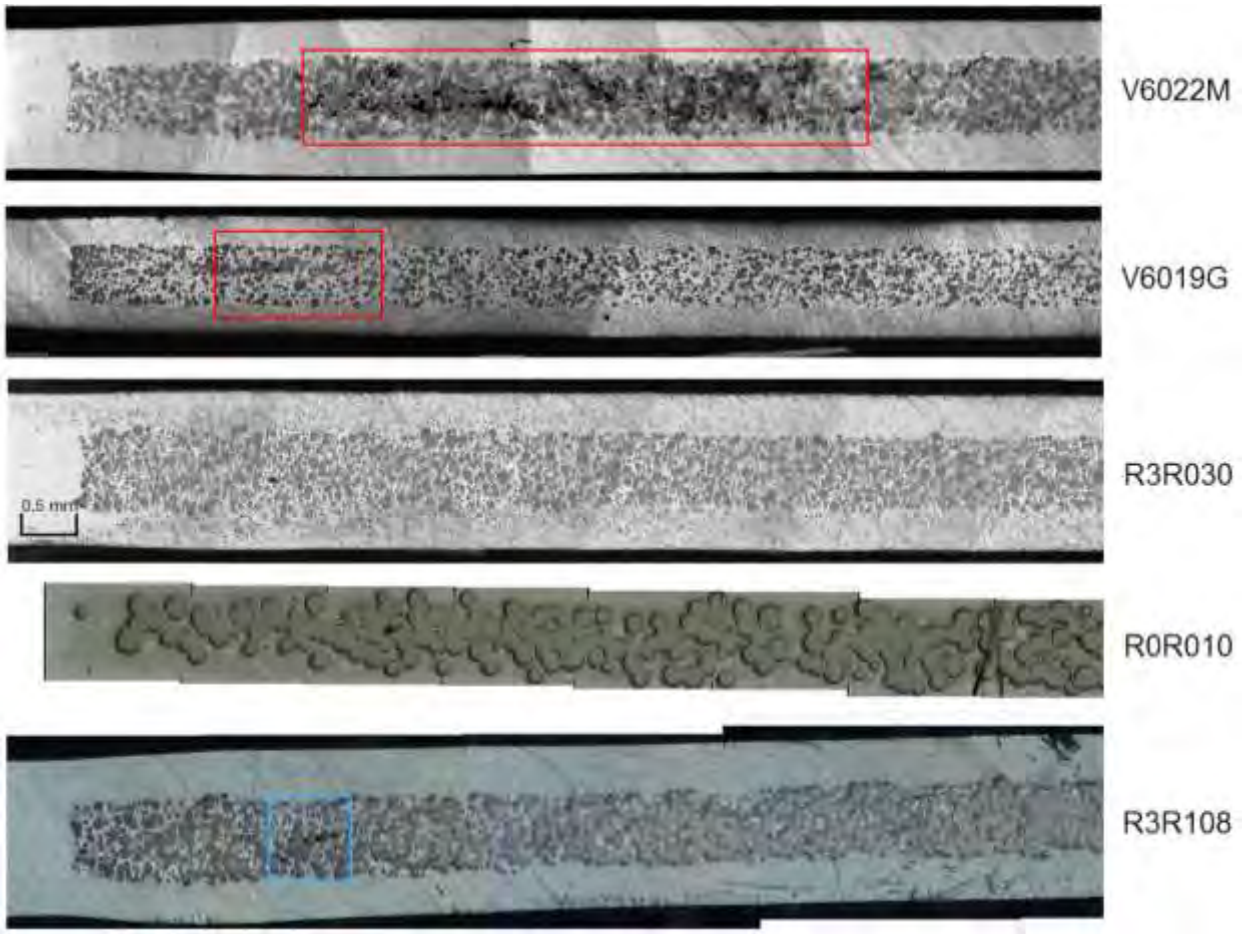

Fig. 1 OM images of fuel meat cross sections from PIE. The red boxes show the pore formed regions and the blue box shows the fractured Al matrix region.

Optical micrographs of cross sections of the five plates are shown in **Fig. 1**. Large pores were observed in V6022M and V6019G. There was no pore development in R3R030. An initial stage of the pore development was seen in R0R010. R3R108 shows cleavage-type fractures in the Al matrix, which is different from the typical pore morphology observed for mostly pure Al-matrix plates. The main cause of the cleavage-type features is attributed to local stress buildup due to fuel swelling, and lack of plasticity in the Al-Si matrix. However, this type of fracture does not appear to lead to breakaway meat swelling from the viewpoint of fuel performance.

3. ABAQUS FEM ANALYSIS

Fuel meat swelling is the primary stress generator, by which mechanical behavior in the meat is predominantly determined. Fuel meat swelling is modeled by combining fission-induced-swelling in U-Mo fuel particles, chemical volume expansion by IL formation, swelling in the IL by fission products accumulation, and volume consumption in the U-Mo and Al matrix due to IL growth [1].

Table 2 Material properties and parameters used for ABAQUS simulations [2].

Plate constituents	Elastic constant (GPa)	Poisson's ratio	Creep rate constant (A) in $\dot{\varepsilon}_c = A\sigma\dot{f}$ (10^{-25} cm^3/MPa)
Al 6061 Cladding	66	0.34	0
U-Mo particle	85	0.34	500
IL	134	0.24	400
Al 1060 Matrix	63	0.33	50

Fuel meat consisting of uniformly-sized U-Mo fuel particles dispersed in the Al matrix in an FCC array was modeled as shown in **Fig. 2**. Microstructural evolution due to IL growth during irradiation was realized by assigning different field variables to the corresponding meshes. The generalized plane strain condition was applied for the FEA modeling based on the observation that plate dimensional changes take place only in the thickness direction. Due to symmetry considerations, analyses were performed only for the biquadratic quadrilateral element to capture the behavior of the full fuel volume.

The microstructural evolution of the fuel meat of V6022M predicted by the ABAQUS simulation is shown **Fig. 3**. As the IL grows and U-Mo particles undergo deformation by creep, mass relocation occurs. The higher creep rate of the IL contributes to the mass relocation that relieves stress peaking at the peak meat thickness location. This phenomenon is further pronounced when the IL forms a continuous phase network in the fuel meat [2]. However, the situation is different for R3R108, in which the IL does not grow to form a continuous phase. In this case, stress relaxation by creep is low, leading to a buildup of stresses in the fuel. This can be seen in **Fig. 4**, where the stress concentration at the thinnest section of the Al matrix, formed by the two closest U-Mo particles, is highest. For V6022M, this stress peaking is effectively relieved by creep, but the stress in R3R108 cannot be relieved. This is consistent with the fracture observed in R3R108.

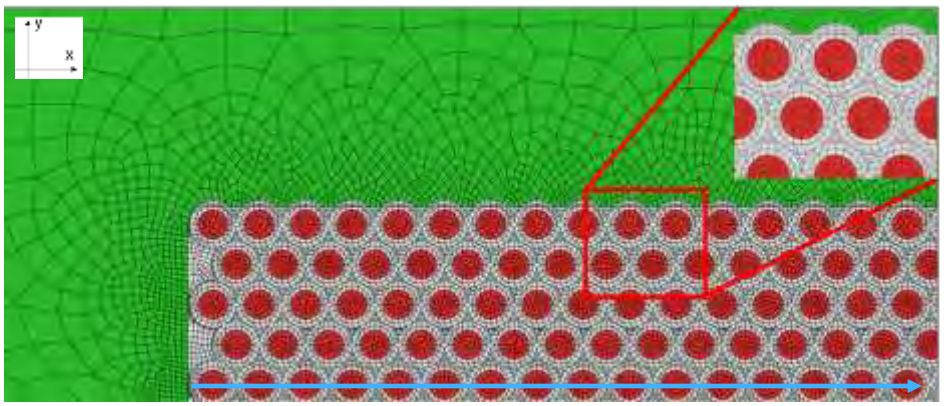

(a) V6022M

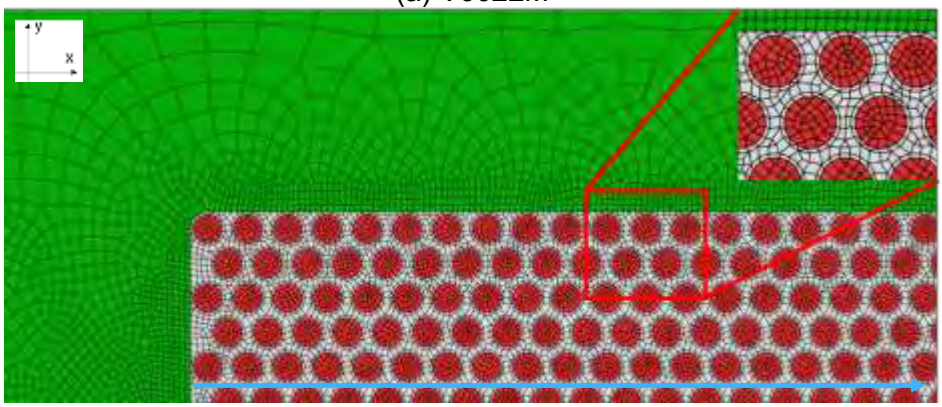

(b) R3R108

Fig. 2 Schematics showing the ABAQUS mesh design and stress analysis path. The blue arrow indicates the stress analysis path.

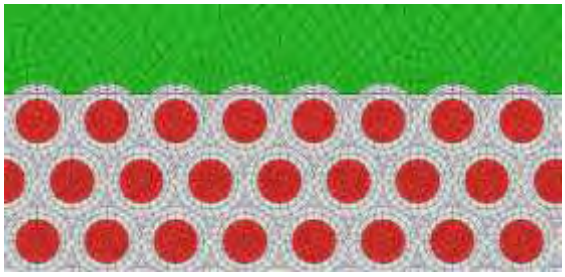

0 – 14 EFPD (IL = 0 μm)

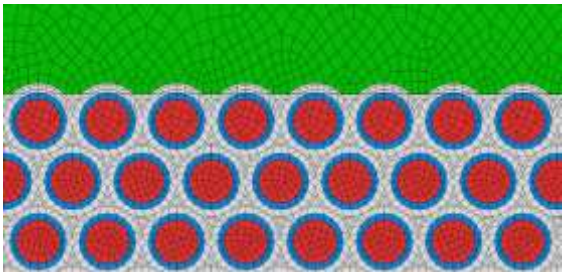

14 – 75 EFPD (IL = 7 μm)

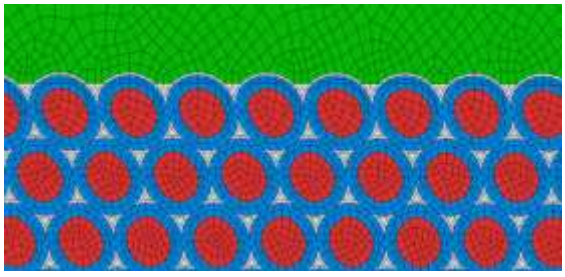

75 – 204 EFPD(IL = 15 μm)

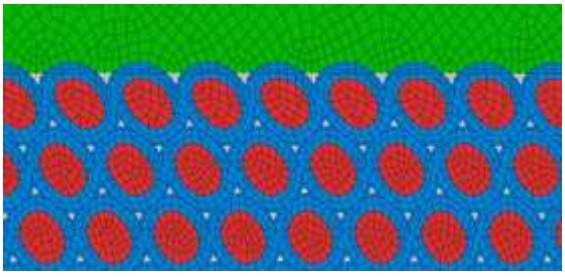

204 – 257 EFPD (IL = 18 μm)

Fig. 3 Microstructural evolution at the peak meat thickness region predicted by ABAQUS simulation for V6022M.

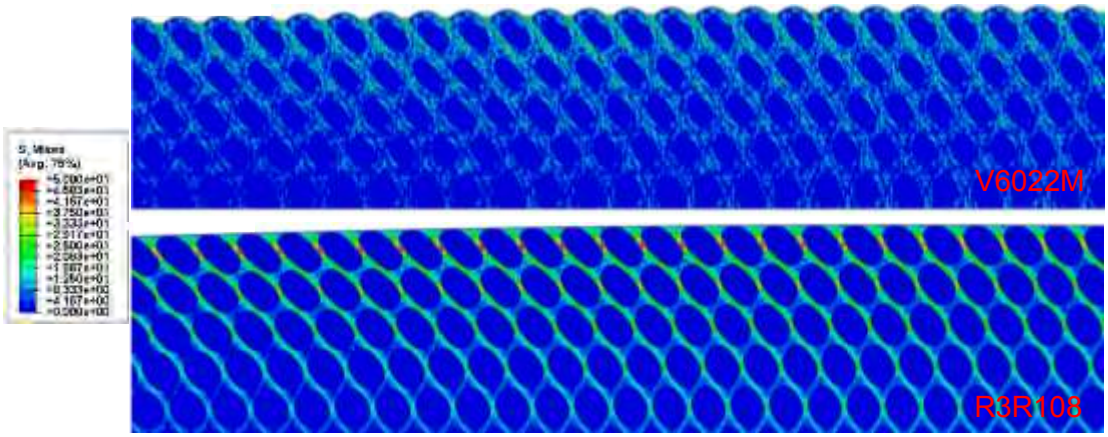

Fig. 4 Equivalent stresses for V6022M and R3R108 predicted by ABAQUS simulations.

The normal stress (σ_{yy}) in the thickness direction along the path shown in **Fig. 2** was predicted by ABAQUS, and is plotted in **Fig. 5**. A positive value of σ_{yy} means that the location is under a tensile stress, while a

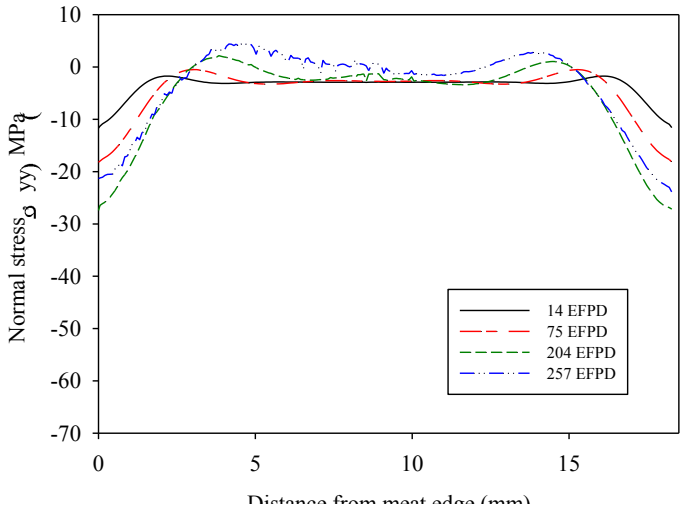

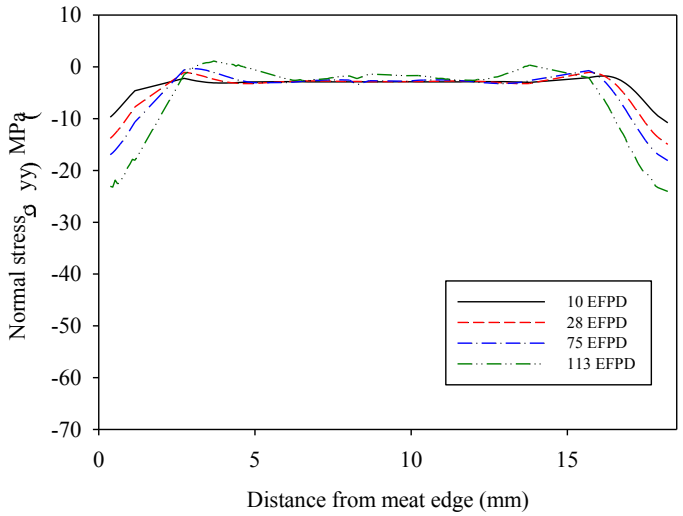

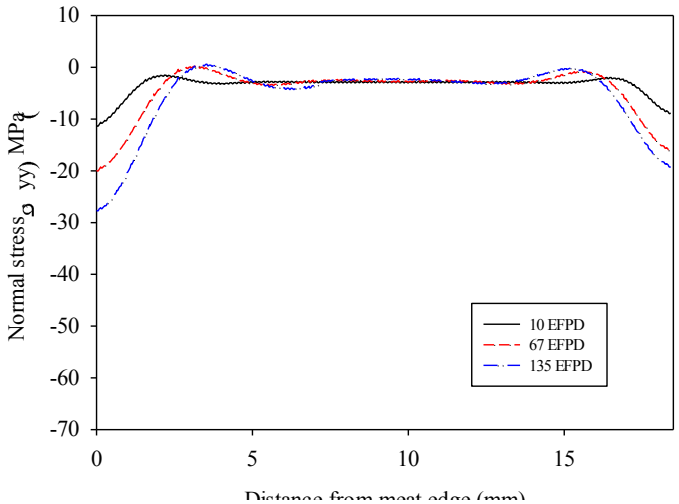

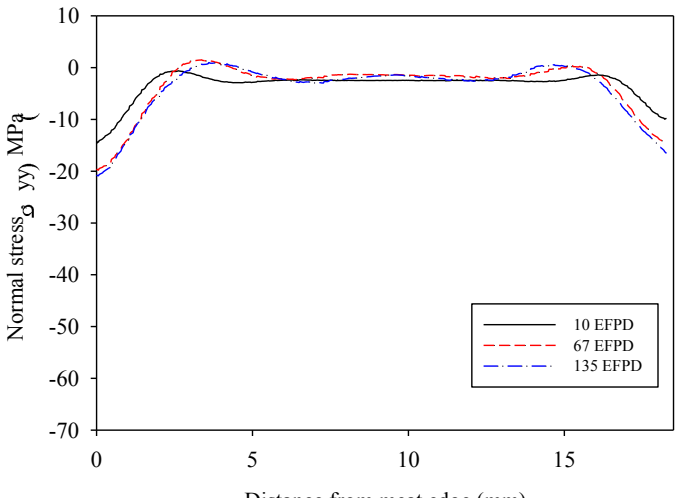

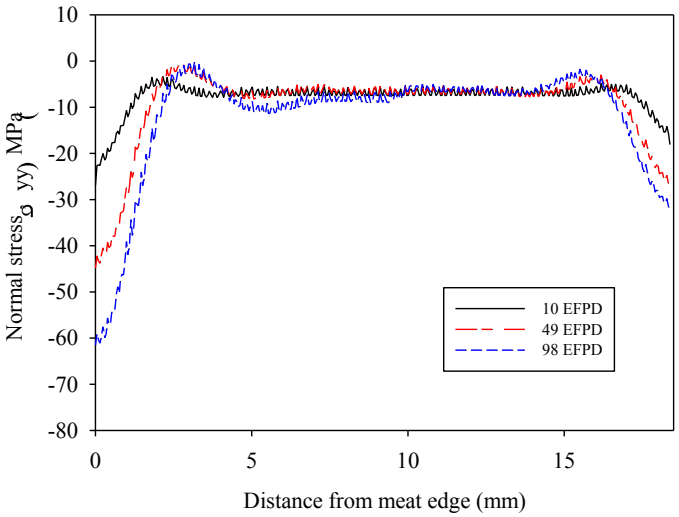

(e) R3R108

Fig. 5 Evolution of normal stress along the path shown in Fig. 2.

V6022M shows that it was under a considerable amount of tensile stress at the region 3 – 7 mm from the meat edge during irradiation, particularly after 75 EFPD. V6019G also exhibited a tensile tress region, although it was much shorter and smaller magnitude than in V6022M. The other plates remained primarily in compressive stress states. The locations where the tensile stress formed, or low compressive stress, at middle of life are consistent with the locations where large pores were observed. This result suggests that the hypothesis that tensile stress promotes pore formation is indeed valid.

It is noticeable in **Fig. 3** that the IL became the continuous phase in V6022M after 75 EFPD. The overall mass relocation by creep is determined chiefly by the continuous phase. When the IL phase becomes the continuous phase, which has a higher creep rate than the Al matrix, more meat mass is transferred toward the meat transverse center, where the magnitude of stress is lowest. When the accumulation of meat mass becomes greater than the critical value at a given location, the stress state changes from compressive to tensile, promoting pore formation and growth. Therefore, IL growth is a valuable indicator to predict large pore formation.

The excellent performance of R0R010 is remarkable. It had the highest fission density among the five plates in this study. Two parameters contributed to its exceptional performance. One is lower U-loading, only 6 gU/cm^3, and the other is the use of larger U-Mo particles. In a previous publication [3], the larger U-Mo particles use was claimed to be the reason for exceptional performance. The ABAQUS simulation in the present study confirmed more specifically that the excellent performance of R0R010 was due to the low IL growth, which kept the vulnerable region in the compressive stress (see **Fig. 5**(d)).

R3R108 showed limited IL growth and was under compressive stress during most of the irradiation. Hence, there are no large pores. However, due to the addition of silicon in the matrix, large fission gas bubbles formed at the U-Mo periphery. R3R108 had a high U-loading of 8 gU/cm^3, which intrinsically reduces the distance between fuel particles as well as the Al matrix thickness between the fuel particles, which enhances stress peaking in the matrix between the fuel particles (**Fig. 4**). Interconnection of the periphery bubbles in the U-Mo particles and stress peaking in the matrix between the U-Mo particles both appeared to promote fractures in the Al matrix.

4. PORE GROWTH MODELING

In addition to the ABAQUS simulation of the stress states within the fuel meat, a model was developed to investigate pore growth within the fuel meat. This section briefly discusses the development of this model.

The pores are assumed to be in mechanical equilibrium in which the pressure in the pore is balanced by the radial stress and surface tension of the pore:

$$P = \frac{2\gamma}{r_{Pore}} + \sigma \tag{1}$$

where P is the pressure inside the pore exerted by gas atoms in the pore, σ is the radial stress at the surface of the pore, γ is the surface tension of the pore and r_{pore} is the pore radius. **Fig. 6** is a schematic illustrating this model.

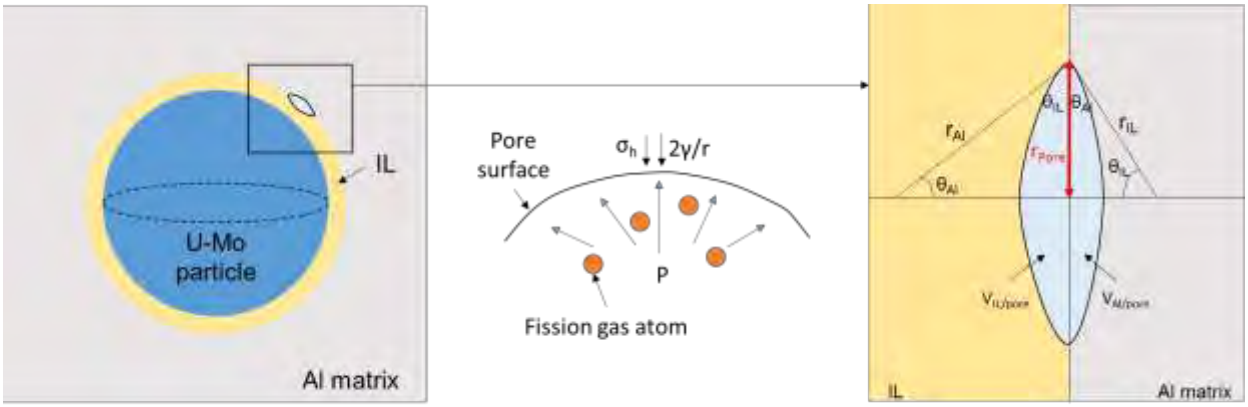

Fig. 6 Schematics of (a) the specific volume element composed of U-Mo, IL, Al matrix with the pore formed at the IL-Al matrix interface, (b) forces on the pore surface, and (c) mechanical equilibrium on the pore surface

The pore radius, r_{pore}, is expressed by:

$$r_{Pore} = \left(\frac{3Q}{4\pi}\right)^{1/3} r_{IL} \tag{2}$$

where $Q = \frac{2\pi}{3}[f(\theta_{IL}) + q^3 f(\theta_{Al})]$ with $q = \frac{\sin\theta_{IL}}{\sin\theta_{Al}}$ and $f(\theta) = 1 - \frac{3}{2}\cos\theta + \frac{1}{2}\cos^3\theta$.

r_{IL} can be found solving the following equation:

$$C_1(t)H^3 - C_2 H + \sigma = 0 \tag{3}$$

where $H = 1/r_{IL}$, $C_1 = \frac{n(t)kT}{Q}$, and $C_2 = 2\frac{\gamma_{IL} f(\theta_{IL}) + \gamma_{Al} f(\theta_{Al})\mathrm{q}}{(1-\cos\theta_{IL}) + q^2(1-\cos\theta_{Al})}$. Here θ is the contact angle (see **Fig. 6**).

The fission gas release rate is calculated considering both recoil release and diffusional release. IL growth is greatly influential to both of these fission-gas-release mechanisms.

Fig. 7 shows preliminary results for porosity growth kinetics for V6022M and R3R108 at their respective locations where most porosity was observed. The symbols are the measured porosity data. V6022M exhibits accelerated porosity whereas R3R108 shows minimal porosity. The predictions are in accord with the measured data.

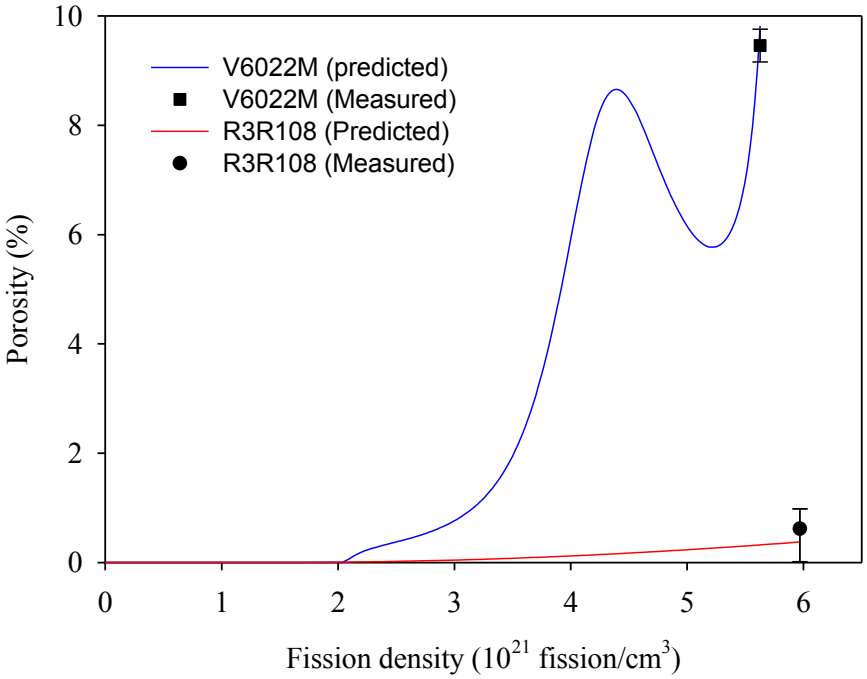

Fig. 7 Preliminary prediction results (lines) for porosity growth kinetics for V6022M and R3R108 at the respective maximum porosity locations. Measured porosities (symbols) at the corresponding locations are also shown.

5. CONCLUSIONS

Mechanical analyses for five miniplates were performed using ABAQUS simulations. The results showed that the normal stress distribution and magnitude in the plate thickness direction were closely dependent upon IL growth. Common for all plates is that the stress is negative (compressive stress) at the plate edge, and approaches zero (stress free) at some locations away from the edge. In some cases at locations away from the edge, the stress state becomes positive (tensile stress). The stress-free locations and tensile stress locations are coincident with the pore formation locations, indicating stress distribution in the plate influences pore growth kinetics. The preliminary results for porosity growth kinetics, predicted from the pore growth model developed in this study, were in fair agreement with the measured data.

ACKNOWLEDGMENTS

This study was sponsored by the U.S. Department of Energy, National Nuclear Security Administration (NNSA), Office of Material Management and Minimization (NA-23) Reactor Conversion Program under Contract No. DE-AC-02-06CH11357 between UChicago Argonne, LLC and the US Department of Energy.

REFERENCES

[1] Yeon Soo Kim et al., J. Nucl. Mater. 465 (2015) 142.
[2] G.Y. Jeong et al., J. Nucl. Mater. 466 (2015) 509.
[3] Yeon Soo Kim et al., J. Nucl. Mater. 454 (2014) 238.

ECONOMY OF BR2 FUEL CYCLE WITH GADOLINIUM AS BURNABLE ABSORBER

SILVA KALCHEVA, EDGAR KOONEN
BR2 Reactor
SCK•CEN, Boeretang, 2400 Mol, Belgium

skaltche@sckcen.be
ekoonen@sckcen.be

ABSTRACT

A preliminary feasibility neutronics study has been performed for HEU (UAlx) and LEU (UMo-dispersed) fuels with various combinations of burnable poisons (within-meat and outside fuel meat). Reactivity and experimental performances, control rod motion, cycle length and fuel burn up (GWD/MTU) prior to discharge are compared in order to assess the fuel utilization. Former analyses have been focused on discrete absorbers located outside the fuel meat. Feasible designs using Cd-wires in the aluminum side plates of the BR2 standard fuel element were proposed for the HEU and for the LEU fuel systems. The necessity to sheath the Cd-wires in order to avoid cadmium solubility brings some technical issues, which increases the fabrication costs. This and also the limitations to manufacture very thin wires (if needed) is the reason to investigate within-meat absorbers, similarly to the ones used in the standard BR2 fuel element. The studies presented in this paper show that the economy of the fuel cycle can be significantly improved by using gadolinium poison in a form of homogeneous mixture with the fuel meat. At the same time, the experimental performances for gadolinium are similar as for the standard poisons (boron and samarium) used in the standard BR2 HEU fuel type. The neutronics calculations are performed by the MCNP6 code.

1. Introduction

A series of studies for the feasibility to convert the BR2 reactor from HEU to LEU fuel have been performed during 2008 – 2012 [1,2]. Upfront to the neutronic conversion feasibility evaluations, an optimization of the burnable absorbers in the fuel assemblies for different LEU fuel systems has been performed. In this optimization project, the nature, quantity (or density, if applicable), geometrical form and localization in the fuel assembly of the burnable absorber have been studied. Four different burnable absorbers in form of wires in the aluminum side plates have been analyzed: Er_2O_3, Gd_2O_3, B_4C and Cd. The final choice made for the new burnable absorber was 36 cadmium wires in the Al side-plates of the standard BR2 fuel element. The optimum wire diameter for the U-7Mo LEU (20% ^{235}U) fuel with density 7.5 g U_{tot}/cm^3 is: Ø = 0.5 mm. The results of these studies have been reported at the RERTR & RRFM conferences [3-5].

In order to avoid cadmium solubility, the Cd-wires have to be sheathed. CERCA studied different methods to sheath the cadmium wires [4]: (i) Al coating by electro deposition or soaking. This solution was abandoned, because it is very difficult to achieve while ensuring the dimensional tolerances as well as the cladding tightness. (ii) Insert cadmium wire into an aluminum sheath, slightly longer, and close it by contraction. This technical solution does not comply with the leak tightness test. (iii) Insert cadmium wires into an aluminum sheath and close it by welding plugs in both ex-

tremities. This technical solution is used for the Japanese fuel elements to ensure the tightness. CERCA masters this manufacturing and has a long experience feedback. As result, CERCA fabricated 2 HEU test fuel elements with Cd-wires which have been successfully irradiated during four BR2 operation cycles [5].

Due to the mentioned technical issues, which increases the manufacture costs, new studies presented in this paper have been performed with gadolinium absorber in a form of homogeneous mixture with the fuel meat for the standard HEU and for the LEU (UMo) fuel types. The reactivity and experimental performances are compared vs. the standard burnable poisons (B_4C and Sm_2O_3) for the HEU fuel and vs. the cadmium wires for the LEU fuel type. The neutronics calculations presented in this paper are performed for the whole core 3-D geometry model of the BR2 reactor using the MCNP6 code [6].

2. Comparison of Burn Up Capabilities of Burnable Poisons

Previous studies for feasibility to operate the BR2 reactor with various fuel types using burnable absorber in form of wires in the aluminum side plates (see Fig. 1) have shown that cadmium had the best burn up characteristics. The other considered absorbers included erbium, gadolinium and boron. The largest core reactivity loss toward EOC was for the erbium poison, while gadolinium and boron had better burn up characteristics but worse than cadmium. It was also concluded that in fuel types with a given combination of density and enrichment, the principle way to improve the reactivity performance of the BR2 core is by decreasing the wire diameter [1-3]. For smaller wire diameter, the reactivity excess at BOC will be higher, and the reactivity performance during the operation cycle will be improved due to the faster burn up in wires with smaller diameter.

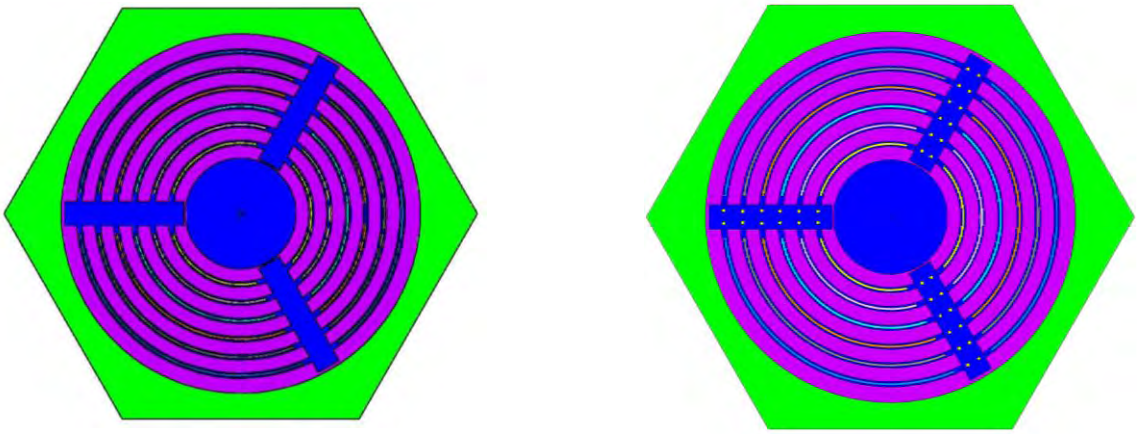

Figure 1. Standard BR2 fuel assembly geometry (left) and with wires in the Al-grooves.

In the present study the performances achieved with fuel types, in which the burnable poisons in form of wires are located outside the fuel meat, are compared to boron & samarium (in form of B_4C & Sm_2O_3) or gadolinium (in form of Gd_2O_3) homogeneously mixed with the fuel meat. The fuel types used in the preliminary analysis for the feasibility of the BR2 reactor operation are summarized in Table 1. The burn up rates of the major burnable isotopes have been calculated by MCNP6 during one operation cycle with duration ~ 24 days. As it is seen from the graphs in Fig. 2, ^{157}Gd acts similarly to ^{149}Sm, burning almost totally in the first 5 days. The burn up rate of ^{155}Gd, compared to ^{157}Gd

is slower, but after 20 days is also totally burnt. The burn up rate of the major cadmium isotope ^{113}Cd strongly depends on the wire diameter, being higher for smaller diameters. The major boron isotope ^{10}B has the slowest burn up rate, burning almost linearly with time.

Table 1. Considered HEU and LEU fuel system parameters.

	HEU fuel assembly		UMo fuel assembly	
Enrichment [%]	93.0	93.0	19.7	19.7
Density [g U_{tot}/cm^3]	1.3	1.3	7.5	7.5
^{235}U mass [grams]	400	400	482	482
^{238}U mass [grams]	30	30	1978	1978
Cd-wire diameter [mm]	-	-	0.5	-
Number Cd-wires (Al side plates)	-	-	36	-
Boron in form of B_4C (fuel meat)	3.8 g	-	-	-
Sm in form of Sm_2O_3 (fuel meat)	1.4 g	-	-	-
Gd in form of Gd_2O_3 (fuel meat)	-	2.5-4.0 g	-	2.5-4.0 g

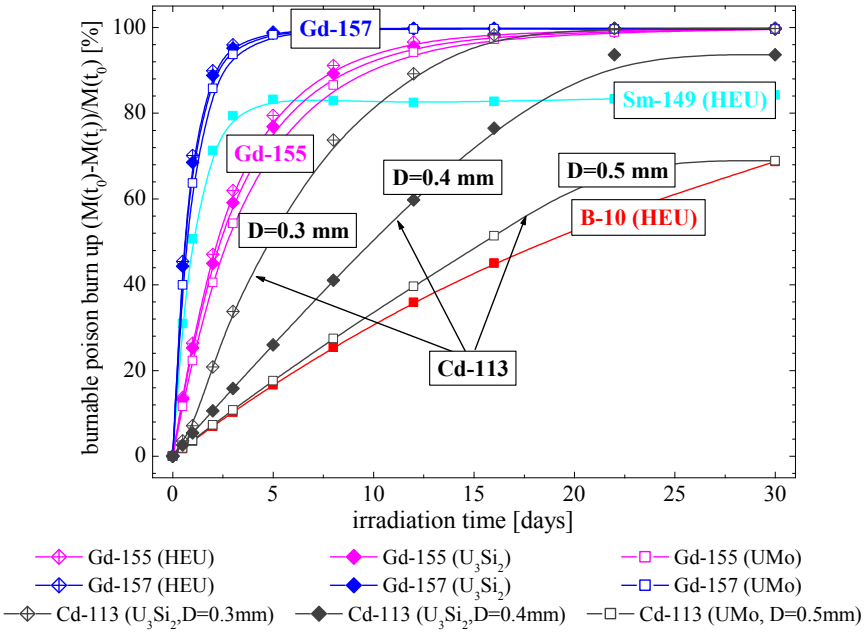

Figure 2. Comparison of burn up rate of different burnable poisons used in the HEU and LEU fuel assemblies.

3. Reactivity Performances

The reactivity performances, such as control rod motion, cycle length and reactivity of a fuel assembly vs. ^{235}U burn up, are compared in this section for the HEU and LEU cores using different

burnable absorber options. Two types of reactor core loads are compared: a representative load, which contains 33 fuel elements and a modified load, which contains 31 fuel elements. The BR2 reactor uses 6 shim-safety control rods to compensate the reactivity changes during operation cycle and at the same time as safety rods to shut down the reactor. The control rod position in "mm" of the control rod motion between fully inserted and totally withdrawn rod is labeled by "Sh" in the graphs in the following sections. The produced energy during an operation cycle is given in MWd, which is equivalent to the average power during the cycle multiplied by the number of the operation days.

3.1. Control Rod Motion and Cycle Length

3.1.1. HEU core

The fuel cycles using burnable poisons, homogeneously mixed with the fuel meat, follow somehow similar tendency, which is characterized with a minimum of the control rod position during the course of the operation cycle. However, the minimum of the CR position in fuel types with Gd_2O_3 in the fuel meat is observed earlier in time (about 3-4 days after BOC) due to the faster burn up of the gadolinium poison compared to boron and samarium. HEU fuel type with 2.5 g/FE Gd poison in the meat is very reactive (low critical control rod position at BOC), characterized with a steep control rod course down during the first operational days. Therefore, in order to respect the safety reactivity margin (> 4.5 $ according with the BR2 Safety Analysis Report) at the minimum of the CR position, different strategies can be applied specifically for the HEU fuel type, such as:

- Loading of absorptive experiments would allow increasing the initial and the minimum control rod critical position.
- Increasing the initial Gd amount in the fresh fuel elements from 2.5 g/FE up to 4.0 g/FE improves the critical height at BOC. However, as it is seen from Fig. 3-left, the minimum critical rod position during the cycle is almost not changed (or very little).
- Removing from the load fresh and/or burnt fuel elements allows increasing significantly the minimum rod position by about 100 mm (see Fig. 3-right).

3.1.2. LEU core

The minimum control rod position for the LEU fuel types with Cd-wires is effective only at the start-up: after the first couple of days, the control rods are almost monotonically withdrawn during the reactor operation. The tendency of the control rod motion with Gd poison in the fuel meat is similar as for the HEU fuel type, however the descending of the rods is less pronounced and in principle the UMo fuel type is feasible for both considered Gd amounts – 2.5 and 4.0 g/FE, as for the representative load (see Fig. 4-left), as well as for the modified load (see Fig. 4-right). In all cases the cycle length with Gd absorber is significantly longer in comparison with Cd-wires.

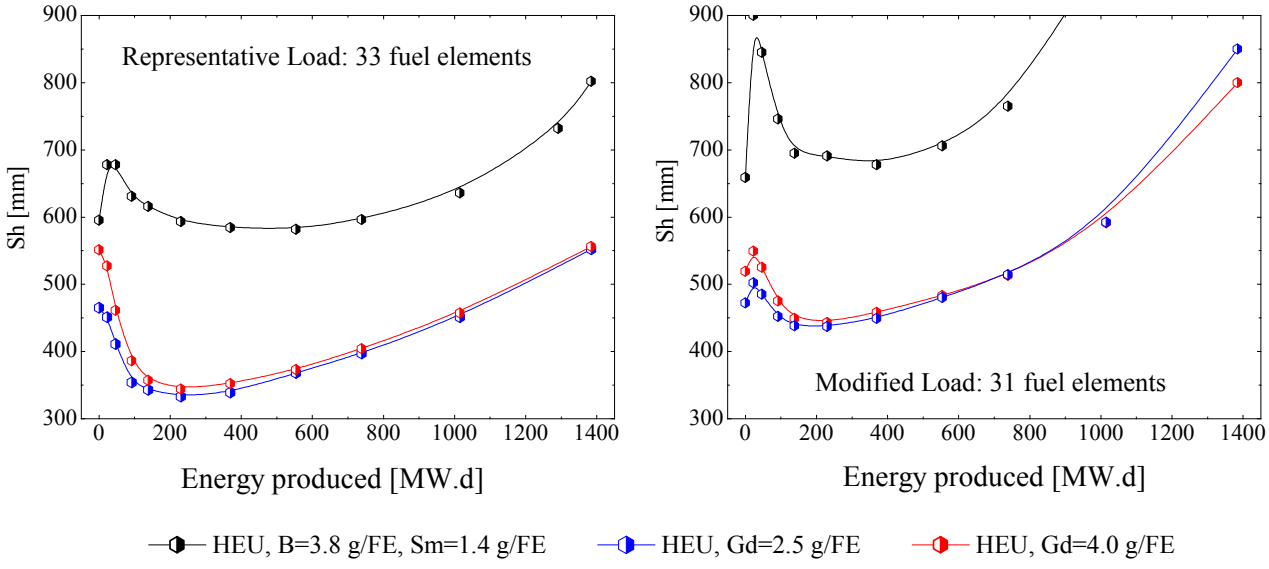

Figure 3. Critical position of the control rod bank vs. produced energy in one BR2 operation cycle with average power P_{BR2}=59 MW and cycle length 24 days for the *HEU cores*: representative load, containing 33 fuel elements (left); modified load, containing 31 fuel elements (right).

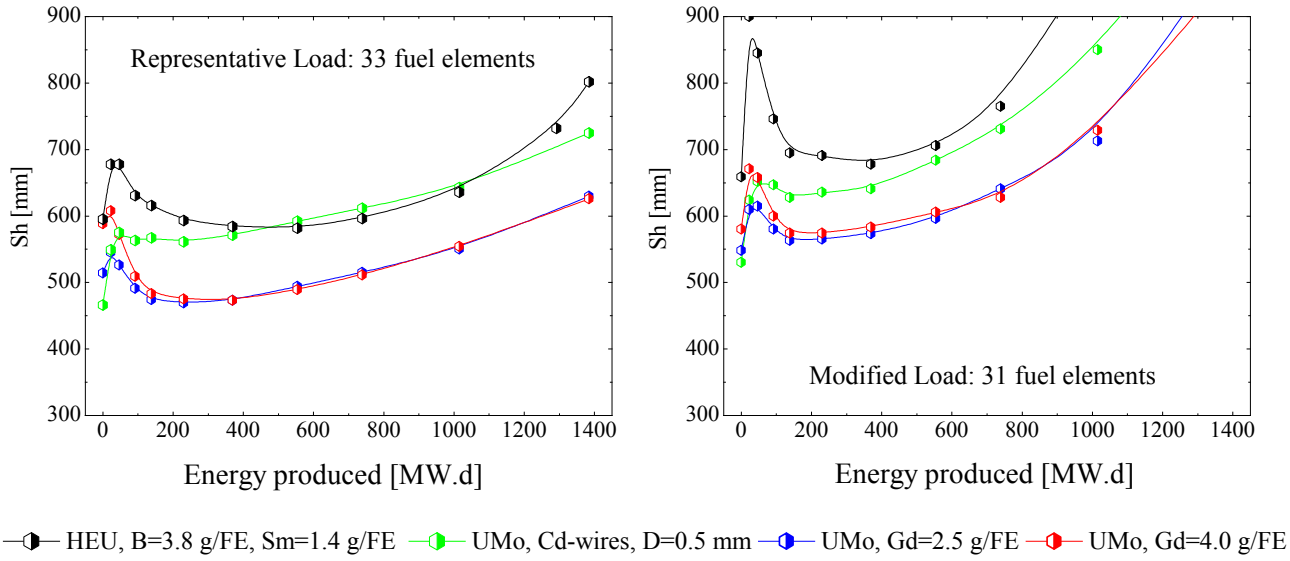

Figure 4. Critical position of the control rod bank vs. produced energy in one BR2 operation cycle with average power P_{BR2}=59 MW and cycle length 24 days for the *LEU cores*: representative load, containing 33 fuel elements (left); modified load, containing 31 fuel elements (right).

3.2. Reactivity of a Fuel Element vs. ^{235}U burn up

The performance graph of the reactivity of a fuel element in dollars [$] as function of the mean ^{235}U burn up [%] has been calculated for the standard HEU fuel and for the LEU fuel type (see Fig. 5). The load of the representative HEU core has been used in the calculations. The methodology for calculation of the reactivity effect is as follows: fuel elements, each with a given mean ^{235}U burn up [%], are loaded in one and the same fuel channel. The reactivity of each fuel element is determined relatively to the reactivity of the fresh [0%] standard HEU fuel element, loaded in the same channel using the following formulae (i=0,…,60% ^{235}U burn up):

$$\Delta\rho(\boldsymbol{HEU_i}) = \rho_{HEU,i}\left(B^5_{HEU,i}\right) - \rho_{HEU,standard}(0\%),$$

$$\Delta\rho(\boldsymbol{LEU_i}) = \rho_{LEU,i}\left(B^5_{HEU,i}\right) - \rho_{HEU,standard}(0\%).$$

As it is seen from Fig. 5, the reactivity of the HEU and LEU fuel elements is maximum for the Gd poison and significantly higher for all ^{235}U burn up values with exception of a fresh fuel element with gadolinium in the fuel meat.

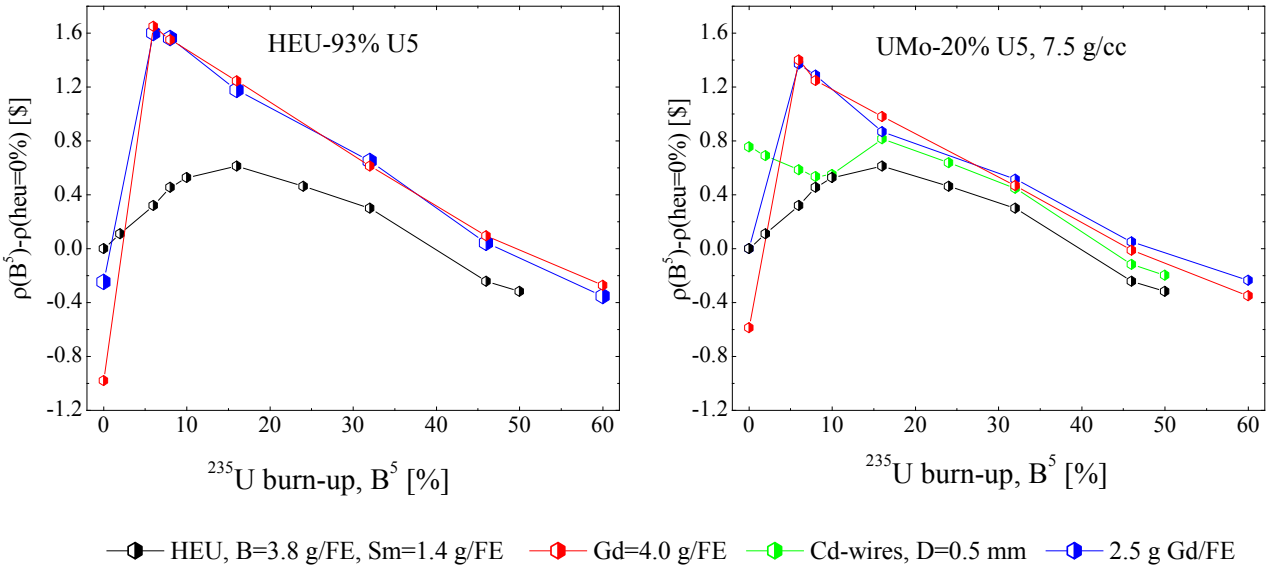

Figure 5. Performance graphs of reactivity of HEU & LEU fuel element vs. ^{235U} burn up.

4. Fuel Cycle Economy

The results about the reactivity performances shown in the Section 3 demonstrate the economic advantages of the gadolinium poison among the other considered options. We have shown that a fuel cycle for a modified core load with reduced number of fuel elements is feasible for the HEU and for the LEU fuel types with Gd poison in the fuel meat. At the same time, the HEU fuel cycle with standard poisons B & Sm has significantly shorter cycle length.

Table 2 summarizes the main results obtained in the Section 3 for the modified core load. The data in the table represent the gain in dollars and days of cycle length for each considered fuel type relatively to the standard HEU fuel with boron and samarium burnable absorbers. The gain in reactivity dollars for fuel elements with different mean fuel burn up is listed in the last row of Table 2. These data represent the reactivity difference between a HEU fuel element with Gd poison (or a LEU fuel element with Cd-wires or with Gd poison in the meat) and a standard HEU fuel element with boron and samarium for different mean ^{235}U burn up values of the fuel element.

Table 2. Reactivity gain (in dollars and days) in HEU and LEU cores relatively to the standard HEU core with standard poisons (boron and samarium) for the *modified core load, containing 31 fuel elements (FE)*.

Fuel type	HEU-93% (UAlx)		LEU-20% (UMo, 7.5 g/cc)		
Burnable absorber	Gd=2.5 g/FE	Gd=4.0 g/FE	Cd-wires D=0.5 mm	Gd=2.5 g/FE	Gd=4.0 g/FE
Reactivity excess (BOC)	+3.85 $	+2.46 $	+3.73 $	+2.46 $	+1.63 $
Cycle length	+5.7 d.	+6.7 d.	+6.0 d.	+8.2 d.	+6.9 d.
Reactivity of fuel element with different ^{235}U burn up (%)	-0.25 $ (0%) +1.09 $ (8%) +0.55 $ (16%) +0.36 $ (32%) +0.29 $ (50%)	-0.98 $ (0%) +1.08 $ (8%) +0.61 $ (16%) +0.35 $ (32%) +0.30 $ (50%)	-0.75 $ (0%) +0.10 $ (8%) +0.20 $ (16%) +0.16 $ (32%) +0.10 $ (50%)	0.00 $ (0%) +0.85 $ (8%) +0.26 $ (16%) +0.21 $ (32%) +0.29 $ (50%)	-0.60 $ (0%) +0.10 $ (8%) +0.36 $ (16%) +0.20 $ (32%) +0.20 $ (50%)

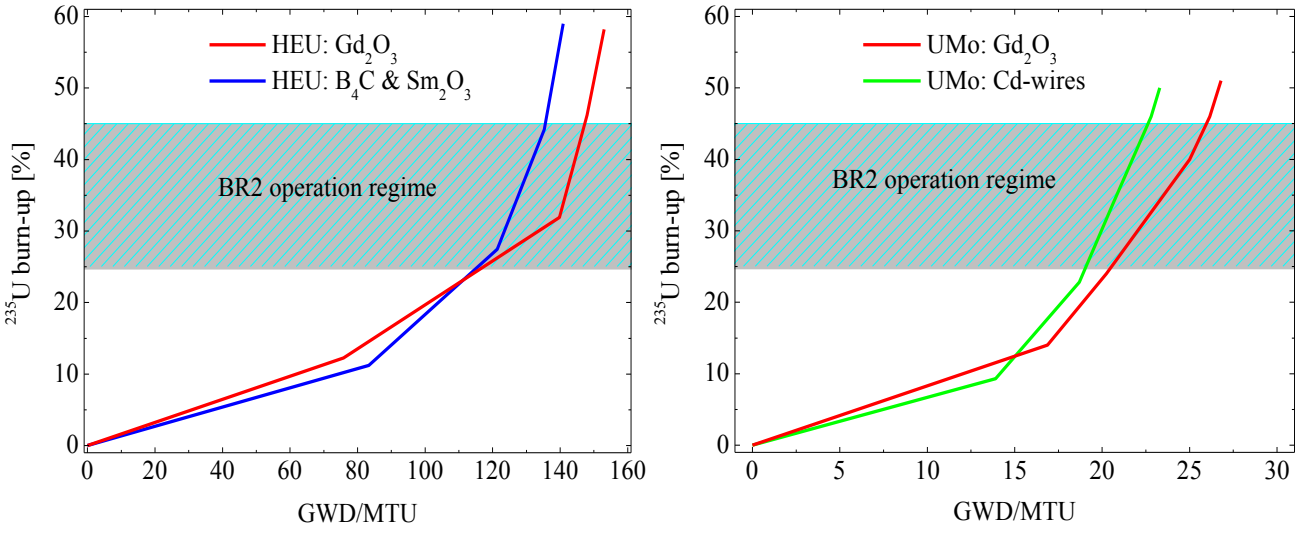

Figure 6. Extended fuel element burn up prior discharge by utilization of Gd as burnable absorber.

As can be seen from Table 2 all burnt elements with Gd poison have significantly higher reactivity values except for a fresh fuel element with Gd poison. Fuels with gadolinium poison in the meat are "more energetic" which is demonstrated in Fig. 6, allowing more efficient uranium utilization by extending the fuel burn up prior discharge.

The MC uncertainties in the calculated k_{eff} are within Δk_{eff}=±0.00005 and the uncertainties in the calculated reactivity values in Table 2 are within $\Delta\rho$=± (0.5% – 1.0%).

5. Experimental Performances

Calculations of thermal, epithermal and fast neutron flux distributions in the axial direction have been performed for representative fuel element channels and for typical experimental positions. The MCNP model of the BR2 core with notation of the reactor channels is given in Fig. 7. Due to the higher ^{238}U content in the LEU fuel types, which is related to the higher total uranium density U_{tot}, the losses of neutron fluxes are essential, especially the thermal flux losses. The higher the U loading per fuel element, the higher thermal flux losses are observed.

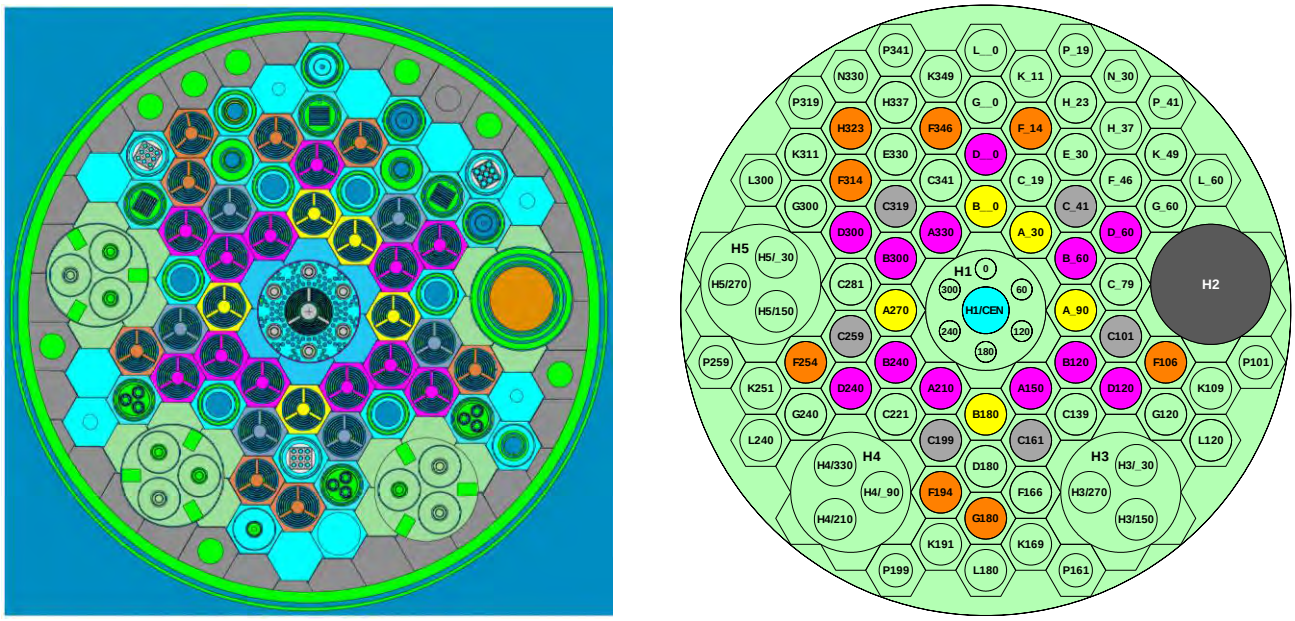

Figure 7. MCNP model of the BR2 reactor core (left) with notation of the reactor channels (right).

Table 3 summarizes the thermal neutron flux losses for the considered HEU and LEU fuels, which were described in Table 1. The fast flux losses in all considered LEU fuels are less pronounced, being about 5% in average for the different channels.

It has been shown in an internal SCK•CEN report that the experimental performances of the HEU

fuel types with Gd poison are similar (or in some instances even better) to the standard HEU fuel type with B & Sm poison. The experimental performances of the LEU-UMo fuel type with Gd poison in the fuel meat are similar to those with the Cd-wires, for which the losses compared to the standard HEU fuel type are in average about 10 to 15%.

Table 3. Percentage losses/gains of thermal neutron flux in representative fuel, reflector and experimental channels relatively to HEU standard fuel (see Fig. 7 for notation of the reactor channels).

Dedicated experimental positions	HEU fuel assembly		UMo fuel assembly	
	B_4C & Sm_2O_3	Gd_2O_3	Cd-wires	Gd_2O_3
Isotope production (core center, H1/0°)	100%	101%	88%	93%
Isotope production (channel E30)	100%	101%	85%	87%
Isotope production (channel G0)	100%	100%	83%	87%
Isotope production (channel G240)	100%	92%	90%	87%
Silicon doping (channel H2)	100%	103%	90%	90%
Irradiation of aging materials (K49)	100%	102%	88%	90%

6. Conclusions

During 2008-2015 a detailed comparative analysis has been performed for the efficiency and absorption capabilities of 3 major candidates as burnable absorber for the new LEU BR2 fuel: Cd, Gd_2O_3, and B_4C. It was shown that the most favorable absorber, used outside of the fuel meat was cadmium. This was due to the fact that for the minimum wire diameter, which could be fabricated ($Ø$=0.3-0.4 mm) cadmium had the highest burn up rate. Gadolinium, boron and other considered absorbers have higher self-shielding effect for such diameters and therefore they need very thin wire diameters ($Ø < 0.3$ mm) in order to have high burn up rate.

Later (current) studies involve analysis of various fuel types (LEU and HEU) with various burnable poisons, homogeneously mixed with the fuel meat: B_4C & Sm_2O_3 as in the standard BR2 fuel, and Gd_2O_3. The studies presented in this paper show that the highest burn up rate has gadolinium due to its 2 major isotopes ^{155}Gd and ^{157}Gd which have very high thermal absorption cross sections and deplete very fast with the fuel burn up. The analysis of the reactivity performances has shown that HEU fuel type with gadolinium within fuel meat has significantly longer (+1 week) cycle length compared to the standard HEU fuel with standard boron and samarium poisons. The LEU fuel type with gadolinium poison inside meat has about 5 to 8 days longer cycle length (depending on the core configuration) compared to fuel type with cadmium wires outside fuel meat.

The preliminary results presented in this paper have shown that fuel types with gadolinium absorber used in a form of homogeneous mixture with the fuel meat have important economic advantages compared to other burnable absorber options.

7. References

[1] S. Kalcheva, E. Koonen, V. Kuzminov, G. Van den Branden and E. Sikik, "Feasibility Report for the Conversion of the BR2 Reactor from HEU to LEU fuel", SCK•CEN-R-5439, August (2012).

[2] B. Guiot, "Improved BR2 Fuel Cycle With Optimized Burnable Absorber", Master Thesis, Mentors: E. Koonen, S. Kalcheva, Promoter: Prof. J. M. Noterdaeme, BNEN, SCK, Belgium. August (2008).

[3] S. Kalcheva, E. Koonen and B. Guiot, "Optimized Burnable Absorber for the BR2 Reactor", *RERTR 2008 – 30th International Meeting On Reduced Enrichment For research And Test Reactors*, October 5-9, 2008, Washington D.C., USA.

[4] N. Franck, S. Kalcheva and E. Koonen, "Cd wires as burnable poison for the BR2 fuel element", *Proceedings of the 13th Int. Topical Meeting on Research Reactor Fuel Management*, Vienna, Austria, March (2009).

[5] S. Kalcheva, G. Van den Branden and E. Koonen, "Reactivity Performance Of Two Prototypes HEU Fuel Elements With Cadmium Wires Irradiated In The BR2 Reactor", *RRFM 2012, Proceedings of the 16th Int. Topical Meeting on Research Reactor Fuel Management*, Prague, Czech Republic, March (2012).

[6] MCNP6, Version 6.1.1beta, LANL, LA-CP-14-00745, Rev. 0. June (2014).

THE EFFECT OF THERMAL CONDUCTIVITY UNCERTAINTIES ON THE OPERATING TEMPERATURE OF U–MO/AL DISPERSION FUEL

F.B. SWEIDAN, Q.M. MISTARIHI, H.J. RYU

Department of Nuclear and Quantum Engineering, KAIST
Yuseong-gu, Daejeon 34141, Republic of Korea

J.S. YIM

Korea Atomic Energy Research Institute
Yuseong-gu, Daejeon 34057, Republic of Korea

ABSTRACT

U–Mo/Al dispersion fuel has been considered one of the most promising candidates for the replacement of highly enriched uranium fuel in many research reactors. The thermal conductivity of nuclear fuel is a very critical parameter for the determination of the operational temperature of the plate-type dispersion fuel. Several models have been developed for the estimation of the thermal conductivity of U–Mo fuel, mainly based on the best fit of the very few measured data without providing uncertainty. In this study, uncertainty ranges of the reported thermal conductivity data of irradiated U–Mo fuel is determined. These uncertainty values are used, alongside with the neutronics and thermal hydraulics uncertainties, to determine the combined uncertainty effect of these parameters on the operational temperature range of U–Mo/Al dispersion fuel.

1. Introduction

The development of low-enriched uranium (LEU) fuels for research reactors has been pursued to replace the use of highly-enriched uranium (HEU) to improve proliferation resistance of fuels and fuel cycles. Reduction of the enrichment requires an increase in the uranium density of the fuel to provide acceptable performance in reactors [1]. U-Mo particles dispersed in an Al matrix (U-Mo/Al) is a promising fuel for conversion of the research reactors that currently use HEU fuels to LEU-fueled reactors due to its high density and good irradiation stability [2].

Dispersion fuel offers an advantage in thermal conductivity over a monolithic fuel design [3]; that is thermal conductivity is proportional to the amount of high thermal conductivity aluminum present in the matrix. The matrix will dissipate heat faster than the lower thermal conductivity fuel phase.

Thermal conductivity is an important parameter in determining the operational temperature of the fuel plate and this property influences available reactor safety

margins. The thermal conductivity of dispersion fuel is primarily dependent upon the thermal conductivity of the matrix material itself, porosity that forms during fabrication of the fuel plates, and upon the volume fraction of the dispersed fuel phase [1]. Several models have been developed for the estimation of the thermal conductivity of U–Mo fuel, mainly based on the best fit of the very few measured data without providing uncertainty ranges. The purpose of this study is to provide a reasonable estimation of the upper bounds and lower bounds of fuel temperatures with burnup through the evaluation of the uncertainties in the thermal conductivity of irradiated U-Mo/Al dispersion fuel.

2. Uncertainty of fuel meat thermal conductivity

The thermal conductivity of U-Mo/Al fuel can be obtained from the simple thermal conductivity model utilizing the three major parameters: density, thermal diffusivity, and specific heat capacity through the following equation [4]:

$$k = \alpha\, C_p\, \rho \ldots (1)$$

where:

- k: thermal conductivity (W/m-K)
- α: thermal diffusivity (mm^2/s)
- C_p: specific heat capacity (J/g-K)
- ρ: density (g/cm^3)

The thermal conductivity uncertainty can be obtained by calculating the combined uncertainty from the respective uncertainty values of specific heat capacity, density, and thermal diffusivity.

Measurement uncertainties of specific heat capacity, density, and thermal diffusivity are adopted from the uncertainties of U-Mo/Al fuel as well as UO_2 fuel that are available in the literature. By combining the uncertainty values of the three parameters, the thermal conductivity uncertainty is obtained.

According to UO_2 fuel thermal properties database, the heat capacity uncertainty is ±2% from 298.15 to 1800 K [4]. These uncertainties are based on the scatter in the data and the percent deviations of the data from the recommended equations. Perkin Elmer Pyris 1 power-compensated DSC is usually used to perform specific heat capacity measurements on the fuel samples as a function of temperature [5].

An AccuPyc 1300 gas expansion pycnometer was used for density determination of U-Mo fuel samples. The density uncertainty according to PNNL-24135 document [5] and UO_2 fuel thermal properties database [4] is considered acceptable if the measured values of the standard weights were within ±1% of the standard values for the entire temperature range.

Thermal diffusivity measurements can be performed using a Netzsch LFA 457 MicroFlash® Laser Flash Apparatus [5]. The instrument was considered in calibration if the iron standard measurements were within ±5% of the expected values. It was also figured out to be the same value by Hay et al. [6] who has identified the thermal diffusivity uncertainty according to the "partial time moments method."

The uncertainty propagation of the three parameters in equation (1) provides the thermal conductivity uncertainty that is obtained from the following equation [7]:

$$\frac{u(k)}{k} = \sqrt{\left(\frac{u(\alpha)}{\alpha}\right)^2 + \left(\frac{u(C_p)}{C_p}\right)^2 + \left(\frac{u(\rho)}{\rho}\right)^2} \ldots (2)$$

By using equations (1) and (2), and the numerical values required for density, thermal diffusivity and specific heat capacity obtained from ref [8], quantity and fractional uncertainties of thermal conductivity are calculated.

The results of uncertainty calculations reveal that the thermal conductivity uncertainty is ±5.48%. These results are used to determine the possible operation temperature ranges of U-Mo dispersion fuel.

3. Operational temperature evaluation of U-Mo/Al fuel

To calculate the operational temperature of fuel meat (T_m), equation (3) is used [1]:

$$T_m = T_c + q''\left(\frac{a}{2\lambda_e} + \frac{b}{\lambda_c} + \frac{c}{\lambda_o}\right) \ldots (3)$$

where:

- T_m: fuel meat operational temperature (^oC)
- T_c: the outer surface of the fuel plate cladding temperature (^oC) (calculated from equation (4)).
- q'': the surface heat flux (W/cm^2)
- a: the half thickness of the fuel meat (cm)
- b: the thickness of the cladding on one side (cm)
- c: the oxide layer thickness.
- λ_e: the effective thermal conductivity of the fuel meat (W/m-K).
- λ_c: the thermal conductivity of the cladding (The thermal conductivity of as-manufactured Al 6061 cladding matrix is 165 W/m-K) [10] .
- λ_o: the oxide layer thermal conductivity (constant at 1.85 W/m-K) [10].

To obtain the value of T_c in equation (3), Newton's law of cooling is used as described by equation (4) [1]:

$$q'' = h\,(T_c - T_b) \ldots (4)$$

where:

- h: the heat transfer coefficient, which was assumed to be constant at 3.03 W/cm^2-K [1].
- T_b is the coolant temperature, assumed to be 40^{o}C based on ref. [11] and ref. [12].

In order to use equation (3) and equation (4) for the determination of the operational temperature of U-Mo/Al fuel, several parameters and equations have to be obtained.

3.1. Fuel plate dimensions

The standard fuel plate dimensions are obtained from NUREG-1313 document [13]. The nominal fuel meat thickness is 0.51 mm and the nominal cladding thicknesses of 0.38 mm. There are fabrication uncertainties regarding fuel meat thickness and uranium density in the fuel meat. The minimum allowable thickness of the cladding is 0.25 mm; the fuel meat thickness range is 0.51 ± 0.26 mm. The acceptable uranium density variations of fuel meat are ± 16%; the uranium density range is 8.0 ± 1.28 g/cm^3 [13].

3.2. Heat transfer coefficient and heat generation (surface heat flux)

The heat transfer coefficient used in equation (4) is assumed to be constant at 3.03 W/cm^2-K. According to a reference by W.L Woodruff [14], the heat transfer coefficient uncertainty, which is based on the spread of data and the fit of the data by the selected correlation, fits within a band of ± 20% for any of the single phase correlations commonly used.

W.L Woodruff [14] stated that since there were no available data for the uncertainties of power and power density, it was assumed that the uncertainty in the power measurements is ± 5% and the uncertainty in power density is ± 10%. These values can be used (if necessary) in the combined uncertainty analysis of the operational temperature calculations as a function of burnup.

Since there is no open data about the fission density as well as the surface heat flux of a research reactor core using U-Mo/Al fuel, it is assumed that the surface heat flux has multiple values ranging between 100 W/cm^2 to 400 W/cm^2 with uncertainty of ±10% that is used for the combined uncertainty study of the operational temperature of U-Mo/Al fuel.

3.3. Outer cladding temperature uncertainty

By modifying equation (4) to be a function of T_c, using the uncertainties of q'' (± 10%) and h (± 20%) stated in the previous section, using T_b as 40^{o}C and applying equation (2). Multiple values of the cladding surface temperature are obtained based on the surface heat flux used, ranging from 73^{o}C at 100 W/cm^2 surface heat flux to 172^{o}C at 400 W/cm^2.

The uncertainty of the outer cladding temperature is obtained by combining the uncertainties of heat flux and the heat transfer coefficient using the same method used for thermal conductivity uncertainty (equation (2) and (4)). The resulting uncertainty of the outer cladding temperature is ± 22%.

3.4. Thermal conductivity of fuel meat as a function of fission density

The data available in ref [1] and ref [8] of the fuel meat (U-7Mo/Al with 8 g-U/cm^3) were used to obtain the thermal conductivity of irradiated U-Mo/Al dispersion fuel as a function of burnup. As can be seen in ref [1], the thermal conductivity of U-Mo/Al dispersion fuel decreases down to approximately 10 W/m-K at a fuel meat fission density of 3.5E+21 when the heat flux is in the range of 200-270 W/cm^2 and the calculated beginning-of-life fuel temperature is in the range of 180-210^{o}C[1].

3.5. Oxide layer thickness growth with burnup

Aluminum alloy cladding experiences oxidation layer growth on the surface during the reactor operation [10]. A prediction of the aluminum oxide thickness of the fuel cladding and the maximum temperature difference across the oxide film is needed for a reliable evaluation of the operational temperature of U-Mo/Al fuel since the temperature difference due to the presence of the oxide layer is high[15].

The oxide growth model developed by Kim and Hofman, et al. [15] which uses a variable rate-law power in a function of irradiation time, temperature, surface heat flux, water pH, and coolant flow rate, was used for estimating the oxide film thickness as a function of burnup. The predicted oxide thickness is sensitive to water pH, and it is assumed that water pH will be evenly distributed in the range of 5.5 ~ 6.2 [10].

The values of the parameters needed to calculate the oxide layer thickness growth as a function of burnup are KJRR data that are listed in ref. [12]. And the conversion of units of burnup was adopted from ref. [16].

Table 1 shows the oxide layer thickness growth as a function of fuel meat fission density, which is obtained by using Kim's model [15]. To obtain the data, assumptions have been used which are average pH value, average heat flux and average cladding surface temperature. Linear interpolation is used to match the

burnup steps with the thermal conductivity steps for operational temperature calculations.

Table 1: The oxide layer thickness as a function of fuel meat fission density.

Fission density (fissions/cm^3)	Oxide Layer Thickness (μm)
0	0.00
1.49E+20	5.56
2.35E+20	7.19
3.34E+20	8.73
4.37E+20	10.37
5.33E+20	11.57
9.44E+20	15.76
1.34E+21	18.49
1.65E+21	20.21
1.92E+21	21.26
2.24E+21	22.24
2.56E+21	22.93
2.83E+21	23.48
3.12E+21	23.93
3.36E+21	24.22
3.50E+21	24.29

The oxide layer thickness at zero burnup is assumed to be zero (no oxide layer formation before operation), although some claddings have a pre-film of the protective oxide layer (of around 5 μm) [1].

The data is obtained at outer cladding temperature of 110^{o}C and a heat flux of 200 W/cm^2. The uncertainty of the oxide layer thickness growth is ± 10% according to ref [15].

3.6. Operational temperature of fuel meat calculations

After obtaining all the required parameters and values for the operational temperature calculations of fuel meat, equations (3) and (4) were used to calculate the operational temperature at different surface heat flux ranging from 100 W/cm^2 to 400 W/cm^2. The results of temperature calculations as a function of fuel meat fission density are shown in Fig. 1.

After obtaining all the required parameters and the uncertainty ranges of thermal conductivity of fuel, heat flux, heat transfer coefficient, fuel meat thickness and the oxide layer thickness, the final goal is to get the distribution of temperatures or upper and lower bounds through the combined uncertainty analysis described in the next section.

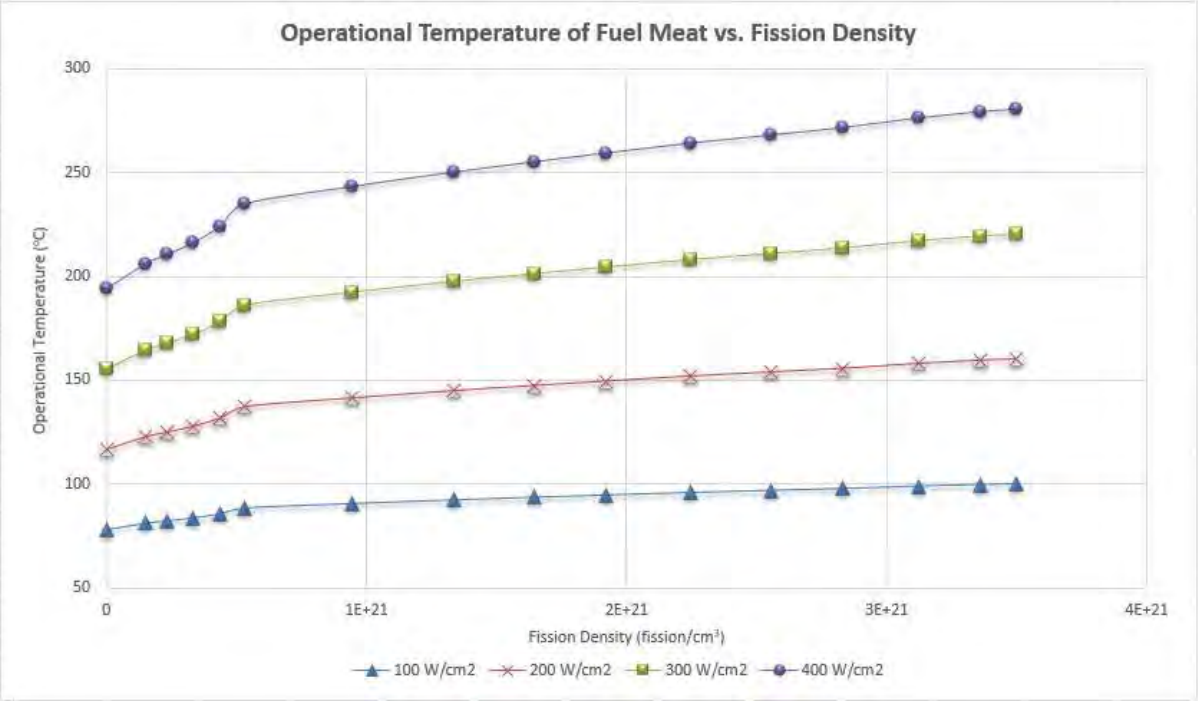

Fig. 1: Operational Temperature of U-Mo/Al Fuel as a function of fuel meat fission density.

4. Combined uncertainty in fuel temperature

The final goal of this work is to get the temperature distribution of upper and lower bounds based on the values of uncertainty of thermal conductivity of fuel, heat flux, heat transfer coefficient, fuel meat thickness and the oxide layer thickness.

The operational temperature of the fuel meat discussed in section 3.6 includes the temperature at four different heat fluxes, for the combined uncertainty analysis, one value of the heat flux is chosen to be 200 W/cm^2 to evaluate the effect of uncertainty values on the operational temperature.

To evaluate the combined effect of all these parameters on the operational temperature distribution, the root of sum of squares (RSS) method is used since these parameters are changing independently [17].

RSS is used and acceptable to combine uncertainties that are independent from each other, and after studying the effect of each parameter on the operational temperature, RSS method is valid to be used assuming that the parameters are independent.

The root of sum of squares (RSS) method, represented as follows [17]:

$$P = P_{base} + Root\left(\sum_i (P_i - P_{base})^2\right) \ldots (5)$$

where:

- P: The combined uncertainty effect of all parameters.
- P_{base}: Operational temperature value of the base model.
- P_i: Operational temperature value after changing a parameter.

Fig. 2 shows the operational temperature distribution as a function of burnup when applying the upper and lower bounds with respect to the base case operational temperature of the fuel meat.

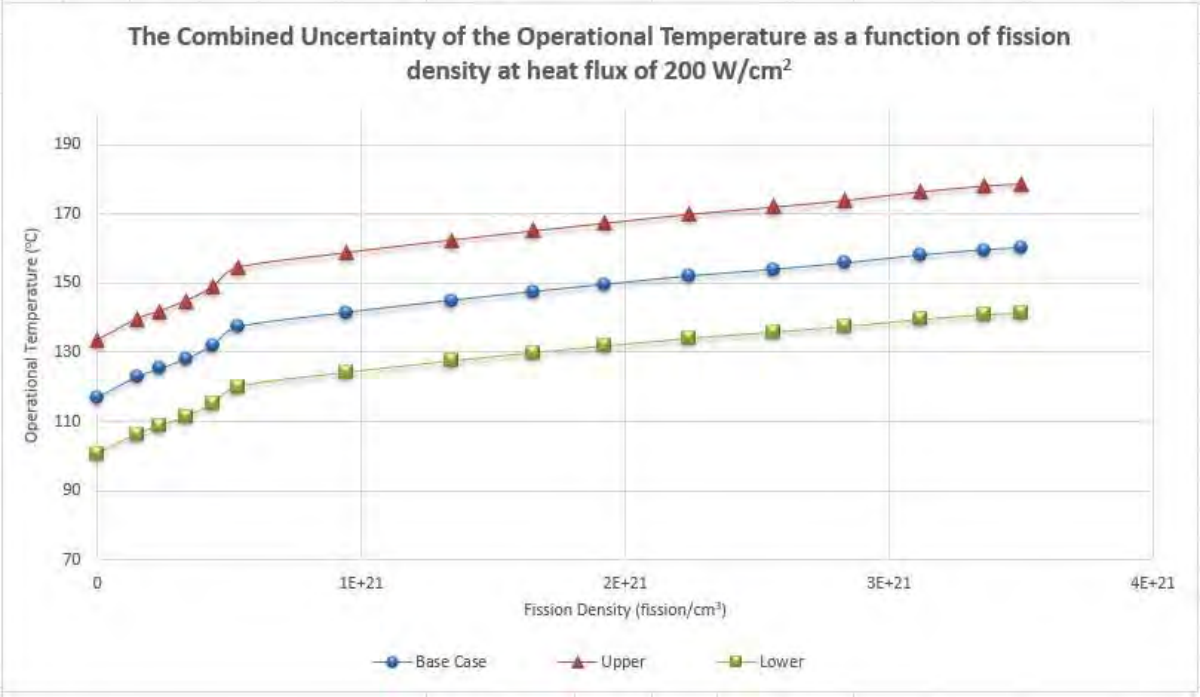

Fig. 2: Operational Temperature Variations of U-Mo/Al Fuel as a function of fuel meat fission density when applying the upper and lower uncertainty bounds compared to the base case.

5. Discussion

The uncertainty analysis results show that the parameter that has the highest impact on the operational temperature of the fuel is heat transfer coefficient, due to its high uncertainty and its direct relation with the cladding outer temperature, ΔT of applying the upper and lower bounds is the highest among all the parameters (27.51°C) and it is constant with increasing burnup.

Fuel meat thickness has the second highest influence among the parameters with a ΔT of 13.05 ^{o}C upon applying the upper and lower bounds of uncertainty. In addition, Heat flux uncertainty shows a higher influence than the oxide layer thickness and the thermal conductivity of fuel as they increase with burnup, the oxide layer thickness has a small effect as ΔT is 4.32 at a fuel meat fission density of 3.50E+21 fissions/cm^{3}.

The parameter that has the lowest impact on the operational temperature is the thermal conductivity of the fuel. It has a ΔT of 2.81^{o}C at the highest burnup value of 3.50E+21 fissions/cm^{3}.

The combined uncertainty results show that when applying all the parameters' uncertainties, the influence on the value of the operational temperature is 16.58^{o}C at the beginning of life and it increases as the burnup increases to reach 18.74^{o}C at a fuel meat fission density of 3.50E+21 fissions/cm^{3}. As a result, these parameters can be used to evaluate the performance of U-Mo/Al fuel depending on which parameter has a high impact on the operational temperature. Fig. 2 shows the results of the combined uncertainty calculations of all the parameters.

Other parameters uncertainties can also be included to evaluate the performance more accurately such as the interaction layer (IL) thermal conductivity, heat flux dependent thermal conductivity and heat flux dependent oxide layer thickness studies.

6. Conclusions

In this study, uncertainty and combined uncertainty studies have been carried out to evaluate the uncertainty of the parameters affecting the operational temperature of U-Mo/Al fuel. The uncertainties related to the thermal conductivity of fuel meat, which consists of the effects of thermal diffusivity, density and specific heat capacity, the interaction layer (IL) that forms between the dispersed fuel and the matrix, fuel plate dimensions, heat flux, heat transfer coefficient and the outer cladding temperature were considered.

After obtaining all the uncertainty values of the required parameters, the thermal conductivity of fuel meat as a function of burnup has been used alongside with the oxide layer growth to evaluate the operational temperature of fuel meat.

The combined uncertainty study using RSS method evaluated the effect of applying all the uncertainty values of all the parameters on the operational temperature of U-Mo/Al fuel. The overall influence on the value of the operational temperature is 16.58^{o}C at the beginning of life and it increases as the burnup increases to reach 18.74^{o}C at a fuel meat fission density of 3.50E+21 fissions/cm^{3}.

Further studies are needed to evaluate the behavior more accurately by including other parameters uncertainties such as the interaction layer thermal conductivity.

Other uncertainties related to heat flux dependent thermal conductivity owing to interaction layer growth, will give more detailed and accurate results for the evaluation of the operational temperature of U-Mo/Al fuel.

Acknowledgments

This study was supported by Ministry of Science, Information and Future Planning (NRF-2015M2C1A1027541) and by the KUSTAR-KAIST Institute, KAIST.

7. References

[1] D.E. Burkes et al., "A model to predict thermal conductivity of irradiated U-Mo dispersion fuel", Journal of Nuclear Materials (2016), doi: 10.1016/j.jnucmat. 2016.01.012.

[2] Y.S. Kim et al., "Thermal conductivity modeling of U-Mo/Al dispersion fuel", Journal of Nuclear Materials 466 (2015) 576-582

[3] D.E. Burkes et al., "Thermal properties of U–Mo alloys irradiated to moderate burnup and power", Journal of Nuclear Materials 464 (2015) 331–341

[4] IAEA-TECDOC-1496, "Thermophysical properties database of materials for light water reactors and heavy water reactors", Final report of a coordinated research project 1999–2005, June 2006

[5] D.E. Burkes et al., "Fuel Thermo-physical Characterization Project: Fiscal Year 2014 Final Report" Office of Material Management and Minimization, PNNL-24135, March 2015

[6] B. Hay et al. "Uncertainty of Thermal Diffusivity Measurements by Laser Flash Method", International Journal of Thermophysics, Vol. 26, No. 6, November 2005

[7] https://www.nde-ed.org/GeneralResources/Uncertainty/Combined.htm

[8] T.K. Huber et al., “The thermal properties of fresh and spent U-Mo fuels: An overview”, RRFM 2015 conference proceedings, pp. 92-103

[9] H.J. Ryu et al. "Performance evaluation of U-Mo/Al dispersion fuel by considering a fuel-matrix interaction." Nuclear Engineering and Technology 40.5 (2008): 409-418.

[10] Y.W. Tahk et al., “Fuel performance evaluation of mini-plate irradiation test of U-7Mo dispersion fuel for KJRR”, IGORR conference proceeding, 2013

[11] D. Jo, and H. Kim. "Safety assessment of U–Mo fuel mini plates irradiated in HANARO reactor." Annals of Nuclear Energy 81 (2015): 219-226.

[12] J.M.Park, “Current Status of and Progress toward Eliminating Highly Enriched Uranium Use in Fuel for Civilian Research and Test Reactors”, the National

Academies of Science, Engineering, Medicine, June 24-26, 2015, Oak Ridge, Tennessee.

[13] NUREG-1313, ” Safety Evaluation Report related to the Evaluation of Low-Enriched Uranium Silicide-Aluminum Dispersion Fuel for Use in Non-Power Reactors”, USNRC, July 1988.

[14] W. L. Woodruff, “Evaluation and selection of hot channel (peaking) factors for research reactor applications” ANL/RERTR/TM-28, Feb 1997.

[15] Y.S. Kim et al.," Oxidation of aluminum alloy cladding for research and test reactor fuel.” Journal of Nuclear Materials 378 (2008) 220–228

[16] S. Van den Berghe, and P. Lemoine. "Review of 15 years of high-density low-enriched U-Mo Dispersion fuel development for research reactors in Europe." Nuclear Engineering and Technology 46.2 (2014): 125-146.

[17] F. Scholz, “Tolerance Stack Analysis Methods”, Boeing Information & Support Services, University of Washington, December 1995.

PIE ANALYSES OF U-MO/AL DISPERSION FUEL WITH DIFFERENT U-MO PARTICLE SIZES

H.J. RYU, Q.M. MISTARIHI

Department of Nuclear and Quantum Engineering, KAIST
Yuseong-gu, Daejeon 34141, Republic of Korea

K.H.LEE, Y.J. JEONG, Y.H.JUNG, B.O.YOO, J.M. PARK

Korea Atomic Energy Research Institute
Yuseong-gu, Daejeon 34057, Republic of Korea

ABSTRACT

The effects of the fuel particle size in U-Mo/Al dispersion fuel were investigated by analyzing the post-irradiation examination results from a series of KOMO irradiation tests at HANARO. Most fuel particles in dispersion fuels fabricated by conventional powder metallurgy processing have been less than 125 μm. It is well known that using a large-sized fuel particle is more beneficial for fuel performance due to the limited fuel-matrix interaction. However, the fuel performance analyses have not been correlated systematically with the irradiation behavior of U-Mo/Al dispersion fuel samples with different particle sizes. The interaction and swelling behavior of the irradiated samples were evaluated from PIE results to demonstrate the benefit of the use of large-size fuel particles for dispersion fuel.

1. Introduction

The dispersion type fuel for research reactors consists of fuel particles dispersed in the pure Al matrix (fuel meat) and covered with an Al alloy cladding. Conventionally, intermetallic compound particles such as U_3Si_2 are mixed with aluminum powder to form the dispersion fuel. Plate-type fuel elements can be fabricated easily by using the powder mixture. The volume fraction of fuel particles was determined by the fuel element specification to satisfy the designed fissile material content. Although it is considered U_3Si_2/Al up to 6.0 g-U/cm^3 can be fabricated [1], the maximum volume fraction which allows the production of fuel elements without much difficulty is seen as less than 45 vol%.

Therefore, for low-enrichment uranium (LEU) fuel with uranium enrichment of 19.75 wt%, the standard uranium density has been 4.8 g-U/cm^3 [2]. The volume fraction of U_3Si_2/Al dispersion fuel is approximately 42.5 vol%, because the uranium density of U_3Si_2 is 11.3 g/cm^3 [3]. When U_3Si_2 particles were fabricated by mechanical pulverization using jaw crushers, hammer mills or ball mills, the size distribution the powder was controlled to facilitate homogeneous deformation during rolling.

Although the average particle size has not been defined according to NUREG-1313 [2], the maximum allowable particle size is between 125 and 150 μm. The recommended allowable amount of fine particles less than 40-44 μm is up to 50wt%. Generally, the quantity of fine particles is between 18 to 40wt%. While there has been no fuel performance issue with the fuel particle size for U_3Si_2/Al dispersion fuel, some fabricators prefer to limit the maximum particle size as fine as 90 μm to enhance the homogeneity of the thickness and density of fuel meat.

The Reduced Enrichment for Research and Test Reactors (RERTR) program aims to replace highly-enriched uranium (HEU) fuel with low-enriched uranium (LEU) fuel to improve the proliferation resistance regarding research reactors. In order to replace HEU with LEU, the low enrichment needs to be compensated with a high U-loading through using a high U-density fuel. Among the proposed high U-density LEU fuels, U-Mo fuel is a promising candidate due to good irradiation stability [4].

The development of U-Mo fuel has been initiated to replace HEU-fueled high-performance research reactors because the uranium density of U-Mo alloys is much greater than that of U_3Si_2. However, the mechanical properties of U-Mo alloys are significantly different from U_3Si_2, particularly regarding the brittleness. Owing to the toughness of U-Mo alloys, the conventional crushing or milling methods cannot be applied to produce U-Mo powder. Although hydriding-milling-dehydriding (HMD) can be used to pulverize U-Mo ingot [5], current engineering-scale production of U-Mo powder relies on a centrifugal atomization technique [6]. In the centrifugal atomization process, spherical U-Mo particles are formed by pouring U-Mo melt over a rotating disk and solidification of the melt droplets spread by the centrifugal force in the chamber. The dispersion type fuel presents a higher thermal conductivity than monolithic type fuel due to the presence of the high thermal conductivity Al matrix.

While the performance of U-Mo fuel was successfully proven for several low heat flux irradiation tests, the severe chemical interaction between U-Mo and Al induced unacceptable breakaway swelling at high heat flux tests [7]. Even during the fabrication of the dispersion type fuel an interaction layer (IL) is formed due to the inter-diffusion between the U-Mo fuel particles and the Al matrix, which is an intermetallic compound $(U,Mo)Al_x$ [8]. During irradiation, the IL becomes amorphous causing a further decrease in the thermal conductivity and an increase in the centerline temperature of the fuel meat [9].

Therefore, many technical solutions, such as Si addition to the matrix and protective coating of U-Mo particles, have been proposed to solve the performance issues of U-Mo/Al dispersion fuel. To reduce the interfacial reaction further, the use of large-sized U-Mo particles has been also proposed to have a smaller surface-to-volume ratio. Because large-sized U-Mo particles can be fabricated by controlling the atomization process, KAERI conducted the KOMO irradiation tests using the U-Mo/Al dispersion fuel with large-sized U-Mo particles. Although the post-irradiation examination (PIE) results of each irradiation test were reported respectively [10], a

comprehensive analysis of the effects of U-Mo particle size on the irradiation performance of U-Mo/Al dispersion fuel has not been presented. The purpose of this study is to compare the irradiation behavior of U-Mo/Al dispersion fuels with different U-Mo particle sizes by using the PIE data of previous KOMO irradiation tests.

2. Description of the KOMO Irradiation Tests using Large U-Mo Particles

The average size of U-Mo powder produced by controlling atomization parameters ranges from 50 μm to 500 μm approximately [6]. After the severe reaction between U-Mo and Al during irradiation was reported, U-Mo/Al dispersion fuel rods with different U-Mo particle sizes were fabricated to investigate the effects of the U-Mo particle size on the irradiation performance of U-Mo/Al dispersion fuel as listed in Table 1. The size-controlled U-Mo particles produced by centrifugal atomization by KAERI are shown in Fig. 1.

Irradiation Test	Fuel System (uranium density)	Standard U-Mo Size (μm)	Different U-Mo Size (μm)	EFPD (day)
KOMO-2	U-7Mo/Al (4.0 g-U/cm^3)	< 125	38 – 63 53 – 106	173
KOMO-3	U-7Mo/Al (4.5 g-U/cm^3)	N.A.	105 – 210 210 – 300 300 – 425	206
KOMO-4 KOMO-4	U-7Mo/Al (4.5 g-U/cm^3)	N.A.	105 – 210 210 – 300 300 – 425	132
	U-7Mo/Al-5Si (5.0 g-U/cm^3)	< 150	210 – 300	
KOMO-5	U-7Mo/Al-5Si (5.0 g-U/cm^3)	< 150	210 – 300	228

Table 1. KOMO Irradiation Tests using Different U-Mo Particle Sizes [10]

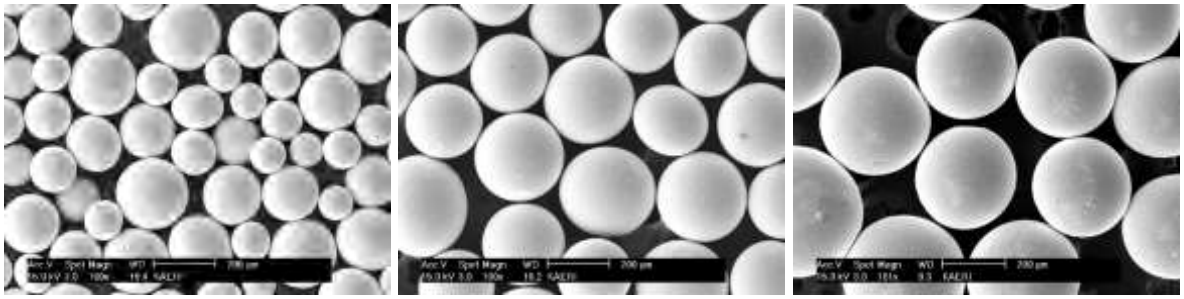

(a) (b) (c)

Fig. 1. Images of atomized U-Mo powder with the diameter range of (a) 105-201 μm (b) 210-300 μm (c) 300-425 μm used in the KOMO-3,-4 irradiation tests at HANARO.

3. Summary of PIE Results

The optical micrographs of U-7Mo/Al dispersion fuel rods with different U-Mo particle sizes present significant changes in the interaction as shown in Fig. 2. When very fine particles with a size range of 38-63 μm were used, the U-Mo particles in the dispersion fuel meat reacted fully with the Al matrix. No isolated U-Mo particles are shown in Fig. 2(a). All dispersion fuel meat was converted to IL. In the dispersion fuel rod with the particle size range of 53-106 μm, unreacted U-Mo particles and unreacted Al were remained as can be seen in Fig. 2(b).

From the KOMO-3 irradiation test, the U-Mo particle size was changed systematically by using the atomized particles with different sizes as shown in Fig. 1. Three U-Mo particle size ranges were used; 105-210 μm, 210-300 μm, 300-425 μm. The IL thickness and the fuel meat swelling measured after irradiation exhibited noticeable trends inversely related to the U-Mo particle size. As shown in Fig. 3 and Fig. 4, the IL thickness and the fuel meat swelling of U-Mo/Al dispersion fuel rods decreased with the increasing particle size.

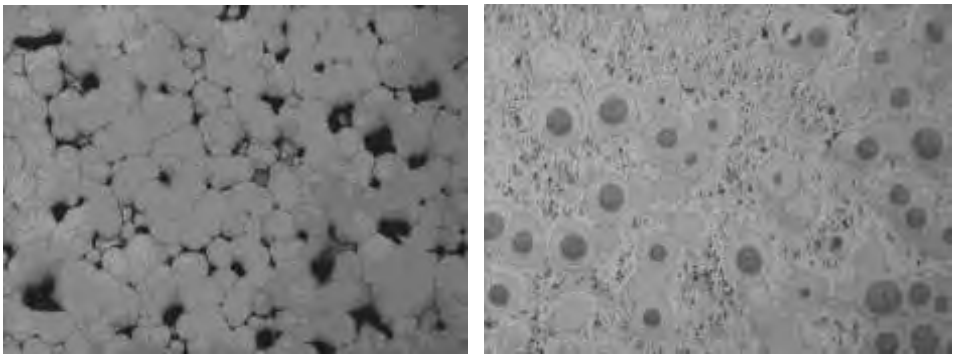

(a) (b)

Fig. 2. Post-irradiation microstructures of U-7Mo/Al dispersion fuel rods with the particle size range of (a) 38-63 μm and (b) 53-106 μm used in the KOMO-2 irradiation test at HANARO.

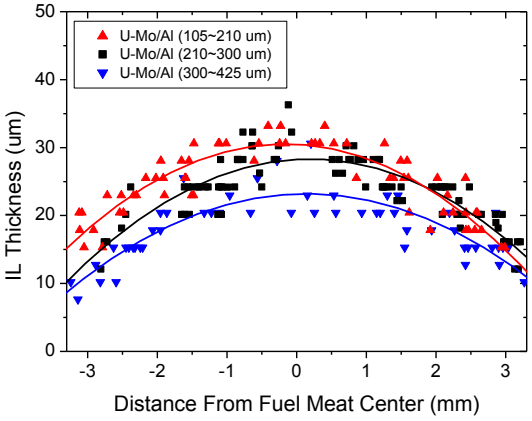

Fig. 3. The interaction layer thicknesses of U-7Mo/Al dispersion fuel rods with an average particle size of 105-210 μm, 210-300 μm, 300-425 μm used in the KOMO-3 irradiation test at HANARO [10].

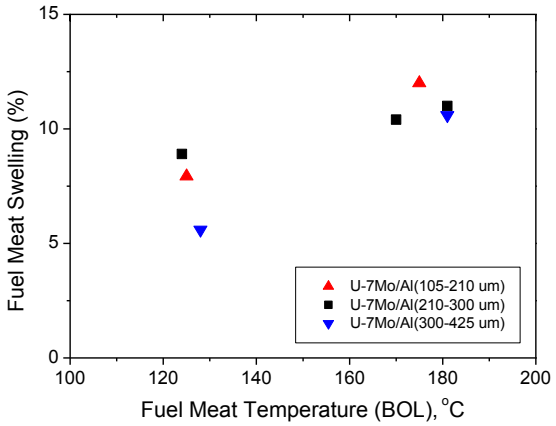

Fig. 4. The fuel meat swelling data of U-7Mo/Al dispersion fuel rods with an average size of 105-210 μm, 210-300 μm, 300-425 μm used in the KOMO-3 irradiation test [10].

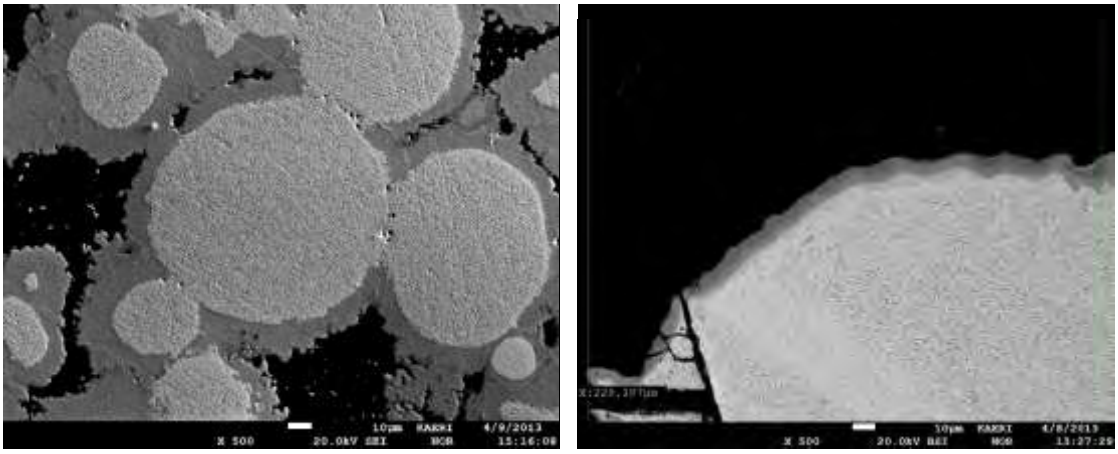

(a) (b)

Fig. 5. Post-irradiation microstructures of U-7Mo/Al-5Si dispersion fuel rods with the particle size range of (a) <150 μm and (b) 210-300 μm used in the KOMO-5 irradiation test at HANARO.

When the matrix was changed from Al to Al-5wt%Si, a similar relation between the IL thickness and the particle size could be observed in the KOMO-5 test. As presented in Fig. 5, U-7Mo/Al-5Si dispersion fuel with a U-Mo particle size range less than 150 μm and a different size range of 210-300 μm shows different IL thicknesses and IL volume fractions.

4. Discussion

The PIE results of KOMO irradiation tests demonstrated that U-Mo/Al dispersion fuel with larger fuel particles led to less interaction and less swelling. The irradiation performance of U-Mo itself is not a function of the fuel particle size if the grain sizes

of U-Mo particles are not so much different. Then, the interaction layer thickness and the fuel particle swelling should not be dependent on the average U-Mo particle size. Only the volume fraction of the interaction phase can be different as the interface-to-volume ratio changes [11].

One reason for reduced swelling for larger U-Mo particle-dispersed fuel can be the contribution of the interaction layers. If the density of interaction layers are smaller than the volume-averaged density of reaction constituents (i.e. U-Mo and Al), fuel meat swelling can occur as a result of the interaction. However, the precise density of the interaction phase has not been known, because of the complicated impacts of amorphization and accumulated fission products [12].

Another possible reason for reduced swelling is associated with the lower fuel meat temperature when larger U-Mo particles are used. It is because more volume fraction of the interaction phase decreases the thermal conductivity of dispersion fuel. As the Al matrix with a high thermal conductivity (~220 W/m-K) is consumed by the interaction, the thermal conductivity of fuel meat decreases. The thermal conductivity of the interaction phase is considered as low as approximately 10 W/m-K [13].

Once the fuel meat temperature is increased with the formation of the interaction phase, thermally activated processes such as interaction layer growth and fission gas bubble growth can be accelerated. Those enhanced interaction layer growth and gas bubble growth match the PIE results for dispersion fuel rods with smaller U-Mo particles.

The effects of fuel particle size on the fuel meat temperature can be simulated by using fuel performance codes if the fuel performance code can estimate the feedback of the IL growth and the fuel meat temperature. Cho et al. used the finite element method (FEM) to calculate the effects of particle size, shape, stereography on the thermal conductivity of U-Mo/Al dispersion fuel [14]. Hayes et al. reported PLATE code calculation results presenting the sensitivity of fuel-matrix interaction and fuel temperature to fuel particle size [15]. As the fuel particle diameter increases from 10 to 100 μm, the fuel temperature decreases from ~280^{o}C to ~170^{o}C. Ryu et al. calculated the centerline temperature for rod-type dispersion fuel as a function of U-Mo particle size from 40 μm to 200 μm [16]. When the particle size is 200 μm the centerline temperature is very stable compared to other fuels with smaller particle sizes. Because of the rod geometry, the centerline temperature of U-Mo/Al dispersion fuel was strongly dependent on the particle size. Burkes et al. also investigated the thermal conductivity modeling of U-Mo dispersion fuel [17]. It was found that the fuel meat thermal conductivity degradation is sensitive to fuel particle size. The IL thickness started to decrease at fuel particle size beyond 127 μm for the calculated beginning-of-life (BOL) fuel meat temperature of 185^{o}C. Ye et al. also simulated the fuel performance of RERTR-5, -6, -7., -9 and AFIP-1 tests with the different average fuel particle size ranging from 50 to 90 μm by using the DART computational code [18].

Even though the possible use of larger sized U-Mo particle will provide more stable irradiation performance of U-Mo/Al dispersion fuel, one of the remaining issues is related to fabrication quality assurance of fuel elements. When larger particles are adopted, the homogeneity of fuel meat may not meet the fuel specification. Therefore, further study to develop the advanced fabrication process with larger U-Mo particles is necessary to improve the U-Mo/Al dispersion fuel performance.

5. Conclusions

The PIE results from the KOMO irradiation tests at HANARO were analyzed to investigate the effects of the U-Mo fuel particle size on the fuel performance. The reduced IL formation by using the large U-Mo particles led to the decreases in the IL thickness and the fuel meat swelling. The modeling and computation provided the interpretation that the decreased IL thickness and the swelling were resulted from the reduced fuel meat temperature because the thermal conductivity of U-Mo dispersion fuel was directly impacted by the IL formation. In order to utilize the advantages of large-size U-Mo particles, modified fabrication processes with larger U-Mo particles should be investigated to improve the U-Mo/Al dispersion fuel performance.

Acknowledgments

This study was supported by Ministry of Science, Information and Future Planning (NRF-2015M2C1A1027541) and by the KUSTAR-KAIST Institute, KAIST. The authors acknowledge the contributions of C.K. Kim, D. B. Lee, S. J. Oh, E. S. Kim, S. C. Kweon, and S. J. Jang for the U-Mo/Al fuel fabrication.

References

[1] J.L. Snelgrove, Qualifications Status of 6-gU/cm^3 U_3Si_2 Dispersion Targets for ^{99}Mo Production. No. ANL/CSE-13/8. Argonne National Laboratory (ANL), 2013.

[2] NUREG-1313, ” Safety Evaluation Report related to the Evaluation of Low-Enriched Uranium Silicide-Aluminum Dispersion Fuel for Use in Non-Power Reactors”, USNRC, July 1988.

[3] J.L. Snelgrove, et al. "Development of very-high-density low-enriched-uranium fuels", Nuclear Engineering and Design, 178 (1997) 119-126.

[4] M.K. Meyer et al., “Low temperature irradiation behavior of uranium-molybdenum alloy fuel”, Journal of Nuclear Materials, 304 (2002) 221-236.

[5] E.E. Pasqualini et al. “Scaling up the production capacity of U-Mo powder by HMD process”, Proceedings of the International Meeting on RERTR, Bariloche, Argentina, November 3-8, 2002.

[6] C.K. Kim et al., “Use of centrifugal atomization process in the development of research reactor fuel”, Nuclear Engineering and Technology, 39 (2007) 617-626.

[7] A. Leenaers, Ann, et al. "Post-irradiation examination of uranium–7wt% molybdenum atomized dispersion fuel", Journal of Nuclear Materials, 335 (2004) 39-47.

[8] H.J. Ryu et al., "Reaction layer growth and reaction heat of U-Mo/Al dispersion fuel using centrifugally atomized powder", Journal of Nuclear Materials, 321 (2003) 210-220.

[9] S. Van den Berghe et al. "Transmission electron microscopy investigation of irradiated U–7wt% Mo dispersion fuel", Journal of Nuclear Materials, 375 (2008) 340-346.

[10] H.J. Ryu et al. "Post-irradiation analyses of U-Mo dispersion fuel rods of KOMO tests at HANARO", Nuclear Engineering and Technology, 45 (2013) 847-858.

[11] Y.S. Kim et al. "Modeling of interaction layer growth between U-Mo particles and an Al matrix", Nuclear Engineering and Technology, 45 (2013): 827-838.

[12] Y.S. Kim and G. L. Hofman. "Fission product induced swelling of U–Mo alloy fuel", Journal of Nuclear Materials, 419 (2011): 291-301.

[13] S.Nazare, G. Ondracek, and F. Thümmler. "Investigations on UAlx-Al dispersion fuels for high-flux reactors", Journal of Nuclear Materials, 56 (1975): 251-259.

[14] T.W. Cho et al. "Thermal conductivity of U–Mo/Al dispersion fuel: effects of particle shape and size, stereography, and heat generation", Journal of Nuclear Science and Technology, 52 (2015) 1328-1337.

[15] S.L. Hayes et al. "Modeling RERTR experimental fuel plates using the PLATE code", Proc. Int. Meeting on Reduced Enrichment for Research and Test Reactors (RERTR), Chicago, Illinois, USA, 5-10 October 2003.

[16] H.J. Ryu et al., “Performance evaluation of U-Mo/Al dispersion fuel by considering fuel matrix interaction”, Nuclear Engineering and Technology, 40 (2008) 409-418.

[17] D.E. Burkes et al. "A model to predict thermal conductivity of irradiated U-Mo dispersion fuel", Journal of Nuclear Materials, (2016).

[18] B. Ye et al. "DART Analysis of Irradiation Behavior of U-Mo/Al Dispersion Fuels", Nuclear Technology, 191 (2015): 27-40.

PRELIMINARY EVALUATION ON THE KJRR FUEL INTEGRITY

J.S.YIM, H.J.KIM, Y.W.TAHK, Y.H.KONG, J.Y.OH

Nuclear Fuel Design for Research Reactor, KAERI

Zip 34057, 111 Daeduok Daero 989 Beon-gi, Yuseong-gu, Daejon, KOREA

ABSTRACT

The KJRR (KiJang Research Reactor) has been under construction since April 2012 in the local government province of KiJang, located near Busan city, in a bid to self-sufficiently provide domestic radioactive isotopes and extend the silicon (Si) doping capacity for coping with the growing industrial power device market and utilizing scientific researches in the neutronics field in Korea. The driver fuel of the KJRR was selected as a U-Mo dispersion fuel, which would be the first kind of a U-Mo fuel in a research reactor ever. Through comprehensive surveillance of the fuel's in-reactor behavior, KAERI has determined a fuel meat of U-7%Mo/Al-5%Si. The KJRR has two kinds of fuel assemblies, 16 Standard Fuel Assemblies (SFAs) and 6 Follower Fuel Assemblies (FFAs), in the core. This paper deals with the design and preliminary evaluation of the fuel integrity of the basic designed KJRR fuels to determine whether it maintains its integrity during its intended reactor operations. It includes the bases of the design criteria and their limits.

1. Introduction

Through a thorough feasibility study on the newly construction of the KJRR, the construction project of the KJRR has launched [**1, 2**] aiming at overcoming the shortage of domestic Radio-Isotope (RI) supply, providing sufficient industrial demand on the neutron transmutation doping and facilitating the utilization of radio-isotope related researches. Since commencing the project, the conceptual design and basic design of the fuel have been completed, which were integrated in the preliminary safety analysis report (PSAR) [3] for being granted construction permit (CP) of the KJRR. As of the end of 2015, the first round of questionnaires are expected to be issued sooner or later by the regulator, KINS (Korea Institute of Nuclear Safety). The KJRR has the following features: an open-tank-in pool type reactor with a lower control rod drive mechanism. The reactor comprises 16 SFAs (Standard FAs) and 6 FFAs (Follower FAs), and thus 22 FAs in total in the core with 6 irradiation holes for the Mo-99 targets. The SFA and FFA as in Figure 1 have the same fuel configuration that stemmed from the similar structural concept of the JRTR FAs other than the fuel meat composition. The fuel meat of the KJRR has U-7Mo/Al-5wt%Si dispersion fuel with two different uranium densities, 8.0 g-U/cc for the 19 inner fuel plates and 6.5 g-U/cc for the two outer FPs. The initial core has three different lesser uranium densities of 5.2, 3.9, and 2.6 g-U/cc, respectively, to reach a fast equilibrium state. The main fuel design parameters are listed in Table 1.

This paper deals with the design and preliminary evaluation on the fuel integrity of the KJRR fuel to determine whether it will maintain its integrity during KJRR's intended operations. It focuses on the results of the preliminary safety analysis with some out-of-pile test results. The basic designed fuel will be finalized by demonstrating the integrity throughout comprehensive irradiation tests both in the HANARO irradiation tests with mini-plates and an LTA irradiation in the ATR in INL. The irradiation plans and status of the qualification with mini plates and an LTA were found in Reference [**4-7**].

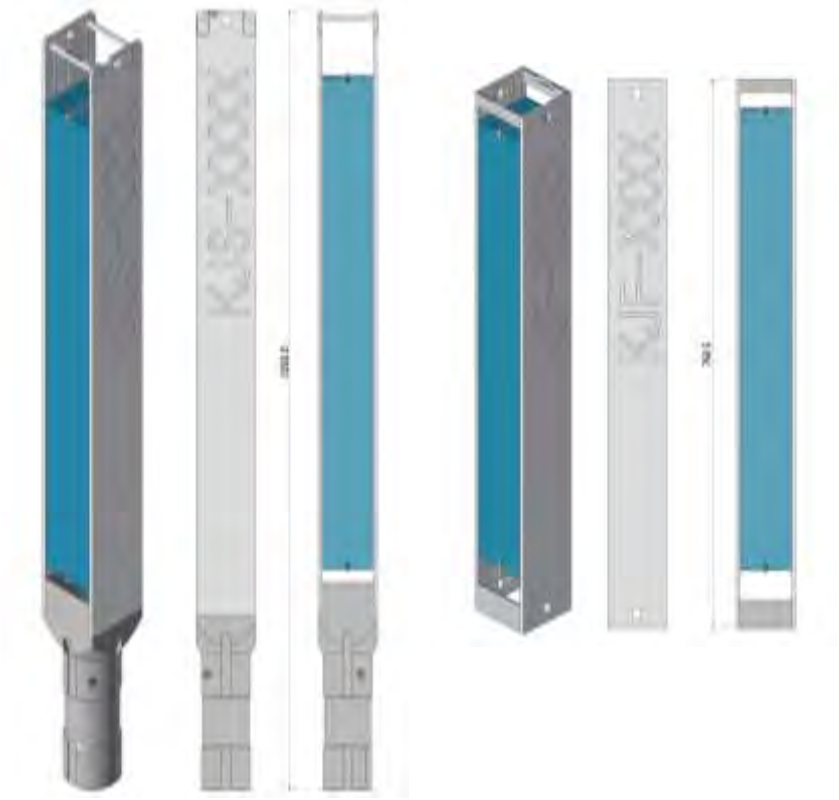

(a) Standard FA (b) Follower FA

Fig. 1 Configuration of KJRR fuels: SFA and FFA

Table 1 Main Fuel Design Paramteres

Parameters	Values
Fuel Meat	LEU less than 20 wt% U-235
	Meat : U-7wt%Mo dispersed in Al-5wt%Si matrix
	Meat dimension (mm) : 62.0 x 600 x 0.51
	Fuel Plate dimension (mm) : 70.7 x 640 x 1.27
Fuel Density	Inner(19)/outer(2) fuel plates(g-U/cm3) : 8.0/6.5
	Initial core (g-U/cm3) : 5.2/3.9/2.6
U 235 mass	FA (g) : 618.34
	FP (g) : 29.98(19 inner FPs)/24.36(2 outer FPs)
FA dimension	SFA (mm) : 76.2 x 76.2 x 1010
	FFA (mm) : 76.2 x 76.2 x 760.5
Material	cladding : Al-6061
	Structural : Al-6061 T6
FA Burnup	average 67.7% U-235 depletion (to be determined later)
Heat Flux(Nominal/maximum)	41.5/137 W/cm^2

2. Design of the KJRR fuel

The design of the KJRR fuel is mainly based on the concept of the JRTR fuel, which has U_3Si_2 dispersed in an aluminum matrix with 4.8 g-U/cc, while the fuel of the KJRR has U-7Mo fuel particles dispersed in an Al-5wt% Si matrix. The meat length of 600 mm in the KJRR fuel is shorter than that of the JRTR, which is 640 mm. The whole length of the KJRR standard fuel assembly is therefore very similar to that of the JRTR.
Basically, the design of the KJRR fuel follows the nuclear safety review guidelines **[8]** in Korea, which mainly refers to NUREG 1537 part 2 [**9**], along with some recently implemented IAEA safety guidelines of NS-R-4 [**10**], and finally, a restructuring and revision reflecting the contents of the SSG-20 [**11**]. In the design of the research reactor fuel, it shall fully comply with the following regulation requirements stipulated in the technical standards for nuclear reactor facilities [**12**] under the Korea Nuclear Safety Act [**13**]. In compliance with the regulation and guidelines [8-11], the design requirements of the FAs in the RRs selected for the operation conditions are as follows: The fuel system shall not be damaged during normal operation and AOO (Anticipated Operational Occurrences). The fuel system damage is never so severe as to maintain a coolable geometry. The number of fuel plate failures shall not be underestimated for the postulated accidents.

2.1 Design Criteria

To ensure the fuel integrity under the intended operation conditions, the fuel design criteria for non-operation including the shipping and handling of FAs, normal operation, and AOO conditions were established. An evaluation of the fuel integrity was then performed to determine whether it satisfies the criteria. Based on the PWR design practices, which have been conducted in Korea, only SSE and LOCA events among the DBAs (design basis accidents) caused by mechanical excitation on the fuels were normally included in the chapter on the fuel design. Meanwhile, for the fuel behaviors under other DBAs, they are dealt with in a separate chapter on a safety analysis in the SAR (safety analysis report).

2.1.1 Design criteria related to fuel performance

To minimize excessive fuel swelling that might cause an undue narrowing of the flow channel between fuel plates, the maximum fuel temperature is set to be less than 200℃ during normal operation conditions. To prevent the fuel from the occurrence of blisters, the temperature shall be less than 400℃ under AOO conditions. The temperature difference across the oxide thickness on the cladding is limited to be less than the spallation temperature of 114℃ to eliminate a possible oxide spallation, which may cause damage to the cladding surface.

2.1.2 Design criteria related to the FA structural integrity

1) Stresses in the non-operation, normal operation, and AOO conditions
During non-operation including fuel handling and transportation, normal operation and AOO conditions, the fuel structural integrity shall be maintained [14].
The stress categories and stress criteria on the FAs established using ASME Sec. III **[15**] as a guide have been successfully applied **[16-18]** in the design of the Korean PWR FAs. However, it has not been well defined for the stress categories and stress criteria for the FAs in research reactors. In a similar way as the FAs in Korean PWR FAs, the stress categories and stress criteria of the FAs for research reactors are set using the KEPIC MN **[19]** (or an equivalent of ASME Sec. III) as a guide, and the stress intensity values of the structural material used in the FAs are presented as follows:
The design stress limits for non-operation and normal and AOO conditions are set as the design criteria to prevent a structural failure owing to excessive stress. For the design limit, the stress intensity limit shall not exceed the design stress intensity value, S_m, for the primary membrane stress,

and 1.5 S_m for the primary membrane stress plus primary bending stress. The primary membrane stress, plus primary bending stress, plus secondary stress shall not exceed 3 S_m. The average primary shear stress shall not exceed 0.6 S_m.

2) Stresses in the design base accidents

The SSE and LOCA events are considered as design base accidents in the FA design to secure a coolable geometry of the FAs. To avoid the loss of coolable geometry of the FAs during a dynamic load occurring as a consequence of the SSE events, the design criteria of the stress are specified in the seismic analysis.

The design criteria and design limit established from the guidance of the KEPIC MNZ (or an equivalent of ASME Sec. III Appendix F) for the stresses during an accident are summarized as the design criterion: A coolable geometry should be maintained during an accident. As for the design limit, the stress intensity limit shall be less than 2.4 S_m or 0.7 S_u for the primary membrane stress, and 3.6 S_m or 1.05 S_u for the primary membrane stress plus primary bending stress. Here, S_u is the ultimate tensile strength. In the KJRR, the mechanical loads from the LOCA on the FA is evaluated as negligibly small so that the LOCA or its combination with the SSE is excluded in the FA structural integrity.

3) Vibration

The resonance vibration of the FAs with respect to the coolant pump blade passing frequency as well as undue vibration of the fuel plate due to coolant flow shall be avoided. The coolant flow velocity obtained using equations **[20-21]** were used for the assessment of the critical flow velocity.

3. Evaluation on the fuel integrity

Ensuring the fuel safety and maintaining the structural integrity of the fuel are the ultimate goal of the fuel design. With respect to the eternal goal of the fuel design, safety and maintaining the fuel integrity were evaluated to determine whether they satisfy the design criteria. The preliminary evaluation results will be updated in accordance with the fuel design progresses, which will finally be demonstrated through irradiation tests and PIEs of the LTA and HAMPs mini-plates.

The KJRR fuel plates are subject to being burned up to average burnup of 67.7% of U-235 depletion. The calculated maximum fuel temperature is less than the design limit so that excessive fuel swelling can be ruled out. Under the AOO condition, the maximum fuel temperature was estimated to be below the design limit so that blistering can be avoided. Oxidation layer build up was estimated using the most updated model by Kim and Hofman **[22]**. The temperature difference across the calculated oxide layer was below the design limit, and thus the possibility of oxide spallation is expected to be eliminated.

An evaluation of the structural integrity of the fuel for non-operation, normal operation, and the AOO conditions were conducted to determine whether they satisfy the criteria. During fuel handling and transportation, the FA is subject to external loads imposed by acceleration or deceleration. The stresses on the FA are calculated using a load of 6g (gravitational acceleration), which is an equivalent load as in the case of the FA for the Korean PWR FAs, which were shown to be far less than the criteria such that the integrity of FAs will be maintained. For the normal operation and AOO conditions, the stresses were also shown to be below the design limits such that the FA structural integrity can be maintained. During the SSE, the stresses on the FA were calculated using the pseudo time dependent grid plate motion obtained from the mechanical reactor design. The stresses during and after the SSE are far less than the design criteria such that the FA structural integrity can be maintained during and after the SSE.

The resonance vibration of the FA due to the coolant pump blade passing frequencies was evaluated, and the results showed that the resonance vibration of the FAs with respect to the pump blade passing frequencies is expected not to occur. A vibration test with a dummy fuel assembly under a coolant flow was conducted and showed that undue vibrations did not occur during normal operating flow conditions. The critical coolant flow velocity was calculated using equations **[20-21]**, and was less than the KJRR coolant flow in the flow channel between fuel plates. Thus, an unstable fuel plate

vibration is expected to not occur.

4. Conclusion

The results of a preliminary evaluation on the fuel integrity of the KJRR were presented. The evaluation is composed of two categories: one for the fuel performance aspect and the other for the mechanical structural aspect. The relevant design criteria were established to secure the fuel integrity for the intended reactor operation conditions. Swelling, blistering, and oxidation criteria were set from a fuel performance point of view, and stresses and vibration were taken into consideration in the structural design criteria. An evaluation of the FA structural integrity during the shipping and handling of the FA were included with the same stress criteria as those under normal operation. The preliminary evaluation results showed that the fuel integrity during the intended operation of the KJRR as well as a non-operational load such as the shipping and handling of the FA will be maintained.
After confirmation of the fuel integrity and its performance through comprehensive irradiation tests of the LTA and mini-plates, the basic design of the KJRR fuel will be finalized and the results will be updated.

References

[1] I.C.Lim, et. Al, Current Status and prospect of Research Reactor utilization in Korea
[2] S.I.Wu, Status of the KJRR Construction Project, Daejeon, IGORR-2013, Oct. 2013
[3] KJRR Preliminary Safety Analysis Report, 2014.11
[4] J.S.Yim, et al., test Plan for mini plates Irradiation and PIE for U-7Mo fuel Qualification, RRFM 2014, Leubuljana, Slovenia
[5] J.S.Yim, et.al, KJRR Fuel (U-7Mo) Qualification plan and its status, RERTR-2016, Seoul, Korea
[6] Y.W. Tahk, H.M. Kim, J.Y. Oh, B.H. Lee, H.J. Kim, J.M. Park, K.H. Lee, Y.J. Jeong and J.S. Yim, "Mini-plate irradiation test and non-destructive analysis of U-7Mo dispersion fuel for KJRR fuel qualification", RRFM 2015, Bucharest, Romania, 19 - 23 April 2015.
[7] Y.W.Tahk et al, Results of HAMP-1 PIE, Seoul Korea, RERTR-2015 (to be presented)
[8] KINS/GE-N10, Vol.2 Nuclear safety review guideline for Research and Training Reactors, KINS, 2014.12
[9] NUREG-1537 Part 2, Guidelines for Preparing and Reviewing Applications for the Licensing of Non-Power Reactors: Format and Content, USNRC, 1996
[10] IAEA, Safety Requirements No. NS-R-4, Safety of Research Reactors, 2005
[11] IAEA, Specific Safety Guide No. SSG-20, Safety Assessment for Research Reactors and Preparation of Safety Analysis Report, 2012
[12] Enforcement Regulation No 13. Technical standards for nuclear reactor facilities, etc., Nuclear Safety and Security Commission, Korea
[13] Korea Nuclear Safety Act, 2014.11.
[14] J.S.Yim, H.J.kim, J.Y.Oh, Y.W.Tahk, B.H.Lee Stress Criteria of Fuel Assembly for structural Integrity in a research reactor
[15] ASME Boiler and Pressure Vessel Code, Section III, 2004, The American Society of Mechanical Engineers.
[16] Final Safety Analysis Report (FSAR), Kori Unit 1, 2, 3 and 4, Korea Electric Power Cooperation
[17] Final Safety Analysis Report (FSAR), Uljin Unit 1, 2, 3 and 4, Korea Electric Power Cooperation
[18] Final Safety Analysis Report (FSAR), Youngkwang Unit 1, 2, 3 and 4, Korea Electric Power Cooperation
[19] Korea Electric Power Industry Code (KEPIC), MN, 2005, Korea Electric Association.
[20] D.R.Miller, Critical Flow velocities for collapse of reactor parallel-plate fuel assembly, KAPL-1954, AEC research and Development Report, Aug. 1958
[21] Carlos Alberto de Oliveira1 and Miguel Mattar Neto, Flow Velocity Calculation to Avoid Instability in a Typical Research Reactor Core, 2011 Int. nucl. Atlantic conference - INAC2011, 2011, Oct.

[22] Yeon Soo Kim, G.L. Hofman, A.B. Robinson, J.L. Snelgrove, N. Hanan, Oxidation of aluminum alloy cladding for research and test reactor fuel, Journal of Nuclear Materials, Vol. 378, p. 220, 2008.

US PROGRESS ON PROPERTY CHARACTERIZATION TO SUPPORT LEU U-10 MO MONOLITHIC FUEL DEVELOPMENT

JAMES I. COLE, BARRY H. RABIN, JAMES A. SMITH, CLARK L. SCOTT, BRADLEY C. BENEFIEL, ERIC D. LARSEN, PAUL R. LIND, DAVID A. SELL
Nuclear Fuels and Materials Division, Idaho National Laboratory
PO box 1625 MS 3818, Idaho Falls, ID 83415-3818, USA

ABSTRACT

The US High Performance Research Reactor program is pursuing development and qualification of a new high-density monolithic LEU fuel to facilitate conversion of five higher power research reactors (ATR, HFIR, NBSR, MIT and MURR) and one critical facility (ATR-C) located in the US. In order to support fabrication development and fuel performance evaluations, new testing capabilities are being developed to evaluate the properties of fuel specimens. Residual stress and fuel-cladding bond strength are two characteristics related to fuel performance that are being investigated. In this overview, new measurement capabilities being developed to assess these characteristics in both fresh and irradiated fuel are described. Progress on fresh fuel testing is summarized and on-going hot-cell implementation efforts to support future PIE campaigns are detailed. It is anticipated that benchmarking of as-fabricated fuel characteristics will be critical to establishing technical bases for specifications that optimize fuel fabrication and ensure acceptable in-reactor fuel performance.

1. Introduction

To support the U.S Department of Energy (DOE), National Nuclear Security Administration (NNSA) mission to reduce the threat posed by the civilian use of highly enriched uranium (HEU) worldwide, the US High Performance Research Reactor (USHPRR) fuel development (FD) program is pursuing development and qualification of a new high-density monolithic U-Mo fuel to facilitate conversion of five higher power research reactors (ATR, HFIR, NBSR, MIT and MURR) and one critical facility (ATR-C) located in the U.S. from HEU to low enriched uranium (LEU). These reactors require higher uranium fuel density than is achievable with dispersion fuel systems used to convert lower power research reactors. The down selected fuel system consists of U-10Mo alloy fuel foils having a thin Zr diffusion barrier interlayer, clad in 6061 Al alloy by hot isostatic pressing (HIP) [1]. Fabrication process development activities are assessing methods to produce the U-Mo foil, apply the Zr barrier foil and optimize HIP strategies to maximize uranium utilization and minimize overall cost. Baseline knowledge of the stresses developed in the fuel plate constituents as well as the strength of the bond interfaces will be important to understanding how fabrication parameters influence fuel performance.

In order to support fabrication development, fuel performance evaluations, generic fuel qualification through the Nuclear Regulatory Commission (NRC), and eventual reactor licensing, a series of irradiation experiments and testing campaigns are being planned. The tests are designed to provide data needed for fabrication process down selection, to establish acceptable fuel performance under normal operating conditions and anticipated transients, and to demonstrate successful scale-up to prototypic reactor-specific fuel element designs. Materials property characterization data considered in the scope of this fuel development effort include mechanical strength of the individual fuel plate constituents, strength and quality of interfacial bonds between the plate layers and residual stresses

developed during fabrication. The same data is needed for the as-irradiated fuel plates to confirm adequate fuel performance and make adjustments to fabrication methods if necessary. This paper describes efforts to develop two specific testing techniques to evaluate the relationship between fabrication variables and fuel performance, and provide needed materials properties data to improve the fidelity of fuel performance models being developed for the US-HPRR FD program. Following a brief overview of the specific techniques for residual stress and bond strength and their implementation in the hot-cell environment, a discussion on the implications the collected data will have on meeting fuel performance requirements is presented.

2. Materials Properties Testing Techniques

2.1 Residual Stress

Monolithic fuel plates are effectively a layered composite system composed of materials with differing mechanical and thermal properties and constrained interfaces. Residual stresses can form as a result of thermo-mechanical processing due to these differing properties, in particular, as a result of cooling from the HIP processing temperature [2]. Tensile and compressive stresses through the thickness of the part ultimately have to balance, so large compressive stresses in one layer will, by necessity, induce large tensile stresses in another. If these stresses exceed the ultimate tensile strength of the material, component failure can result.

Fuel performance modeling results suggest pre-irradiation residual stresses from fabrication do not significantly influence irradiation performance because these stresses are relaxed very quickly during initial irradiation. However, post-irradiation residual stresses (developed during reactor shutdown) are believed to play an important role in causing fuel failures at high burnup [3]. It is also important to understand if the proposed alternate fabrication processes, i.e. application of Zr by electroplating or plasma spraying, have an effect on the post-irradiation stress state.

A variety of techniques can be employed to measure residual stresses in as-fabricated, unirradiated fuel plates and many of these techniques are non-destructive. For example, monolithic fuel plates have been examined using diffraction techniques [4]. In general, these methods cannot be readily implemented in a hot-cell environment for use on irradiated fuel specimens.

The US-HPRR FD program has explored alternate methods of measuring residual stresses. Several destructive measurement techniques are available and, of these, the incremental slitting or crack compliance technique developed at Los Alamos National Laboratory seemed the most amenable to hot-cell adaptation [5]. This technique uses incremental slitting of the plate and measures the deflection to calculate the residual stress. Typically, in non nuclear applications, the slits are made with electric discharge machining [6] and deflections are measured using strain gauges. However, due to the need to operate the system remotely, the method has been adapted to facilitate hot cell deployment. The EDM slitting has been replaced by a small milling tool, and the strain gauges been replaced by non-contacting displacement transducers. The schematic shown in Figure 1 shows a simplified version of the setup with all of the essential elements.

The measurement is made by clamping the fuel plate on one end vertically, then milling a slit across the width of the plate. As the residual stress is relaxed, the end of the plate opposite the clamp will deflect, and the extent of deflection is measured by the transducer. The direction of the deflection will be dictated by the nature of the residual stress, tensile or compressive. The milling tool depth is incremented (~10 microns for this application) and another slit is made. In this manner a 1-D through plate profile of residual stress can be mapped. Of particular interest is the extent of the stress that develop at the interfaces

between the cladding, Zr barrier layer and the U-Mo fuel, and how these stresses relate to bond strength.

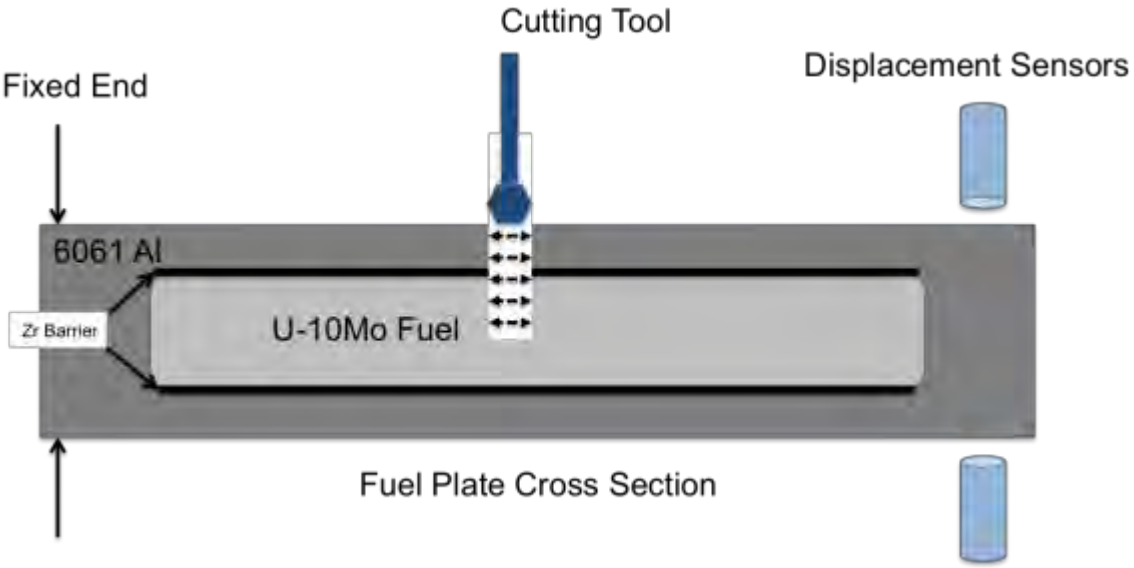

Figure 1 Schematic of slitting residual stress measurement system.

In order to be effectively utilized for testing of highly irradiated fuel plates, the equipment has to be adapted from its conventional configuration, to a configuration that can be readily used inside of a hot-cell with remote manipulators. The customized system being developed incorporates a heavy baseplate to reduce vibration, a clamping jig to hold the sample, displacement sensors and a cutting tool. The sensors and the cutting tool are fully motion controlled to allow precise positioning and calibration. Eddy current sensors were chosen for the displacement measurements, rather than capacitive displacement sensors, as they were deemed to be more robust in a high radiation environment.

Both this system and the bond strength system (discussed below) require installation of new feed-throughs into the Hot Fuels Examination Facility (HFEF) hot cell in order to provide instrument control and minimize the amount of materials that have to be introduced into the hot-cell to conduct the testing. The residual stress-system will have a footprint that can be accommodated within the HFEF containment box, which is an area separated from the main HFEF cell and kept at negative pressure. Operations that generate larger quantities of fines and debris such as cutting, grinding and polishing are frequently conducted in the containment box to minimize contamination levels in the rest of the cell.

2.2 Bond Strength

Acceptable interfacial bond strength between fuel and cladding will be critical to maintaining fuel integrity during irradiation. A variety of techniques can be used to measure bond strength (peel test, double cantilever test, bulge test, etc.) that require significant set-up and hands on sample manipulation. However, for the monolithic fuel plates being tested in a hot-cell, a customized laser shock/ultrasonic testing system has been developed by the INL, in partnership with the National Research Council of Canada Corporation (NRC). This system employs a non-contact method using a high power laser pulse to induce an acoustic shockwave in the test piece. The generated wave is a compressive shockwave and when it is reflected off the back surface of the piece it becomes a tensile wave that can de-bond internal interfaces [7-8]. The velocity of the shockwave is detected on the back side of the plate and can be related to the internal stress. By incrementally increasing the laser power and using laser-UT scanning between shots to detect the occurrence of the de-bond, the tensile stresses to induce the de-bond can be qualitatively estimated. The magnitude of the

measured de-bond stress can be compared, for example, for different fuel plate fabrication conditions, however, it's important to note that these stresses are not directly comparable to, for example, the stress that would be measured in a tensile test, because of the very high strain-rates associated with laser-induced shockwaves.

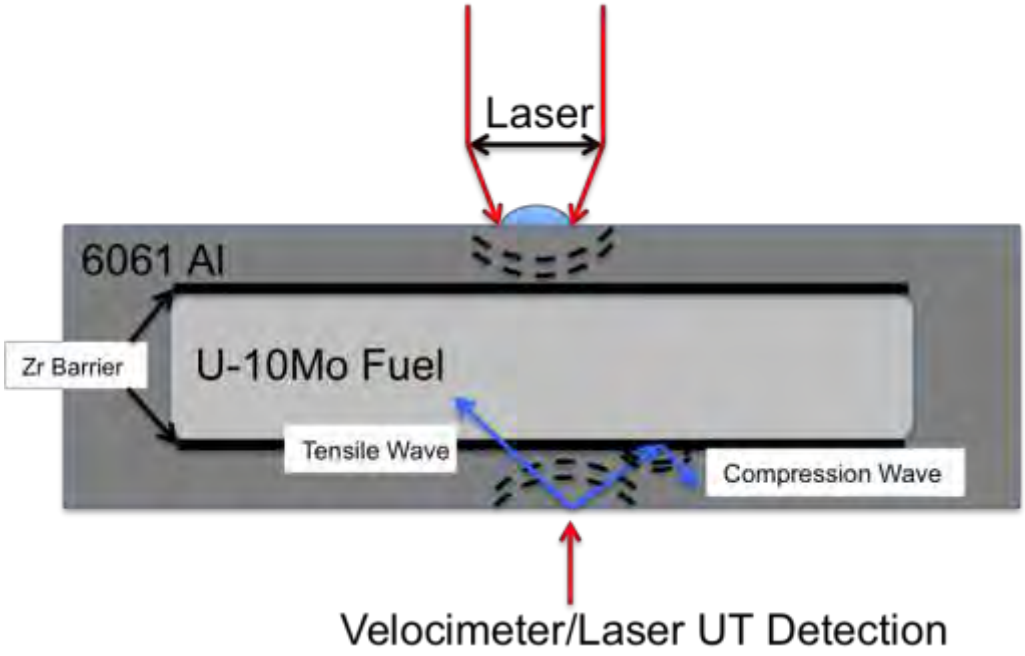

Figure 2 Schematic of laser shock bond strength measurement.

The system is able to determine at which fuel-cladding interface within the fuel plate the debond occurs, however,, the resolution is not adequate to identify whether the failure occurs at the Zr-cladding or fuel-Zr interface. Further evaluations of the debonds created can be made using metallographic examinations. For post-irradiation bond strength testing, localized bond-strength evaluation as a function of fission density within a fuel plate will provide valuable data on the evolution of bond strength during irradiation and the resistance of fuel plates to delamination.

The laser shock system is currently undergoing modification for hot-cell use. The rather complex optical paths of the laser shock and laser-UT scanning system has required fabrication of a large diameter hermetically sealed feed through to accommodate the optical fibers. Qualification of the system for in-cell use has entailed ensuring the laser optical paths can be run through the feed through and maintain signal integrity. Initial testing of this modified system is on-going.

3. Initial Testing Results and Fuel Performance Considerations

As mentioned previously, a prototype (proof of principle) residual stress system was developed and tested at LANL. Based on modifications of this design, a new system has been assembled for hot-cell implementation and is currently undergoing qualification testing at INL. Initial results for a surrogate fuel sample that consists of an aluminum clad stainless steel foil bonded using friction stir welding are shown in Figure 3. Deflections as a function of slit depth illustrate a change in the sign of the stresses at the internal interfaces. These initial results show promise in being able to measure residual stresses in-cell. Further analysis is being conducted to calculate the residual stresses in the surrogate plate from the measured deflections. Following further system refinement, tests will be conducted on HIP processed plates to ascertain baseline residual stress states prior to irradiation.

It is important to understand the baseline residual stress state of the as fabricated fuel plates to evaluate whether the fabrication processes have introduced stresses into the fuel plate that might enhance chances for debonding during irradiation. As the plate is composed of three disparate materials, the thermal history will introduce differential thermal expansions and result in stress gradients through the plate thickness. Most of these stresses are predicted to be relaxed during the initial stages of irradiation, but additional stresses will be imposed during irradiation as the fuel swells, cladding deformation occurs, and as the fuel plate cools during reactor shut down. Post-irradiation residual stress examinations will aid in the determination of likely stress concentrators and with additional property measurements (e.g. hardness, bend testing, bond strength) give a good indication if any of the fuel plate constituents are near the failure limits.

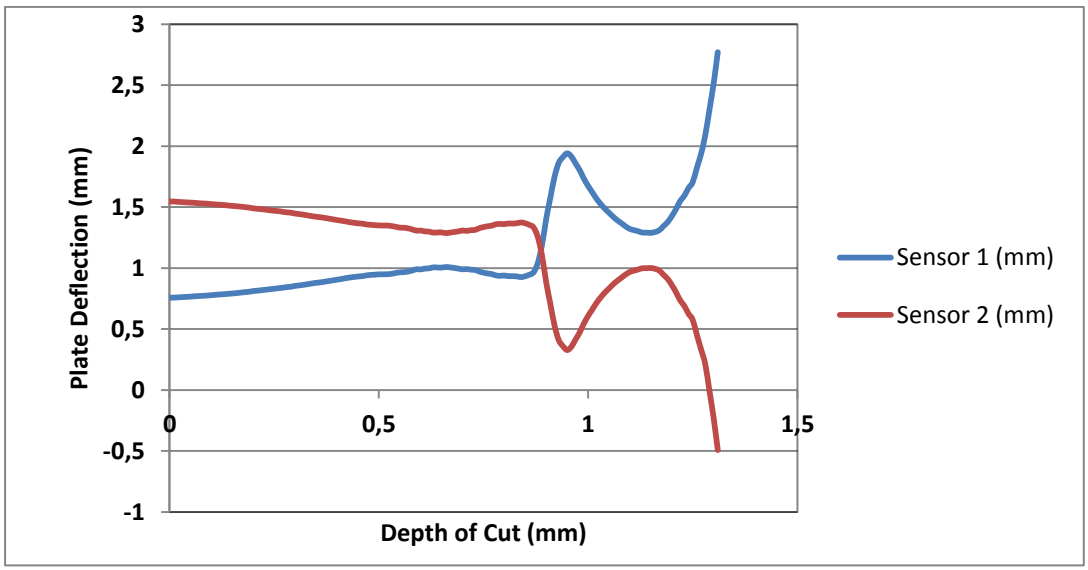

Figure 3 Sample deflection vs slit depth for surrogate fuel plate generated during initial system qualification tests.

Initial testing of the laser shock/UT system was conducted on surrogate fuel plates similar to those used for residual stress (Al cladding with SS foil) to determine if bond quality could be effectively discerned. In this case the fuel plate was HIP bonded and the circular features in the image provided in Figure 4 indicate where the laser shock tests were conducted. Signal analysis indicates that tests conducted in the clad-clad region did not de-bond the interface (locations 1 and 2), while the larger dark circles in the surrogate fuel region (locations 3 and 4) indicate fuel-clad de-bonding. In this particular sample, it is anticipated that bonding should be weaker as the samples were intentionally contaminated with a parting agent.

In a further series of tests actual HIP'ed fuel plates containing U-Mo fuel were examined. Surface velocity at the back side of the plate was measured as a function of shock laser energy to discern the threshold for de-bonding. In some cases, as the graph in figure 5 shows, de-bonding occurred at a lower measured back surface velocity than a previous measurement. Thus, this measurement could not provide an accurate de-bond threshold. Efforts are on-going to refine correlations between measured surface velocity and actual de-bond stress by comparing with results from other tests [10] as well as thermo-mechanical modeling. Overall, the initial testing of samples that had known regions of good bonding and poor bonding could be discerned with the system, and the system is now undergoing qualification for in-cell implementation.

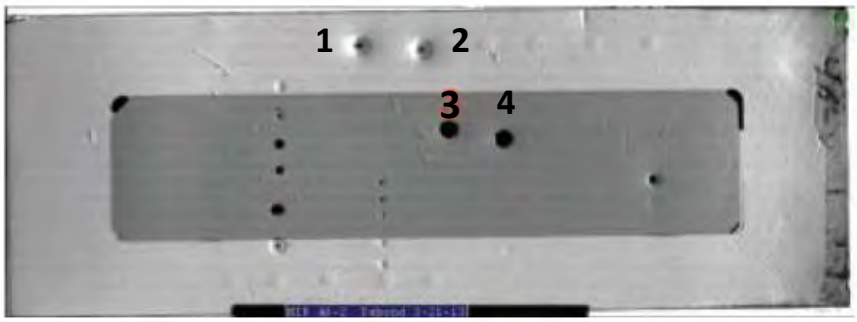

Figure 4 Image of fuel plate following laser shock testing showing regions of good bonding and poor bonding [REF].

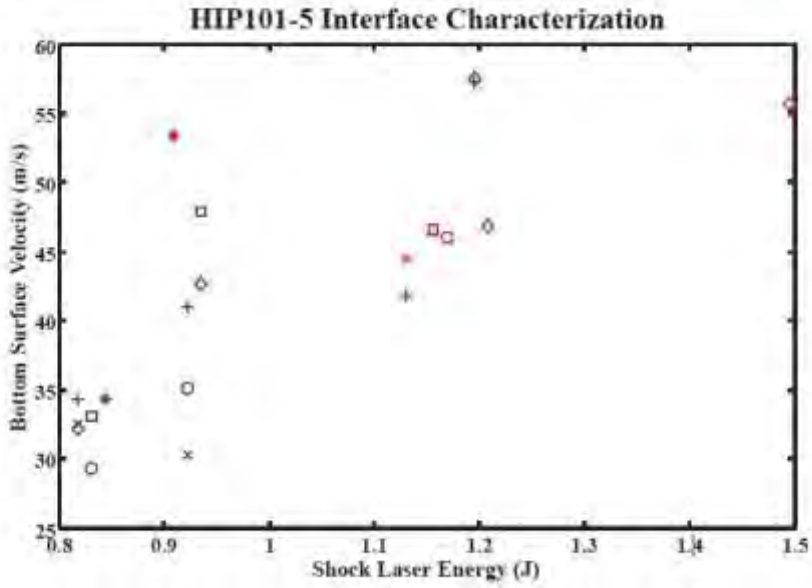

Figure 5 Measured bottom surface velocity as a function of shock laser energy for an RERTR-12 HEU mini-plate. Each symbol represents a separate test locations with red symbols indicating a de-bond occurred.

The primary functional requirements for monolithic fuel are mechanical integrity, geometric stability, and stable and predictable behavior. Residual stresses both prior to and developed during irradiation are important relative to possible fuel plate delamination failures, in-reactor pillowing, or cladding breach. It is important to understand if the peak stresses developed in the fuel on reactor shutdown can exceed the ability of the fuel to accommodate the stresses. It is also important to understand the relationship between the post-irradiation residual stress state and the fuel-cladding interfacial bond-strength, since local failure at these interfaces could potentially lead to fuel plate delamination.

4. Conclusions

The US HPPR program is undertaking a comprehensive effort to develop and qualify a new fuel form. As part of this effort, new testing techniques to measure fuel-cladding bond strength and residual stresses are being developed and adapted for hot-cell use that will ensure fuel properties are well understood and potential failure precursors are identified to the extent possible. In combination with fuel performance modeling, behavior of this new fuel type should be known with a high degree of confidence. A significant outcome of this program will be the qualification and eventual licensing of a new plate-type fuel system for use in research reactors through the NRC for the first time in nearly 3 decades.

5. Acknowledgements

The U.S. Department of Energy, Office of Material Management and Minimization, National Nuclear Security Administration, under DOE-NE Idaho Operations Office Contract DE-AC07-05ID14517, supported this work. A contractor for the U.S. Government authored this summary. The publisher, by accepting the article for publication, acknowledges that the U.S. Government retains a nonexclusive, paid-up, irrevocable, worldwide license to publish or reproduce the published form of this manuscript, or allow others to do so, for U.S. Government purposes.

6. References

1. A.B. Robinson, et al., Irradiation Performance of U–Mo Alloy Based “Monolithic Plate-Type Design Selection Update”, Idaho National Laboratory, INL/EXT-09-16807, Rev.1, July 2013.
2. Hakan Ozaltun, “The Effects of Fabrication Induced Stress Strain-States on the Irradiation Performance of Monolithic Mini-Plates”, Proceedings of the ASME 2015 International Mechanical Engineering Congress & Exposition, IMECE2015, November 13-19, 2015, Houston, Texas, paper 53050.
3. H. Ozaltun, P. G. Medvedev, A. B. Robinson, B. H. Rabin, “Shutdown-Induced Tensile Stress in Monolithic Miniplates as a Possible Cause of Plate Pillowing at Very High Burnup” , RRFM2014, Paper A0101.
4. D.W. Brown, D.J. Alexander, K.D. Clarke, B. Clausen, M.A. Okuniewski and T.A. Sisnerosa, “Elastic properties of rolled uranium–10 wt.% molybdenum nuclear fuel foils”, Scripta Materialia 69 (2013) 666–669.
5. Prime, Michael B., Lovato, Manuel L., Alexander, David J., Beard, Timothy V., Clarke, Kester D., Folks, Bo S., “Incremental Slitting Residual Stress Measurements for a Hot Cell”, Los Alamos National Laboratory, LA-UR-14-23273.
6. Hill, M. R., 2013, "The Slitting Method," Practical Residual Stress Measurement Methods, G. S. Schajer, ed., John Wiley & Sons, Ltd, pp. 89-108.
7. Perton Mathieu, Lord Martin, Jean-Pierre Monchalin, and Guy Rousseau, Laser Shock/ultrasonic Testing System Instructions Manual and Documentation, National Research Council of Canada.
8. Smith, James A.; Rabin, Barry H., Perton, Mathieu, Lévesque, Daniel, Monchalin, Jean-Pierre, Lord, Martin, “Laser Shockwave Technique For Characterization Of Nuclear Fuel Plate Interfaces,” RERTR 2012 — 34th International Meeting On Reduced Enrichment For Research And Test Reactors, Warsaw Marriott Hotel Warsaw, Poland, October 14-17, 2012.
9. D.E. Dombrowski, C. Liu, M.L. Lovato, D.J. Alexander, K.D. Clarke, N.A. Mara, W.M. Mook, M.B. Prime, D.W. Brown, B. Clausen, “Experimental Investigation Of Bonding Strength And Residual Stresses In Hip Clad Fuel Plates”, Advances in Powder Metallurgy and Particulate Materials - 2013, Proceedings of the 2013 International Conference on Powder Metallurgy and Particulate Materials, PowderMet 2013, p 1134-1148, 2013.

MCNP CALCULATION OF CORE PHYSICS PARAMETERS OF NIRR-1 LEU CORE USING MANUFACTURER'S RECOMMENDED VALUE OF 13% ENRICHED UO_2 FUEL

K. IBIKUNLE[1], Y.V. IBRAHIM[2] S.A. JONAH[2]

1 Department of Physics, Ahmadu Bello University, Zaria, Nigeria
2 Centre for Energy Research and Training, Ahmadu Bello University, Zaria, Nigeria

Email: jonahsa2001@yahoo.com

ABSTRACT

As part of the on-going worldwide effort of converting Miniature Neutron Source Reactors (MNSRs) from highly enriched uranium (HEU) core (i.e. > 90% enrichment) low enriched uranium (LEU) cores (i.e. < 20% enrichment) under the auspices of the International Atomic Energy Agency (IAEA) and the Reduced Enrichment for Research and Test Reactors (RERTR) programme, the modification of Nigeria Research Reactor-1 (NIRR-1) has been embarked upon since 2006. In this work, the MCNP code has been used to recalculate core physics data of NIRR-1 on the basis of manufacturer's recommended enrichment of 13% as against 12.5% enrichment initially proposed for the conversion of MNSRs. The following reactor core physics parameters were computed for the 13% enriched UO_2 LEU fuel; number of fuel pins required to provide clean cold core excess reactivity (ρ_{ex}) of between 3.5 – 4.0 mk, control rod (CR) worth, shut down margin (SDM) and kinetics data (i.e. effective delayed neutron fraction, β_{eff} and prompt neutron lifetime, l_f). Results are compared with experimental and calculated data of the current HEU core. Data obtained indicate that 341 fuel UO_2 pins and nine Zirc-alloy claddings would provide a cold core excess reactivity of 4.91 mk, which compares well with the calculated value of 4.76 mk and a measured data of 4.97 mk for the current HEU core.

1.0 Introduction

The Nigeria Miniature Neutron Source Reactors (MNSR) code named the Nigeria Research reactor-1 (NIRR-1) is a low power, tank-in-pool research reactor currently fueled with about 1 kg of HEU. NIRR-1 is currently in its first fuel cycle and was designed mainly for neutron activation analysis and production of some short-lived radioisotopes [1, 2]. Over the years, studies under the aegis of the International Atomic Energy Agency's (IAEA) Coordinated Research Project (CRP) and the Reduced Enrichment for Research and Test Reactors (RERTR) programme have been performed to convert MNSRs in general and NIRR-1 in particular to LEU [3, 4]. The MNSR is a compact low-power research reactor designed mainly for training and research. The prototype MNSR was built by the China Institute of Atomic Energy (CIAE), Beijing, China and was critical in 1984. Subsequently, the commercial versions of the reactor have been installed in China, Ghana, Iran, Nigeria, Pakistan and Syria. The nominal power of MNSR is approximately 30 kW and they have common operational, utilization and spent fuel management issues. The cores are fueled with HEU (>90% enrichment) consisting of a total ^{235}U loading of approximately 1 kilogram. In 2005, the IAEA in collaboration with RERTR program organized a Technical Meeting of owner organizations of MNSR and SLOWPOKE reactors to discuss issues related to conversion to low enriched uranium (LEU) as part of the global efforts at minimizing the civil use of HEU. Thereafter, the CRP entitled "Conversion of MNSRs to LEU" was initiated in 2006. A major objective of the CRP was to perform feasibility studies to identify a single fuel for the conversion to LEU. Results of the feasibility studies performed on NIRR-1 showed that the reactor would run on LEU UO2 fuel with 12.5 % enrichment [3, 4]. In this work, the MCNP code was used to evaluate the neutronics data of LEU-UO_2 fuel on the basis of manufacturer's recommended enrichment of 13% to recalculate core physics data of NIRR-1 as against 12.5% enrichment initially proposed for the conversion of MNSR.

2.0 Materials and Method

As part of the feasibility studies to convert NIRR-1 to LEU, an MCNP model of current HEU core of the reactor was developed. Detailed geometry of the HEU fueled core of the Nigeria Research Reactor-1 (NIRR-1) was created in a three-dimensional, Cartesian coordinate system. An MCNP input deck was constructed using detailed engineering drawings of the reactor. The core centre was taken as the origin (0, 0, 0) in the x- and y-plane and the center of the fuel pin in the z-plane. Individual cells were defined explicitly for each of the following reactor components; 347 fuel pins and three Al dummies, control rod, light water moderator, grid plates, Be reflectors, shim tray, irradiation channels, reactivity

regulators, fission chambers, startup guide tube also known as slant tube. The temperature measuring devices were defined as separate cells and all details of the aluminum support structure, reactor vessel as well as the reactor pool and the stainless steel liner were also included. The parameters of the reactor used in constructing the MCNP model were taken from the final SAR [5] and results have been published in Ref. [2]. Geometric representation of the reactor in the input deck as read by MNCP code and is depicted in Fig. 1.

The design data of the HEU, LEU- 12.5% and LEU 13% are presented in Table 1. All the calculations were performed as a KCODE source problem for criticality calculations using the MCNP code on the basis of half a million particles in 400 cycles. The following reactor core physics parameters were computed for the 13% enriched UO_2 LEU fuel; number of fuel pins required to provide clean cold core excess reactivity (ρ_{ex}) of between 3.5 – 4.0 mk, control rod (CR) worth, shut down margin (SDM) and kinetics data (i.e. effective delayed neutron fraction, β_{eff} and prompt neutron lifetime, l_f). The data obtained are compared with the results for measured and calculated data for the HEU core as well as calculated for the 12.5% enrichment.

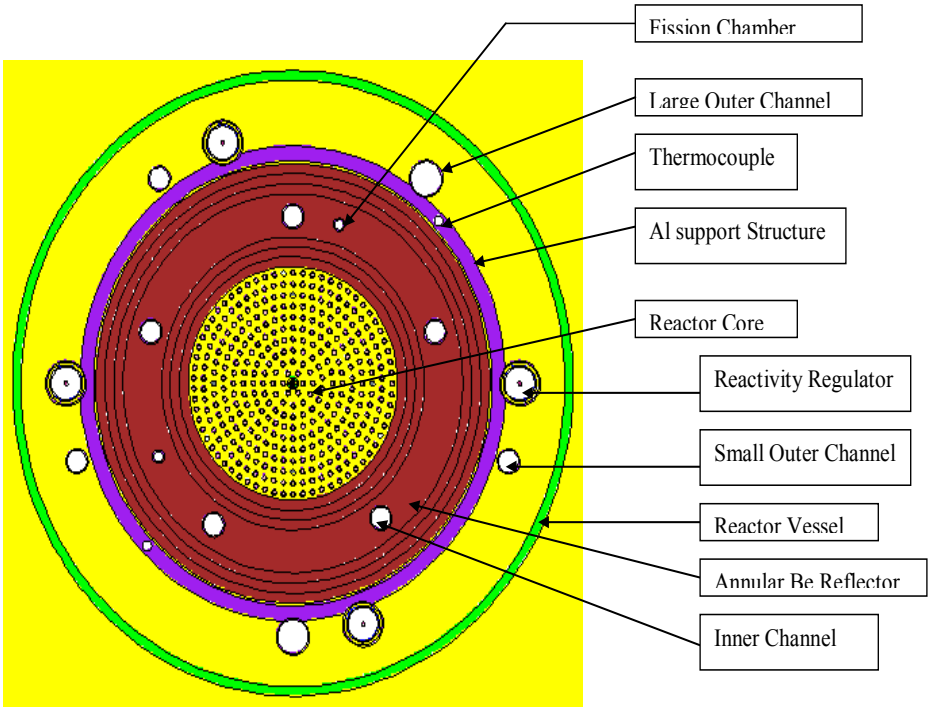

Fig. 1 A geometric diagram of NIRR-1 in the x-y plane from MCNP

Fuel Type/Enrichment (%)	Density of Meat/U (g/cc)	Meat Diameter (mm)	Clad material/Thickness (mm)	No. of fuel pins
HEU-U-Al4/90.2	3.456/0.92	4.3	Al/0.6	347
LEU-UO2 Pellets/12.5	10.6/9.35	4.3	Zr/0.6	348
LEU-UO2 Pellets/12.5	10.6/9.35	4.3	Zr/0.6	348

Table 1 Design data of HEU and LEU fuel options

3.0 **Results and Discussion**

Results of number of fuel pins required to provide clean cold core excess reactivity of 3.5 – 4.0 mk as a function of multiplication factor, k_{eff} are displayed in Figure 2. As can be seen in the Figure, 341 fuel UO_2 pins and nine Zirc-Alloy

claddings would provide a k_{eff} of 1.00493, which is equivalent to 4.91 mk clean cold core excess reactivity. This values compares well with the calculated value of 4.76 mk and a measured data of 4.97 mk for the current HEU core. This value of 4.97 mk was reduced to 3.77 mk via the introduction of Cd string worth -1.2 mk in one of the unconnected irradiation channels [5]. The number of fuel pins required to provide the same clean cold core excess reactivity for the 12.5% enrichment was found to be 348 fuel UO_2 fuel pins and two Zirc-Alloy claddings.

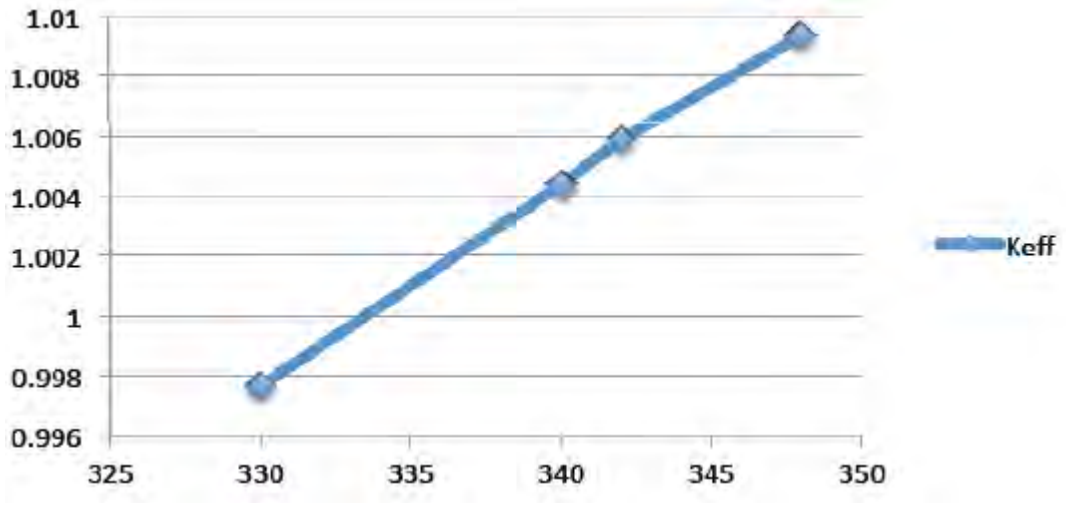

Fig.2 A plot of Multiplication factor, k_{eff} versus number of fuel pins

Detailed results of core physics data obtained for HEU and candidate LEU cores are given in Table 2. The calculated data of control rod worth, shut down margin and clean cold core excess of the HEU and candidate LEU cores compare well with measured data for the current HEU core. The kinetics parameters of the fuel options were calculated using the adjoint method (KOPTS) and by turning 'on" and "off" the physics card (TOTNU) option and are presented in Table 3. The adjoint method derives from the reactor point kinetic equation and employs an enhanced feature of the MNCP in version 5-1.6 to calculate the kinetics parameter. For the effective delayed neutron fraction, β_{eff}, the calculation was performed using the KOPTS and TOTNU card options. Furthermore, the prompt neutron lifetime, l_f of the fuel options were calculated using the adjoint method. The β_{eff} data are in good agreement with MNSR's manufacturer's quoted values. However, the manufacturer's quoted value of 8.12×10^{-5} for l_f deviates from calculated data for the three fuel options in this work. It should be noted that the diffusion code 'EXTERMINATORS" was used by the CIAE to calculate the

kinetics parameters quoted by the manufacturer. Based on the recommended enrichment of 13% of LEU UO_2 fuel option, 341 fuel pins and nine Zirc-alloy claddings would be required to provide core physics data comparable with the current HEU core for the conversion of NIRR-1 to LEU. Further investigation are needed with regards to the thermal hydraulics data and radiological analyses of the 13% LEU fuel option in order to ascertain its suitability for the conversion of NIRR-1 to LEU.

	HEU-347 90.2% Measured	HEU-347 90.2% Calculated	LEU-348 12.5% Calculated	LEU-113.0% Calculated
k_{eff} Rod out	-	1.00476	1.00476	1.00493
k_{eff} Rod in	-	0.99709	0.99712	1.099727
Clean coal core excess reactivity, ρ_{ex} (mk), k_{eff}-$1/k_{eff}$	4.97	4.737	4.737	4.91
Control rod worth, ρ_w (mk) $K_{out} – k_{in}/(k_{out}.k_{in})$	7.0	7.66	7.63	7.61
Shut down margin, SDM (mk) $\rho_w - \rho_{ex}$	2.03	2.92	2.89	2.76

Table 2 measured and calculated core physics data of reference HEU and candidate LEU fuels

Kinetics parameters	CIAE quoted data	HEU 90% (347)	LEU 12.5% (348)	LEU 13% (341)
β_{eff} KOPTS)	0.0081	0.00837±0.00009	0.00836±0.00009	0.00841±0.00009
β_{eff} (TOTNU)	0.0081	0.00849±0.00009	0.00843±0.00009	0.00845±0.00009
$_{lf}$ (KOPTS) (μs)	81.2	56.09±0.09	47.2209±0.09	49.60±0.09

Table 3 Comparison of calculated kinetics parameters for the reference HEU and LEU options

4.0 References

[1] Jonah S.A., Balogun G.I., Umar I.M., Mayaki M.C. Neutron Spectrum Parameters in Irradiation Channels of the Nigeria Research Reactor-1 (NIRR-1) for the k_0-NAA Standardization Method, *J. Radioanal. Nucl. Chem.* 266, (2005), 83-88

[2] Jonah S. A., Liaw J. R., Matos J. E., Monte Carlo Simulation of Core Physics Parameters of Nigerian Research Reactor-1. Annals of Nuclear Energy 34 (2007) 953-957

[3] IAEA TECDOC 2014, NIRR-1 Final Report on CRP for the Conversion of MNSR, in press

[4] Nigeria Research Reactor-1 (NIRR-1) Final Safety Analyses Report (SAR) CERT/NIRR1/SAR/02, CERT, 2005

[5] Jonah S. A., Ibikunle K, Li Y. A Feasibility Study of LEU Enrichment Uranium fuels for MNSR conversion using MCNP, Annals of Nuclear Energy, 36 (2009) 1285-1286

6.0 Acknowledgements

The work was performed under the aegis of the IAEA Coordinated Research Project CRP No.NIR\13934 entitled “Conversion of MNSR to LEU” 2006 -2012. The authors are highly indebted to the Reduced Enrichment for Research and Test Reactors (RERTR) at the Argonne National Laboratory (ANL), USA.

PVD-BASED MANUFACTURING PROCESS OF MONOLITHIC LEU FOIL TARGETS FOR 99MO PRODUCTION

T. HOLLMER, B. BAUMEISTER, C.STEYER, W. PETRY

Technische Universität München, Forschungs-Neutronenquelle Heinz Maier-Leibnitz (FRM II)
Lichtenbergstr. 1, 85748 Garching bei München

ABSTRACT

The complete fabrication process of cylindrical LEU foil targets for 99Mo production was demonstrated using newly developed manufacturing methods and depleted uranium as a surrogate for LEU. In this process, the uranium as well as the interlayer is directly applied to the inner side of the outer cladding aluminum cylinder by cylindrical magnetron physical vapor deposition (sputtering). The setup was parametrized and a layer growth algorithm was developed to be able to calculate the layer thickness in real time or to simulate different coating procedures. By adjusting the process parameters, the mechanical properties of the produced foils, their thickness homogeneity and the material utilization were optimized. In this way, self-supporting uranium foils with a good mechanical strength and a high thickness homogeneity were produced. By the application of a suitable interlayer material, these uranium foils were easily separable from the aluminum cladding. The material utilization of the uranium sputter process was above 90%.

1. Introduction

^{99m}Tc is the most widely used radioisotope in nuclear medicine for diagnostic imaging worldwide. It results from the beta minus decay of ^{99}Mo, which is mainly produced by fission of ^{235}U in irradiation targets using high-flux nuclear reactors. The monolithic cylindrical LEU target provides a multitude of advantages over conventional dispersion targets, such as the higher uranium density or the minimization in volume of highly radioactive liquid waste during processing. To make the fabrication of these targets industrially feasible, a novel manufacturing process was developed. In contrast to conventional production techniques where the uranium foil is pre-produced by rolling or casting [1,2], in this process the uranium foil is directly produced in the outer cladding cylinder by PVD deposition. Thereby a cylindrical uranium sputter target is evaporated by a bombardment of argon ions. In the same way, the interlayer material, which allows a separation of the uranium foil from the cladding after irradiation, can be deposited. To realize this process, an advanced cylindrical sputter device was developed. The necessary ions are generated by a low pressure dc plasma. To increase the ionization density, the plasma is magnetron enhanced, meaning that the electrons are trapped in the plasma region by an additional magnetic field. To produce the necessary cylindrical uranium targets for the sputter procedure, a casting process was developed. Using an arc melting furnace, sputter target with a high density of 98.8% in average and a good surface quality were produced. In a final step, the successful assembly of the coated target was demonstrated. Therefore, a hydraulic forming device was built and successfully tested. The principle of the developed manufacturing process and the dimensions of the irradiation target are shown in figure 1. The dimensions were slightly

altered from the original Y-12 design to metric units in order to simplify the machining of components.

This paper will focus on the coating process. For further details and a description of the casting process and the target assembly, reference is made to [3].

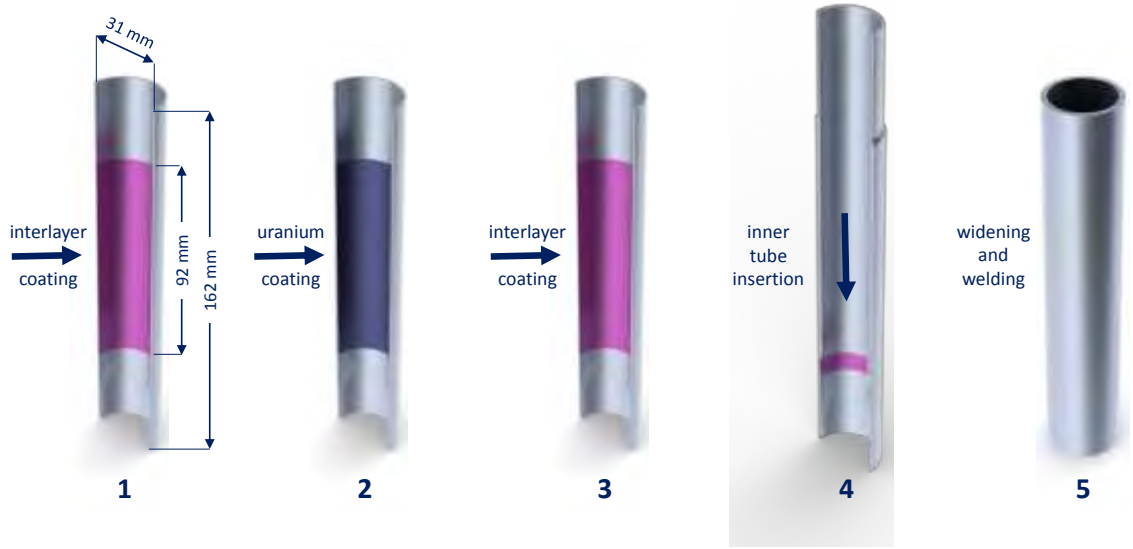

Figure 1: *The irradiation target manufacturing procedure by PVD coating.*

2. Instrumentation

A schematic of the sputter apparatus is shown in figure 2. It consists of a cylindrical PVD target (a), which is mounted in a water cooled heat sink (b). The target is electrically isolated from the heat sink and connected to a dc power source, providing up to 800 V and 2 kW. On both ends of the sputter target, a ceramic electron reflecting surface (c) is attached. Due to an electrostatic charge, these surfaces trap the plasma generating electrons in the volume around the target. In this way the plasma is well localized and its ionization density is significantly increased.

The sputter source can be moved along the central axis of the substrate (d), the outer cladding cylinder. To prevent the outer ends of the cladding cylinder to be coated, re-usable aluminum coating shields (e) are installed.

All these components are located inside a vacuum vessel, which allows the establishment of a suitable argon process atmosphere. The process pressure is determined by a dynamic equilibrium between a controlled argon inflow and a constant outflow using a two stage pumping system. The vacuum vessel is surrounded by a magnetic coil (f), which both provides a magnetic field of up to 120 mT for the magnetron PVD process and allows controlling the substrate temperature. Latter is realized by the coils' ohmic heating and a PID controller, which controls a cooling water flow through the coil. This permits the adjustment of the coil temperature from 20°C to 90°C.

Due to the design of the sputter device, both the magnetic field and the gas pressure show a dependency on the position of the sputter source. Since these two parameters have a strong influence on the sputter process, the position dependency is eliminated by a PLC controlled adjustment of field and pressure according to the sputter source position. Thereby, a uniform sputter process and, as a result, a homogenous layer thickness can be realized.

To allow a save handling of the uranium and to prevent the produced samples from oxidation, the set-up is mounted on a glove-box with a highly pure argon atmosphere. The complete sputter process is PLC controlled and can be performed fully autonomous.

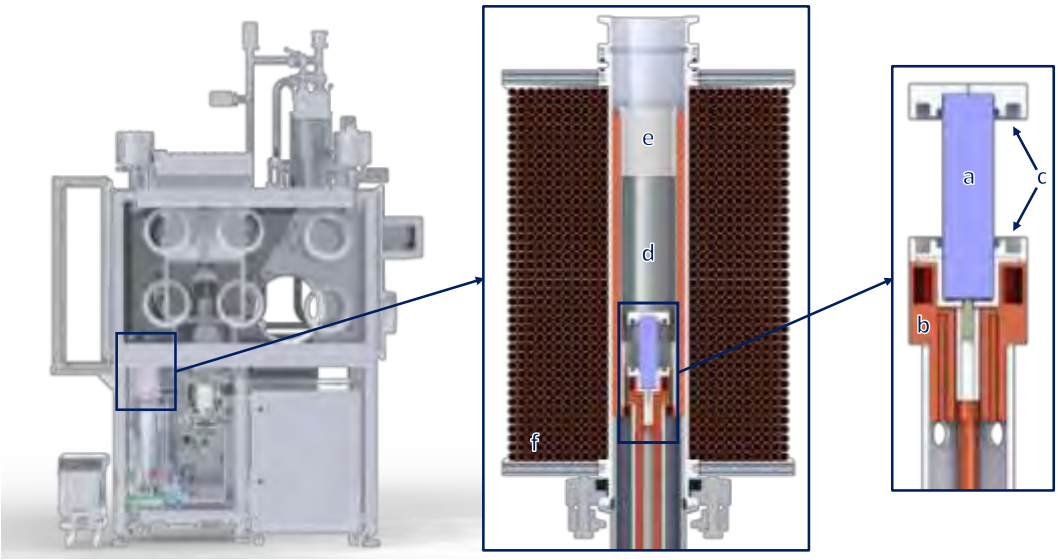

Figure 2: *The cylindrical PVD device.*

3. Process parameters and results

To make the PVD process feasible for the irradiation target production, it was aimed to produce uranium foils with a high mechanical strength and homogeneity. Due to the desired possibility to disassemble the target after irradiation, the produced foils need to be self-supporting and separable from the substrate. Furthermore, the sputter process has to be fast enough to allow the irradiation target production in a reasonable amount of time. These four objectives (layer quality, homogeneity, adhesion and sputter rate) can be controlled by adjustable process parameters: sputter power, magnetic field, gas pressure, the application of an interlayer and the movement of the sputter source. The dependency of all these parameters is shown in figure 3.

Before performing the coating experiments with uranium, the sputter device was extensively parameterized using copper as surrogate material. Due to a similar melting point of both materials, their layer formation in the PVD process is comparable. Therefore, the optimal process parameters gained for copper could successfully be transferred to the uranium sputter process.

Sputter rate

The sputter rate is defined as the eroded mass per time. It is influenced by the applied electric power, the gas pressure and the magnetic field. The magnetic field traps the plasma generating electrons on cycloidal-like path around the sputter target. Up to a certain point, a higher field strength leads to a more efficient trap of the electrons in the system. This increases their residence time in the plasma and, therefore, the ionization density. Due to the higher ionization density, more ions are created and the sputter rate increases. Therefore, high field strength is preferable. The applicable field however, is determined by the limited cooling of the coil. In the given set-up, a magnetic field of 85 mT proved to be the ideal compromise between high sputter rate and possible heat dissipation. Therefore, the magnetic field strength was kept constant in all experiments.

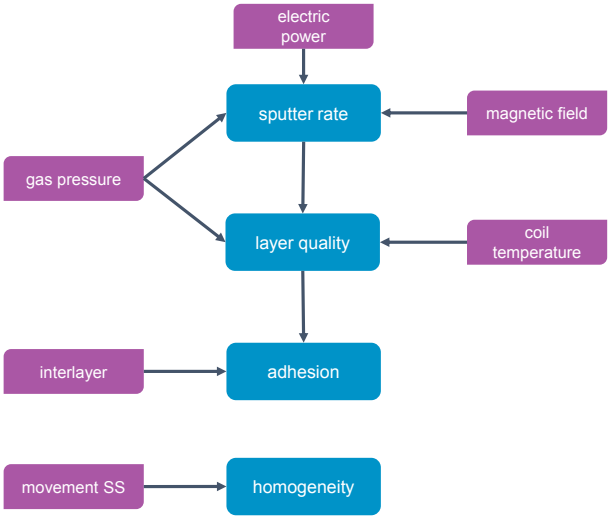

Figure 3: *Objectives of the PVD process (blue) and their dependencies on the adjustable process parameters (purple).*

The gas pressure is indirectly proportional to the sputter rate. At high pressures, the mean free path of the sputtered target atoms is reduced. This causes a higher residence time in the plasma region, which leads to an increased ionization probability of the target atoms. In this case, the target atoms are accelerated back towards the target and the effective sputter rate is reduced. Therefore, the gas pressure was kept as low as possible. Limiting factor is the stability of the plasma. At low pressures, the necessary voltage to sustain the plasma increases. This leads to more electric arcs and, therefore, a low stability of the process. As a compromise, the pressure was fixed to 0.035 mbar.

The main parameter to influence the sputter rate is the applied electric power. Following formula has proven to accurately describe the dependency of the sputter rate R on the electric power P and electric current I

$$R = aP\frac{I}{I+b} \tag{1}$$

The parameters a and b are material specific and were determined by comparing the measured mass difference of the sputter target before and after the coating procedure with the calculated mass difference

$$m = \int R(t)dt \tag{2}$$

In the current set-up with a magnetic field of 85 mT and a pressure of 0.035 mbar, the parameters were determined to be $a = 0.120\frac{mg}{W\,min}$ and $b = -50.99\,mA$ for uranium. The consideration of the electric current in equation (1) increases significantly in accuracy of the discretion of the sputter rate R compared to a simple linear dependency on P. By using equation (1), the maximum deviation between the measured and the calculated values stayed below 1.6% for sputtering uranium. Figure 4 compares measured and the calculated values. For comparison, the simple linear dependency on P is also shown.

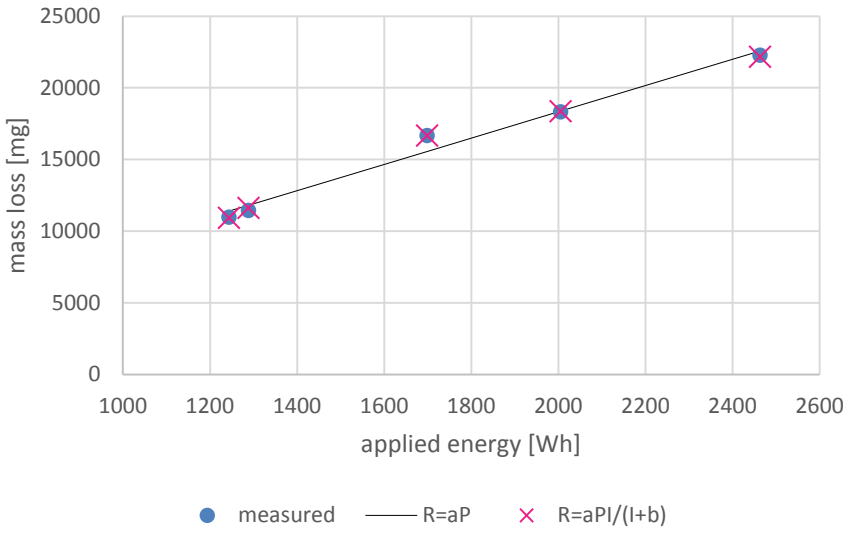

Figure 4: *Comparison of the calculated and the measured target mass loss for different uranium sputter procedures.*

In the current set-up, the maximum sputter rate is determined by the limited cooling of the sputter target. In case of uranium, the maximum power was set to 90 W to prevent the sputter source from damage. However with an improved cooling system, significantly higher powers can be achieved. The sputter rater can be further improved by using krypton instead of argon as sputter gas due its better mass ratio to uranium. With these two measures, the necessary time to produce an irradiation target can be reduced from currently 24 h to 8 h.

Layer quality

The quality of the deposited layers depends on the type of layer growth. It grows by successive nucleation of atoms on previous deposited material. Layers deposited atom-by-atom, like sputter coating, generally grow in a columnar structure. The form of the columnar growth mainly depends on the mobility of the ad-atoms. In a given system, this mobility can be controlled by the substrate temperature and the inert gas pressure. A high substrate temperature and a low gas pressure lead to more compact and denser layers, what results in a higher mechanical strength. Since the gas pressure was kept constant, as detailed before, the important parameter for the layer quality is the substrate temperature. This temperature can be influenced in two ways: the temperature created by the magnetic coil and, due to the low target substrate distance, the intensity of the sputter plasma. Latter is controlled by the applied electric power.

It could be shown that the uranium layer quality strongly depends on the substrate temperature. While at low temperatures the deposited layer are brittle and tend to crack when exposed to air, layers deposited at high temperatures show a high mechanical strength and no signs of cracking. Good results were achieved using a coil temperature of 90°C and a sputter power of 90 W. The actual substrate temperature could not be determined, but is significantly higher than the 90°C due to the heating caused by the plasma. A microscopy of an aluminum-uranium-aluminum multilayer deposited with these settings is shown in figure 5. As one can see, the layers show no signs of cracking or inhomogeneities. The separation of the upper aluminum layer is caused by a contraction of the mounting resin used to prepare the microscopy sample.

Figure 5: *Microscopy of a sputtered Al-U-Al multilayer.*

Homogeneity and material utilization

As described in chapter 2, the dependency of the sputter parameters on the position of the sputter source was electronically eliminated. Therefore when using constant sputter parameters, the layer homogeneity only depends on the movement of the sputter source.

The layer thickness F can be calculated by

$$F(z) = \frac{\epsilon_C}{2\pi\rho r_i} \int f(z, z_S(t)) R(t)\, dt \tag{3}$$

where z is the axial position of the substrate, z_s the position of the sputter source, R the sputter rate according to equation (1), ρ the material density, r_i the inner diameter of the substrate cylinder and ε_c the coating efficiency. The coating efficiency is given by the mass of the material deposited on the substrate compared to the total eroded mass. This efficiency is mainly determined by the material deposited on the electron reflecting surfaces. The function f is the deposition distribution of the sputter source and is a normalized, material dependent function and describes the thickness distribution of the deposited material. This distribution can well be described by following formula

$$f\big(z, z_S(t)\big) = \frac{mm}{4c}\left[\frac{c - (z - z_S(t))}{\sqrt{(c - (z - z_S(t)))^2 + d^2}} + \frac{c + (z - z_S(t))}{\sqrt{(c + (z - z_S(t)))^2 + d^2}}\right] \tag{4}$$

with c and d being material dependent variables. These variables were determined by measuring the thickness distribution resulting of a non-moving sputter source by microscopy. At a pressure of 0.035 mbar and a magnetic field of 85 mT the parameters were determined to be $c = 12.26\, mm$ and $d = 3.98\, mm$.

The calculation of the thickness using equation (3) was validated by comparing sputtered thickness distributions with calculated ones. Figure 6 shows a typical sputter procedure of uranium and the resulting thickness distribution. The plot shows both the measured values and the values calculated according to equation (3). As one can see, both distributions are in very good accordance. Therefore, the formalism can not only be used to follow the grown layer thickness distribution in real time but also to simulate different movements of the sputter source. It showed that very homogenous layer can be produced when using a constant up and down movement of the sputter source during the coating procedure. In the given example, the resulting thickness shows a high homogeneity with a maximum deviation of less than 1.6% in the range from -30 mm to + 30 mm.

The material utilization of the coating process is defined by the material loss on the coating shields (figure 2, e) and the coating of the electron reflecting surfaces (c). Latter is given by ε_c

in equation (3), which is approximately 95%. The material loss on the coating shields can be determined by the maximum oscillation of the sputter source. Up to a movement from – 35 mm to +35 mm, no significant coating appears. At a normal movement from -45 mm to +45 mm, the average material utilization is approximately 92%. However, the deposited uranium on both the electron reflecting surfaces and the coating shields can be removed. By recycling this material in the sputter target production, the material utilization can be increased above 95%.

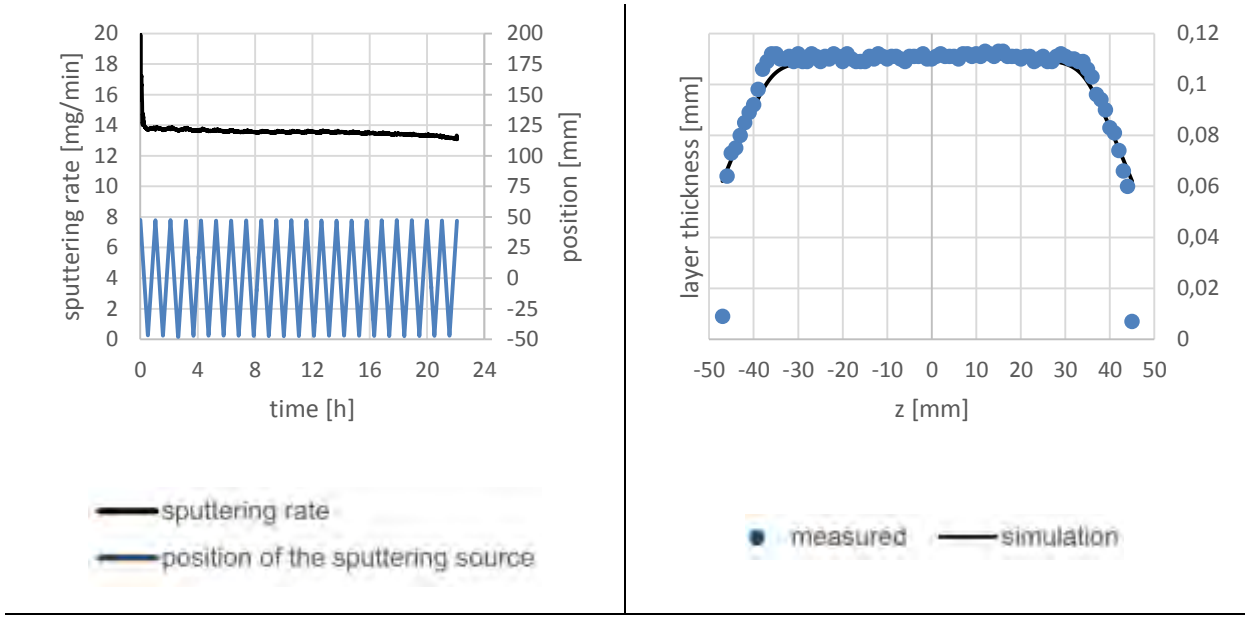

Figure 6: *Typical uranium coating procedure and resulting thickness profile.*

Adhesion

The adhesion of sputtered layers can be controlled in two ways: by its layer quality and/or by applying a suitable interlayer. Layers with a poor quality also show a poor adhesion to the subjacent substrate. This can be used to produce separable foils by first coating a layer with poor quality followed by a layer with high quality. This approach was tested with copper layers. It showed that the layers could easily be removed, however the removal was not free of residues.

To control the adhesion of the uranium layers, experiments with aluminum and graphite interlayers were performed. In case of aluminum, the interlayer was sputtered in the same way as the uranium layer. In contrast, the graphite was applied by spraying and a subsequent drying step. In both cases, the uranium layers are easily removable without any residues. As an example, a sputtered Al-U-Al multilayer is shown in Figure 7. The outer aluminum layer has a thickness of approximately 20 µm, the uranium layer of 140 µm and the inner aluminum layer of 5 µm. After the coating process, the substrate cylinder was cut in shorter segments, cut open on one side and bent up. The resulting uranium foil came off easily from the outer aluminum layer, while the inner aluminum layer stuck to the uranium. The uranium foil showed a good mechanical strength and flexibility. After an exposure to air of approximately 30 minutes, the foil showed a tarnish typical to uranium (see figure 7). However, no signs of mechanical impairment due to oxidation could be observed; even after an exposure time of several days.

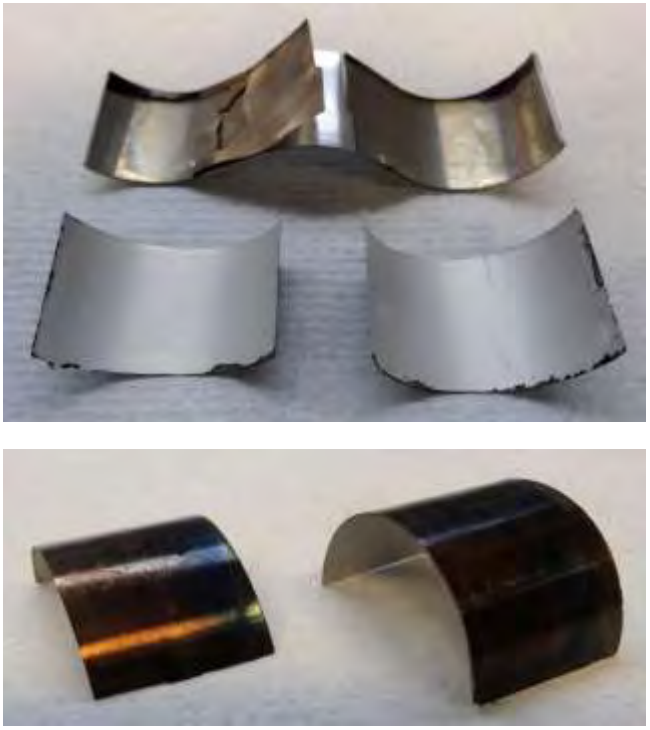

Figure 7: *Sputtered uranium foil with two aluminum interlayers.*

4. Conclusion

Within the presented work, a complete PVD based manufacturing process of cylindrical LEU foil targets was demonstrated. Figure 8 shows the developed process from a potentially oxidized uranium ingot to a completely assembled and welded irradiation target. A detailed description of the single manufacturing steps can be found in [3].

It was the aim of this study, to demonstrate the feasibility of PVD coating for the production of cylindrical LEU foil targets. Therefore, a demonstration PVD reactor was developed, which allowed to study the relevant sputter parameters. The apparatus was extensively characterized and, in this way, the process could be well understood. The developed theoretical description of the layer thickness is based on only four different material parameters and allows the simulation of different movement profiles and a real-time process observation.

A major requirement for the feasibility of the presented manufacturing technique is the separability and the mechanical stability of the produced foils. As described in chapter 4, the mechanical strength of the foils mainly depends on the coating temperature. By applying sufficient values, mechanically stable uranium foils were produced. These foils were self-supporting and showed no mechanical impairment due to oxidation.

It was also demonstrated that the adhesion of the uranium layer to the substrate can successfully be controlled by the usage of a suitable interlayer. Experiments were performed using aluminum and graphite. In both cases the produced foils were easily separable from the subjacent substrate.

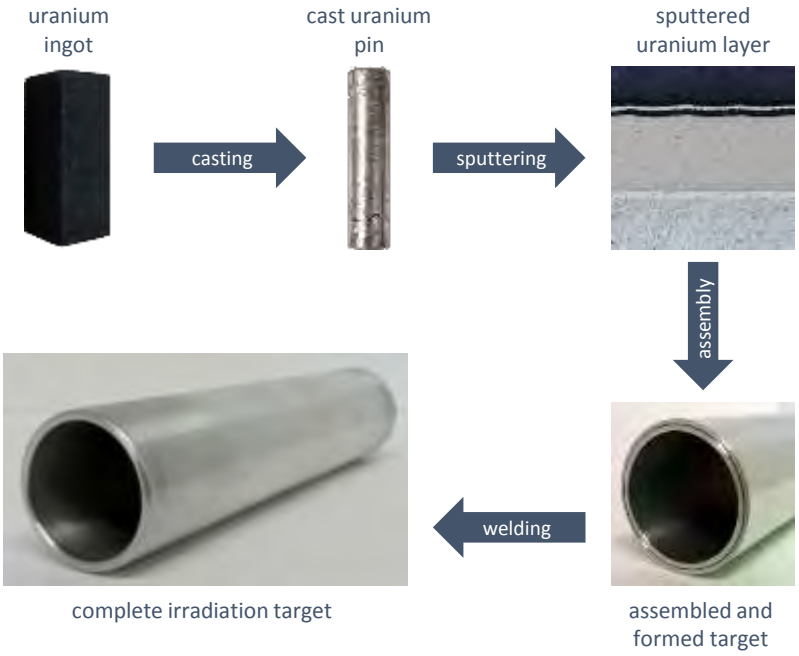

Figure 8: *The complete irradiation target manufacturing process by PVD coating.*

The developed coating process features three major benefits. The first benefit is its high degree of flexibility. Thickness, length and mass of the uranium foil and the interlayer material can easily be modified. This can be used to optimize the irradiation target and the overall cost efficiency. A second important advantage is the high material utilization. For the uranium pin casting an efficiency of 95% was achieved. Together with the maximum sputter efficiency of 92% for uranium, this results in an overall efficiency of 87%. These numbers do not consider any material recovery from the electron reflectors, which would lead to a further increase. A third advantage of the presented technique is the high degree of automation. After loading the target and the substrate in the PVD reactor, the process is PLC controlled and fully autonomous.

In summary it can be concluded that the presented technique proved to be suitable for the irradiation target manufacturing. Therefore, further development will take place, which is oriented towards an industrial application.

5. References

[1] L. Jollay, J. Creasy, C. Allen, G. Solbrekken, “Equivalent Fission Mo-99 Target without Highly Enriched Uranium”, Mo-99 Topical Meeting, Santa Fe, USA, 2011.

[2] C. Kim, “KAERI Recent Activities on Research Reactor Fuel”, IWG consultancy meeting, Vienna, Austria, 2010.

[3] T. Hollmer, “Development of a PVD-based manufacturing process of monolithic LEU irradiation targets for ^{99}Mo production”, PhD thesis, Technische Universität München, Germany, 2015.

JM-1 RESEARCH REACTOR CONVERSION DEMONSTRATED AT POLYTECHNIQUE MONTREAL

CORNELIA CHILIAN, ALTAN MUFTUOGLU
Department of Engineering Physics, Polytechnique Montreal
Quebec, Canada

ABSTRACT

Recently, JM-1, the Jamaican SLOWPOKE reactor was converted from HEU to LEU. This complex process was directed by the Material Management and Minimization Conversion Program of the US Department of Energy's National Nuclear Security Administration. Over the years, much of the expertise for converting and commissioning a SLOWPOKE reactor had been lost. To ensure safety and efficiency and also to facilitate the conversion, it was necessary to conduct trial runs with non-reactor materials before performing real operations on the reactor itself. Therefore, Polytechnique Montreal identified, designed, manufactured and assembled all the tools and equipment required for the conversion as well as a mock-up of the JM-1 reactor, which was installed in a realistic environment at the Polytechnique Montreal SLOWPOKE Laboratory. The tools, equipment and the mock-up passed several safety tests to confirm their functionality, and served for extensive dry runs performed by the conversion team and employees of Polytechnique Montreal. All findings, comments and lessons learned were implemented not only to further improvements of the tools, techniques and procedures, but also to facilitate the actual conversion work.

1 Introduction

The SLOWPOKE-2 reactor is a 20 kW reactor used mostly for research in a wide variety of disciplines involving neutron activation analysis and radioisotope production. Between 1976 and 1984, Atomic Energy Canada Ltd. (AECL) commissioned seven High Enriched Uranium (HEU, 93% U-235) SLOWPOKE-2 reactors, including JM-1 [1,2] at the International Center for Environmental and Nuclear Sciences (ICENS) of the University of the West Indies (UWI) in Kingston, Jamaica. The one at Polytechnique Montreal was converted to Low Enriched Uranium (LEU) in 1997 by AECL [3,4]. In 2009, Jamaica, with support from the International Atomic Energy Agency (IAEA), submitted a formal request to both the Global Threat Reduction Initiative (GTRI) and the Reduced Enrichment for Research and Test Reactor (RERTR) programs for the conversion of the JM-1 reactor from HEU to LEU. Since the inception of RERTR, Argonne National Laboratory (ANL) has provided technical coordination and support for the Conversion Program, including Jamaica's research reactor.

The operations needed to convert a SLOWPOKE reactor from HEU to LEU are quite unique. In addition, the equipment used for the conversion at Polytechnique Montreal in 1997 is no longer available and much of the expertise gained in 1997 had been lost. Therefore, in order to ensure the safe and efficient conversion of the JM-1 reactor, it was necessary to acquire all new equipment and to conduct trial runs with non-reactor materials before performing the operations on the reactor itself. Thus, in April 2015, ANL selected the personnel of the Slowpoke Reactor Laboratory at Polytechnique Montreal to provide the environment and the expertise for tooling, testing and rehearsing of JM-1 conversion activities. It was decided to use a mock-up of the JM-1 reactor for tool development, familiarization with the equipment, assessment and development

of procedures, testing of tools and qualification of equipment as well as training of the personnel involved in the conversion of the Jamaican reactor.

2 Objectives

The main goal of this work was to demonstrate the operations for converting the JM-1 (SLOWPOKE-2 type) reactor from HEU to LEU. Therefore, the first objective was to build a mock-up of the JM-1 reactor including all necessary details. The major components of this mock-up are: the upper part of the reactor container (top plate, top plate support and guide plates); the lower section of the reactor (the critical assembly), the container; the lower section support; major guide tubes (including irradiation and thermocouple); the control rod drive mechanism; the access platform. The second objective was to identify and fabricate all the tools and equipment necessary for the demonstrations of the JM-1 irradiated core removal and fresh core loading operations, as tools for shim and shim tray removal, guides for commissioning rod, neutron source and neutron ion chamber and BF3; the commissioning rod drive mechanism; LEU grapple tool; LEU dummy fuel cage and dummy fuel pins and riveting tools. The third objective was to safely install and align the mock-up reactor without interfering with the existing operating reactor and its structure. Finally, the last objective was to demonstrate the tools and equipment and to conduct trial runs with non-fissile materials in the pool of the SLOWPOKE reactor at Polytechnique Montreal in order to gain expertise before converting the real reactor at ICENS, Jamaica.

3 JM-1 Reactor Mock-up

Polytechnique Montreal designed and fabricated the components of a mock-up assembly, representative of the JM-1 reactor vessel. This mock-up was used to perform joint studies of the techniques and procedures required to remove the HEU core from the JM-1 reactor and to load the LEU core.

3.1 Challenges

SLOWPOKE-2 reactors are pool type nuclear research reactors. The reactor core at Polytechnique Montreal is located under 4.4 m of water and rests on the bottom of an aluminium container (vessel) suspended in the pool from I-beams. The pool is 2.5 m in diameter and 6 m deep. The mock-up for demonstrations had to be installed securely next to the operating SLOWPOKE-2 reactor (1.12 m from centre to centre) without interfering with the operating reactor structure, systems and components. The bottom section of the mock-up needed to be installed and levelled on an uneven pool floor and aligned with the vessel top plate which is 5 m above.

3.2 Mock-up Design and Fabrication

The lower section assembly (critical assembly) and the upper section assembly are made entirely of aluminium and assembled with zinc coated stainless steel bolts and nuts if not welded. The lower section of the mock-up, shown in Figure 1, is supported by a table which also serves as the bottom of the reactor vessel. The dummy HEU core, aluminium 5.2 kg, was already manufactured in 1997 during the reactor conversion at Polytechnique Montreal. The removable shim tray, shown in Figure 1, is made from rolled aluminium sheet, welded at the seam, and has two J notches for the shim tray tool.

The mock-up top plate is 13 mm thick (38 mm thick in the real reactor) with a central hole and 10 irradiation tube holes, 6 of which are used to support irradiation tube assemblies and the others are closed by cover plates. Beneath the central hole, the boomerang shaped control rod motor support plate is attached as shown in Figure 2. In a real SLOWPOKE reactor, this boomerang shaped plate is welded in place and cannot be removed and it is an important obstacle when removing a used reactor core up through the central hole.

Figure 1 - Mock-up lower section assembly including support table

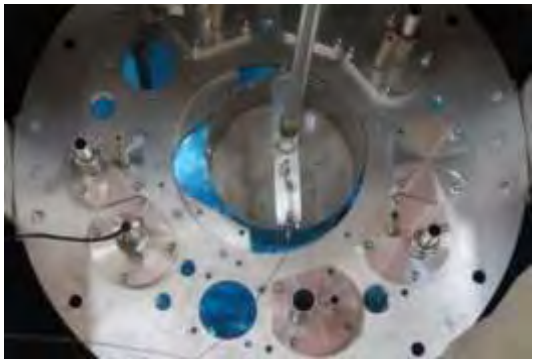

Figure 2 - Mock-up top plate with control rod support plate and shim tray

The aluminium angle support beams are bolted to a large semi-circular support plate (shown in Figure 3) which covers half the pool just above the I-beams. The top plate is suspended below the support beams using aluminium plates and angles. It is important to mention that the commissioning rod drive system support frame (not seen in the Figure) is also attached to these angle support beams.

3.3 Mock-up Assembly and Installation

The mock-up was installed using four winches and cables, the four handles were used to lower the table and the mock-up lower section assembly, weighing 160 kg, to the bottom of the pool. Levelling, within 0.2°, was achieved by measuring the distances to the pool bottom and adjusting the lengths of the table legs. For the reactor vessel walls, five 60 cm diameter 1.5 m long galvanized steel ducts were used. The first section was attached to the table when the mock-up was above the pool and the other sections were added as the mock-up was lowered. The fifth section was cut to length, attached to the fourth section and then attached to the top plate. The top plate was secured in place, suspended from the frame by support plates. Then the six irradiation tube assemblies were added as shown in Figure *2* and Figure 3 with outer tube assembly no.6 in socket no.9 as in JM-1. The mock-up control rod with cable, its support plates and motor were installed as shown in Figure 4. Finally, the mock-up vessel, including all components necessary to perform the disassembly and core removal exercises, were proved to be ready for dry run operations.

3.4 Mock-up removal process

After the demonstrations, the mock-up was removed from the pool. First, all tubes going from the top plate to the lower section were removed one by one. Then the top plate and its support were removed. Finally, the cables of the four winches, connected to the eyelets of the support table handles and used to raise the lower section and the vessel walls. The vessel walls were disassembled step by step due to space limitations while lifting the mock-up from the bottom of the pool. After each step, radiation measurements were conducted on every part. As expected from design criteria, it was observed that there was minimal activation even for the parts of the mock-up closest to the reactor.

3.5 Tools for Reactor Disassembly and Removal of the HEU Core

The tools required to prepare the JM-1 reactor for removal of the HEU core are non-standard, their main design criteria was safety of the JM-1 core conversion, and they were designed and manufactured for demonstration purposes. They include the shim tray tool, the shim handling tool and shim pick up tools. The shim tray tool, shown in Figure 5, was fabricated according to the design drawings and improved according to today's machining capabilities. It has three 2 m

Figure 3 - Top plate assembly with support beams

extension tubes attached by threaded brass collars.

The shim handling tool, partially shown in Figure 4 uses a suction cup to pick up the shims. It has three concentric 2 m tubes which can be extended to pick up shims below 5 m of water. It is operated by two people. A reversible vacuum pump with pressure gauge is first used at positive pressure to expel the water and then at negative pressure to provide suction and finally at positive pressure to release the shim. In addition, short and long shim pickup tools are used to handle the shims outside of the pool and to retrieve possible dropped shims.

3.6 HEU Core Removal Dry Runs

Following the successful completion of the mock-up installation and tool shakedown tests, dry runs were conducted in two sessions at Polytechnique Montreal, on July 14-17, 2015 and August 12-14, 2015. The scope of these exercises was to simulate the partial disassembly of the JM-1 reactor vessel to prepare it for the HEU core removal, and to simulate the lifting of the HEU core from the reactor vessel using the dummy HEU core.

Figure 4 - Shim removal process

First, the shim handling tool was demonstrated to pick up a shim from the shim tray, raise it out of the water and out of the mock-up vessel and place it on a paper towel on the platform. The short shim pickup tool was then used to place it quickly in a shielded container. Later, the same tools were used to re-install shims of various thicknesses in the shim tray. In addition, a shim was dropped intentionally to the bottom of the mock-up vessel and lodged at an angle in the shim tray. It was picked up successfully with the debris grapple tool.

After the removal of all the shims, the shim tray tool was demonstrated to unlock the shim tray from the retaining ring and remove it from the vessel. It was later put back in place. The removal of the shim tray through the hole in the top plate, shown in Figure 4, is delicate since the dimension of the central opening in the top plate is not round and is close to the shim tray diameter.

Irradiation tube no.5 needs to be removed in order to install the commissioning rod guide tube. The bottom end of the irradiation tube assembly sits in a hole in the annular reflector and the top end of the assembly is fixed to the top plate with the irradiation tube hole cover plate. The irradiation tube hole cover plate is never removed from the irradiation tube assembly because it holds the two tubes (capsule tube and return air tube) at the proper orientation. The cover plate of irradiation tube assembly no.5 was unbolted from the top plate and the entire tube assembly was lifted out of the hole and was placed in the pool and attached to the I-beam. The irradiation tube assembly no.5 was then re-installed in its hole in the top plate and the bottom end was put back in the hole in the annular reflector. The cover plate was aligned on the top plate which automatically aligns the tube assembly.

Figure 5 - Shim tray tool

It is important to keep the control rod, cable, pulley and motor intact so that when they are re-installed the length of the cable will be unchanged. The semi-circular support plate of the control rod motor was unbolted from the lip of the top plate and the motor, cable and control rod were raised. Two people were needed to raise it, taking care not to tangle the cable. It was judged that two short shim pickup tools were needed to handle the radioactive (on the real reactor) control rod. For storage and shielding during the conversion activities, the rod was placed at the side of the pool, lowered into the water on its cable and then the motor and its support plate were fixed in place with the control rod suspended near the bottom of the pool.

Two people were needed to re-install the control rod. It was lowered into the mock-up vessel, suspended by its cable, taking care not to kink the cable while feeding it through the top plate central hole. The rod was easily inserted into the central hole of the shim tray. The semi-circular support plate of the control rod motor was bolted to the boomerang-shaped lip of the top plate. On the real reactor the electrical cables would be reconnected at this point.

4 Commissioning Tools and Equipment

4.1 Fabrication and Coordination of Commissioning Tools and Equipment

Here, brief descriptions of the fabricated equipment are given:

Cd shutdown capsules: Two Cd shutdown capsules were made from 0.5 mm thick Cd sheet by rolling and they are enclosed in a 7 mL polyethylene irradiation vial which is heat sealed.

Inlet water thermocouple support tube: It is made from three sections of aluminium tubing connected by Swagelok connectors. It fits in large outer irradiation tube socket no. 7. The top of the tube is closed around the thermocouple wire by an airtight plug.

Commissioning rods: Two commissioning rods were made by rolling 0.81 mm thick Cd sheet absorber and installed in aluminium housing which is welded to make it watertight. Rod 1 has aluminium rod inside the Cd absorber and Rod 2 has polyethylene. The mass of Cd in rod 1 is 99.025 g and the total weight of rod 1 is 450 g. The mass of Cd in rod 2 is 99.135 g and the total weight of rod 2 is 287 g.

Neutron source tube: Since the JM-1 neutron source (Am/Be of 185 mCi, QSA Global, Inc. Model No. X.3) was too large for an inner irradiation tube, a water proof neutron source guide tube was fabricated from three sections of aluminium tube. The bottom end was machined so that it will fit in irradiation site no.1. The bottom end is closed by a welded aluminium disk.

Dummy neutron source: An accurate copy of the neutron source was fabricated from stainless steel. The dummy source was lowered to the bottom of the tube with a stainless steel cable and fixed at the desired height at the top end of the tube using an aluminium plug and a collet head which can be tightened on the cable at the top of the plug.

LEU core lifting tool: It has three 2 m extension tubes and used to lower the core into the reflector during fuel loading. The tool locks into the central spindle of the fuel cage with a bayonet connector.

Ion chamber tube assemblies: Two identical ion chamber assemblies were fabricated including container tube, extensions with O-rings and load-bearing and pivot sections. The load-bearing section is used to attach the tube of the ion chamber assembly to a U-shaped bracket on the reactor support frame so that the container tube can rotate and be positioned with the ion chamber at the desired angle and height relative to the reactor.

List of additional commissioning equipment:

- Inlet water thermocouple (J-type) with readout and digital recorder (Yokogawa, model GX20)
- Commissioning rod motor drive (with stepping motor, gearhead, pulley, cable, position readout, controller, support)
- 2 ion chamber sets (7.62 cm diameter LND model 50460 ion chambers, HV cables, signal cables, HV power supplies, electrometers, signal digital recorder Yokogawa, uninterruptable power supply, connecting cables/fittings)
- 2 picoammeter (Keithley model 6485)
- 2 BF3 detector sets (cables, HV power supplies, NIM bin power supply, preamps, amps, discriminators, scaler-counters, connecting cables/fittings)

4.2 Commissioning Tools and Equipment Tests

The list of all the tests performed with the tools and equipment is too extensive to be presented here. So we choose to list only some specific tests:

- Solidity of the shim tray tool was tested several times in case it is stuck or hits an obstacle during the removal of the tray from the top of the reactor.
- Shim handling tool was tested to hold the vacuum at least 10 minutes for safe removal of the shims from under 5 m of water. Also, tool was inclined and shaken while holding the wet shim. No vacuum leak was observed.
- LEU core lifting tool's no failure functionality was important since it will be used several times during the reactor commissioning. In addition, operator should be able feel if the tool is snapped on the core's J slots or not. During the tool commissioning, tightness of the spring was adjusted according to operator's preference.
- Ion chamber sets and BF3 detectors were tested both with source on bench and near reactor at low power. A ground loop problem was eliminated by isolating the detector and cable connector from the housing using plastic foam insulation.
- Ion chamber and BF3 tube assembly installations were tested for water leaks.
- Commissioning rod motor drive successfully was raised and lowered both commissioning rods below water in the guide tube at the required speed of 12.7 mm/s.
- Commissioning rod position readout was tested. During the first test, when the readout indicated a displacement of 8.00 inches (203.2 mm), the actual displacement of the cable was measured by a digital calliper to be 199.6 mm. The readout software was modified to correct this 1.7% error and further tests confirmed that readout of 8.00 inches corresponds to a displacement of the cable of 8.00 inches. The speed was confirmed by stopwatch to be 12.7 mm/s.

4.3 Commissioning Dry Runs on Mock-up and with Polytechnique SLOWPOKE

Neutron source manipulation: During commissioning of the JM-1 reactor with LEU fuel, at the beginning of fuel loading, it will be necessary to place the chosen neutron source at the bottom of a guide tube replacing the irradiation site no.1 in the beryllium reflector. When the reactor approaches criticality and the multiplication factor increases, the neutron source will be moved to an outside position from the reactor core to reduce the signals of the ion chambers.

During the exercises, the lower end of the neutron source tube was placed at the bottom of irradiation site no.1 in the annular reflector of the mock-up. The top end was fixed in place by the cover plate. The dummy source was lowered to the bottom of the tube until the calculated length of cable had been lowered and it was felt that it had touched the bottom of the tube. When the cable was slightly slack, an indicator was attached to the cable at the top of the tube to mark that the source was at the bottom.

To place the dummy source farther from the core, the cable was pulled up 61 cm, a second indicator was attached to the cable, and the cable was fixed at this position using the aluminium

plug at the top end of the tube and the collet head tightened on the cable at the top of the plug. The same approach of placing the source at the bottom of the tube and then fixing it at the desired height was used in 1997 during the conversion of the Polytechnique Montreal SLOWPOKE reactor. However, the source guide tube, plug and collet were developed to suit the ANL neutron source dimensions, to reduce the eventual neutron streaming through the guide tube, and to improve the positioning of the neutron source relative to the critical assembly.
Commissioning rod manipulation: The lower end of the commissioning rod guide tube was installed in the hole of the annular reflector of the mock-up corresponding to the irradiation site no.5. The guide was fixed at the top end using the commissioning rod guide tube cover plate. The procedure to place the tube at the proper height was demonstrated and validated during the dry runs. Once the guide was installed, the participants bolted the commissioning rod motor support frame to the mock-up top plate frame using the four holes designed for this purpose.
The commissioning rod with polyethylene core was lowered on its cable to the bottom of the guide tube, and the upper end of the cable, slightly slack was placed and attached on the pulley. Finally, command console reads out the position relative to the bottom of the hole.
The commissioning rod position controller and monitoring unit was used to move the rod up and down and to readout its position. The IN and OUT pushbuttons were used to move the rod from 0 to 30.5 cm at a speed of 12.7 mm/s. The speeds moving up and down were found to be acceptable and the weight of the rod in water was sufficient to keep the cable taught. It was demonstrated that the rod could be easily placed at any desired position within 0.18 mm. The zero was set using the ZERO button. Then the rod would move over a range (0 to 203.2 mm) relative to this zero and the lights indicates when the rod was at one of the limits.
Manipulation of ion chamber assemblies: The LND ion chambers available have the serial numbers 97-11 and 14-48. Ion chamber 97-11 was installed in housing no.1 with its high-voltage and signal cables. As previously verified during the tools shakedown activities, no water leaks were observed during any of the operations.
The assembly was installed in the designated bracket of the reactor top plate support frame. The technique to insert the pivot pin in the pivot hole at the reactor core level was demonstrated to the conversion team and it was practiced several times. The assembly rotated easily and could be positioned at any of the 19 positions, over 180° at 10° intervals.
Measurement of fluxes of sub-critical reactor with ion chamber sets and source: Ion chambers 97-11 and 14-48 were installed one after another in the support on the east side of the Polytechnique Montreal SLOWPOKE reactor and were used to measure the neutron flux at several positions with the reactor sub-critical. The ion chamber high voltage was set at +500V, and the Keithley picoammeter was used to measure the current from the ion chamber, further acquired by the Yokogawa recorder.
The neutron source is photoneutrons produced in the Be reflector by gamma-rays from decaying fission products; these are multiplied by the sub-critical reactor. The signal from the ion chamber is also partly due to fission product gamma-rays. The reactor had been shut down five days before these measurements. Table 1 shows the measured currents at various positions. Position 1 is closest to the reactor, position 10 is with the housing at a 90° angle, and position 19 is the most distant from the reactor. It can be seen that ion chamber 97-11 has slightly greater sensitivity than ion chamber 14-48.

Position	Angle (º)	Current (μA)	
		97-11	14-48
19	180	37	35
10	90	138	127
1	0	1994	1460

Table 1 - Currents measured by ion chambers 97-11 and 14-48 at various positions

Manipulation of BF3 detector sets (sub-critical reactor): Two 25 mm diameter BF3 detectors were available, one 250 mm long and one 350 mm long. The 250 mm detector was installed in housing no.2 with its cable. The detector and the cable connector were surrounded by bubble

wrap to prevent contact with the housing and the creation of a ground loop. Each housing can be rotated on a pivot (over 180° at 10° intervals) to place the detector at 19 reproducible positions ranging from 368 mm (position 1) to 775 mm (position 19) from the axis of the reactor (or 63 mm to 470 mm from the exterior of the aluminium reactor container). After removing the assembly with the ion chamber, the assembly with the BF3 detector was installed in the same designated bracket of the Ecole Polytechnique SLOWPOKE reactor. Assembly no.2 rotated easily and could be positioned at any of the 19 positions.

Figure 6 - Dummy LEU fuel cage with dummy fuel pins

Measurement of fluxes of sub-critical reactor with BF3 detector sets and source: The 250 mm BF3 detector was used with its electronics package no. 2. The high voltage was set at +1500V, and the gain of the amplifier was adjusted so that the pulses corresponding to 2.31 MeV deposited in the detector had an amplitude of 1.5 V as seen on an oscilloscope. If a neutron is captured near the wall of the detector, the pulses had lower amplitude because part of the kinetic energy of one of the nuclei produced is deposited in the wall and not in the gas. The discriminator was set at 0.5 V in order to reject pulses from fission product gamma-rays.

The 250 mm BF3 detector was used to measure the neutron flux at several positions with the reactor sub-critical. The relative neutron flux was given by the BF3 detector count-rate.

Manipulation of commissioning rod worth by absorption of neutrons from a neutron source: Two commissioning rods were tested. In both, the absorber is a 0.81 mm wall-thickness Cd tube 0.95" diameter and 190 mm long. Measurements were performed to demonstrate that the two rods absorb neutrons. The 254 mm BF3 detector with its electronics and a neutron source were used to conduct the tests on the workbench. The BF3 detector and the neutron source were surrounded by moderator. With only an air gap between source and detector, the observed count-rate was 3900 cps. When either of the two commissioning rods was inserted between source and detector the observed count-rate decreased by approximately 20%.

5 Dummy LEU reactor core and assembly tools

5.1 Fabrication of Dummy LEU Core Components

Dummy LEU core is the one of the most important part of the demonstrations. It consists of LEU mock-up cage, dummy pins and masks for sequential loading, Figure 6. Other than the dummy core itself, tools for assembling and loading the LEU fuel pins, such as collet holding tool, anvil and riveting punch, were also designed and fabricated by Polytechnique Montréal to practice loading the pins into the fuel cage (shown in Figure 7) and to determine the best method for securing the fuel pins to the lower grid plate of the fuel cage. At the end, this dummy LEU simulates the core installed in the JM-1 reactor.

For the dummy LEU fuel cage, the top plate, the bottom plate, the central tube, the posts, the top pins and the feet were machined from SS 304 which has hardness similar to Zircalloy-4. These parts were assembled and welded together as shown in Figure 6. The top plate and the bottom plate each have more than 1000 holes that were machined to approximate the mass and hydraulic resistance of real LEU core.

Figure 7 – Loading the dummy LEU pins into the dummy fuel cage

The core lifting tool, shown in Figure 8, was designed and manufactured to fit both the dummy HEU and dummy LEU core assemblies. The main body of the tool is made from aluminium rod 21 mm diameter and 200 mm long. At first, aluminium was used as the sleeve material as in the original AECL design drawings. However, it was observed that the sleeve would not slide smoothly after several operations. Moreover, it was impossible to see if the tool has locked in the fuel cage properly at the bottom of the pool. Therefore, for better functionality of the tool, the sleeve material was changed to brass and tolerances were tightened to keep the concentricity.

5.2 LEU Core Installation Dry Runs

A total of 180 stainless steel fuel pins, 26 Zircaloy fuel pins and 3 sets of six masks (3 top, 3 bottom) were made available. Fuel pins are loaded according to the masks placed on the top and bottom of the fuel cage. The threading needle and the brass collet tool were used, shown in Figure 7 to hold the pin and to guide it into the desired position. To fix the pin in place, one person held the flat end of the cylindrical anvil against the top end of the pin and another person riveted the bottom end by peening with the hammer and punch.

Figure 8 – Dummy LEU core and core lifting tool

The dummy LEU core was built following the pattern of the masks and the 15 steps of the LEU fuel loading procedure. For the first few pins there was no difficulty placing the flat end of the cylindrical anvil against the top end of the pin to rivet the bottom end, but after many pins were installed it was difficult to ensure that the anvil was solidly touching the top of the pin to be riveted and not the others surrounding it. The anvil was therefore modified. One end was machined to create a raised central disk 10 mm in diameter and 3 mm thick with a flat recess machined 1 mm into this disk. With this modification, the flat recess could be placed on the pin to be riveted and the anvil would not touch the other pins. 18 of the 26 Zircaloy pins were loaded in the dummy cage. The other 8 were sent for further practice at JM-1 to be used before the real fuel loading. It was observed that riveting the Zircaloy pins required about the same force with the hammer as the stainless steel pins. A total of 190 pins were loaded. The almost fully loaded dummy cage with 190 fuel pins and weighing 8.8 kg was installed in the mock-up reflector using the available fuel cage handling tool.

After installing the dummy LEU core into the mock-up reactor critical assembly, the shim tray tool with its extension tubes was used to install the shim tray above the loaded dummy fuel cage. The reason for doing this was to verify that the shim tray would still fit in place even with the loaded LEU fuel cage which has fuel pins 7 mm longer than the HEU fuel pins. There was no indication that the shim tray was touching the tops of the fuel pins. The shim tray was then removed and brought to the surface. Its bottom was checked for eventual scratches from fuel pins, but none were identified.

6 Conclusion

The dry-runs were divided into four different categories: HEU core removal from reactor vessel,

tools and equipment manipulation for commissioning of LEU reactor, fuel pin loading and LEU core insertion into reactor vessel. All of these categories were first demonstrated by Polytechnique Montreal personnel and later the conversion team practiced until they felt comfortable with the process, equipment and tools. All questions of the conversion team were answered, and some minor recommendations on the tooling were dealt with to improve the tools and the smoothness of the process. The ability to carry out a detailed practice conversion ahead of time allowed the conversion team to adjust and streamline the processes and procedures, eliminating many unknowns during the actual conversion. All the JM-1 reactor conversion tools demonstrated performed successfully and according to the designed purpose. These demonstrations led to the optimization of the HEU to LEU conversion of the Jamaican JM-1 reactor that was successfully completed at the beginning of October 2015.

Acknowledgments

Among all the individuals who helped us during this project, the following contributors are specifically appreciated: Greg Kennedy former director of Polytechnique's SLOWPOKE reactor, Jean-Claude Juneau technician, Professor Alberto Teyssedou, Cyril Koclas and Cristina Cimpan research associates, George Burbidge and Manfred Müeller former SLOWPOKE reactor engineer and reactor technician respectively, personnel of machine shops of University of Montreal and Polytechnique Montreal. The work presented in this project was possible due to the financial support of ANL.

References

[1] J. Preston, C. Grant. *The Status of HEU to LEU Core Conversion Activities at the Jamaica Slowpoke*. CNL Nuclear Review, 2014, 51-55.

[2] C.N. Grant, J. Preston, C. Chilian, G. Kennedy. *SLOWPOKE-2 Refuelling – Past Experience and New Challenges*. Transactions of the RRFM 2013, St. Petersburg, Russia, 106-114.

[3] G. Kennedy and J. St. Pierre, L.G.I. Bennett and K.S. Nielsen, *LEU-Fuelled SLOWPOKE-2 Research Reactors: Operational Experience and Utilisation*, Transactions of the International Meeting on RERTR, San Carlos de Bariloche, Argentina, 2002.

[4] Hilborn JW, Townes BM. 1987. Converting the SLOWPOKE Reactor to Low-Enrichment Uranium Fuel. J. Radioanal. Nucl. Chem 110, 385-390.

Utilisation

Preparing JHR international Community through the developments of the first experimental capacity

Christian Gonnier ; Gilles Bignan ; Jérôme Estrade ; Catherine Santucci ; Daniel Parrat ; Thomas Le Jolu ; Stéphane Gaillot (1) ;

Marek Miklos (2) ; Abderrahim Al-Mazouzi (3) ; Petri Kinnunen (4)

(1) CEA: French Atomic and Alternative Energies Commission-France

(2) UJV/CVR –Rez Research Centre-Czech Republic

(3) EDF-Les Renardières Research Centre- France

(4) VTT Technical Research Centre of Finland

Corresponding author: christian.gonnier@cea.fr

Abstract

The Jules Horowitz Reactor (JHR) is a new Material Testing Reactor (MTR) currently under construction at CEA Cadarache research center in southern France to become one of the major research infrastructures for scientific studies dealing with nuclear materials and fuels behavior under irradiation. It is consequently identified for this purpose within various European road maps and fora; ESFRI, SNETP, NUGENIA… The reactor is also being optimized for medical Isotope production.
The reactor is designed to host various R&D programs dedicated to the optimization of the operation of the existing Nuclear Power Plants (NPPs), to assess the irradiation induced ageing of the non-replaceable and safety related components of the operating NPPs, to support the improvement, development and deployment of the third generation of NPPs as well as small modular reactors (SMR). It will also offer irradiation capabilities for GEN IV and fusion technologies.
Its flexibility is an asset to address the needs expressed by the scientific community (R&D institutes, Technical Support Organizations…) and the Industry (utilities, fuel vendors…).
Consequently, the JHR facility will become a major scientific hub for cutting edge research on fuel and material investigations.

JHR is fully optimized for testing materials and fuels under irradiation in normal and off-normal conditions:

- with high thermal and fast neutron flux capacities to address existing and future NPP needs,
- with highly flexible irradiation loops producing operational conditions compatible with the various power reactor technologies,
- with major innovative embarked in-pile and on-line instrumentation associated with out-of-pile analysis,
- with various non-destructive examination benches and analysis laboratories to perform state-of- the-art R&D experiments and to obtain reliable and quantitative results with high spatial resolution and precision.

JHR is designed, built and will be operated as an international User's Facility open to international collaboration.

To achieve this objective, JHR Project has:

- set up an International Consortium, for close partnership between the funding organizations
- Extended the collaboration to some international partners to help in the development of the first fleet of experimental devices,
- gathered an international scientific Community for exchange of information and knowledge including scientific and technical seminars to identify and prioritize the topics of interest,

- organized within this international Consortium 3 Working Groups, namely on fuel, material and technology issues to provide recommendations and guidance regarding the reactor experimental capacity including hints on the facilities to be developed versus potential R&D needs,
- prepared within these 3 Working Groups a proposal for the first JHR International Program, intended to be open to non-members of the JHR Consortium.

This paper will give an update of the on-going work performed to build the first JHR experimental capacity. It will also illustrate the main outcome of the 3 Working Groups regarding the R&D needs. Finally and most importantly, it will describe the first proposal of joint international program under preparation.

1. OBJECTIVES OF THE WORKING GROUPS

The Fuel, Materials and Technology Working Groups (FWG, MWG and TWG) gather scientific representatives and experts from the JHR Consortium members. Their role is to give orientations and recommendations, as a technical support and without commitment, to the future "International Advisory Group" (IAG) indicated on the Consortium Agreement, to prepare future programs in JHR.
As this IAG is not yet in existence, the objective of the WGs is to advise the Governing Board (GB) on potential scientific topics of interest for future R&D programs in JHR, through proposal of joint international program(s) or multi-lateral program(s). It is interesting to quote that such future programs could be open to non-Members of the Consortium, to enlarge the scientific community on JHR.

2. WORKPLAN SET UP BY WORKING GROUP PARTICIPANTS

To reach the above objective, participants integrated some orientations from the GB:

- Develop matrix experiments for future programs in JHR,
- Initiate in a short term future new R&D programs which could start in existing MTRs and/or in hot cell Laboratories, according to their possibilities, in order to be continued in the JHR at a larger stage and with the added value of the JHR,
- Establish a roadmap detailing how to address this matrix of experiments, considering either existing devices for "qualification experiments" in existing facilities or in the JHR fleet of experimental devices currently under design, or if necessary development of new components,
- Consider the cost/benefit analysis in a second stage,
- Allow strong interactions and cross-fertilization between the WGs.

Based on these orientations, MWG and FWG members decided to examine successively following points:

- Identify open issues in the field of nuclear fuel and nuclear materials development and qualification, by each member, taking into account their scientific and/or industrial interest(s),
- Discuss in depth topics of common interest between the participants of the same WG,
- Define criteria to elaborate a "ranking grid" to have a more quantified and detailed evaluation of interest experiments from participants, with the aim to set up a comparable grid for fuel and materials irradiation experiments:
    - Fuel / Materials types,
    - Reactor systems considered,
    - Experimental objectives and main irradiation conditions,
    - Availability and constraints of JHR experimental devices,
    - PIE to perform,
    - …
- Comment, amend and complete the «ranking grid », then assess it and set up a "priority list" based on received answers,
- Select a first set of potential joint or multilateral experiments in JHR, with special attention to programs which could fulfill the needs of both FWG and MWG,
- Consider the feasibility of these first programs, in particular the possible role of existing MTRs associated with (hot)-labs as support for qualification and/or benchmarking experiments and the added value offered by the JHR.

To help to set up this roadmap, the Technology WG provided a description of the JHR experimental capacity available at the reactor start-up and gave the main operating parameters of JHR fuel and material irradiation devices. Moreover the Technology WG checks the good compliance of the experimental capacity under development versus these potential needs expressed by the FWG and MWG.

3. IDENTIFICATION OF OPEN ISSUES IN THE FIELD OF FUEL DEVELOPMENT AND QUALIFICATION

In the fuel domain, 12 topics of interest were identified, accompanied by specific needs and recommendations expressed by participants during the two first meetings. These topics and comments allowed to elaborate and structure the ranking grid and to orientate the range of main irradiation parameters in future irradiation programs. A few topics are cross-cutting with cladding and assembly skeleton materials when coupled effects are active (clad internal corrosion, power ramp…).

A generic question was discussed in the both groups about in-pile experiments dealing with severe accidents experiments (and at least beyond LOCA conditions): it has been decided to not consider this topic in the first phase of the work, mainly because the JHR experimental capacity doesn't integrate such possibility during its first years of operation. However, an internal study has been done by JHR team detailing constraints related to implementation of such experiments: progressive adaptation of the JHR reactor block versus increasing complexity of an integral experiment, consequences on other experiments simultaneously present in core and in reflector…

3.1 Fuel development for Gen II-III power systems

This topic includes new fuel concepts actually under development with the aim to be more tolerant to accidental transients (Enhanced Accident Tolerant Fuels, or "E-ATF").

- LWR fuel material basic properties:
  - thermal and irradiation properties (thermal conductivity, creep, local oxygen potential… mainly at high burn-up),
  - fission products (FP) and He distribution and effects on the microstructure (e.g. FP compounds formation),
  - irradiation effects at beginning of life (BOL) for new concepts (cracking, sintering…).
- Integral LWR fuel element performance study in normal operation :
  - fuel rod integral performance (select new candidates and comparison with reference materials),
  - cladding and fuel assembly structural materials performance in specific chemistry conditions (innovative claddings, hydrogen pick-up and distribution, corrosion and cruds, deformation).
- Integral LWR fuel element performance in high demanding conditions:
  - burn-up extension of pre-irradiated rods,
  - power up-rates, power cycling, load following and Extended Reduced Power Operation (ERPO).
- LWR fuel testing up to limits as in incidental conditions:
  - power ramps (crack initiation and propagation, clad integrity thresholds, pellet-cladding chemical interaction, FP release and radiological source-term),
  - power to melt (fuel melting centerline temperature based on a progressive approach),
  - lift-off (mechanisms and acceptable rod overpressure limits),
  - axial transport of gases (fuel-clad gap hydraulic conductance determination, axial effects and cycling effects),
  - dry-out (controlled approach of dry-out conditions),
  - failed fuel behavior in normal operation and on the long term, including operational transients (failure development (Delayed Hydride Cracking), radioactive source term, fuel degradation…) and use of advanced cladding material (e.g. SiC, Mo, coated…).
- LWR fuel behavior in accidental conditions:
  - LOCA-type conditions (clad ballooning, burst, and hydriding, fuel fragmentation, pulverization and ejection, grid effects, radioactive source term, bundle geometry after quenching…),
  - specific off-normal conditions (fast transients activating similar phenomena as a reactivity insertion accident RIA, cladding integrity, interaction with coolant…).
- Integral LWR fuel bundle performance study:
  - fuel bundle behavior / guide tubes and grids: grid-spring interaction, Stress Corrosion Cracking, guide tubes axial creep, effect of rod bowing),

- control rods and burnable absorbers: thermal-mechanical and geometrical evolutions, neutron absorber consumption).
- High conversion LWRs:
  - integral fuel performance study (fuel element concept validation, high burn-up objectives).
- Fuel for future SMR concept

3.2 Fuel development for Gen IV power systems

- Fuel for power fast reactors:
  - thermal-mechanical fuel properties at BOL (basis properties, central hole formation, gap size evolution, margin to central melting…),
  - thermal-mechanical fuel properties during irradiation and at end-of-life (EOL) (basis properties, clad corrosion…),
  - fission product effects (FP retention, "joint oxide-gaine" (JOG) formation, fissile-fertile interaction),
  - integral fuel performance for sodium fast reactor (SFR) – type concept (high burn-up conditions, FP chemical behavior, behavior in transients…),
  - integral fuel performance for accelerator-driven system (ADS) – type concept (fuel-coolant interaction, fuel-cladding chemical interaction, behavior in transients…),
  - integral fuel performance for gas fast reactor (GFR) – type concept (high burn-up conditions, FP chemical behavior, behavior in transients…).
- Minor actinide transmutation:
  - fuel material selection (fuel swelling and gas release versus manufacturing process and actinide content ; transmutation efficiency),
  - fuel material characterization in normal conditions (temperature evolution, He release…),
  - fuel material characterization in transient conditions (temperature evolution, He release…),
  - specific transmutation concepts (fuel swelling and gas release versus actinide content, transmutation efficiency…).
- Particle fuel concept:
  - fuel performance and burn-up effects (fission product permeation and release, particle reliability rate, release of other gases…).

3.3 Development of driver core for research reactors

- Fuel performance assessment and qualification (high burn-up performance, cladding oxidation, fuel microstructure evolution, cladding integrity in transients…).
- Fuel assembly qualification (fuel element geometry evolution, mainly at high burn-up…).

3.4 Fuels of interest

Power reactor system	Types of fuel
Gen II-II fuels	• UO_2 • Integral Burnable Absorber UO_2 (e.g. UO_2-Gd_2O_3) • Additive UO_2 • LWR MOX and reprocessed U • Thorium fuel • High Density (xC, xN) • Enhanced Accident Tolerant Fuels (E-ATF) innovative concepts (new geometry, fuel with additives, Vipac, micro-cell, particle fuels…)
Gen IV fuels	• UO_2 • $(UPu)O_2$ • Thorium fuel • Carbide fuel • Nitride fuel • Minor actinide ("MA") bearing fuel, homogeneous or

	heterogeneous concepts • Particle fuel
Fuel for research reactors	• UAl_x • U_xSi_y • UMo • Other fuel concepts • Plate geometry (plane, curved) / Rod geometry

4. IDENTIFICATION OF OPEN ISSUES IN THE FIELD OF MATERIALS DEVELOPMENT AND QUALIFICATION

MWG members identified following items as basis and common requirements:

- Ensure a comprehensive mastering and follow-up of the irradiation conditions in terms of local neutron flux and spectrum, temperature homogeneity and thermal gradients,
- Realize instrumented tests on loaded (monotonic, cyclic, …) specimens (different geometries) under well controlled conditions including control of the chemistry and temperature of the medium,
- Control and monitor of temperature even under shutdown conditions,
- Provide the possibility to un/re/load irradiated materials in the JHR experimental devices,
- Measure as precisely as possible the deposited local energy and its field variation with the power (local gamma heating …),
- Define an experimental validation program (in continuity with OSIRIS).

4.1 Cladding

- In-pile mechanical behavior of cladding:
  - Mechanical behavior (creep test) with on-line biaxial control (stress and strain),
  - Effect of environment on mechanical behavior (various LWR environments).
- Dose accumulation effect on cladding (Gen II/III, Gen IV):
  - Effect of irradiation on microstructure, hardening, embrittlement, creep (Gen II/III),
  - Effect of irradiation on microstructure, swelling, embrittlement, creep (Gen IV).

4.2 High demanding conditions:

- LWR fuel assembly behavior in accidental conditions (LOCA).

4.3 Reactor Pressure Vessel (RPV) / Internals:

- **RPV**
  - Dose accumulation (Gen II/III, Gen IV): Irradiation effect on the microstructure and mechanical properties.
- **Internals**
  - Dose accumulation (Gen II/III, Gen IV),
  - Environnent effect (LWR),
  - Mechanical behavior (in pile).

4.4 Absorbers:

- Dose accumulation (Gen II/III, Gen IV)
  - Effect of irradiation on microstructure,
  - Overall behavior (degradation, swelling, etc..).

4.5 Materials of interest

Power reactor system	Materials of interest
Gen II/III materials	• Zr-based alloys (cladding) • E-ATF claddings (Coated Zr, Coated Mo, SiC sandwich, SS claddings, etc.) • Low alloy Steels (RPV) • Austenitic stainless steels (Internals) • Absorber
Gen IV materials	• Ferrito-martensitic stainless steels (cladding) • Austenitic stainless steel (cladding) • ODS steels (cladding) • Stabilized zirconia (coating of pressure tubes) • Graphite • Absorber (B_4C)

5. Position Paper: first proposal for a JHR International Joint program

After 3 years of fruitful scientific and technical exchanges, the Working Groups have finalized a synthesis document (internally distributed to the Board Members in December 2015) gathering a reminder of possible experiments in JHR with associated stakes; it also gives indication on level of interest for each topic and proposed further developments.

Fuel and Materials WG participants have followed three successive steps, namely:

1. Identify open issues in the field of nuclear fuel and nuclear materials development and qualification, taking into account their potential scientific and/or industrial interest(s),

2. Elaborate and assess a "ranking grid" in order to set up a list of participant's common interests,

3. Define and elaborate first common experiments aiming at validating/benchmarking either the experimental devices under development and/or the irradiation parameters expected in specific locations within JHR.

For this last point, It appears a consensus within the 3 Working Groups to define between now and the first operation of the JHR some "pre-JHR" Experiments of common interest with added value in terms of either qualifying the experimental conditions or explore the performance limits of the devices. These qualification experiments will be proposed in existing MTRs and/or hot cell laboratories, according to their possibilities and for starting a first international joint program in the coming years before continuing it in JHR.

Thus, the two first common experiments, identified for further development, are the following:

- Fuel Working Group members proposed power-ramp experiments as a first choice, including irradiation process qualification and benchmarking objectives (in order to point out the added value of the JHR experimental capacity on this domain) without considering any industrial fuel qualification (analysis of the phenomena involved in a power-ramp without trying to reach operating limits). This is linked to a potential important topic for utilities as Nuclear Power Plant may be in the future more solicited for electricity need follow-up thus putting the fuel under more demanding power transients.
- Material Working Group members focused on irradiation effects on Internals and more specifically on checking the effect of ratio between epithermal neutron flux and fast neutron flux on their mechanical properties. This specific point (which will be addressed in JHR with high performances) appears of particular interest for harmonizing interpretation of such physical parameters versus dpa (displacement per atom) thus having an impact for NPP both for Internals components management and for Long Term Operation. In fact, previous experiments have shown that the nature of the neutron spectrum may affect damage accumulation kinetics (e.g. segregation, bubbles/voids formation, precipitation …) and

hence influencing the response of the material when subjected to external stresses in primary water environment.

It has also been underlined that such program proposals are of exploratory nature without any commitment and therefore could be open to non-Members of the Consortium to enlarge the scientific community around JHR.

5.1 FIRST FUEL EXPERIMENTAL JOINT PROGRAM

Fuel WG members agreed to propose power ramp – type experiments on a PWR sample (the JHR experimental devices in view for this "pre-JHR" experiments is the ADELINE device), with following features and objectives:

- This program will firstly include irradiation process qualification and benchmarking objectives, in order to point out the added value of the JHR in terms of :
    - Maximum linear power reachable on an experimental rod at a given burn-up,
    - Flexibility of the irradiation process, with a high independency from the MTR operation (e.g. rod loading/unloading during the reactor cycle),
    - Capability for test section instrumentation (on-line measurement of parameters such as clad elongation or internal gas pressure),
    - Quick checking of the rod "as tested" by on-site non-destructive examinations (NDEs).

5.2 FIRST MATERIAL EXPERIMENTAL JOINT PROGRAM

In the context of addressing some specific characteristics of JHR, the Material Working Group (MWG) identified among others, the need to:

- Ensure a comprehensive mastering and follow up of the irradiation conditions in terms of local neutron flux and spectrum, temperature homogeneity and thermal gradients ;
- Define an experimental validation program to ensure the continuity with OSIRIS

Consequently, MWG members agreed to focus this first experiment on the qualification of the MICA and OCCITANE devices under development. The specifications of these two devices indicated that the ratio (Rs) between epithermal neutron flux (E>0.1 MeV) and fast neutron flux (E>1 MeV) might be different according to their location in the reactor: for instance, MICA device (Rs around 2 in the core) and/or OCCITANE device (Rs around 3 in the reflector). Thus, it appears of paramount importance to check out the effect of this ratio especially when considering the, irradiation effect on Internals.
In fact, this ratio is of particular interest to:

- address key physical parameters such as dpa (displacement per atom),
- underpin the effect of the spectrum on the irradiation damage accumulation kinetics/nature,
- allow the transferability of experimental data between operating MTRs and future JHR,
- define the necessary instrumentation and PIE to assess the microstructural changes and their effect on mechanical properties of the material when in contact with the primary environment.

6. CONCLUSION AND RECOMMENDATIONS

During these last 3 years, the Working Groups set-up by the Governing Board have produced significant amount of work which are summarized in the various minutes of meetings and in the documents indicated here in reference.

One of the most important point is that it has helped creating a “JHR Scientific and Technical Community” allowing scientists from all Consortium Members to exchanges their future interest in the JHR.

It is also important to pinpoint the fact that a consensus arises from the 3 Working Groups to go-ahead with “Pre-JHR” experiments in existing MTRs for the benefit of the future JHR experimental capacity; this is the main outcome described in this “position paper”.

To enhance the scientific community around JHR, it is proposed by the 3 WGs to enlarge the potential number of partners associated to this first International Joint Program; this is the main reason of having the next JHR seminar (April 2016-Marseille) embedded with the NUGENIA forum: it will give us a very good opportunity to present the main outcomes of the WGs and to present in detail this proposal of Joint Program to potential partners who are non-member of the Consortium.

CURRENT AND FUTURE UTILISATION OF MARIA RESEARCH REACTOR

G. KRZYSZTOSZEK
Department of Nuclear Facilities Operation, National Centre for Nuclear Research
A. Sołtana 7, 05-400 Otwock – Poland

ABSTRACT

The high flux research reactor MARIA is operated at the National Centre for Nuclear Research. It is a water and beryllium moderated reactor of pool type with graphite reflector and pressurized channels containing concentric tube of fuel element. It has been designed to provide high degree of flexibility. The reactor conversion was fully completed in August 2014.
MARIA reactor is mainly used for irradiation materials used in radioisotope production for "Polatom" Centre and Mallinckrodt Pharmaceuticals company.
The current supply of Mo-99 for nuclear medicine is around 2100 six days Ci/week. MARIA reactor offers special irradiation in converter of 14 MeV neutrons. For future we propose BNCT research/training station for: radiobiology, boron carriers, dosimetry, treatment planning systems

1. Description of MARIA reactor

The high flux research reactor MARIA is a water and beryllium moderated reactor of a pool type with graphite reflector and pressurised channels containing concentric six-tube assemblies of fuel elements. It has been designed to provide high degree of flexibility. The fuel channels are situated in a matrix containing beryllium blocks and enclosed by lateral reflector made of graphite blocks in aluminium cans. The MARIA reactor is equipped with vertical channels for irradiation of target materials, a rabbit system for short irradiations and six horizontal neutron beam channels. The MARIA reactor reached its first criticality in December 1974. The reactor was in operation until 1985 when it was shut down for modernization. The modernization encompassed refurbishment and upgrading of technological systems such as:

- enlargement of beryllium matrix,
- inspection of the graphite bocks,
- upgrading of ventilation and temperature systems.

The second step of upgrading the technological system was done from 1996-2002 (during regular maintenance) and it was consisted with: replacement of heat exchangers, replacement of instrumentation and control system, upgrading of radiation protection system, modernization of fuel element integrity monitoring system. The reactor was fully converted from HEU to LEU fuel in the end of August 2014. In the end of March MARIA reactor received the new license for reactor operation till 2025 year.
The main characteristics and data of MARIA reactor are as follows:

- nominal power 30 MW(th),
- moderator H_2O, beryllium,
- cooling system channel type,
- fuel assemblies:
  - material U_3Si_2
  - enrichment 19,75%
  - cladding aluminium
  - shape five concentric tubes
  - active length 1000 mm.

- output thermal neutron flux
  at horizontal channels $3 \div 5 \times 10^9$ n/cm^{2}s

The main areas of reactor application are as follows: production of radioisotopes, testing of fuel and structural materials for nuclear power engineering, neutron radiography, neutron activation analysis, neutron transmutation doping, research in neutron and condensed matter physics. For today the NCBJ has a program for MARIA research reactor operation till 2030.
MARIA reactor core contains the fuel assemblies which are installed in pressurized channels embedded in matrix sockets. The matrix is composed of beryllium blocks which are fastened to the support slab in reactor pool on the level +2.75 m. Beryllium blocks of the core matrix as well as the graphite blocks creating the radial reflector are positioned in the sockets of separator slab on the level – 1.4 m (6x8) Fig.1 and Fig. 2.

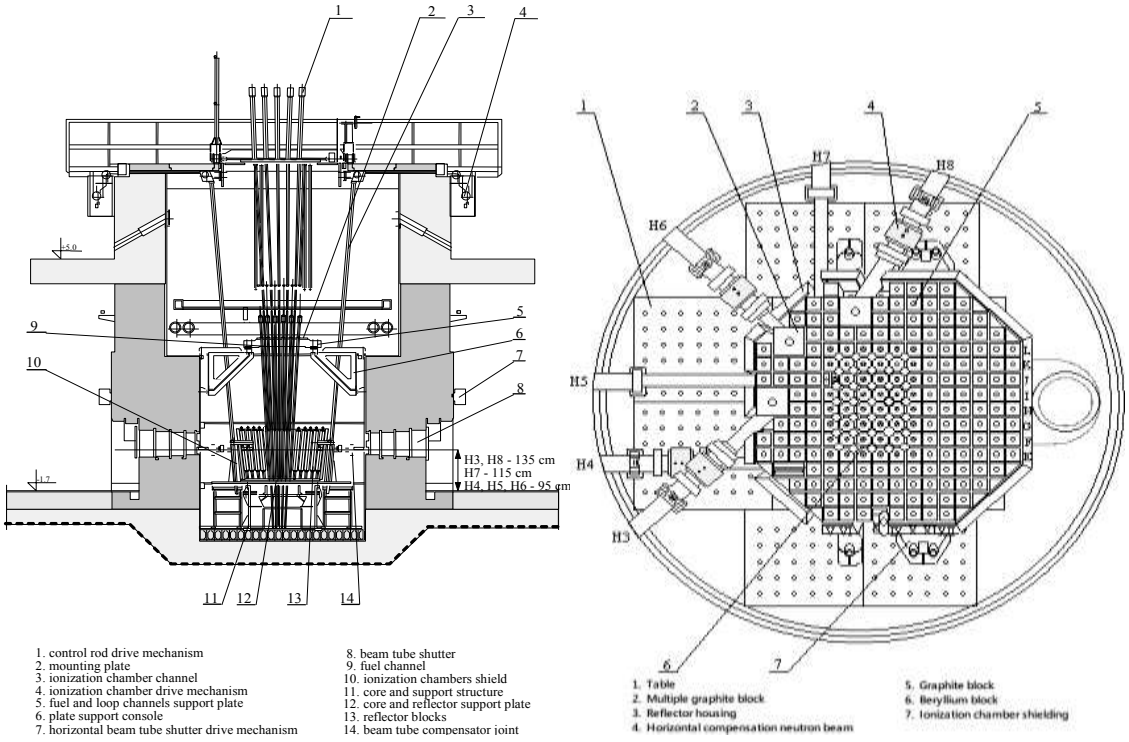

a) b)

Fig. 1: a) vertical cross-section of the reactor pool, b) top view of the reactor core and reflector.

2. Reactor Operation

In 2015 the reactor completed 36 operation cycles at power levels from 30 kW to 25 MW (Fig. 2). The overall operation time: 4806 h.

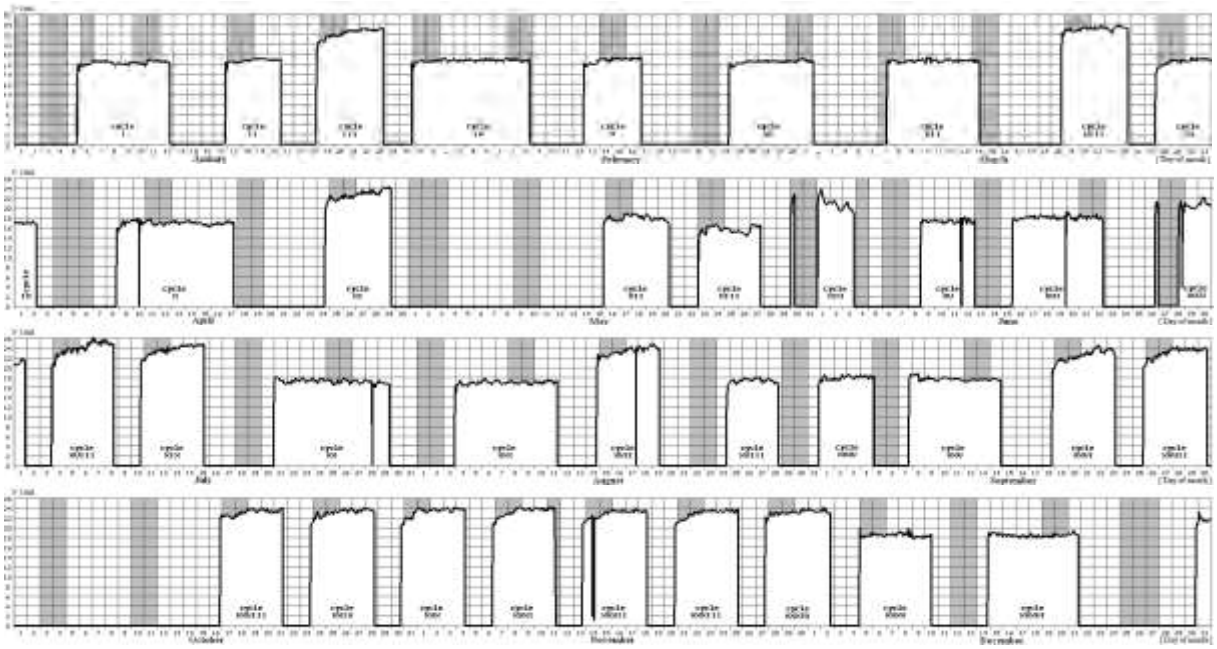

Fig. 2. Schedule of the reactor MARIA operation in 2015.

The main activities carried out in MARIA reactor were focused on:
- irradiation of target materials in vertical channels and in rabbit system,
- neutron scattering condensed matter studies with neutron beams from reactor horizontal channel,
- neutron radiography studies,
- neutron modification of crystals and minerals.

In 2015 the MARIA reactor was operated successfully. The reactor scram was activated 8 times and in 2 cases the shortening of the operation cycle was necessary.
Operational availability factors were following:

$$A1 = \frac{OT}{NH} \cdot 100\% = 98\%$$

$$A2 = \frac{OT}{8760} \cdot 100\% = 54{,}5\ \%$$

where *OT* (operational time) denotes the number of hours on power and *NH* is the sum of number of hours on power and the number of unscheduled shutdown.
The total emissions of radioactive materials to the environment were:
- inert gases (mainly ^{41}Ar): $9.3 \cdot 10^{12}$ Bq, i.e. 0.9% of the limit determined by the NAEA,
- iodine: $3.2 \cdot 10^{7}$Bq, i.e. 0.6% of the limit determined by the NAEA,
- ^{88}Rb and ^{138}Cs: $8.4 \cdot 10^{6}$ Bq.

Neutron irradiation services provided at the MARIA research reactor include mainly radioisotope production, neutron activation analyses and biomedical technology.
Irradiation services are performed in various facilities constructed in the MARIA reactor, depending on the required neutron flux levels, irradiation times, target mass and geometry. The standard vertical in-core isotope channels as well as the special ones equipped with hydraulic transport system are in operation.
For the domestic customers the targets of S, TeO_2, Lu_2O_3, Yb_2O_3, Cu, Se, $SmCl_3$ and KCl were irradiated (Fig. 3). Most of them were produced for the POLATOM Radioisotope Centre
Total annual isotope production reached 1480 TBq.

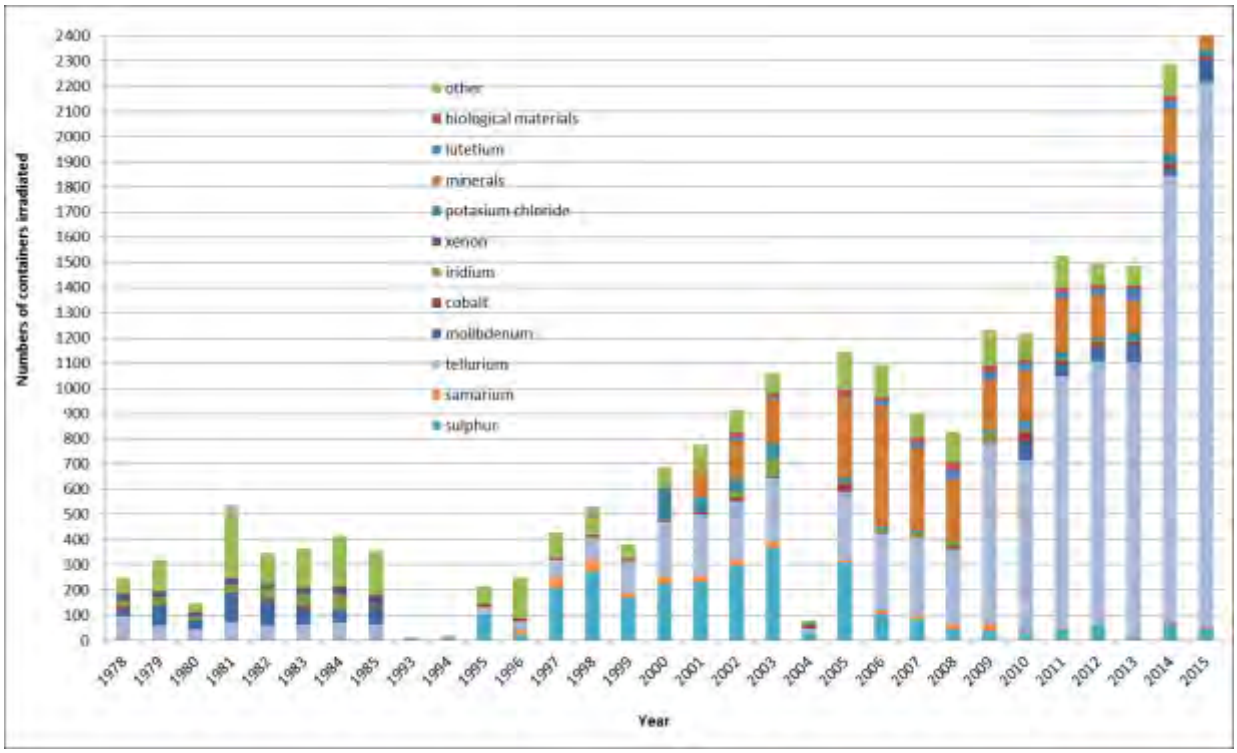

Fig. 3 Distribution of target materials irradiated

3. Current status of Mo-99 production in the MARIA reactor

In the period March 2010 to December 2015, 94 irradiation cycles in the MARIA reactor were conducted. In all cycles were irradiated 1448 HEU plates.

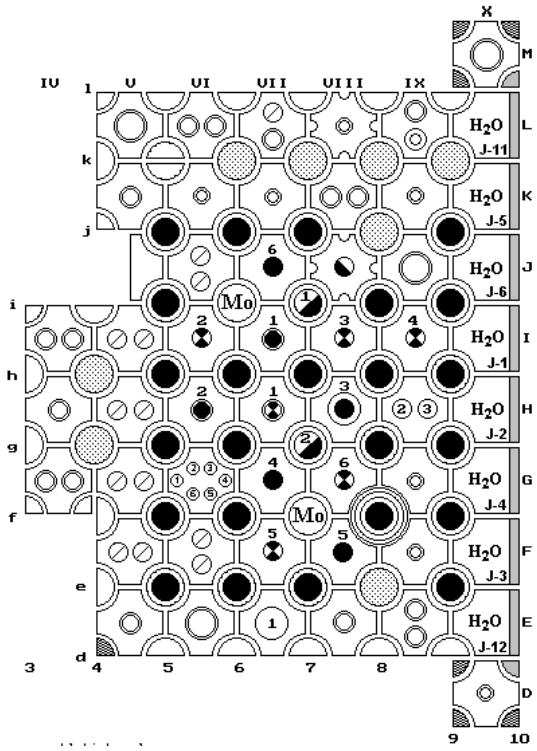

Fig. 4. A typical configuration of the MARIA reactor core with molybdenum channels.

Irradiations were conducted in two different locations of molybdenum channels (f-7 and i-6) and different configurations of the core. The typical configuration of the core for irradiations of molybdenum channels is shown in Fig.4.
The details of irradiation cycles of uranium plates in the Maria reactor are presented below:

	8 plates	**12 plates**
- power generated in molybdenum channel:	170-200 kW	240-250 kW
- activity reached (EOI):	7000-8000 Ci	9500-10000 Ci
- time of irradiation:	120 hours	120 hours
- flow rate of cooling water:	25 m^3/h	25 m^3/h
- temperature difference:	4-6 °C	8-9 °C
- cooling time of irradiated plates before transfer to the hot cell	12-15 hours	12-15 hours

The technological parameters of MARIA RR core are shown in *Fig.5*.

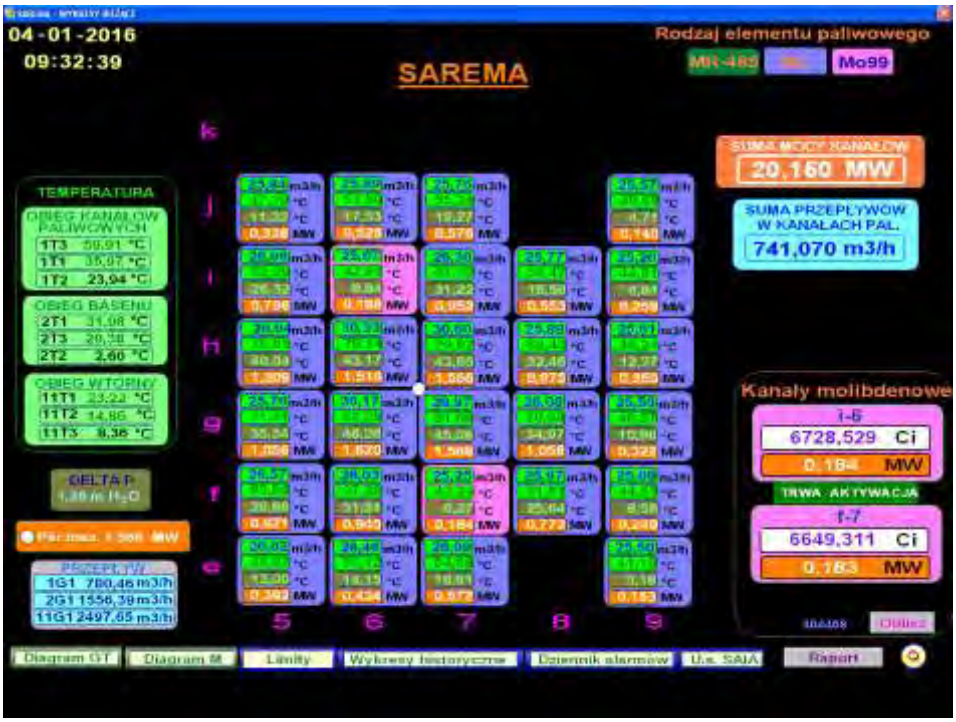

Fig. 5. Diagram of MARIA RR core.

3.1. Irradiation program of HEU IRE targets in MARIA

In the beginning of 2014 we have started cooperation between NCBJ and IRE, Belgium to develop the technology of U-targets irradiation, handling and loading to the AGNES transport containers and then expedition of irradiated targets to the processing facility in Flerus (Belgium).
The scope of program includes:

- safety analysis (neutronic, thermohydraulic in steady states, transient and emergency situation),
- technology of irradiation handling and reloading of irradiated targets:
  - manufacturing and commissioning of an irradiation facility,

- licensing process (interaction between NCBJ and Regulators Authority
- training of MARIA reactor operators,
- hot tests.

We plan to irradiate HEU IRE targets tubes in position h-8 of MARIA reactor core, Fig. 4.
In one channel will be irradiated 9 tubes and total power generated in these tubes will be around 190 kW during 120 hours of irradiation time. We assume that activity of molybdenum will be 107 - 6 day Ci per target.

3.2. Certification of LEU target

Under supervision of the Mallinckrodt Pharmaceuticals and with collaboration with HFR and BR2 reactors we are developing irradiation and transport technology of a new designed Low Enriched Uranium (LEU) targets for molybdenum production.
In order to support the qualification of the new LEU targets at MARIA reactor the following activities must occur:

- modification of the design existing molybdenum channel and manufacturing of the new parts;
- upgrading of expedition devices;
- modification of existing equipment in the hot cell;
- adaptation of the hosting device for MARIANNE transport container;
- licensing process.

Testing irradiation is predicted in the second part of 2016.

4. Research activities in MARIA

4.1 Collaboration between NCBj and CEA, France

In September 2014 and November 2015 the NCBJ in collaboration with CEA and AMU, France have evaluated of gamma heating in research reactors.
The scope of works consist of:

- gamma heating measurements in MARIA,
- development n-gamma transport model for MARIA reactor,
- development of in-core measurements capabilities.

With cooperation between MARIA and JHR, Cadarache we are working on development of new beryllium poisoning calculation model which consist of:

- validation of poison concentration calculations (Li-6, He-3, H-3) in beryllium samples irradiated in the reactor,
- possibility of beryllium blocks usage extension.

The results will be used in MARIA and JHR reactors.

4.2 The thermal to 14 MeV neutron converter

The first tested operation of the converter in the MARIA reactor was launched in September 2014. The neutron energy spectrum inside the converter depends on its location in the reactor core. In the chosen location, during testing opertaions the 14 Mev neutron flux density was estimated to be over $10^{9}cm^{-2}s^{-1}$, whereas fast fission neutrons inside the converter achieved $10^{12}cm^{2}s^{-1}$ and thermal neutrons were reduced down to $10^{9}cm^{2}s^{-1}$. The neutron flux densities were measured by means of the activation method.

5. Future of MARIA reactor

5.1 Neutron beam studies

We started upgrading of experimental hall for new spectrometers from Zentrum Berlin Helmholts (HZB). The three out of five instruments below will be delivered to MARIA reactor:
E1 – Triple axis spectrometer
E2 – Flat-Cone and powder diffractometer
E4 – TwoAxis Diffractometer
E5 – Four-Circle Dffractometer
E6 – Focusing Diffractometer

5.2 Irradiation of target materials

MARIA will continue irradiation of HEU and LEU targets for molybdenum production. We will cooperate with CR POLATOM on continuous irradiation of target materials for radioisotope production.

5.3 Epithermal neutron source

In 2013 a programme aimed a neutron beam for many different applications was resumed. It would be epithermal neutron beam of flux density exceeding $10^9 ncm^{-2}s^{-1}$. Two of eight horizontal research channel at MARIA reactor were allocated to a training and research station, Fig.6. In 2014 it was decided to construct a new fission converter, powered by uranium fuel plates made for this purpose.

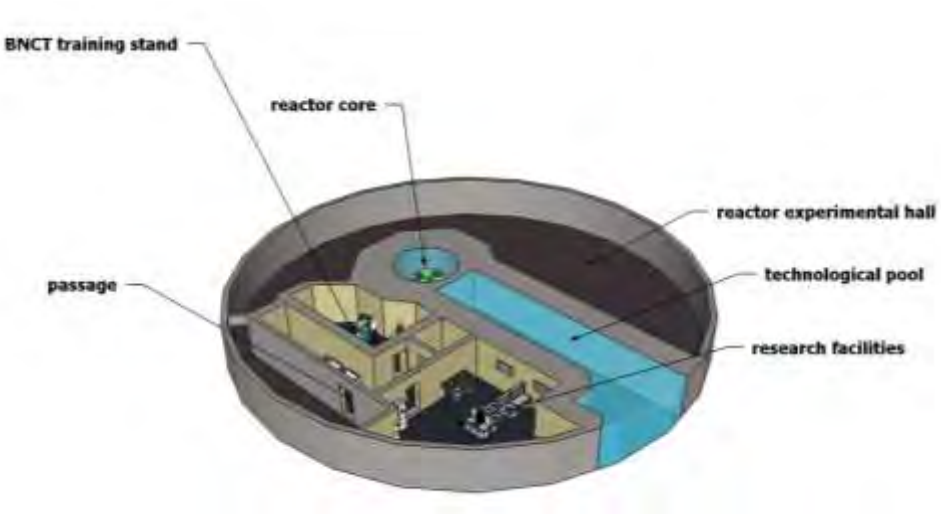

Fig. 6 Fission converter based research /training station at the MARIA research reactor.

A series of studies are being carried out to prepare the neutronic, thermal – hydraulic and engineering design of the converter.
BNCT combines many different fields of research . Beyond the irradiation facilities the second important issue is the boron carries. Neutron capture ^{10}B-containing compounds should cause preferential killing of tumour cells and induce therapeutic effects. There is a strong group of scientists in Poland with significant achievements in this area and they report the need for irradiation experiments on the use of boron compounds,. Also, for the development of many other research areas, it is necessary to conduct research using a high intensity epithermal neutron source, e.g.: dosimetry, electronics, technical equipment, radiobiology, molecular biology.

6. Conclusion

From the 2010 when we started irradiation of HEU U-targets MARIA research reactor is in the supply chain to ensure a reliable supply of molybdenum-99 for nuclear medicine.
Reactor was fully converter from HEU to LEU fuel in August 2014.
MARIA reactor will be operated at least to 2030. Basic technological systems of reactor (main pumps, heat exchangers, dosimetry) upgraded. Moveable components of reactor: core and reflector will allow to prolong operating lifetime of reactor. All HEU spent nuclear fuel elements were exported to Russian Federation.

Design improvement of capsule for a higher neutron irradiation fluence

K.N. CHOO, M.S. CHO, S.W. YANG, T.H. Yang, M.S. Kim
Korea Atomic Energy Research Institute 1045 Daedeokdaero, Yuseong-gu, Daejeon 305-353, Korea

S.H. Hong
Department of Mechanical Design Engineering, Chungnam National University, 79 Daehangno, Yuseong-gu, Daejeon, Korea

ABSTRACT

To scope the user requirements for a higher neutron irradiation fluence, several efforts using an instrumented capsule have been performed at HANARO. During the last three years, a long-term irradiation capsule technology of up to 3 dpa (displacement for atom) was developed at HANARO. The new capsule technology was successfully applied for neutron irradiation of the core materials (graphite, beryllium, and zircaloy-4) of research reactors as a part of the National Research Reactor Development Project. The long-term irradiation capsule technology was scheduled to extend its capability to up to 5 dpa for the next three years starting from this year, particularly for the irradiation of materials of future nuclear systems. 5 dpa is equivalent to irradiation testing for 15 cycles at HANARO. An improvement of the capsule technology will be performed based on safety analysis and a design optimization of the irradiation capsule. However, for a higher neutron fluence exceeding 5 dpa, new capsule technologies including flux-boosting, re-irradiation, and re-instrumentation are under plan as the next 5-year R&D project starting from 2017 at HANARO.

1. Introduction

The High Flux Advanced Neutron Application Reactor (HANARO), located at the Korea Atomic Energy Research Institute (KAERI) in Korea, has been operating as a platform for basic nuclear research in Korea, and the functions of its systems have been improved continuously since its first criticality in February 1995. To support the national research and development programs on nuclear reactors and nuclear fuel cycle technology in Korea, irradiation facilities have been developed and actively utilized for the irradiation tests requested by numerous users [1-3]. Most irradiation tests have been related to national R&D relevant to present nuclear power reactors such as the ageing management and safety evaluation of the components. HANARO has recently supported national R&D projects relevant to new nuclear systems including System-integrated Modular Advanced Reactor (SMART), research reactors, and future nuclear systems. HANARO has successfully contributed to the development of national nuclear technology [2].

Following the experience with HANARO, KAERI has been constructing a new research reactor, which is named the KIJANG Research Reactor (KJRR). The KJRR is due to start up in 2019 and will be mainly utilized for isotope production, NTD (Neutron Transmutation Doping) production, and the related research activities. Therefore, HANARO will specialize more on irradiation research of nuclear materials.

To effectively support the national R&Ds relevant to the present NPP, research/SMR reactors, and future nuclear systems, the development of advanced irradiation technologies is being preferentially developed at HANARO. Especially, irradiation technologies for high neutron fluence are inevitably required for the characterization of

nuclear fuel and material performance of future nuclear systems. To scope the user requirements for a higher neutron irradiation fluence, several efforts using an instrumented capsule have been performed at HANARO.
In this paper, the on-going design improvement of irradiation capsule for a higher neutron irradiation fluence at HANARO are described, and future plan for a much higher neutron fluence is discussed.

2. Irradiation at HANARO

2.1 Irradiation Capsule

HANARO, a 30 MW open-pool type multipurpose research reactor, has been operated as a platform for nuclear researches in Korea. Both the general design features and detailed information about this reactor are available on the HANARO home page (http://hanaro.kaeri.re.kr). Table 1 shows the characteristics of the reactor test holes for a fuel/material irradiation at HANARO [4].

Location	Hole		Inside Dia. (cm)	Neutron Flux (n/cm^2 . sec)	
	Name	No.		Fast Neutron (>0.82 Mev)	Thermal Neutron (<0.625 ev)
Core	CT IR OR	1 2 4	7.44 7.44 6.00	1.95×10^{14} $1.80/1.76 \times 10^{14}$ $1.92 \sim 2.01 \times 10^{13}$	4.30×10^{14} $3.83/3.80 \times 10^{14}$ $2.94 \sim 3.30 \times 10^{14}$
Reflector	LH HTS IP	1 1 17	15.0 10.0 6.0	7.35×10^{11} 1.72×10^{11} $1.43 \times 10^{9} \sim 2.17 \times 10^{12}$	9.72×10^{13} 8.82×10^{13} $2.16 \times 10^{13} \sim 1.81 \times 10^{14}$

Table 1. Characteristics of the Test Holes for a Material Irradiation at HANARO

Various neutron irradiation facilities, such as rabbit irradiation facilities, capsule irradiation facilities, and neutron transmutation doping (NTD) facilities, have been developed. Among the irradiation facilities, the capsule is the most useful device for coping with the various test requirements at HANARO. Therefore, it has played an important role in the integrity evaluation of reactor core materials and the development of new materials through irradiation tests of specimens such as a reactor pressure vessel, reactor core structural materials, and fuel assembly parts at HANARO. Figure 1 shows the reactor core of HANARO with an irradiation capsule installed in the central test (CT) hole.

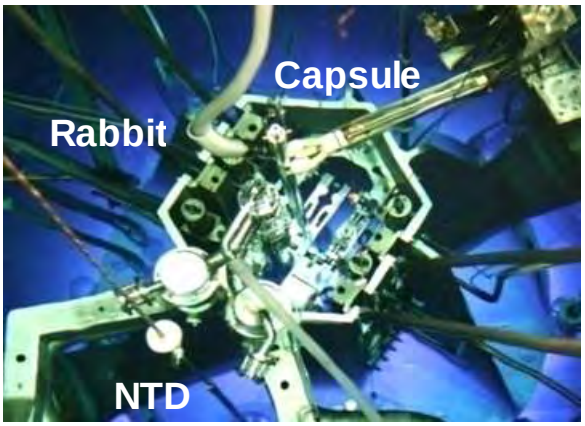

Figure 1. Reactor core of HANARO with a capsule installed in the CT hole

A standard HANARO material irradiation capsule consists of three main parts connected to each other: a protection tube, a guide tube, and the capsule's main body, as shown in Figure 2. The main body including the specimens and instruments is a cylindrical shaped stainless steel (STS) tube of 60 mm in diameter and 1170 mm in length. The main body has 5 stages with independent micro-electric heaters, and contains thermocouples and neutron fluence monitors to measure the temperature and the fast neutron fluences of the specimens, respectively. Heaters and thermocouples are connected to a capsule temperature control system through a guide tube. The remaining space in the closed capsule was filled with He gas and the temperature of the specimens was controlled in the range of 300-500℃ during reactor operation cycles at HANARO. The temperature of the specimens during irradiation is initially increased by gamma heating, roughly adjusted to the optimum condition by a gas control system, and then finally adjusted to a desired value by micro-electric heaters.

Figure 2. Standard material irradiation capsule at HANARO

3. Improvement of irradiation capsule for a higher neutron fluence

3.1 User requirement and R&Ds

The development of future nuclear systems such as VHTR, SFR, and Fusion reactors is one of the most important projects planned by the Korean government. The environmental conditions for these reactors are generally beyond present day reactor technology, especially regarding higher neutron fluence. Table 2 summarizes the required irradiation testing from HANARO users. To effectively support the national R&Ds relevant to the future nuclear systems, the development of advanced irradiation

technologies concerning higher neutron fluence is being preferentially developed at HANARO. During the last three years, a long-term irradiation capsule technology of up to 3 dpa (displacement for atom) was developed at HANARO. The new capsule technology was successfully applied for neutron irradiation of the core materials (graphite, beryllium, and zircaloy-4) of research reactors as a part of the National Research Reactor Development Project. The long-term irradiation capsule technology was scheduled to extend its capability to up to 5 dpa for the next three years starting from this year, particularly for the irradiation of materials of future nuclear systems. 5 dpa is equivalent to irradiation testing for 15 cycles at HANARO.

	Specimen	Irradiation Temperature	Test Hole	Irradiation Cycle	Year	User
1	Fusion Structural Mats (ARAA) (Fe-9Cr alloy)	300~350℃	CT	8	2016	KAERI
2	Fusion Structural Mats ARAA Welds	320℃	CT	>8 (15)	2017	KAERI
3	Accident-Resistant Nuclear Fuel Cladding (Zr)	300℃	CT	4~6	2016	KAERI
4	Cladding Alloys for PWRs	350~400℃	CT	2~4	2016	University
5	VHTR Reactor Core Mats (Fe Alloys)	300~1,000℃	CT	8~24	2017	KAERI
6	Long Life SPND	300℃	OR	8~24	2016	KHNP
7	U-Mo Nuclear Fuel		OR	8	2016	KAERI
8	Epoxy, SiC Epoxy	~200℃	OR	8	2017	KAERI
9	Fission Mo		OR	1	2016	KAERI
10	Th-based Nuclear Fuel		OR	8~24	2018	KAERI
11	SiC Composite	900~1,600℃	OR	8	2018	KAERI
12	SFR Structural Mat.s (ODS)	300～500℃	CT	>8	2017	KAERI
13	Low Alloy RPV Mat.s	300℃	OR	2	2016	KAERI

Table 2. Current user requirements for irradiation testing at HANARO

3.2 Design improvement of capsule for 3 dpa

There is a forced upward coolant flow in the core of HANARO. All of the inserted structures in the core including the irradiation capsule are required to satisfy the pressure drop criteria of 209 kPa at HANARO. Because of the up-stream of the coolant in the reactor, the instrumented capsule is fixed or supported at four points, which are the bottom and top of the main body, the top of the reactor chimney, and the capsule robot arm's site. HANARO instrumented capsules have been irradiated within 1.5 dpa. Recently, as part of the research reactor development's project, irradiation testing of materials used as core materials in a research reactor, such as graphite, beryllium and zircaloy-4, has been required for up to 3 dpa at a low temperature (<100°C). Therefore, the first irradiation capsule for 3 dpa was designed for an irradiation testing of materials

used as core materials in a research reactor.
However, as the irradiation capsule is exposed into a very high pressure coolant flow of 19.6 kg/s during an irradiation testing, it has been suspected to be vulnerable to a vibration-induced fatigue cracking. The source of stress causing the fatigue cracking is generally proportional to the vibration displacement of the capsule. And all of the inserted structures in the reactor core including the irradiation capsule are recommended to satisfy the vibration displacement criteria of 300μm due to the design characteristics of HANARO. Therefore, the 'Reactor Safety Review Committee of HANARO' required a vibration and out-pile endurance testing for a new-designed capsule in the out-pile testing facility simulating HANARO operating environment. Through out-pile performance and endurance testing of the capsule before HANARO irradiation testing in the HANARO out-pile test facilities, an optimized design of the capsule was determined [5]. By changing the material from STS 304 to STS 316L and welding by EB welding method fabricating for the rod tip of the capsule, the endurance life of the rod tip of the capsule was greatly extended in the out-pile test. STS 316L is selected due to a superior properties than STS 304 in terms of welding [6,7], EB welding is considered to have a narrow welding area than previous TIG welding, resulting in a less harmful distribution of residual stress in the welding area [8].
Based on the out-pile test results, an irradiation capsule (named as 11M-21K according to HANARO capsule numbering system) was designed and successfully irradiated up to eight reactor operation cycles (equivalent to 3 dpa) at low temperature (<100°C) at HANARO [9]. Figure 3 shows a variation of the temperatures of the specimens of the 11M-20K capsule during the last irradiation cycle among eight irradiation cycles. After the irradiation for eight cycles, the rod tip of the capsule was also examined to see any occurrence of fatigue cracks or defects. No cracks or defects were found in the rod tip of the irradiated capsule. Therefore, the new capsule design was proved to be safe for irradiation of up to eight cycles at HANARO.

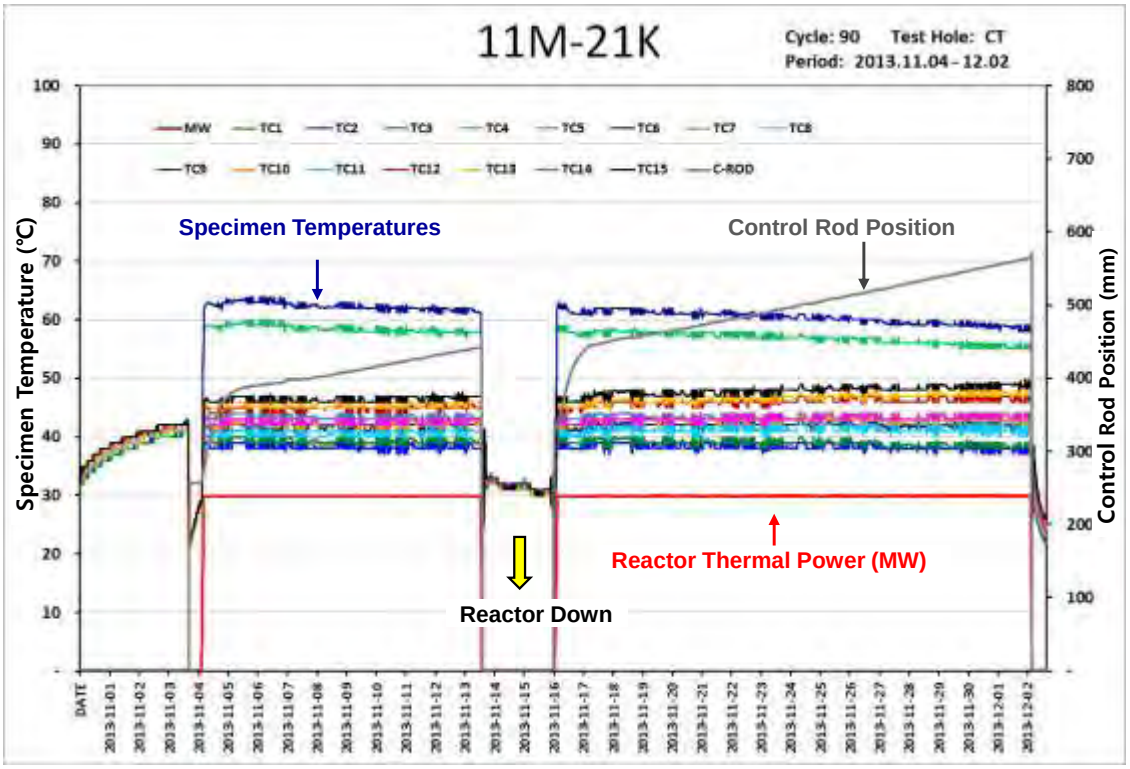

Figure 3. Variation of the temperature of the 11M-21K capsule irradiated in the central hole of HANARO (8th Cycle)

3.3 Design improvement of capsule for 5 dpa

Although the design improved capsule was proved to be sound up to 3 dpa, it seems still to be susceptible to the fatigue cracking of the rod tip of the capsule for a higher dpa irradiation. Actually, the improved rod tip was failed after 203 days (equivalent to 3 dpa at HANARO) under the 110% accelerated condition of normal reactor coolant flow. Figure 4 shows the failed parts of the capsule and the fracture surfaces of the rod tips. The fracture seems to be occurred at around the boundary of weld end and the fracture surface shows the typical appearance of fatigue fracture in the literature [10,11]. A lot of cracks initiated at near the surface propagated towards center, and finally a ductile fracture occurred in the rod tip of the EB welded STS 316L. Considering the increased vibration of this capsule and the typical failure appearances of the rod tips [5], these cracks seem to be initiated and progressed by vibration-induced fatigue cracking. Therefore, the failure of the rod tip can be concluded to be caused by a vibration-induced fatigue cracking during irradiation testing.

Figure 4. The failed rod tip of the capsule during the out-pile test

The applied stresses on the rod tip were analyzed using the ANSYS program. The position having the highest values was nearly matched with the failed location, as shown in Figure 5. The applied stresses on the rod tip can be classified into stresses by designed bottom spring, by coolant upward flowing, by capsule vibration, and welding residual stress. The maximal stresses due to the first three factors were estimated as 5.4 MPa, 132.9 MPa, and 161 MPa, respectively. These stresses do not exceed the known fatigue strength of stainless steels (~300 MPa [12]). Residual stress by welding is another possible stress and it is known to be occurred up to about 300 MPa [13]. Therefore, the combination of these stresses can be enough to cause the fatigue failure of the rod tip of the capsule.

Based on the failure analysis, another design of the rod tip of the capsule was made for 5 dpa irradiation, as shown in Figure 6. To decrease the applied stress on the rod tip, the diameter of the rod tip was increased from 8.0 mm to 9.0mm and the height of the tapered part of the rod tip was decreased from 0.5 mm to 0.2 mm. It results in a

decrease of 22.6% of the applied stress in the same condition. The gap (gap 1 in Figure 6) between the rod tip and the bottom end guide, and the gap (gap 2) between the rod tip fixture guide and the bottom end guide were decreased from 0.05 to 0.025 mm and from 0.15 mm to 0.05 mm, respectively, to suppress the applied stress by constraining the vibration of the rod tip. The length of the rod tip was increased by 7mm to position the weld part of the rod tip above the stressing position. It will eliminate the effect of residual stress by welding fundamentally.

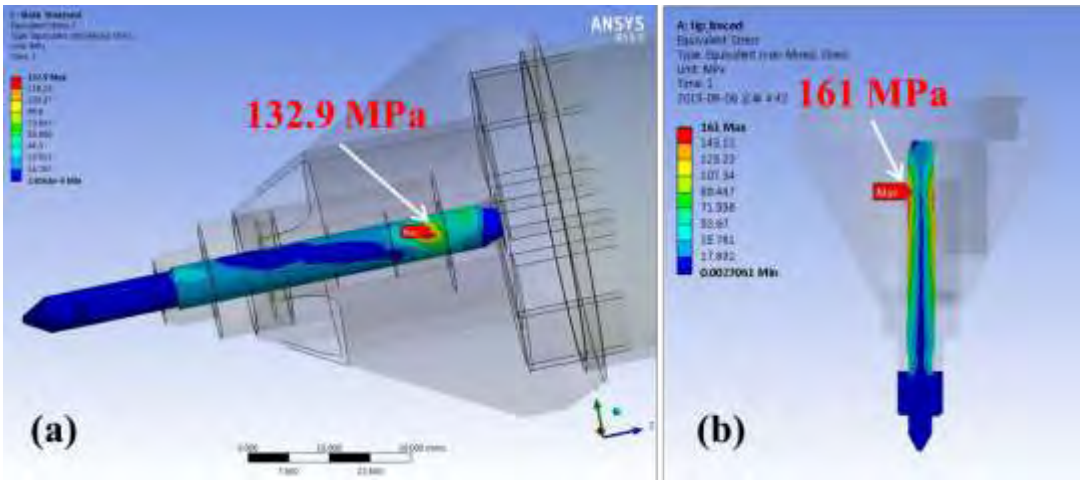

Figure 5. Stress analysis on the rod tip of the capsule during the out-pile testing using ANSYS program: (a) stress by coolant up-flow, (b) stress by capsule vibration

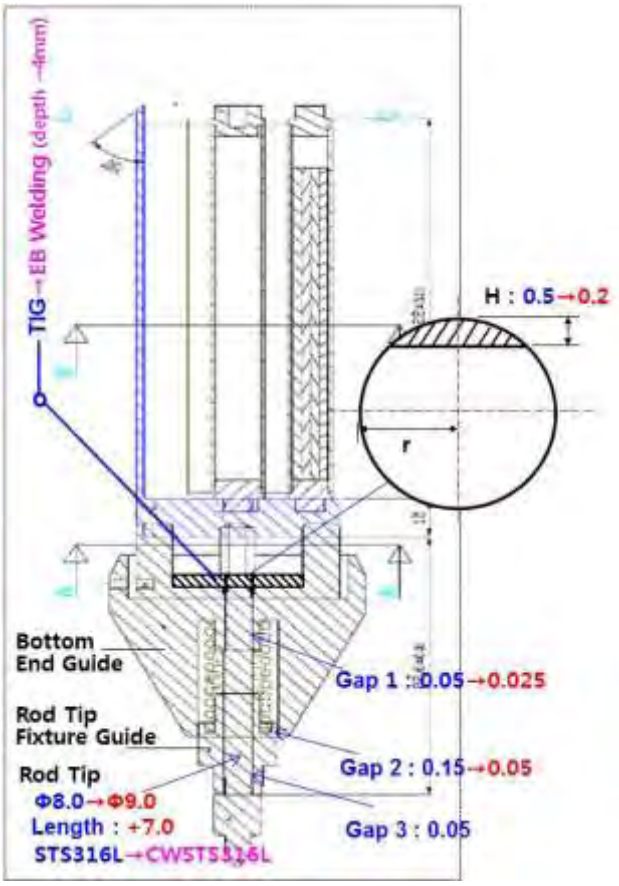

Figure 6. The improved design drawing of the capsule bottom part for 5 dpa irradiation

4. Future Works

The safety of the new capsule should be fully checked before irradiation testing. Out-pile performance and endurance testing should be performed before HANARO irradiation testing. The new rod tip of the capsule will be out-pile tested up to 450 days equivalent to 5 dpa irradiation in the reactor. Up to 5 dpa irradiation, improvements of the capsule technology have been performed based on a design optimization of the irradiation capsule. However, for a higher neutron fluence exceeding 5 dpa, new capsule technologies including flux-boosting, re-irradiation, and re-instrumentation are under plan as the next 5-year R&D project starting from 2017 at HANARO. It will scope the user requirements for the National R&Ds on next generation nuclear power plants, as shown in Figure 7.

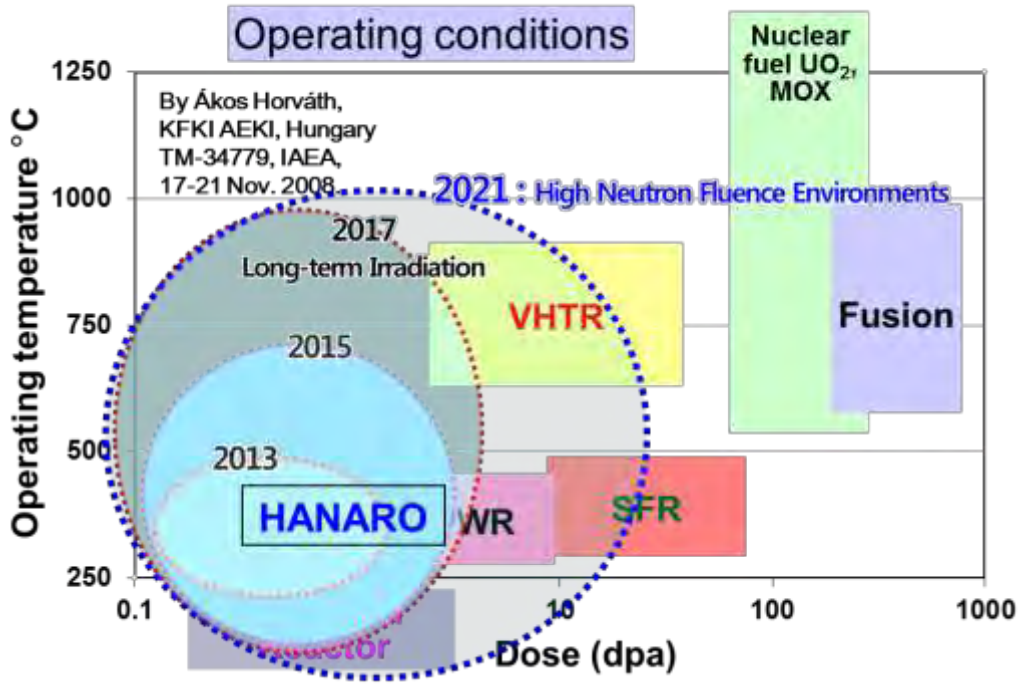

Figure 7. Strategy of development of irradiation technology for a higher neutron irradiation at HANARO

5. Conclusions

Several R&D efforts for a higher neutron irradiation have been performed at HANARO. At first, a long-term irradiation capsule technology of up to 3 dpa (displacement for atom) was developed at HANARO during the last three years. For an extended endurance life of the rod tip of the irradiation capsule, susceptible to a vibration-induced fatigue cracking, the material of the rod tip was changed from STS 304 to STS 316L, and the welding method was also changed from TIG welding to EB welding. The new designed capsule was successfully applied for neutron irradiation of the core materials (graphite, beryllium, and zircaloy-4) of research reactors up to 3 dpa irradiation as a part of the National Research Reactor Development Project. To scope user requirements for the irradiation of materials of future nuclear systems, more improved long-term irradiation capsule technology of up to 5 dpa is under development for the next three years starting from this year. 5 dpa is equivalent to irradiation testing for 15 cycles at HANARO. The second improvement of the capsule technology have been performed based on safety analysis and a design optimization of the irradiation capsule to reduce applied stress on the venerable rod tip of the capsule. However, for a higher neutron fluence exceeding 5 dpa, new capsule technologies including flux-boosting, re-irradiation, and re-instrumentation are under plan as the next 5-year R&D project starting from 2017 at HANARO.

Acknowledgements

This work was supported by the National Research Foundation of Korea (NRF) grant funded by the Korea government (MSIP) (No. 2013035822).

References

1. K.N. Choo, et. al., “Material Irradiation at HANARO, Korea,” Research Reactor Application for Materials under High Neutron Fluence, IAEA-TECDOC-1659, 2011, IAEA.
2. K.N. Choo, et. al., "Contribution of HANARO Irradiation Technologies to National Nuclear R&D," *Nuclear Engineering and Technology*, **46**, 4, 501 (2014).
3. M.S. Cho, et al., “Material Irradiation by Capsules at HANARO,” *Nucl. Technol.*, to be published.
4. K.N. Choo, et al., “Measurement and Evaluation of the Irradiation Test Parameters for a Specimen in a HANARO Material Irradiation Capsule,” *IEEE Transactions on Nuclear Science*, **57**, 2642 (2010).
5. B.G. Kim, et. al., “Design and Fabrication Report on Capsule (11M-19K) for Out-pile Testing of Research Reactor Materials at HANARO,” KAERI Report, KAERI/TR-4610/2012 (2012).
6. J.M. Keisler, er al., “Statistical models for estimating fatigue strain-life behavior of pressure boundary materials in light water reactor environments,” *Nucl. Eng. Des.,* **167**, 129 (1996).
7. D. Harish Kumar, et al., “A review on critical aspects of 316ln austenitic stainless steel weldability,” *Int. J. Mat. Sci. App.*, **1**, 1 (2012).
8. Jiamin Sun, et al., “A comparative study on welding temperature fields, residual stress distributions and deformations induced by laser beam welding and CO_2 gas arc welding,” *Materials and Design*, **63**, 519 (2014).
9. S.W. Yang, et. al., “The Irradiation Test Report for Research Reactor Materials at HANARO,” KAERI Report, KAERI/TR-5494/2014 (2014).
10. G.F. Vander Voort, “MACROSCOPIC EXAMINATION PROCEDURES FOR FAILURE ANALYSIS,” *Metallography in Failure Analysis*, p. 60, James L. McCall and P.M. French, Ed., Plenum Press, New York and London (1978).
11. R. Avilés, et al., “Influence of low-plasticity ball burnishing on the high-cycle fatigue strength of medium carbon AISI 1045 steel,” *Int. J. Fatigue*, **55**, 230 (2013).
12. Sergei A. Shipilov, “Solving some key failure analysis problems using advanced methods for materials testing,” *Eng. Failure Analysis*, **14**, 1550 (2007).
13. J. Sun et al., “A comparative study on welding temperature fields, residual stress distributions and deformations induced by laser beam welding and CO_2 gas arc welding,” *Materials and Design*, **63**, 519 (2014).

OUT-OF-PILE TESTING OF THE CALIPSO IRRADIATION DEVICE FOR THE JULES HOROWITZ REACTOR

D.J. MOULIN, P. CHARVET, F. CHALLET, G. CHAUMONT

CEA, DEN, Department of Nuclear Technology,
F-13108 Saint-Paul-Lez-Durance - France.

ABSTRACT

The CALIPSO device is a NaK liquid metal loop for material irradiation in the core of the Jules Horowitz Reactor. A prototype for out-of pile testing was manufactured and a specific experimental facility called SOPRANO was built at the CEA Cadarache centre. Since September 2013, the qualification of the prototype over all its operating range has been carried out.
After a short recall on the CALIPSO device and its operating principle, the main results of the experimental campaigns are presented in this paper.
The electromagnetic pump showed very good time stability and reproducibility all along the campaigns to control NaK flowrate up to 0.5 kg/s.
Concerning thermal behaviour, the modularity of the heat exchanger is very efficient to enlarge the temperature operating range. For instance, the targeted 450°C NaK temperature was obtained with the shorter heat exchanger configuration. Besides, by controlling the electrical power parameters, one could flatter the NaK temperature profile in the test channel down a few degrees over the 765 mm heating length of the electrical rod.
These experimental campaigns were necessary to qualify the overall behaviour of CALIPSO and to characterize the main components. Most of the results are consistent with the expected values. The objective of reducing the thermal gradient in the flowing NaK along the sample zone has been achieved. Therefore, it confirms the adequate design of CALIPSO to perform irradiation of material samples with an accurate control of the coolant temperature conditions over a large range of heating power.

1. Introduction

Test devices in research reactors such as the Jules Horowitz Reactor, are designed to provide specific experimental conditions to study material behaviour under irradiation (1). Among them, the CALIPSO device is a Sodium-Potassium (NaK) liquid metal loop for material irradiation in the reactor core. Its design and thermal performances have been presented in previous congresses (2), (3). Two out-of-pile hard mock-ups were manufactured; one concerning the prototype of the in-core part (4) and the other one concerning the prototype of the head (5). At the same time a new experimental facility called SOPRANO was developed and built at the CEA Cadarache centre (4). Since September 2013, the qualification in realistic conditions of the prototype with NaK has been carried out. After a short recall on the CALIPSO device and its operating principle, the main results of the experimental campaigns are presented.

2. General description of CALIPSO

An important requirement for experimental conditions in test devices with a lot of samples is to keep the temperature distribution homogeneous. In the case of CALIPSO, the accurate temperature control of the samples is possible by the mean of a small in-core loop of circulating NaK. This device encloses in a confined space all the components needed to ensure a forced convection flow in the test section that is to say a pump, an electrical heater, and a so-called heat exchanger.
The overall length of the in-core test device is 6500 mm and its outer diameter is 33 mm in the lower part so that it can fit into the central hole of JHR fuel elements (Figure 1). It is

composed of two main parts: the containment rig and the sample-holder. The containment rig is the outer shell of the test device that houses fluids. The sample-holder is plugged into the containment rig through the circular opening situated in the upper part. It holds the material samples to be irradiated and the specific experimental instrumentation such as thermocouples, radiations sensors, pressure sensors, strain gauges, displacement transducers, etc. It is in the lower part of the containment rig, where the internal diameter is only 24 mm, that samples and instrumentation are immerged in the experimental fluid (NaK).

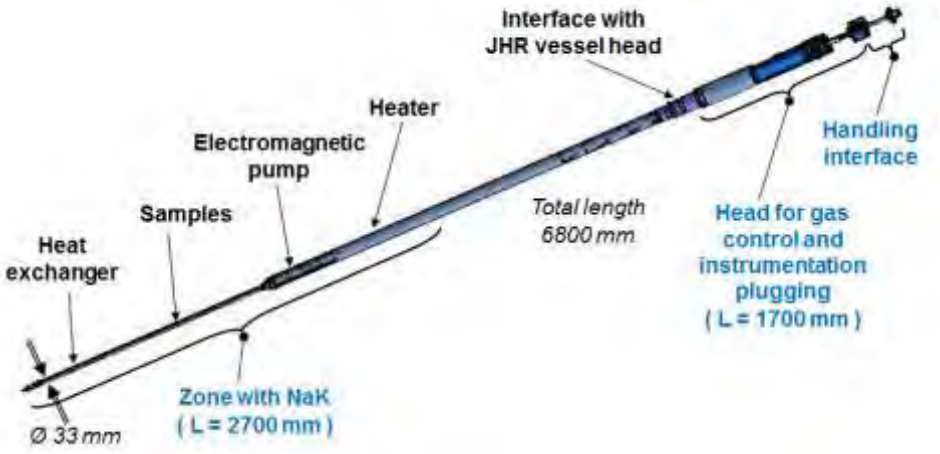

Figure 1 : General view of CALIPSO

3. Operating principle

The description of the operating principle is illustrated by a schematic view given Figure 2.
Material samples ❸ are located in the central channel of the test device in the 600 mm-long active zone of the reactor core **(A)**. Gamma and neutron radiations induce heating of materials.
A very compact annular electromagnetic pump (EMP) ❹ makes NaK flowing down around samples. It is a 500 mm-long and 78 mm-large component located in the containment rig ❶ just above the active zone.
An electrical heater ❺ is situated in the NaK above the pump. It is necessary to control the temperature operating conditions in the sample zone. Its maximum power is 18 kW over a total length of 400 mm.
Internal heat transfer between NaK counter-flows occurs through the separator shell ❼. And thermal equilibrium of the system is obtained by heat loss to the water of the reactor primary circuit **(B)** through the Helium gas gap **(C)**.
A 700 mm-long component called heat-exchanger ❻ is located at the lower part of the sample-holder ❷, below the active zone. It is designed to be configured in hot cell before irradiation in order to have the NaK flow return at a variable altitude, thus to provide a variable area of heat exchange (Figure 3).

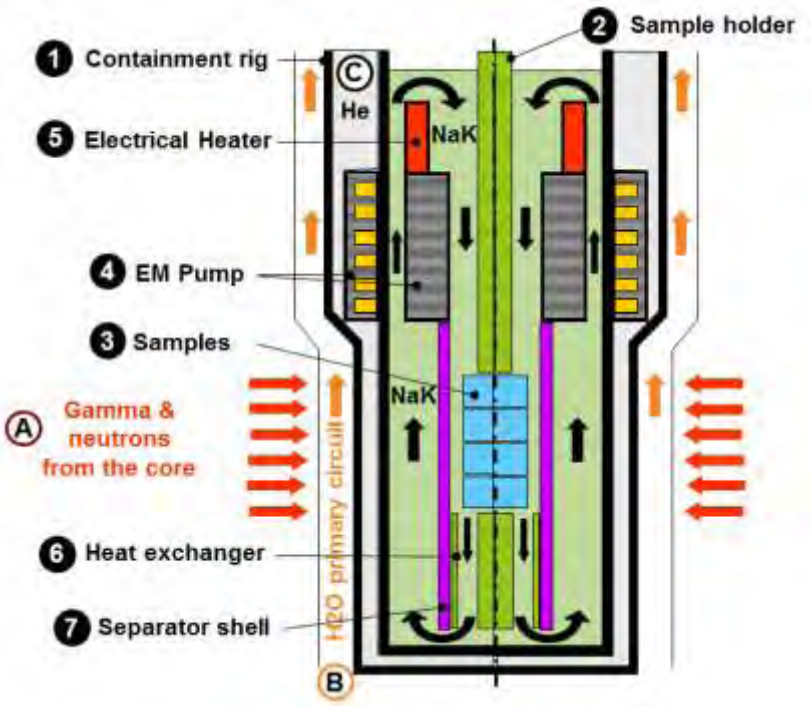

Figure 2 : Schematic view describing the operating principle

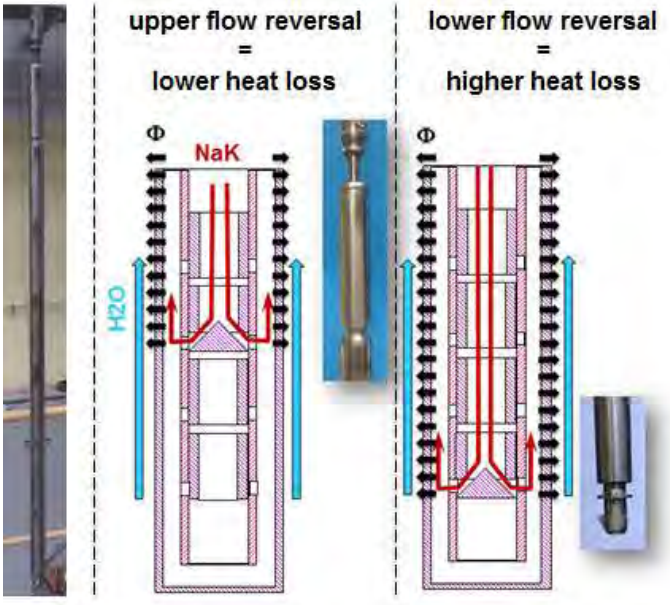

Figure 3 : Modular heat exchanger

4. The prototype of CALIPSO and the qualification facility

The prototype of CALIPSO consists in the bottom part of the actual test device. It is composed of all the components entering into the NaK loop with the same geometry (Figure 4). To simulate nuclear heating, a 765mm-long 20kW-powered electrical heating rod replaces the actual sample holder (Figure 5).

The prototype is also highly instrumented with 48 thermocouples for coolant and material temperature measurements. Pressure measurements at the inlet and the outlet of the pumping channel are effective thanks to small tubes connected to external pressure sensors.

Figure 4 : The outer flask and the electromagnetic pump on the inner flask

Figure 5 : Electrical rod with thermocouples clamped on the cladding

The SOPRANO facility is an operating platform with different components and circuits, built to perform experimental testing on the mock-up of CALIPSO and to allow operations with NaK (Figure 6).

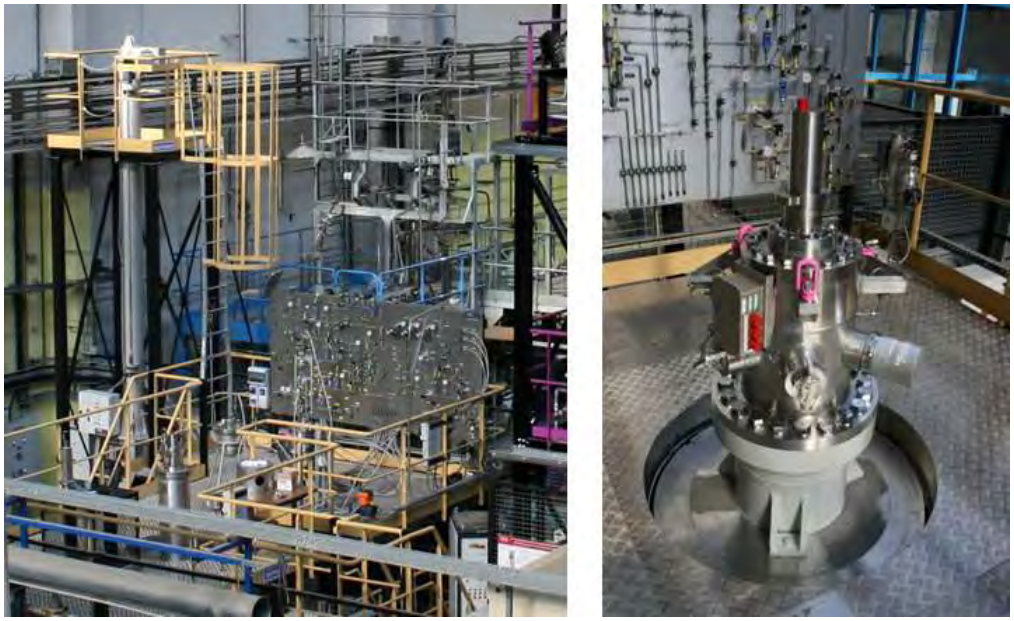

Figure 6 : Pictures of the SOPRANO facility

5. Experimental program

The first goal of the experimental program was to characterize the EMP by measuring the NaK differential pressure between the outlet and inlet of the pumping channel. This is correlated with the NaK flowrate through the total pressure drop of the integrated loop. By varying the power supply of the pump (voltage and frequency), it is possible to cover a large range of NaK flowrate.

A second goal was to evaluate the overall thermal performances of the device by changing the power supply of each electrical heater and recording all electrical parameters. Several

thermocouples are immerged in the NaK and others clamped on the main components (Figure 5). Thus, a very accurate monitoring of the test device temperature is carried out during experimental campaigns. Furthermore, by changing the heat exchanger length, one can reach different operating conditions regarding pressure drops and thermal balance. Since September 2013, three heat exchanger configurations were tested corresponding to 3 specific experimental campaigns (Table 1).

Campaign #	Dates	Configuration
1	Sep.- Oct. 2013	Long-length heat exchanger
2	Jan.- Apr. 2014	Short-length heat exchanger
3	Oct.- Dec. 2014	Medium-length heat exchanger

Table 1 : Characteristics of the experimental campaigns

6. EMP characteristics

First of all, the EMP showed very good time stability all along the campaigns. As an example, Figure 7 shows a 5 hour-long steady state operation at 320°C.

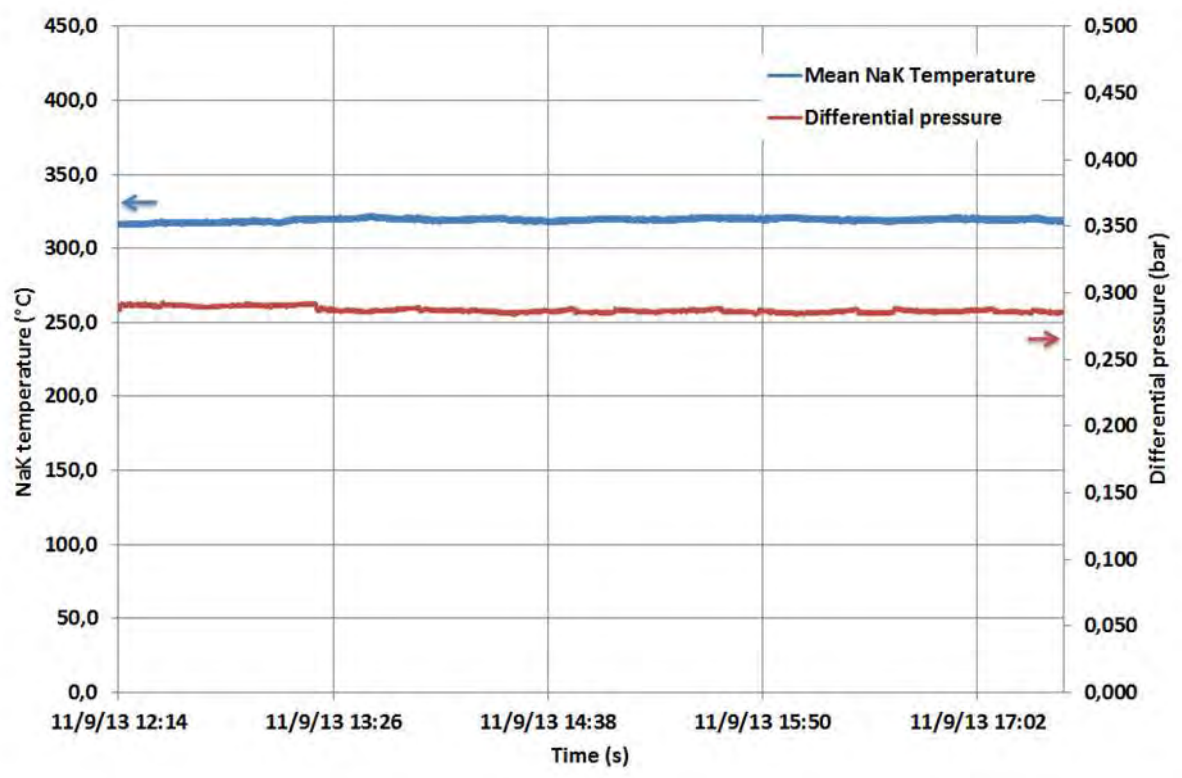

Figure 7 : Example of a 5 hour-long steady state EMP operation

Concerning pump operating characteristics in the test device, it can be noticed (Figure 8) that the differential pressure decreases while the heat exchanger length is smaller. This is obviously consistent with the change of linear pressure drop in the annular tube of the heat exchanger. Maximal load pressure is 0.9 bars. It was obtained with the long heat exchanger. Absolute uncertainty on differential measurement is ± 0.003 bar.

There is no flowrate sensor in the prototype. However flowrate can be evaluated based on the measured differential pressure and correlations from pressure drop calculations using computational fluid dynamics (CFD) software. In such a way, an estimation of flowrate absolute uncertainty is ± 0.02 kg/s. By processing data from differential pressure, it is

possible to plot flowrate versus EMP power supply (Figure 9). The curves fit quite well whatever the heat exchanger configuration, and a maximal value of 0.5 kg/s can be reached.

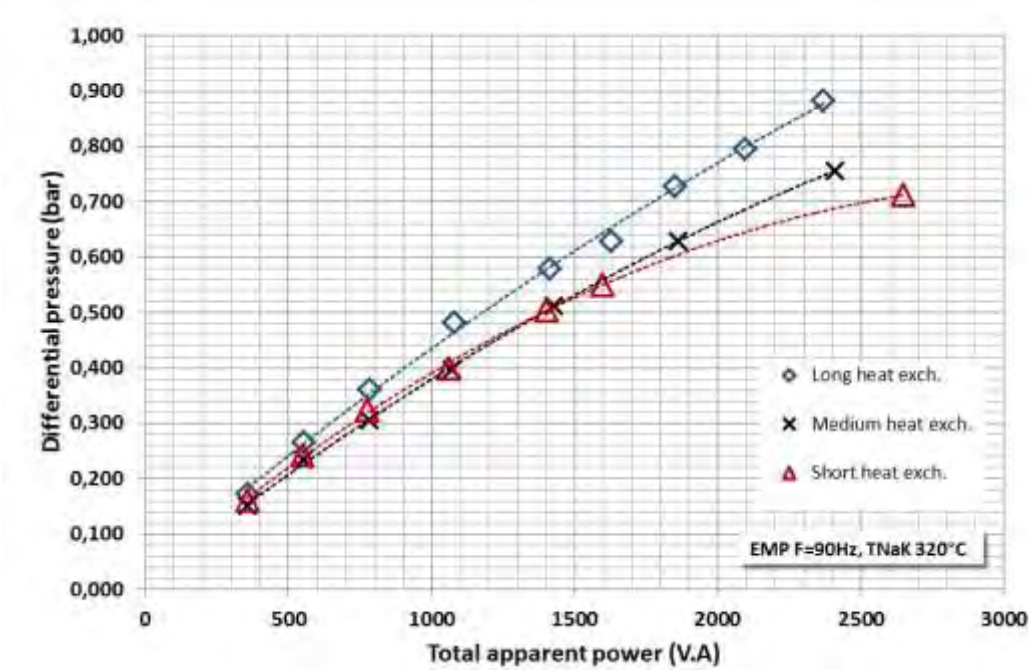

Figure 8 : Pump operating characteristics in the test device

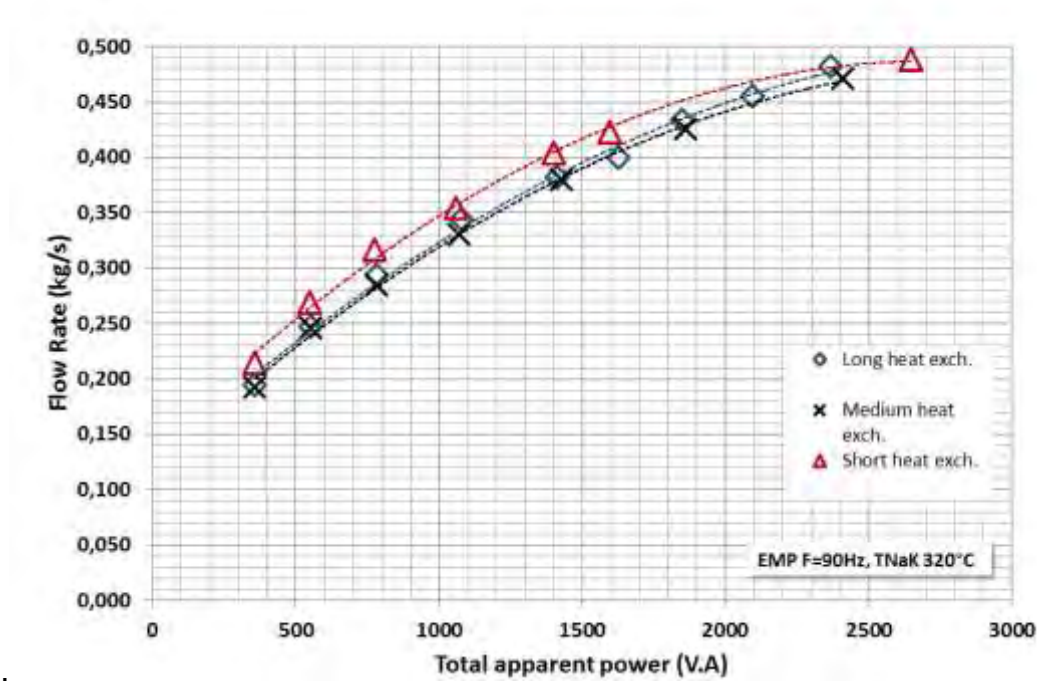

.

Figure 9 : Flow rate in the test device

7. Thermal performances

Figure 10 plots maximal NaK temperature versus heating power for the three tested configurations. As expected, to reach the same temperature level, smaller heating power is necessary with the short-length heat exchanger. Thus, the 450°C maximal NaK temperature can only be obtained with this configuration while it is 350°C with the others.

However, it cannot be observed any significant difference between long length and medium length curves. The reason is not well known and an additional experimental campaign should be necessary to investigate this phenomenon.

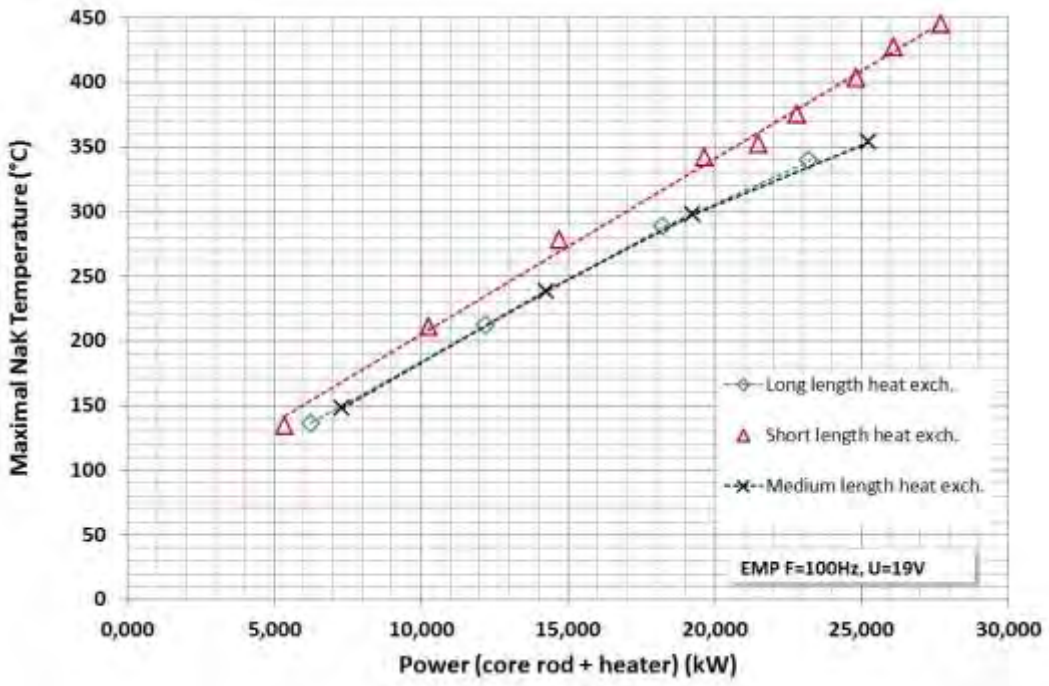

Figure 10 : Maximum NaK temperature (EMP F=100Hz, U=19V)

Calculation showed that the ability of reducing the thermal gradient in the flowing NaK along the sample zone could be controlled by the power of the electrical heater in regards of the nuclear heating in the sample zone (3).
In the prototype, the thermal gradient is evaluated by the differential temperature measured between thermocouples clamped on the rod upward and downward the heating zone. Given a NaK flowrate value and a rod power level, the electrical heater input could be adjusted to have the thermal gradient close to zero. The optimum power sharing is roughly 1/3 electrical heater and 2/3 heating rod. Besides, in such a condition, the NaK temperature profile in the test channel flattened down a few degrees over the heating zone. Figure 11 gives an example of power sharing impact on NaK temperature profile.
Sensitivity tests to NaK flowrate variation and rod power changes were carried out to check the loop feedback controller on the electrical heater. Results show good stability of NaK temperature and only small deviation from the optimum temperature profile.

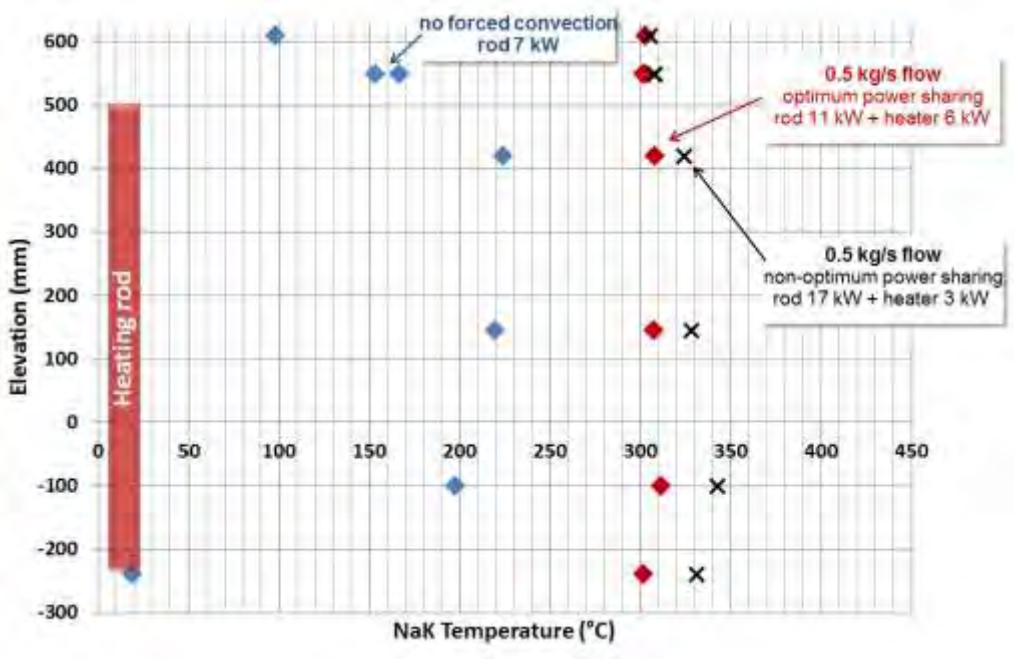

Figure 11 : Impact of power sharing on NaK temperature profile

8. Conclusion

These experimental campaigns were necessary to qualify the overall behaviour of CALIPSO and to characterize the main components. Most of the results are consistent with the expected values. The EMP showed very good time stability and its operating characteristics allowed reaching the 0.5 kg/s targeted flowrate. The modularity of the heat exchanger is quite efficient to enlarge the temperature operating range. The objective of reducing the thermal gradient in the flowing NaK along the sample zone has been achieved. Therefore, it confirms the adequate design of CALIPSO to perform irradiation of material samples with an accurate control of the coolant temperature conditions over a large range of heating power.
Future experimental work will focus on component reliability under long operating time. Concerning the design of the actual irradiation device for the Jules Horowitz Reactor, some improvements are necessary to take into account feedback from the manufacturing and the testing of the CALIPSO prototype.

9. References

(1) C. Colin, J. Pierre, C. Blandin, C. Gonnier, D. Moulin, M. Auclair, F. Rozenblum, Experimental devices in Jules Horowitz Reactor dedicated to the material studies in support to the current and future nuclear power plants, *European Nuclear Society, RRFM/IGORR 2012 Joint Meeting, Prague, Czech Republic, March 18-22, 2012*

(2) D. Moulin, C. Biscarrat, S. Christin, G. Laffont, A. Morcillo, E. Pluyette, F. Rey, Design of a flowing-NaK experimental device for in-core irradiation in the Jules Horowitz Reactor, *European Nuclear Society RRFM 2009, Vienna, March 22-25, 2009*

(3) D.J. Moulin, S. Christin, Ch. Biscarrat, Thermal assessment of the CALIPSO irradiation device for the Jules Horowitz Reactor, *IGORR 13, Knoxville, TN, USA, September 19-24, 2010*

(4) D.J. Moulin, F. Delassalle, L. Ayrault, An experimental facility to qualify the CALIPSO mock-up and NaK processes for the Jules Horowitz Reactor, *European Nuclear Society, RRFM/IGORR2012 Joint Meeting, Prague, Czech Republic, March 18-22, 2012*

(5) D.J. Moulin, A. Morcillo, S. Gay, X. Mognot, J. Pierre, Head for gas control and instrumentation plugging of a test device for the Jules Horowitz Reactor, *International conference ANIMMA Advancements in Nuclear Instrumentation Measurement Methods and their Applications, Marseille, France, June 23-27, 2013*

Status and Scientific Use of the TRIGA Research Reactor at the University of Mainz

CH. GEPPERT, K. EBERHARDT, S. KARPUK
Institut für Kernchemie, Johannes Gutenberg-Universität
Fritz-Straßmann-Weg 2, 55099 Mainz, Germany

ABSTRACT

The Johannes Gutenberg-University in Mainz, Germany, pursues a TRIGA mark II reactor (Forschungsreaktor Mainz = FRMZ). The FRMZ provides a maximum thermal power of 100 kW in steady state operation mode. Alternatively, it can be operated in pulsed mode with pulse strengths of up to 2.0 $, which represents about 250 MW of pulse peak power in a timeframe of 30 ms. The reactor is predominantly requested in continuous operation mode. However, in recent years the focus in utilization is gradually moving toward pulsed operation.

The FRMZ is utilized for a wide scientific spectrum. Traditionally the FRMZ is employed for neutron activation analysis as a tool for trace analysis or for nuclear chemistry studies of radioactive isotopes. In the last years the FRMZ benefited from the participation in the PRISMA cluster of excellence, which aims for experiments of precision physics, fundamental interactions and structure of matter. Inside the PRISMA cluster of excellence, the FRMZ contributes with two long-term experiments. The TRIGA-SPEC collaboration is studying the ground state properties of short-lived radioactive nuclei by means of Penning-trap mass spectrometry and collinear high-resolution laser spectroscopy. The second pillar within PRISMA is the development and refinement of sources for ultra-cold neutrons (UCN). Therewith the FRMZ is currently in the transition phase becoming a future UCN user facility for scientific users from all over the world. In preparation of a user facility, the first regular two-shift operation was introduced, allowing for a more efficient use of beam time for external users and guests at the FRMZ.

Beside the scientific goals, the FRMZ is playing an active role in the education and maintenance of nuclear (technology) competence. Beside the regular production of radioactive samples for nuclear chemistry laboratory courses for students, the FRMZ is providing an exclusive and greatly demanded reactor training course, in which students as well as guest reactor operators are getting a one-week hands on course at the TRIGA mark II reactor and finally operate the reactor by themselves for various experiments.

1. Introduction

The TRIGA mark II reactor (Forschungsreaktor Mainz = FRMZ) at the Johannes Gutenberg University is, together with the reactor BER II of the Helmholtz Zentrum in Berlin and the FRM2 of the Technische University München, one of only three research reactors within Germany which provides thermal power capacities of above 50 kW. Although the FRMZ is with only 100 kW thermal power the weakest of these three reactors, it provides a large range of possible applications, is well utilized and benefits from its inherently safe reactor design.

1.1 History

The purchase and installation of the FRMZ was initiated by Prof. Fritz Straßmann in the mid-1960s. Last year, on 3rd of August 2015, the FRMZ celebrated the 50th anniversary of operation. Except one major revision of the water cooling circuits in 1995, the reactor was operated during these 50 years without longer interruptions. The official inauguration of the reactor was conducted with the first pulsed operation triggered by Nobel laureate Prof. Otto Hahn himself (see Fig. 1) on 3rd of April 1967. Since that time the FRMZ reached pulse number 20’000 in October 2015. According to information from the IAEA [1], the FRMZ therewith holds the world records on reactor pulses.

Figure 1: First reactor pulse triggered by Prof. Otto Hahn on the occasion of the official FRMZ inauguration on 3rd of April 1967.

1.2 Capacity Utilisation

In the past decades the FRMZ was predominantly requested in continuous operation mode (80%), whereas in recent years an increased demand in pulsed operation mode is observed due to new and modern neutron physics applications, as described in section 1.4.4.

The University of Mainz initiated the so-called PRISMA cluster of excellence [2] which was granted in 2012. In the framework of this cluster, the FRMZ is one of the instrumental pillars of the proposal providing an international user facility for experimentalists all over the world. Benefiting from that, the reactor staff was strengthened by two new reactor operators. With this recruitment a regular two-shift operation was introduced in 2015: for twelve weeks per year the FRMZ is accessible for PRIMSA experimentalists from 7:30 to 0:00 (Monday to Thursday) and 7:30 to 18:30 on Fridays.

Due to intensive requests of the FRMZ operation by internal and also university-external users, the FRMZ is often operated in parallel utilisation for two or even up to three applications at the same time. Despite a four weeks break in operation in 2015, due to a replacement of the FRMZ secondary water circuit cooling-tower, the reactor was available for experiments on about 200 days. About 60 % of that time were used by fundamental research experiments (see section 4.4) of the PRISMA cluster. Summarizing normal operation as well as two-shift operation in this timespan a total sum of 1513 pulses were triggered in 2015.

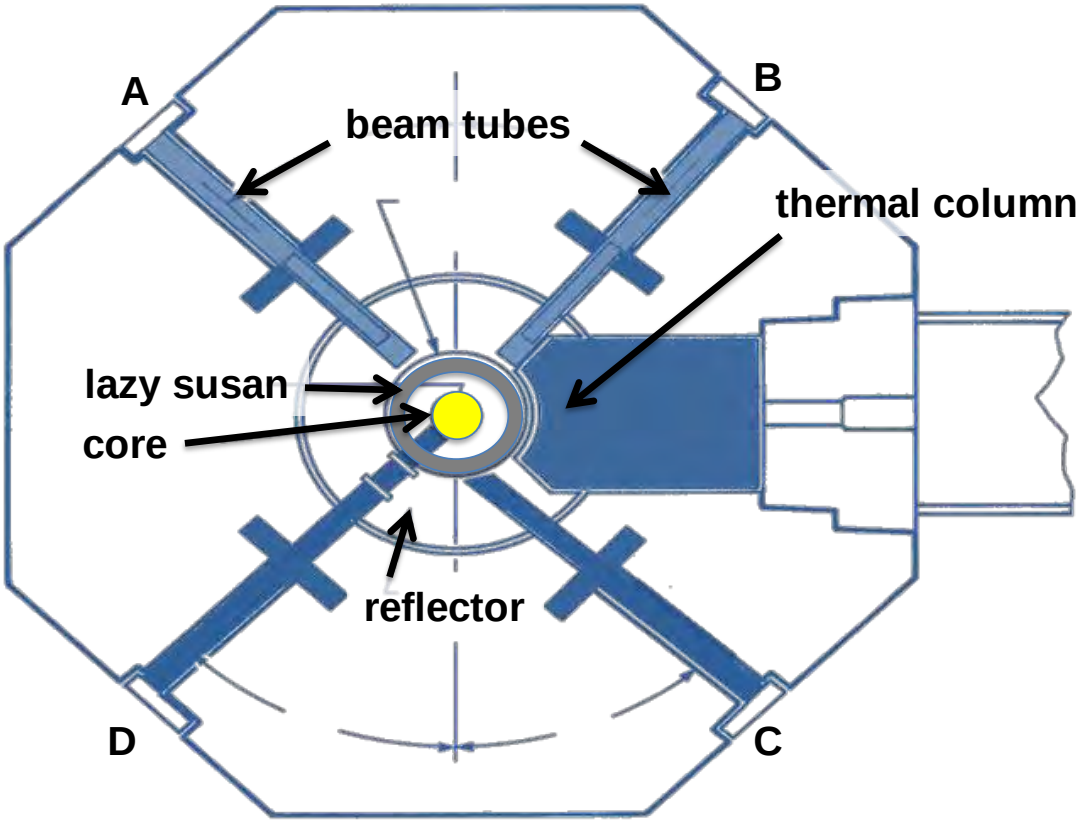

Figure 2: Simplified cut drawing (Slightly above the core center) showing the experimental stations: lazy susan system and beam tubes.

2. Layout

The FRMZ is a standard TRIGA mark II swimming pool reactor from General Atomic. It provides a lazy-susan-system embedded inside the outer reactor reflector (see Fig.2) which can receive up to 80 sample capsules in 40 positions. Furthermore, the FRMZ is equipped with four beam tubes which are penetrating through the biological shield and can be used as caves for experiments close to the reactor core. All beam tubes have the same inner diameter of 150 mm but to their various layout in regard to the reactor core they provide slightly different neutron spectra. Beam tubes A to C stop in front of the reactor reflector housing. While beam tubes A to B have a radial configuration, the axis of beam tube C is pointing only tangentially to the reactor core. Beam tube D again is in radial configuration but is completely penetrating through the reflector, stopping directly in front of the reactor core.

Additional to the irradiation facilities shown in Fig. 2, the FRMZ is equipped with three pneumatic transfer systems (rabbit systems) in the outer periphery of the core and one central irradiation position in the centre of the core, providing the highest neutron flux of about $4x10^{12}$ per square-centimetre and second at 100 kW thermal power.

The FRMZ is controlled and operated by three control rods. A shim rod in combination with an optionally automated regulation rod allow for well stabilized operation at any power level between a few 10 mW up to 100 kW of thermal power. Once the reactor is stabilized on 50 W thermal power, an additional transient rod (pulse rod) can be expelled within a few 10 ms out of the core, pneumatically driven by about 5 bar of pressurized air and the reactor reaches prompt criticality. This stops again after about a few 10 ms to 100 ms due to an sudden increase of the fuel element temperature in combination with the negative temperature gradient of the fuel element ZrH matrix moderation capabilities [3]. Depending on the expelling distance this procedure generates short neutron pulses with excess reactivities between typically 2.0 $ to 1.25 $, respectively. Fig. 3 shows a time spectrum of a typical 2 $ neutron pulse by recording the Cherenkov light in the reactor pool

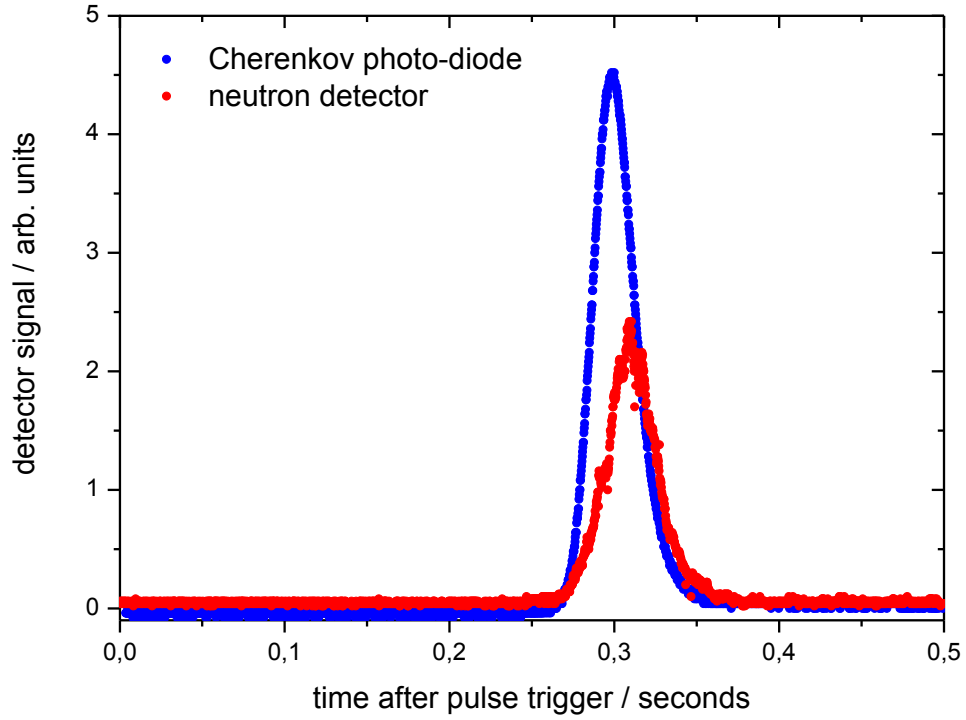

Figure 3: Recording of a 2 $ neutron pulse at the FRMZ by a fast photo diode above the reactor tank and a fast neutron detector inserted into the thermal column of the reactor.

as well as the neutron pulse time-structure recorded by a fast neutron detector. During the 25 ms duration of the 2.0 $ pulse, the peak reactor power increases up to 250 MW.

3. Fuel

The reactor has a so-called “life-time-core” which is currently equipped with 76 fuel elements. The uranium is embedded in a ZrH matrix and contributes to only 8% of weight of the fuel elements. The enrichment of fuel elements is below 20% (LEU fuel). More than 90 % of the initially inserted fuel elements are still in use today. Every two to three years, depending on the utilisation of the FRMZ, fresh fuel elements are inserted replacing graphite placeholders. Based on this moderate “consumption” of fuel elements together with an internal reservoir of unused fuel elements at the FRMZ, we predict between 15 to 20 years’ security of supply.

4. Utilisation

The embedment of the FRMZ into a nuclear chemistry institute and its inherent safety of a TRIGA type reactor allows for a wide range of applications. Fig. 4 gives a condensed overview, which will be exemplary discussed in the following subsections.

4.1 Educational Courses

As integral part of the university’s institute for nuclear chemistry, the FRMZ is used for training and education of students in various ways. For the traditional nuclear chemistry lab courses, the FRMZ is used for the production of radioactive (tracer-) isotopes such as Na-24, P-32, Np-239, Cu-64, Os-190m isomer, and fission products for demonstration experiments in nuclear chemistry and –physics. Furthermore, the infra-structure of the FRMZ is used for radiation protection curses not only for students, but also for a wider public. Special trainings are provided e.g. for school teachers and specialized fire fighters.

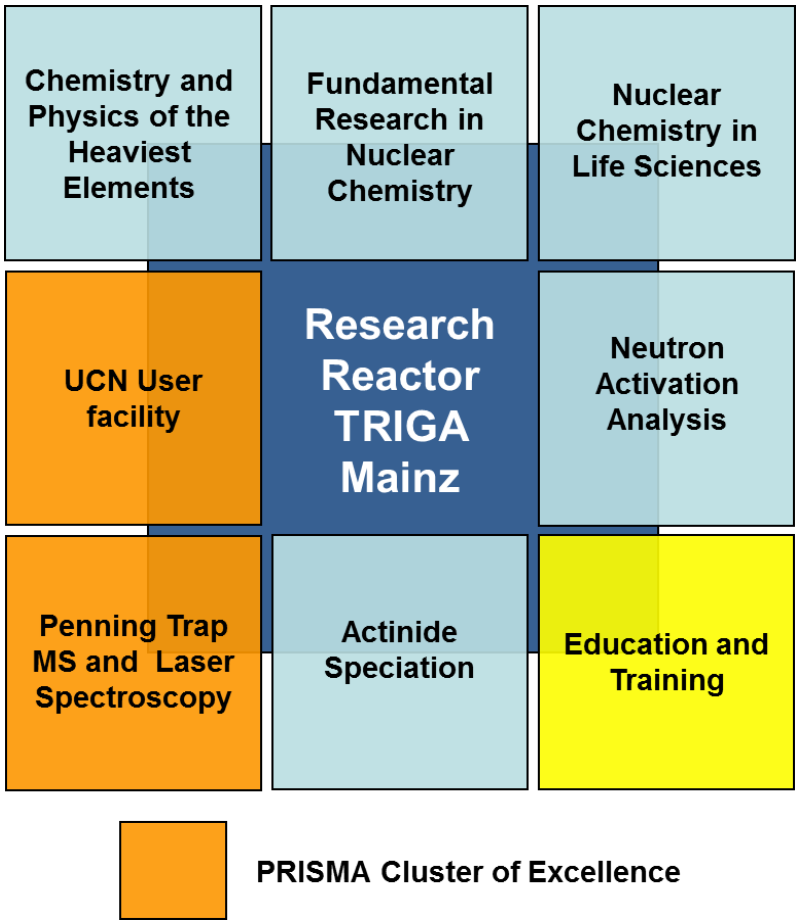

Figure 4: Overview of the various applications of the FRMZ at the Johannes Gutenberg-University.

4.2 Professional Training

A unique application is the so-called “Reaktor-Praktikum”. In this hand-on reactor training the participants get an inside in the working field of reactor operator. Within the training the participants are performing under supervision the daily check-lists of the complete reactor facility w/o an w/ artificially inserted failures of components. They are introduced in fuel element handling, irradiation of samples etc. and finally operating the reactor by themselves. The reactor operation training course is offered twice per year for groups of typically eight students.

In the recent past this course has also become part of professional reactor operators training. E.g. prospective reactor operators in Switzerland, which are trained in reactor courses at the Paul Scherrer Institut (PSI) in Villigen, are attending a one-week lasting, slightly modified reactor training course specially adapted to their previous experiences at reactor facilities.

4.3 Applied Sciences

The various irradiation facilities inside the core (pneumatic delivery stations and central irradiation position) are traditionally used for instrumental neutron activation analysis (INAA). First highlight in the history of the TRIGA Mainz was the INAA of lunar rock samples from the Apollo 11 mission only a few months after the landing on the moon. These experiments were conducted in collaboration with the Max-Planck-Institut für Chemie in Mainz [4]. Since these studies the method of INAA was used and is still used for modern problems of their time. Current applications of INAA include the determination of the contamination of silicon with transition metals in the original wafer material that play a crucial

part in the production of solar cells. After first feasibility studies [5], INAA is currently used in the context of an ongoing PhD thesis for the investigation of the silicon purity during the production process of solar cells. On a different field of application, the precise knowledge of the irradiation sample compositions allows for the determination of the neutron absorption cross sections. With this approach the neutron capture cross section of Fe-60 [6] was recently studied in a collaboration at the FRMZ under the guidance of the University Frankfurt. An incomplete listing of other current applications of the FRMZ for applied scientific studies are:

- monitoring of (trace-)elements in agricultural studies, e.g. the chronological development of element concentrations during the growth, ripeness and fermentation of grapes and wine by INAA [7],
- archaeological provenance studies on roman lime stone samples by INAA,
- tests of radiation hardness of electronic components (detectors, circuits etc.) by irradiation close to the reactor core,
- application of INAA for trace element analysis in e.g. ore, clay minerals, coal, airborne dust particles in environmental studies
- ….etc.

4.4 Fundamental Research

In the last 50 years the focus of the fundamental research at the FRMZ continuously changed. Currently three main fields are studied at the FRMZ:

Fission fragments that are produced in a target chamber in beam port A of the FRMZ and transported by an attached gas jet system can be used to develop and evolve fast chemical separation and detection systems, as they are used for the **chemical investigations of the super heaviest elements** (SHE, Z> 103). Based on this development platform at the FRMZ, new methods have been applied at so-called “in-flight” radioactive ion-beam facilities. A recent example is the first preparation of an organic-SHE compound [8], a seaborgium hexacarbonyl complex ($Sg(CO)_6$) as produced at the RIKEN accelerator centre in Japan.

Another application of the fission fragment production in beam port A is the precision mass spectrometry and laser spectroscopy of short-lived radioactive isotopes. Aiming for the ground state properties of these nuclei, the **TRIGA-SPEC** collaboration [9] applies a cryogenic Penning trap to measure the mass (binding energy) of the nuclei and a collinear laser spectroscopy beam section applying high-resolution continuous-wave laser systems for measuring the shape (charge radius, dipole moment, quadrupole moment and spin) of the nuclei of interest. As both individual experiments have reached an advanced evolution stage, which is documented by various off-line measurements [10][11], the common coupling of both experiments on the gas jet system is still under development.

The largest contingent of experimental time is currently requested for the developments on the production and **experiments with ultra-cold neutrons** (UCN). UCNs have by definition kinetic energies below 300 neV which corresponds to a temperature below 3.5 mK. In collaboration with the Institut für Physik at the University of Mainz and with the Technische Universität München two sources for UCN have been developed at the beam tubes D and C, respectively. While the UCN source at beam tube D is used for pulsed operation, the UCN source at beam tube C is aiming for continuous reactor operation. Both sources will be available within the PRISMA’s cluster of excellence user facility (see section 1.1.2). One of the first planned experiments will be the measurement of the neutron lifetime within the so-called Tau-SPEC spectrometer [11].

5. Outlook and Conclusion

After 50 years of operation the FRMZ is still an intensively used university research reactor with a wide-spread portfolio of applications. Due to its special fuel and the corresponding inherent safety, the TRIGA reactor is a unique tool for the education and training of young students and operators. The FRMZ contributes therewith to the conservation of competence in nuclear chemistry and technology in Germany. Due to the concept of a life-time-core of the FRMZ with only moderate fuel consumption in combination with a reservoir of fresh fuel elements, an ongoing operation for next 15 to 20 years is possible, looking for the exciting evolution of the currently developed experiments and new scientific challenges and applications.

6. References

[1] D. Ridikas, Research Reactor Officer, Physics Section, International Atomic Energy Agency (IAEA), Vienna, private communication to K. Eberhardt

[2] For more information, see homepage of the PRISMA cluster of excellence: http://www.prisma.uni-mainz.de

[3] R.S. Stone et al., Nuclear Science and Engineering 6 (1959) 255-259

[4] H. Wäncke et al., Science 167 (1970) 523-525

[5] J. Hampel et al., Applied Radiation and Isotopes 69 (2011)1365–1368

[6] T. Heftrich et al., Physical Review C92 (2015), 015806

[7] M. Feige et al., Radiochimica Acta 102 (2014), 333–349

[8] J. Even et al., Science 345 (2014), 1491-1493

[9] J. Ketelaer et al., Nuclear Instruments and Methods A594 (2008), 162-177

[10] M. Eibach et al., Physical Review C89 (2014), 064318

[11] C. Gorges et al., Journal of Physics B48 (2015), 245008

[12] For more information, see: www.prisma.uni-mainz.de/1041.php

RA-6 ONLINE + IRL: AN EFFECTIVE COLLABORATION BETWEEN CNEA AND IAEA FOR THE DEVELOPMENT OF A RESEARCH REACTOR EDUCATION REMOTE TOOL

P. CANTERO, D. MANGIAROTTI, F. BROLLO, F. SANCHEZ, J. LONGHINO, N. CHIARAVIGLIO, H. BLAUMANN

Nuclear Engineer Division – Nuclear Energy Department – National Atomic Energy Commission (CNEA)

Centro Atómico Bariloche, POB 9, Exequiel Bustillo Avenue 9500, R8402AGP, S. C. de Bariloche, Argentina

A. BORIO DI TIGLIOLE, J. VYSHNIAUSKAS

Research Reactor Section - Division of Nuclear Fuel Cycle and Waste Technology - Department of Nuclear Energy - International Atomic Energy Agency (IAEA) - Vienna International Centre, PO Box 100, 1400 Vienna, Austria

ABSTRACT

The Nuclear Engineering School at the Balseiro Institute (IB) was established in 1977. The RA-6 research reactor, designed and constructed to support the teaching activities at the IB, was inaugurated on 26 of October of 1982. As part of the academic program in nuclear engineering at the IB, a reactor experiment course, *Laboratory II*, was developed and integrated into the last academic year of nuclear engineering students. At the first part of this course, the students are introduced to research reactor design and utilization and perform a series of standard experiments at the RA-6. In the second part of the course, the students develop the solution to an engineering challenge, proposed for the professors and related to the RA-6, via the development of an experiment.

To enhance the extent of this course and of other similar programs at the RA-6 reactor, the CNEA has developed with partial financial support by the IAEA a data acquisition tool, the *RA-6 Online*, aiming to give students digital access to all the data necessary to perform the reactor experiments. Each student has access to an interactive and customized link to the reactor operation data, allowing the student to follow the practice in a personalized way and to have all the reactor operation information to post-process the laboratory data when needed.

Within the framework of internet-based nuclear education, in 2011 the IAEA started working on the development of the Internet Reactor Laboratory (IRL), a project financially supported by the US Department of State via Peaceful Uses Initiative (PUI) funds, IAEA regular budget and TC projects. The main objective of the project is to provide access to students in countries with no possibility of using a research reactor to remotely perform research reactor experiments.

Both, the *RA-6 Online* and the IRL, share the mechanism and the scope. This concurrence anticipated a fertile arena for collaboration between institutions to increase the outreach of a unified educational tool. Along these lines, the IAEA and CNEA held discussions in 2011 for the possibility of a concrete collaboration in this field. In 2013, an agreement between CNEA and IAEA was signed, establishing the legal framework of the IRL project in Latin America, which uses the RA-6 reactor as host reactor, and the *RA-6 Online* as the platform for the IRL project. The agreement includes the broadcasting of six reactor experiments developed for Laboratory II to academic institutes within Latin America.

In this paper, the set-up and scope of the *RA-6 Online* platform will be described, and its integration within the IRL scheme of the IAEA. Additionally the scope of the IRL, its implementation around the world and related IAEA's activities will be described. Finally, the future work plan and planned broadcasting schedule will be mentioned.

Introduction

The Nuclear Engineering School at the Balseiro Institute (IB) was established in 1977. Since then, around 10 to 15 students acquire the degree in nuclear engineering every year. The academic activities at IB require a strong academic background on math and physics and a very fluid and fruitful interaction with research laboratories and researchers in the Bariloche Atomic Center (CAB). This scheme has shown to be very effective giving the students a complete education that includes strong theoretical basis and the knowledge of applied technics in research and development.

In this scheme, the last semester of the Nuclear Engineering career inserts the RA-6 Reactor as the main laboratory for the students and a whole course takes place in the reactor: Laboratory II.

The RA-6 Research Reactor, Figure 1, was designed and constructed to support the teaching activities at the IB, and was inaugurated on 26 of October of 1982. It is an open pool type reactor, 1MW thermal power, moderated and refrigerated for light water. The core, with variable configuration, is composed for MTR type fuel elements, originally HEU and then converted to LEU at 19.7%. As academic laboratory, the RA-6 has supported the education and training of hundreds Argentinian and foreign professionals as physicists, engineers,

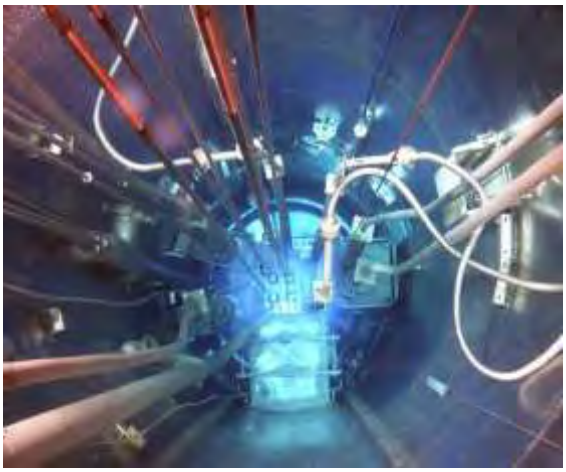

Figure 1: RA-6 pool, core, nuclear instrumentation, reactivity control system and other pool internals on the left. On the right, RA-6 reactor experimental hall and reactor block.

nuclear radiochemicals and experts in materials.

Laboratory II is a reactor experiment course, developed specifically for and integrated into, the last academic year of the nuclear engineering degree. At the first part of this course, the students are introduced to research reactor design and utilization and perform a series of standard experiments at the RA-6. Those experiments focus on the design of main systems of the reactor, reactor physics and reactor operation. Related to system design the experiences introduce the students into concepts as design basics, design criteria, design standards application, safety functions and regulatory aspects.

In the second part of the course, the students apply their acquired theoretical knowledge to propose a solution to an engineering-based challenge concerning the RA-6. The proposal is implemented via the development of an experiment at the reactor. During the past years, the students have developed solutions to different challenges, some of these are:

- Primary cooling system activity measurement
- In core flux spectrum measurement
- Primary cooling system void fraction measurement
- Power estimation via Cherenkov effect
- Automatic power control via plant modeling and regulation rod control
- Z(t) measurement for first shutdown system

The ***underlying concept in teaching at Laboratory II*** course is that the main learning and formative activities for the students are to perform the experiences, analyzing and processing data from the reactor variables, taking decisions and finally making their own conclusions based on the experience methods, the dynamics, etc. The idea behind this, is to position the students as major actors in all the activities performed within the course.

To enhance the extent of this course and of other similar programs at the RA-6 reactor, the CNEA has developed with partial financial support by the IAEA a data acquisition and integral management tool, the ***RA-6 Online***.

The aim of the RA-6 Online platform is to give the students digital access to all the reactor operation information on-line to perform the experiences and to post-process the laboratory data off-line when needed. Each student has access to an interactive and customized link to the reactor operation data, allowing the student to perform the practice in a personalized way.

The RA-6 Online platform was developed with this concept as the design basis and thinking that it would have to support both, local and remote students maintaining ***the underlying concept in teaching at Laboratory II***.

RA-6 Online – The platform

The RA-6 Online follows the main principle of allowing the remote students to perform the experiences as if they were in the RA-6 Reactor itself. In order to do so the signals of the RA-6 Reactor are replicated via internet and a videoconference (VC) link is provided to allow, when needed, the interaction with the installation and professors. In a typical experiment the students follow the evolution of the reactor signals in their own computers or personal laptops and the instructor guides them through the physics and theoretical basis. In a screen they can see and hear the professor at the reactor who interacts with the reactor operators and interprets any input, questions or requests of the students.

The RA-6 Online system has the following layers:

- Data acquisition, hardware based. This layer is dedicated to acquire electrical signals representing the reactor operation variables. There is no possibility of control or perturbation of the reactor variables.

- Data management, software based. This layer includes the databases and storing configuration, calibration and historical record.
- Data publishing, with a dedicated web platform developed to interact with the users in an intuitive and friendly way.
- Videoconference. Allows the link between the remote classroom and the reactor. The VC system contributes to the feeling of the remote students as if they were present at the reactor building. The VC system also allows the local professors to guide the remote students in the development of the experience.

Data acquisition

The RA-6 reactor has a terminal block room where all of the field signals are gathered. Some are connected to the main control console, where they provide to the operators all the required information to run the plant. Those signals and some others, produced locally for the control and protection logic, are processed and filtered in an interactive computer software with multiple screen called SEAD (Data Acquisition Electronic System) dedicated to support the operators. All of these signals - and some more - are isolated and acquired in the RA-6 Online system with CompactRIO™ equipment. Through a dedicated terminal block of over a thousand terminals, the signals are gathered, isolated and sent to the four acquisition modules of the CompactRIO™. Thanks to its modular and scalable characteristics, the system allows to increase the number of signals for future application.

The CompactRIO™ data acquisition system performs some of the signal processing needed. The data is acquired every 100 ns and published with NI Shared Variables™ on the dedicated local area network. This database includes not only the raw data but also the same signal filtered and calibrated in engineer units. In the CompactRIO™ the values of those signals that have a logarithmic calibration are calculated. For those that need a fast processing and acquisition the integrated FPGA is utilized: the signal corresponding to the Start-Up Pulses -generated by the fission chambers have a typical pulse width of 50ns so they are acquired through a prescaler divisor by 8.

The dedicated local area network consist of a switch with three LANs. In one of them the acquisition equipment is connected only to the data server, in the second one the web server is accessible for control and upgrades, and the third one is the only one with internet access and is used for the publishing the web server.

Data management

Utilizing NI Shared Variables™, the data acquired is published in the dedicated network between the CompactRIO™ and the data server. There, the raw and calibrated signals are stored with its timestamp. In order to reduce the storage capacity utilized, a 0.1% dead-band is applied.

The data storing is performed with a dedicated virtual machine.

Data publishing

The data publishing is performed with a web platform that is accessed via Internet. The server runs in a dedicated virtual machine that allows for fast and safe restoration to previous configuration save points.

Software's modules were constructed on NI LabVIEW™ for the user management. The information of each user is saved in a SQL database, with its password, experience assigned and time frame.

When a user opens the webpage to access the platform, he is requested to log in, providing his user and password (Figure 2).

Figure 2: Web Platform, welcome screen and log in interface

Once the user has logged on, he can navigate through different screens, accessible from the menu screen (Figure 3). From there he can access the live data of the Reactor, go to the data download configuration or analyze the reference bibliography.

Figure 3: Web Platform, home menu with access to the different screens

In the Live data screen, the user has all necessary data to perform the programmed experience (Figure 4). On the right side of the screen are displayed the position of the four control rods and the security rod, above that the local time in Bariloche is shown. On the left side, the user has a graph with the evolution of significant signals, and he can choose different groups of signals to analyze.

Figure 4: Web Platform, live data screen with all necessary data to perform an experience

Figure 5 shows the way the user can access the historical data. With a set of buttons and a slider, the user can change the zoom level.

Figure 5: Web Platform, historical data of the experience

Figure 6 shows the different signals groups. Those groups include the start-up signals (linear, logarithmic and its derivative), the power signals (linear, logarithmic and its derivative), conventional (core inlet and outlet temperature) and the evolution of the position of the control rods.

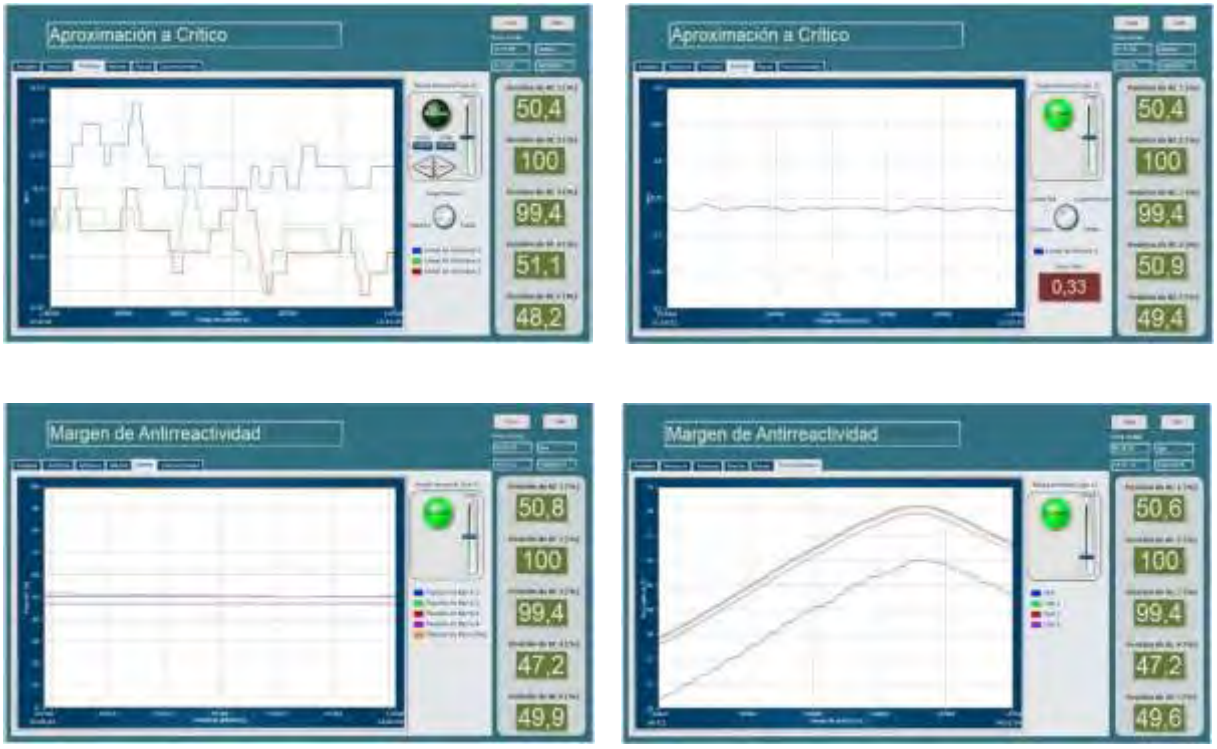

Figure 6: Web Platform, historical data of the experience

The user also have the option to download the data set of the experience for data processing and in depth analysis. The user can choose the group of signals and the time frame, as shown in Figure 7

Figure 7: Web Platform, data set download

Videoconference

The videoconference system allows the local professors to guide the remote students in the development of the experiments with the moderation of the remote instructor. The local professors are located at the training control room, with a multipoint video conference system and three screens, two dedicated to aid them in the explanations and one that allows the local instructors to observe his remote audience. The VC settings at the training control room are shown on the Figure 8.

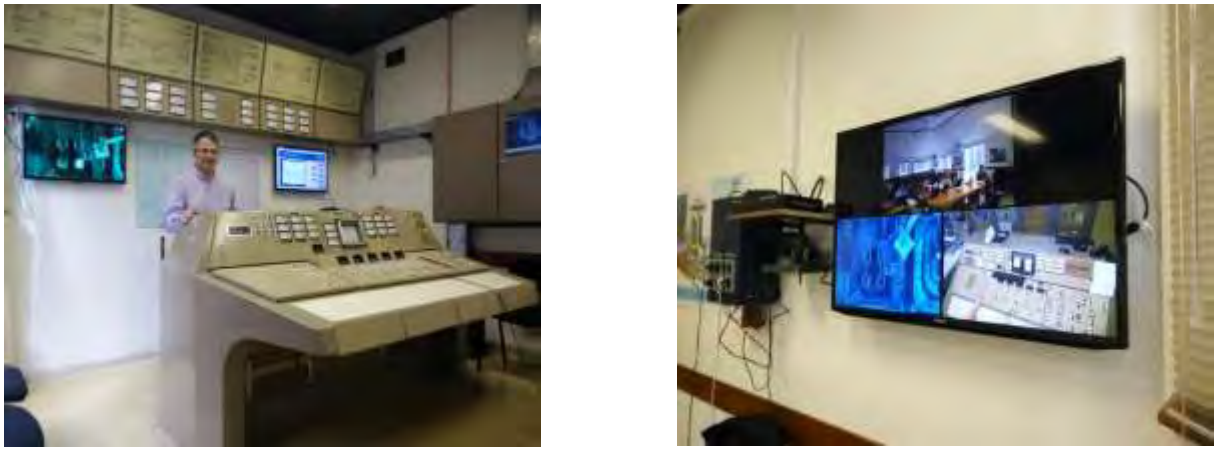

Figure 8: Training console, professor and aiding screens (left) and video conference management screen (right)

In the main control room there is one VC equipment dedicated to capture the operation of the Reactor and to facilitate the communication with the operators. Figure 9 shows the main control room and the operators, with the video conference screen.

CNEA and IAEA cooperation for the establishment of the IRL Project in Latin America

On the 4th of April 2013, the CNEA and the IAEA signed an agreement concerning the establishment of the Internet Reactor Laboratory (IRL) project in Latin America. The agreement establishes the basis for the collaboration between institutions, and defines the role of each one. The agreement also defines the third part of the collaboration: the remote institutions participating in the IRL in Latin America.

Figure 9: Control Room, operators and main console (left), and video conference management screen (right) next to the plant control screens

The main aspects of the agreement are:

- IAEA financially supports the project, procuring the new equipment needed to establish the IRL in Latin America using the RA-6 Reactor as Host Reactor.
- IAEA covers the fee of each transmission to three guest institutions participating in the project for a period of 5 years.
- IAEA financially supports a training and orientation workshop for the principal instructors from the Guest Institutions
- CNEA, with its RA-6 Reactor acts as Host Institution for IRL project in Latin America.
- CNEA installs all the equipment needed to support the IRL project in Latin America.
- CNEA procures the internet infrastructure needed to support the IRL project in Latin America.
- CNEA develops the software and hardware software to support the IRL project in Latin America. IAEA will support this development if needed.
- CNEA will provide live video signals from the Host Reactor control room to facilitate interaction between the operator, students and instructors at Guest Institutions.
- CNEA will broadcast the six following experiments once a year during five years to the remote institutions.
    1. Nuclear instrumentation in a Research Reactor;
    2. Critical approach;
    3. Control rod calibration;
    4. Control rod reactivity measurement (rod drop);
    5. Temperature reactivity coefficient; and
    6. Void coefficient calculation.
- CNEA will provide the necessary curriculum and laboratory protocols for each of the six core experiments to the Guest Institutions.
- The agreement identifies three potential Guest Institution:
    - Cuba,
    - Ecuador,
    - Uruguay,

  then extended to seven, including:
    - Bolivia,
    - Colombia,
    - Universidad del País Vasco – Spain,
    - Universidad Politectnica de Madrid – Spain,

  But maintaining the quota of three simultaneous guests attending to a session.

The work plan.

Within the context of the agreement, CNEA and IAEA started the implementation of the work plan. In March 2015, the RA-6 Online was ready to start the tests.

In September 2015, CNEA hosted the training and orientation workshop for the principal instructors from the Guest Institutions. The workshop had the participation of the IAEA, and the main professors of the Universidad Mayor de San Andres, Bolivia; the Escuela Politécnica Nacional de Ecuador; the Universidad Nacional de Colombia; the Instituto Superior de Tecnologías y Ciencias Aplicadas, Cuba; the Universidad Politecnica de Madrid, Spain and Universidad del Pais Vasco, Spain.

During the workshop, the CNEA staff introduced the remote instructors to the RA-6 reactor as a machine. This activity was of great relevance in order to familiarize the remote instructors to the RA-6 reactor, the future laboratory of the experiments.

Also during the workshop, the CNEA staff presented the six protocols developed to use in the IRL in Latin America. The local and remote instructors analysed the protocols and their implementation in the IRL platform.

After that, the host institution presented how they intend to include the IRL activities into the curricula of their institutions.

Finally the CNEA staff conducted 2 reactor experiments out of the 6 that will be transmitted during the IRL project, acting as local and remote instructors in order to show the participants how should be the dynamic of the sessions to be broadcasted by the IRL for Latin America. Figure 10 shows on the left the remote setup with the instructors from guest institution performing the experience. It can be seen that each remote instructors has the complete set of signals on their laptops. On the right part of Figure 10 the local instructor from the CNEA can be identified conducting the experience from the training control room at the RA-6 reactor.

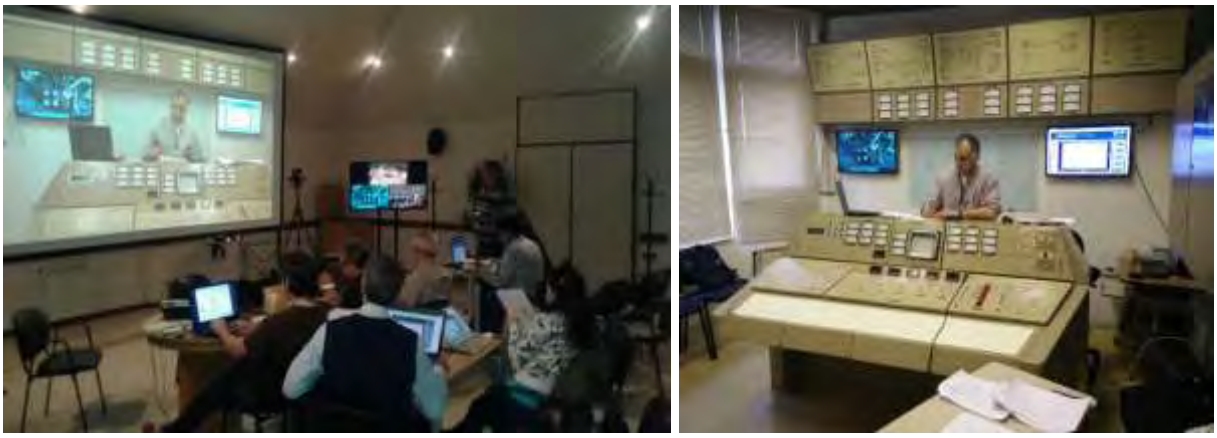

Figure 10: Transmission during the Orientation Workshop conducted in Bariloche, Argentina in September of 2015.

Based on the availability of the RA-6 reactor and the academic curricula of the participating guest institutions at the training and orientation workshop, the participants agreed on officially commencing with the transmissions on the second semester of 2016.

The Internet Reactor Laboratory by the IAEA

With the initiative of the US Department of State, the IAEA was involved in bilateral efforts between the US and Jordan in 2010 to establish a cooperation on an online-based nuclear education program. The aim was to transfer nuclear reactor knowledge from the North Carolina State University (NCSU) in particularly their research reactor experimentation on nuclear engineering to the Jordan University of Science and Technology (JUST) via the internet. After few years of efforts the NCSU's PULSTAR research reactor was authorized to provide nuclear education experiments sent via online transmissions to students of the JUST. This initiative is regarded as the first international iteration of the IRL project, later developed and expanded by the IAEA with financial support from the US Department of State.

Figure 11 Connection between the NCSU and students of JUST taking part in a practical research reactor experiment using NCSU's PULSTAR reactor, February 2014. (Photo: GIG HOUSE)

In 2011, with the receipt of the donor's financial funds the IAEA started implementing the program titled "Increasing the Global Supply of Nuclear Education and Training Programmes through Research Reactor Facilities". The IRL project and other activities related to the utilization of research reactors for education and training were incorporated within this Peaceful Uses Initiative program.

Scope and Regional Implementation of the IRL

Within the programmatic priorities of the IAEA the IRL is intended to increase the global supply of nuclear education, promoting the utilization of research reactors around the world. The scope of the IRL is of strengthening education and training programs at IAEA Member States and also contributing to the future development of human resources which will be performing work in the field of nuclear science and technology. It can also be seen as a cost-effective way to expand the nuclear education for groups of students or trainees that would not normally have access to a research reactor during their enrollment in an academic program of nuclear related fields. It can also help Member States to strengthen their training capacities and evaluate their human capital needs for ensuing future (research or power) reactor projects.

The IRL project was launched to be implemented following a regional approach. With the idea of finding and identifying counterparts to implement the project in Africa, Asia, Europe and Latin America, the Research Reactor Section (RRS) at the IAEA started involving IAEA Member States to find available research reactor facilities with demonstrated experience in nuclear education to host such a program and perform research reactor experiments. On the other end, the IAEA also initiate to look for suitable guest institutions with the potential of incorporating such experiments into existing academic curricula. Due to the different characteristics of research reactors chosen as host reactors for the project, the IRL experiments may vary from one region to the other, however the experiments are generally aimed at advanced undergraduate or postgraduate level nuclear engineering or nuclear physics students.

In Latin America, the CNEA RA-6 reactor in Centro Atomico de Bariloche –CAB - (Argentina) was identified as the host reactor for the project. Within this framework and a legal agreement in place, the IAEA provided to CNEA relevant hardware and software equipment to strengthen CAB infrastructure to be able to transmit the IRL experiments to guest institutions. The financial support also includes covering the fees of each transmission to the three guest institutions participating in the project for a period of 5 years.

In September 2015, the IAEA, in cooperation with CNEA, organized the kick-off meeting of the IRL project in Latin America. The meeting was hosted by CNEA and attended by the professors from the guest institutions involved in the project and an IAEA representative.

During the meeting, a work plan agreed among all participants indicates that the IRL transmissions are to commence in September of 2016.

Conclusions

A successful collaboration between the Argentinian National Atomic Energy Commission and the International Atomic Energy Agency was presented. Both agencies joint their effort while holding similar projects to generate an on-line teaching platform for reactor experiments course. The RA-6 Online from CNEA was pursuing to create a platform where the relevant measured signals of the RA-6 reactor were available. On the other side IRL project is looking to provide teaching resources to those countries without access to experimental reactors that serves teaching purposes.

However it does not replace real hands on experimentation at a research reactor facility, the IRL project is a cost-effective option to include practical reactor experiments into existing university nuclear curricula. With the work of the IRL, the IAEA intends to promote similar bilateral cooperation among research reactors and universities in Latin America and other regions. It also promotes the expansion of the transmissions beyond the timeline of the IRL agreement and outside of the financial support of the IAEA, so guest institutions can build one-on-one partnerships with host reactors for future transmissions.

Implementation of a Fission Gas Release and Monitoring Loop at the PULSTAR Reactor

A. I. Hawari, M. Liu, M. R. Smith
Nuclear Reactor Program, North Carolina State University
Raleigh, North Carolina, 27695, USA

J. M. Harp, G. Pastore, R. L. Williamson
Idaho National Laboratory, Idaho Falls, ID, 83415, USA

ABSTRACT

A fuel irradiation and fission gas release (FGR) measurement loop is under implementation at the PULSTAR reactor. In various fuel performance analysis computational tools, physical models are used that describe the release of fission gases (i.e., krypton and xenon) to aid in predicting macroscopic fuel behavior, e.g., fuel swelling and pellet cladding mechanical interaction. However, for important fuel types such as uranium dioxide and uranium silicide fundamental data on intra-granular fission gas diffusion remain inaccurate or nonexistent. To study this phenomenon, a loop for irradiating fuel samples and sweeping and detecting the released fission gases has been designed and is currently being set up to operate in beamport #1 of the PULSTAR reactor. The main components of the loop include a sample holding and heating chamber, a sweep gas flow system, an HPGe gamma-ray detection system, and a sweep gas venting system. In addition, other equipment are used for neutron flux monitoring, gas flow monitoring and control, gamma-ray signal processing, and HPGe detector shielding. To support the implementation of the FGR loop, design analysis using the MCNP neutronic code and the multi-physics COMSOL code was performed. The MCNP analysis was based on accurate models of the coupling between the PULSTAR core and beamport #1 and produced the fission gas birth rate (B) in a fuel sample for a given thermal neutron flux and fuel mass. COMSOL was used to simulate sample heating and the sweep gas flow system to predict the release rate (R) of the produced fission gas and to infer detectability for set temperature and flow conditions. The MCNP simulations showed that at the expected sample location a thermal neutron flux of nearly 5×10^{12} n/cm^2·s will be available to perform the irradiations. In addition, the COMSOL simulations showed that for fuel samples (e.g. uranium dioxide) with a mass less than few grams and enrichment less than 10% in U-235, the temperature of the sample will be controlled by the heating system (as opposed to the fission process). Furthermore, it was shown that at a given temperature, the sweep gas flow rate can be set to produce reasonable fission gas gamma-ray signal at the HPGe detector. At this stage, the components of the loop are being assembled to produce a system that is capable of performing fission gas release-to-birth (R/B) measurements with close control of the experimental conditions including the temperature to allow accurate assessment of fission gas diffusional behavior in nuclear fuel.

1. Introduction

Modern nuclear fuel performance analysis computational tools aim at establishing a predictive approach for examining macroscopic fuel behavior due to fission gas induced swelling and the associated pellet cladding mechanical interaction (PCMI). In general, macroscopic fuel behavior is highly sensitive to understanding microscopically driven

phenomena, which in this case is the release of fission gas (i.e., Kr and Xe) from the fuel. Previous studies identified the uncertainties associated with the intra-granular fission gas diffusion coefficient as most limiting for the accuracy of fission gas release calculations [1]. In particular, it was concluded that, in order to improve fission gas release as well as gas induced swelling predictions using fuel performance codes, a better characterization of the diffusion coefficient is needed. Figure 1 shows fission gas release predictions in comparison to measured data.

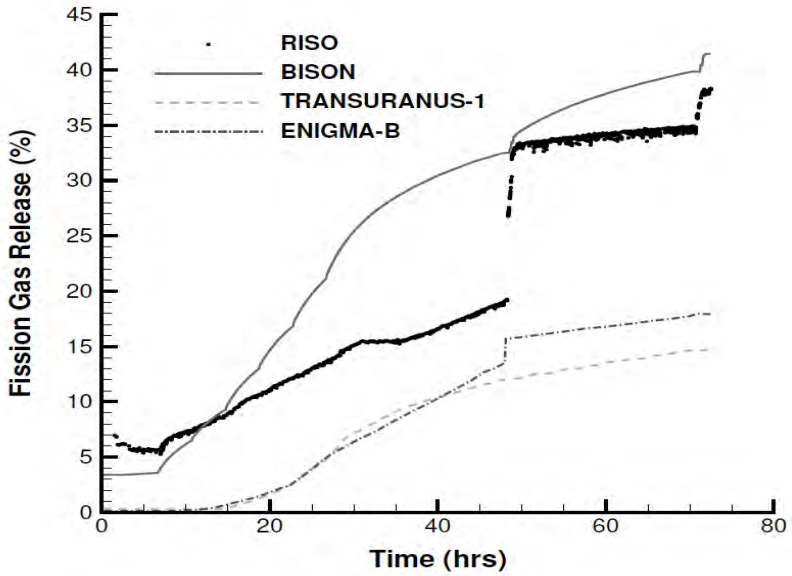

Fig. 1. Fission gas release from UO_2 fuel in a ramp test (RISO) as predicted by the computer codes BISON, TRANSURANUS-I and ENIGMA-B [1].

This work explores the implementation of an on-line fission gas release and measurement loop at the North Carolina State University (NCSU) PULSTAR reactor. A unique characteristic of this loop is the ability to control the temperature of the fuel samples during irradiation to establish a more accurate correlation between the irradiation conditions and an observable such as the intra-granular gas diffusion coefficient.

2. Loop set up at the PULSTAR reactor

A layout of the PULSTAR reactor is shown in Fig. 2. Beamport #1 is chosen as the location of the fission gas release loop. Samples of uranium dioxide (UO_2) and uranium silicide (U_3Si_2) will be prepared for irradiation in this loop. The samples will be positioned to assure exposure to the maximum available neutron flux in the beam tube. Analysis using the MCNP6 code shows that a neutron flux greater than 5×10^{12} n/cm^2·s can be reached outside of the reactor core and within beamport #1 to support the irradiations [2]. The neutron flux energy distribution is also shown in Fig. 2. Measurements are currently underway to verify the flux data as predicted by MCNP6.

Outline of the design of the fission gas release and measurement loop is shown in Fig. 3. The main components of the loop include the sample holding and heating furnace, the sweep gas (e.g., helium) flow sand venting systems, and instrumentation for neutron flux monitoring and temperature and sweep gas flow control. In addition, the current design considers using fuel samples of uranium dioxide (UO_2) and uranium silicide (U_3Si_2) with ^{235}U enrichment reaching 10% by weight. The samples will consist of fuel microspheres with radii of 0.1 to 1 mm. The “in-pile” experiment is designed so that the fission product gases can be continuously collected throughout the experiment using the helium sweep gas, which will circulate through the fuel sample(s) and carry the release fission gas to a gamma-ray detection

and spectrometry system that is setup at the exit of the loop. This system will be configured to detect the gamma-ray signatures and intensities of Kr and Xe as observables that are correlated with the experimental conditions (i.e., neutron flux and temperature) to extract fission gas release information.

A unique aspect of the loop described above is its ability to control the temperature of the sample independent of the fission rate. To verify this control, simulations using the COMSOL multi-physics package were performed that included a number of spheres held at a given surface temperature with an internal power source (representing fission) and in the existence of helium sweep gas flow [3]. The results of this investigation indicated that for the samples that will be used in this work (e.g., microspheres varying in diameter from 10 to 1000 micrometers) the temperature will be completely controlled by the furnace. The contribution of the fission heat source is negligible (See Fig. 3).

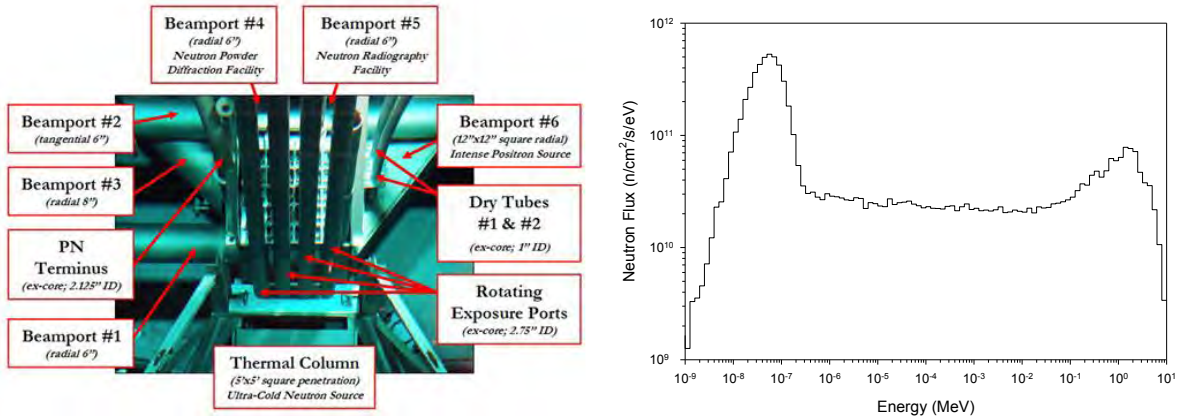

Fig. 2. A layout of the PULSTAR reactor core and its surrounding region showing various irradiation locations including beamport #1 (left). The neutron flux energy distribution in beamport #1 (right).

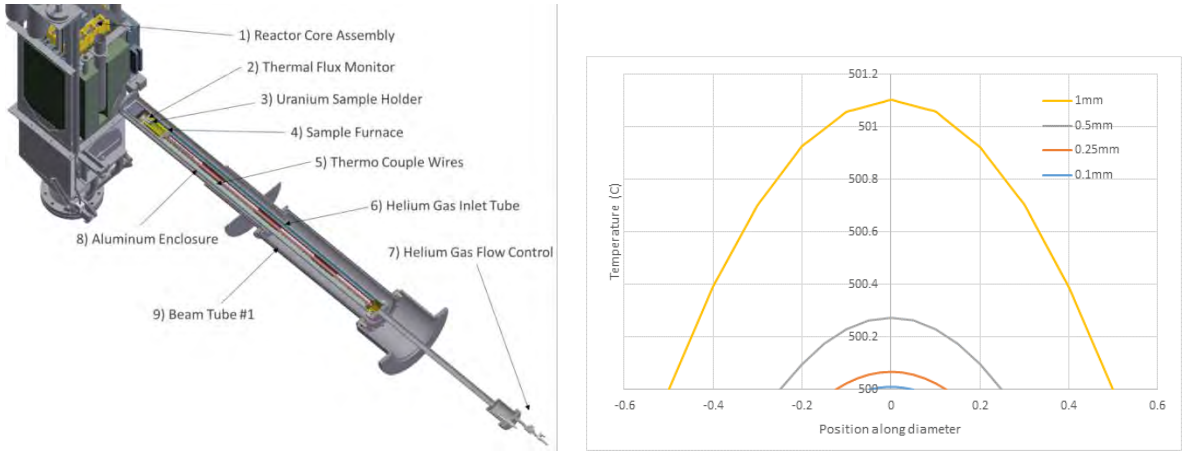

Fig. 3. The layout of the fission gas release and measurement loop at the PULSTAR reactor (right). The loop will be implemented in beamport #1 of the reactor. The results of the COMSOL model for a sample of 1000 UO_2 spheres with diameters varying between 100 and 1000 μm and a surface temperature of 500 °C (right).

3. Assessment of experimental observables

The primary observable that will be measured using the implemented loop is the fission gas release rate (R) as a function of temperature. The release rate will be compared to computationally estimated fission gas birth rate (B) to establish what is commonly known as

the release-to-birth (R/B) ratio, which may be related to various theoretical gas release models to explore release mechanisms, e.g., through diffusion or otherwise.

As a representative case, analysis was performed to estimate R for the ^{138}Xe gaseous fission product, which has a half-life of 14 minutes, emits reasonably intense gamma-rays with energies extending up to 2 MeV, and has negligible transmutation in a neutron field. Under steady state irradiation conditions, the R/B ratio for this radionuclide may be estimated using the formulation of the equivalent sphere model given by [4,5]

$$\begin{aligned} R/B &= 3\sqrt{\frac{D}{\lambda a^2}}\left[\coth\left(\sqrt{\frac{\lambda a^2}{D}}\right)-\sqrt{\frac{D}{\lambda a^2}}\right] \\ D' &= \left(\frac{500}{d}\right)^2 10^{\left[-7.97-\left(1920/T\right)\right]} \qquad T<1173\,\mathrm{K} \\ D' &= \left(\frac{500}{d}\right)^2 10^{\left[-2.60-\left(8220/T\right)\right]} \qquad T>1173\,\mathrm{K} \end{aligned}, \tag{1}$$

where, D is the diffusion coefficient, λ is the decay constant, a is the sphere radius, D' is the reduced diffusion coefficient defined as D/a^2, d is the sphere diameter, and T is temperature. Furthermore, B was estimated using MCNP6 calculations of the steady state fission rate density in a representative spherical sample of UO_2 with 100 μm diameter. In this case, the neutron flux energy spectrum given in Fig. 2 was used and a density of 5.6×10^{12} cm^{-3} s^{-1} was obtained. This results in a steady state production of ^{138}Xe of 3.6×10^{11} cm^{-3} s^{-1}. Assuming a sample size of 1000 microspheres and a diameter of 100 μm, the steady state release rate at various temperatures is given in Table 1 below.

Temperature (K)	R (Xe atoms/s)
673	4×10^3
873	1×10^5
1073	7×10^5
1273	1×10^6
1473	2×10^6

Tab 1: Temperature dependent release rates as predicted using Eq. 1.

	Predicted Count Rate at Various Temperatures				
Gamma-ray energy (keV)	673 K	873 K	1073 K	1273 K	1473 K
258	1	30	230	570	700
434	0.8	20	150	360	460
1768	0.6	16	120	300	380
2015	0.5	12	90	220	280

Tab 2: Predicted temperature dependent count rates. The count rate is calculated as $\varepsilon\Gamma R$, where ε is the detector efficiency and Γ is the gamma-ray absolute intensity.

As mentioned above, the detection of the released radionuclides that are carried by the sweep gas will be performed using a high resolution gamma-ray spectrometry system (e.g., using an HPGe detector). The counting arrangement that is currently under design aims at achieving an absolute counting efficiency of at least 0.1%. Assuming that the travel time of the released radionuclide (e.g., ^{138}Xe) to the detector and its counting time to be significantly less than its half-life, the predicted count rate for various emitted gamma-rays was found to depend on temperature and can range from a few counts per second to hundreds of counts per second (see Table 2 above). These count rates are distinguishable from the background in the experimental area of the PULSTAR reactor, which indicates the feasibility of using this

experimental set up for collecting fission gas release data. Figure 4 shows the gamma-ray spectrometry setup and initial assessment of background levels in the vicinity of beamport #1 in the PULSTAR reactor bay area. Further enhancement of the detection arrangement will be pursued to assure achieving optimal signal to noise conditions.

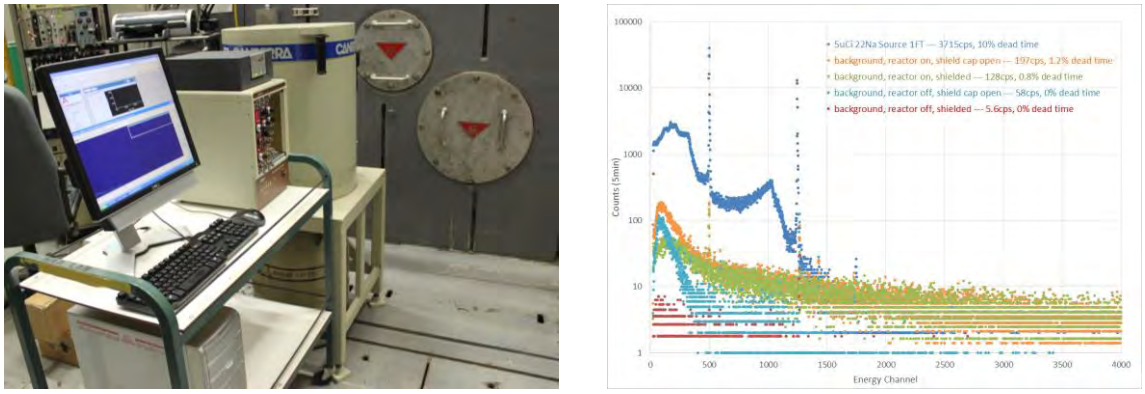

Fig. 4. The gamma-ray spectrometry setup at beamport #1 of the PULSTAR reactor (left) and results of background radiation assessment near beamport #1 (right). For shielded conditions, the background levels are well below expected signal levels.

4. Conclusions

Analysis was performed of an "in-pile" fission gas release experiment that is currently under implementation at the NCSU PULSTAR reactor. Using MCNP6 calculations and COMSOL simulations, the fission rate density and temperature distributions in UO_2 microspheres were estimated. To explore the feasibility of detecting fission gas isotopes, estimates of R/B for ^{138}Xe were obtained using the equivalent sphere model and combined with MCNP6 predicted B values to calculate R. Assuming detection using a typical gamma-ray spectrometry HPGe system, it was conclude that reasonable count rates will be achieved to allow extraction of release information and the related intra-granular diffusion coefficient. At this stage, accurate assessment is underway of the performance of various loop components to set the final design criteria in support of loop fabrication.

5. References

1. G. PASTORE et al., "Uncertainty and sensitivity analysis of fission gas behavior in engineering-scale fuel modeling," *J. of Nuclear Materials*, **456**, 398 (2015).
2. J. T. GOORLEY et al., "Initial MCNP6 Release Overview MCNP6 Version 1.0," LA-UR-13-22934, Los Alamos National Laboratory (2013).
3. See http://www.comsol.com/comsol-multiphysics.
4. D. R. OLANDER, *Fundamental Aspects of Nuclear Reactor Fuel Elements*, National Technical Information Service, Springfield, VA (1976).
5. D. PETTI et al., "Development of Improved Models and Designs for Coated-Particle Gas Reactor Fuels," INEEL/EXT-05-02615, Idaho National Laboratory (2004).

"QUALIFICATION OF POWER DETERMINATION FOR F&M EXPERIMENTS IN RESEARCH REACTORS"

B. Yu. Volkov
Division Nuclear Technology, Physics and Safety (NTPS)
IFE-Institutt for energiteknikk (Norway)
OECD Halden Reactor Project
www.ife.no

ABSTRACT

Fuel and materials R&D programmes usually include different types of in-pile tests in research reactors that can simulate the real operational conditions of commercial NPPs. The general objective of these tests is to investigate fuel behaviour under normal, operational transients and accidents conditions. The main goal of these tests is to study the fuel thermal performance and mechanical behaviour by means of in-pile measurements such as fuel temperature, fuel and cladding elongation, internal rod pressure and some other specific parameters during irradiation. An integral part of the analysis of the data obtained from these experiments is an accurate power determination with respect to NPPs.
This paper presents a general approach for the qualification of test fuel power determination for different fuels experiments, which is based on the experience derived from the Halden reactor (HBWR) tests over many years:

- Steady-state experiments in PWR and BWR test loops
- Transient power ramp tests
- LOCA tests

Also considered are some factors that affect the quality of the test fuel power determination which not only originate from the accuracy of the primary measurements but also depend on the design of the irradiation device and position of instruments, test conditions and calibration methodology.
The experimental capabilities in the Halden reactor are constantly upgraded in order to enhance the quality of in-pile experiments and the power determination technique. The experience derived from the long term fuel and materials experimental programme at the Halden reactor may also be used by other research organizations, in particular for power qualification of fuels irradiation tests.

1. Introduction

Power determination is an important part of any fuel performances experiments in research reactors both for safety and for analysis of the test fuels and materials behaviour. The thermal power measurements are based on the conventional methodology used in many research reactors including Halden reactor [1]. The main approach for qualification of these measurements is usually based on "Guide to the Expression of Uncertainty in Measurements" [2] issued under the auspices of several international organizations for standardization.
One of the important parts of the qualification is the experience with or general knowledge of the processes, behaviour and properties of relevant materials employed for the experiments. An analysis of the data obtained from actual in-pile experiments performed in the Halden reactor shows that a quality of the power determination are not only originated from the quality of the instrumentation but also dependent on the rig design, position of the instruments in the rig, test conditions, capability of the test fuel to generate power and some other specific factors. The main goal of the paper is to share some experience with power determination for different types of the Halden F&M tests with emphasis on specific phenomena which can affect accuracy of power determination in RR with respect to commercial NPPs.

2. Types of fuel and material tests in research reactors

Power generation and time of fuel operation define the energy production and thereby the level of fuel utilization within NPPs. Fuel vendors, within the licensing process, establish a design limit for the fuel they supply, which restricts power rating and fuel discharge burnup. To determine both these parameters some in-pile experiments are usually performed in RRs like the Halden Reactor [3]. In generally, the experiments can be divided on several types where correct power determination is important and has some specific features.

Steady-state basic irradiation tests

The main part of the steady-state tests is to correct determination of test fuel burnup which is actually determined as an integral of the heat generated by the fuel. Some example of the tests performed in the Halden Reactor with respect to power and burnup determination:

- Tests for determination of FGR threshold which may restrict a power (LHR) of the commercial fuel with burnup : **FGR threshold ~ f(TF (LHR), Bu)**
- Fuel thermal conductivity degradation tests with burnup: ***λ fuel ~ f(Bu(ALHR))***

Transient tests

Specific feature of the transient tests is fast changes of the nuclear power to determine pellet-cladding mechanical (PCMI) failure thresholds as a function of terminal power, power ramp rate for fuel with different burnups [3]. The precise power determination for this type of the tests is important and in some cases is difficult because of transient effects.

Accident simulation tests

Accident simulation tests are performed to find power-burnup limits with real safety margins.

- The HRP series of LOCA simulation test where target max cladding temperature is provided by fuel heat generation power to simulate deposited energy: ***Tmax (LOCA)~ f(Deposited energy)~f(ALHR in RR)*** as shown in *Figure 1* .
- Dry-out tests were performed in Halden to study occasional cladding overheating which directly dependent on CHF (critical heat flux) determined during the tests.

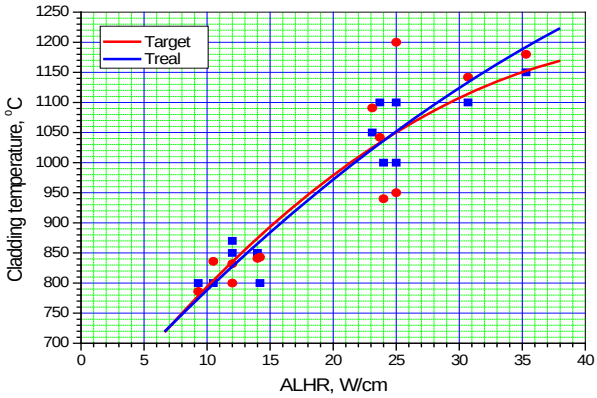

Figure 1 Cladding temperatures as a function of ALHR in Halden LOCA test

3. Approach for qualification of power determination in F&M tests

Any kind of direct and indirect measurements (based on calculations) should be performed with certain accuracy and precision. It is obviously, if measurements do not provide required accuracy, the time (and money) to perform the experiment is wasted. In other hand, if too much effort was done trying to provide measurements with accuracy higher than need, then time (and also money) was also wasted.

The main approach for qualification of in-pile measurements for determination of the thermal power released by nuclear fuel in RR should be in compliance with those in commercial NPPs. According to the international recommendation [2], so-called Type B standard uncertainty (not statistical equivalent of the standard deviation (Type A)) should be employed for a scientific judgement of the following available information:

- Uncertainties of the measuring instruments specified by manufacturer
- Quality of the measurements technique and resolution of Data Acquisition System;
- Experience with or general knowledge of the processes, behaviour and properties of relevant materials;

3.1 Principles of power determination for R&M tests

The thermal power generated in the test devices (rigs) may be subdivided into the power generated by the fuel itself (due to fission, gamma- and beta-decays and etc.) and the power generated by gamma and neutron capture by structural materials.
Correct determination of the thermal power may be affected by heat losses due to unperfected insulation of the test rig. Some specific phenomena can also influence the correct determination of thermal power released by fuel in the test channel. Knowledge of these phenomena can help to reduce or avoid systematic effect on uncertainties (δQ):

$$Q_F = Q_{th} + Q_{loss} - Q_\gamma \pm \delta Q \tag{1}$$

Thermal power balance in the test rigs of any RR is simply determined by the coolant enthalpy rise (based on temperature and pressure measurements) and coolant mass flow:

$$Q_{th} = (h(TO,P) - h(TI,P)) \cdot \dot{m} \tag{2}$$

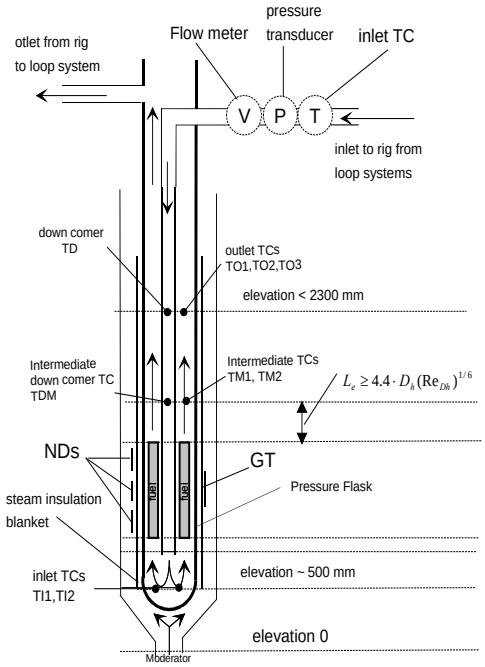

Figure.2 Typical fuel test rig and instrumentation used for loop tests

Schematic view of typical rig in water cooled loops employed in RR for F&M test is shown in *Figure.2* with instrumentation installed for power calibration. The mass flow rate is determined using volume or mass flow meters, pressure transducer and temperature detector installed in the loop system at inlet to the rig. One or two of down comer thermocouples (TD1…) are installed at the same axial position as the outlet thermocouples. In addition, intermediate down comer and intermediate outlet thermocouples are usually mounted in the level between fuel top and outlet TCs. This allows not only reliable temperature measurements but also heat losses from the test channel to be accounted for the calorimetrical power calibration. The outlet (TO1…) or intermediate thermocouples (TM1…) are usually mounted far enough from the fuel top in order to provide temperature measurements of equilibrium flow in utlet. Inlet thermocouples (TI1…) are fixed in the bottom of the rig accomplishing the temperature measurements for the power calibration. In order to reduce heat loss to a moderator (surrounded the test rig) the pressure flask may be surrounded by steam blanket generated (in specially designed outer shroud) due to higher loop temperature than in the moderator. Gamma thermometers (GT) and neutron detectors (NDs) may also be incorporated into the rig to monitor gamma and thermal neutron fluxes for on-line fuel power determination:

$$Q_F \cong KG \cdot NDAVG \tag{3}$$

where: $KG = \dfrac{Q_{FC}}{NDAVG}$,is the power calibration factor determined during special calibration routine accounting for thermal balance power Eq (1) and NDAVG is the average signal recorded by all SPNDs both during calibration and experiment.
The in-pile and out-of-pile instrumentations as well as data acquisition system (DAS) employed in RR should be specified for qualification of the primary measurements used for test fuel power determination and calibration which uncertainties are based on propagation of the errors from these measurements [1,2].

3.2 Calibration procedures

The calibration includes the following procedures: (a) inter-calibration of outlet and inlet thermocouples and (b) power calibration. Both these procedures are carried out to achieve a zero heat transfer with environment by means of the coolant temperature variation.

Inter-calibration of thermocouples

In order to reduce systematic effect of instrumental uncertainties on power calibration the so-called inter-calibration of thermocouples is carried out to set to zero the balanced thermal power at hot-stand-by (HSB) conditions without nuclear heating. The corrections of the downcomer and outlet thermocouples against average inlet temperature are determined at the conditions of zero balanced heat in test rig.
Examples of this inter-calibration before and after corrections (reference plot) are shown in *Figure 3*.
The linear regression analysis of the plots allows an uncertainty of this procedure to be estimated. Statistically, the inter-calibrations of the in-core thermocouples are performed in the Halden reactor with typical deviation better than:± 0.05 ^{o}C.

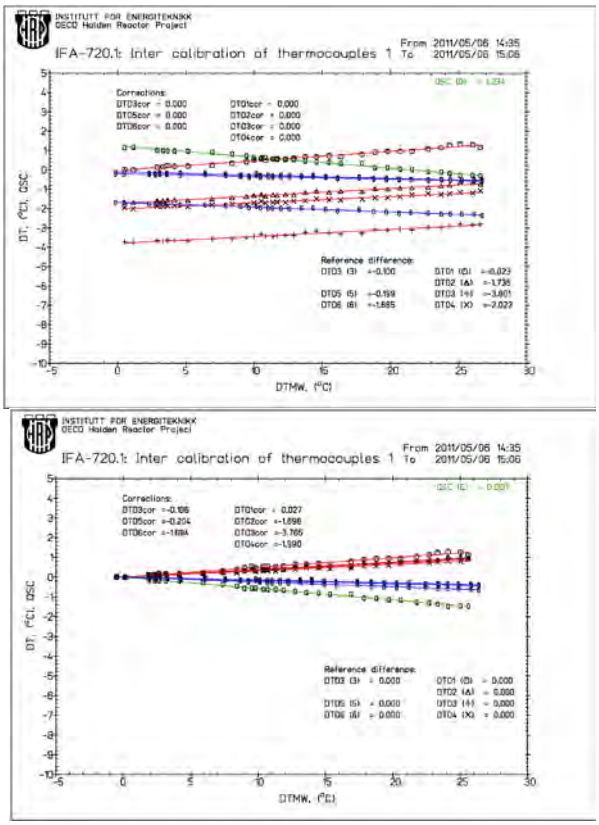

Figure 3 Example of the inter-calibration of thermocouples before and after corrections

Power calibration and its verification

The power calibration routine has been developed in order to eliminate from the balanced thermal power the heat loss to the environment due to imperfection of rig's insulation. The test rig is usually cooled down and axial thermal balance of the heat exchange with moderator is vanished due to approaching of the weighted average coolant temperature (*DTMW*) in the rig to the average surrounded moderator temperature. This procedure improves the test power determination but itself can produce some uncertainties with random effects.

$$Q_{loss} = k_{loss} \cdot \Delta L \cdot (\overline{T} - T_{\mathrm{mod}}) = k_{loss} \cdot \Delta L \cdot DTMW \quad (4)$$

where: K_{loss} is the linear heat transfer coefficient from coolant to the moderator;

ΔL is the distance between inlet and outlet thermocouples.

The verification of this procedure was performed using electrical heater in the LOCA test rig (*Figure 4*). The standard deviation of the calorimetrically measured power vs electrical heater during power calibration procedure at hot stand-by condition without nuclear heating was evaluated ±0.075 kW which is associated with random effect on power determination. The result of power calibration of the heater is shown in *Figure 5*.

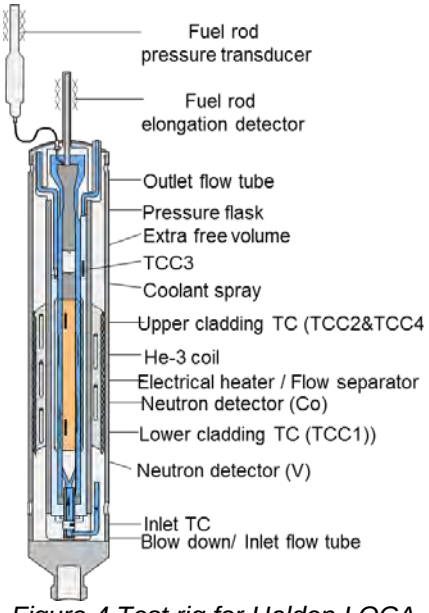

Figure 4 Test rig for Halden LOCA tests

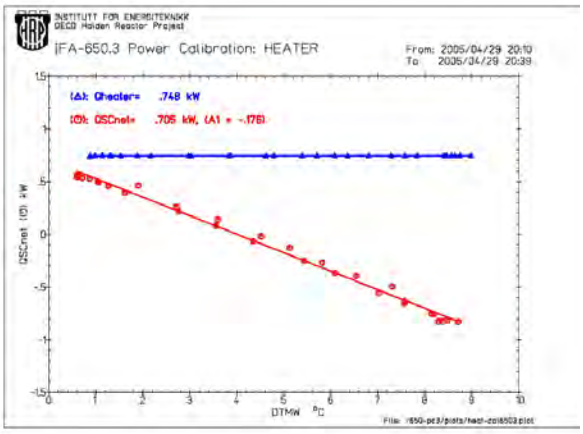

Figure 5 Verification of power calibration routine using el. Heater in LOCA test rig

3.3 Gamma heating in the structural materials

The thermal power released in the test channel due to external gamma heating in the structural materials should be subtracted from the total thermal power in the rig according to Eq. (1). In general, the gamma heating is dependent on several factors as reactor power, position of the rig in the reactor core (radial gamma flux), rig design (mass of the structural materials in the rig) and some other specific factors. The calculations are usually performed with computer program where the following general formula is applied:

$$q_{\gamma(i)} = G \cdot \sum_{j=1}^{N} \left(M_j \alpha_j \right) \cdot \gamma(i) \qquad (5)$$

G *is the rate of gamma heat power measured in the test rig by gamma thermometers (or calculated on the data previously measured) [W/g];*
N *is the number of components in the axial segments "i" ;*
Mj *is the mass of the component "j";*
αj *is the absorption factor of the material of the component "j";*
γ(i) *is the axial gamma flux profile for axial segment (i).*

Relative uncertainty of the fuel power can be estimated by means of the correlation modified for the analysis of the gamma heating as follows:

$$\delta_F = \frac{u_F}{Q_F} = \frac{\sqrt{u_{th}^2 + u_\gamma^2}}{Q_F} = \frac{\sqrt{(Q_{th}\delta_{th})^2 + (Q_\gamma \delta_\gamma)^2}}{Q_{th} - Q_\gamma} = \frac{\sqrt{(\delta_{th})^2 + (\delta_\gamma \cdot (Q_\gamma / Q_{th}))^2}}{(1 - Q_\gamma / Q_{th})} \qquad (6)$$

u_{th} and δ_{th} are the combined standard deviation and relative uncertainty of net thermal power generated in the rig;
u_γ and δ_γ are the standard deviation and relative uncertainty of gamma heating in the rig;

The effect of gamma heating uncertainty on combined uncertainty of test fuel power determination is shown in *Figure 6*

In order to improve accuracy of power determination for F&M tests in RRs with high gamma flux it is necessary to improve a gamma heating power determination.

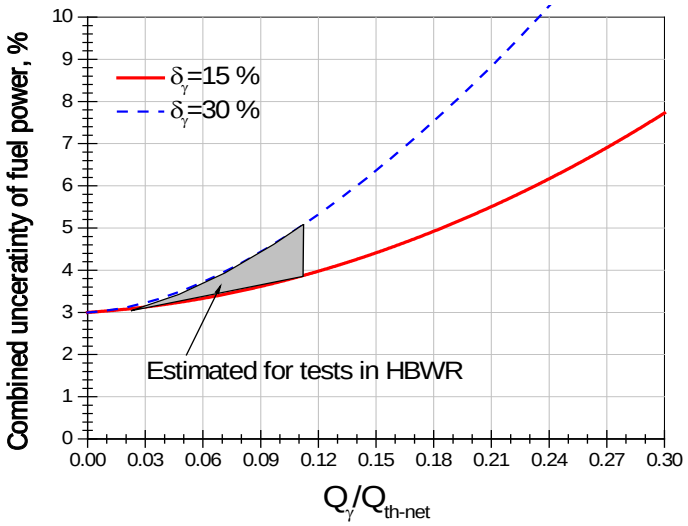

Figure 6 Effect of gamma heating on combined uncertainty of test fuel power determination

4. Specific effects influencing thermal power determination in F&M tests

4.1 Rig design and problem of mixing flow at outlet

The cross-sectional weighted average or so-called equilibrium temperatures at inlet and outlet of the channel must be used for thermal power determination. However, there is a temperature gradient across the coolant flow due to hotter stream generated by the fuel and colder wall of pressure flask separating the test rig from the moderator. In this case, some special arrangements for the rig design at outlet should be made. For example, coolant outlet thermocouples should be elevated far enough from the fuel top to the position where the hot and cold streams merge developing fully mixed flow as shown schematically in *Figure 7* . This distance (called mixing-length) can be calculated as a function of rig's hydraulics using the following correlations adopted from [4] for circular tube:

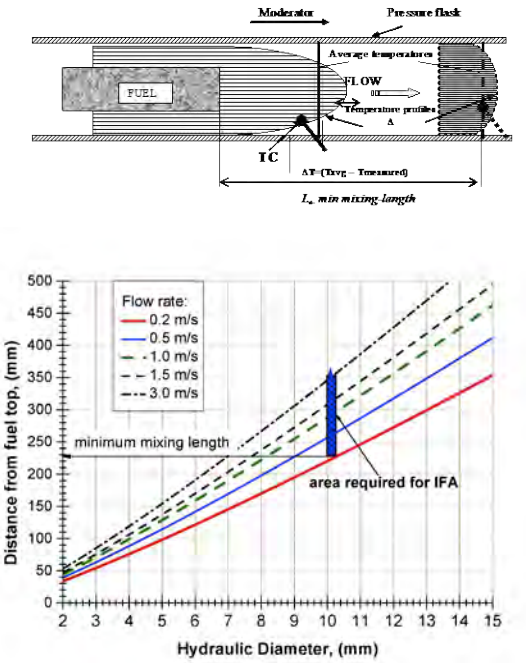

Figure 7 Schematic view and calculation of the mixing length in test rig

for laminar flow (Re < 2300):

$$L_e \geq 0.06 \cdot D_h \, \mathrm{Re}_{Dh} \qquad (7)$$

for turbulent flow (Re > 2300):

$$L_e \geq 4.4 \cdot D_h (\mathrm{Re}_{Dh})^{1/6} \qquad (8)$$

where: D_h is the hydraulic diameter;

L_e is the mixing length of flow (here the minimum distance from the fuel top);

$Re_{Dh} = (w\, D_h / \nu)$ is the Reynolds number.

4.2 Fission beta effect on NDs position in test rigs

High energy fission betas are able to penetrate fuel rod cladding, water and reach Vanadium-SPND emitter through the structural material (sheath and insulator), and thus affect the generated by V-SPND current. This effect is observed when the distance between the V-SPND and the fuel rod is too small (less than 5 mm) [5].

The investigation of this effect was performed using a reactor scram data with time resolutions of 0.5 sec to record the V-SPND current. A typical ND signals recording before and just after the scram is shown in *Figure 8*. Since the fission betas contribute negatively to the SPND current at nuclear power the signal dramatically increased just after the scram while the signal due to the neutrons remains relatively high because of the slow time constant of the Vanadium signal. This explains while the signal transiently increases at the moment of the scram.

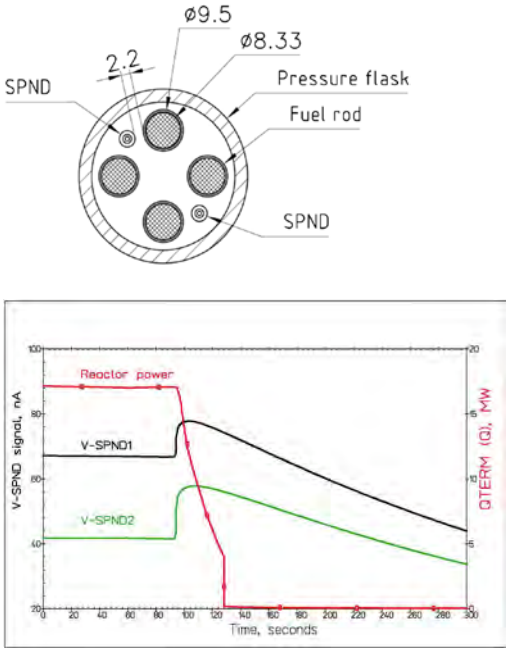

Figure 8 Effect of fission beta from fuel on V-SPND signal

4.3 Transient effect

The coolant cooling down or heat up in the rig is usually performed very slowly and this procedure may be considered as steady-state. Nevertheless, this cooling transient may produce some uncertainties with systematic effect for power ramps, which is dependent on the cooling or heat up rates and coolant flow rate as well as on thermal capacity of the materials used for test rig production.

The accurate assessment requires sophisticated numerical or model calculations but for uncertainty estimate, so-called "lumped capacitance" model [6] may be applied despite its domain of applicability (Biot number Bi=αl/λ<<1.0) can be out of the range for some test conditions. According to this model, response of temperature distribution on cooling transient is assumed to be dependent on specific capacity of the rig's materials and to be independent of the thermal conductivities of these materials. A particular point of interest for thermal power determination is a variation of the temperature rise along the channel, which can be calculated as a function of elapsed cooling time with the following assumptions:

- inlet and outlet coolant temperatures are recorded at the same time;
- response time of the coolant thermocouples is small (< 0.1 s) and it is not accounted for estimations;

It is also assumed that inlet coolant temperature (T_{in}) linearly decreases with constant rate (a) as a function of transient cooling time (τ):

$$T_{in}(\tau) - T_{in}(0) = \Delta T_{in} = -a\,\tau \tag{9}$$

According to the "lumped capacitance" model, the non-steady-state energy equation regarding to the wall temperature variation can be written in the following form:

$$\frac{d(\Delta T_w)}{d\tau} + \frac{hA}{(\rho c V)_w}(\Delta T_w - \Delta \overline{T}) = 0 \tag{10}$$

$(\rho c V)_w$ is the "lumped capacitance" calculated as a product of density, specific heat capacity and volume of materials incorporated into the rig, respectively;

h is the average heat conductance coefficient of the wetted surface of the rig;

A is the area of the wetted surface in the rig.

The thermal power variation can be derived from the energy balance equation accounting for only energy stored due to heat capacity of the materials in the rig and released at cooling down:

$$C_p \dot{m}(\Delta T_{out} - \Delta T_{in}) = hA(\Delta T_w - \Delta \overline{T}) \tag{11}$$

C_p is the heat coolant capacity at constant pressure;

$\dot{m}$ is the mass flow rate.

The left part of this equation can be considered as a power uncertainty (due to cooling transient), which can be determined using the differential Eq. (10) for determination of "bulk" wall temperature variation.

The average temperature can be re-written in the following form:

$$\Delta \overline{T} = \Delta T_{in} + \frac{(\delta T_{cap} + \delta T_{trans})}{2} \tag{12}$$

where: δT_{cap} and δT_{trans} are the deviations of temperature due to rig thermal capacity and transition time due to cooling transient

In result of solution of the equation (11) and (10) for the late stage of the cooling, the transient deviation of the temperature rise becomes to be independent of time and combine deviation of outlet temperature can be calculated as follows:

$$\delta T_{\Sigma} = \delta T_{cap} + \delta T_{trans} = a\left\{\frac{(\rho c V)_w}{C_P \dot{m} - hA/2} + \frac{L_{TC}}{\omega}\right\} \tag{13}$$

where: L_{TC} is the distance between inlet and outlet thermocouples;

ω is the average flow velocity between inlet and outlet thermocouples.

The analysis shows that transient power deviation could be substantial with high cooling rates >3°C/min for high capacity rigs (with several fuel rods and with massive of the structural materials). The effect of coolant transient on deviation of power determination due to "lamped capacitance" model of high and low capacity rigs used in HB WR during cooling is shown in *Figure 9*.

The deviation of the temperature rise at heat up can be obtained using the same way but the value will be negative and transient effect on power determination does not account for conductivity of the materials incorporated into the rig which may reduce the deviation of the thermal power determination due to rig "lumped capacitance" under cooling transient.

The transient uncertainty may be reduced if the following conditions are met:

- Short distance between inlet and outlet thermocouples;
- Low mass of structural materials with high thermal capacity;
- Higher flow velocity through the fuel assembly;

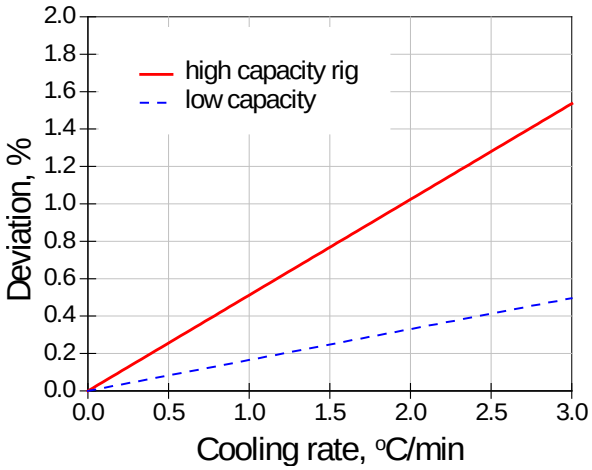

Figure 9 Deviation of power determination as a function of cooling rate for different heat capacity rigs

4.4 Helium-3 heat release in power ramp test

The test rig designed in Halden for power ramps is able to move rods one by one from low flux position to the ramp position schematically shown in *Figure 10*. This special rig design made it possible to analyse the heat generation sources in the ramp position without fuel rod including the gamma heating and energy release due to He-3 neutron absorption. The ramp channel was thermally insulated by He-3 chamber and power can thus be specified more precisely when pressurizing/depressurizing He-3 system.

It is known that He-3 gas due to neutron absorption releases some energy according to the following nuclear reaction:

$$n + {}^{3}He \rightarrow {}^{3}H + p + 0.764\ MeV \qquad (14)$$

The power generated by this reaction in the He-3 chamber is a function of neutron flux and number of gas atoms which dependents on temperature and pressure. The following function was used to evaluate the power generated by He-3 neutron absorption:

$$Q_{He-3} = \frac{E \cdot P_{He-3} \cdot V_{ch} \cdot \sigma_a \cdot \varphi}{k \cdot T} \qquad (15)$$

E is the energy of a single *(n,p)* reaction (Eq. 15) as a function of energy of thermal neutrons;
P_{He-3} is the He-3 pressure in the rig chamber;
V_{ch} is the volume of He-3 chamber;
σ_a is the microscopic cross section of *(n,p)* reaction is a function of neutron energy;
k id the Boltzmann constant (1.38 10^{-23} J/K);
T is the temperature of He-3 gas in chamber (K);
φ is the thermal neutron flux in the He-3 chamber.

The theoretically determined power of He-3 neutron absorption (Eq. 15) has been adjusted to the experimental data derived from the in-pile measurements during calibration procedure for the ramp rig in HBWR as shown in *Figure 10*. The adjustment factor shows how much the heat released in the He-3 chamber contributes to the power measured in the ramp position.

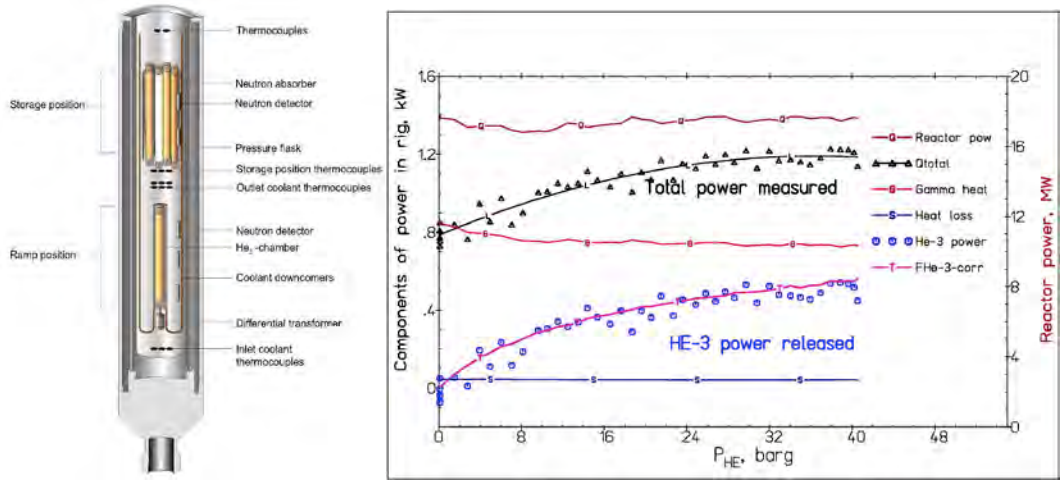

Figure 10 Ramp rig designed with He-3 chamber and power generated in the rig with empty ramp position

4.5 Other effects under investigations

Several other effects may also affect an accuracy of test fuel power determination and may be related to specific test conditions in RRs.

Hydrogen effect on Vanadium SPND measurements

In the PWR loop tests, a clear effect of the dissolved H_2 content on V-SPND signal has been noticed [5]. However, the V-SPND signals are not regular and can vary significantly from case to case both with very slow variations and faster variations as shown in *Figure 11*. The deviation of the signals can varied from 1% to 40 % with both negative and positive effect.

It is suspected permeability of H_2 into the V-SPND by diffusion mechanism under high temperature. The investigations are ongoing with emphasis on tests conditions rig design and other SPND types.

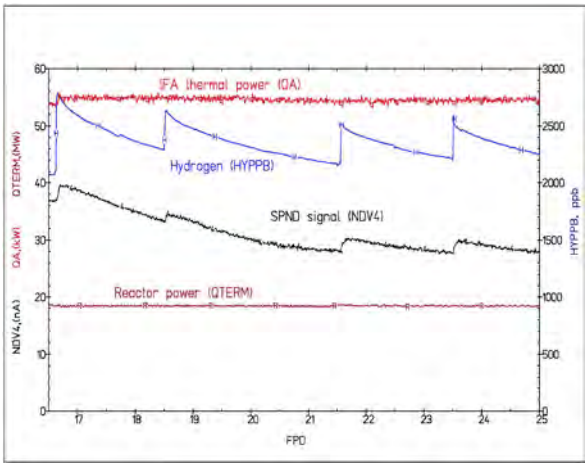

Figure 11 Effect of hydrogen injection in PWR loop on V-SPND signals

Ambient temperature effect on calibration factor

The power calibration factor can be affected due to a temperature deviation of the neutron fission and capture cross sections in fuel and in SPNDs. The Westcott g-factor [7] may be used for correction of this deviation:

$$\Delta KG_T = \frac{\Delta Q_{fuelT}}{\Delta ND_T} \approx \sum_i^n \frac{g_i(T_1)}{g_i(T_2)} \cdot \xi_i \qquad (16)$$

This effect is more pronounced for Pu-239 than for UO_2 fuel as shown in Figure 12.

Investigations are continuing but preliminary estimation shows that this phenomena may contribute of about 1.5 % to the combined uncertainty of power determination in RRs.

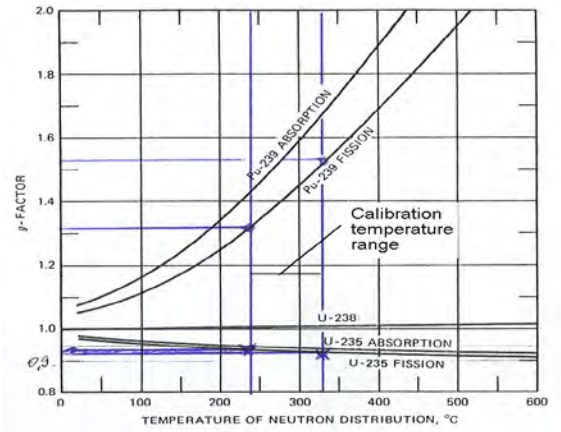

Figure 12 Westcott g-factor for fissile materials as a function of temperature [7]

5. Conclusions and recommendations

Main sources of power determination uncertainty in RRs:

- test rig design, quality of primary sensors and their position;
- heat loss;
- gamma heating in the structural materials;
- specific effects in RRs influencing the accurate power determination in the in-pile tests.

Some recommendations may be proposed for the power determination technique in RRs:

- optimisation of sensors sensitivity and their positions in tests rigs;
- careful investigation of the phenomena which may affect the correct power determination for the F&M tests in RRs;
- development of power calibration methodology accounting for transient, ambient temperature and water chemistry effects.

The experimental capabilities in the Halden reactor are constantly upgraded in order to meet enhanced requirements with high quality of the in-pile F&M experiments that demand the detailed qualification of the power determination technique. According to the experience from different kind of the in-pile tests performed, the combined power determination uncertainty in RRs should be better that ± (2.5-6.0)% with respect to the power rating determined at NPPs whereas standard deviation (with one sigma) should be in the range of ±(0.2–1.0) kW.

6. References

[1] B.Volkov, J.K. Liverud “Qualification of test fuel power calibration in HBWR», Halden Reactor Project, HWR-845, February 2007,

[2] “Guide to the Expression of Uncertainty in Measurement”, ISBN 92-67-10188-9, ISO (International Organisation for Standardization), corrected and reprinted in 1995.

[3] B. Volkov, W. Wiesenack, M. McGrath „Halden Fuel and Material Experiments Beyond Operational and Safety Limits“, WRFPM2014, Sendai, Japan September 14-17, 2014, Paper 1000140.

[4] F. M. White “Fluid Mechanics”, Second edition, McGraw-Hill, 1988.

[5] R. Van Nieuwenhove, “Effect of fission betas, activated structure and hydrogen on Self Powered Neutron Detectors”, IEEE transactions on nuclear science, vol. 61, no. 4, August 2014

[6] A. Bejan “Heat Transfer”, J.Wiley & Sons, Inc., 1993

[7] S. Glasstone, A. Sesonske “Nuclear Reactor Engineering” 4-th ed. Chapman & Hall Inc., 1994.

LOW POWER RESEARCH REACTOR TO IMPEL CREATION OF NATIONAL INFRASTRUCTURE

R.O. MAZZI
Nuclear Projects Division, INVAP
Cmte. Luis Piedrabuena 4950, (8400) S.C. de Bariloche (RN) – Argentina

ABSRACT

There are multiple reasons why a country with scarce or limited development, decides to make a qualitative leap in nuclear technology, be it in the areas of R&D, nuclear applications, nuclear generation or a combination of the three.
Implementing a nuclear programme requires developing a National Infrastructure aimed at ensuring the safe and secure use of the nuclear technology for workers, members of the public and the environment, and to ensure the international community about its commitment to peaceful use.
The initial stage —preparation of feasibility studies, concluding agreements with other countries and international organizations, and adoption of laws and regulations— can be carried out using the experience and support of international organizations and through specific cooperation agreements with regulatory bodies of other countries.
Establishing a mature Regulatory Authority with the ability to develop and apply technical criteria requires also a number of experienced professionals which are not normally available in a country starting nuclear activities.
The experience of many countries shows that developing such infrastructure is not straight forward and can take several years that frequently turn into decades.
Choosing the right strategy is the key to achieve good results in the shortest time.
Some aspects of the basic scheme, which aims to generate a National Infrastructure through cooperation with foreign organizations as a prelude towards having a nuclear installation are discussed.
In contrast to the case applied by UAE in which the creation of a National Infrastructure relies on a large number of international experts, this paper supports the idea of maximising the involvement of newcomer´s staff from early stages of the project.

A low power research reactor designed by INVAP (LPRR), with distinguished features here described, can be used to impel the creation of national infrastructure in newcomers countries.

1. Introduction

A recent report[i] describing the status of nuclear energy shows that by January 2016, 31 countries are operating 440 Nuclear Power Plants (NPP) with a total installed capacity of 380GWe and 240 Research Reactors (RR), and about 180 small reactors, used to power 140 ships-submarines, are operating in 56 countries.

Armenia, Bulgaria, Slovakia, Spain and Sweden operate NPP but not RR. So a total of 61 Countries out of 193 UN's Member States have some degree of development regarding Nuclear National Infrastructure (NNI), and more than two thirds of states worldwide (132) have no nuclear infrastructure at all. Africa, the Middle East, Asia, Central and South

America, and a number of countries/Islands in the pacific are the areas with higher number of countries in this condition.

In recent years, Belarus, Jordan, KSA and UAE began the construction their first nuclear installation. According IAEA[ii] some 20 "newcomers" are currently making plans to initiate nuclear activities in the near future.

IAEA paid considerable attention to the challenges faced by newcomers and established four different phases[iii]: 1) Pre Project, 2) Project decision making, 3) Construction and 4) Operation to Decommissioning. Nineteen different issues were identified, with specific requirements and conditions recommended prior to the beginning of each phase.

It can take decades to build mature and efficient organizations necessary to define and implement all the stages of a nuclear program, even with a limited scope.

Building up the human resources in quantity and quality to cover the needed technical specialities requires hundreds to be trained; nuclear facilities are important to provide them with the practical experience in real world conditions.

Construction of a relevant facility (i.e. a Multi-Purpose Reactor or Nuclear Power Plant) could take between 6 to 8 years and requires a significant budget (i.e. some hundreds millions USD for MPR to thousands millions USD in case of NPP).

Before embarking in a nuclear program, a newcomer shall answer some key questions that are relevant to establish the appropriate policies.

The adoption of a legislative and regulatory framework, nuclear technology, goals for R&D plan, characteristics of nuclear installations; schemes for management, regulations, licensing, nuclear and radiological safety, operation; and policies on QA/QC, procurement, fuel cycle, waste, environmental, stakeholders, etc. have an impact for the long term. So, even if the procurement of the new facility is made through the "turnkey" modality, it is valuable that the country will have its own resources to address these issues.

The larger the size and complexity of the project, the more difficult it turns for a newcomer to grasp the necessary knowledge to decide on those questions. Thus, they must largely rely on the advice and judgement of foreign experts.

When launching a nuclear program, newcomers are faced with the need to choose between two competing options:

a) Start with the construction of the first nuclear installation and rely on international expert advice to bridge the gap on National Infrastructure
b) Start developing human resources to "narrow the gap" on National Infrastructure and delay the decision of building the first nuclear facility until some experience is gained by the local staff

International and governmental organizations, nuclear builders and international experts can contribute to "bridge/narrow the gap", particularly from the early project's stages (pre-bidding stages) until Commissioning, but "filling the gap" is a more difficult question to solve, that requires longer times and effort.

2. Two common approaches to build national infrastructure

UAE's case is representative of a country having no previous nuclear experience that decides to launch an ambitious program on nuclear energy without interest in R&D activities.

The rally of events shows that: The Government adopted its Nuclear Policy in 2008 to develop nuclear energy; one year later it enacted the Federal Act and created the Federal Authority for Nuclear Regulation (FANR) and Emirates Nuclear Energy Corporation (i.e. the UAE's Nuclear Energy Program Implementation Organization (NEPIO). ENEC awarded the prime contract in 2010 for the construction of 4 APR-1400 to be built in Bakarah near Abu

Dhabi. The first concrete pouring of Unit 1 was done in 2012 and connection to the grid is now planned to 2017[iv].

Construction Licensing of Units 1 & 2 and review of the PSAR was completed in 18 month.

An International Advisory Board (IAB) advised the government on key technical issues. FANR hired more than 60 experts for its own staff and technical matters, including safety reports, and reviews were made by 3 International Consulting firms – TSO, with participation of other 150 experts.

The training of FANR's local staff was largely oriented to routine inspections and audits of the four APR-1400 NPP. ENEC also built two full scale APR-1400 simulators at Bakarah.

A different approach is applied when the target encompasses a R&D program: i.e. to build up local resources and when some knowledgeable basis exists, to launch a construction program.

IAEA fosters regional collaboration throughout the "Project to Enhancement of Utilization of Research Reactors" sharing the use of existing facilities among members of the scientific community.

The above is a useful tool to develop local specialists, in particular to those countries that are doubtful about initiating a nuclear program. But, without a nuclear facility, the process of building up a local staff by training exclusively in foreign facilities might become difficult and non-converging. Some of the reasons that make it rational to build a nuclear installation to develop NNI are:

- A new construction produces momentum for developing NNI
- Training efforts are easy to be focused to a number of goals
- Universities, industry and scientists are prone to get involved in national endeavours
- Incentives to maintain qualified staff in the country
- Developing indigenous training capabilities for sustaining activities in the long term
- Creating and developing a national technological culture
- Becoming a scientific and technological hub for the region
- Typical times to build up experienced staff are too long for most countries

The larger the size and complexity of the project, the larger is the dependence on external experts, so choosing the right project´s characteristics is a relevant matter for newcomers to consider.

3. INVAP´s experience in supporting the development of NNI

In the last 40 years, INVAP has been involved in various research reactor projects delivered to countries with different infrastructures.

INVAP provides training as part of the project activities. The extent and scope of the support in each case is adapted to the country needs, taking into account the pre-existing development at the time the project starts.

Table 1, shows a summary of all the research reactor projects of INVAP and the type of assistance provided.

To those countries with almost no initial nuclear infrastructure (i.e. Peru, Algeria, KSA); INVAP provided technical support on sitting and design specifications.

The project itself was used as a valuable tool to boost an education and training programme to develop human resources.

A typical program required a number of trainees (i.e. between 20 and 50) with a solid background in physics and mathematics.

During the first year they received education in nuclear technology, nuclear engineering and its applications, in one of the various training centres in Argentina (i.e. Balseiro and Dan Bennison Institutes or Buenos Aires University).

At the second year, INVAP conducts "on the job training" in different specialities (i.e. licensing, operation, practices and applications), facing trainees with true problems of design, supervised by experienced specialists working at the project.

During the design and licensing phase, the trainees, appointed to perform regulatory or engineering activities at the return to their country, receive "On the Job Training" in nuclear design and safety issues, and participate in critical review meetings and preparation of the safety reports.

Facility	Owner	Training Term	Details of assistance to the Owner
RP-10[v] (10MW MPR)	IPEN (Instituto Peruano de Energía Nuclear)	1977-78	• Specs RP-10: CNEA • Licensing: IPEN CNEA/ARN • Construction: CNEA-INVAP • Training: 150 Junior/Senior Staff (300Mm Arg. RA-3), 1200 Mm in Lima Peru at RP-0 (supplied earlier to RP-10)
NUR (1 MW MPR)	HCR (Haut Commissariat a la Recherche), Algeria	1988	• Specs INVAP • Licensing HCR – CNEA/ARN • Construction INVAP • Training: 20 Junior & Senior Staff, 240mM Arg., Design, Safety, O&M " *On the Job training"* INVAP-RA-6
TRR (LEU core replacement and I&C Refurbishing)	AEOI (Atomic Energy of Iran)	1990-91	• Supported by IAEA • Training: 3 Seniors O&M Staff, 4 month at INVAP-RA-6
ETRR-2 (MPR 22 MW) FMPP	AEA (Atomic Energy Authority of Egypt)	1996-2000	• Specs: AEA, International experts / INVAP • Licensing: National Center of Nuclear Safety and Radiation Control (NCNSRC), IAEA Expert team and independent reviewers, ARN (Arg) • Training: 40 Junior and 10 Seniors Staff " *On the Job training"*
OPAL (Reactor de Investigación de ANSTO)	ANSTO, Australia	2004	• Specs: ANSTO (performance based) • Licensing: ARPANSA • Training: four Senior Staff (instructors) and course´s materials for training operators on site. INVAP
RPF (Radioisotope Plant)	AEA (Atomic Energy Authority of Egypt)	2008	• Specs: CNEA • Licensing: National Center of Nuclear Safety and Radiation Control (NCNSRC), assistance of IAEA Expert team and reviewers, ARN (Arg) • Training 20 Staff , 1 year on Safety, O&M " *On the Job training"* CAE-CNEA and INVAP
LAEE I&C (Tajoura Research Reactor)	Libyan Atomic Energy Establishment	2010	• Training 20 Staff, 20 weeks on at IDB (I. Dan Beninson) Buenos Aires
LPRR (Low Power Research Reactor)	KACST (King Abdullah City for Science and Technology, KSA)	2010-2014	• Specs: INVAP • Licensing: KACST, assisted by STUK • Training 20 Staff Nuclear Eng. and Technology and " On the Job training" IB-CNEA and INVAP • 17 Staff from KACST + KACARE Nuclear Eng. design, INVAP • LPRR Staff O&M training contract waiting for green light
NUR/UDEC (Power upgrade and refurbishment)	COMENA, (Commissariat à l'Energie Atomique Algeria)	2015-6	• 23 Staff Eng. Design, Safety, 1 year "on the job training" INVAP

Table 1. Project related activities for development National Infrastructure

In some cases, ad-hoc agreement between regulatory bodies of both countries is signed to provide " On the Job Training" on regulatory issues and regulations at the Argentinean Regulatory Body (ARN).

Staff aimed at O&M receives "On the Job training" at RA-6 (1MW MPR) and jointly with engineering staff and users are encouraged to participate actively during the commissioning phase, close to INVAP´s specialists.

On the other hand, countries having well developed nuclear organizations are supported in specific and well defined areas. For example, during the RRRP[vi] project (Australia), INVAP developed the "design´s technical specifications" in order to comply with the "performance specifications" established by ANSTO for the bidding. INVAP prepared the PSAR and technical reports, including the Commissioning Plan, for the licensing phase, and trained a number of Senior Staff (Instructors) on RRRP´s O&M to allow them to provide further training to ANSTO operators' crew.

A new reactor project represents a unique and rich opportunity to learn nuclear technology and understand fundamentals of the design and safety.

For that reason, it is recommended that new comer´s staff be able to have as much involvement as possible in the project activities from the early stages until commissioning.

Even when large facilities are in the radar of a newcomer, starting with the construction of one small research reactor is largely beneficial in order to have a wider and more solid knowledgeable basis before launching the major project.

With an eye on those problems, INVAP developed a Low Power Research Reactor (LPRR) aimed at "filling the gap" of national infrastructure for new comers. The first of a kind is already designed and ready for construction in Riyadh, KSA.

4. LPRR to Impel Nuclear National Infrastructure

Low Power Research Reactor (LPRR) is designed by INVAP for education and training capabilities in nuclear physics and nuclear engineering; but LPRR´s distinguished features, particularly regarding design, safety, operation and user´s capabilities, present the opportunity to shorten the time for developing indigenous resources towards creating national infrastructure.

Training in Nuclear Safety and Licensing, O&M, Scientific applications of neutrons, RR Based Production, can be conducted from "early stages of the project", "in-house" and almost "autonomously".

Fundamentals design criteria are:

- Large safety margins
- Simple systems
- Easy operation
- Wide range of experiments
- I&C criteria similar to RR
- Experimental Practices featuring larger RR´s

Basic technical data

- Open Pool Type
- Maximum Thermal Power 100 KW
- Fuel pin rods ^{235}U (e < 2.5%)
- Core variable cooled by natural convection
- Moderator: Light Water
- Irradiating flux > 10^{12} n/cm^2/s
- Beam flux > 10^8 n/cm^2/s

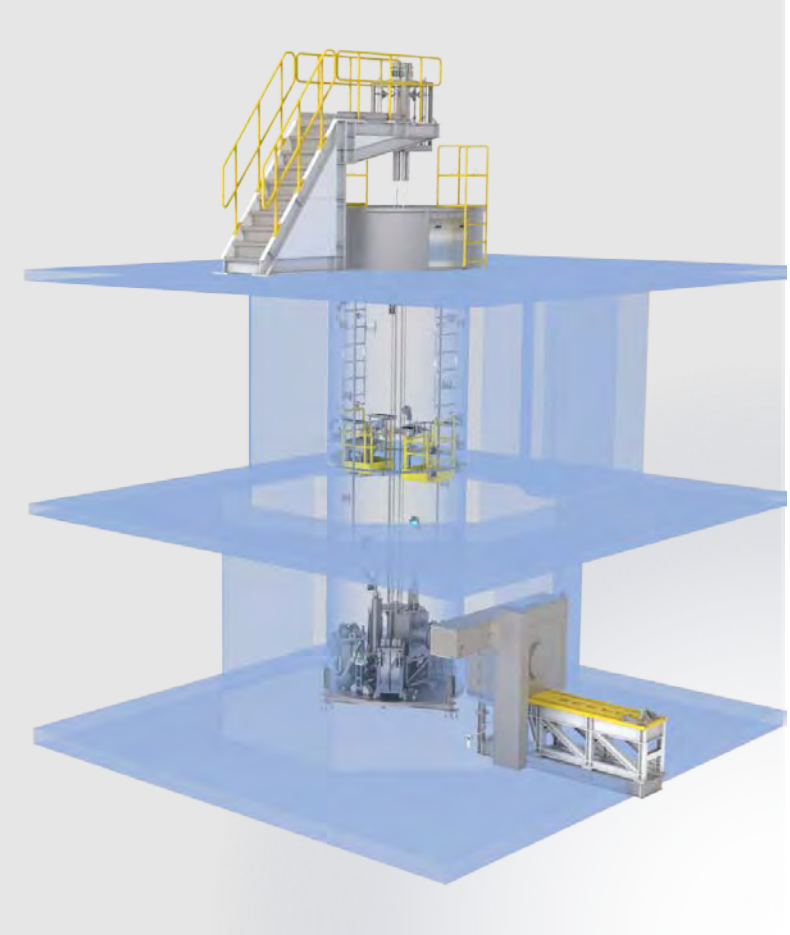

Figure 1: Representation of the reactor assembly:
(Block, Operating Bridge, Pool, Core and Beam Shutter)

Choosing LPRR as the first nuclear installation compared with choosing a larger MPR or a NPP in one step, increases greatly the chances of young staff to participate in the design, licensing and construction activities of the project. Some of the main reasons are highlighted below.

4.1. Size of the project

LPRR overall project size is substantially reduced compared with a large MPR, so do cost, time and resources necessary to fill up staff´s positions.

Construction program of LPRR could be achieved in 3.5 to 4 years, meaning that the country could save two years or more to start building up indigenous resources.

Construction cost of LPRR could be set between 15% and 30% of large MPR and relevance is far less compared with a NPP.

Two steps option presumes an additional cost for the construction of the LPRR. Nevertheless, the country will benefit from the fact that the decision on a much larger investment can be done some years later supported by a more knowledgeable basis.

The above also reduces the stress on financing and the need for large structures to manage the project, and consequentially it reduces overall risks.

4.2. Simplified Safety Analysis

LPRR is designed with ample margins to “critical/important to safety” phenomena and is furnished with a low number of safety systems.

A thorough Safety Analysis of the LPRR design does not require detailed computer code modelling or complex fault three diagrams due to reduced number of systems.

In normal or abnormal scenarios, compliance with safety limits can be understood and verified by young graduates by using simple analytical methods, providing to the local staff a direct knowledge on the applicability of the basic safety criteria.

Some of the features concurrent to that goal are:

1. Core excess reactivity is less than beta so prompt critical scenarios are ruled out
2. 100% control rod shutdown margin is several times above the minimum required and as much as seven times for single fail[vii]
3. Fuel assembly is limited to one single fuel rod and can be removed one at a time, so reactivity steps during core configuration changes are tens pcm, well under shutdown margin
4. Fuel rod design based on PWR´s with ample margins regarding operating values
5. Core cooled by natural convection avoids cost down analysis and LOFA
6. Large volume of water with low operating temperature ~20ºC provides high thermal inertia and mild thermal transients. No thermal stress on cladding, structures, materials, and no safety related cooling systems.
7. Limited radioactive inventory for the lifetime (i.e. comparable to a medical Co-60 source), off site impact for accidental condition (mechanical damage) not relevant

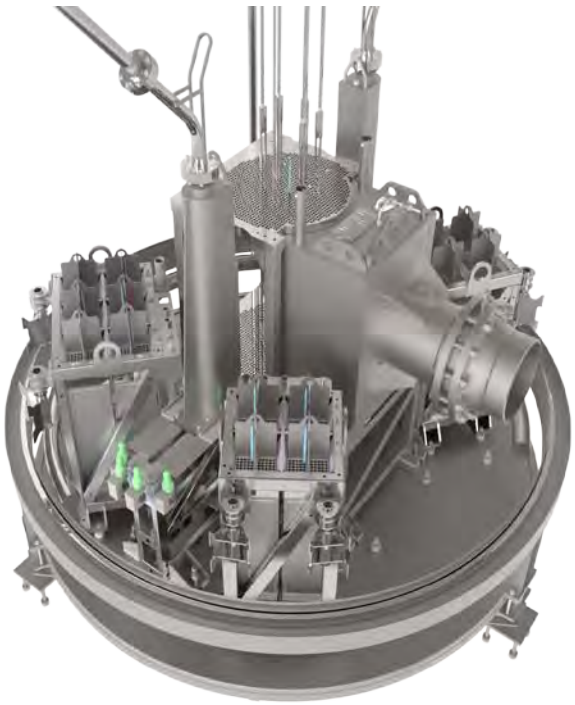

Figure 2: View of the Core and Pool Internals

4.3. I&C Criteria as in large MPR

Even when a reactor trip failure has no adverse consequences to the reactor and staff, the Reactor Protection System at LPRR is designed following the same criteria as applied in OPAL/RA-10: “Fail Safe”, “Single Fail Tolerant”, “Redundant”, “Independent” and “Functional Isolated”.

4.4. Operating environment resembling large RR´s

LPRR is furnished with a Control Room designed with modern Human Machine Interfaces criteria that resembles that used by large research reactors.

The main console is furnished with HD-LCD´s touch screen to display process diagrams, logbook, control loops and status of the plant and allows operators to change the status of active systems. The reactor monitoring system and the radiation monitoring system allows the operator to supervise and follow up all relevant parameters.

Safety related I&C are displayed through a separate hard wired console.

The main console is also replicated in a separate room for training purposes, allowing trainees to follow up reactor conditions while a limited control is tutored from the main console.

Figure 3: View of the Reactor Console

4.5. Applications and uses

One aspect not easy to address is the development of human resources demanding the use of reactor for R&D applications and production techniques and procedures based on the use of neutron irradiation and beams.

On top of the traditional application of the low power reactors (i.e. Education and Training for Physics and Engineering Carriers, Neutron Activation Analysis, Target Irradiation, radioisotope production), INVAP furnished LPRR's design with a set of facilities aimed at developing skills necessary to make advantageous use of larger Research Reactors.

Some of the basic design features in this regard are:

- Transport Rabbit for NAA
- In Core and Graphite Column Irradiating position
- Removable Central Core Grid block
- Graphite Column
- Neutron Beam with Rotating Shutter
- Radiochemical Lab and Multipurpose Hot Cell for radioisotope separation (non-commercial scale), Some of them are: ^{24}Na, ^{35}S, ^{42}K, ^{64}Cu, ^{82}Br, ^{198}Au

5. Other general characteristics

The following characteristics will also contribute to facilitate operation and use simplified procedures:

- Fuel Uranium enriched < 2.5%
- Low radiation levels in all occupancy areas
- Low activation levels of liquids and materials
- Max Fuel BU< 2% means almost no-spent fuel during lifetime
- Working platforms and tool inside pool tank

These features provide O&M Staff with a useful tool to instil Safety Culture and to introduce them to the more complex environment found in larger nuclear facilities.

6. Conclusion

More than one hundred countries have no nuclear development and lack almost completely the national infrastructure. Twenty countries of this group are currently evaluating having a nuclear installation in the following years.

From the experience gathered by INVAP, in the last 40 years supporting countries with different national infrastructure, the following can be stated:

- Medium or large facilities face the governments with challenges beyond capabilities of a newcomer's staff, so strategic decisions relevant to the country must largely rely on external expert advice with minimum or no involvement of local staff
- Even when a program is based on turnkey procurement, developing in-house capabilities for education and training underpins sustainability for operation and development, sourcing a qualified staff with common technological culture
- The construction of the first nuclear facility provides a unique and valuable opportunity for a newcomer to learn fundamentals of nuclear technology and to develop its own licensing, engineering and operating criteria.
- The larger the size and complexity, the less are the chances of local staff to get involved in this process
- A low power reactor as the first project results effective to impel the creation of National Infrastructure, since it allows an early deployment of qualified indigenous staff, reduces the overall project's risks and provides the newcomer with a more solid knowledgeable basis for decisions to be taken in further developments

INVAP design of LPRR aims at closing the existing gap of NNI in newcomer countries with the objective of developing a program in R&D and applications of Nuclear Energy. Newcomers are provided with the following benefits:

- Capabilities for education and training in nuclear physics and engineering are broaden and powered to match specific needs
- LPRR's project allows local staff to gain experience in the modality "On The Job" and "Learning by Doing" in all stages, particularly in regulatory, licensing and engineering issues

- Safety Design, Control and Operating characteristics of LPRR provides a working environment capable to instil nuclear culture and operating practices adopted by larger nuclear facilities
- Experimental facilities for R&D with neutrons beams and other scaled procedures for neutron based products allow to have a better understanding of facts behind the technology to support the establishment of a more ambitious R&D plan

7. References

[i] Nuclear Power in the World Today, WNA (January 2016)

[ii] WNA Emerging Nuclear Energy Countries. WNA (Jan 2016)

[iii] IAEA NP-T-5.1 Specific Considerations and Milestones for a Research Reactor Project

[iv] WNA Nuclear Power in the United Arab Emirates, WNA (Sept 2015)

[v] R. Radichella, El Proyecto Perú. Revista CNEA Año 8 # 29-30, Ene-Jun 2008

[vi] RRRP is the former name of OPAL research reactor designed and built by INVAP for ANSTO (Australian Nuclear Organisation). ARPANSA (Australian Radiation Protection and Nuclear Safety Agency) was the licensing authority.

[vii] ARN. AR 4.2.2 Rev. 1 Diseño de reactores de Investigación

FEASIBILITY STUDY OF INSTALLING A THERMAL TO 14 MeV NEUTRON CONVERTER INTO A RESEARCH NUCLEAR REACTOR

LUKA SNOJ, IGOR LENGAR, ANŽE JAZBEC, VLADIMIR RADULOVIĆ, GAŠPER ŽEROVNIK[1]
Reactor Physics Department, Jožef Stefan Institute
Jamova 39, 1000 Ljubljana – Slovenia

ALJAŽ KOLŠEK, PATRICK SAUVAN, FRANCISCO OGANDO, JAVIER SANZ
Universidad Nacional de Educacion a Distancia, Ingenieria Energetica
Calle Juan del Rosal 12, ES-28040 Madrid – Spain

ANDREJ TRKOV
International Atomic Energy Agency, Vienna International Centre, 1400 Vienna, Austria

ABSTRACT

A deuterium-tritium (DT) based thermal-to-fast neutron converter will be installed into the TRIGA reactor at the Jožef Stefan Institute. This paper presents preliminary results of a feasibility study where different aspects have been addressed. The thermal column is the most appropriate irradiation position for the DT converter in the reactor. From potential active converter materials, LiD yields the most 14 MeV neutrons. Lithium enrichment affects the required thickness of the active converter material, but not significantly the 14 MeV neutron yield. For coupled neutron-tritium transport calculations, the modified MCUNED code was used. Relevant DT neutron activation monitor materials for spectrum unfolding have been identified and neutron flux criteria established.

1. Introduction

The demand for experimental devices for irradiation with 14 MeV neutrons, which are especially important for fusion related applications, is increasing. Conventional neutron generators require laboratory space and maintenance. In the literature one can find documents, which pursue the idea of using the ^{6}Li(n,t)^{4}He reaction in a blanket of lithium in a deuterated environment, placed in a thermal reactor irradiation channel to obtain a neutron source with enhanced 14 MeV component in the neutron spectrum.

The idea of a thermal neutron driven neutron generator has been addressed by different authors. One of the earliest reports is by Frigerio [1], who proposed to use such a device for neutron activation studies. In 1976 Napier *et al.* [2] described an operating device, including the construction details. Two years later Eckhoff *et al.* report [3] that such a device is not as effective as initially believed (referring to Napier's work), and Wysocki *et al.* argue [4] that the flux magnitudes reported for a LiOD-D_2O converter indicate that such a device offers little if any

[1] Currently at Institute for Reference Materials and Measurements, Geel, Belgium

advantage over fission spectrum neutrons. Both statements are probably true, in view of the authors' objectives to use irradiation devices for analytical work and considering the status of nuclear data at the time. Since then, the activation method has been greatly improved for routine applications and the status of nuclear data is incomparable. Limitations of the activation method have been reached, where complementary information from high-threshold reactions could be useful to extend the range of applicable elements and increase the reliability and the detection limits of the method. Furthermore, the present objectives are also studies of the activation properties of new structural and special-purpose materials in complex spectra, which include a 14 MeV component as well as neutrons at lower energies from the slowing-down in surrounding materials and coolants. The spectrum of the 14 MeV converter device is quite representative of many such environments. Napier's device was operated and tested on a TRIGA reactor similar to the one at JSI, so the construction details and the results of experimental measurements are highly relevant and valuable. A more detailed theoretical investigation was reported by Miller *et al.* [5], including some optimization studies. These can serve as the starting point and guideline for further studies, using state-of-the-art computational methods and nuclear data. Theoretical basis and activities needed for design and installation of such converter into the Jožef Stefan Institute (JSI) TRIGA Mark II reactor has already been described [6]. As in all such demanding projects, neutronics calculations are required to support the physics, safety and engineering efforts. In this paper we present the first results of a series of thorough analyses performed in an effort to optimize, design and install a DT neutron converter by using state-of-the-art computational methods (i.e. Monte Carlo methods for particle transport) and nuclear data.

This paper is organized as follows: In the first part of the paper we present the state-of the-art computational methods used for optimization studies. In the second part we present first preliminary results of the analyses focused in three main fields: optimization of the DT neutron yield with respect to irradiation position in the reactor, optimization and design of the target (including the choice of the converter material) and safety analyses. In the third part of the paper we identify neutron monitors suitable for monitoring the DT neutrons and present acceptability criteria for the DT converter.

2. Application of MCUNED

2.1 Code description

Because the neutron conversion process involves the production and reaction of charged particles (tritons), MCUNED code has been selected for the calculations, since it is uniquely suited for the description of the coupled neutron and charged particle transport needed for such calculations. MCUNED has been originally developed at the UNED to perform transport calculations in deuteron accelerators facilities. The code is an MCNPX extension providing two new features [7]:

- it allows using light-ions evaluated nuclear data library for ion transport like MCNPX does with the proton library,
- it includes a variance reduction technique for the production of secondary particles induced by light-ion nuclear reaction.

Since MCUNED is derived from MCNPX (they have the same code core), the MCUNED input is fully compatible with any MCNPX input, and its transport techniques are as reliable as in the original code. Likewise, MCUNED keeps all the MCNPX original capabilities, such as flexibility in definition of the particle source, in the definition of the geometry of the system, nuclear responses, etc. The use of the evaluated library extension allows transporting accurately light-ions also at low energies, where most nuclear models fail to produce reliable results. Indeed, at low energy, nuclear models for ion interaction implemented in the transport part of the code are not valid and the only way to perform ion transport is to use evaluated nuclear data. At low ion energies, due to the very short path of ions, the probability of nuclear interaction is very low and so is the secondary particle yield. In Monte Carlo calculation, this requires a large number of source particle (ions) histories to obtain few secondary particles. The variance reduction technique implemented in MCUNED increases significantly the number of secondary histories produced and allows saving computing time when light-ions are transported.

2.1.1 New developments for neutron converter application

In order to apply MCUNED for neutron converter simulations, code and DT libraries modifications were required. In the present work we are interested in the fast neutrons production by DT reaction, where tritons are secondary particles produced by n+Li reactions. To reproduce the global process all particles production steps (tritons and fast neutrons) have to be considered in the same simulation. In this case, the variance reduction for the fast neutron production during the triton transport is a valuable technique to improve the efficiency of the calculation. Unfortunately, since MCUNED was originally developed for accelerator-oriented applications, the variance reduction was only applied when ions were source particles and the former version of MCUNED was unable to use the variance reduction with tritons as secondary particles. Therefore, modification of MCUNED source code has been implemented to solve this problem.

In this application, the fusion reaction is achieved using triton as a projectile and deuterium as target. This means that the transported particle is the triton and the data library needed to take into account the fusion reaction should have triton as incident particle. For the DT reaction only evaluated library with deuteron as a projectile exists. A library with triton as a projectile has been processed using data of the deuteron library. In the center-of-mass (CM) frame, reaction cross section is identical whether the projectile is deuteron or triton, but in evaluated libraries reaction cross section is expressed with respect the projectile energy in the laboratory frame. In order to generate a DT library considering triton as incident particle, the DT library with incident deuteron has to be rescaled considering the corresponding triton energy in the lab frame.

3. Preliminary calculations

The primary (reactor) neutron transport has been simulated using the existing MCNP5 [8] JSI TRIGA model [9].The calculated neutron fluxes and spectra have then been used in MCUNED to simulate the triton transport in the selected breeding materials and estimate the DT neutron yield. In the first step, the irradiation location in the reactor, optimal with respect to several requirements, has been chosen. Later, the design (i.e. geometry and active material) of the DT converter device has also been optimized.

3.1 Triton Yield at Various Locations

Since the contribution of epithermal neutrons to triton production is negligible, the triton spectrum is not sensitive to the neutron spectrum in the irradiation channel, thus being approximately independent of the positioning of the DT converter in the reactor. Therefore, we may assume the 14 MeV neutron yield is proportional to the triton yield, which has been thoroughly investigated in Ref. [10]. The irradiation channel locations in the JSI TRIGA reactor are thoroughly characterized in Ref. [9]. For this study, position in the core, reflector, and outside have been considered. For tritium production in the TRIGA reactor, only isotope ^{6}Li is relevant since the production from ^{7}Li is negligible, mainly due to huge difference in the spectrum-averaged tritium production cross sections of these two isotopes in the well-thermalized neutron spectrum in TRIGA. The primary objective was to maximize the tritium production, however the amount of material (lithium) used and feedback effect on the reactor reactivity was also considered. Firstly, optimal irradiation channels have to be identified. High triton yield and small effect on the multiplication factor have been optimized. Each irradiation channel was filled with natural lithium (containing 7.59 at. % of ^{6}Li). The calculated reaction rate densities per reactivity change are compared in Figure 1. The most appropriate channels are located farthest from the graph origin in the bottom-left corner. These channels are: Central irradiation channel, Channel F22 (both in the reactor core), and irradiation channels inside the reflector (e.g. IC40).

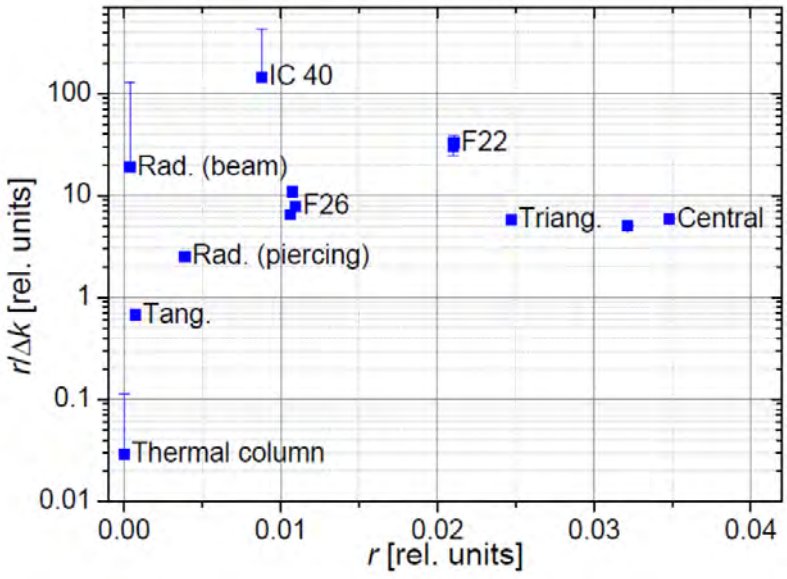

Fig. 1. Reaction rate density versus change in reaction rate density per multiplication factor change due to inserted natural lithium.

Due to large thermal absorption cross section, there is a very significant flux depression inside lithium. Consequently, for thicker (i.e. a few mm) samples, the reaction rate becomes proportional to the sample surface area rather than volume. Hence different shapes of targets like hollow cylinders (O-profiles) were tested inside the central channel. The analysis was performed for the central channel only as it exhibits the highest triton yield. However, tritium production is the largest when 40 irradiation channels in rotary groove were completely filled with Li targets. In the final decision for the position of the DT converter, two additional factors were taken into account. The size of the irradiation location is important to maximize 14 MeV neutron yield and use of larger samples for fast neutron activation. Furthermore, fast neutrons originating from the reactor interfere with the DT fusion neutrons and slightly alter the spectrum around the 14 MeV peak - reducing the fraction of the fast reactor neutron enables cleaner measurements of the activation reaction cross sections in the DT neutron spectrum which is important for fusion applications. The application requires a well-thermalized neutron flux, however, the thermal neutron flux inside the Thermal Column (ThCol) decreases with the distance from the reactor core. Therefore, the DT converter was placed at the end (position closest to the reactor core) of the ThCol port and because the TRIGA Mark II research reactor features several ex-core irradiation facilities, one could also add some additional moderation in the form of heavy water to improve the results. Figure 2 shows two alternative positions inside the Tangential Channel (TangCh) and the Radial Piercing Port (RPP) filled with heavy water and inserted DT converter.

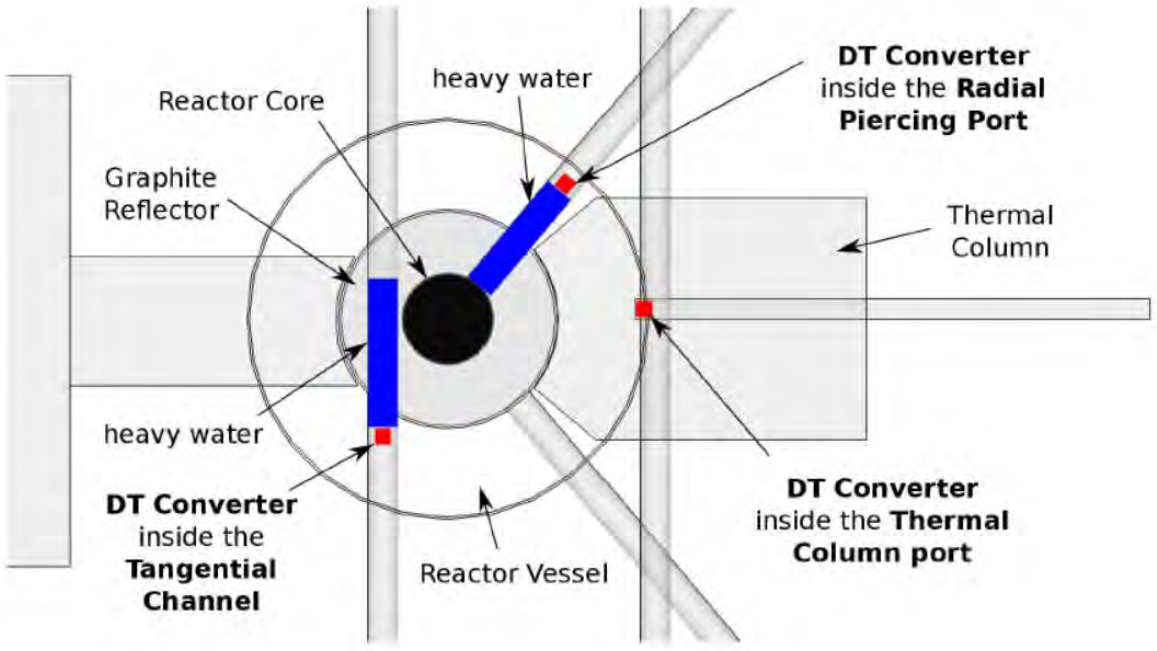

Fig. 2. Various possible irradiation positions inside the TRIGA reactor, two of them featuring additional heavy water moderation.

Calculations were carried out separately in order to eliminate the influence of one converter setup on the other. ThCol has proven to be the best irradiation position to design a DT

converter, because Figure 3 shows a fewer number of background fast neutrons as inside the TangCh, and around 10 times higher 14 MeV neutron flux as inside the RPP. The use of the DT converter inside the ThCol port increases the fast neutron flux between 10 MeV and 20 MeV by a factor of 18.5 to achieve the value of around 6.0×10^6 $cm^{-2}s^{-1}$. Finally, taking all that into account the Thermal Column has been chosen as the location for the DT converter.

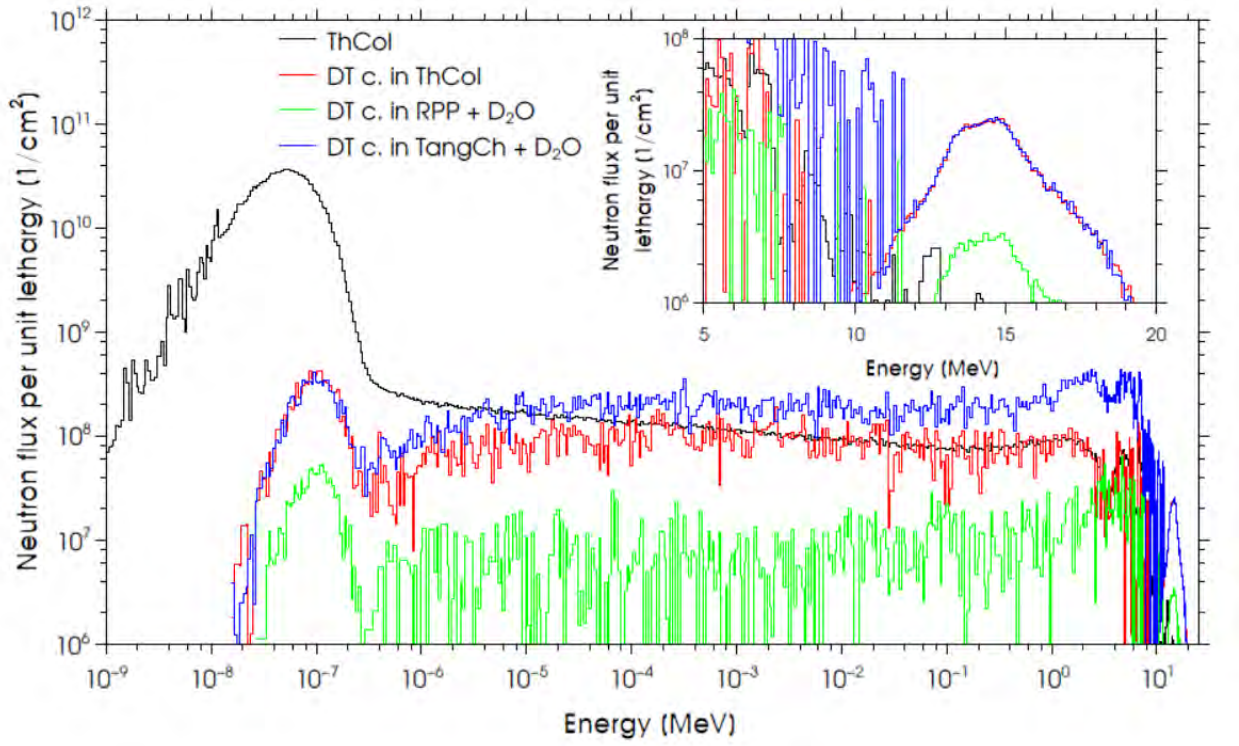

Fig. 3. Spectra inside the DT converter placed in various irradiation facilities and with additional moderation compared with neutron spectrum inside the ThCol without DT converter.

3.2 Optimization and Design of New Device

3.2.1 Tritium breeding materials

In a given external neutron field (which is defined by the choice of the location in the reactor), the 14 MeV DT neutron yield primarily depends on the converter material. The main factor defining the converter efficiency is the probability that a triton, produced within the converter, fuses with a deuteron before being slowed down by the Coulomb field. A study has been carried out by modeling a 1D slab breeding material irradiated by thermal neutrons [11]. The observables: fast-to-thermal neutron ratio n_f/n_{th} and the so-called "neutron production range" which is defined as the depth until where 99% of the fast neutrons are born are shown in Table 1. The lithium enrichment primarily affects the production range (i.e. the required breeding

material thickness) but only slightly influences the fast neutron yield. Due to its high cost the use of enriched lithium is justified only if the space in an irradiation channel is very limited.

Table 1. Fast neutron yield for different breeding materials.

Material	Li enrich.	n_f/n_{th}	Neutron prod. Range [cm]
LiD	Nat. 20%	1.8×10^{-4} 1.7×10^{-4}	1.4 0.6
LiOD solid	Nat. 20%	7.7×10^{-5} 7.6×10^{-5}	2.1 0.9
$LiAlD_4$	Nat. 20%	1.7×10^{-4} 1.7×10^{-4}	4.5 2.7
LiOD(9 wt. %) + D_2O	Nat. 20%	1.1×10^{-4} 1.4×10^{-4}	4.8 4.6
LiOD(15 wt. %) + D_2O	Nat. 20%	1.4×10^{-4} 1.5×10^{-4}	4.7 4.1
LiOD(30 wt. %) + D_2O	Nat. 20%	1.4×10^{-4} 1.4×10^{-4}	4.1 2.4

Table 1 shows that the best candidates with respect neutron yield for breeding material are LiD or $LiAlD_4$. For LiD less breeding material is necessary to produce the same amount of fast neutrons. This difference is due to the lower ^6Li concentration in $LiAlD_4$. The reason why the neutron yield does not vary with the deuterium concentration (considering that all thermal neutrons produce triton) is because the triton path length varies from a material to other depending on its density. The deuteron concentration is balanced by triton range and the neutron yield is ruled by the product of both magnitudes rather than only deuterium concentration. It has also been shown that the effect of the impurities on the 14 MeV neutron yield is negligible [11].

3.2.2 Geometry of the DT converter

The TRIGA MCNP model features several ex-core irradiation facilities, however, experience from previous irradiations have shown that the best place to achieve well-thermalized neutron flux with as low as possible fast (fission) neutron background is in the Thermal Column. In order to increase computational efficiency, the Thermal Column in the TRIGA MCNP model was divided into 10-cm long cells, in which the neutron spectra were calculated in 640 energy groups. These neutron spectra were used in a simplified model of the irradiation channel with a spherical neutron source, isotropic and inward directed. DT converter in the simplified model was constructed with stainless steel inner/outer 1 mm thick wall and the space between was filled with ^6LiD (Figure 4).The final design of the DT converter is cylindrical with outer diameter of 80 mm and height of 106 mm, respectively. All results of the below study can easily be translated to natural LiD (which will finally be used) with increase of the breeding material thickness according to the neutron production ranges from Table 1.

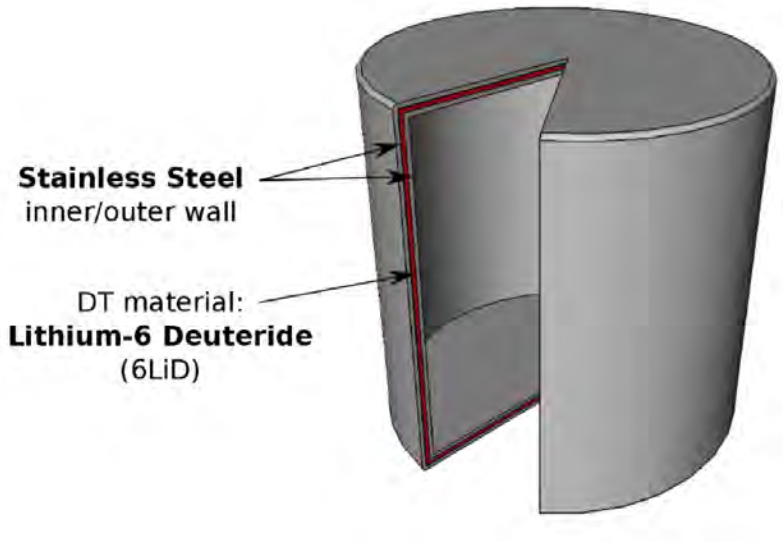

Fig. 4. Schematic presentation of the DT converter.

Stainless steel is an excellent choice for a DT converter housing due to its high corrosion resistance and good mechanical properties. However, the choice of DT material is a much more difficult task, because lithium reacts violently with water and is corrosive. Preliminary calculations have shown that LiD has the advantage over the other tested materials (i.e. $LiAlD_4$, LiD, LiOD, and LiOD in D_2O) in terms of 14 MeV neutron production and/or required thickness, but chemical compatibility with stainless steel has not been determined yet. ^{6}Li is an excellent neutron absorber and when bombarded with neutrons, it produces tritons with energy around 2.7 MeV with a very short penetration depth. Therefore, it is important to determine the depth at which saturation occurs, so the first process of optimization includes the DT material thickness variation for ^{6}LiD with density of 0.78 g/cm^3. During the optimization process, the thickness of DT layer was varied, but the outer dimensions of the DT converter were kept the same. Due to substantial absorption in the thermal region, the 14 MeV neutron flux inside the converter capsule first increases with thickness, however at larger thicknesses, when the majority of the thermal neutrons are converted to 14 MeV, the fast neutron absorption becomes the dominant effect and the 14 MeV neutron flux inside the converter capsule starts to decrease.

For this particular material composition the 14 MeV neutron production is the highest at the thickness of around 0.1 cm. Finally, the following design of the DT converter was adopted: stainless steel cylindrical shell with inner/outer 1 mm thick wall, filled with 1 mm thick layer of ^{6}LiD. Final calculations were performed with the full JSI TRIGA Mark II reactor MCNP model, into which the optimized DT converter has been inserted (Figure 5).

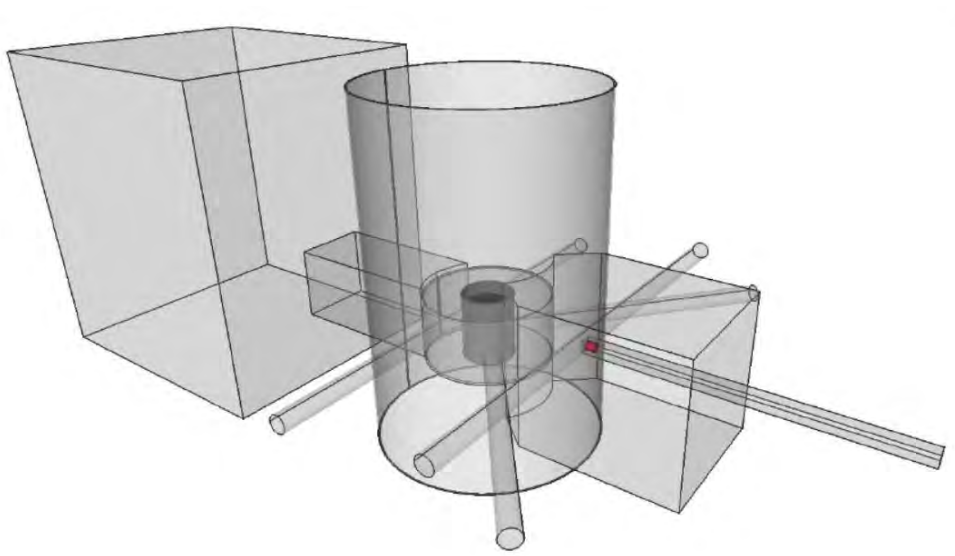

Fig. 5. Designed DT converter placed inside the Thermal Column port in TRIGA.

3.3 Safety Analysis

3.3.1 Criticality

Since lithium is a strong thermal neutron absorber, it has a similar effect on the reactor as control rods - it causes decrease of the reactor reactivity and local (thermal) flux depressions. As already explained in Section 3.1, placing lithium in irradiation channels in the reactor core causes significant decrease of the multiplication factor. However, the impact of the DT converter in the thermal column on the reactor operation is negligible.

3.3.2 Pressure build-up

When a neutron reacts with lithium inside LiD molecule, three atoms are released (D, T, and ^{4}He) and form a gas. For the following evaluation we can assume that all atoms stay inside stainless steel capsule and that the volume of consumed LiD can be neglected. Using the MCNP model of TRIGA reactor with DT converted placed inside the thermal column, the reaction rate for tritium production was calculated, from which the gas production rate can be calculated.

Since LiD is powder like material, we assumed that there is 1 cm^3 of air inside LiD (3% of the whole volume). Assuming ideal gas law, at full reactor power (250 kW) the pressure builds up to around 1 kPa/day. Pressure build-up is thus non-negligible and will have to be taken into account when designing the actual capsule.

3.3.3 Heating

Using the same computational model as above and taking into account the heat produced by neutrons and tritons inside LiD and stainless steel, the whole device emits around 2 W of heat.

Heating produced by DT converter does not have any negative impact on nuclear safety and can therefore be neglected.

4. Selection of dosimeters, acceptance criterion for the fast neutron flux

A requirement for a thermal to 14 MeV neutron converter is to provide a sufficiently high fraction of fast neutrons to enable measurements of activation rates for a variety of standard and new candidate threshold reactions. Therefore the determination of an acceptance criterion for the fast neutron flux inside the converter capsule has been carried out as an integral part of the present study. A calculation of the reaction rates has been performed with the RR_UNC code [12] using the neutron spectrum shape inside the converter capsule obtained from a calculation with the MCUNED code displayed in Figure 6, and the standard dosimetry cross section file IRDFF [13, 14].

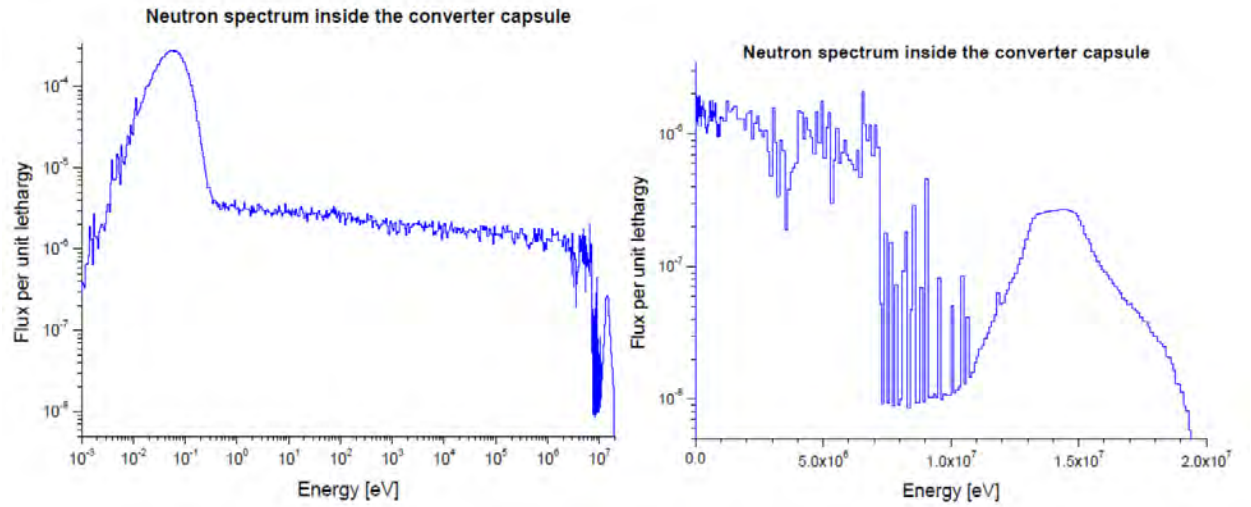

Fig. 6. Neutron spectrum inside the converter capsule, located in the thermal column of the JSI TRIGA reactor, in lethargy scale.

A selection was made (see Table 2) of the reactions most sensitive to the energy region around 14 MeV and with the highest calculated reaction rates. In addition, the computation has been performed for the $^{27}Al(n,\alpha)^{24}Na$, $^{27}Al(n,p)^{27}Mg$ and $^{197}Au(n,\gamma)^{198}Au$ reactions for a sample of the standard neutron flux monitor material Al-0.1%Au, available from the Institute for Reference Materials and Measurements (IRMM-530R). For the selected threshold reactions, the ratios of the reaction rates induced in samples of pure materials (or commonly available reference materials in case of sodium and fluorine), in the form of disks 1 cm in diameter and 1 mm in thickness, relative to the reaction rate of the $^{197}Au(n,\gamma)^{198}Au$ reaction in a sample of Al-0.1%Au of the same dimensions, were computed using the neutron spectrum shape as displayed in Figure 6.

The reaction rates per target atom for the threshold reactions are some 6-8 orders of magnitude smaller than the $^{197}Au(n,\gamma)^{198}Au$ reaction rate. However, in contrast to the activation of strong resonance absorbers, where the flux depression and resonance self-shielding effects play a very strong role and dictate the use of small/thin samples with low contents of the relevant materials, in threshold reaction activation measurements, samples of pure material and larger dimensions/masses can be employed. Therefore, with a careful sample choice, the induced activities from the threshold reactions can be made high enough for gamma spectrometry

measurements of good quality (i.e. with low statistical uncertainties). As can be seen in the rightmost column in Table 2, the reaction rates in actual samples are only 3-4 orders of magnitude smaller than the $^{197}Au(n,\gamma)^{198}Au$ reaction rate in a sample Al-0.1%Au) of the same dimensions. In the calculated results, the fraction of the neutron flux at energies above 10 MeV inside the converter capsule is approximately 1.3×10^{-4}, and the highest attainable absolute neutron flux value is approximately 10^6 $cm^{-2}s^{-1}$. In the measurement procedure, low activities can be compensated somewhat by extending the measurement times and performing the measurements at smaller sample-detector distances. On the basis of the present calculations, an acceptance value for the fast neutron flux (above 10 MeV) of 10^6 $cm^{-2}s^{-1}$ inside the converter capsule can be recommended.

Table 2. Reaction selection, calculated reaction rates per target atom relative to the $^{197}Au(n,\gamma)^{198}Au$ reaction rate, reaction rates in samples 1 cm in diameter and 1 mm thick, relative to the $^{197}Au(n,\gamma)^{198}Au$ reaction rate in a sample of Al-0.1%Au of the same dimensions, inside the DT converter capsule, placed in the Thermal Column of the JSI TRIGA reactor. The E50% value is the incident neutron kinetic energy at which the cumulative reaction rate reaches 50% of its total value.

Target	Reaction	Product T1/2 [h]	E50% [MeV]	RR/atom rel. to $^{197}Au(n,\gamma)$	Sample	Density [g/cm3]	Sample RR rel. to $^{197}Au(n,\gamma)$ in AlAu
^{197}Au	(n,γ)	64.68	42 meV	1	Al(Au)	2.70	1
^{27}Al	(n,p)	0.16	6.52	5.83×10^{-7}	Al(Au)	2.70	4.25×10^{-3}
^{27}Al	(n,α)	15.00	13.40	2.32×10^{-7}	Al(Au)	2.70	1.69×10^{-3}
^{93}Nb	(n,2n)	243.6	14.18	6.66×10^{-7}	Nb	8.57	4.48×10^{-3}
^{127}I	(n,2n)	310.32	14.27	2.13×10^{-6}	I	4.93	6.03×10^{-3}
^{65}Cu	(n,2n)	12.70	14.45	1.26×10^{-6}	Cu	8.96	8.96×10^{-3}
^{55}Mn	(n,2n)	7490.9	14.46	9.79×10^{-7}	Mn	7.21	9.38×10^{-3}
^{59}Co	(n,2n)	1700.6	14.49	9.62×10^{-7}	Co	8.90	1.06×10^{-2}
^{63}Cu	(n,2n)	0.16	14.71	6.50×10^{-7}	Cu	8.96	2.06×10^{-3}
^{90}Zr	(n,2n)	78.41	14.84	8.88×10^{-7}	Zr	6.52	2.38×10^{-3}
^{19}F	(n,2n)	1.83	14.85	5.62×10^{-8}	CaF_2	3.18	3.34×10^{-4}
^{52}Cr	(n,2n)	664.86	14.98	4.25×10^{-7}	Cr	7.19	3.59×10^{-3}
^{58}Ni	(n,2n)	36.60	15.11	4.22×10^{-8}	Ni	7.81	2.80×10^{-4}
^{23}Na	(n,2n)	22800	15.35	4.26×10^{-8}	NaCl	2.17	2.93×10^{-4}
^{46}Ti	(n,2n)	3.08	15.90	6.16×10^{-8}	Ti	4.51	3.47×10^{-5}

5. Conclusion

Different aspects of installing a DT converter device into the TRIGA reactor have been studied. Due to the well-thermalized neutron spectrum, the thermal column is the most appropriate irradiation position in the reactor. From the full range of relevant materials, LiD yields the most 14 MeV neutrons. Lithium enrichment affects the required thickness of the active converter material, however it does not significantly affect the 14 MeV neutron yield. Therefore, due to economical reasons natural lithium is to be used. Stainless steel capsule was designed to enclose the DT converter, and its chemical compatibility with adjacent materials has to be verified. For coupled neutron-tritium transport, modified MCUNED code was used to accelerate

the convergence. DT neutron spectrum relevant monitor materials for neutron activation analysis have been identified and neutron flux criteria established.

Acknowledgments

This work was partially supported by the International Atomic Energy Agency within the framework of technical cooperation project SLO/1/006.

References

[1] N. A. Frigerio, “Conversion of Reactor Neutrons to 15 MeV with LiD”, Proceedings of Radiobiological applications of neutron irradiation, Vienna, Austria, December 6, STI/PUB-325: pp. 51-6 (1971).

[2] B. A. Napier et al., “`Design of an in-core fast neutron generator", Nucl. Instr. Meth. A, 138(3), pp. 463-465 (1976).

[3] N. D. Eckhoff and J. F. Merklin, `”On the utility of an in-core fast neutron generator - A response”, Nucl. Instr. Meth. A, 156(3), pp. 607 (1978).

[4] C. M. Wysocky and H. C. Griffin, “On the utility of an in-core fast neutron generator”, Nucl. Instr. Meth. A, 156(3), pp. 605-606 (1978).

[5] W. H. Miller, W. S. Law, and R. M. Brugger, “Thermal neutron driven, 14.1 MeV neutron generators”, Nucl. Instr. Meth. A, 216(1-2), pp. 219-226 (1978).

[6] A. Trkov, L. Snoj, and G. Žerovnik, “Feasibility Study and Installation of Thermal Neutron Driven 14 MeV Neutron Converter into the TRIGA Research Reactor”, Proceedings of the International Conference Nuclear Energy for New Europe 2011, Bovec, Slovenia, September 9-12, Nuclear Society of Slovenia, pp. 406.1-406.6 (2011).

[7] P. Sauvan, J.Sanz, and F. Ogando, “New capabilities for Monte Carlo simulation of deuteron transport and secondary products generation”, Nucl. Instr. Meth. A, 64, pp. 323-330 (2010).

[8] X-5 Monte Carlo Team, “MCNP^{TM} - A General Monte Carlo N-Particle Transport Code, Version 5”, LA-UR-03-1987 (2004).

[9] L. Snoj, G. Žerovnik, and A. Trkov, “Computational analysis of irradiation facilities at the JSI TRIGA reactor”, Appl. Rad. Isot., 70, pp. 483-488 (2013).

[10] A. Jazbec, G. Žerovnik, L. Snoj, and A. Trkov, “Analysis of tritium production in TRIGA Mark II reactor at JSI for the needs of fusion research reactors”, Atw. Int. Z. Kernenerg., 58(12), pp. 701-705 (2013).

[11] P. Sauvan and J. P. Catalan, “Parametric Analysis of Tritium breeder for neutron converter”, IAEA Document TECF3IR-SLO 1006-02-05, June 2013 (updated November 2013).

[12] A. Trkov, “The RR_UNC code - Calculation of uncertainties in reaction rates”, unpublished.

[13] R. Capote et al., “Updating and Extending the IRDF-2002 Dosimetry Library”, J. ASTM Int., 9(4), (2012).

[14] E. M. Zsolnay et al., “Summary description of the new international reactor dosimetry and fusion file (IRDFF release 1.0)”, – IAEA Technical report INDC(NDS)-0616 (2012).

MAXIMIZING UTILIZATION OF NEUTRONS AT A RESEARCH REACTOR BY EMPLOYING AUTOMATION OF IRRADIATION AND COUNTING PROCEDURES FOR THERMAL AND EPITHERMAL NAA, CYCLIC NAA AND COMPTON SUPPRESSION

S.LANDSBERGER, S.BIEGALSKI, B.COPPLE, L. WELCH

University of Texas, Nuclear Engineering Teaching Lab, Pickle Research Campus, R-9000, Austin, Texas, USA 78712

ABSTRACT

One major realistic improvement in neutron activation analysis is the automation of irradiation and counting facilities. Incorporating thermal and epithermal neutrons for short-, medium- and long-lived NAA can truly expand the array of elements that can be determined. The addition of Compton suppression techniques can still further drastically lower detection limits for elements not traditionally determined by routine NAA methods. At the Nuclear Engineering Teaching Laboratory at The University of Texas we have significantly developed capabilities in employing thermal and epithermal irradiation procedures including cyclic activation analysis. Automated counting procedures for Compton suppression and prompt-gamma have significantly reduced personnel time and human errors.

1. Introduction

Neutron activation analysis (NAA) is truly a unique analytical method in that there is an array of parameters that may influence the uncertainty of the final results coupled with the need to wait for extended periods of time to determine longer-lived isotopes for a complete study of the elemental composition of samples. While in the 1960's NAA was the undisputed multi-elemental technique of analysis the last twenty years has shown that other methods notably inductively coupled plasma- atomic emission spectrometry (ICP-AES), inductively coupled plasma- mass spectrometry (ICP-MS) and to a lesser extent particle induced x-ray emission (PIXE) and x-ray fluorescence (XRF) have gained a lot in popularity for research and commercial applications. Furthermore, there are fewer research reactors available for reliable access involving commercialization of NAA services or long-term academic investigations. Enhancement of research reactors utilization via NAA is seriously hampered by the lack of automation in hardware and software. As well, many facilities have not fully exploited the use of epithermal neutrons to ameliorate the set of elements that can be determined in a routine fashion. Other instrumentation methods such as Compton suppression in conjunction with thermal and epithermal neutrons can also be effectively employed to dramatically improve signal to noise ratios as compared to routine NAA. At The University of Texas we have endeavoured to increase efficiency of NAA by exploring several facets of automation of irradiation and counting facilities, and to use of epithermal neutrons and Compton suppression to reduce background.

All these methods have allowed the University of Texas to have one of most dynamic laboratories which includes a very comprehensive set of elements that typically cannot be achieved by routine NAA.

2. Automation of irradiation facilities

Automation is any process that reduces the need for operator intervention. An ultimate concept would be to remove the need for any human intervention, with *machine* talking to *machine* controlled by software. As many independent modules should be created as possible, to give the analyst the greatest flexibility in its use in a given situation. Automation in NAA can enhance the revenue-generating capabilities of a laboratory, raise the socio-economic benefits and increase reactor utilization. All of these areas can increase the visibility and impact of the facility. New markets may be opened by increasing capacity or particular limiting steps may be overcome. Automation is of most benefit where large numbers of similar samples need to be analyzed or may also be advantageous where there is a high demand to run small batches of samples. For example, throughput is significantly increased if jobs can be run around the clock, rather than being limited to running during working hours.

2.1 Overview of NAA facilities

The 1.1 MW TRIGA reactor, situated in the Nuclear Engineering Teaching Laboratory, has several in-core facilities for irradiation as can be seen in Figure 1. The first is the pneumatic tube system for short-lived NAA; the second is the 3-L (3 fuel elements that have been removed) facility that is primarily used for epithermal irradiations with a cadmium-lined tube and the RSR (rotary specimen rack) which is used for long irradiations with thermal neutrons. The pneumatic tube system can also be placed inside the 3-L facility for short-lived NAA with epithermal irradiations.

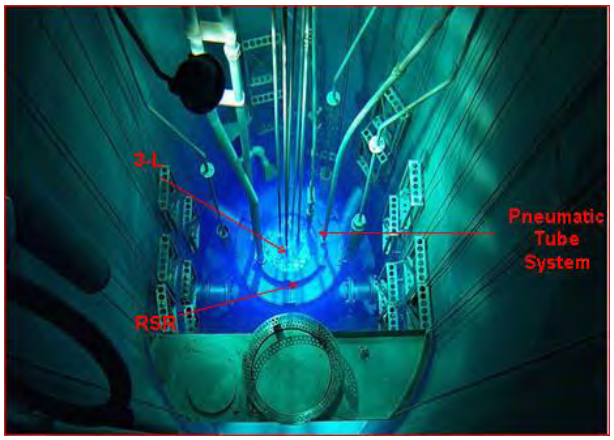

Fig. 1 TRIGA reactor showing three irradiation facilities

The prompty gamma facility as seen in Figure 2 can be used with and without a cold source. A complete description of the facility has been previously published (1).

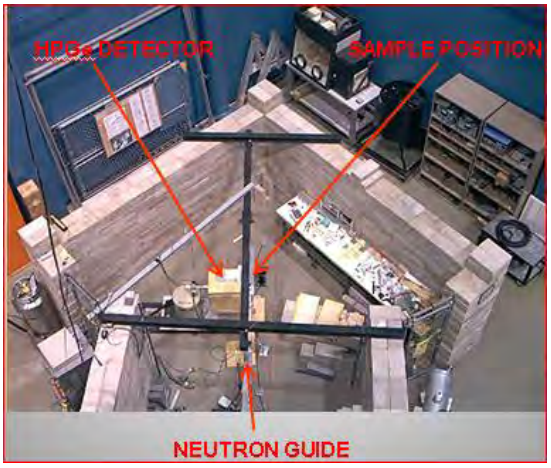

Fig 2. Prompt gamma facility

2.2 Irradiation timing for short-lived NAA

One critical step in the automation of NAA is the precise accounting of irradiation times for short-lived isotope production. This is particularly true for durations in the order of seconds. For instance a one second uncertainty in a 10-second irradiation leads to an automatic 10% uncertainty in the final result. While this uncertainty decreases with longer irradiation times, often this is not possible due to the activity of the returning sample. We have incorporated an automated electronic system as seen in Figure 3 that can accurately determine the irradiation time within 0.1 seconds. The top module displays the irradiation time while the bottom modules display the decay times. In such a system the worker can irradiate up to two samples, with one sample being irradiated while the other one is being counted. This type of procedure has greatly increased the number of samples processed in one day.

Fig. 3 Electronic modules for irradiation and dual decay times

2.3 Irradiation automation for prompt gamma activation analysis

For the prompt gamma facility we have incorporated an automated sampler changer. The key goals of this project were the following:

1. Reduce the amount of additional material in the beam line.
2. Reduce the time required to change samples from ~7 min to fewer than 10 sec.

3. Create a system that would be fully automated requiring no user interaction, i.e. a system that can communicate with the existing detector software.
4. Create a system that would have a capacity of up to eight samples.

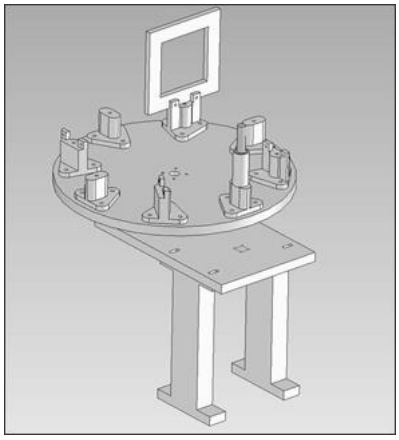

Fig. 4 Automated irradiation facility for prompt gamma activation analysis

The sample changer is controlled through the GENIE PC-2000 gamma-ray spectroscopy software. Gamma-ray spectrum live time and the number of samples are initially user defined. The system then automatically acquires spectra, saves the spectra, advances the samples, and initiates new spectral acquisitions.

2.4 Cyclic activation analysis

The emlpoyment of cyclic activation analyis is rather limited in the number of elements that can be determined as compared to routine NAA. However it has has proven to be useful in several analytical situations (2-3) particulary for fluorine, oxygen, selenium, silver using both thermal and epithermal neutrons. We have devloped a comprehensive irradiation facility that is capable of handling up to thirty samples. An overview on the system and the computer controlled comands are depicted in Figure 5.

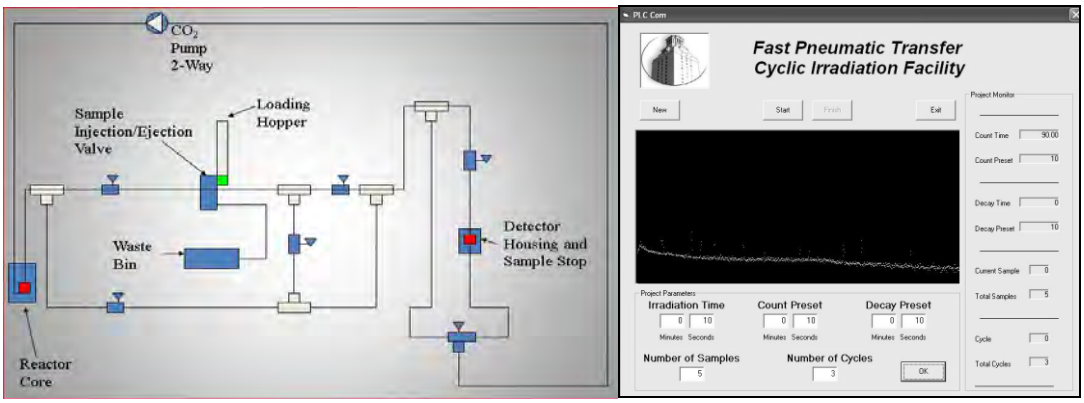

Figure 5 Overview of cyclic activation system (left) and irradiation, decay and counting control system

3. Epithermal NAA

The rate of neutron interactions R_i of type *i* is obtained by integrating the product of the interaction cross-section $\sigma_i(E)$, the neutron flux $\varphi(E)$ and the number of target nuclei N over the energy range of the incident neutrons.

$$R = N\int_0^\infty \sigma_i(E)\varphi(E)dE \qquad (1)$$

Concentrating on only radiative capture reactions, the reaction rate is generally broken into three terms which depend on the energy ranges (thermal, epithermal, and fast) of the incident neutrons.

$$R = R_{th} + R_{epi} + R_{fast} \qquad (2)$$

Many nuclides, especially those with low atomic number, have neutron capture cross sections that are proportional to 1/v at energies below 0.5 eV, where v is the speed of the neutron. Generally the thermal cross section σ_{th} corresponding to the thermal neutron energy (0.025 eV) is used to determine the thermal reaction rate R_{th} due to the thermal flux $ø_{th}$.

$$R_{th} = N\int_{th} \sigma(E)\varphi(E)dE = N\sigma_{th}\phi_{th} \qquad (3)$$

Resonance peaks dominate the neutron capture cross sections at energies in the epithermal range between 0.5 eV and 0.5 MeV. The epithermal neutron flux φ_{epi} in a water moderated reactor like the TRIGA follows a 1/E distribution. Since the epithermal capture cross-section φ_{epi} varies rapidly, the radiative capture integral I_0 is used to refer to the cross section. The epithermal reaction rate R_{epi} can be calculated:

$$\begin{aligned} R_{epi} &= N\int_{epi} \sigma(E)\phi(E)dE \\ &= N\int_{epi} \sigma(E)\Phi_{epi}(E)dE/E \\ &= N\Phi_{epi}\int_{epi} \sigma(E)dE/E \\ &= N\Phi_{epi}I_0 \end{aligned} \qquad (4)$$

where the epithermal flux Φ_{epi} is in units n/(s-cm^2-ln(E)). The fast reaction rate R_{fast} is negligible because the capture cross section at high energies is very small. The radiative capture reaction rate can then be written as:

$$R = N\sigma_{th}\Phi_{th} + NI_0\Phi_{epi} \qquad (5)$$

In reactor based thermal irradiations, both terms in the above equation are important. The thermal reaction rate term is eliminated for epithermal irradiations. By employing a cadmium filter, neutrons below energy 0.4 eV are removed from the flux. Irradiations executed in this manner are called epithermal, although epicadmium is more correct. In the epithermal region neutron cross-sections do not strictly follow the 1/v rule. Some elements possess large resonance peaks superimposed on the 1/v continuum in the epithermal range. Such a stable isotope is said to have a large resonance integral I_o. Elements with large resonance integral to thermal neutron cross section

ratios, I_o/σ_{th}, are very sensitive to epithermal neutron activation analysis. Table 1 exhibits the various nuclear reactions and their respective I_o/σ_{th} values.

Table 1 List of some large resonance integral to thermal neutron cross section ratios

Nuclear Reaction	**I_o/σ_{th},**
$^{59}Co(n,\gamma)^{60m}Co$	1.91
$^{186}W(n,\gamma)^{187}W$	12.80
$^{75}As(n,\gamma)^{76}As$	13.56
$^{109}Ag(n,\gamma)^{110}Ag$	15.38
$^{115}In(n,\gamma)^{116m}In$	16.33
$^{81}Br(n,\gamma)^{82}Br$	18.52
$^{127}I(n,\gamma)^{128}I$	23.71
$^{121}Sb(n,\gamma)^{122}Sb$	33.90
$^{68}Zn(n,\gamma)^{69}Zn$	43.06
$^{124}Sn(n,\gamma)^{125}Sn$	61.54

.

In neutron activation analysis the major interferences that lead to high backgrounds typically come from the following reactions: $^{23}Na(n,\gamma)^{24}Na$, $^{27}Al(n,\gamma)^{28}Al$, and $^{37}Cl(n,\gamma)^{38}Cl$ and $^{55}Mn(n,\gamma)^{56}Mn$ for short-lived isotopes; $^{23}Na(n,\gamma)^{24}Na$ and $^{81}Br(n,\gamma)^{82}Br$ for medium-lived isotopes; and $^{45}Sc(n,\gamma)^{46}Sc$, $^{59}Co(n,\gamma)^{60}Co$, and $^{58}Fe(n,\gamma)^{59}Fe$ for long-lived isotopes. There may other circumstances that lead to high continuums notable coming from engineering (e.g. semiconductors) or ore specimens. It is interesting to note that the reactions that lead to high backgrounds with the exception of $^{81}Br(n,\gamma)^{82}Br$, have low resonance integral to thermal neutron cross section ratios which ultimately yields significantly lower backgrounds due to the Compton scattering when using epithermal neutrons.

The comparison between thermal (top) and epithermal (bottom) NAA of an Arctic air filter is shown Figure 6. The use of epithermal neutrons decreases the Compton continuum due to $^{23}Na(n,\gamma)^{24}Na$, $^{27}Al(n,\gamma)^{28}Al$, and $^{37}Cl(n,\gamma)^{38}Cl$ reactions and allows the determination of ^{116m}In with a very good signal to noise ratio.

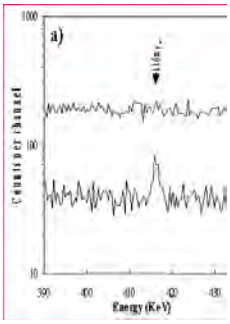

Fig 6. Comparison of themal vs epithermal NAA for the determination of ^{116m}In

4. Compton Suppression NAA

Since the early 1990's Compton suppression NAA (CSNAA) has gained a lot of recognition that it can significantly decrease backgrounds allowing the detection of radionuclides not normally reliably determined. Compton suppression works well for unstable isotopes that emit only one gamma ray such as ^{137}Cs. Some radionuclides that have two or more gamma-rays in their decay can also benefit from CSNAA, if one of them has weaker coincidences with the remaining gamma-ray(s). The radionuclides ^{76}As (559 keV) and ^{122} Sb (564 keV) are two such cases in point. It is interesting to observe that radionuclides that have coincident gamma-rays also are suppressed since the electronic set up is incapable of distinguishing events between Compton scattering and gamma-gamma coincidence. In fact this is very advantageous since the radionuclides that give rise to high backgrounds have strongly coincident gamma-rays: These photons include: 1173 and 1332 keV of ^{60}Co, 1642 and 2167 keV of ^{38}Cl, 889 and 1120 keV of ^{46}Sc, 554 keV and multitude of γ's of ^{82}Br and 846,1810 and 2112 keV of ^{56} Mn. In certain cases typical spectral interferences are also reduced or nearly eliminated such as the case of determining Cd through it 334 keV photon and the interference of the 336 keV photon from ^{239}Np. Cd is determined from the ^{114}Cd(n,γ)^{115}Cd $\rightarrow$ ^{115m}In reaction while U is determined from the ^{238}U(n,γ)^{239}U $\rightarrow$ ^{239}Np reaction. A typical Compton suppression system is shown in Figure 7a with its instrumentation shown in Figure 7b (ORTEC hardware). However, Canberra has a more integrated system with less modules and a completely integrated system by PIXIE is shown in Figure 7c.

Fig. 7a
Compton system

Fig. 7b
Compton electronics

Fig. 7c
PIXIE XIA integrated system

To show the usefulness of Compton suppression Figure 8 shows the spectra for short-lived NAA of a coal sample irradiated with thermal and epithermal neutrons with and without Compton suppression and a more detailed depiction of the determination of ^{160}Tb using the 879 keV gamma-ray and the ^{58}Co using the 811 gamma-ray. Nickel is determined using the ^{58}Ni(n,p)^{58}Co reaction. As can be see the backgrounds dramatically decrease as one uses Compton suppression. While not all stable isotopes have large resonance integral to thermal neutron cross section ratios it very useful to acquire data in both modes as to maximize the number of elements that can be reliably determined.

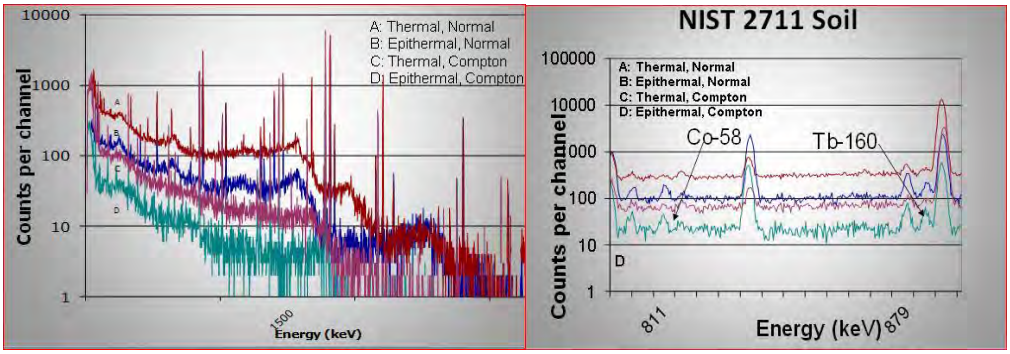

Fig. 8 General spectra structure of short-lived radionuclides (left) comparison of thermal and epithermal NAA with and without Compton suppression for the detemination of nickel and terbium (right)

5. Sample Changer

While sample changers have a long history of use in gamma-ray spectroscopy they have not been utilized with Compton suppression systems. This is due to the unique problems associated with replacing a sample that is completely surrounded by a combination of detectors. Motion required by the sample changer is dependent on three linear slides driven by stepper motors. One produces the motion that loads the sample vial onto a sample holder fitted to the top of the germanium detector. Two other stepper motor driven slides provide the vertical and horizontal motion required to move the germanium detector between the sample loader and the inside of the shield structure. Limit switches control the extent of vertical travel. A single switch determines the lower limit. The required upper height is different depending on whether the detector is being lifted into the shield or up to the sample loader. Therefore, two separate upper limit switches wired in series are used. For horizontal movement, there is a back limit switch that places the detector directly under the shield's entry point. This horizontal position and the bottom vertical position are initialized as coordinates (0,0). Moving the detector to the point under the sample loader is accomplished by sending the motor forward a specific number of steps. The detector can be moved to a more forward position before it encounters the forward limit switch (Figure 9c). This facilitates easier maintenance and removal of the detector. Before the first sample is loaded, the detector is moved completely down and then back, stopping just under the shield. The zero coordinates are initialized and the detector is then returned to the sample loader. This is where the cycle normally begins. A stepper motor controlled linear slide (Figure 9b) moves the sample vial out of the sample loader and onto the sample holder affixed to the germanium detector. This displaces the previous sample, which is then pulled down the exit guide by gravity. Sample holders of different heights are available to accommodate four different counting geometries. The sample loading mechanism is shown in Figure 9b. The

germanium detector is moved, by a vertical slide (Figure 9d), down and below the shield table. It is then carried by a horizontal slide underneath the shield (Figure 9a). The vertical slide then raises the detector into the shield structure. Once data acquisition has been completed, the detector is again lowered to the bottom limit switch, moved forward to the correct distance, and raised until the sample loader limit switch stops it. The computer that does the data acquisition also controls the sample changer through stepper motor controllers (Figure 9e) connected to its serial port. OPRTEC Maestro MCA emulation software is used to communicate with two multichannel buffers connected to the computer.

Fig 9. (a) Detector on transport (b) Sample loader (c) Horizontal slide (d) Vertical slide (e) Stepper motor controllers

6. Conclusions

We have judiciously maximized the use of neutrons through automation of irradiation and counting hardware and software in conjunction with thermal and epithermal neutrons and Compton suppression. Not only the array of elements has been significantly increased, but also detection limits and counting uncertainties have decreased and spectral interferences have also been decreased in for several radionuclides.

10. References

(1), Zs. Révay, R. K. Harrison, E. Alvarez, S. R. Biegalski and S. Landsberger, “Construction and Characterization of the Redesigned PGAA facility at The University of Texas at Austin”, Nuclear Instruments and Methods in Physics Research A, **577**, 611-618 (2007).

(2) N. M. Spyrou and S.A. Kerr “Cyclic Activation: The Measurement of Short-lived Isotopes in the Analysis of Biological and Environmental Samples: Journal of Radioanalytical and Nuclear Chem. **48,** 1979 169-183 and references therein

(3) N. Rodriguez, M. D. Yoho and S. Landsberger, “Determination of Ag, Au, Cu and Zn in Ore Samples from Two Mexican Mines by Various Thermal and Epithermal NAA Techniques” , J. Radioanal. Nucl. Chem. **307,** 955-961 (2016).

(4) B. Canion and S. Landsberger “Determining Trace Amounts of Nickel in Plant Samples by Neutron Activation Analysis”, J. Radioanal. Nucl. Chem., **296,** 315-317 (2013).

(5) B. Canion and S. Landsberger, “Determination of Zinc in Geological Samples Using Compton Suppression and Epithermal Instrumental Neutron Activation Analysis” J. Radioanal. Nucl. Chem., **296,** 379-382, (2013).

(6) Y. A. Ahmed, S. Landsberger, D.J. O’Kelly J. Braisted, H. Gabdo, I.O.B. Ewa, I.M. Umar and I.I. Funtua, “Compton Suppression Method and Epithermal NAA in the Determination of Nutrients and Heavy Metals in Nigerian Food and Beverages”, App. Radiat. Isotop. **68,** 1909-1914 (2010).

OPTIMIZING PALLAS REACTOR UTILISATION TO SUPPORT AN ECONOMICALLY VIABLE BUSINESS CASE

DAVID ZEKVELD

Market Intelligence Analyst, Business Case & Financing, PALLAS
Comeniusstraat 8, 1092 KB Alkmaar, The Netherlands

ABSTRACT

Stichting Voorbereiding Pallas-reactor, PALLAS, aims to realize a multi-purpose reactor to replace the current High Flux Reactor (HFR) in Petten, which has been in operation for over fifty years and is now approaching the end of its economic life. It is the goal of the PALLAS project to deliver a fully privately financed, owned, operated and utilised research reactor, with a safe, state-of-the-art and multi-purpose design enabling a world-leading position in the radio-isotope market and facilitating R&D in the field of nuclear technology.

PALLAS financing consists of two phases: a publicly funded phase of about five years followed by a privately funded phase. Phase one consists of preparing a design and obtaining the necessary licenses. For this phase the government has granted a loan of 80 million euros. The first phase also involves attracting private resources to realize the construction and commissioning of the PALLAS reactor. This requires the development of a sound business case as a basis to eventually finance the PALLAS project based on private capital. The second phase involves the actual construction and commissioning of the PALLAS reactor. This paper summarizes key elements of the PALLAS business case and financing project.

1. Introduction

The PALLAS project organisation was part of NRG, a subsidiary institute of the Energy research Centre of the Netherlands (ECN), until the end of 2013. As of December 16, 2013 the activities of PALLAS have been incorporated in an independent foundation, the 'Stichting Voorbereiding Pallas-reactor', referred to as 'PALLAS' from this point forward. The PALLAS project organisation was funded from the early 2000's until the end of 2013 by investments from NRG and Dutch government. In 2012, the national government (Department of Economic Affairs) and the province of North Holland provided an investment of €40M each to lead PALLAS through its first phase, specifically to obtain a detailed design and a license.

The PALLAS-reactor will be a pool-type reactor design based on proven technology (see Schematic of PALLAS-reactor Figure 1). The PALLAS-reactor will be optimized for production of medical and industrial isotopes and conducting nuclear technology research. The most important feature of PALLAS-reactor is its operational flexibility; the design of the core shall ensure that it can respond to changing markets. This paper focuses on the aspects of defining and optimizing the PALLAS reactor utilisation to support the economically viable Business Case.

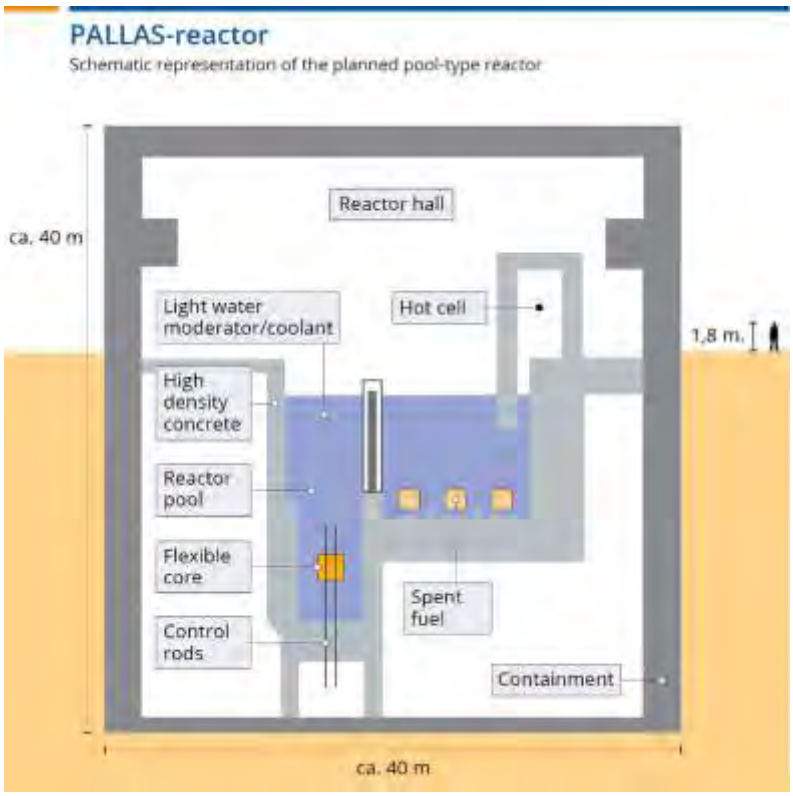

Fig 1: Schematic representation of the PALLAS reactor

2. PALLAS at Onderzoekslocatie Petten

The PALLAS-reactor will be located near the village of Petten in the province of North Holland at the "Onderzoekslocatie Petten" (OLP) site (translated as "Research Site Petten"). Organizations such as NRG, Mallinckrodt, ECN, and the European Commission's Joint Research Centre and the Institute for Energy and Transport (JRC-IET) all have operations at the OLP site. PALLAS will provide an integral asset for the continued success of these organizations by providing a replacement for the HFR. The design of the PALLAS-reactor shall seek to optimize interfaces with existing facilities and customers at OLP.

Fig 2: Onderzoekslocatie Petten (OLP) - PALLAS's future location

The existing facilities, experienced staff and organizations currently on the OLP site make it an ideal location for the PALLAS-reactor (Reference 1). The OLP site has the following interfacing nuclear facilities:

- High Flux Reactor (HFR) which will be replaced by the PALLAS-reactor;
- Hot Cell Laboratories (HCL)
- Molybdenum Production Facility (MPF);
- Decontamination and Waste Treatment Facility (DWT);
- Jaap Goedkoop Laboratory (JGL) for research into new radioisotopes;
- Waste Storage Facility (WSF);

The construction of the PALLAS-reactor by 2024 will ensure that medical isotope production and research activities can seamlessly transition to PALLAS-reactor and ensure business and research continuity for the organizations located in Petten.

PALLAS will support the Dutch Isotope Valley (DIVA) initiative and provide benefits to the Dutch medical isotope industry beyond the boundaries of the OLP site. NRG, URENCO and TU Delft have formed DIVA to ensure that The Netherlands continues to be a leader in the production of medical isotopes. PALLAS is preparing a vision on research to provide assurance that PALLAS will not only be a leader in the safe production of medical isotopes, but also contribute and benefit from the research and development of new medical isotopes and improving effective use of current isotopes.

3. PALLAS Organization

The PALLAS foundation is organized into two primary teams, Design and Licensing (D&L) team and Business Case and Financing (BC&F) team. Each team is responsible for the respective projects and fulfilling the objectives:

- *D&L Objective* – to prepare detailed design and obtain requisite licenses;
- *BC&F Objective* – to prepare an economically viable Business Case and obtain financing.

The D&L and BC&F projects are proceeding in parallel with significant interaction and communication between the teams. BC&F proposes the most economically viable quantity of radioisotopes / experiments (PALLAS's "products") and D&L evaluate the proposed "products" impact on design. The interaction between the teams is iterative and the process of interaction between the organizations is further described in Section 6 of this paper.

4.The PALLAS Business Case

The PALLAS Business Case is a fundamental deliverable of the PALLAS project with the primary function of attracting private investment in the PALLAS project. During the preparation of PALLAS-reactor Design Requirements, the Business Case is used to influence both design and product selection to maximize economic viability and optimize full lifecycle costs (design, construction, operation and decommissioning) of the reactor.

The PALLAS Business Case has continually evolved since the PALLAS project inception in early 2000's at NRG. Over the past five years, several major updates to the business case have been made in submission to key stakeholders (e.g., the Dutch government). As PALLAS originated as a project within the NRG organization, the previous business cases were built on the NRG product portfolio and therefore has a realistic market assessment based on performance and market projections at NRG. The formation of the independent entity of PALLAS allows for the BC&F team to independently verify previously made market

and growth assumptions in the Business Case and expand PALLAS product offerings beyond those of the HFR. The last major revision was issued in May 2012. An update to the business case was made by PALLAS organization in June of 2015.

Throughout 2016, PALLAS will be engaging in a tendering process for the selection of the reactor's DNI under the European Union Procurement Directives. This process allows PALLAS to have dialogues with the vendors on a variety of topics prior to issuing a formal request for tender. The dialogues will be an opportunity for the PALLAS BC&F team to further validate and challenge the assumptions in the business case.

PALLAS will be issuing an updated Business Case to stakeholders near the end of 2016. The next revision of the Business Case shall be updated to:

- reflect current market analysis;
- validate previous business case assumptions (to extent possible);
- incorporate feedback from vendor Competitive Dialogues;
- incorporate a new "vision on research"; and,
- update cost estimates (e.g., CAPEX, OPEX, decommissioning) based on new assumed reactor specifications.

5. Financing PALLAS Reactor

The statutes of PALLAS state that PALLAS should be financed out of private sources (private financing) or 'open' public funding sources. To fulfill the financing objective PALLAS has prepared a financing strategy to approach the market of private investors, including both equity and debt financing. The mandate to seek private investment is consistent with a shift in utilisation of the current HFR in Petten from a subsidized public research use to commercial production. A privately financed reactor is also consistent with the principles of Full Cost Recovery for the production of Molybdenum by the Organization for Economic Co-operation and Development (OECD) Nuclear Energy Agency (Reference 1).

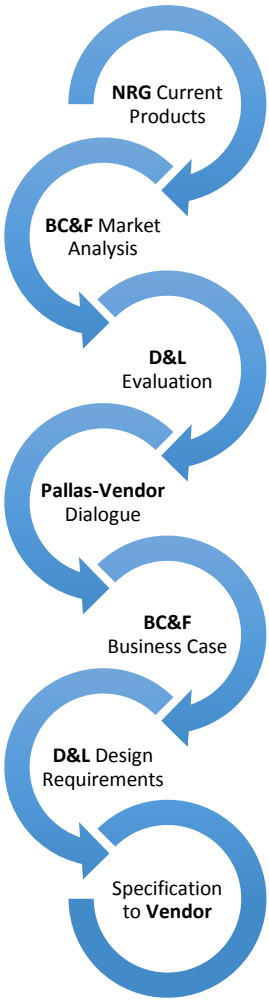

6. PALLAS reactor utilisation

Optimizing the economic viability of the PALLAS-reactor is achieved by: selecting products to maximize profitability; ensuring the proposed design has flexibility to meet changing market demand; and, minimizing capital expenditures (CAPEX) and operating expenditures (OPEX). The PALLAS Business Case is based on revenues from four key complementary product areas:

- Medical Isotopes;
- Industrial Isotopes;
- Irradiation and testing services; and,
- Innovation and research services.

The product selection is being refined through an iterative process between business case and design teams. PALLAS considers NRG's current diagnostic medical isotope product spectrum and therapeutic medical isotope products to be the starting point for PALLAS business case market analysis (see full radioisotopes offered by NRG in Appendix A). The PALLAS Business Case incorporates a full life cycle approach to estimating costs and specifies requirements to optimize costs throughout reactor life (e.g., specifying a requirement that reactor be designed for safe and cost effective decommissioning).

The PALLAS Business Case will take the HFR isotope products (Appendix A) as the starting point for PALLAS's product offerings. PALLAS will endeavor to offer products that will service the current NRG customer base. Market analysis will be performed to identify further products and then evaluate the revenue of the potential products in contrast to CAPEX and OPEX costs. Once the BC&F team has proposes a profitable product assortment, the D&L team shall review the proposed isotopes and determine the feasibility of producing the specified isotopes and quantities. The product specification shall be discussed by the PALLAS BC&F and D&L teams with potential vendors through the Vendor Dialogues as part of the tender process

After the vendor dialogue and further market research, the BC&F will propose a new set of radioisotope products and quantities. The D&L team shall propose a bounding envelope for the suite of isotopes and identify significant "outliers" in terms of impact on CAPEX, OPEX, operations, etc. The bounding production envelope will be used as the basis for the final Design Requirements issued to the vendors through the formal Invitation To Tender process.

7. Opportunities and Challenges

PALLAS is incorporating economic viability into the design process and capitalizing on the existing infrastructure and assets on the OLP site. This design focus includes optimizing interfacing onsite processes; such as the interfaces with the existing onsite Molybdenum Processing Facility (MPF) to maximizing molybdenum output and minimizing loss by virtue of decay. Located at Petten, PALLAS will have the option to also provide irradiated targets to other nearby processing facilities. PALLAS's location will provide good access to the North American and European isotope markets.

The business and design teams endeavor to maximize the flexibility of the isotopes and irradiation services offered to meet market demand, while minimizing CAPEX and OPEX costs. The design of PALLAS prioritizes the safe and reliable production of quality isotopes to meet customer demands.

PALLAS currently observes market challenges in achieving Full Cost Recovery pricing of Molybdenum and considers this to be a challenge to the PALLAS business case. Based on OECD NEA reports, the principles of Full Cost Recovery have been accepted by participating the governments of participating countries. PALLAS remains optimistic that Full Cost Recovery will be achieved before PALLAS enters the market in 2024.

Appendix A

Isotope	Medical Application
Chromium-51	Used to label red blood cells and quantify gastro-intestinal protein loss.
Iodine-131	Adrenal imaging.
Molybdenum-99	Mo-99 is the parent for Tc-99m generator used for a broad range of imaging in serious medical conditions: all areas of oncology, cardiology, kidney function, brain function, brain disorders, lung function, infection detection, thyroid function, bone disorders.
Xenon-133	Imaging for lung function.

Table 1: Diagnostic Medical Isotopes currently produced by NRG

Isotope	Medical Application
Cobalt-60	High dose rate brachytherapy.
Copper-64	Used to study genetic diseases affecting copper metabolism, such as Wilson's and Menke's diseases.
Erbium-169	Arthritic conditions.
Gold-198	Head and neck cancer, tongue and mouth cancer (low dose rate brachytherapy).
Holmium-166	Liver cancer. Used in clinical trials in Europe for new blood cancer treatment.
Iodine-125	Prostate cancer.
Iodine-131	Thyroid, lung, brain and liver cancer, non-Hodgkin
Iridium-192	Various cancer therapies, e.g. cervical cancer, lung cancer (high dose rate brachytherapy) and head and neck cancer.
Lutetium-177	Cancer therapy of solid tumors, ovarian and neuroendocrine cancer.
Phosphorus-32	Treatment of excess red blood cells.
Rhenium-186	Metastatic bone pain relief and arthritic conditions.
Samarium-153	Metastatic bone pain relief (palliative care) and in development for treatment of bone cancers.
Strontium-89	Metastatic bone pain relief.
Yttrium-90	Liver cancer, arthritic conditions and metastatic bone pain relief.

Table 2: Therapeutic Medical Isotopes currently produced by NRG

(Reference 3)

References

1. NRG, Report no. 25192/12.113089, “Complementary Safety Margin Assessment Onderzoekslocatie Petten" February 2012.
2. OECD NEA, Report no. 6985, “The Supply of Medical Radioisotopes: the Path to Reliability”, , 2011. Available at: www.oecd-nea.org/
3. NRG, Factsheet, “Overview of Medical Isotopes”, September 2015. Available at: https://www.nrg.eu/fileadmin/nrg/Afbeeldingen/producten/3._Isotopes/Factsheet_Medical_Isotopes_DEF_oct_15.pdf

ZERO POWER REACTOR AGN-201K FOR UNIVERSITY EDUCATION

MYUNG HYUN KIM
Reactor Research & Education Center, Kyung Hee University
1732 Deogyeong-daero, Giheung-gu,Yongin-si, Gyeonggi-do, 17104, Rep. of Korea

ABSTRACT

AGN-201K in Kyung Hee University is only one university reactor in Republic of Korea. It has been open to all university students for a credit course or short term training course since 2009. More than 15 universities have nuclear engineering programs both for undergraduate and graduate programs. Most of them educate reactor physics and other related courses for fission technologies. Compared with 5 years ago, demand of student training with research reactors has been grown.
Regular training courses as winter or summer camp have been repeated 49 times during last 7 years. Most of them are carried out during 5 days based on request of visiting universities. All students should stay at dormitory for five days and attend 6 experimental modules. All experiment modules consist of lecture, experiment and student presentation. Even though schedule was tight and duty of students was quite large, satisfaction level of participants has been very high.
In this paper, three topics will be introduced. The first topic of this paper is the contents of experimental courses. Six experimental modules are designed to simulate physics test in nuclear power plants. The second topic is activities related to domestic and international training courses. Recently international collaboration programs were performed with UAE and Japan. Strong collaboration with Japanese universities for student education has been wanted after the temporary shutdown of all university reactors in Japan caused by re-inspection according to new safety regulation. The third topic with AGN-201K is the future works planned for international education network.

1. Introduction

Right now, there are two research reactors in operation in Republic of Korea. The first one is a 30 MWt heavy water moderated/cooled pool-type reactor, HANARO and the second is a zero power educational reactor, AGN-201K. A new multi-purpose 15 MWt reactor, KJRR is ready to be constructed with the time goal to be operational on April 2017. However, this project is now delayed because of objection of local assembly.[1] Therefore, AGN-201K in Kyung Hee University is now and will be the only facility open to students for training and education. Specific role of this reactor can be forecasted with the following historical perspectives.
Nuclear R&D in Korea was started at 1958 and 1959 when department of nuclear engineering was founded at two universities, Hanyang University and Seoul National University. At the same time nuclear act had become effective and KAERI was founded. In the period of 1960's first research reactor, TRIGA-mark II was built at KAERI and uprated from 100KWt to 250KWt. Second one, TRIGA mark-III (2 MWt) was commissioned in 1972. Thereafter TRIGA Mark-II was dedicated for training and education for two university students.
Late 70's and 80's is a period of initiation and expansion of Korean nuclear industry. Four more universities opened nuclear engineering departments and operation of the 1st NPP was started in 1978. An engineering company KOPEC, a regulatory body, KINS and a nuclear fuel manufacturing company KNF were established. A zero power reactor, AGN-201 installed at Colorado State University was moved to Kyung Hee University (KHU) at 1982, but utilization programs was limited to KHU students only. [2]
1990's and 2000's is a period of chaos but steady-growth. Because of strong anti-nuclear movement initiated after TMI and Chernobyl, many national projects were delayed and

cancelled. KAERI was moved from Seoul to Daejon science town with the construction of new reactor, HANARO. Two TRIGA reactors at Seoul were shutdown in 1995 and lately they were completely decommissioned. After 1995, there were no research reactors available for education and training. In the period of 2003 to 2008, selected students from 6 universities were sent to Kyoto University Critical Assembly in Reactor Research Institute every year for 10 days reactor experimental training. This activity was an excellent example of international collaboration in education between Japan and Korea. Recognizing the need of a university training reactor at national level, KHU started refurbishment project on AGN-201 aiming for nationally open facility. After 2008, reactor research and education center was established and began to serve educational programs with AGN-201K (a new name for a refurbished reactor).

Recently a nuclear renaissance was started in Korea after December 2009 when Korean nuclear consortium succeeded in UAE NPP contracts. With a new national expansion policy of nuclear energy, sudden impact was given in Korean nuclear society with high demand of supply. One of the demanding issues was human resource development. In the year of 2015, the nuclear engineering programs were going on in 15 different universities. Duty of AGN-201K should become heavier only in need of education programs.

The same kind of expansion in nuclear engineering programs in universities s found in Asia – particularly China and Malaysia and also in Arabic countries.

In this paper, role of AGN-201K is reviewed for current and future utilization in education and training. At the next section, unique and favorable features of this reactor is addressed. At the last part of this paper, upcoming plan for multi-national remote internet training is introduced.

2. Unique Features of AGN-201K

Two times refurbishment were done by research fund during the period of 2004 through 2007 and 2011 through 2012. Reactor power was uprated from 0.1 watt to 10 watt with additional shielding walls and doors. Maximum thermal flux at the beam port is about 3.0×10^{8} #/cm^2-sec at the permitted maximum power. It is quite low for research but high enough to measure neutrons and gammas inside and outside of reactor. Because of low radiation level, students can access near to the reactor and closer as compared to most of research reactors in national institutes. Components for I&C and safety features were repaired and added in order to comply with standing safety regulations and rules. A new digital monitoring console(DMC) was installed side by side in parallel to the original analog operating console(AOC), used by licensed operators. All signals at AOC are connected to DMC. Students can manipulate two control rods at the DMC under the supervision of operators at the AOC. It provide good experience about reactor operation and how reactor is protected against accidents.[3]

Fig 1. DMC and AOC at the operating room

It is found that conditions of AGN-201K now be perfect for the student education. First of all, low-power operation near to zero power is not good for research but ideal for education. There is enormous margin to fuel melting under any kinds of transients. Temperature

reactivity feedback is very strongly negative. Homogeneous core made of LEU oxide powder mixed with polyethylene is free from cladding problem such as PCI resulting in capability of fast power increase. Under the regulation, fast power increase itself is banned but student is allowed to change power at separate console, DMC with full confidence of safety by operator at the safety console, AOC. All control action done by student can be override by operator in AOC. Therefore DMC is a platform to be used by students without operation license.
The second advantage of this reactor is all-in-one information panel at DMC. Students can monitor all kinds of nuclear instruments; 7 neutron detectors (two fission chambers, one He-3, four ionization chambers) and neutron and gamma area monitoring signals at three locations. All data can be read by old fashioned gauges, digital reader, log-paper meter and graphs at screen with recorded database. Students can compare analog system with modern system.

3. Education Programs for Reactor Experiment

Table 1 shows structure of one-week course with six experiments. 4 experiments are well-known traditional experiments shown in many reactor training programs. The first and the last one are very unique experiments in AGN-201K.
Experiment-1 is the introductory practice to make students understand nature of reactor and all instruments. Each student has a chance to manipulate control rods to change the power level to the given target power level. Before and after the operation, student operator should read data from DMC; count rate or ampere from 4 neutron detector channels, control rod positions and dose at 4 radiation monitors. Based on the theory, students should confirm that control rod position for criticality are not changed after the change of power level because this reactor do not have any reactivity feedback from xenon and temperature. Another objective of this experiment is to find the linearity of all detectors expecting count rates proportional to power level.

	Title of Experiments	Activity Goals
1	Understanding RRs & AGN-201K, Reactor Operation Practice	Relation between criticality & power level
2	Measurement of Reactor Period	Handling of measurement errors, Calculation of reactivity with Inhour eq.
3	Critical Mass Approach Experiment	Experiment for subcriticality measurement
4	Control Rod Calibration	Rod swap method & Rod drop method
5	Thermal Flux Measurement	NAA with gold wire, Evaluation of Cd ratio, MCA counting with HPGe Detector
6	Measurement of Reflector Effect & Temperature Feedback Effect	Compare with design data (ITC) Compare graphite with water

Tab 1: Course contents of reactor experiment

Experiment-2 is the preliminary training to Experiment-4. In this experiment, Inhour equation and reactor period is explained. Given the reactivity change, students should measure an asymptotic period of reactor under the power transient and calculate the reactivity value with an Inhour equation. For this simple activity, each student has a different role independently. Each student read one value from up to 6 different detector signals. Three different methods of data processing were suggested in order to pick up the period from 20 measurement; least square fitting, slope between two points, and statistical average. Therefore, students can compare results from three fitting methods, 6 detector signals for different runs initiated with different reactivity insertion.
Experiment-3 is the traditional criticality search experiment. Experimental procedure is the same as for search of critical rod position. Material of control rods in AGN-201K is the same

as of core (homogeneous mixture of fuel and moderator) material. Insertion of control rod from bottom to the top is an action for power increase in AGN-201K. Therefore, stepwise raise of control rod position near to the critical position is corresponding to addition of fuel, i.e. increase in fissile mass near to the critical mass. A response of inverse multiplication (1/M) curve was compared with two different detectors.
Experiment-4 is the most painstaking experiment comprised of three subtasks as a full day activity. The first subtask is a period measurement method. For each stepwise rod insertion, period is measured from each transient and then reactivity insertion is calculated. After summing up all data from 6~8 runs, an integral rod worth curve is produced for the fine control rod (FR). The second subtask is a swap method. After the measurement of period for a specific transient, reactor should be adjusted back to critical condition by moving the other control rod (here CR, coarse control rod) to the opposite direction instead of pulling back the FR to the initial position. After summing up all data from 6~8 runs, differential rod worth curves are produced for both FR and CR. The third subtask is the rod drop experiment. From the critical position, all control rods are drop by a manual trip and count rate change is recorded at every 5 seconds. After fitting the power drop profile, reactivity change can be predicted by prompt drop approximation.
Experiment-5 is the measurement of absolute level of thermal flux in the core and thermal flux distribution inside of the core. This is performed by neutron activation of gold (Au-197) wire attached along the glory hole. Gamma rays from Au-198 are measured by HPGe detector systems with multi-channel analyzer. Because of time requirement for irradiation and cooling before gamma measurement, schedule of this experiment is overlapped and separated during the other experimental schedule.
Experiment-6 is done at the last turn. Measurement of isothermal temperature feedback coefficient is done over the 5 days distance. Critical control rod position of FR is measured at the first day and the last day with intentional temperature change of core. Reactivity difference is then calculated using integral rod worth curve obtained in Experiment-4. Additional experimental run is done for reflector effect. Thermal column was replaced from from water to graphite and the reactivity difference was also measured to see the choice of reflector material.

Fig 2. Student Operation during Exp-1

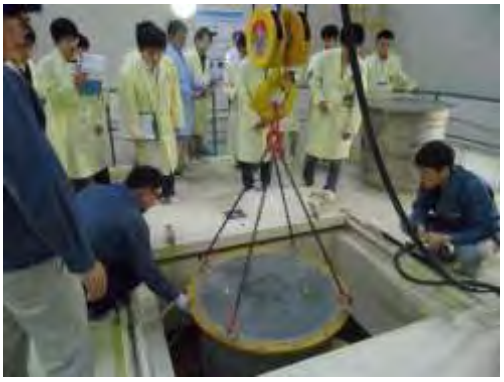

Fig 3. Exchange of Thermal Column for Exp-6

4. Educational Achievement

Reactor Research & Education Center (RREC) is now serving a national student training center open for all universities. Regular one-week short courses have been provided to visiting universities as dormitory-housing programs. Table 2 shows a whole achievement record in education service. Through 49 times courses, there has been 511 participants. Domestic training courses were given to 351 students from 10 visiting universities and 79 students from KHU. 19 courses were preceded in English for both foreign students and Korean students. 9 courses were provided for foreign students from UAE, Malaysia, Jordan and Japan.

Questionnaire records from all participants have been monitored. Satisfaction level from all participating groups are very high except for complain about busy schedule.

	# of Courses	# of Trainee
KHU students	6	79
domestic visitors	34	351
foreign participants	9	81
	49	511

Tab 2: Course records done since January 2009

5. International Collaboration

As shown in Table 3, there are three kinds of foreign participants up to now. The first visitors are from Khalifa University of Science, Technology and Research (KUSTAR) when they sent their students to partner institute KAIST. This program was done as HRD contract between UAE and Korea. They visited three times during period from 2011 to 2013. The second case are temporary visitors to KAERI as their OJT. Two group of trainee from Jordan and Malaysia visited at 2012 and 2015. This case is expected to be continued by Saudi Arabian visitors to KAERI. Third case is student dispatch from Japan. After Fukushima accident, Kinki University initiated an international student training program between Korea and Japan. UTR in Kinki, KUCA in Kyoto University and AGN-201K in KHU is designed to be shared for student training including environmental radiation monitoring program near to Fukushima site. Participants are Kyung Hee University from Korea, Kyoto University, Nagoya University, Kyushu University and Kinki University from Japan. In early 2014, a new nuclear safety regulation stopped all research reactors in Japan for reevaluation under the new rules. Thereafter, KHU became a host university for reactor experiment. Four 4 days training were provided to Japanese students at 2014 and 2015. Korean students joined to Japanese group at Fukushima site for radiation measurement experiments. This program was spot-lighted in Japanese community in many different aspects. It is expected to be continued as a successful international collaboration in education and training.

Visitors	Program	# of Courses	# of Trainee
Japanese Universities	Kinki University	4	41
KUSTAR Graduate students	KAIST-KUSTAR	3	16
Jordan Atomic Energy Commission	KAERI OJT	1	18
Malaysian Nuclear Agency	KAERI OJT	1	6
		9	81

Tab 3: Visitors from foreign countries since January 2009

Fig 4. MNA from Malaysia

Fig 5. JAEC from Jordan

5. Future Plans

Recently, KHU is discussing with IAEA for the establishment of cyber broadcasting equipment for Internet Reactor Laboratory (IRL) program. IRL in KHU is designed to be an asian hub for remote education. This program will be under the Asian Network for Education in Nuclear Technology (ANENT). Korean site is favorable to cover the range from Far East Asia to Middle East Asia because of smaller time zone difference.
During the period of 2013-2014, AGN-201K was used for public education. School teachers were invited to KHU experience summer camp. Total 155 teachers participated to 7 courses. It was very effective in public communication and education. Lots of information were provided them. This program was stopped in 2015 because of limit in work-time and budget. We are facing now quantum jump in education and training demand from 15 domestic universities. This is another problem of budget and man power to be allotted.
Korean regulation to the research reactors became more strict and wide. Periodic safety review is forced to all research reactors including many new regulations against fire, disasters and others. AGN-201K in university cannot be an exception on this matter. Extensive efforts is required for inspections just like Japanese research reactors.
Serious discussion is under way with government office to solve these problems to be ready to solve in a few years.

References

[1] I.C.Lim, H.S.Jung, K.H.Lee, S.J.Park and M.H.Kim, “Current Status and Prospect of Research Reactor Utilization in Korea,” Joint IGORR 2013 & IAEA Technical Meeting, Daejeon, Korea, October 13-18, 2013.
[2] Document: Educational Experiments Utilizing The AGN-201 Nuclear Reactor, AGN REPORT No.16, Aerojet General Nucleonics, January 1957.
[3] Myung Hyun Kim, "Utilization of AGN-201K for Education and Research in Korea," Research Reactor Fuel Management (RRFM-2011), Rome, Italy, March 20-24, 2011.
[4] Myung Hyun Kim, "Role of A Zero Power Reactor, AGN-201K for Education & Training in Rep. of Korea,“ Technical Meeting (TM) for the Development of a Compendium on “Research Reactors Utilization for Higher Education Programmes”, Vienna, Austria, June 16-20, 2014.

MEASUREMENT OF POSITIVE TEMPERATURE COEFFICIENTS OF REACTIVITY FOR RACK-LIKE ARRANGEMENTS OF REACTOR FUEL IN THE NEPTUNE ZERO ENERGY FACILITY

S P WALLEY, P S BEAN, I P SAINSBURY, D F GILL*, D A SOTTOSANTI*, M L ZERKLE*, D J KELLY**,

Rolls-Royce, Derby DE21 7XX

** Bettis Atomic Power Laboratory, United States, PA 15122*

*** Knolls Atomic Power Laboratory, United States, NY 12301*

ABSTRACT

It is a common expectation in criticality safety analyses for LWR fuel that modelling water at its peak density will maximise the reactivity. However, positive temperature coefficients of reactivity at near ambient temperatures are predicted for some arrangements of fuel in (for example) storage ponds for systems that exhibit a negative temperature coefficient during reactor operation. To provide validation of these positive coefficient predictions, measurements of temperature coefficients of reactivity have been made on fuel arrangements where this characteristic is predicted. The experimental set-up featured pairs of light water moderated uranium fuel assemblies where the effective separation between the assemblies was progressively increased. Temperature coefficients were measured in the range of 20-50°C and compared with predictions obtained from Monte-Carlo codes used for criticality and reactor physics.

1 Introduction

The Neptune reactor located at Rolls-Royce, Derby is an unpressurised zero-energy (maximum 300W, normally <100W) facility that can be used to operate a wide range of light water moderated critical assemblies. Reactivity control is either by control rod movement or moderator height adjustment. The moderator can be heated using an auxiliary circuit. The reactor is used primarily for reactor physics design and criticality methods validation.

2 Temperature Coefficients of Reactivity

The temperature coefficient of reactivity of most light water moderated and cooled reactors is designed to be negative for reasons of safety. A negative coefficient tends to occur naturally as the reduction in water density associated with an increased temperature will increase leakage and reduce moderation, generally leading to a reduction in reactivity. However, as shown by Zerkle and Copinger (Reference 1), pond storage arrangements of light water reactor fuel assemblies can exhibit a positive temperature coefficient even though the reactor core has a negative coefficient using the same assemblies.

3 Experimental Arrangement

A set of six experiments were devised to measure the temperature coefficient of reactivity at temperatures that might be seen in a storage pond for an arrangement of uranium fuel assemblies that were predicted to exhibit a positive temperature coefficient. Pairs of fuel assemblies were constructed such that the effective distance between the assemblies was varied. This was achieved by reconfiguring the fuel within the assemblies to change the gap between the fuel regions as shown in Figure 1. The fuel assemblies were nominally identical with assembly 2 positioned so that it formed a reflection of assembly 1, as shown. The fuel content of the fuel assemblies was increased with increased effective separation in order to maintain a critical arrangement.

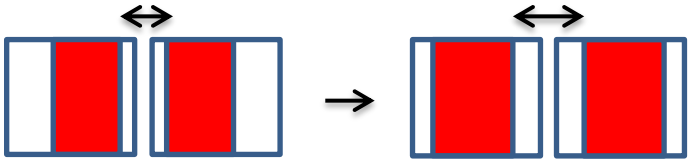

Figure 1 – Schematic of Fuel Arrangement Showing the Increase in Effective Gap

4 Experimental Procedure

For each of the six experimental configurations an initial criticality was achieved using rod control, after having fully flooded the reactor using water at ambient temperature. During the approach and following criticality, various safety parameters were measured, including a reactor power determination using fission chambers positioned close to the fuel assembles, as shown in Figure 2. For the subsequent reactor operations in which the moderator was heated, these fission chambers were removed.

In general the heating operations were performed by flooding the reactor, taking the reactor critical using control rods in a routine manner, and then raising the moderator temperature using the heating circuit while keeping the reactor critical with small control rod movements.

In cases where the required temperature was not achieved in a single day of reactor operation, the heated moderator was dumped to a holding tank overnight and then used to re-flood the reactor the next day. The overnight temperature drop then provided some overlap between measurements.

The temperature coefficient of reactivity was determined in the following two ways. The first (denoted indirect) was to measure the reactivity worth of the control rod bank by measuring the reactivity effect of small insertions and withdrawals of the two individual control rods (one in each assembly) at the critical height for a number of temperatures. The temperature coefficient of reactivity was then calculated as the change in critical height between adjacent pairs of critical heights/temperatures multiplied by the average of the control rod bank reactivity worths measured at the two temperatures and divided by the temperature change between the two measurement points, i.e. $(H_1-H_2)(W_1+W_2)/2(T_1-T_2)$.

The second method (denoted direct) was to periodically lower the control rods during the warm-up to give a reactivity of approximately -0.0004 (delta-k) and then, at the temperature at which the earlier rod position is close to being the critical rod position, determine the reactivity at exactly the same rod position. The temperature coefficient was then calculated as $(\rho_1-\rho_2)/(T_1-T_2)$. Reasonable agreement was seen between the two methods.

The reactivity was determined using a bespoke reactivity meter (RM) connected to an ion chamber located about 150mm from the face of one of the fuel assemblies as indicated schematically in Figure 2.

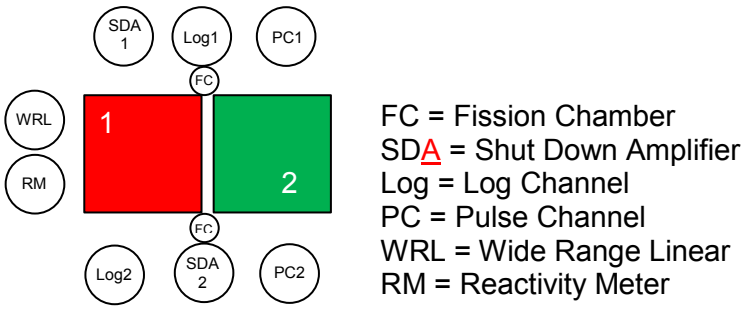

Figure 2 – Schematic of Core and Detector Arrangement

5 Experimental Results

Graphs of the control rod height versus temperature for each of the six configurations are shown in Figures 3 to 8. The separation between the fuelled regions in the adjacent assemblies for each arrangement is shown in Table 1. Temperatures were measured using a resistance thermometer (RT) or one of the thermocouples (Mid S).

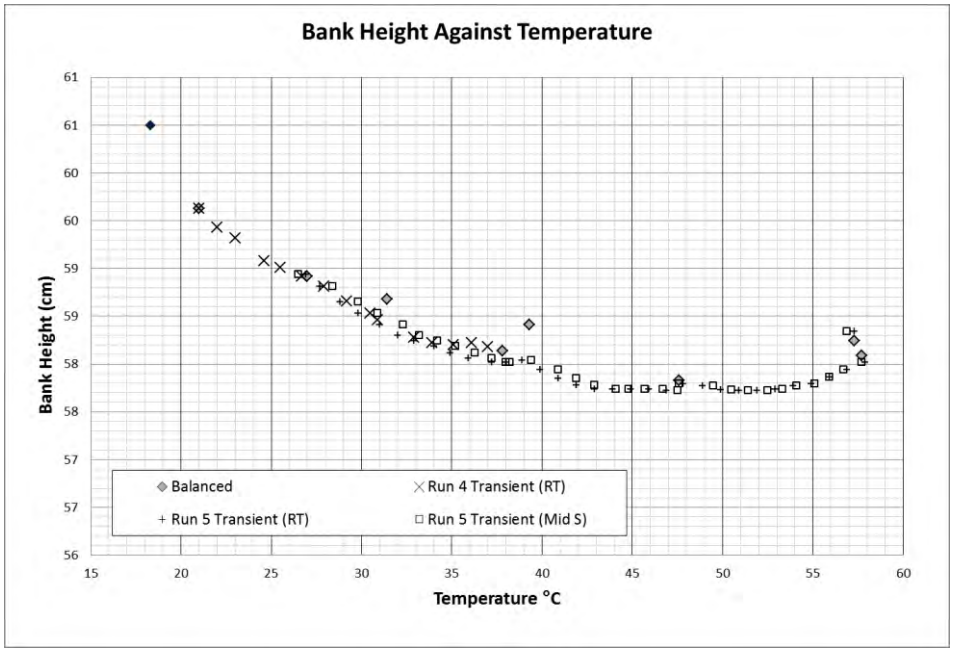

Figure 3 Configuration A, Critical Height v Temperature

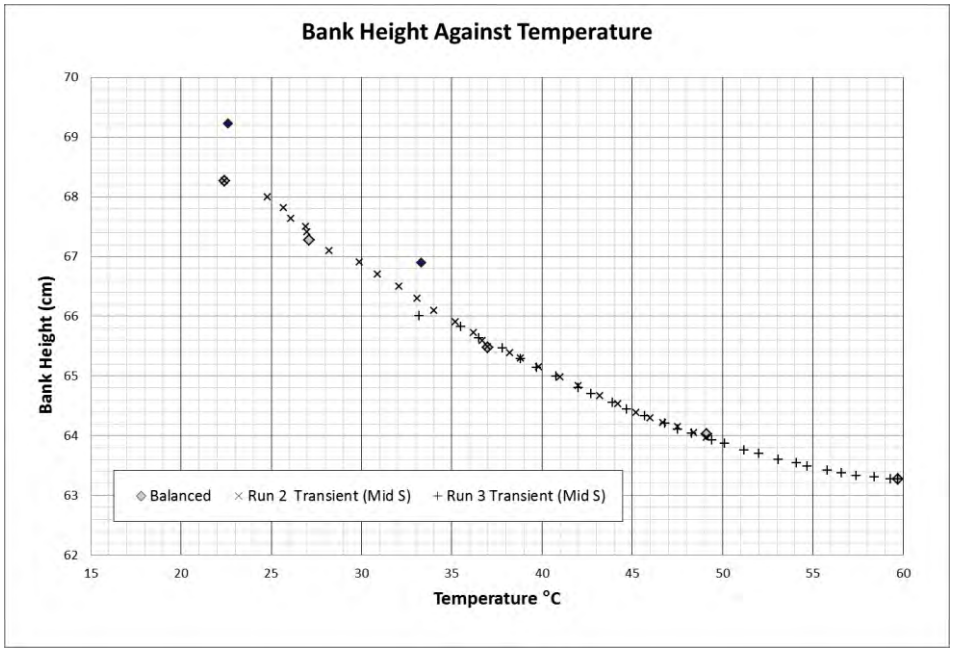

Figure 4 Configuration B, Critical Height v Temperature

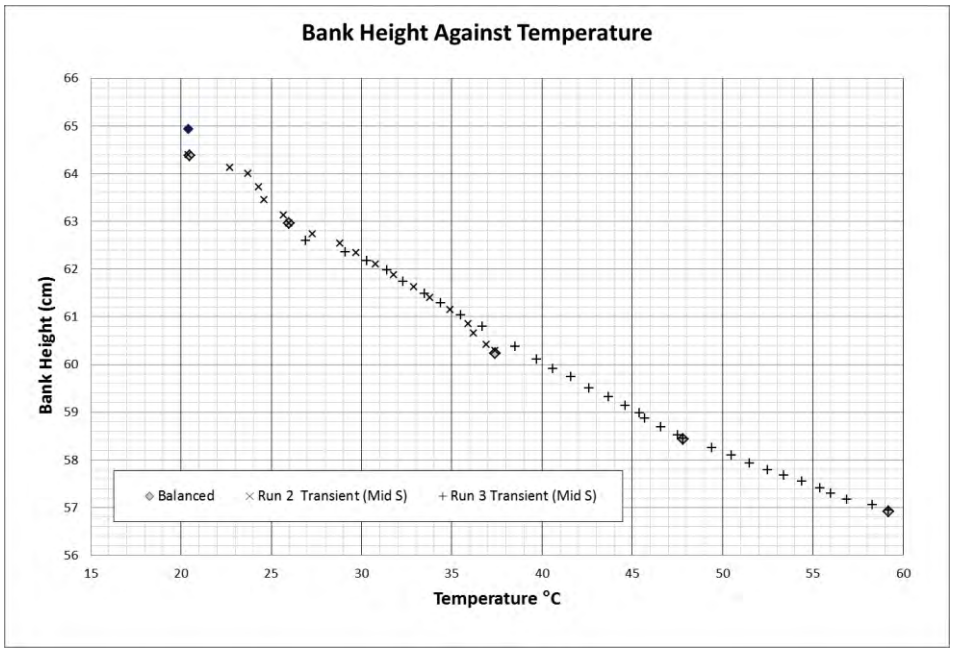

Figure 5 Configuration C Critical Height v Temperature

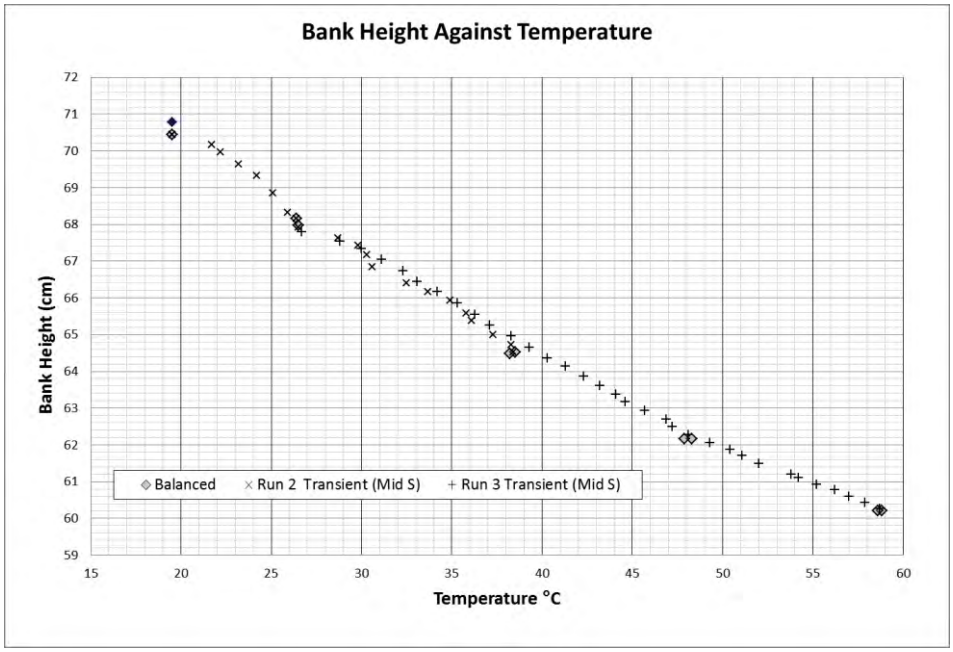

Figure 6 Configuration D, Critical Height v Temperature

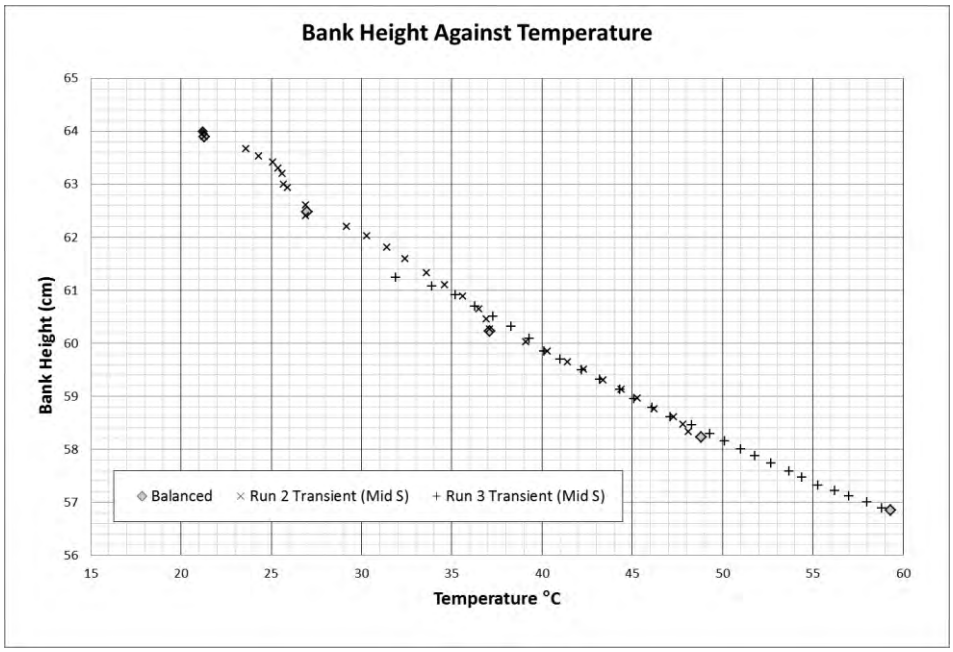

Figure 7 Configuration E2 Critical Height v Temperature

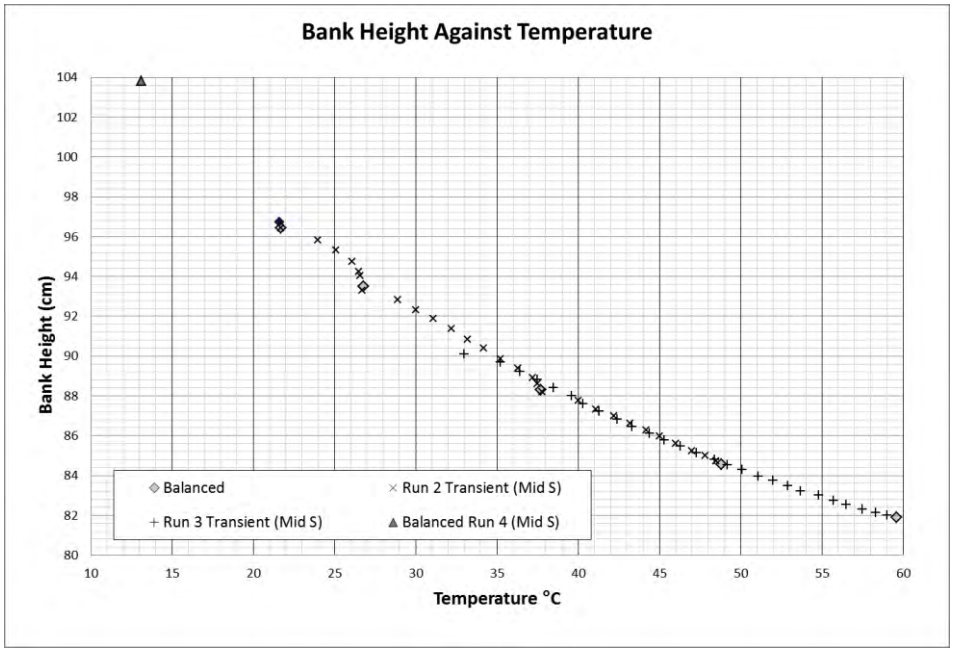

Figure 8 Configuration F2 Critical Height v Temperature

Table 1 Effective Gaps

Configuration	Effective Gap (mm)
A	22.5
B	44.3
C	66.1
D	87.9
E2	109.7
F2	131.5

The data points labelled ‘balanced’ were obtained after the moderator heating was paused for a few minutes until steady conditions were obtained. The remaining data points were taken as the moderator heating progressed with frequent small adjustments to the rod positions to keep the reactor just critical. The ‘balanced’ data point in the darker shade

denotes the presence of the fission chambers. The triangle data point in Figure 8 is an additional measurement taken in the winter after the end of the original experimental programme.

It can be seen from the slope of the critical height versus temperature that all the configurations exhibited a positive temperature coefficient, but Configuration A has a small negative temperature coefficient at about 55°C.

Temperature coefficients produced by the direct measurement method are shown in Figure 9 where it can be seen that their magnitude first increases and then decreases as the effective gap between the fuel assemblies increases.

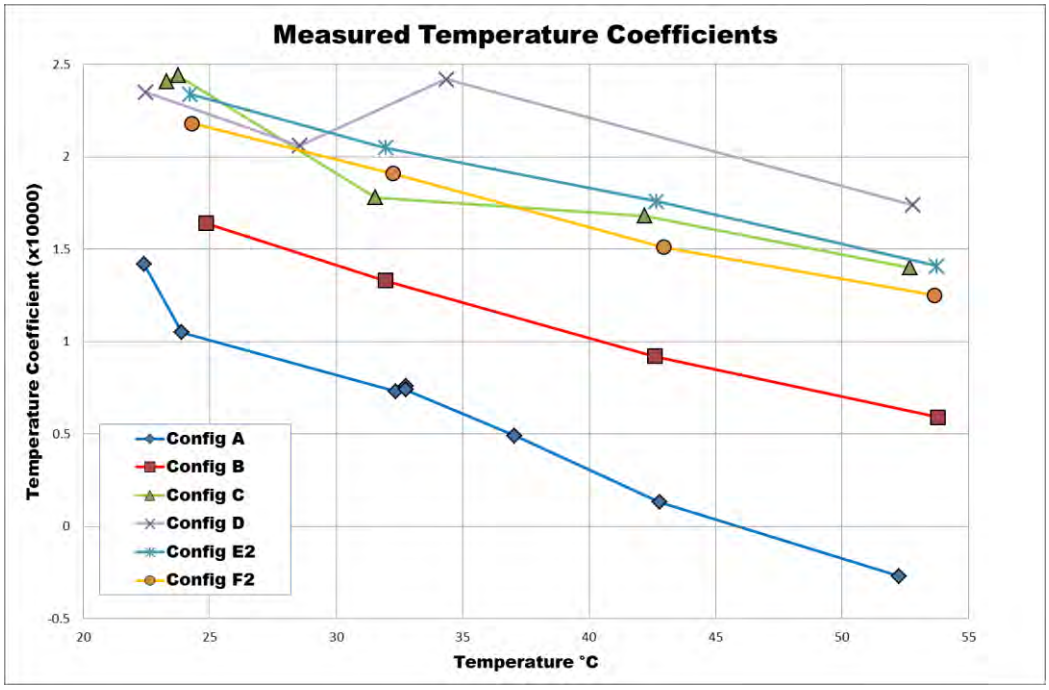

Figure 9 Measured Temperature Coefficients v Temperature

6 Theoretical Predictions

6.1 Tools and Methods

The Monte Carlo code MC21 (Reference 2) with an ENDFB7.1 based nuclear data library was used to design the fuel arrangements. In addition, safety parameters (1 stuck rod shut down margins, water and control rod reactivity worths, detector responses) required for assessment prior to Neptune core build and operation were also calculated using the MONK Monte Carlo code (Reference 3) and an in-house Sn transport theory code suite similar to WIMS (Reference 4), both with a JEF2.2 based nuclear data library. All methods predicted positive temperature coefficients of reactivity.

The models only represent the fuelled regions of the core in detail. The structure of the fuel assembles above and below the fuel is represented approximately and the detectors are not modelled.

6.2 Comparison with Measurements

Figures 10 to 15 show the measured temperature coefficients from each configuration along with theoretical predictions. The predictions are subject to stochastic uncertainty of the order of 15% for MONK and 5% for MC21. The MONK calculations used WIMS format multi-group nuclear data.

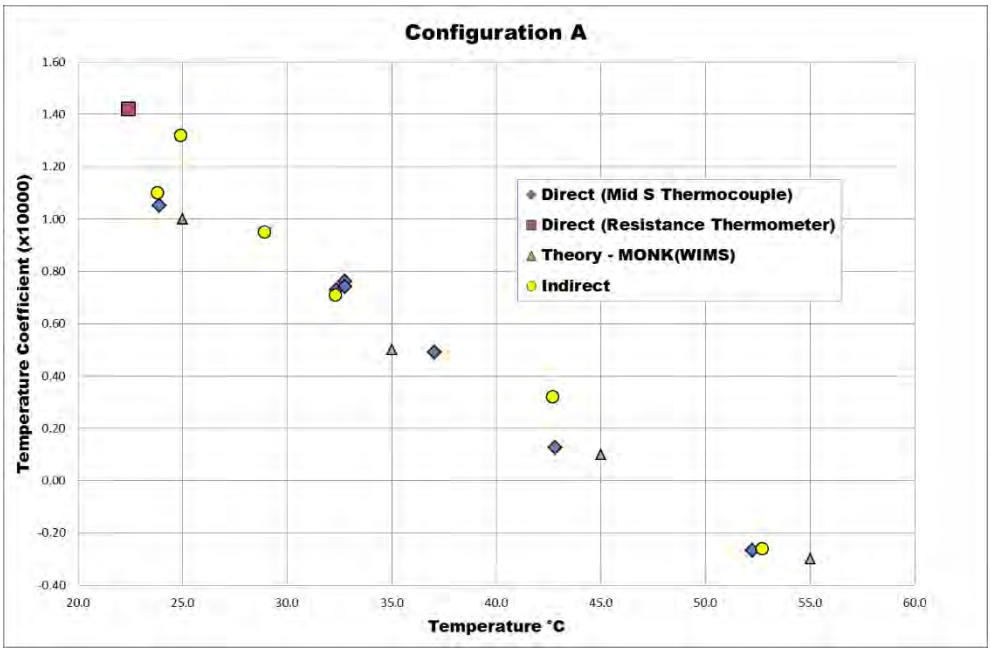

Figure 10 Configuration A, Temperature Coefficient v Temperature

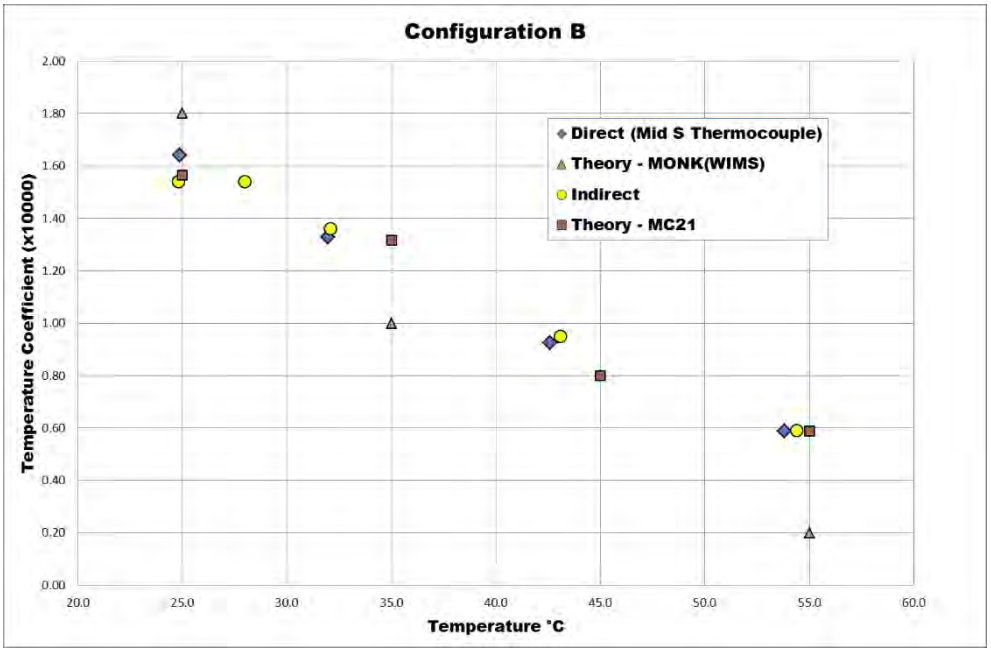

Figure 11 Configuration B, Temperature Coefficient v Temperature

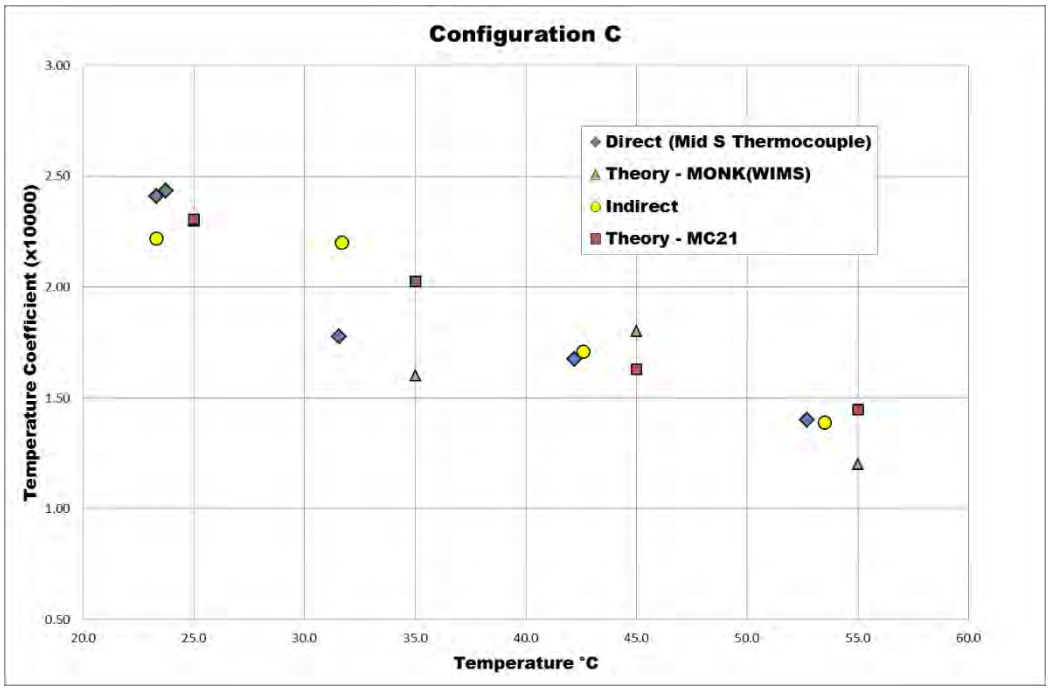

Figure 12 Configuration C, Temperature Coefficient v Temperature

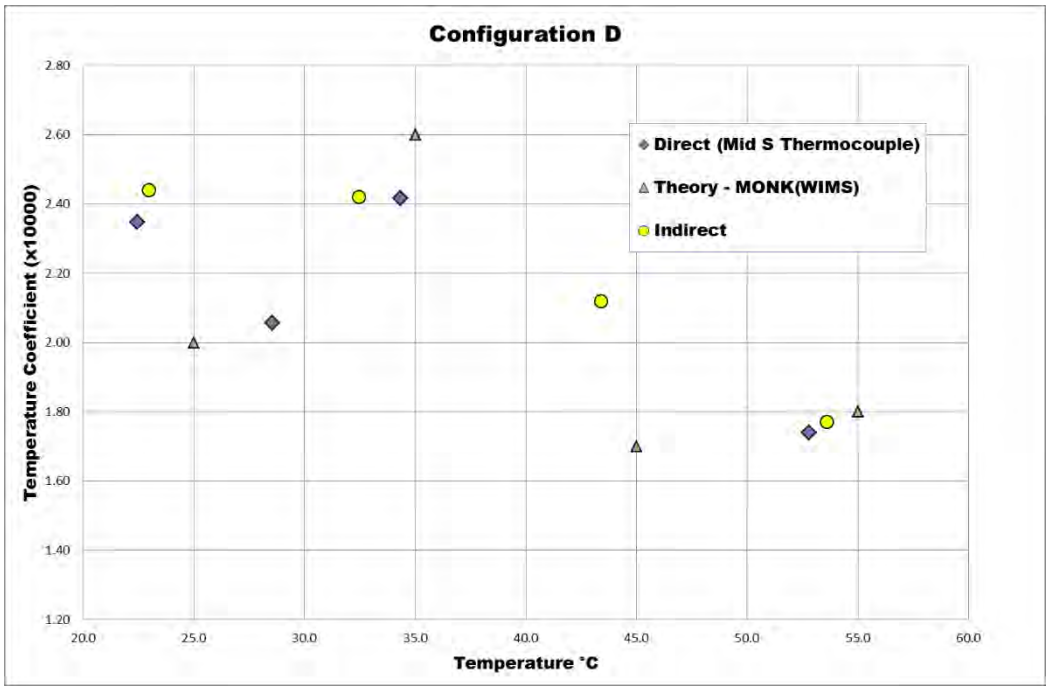

Figure 13 Configuration D, Temperature Coefficient v Temperature

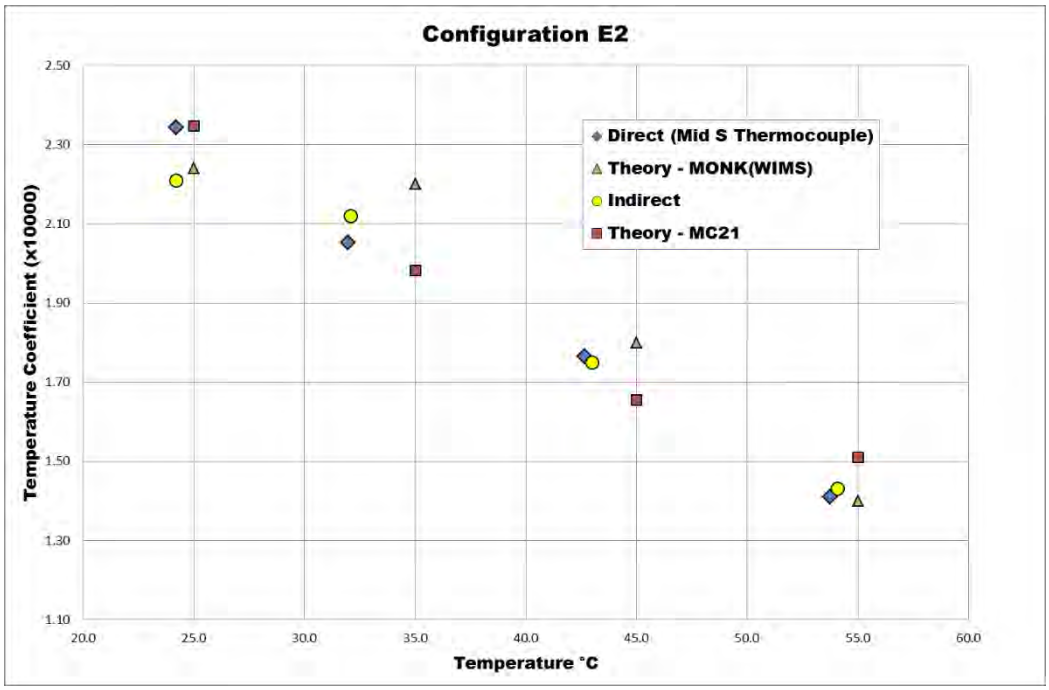

Figure 14 Configuration E2, Temperature Coefficient v Temperature

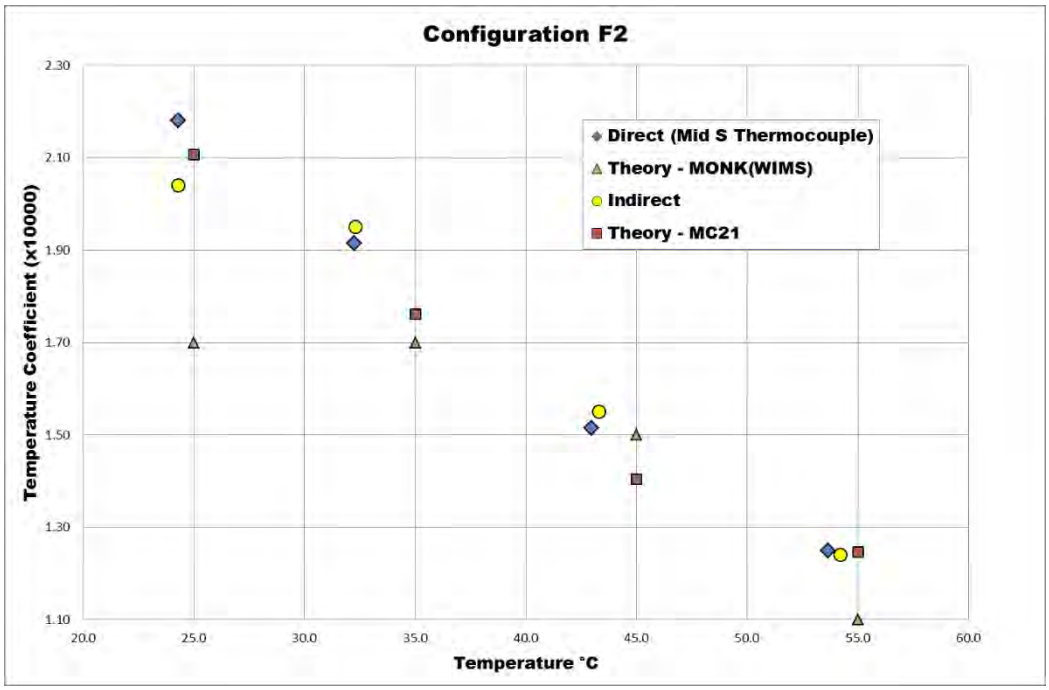

Figure 15 Configuration F2, Temperature Coefficient v Temperature

7 Discussion

7.1 Experimental Observations

A number of points of interest were noted during the experimental programme, as follows:

- In some cases (see shaded diamonds in Figures 3 to 8 at low temperatures, particularly Figure 3 and Figure 8) it was noticed that there was a difference in critical heights between the initial criticality and subsequent reactor operations. This was attributed to the presence of the fission chambers adjacent to the fuel assemblies in the initial reactor operation of each configuration and confirmed by subsequent measurements. This had not been observed for previous Neptune cores and is

attributed to the thermal flux peaking in the effective gap between the two fuel regions.

- It was necessary to re-instate the heating and cooling system that had not been used for many years. An assessment using modern safety methods revealed hazards that had (presumably) not been considered significant by the original designers, this resulted in the cooling part of the circuit remaining isolated.

- Occasional bubbles from the heating system were observed emanating from under the core base plate while heating. These were assessed as having negligible reactivity effect and no disturbances of the neutron detector signals were observed.

- Nine thermocouples were placed at different positions adjacent to the fuel assemblies. These indicated that the moderator temperature was fairly uniform.

7.2 Positive Temperature Coefficients

The measured positive temperature coefficients are relatively large in magnitude. It was noted during the design of the experiments that the presence of fixed neutron poisons within or adjacent to the fuel generally destroys the effect. This agrees with previous experience in the criticality assessment of storage racks with flux traps, which showed a positive temperature coefficient if the absorber material forming the flux trap was absent.

Note that both methods of deriving the temperature coefficient use non-zero values of reactivity obtained from the reactivity meter. Thus there is a dependence on the delayed neutron data used in the meter to solve the inverse point kinetics equation. Current perception is that this leads to an over-estimate of reactivity by a few percent as modern evaluations of the delayed neutron fraction are lower than that hard-wired into the reactivity meter.

Reference 1 indicates that the positive coefficient has two main contributions, from the increased neutron coupling between the two fuel assemblies as the water density decreases (although the overall leakage increased with temperature) and from the detail of the thermal neutron scattering and hence neutron spectrum and associated parasitic absorption. The measurement does not separate the effects but the reasonable agreement with prediction suggests that both are fairly well calculated by modern codes and data.

8 Conclusion

Positive temperature coefficients of reactivity have been measured for a number of rack-like configurations of light water moderated uranium fuel in the Neptune facility. Reasonable agreement is obtained with predictions made using Monte Carlo codes used for reactor physics and criticality assessments.

References

1 Michael L Zerkle and Thomas E Copinger, Evaluation of an Unexpected Reflector Temperature Effect for Water-Isolated Array Configurations, International Conference on Nuclear Criticality and Safety (ICNC 2015), 2015, Charlotte, North Carolina, September 13-17.

2 D P Griesheimer et al, MC21 v 6.0 – A Continuous-Energy Monte Carlo Particle Transport Code with Integrated Reactor Feedback Capabilities, Ann. Nuclear Energy, 76, pp. 29 – 40 (2015).

3 MONK – A Monte Carlo program for nuclear criticality safety and reactor physics analyses, answerssoftwareservice.com/monk

4 WIMS – A general purpose Reactor Physics Program for Core Physics Calculations, answerssoftwareservice.com/wims

FUTURE EXPERIMENTAL PROGRAMMES IN THE CROCUS REACTOR

V. LAMIRAND, M. HURSIN, P. FRAJTAG, A. PAUTZ
Laboratory for Reactor Physics and Systems Behaviour (LRS)
École Polytechnique Fédérale de Lausanne (EPFL)
CH-1015 Lausanne – Switzerland

M. HURSIN, G. PERRET, O. PAKARI, A. PAUTZ
Laboratory for Reactor Physics and Systems Behaviour (LRS)
Paul Scherrer Institut (PSI)
CH-5232 Villigen – Switzerland

ABSTRACT

CROCUS is a teaching and research zero-power reactor operated by the Laboratory for Reactor Physics and Systems Behaviour (LRS) at the Swiss Federal Institute of Technology (EPFL). Three new experimental programmes are scheduled for the forthcoming years.

The first programme consists in an experimental investigation of mechanical noise induced by fuel rods vibrations. An in-core device has been designed for allowing the displacement of up to 18 uranium metal fuel rods in the core periphery. The vibration amplitude will be 6 mm in the radial direction (±3 mm around the central position), while the frequency can be tuned between 0.1 and 5 Hz. The experiments will be used to validate computational dynamic tools currently under development, which are based on DORT-TD and CASMO/S3K code systems.

The second programme concerns the measurement of in-core neutron noise for axial void profile reconstruction. Simulations performed at Chalmers University have shown how the void fraction and velocity profiles can be reconstructed from noise measurements. The motivation of these experiments is to develop an experimental setup to validate in-core the method in partnership with Chalmers University.

The third experimental programme aims at continuing the validation effort on the nuclear data required in the calculation of GEN-III PWR reactors with heavy steel reflectors. This is a collaboration with CEA Cadarache that extends the results of the PERLE experiments carried out in the EOLE reactor at CEA. Scattering cross sections at around 1 MeV will be studied separately by replacing successively the water reflector by sheets of stainless steel alloy and pure metals – iron, nickel, and chromium. Data will be extracted from the measured flux attenuation using foils in the metal reflector and from the criticality effects of these reflectors.

In parallel to the three reactor experiments, we develop in-core detectors and measurement systems. Following the last development of a neutron noise measurement station in pulse mode, a second neutron noise station in current mode is being designed. In current mode the reactor can be used at higher power without dead time effects. It allows faster measurement time or lower results uncertainties. Finally, a joint development of a full new detection system based on chemical vapour deposited (sCVD) diamond has been started with the CIVIDEC instrumentation start-up company. A first prototype has been tested in November 2015 in CROCUS. One of the main purposes is to work on the discrimination of gammas, thermal

and fast neutrons for demonstrating the interest of this detector type in a mixed neutron-gamma field.

1. Introduction

This last decade, the CROCUS reactor operated by the LRS at EPFL was primarily used for teaching purposes. Only a few research collaborations with the Paul Scherrer Institute (PSI) were carried out on safety analysis [1] and neutron noise measurements [2]–[5]. After the closure of the PROTEUS research reactor at PSI in 2011, CROCUS was and remains as of today the only zero-power reactor in Switzerland. As of national interest, PSI and EPFL agreed to develop new research experimental programmes in the CROCUS reactor. An extensive review of possible experiments was carried out in 2015 [6] and resulted in the selection of three new experimental programmes. From their design, the programmes were carried out in the framework of national and international cooperations with renowned research institutes and universities, such as PSI, CEA and Chalmers University, which pledge for their usefulness for the international community. In parallel to these experimental programmes and supporting their needs, the LRS initiated the development of new instrumentations and measurement methods. This article presents in turn CROCUS, the selected experimental programmes and the activities to develop the reactor instrumentation and measurement methods.

2. The CROCUS reactor

CROCUS is an experimental zero-power reactor, uranium-fuelled and water-moderated, mainly dedicated to teaching radiation and reactor physics [7], [8]. It is licensed for operating at 100 W, i.e. ~$2.5 \cdot 10^9$ $n.s^{-1}$ at the core centre. Power is controlled either by water level using a spillway, or two B_4C absorber control rods, with an accuracy of ±0.1 mm (equivalent to approximately ±4 pcm) and ± 1 mm respectively. It operates at room temperature using a controlled water loop with secondary and tertiary circuits, two heat exchangers and an electrical heater.

The core is located in an aluminium vessel of 130 cm diameter and 1.2 cm thickness (see Fig 1). It is filled with demineralised light water used as both moderator and reflector. Its active part has the approximate shape of a cylinder of about 60 cm in diameter and 1 m in height. It consists of two interlocked fuel zones with square lattices of different pitches:

- an inner zone of 336 UO_2 rods with an enrichment of 1.806 wt.% and a pitch of 1.837 cm,
- an outer zone of 172 U_{metal} rods in nominal configuration, 0.947 wt.% and 2.917 cm,
- a water gap between the two zones because of the two different pitches.

Both uranium fuels consists of a 1-m pile of cylindrical pellets cladded in aluminium. The rods are maintained vertically by two octagonal aluminium grid plates spaced 1 m apart. The grids have a 0.5-mm cadmium layer to limit axial neutron leakage, with the active zone of the fuel starting above the lower cadmium layer.

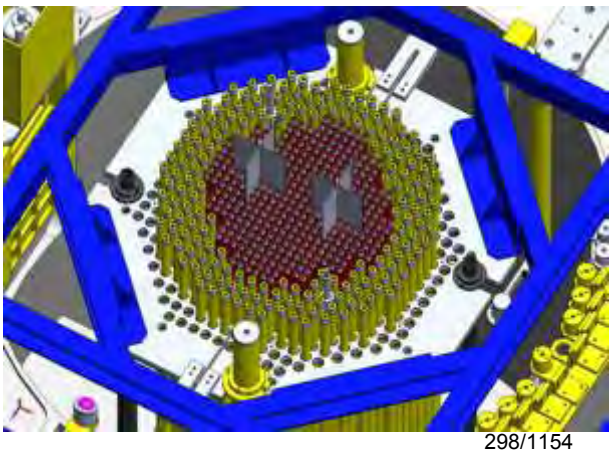

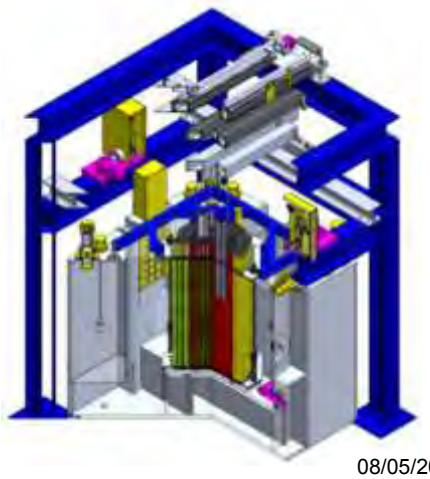

Fig 1: Top view of CROCUS core with fuel rods and systems such as cruciform safety blades and control rods (left); cross-section view of the full reactor with core and structures (right).
The six independent safety systems consist of two cruciform-shaped cadmium blades and four expansion tanks. The safety blades are held by electromagnets for top to bottom gravity insertion. The expansion tanks trap air when valves are closed, allowing a fast drop of the water level when opened. Any of these systems allow shutdown within less than a second.

3. New experimental programmes in CROCUS

3.1. COLIBRI experiments - Investigation of mechanical noise induced by fuel rod vibrations

The motivation for this investigation is the increased amplitudes in the neutron noise distributions recorded in ex/in-core detectors that have, in recent years, been observed during normal operation conditions in Siemens pre-Konvoi type of PWR reactors. Several potential explanations have been put forward, but no definitive conclusions could yet be drawn. Among others, changes in fuel assembly vibrations patterns, due to recent modifications of assembly structural designs, were pointed out as a possible primary cause. Such mechanical noise is suspected to arise from vibration of groups of fuel assemblies.

In this context, the aim of the COLIBRI programme is to carry out rod vibration experiments in CROCUS with different numbers of rods and different displacement amplitudes and frequencies. The vibration amplitude will be 6 mm in the radial direction (±3 mm around the central position), while the frequency can be tuned between 0.1 and 5 Hz, i.e. the frequency range in which the neutron flux fluctuations are most pronounced. A device meeting these requirements has been designed and manufactured (Fig 2). A first test has been carried out of pile in January 2016 with dummy fuel rods. The device allows oscillating single or groups of up to 18 fuel rods simultaneously.

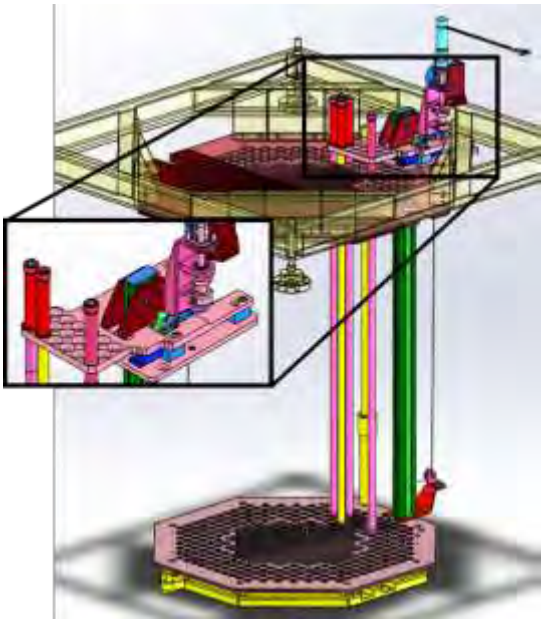

Fig 2: CROCUS Oscillator for Lateral Increase Between u_m Rods and Inner zone (COLIBRI).

Preliminary CASMO and MCNP calculations were performed to dimension the system. Moving 18 U_{metal} rods in CROCUS in the radial direction by ± 3 mm resulted in a reactivity change of ± 8 pcm with a 3 pcm uncertainty. Such a perturbation translates into a neutron

flux variation that is large enough to be measured and interpreted with standard noise post-processing techniques. Considering for instance cross-power spectral density technique (CPSD), such a perturbation will generate a Dirac peak at the frequency of oscillation whose amplitude is about three times larger than that due to neutron noise – as measured in previous experiments [2].
The programme is planned to start in summer 2016. The safety assessment was performed and the licensing process will be started after the test phase with dummy fuel rods. In parallel to this experiment, computational dynamic tools – based on DORT-TD and CASMO/S3K – are currently developed at LRS to help understand the source of the additional amplitude of the noise. The experiments planned at CROCUS will be used for the first validation of the code.

3.2. VOID - Void fraction determination using neutron noise measurements

The measurement of in-core neutron noise for axial void and velocity profiles reconstruction has been demonstrated theoretically at Chalmers University assuming an idealised 1D bubble distributions measurements [9], [10]. The motivation of these experiments is to develop a setup to validate experimentally the method in-core in collaboration with Chalmers University.

The method will be tested in clean conditions in CROCUS. A square Plexiglas tube of 5x5 cm^2 located at the periphery of the core will be filled with a known void density. The axial void profile is controlled thanks to nozzle injecting air bubbles at several different elevations (see Fig 3). The airflow rate at the different elevations will be adjustable to reproduce several axial void profiles of interest – such as that of a BWR with 80 % void at the top of the channel. We will measure the void distribution at five axial elevations using the neutron noise measurement station developed at LRS [2]. The results will be compared with the same void profiles measured in a copycat channel outside of the core using standard techniques for two-phase flow visualization, like X-ray imaging.

After designing the experiments and purchasing the required hardware components last year, the safety case for this experiment will be submitted to the authorities this year. Preliminary calculations with MCNPX showed that the increase of reactivity due to an inadvertent filling of the tube (worst case scenario considering it fully voided at first) is lower than the +20 pcm excess reactivity operation limit, which should be no problem from a safety point of view.

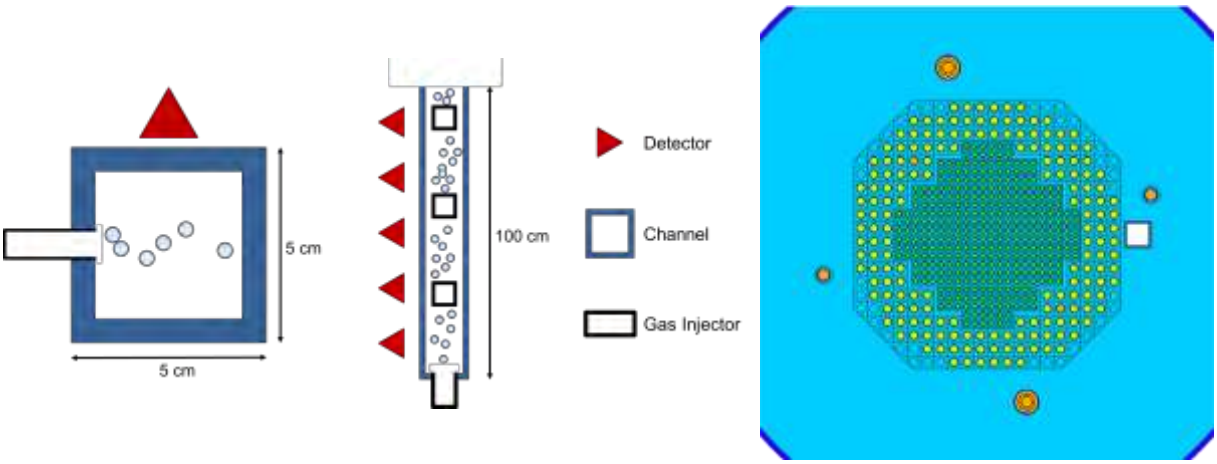

Fig 3: Top and side view of the bubbling channel (left) and location in the reflector of the CROCUS reactor (right).

3.3. PETALE experimental programme - Qualification of reflector materials for GEN-III reactors

CEA Cadarache performed an experimental programme in the EOLE reactor – PERLE – whose main purpose was to validate the nuclear data required in the calculation of GEN-III PWR reactors with heavy steel reflectors and to characterise reactor parameters such as reflector savings [11]. The PERLE experiments featured a large stainless steel buffer around a UO_2 core. Reactivity effects, reaction rates in the pin at the interface of the core and the reflector, and attenuation in the stainless steel block were measured. The latter measurements were carried out with different foils and fission chambers to assess the attenuation of the flux over different energy domains, which is sensitive to the elastic and inelastic cross-section of ^{56}Fe. These experiments showed that the ^{56}Fe nuclear data were rather well predicted in JEFF-3.1.1 and that optimized variance-covariance files could be issued.

In collaboration with CEA, the PETALE experiment in the CROCUS reactor aims to continue the validation effort on the ^{56}Fe cross-sections and its resonant behaviour and to extend the validation to the Ni and Cr isotopes by studying separately their scattering cross-sections around 1 MeV. To this end, the neutron attenuation in sheets of various thicknesses located close to the CROCUS fuel will be measured using dosimeters (foils) and possibly fission chambers. In addition, reactivity worth will be measured by the change of water level necessary to reach criticality.

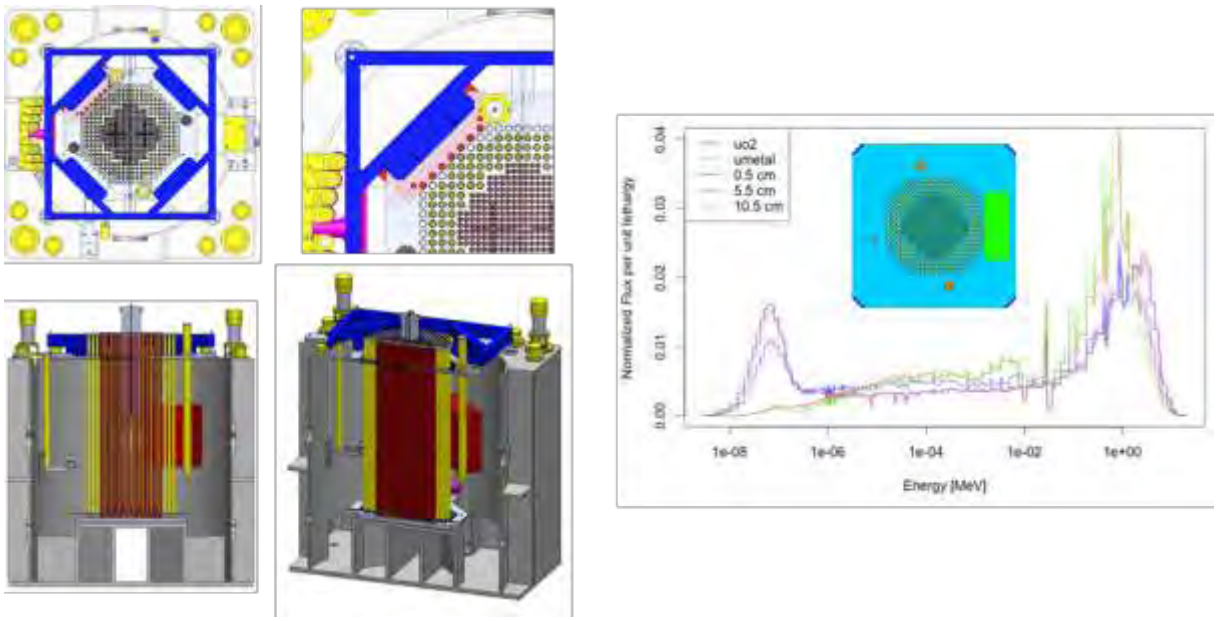

Fig 4: Top and side view of the CROCUS reactor with the positioning of the reflector sheets in red (left) and flux per unit lethargy at different location in the reflector sheets and in the UO_2 and U_{metal} pins (right).

The system to position the sheets is currently being designed. The system will allow positioning with high precision up to eight 30×30×2 cm^3 sheets next to the reactor core to maximise the flux (Fig 4 - left). The total thickness is up to 16 cm, which is representative of the optimal 20−cm reflector thickness in nuclear power plants. The system is located in CROCUS water reflector but is filled with air for the flux attenuation in the sheets to remain unperturbed. The sheets are manufactured from stainless steel, pure Fe (99.85%), Ni (99.7 %), and Cr (99.95 %) and were purchased in 2015. Activation foils will be located between the sheets. Their positions need to be well known because of the strong flux gradient.

In addition, several aspects of the PETALE experiments were investigated with MCNP in 2015. The reactivity effects resulting from the insertion of the sheets were shown to be well below the operating limit of 200 pcm: the larger reactivity worth (iron sheets) is +45 pcm. The flux level and spectra and the activity of foils of interest have been assessed (Fig 4 - right). Results showed that despite the low power of CROCUS, the activity in most foils sensitive to the thermal energy range is high enough to be measured with the LRS-EPFL HPGe stations. Regarding dosimeters with very low activity, due to the limited fast flux component in CROCUS, other possibilities were prospected, e.g. counting in CEA remote low-activity laboratories.

4. Development of measurement methods and new instrumentation

4.1. Neutron noise measurement in current mode

Neutron noise measurement techniques were developed in collaboration with swiss*nuclear* and PSI and applied in CROCUS. The acquisition was performed in pulse mode with BF_3 detectors and the data stored in multichannel scalers and post-processed to yield the Feynman-α and Power Spectral Density curves [2]–[5]. An inherent limitation of the pulse mode acquisition is the dead time of the detector at high count-rate, which set a lower limit on the measurement time. Acquisitions in current mode bypass this limitation by observing the current oscillations around a mean value without isolating each single detection event. The mean current and its variations need to be read with high precisions – typically in the range of 1 nA to 1 µA. Generally the continuous and fluctuating parts of the current are amplified and converted into voltage signals before being analysed, similar to what is performed for the pulse mode acquisitions.

The project aims at building the measurement station in current mode, testing it in the CROCUS reactor and comparing its results with the previous measurements performed in pulse mode. The first stage is concerned with the definition of the specifications of the amplifier (gain, bandwidth, range of input and output signals, etc.), and the definition of the measurement set-up (detector types, location of detectors, power of the reactor, etc.) [12].

MCNP simulations were performed for 1 g ^{235}U fission chambers (Photonis CFUL01) and ^{3}He detectors located in periphery of the CROCUS core and for four BF_3 detectors located in the periphery and control rod positions that were used during the pulse mode measurements (see Fig 5). Based on the thermal efficiency of the detectors and the impinging flux determined in the MCNP simulation the power needed to have a measurable current and Power Spectral Density curve were estimated. As an example, to achieve a current in the detector of 100 nA – typical value obtained in previous experiments – a power level of 0.3 W was sufficient for the CFUL01 detector, whereas a power of 15 W and 30 W were required for the ^{3}He and BF_3 detectors. The corresponding PSD levels were $2.1.10^{-20}$, $2.8.10^{-22}$ and $1.2.10^{-20}$ A^2/Hz for the CFUL01, ^{3}He and BF_3 detectors, respectively. These levels need to be higher than the level coming from the background noise to have a sufficient signal-to-noise ratio. Values for the required power to yield sufficiently high currents and PSD levels will be used to dimension the amplifier and select the measurement set-up.

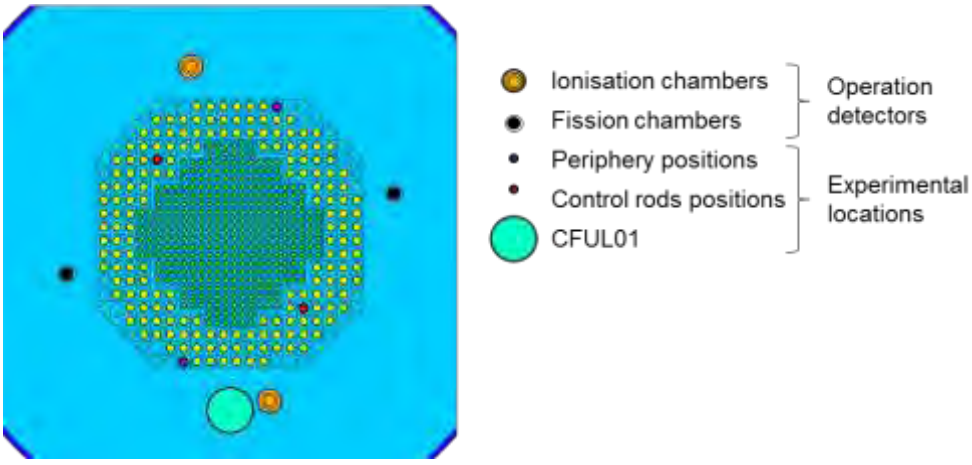

Fig 5: CROCUS model with considered detector locations for neutron noise measurement in current mode.

4.2. sCVD diamond detector and acquisition system

Chemical vapour deposited (sCVD) diamond detectors are currently under study in the nuclear community (e.g. [13]). Their fast response, their ability to withstand high irradiation fluxes and additionally the envisaged possibility to perform simple neutron spectrometry, make them good candidates for in-core measurement. [14]–[16] The LRS started the joint development of a full new detection system based on this material with the CIVIDEC start-up. A first prototype was tested in November 2015 in CROCUS (see Fig 6). The campaign results will be published early 2016. One of the main purposes of the future experiments is to work on the discrimination of gammas, thermal and fast neutrons for demonstrating its possible use in a mixed radiation field like that of CROCUS.

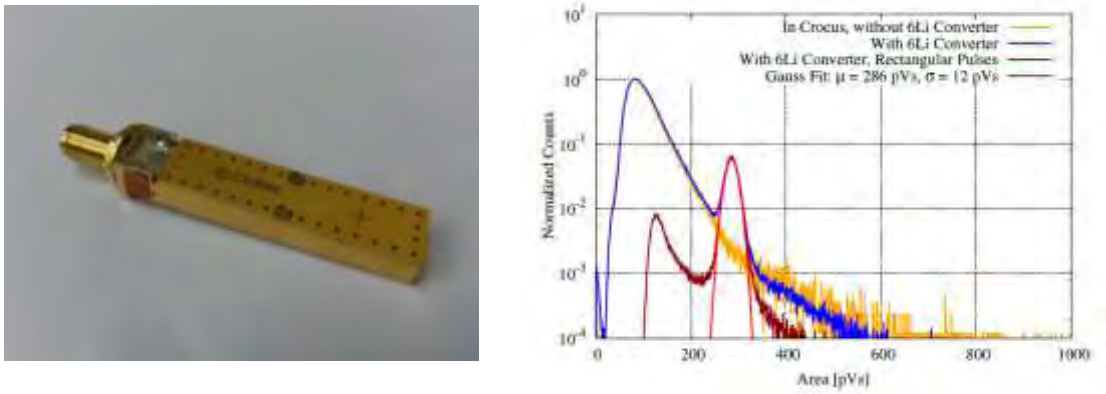

Fig 6: Diamond detector manufactured by CIVIDEC (left) and example of pulse shape discrimination based on measurements in CROCUS (right).

5. Conclusion

In the last decade, the CROCUS reactor was primarily used for teaching purposes. After the closure of the PROTEUS research reactor, it became the only remaining research reactor in Switzerland. As a result, and to keep experimental reactor physics competence in Switzerland, the Laboratory for Reactor Physics and Systems Behaviour at PSI and EPFL decided to increase research activities in CROCUS. In parallel to the existing research experiments for safety analysis and neutron noise measurement, the LRS selected three new experimental programmes. The programmes are related to neutron noise theory, measurements and applications, and to nuclear data for reactor technology. These programmes benefit from strong interactions with national and international research institutes and universities. The first programme will start by the end of 2016, alongside the development of new instrumentation. This effort supports the nuclear competence sustainability in Switzerland and provides a rare place for experiments in zero-power reactors in Europe.

6. References

[1] A. Rais, D. Siefman, G. Girardin, M. Hursin, and A. Pautz, “Methods and Models for the Coupled Neutronics and Thermal-Hydraulics Analysis of the CROCUS Reactor at EFPL,” *Sci. Technol. Nucl. Install.*, vol. 2015, 2015.

[2] V. Roland, G. Perret, G. Girardin, P. Frajtag, and A. Pautz, “Neutron noise measurement in the CROCUS reactor,” in *Proc. IGORR 2013*, 2013, pp. 2–7.

[3] G. Perret, “Delayed Neutron Fraction and Prompt Decay Constant Measurement in the MINERVE Reactor using the PSI Instrumentation,” in *ANIMMA 2015*, 2015.

[4] G. Perret, G. Girardin, P. Frajtag, and M. Hursin, “Decay constant and delayed neutron fraction measurements in CROCUS,” TM-41-14-02, 2014.

[5] G. Perret, “Delayed neutron fraction and generation time measurements at the zero-power reactor MINERVE - PSI results,” TM-41-14-21, 2015.

[6] V. Lamirand, G. Perret, M. Hursin, P. Frajtag, and A. Rais, “Experimental prospects of the LRS,” RT-100-113-15-02, 2015.
[7] J. M. Paratte, R. Früh, U. Kasemeyer, M. a. Kalugin, W. Timm, and R. Chawla, “A benchmark on the calculation of kinetic parameters based on reactivity effect experiments in the CROCUS reactor,” *Ann. Nucl. Energy*, vol. 33, no. 8, pp. 739–748, May 2006.
[8] U. Kasemeyer, R. Früh, J. M. Paratte, and R. Chawla, “Benchmark on Kinetic Parameters in the CROCUS Reactor,” in *Volume IX*, no. 4440, OECD, Ed. 2007.
[9] V. Dykin and I. Pazsit, “Simulation of in-core neutron noise measurements for axial void profile reconstruction in boiling water reactors,” *Nucl. Technol.*, vol. 183, pp. 354–366, 2013.
[10] G. Kosaly, “Noise Investigations in Boiling-Water and Pressurized-Water Reactors,” *Prog. Nucl. Energy*, vol. 5, no. 1979, pp. 145–199, 1980.
[11] C. Vaglio-Gaudard, A. Santamarina, P. Blaise, O. Litaize, A. Lyoussi, G. Noguère, J. M. Ruggieri, and J. F. Vidal, “Interpretation of PERLE Experiment for the Validation of Iron Nuclear Data Using Monte Carlo Calculations,” *Nucl. Sci. Eng.*, vol. 166, pp. 89–106, 2010.
[12] O. Pakari, “Neutron noise measurement in current mode,” Semester project ETHZ/EPFL, 2015.
[13] P. Kavrigin, P. Finocchiaro, E. Griesmayer, E. Jericha, A. Pappalardo, and C. Weiss, “Pulse-shape analysis for gamma background rejection in thermal neutron radiation using CVD diamond detectors,” *Nucl. Inst. Methods Phys. Res. A*, vol. 795, pp. 88–91, 2015.
[14] M. Angelone, M. Pillon, G. Prestopino, M. Marinelli, E. Milani, C. Verona, G. Verona-Rinati, G. Aielli, R. Cardarelli, R. Santonico, R. Bedogni, and A. Esposito, “Thermal and fast neutron dosimetry using artificial single crystal diamond detectors,” *Radiat. Meas.*, vol. 46, no. 12, pp. 1686–1689, 2011.
[15] M. Pillon, F. Andreoli, M. Angelone, A. Milocco, and R. Cardarelli, “Development of an high resolution neutron spectroscopy system using a diamond detector and a remote digital acquisition methodology,” *Fusion Eng. Des.*, vol. 89, no. 9–10, pp. 2184–2188, Oct. 2014.
[16] P. Lardon, C. Mer, P. Delacour, B. Bazin, D. Tromson, S. Normand, M. Nesladek, F. Foulon, and P. Bergonzo, “Investigations of high quality diamond detectors for neutron fluency monitoring in a nuclear reactor,” *Diam. Relat. Mater.*, vol. 15, no. 4–8, pp. 815–821, Apr. 2006.

THE INTERNET REACTOR LABORATORY PROJECT: STATUS AND EXPERIENCE OF THE ISIS RESEARCH REACTOR

F. FOULON
National Institute for Nuclear science and Technology
French Atomic Energy and Alternative Energies Commission (CEA)
91191 Gif sur Yvette, France

BORIO-DI-TIGLIOLE, A. VYSHNIAUSKAS-GOMEZ
Research Reactor Section, Division of Nuclear Fuel Cycle and Waste Technology,
Department of Nuclear Energy, International Atomic Energy Agency, 1400 Vienna, Austria

ABSTRACT

The International Atomic Energy Agency (IAEA) implements several international initiatives to support Member States in acquiring access to high quality nuclear education opportunities. Even though it does not replace the effectiveness of hands-on training, internet based education and training is becoming a cost-effective option for complementing academic and vocational education. The Internet Reactor Laboratory (IRL) project from the IAEA gives the opportunity to countries without research reactors to access reactor laboratories for the development of their human resources. For the implementation of the IRL project in Europe, the IAEA has been working with the French Atomic Energy and Alternative Energies Commission (CEA). Under the agreement signed between the IAEA and CEA, the ISIS reactor located at Saclay CEA Centre in France will carry out IRL experiments to institutions located in Africa and Europe. This paper provides the background and the status of the IRL project implementation at the ISIS reactor.

1. Introduction

The International Atomic Energy Agency (IAEA) implements several international initiatives to support Member States in acquiring access to high quality nuclear education opportunities. Even though it does not replace the effectiveness of hands-on training, internet based training and education has become a cost-effective option for complementing academic and vocational education. With this in mind, the IAEA has been working on the Internet Reactor Laboratory (IRL) project which aims at providing virtual access to research reactor experiments connecting, via the internet, an operating research reactor in a country with universities classes in other foreign countries.

For the implementation of the IRL project in Europe and neighbouring countries, the IAEA has been working with the French Atomic Energy and Alternative Energies Commission (CEA) and its integrated higher education institution, the National Institute for Nuclear Science and Technology (INSTN).

This paper gives an overview of the IRL project from the IAEA. It describes the INSTN's education and training activity on research reactors and in particular on the ISIS reactor. The paper presents the characteristics of the ISIS reactor and describes the broadcasting system implemented on the reactor for the IRL. It also describes the content of the internet-based reactor experiments that will be broadcasted from 2016, giving the status of the IRL project implementation on the ISIS reactor.

2. The IRL Project from the IAEA

The IAEA has various activities in the area of nuclear education and training for the development of the human capital using research reactors. The IAEA, mainly via the Peaceful Uses Initiative project 'Increasing the Global Supply of Nuclear Education and

Training Programmes Through Research Reactor Facilities' supported by US Department of State funds, is developing the IRL project which aims at providing virtual access to research reactor experiments, connecting, through the internet, an operating research reactor in a country (host reactor) with universities classes in other countries (guest institutions).

The IRL project is intended to increase the global supply of nuclear education based on the use of research reactors. It offers an additional option to access operating research reactors around the world and carry out education and training activities through the internet. Such a project delivers its maximum benefit to countries that are engaged in educating human capital for future nuclear programmes (power and non-power) but that do not have access to suitable research reactor facilities. The IRL project is aimed at advanced undergraduate or postgraduate level nuclear engineering or nuclear physics students. It is now in the final stage of its implementation in Europe (on the ISIS reactor, in France) and in South America (on the RA-6 reactor, in Argentina), while an extension in the Asia and Pacific region is foreseen.

For the implementation of the IRL project in Europe, the IAEA has been working with CEA since 2013. Based on the demonstrated experience of the INSTN in the area of nuclear education utilizing the ISIS training reactor, this reactor was identified as the candidate to act as the host reactor of the IRL project in Europe. From 2016, the reactor will provide internet-based reactor experiments to students from other countries in Europe and Africa. Currently, the countries participating in the IRL as guest institutions are Belarus, Lithuania, Tanzania and Tunisia.

3. INSTN's education and training activity

The INSTN was created in 1956 with the objective of providing students and professionals a high level of qualification in disciplines related to nuclear engineering. In this frame, the institute carries out education and training (E&T) programs on nuclear reactor theory and operation. From the very beginning, the INSTN's strategy has been to complete theoretical courses by training courses and laboratory works carried out on an extensive range of training tools that included a critical assembly, training reactors, instrumentation laboratories as well as, software applications, calculation codes and simulators.

From 1961 till 2007, the INSTN operated its own training reactor, ULYSSE, an Argon type 100 kW reactor. In 2007, the E&T activity was transferred on the ISIS research reactor, which went through a major refurbishment from 2004 till 2006 to ensure this activity.

Today, ISIS research reactor is an essential tool for the E&T programs organised by the INSTN from CEA. A large panel of training programs (duration ranging from 3 to 30 hours) are conducted on the ISIS reactor. They include:

- Fuel loading supervision (loading of the last 4 fuel assemblies)
- Approach to criticality (by moving up one control rod)
- Reactor start up and stabilization at low power
- Changes around criticality, manual and automatic control
- Core reactivity change related to experimental devices
- Study of the reactivity effect related to the local modification of the moderation factor
- Plotting a calibration curve (doubling time measurement, rod swap, …)
- Measurement of the total worth of a rod by the rod drop technique
- Study of a fast reactivity transient to show the role of the precursors on the reactor control
- Study of the temperature effects (Doppler, water expansion, temperature coefficient, self-stabilization)

- Study and setting of the neutron detection systems used for reactor control
- Cartography of the neutron distribution in the core
- Hands on the use of radiation protection equipment on the facility
- Reactor operation under the supervision of the instructor and reactor staff

The training courses are integrated both in academic degree programs and continuing education programs for professionals, which include:

- an international Master in Nuclear Energy held at the INSTN,
- a one year specialization course in Nuclear Engineering held at the INSTN,
- modules of Master's degrees from three Swedish universities,
- a 8 week qualifying course for the operators of research reactors,
- 1 to 2 week regular courses related to the principle, the operation, the safety and the neutronics of nuclear reactors,
- courses organized to respond to the specific need of the nuclear industry and nuclear programs (inspectors from the French regulator body, engineers from ENEL – Italy, project managers from EVN – Vietnam, young scientists from CTGPC – China, students from KAU – Saudi Arabia, professors from the Polish Universities - train the trainees program).

4. Description of the ISIS reactor and its broadcasting system

The ISIS research reactor is an open core pool type reactors, with a nominal power of 700 kW. The core (see Figure 1) contains 38 fuel assemblies, 6 control rods, 7 Beryllium assemblies, as well as 5 experimental cases. The MTR (Material Testing Reactor) type fuel, in silicide U3Si2Al form, is enriched at 19.75 %. Above the core a stainless steel chimney separates the water from the primary water loop from the rest of the pool. The reactor can be operated either in natural convection, the power being limited to 50 kW, or in forced convection. A gate, which is placed on one side of the chimney, can be removed to load or unload fuel assemblies or experimental devices between the pool and the core.

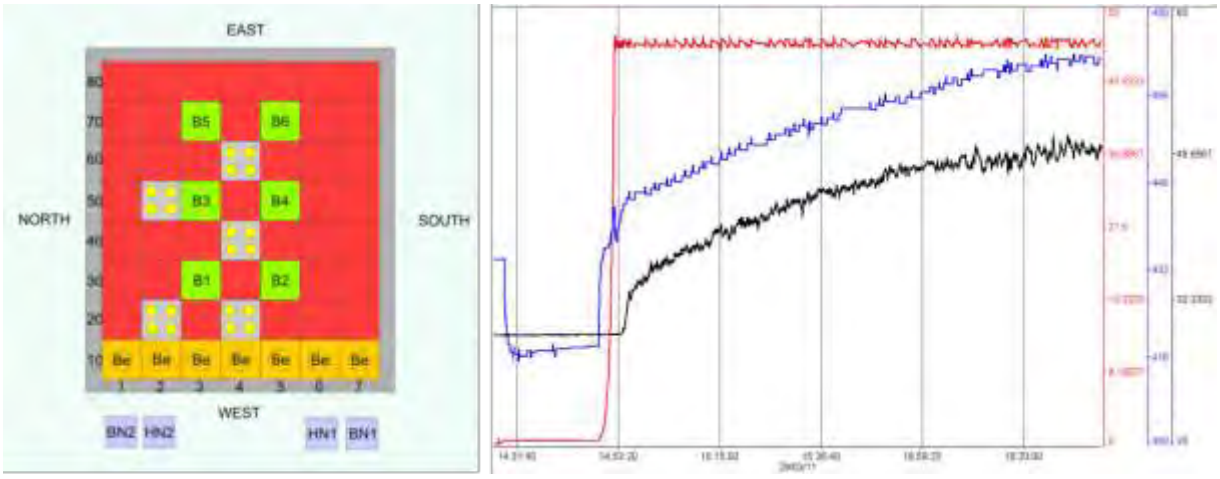

FIG. 1. Schematic of the core (left hand side) and histogram of the reactor power in red, position of the regulating rod in blue and water temperature in black (right hand side).

The control system and the control room of the reactor went through a major upgrade and refurbishment in 2006. A supervision system was specifically developed and the safety system was adapted to this specific activity. This supervision system shows the state and records the parameters of reactor. For each experiment, the parameters to be displayed to

the trainees are chosen by the lecturer. Figure 1 shows the histogram of the reactor power, position of the regulating rod and water temperature during the study of the temperature effect. It can be used to show and discuss the successive influence of the Doppler effect and water expansion effect on the critical position of the control rod. It can also be used to calculate the temperature coefficient of the reactor.

An important feature of training reactors is the ability for on-site trainees to operate the reactor under the guidance and supervision of the reactor staff, the ISIS reactor has been equipped for accompanied reactor operation.

In 2014, with the aim of enhancing the access to the practical courses carried out on the ISIS reactor, the INSTN integrated a videoconference system on the ISIS reactor. The decision to go for the transmission of only video signals out of the computer from the supervision system was dictated by security issues, i.e. to guaranty that no action can be conducted through internet on the control system of the reactor. Also the transmission of common video signal through a standard video system makes easy the reception and display of the information at the guest institutions.

The equipment implemented on the reactor includes a video conference system that can send in parallel two video signals. The schematic in Figure 4 shows the principle of the system that was implemented on the ISIS reactor.

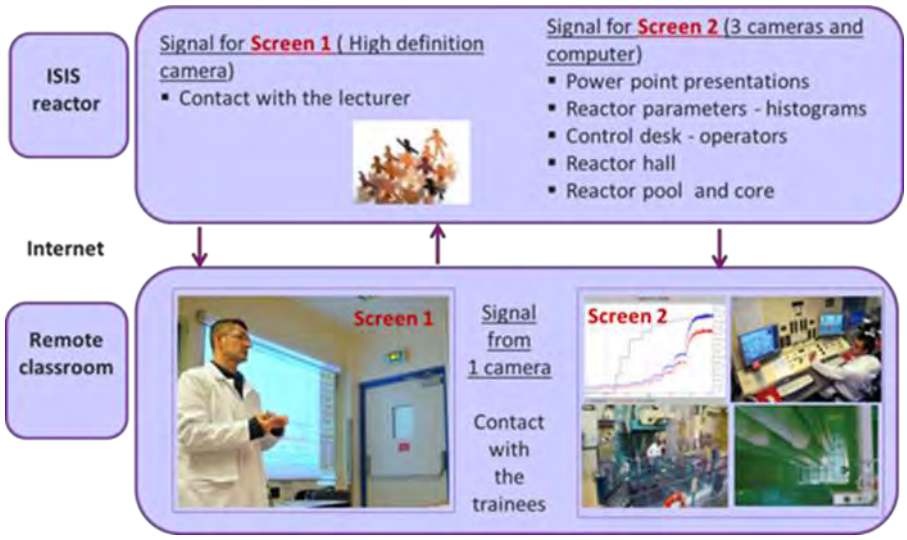

FIG. 2. Schematic representation of the video conference signal implemented on the ISIS reactor.

The first signal corresponds to the signal of the camera from the video conference system. This camera installed in the control room is the major link between the team at the host reactor and the trainees at the guest institution. The camera has pre-set positions allowing the camera to zoom at specific views (control desk, lecturer paper board, etc.) according to the needs of the experiment.

The second signal comes from an internet broadcast dedicated computer that receives four different video signals: the video signal from the slave computer of the supervision system and the video signals from three cameras installed on the facility and looking at the reactor hall, in the core and at the control desk. Concerning the video signal from the slave computer, it can be used to show the following information:

- pages from the supervision system used by the operator to follow the state of the different systems of the reactor (control rods, neutron detection systems, cooling system, safety system…),

- graphs from the supervision system showing the time evolution of selected parameters for each experiment,
- power point presentations,
- tables of selected data recorded by the supervision system,
- curves plotted using the recorded data after calculation,
- films to introduce or illustrate some experiments or phenomena.

Based on the particular experiment which is conducted, the host instructors can choose the images and information to be transmitted as a second video signal.

The two signals, from the camera of the videoconference system and from the internet dedicated computer, are broadcasted to students and trainees through the internet. Thus, from a remote classroom the lecturer and trainees are able to follow the parameters of the reactor and to interact with the reactor team (lecturer and operators) to conduct the experiment on the reactor.

5. Laboratories broadcasted in the frame of the project

In the frame of the IRL project, the ISIS reactor will perform and transmit every year five experiments, called ‘core experiments’, related to:

(1) fuel loading,

(2) approach to criticality and reactor start-up,

(3) reactivity effect of devices, rod calibration,

(4) study of a fast transient in reactivity, temperature effect, Operational limits and conditions,

(5) neutron detection systems, neutron flux mapping.

Each core experiment, with duration of three hours, will be broadcasted live from the ISIS reactor in parallel to the guest institutions involved in the project. Up to six guest institutions are expected to be able to join the experiments. In order to ensure the effectiveness of the laboratories, the host instructor in the ISIS control room will conduct the laboratory and interact both with the operating team of the reactor and with the guest instructor at each institution that will serve as the main interface with the students in the remote classroom.

6. Status of the project on the ISIS reactor

Currently, the IRL project is in its initial implementation stage in Europe and in Latin America, after several years of preparing legal agreements, including the procurement, delivery and installation of the equipment. The reactor experiments are expected to be broadcasted in the second half of 2016. In these two regions, the RA-6 reactor in Argentina and the ISIS reactor in France will be acting as the host reactors, respectively.

Concerning the project implementation in Europe, after the signature of the agreement between the IAEA and CEA in September 2014, the equipment necessary for the IRL has been installed on the ISIS reactor at the end of 2014. During the year of 2015, the legal agreements between the IAEA and the guest institutions were finalized. All agreements have been signed with project counterparts in Belarus, Lithuania, Tanzania and Tunisia. Within the majority of these agreements, the IAEA commits to provide financial support for the procurement of the equipment to the participating guest institutions.

As part of the agreement between the IAEA and the CEA, a training and orientation workshop for professors from the guest institutions was organized at CEA in October 2015.

The main objective of the workshop was to prepare the guest institutions for the first transmissions of the IRL experiments going through the following tasks:

- to provide on-site practical demonstration of the reactor experiments that will be broadcasted in order to familiarize the professors with the IRL experiments;
- to train the professors on how to deliver the IRL experiments within their academic courses (technical and pedagogical aspects
- to share information on existing academic programs both at the host institute (INSTN) and at the guest institutions;
- to share experience and lessons learned on how to integrate these experiments into nuclear engineering and, eventually, nuclear physics curricula;
- to discuss the technical and logistic issues related to the internet broadcasting system;
- to discuss and develop the timetable for the transmission of the experiments during the academic year 2015/2016.

The workshop was attended by one or two professors from each guest institutions and was leaded by five professionals from CEA. The professors invited to attend this consultancy meeting were those expected to prepare the students and to teach the IRL experiments within their academic programs.

The workshop was organized in such a way that, after a general presentation and visit of the ISIS reactor, the guest instructors attended and experienced the three first laboratories at the reactor, in the reactor hall or control room. This was a way for them to get familiar with the reactor characteristics, reactor operation, as well as with the recording and display of the reactor parameters carried out by the supervision system.

For the last two laboratories, the guest instructors attended the experiments in a video conference room next to the ISIS reactor. This was a way to train the guest instructors in having only the information broadcasted through internet for the delivery of the experiments at their guest institution. This test had a positive feedback. It showed that the information available through the internet connection together with the interactions between the host team and the guest instructors provided adequate information for the effectiveness of the IRL.

The workshop has been followed by connectivity tests carried out simultaneously from the ISIS reactor to the guest institutions, early in 2016. These will be followed by the broadcast of a first three-hour experiments in the first semester of 2016, before the five core experiments described in § 5 will be performed and broadcasted at the autumn 2016.

.

7. Conclusion

The IRL appears to be a powerful tool, complementary to the on-site reactor training courses, for the development of the human resources needed for nuclear programs. Keeping in mind that the IRL cannot replace real hands-on experimentation at a research reactor, the IRL is seen as a cost-effective way to expand the nuclear education for groups of students or trainees that would not normally have access to a research reactor during their education. It can also help states to better train and evaluate their human capital needs for ensuing future (research or power) reactor projects. After the IRL's implementation on the ISIS reactor in 2014, the performing and broadcasting of the IRL experiments from the ISIS reactor will start in 2016. This will contribute to the increase in the global supply of E&T on research reactor for the nuclear education and training programmes. The first test carried out delivering the experiments to the instructors from the guest instructors located in a remote video conference room has shown the effectiveness of the IRL experiments in getting an insight

into the reactor principles and operation. Thus the IRL is expected to provide a valuable contribution to the quality of the educational programmes at the guest institutions.


RRFM
EUROPEAN RESEARCH REACTOR CONFERENCE 2016
IGORR
BERLIN
13 - 17 March 2016
GERMANY

Safety

CHARACTERIZATION OF THE OPERATING STRATEGY AND SAFETY MARGIN AT NOMINAL WORKING CONDITIONS OF THE MADISON EXPERIMENTAL SYSTEM IN THE JHR RESEARCH REACTOR.

Y. WEISS
Rotem Industries LTD, Mishor Yamin, D.N Arava 86800, Israel

S. BOURDON, P. JAECKI, C. GONNIER, C. BLANDIN
French Atomic Energy Commission (CEA) - Cadarache Centre, France

ABSTRACT

The Jules Horowitz Reactor (JHR) is a high performance Material Testing Reactor (MTR) under construction in southern France (CEA Cadarache). JHR will host a set of fuel and material test facilities for the nuclear industry or other organizations. In the qualification studies domain, the MADISON test device **("Multirod Adaptable Device for Irradiation of experimental fuel Sample Operating in Normal conditions")** dedicated to qualify fuel and clad at nominal working conditions of two reactors types, Pressurized Water Reactors (PWR) and Boiling Water Reactors (BWR). The fuel channel diameter of the In-pile device is designed to test potentially any number of fuel samples, ranging from one to eight arranged in various geometry. This work will present the calculation results obtained with the fuel channel first design, of four fuel samples arranged in a row. The paper will briefly describe the JHR project, the objectives and the main characteristics of the test device for general background. Taking into account the design of Madison (with the first proposed fuel channel design, simulating the PWR case), the high-pressure loop and the low-pressure circuit parts were simulated using the CATHARE2 code and used to check the thermal-hydraulic performance and the consistency with the specifications. A set of calculations (parametric study) allowed to define the operating range of the loop (correlation was established to meet the chosen fuel channel working temperature, by adapting the control valves position) and to analyse the safety margin. It was found that the safety margin determined by the DNBR limit is greater than 1.3 for all range of operating conditions and that the proposed channel design is robust. The calculated CHF was performed with several updates of the Groeneveld Look Up Table (LUT) correlation. Working with the 2006 Groeneveld updated correlation the CHF value is 40% higher compared to the 1986 correlation. The work presents a non-dimensional correlation/law between the operating water temperatures at the inlet of the fuel channel and the flow partition at the main heat exchanger bypass. The paper will also present the studies dedicated to LOFA and LOCA accidental situations with the proposed design. These studies take benefit of two types of calculation: CATHARE2 code for the integrated system calculations and COMSOL for specific local phenomenon calculations.

1. Introduction

The Jules Horowitz Reactor (JHR) is a Material Testing Reactor (MTR) under construction at the CEA/Cadarache (France) and will be an important international user facility for R&D in support to the nuclear industry, research organizations, regulatory bodies and Technical Support Organization (TSO), and academic institutions [1], [2].

This facility based on a 100 MWth pool reactor compact core cooled by a slightly pressurized primary circuit. The core tank is located in the reactor pool. A typical reactor cycle expected to last 25 days, and CEA targets to operate the reactor 10 cycles per year. The nuclear facility comprises a reactor building with all equipment dedicated to the reactor and experimental devices and an auxiliary building dedicated to tasks in support to reactor and experimental devices operation.

The reactor building is designed to provide the largest experimental capacity possible with the largest flexibility. One-half of this building is dedicated to the implementation of equipment in support to in-pile irradiations. This corresponds to 700 m^2 over 3 floors for implementation of experimental cubicles and 490 m^2 over 3 floors for instrumentation and control equipment.

CEA is developing a set of test devices aiming at testing materials and fuels under irradiation [3]. More specifically, in the qualification studies domain, the MADISON test device **("Multirod Adaptable Device for Irradiation of experimental fuel Sample Operating in Normal conditions")** is dedicated to qualify fuel and clad in nominal working conditions of two reactors types, Pressurized Water Reactors (PWR) and Boiling Water Reactors (BWR. Such a family of experiments in the JHR will be devoted in priority to better understand mechanisms governing the current types of fuel sample behaviour and new ones during present or future nominal working conditions (chemistry; THy conditions, fuel burn up,…) [4].

Such experiments will allow characterizing fuel properties (mechanical properties, microstructures, fission gas release), it will allow performing comparisons of different fuel microstructures or performing re-irradiation of fuel samples before other tests (ramp tests for example). For the clad it will allow characterizing clad corrosion, creep phenomena, crud deposits. Acceleration in burn up aging of the fuel sample (for example by increasing the power density while reducing the fuel diameter) is another important objective of the device.

MADISON is developed with **IFE** team (Institute For Energy Technology in Norway), operating the **Halden boiling water reactor**, taking benefit of the experience of this institute in the design and operation of LWR experimental loop. It will allow performing experiments of high precision (follow up of fuel power, primary fluid thermal-hydraulics and chemical conditions). The in-pile test device is compatible with the systems available in the JHR to perform post-irradiation testing and examination on samples. The MADISON facility expected to be in operation just after the JHR commissioning.

This work will present the results obtained with the fuel channel first design, of four fuel samples arranged in a row. After the objectives of the test device and the device main characteristics, the paper will present the operation domain deduced from the parametric study, the steady state safety margins (DNBR) in the nominal range of operating conditions and some first main safety study scenarios regarding LOCA and LOFA for the system.

2. Device main characteristics

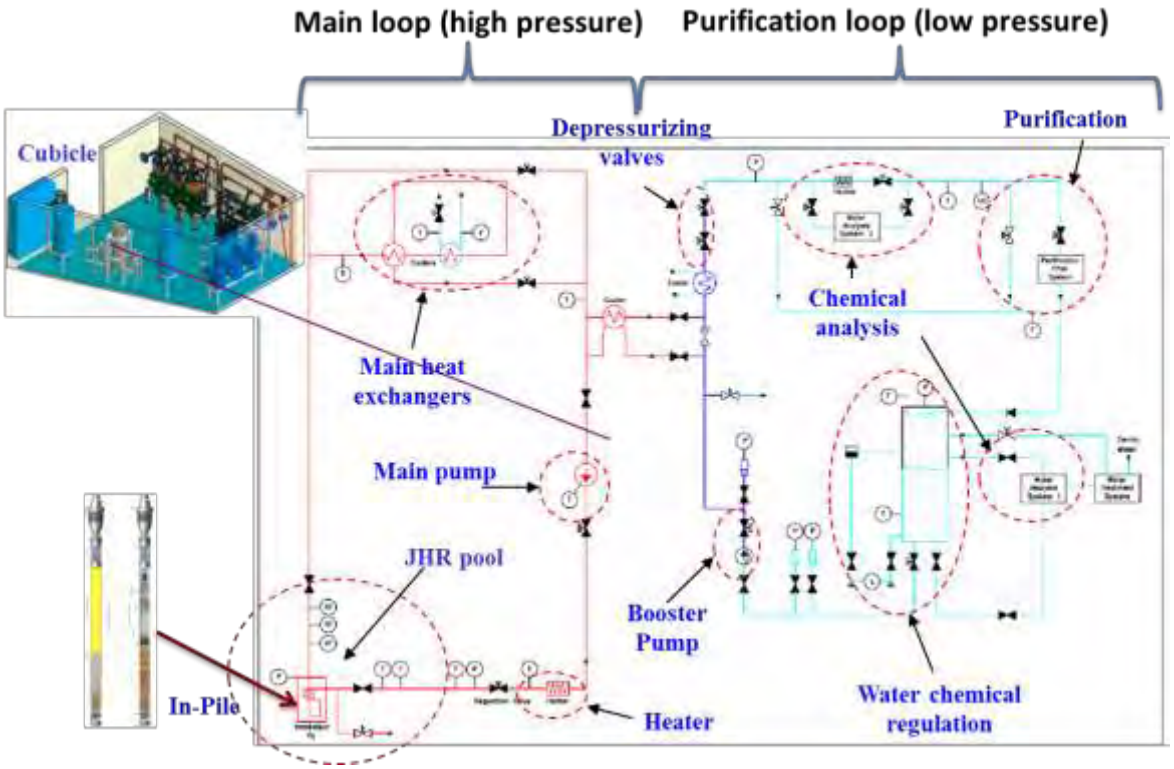

Figure 1, Schematic description of the MADISON system

The system can be divided in two major parts the in-pile device and the cubical as can be seen from Figure 1. The in-pile device contains the fuel samples and is located in a dedicated channel of the beryllium reflector in the reactor pool. The cubicle contains the high-

pressure circuit (heat exchangers, main pump, heaters, control valves and maintenance valves) of the loop and the low pressure purification and water treatment loop

2.1. In-pile components (in pool components)

The in-pile part of the device will be installed in a water channel of the reflector (see Figure 2). The in-pile device is fixed on the displacement system allowing a radial movement of about 45 cm. The power is therefore controlled by the distance between the sample and the core vessel.

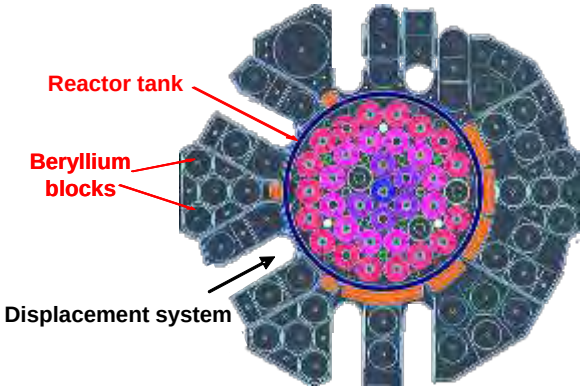

Figure 2, Location of the MADISON test device in the Berylium reflector.

The fuel channel diameter of the In-pile device is designed to potentially test any number of fuel samples ranging from one to eight arranged in different geometries.

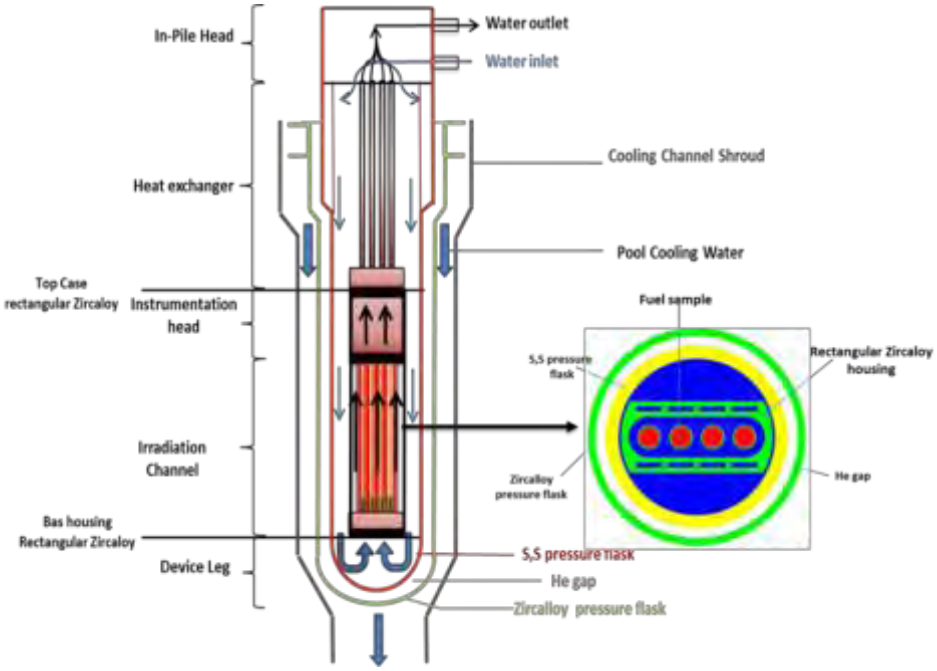

Figure 3, schematic description of the In-pile device.

As mentioned, the work will present the calculation results obtained with the fuel channel first design, of four fuel samples arranged in a row. Figure 3 presents the final design cross section of the fuel channel used in the schematic description of the in-pile part in the CATHARE2 model. The lower part of the device, with the smaller diameter, contains the fuel rods and is located under the neutron flux area.

The in-pile device consists in a double flask. The internal flask is made of stainless steel, while the outer flask is made with Zircaloy. The inner flask is a pressure flask designed to withstand the internal pressure and which characteristics allow to be representative of power plant conditions, while the outer flask is a second envelope whose functions are to form a gas gap and to serve as a radiation shield lowering the gamma heating power in the inner structures of the device. This gap is filled up with helium and plays the role of thermal insulation between the hot inner parts and the water of the pool surrounding the device. To detect potential leakage in the flasks the pressure in the gas gap is monitored. The gas gap is about 6 mm and enables to transfer heat toward the pool that can serve as a heat sink for accidental situations.
A sample holder at the centre of the device holds the fuel samples. A flow separation housing , made of Zircaloy, is installed in the pressure flask, forming two channels, a hot channel surrounding the fuel samples and a cold channel ("Downcomer") between the separator and the inner flask (see Figure 3). The forced flow from the cubicle is flowing down to the bottom of the device and returns upward cooling the fuel in the fuel channel in the inner part of the separation housing. From the fuel channel the hot cooling water passes through a heat exchanger to condense all the steam that can potentially formed in the fuel channel (specially for BWR applications of the test device), by exchanging heat with the down coming forced flow at the outer side of the separation housing . For simulating the PWR conditions, the operating range is 250°C to 320°C for the water temperature at the fuel channel inlet and the pressure is 155bar.

The outer flask is cooled by forced convection. The In-Pile device is connected to the reactor pool wall by flexible hoses and dedicated penetration instrumentation enables to connect the pipes to the cubicle.

2.2. The cubicle (out of pool components)

The cubicle contains the high-pressure circuit (Main and secondary heat exchangers, main pumps, heaters, control valves and maintenance valves) and the low-pressure purification loop. The purification loop consists of chemical treatment for the water in the system, preheating heat exchangers for the “feed and bleed” system, auxiliary feed water pumps and accumulators. The heat exchangers of the primary system are designed by a special arrangement of a two stage cooling, to reduce the high temperature gradients in construction materials.

2.3. Operating procedure and control

The three regulated parameters in the high-pressure loop are the water temperature at the fuel channel inlet, the pressure and the mass flow rate in the loop. The inlet temperature to the fuel channel is regulated by the flow-partition between the main loop heat exchanger and its bypass. A heater makes possible a final and more accurate adjustment of the inlet temperature. The loop pressure is regulated via a “feed and bleed” system allowing controlling the net flow rate exchange between the high-pressure circuit and the low-pressure circuit. The mass flow rate in the primary system is controlled by the pump bypass valve that can give any desired flow rate in the range between 0.4 kg/s to 0.8 kg/.

3. Characterization of the steady state operating condition

3.1. Operating strategy characteristics

A parametric study was performed by simulating the high-pressure loop and the low-pressure circuit parts using the CATHARE2 code. A set of calculations performed with different mass flow rate combinations, through the main heat exchanger and its bypass branch valves were conducted. For each fuel power, each total mass flow rate, and combinations of the valves setup (i.e. a given partition of the flow between the two branches), the calculation provided the channel inlet temperature of the water.

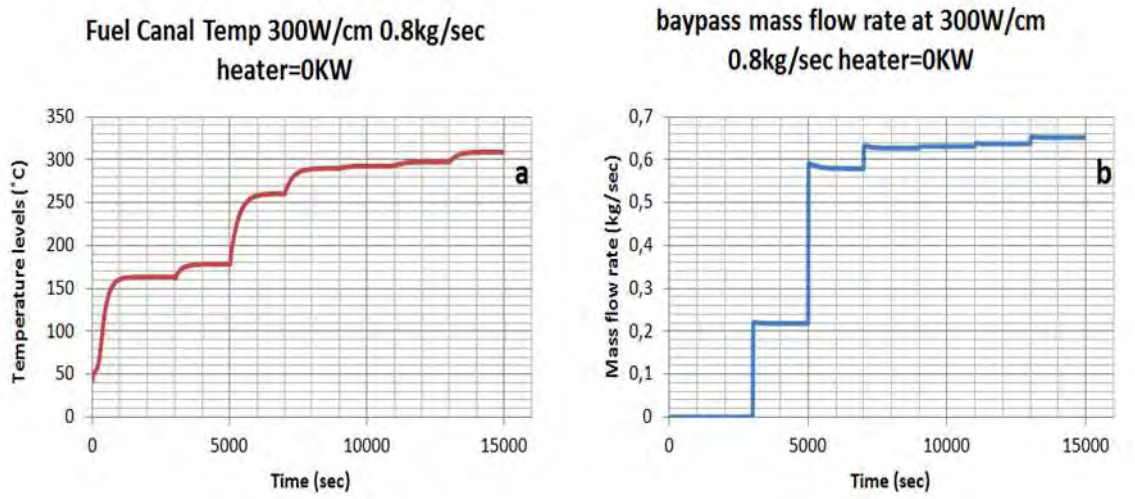

Figure 4, a typical multilevel operating calculation a) temperature b) bypass mass flowrate, as a function of time.

Figure 4 presents typical multilevel steady state operating temperature results of the calculations for a given total power in the loop. Some more calculations were conducted for different linear power values with the same power level of the heater, for different combinations of flow partition. Figure 5 presents the results of the parametric study with different power levels as a function of the bypass branch mass flow rate. This figure provides operating characteristics depending on fuel nuclear powers and electrical power of the heaters (the lines are parallel to each other). According to the presented results and the parallel tendency of the different curves one can normalize the results to get a law/correlation to the operational control of the system.

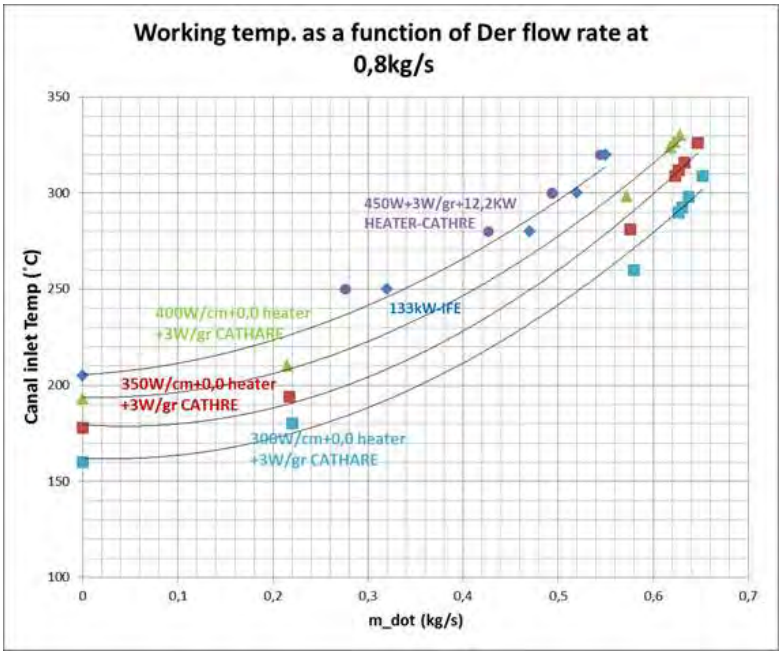

Figure 5, parametric study results for different working power levels an some of IFE calculated results

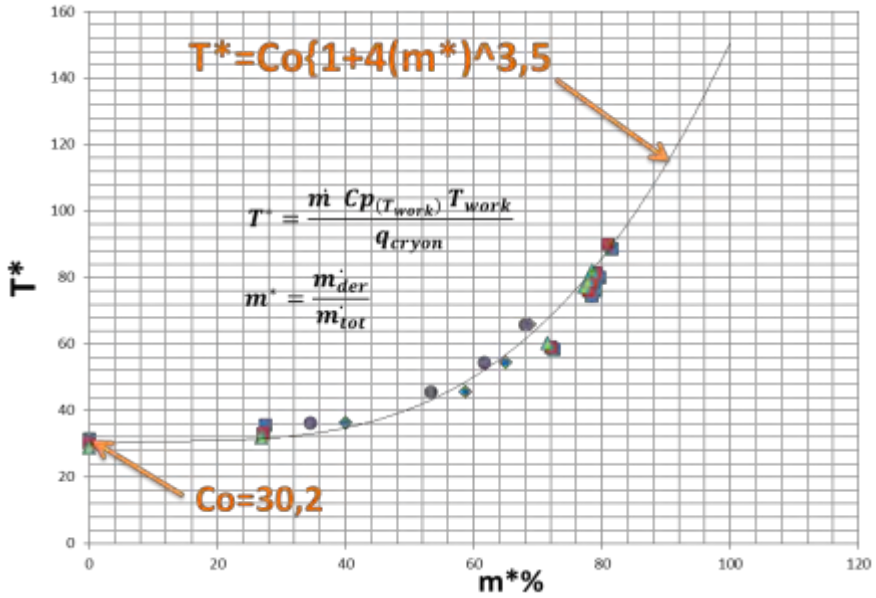

Figure 6, Normalized results and the fitted correlation for the system operational strategy.

Equation 1 presents the suggested normalized parameters of the correlation as:

$$T^* = \frac{\dot{m}\ Cp(T_{work})\ T_{work}}{q_{cryon}} \quad and \quad \dot{m}^* = {\dot{m}_{Bypass}}/{\dot{m}} \tag{1}$$

Were T_{work} is the chosen water temperature at the fuel channel inlet, q_{cryon} is the total power of the fuel, $\dot{m}$ is the total loop mass flow rate, $\dot{m}_{Bypass}$ is the mass flow rate in the bypass branch of the heat exchanger and $Cp(T_{work})$ is the heat capacity of the water at the inlet temperature of the fuel channel. Figure 6 presents the normalized characteristic of the circuit found from the study.

The design calculations performed by IFE are in fair agreement with the normalized characteristic (See Figure 6). Generally speaking, the CATHARE2 model is in good agreement with the calculated points reported by IFE for the design studies of the loop.

3.2. Nominal condition safety margin

Calculations with CATHARE2 where conducted to study the DNBR margin (limitation to avoid dry out in nominal working conditions), for the bounding case conditions of the PWR operating domain with 9.5 mm fuel samples, at 155 bar and 450 W/cm maximum power.

Results show that using the built-in CHF correlation in CATHARE2 (Groenveld table, 1986) gives a DNBR of 1.5 which gives a satisfactory safety margin. A parametric study was conducted to give the cladding temperature, limiting fluid temperature at the outlet, void fraction at the outlet and the DNBR.

The MADISON test device thermal-hydraulics operating conditions were studied in the range of the fuel channel parameters water mass flow rate: 0.5 kg/s < Q < 1.2 kg/s, Fluid temperature at the channel inlet: 250°C < T < 320°C, Pressure at the channel inlet : P = 155 bar, max. linear power at the mid plane : 450 W/cm and gamma power in the structures : 3 W/g. The mass flowrate range and the water temperature range (at the fuel channel inlet) define the operating window.

Simulation were done with the CATHARE2 code, using the built in correlations and various specific assumptions (the annulus and other updated CHF corrections) Figure 7 presents typical results obtained with the updated 2006 Groeneveld LUT. In this case, CHF is 40% higher than the value deduced from the CATHARE2 built in 1986 correlation.

The 2006 CHF Tables are not introduced in the CATHARE2 code consequently, the estimation of the DNBR was performed in post-processing mode.

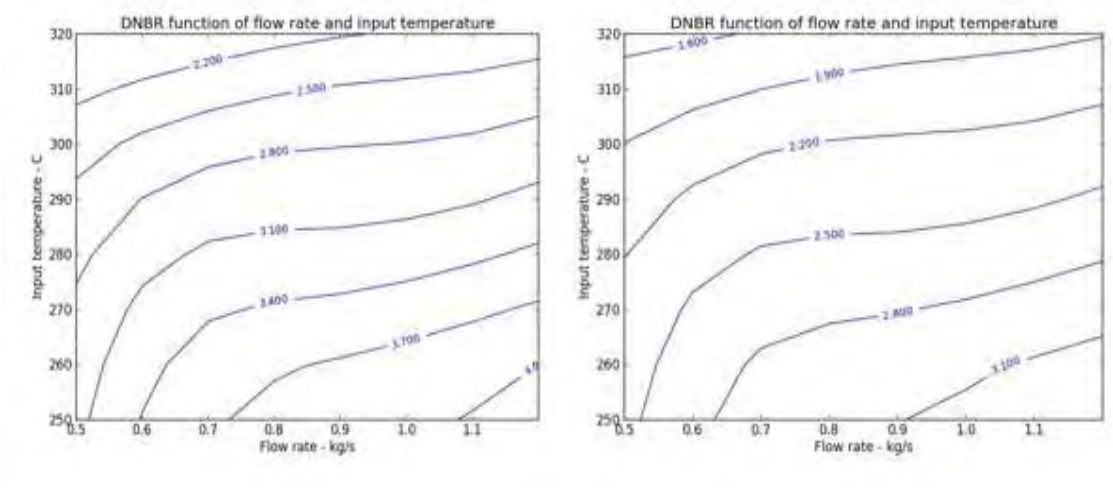

Figure 7, typical DNBR values as a function of operating condition: - a) central rods b) outer rods, using 2006 Groeneveld CHF Tables.

4. First studies dedicated to accidental situations

Models simulating the LOCA and LOFA transient scenarios were developed in CATHARE2 [5], with fuel thermo-mechanical model to perform a parametric safety study. A complementary study dedicated to the LOCA transient has been performed with a 2D model built with COMSOL. Some results of this last study are presented herein.

4.1. LOCA scenario

The high-pressure loop and the low-pressure circuit were simulated using the CATHARE2 code. The code handles two-phase flow and corresponding heat transfer simulation. A fuel model (fuel-clad heat transfer, cladding oxidation, clad ballooning and burst) is implemented in the code to take into account the thermo-mechanic behavior of the fuel. A dedicated subroutine was developed to calculate the radiative heat transfers between fuel rods and the shroud (made of Zircaloy) during the dry-out phase of the LOCA scenario.

The fuel and clad parameters are described in Table 1. Reactor shutdown was triggered by the detection of low pressure in the test device (113 bar) and a function determining the evolution of neutron and gamma power after the reactor shutdown was introduced in the CATHARE2 model.

Fuel Parameter	Value
Clad outside diameter	9.5 mm
Clad thickness	0.57 mm
Clad Inside pressure	58.5 bar
Gap between the fuel and clad	0.001mm
Initial inside oxidation layer	0.1µm
Initial outside oxidation layer	0.63µm

Table 1, fuel parameters that was implemented in the CATHARE model

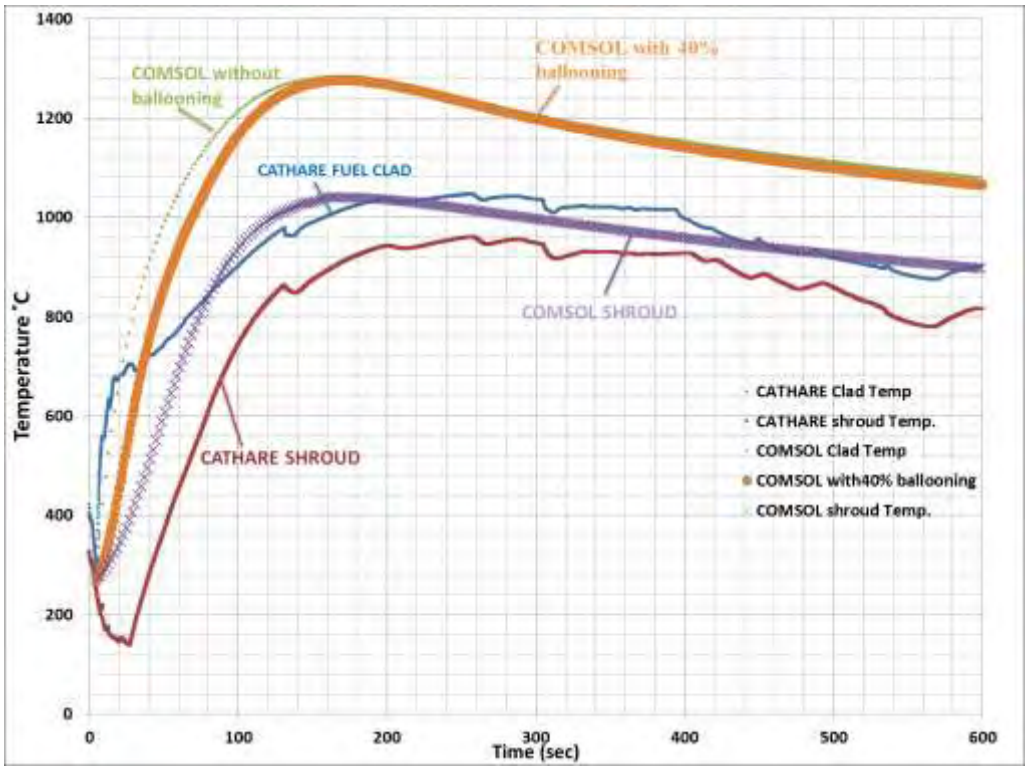

Figure 8, typical temperature behaviour during LOCA scenario calculated by CATHRE with comparison to the COMSOL results.

The radiation subroutine models the radiative heat transfers between all parts of the in-pile device. The radiation model between the fuel samples and its surrounding fuel channel (shroud) was determined by an equivalent thermal resistors network, which enabled to write a set of algebraic equations for the unknown gray body potentials (the radiosity).

The set of algebraic equations were solved symbolically for the gray body potentials of each surface in the fuel channel, and were implemented in the radiation subroutine. The equivalent network describes the relations between the black body potential and the radiosity of the gray body surfaces. The model takes into account the view factors between five existing surfaces (4 fuel samples in a row and the shroud as the fifth area). The radiative exchanges are supposed to take place as soon as the void fraction is higher than 0.97.

Figure 8 presents the results obtained compering between the models. The coupled calculation between the thermal-hydraulic two-phase calculation during depressurization and the radiation heat exchange shows that there is a satisfactory margin preventing runaway oxidation of the cladding in Zircaloy (using a best estimate correlation).

As a crosscheck, a 2D model was built in COMSOL Multiphysics®. The model is built as a cross section at the core mid-plane of the in-pile device. This finite element transient analysis model takes into account thermal radiation exchanges between all the surfaces as well as the oxidation kinetics between steam and Zircaloy, solved by adding a dedicated differential equation. Fuel ballooning is not modelled but can be simulated by changing the input geometry. The emissivity of the clad is taken to be about 0.8 (oxidized Zircaloy) and the oxidized Stainless steel (S.S) emissivity of about 0.5.

The CATHARE2 results are compared to the COMSOL model in Figure 8. As can be seen, the results are in good agreement for the first 20 s as the clad geometry is preserved (COMSOL no ballooning line). The COMSOL model with the ballooned geometry of about 40% increases the heat-transfer and the oxidation area, but doesn't take into account the thermo-hydraulic effect of the shroud cooling during depressurization. It results in higher temperature levels of the clad for the short period of the scenario compared to CATHARE2 simulations.

It was found using the CATHARE2 code that the clad temperature during a LOCA scenario is sufficient for the range of foreseen operating conditions and that the proposed channel updated design is robust.

Cross checking the results with a FEA calculation (COMSOL), it was found that the clad temperature is higher as an outcome of the uncoupling with the two-phase cooling effects. The CATHARE2 model with the shroud cooling during depressurization, coupled to the radiation heat exchange and fuel thermo-mechanics behaviour predicts a more realistic picture of the problem. The conservative COMSOL model shows that for the short and the long period of the scenario there is a satisfactory margin preventing runaway oxidation of the fuel.

4.2. LOFA scenario

A model developed in CATHARE2 has been used to simulate the Loss Of Flow Accident scenario (stop of the main pumps of the primary system). In this scenario, reactor shutdown is triggered after a pre-defined delay time of 1.5 s due to the I&C treatment. The loop switches to the safe-state mode (heater shutdown and closing the bypass line of the main heat exchanger).The possible residual flow due to make-up pumps in the low pressure circuit has been taken into account. Calculations where performed with two initial steady state operating conditions, the case with 250°C and the high temperature case of 320°C. Figure 9 presents the results with the different cases.

As can be seen from the results, there is almost not any detectable difference in the clad temperature, between the 250°C cases (with and without make-up pump operation). The clad temperature reaches significantly higher values for the hot case (320°C). In any case, the transient leads to an increase of the pressure in the primary system during the scenario (consequence of temperature increase of the water and void formation in the fuel channel). Complementary study will be conducted to analyse the possibility of the safety-valves opening or by studying the impact of the size of the accumulators on the pressure evolution.

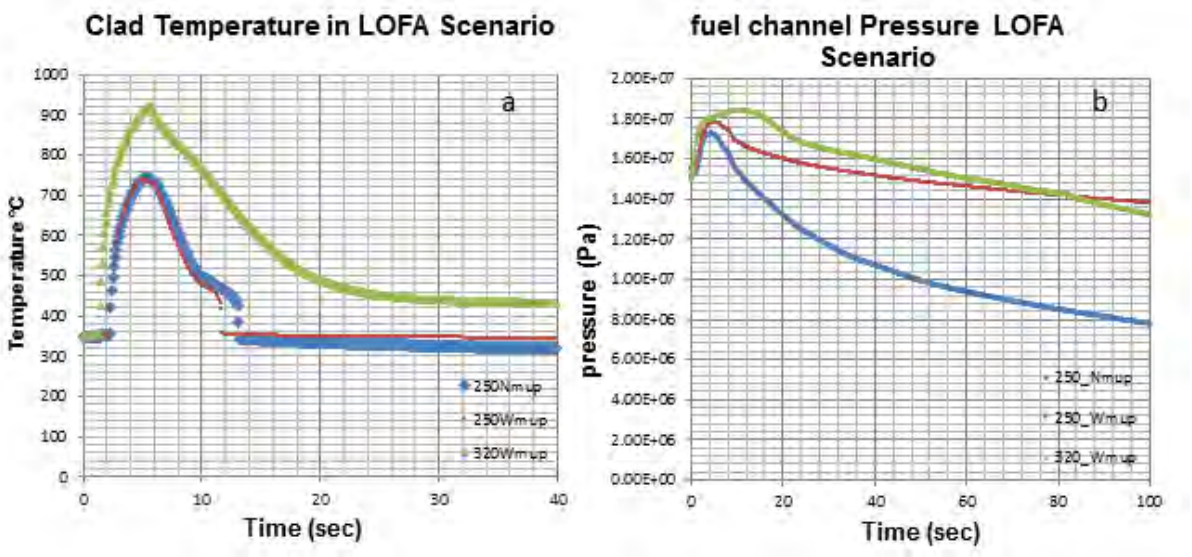

Figure 9, typical temperature (a) and pressure (b) behavior during LOFA scenario as a function of time.

5. Summary and conclusion

The study dedicated to nominal conditions confirmed the design of the loop and showed significant safety margins. A correlation/law was derived from the parametric study to get any desired nominal operating conditions and can serve to control the system.

It was found, that the safety margin determined by the DNBR limit is greater than 1.3 for all range of operating condition and the proposed channel design is robust. The calculated CHF was performed with several updates of the Groeneveld Look Up Table (LUT)

correlation. Working with the 2006 Groeneveld updated correlation one can get a CHF value 40% higher compared to the 1986 correlation.

In the case of LOCA, the shroud cooling during depressurization in the CATHARE2 model, coupled to the radiation heat exchange and fuel thermo-mechanics behavior allows predicting an acceptable transient without runaway Zircaloy reaction.

The conservative COMSOL model approach confirms this conclusion.

During the LOFA scenario, the maximum clad temperature found to be around 900°C, for the range of operating conditions. This calculated result gives confidence in the consequences of such an accident. Additional parametric studies and investigations will be performed to possibly suggest some updates of the design (accumulator volume, pressure controlling valves) to compensate for the pressure increase in the system.

6. References

[1] G. Bignan, J. Estrade, “The Jules Horowitz Reactor: a new high performances European MTR (Material Testing Reactor) with modern experimental capacities: toward an international user facility”, International Group on Research Reactors - IGORR 2013, October, 13-18, 2013, Daejeon, Korea.

[2] G. Bignan, J.C. Brachet, G. Ducros, C. Gonnier, D. Parrat, M. Tourasse, “The OECD/NEA future Jules Horowitz Reactor International Program built by the Nuclear Energy Directorate of CEA”, Enlarged Halden Program Group Conference, March, 10-15, 2013, Storefjell, Norway.

[3] C. Blandin, P. Roux, T. Dousson, L. Ferry, D. Parrat, C. Gonnier, “LWR fuel irradiation hosting systems in the Jules Horowitz reactor”, LWR Fuel Performance Meeting 2013, September 2013, 15-19, Charlotte, NC, USA.

[4] P. Roux C. Gonnier, D. Parrat, C. Garnier, The MADISON experimental hosting system in the future Jules Horowitz Reactor”, 13th International Group On Research Reactors (IGORR 13), September, 19-23, 2010, Knoxville, Tennessee, USA.

[5] G. Geffraye, O. Antoni, et al., CATHARE 2 V2.5 2: A single version for various applications, Nuclear Engineering and Design, 241, 4456–4463, 2011.

ACCIDENT SCENARIO DEVELOPMENT OF THE NUCLEAR RESEARCH REACTOR 'HANARO' FOR A FULL-SCALE NUCLEAR EMERGENCY EXERCISE

G.Y. LEE, B.S. KIM, H.C. Lee, J.S. Kim
Emergency Preparedness Department, Korea Atomic Energy Research Institute
989-111 Daedeok-daero, 34057 Daejeon – Korea

ABSTRACT

Korean government imposed the obligation of a nuclear emergency exercise with local government to the research reactor operator who operates more than 2MW thermal power. Korean government requests an accident scenario requiring off-site protective action in case of a full scale exercise. Recently the emergency planning zone of HANARO research reactor was expanded from radius 800m to 1500m, so the number of residents inside EPZ was increased from about 3,000 to about 39,000. To test and improve emergency response capabilities, the HANARO accident scenario for full scale emergency exercise was developed by using ORIGEN2 code, MELCOR code, dose assessment code and calculation equation suggested IAEA technical document.
The inventory was calculated by ORIGEN2 on the fixed flux condition. The simulated accident condition was channel blockage in core and fire in reactor hall. The release fraction of nuclide from core by channel blockage was chosen based on the NUREG-1465 source-term, but then only the early-in-vessel source-term was considered because the reactor core is still located inside reactor pool. The reactor pool and building structure, flow path was designed by MELCOR code to simulate of diffusion of the nuclide released from the core. The source-term by the simulated accident condition was also calculated by MELCOR code, but the data such as air concentration and dose rate in reactor hall was calculated by using dose conversion factor supplied by IAEA document. The environmental data such as air concentration, dose rate by cloud shine and ground shine, deposition concentration was calculated by using dose assessment code based on Gaussian plum model developed by KAERI. The dose rate data produced for environment was established to fit to the declaration of the general emergency to lead taking a protective action for the residents inside EPZ. The accident scenario developed was applied on-site full scale emergency exercise in 2015, and this scenario will be applied to on- and off-site full scale emergency exercise on September in 2016.

1. Introduction and requirement of nuclear emergency exercise

The purpose of a nuclear emergency exercise is to prove and increase the emergency response capabilities in a nuclear emergency situation according to an accident. So to accomplish this purpose, realistic accident scenario should be developed. In Korea, the licensee who operate nuclear reactor more than 2MW thermal power should performance on-site scale nuclear emergency exercise every year and regional scale nuclear emergency exercise including off-site organizations every two years. The on-site scale nuclear emergency exercise was held in 2015 and regional scale nuclear emergency exercise will be held in 2016 for HANARO research reactor. To implement the exercise realistically, the exercise scenario was developed by using ORIGEN2, MELCOR and KAERI dose assessment computer code. The methodology of developing of the exercise scenario and data was described in this paper.

2. Development of exercise scenario

2.1 Core inventory calculation

The SAR of HANARO reactor only considers the nuclides of noble gas and iodine as released radioactive materials by a limiting accident, but some documents mention the radioactive particles such as cesium as the released materials by a fuel damage accident. To obtain the inventory data needed, the reactor inventory was recalculated by using ORIGEN2 computer code. The HANARO Core is composed 20 bundles of 36-rod-assemblies and 8 bundles of 18-rod-assemblies. The most severe limiting accident of HANARO is the fuel damage of one bundle of 36-rod-assembly by flow blockage, so the inventory of one bundle of 36-rod-assembly was calculated. After loaded in core, 36-rod-assembly is burned 28 days and decayed 7 days as one operation cycle, this cycle is repeated to 210 day, so this operation pattern was applied in the inventory calculation. And the 36-rod-assembly is burned in the same neutron flux condition, so the fixed neutron flux condition as 7.00E+14 n/cm^2-sec was adapted as calculation condition. The total inventory of each elements such as Kr, Xe, I, Br, Cs, Rb was decreased to the end of operation, but some nuclides such as Rb-86, 88, Br-80, 80m, 82, Kr-85, I-128, Cs-132, 134, 134m, 135, 135m, 136, 137, Xe-129m, 131m, etc. were increased to the end of operation, so the inventory of the end point of the reactor operation was chosen as the accident inventory. The total inventory of major element was described as under table.

Elements	Inventory(Ci)	Elements	Inventory(Ci)
Br	1.019E+05	I	3.305E+05
Kr	1.798E+05	Xe	2.567E+05
Rb	2.451E+05	Cs	2.352E+05

Table 1. The inventory of the 36-rod-assembly burned to 196 days

2.2 Diffusion in reactor hall and Source-term calculation

To calculate the diffusion inside the building and source-term after the limiting accident occurred, the HANARO reactor building was designed by MELCOR computer code and each control volume (CV) was considered as under described figure.

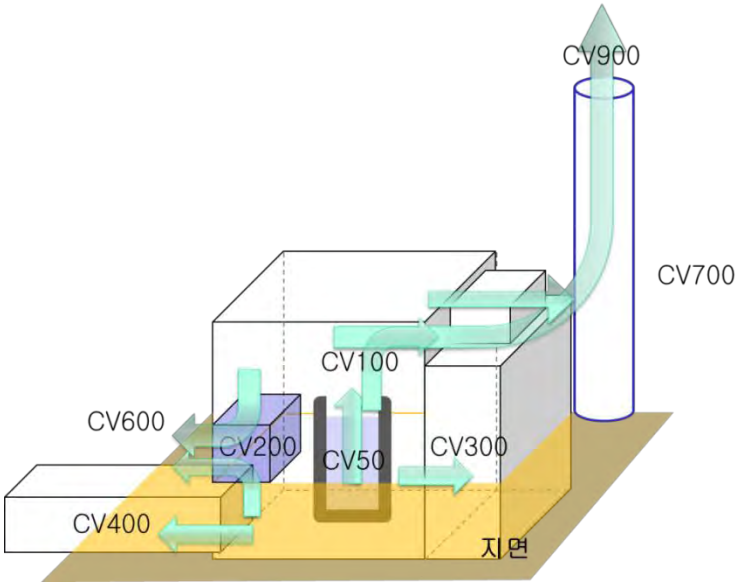

Figure 1. HANARO building structure and control volume for MELCOR calculation

HANARO building was designed and constructed to meet the leak rate as 600m^3/hr at the

25mmWG positive pressure inside the building, so all flow paths which air can flow were searched and designed by MELCOR code, as a result the leak rate in the 25 mmWG inside the reactor building was calculated as under described figure, it fit the reactor building condition.

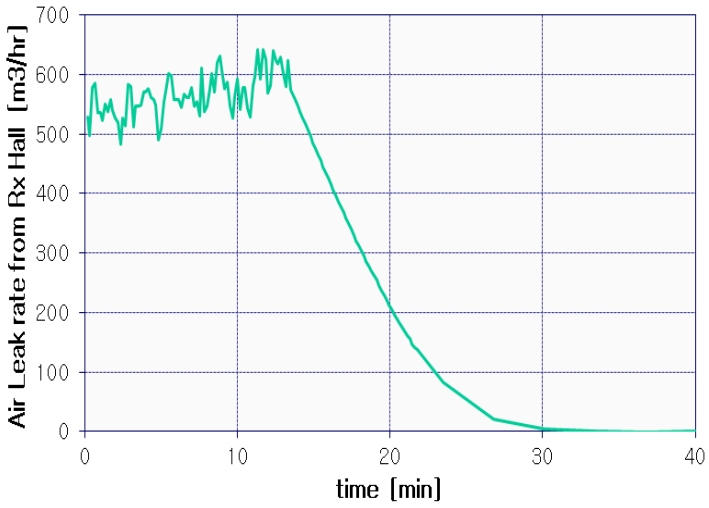

Figure 2. Air Leak rate from reactor hall in 25 mmWG positive pressure

To simulate the diffusion of the fission products by an flow channel blockage accident, the diffusion of the 1kg noble gas as Xe and 1kg aerosol as Cs in 10 minutes was simulated inside reactor pool. And a fire condition inside reactor hall to increase source-term from reactor building to environment was designed as under described figure.

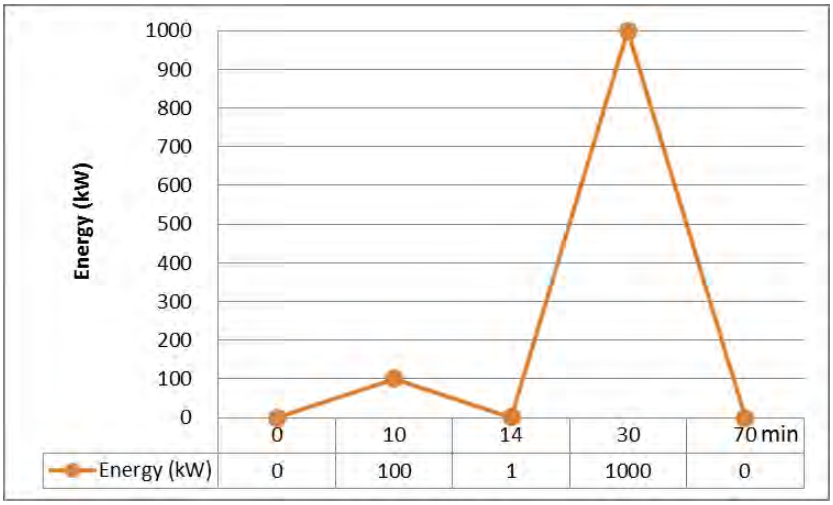

Figure 3. Fire condition in reactor hall

In fire condition, energy is increased to 10minutes and decreased to 14 minutes, after that the energy is again increased to 30minutes and then decreased to 70 minutes, it means the firefighting action by self-fire brigade in the first step, and the firefighting action by professional firefighter in the second step. And also the wind condition outside the reactor building was considered in the MELCOR code input data.

We obtained the diffusion data of noble gas and aerosol as under described figures as the MELCOR simulation result according to the simulated accident condition.

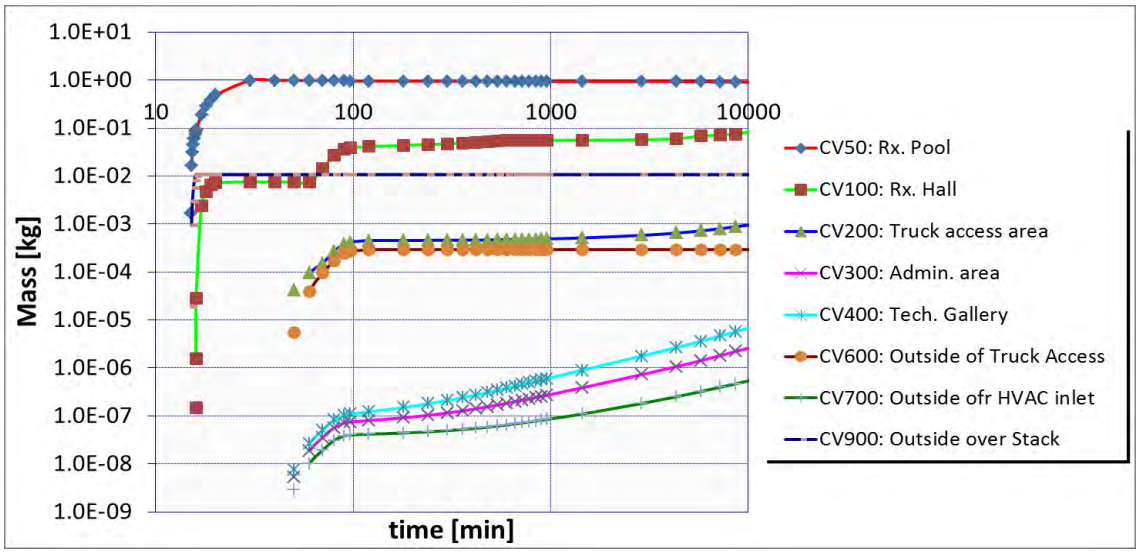

Figure 4. The diffusion of noble gas in each control volumes

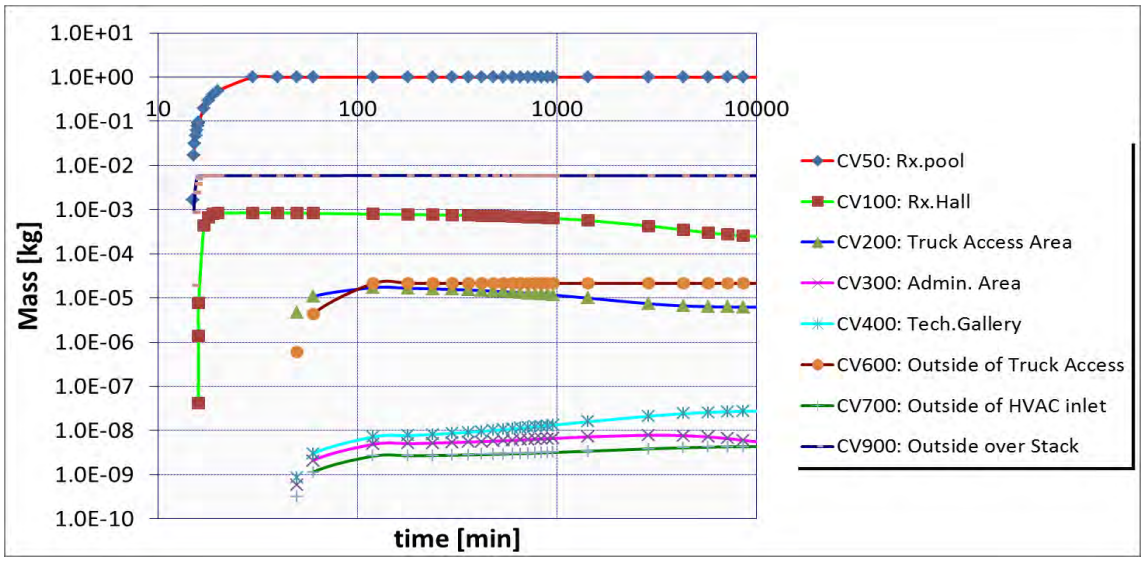

Figure 5. The diffusion of aerosol in each control volumes

The data calculated above figures were considered as fraction, so radioactive concentration, radiation level, etc. were calculated using under equation based on the above calculated data, and also source-term was calculated using the mass outside the building in above figures.

1) Reactor pool concentration of radioactive materials

$$(Vapor\ fraction * \sum_{vi} A_{o,vi} (\frac{1}{2})^{\frac{t}{T_{vi}}} + Aerosol\ fraction * \sum_{ai} A_{o,ai} (\frac{1}{2})^{\frac{t}{T_{ai}}}) / Pool\ volume$$

2) Radiation level over reactor pool top

$$\dot{D} = 2\pi \cdot CF_1 \cdot A_s \cdot \ln \frac{X^2 + R^2}{X^2}$$

3) Reactor hall concentration of vapor and aerosols(particle and iodine)

$$(Vapor\ fraction * \sum_{vi} A_{o,vi} (\frac{1}{2})^{\frac{t}{T_{vi}}}) / Rx\ Hall\ volume$$

$$(Aerosol\ fraction * \sum_{hi} A_{o,hi} (\frac{1}{2})^{\frac{t}{T_{hi}}}) / Rx\ Hall\ volume$$

4) Reactor hall radiation level

$$(Vapor\ fraction * \sum_{vi} A_{o,vi}(\frac{1}{2})^{\frac{t}{T_{vi}}} * CF_{vi} + Aerosol\ fraction * \sum_{ai} A_{o,ai}(\frac{1}{2})^{\frac{t}{T_{ai}}} * CF_{ai}) / Rx\ Hall\ volume$$

5) Stack monitor air concentration of vapor and aerosols(particle and iodine)

$$(Vapor\ fraction\ rate * \sum_{vi} A_{o,vi}(\frac{1}{2})^{\frac{t}{T_{vi}}}) / Volume\ emission\ rate$$

$$(Aerosol\ fraction\ rate * \sum_{hi} A_{o,hi}(\frac{1}{2})^{\frac{t}{T_{hi}}}) / Volume\ emission\ rate * filter\ efficiency$$

The sample of calculation data using above mentioned equation was described as under table.

Time	Rx. Pool Concentration	Rx. Pool top Radiation	RCI Duct Radioactivity	Rx. Hall Concentration			Rx. Hall Dose rate	CM Dose rate
				Gas	Particle	Iodine		
	kBq/m3	nGy/hr	cpm	uCi/cc	uCi/cc	uCi/cc	mSv/hr	mSv/hr
H+00:00	0	1.02E+03	162	0	3.82E-11	1.97E-11	2.00E-04	2.02E-06
H+00:15	1.76E+10	5.37E+08	37,604,300	0	3.82E-11	1.97E-11	2.00E-04	2.02E-06
H+00:16	9.76E+11	2.98E+10	89,628,850	1.22E-04	1.30E-01	1.62E-04	1.12E+00	1.13E-02
H+00:17	2.00E+12	6.10E+10	170	1.02E-02	7.15E+00	8.84E-03	7.72E+01	7.80E-01
---	---	---	---	---	---	---	---	---
H+4320:00	9.40E+09	2.87E+08		4.44E-04	3.82E-11	1.97E-11	1.44E-02	3.44E-04
H+8760:00	8.76E+09	2.67E+08		4.30E-04	3.82E-11	1.97E-11	1.40E-02	3.40E-04

Table 2. Sample of calculated data

2.3 Dose assessment and calculation of environmental data

The environmental impact was assessed by KAERI dose assessment code and the environmental data such as dose rate, air concentration, ground concentration, etc. was produced. The graphical dose assessment results were described as under figures.

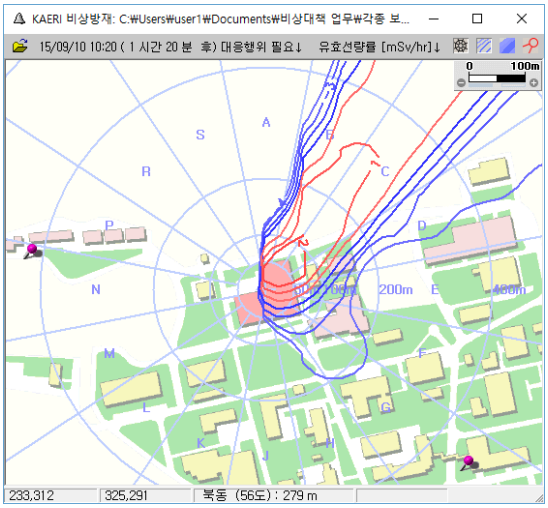

Figure 6. Dose rate by release

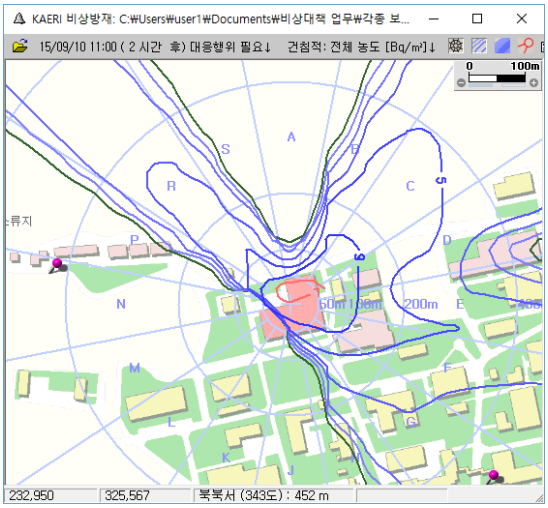

Figure 7. Ground contamination by release

To calculate the environmental impact by using dose assessment code, the real weather data

observed in the KAERI metrological tower was used.

3. Applying to the nuclear emergency exercise and future plan

The exercise scenario and data was applied in the on-site full scale nuclear emergency exercise held on 10 September 2015. In the exercise, emergency declaration at the control room and the operation of emergency response organization, firefighting, the radiation survey around the facility and KAERI site, protective action for the non-essential workers, medical treatment, recovery action, etc. were simulated.
The exercise scenario and data will be somewhat modified and will be used in the regional scale full scale nuclear emergency exercise including off-site organizations on September 2016.

4. References

[1] A.G. Croff, “A User’s Manual for the ORIGEN2 Computer Code”, ORNL/TM-7175, ORNL, 1980
[2] R.O. Gauntt, etc., “MELCOR Computer Code Manuals”, NUREG/CR-6119, U.S. NRC, 2005

A case study SAFARI-1: Implementation of the safety classification in the existing facilities using a graded approach.

[1] *K Moodley & DAH Arndt*, *SM Malaka*
SAFARI-1, Necsa, Pretoria, South Africa
Email: Sammy.malaka@necsa.co.za

Abstract. The existing research reactor plants are grappling with implementing the safety classification as defined in the IAEA document as it is deemed to be more relevant to NEW PLANTS. It is likely that a "traditional" functional analysis will be performed for new facilities using a top-down approach during the design process, however on the other hand for existing facilities, in particular old research reactors like SAFARI-1 and NRG-Petten etc, are not likely to have a formal functional analysis in place, and it is vital that some innovative approach be in place to address this, hence the content of this paper to address this deficiency and still maintain ***safety objective and principles of protection and safety***.

Key words: SSC, Safety Classification, Safety Function.

1. Introduction

The need to classify *structures, systems and components* (SSCs) according to its importance to safety is not unique to research reactors and in particular the 50 year old SAFARI-1 research reactor. The method has been recognized since the early days of reactor design and operation. According to [2] *the methods for safety classification of (SSCs) have evolved in the light of experience gained in the design and operation of existing plants.*

Although the concept of a safety function as being what must be accomplished for safety has been understood for many years, the process by which SSCs important to safety can be derived from the fundamental safety objective has not been described in earlier IAEA Safety Guides dealing with SSC classification. Therefore, the classification schemes used in practice to identify those SSCs deemed to be of the highest importance to safety have, for the most part, been based on experience and analysis of specific designs.

For existing facilities with no formal functional analysis in place, it is suggested that a "modified" functional analysis be performed in a bottom-up manner, with top-down traceability shown afterwards. This would imply the following steps:

- Identify the SSC for which safety classification is required.
- For each SSC, identify all functions that are performed directly from the existing plant.
- For each SSC function, determine if it supports the MSF (Main Safety Function) (and is therefore a SSF (SCC Safety Function) or if it is a non-safety function.
- Then allocate all SSFs to the appropriate MSFs.

After all SSC in the plant are classified, perform a top-down completeness check to ensure that every MSF is performed by at least one SSC in the plant. It should be emphasised that, with so many SSC and so few MSFs, the completeness check is almost guaranteed to be satisfied.

This paper will present practicality approach taken to implement the safety classification for existing facilities in particular the SAFARI-1 research reactor organisation starting with SSC important to safety in a graded approach.

[1] *K Moodley & DAH Arndt* are the main contributors of the SAFARI-1 Safety classification methodology

2. Methodology

The process followed for the classification of SAFARI-1 SSCs is based on the principles and process defined [3]: *Plant safety functions are categorised according to their significance with regards to nuclear safety during the plant states i.e. operating and accident conditions. SSCs are classified according to their contribution in delivering the required plant safety functions. The safety classification of SSCs allows for a graded approach to the design, quality and management requirements of SSCs related to the life cycle stages of a facility.*

According to [3] SAFARI-1 is a Hazard Level 3 facility that requires a full safety classification, with the potential for SC-1, SC-2, SC-3 and Non-classified SSC. SAFARI-1 is an existing facility with a detailed Safety Analysis Report that includes a Deterministic Safety Assessment (DSA) and Probabilistic Safety Analysis (PSA). A preliminary SSC safety classification was performed and is being systematically updated to include the applicable results and references of the later performed PSA.

The methodology take into account the both the quantitative results of events analysed in the PSA as well as the qualitative information evaluated by an interdisciplinary workgroup of individuals with relevant qualifications and experience related to the facility The specific safety classification process applied to SAFARI-1 is shown in Figure1.

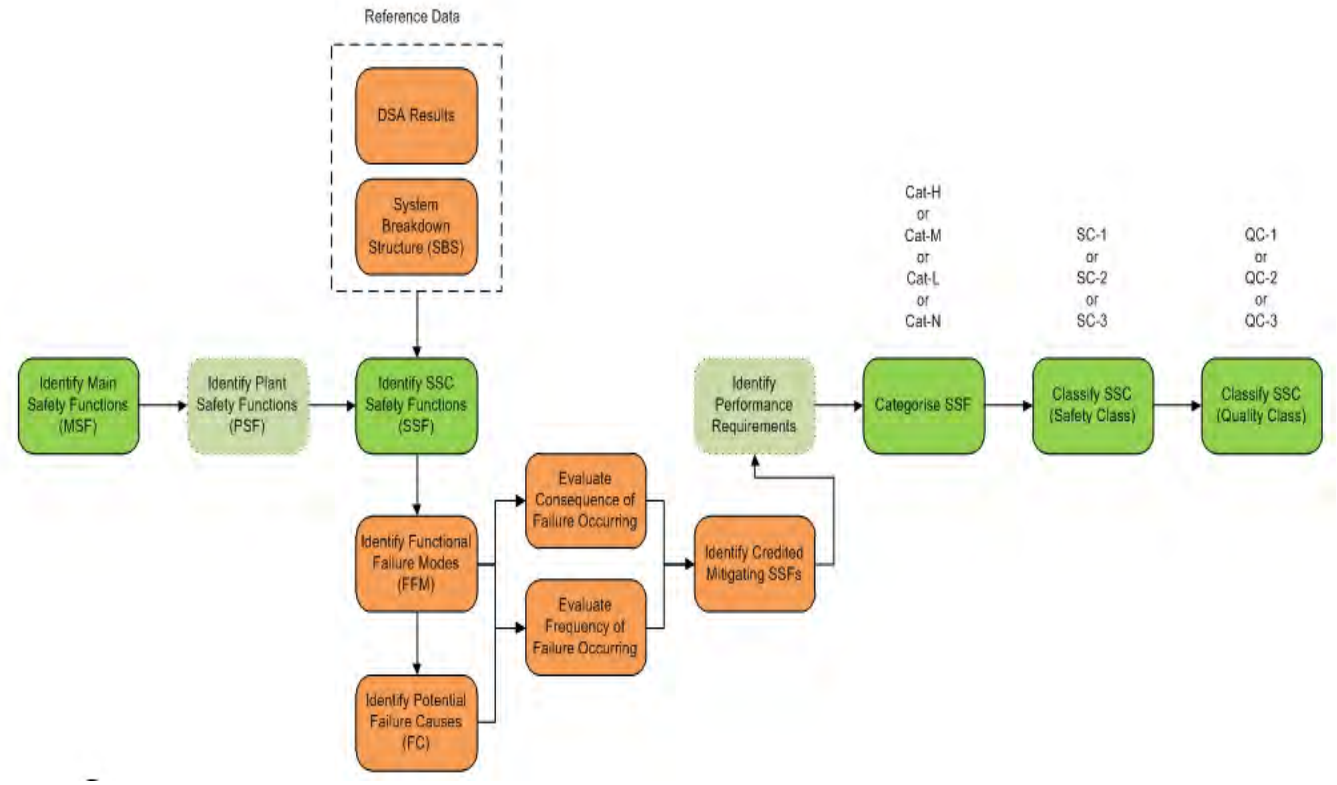

Figure1: Methodology Process over view

The methodology requires that an identification of the specific performance requirements of SSC based on its functions is taken into account. When required, the performance requirements for any SSC can be derived from seeing the important Functional Failure Modes and Failure Causes. While considering the failure modes, consideration was given not only to total failure of the function, but also to unwanted changes in performance of the function.

3. Safety Functions, Failure modes and Cause

3.1. MAIN SAFETY FUNCTIONS

The Main Safety Function (MSF) listed in [3] for the reactor facilities (viz. “Control reactivity”, “Remove heat” and “Contain/confine radionuclides”) cover only the Basic (Fundamental) Safety Functions as per IAEA NS-R-4. In order to ensure that all functions important to safety for SAFARI-1 are considered, two additional functions (“Prevent uncontrolled criticality” and “Shield radiation”) are added to ensure that the main safety goal of protecting the worker, public and environment against the harmful effects of radiation is achieved. The functions are shown in Figure 2 below

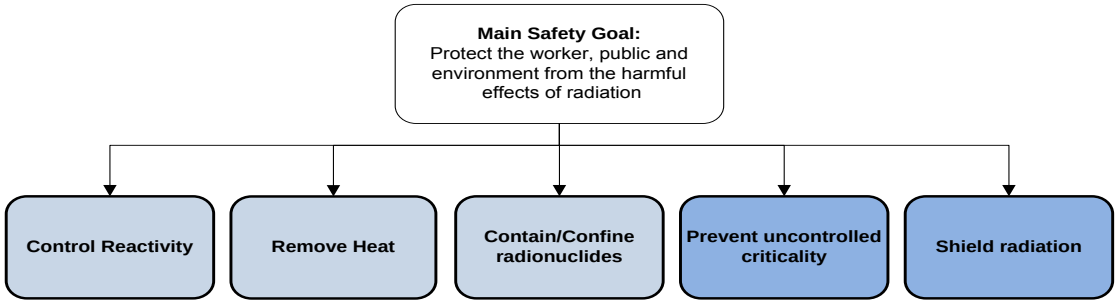

Figure 2: Main Safety Function

3.2. PLANT SAFETY FUNCTIONS

As indicated in the introduction that SAFARI-1 is an existing facility and has just celebrated 50 years of existence, and thus not a new facility under design, the downward flow of safety functions from MSFs through Plant Safety Functions (PSFs) to SSC Safety Functions (SSFs) is not performed by doing a functional analysis. Instead, SSFs are directly identified from the existing SSC in the facility, thereby ensuring that the functions under evaluation reflect the real status in the plant. SSFs are functions that contribute to any of the MSFs (identified in Figure 2 above), and in turn, to the main safety goal. The relationship between the MSFs, PSFs and SSFs are indicated in Table 1 (The list in the table is not exhaustive).

Main Safety Function (MSF)	**SAFARI-1 Specific Safety Function (PSF)**	**SSC Safety Function (SSF)**
Confinement (“Contain/confine radionuclides” and “Shield radiation)	Maintain control of radioactive releases from irradiated fuel transported and stored outside the reactor but within the facility.	• Fuel Assemblies, • Fresh Fuel Vault
	Maintain control of environmental conditions within SAFARI-1 for personnel habitability necessary to allow performance of operations beneficial to safety.	• LA Tanks, Pipes, Valves & Pump • Area Monitoring System, • :K1-K7 Activity Monitoring
	Limit the discharge or release of radioactive waste and airborne radioactive material to below prescribed limits and ALARA	• Primary System Strainer, • MA Tanks, Pipes, Valves & Pump
Reactivity Control (“Prevent uncontrolled criticality” and “Control reactivity”	Maintain core geometry.	• Reactor Vessel Assembly, • Grid Plate Assembly ,
	Prevent unacceptable reactivity transients or insertions	• Gamma Safety Channel, • Process Instrumentation
Heat Removal	Maintain an active heat transfer path from the core.	• Beryllium reflector Elements, • Non-neutronic Core Components
	Maintain a passive heat transfer path from the core.	• Reactor Vessel Assembly,
	Prevent excessive power levels in the core.	• Neutron Safety System, • Gamma Safety Channel

Table 1: The relationship between the MSFs, PSFs and SSFs

3.3. SSC SAFETY FUNCTIONS

SAFARI-1 developed an SBS (System Breakdown Structure), this is used as a representation of the facility, and lists the SSC of the facility in a hierarchical structure. The advantage of this structure is that it can be expanded to the level necessary for each SSC, allowing more detailed evaluation of systems that are important to safety and avoiding complex evaluation of systems with little or no safety significance. During the assessment, evaluators are prompted to identify all functions performed by the SSC under consideration that may contribute to one or more of the MSFs. The safety functions performed or supported by each SSC are listed as SSFs, with a description of their contributions to the MSFs and in turn, to the main safety goal.

SSF-	**1**	Control neutron leakage (reflection)
SSC		Beryllium reflector system
SSF Description		The low absorption cross-section and large scattering cross-section of beryllium make it a good moderator and enable the reflector elements to effectively reflect leaking neutrons back into the core. This reduces the neutron leakage rate from the core, which is a factor in the effective multiplication coefficient, and hence contributes to the core reactivity.
SSF-	**3**	Maintain core geometry
SSC		Beryllium reflector system
SSF Description		Support the geometry of the reactor core to maintain a constant configuration.
SSF-	**7**	Contain fission products
SSC		Fuel assemblies, Control rod fuel sections
SSF Description		Contain fission products within the fuel plate cladding.
SSF-	**XXX**	Safety Function
SSC		System, Structure and Component
SSF Description		Safety Function Description.

Table 2: The *SSC SAFETY FUNCTIONS (SSF) descriptions*

3.4. FUNCTIONAL FAILURE MODES

Functional Failure Modes (FFMs) are the ways in which SSC fail to meet a performance requirement. FFMs therefore include not only the total inability for the function to be performed, but also the incorrect performance of the function. Each SSF is evaluated for potential Functional Failure Modes (FFMs). Each SSF is evaluated for potential Functional Failure Modes (FFMs

3.5. FAILURE CAUSES

Potential Failure Causes (FCs) of the FFMs are described to provide some insight to the frequency of occurrence of the FFMs. The FCs also provides information on the important characteristics of the related SSC. The possible FCs for each FFM are defined and discussed in Table 3.

SSF	**1**	Control neutron leakage (reflection)	
SSC		Beryllium reflector system	
SSF Description		The low absorption cross-section and large scattering cross-section of beryllium make it a good moderator and enable the reflector elements to effectively reflect leaking neutrons back into the core. This reduces the neutron leakage rate from the core, which is a factor in the effective multiplication coefficient, and hence contributes to the core reactivity.	
FFM	1.1	FFM Description:	Changes to reflection characteristics.
FC	1.1.1	FC Description:	Incorrect material used during manufacture of the reflector elements.

	Frequency:	AOO	
	Justification:	Manufacturing defects may occur, despite quality control measures being implemented. These defects may initially go undetected (i.e. latent defects) and cause failures later within the lifetime of the reactor.	
	Consequence:	None	
	Justification:	Any reasonable material substitution will only result in unchanged or decreased reactivity in the core. NOTE: Substitution of beryllium in the reflector element with highly enriched uranium, for example, is not considered possible here.	
FC	1.1.2	FC Description:	Changes in the material properties due to irradiation or temperature effects.
	Frequency:	AOO	
	Justification:	Material changes are well documented and known to occur within the lifetime of the reactor.	
	Consequence:	None	
	Justification:	Material changes occur over very long periods and may be detected through trends based on proper monitoring and recording of process parameters. However, even if material changes go unnoticed, it still will not lead to increased reactivity in the core and is expected to have no safety consequences, since irradiation of the reflector elements actually results in a slight decrease in reactivity over time.	

Table 3: The possible FCs for each FFM

Each FC is evaluated to determine the unmitigated consequence of the functional failure. Since a detailed analysis is not available for each failure, the consequence is judged to be in one of a number of categories. A brief justification is provided to state the rationale for the selected consequence level. The definitions of High, Medium and Low consequences are presented in Table 4.

Consequence	Description	Typical Condition
High	Significant radiological release Public exposure ≥ 1 mSv and/or Worker exposure ≥ 50 mSv	e.g. Severe core damage
Medium	Moderate radiological release 0.25 mSv ≤ Public exposure < 1 mSv and/or 20 mSv ≤ Worker exposure < 50 mSv	e.g. Moderate core damage
Low	Some radiological release Public exposure < 0.25 mSv and/or Worker exposure < 20 mSv	e.g. Minor core damage
None	No nuclear safety impact.	No core damage

Table 4: Consequence quantification

The consequences of each FFM are conservatively estimated, and therefore only a short justification is typically provided where higher (more severe) consequences are assumed. Where lower (less severe) consequences are assumed, a more comprehensive justification may be provided.

The following rules are applied when the consequences of failure are determined and specified:

- *A safety function may have different consequence levels for different FCs, but these levels shall be restricted to High, Medium or Low.*
- *For a non-safety function, the consequence level shall be None for all FCs.*

The frequency of each FC leading to a given consequence is evaluated in accordance with [3]

Failure Causes that are expected to occur within the lifetime of the reactor ($f \geq 10^{-2}$ p.a.) are listed as being within the AOO domain. The remainder fall either within the DBA domain ($10^{-6} \leq f < 10^{-2}$ p.a.), or outside DBA and therefore in the BDBA domain ($f < 10^{-6}$ p.a.). A justification is provided to support the stated frequency domain. Where possible, the justification is supported by a reference to the PSA, the Equipment Reliability Database Report or the Initiating Events Report

Where failure of a SSF may lead to a certain consequence level, a different SSF may be credited to mitigate the failure, provided that the mitigating SSF inherits at least the safety category corresponding to the consequence of the failure. SSFs are therefore categorised according to the consequence of only those failures that they are credited for.

4. Safety Classification of SSC

In [1], classification is a specific type of grading applied to SSCs or to activities. It is a method of grouping items with similar characteristics or functions for the purpose of identifying appropriate requirements, codes, and standards to be applied to their design, manufacture, construction, operation and maintenance.

The safety classification of the SSC is defined according to the safety importance of the SSFs they are credited to perform or contribute to. Normally, there is a direct relationship between the SSF safety categorisation and SSC safety classification as defined by the SAFARI-1 methodology.

4.1. SSC SAFETY FUNCTIONS CATEGORISATION

Each SSF is categorised based on the reduction of risk which the specific function provides, keeping in mind that the unmitigated consequences arise from loss of the SSF. Three levels of safety categories are defined for SSFs in [3], Cat-H, Cat-M and Cat-L, where the respective categories indicate a high, moderate and low significance to nuclear safety. The categorisation of SSFs is done according to the safety criteria presented graphically in Figure 3 below.

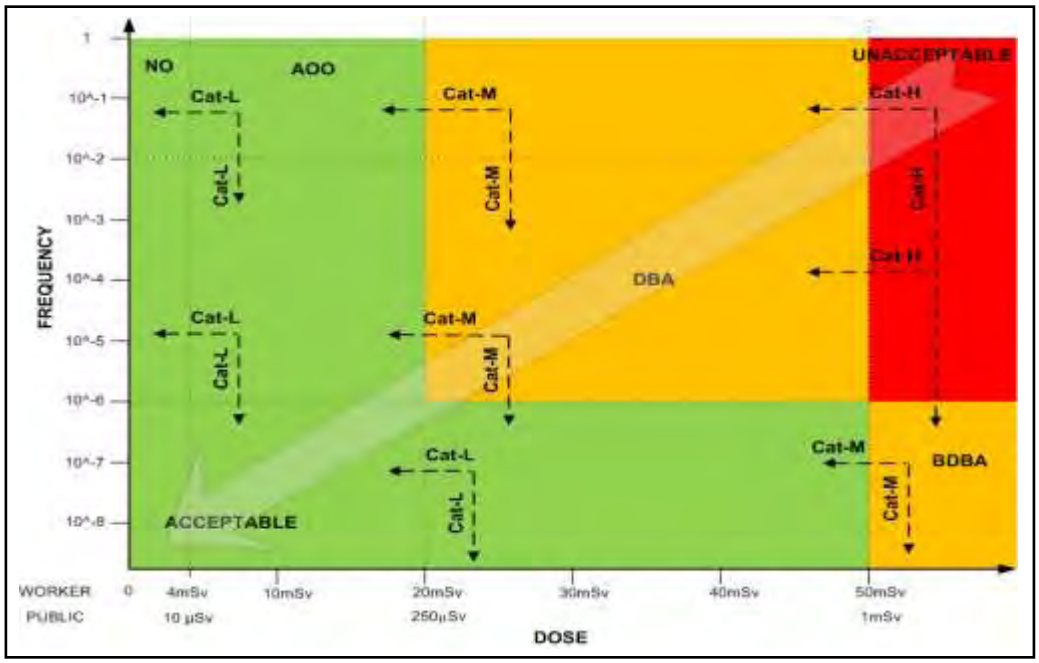

Figure 3: Nuclear Safety Criteria

The colour scheme (shading) is modified slightly in Figure 3, so that those regions of the risk matrix diagram which correspond to the same safety category are represented by the same colour, viz. red for Cat-H, orange for Cat-M and green for Cat-L.

Any function which contributes towards achievement of the main safety goal is a safety function, and therefore, shall not be categorised as Cat-N. The lowest safety category assigned to a safety function shall be Cat-L.

4.2. SSC SAFETY CLASSIFICATION

In cases where only one SSC provides certain functionality, there is a one-to-one relationship, as follows:

Cat-H SSF ⟶ SC-1 SSC

Cat-M SSF ⟶ SC-2 SSC

Cat-L SSF ⟶ SC-3 SSC

Cat-N SSF ⟶ SC-n SSC (i.e. Non-classified SSC)

Where a SSC performs more than one SSF, it is classified according to the function of highest safety significance. Where two or more SSC provide a certain functionality, then the SSC safety classifications can be dropped one level, but only if redundancy, diversity, independence and separation (RDIS) is provided and the redundant SSC has the same integrity as the first one. However, no SSC is assigned a safety classification lower than SC-3, even if more than one SSC provides a certain functionality. Table 4 indicate the non-exhaustive list of SAFARI-1 classified systems.

Item ID	Level	SSC Description	SSF Category	SSC Safety Class
007139	1	**Reactor System**		SC-1
039392	2	Reactor Structural System		SC-1
008747	3	Lower Bearing Plate	Cat-H	SC-1
008746	3	Grid Plate Assembly	Cat-H	SC-1
105008	4	Control Rod Fuel Section	Cat-M	SC-2
007145	3	Primary Pumps	Cat-L	SC-3
007137	1	**Cooling System**		
111064	3	Primary Pump Outlet Valves (Motorised)	Cat-L	SC-3
039401	1	Storage System		SC-1
039408	2	Chemicals Storage System	Cat-N	SC-n
039414	3	Regeneration Chemicals Store		SC-n

Table 4: SAFARI-1 SSC Safety Classifications

The Table indicates the SSFs performed by each SSC, the category of the SSF of highest safety significance, and the resulting safety class. The “Item ID” is the capturing identification number of the item, while the “Level” indicates the hierarchical level of the item in the System Breakdown Structure.

5. Graded Approach

The approach followed was based on Graded Approach for Research Reactors, as specified mainly in the Safety Requirements document NS-R-4 and the General Safety Requirements document GS-R-3. The Graded Approach is used to determine the appropriate manner to comply with a safety requirement; it is not used to provide relief from a requirement.

Any grading performed should ensure that safety functions and Operating Limits and Conditions are preserved and that there are no negative effects on the facility staff, the public, or the environment.

6. Discussions and Conclusions

The SSF safety categorisation translates to the SSC safety classification according to the rules given Section 4.2. The final SSC safety classification is summarised in Table 4. Some SSC were not considered to contribute to nuclear safety functions, and were therefore not analysed. With failure of these SSC having no nuclear safety consequences, the SSC are also classified as SC-n.

The classification process dictates that:

- Where a SSC is decomposed and analysed on the next lower level, the SSC inherits the highest safety classification of its sub-components.
- Where a higher level SSC is classified, but not decomposed any further, then all of its sub-components conservatively inherit the classification of the "parent" SSC. Where the need arises to classify a specific lower level SSC, for example, for modification, utilisation or procurement purposes, a more specific classification of that SSC is then performed.

It should be emphasised the graded approach adopted by the SAFARI-1 safety classification and as per [3] is that

- Any failure of items important to safety in a system in a lower safety class will not propagate to a system in a higher safety class.
- Equipment that performs multiple functions shall be classified in a safety class that is consistent with the most important function performed by the equipment.
- The categorisation of safety functions should take no account of any redundancy, diversity or independence within the design."

The adequacy of the safety classification should be verified using deterministic safety analysis, which should be complemented by insights from probabilistic safety assessment and/or supported by engineering judgement.

Consistency between the deterministic and probabilistic approaches will provide confidence that the safety classification is correct. Generally, it is expected that probabilistic criteria for safety classification will match those derived deterministically.

References:

[1] IAEA – TECDOC-1740 Use of a Graded Approach in the Application of the Management System Requirements for Facilities and Activities
[2] Safety Classification of Structures, Systems and Components in Nuclear Power Plants- SSG-30
[3] SHEQ INS 0890: Necsa Safety Classification of Structures, Systems and Components

EFFECT OF ION IRRADIATION ON THE CORROSION OF AN AlFeNi ALUMINIUM ALLOY

D.NABHAN, B.KAPUSTA, K.COLAS

Département des Matériaux pour le Nucléaire, CEA Saclay,

91 191 Gif sur Yvette Cedex - France

N.DACHEUX

ICSM, UMR 5257 CNRS / CEA / UM2 / ENSCM

Site de Marcoule, *Bât 426, BP 17171, 30 207 Bagnols/Cèze – France*

ABSTRACT

AlFeNi is an aluminium alloy used for fuel cladding in some high flux research reactors because of its good corrosion behavior in water at high temperatures. Up to now, the in-reactor corrosion kinetics were evaluated directly on fuel plates irradiated in nominal conditions, but a lack of data was identified on the in-pile corrosion behavior at incidental temperatures (above 100°C). In order to simulate the effect of neutron irradiation on the corrosion kinetics of this alloy and on the structure of the hydroxide film formed in the water environment of a reactor core, ion implantation was performed on un-corroded and pre-corroded AlFeNi samples. Al^+ ions with an energy of 1.6 MeV were implanted on un-corroded samples to a damage level of 36 dpa (displacement per atom) which corresponds to a few reactor cycles. The pre-corroded samples were irradiated up to 18 dpa. To simulate radiation damage in an oxidizing environment, O^+ ions were implanted with an energy of 1.4 MeV in both un-corroded and pre-corroded samples creating damage up to 18 dpa. Following irradiation, all samples were corroded in water at 140°C and pH 5.2 for different durations. The oxide layers were characterized at different scales using various techniques (electron microscopy, X-ray diffraction, Secondary Ion Mass Spectrometry). An evolution of the metal microstructure was observed only at the highest Al^+ damage (36 dpa) by TEM analysis, which revealed the formation of thin precipitates, in good agreement with literature. Samples that were irradiated in the as-received state and then corroded presented an acceleration of the weight gain for a constant oxide thickness when compared to unirradiated corroded specimens. Our results suggest the densification of the oxide layer formed after metal irradiation, and slower anionic diffusion through the inner oxide. On the contrary, irradiation of the oxide layer leads to an increase of the corrosion kinetics, not only in terms of weight gain but also of oxide thickness. These results suggest that the damaged oxide layer contains diffusion paths leading to enhanced cationic diffusion from the metal, and subsequently to faster anionic diffusion. In addition, an amorphisation of the crystalline boehmite layer was observed on these pre-corroded samples. The corrosion kinetics behavior is thus different for samples irradiated in the metal compared to samples irradiated in the oxide. The results obtained in this study suggest that a high fast neutron flux at the initial phases of corrosion can be beneficial to limit end-of-life fuel plate corrosion.

1. Introduction

In the past, numerous correlations have been proposed to predict the oxide thickness on aluminum fuel claddings in the research reactors [1-6]. Most of these models have been established from results obtained in the ANS corrosion loop with a thermal flux through the cladding, but without neutron flux. The comparison between oxide thicknesses measured on irradiated fuel plates and those estimated with the models shows in some reactors a good agreement, thus suggesting that the effect of the neutron flux on the corrosion kinetics could be much smaller than that of a high thermal flux. But in other reactors the established correlations applied in the temperature, pH and thermal flux range for which they are valid, do not fit correctly the experimental results. Only the Kritz correlation [2] was

fitted on oxide thicknesses measured on fuel plates in reactor, but the set of used parameters - time, temperature and thermal flux - does not take into account the neutron flux, implicitly supposing that the thermal flux through the cladding is prevalent on the corrosion rate. However when applied to fuel cladding in other reactors, discrepancies arise which seem to reveal that the neutron flux could have an important effect on the corrosion kinetics.

In order to estimate this effect, we simulated the neutron damage on an AlFeNi cladding with ion irradiation of some as-received AlFeNi and pre-corroded samples.

2. Materials and experimental methods

Coupons-shaped samples and 3 mm diameter discs were prepared from rolled AlFeNi sheets that were manufactured by CERCA (Roman, France). The initial sheets were annealed after cold-rolling.

In order to study the effect of ion-irradiation and implantation on the microstructure and the corrosion of AlFeNi, several irradiation runs were performed on as-received samples and on pre-corroded samples. The irradiation runs were performed at the JANNuS Irradiation Platform at CEA-Saclay.

A schematic diagram representing the experimental plan used for the irradiation experiments is presented in Figure 1. As can be seen in this figure, as-received samples were irradiated up to 5.25 x 10^{16} ions.cm^{-2} with 1.6 MeV Al^+ ions which corresponds to 36 dpa (displacement per atoms). These samples then underwent corrosion experiments at various durations as described in the following paragraph. Pre-corroded samples have been irradiated up to 4.24 x 10^{16} ions.cm^{-2} with 1.4 MeV O^+ (18 dpa). Another set of pre-corroded samples have been irradiated up to 2.63 x 10^{16} ions.cm^{-2} with 1.6 MeV Al^+ (18 dpa). This allowed us to compare the effect of various implantation ions, in particular oxygen which is an essential part of the corrosion mechanism. All irradiation experiments were performed at 140°C in order to be at the same temperature than the corrosion experiments and avoid irradiation defect annealing during corrosion.

The corrosion experiments of the pre-irradiated metal samples and of the as-received samples destined to be irradiated have been performed in 316L steel autoclaves of 160 mL. All corrosion experiments were performed at 140°C and a pH of 5.2 which are realistic conditions for incidental operation of fuel cladding in the research reactors. Temperature was controlled with thermocouples and the inside of the autoclaves was coated in Teflon in order to perform acid-media corrosion. The weight gain was measured with a precision up to 10^{-4} g. Oxide thickness and surface observations were performed by Scanning Electron Microscopy (SEM) (FEG JEOL JSM-7001FLV). Additional observations were performed by X-Ray Diffraction (Bruker D8 Advance) and Transmission Electron Microscopy (FEI TEcnai 30 G2 300 kV).

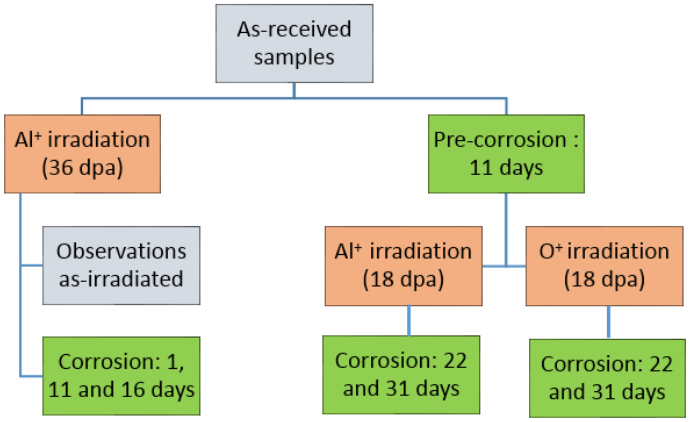

Figure 1 : Schematic representation of irradiation and corrosion experiment on AlFeNi samples presented in this study.

3. Results and discussion

3.1. Impact of metal irradiation on microstructure and corrosion kinetics

In order to study the impact of irradiating the metal on corrosion, Al^+ irradiation experiments have been performed prior to corrosion experiments. TEM examinations have been performed on AlFeNi metal sample in three states: as-received, irradiated up to 18 dpa with Al^+ and irradiated up to 36 dpa with Al^+. The micrographs from the examinations are presented in Figure 2. It can be seen that irradiation

to the lower dose (18 dpa) does not have a strong impact on the metal microstructure whereas irradiation up to 36 dpa leads to the formation of small needles (however it should be noted that the TEM thin foils were prepared at a position which does not correspond to the maximum ion-irradiation damage).

After irradiation, corrosion experiments were performed on the 36 dpa irradiated metal samples for different durations (1, 11 and 16 days). SEM observations of the oxide surface for unirradiated samples and metal-irradiated samples are reported in Figure 3. The aluminum hydroxide crystals forming the surface of the samples [7, 8] seem to be strongly affected by irradiation: in the case of ion-irradiated samples, the crystals are coarser with apparent smaller density. This difference could be due to a change in the corrosion mechanism or oxidation kinetics with irradiation of the metal matrix.

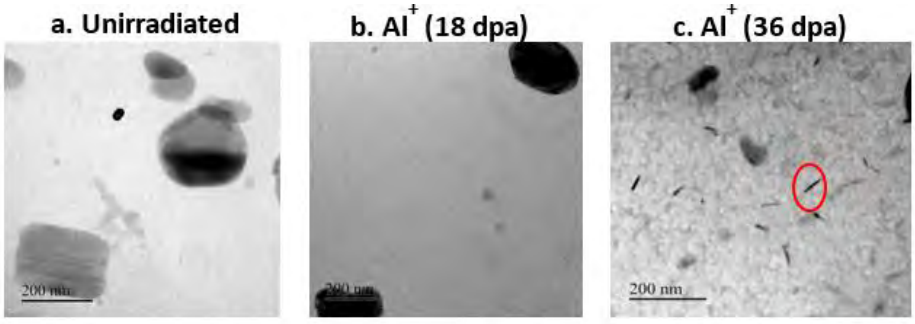

Figure 2 : TEM observation of AlFeNi samples: a. unirradiated ; b. irradiated with Al^+ ions up to 18 dpa ; c. irradiated with Al^+ ions up to 36 dpa.

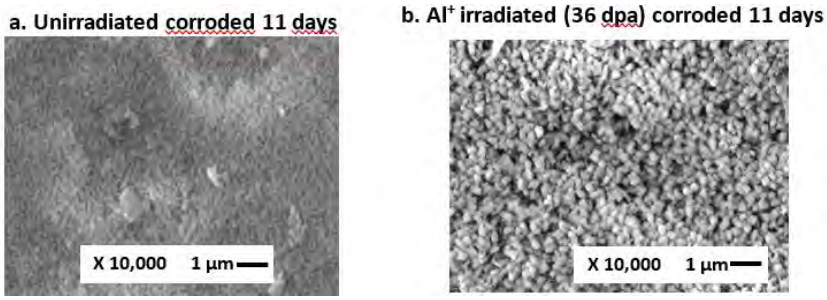

Figure 3 : SEM observation of oxide surface of AlFeNi samples after 11 days of corrosion at 140°C and pH 5.2 : a. unirradiated sample ; b. sample irradiated up to 36 dpa with Al^+ ions.

In order to study the oxidation kinetics and corrosion mechanisms of metal-irradiated samples, the weight of the samples was measured before and after corrosion experiments. In addition the oxide layer thickness was evaluated from SEM micrographs of samples embedded edge-on in resin. As can be seen in Figure 4, the oxide layer of the pre-irradiated samples is thicker than the as-received material for the short corrosion duration (1 day) while it is similar for the two types of samples for longer corrosion durations (11 and 16 days). The weight gain however is much more important for the metal-irradiated samples. This implies that the corrosion kinetics are initially faster for irradiated samples and that the formed oxide is much denser for the corroded irradiated samples than for the unirradiated metal.

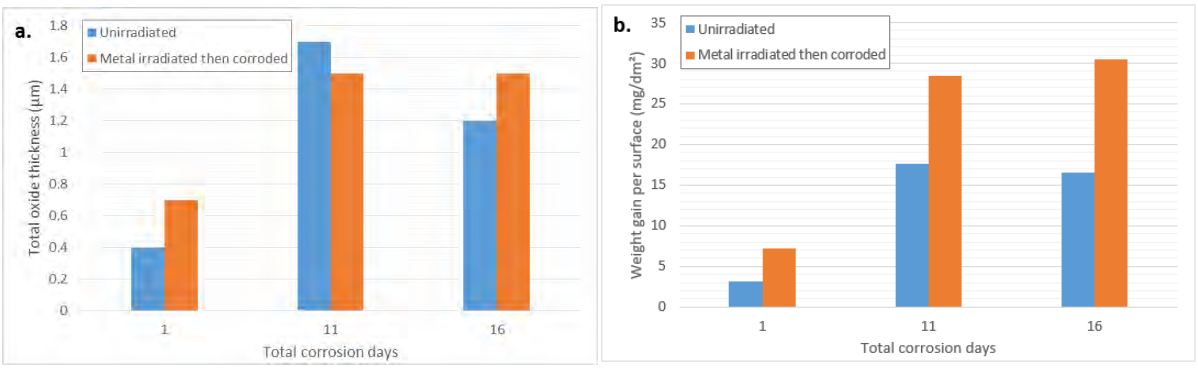

Figure 4 : a. Total oxide thickness versus corrosion time for unirradiated and pre-irradiated samples; b. weight gain versus corrosion time.

3.2. Impact of oxide irradiation on microstructure and corrosion mechanisms

During corrosion in reactor, irradiation affects not only the metal matrix but also the corrosion layer itself. In order to study the impact of irradiation on the oxide layer and on the corrosion kinetics, irradiations were performed on samples pre-corroded up to 11 days (140°C, pH 5.2). Grazing angle XRD patterns acquired on pre-corroded samples and on pre-corroded then irradiated samples (18 dpa with Al^+) are presented in Figure 5. The X-ray diffraction (XRD) pattern reveal that the oxide phase formed at 140°C on AlFeNi crystallizes with the boehmite structure which is consistent with previous literature results [7-9]. The boehmite lines however disappear for the irradiated samples suggesting an amorphization of the irradiated oxide layer. XRD patterns performed after re-corroding the irradiated samples show that the new oxide layer formed during post-irradiation corrosion experiments is constituted of boehmite.

The microstructure of the oxide layers is also significantly affected by oxide irradiation as shown in Figure 6. For unirradiated samples corroded for 33 days the oxide layer is constituted of two sub-layers: a dense inner layer with un-oxidized precipitates and a crystal-shaped outer layer constituted of aluminum hydroxide (as shown from the surface point of view in Figure 3). However, oxide-irradiated samples (pre-corroded 11 days, irradiated then re-corroded 22 days) present a triple layer oxide structure: both dense, precipitate rich inner layer and hydroxide crystal outer layer remain but a new intermediate layer appears in between. This intermediate layer is likely to be the initial irradiated oxide layers based on the measured dimensions.

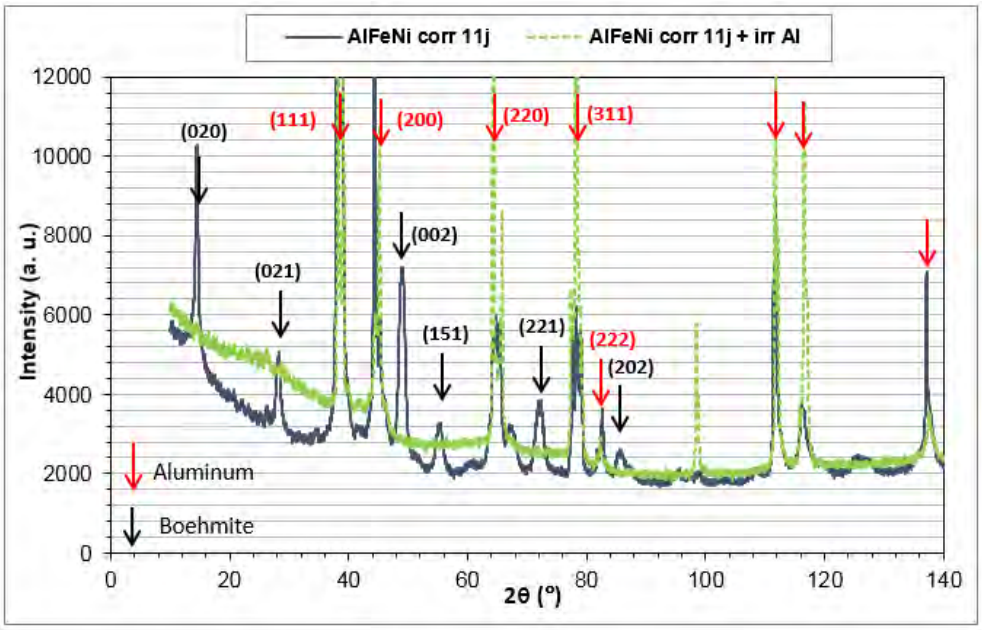

Figure 5 : XRD patterns of pre-corroded AlFeNi samples (11 days, 140°C and pH 5.2 – full line) and of a twin sample irradiated after corrosion (11 days, 140°C and pH 5.2 then irradiated with Al^+ ions up to 18 dpa – dotted line).

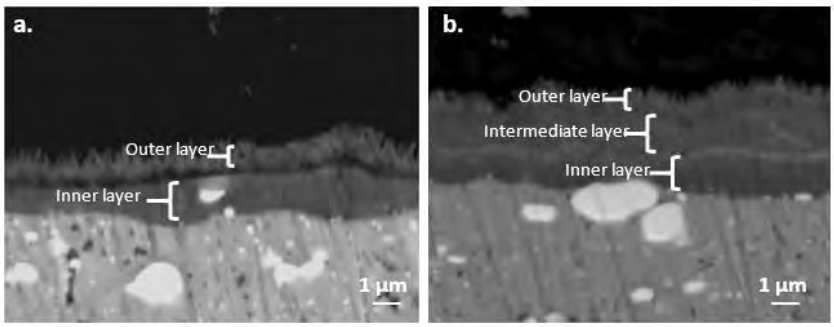

Figure 6 : SEM micrographs of AlFeNi corrosion layers (140°C and ph 5.2): a. for a sample corroded for 11 + 22 days; b. for a sample corroded for 11 days, irradiated with O^+ at 18 dpa then re-corroded for 22 days.

The impact of oxide irradiation on the corrosion kinetics is studied in the same way than for the metal irradiated samples by measuring weight gain and oxide layer thickness for unirradiated samples, pre-corroded (11 days) then irradiated then post-corroded samples. As can be seen from the results

presented in Figure 7, both the oxide layer thickness and the weight gain increase significantly for irradiated oxide layers compared to unirradiated samples. There does not seem to be a large difference between Al^+ and O^+ irradiated samples for the studied conditions. These results suggest higher corrosion rate for the oxide irradiated samples which could be due to the fact that the oxide layer damaged by the irradiation is less protective than the unirradiated one. This leads to greater cationic diffusion from the metal and in turn to accelerated anionic diffusion and overall greater corrosion kinetics.

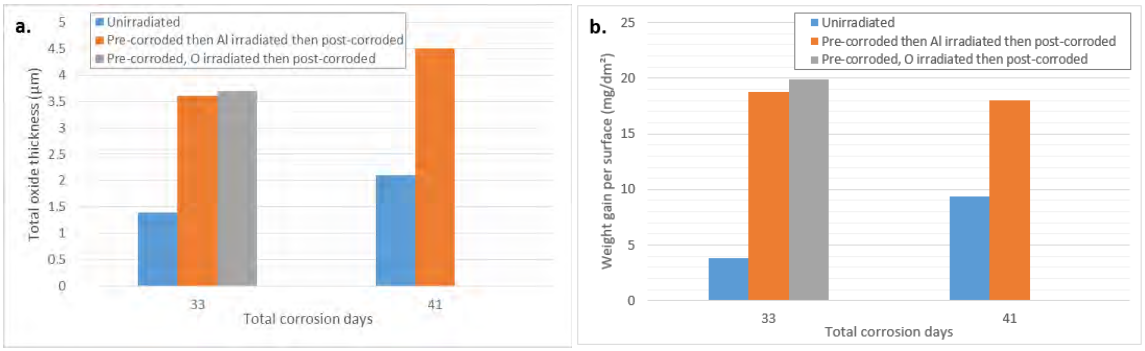

Figure 7 : a. Total oxide thickness versus corrosion time for unirradiated and oxide-irradiated samples; b. weight gain versus corrosion time.

3.3. Comparison to corrosion under neutron irradiation

In order to compare the observations presented in this study on ion-irradiated samples, a comparison to neutron irradiated samples is discussed in this section. Two AlFeNi samples in particular are of interest as seen in Figure 8:

a. The FLOREAL irradiation was performed in the Osiris reactor at ~43°C. The observed sample has received a fast neutron dose of 11 x 10^{20} n.cm^{-2}. The pH in the reactor was approximately 6. The residence time of this sample in the reactor is approximately ~60 days.

b. The SHARE irradiation was performed in the BR2 reactor [10, 11]. For these experiments, samples were representative of fuel cladding and were at higher temperature than the FLOREAL experiment: ~90-140°C at the cladding surface. The reactor pH is 6 and the water flow rate is 11 m/s. The studied sample exhibited an average burnup of 1.3 x 10^{21} fissions.cm^{-3} and was submitted to three irradiation cycles of ~23 days each.

Observations on the aforementioned neutron irradiated AlFeNi samples have revealed a duplex structure of the oxide layers which are subdivided into one dense layer with Fe-Ni precipitates visible and another dense layer without visible precipitates (Figure 8). Analysis of several samples with various irradiation times also revealed a densification of the oxide layer similar to that observed for ion-irradiated samples. In addition, an acceleration of the corrosion kinetics under neutron irradiation is also clearly demonstrated given the thickness of the oxide layers on the observed samples. This acceleration is also observed for ion-irradiated samples although it is not as strong as for neutron irradiated samples likely because ion irradiation and corrosion experiments are not performed simultaneously.

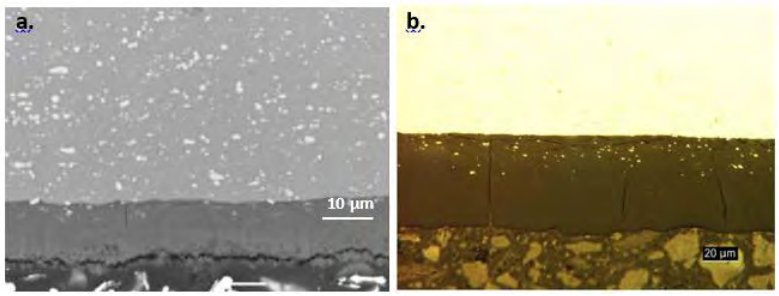

Figure 8 : Micrographs of neutron irradiated AlFeNi samples: a. FLOREAL irradiation in Osiris reactor; b. SHARE irradiation in BR2 reactor [10, 11].

4. Conclusions

In order to understand the impact of irradiation on the oxidation behavior of the AlFeNi fuel plates, various ion-irradiations and corrosion experiments were performed in this study. Two separate effects of irradiation were investigated: the impact of metal matrix irradiation and of oxide layer irradiation on corrosion behavior.

The main results from the metal-irradiated samples are summarized as follows:

-Metal irradiation up to 36 dpa with Al^+ created thin needle shaped precipitates;

-The surface layer of the metal-irradiated oxide is affected by irradiation (coarser crystals);

-The corrosion kinetics are initially accelerated for metal-irradiated samples, then a densification of the oxide layer occurs.

Examinations on pre-corroded then irradiated and post-corroded samples led to the following conclusions:

-The oxide layer amorphizes under irradiation. The newly formed oxide layer during post-corrosion is crystalline boehmite. The resulting oxide layer is sub-divided into 3 layers;

-The corrosion kinetics are much faster for ion-irradiated samples than for unirradiated samples suggesting a much less protective layer under irradiation.

The comparison of the results obtained with ion-irradiation to those obtained for neutron irradiated samples has also been discussed in this study. Similarities have been evidenced: densification of the oxide layer, accelerated corrosion kinetics. However, the observed effects are much more drastic for neutron irradiated samples which could be due to the fact that corrosion and irradiation happen simultaneously in reactor. It is suspected that the effect of neutron flux is a major factor on corrosion kinetics and must be carefully considered in order to develop a predictive understanding of the corrosion behavior of AlFeNi fuel cladding.

5. References

1. Griess, J.C., H.C. Savage, and J.L. English, *Effect of heat flux on the corrosion of aluminum by water. Part IV: Tests relative relative to the advanced test reactor and correlation with previous results*, 1964, ORNL: Oak Ridge, TN, USA.
2. Ondrejcin, R.S., *Evaluation of Mark-22 cladding*, 1983, Savannah River Laboratory.
3. Pawel, R.E., et al., *The corrosion of 6061 aluminum under heat transfer conditions in the ANS corrosion test loop.* Oxidation of metals, 1991. **36**(1/2): p. 175-194.
4. Pawel, R.E., D.K. Felde, and M.T. McFee. *The development of an improved correlation for corrosion product growth on aluminum alloy fuel cladding for the advanced neutron source*. in *Sixth International Symposium on Environmental Degradation of Materials in Nuclear Power Systems - Water Reactors*. 1993. San Diego, CA, USA.
5. Kim, Y.S., et al. *Prediction model for oxide thickness on aluminum alloy cladding during irradiation*. in *International Meeting on Reduced Enrichment for Research and Test Reactors*. 2003. Chicago, IL, USA.
6. Kim, Y.S., et al., *Oxidation of aluminum cladding for research and test reactor fuel.* Journal of Nuclear Materials, 2008. **378**: p. 220-228.
7. Wintergerst, M., et al., *Corrosion of the AlFeNi alloy used for the fuel cladding in the Jules Horowitz research reactor.* Journal of Nuclear Materials, 2009. **393**: p. 369-380.
8. Nabhan, D., et al., *Effects of pH, surface finish and thermal treatment on the corrosion of AlFeNi aluminum alloy. Characterization of oxide layers.* Journal of Nuclear Materials, 2015. **457**: p. 196-204.
9. Vargel, C., *Corrosion de l'aluminium*. Matériaux1999: Dunod.
10. Leenaers, A., et al. *Post-irradiation examination of AlFeNi cladded U_3Si_2 fuel plates irradiated under severe conditions*. in *11th International Topical Meeting Research Reactor Fuel Management (RRFM) and Meeting of the International Group on Research Reactor (IGORR)*. 2007. Lyon, France.
11. Leenaers, A., et al., *Post-irradiation examination of AlFeNi cladded U_3Si_2 fuel plates irradiated under severe conditions.* Journal of Nuclear Materials, 2008. **375**: p. 243-251.

ACQUISITION OF A SAFE MULTI-PURPOSE REACTOR

MARISA VAN DER WALT, DESIGN CONTROL MANAGER
Design and Licensing Project, Pallas
Comeniusstraat 8 Alkmaar,
PO Box 1092, 1810 kb Alkmaar, the Netherlands

ABSTRACT

PALLAS (Stichting Voorbereiding Pallas-reactor) aims to realise a multi-purpose reactor to replace function of the current High Flux Reactor (HFR) in Petten, which has been in operation for over fifty years and is now approaching the end of its economic life.

The acquisition of a new reactor requires the establishment of a framework to oversee the safety management and technical development thereof. This framework is based on systems engineering principles, regulatory requirements and IAEA standards. A tailored acquisition model is used to facilitate project delivery and integration with the licensing process.

Systems engineering principles are used for the development of the user requirements specification. The user requirements specification is based on a set of functional requirements derived from a functional breakdown structure. The top level function of the functional breakdown structure represents the PALLAS mission. The lower level functions enable the top level function. As part of the functional breakdown structure the main safety functions and specific safety functions are identified. These safety functions form the basis of the safety concept. A safety concept is developed to support the safety management and licensing process by mitigating potential design risks. From this the design basis and preferences are derived.

1 Introduction

The main purpose of the PALLAS Reactor is to be a multi-purpose reactor capable of producing medical and industrial radioisotopes and conducting nuclear technology research (private and public). The PALLAS project team is responsible for the establishment of a safe and cost effective reactor that will encourage investment by being a profitable, self-sustainable production facility.

1.1 Approach

The approach followed within this paper is presented in the following figure:

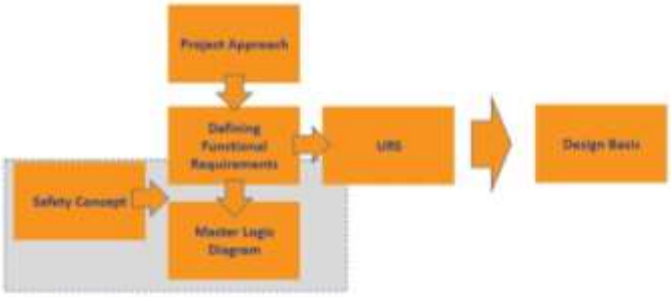

Figure 1: PALLAS Acquisition Model

Firstly, the project approach is presented. This includes the intelligent customer, acquisition model and the tender process of PALLAS. Secondly, to enable a tender process a user requirements specification was developed as part of the tender documents. The user requirements are based on functional requirements derived from functional breakdown structure. Thirdly, as input to the user requirements specification and use of the functional breakdown structure a safety concept was developed to facilitate safety within the design. From these input the design basis can be derived from.

1.2 Intelligent Customer

PALLAS is an Intelligent Customer, which entails overseeing project execution, developing the business case, establishing financing, defining the user requirements, performing design reviews to ensure conformance to the user requirements and managing the licensing process. This is being done with a small number of PALLAS employees working together in an integrated team with the employees of an Owners Engineer providing both permanent and as-needed back-office support. For the support on licensing and the design of the off-plot scope (balance of plant) a second engineering firm has been contracted. Both parties where appointed during 2015.

1.3 Acquisition Model

To enable the PALLAS mandate a tailored acquisition model is used, as presented in Figure 1. This approach is generally applied within a systems engineering environment and is used to facilitate acquiring design, construction, commissioning and operation of the PALLAS-reactor. This model is used as the basis for project planning and supports the integration of design, construction, commissioning and operations with the processes for the Dutch Nuclear Energy Act. For the PALLAS Project two nuclear licences are required: one for construction and one for operation.

With regards to the design process, the design will be managed in different design stages, namely the pre-conceptual design (as part of the bid proposal), conceptual design, basic design and detail design.

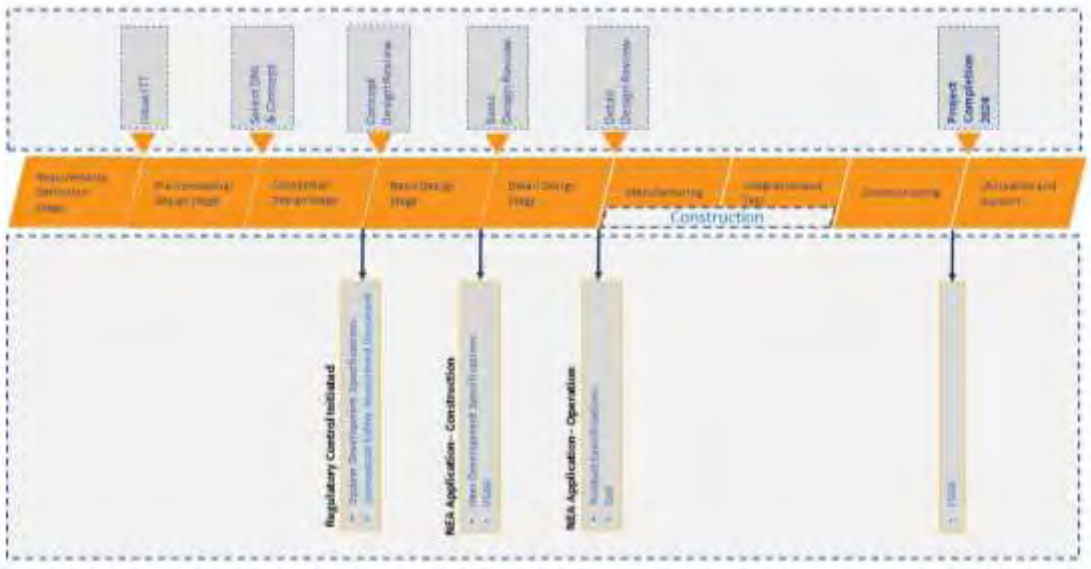

Figure 2: PALLAS Acquisition Model

As presented in Figure 2 design reviews are performed to assess technical progress during the design process and to provide PALLAS with an independent and objective opinion of the issues under review. Although design reviews have specific goals, they generally:

- Confirm up- and downwards traceability of requirements
- Verify validity and quality of requirements.
- Confirm that the output baseline of a stage satisfies the input requirements of that stage.
- Identify implementation alternatives
- Investigate selected design
- Investigate results of analyses and studies
- Assess risk associated with a selected design
- Ensure interface management with the off-plot scope design
- Authorise the next stage.

During these design reviews possible shortcomings are identified and corrective actions documented.

1.4 Tender Process

The Tender Phase of the Designer Selection Process, which will be launched during 2016, will be conducted under the EU Negotiated Procedure. The Tender Phase comprises two principal activities: Dialogue and Tendering.

The Contract will be a requirements based contract with the PALLAS requirements being defined in its User Requirements Specification (URS) which will form part of the Contract.

2 Requirements Definition

Following system engineering principles and the acquisitions model (Figure 1), within the functional architecture, a high level Functional Breakdown Structure (FBS) for the PALLAS-reactor was developed as basis for the User Requirements Specification.

2.1 Justification of Approach

One of the main reasons PALLAS pursued the FBS approach to define the user requirements was to ensure rigorous design control by enabling functional configuration audits throughout the product lifecycle. With regards to oversight of the project, development of the FBS serves as a guide to develop a Work Breakdown Structure for the selected designers of the PALLAS reactor and for PALLAS itself.

Within the design process the FBS provides a view on those systems, structures and components (SSCs) needed to perform the functions. It also allows the designer freedom to optimise the technical solutions to enable a function. Furthermore, this approach supports the identification of the personnel skills required for development and operation of the reactor. The FBS allows system engineering activities to completely integrate each discipline and furnishes a framework that will prevent over- and under-specification of requirements, as all SSCs are aligned with the identified functions.

Main safety functions and specific safety functions are derived within the FBS. The safety functions are used to classify the safety-class SSCs (paragraph 3.4). The FBS therefore heavily supports the development of the safety case, forming an integral part of the process of identifying the systems that can be credited in the development of the safety case.

2.2 PALLAS FBS

The FBS is a hierarchical structure of functions that enables the main function as presented in Figure 3. The functional architecture identifies and structures the allocated functional and performance requirements. The top level FBS for PALLAS is defined as follows:

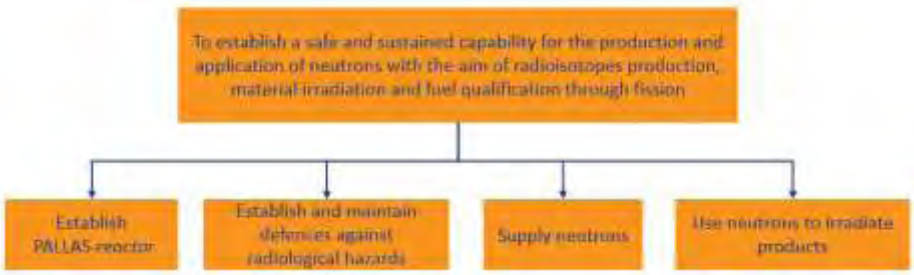

Figure 3: High-level PALLAS-reactor Functions

The lower level functions are required to enable the top level function and for this reason it was decided to break the lower level functions down into the establishment of the plant (PALLAS-reactor), dedicated safety functions, the supply of neutrons (which refers to the reactor) and the utilisation of the neutrons. The establishment of the plant entails the construction, manufacturing, commissioning and operation of the PALLAS-reactor. It will be part of the designer's responsibility to further the development of the functional breakdown structure.

2.3 Functional Requirements

The process of deriving the functional requirements from the FBS is presented in Figure 4.

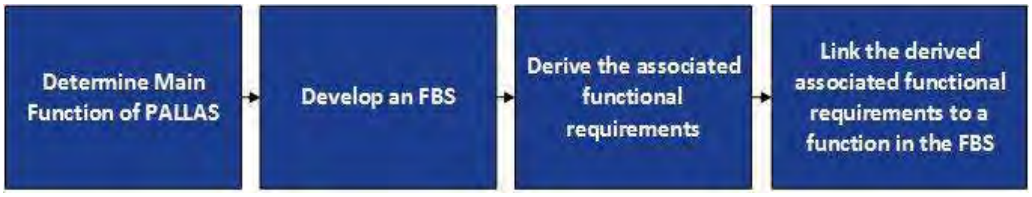

Figure 4: Deriving Functional Requirements

2.4 Non-functional Requirements

The Non-Technical URS defines the work packages and activities to be carried out by the designers.

2.5 Requirements Management

All requirements are managed within a requirements management tool. This forms part of an initial effort to perform configuration management over the full product life cycle. The requirements management tool being used is Relatics. This tool will enable:

- management of each requirement as a configuration management item
- unique identification of a requirement
- full traceability of the requirements
- preservation of all technical communications with the Tenderers
- a common platform on which PALLAS and Tenderers can work
- the restructuring of requirements as and when required
- providing each Tenderer with a secure workspace to which only PALLAS will have access
- real time update of requirements

3 Safety Concept

The main safety objective of PALLAS is to protect the public, workers and the environment and for this reason it is required to ensure the prevention and mitigation of safety risks by maintaining the fundamental safety functions and by implementation of design provisions.

The PALLAS safety concept is based on the Dutch Safety Requirements (DSR) and the main goal of the concept is to implement requirements to maintain the fundamental safety functions. The approach is therefore used to mitigate the potential risks within the design. The safety concept focuses on the technology and must be applied throughout the entire plant life cycle.

By implementing the safety concept within the design assurance of reactivity control, minimization for radiological impact and sufficient heat removal are achieved. The following figure presents the application of the DSR within the safety concept on a high level:

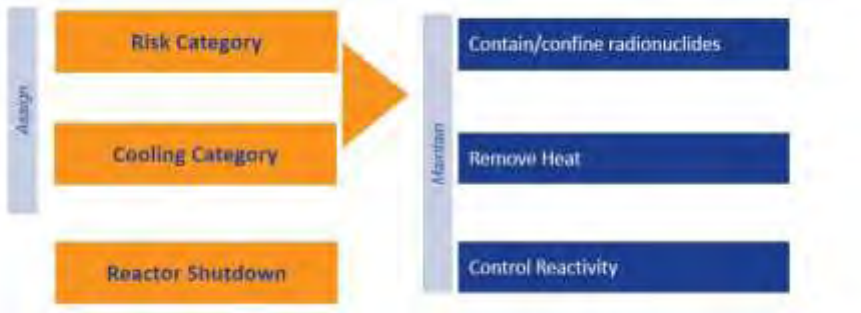

Figure 5: Maintaining Fundamental Safety Functions

As the DSR is based on safety requirements for nuclear power plants, grading of the requirements is necessary to account for the large difference in thermal power when compared to a research reactor. When a requirement is graded sufficient justification needs to be provided. Justification for grading of a requirement is based on the hazard level of the plant, deterministic safety analysis, probabilistic safety assessments, experiments and engineering judgement.

3.1 Risk mitigation

In addition to the inclusion of design provisions and maintenance of safety functions further measures shall also be implemented to mitigate safety risk (Figure 6). These measures are input to the PALLAS user requirements specification.

Figure 6: PALLAS Safety Concept

3.2 Risk Category

As presented in the DSR, grading requires the determination of the plant hazard level. The plant hazard level is used to assign a risk category to the facility. The risk category takes radiological impact into account and represents the fundamental safety function 'confinement of radioactive materials'. Factors including, but not limited to, the reactor power, amount and enrichment of fissile and fissionable material, source term, spent fuel elements, high pressure systems, type of fuel etc. are taken into account when determining the hazard level. The systematic approach to selection of risk category shall be justified and presented to the regulator for acceptance.

3.3 Cooling Category

The reactor shall be designed according to cooling category two, as per the DSR. Cooling category two is defined as follows: After shut-down from full power operation the reliability of passive cooling systems must be ensured to remove the residual heat from the reactor core to an ultimate heat sink. In the worst case scenario cladding failure and melting of fuel element shall be considered.

3.4 Master Logic Diagram

This paragraph describes one of the valuable uses of the FBS. A master logic diagram methodology (as presented in Figure 7) is followed to assess the risk of failure of a safety class SSC. The methodology has three main outcomes as described in the following sections, namely the Functional Breakdown Structure (as per paragraph 2), risk assessment and classification.

The risk assessment uses the SSC safety functions (SSF) identified in the Functional Breakdown Structure as a starting point. Consequently, each SSF is evaluated for potential Functional Failure Modes (FFMs). The FFMs are the ways in which the SSC fail to meet a performance requirement. FFMs therefore include not only the total inability for the function to be performed, but also the incorrect performance of the function.

Next, the process requires the identification of Failure Causes (FC), which are described to provide some insight to the probability of occurrence of the FFMs. The FCs also provide information on the important characteristics of the related SSC. Once the FCs have been identified it is necessary to evaluate the consequence of Functional Failure Modes which in turn is used to determine the unmitigated consequence of the functional failure. Following this the Probability of Functional Failure Mode is evaluated (the probability of each FFM leading to a given consequence is assessed). This should be justified by equipment reliability data and initiating events.

At this stage it is possible to identify credited mitigation SSC Safety Functions - where failure of a SSF may lead to a certain consequence level a different SSF may be credited to mitigate the failure, provided that the mitigating SSF inherits at least the safety category corresponding to the consequence of the failure. SSFs are therefore categorized according to the consequence of only those failures that they are credited for.

Only now, when the performance requirements of the SSC can be established, the SSF is categorised (for example high, medium, low or non) and used as input to the SSC classification. The SSC classification is presented as:

Cat-H SSF	----->	SC-1 SSC
Cat-M SSF	----->	SC-2 SSC
Cat-L SSF	----->	SC-3 SSC
Cat-N SSF	----->	SC-non SSC

The Master Logic Diagram is presented below:

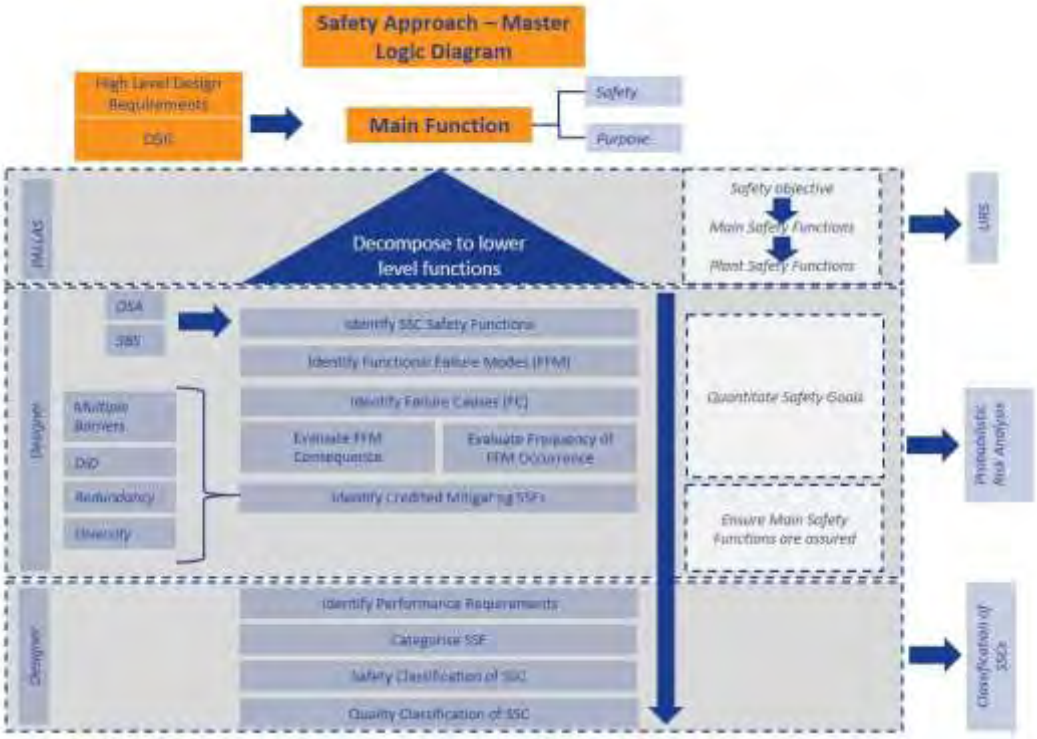

Figure 7: PALLAS Master Logic Diagram

4 Basis of the PALLAS Design

To strengthen the safety, availability, reliability and economic performance of the PALLAS reactor it is necessary to have the highest level of proven technology and use Commercial of-the-shelf (COTS) items in accordance with best engineering practices.

4.1 Simplistic Design

A simplistic design is preferred which entails the following:

- Using the minimum number of structures, systems and components (e.g. pumps, valves, instruments, electrical components etc.) to comply with functional requirements

- Having a simplified plant layout, pipe routing and equipment arrangement to facilitate construction and maintenance
- Simplifying the system design and control logic
- Simplifying manoeuvring, loading and unloading of irradiation facilities

4.2 Flexibility

PALLAS acknowledges changing future markets and therefore, to attract investors and customers, the design needs to be flexible, enabling adaptation of the PALLAS Reactor to address current and future business requirements.

4.3 Design Requirements and Preferences

The reactor will be required to have a thermal power as low as possible and the fast and thermal flux levels are to be optimised with respect to the future customer requirements. The choice for selection of reflector should be based on the safest and most economically feasible option. Depending on the practicable power density, the preference of PALLAS is to have a non-pressurised open pool reactor. With regards to the shutdown of the reactor, first and second shutdown systems are required. One of the main requirements is the prevention of common cause failure between the two systems during displacement of the core due to internal or external events.

With regards to reactor fuel, it should be low enriched U3Si2 fuel. The PALLAS Reactor should be able to be converted to UMo in the future.

4.4 Radioisotope Production

The PALLAS reactor should enable the production of Mo99 and other isotopes. At this moment it is foreseen that Mo99 can be considered as a priority product as it is currently anticipated to be the highest revenue-generating product by PALLAS.

4.5 Experiments

Experiments to be considered in the PALLAS reactor design are positioned towards fuel, material qualification and degradation studies including material testing for irradiations performed with a homogeneous-constant temperature distribution, thermal neutron irradiations and fast neutron irradiations. Due to the uncertainty in the market different options are under consideration, including loops required for fuel improvement/ ramping/ qualification.

4.6 Value Chain

PALLAS aims to have a competitive value chain. Important factors to consider are minimising time losses, adding value to customers, monitoring of processes and improved ergonomics. In terms of production the following elements need to be considered:

- Customer/user needs are to taken into account regarding irradiation duration, cooling requirements and delivery schedule.
- Limiting unforeseen shutdowns
- Enabling safe, fast restart after an unplanned shutdown
- Adjustable cycle durations depending on market demands
- Ensure continuous reactor operations
- Dry vs. wet loading of products

4.7 Life Cycle Costs

Life cycle costs and return on investment should be taken into account when determining the optimal plant life time and cycle duration. PALLAS Reactor plant life time should be at least 40 years.

4.8 Availability

To enable a viable business case PALLAS Reactor needs to have an availability of more than 300 Full Power Days (FPD). The reactor cycle duration is a function of customer needs and maintenance requirements and for this reason needs further optimisation. PALLAS suggests a cycle duration of 28/31 days per cycle which is similar to the HFR design.

4.9 Operating Philosophy

With regards to the PALLAS operating philosophy, the designers are required to propose an optimal strategy in terms of safety and cost. Aspects to be considered are operators' roles and responsibilities, how the PALLAS Reactor will be operated in normal and abnormal conditions, the composition of operating crew, the skills and capabilities of reactor operators and equipment or auxiliary operators, how the crew is expected to handle anticipated and unanticipated transients, maintenance requirements and human factor aspects in the facility.

4.10 Inspectability and Maintainability

With regards to inspectability and maintainability of the PALLAS Reactor the preference is to have:

- Effortless removal of core internals and structures during normal maintenance periods
- Low maintenance equipment
- Online maintenance and inspection (where possible)
- Online monitoring
- Reduction of occupational exposure
- Facilitate access to equipment (ease of access to several areas during operation as well as during outages)
- Maintenance performed under satisfactory work conditions
- Use of automated maintenance and inspection machines
- Ease of exchanging components
- Ease of measuring and monitoring parameters
- ALARA dose rates and exposure-time at maintenance locations
- Ease of isolating parts or components by having spare capacity / multiple redundancy
- Waste production minimisation
- Online testing and equipment to be able to do self-testing

4.11 Instrumentation and Control

With regards to instrumentation and control the designers will be expected to propose the ratio and distribution between digital and analogue technology in accordance with safety and cost optimization.

4.12 Electrical Supply

The main electrical supply is provided by Off-Plot-Scope-infrastructure and all systems inside the NI by the DNI. Active cooling will be required during normal operation and passive cooling in loss of off-site power. There should be limited needs for uninterrupted power supply and emergency power supply in order to limit investment cost.

Highlights of Regulatory Aspects of Research Reactors in the Russian Federation: from Fukushima to Future

Alexander Sapozhnikov

Federal Environmental, Industrial and Nuclear Supervision Service of Russia,
109147 Moscow, Taganskaya, 34, Russia

ABSTRACT

The experience available from the Fukushima Daiichi NPP accident is crucial and equally applicable to research reactors, including associated facilities (first of all spent fuel storages), when subjected to extreme external events. A set of design extension conditions are to be derived with the aim of enhancing capabilities of the research reactors to withstand more severe accidents without unacceptable radiological consequences. In solving the above stated problem and in view of improving application of the defence in depth concept at nuclear research facilities an exhaustive review of the complementary safety assessments of research reactors in the Russian Federation has been performed with due account to feedback from the Fukushima Daiichi NPP accident. The report presents main results of this regulatory review with the emphasis on such issues as regulatory aspects, safety requirements and emergency communication.

1. Introduction

Following the accident at the Fukushima-Daiichi Nuclear Power Station (F-D accident) the community of research reactors (RRs) stakeholders, operators and regulators has supported an initiative to re-evaluate and update safety status of the facilities facing a possibility of extreme external events. The preliminary results of this initiative activities were discussed at the International *Conference on Research Reactors: Safe Management and Effective Utilization,* held 14-18 November 2011 in Rabat, Morocco. Complementary safety reassessments were performed at research reactors, spent fuel pools, and other associated facilities, based on graded approach and taking into account the potential hazard associated with a specific facility or activity. The objective of the reassessment was to evaluate robustness of the existing facility against the impact of credible extreme events, and, if it needs, take measures to enhance RR safety. Rostechnadzor[1] reviewed safety reassessments, performed by operating organizations in order to evaluate their compliance with the established set of enhanced safety requirements and with current reference basis for licensing of nuclear research facilities (NRFs)[2] and activities, specified in the established programme for complementary safety reassessment (stress-test). The review of safety reassessments of NRFs did not identify any gaps in the national regulatory framework or necessity to take urgent measures to change NRF safety requirements. The findings from these reviews were discussed with operating organizations, introduced at international technical meetings, and reported to RR community as presented in Ref. [1-4]. The report introduces a proactive approach taken by Rostechnadzor in order to update NRF safety requirements in light of the lessons learned from the F-D accident, taking into account recommendations of the IAEA IRRS missions, new and forthcoming IAEA safety standards and other documents related to safety of research reactors [5-7]. It is shown that the national regulatory framework and the NRFs reference licensing basis are consistent with the IAEA

[1]The Federal Environmental, Industrial and Nuclear Supervision Service (Rostechnadzor) - the state regulatory authority in the field of the use of atomic energy.

[2] NRF - nuclear research facility including research nuclear reactors, critical and subcritical nuclear stengs, and related complex of premises, structures, systems, elements, experimental facilities, and personnel that are in boundary of territory (NRF site) defined by the design for utilization of neutrons and ionizing radiation for research purposes.

safety standards, sustain safety enhancement and may be applied to the both - refurbishment of operating NRFs and commissioning of new 100-150 MW (th) facilities for future research.

2. Main Findings and Outcomes of NRF Safety Reassessments in Russia

Organizational and technical aspects of the NRF complementary safety reassessment covered design features and procedures, site specific hazard, analysis of the extreme external events (including their combination and consequential events), and assessment of sufficiency of emergency preparedness and emergency management. Reassessments of safety of NRFs were made in two steps, and were performed totally for 37 NRFs and 15 associated facilities. The results of review of Rostechnadzor have not revealed the necessity to upgrade current licensing basis, because most of the safety aspects had been analyzed before the F-D accident. In fact, safety reassessments of the NRFs are performed every 5-10 years, inspections at facilities are carried out systematically in planned regime and main safety aspects are monitored in continuous supervision. In general the safety reassessment of NRFs showed that:

- The technical and administrative measures taken in design basis of NRFs provide safety of personnel and population in case of design basis accidents (DBA) and those beyond design basis accidents (BDBA) that have been reviewed in safety analysis report (SAR);
- In case of BDBA scenarios, considered in the design and evaluated in SAR, the projected doses of radiation exposure to population will not exceed the criteria for public evacuation.

Careful analysis of the extreme external events, including their combination and consequential events identified the need of safety improvements at some facilities that were implemented. Most important of them were installation of new antiseismic diesel generators and additional pumps for emergency cooling.

The reassessment of the consequences of the impact of BDBA events on storages of spent fuel (SF) showed that:

- Storages of SF at many reactors were put in operation long time ago, their loading is high and terms of SF storage are long;
- Coating of SF storage pools at many facilities may be not sufficient to keep pool integrity and exclude penetration of the radioactive water from pool into a ground water under extreme external events. To avoid the mentioned consequences additional measures for safety enhancement have been determined and implemented including the removal of the SF from the site for reprocessing.

Although the complementary safety reassessment of NRFs did not identify the necessity of urgent changes in NRF safety requirements, it has revealed areas for long-term updating of the regulatory framework such as: extension of groups of BDBAs for analysis (design extension conditions); strengthening of emergency power supplies; setting specific system for predicted shutdown in case a parameter of extreme external process reached the dangerous values; modifying emergency planning, in particular, for RRs with potential off-site consequences; improving communication of emergency information; and clarification of roles and duties of Rostechnadzor's officials during an accident. A technical brief of recent and future enhancements of regulatory framework is given below.

3. Improving of Regulatory Framework

3.1. Recent Fundamental Amendments to the Atomic Act

In the Russian Federation a number of fundamental principals are established in the federal laws but not in safety standards. In view of feedback of the IAEA IRRS missions to the Russian Federation [8] the following fundamental amendments were implemented in 2011-2013 to the Federal Law on the Atomic Energy Use (Atomic Act):

- Priority of nuclear legislation over legislative requirements in other areas (e.g. in industrial safety);
- Legal status of the Regulatory Body with regard to its authorities and independence;
- Activities subject to licensing;
- The state-level oversight, including establishment of continuous supervision;
- The Institution of "Scientific and Technical Support Organization" for the authorized Safety Regulatory Authority;
- Strengthened responsibility for violation of legislation in the field nuclear energy;
- The opportunity for operating organization to have a combined license for carrying out several types of activities in relation to one or several facilities;
- *The legal status of "Safety Guides" issued by the Regulatory Authority;*
- *Adoption of graded approach to safety regulation depending on a potential facility (activity) hazard;*
- *Requirements for conducting periodic safety reviews of nuclear facilities and fuel storages.*

Relevant amendments in procedures for licensing, state safety oversight, and developing of safety standards and safety regulations (guides) were enforced by subsequent decrees of the Government of the Russian Federation in 2012-2013, including:

- Provisions on Licensing in the Field of Nuclear Energy Use (2013);
- Provisions on the Federal State Supervision in the Field of Nuclear Energy Use (2012);
- Provisions on the Regime of Permanent State Supervision at Nuclear Facilities (2012);
- List of Nuclear Facilities Subject to Permanent State Supervision (2012);
- On Specifics of Standardization in the Field of Nuclear Energy Use (2013);
- On Development and Approval of Federal Regulations (2012).

3.2. Current State of the System of NRF Safety Regulations

The safety objectives, principles, criteria and requirements, which are mandatory for the performance of activities in the field of atomic energy use, were established in the safety regulations. The system of safety regulations includes two hierarchy levels as Ref. [9]:

- General safety provisions for each type of the nuclear facilities (Nuclear Power Plant, Nuclear Research Facilities, Nuclear Installation on Ships, Nuclear Fuel Cycle Facility, Radioactive Sources);
- Safety standards pertaining to types of activity:
    - Common for all types of nuclear facilities/activities (for example, Requirements to Quality Assurance Program of Nuclear Facilities, NP-090-11; Accounting of External Natural and Man-Induced Impacts on Nuclear Facilities, NP-064-05);
    - Specific requirements for each category of nuclear facilities/activities (for example, safety requirements for the facility siting, design ect.).

The system of safety standards developed by Rostechnadzor incorporates 86 documents, including 9 safety standards specifically for NRFs:

- General NRF Safety Regulations (NP-033-11);
- Rules on Nuclear Safety of Research Reactors (NP-009-04);
- Rules on Nuclear Safety of Critical Stands(NP-008-04);
- Rules on Nuclear Safety of Pulse Reactors (NP-048-03);
- Rules on Nuclear Safety of Subcritical Stands (NP-059-05);
- Requirements to the Content of NRF Safety Analysis Report (NP-049-03);
- Provisions on Investigation and Reporting on Anticipated Operational Occurrences and Accident at NRFs (NP-027-10);
- Requirements to the Content of Plan of Actions to Protect Personnel in Case of an Accident at NRF (NP-075-06);
- Safety Rules on Decommissioning of NRFs (NP-028-01).

Furthermore, the system of safety standards comprises the documents, which are developed and approved by other regulatory bodies of the Russian Federation (for example, Radiation Safety Norms, NRB-99/2009; Sanitary Rules of RRs, SP IR-03).

Rostechnadzor has developed and issued a set of national safety guides, which provide recommendations and guidance on how to comply with the safety requirements established by safety standards.

4. Licensing of Commissioning New NRFs

At present Rostechnadzor conducts state safety regulation of 65 NRFs, two of them are the research reactors under commissioning as international centers for research: RR “PIC” in Konstantinov Petersburg Nuclear Physics Institute (PNPI), Gatchina, Leningrad region, and RR “MBIR” in Joint Stock Company “State Scientific Center – Research Institute of Atomic Reactors” (JSC “SSC RIAR”), Dimitrovgrad, Ulyanovsk region.

The research reactor “PIK” – is tank, water-water type with heavy water reflector, power 100 MW, maximal flux of thermal neutrons $5 \cdot 10^{15}$ $n/sm^2 \cdot sec$. The proposed date of operation at power is 2020. The reactor “PIK” is intended for a wide range of research tasks specified in long-term nuclear science and technology programme. The facility is equipped with 22 beams for research purposes, has three sources of cold neutrons, and 50 stations for research (condensed matter physics, nuclear physics, elementary particle physics), and includes hall of horizontal channels and neutron guides and hall for neutron scattering. The decision on the reactor commissioning was taken in 1969. The commissioning of the reactor was started in 1976. After Chernobyl accident there was a decision on facility reconstruction, but it was postpone due to economic reasons. Rostechnadzor issued the first licence on commissioning of the reactor in January 2000. Further works on design modification were completed in 2006. At present design includes three stages of the facility startup: 1) start-up till power 100 KW, 2) power start-up till 100 MW, 3) finalization of experimental basis. The results of peer review in licensing of RR “PIC” were discussed at the session of Scientific and Technical Board of Rostechnadzor with participation of competent authorities and stakeholders on 30 September 2009. The facility was licenced for operation in 2010 at power 100 W and the first physical start-up of facility was performed in February-March 2011. Currently the facility is under preparation for start-up at power 100 KW. The licence on commissioning activity is valid till 31 December 2021, the activity for facility operation is carried out within the new license issued on 30 December 2015 and valid till 30

December 2022. The availability of two licenses allows the operating organization to undertake both activities on construction and commissioning as well as equipment testing. The design includes reinforcement of reactor buildings against earthquakes and implementation of additional monitoring instrumentation including seismic detectors with associated action to shut down the reactor; specified equipment and procedures for mitigation of severe accident consequences, and probabilistic safety analysis as a complementary tool for safety assessment. Following the lessons learned from the F-D accident the peer review during the licensing process covered analysis of additional groups of BDBA, including crash of aircraft at reactor building accompanied by fire; facility blackout with failure of emergency power supplies; loss of ultimate heat sink; break of the wall of the reactor vessel, and other extreme external events and their combination with impact at all related facilities.

The research reactor MBIR – is Multipurpose Sodium Fast Research Reactor, power 150 MW, maximal neutron flux $5{,}3 \cdot 10^{15}$ n/(sm^2•sec), designed lifetime – 50 years. The proposed commissioning date is 2020. The new facility MBIR is intended to replace the world's unique fast research reactor BOR-60, which was put in forth in 1969 and has licence valid untill 29 January 2019. Modern facility will have new opportunities for testing material and fuel as well as a wide range of post-irradiation examinations needed for study innovative nuclear power reactors and capabilities of closed nuclear fuel cycles. The facility commissioning is implemented within frame of the Federal Target Programme «New Generation of Nuclear Power Technology for 2010 - 2015's and up to 2020» (2010). The licence for facility sitting (engineering research and other activity) is issued on 25 June 2014 and valid untill 25 June 2019. Owing to lack of a specific standard for NRFs sitting, the standard "Sitting of NPP. General Criteria and Safety Requirements" (NP-032-01) was applied in the reference licensing basis for peer review of the facility. The results of peer review in licensing of RR "MBIR" were discussed at the session of Scientific and Technical Board of Rostechnadzor with participation of competent authorities and stakeholders on 25 June 2015. The activity on commissioning of the facility is carried out within the license issued on 8 May 2015, which is valid until 8 May 2025.The peer review of facility licensing on commissioning of the facility covered 72 safety documents including interim SAR that consists of 24 volumes. Following the lessons learned from the F-D accident the peer review during the licensing process covered analysis of additional groups of BDBA, including crash of aircraft, facility blackout with failure of emergency power supplies, lost of integrity both of main tanks and safety vessel plus fire in the reactor vault, criticality during handling and storage of nuclear fuel, falling of equipment and building structures on overlapping of compartments nuclear fuel storage or on the nuclear fuel inside storage, flooding of nuclear fuel storage.

The development of new safety standard ***"Sitting of NRFs. General Criteria and Safety Requirements"*** and new safety standard ***"Requirements to Emergency Power Supplies of NRFs"*** was recognized to include in a long-term plan on updating of safety standards as presented in Ref. [10].

5. Improvement of NRF Safety Requirements

Consistency and adequacy of the established safety requirements and guidance are confirmed by successful operation of NRFs. The IAEA IRRS missions, held in the Russian Federation in 2009 and 2013, stressed efficiency of a regulatory framework as a whole. However, the improvement of safety requirements is ongoing process because of the changes to the atomic energy legislation due to following two factors:

- Need to incorporate recommendations of international organizations, progress in science, industry and technology, and national and international experience (good practice on the safety regulations, findings, lessons learned from accidents);

- Need to ensure safety design and commissioning of new types of reactors and other nuclear facilities and (or) activities (performance of works, services) in the field of atomic energy use.

In this light, Rostechnadzor carries out the systematic review and analysis of the national regulatory basis.

5.1. Incorporation of National and International Experience and Good Practices

Generally the set of national NRF safety standards is full, consistent with the IAEA Safety Standards and sustain enhancement of NRF safety. The recent enhancement of safety regulatory system is given below.

New Safety Standard ***"Periodic Safety Reviews for NRFs" (NP-092-14)*** was issued on 19 February 2015. Following to Principle 3 in Ref. [11] safety has to be assessed and periodically reassessed throughout the lifetime of facilities and activities, consistent with a graded approach. Following to an article of the Atomic Act (see item 3.1 above) the national standard has been developed that specifies requirements to PSR of NRFs licensed for operational period more than 10 years apart from the facilities that are in a final shutdown mode or in decommissioning state. The complex task of PSR is subdivided into several important aspects of safety. A level of facility safety is determined by a global assessment reflecting the combined effect of all specified safety factors.

New Safety Guide ***"Recommendations on development of probabilistic analysis of NRFs"*** is in approving process. The safety guide provides recommendations and guidance of the Rostechnadzor on how to comply with the safety requirement established by safety standard "General NRF Safety Regulations" (NP-033-11). There is requirement that a likelihood of maximal radioactive release requiring urgent protective actions for public shall not exceed 10-7 1/per year. The compliance with this requirement should be reflected in the SAR. The safety guide contains guidance for determining the cumulative probability of the accidental releases of radioactivity, that lead to exceeding the doze limits values for population established by the safety standard "Norms of Radiation Safety" (NRB-99/2009). Probabilistic Safety Analysis (PSA) is recommended for those nuclear facilities that have potential for accidental radioactive release resulting in the need for warranting urgent protective actions for population.Based on graded approach the fact that radioactive release and risk to exceed established doses are negligible shall be justified through deterministic analysis. The safety guide includes recommendations on scope and contests af the PSA, methods of specific PSA tasks and format of reported documents.

New Safety Guide ***"Preparation and Transmission Data of the Automated Information Support System to Control of NRFs while Normal Operation and Emergency" (RB-077-12)*** was issued on 22 November 2012. The safety guide provides recommendations and guidance of the Rostechnadzor on how to comply with the safety requirements established by safety standard "Provisions on Investigation and Reporting on Anticipated Operational Occurrences and Accident at NRFs" (NP-027-10) to enhance quality and efficiency of information exchange. The safety guide recommends to implement in operating organizations the Informational Support Centers, which may be integrated in automated information system at local and federal levels for monitoring state of NRFs in normal operation and in emergency.

5.2. A Long-Term Plan for Updating of Safety Standards

To provide for harmonization of safety and security requirements with recommendations of international organizations, keeping their consistency and stability, Rostechnadzor drafted *"Concept for Improvement of Normative Legal Regulations of Safety and Standardization in*

the Field of Nuclear Energy Use" Ref. in [10] that is now in the process of approving by relevant competent authorities and stakeholders. When developing new NRF safety requirements, the relevant IAEA recommendations and standards are required to be examined and taken into account. A technical brief of safety requirements for NRFs that are being reviewed by Rostechnadzor are highlighted below.

The safety standard ***"General Safety Regulations for NRFs" (NP-033-11)*** belongs to a high hierarchy level and defines general requirements to all types of NRFs at all stages of their life time. The standard specifies that the dose limits for occupational and public exposure, and established discharge levels of radioactive substances in the environment must not be exceeded during facility operation, anticipated operational occurrences and DBA, and the consequences of BDBA, if they do occur, may be mitigated. The defense-in-depth concept is applied to ensure adequate protection. The general safety requirements cover technical and organizational measures that shall be taken to support effectiveness of independent defence levels against anticipated operational occurrences and possible accidents resulting from equipment failure, human behavior or action, and events induced by external hazards. The system of technical and organizational measures shall be provided at five levels of defence. The number of implemented physical barriers on the ways of harmful impact of radiation, nuclear materials or radioactive substances to the environment and measures supporting effectiveness of these barriers shall be defined by the design. The adequacy of applied physical barriers, technical and organizational measures of defense-in-depth protection shall be justified in the design and analyzed in the NRF SAR.

Graded approach and integrated management system shall be applied. Global safety requirements to structures, systems and components important to safety (SSC) make focus on maximal use of inherent safety features of the facility design, including large margin for operational parameter; application of proper structural materials; use of self-quenching effect for process variables; installation of passive protection systems to avoid power supply (including installation of passive components in the cooling systems); providing of inertial emergency process with time enough for personnel intervention, and prevention of BDBA becoming DBA and BDBA transient in severe accident. The revision of this safety standard is not planned until 2023.

The safety standards ***Nuclear Safety Rules (NP-009-04), (NP-008-04), (NP-048-03), (NP-059-05)*** reflect design specific of the core, protective, localizing, control and supplying safety systems, including extent of the cooling requirements, structures for confining radioactive substances, handling with nuclear fuel and materials, requirements to experimental facilities and works. The nuclear safety requirements have been developed in the separate safety standards specifically for research reactors with steady-state neutron flux; pulse research reactors, including self-quenching (burst-type, aperiodic) and with reactivity modulation (batch-type, periodic); critical stands; subcritical stands.

The safety standard ***"Rules on Nuclear Safety of Research Reactors" (NP-009-04)*** is under revision. The following additional safety requirements are proposed to include in the draft:

- The analysis of the SSC in response to impact of combination of external natural and man-made origin events specified for facility site along with the impact of other NRFs located at the site;
- Groups of BDBA for analysis shall be extended based on deterministic approach including NRF blackout, loss of the ultimate heat sink;
- Emergency power supplies shall ensure safe core cooling, safe localizing of radiation, and continuity of facility monitoring in emergency;

- Installation of the monitoring instrumentation including seismic detectors connected to the reactor protection system shall be provided.

The safety standard ***"Rules on Nuclear Safety of Critical Stands" (NP-008-04)*** is in approving in 2016. The following additional safety requirements to design (operational) documents are proposed to include in draft:

- The values of parameters of external impacts of natural and man-made origin requiring facility scram;
- The analysis of the SSC in response to impact of combination of external natural and man-made origin events specified for facility site.

The safety standard ***"Requirements to the Content of NRF Safety Analysis Report" (NP-049-03)*** is under revision. The safety standard defines requirements to information, which has to be submitted to Rostechnadzor for the review and assessment of SAR. In SAR shall be included features of initial design, modifications, and current state of the NRF, results of adjustment and tests of systems, facility criticality and facility starting-up, correction of design and amendments in documents, management programme, safety analysis covering DBA and BDBA. The acting safety requirements were evaluated in respect to international practice. These concerns:

- Characteristics of Aria and Site of NRF
    - Potential external impacts, external events, having potential frequency 10^{-6} per year and more;
    - Monitoring of external events impacts, maximal values of hydro meteorological, geological and engineering-geological processes and phenomena determined on a time interval equal to 10,000 years and are considered in the design.
- Buildings and Structures
    - Shall withstand to natural and man-induced external impact;
    - Will not have inadmissible damages in normal operation and violations due to external impacts of maximal design values;
    - Will provide confining of radioactive substances, so that possible release in environment at DBA does not exceed a permissible level.
- Analysis of Accidents
    - DBA, list of postulated initiating events, requirements to analysis;
    - *Recommended* groups of BDBA for analysis:
        a) Accidents, caused by unauthorized insertion of high positive reactivity as a result of superposition of a number of failures or personnel errors, which may be accompanied with reactor core damage and nuclear fuel melting.
        b) Accidents, where the initiating events of design-basis accidents are accompanied by complete failure of the scram system and by the failure of any one component of confinement system or by the false decision to control this system.
        c) Accidents, caused by the complete black-out of the facility (complete disappearance of system and emergency power supply) and accompanied by the failure of any one component of confinement system or by the false decision to control this system.
        d) Loss of coolant of research reactor, leading to the "bared" core and complete failure of emergency cooling system and also the failure of any one component of confinement system or by the false decision to control this system.

The *requirement* to analyze design extension conditions, which cover groups BDBA listed above, and the following additional BDBA groups are proposed to include in draft:

e) The accidents caused by full loss of NRF electrical power supplies (NRF blackout) including off-site power sources (electrical grid), ordinary back-up generators (diesel generator, gas turbine ect.), other diverse back-up sources (battery).

f) The accidents caused by loss of primary ultimate heat sink that provide heat removal from the reactor, pool of temporary spent fuel storage and irradiated samples.

g) The accidents caused by simultaneous impact of several external factors with maximum values of the parameters.

h) Accidents caused by the inability of the personnel to implement emergency measures when initial events of DBA accidents happened.

The safety standard *"**Requirements to the Content of the Plan of Actions to Protect Personnel in Case of an Accident at NRF" (NP-075-06)*** is under revision. The safety standard applied to NRFs of any type and any category of potential radiation hazard in commissioning, operation or decommissioning phaze. The Action Plan for protection of personnel in case of an accident at NRF (Action Plan) shall be developed by the operating organization and agreed on with all organizations, having responsibilities during elimination of accident consequences. An operating organization having several NRFs shall provide for development of the specific (facilities-related) personnel protection action plan for each NRF being a component part of the Action Plan. The Action Plan shall be mutually agreed on with the action plan for protection of the population in case of an accident at NRFs in terms of timely annunciation of an accident (occurrence) hazard, scope and frequency of the information transmitted, and coordination of activities. The following additional safety requirements are proposed to include in draft of the safety standard:

- Time for notification and providing updated information to the off-site local administration and notification point with the authority and responsibility to take urgent protective action within the precautionary action zone and urgent protective action planning zone;
- Measures identified for certain scenarios of "Emergency preparedness" and "Emergency situation";
- Templates of information (tables, forms ect.) that should be implemented in emergency;
- Arrangements performed for delivery additional emergency staff out of the facility site according to scenario of an emergency, if required;
- Procedures determined for communication and information exchange with notification point, public, and mass media.

6. Conclusion

Taking in consideration the fact that the F-D accident happened at the licensed facility, the regulatory framework and the reference licensing basis of nuclear facilities and/or activities are the subject for upgrading/improving on ongoing basis. Rostechnadzor carries out the systematic review of the national system of regulations to achieve its best consistency with the IAEA fundamental safety principles and international good practices. The results of review demonstrate that:

- In general the set of Russian safety standards and other regulatory documents is in good consistence with the IAEA safety standards and sustain enhancement of NRF safety;
- Planned improvements of Russian national regulatory framework are based on the proactive approach and in line with measures for strengthening international cooperation and regulatory competence;
- Comprehensive and systematic safety assessments are carried out periodically throughout the lifetime of facilities and activities, in consistence with a graded approach;
- Clear and transparent system of interaction between the Operating Organizations, Regulatory Body and Expert Organizations provides for high quality of NRFs safety documents and should be considered as a good practice.

7. References

[1] The 14-th meeting of the International Group of Research Reactors (IGORR)/16-th European Research Reactor Conference (RRFM) RRFM/IGORR 2012, Czech Republic, Prague, 18-22 March 2012, (CD-ROM).

[2] The European Research Reactor Conference RRFM 2013, St. Petersburg, Russia, 21 - 25 April 2013, Transactions.

[3] The European Research Reactor Conference RRFM 2015, 19 - 23 April 2015, Bucharest, Romania, Transactions.

[4] International Conference on Research Reactors: Safe Management and Effective Utilization IAEA-CN-231, 16-20 November 2015, Vienna, Austria (CD-ROM).

[5] INTERNATIONAL ATOMIC ENERGY AGENCY, Safety Reassessment for Research Reactors in the Light of the Accident at the Fukushima Daiichi Nuclear Power Plant, Safety Reports Series № 80, Vienna, IAEA (2014).

[6] INTERNATIONAL ATOMIC ENERGY AGENCY, Preparedness and Response for a Nuclear or Radiological Emergency, General Safety Requirements, IAEA Safety Standards Series GSR Part 7, IAEA, Vienna (2015).

[7] INTERNATIONAL ATOMIC ENERGY AGENCY, Safety of Research Reactors, Draft Specific Safety Requirements DS476, 2014-12-06.

[8] The Order of the Rostechnadzor from 22 December 2014 № 593 “On Approval of Action Plan of Rostechnadzor on Implementation from the IAEA IRRS Follow-up Mission in the Russian Federation of November 2013”, http://en.gosnadzor.ru/international/

[9] The Order of Rostechnadzor from 04 September 2013 № 385 “On Approval of Item II “The State Safety Regulation in the Nuclear Energuy Use” of the List of Legislative Acts and Regulations Related to Federal Environmental, Industrial and Nuclear Supervision Service of Russia (P-01-01-2013)”.

[10] “Concept of Improvement of Safety Regulation and Standardization in the Field of Nuclear Energy”, Scientific and Engineering Centre for Nuclear and Radiation Safety, Nuclear and Radiation Safety. 2014. № 1(71) (in Russian) http://www.secnrs.ru/publications/nrszine/1-71-2014/pr-2.pdf

[11] INTERNATIONAL ATOMIC ENERGY AGENCY, Fundamental Safety Principals, IAEA Safety Standards, Safety Fundamentals SF-1, Vienna, IAEA (2006).

EVALUATION ON SEISMIC INTEGRITY OF HTTR CORE COMPONENTS

MASATO ONO, KAZUHIKO IIGAKI, YOSUKE SHIMAZAKI,
DAISUKE TOCHIO, ATSUSHI SHIMIZU, HIROYUKI INOI,
SHIMPEI HAMAMOTO, SHOJI TAKADA and KAZUHIRO SAWA
High Temperature engineering Test Reactor, Japan Atomic Energy Agency
4002 Narita-cho, Oarai-machi, Higashi-ibaraki-gun, Ibaraki, 311-1393, Japan

ABSTRACT

Japan Atomic Energy Agency (JAEA) has carried out research and development to establish the technical basis of High Temperature Gas-cooled Reactor (HTGR) by using High Temperature engineering Test Reactor (HTTR). The HTTR is graphite-moderated and helium gas-cooled reactor with prismatic fuel elements and hexagonal blocks. Here, the graphite block is brittle materials and might be damaged by collision of neighboring blocks by the large earthquake. A seismic observation system is installed in the HTTR site to confirm a behavior of a seismic event. Seismometers are installed in the surrounding foundation at the reactor building. On March 11th, 2011, off the Pacific coast of Tohoku Earthquake (2011 Tohoku Earthquake) of magnitude 9.0 occurred. After the accident at the TEPCO's Fukushima Daiichi Nuclear Power Station, the safety of nuclear reactors is the highest importance. To confirm the seismic integrity of HTTR core components, the seismic analysis was carried out using the evaluation waves based on the relationship between the observed earthquake motion at HTTR site and frequency transfer function. In parallel, confirmation tests of primary cooling system on cold state and integrity confirmation of reactor buildings and component support structures were also carried out.

In the evaluation a simple evaluation method was applied by using the response magnification factor analysis based on the calculated stress at the design stage. Because graphite is a brittle material, the stress is assumed in the linear range. To calculate the stress, the calculated stress at the design stage was multiplied to the ratio of the analytical results of seismic force to those at the design stage. The seismic acceleration and the impact force between the graphite blocks are calculated by the seismic analysis of the graphite structure. The calculated stress by the response magnification factor analysis was compared with the criteria.

As a result, it was found that the stress values of graphite blocks satisfied an allowable value, and the integrity of the HTTR core components was ensured. The integrity of HTTR core components was also supported by the operation without reactor power in cold conditions of HTTR. The obtained data was compared with the normal plant data before the earthquake. As the result, the integrity of the HTTR facilities was confirmed.

1. Introduction

The safety of nuclear reactors is a prime concern after the accident at the TEPCO's Fukushima Daiichi Nuclear Power Station. A new concept of the High Temperature Gas-cooled Reactor (HTGR), so-called the Naturally Safe HTGR, is proposed as a challenge to assure no event sequences to the harmful release of radioactive materials even when the design extension conditions occur by deterministic approach based on the inherent safety features of the HTGR.

Japan Atomic Energy agency (JAEA) constructed and has operated the first High-temperature Gas-cooled Reactor (HTGR) named High Temperature engineering Test Reactor (HTTR) [1], of which the reactor thermal power is 30MWt and the reactor maximum

outlet coolant temperature is 950℃ at the Oarai Research and Development Center for the purpose of establishing and upgrading technologies of HTGRs as well as nuclear heat utilization. The safety demonstration tests using the HTTR have conducted for demonstrating inherent safety features of HTGRs. In the safety demonstration test, it was performed that the loss of forced cooling (LOFC) through the core by trip of the circulators without reactor scram at the reactor thermal power 9MW in Dec. 2010. As the result of the test, it was confirmed that the reactor power was naturally lowered to a stable state without any abnormal fuel temperature rise [2].

The reactor core of HTGRs is composed of graphite blocks which withstand in high temperature. On the other hand, the graphite block is brittle material and might be damaged by a collision of neighboring blocks by the large earthquake such as the Great East Japan Earthquake. In order to confirm integrity of the graphite blocks in the HTTR, a safety evaluation was carried out against the Great East Japan Earthquake. In the evaluation, a seismic analysis was carried out to focus on the reactor core graphite blocks by the response magnification factor analysis by using the measured seismic waves in the HTTR site. In parallel, the confirmation test of primary cooling system was carried out without reactor power in cold condition in 2011, 2013 and 2015 [3,4]. Furthermore, nine control rod guide blocks were taken out from reactor core to exchange neutron start-up sources. Visual inspection was carried out for the three of 9 blocks to confirm its integrity, especially important components in terms of reactor shutdown.

This paper describes the safety evaluations of reactor core components against the Great East Japan Earthquake.

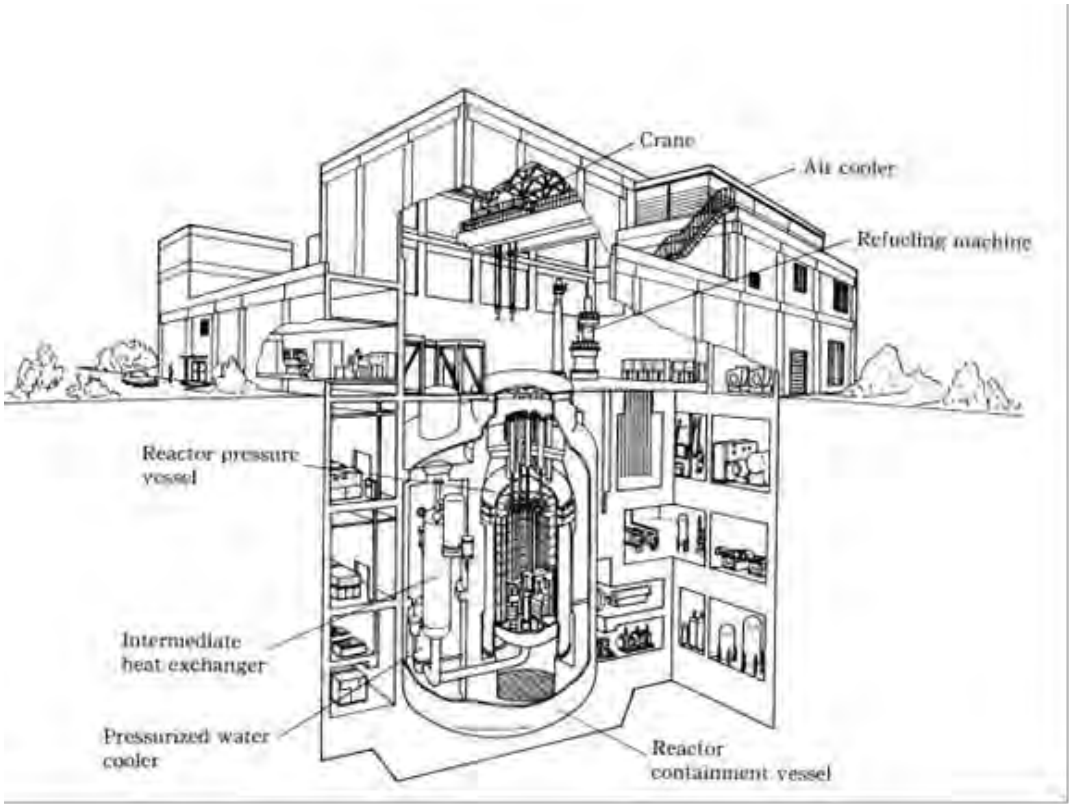

Fig. 1 Bird's-eye view of the HTTR reactor building

2. Outline of HTTR

The HTTR is a helium-gas cooled graphite moderated reactor and the fuel is a TRISO coated fuel particle which is Tri-isotropic type with four coating layer with the maximum diameter of 1mm. The bird's-eye view of the HTTR is shown Fig. 1.

The reactor building, which has two floors above the ground (24.2m) and three floors under the ground (30.5m), covers an area of 50m ×52m and is made of a reinforced concrete, and the foundations are supported directly on the stable ground.

The reactor containment vessel made of steel, 30m in height and 18.5m in diameter, is located nearly center in the reactor building. The inner concrete is installed in the reactor containment vessel.

The reactor core is shown in Fig. 2. The reactor pressure vessel (RPV), 13.2m in inner height and 5.5m in diameter, consist of a vertical cylinder, hemispherical top and bottom heads. The RPV is supported by the RPV skirt, stabilizers, and stand-pipe support beams. The RPV skirt is welded to the outside of the bottom head closure. The stabilizers surround the outside of the RPV cylinder and are supported by the side concrete. The stand-pipe support beams are located near the top of the stand-pipe.

The reactor core consists of core components, reactor internals, reactivity control equipment and the RPV. The core components consist mainly of hexagonal fuel blocks, control rod guide blocks and replaceable reflector blocks. The fuel element of the HTTR is a so-called pin-in-block type. One column is a row of prismatic hexagonal blocks piled up axially. The fuel blocks are 360mm in across flats and 580mm in height. Three dowel pins are installed on the top face, and they are engaged with the dowel sockets in the bottom face of the other block located above. The dowel arrangement ensures the correct orientation of fuel blocks within the column each other.

The reactor internal consists of graphite and metallic core support structures. They support and arrange the core components, such as fuel elements and replaceable blocks, within the RPV. The graphite core support structure consists of permanent reflector blocks, hot plenum blocks, core support posts, core bottom structures and so on. The permanent reflector block array surrounding the replaceable reflector block is composed of large polygonal graphite blocks fixed by key elements and core restraint mechanisms. The core support assembly is shown in Fig. 2. The hexagonal hot plenum block array is composed of two axial layers. This structure provides lateral and vertical positioning and support of the core array. The hot plenum block assembly contains passages, which collect the primary coolant flow from the outlet of the columns and distribute it into the high temperature plenum beneath the hot plenum blocks. The core support posts located between the hot plenum blocks and the core bottom structures provide a hot plenum space where the hot core outlet helium gas can be mixed uniformly. The metallic core support structures are composed of the core support plates, the core support grid and the core restraint mechanisms. The core support plate and the core support grid are placed below the thermal insulation layers. The core restraint mechanism surrounds the permanent reflector blocks.

3. Seismic observation system of HTTR site

A seismic observation system was installed in the HTTR site to confirm a behavior of a seismic event [5]. Seismometers were installed in the surrounding foundation at the reactor building north in the depths of 250 m, 30 m, and at the reactor building south in the depths of 94 m, 30 m, 1 m, and at the reactor building west in the depths of 174 m, 95 m, 32 m, 1 m, and installed in the reactor building at the positions of B3F, B1F, 1F and 2F and in the inner concrete at the positions of B3F and B1F. The positions of seismometers in the surrounding foundation and in the reactor building are shown in Fig. 3. The maximum accelerations of the observed seismic waves in the measuring positions in reactor building at the Great East Japan Earthquake are shown in Table 1 [6].

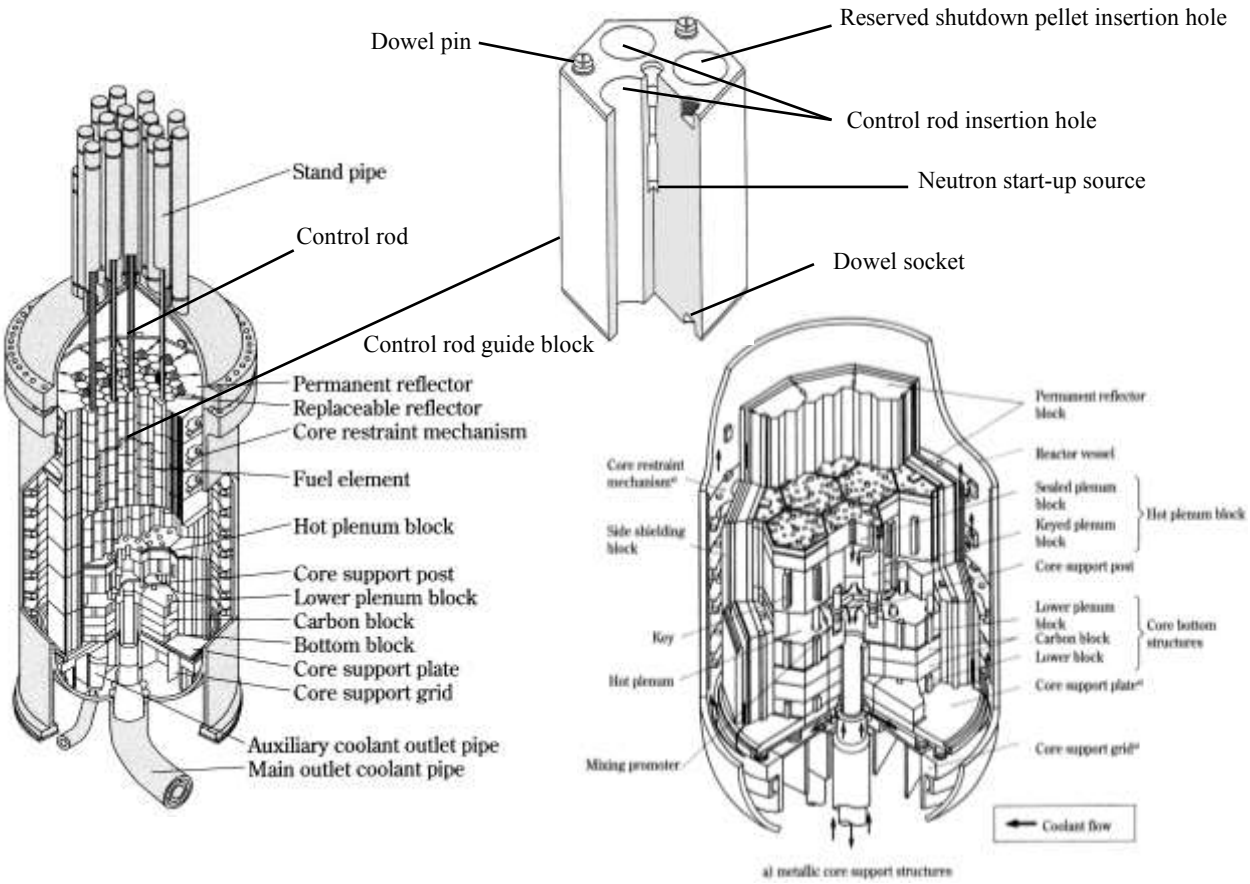

Fig. 2 Cutway view of reactor core and core support assembly of the HTTR

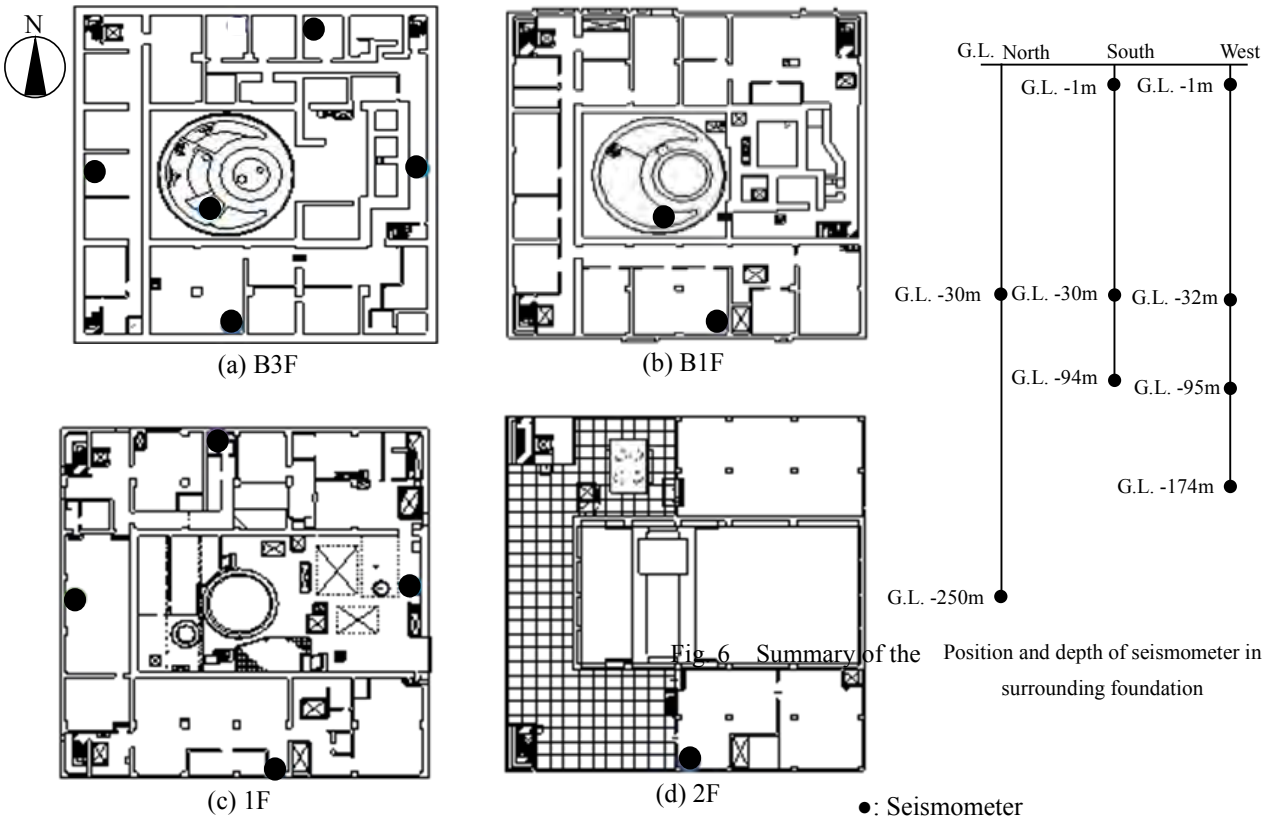

Fig. 6 Summary of the

Fig. 3 Seismometer position at the HTTR reactor building and surrounding foundation

Table 1　Maximum acceleration of observed seismic wave

Location	Floor	Max of acceleration (m/s^2)		
		North-South	West-East	Up-Down
Reactor building	2F	5.19	3.24	2.30
	1F	3.27	2.94	2.87
	B1F	2.58	2.21	1.84
	B3F	1.98	2.22	1.92
Inner concrete	B1F	3.60	2.71	2.58
	B3F	1.96	1.99	2.13

4. Seismic evaluation for graphite structure

4.1 Procedure of seismic analysis for graphite structure

The seismic analysis of graphite structure was carried out by using the conventional design method. As shown in Fig. 4, the procedure of analysis is as followings; first, the seismic analysis of reactor building is carried out based on the observed seismic waves during the earthquake. Second, the seismic analysis of RPV is carried out by using the analytical result of reactor building. Third, the seismic analysis of the structure in reactor core is carried out by using the analytical result of pressure vessel. These three seismic response analyses are carried out by the time history response analysis. Finally, the stress analysis is carried out by the response magnification factor method.

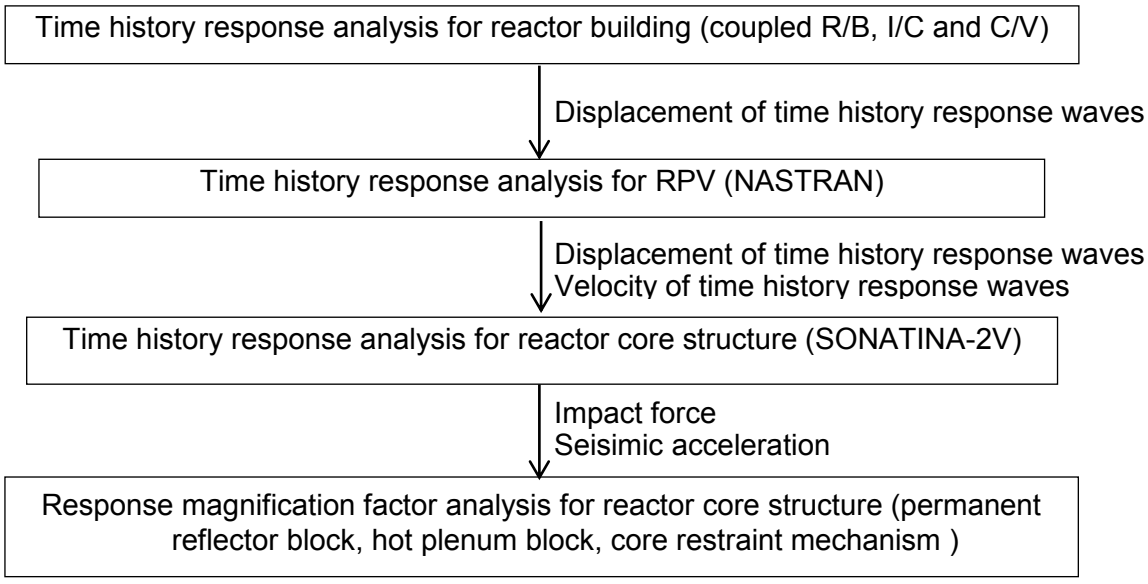

Fig. 4　Procedure of seismic analysis

4.2 Estimation of input waves at the foundation basic ground

The input seismic motion at the foundation basic ground for the analysis of reactor building was calculated from the observed seismic wave at the upper end of foundation and the frequency transfer function of foundation.　Figure 5 shows the concept of estimation method of input seismic motion.

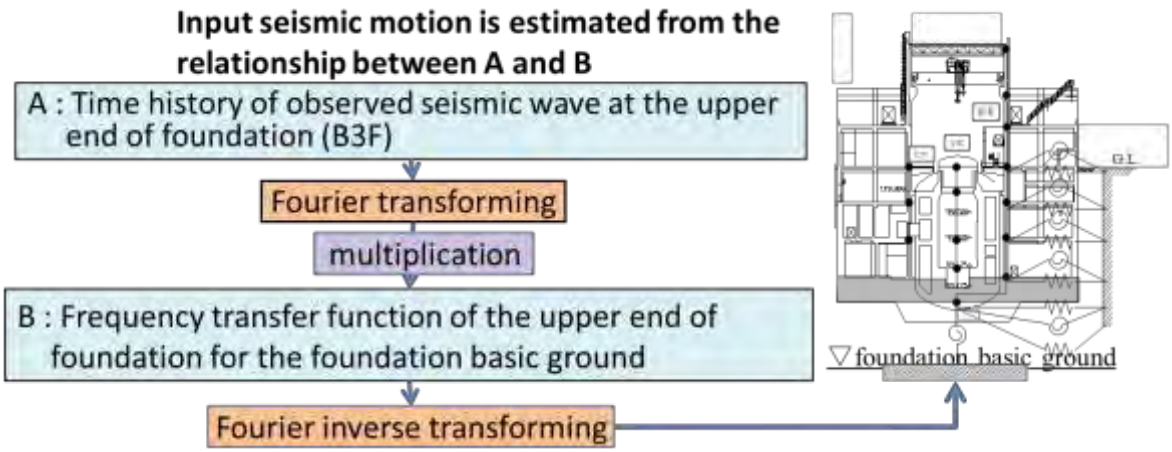

Fig. 5 Concept of estimation method of input seismic motion

4.3 Analytical method

4.3.1 Reactor building

The structure consists of three parts; the reactor building (R/B), which is connected to surrounding soil, the inner concrete (I/C) and the containment vessel (C/V). These parts are structurally isolated on the common base mat. Here, the R/B and the I/C are made of reinforced concrete, and the C/V is made of steel. Each part is modeled by the elastic beam with lumped masses as shown in Fig. 6.

4.3.2 Reactor pressure vessel

An analytical model of the RPV was modeled by multi-mass model which simulates stand pipes, cylinder body and skirt. The analysis was carried out by time history response method by using the NASTRAN, which is a generic FEM code for structural analysis [7]. The analytical model is shown in Fig. 6. The input seismic waves are the time history of seismic waves which are obtained by the seismic analysis of the reactor building. The input positions are the support beam, stabilizer and foundation of I/C.

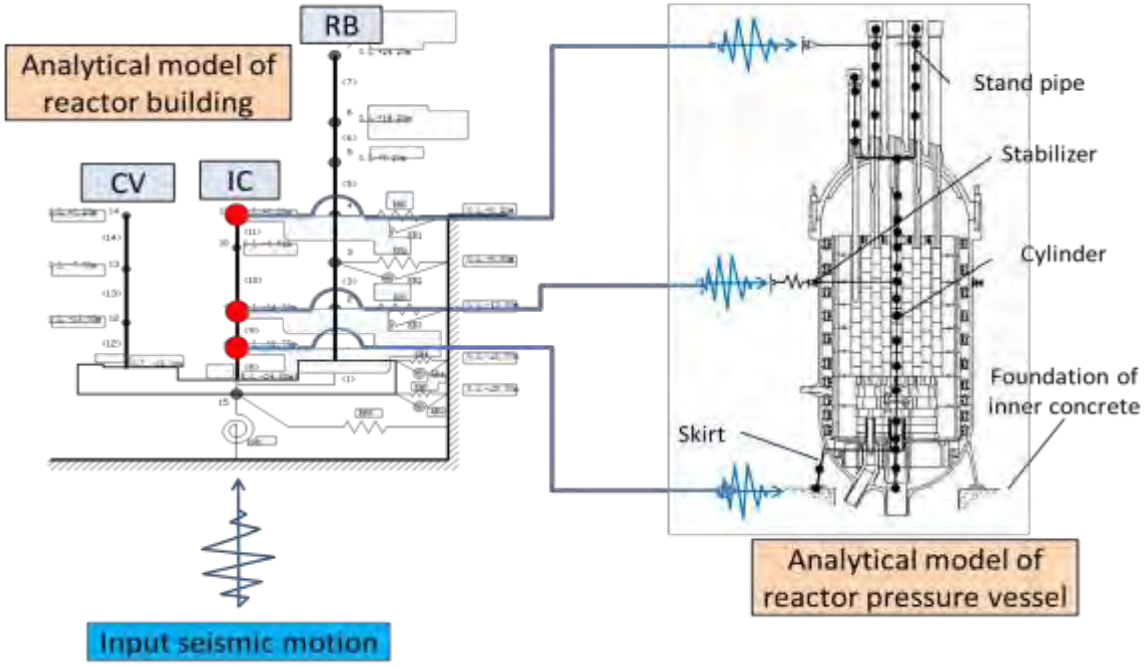

Fig. 6 Analytical model of reactor building and RPV

4.3.3 Reactor core structure

The analytical model of reactor core structure is simulated by graphite blocks with a spring mass, which is a two-dimensional vertical cross-sectional model of the fuel columns in the core as shown in Fig. 7. The graphite blocks above the hot plenum blocks are laterally supported by the core restraint mechanisms and permanent reflector blocks in the model. The analysis is carried out by using the computer program for seismic analysis of two-dimensional vertical cross-section HTGR core, named SONATINA-2V [8]. The HTTR core is a build-up structure, and gaps are provided between the blocks. For this reason, the analysis is a nonlinear calculation that takes into account of the collision between blocks.

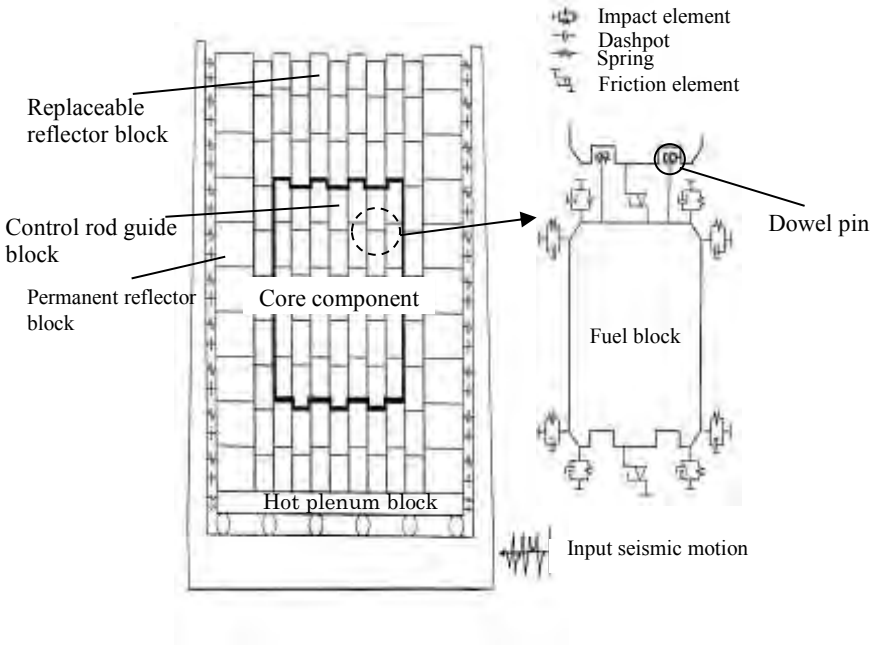

Fig.7 Analytical model of reactor core structure

4.3.4 Evaluation

The integrity of the graphite structure was carried out by a simple evaluation method by using the response magnification factor analysis based on the calculated stress at the design stage. Because graphite is a brittle material, the stress is assumed in the linear range. To calculate the stress, the calculated stress at the design stage was multiplied to the ratio of the analytical results of seismic force to those at the design stage. The seismic acceleration and the impact force between the graphite blocks are calculated by the seismic analysis of the graphite structure. The calculated stress by the response magnification factor analysis was compared with the criteria.

4.3.5 Result

Table 2 shows sum of the calculated membrane stress, bending stress and peak stress of the core components. Because of two-dimensional, the seismic force was input in the horizontal two direction of graphite block, which is higher than the actual one. The input force is a distributed force which is implemented on the surface of graphite block to be lowered because the actual graphite block is a hexagonal cross section. Therefore, the two-dimensional analytical model evaluates safely with sufficient margin. It was confirmed that the calculated stress satisfied the evaluation criteria to keep the structural integrity

against the Great East Japan Earthquake.

Table 2
Analytical results (sum of the membrane stress, the bending stress and the peak stress)

component	Dowel pin	Control rod guide block (Active core region)	Permanent reflector block (side)	Replaceable reflector block
Analysis(MPa)	5.6	12.8	2.5	10.0
Design criteria(MPa)	14.1	20.0	3.0	17.4

5. ADDITIONAL CONFIRMATION

5.1 PERFORMANCE CONFIRMATION TEST

The active components of cooling system were operated to obtain the plant data by the several operations without reactor power in cold condition of HTTR in 2011, 2013, 2015 [3,4]. The obtained data was compared with the normal plant data before the earthquake. As the result, the integrity of the HTTR facilities was confirmed as shown in Fig. 8, obtained in 2013. If the graphite block in reactor core is damaged by the earthquake, flow channel is blocked by the fragments of graphite blocks. Therefore, the differential pressure of core was compared with the past data. As the results, the two data agreed well, and thus it was confirmed that the differential pressure of the core was in the normal range. Thus, the integrity of reactor core, which was confirmed through the seismic evaluation mentioned above, was also supported by the results from the operation without reactor power in cold conditions.

5.2 INSPECTION OF GRAPHITE BLOCK

In order to obtain positive proof of result of seismic analysis, nine control rod guide blocks were taken out from reactor core when neutron start-up sources were exchanged. Three of 9 blocks were carried out by visual inspection. The integrity of the blocks were confirmed, especially important components in terms of reactor shutdown were confirmed. Blocks have been taken out for the first time since the great earthquake.

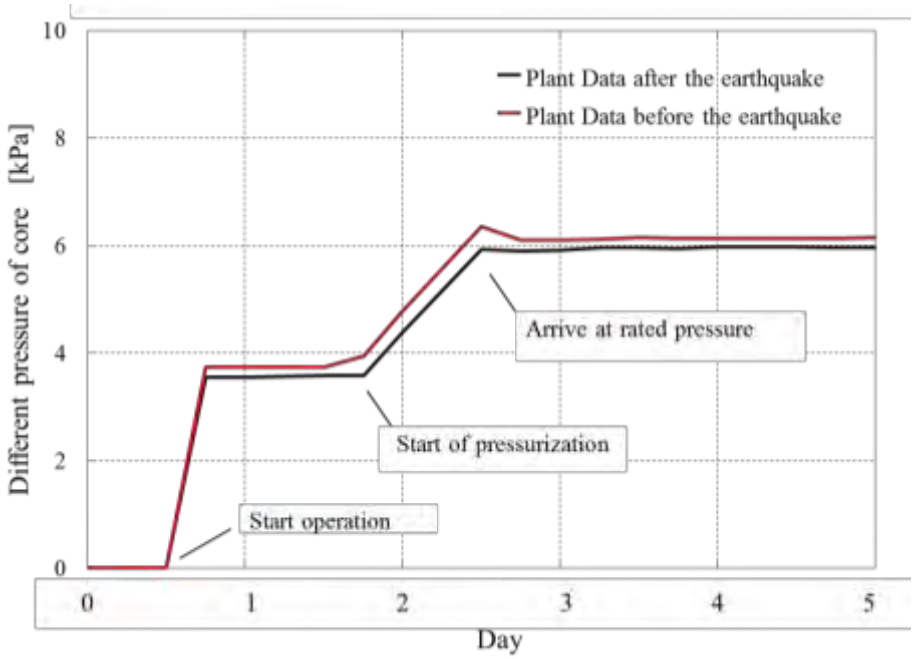

Fig. 8 Comparison of differential pressure of core

6. Conclusion

In order to confirm the integrity of the graphite structures in reactor core of HTTR after the Great East Japan Earthquake that occurred on March 11, 2011, the safety evaluation was carried out by the seismic analysis by using the observed seismic waves in the HTTR site. The stress was evaluated by the response magnification factor method. As the results of the evaluation, the generated stress in the graphite blocks in the reactor core at the earthquake were well below the allowable values of safety criteria, and thus the structural integrity of the reactor core was confirmed. The integrity of reactor core was also supported by the visual inspections of facilities and the operation without reactor power in cold conditions of HTTR.

References

[1] Saito, S., Tanaka, T., Sudo, O., et al., “Design of High Temperature Engineering Reactor (HTTR)”. JAERI-1332, Japan Atomic Energy Research Institute (1994).

[2] Takada, S., “Initiation of safety demonstration test of loss of forced cooling by HTTR; Completion of the first test of loss of forced cooling”. Transactions of the Atomic Energy Society of Japan, 53(3), 167-168 (2011) (in Japanese).

[3] Ono, M., Tochio, D., Shinohara, M., et al., “Plant Data Evaluation of Performance Confirmation Test in HTTR after Tohoku-Pacific Ocean Earthquake”. JAEA-Technology 2012-004, Japan Atomic Energy Agency (2012) (in Japanese).

[4] Ono, M., Shinohara, M., Iigaki, K., et al., “Reconfirmation of facilities/instruments integrity by cold test of HTTR”. JAEA-Technology 2013-042, Japan Atomic Energy Agency (2014) (in Japanese).

[5] Iigaki, K., Hanawa, S., et. al., “Seismic design”. Nuclear Engineering and Design 233 59-70 (2004).

[6] JAEA, available from <http://www.jaea.go.jp/02/news2012/121102/be03.pdf> (in Japanese).

[7] “ Femap with NX Nastran version 10.2J user’s guide “, Numerical Simulation Tech Co., Ltd. (NST) (2011) (in Japanese).

[8] Ikushima, T., “SONATINA-2V a computer program for seismic analysis of the tow-dimensional vertical slice HTGR core”. JAERI-1279, Japan Atomic Energy Research Institute (1981).

SOME SUGGESTED METHODOLOGIES FOR USE WHEN PERFORMING PERIODIC SAFETY REVIEWS AND SAFETY REASSESSMENTS FOR RESEARCH REACTORS

M W SUMMERFIELD
Technical Support Group, Nuclear Operations, ANSTO
Lucas Heights Science and Technology Centre, Lucas Heights, NSW 2234, Australia

ABSTRACT

In presentations at previous IGORR Conferences, I have covered the overall project management of a Periodic Safety Review (PSR) of the OPAL reactor, the use of a fault schedule approach in the review of the deterministic safety assessment as part of the PSR and the safety reassessment of OPAL in light of the Fukushima Daiichi NPP accident. This paper presents some additional lessons learned that may be useful to research reactor operating organisations performing either a PSR or a safety reassessment on their own facilities. It is based not only on experience with the PSR and safety reassessment of OPAL but also on feedback received during the course of various IAEA Expert Missions and Technical Workshops on these subjects. Topics covered include the project management of a PSR, the review of codes and standards, evaluating the status of SSCs, the use of a fault schedule to assess beyond design basis events, the Global Assessment and how to identify common themes and root causes across different safety factors, and what traps to avoid when documenting findings and identifying recommendations or observations.

1 Introduction

Many countries now require the research reactor operating organisations to perform Periodic Safety Reviews (PSRs) over the life of the facility at regular intervals. However, to date, the only international guidance available has been the IAEA safety standard for the *Periodic Safety Review of Nuclear Power Plants* (previously NS-G-2.10, now SSG-25) that as the name implies, was specifically intended to be used for nuclear power plants. Whilst this guidance can be used to perform a PSR for a research reactor through an appropriate application of a graded approach to safety requirements (e.g. as outlined in IAEA SSG-22), a number of research reactor operators have requested the IAEA to provide more specific guidance for performing a PSR for a research reactor, particularly for smaller research reactors with limited resources. Such a guidance document is currently being prepared by the IAEA and it is intended that it will include practical guidance, methodologies and techniques on performing a PSR for a research reactor.

This paper and associated presentation provides some practical lessons learned that may be useful to research reactor operating organisations when performing either a PSR or a safety reassessment on their own facilities. It is based not only on previous experience with performing a PSR and a safety reassessment for a research reactor but also on feedback received during the course of various IAEA Expert Missions and Technical Workshops on these subjects. Topics covered include the use of a fault schedule to both evaluate the adequacy of a deterministic safety assessment and to subsequently assess beyond design basis events, how to identify common themes and root causes across different safety factors, and what traps to avoid when documenting findings and identifying recommendations or observations. Reference will also be made to papers presented at previous IGORR Conferences, including the papers *Application of Fault Schedule to the Period Safety Review of the OPAL Deterministic Safety Case* as presented at the joint RRFM/IGORR Conference in Prague, Czech Republic in March 2012 and *The Periodic Safety Review of ANSTO's OPAL Reactor* presented at the IGORR Conference in Daejeon, South Korea in October 2013. This paper will also identify some aspects that may be beneficial in relation to

performing a safety reassessment of a research reactor, expanding on the information provided in the presentation *The Safety Reassessment of ANSTO's OPAL Reactor: Application of the Guidance Contained in IAEA Safety Reports Series No.80* given at the IGORR Conference in San Carlos de Bariloche, Argentina in October 2014.

2 Project Management and Organisation

As previously advised in my paper *The Periodic Safety Review of ANSTO's OPAL Reactor* presented at the IGORR Conference in Daejeon, South Korea in October 2013, setting up an appropriate project management structure and organisation is fundamental to the success of performing a PSR. Subsequent experience has identified a number of additional lessons as follows:

- A clear definition of the scope and terms of reference of the PSR, including agreement with the appropriate Regulatory Body, is fundamental to successfully performing a PSR. SSG-25 recommends that this should be documented in a PSR Basis Document but alternatives may be equally appropriate, depending on the individual organisation's requirements.
- A clear definition of the roles and responsibilities of the organisations and the individual staff involved in the PSR is beneficial. In particular, who is responsible for the review of specific Safety Factors and how they interact and interface with other reviewers should be clearly defined. As above, this may be documented in the PSR Basis Document or its equivalent.
- The interface with the Regulatory Body also needs to be clearly defined so as to ensure that both the operating organisation and the Regulatory Body have a clear understanding of what is expected from both parties. Again, this may be documented in the PSR Basis Document or its equivalent.
- The appropriate use and involvement of resources, particularly non-professional staff (technicians, fitters, etc.) and support staff, is often very beneficial to a successful PSR. For example, maintenance technicians often have a very good knowledge of the actual state of the as-built plant through their experience maintaining the plant that is not always recorded formally.

For OPAL, we developed specific Task Briefs for each Safety Factor that identified not only the scope and terms of references in relation to the review of the Safety Factor but also the deliverables expected from the reviewers. We also appointed a dedicated Project Manager to manage the project and coordinate the separate review activities. The Project Manager was also able to oversee the individual review activities and identify areas where review teams needed to coordinate their activities. We also allocated appropriate administrative support, including a technical writer whose job was to put together the overall PSR report based on the deliverables provided by the reviewers assessing the individual safety factors. This enabled the reviewers, who were generally section or group heads, to concentrate on the technical reviews providing their deliverables and not be distracted by writing reports.

3 Review of Codes and Standards

According to SSG-25, the review of applicable codes and standards is required under Safety Factor 1 in order to assess the level compliance of the facility with the current codes and standards, which may have changed significantly since the facility was originally constructed. The main difficulties with this are the large number of codes that may need to be reviewed and the fact that very few standards organisations actually identify he changes to the individual clauses as a standard is revised. These means that (as stated in SSG-25), a clause-by-clause review of the applicable standards is normally required. Furthermore, actually determining which codes and standards, and particularly what revisions of those codes and standards, were used during the original construction may in itself require significant resources. For this reason, when building a facility, or undertaking modifications

to it, it is important to keep a copy of the version of each code or standard used which was current at the time of design. Without access to these, it is very difficult to establish a baseline against which to do the assessment.

In the case of the OPAL, the size and difficulty of this task was recognised early on and a separate task brief prepared covering this review. This task brief identified the codes and standards to be reviewed, which was limited to those with an impact on nuclear safety. In addition, it was decided that the best option to perform the actual review would be to recall as a contractor the now retired ANSTO staff member who was responsible for the codes and standards used during the construction of OPAL. This enabled the project to take advantage of not only the former staff member's expertise on codes and standards but also their intimate knowledge of OPAL and how those codes and standards were applied during construction. Even so, it was found that this review was one of the single biggest tasks of the PSR and an operating organisation intending to perform a PSR on their own facility should take this into consideration.

4 Evaluating the Actual Condition of SSCs

Safety Factor 2 of SSG-25 covers the evaluation of the actual condition of the Structures, Systems and Components (SSCs) important to safety so as to determine whether they are capable and adequate to fulfil their required safety function. This section of SSG-25 goes on to outline the scope and tasks and the methodology but here are a couple of points that may be useful in performing the actual review:

- What SSCs are to be considered needs to be clearly identified as do their design safety requirements. For older plants, it is not always clear what are the SSCs important to safety and what is the safety function they are required to fulfil. Even for newer plants, differentiating between a SSC's safety function and operational design requirements is not always clear.
- As indicated previously, the use of the expertise and knowledge available in non-professional staff such as maintenance technicians and fitters is likely to make a significant contribution to the review of this Safety Factor. A particular issue to look for is where maintenance technicians implement "work-arounds" that are not formally identified in the plant procedures or instructions in order to keep the plant operational.

In the case of the OPAL PSR, the assessment of the condition of each SSC was performed in four steps as follows:

a. Identify the maintenance, surveillance, inspection and testing activities performed to date that provide information on the condition of the SSC, including routine and corrective maintenance tasks.

b. Identify significant issues or problems encountered, or modifications done, to the SSC to date that provides additional information on the condition of the SSC.

c. Based on available information, assess and provide a summary description of the present condition/status of the SSC and whether it is adequate to meet its design requirements.

d. Identify recommended actions to be completed or considered to assure or improve SSC condition into the future.

This information was reported in a tabulated form to ensure consistency.

It should also be noted that the review of this Safety Factor often has significant interfaces with the reviews of other Safety Factors identified in SSG-25. The most obvious of these is Safety Factor 4 in relation to ageing management but from the OPAL PSR experience, significant interfaces also arise with Safety Factor 8 relating to safety performance, Safety

Factor 10 relating to organisation and management systems and Safety Factor 11 relating to procedures.

5 Use of a Fault Schedule

The paper *Application of Fault Schedule to the Period Safety Review of the OPAL Deterministic Safety Case* presented at the joint RRFM/IGORR Conference in Prague, Czech Republic in March 2012 outlined the way that a fault schedule could be used as a means of independently reviewing a research reactor's deterministic safety case. It should be noted that a fault schedule is defined as *"a comprehensive schedule of initiating events which have the potential to give rise to a radiological release, together with the corresponding lines of protection"*. It is not simply a list of postulated initiating events and as such, it is a tool that enables verification of the adequacy of the deterministic safety case and also facilitates understanding by non-safety specialists.

Subsequent to the PSR, a separate safety reassessment of OPAL was performed in accordance with *IAEA Safety Report Series No.80: Safety Reassessment of Research Reactors in the Light of the Fukushima Daiichi NPP Accident*. This made use of the fault schedule prepared for the PSR but focused on those postulated initiating events that had previously been identified as beyond design basis or incredible. This application is discussed separately in section 8 below. However, it is an example of where performing a PSR can have unanticipated benefits from a safety perspective.

6 The Global Assessment

SSG-25 recommends that the overall Global Assessment section be prepared following completion of the reviews of individual Safety Factors by an interdisciplinary team that is independent of those reviewing the individual Safety Factors . It also recommends that this section should identify interface issues, overlapping issues and omissions both within and between Safety Factors so as to determine whether additional or grouped safety improvements arising from more than one Safety Factor are appropriate. However, for many research reactor operating organisations, compliance with this guidance is often difficult if not impossible due to resource limitations, both financial and human. Limited staffing numbers also tends to mean that there is a reliance on a relatively small number of highly knowledgeable and experienced staff to perform the review of individual Safety Factors with nobody "independent" left within the operating organisation to prepare the Global Assessment. The fact that most research reactors are effective unique designs compounds this difficultly since it is often difficult to bring in an appropriate expert from another research reactor who is knowledgeable on the reactor being assessed.

In the case of the OPAL PSR, the Global Assessment was mainly written by the Project Manager, who oversaw the review process against the individual Safety Factors but did not have direct responsibility for any specific review. The General Manager, Nuclear Operations, who had ultimate responsibility for the PSR, also contributed to the Global Assessment even though he was also responsible for the review against one of the Safety Factors. It was considered that this approach was the best compromise between the guidance of SSG-25 and the fact that there were no suitably expert ANSTO staff available who were not already involved in the PSR and the review of the individual Safety Factors.

Although not specifically identified in SSG-25, the identification of common themes and root causes across multiple Safety Factors is an aspect of a PSR that may be requested by a Regulatory Body. It may be covered in the Global Assessment through the consideration of interface issues, overlapping issues and omissions but in the case of the OPAL PSR, the Regulator commented that the Global Assessment was insufficient in this respect. As such, it was necessary to prepare a Supplement to the PSR that addressed this comment (among others). This was done by two separate people (one of whom was not involved in the original PSR) reviewing the list of recommendations and allocating one or more keywords or

themes for each recommendation. The resultant set of keywords and themes was then reviewed and rationalised and the common themes and root causes thus identified. The benefit of this approach, as opposed to simply reviewing the individual Safety Factor reports and trying to identify common themes and root causes, was that it was systematic, repeatable and demonstrable in a documented form.

7 Findings and Recommendations

SSG-25 recommends that the Global Assessment should collate the findings and recommendations from the reviews of the individual Safety Factors and categorise or prioritise them as appropriate with respect to their safety significance. Whilst this sounds simple and straightforward, there are some lessons to be learned as follows:

- Findings can be positive as well as negative and should include any good practices identified during the course of the PSR. An overly negative PSR can have an adverse impact on the safety culture of the operating organisation unless very carefully managed.
- The categorisation of findings and recommendations should be done in accordance with an agreed and documented set of criteria that may be set out in the PSR Bases Document referred to previously. These criteria may be based on deterministic analysis, PSA, engineering judgement, cost-benefit analysis, risk analysis or a combination of these methods.
- Recommendations should be clearly written as recommendations and not as actions since actions should be defined by the operating organisation line management to address the recommendations. As an associated point, do not assume that every recommendation will have a corresponding action as recommendations may be rejected by the operating organisation line management if there is appropriate justification (e.g. the potential increase in safety is not sufficient to justify the cost involved).

As indicated above, whilst the categorisation of recommendations in relation to their significance to safety should be done as part of the PSR, the subsequent identification and prioritisation of actions to implement the recommendations should be done by line management. This is necessary as performing actions generally requires resources (human, material, and funding), the source of which is normally limited and subject to multiple and often conflicting demands. As such, a recommendation allocated a high safety category does not necessarily result in high priority or high urgency actions.

In the case of the original OPAL PSR, 124 recommendations were identified, although a number of recommendations also had subsidiary recommendations that meant that a total of 226 individual recommendations were identified. However, 28 of the top level recommendations were effectively related to the same topic of the need to develop appropriate long term maintenance strategies and associated integrated logistic support provisions for 28 different SSCs. Furthermore, this issue was something that had been previously identified and plans were in place to address this issue as part of the overall ANSTO Reactor Operations strategic plan to implement a formal Maintenance Strategy for OPAL that is intended to generally be compliant with the guidance contained in ISO 55001.

All the recommendations arising from the OPAL PSR were allocated to three categories as follows:

1. Areas where improvements are essential: ;
2. Areas where improvements should be considered; and
3. Observations, where improvements could be beneficial.

Note that the 28 top level recommendations relating to the development and implementation of a formal Maintenance Strategy for OPAL were identified as Category 1 and that this categorisation was also consistent the operational importance of developing and implementing such a strategy for OPAL. In addition, a further 28 top level recommendations were also identified as Category 1 and many of these recommendations had similar significant operational benefits. Of the remaining top level recommendations, 60 were identified as Category 2 and only 8 identified as category 3. However, the highest category did not automatically mean that the resultant actions had the highest priority or highest urgency. Again using the example of the 28 top level recommendations relating to the development and implementation of a formal Maintenance Strategy for OPAL, this resulted in a total of 149 separate actions and is a long term activity with the completion dates for some actions not scheduled until 2018. Note that as of the end of 2015, 32 of these 149 actions were complete, 20 have been superseded by other actions or by modifications that make the action redundant, 74 are being progressed and 23 have not been started. Of the 23 that have not been started, these are generally low priority actions that involve major capital investment.

8 Safety Reassessment

In 2014, the IAEA published Safety Report Series No.80: *Safety Reassessment for Research Reactors in the Light of the Accident at the Fukushima Daiichi Nuclear Power Plant*. This document provides a set of suggestions and methods for performing a safety reassessment for a research reactor, taking into consideration the available feedback from the Fukushima Daiichi NPP accident. The IAEA strongly encourages the research reactor operating organisations in Member States to perform such a safety reassessment (or its equivalent) if they have not already done so.

As described in the presentation *The Safety Reassessment of ANSTO's OPAL Reactor: Application of the Guidance Contained in IAEA Safety Reports Series No.80* given at the IGORR Conference in San Carlos de Bariloche, Argentina in October 2014, the OPAL PSR was underway when the Fukushima Daiichi NPP accident occurred. A preliminary assessment of the implications of the accident for OPAL was performed at that time but due to a lack of formal guidance on what a safety reassessment should actually consist of, such a safety reassessment was not performed until the issuing of IAEA SRS No.80. This had the unintended benefit of subsequently enabling the results of the full OPAL PSR to be utilised as part of the safety reassessment. In particular, the safety reassessment of the facility with respect to the adequacy of the design basis was effectively considered under Safety Factor 5 of the PSR whilst the review of site characteristics was effectively considered under Safety Factor 7. As such, the safety reassessment could concentrate on those aspects not covered directly by the PSR whilst making use of the methodology and results of the PSR.

The main example of utilising the PSR to facilitate the safety reassessment was the use of the fault scheduled prepared for the PSR to assess potential beyond design basis events. This was done by effectively assessing postulated initiating events that had previously been identified as beyond design basis as if they were design basis events and determining whether the level of protection provided was sufficient to prevent a large scale release of activity. As such, it was possible to assess the capability of the plant to withstand or cope with postulated initiating events regardless of whether the events were actually within the design basis or not.

In practice, the main result of the OPAL safety reassessment was the determination that many of the nominally beyond design basis initiating events appeared to be within the plant's capabilities although this would need to be confirmed by analysis of the specific event sequences. For example, the total loss of all AC power (both offsite and onsite) for more than 30 minutes and less than 10 days was identified in the original safety analysis as a beyond design basis event. The safety reassessment indicated that a more appropriate

event would be the total loss of AC power for up to 15 days (the “ever-safe” time for the OPAL fuel assemblies) and that this is within plant capability without fuel damage.

9 Conclusions

This paper presents some lessons learned that may be useful to research reactor operating organisations performing either a PSR or a safety reassessment on their own facilities. It is based not only on experience with the PSR and safety reassessment of OPAL but also on feedback received during the course of various IAEA Expert Missions and Technical Workshops on these subjects. It is not intended to be a comprehensive list of all lessons learned but rather just a number of areas where other research reactor operating organisations performing either a PSR or a safety reassessment on their own facilities may benefit from previous experience.

DEVELOPMENT OF EVACUATION TIME ESTIMATES ON RESEARCH REACTOR 'HANARO'

BONGSEOK KIM, GOANYUP LEE
Emergency Preparedness Department, Korea Atomic Energy Research Institute
989-111 Daedeok-daero, 34057 Daejeon – Korea

ABSTRACT

HANARO is a multi-purpose research reactor which is operated by Korea Atomic Energy Research Institute (KAERI). Its thermal output is 30 MW, which is categorized as high hazard, according to IAEA Safety report, series NO.41.
KAERI has two facilities for emergency responses. One is the Technical Support Center (TSC), located near HANARO and the other is the Emergency Operation Facility (EOF), which is located 800m from HANARO. These facilities are equipped for dealing with emergency response activities. KAERI has also established an Emergency Planning Zone (EPZ) for any radiological emergency.
EPZ of HANARO was established within 800ms of KAERI's site. However, after the Fukushima accidents, people belonging to an environmental organization and living near the nuclear facility, have insisted that the government must expand the EPZ distance criteria. The government have finally agreed to this. Thus, EPZ in Korea has expanded considerable, from 800ms to 1500ms. The new EPZ exceeds the KAERI site and includes the people who live near KAERI. KAERI has also included new emergency plans and protective action for the public and all who live near the KAERI site.
Protective action for the public can be divided into three types of action. One is a distribution of KI, and another is sheltering houses, while the third is Evacuation. This study deals with evacuation. Evacuation is an essential protective action in the case of high radiation exposure. People need to be evacuated speedily in this case the aim of the study is to estimate the timing of evacuation, once the radiological emergency had begun. A dataset is needed for this study, including, population figures, geographic characteristics. Road networks, traffic volumes etc. The result of this study can be used to establish if the protective action is effective and, more importantly, adequate.

1. Introduction

HANARO has been operated as multi-purposed research reactor since 1995. HANARO is used by with various facilities like Neutron Beam Facilities, Cold Neutron Research Facilities, Capsule Irradiation Test Facility, Fuel Test Loop. Thermal output of HANARO is 30 MW which is higher output among research reactor. And, its output is categorized as high hazard, according to IAEA safety NO. 41.

KAERI prepare emergency response facilities to response for the emergency situation of HANARO and other facilities. KAERI has two types of emergency response facilities. One is the Emergency Operation Facility (EOF), and other is the Technical Support Center (TSC). EOF is located 800m from HANARO. And, In EOF, there is stocked many articles of emergency response. Also, EOF has rooms for debate and decision making of protective action for the emergency. TSC is located near HANARO and this facility has a lot of articles of emergency response for the on-site situation, like, filtered-mask, anti-contamination clothing and portable radiation instrument. The role of TSC is supporting the emergency response for the on-site situation.

Before 2015, EPZ of HANARO was established within 800m, its distance criteria were 800m. And, only KAERI's site is applied EPZ of HANARO. But, after Fukushima accident, many people in Korea are

concerned about the safety of nuclear facility and demand countermeasure in case of radiological emergency. Also, people belonging to an environmental organization and living near the nuclear facility, have insisted that the government must expand the EPZ distance criteria. Moreover, politicians who are based on these area, made an issue of EPZ in National Assembly. For constantly have been pushing the government for years to expand the EPZ distance criteria. The government finally have agreed to this issue. Thus, revised law is enacted, which include new distance criteria of EPZ. For research reactor, distance criteria are expanded from 800m to 1500m. So, EPZ is newly set in 2015 through discussion between KAERI and Local government and other stakeholders.

In revised law, distance criteria of EPZ are 1500m. According to this criteria, New EPZ is including residential area, commercial area, and agricultural area. So, there are people who have to protect from radiological effect. KAERI should have the emergency plan to protect public. Also, evacuation is one of the protective action for public. Therefore, KAERI develops the Evacuation Time Estimate on residents to establish the protective action adequately.

2. Background

Figure 1. Map of HANARO and EPZ area

Newly expanded EPZ include the residential area where live people. Former EPZ include only KAERI's site, so there is no resident. But, newly expanded EPZ including public people. Whole EPZ area is 6.825km^2, and the number of population in EPZ is 38,000. Newly set EPZ include apartment block, and

its height is around 15 ~ 20 floor. So there is high-density population area.

3. Methodology

The simulation program used for estimate the evacuation time on residents in EPZ is VISSIM of PTV. VISSIM is micro traffic simulation program, which can simulate the traffic situation as micro moving of car. With this program, it can be that analyzing and estimating of evacuation time in EPZ through input data such as road network, traffic demand data, demographic data, etc.

To build road network data, it is needed to be input the road network characteristics like geometry structure of road, saturation flow rate, the number of lanes, lane width. And, these data is collected from satellite images and local government data base. Also, in this study, road network data is built not only in EPZ area but outside area of EPZ, because evacuation is not only happening in EPZ area. Evacuation will be conducted from in EPZ area to the destination.

Figure 2. Road Network of Evacuation Time Estimate Modeling

Designated destination is Daejeon Convention Center, which is located approximately 6km from HANARO. Daejeon Convention Center is held a lot of events. And, there is plenty of room for these events. Because of this, we designate this facility as a destination of evacuation.

In this study, Evacuation route is planned that car move to designated destination from 2 different zones in EPZ. And, there is no cross traffic conflict among the cars. But, there is cross traffic conflict between car and pedestrian. For this spot, assume that 10 seconds pedestrian signal in 2-minute cycle. This assumption makes pedestrian can go their destination by walk. Also, there is two different evacuation route each zone. The driver can choice their route individually.

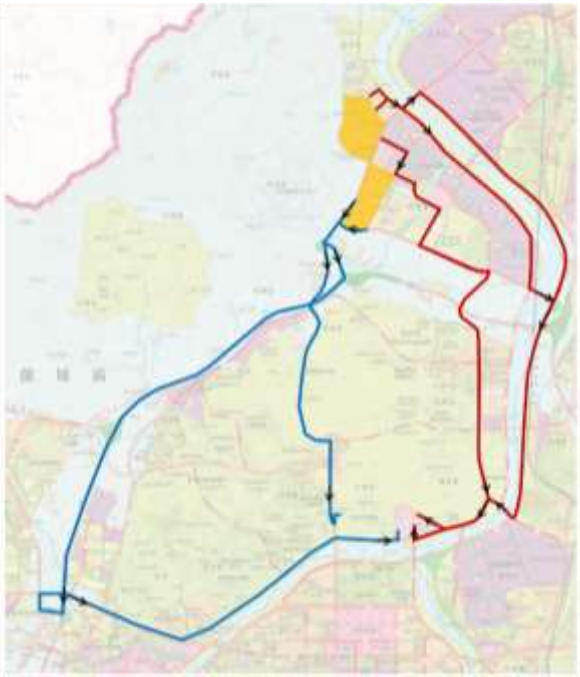

Figure 3. Evacuation Route for Residents

The number of origin point for trip generation is composed of 18 points for Evacuation Time Estimate modeling. Also, calculating the traffic demand according to the population of each origin point. In other words, Evacuation Time Estimate modeling is composed by 18 origin point and 1 destination point in this study.

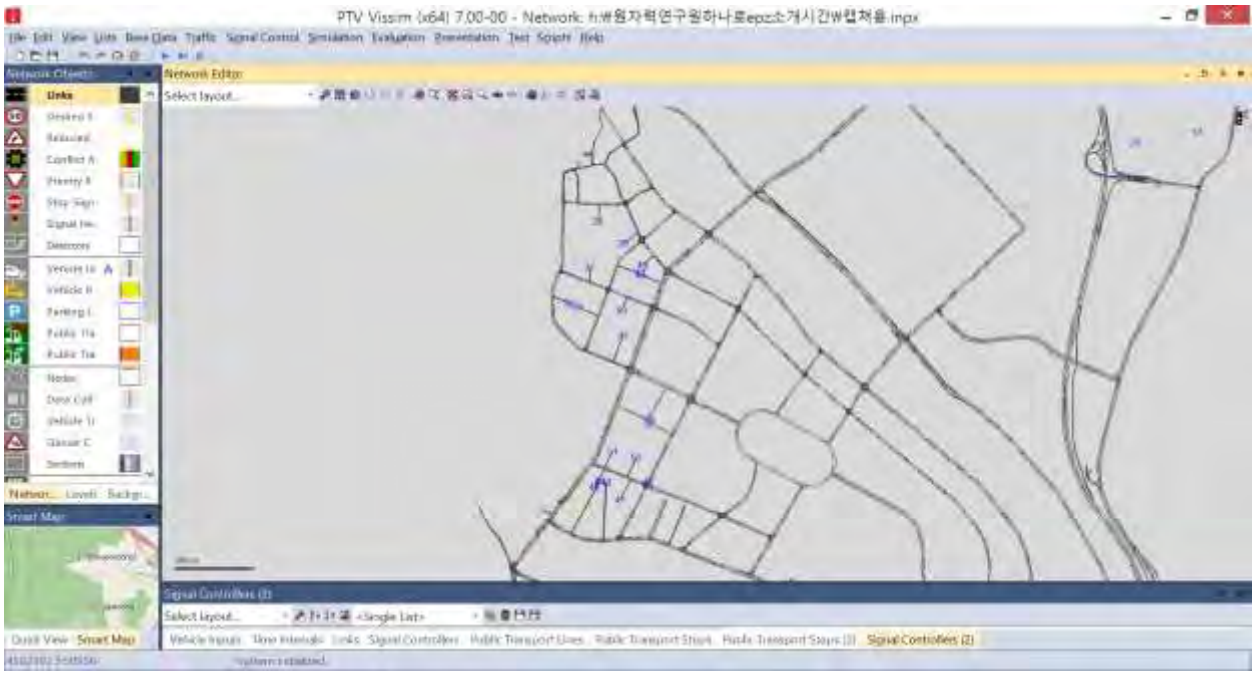

Figure 4. Trip Generation Points

In case of evacuation, people use their own car to evacuate. But, there are people who do not have their own car. These people is transit-dependent population. Transit-dependent population cannot evacuate themselves. Therefore, planner should consider supplying the public transportation for this people. In this

study, transit-dependent population in EPZ evacuate by public transportation. These people ride the public transportation at designated school. So, school function as first assembly place and terminal. Actually, local government have a plan for supply the bus for transit-dependent population in case of radiation emergency. Assuming that, each bus is taken 40 people in this modeling.

Figure 5. Public Transportation Line for Transit-dependent population

In this study, the varying of time and traffic demand are represented as some scenario for Evacuation Time Estimate modeling. According to this, modeling is conducted in two scenarios as midday and evening.

The difference between midday and evening is the movement of the population according to the time of day. In case of evening scenario, most population are in their home. And, assuming that most household can use their own cars for evacuation in evening time except transit-dependent population. Also, public transportation supply plan is reflected on this scenario. In case of midday, there is more variation of population than evening time. Because people's activity happen mostly in midday and uncertainty of traffic demand on midday is increased. Therefore, midday scenario considers various condition in traffic demand. In this study, midday scenario assumes 3 different conditions. Each condition is represented car used rate in the evacuation. Usually, people used the car in midday only one person and their kids in school.

scenario	Ratio of car using	Number of vehicle	Number of public transportation
evening	0	13706	14
midday	30%	4112	552
	50%	6853	339
	70%	9594	126

Table 1. Number of traffic demand

Also, midday scenario reflects traffic demand in KAERI site, the number of KAERI staff is more than 3500. So, in case of radiation emergency staff will evacuate immediately except the emergency response team.

And most people commute their own car, so an average number of people in each car is 1.2. So, traffic demand of KAERI site is approximately 3000.

In addition, Evacuation Time Estimate model simulate the traffic congestion through background traffic volume data and signal time data.

According to disaster study, In case of emergency situation, trip generation distribution is similar to Rayleigh distribution. In this study, assuming that trip generation distribution followed Rayleigh distribution. And average prepare to leave time is 30 minute, and last time of prepare to leave is 120 minute.

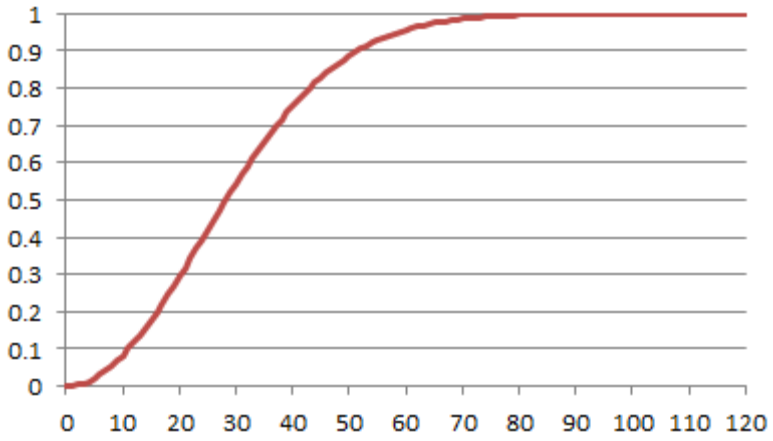

Figure 6. Rayleigh Distribution

4. Result

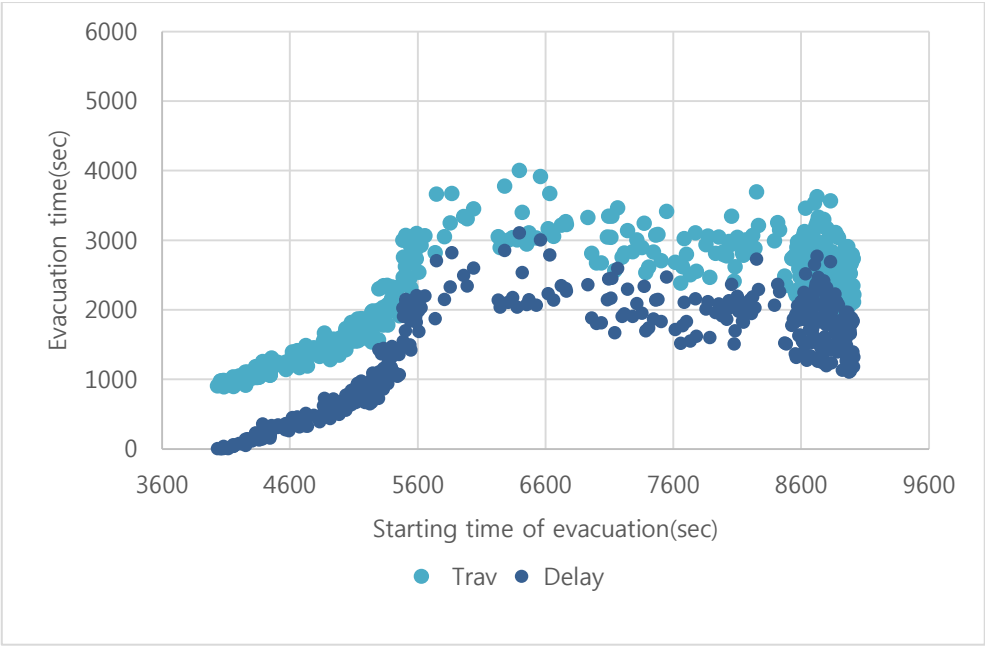

Figure 7. Distribution of evacuation time

This is the result of Evacuation Time Estimate modeling. This graph is represented that midday scenario (70% car using). And, this is only one route represent. This graph means that evacuation time is relate on that the time of leaving. The first evacuees take a short time for evacuation, however, after traffic

congestion occur, many evacuees take a long time for evacuation.

	Total Travel Time	Total evacuation Time	Average Evacuation Time
Min	26,019,215	12,705	1,870
Max	31,024,198	14,045	2,233
Mean	28,330,633	13,338	2,027
Std.dev	1,231,169	325	87

Table 2. Result of simulation (evening scenario)

	Total Travel Time	Total evacuation Time	Average Evacuation Time
Min	20,180,658	9,793	1,594
Max	23,588,351	10,453	1,833
Mean	21,845,769	10,141	1,706
Std.dev	783,339	150	56

Table 3. Result of simulation (midday scenario, 70% using car)

	Total Travel Time	Total evacuation Time	Average Evacuation Time
Min	12,677,181	9,243	1,236
Max	14,277,835	9,360	1,397
Mean	13,594,257	9,316	1,318
Std.dev	384,212	29	36

Table 4. Result of simulation (midday scenario, 50% using car)

	Total Travel Time	Total evacuation Time	Average Evacuation Time
Min	6,369,008	9,266	826
Max	8,346,599	9,381	1,051
Mean	7,263,670	9,318	932
Std.dev	491,564	26	59

Table 5. Result of simulation (midday scenario, 30% using car)

This table shows the result of Evacuation Time Estimate modeling. And, each table stands for each scenario. In this study, there is 4 type of scenario. Each scenario has different traffic demanding. Because of difference car using rate. Total travel time means that the sum of whole evacuation time of each car. And, total evacuation time means that the time lap from starting time of evacuation to completion time of evacuation. Finally, average evacuation time means that mean time of each car for evacuation.

Total evacuation time and average evacuation time increase with car using rate. But, some scenario has a similar result even though different car using rate. Especially, 50% using car and 30% using car scenario have a similar result of total evacuation time. But, there is a difference of average evacuation time. This result means that the difference possibility of exposure to the radioactive material during the evacuation. Therefore, the less car using rate during the evacuation, the safer for people who evacuate during the radiological emergency.

5. Conclusion

Based on simulation result, Total evacuation time is similar according to different scenario. But, Average evacuation time and total delay are totally different according to each scenario. These differences will make a huge effect on people's health. Because it can be caused different radiation exposure.

6. References

[1] "Criteria for Development of Evacuation Time Estimate Studies", NUREG/CR-7002, SNL, 2011
[2] "Development of Evacuation Time Estimate Studies for Nuclear Power Plants", NUREG/CR-6863, SNL, 2004

FRENCH POST-FUKUSHIMA COMPLEMENTARY ASSESSMENTS - GENERAL APPROACH AND RESULTING SAFETY IMPROVEMENTS FOR THE HIGH FLUX REACTOR LOCATED IN GRENOBLE

E. GROLLEAU, A-C JOUVE, S. KANAMORI
Institut de Radioprotection et de sûreté Nucléaire (IRSN)
Fontenay-aux-Roses, France

ABSTRACT

Following the accident that occurred on the Fukushima Daiichi nuclear power plant on March 11th 2011, the licensees of French nuclear facilities were asked to engage a safety reassessment of their facilities with the aim of evaluating their capacity to withstand extreme situations beyond design basis assumptions. These specific reassessments, called Complementary Safety Assessments (CSAs), were carried out on the basis of the specifications for the stress tests requested by the European Council. In France, these reassessments included all nuclear power plants in operation but also fuel cycle facilities and research reactors. This paper presents the analysis performed by French licensees in the framework of CSAs and the opinion of the Institute of Radiological Protection and Nuclear Safety (IRSN) which has been largely involved in the review of the CSAs. Then, the paper introduces the concept of "hardened safety core" firstly defined by IRSN and presents a concrete implementation of the "hardened safety core" based on the example of the High Flux Reactor (RHF), which is a research reactor located in Grenoble (France) and operated by the Laue-Langevin Institute (ILL).

1. Introduction

Following the accident that occurred on the Fukushima Daiichi nuclear power plant on March 11th 2011, the French Nuclear Safety Authority (ASN) requested the French nuclear licensees, by the mean of regulatory decisions taken on May 2011 [1], to carry out a reassessment of their facilities in the light of the Fukushima accident. These reassessments, called Complementary Safety Assessments (CSAs), were based on the specifications attached to the aforementioned decisions and were consistent with the specifications for the stress tests requested by the European Council.

The aim of the CSAs carried out in France is to take into account the lessons learned from the events that hit the Fukushima Daiichi nuclear site by evaluating the capacity of nuclear facilities to withstand extreme situations beyond design basis assumptions. The scope of CSAs included nuclear power plants in operation or under construction as well as nuclear facilities considered to be high-priority[1] like the High Flux Reactor (RHF) in Grenoble, the Osiris reactor in Saclay, the Jules Horowitz Reactor (under construction in Cadarache) and main fuel cycle facilities such as La Hague (AREVA) facilities.

The Institute of Radiological Protection and Nuclear Safety (IRSN), which is the main technical support organization of the ASN, has been largely involved in the review of the CSAs carried out by licensees. In that context, IRSN conducted extensive technical discussions with licensees.

[1] The French CSAs were carried out by sorting nuclear facilities into three categories depending on their vulnerability to the phenomena which led to the Fukushima accident and the importance and scale of any consequences of an accident affecting them.

2. The French CSAs general approach

2.1 The French nuclear safety approach

The general safety demonstration approach for French nuclear facilities consists in constantly seeking for safety improvement. Enhancing safety relies on:

- taking into account the operating facilities feedback;
- the periodic safety reviews which are an obligation for all French nuclear facilities since 2006, including compliance review and safety reassessment accordingly to up-to-date safety standards and practices;
- the development and the updating of scientific and technical reference repositories.

Nuclear facilities design and specifications must lead to the deployment of technical and organizational provisions allowing the management of the operation-related risks (under normal or accidental situations) including the ability of facilities to withstand the hazards (of internal or external origin) which may affect them. Specifications are likely to be modified throughout the facilities life, especially thanks to the periodic safety reviews.

The safety demonstration in France is mainly based on the defense-in-depth principle articulated around five levels. This principle aims at designing the facilities in order to prevent incidental or accidental situations and to foresee the adequate provisions to mitigate the consequences of such situations. In this context, the safety analyses established in France are carried out accordingly to a deterministic approach, supplemented, when relevant, by probabilistic studies.

All justifications and analyzes produced by licensees of nuclear facilities require the clear definition of assumptions and input data with related uncertainties. For instance, these assumptions and data concern the hazards characteristics which are taken into account in the safety demonstration (intensity, duration, etc.) or combinations of hazards that it is reasonable to consider for the demonstration. These characteristics are regularly reassessed in the light of new technical and scientific knowledge.

2.2 The objectives and the implementation of CSAs

The approach of CSAs engaged after the Fukushima-Daiichi accident assumes that very unlikely severe accident situations may be caused by natural external hazards with higher intensity level than those considered until then in the safety demonstration. The main natural hazards considered in CSAs are extreme earthquake, flooding and climatic phenomena. Extreme situations such as the total loss of electrical supplies or the total loss of cooling sources have also been postulated in CSAs with more degraded assumptions than those previously considered in the safety demonstration (duration of sources loss, numbers of facilities concerned in the same time on a given site, etc.).

The prime objective of CSAs is to assess the response of nuclear facilities in the event of an extreme hazard or an extreme situation (as above mentioned) which would affect them. In France, the analysis has been focused on the identification of potential cliff-edge effects, that is to say, the risk that a small variation of a characteristic related to a hazard or to a degraded situation will lead to a brutal change of the facility behavior, combined in most of cases with large radiological consequences.

To this effect, the French licensees of nuclear facilities have presented analyses of robustness based on an evaluation of safety margins, in terms of resistance of civil engineering structures or equipment, estimated from the design technical specifications (input data related to dimensioning methods or assumptions taken to the seismic spectra used in design studies) or to the construction (equipment anchorages, structural gaps

between civil engineering structures) of facilities. This safety margin assessment, mostly based on single margin factors evaluated with an engineer appreciation, has enabled licensees to assess the robustness of their facilities and, where appropriate, to identify points of weakness and some required facility reinforcements.

In 2011, IRSN has estimated [2] that given the uncertainties related to the levels of extreme hazards to be considered and because of simplified approaches implemented for CSAs for assessing the behavior of the facilities, it was not possible to conclude, with a sufficient degree of confidence, on the robustness of facilities facing extreme hazards. In that way, IRSN recommended that additional studies, based on codified technical rules and methods, had to be implemented to accurately identify the reinforcements that may be required to ensure the resistance of nuclear facilities against extreme hazards and situations.

However, the important work done by the operators licensees for CSAs in a very short time allowed to identify the systems, structures and components (SSCs) of facilities whose loss or failure may lead to a cliff-edge effect in terms of radiological or toxic consequences. These SSCs are directly involved in the control of fundamental safety functions namely, for the reactors, the reactivity control, the fuel cooling control and the containment of dangerous materials. In addition, these SSCs can be classified in one of the different levels of defense-in-depth (prevention of an accident, mitigation of the accident consequences and crisis management) according to their role for safety. From the point of view of IRSN, the identification by licensees of the SSCs whose loss or failure is likely to lead to a cliff-edge effect was globally satisfactory.

Finally, the CSAs determined, for the facilities for which a risk of cliff-edge effect had been identified, a set of material provisions necessary to enable the facility to withstand hazards or situations with higher intensity levels than those considered so far. This set of provisions, completed by organizational measures, constitutes what IRSN has called the post-Fukshima "hardened safety core” [2].

3. The “hardened safety core” concept

The “hardened safety core” (HSC) must ensure ultimate protection of nuclear facilities with the three following objectives:

- prevent a severe accident or limit its progression;
- limit large-scale releases in the event of an accident which was not possible to control;
- enable the licensee to perform its emergency management duties.

The HSC may be composed of existing SSCs, that might require to be strengthened, and new SSCs that should be designed and sized to withstand extreme situations. In a general way, IRSN considers that choices regarding the definition of the SSCs of HSC and the related technical requirements must guarantee, with a high level of confidence, the ability to ensure their functions in the event of extreme situations.

To this purpose, the required intensity levels to be retained to characterize extreme hazards and situations (intensity, duration, etc.) have to be defined, and also the methods implemented to justify the resistance and the operability of SSCs of the HSC under extreme conditions. It is on the basis of these data that it will be possible to demonstrate that the main safety functions will be ensured in the event of extreme situations.

Then, characterization of extreme seismic and flooding hazards, as well as extreme climatical conditions is necessary. In the same time, it must be taken into account the possible effects induced by these extreme natural hazards.

The paragraph 4 presents the implementation of the “hardened safety core” concept to the High Flux Reactor located in Grenoble, France.

4. The hardened safety core of the High Flux Reactor

4.1 Description of the facility

The High Flux Reactor (RHF) is a research reactor located in the immediate vicinity of Grenoble city (France). First diverged in 1971, this reactor aims at providing, through channels pointing directly towards the reactor core, neutrons source for the purposes of fundamental research mainly devoted to the exploration of matter. This reactor, operated by the Laue-Langevin Institute (ILL), developes a maximum thermal power of 58.3 MW. The reactor core *(see FIG.1)*, cooled by heavy water, is composed of one fuel element made of highly-enriched uranium and aluminum alloy. The reactor is operated by cycles of approximately 50 days. Immediately after the reactor shutdown, the passage in natural convection allows, thanks to the calorific capacity of the reactor pool, to cool the core without need of electrical power supply or external cooling source.

The reactor building is made of a double enclosure *(see FIG.2)*, one in a 40-cm thick concrete wall (internal enclosure), the other in a 1.1-cm thick metal lining, the annular space between both enclosures being pressurized at 135 mbar.

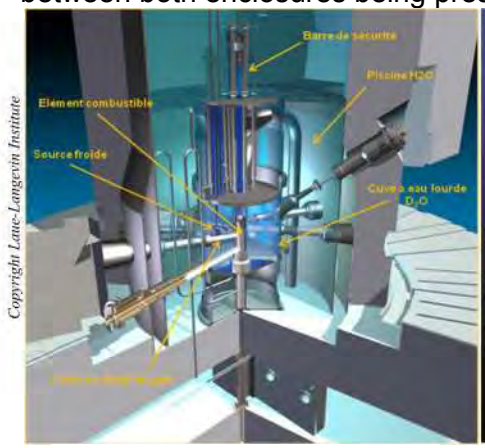

FIG.1. RHF reactor core

FIG.2. RHF building reactor

4.2 IRSN review of RHF hardened safety core defined by ILL

As previously mentioned, IRSN reviewed the demonstration carried out by the operators to identify the SSCs of their facilities whose failure might lead to a cliff-edge effect in case of extreme hazards or extreme situation. For ILL this identification has been made on the basis of scenarios related to core melt accidents (severe reactivity accident or loss of fuel cooling accident). In that way ILL retained as scenarios that could lead to a cliff-edge effect such as BORAX-type accident and accidents of fuel melting (in air or in water) cumulated to a degradation of the building containment function. From these scenarios, ILL has identified the SSCs whose failure may lead to important radiological consequences to the public and the environment. IRSN review has confirmed that ILL realized an approach matching the specifications of the CSAs, while underlying the effort made to perform an exhaustive search of cliff-edge effects scenarios taking into account all possible initial states of reactor operation.

In 2012, as a following of the CSA of RHF, ILL has proposed to implement a hardened core of material provisions and organizational measures aims at ensuring the control of the basic safety functions in the event of extreme hazards. On the basis of the conclusions of the HRF CSA, the main hazards to be considered are the extreme earthquake and the extreme flooding (induced by the failure of dams located in the mountains surrounding Grenoble), as

well as the induced effects (explosion of internal or external origin, fire, etc.). Thus, ILL defined, in a first approach, the HSC of RHF as described below, relying on the levels 3 to 5 of the defense-in-depth principle:

The **"prevention of severe accident" part of the HSC** (level 3 of defense-in-depth):

- the reactor emergency shutdown system (new system called ARS[2]) based on earthquake detection (0,01g) aims at stopping the reactivity inside the core;
- the core water supply safeguard systems (existing core water supply systems called CRU and CES, completed by a new groundwater supply system called CEN);
- the emergency fuel lowering system (system called PUC which is an already existing system) for setting the fuel element being handled in a safe position in the fuel storage pool.

The **"mitigation of severe accident" part of the HSC** (level 4 of defense in depth):

- the concrete enclosure building with the related automatic containment isolation devices (system called SIE);
- the containment depressurization seismic circuit (new system called CDS) which will ensure the extraction and the filtration of contaminated air from the reactor building in case of severe accident.

The **"emergency management" part of the HSC** (level 5 of defense in depth):

- the bunkered emergency control room (new room called PCS3 located in a new building) which will permit to ensure the control of the aforementioned active systems, the general monitoring of the reactor after accident (temperature and pressure measures, pools water level measures, radioactive releases control, etc.) and the emergency management duties (communication with national and local authorities, communication and information exchange with IRSN, etc.).

During the technical discussions with licensees, IRSN has indicated to ILL that the HSC will be useful only if passive SSCs of RHF were not completely deteriorated after an extreme aggression (for instance the pool walls or the beam tube structures total failure would make any water supply vain). ILL agreed with this point and decided to modify the content of the HSC of RHF by including "passive" SSCs necessary to achieve basic safety functions.
From this point on, the HSC of RHF is defined as described in Table I below [4].

Table I: SSCs of the hardened safety core of RHF

« Active » HSC	***« Passive » HSC***
• Emergency reactor shutdown system (ARS) • Ultimate "drench" circuit (CRU) in association with the emergency water supply circuit (CES) • Underground water supply circuit (CEN) • Emergency fuel lowering system (PUC) • Automatic containment isolation system (SIE) • Containment depressurization seismic circuit (CDS) • PCS3 (means of control and monitoring required for the management of crisis)	• Primary core enclosure and related supporting structures • Fuel handling container • Natural convection flappers • Civil engineering structures and lining of the fuel storage channel and reactor pool • Neutron beam tube nozzles • Concrete reactor enclosure • PCS3 (room and supporting building)

[2] A reactor shutdown system was of course already in place but not designed to withstand strong earthquakes (I&C in particular). The new ARS system will permit to ensure the reactor shutdown including during the strongest solicitations of an extreme earthquake.

It must be underlined that all new "active" SSCs of HSC satisfy the single failure criterion. Thus, CEN circuit (underground water supply), CDS circuit (which manages the depressurization of reactor building and the accidental release) and all electrical power supplies and monitoring devices required for PCS3 crisis management are redundant.

At the end of technical exchanges with ILL, IRSN concluded that principles and safety requirements chosen by the licensee for the definition, the design and the realization of the HSC of RHF were satisfactory. This is likely to meet the expectations of IRSN who considers that the objective of the hardened safety core is to confer on nuclear facilities (and therefore to RHF in particular) a better robustness to withstand situations not considered up to now in safety demonstrations.

4.3 Characterization of extreme hazards to design the HSC

One fundamental aspect related to the implementation of HSC is to characterize the extreme hazards which will be used to design and size new SSCs of HSC and to justify existing SSCs of HSC. In the case of RHF, it is thus necessary to define the levels of extreme earthquake and extreme flooding to be considered, knowing that RHF site is particularly exposed to such hazards. Then, it is also required to evaluate the damages induced (secondary effects) which may affect the facility.

4.3.1 The extreme earthquake

The ASN has fixed the general requirements that must meet the levels of seismic solicitation considered for the SSCs of HSC. Thus, the requirements to be fulfill by the HSC seismic response spectrum (giving the answer in acceleration of a simple oscillator placed on the ground affected by the earthquake) are as follows:

- be 50% higher than the seismic spectrum chosen as a reference to the design of new nuclear facilities (determination method of this spectrum is specified in a fundamental safety rule published by the ASN in 2001 [3]);
- be conservative of spectra defined accordingly to a probabilistic manner with a return period of 20 000 years;
- take into account the possible effects due to the facility location including the nature of the soil.

These requirements had to be declined to the site of RHF. To this purpose, several technical discussions were held between IRSN and ILL from 2013 to 2014 in relation with the definition of the seismic spectra to be retained for the HSC. These exchanges were particularly focused on the input data (such as the seism-tectonic zoning, the predictive equations of seismic movement, the seismicity rate) used for the probabilistic assessments of seismic spectra (also called PSHA for Probabilistic Seismic Hazards Assessment[3]) and on the multiplicative coefficients to apply for taking into account specific site related effects (the site of RHF is located in a paleo-sedimentary valley).

On the base on its own calculation models, IRSN has estimated that the seismic spectra defined by ILL for the HSC of RHF (a reference spectrum and a simplified spectrum with a Eurocode 8 type form easier to use for some design studies) meets the requirements fixed by the ASN for the HSC.

The seismic spectra finally obtained for the HSC of ILL are shown on the *FIG.3* hereafter. This figure shows the two forms of seism spectrum retained by ILL compared to the envelope

[3] PSHA are a mathematical approach combining models for the location and size of potential future earthquakes with predictions of the potential intensity caused by these future earthquakes.

of the SMS[4] spectra of RHF, increased by 50 %, taking into account specific related site effects.

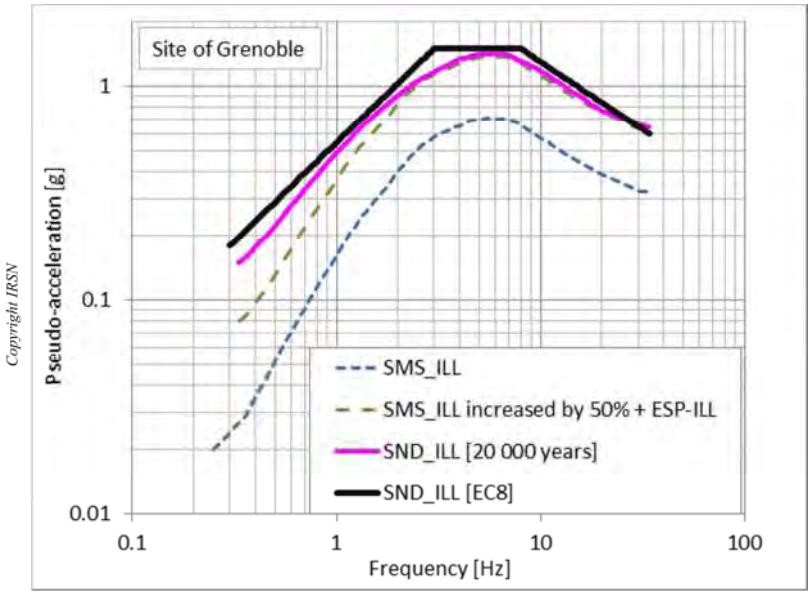

FIG.3. Spectra defined by ILL for the hard safety core (HSC) of RHF (in pink: spectrum associated with a period of return target of 20,000 years taking into account specific site effects - in black: spectrum of simplified type "Eurocode 8" - in green dashed: the envelope of the SMS spectra for RHF, increased by 50 %, with specific site effects taken into account - in blue dashed: the envelope of the SMS spectra for RHF)

4.3.2 The extreme flooding

The flooding hazard has firstly to be assessed in terms of height of water level which may occur at RHF site in the event of an extreme hazard. In order to estimate the height of water level, ILL assumed a scenario combining the total simultaneous break of four dams located on the Drac river upstream of RHF (*see FIG.4*).

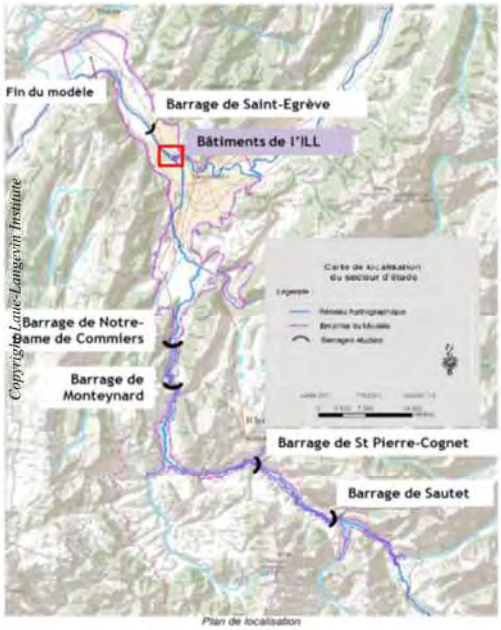

FIG.4. Localization of the four Drac river dams that have been supposed to be breakdown in the scenario of extreme flooding of RHF site

[4] The SMS (Séismes Majorés de Sécurité) are considered to be the most aggressive earthquakes to be retained when sizing a nuclear facility. The SMS are defined based on the "Maximum Historically Probable Earthquakes" (Séismes Maximaux Historiquement Vraisemblables - SMHV) considered as the most penalising earthquakes liable to occur over a historical period. The SMS is deduced from the SMHV by the following equation in terms of intensity (I) on the site: I(SMS) = I(SMHV)+1.

IRSN considered that the scenario defined by ILL was relevant with regards to the Fukushima accident feedback. This scenario leads to assume that a maximum 6 meters high wave of water is coming down RHF inducing a total flooding of site. The maximum height of water is taken into account by ILL for the demonstration that RHF will withstand such extreme conditions. For instance, the location of new SSCs of HSC has been defined by considering the water height and the throughlets of the reactor buildings have been protected from flooding. The PCS3 has also been designed such in a manner that it will not be flooded under extreme conditions.

Another aspect relating to the extreme flooding concerns the risks induced by large and heavy debris carried along by water which can impact the reactor building and the new PCS3 building. On this point, ILL postulates the impact of a 20-ton truck which would come hitting buildings. Thus ILL has designed and sized the PCS3 building taking that risk into account. IRSN is currently reviewing the studies carried out by ILL.

Finally IRSN recommended that ILL assesses the risks of the soil being washed away when the flooding wave is coming on RHF site. In order to prevent from that risk, ILL has provided provisions such as:

- the 4 meters-depth burial of electrical and control-command cables between the building reactor and the PCS3;
- the setting of sheet piling designed to protect the civil structure foundations of buildings;
- the building of plane concrete zones surrounding main buildings for guiding the flood flow.

4.3.3 Induced risks (secondary effects)

ILL has also taken into account the risks that may result from extreme hazards as earthquake (secondary effects). For example, aggravating events such as external explosions coming from industrial plants located in the environment of RHF site have been considered for the design and the sizing of the new SSCs of HSC or the verification of existing SSCs of HSC. Thus the PCS3 has been designed to withstand the blast from an explosion which would arise from the yard to a few hundreds of meters from the site of ILL.

Furthermore ILL has modified general electrical supply system by providing a specific device which will shut down all electrical sources in the building reactor in the case of extreme earthquake or flooding to prevent induced internal fire risks.

Finally provisions have been set by ILL to protect workers assuring emergency management at the PCS3 from potential cloud of toxic substances which would affect RHF site as a result of the explosion of hazardous gas stored on the industrial platform located at the south of Grenoble.

4.4 The building and the setup of RHF hardened safety core

Since 2012, ILL has placed special emphasis on the strengthening of RHF decided as a result of the accident of Fukushima. The implementation of the HSC must be completed at the end of the first quarter 2016.

In summer 2015, the state of progress of the implementation of the HSC of RHF is as described hereafter.

SSCs related to the "prevention" of severe accidents:

- The new equipment of the water underground circuit CEN (*see FIG.5*) are installed and tested (pumps, suction strainers, piping, power supplies, monitoring and control systems);

FIG.5. Suction strainers of the new CEN system

SSCs related to the "mitigation" of the consequences of severe accidents:

- The containment depressurization seismic circuit CDS (*see FIG.6*) is installed and tested (ventilators, HEPA[5] filters, iodine filters, pipes, isolation valves, chimney on the roof of reactor building);

FIG.6. New CDS circuit: parts located outside the reactor building

SSCs related to "emergency management":

- The PCS3 (*see FIG.7*) has been built between 2012 and 2013 and its equipment, as well as the cable connections between the new building and the reactor, was installed between 2013 and 2014 (*see FIG.8*). Since the beginning of 2015, all relevant information for emergency management are available at the command post of PCS3 (water level in the reactor pool and fuel storage, radioactivity measures in the reactor building, wind speed and direction, communication devices, etc.). Moreover, equipment required for the human habitability of PCS3 in situation of accident is already installed (air conditioning systems, HEPA and iodine filters, NBC[6] filtration

[5] High Efficiency Particulate Air.
[6] Nuclear, Biological, Chemical.

system, etc.). Nevertheless the control of the active systems of the HSC (CEN, CDS, etc.) from the PCS3 is not yet possible since it still requires an authorization from the ASN.

FIG.7. External view of new PCS3 (building) and emergency control

FIG.8. Communication tools and air conditioning systems of PCS3

5. Conclusion

As a result of the accident of Fukushima-Daiichi, Complementary Safety Assessments (CSAs) have been carried out by licensees of French nuclear facilities to evaluate the behavior of these facilities with regard to extreme hazards and situations, mainly targeted on the earthquake, flooding, climatic phenomena and the total loss of power supplies and sources of fuel cooling.

The review by IRSN of these CSAs has led to the emergence of the concept of “hardened safety core (HSC)” whose objective is to enhance the resistance of nuclear facilities to extreme hazards of extreme situations whose main characteristics are superior to those considered up to now in safety demonstrations.The Laue-Langevin Institute (ILL) has fully developed the concept of HSC for the High flux reactor (RHF) and many technical exchanges with IRSN have been done since 2011 playing an important part in the definition and the implementation of the HSC in the facility.

IRSN considers finally that the reinforcements of existing SSCs made by ILL and the new SSCs put in place on RHF are likely to significantly improve the robustness of the reactor in the event of extreme natural hazards.

6. References

[1] *ASN, Decisions requiring that French Nuclear Facility Licensees conduct a Complementary Safety Assessment of their Basic Nuclear Installations in the light of the accident that occurred on the Fukushima Daiichi Nuclear Power Plant (2011).*

[2] *IRSN, Report No. 679 (November 2011).*

[3] *ASN, Fundamental Safety Rule No. 2001-01 concerning basic nuclear facilities (2001).*

[4] *IRSN, Report No. 2013-00005 (March 2013).*

APPLICATION OF SAFETY REASSESSMENT IN THE LIGHT OF FUKUSHIMA DAIICHI ACCIDENT TO NEW DESIGNS: THE RA-10 REACTOR CASE

P. RAMIREZ, P. CANTERO, F. BROLLO AND H. BLAUMANN
National Atomic Energy Commission (CNEA)
Centro Atómico Bariloche, Postal Box 138, Exequiel Bustillo Avenue 9500, R8402AGP, S. C. de Bariloche, Argentina

ABSTRACT

The lessons learned from severe accidents, such as the Accident at the Fukushima Daiichi Nuclear Power Plant, are a very important input that need to be taken into account in reassessing the safety of nuclear installations, including research reactors, particularly for defining and implementing measures to prevent and mitigate accidents. Due to the fact that many research reactors are operational since many decades ago, their designs usually do not comply with IAEA standards and the defence in depth principle and therefore safety reassessment recommendations focus particularly on those installations. Nonetheless, the lessons learned from severe accidents are also a key opportunity for research reactors at the design stage. At this stage, the safety reassessment results can be used to ensure that structures, systems and components important to safety are properly designed and the opportunities for improving the safety aspects of the design can be incorporated more easily than for existing facilities.

The RA-10 reactor is a planned 30 MW research reactor for radioisotope production and neutron beam research. The RA-10 reactor project has conducted a safety reassessment in the light of the Accident at Fukushima Daiichi by following the recommendations provided by IAEA in the Safety Reports Series No. 80. In this paper, the main aspects and results of the safety reassessment conducted for the RA-10 reactor are presented and discussed. Emphasis is given on how the results of the safety reassessment were used in the review and improvement of the design characteristics of structures, systems and components important to safety of the reactor and on emergency preparedness and response. Particularly, details will be given on the review of the flooding design basis for the reactor site and provisions adopted against the flooding event, the modifications introduced to the water injection system and long term cooling systems, the discussion of the analysis conducted for a beyond design basis where it is assumed that a black-out scenario takes place during an extended time period. Finally, the main conclusions gained from this safety reassessment to a new design and the future work will be discussed.

1. Introduction

Incorporating the lessons learned from accidents at other facilities is an important process to enhance safety of reactor facilities. This process may be difficult to implement when the facilities are not similar or are intended for different purposes, such as the case of nuclear power plants and research reactors. In those cases, a guideline to conduct this process is necessary.

This paper presents the results of the reassessment conducted for the RA-10 reactor, currently at the design stage. The reassessment incorporated the lessons learned at the Accident at Fukushima Daiichi by following the recommendations provided by IAEA in the Safety Reports Series No. 80 [1]. In line with this, the paper follows the structure of this guideline.

In section 2, requirements used in the safety reassessment are discussed. In section 3, the reassessment of the facility is presented. As the reactor has recently completed the safety assessments necessary to apply for the construction license, those safety evaluations were used as review of the design basis. The analysis conducted for an extended station black out event is presented in this section. In section 4, highlights of the site reassessment are discussed, including the complementary site studies conducted to revaluate the flooding level design basis. In section 5, the reassessment of the emergency preparedness and response is discussed and an example of a design change in the Emergency Water Injection System to allow feeding water from outside the reactor building is discussed as an example of the results of the reassessment. Finally, in section 6 the conclusions of the safety reassessment are presented and discussed.

2. Requirements for the Safety Reassessment

Regarding the measures adopted by ARN, the Argentinean regulatory body, it was required that the Argentinean nuclear power plants in operation undergo a number of inspections, reviews and verifications aimed to verify their capability to withstand the occurrence of events considered within the design basis as well as beyond the design basis events. ARN also required that the nuclear power plants in operation and under construction to conduct an Integral Safety Evaluation (stress tests) with the objective of detecting weaknesses and implementing the corresponding upgrades. Such inspections, reviews, verifications and the integral safety evaluation followed the recommendations of interational organizations such as WANO and the FORO [2].

The regulatory body imposed no specific requirements to conduct a safety reassessment for research reactors. It is worth noticing that argentine regulations adopt a risk based approach for the evaluation of the safety of nuclear installations, including research reactors. Therefore, the safety assessment of research reactors includes the consideration of event of very low frequency of occurrence and high severity. Notwithstanding this, the project decided to conduct a safety reassessment of the design of the RA-10 reactor in the light of the accident at the Fukushima Daiichi Nuclear Power Plant. It was also decided that the reassessment will be conducted in accordance with the requirements of IAEA Safety Report Series 80.

3. Reassessment of the Reactor Facility

3.1. Review of the Design Basis

The main objective of the review of the design basis is to ensure that the fundamental safety functions can be fulfilled. Since the RA-10 reactor is at the design stage, a complete safety evaluation has been conducted for the facility complying with national regulations [3, 4] and IAEA standards [5, 6 and 7]. The safety assessment included the elaboration of safety analyses both deterministic and probabilistic used complementarily in the risk assessment of internal failures capable of affecting radiation sources including: the reactor core, the experimental devices and the irradiated fuel assembly storage. The safety assessment also included the conduct of evaluations of engineering factors important to safety related to: the adequate implementation of the design principles adopted with emphasis on assessing the adequate implementation of the defense in depth principle and the performance of SSC important to safety in order to demonstrate that they can fulfil their assigned safety functions.

In order to ensure completeness and in compliance with regulatory standards [3, 4], initiating events were identified, selected and postulated through the systematic application of a specific procedure. Initiating events and the sequences originated from them were incorporated within

the scope of the safety analysis, the evaluation of factors important to safety or a combination of both. The initiating events proposed by regulatory guidelines [8] and IAEA [6, 7 and 9], operational experience and derived from other analysis techniques were included to be assessed. It is worth noticing that the referred initiating event lists include the consideration of external events.

The design of the RA-10 includes the provision of safety systems to cope with design basis events including: a reactor protection system, a first shutdown system, a natural circulation cooling system for the core and the experimental devices. For all design basis events the design of the safety systems ensures that no damage occurs to the core. The design also provides safety systems for extended design basis events (i.e. low frequency events involving the failure of one design basis safety system or severe accidents) which include a second shutdown system, an emergency water injection system, a long term cooling system, the confinement system, a post-accident monitoring system, an alternative control room and an emergency power supply system. All the systems include in their design basis the consideration of external events, particularly those with components outside the reactor building.

From the review of the design basis and the reassessment of the site characteristics, the flooding design basis determined by the new site studies was adopted. In order to cope with the design basis flooding, a “dry site” strategy was adopted and therefore the level of the facility will be raised above the flooding design basis level by means of a terrain fill.

The review of the emergency response and preparedness demonstrated that the postulated scenarios, which included a very low frequency severe accident scenario, covered the possible outcomes of accident sequences.

Other modifications to the design emerging from the assessment were: the identification of water sources within the facility and the possible ways to use them as make up water to the reactor pool in case of emergency, the provision of emergency power supply to equipment involved in long term cooling of the core and experimental devices and the provision of emergency power to ventilation systems to improve and optimize the response of containment systems.

3.2. Assessment of the Consequences of Beyond Design Basis Events

The reassessment results of the site, which will be discussed in section 4, showed the potential for a flooding affecting the site. As discussed in the previous section, provisions were included in the reactor facility design in order to withstand the design basis flooding adopted after the reevaluation. In order to assess the robustness of the design, the consequences on the reactor for a beyond design basis flooding exceeding the design basis provisions was analyzed. If such an extreme flooding occurred, both normal and emergency power supply would be affected and eventually lost, thus resulting in a black out event. Such an event would affect the power supply for the duration of the flooding event and it may take several days until power can be reestablished to the facility. It is assumed in this analysis that the power supply is affected for a long-term, i.e. a period of time of one week or more.

The loss of the normal power supply will result in the full insertion of the control rod plates which are the reactor first shutdown system. After 30 minutes, the interruptible power supply will be lost and this would result in the inherent triggering of the second shutdown system consisting in the partial dump of the heavy water reflector contained in the reflector vessel which surrounds the reactor core. Therefore, in this event the shutdown function is achieved successfully. The radioactive material of the core is contained in the fuel assemblies which will need cooling in order to ensure the confining of the radioactive material of the core. The black-out event affects

the cooling systems that use normal or emergency power. Therefore, the analysis does not take into account the availability of any forced circulation cooling system, including the primary cooling system and the pools cooling system. Conservatively, the analysis assumes that both power sources are lost simultaneously. When power is lost, the flywheels provided to the primary pumps allow them to provide a coast down cooling flow to the core and, when the decays away, allows the opening of flap valves and a smooth establishment of natural circulation cooling which constitutes the emergency core cooling system of the reactor. The safety analysis previous to this analysis demonstrated that the natural circulation cooling was adequate to provide cooling to the core in the short term [reference]. The analysis described in this section, conducted for the extended black out event, is intended to evaluate the time period that the core can be cooled relaying only on natural circulation.

A nodalization for the RELAP5/MOD3.3gl code, developed by Safety Nuclear Department of the Bariloche Atomic Center, was used in order to perform the simulation.

The analysis was performed in two stages. Using a RELAP model, a 29 hours simulation of the transitory “black out event”, with the success of the Fist Shutdown System and the natural circulation cooling system was performed to analyze the first stage of the transient. The second stage after the 29 hours the RELAP model becomes no longer appropriate to describe the pool boiling phenomena. To continue the analysis of the second stage, the results of the first stage were extrapolated to estimate the core cooling conditions and the emptying lapse of the reactor pool due to the evaporation of the coolant, corresponding to the interval in which the coolant level drops from its nominal value to the upper level of the reactor core.

For the analysis of core cooling, the attention was directed toward the phenomenon of Burn-Out, which is the most important in the long-term, when the mass flow of coolant and the core heat flux are low. A verification of the Burn-Out Margin, which is adopted as acceptance criterion for the cooling of the reactor, was made following the correlations scheme proposed by Sudo and Kaminaga in order to estimate the critical heat flux as a function of the mass flow values.

The analysis concludes that the design meets the safety objectives, demonstrating that the reactor is properly extinguished and cooled by natural circulation in the reactor pool during a period of 10 days. The thermal-hydraulic acceptance criteria are verified during that period of time.

From the analysis emerged that, for this event, the coolant in the reactor pool will reach the saturation temperature. Therefore, the reactor pool liner was verified to withstand the loads imposed by this event, allowing the pool to contain the coolant during the duration of the event. Compliance with the stress limits required by ASME III service level D was used as acceptance criterion for this verification.

4. Site Reassessment

4.1. Review of Site Characteristics

The RA-10 reactor will be constructed at the Centro Atómico Ezeiza (CAE) site. The site has 8.322.584 m2 where CNEA, the site owner, runs a number of facilities, including the RA-3 research reactor that will be eventually replaced by the RA-10 reactor, nuclear fuel manufacturing facilities and radioactive waste storage facilities, among others.

The safety assessment conducted for the RA-10 reactor included the evaluation of external events that have the potential of affecting the site. The safety assessment of the site included

main objective was to identify those external events, both natural and man induced, that may affect the safety of the future reactor and establish the design basis for those events that have to be taken into account in the design. The derivation of the design basis for the external events was conducted following the recommendation of IAEA guidelines [referencias]. The site safety assessment also provided the appropriate justifications for those external events that were deemed as not having potential enough to affect the safety of the reactor [10].

The reassessment of the site comprised three major steps. Firstly, a review of the completeness of the external events considered in the site evaluation was conducted using the list of external events provided by IAEA guidelines as completeness criterion [6]. Secondly, the design basis adopted for the different external events were reviewed in order to ensure that the appropriate design basis have been adopted. Finally, it was ensured that the external events excluded from further analysis for the site have the appropriate justifications for their exclusion.

From the reassessment it could be demonstrated that the external events analysed for the CAE site comprise a complete spectrum of events, including all the external events recommended to be taken into account by IAEA NS-R-4.

Regarding the design basis adopted for the external events capable of affecting the site, it was found that the evaluation of the seismic hazard required a more detailed study than the one performed in the first version of the site evaluation studies and to fully comply with international recommendations for this type of studies [referencia]. A detailed seismic hazard study was conducted which allowed to define a suitable design basis for the seismic hazard in terms of the peak seismic acceleration and its return period. The argentine regulation required that the safe shutdown seismic level (usually known as SL-2 level) has a probability of occurrence lower than 10-3 per year. The design basis adopted corresponded to a seismic event with a return period of 10000 years, therefore complying with the regulatory requirement, and the study determined an horizontal peak seismic acceleration of 1.15 g. For the vertical peak seismic acceleration, a value of 0.5 of the horizontal peak seismic acceleration was adopted.

From the reassessment it also emerged that the design basis for extreme flooding required a further study. In the original site evaluation studies, a 7.5 m over the reference flooding level corresponding to a 50 year return period was adopted. From the reassessment of this study it was concluded that, being the site susceptible to flooding induced by rainfall, the flooding design basis should be changed take into account the potential of an extreme flooding at the site. Consequently, a new hydrogeological study for the site was developed to establish to reassess the flooding level design basis. Details on the study performed are given in the next section.

4.2. Site-wide Events

An hydrogeological study of the CAE site was performed being one of the main objectives of this study to reassess the flooding hazard at the site. For this study, a geographical information system was implemented, historical meteorological and hydrological data of the site was gathered and analysed, surface and underground hydrological characteristics which included the identification and characterization of water courses were determined, and a site model to evaluate the amount of rain precipitation that becomes surface water and goes to the site water courses was elaborated. Extensive field work was required for the study of geographical, hydrological and geological characteristics of the site, involving site surveying, underground water and borehole drillings.

One of the main results of the study emerged from the characterizations of the interaction between surface and underground water. Underground water is found near the surface and

water courses in the area are generated from underground water emerging to the surface. This result in the soil of the site being practically saturated with water and therefore any rainfall would become surface water making the site susceptible of being susceptible to flooding generated by extreme rainfalls.

This study allowed redefining the flooding level design basis by calculating the flooding that would be induced by the heaviest rainfall registered in the last years in the area, assuming that such a rainfall occurs at the site. The available historical information only allowed determining that such a flooding induced by rainfall would have a return period higher than 100 years. The flooding level design resulting from the new study was 11.35 m.

5. Reassessment of the Emergency Preparedness and Response

The reassessment of the emergency preparedness and response included assuring that for all the emergency scenarios, the organizational arrangements, training programmes, emergency equipment, design features aimed to facilitate emergency response and accessibility to the site is suitable.

Particularly for the case of extreme flooding, a scenario where the access to the reactor site is impaired or directly impossible is included to the original set of emergency scenarios. For this case, the analysis presented in section 3.2 demonstrated that for the lapse of 10 days the reactor the fundamental safety functions can be established. During that lapse of time, no additional support from off-site emergency organizations would be necessary and therefore the RA-10 will not compromise the response of those organizations to support the emergency response to other facilities present at the site. After 10 days, it is necessary to provide water make up to the reactor pool were the core is located and to the service pool where the spent fuel is stored. One of the reassessment recommendations was to add a line connecting the Emergency Water Injection System with a fire hydrant type connection located outside of the reactor building which will allow a fire truck to feed the reactor and service pools with external water coolant through this connection. It is worth noticing that the site studies detailed in section 4.2 estimates that emergency access to the RA-10 reactor site will be available after 10 days. This new scenario and the detailed emergency response procedures will be developed in a future stage of development of the project and will be include in the emergency training programmes.

6. Conclusions

The reassessment conducted for the RA-10 reactor provided useful information to enhance the RA-10 reactor, currently at design stage. The possibility of conducting this assessment at this early stage allowed introducing changes in the flooding design basis, allowing incorporating protective measures, a terrain fill to raise the level of the whole facility, to cope with this event. Such a change would be impossible for a reactor in operation.

The reassessment also allowed incorporating design changes to safety systems of the reactor such as the case of the connection of the Emergency Water Injection System to allow feeding this system with water sources from outside the reactor. Such a change, although not impossible, is much more expensive and would require the facility to go off-line in order to implement the changes.

The site reassessment provided useful results allowing identifying the need for further studies, as the hydrogeological study developed for the RA-10 which complemented the studies

conducted for the original site assessment. It is also easier at this stage to translate into design solutions the results of such complementary site studies.

The assessment of an extended station black-out scenario, demonstrated the robustness of the facility for this beyond design basis event, demonstrating that the fundamental safety functions can be properly achieved. From this assessment emerged the need to verify that the reactor and service pool and the safety related internal components can withstand the load conditions imposed by this event.

The emergency planning and procedures will be developed in detail in a future project stage, the reassessment results on this regard constitute a very valuable input to ensure that all emergency scenarios and the response requirements will be properly taken into account by the emergency plans and procedures.

Finally, it was concluded that, in order to conduct a complete and useful reassessment in the light of accidents occurred at other facilities, the reassessment should follow a consistent and complete list of requirements and guidelines. When those requirements and guidelines are not available for research reactors from the regulatory body, the use of reassessment requirements for nuclear power plants can be difficult to adapt for use in a research reactor reassessment. In this case, IAEA in the Safety Reports Series No. 80 provided a complete and consistent guideline to conduct the reassessment of a research reactor, ensuring that a commensurate effort is made for consistently with the potential risks imposed by the reactor facility.

7. References

1. INTERNATIONAL ATOMIC ENERGY AGENCY, Safety Reassessment for Research Reactors in the Light of the Accident at the Fukushima Daiichi Nuclear Power Plant, IAEA Safety Report Series No. 80, IAEA, Vienna (2014).
2. AUTORIDAD REGULATORIA NUCLEAR, Report of the Evaluation and Analyses Conducted for the Argentinean Nuclear Power Plants, ARN, Buenos Aires (2012).
3. AUTORIDAD REGULATORIA NUCLEAR, Design of Nuclear Research Reactors, Regulatory Standard AR 4.2.2, Revision 1, Buenos Aires, Buenos Aires (2002).
4. AUTORIDAD REGULATORIA NUCLEAR, Accident Related Radiological Criteria in Nuclear Research Reactors, Regulatory Standard AR 4.1.3, Revision 2, Buenos Aires (2002).
5. INTERNATIONAL ATOMIC ENERGY AGENCY, Safety Assessment for Facilities and Activities, IAEA General Safety Requirements Part 4 No. GSR Part 4, Vienna (2009).
6. INTERNATIONAL ATOMIC ENERGY AGENCY, Safety of Research Reactors, IAEA Safety Requirements No. NS-R-4, Vienna (2005).
7. INTERNATIONAL ATOMIC ENERGY AGENCY, Safety Assessment for Research Reactors and Preparation of the Safety Analysis Report, IAEA Specific Safety Guide No. SSG-20, Vienna (2012).
8. AUTORIDAD REGULATORIA NUCLEAR, Design of Nuclear Research Reactors, Regulatory Guide AR 4, Revision 0, Buenos Aires (2003).
9. INTERNATIONAL ATOMIC ENERGY AGENCY, Safety Analysis for Research Reactors, IAEA Safety Report Series No. 55, Vienna (2008).
10. P. RAMÍREZ, M. CAPUTO, R. HILAL, M. GIMENEZ AND M. GRINBERG, RA-10 Project Safety Assessment and Licensing Process, International Group On Research Reactors Conference 2014, San Carlos de Bariloche (2014).

SAFETY REASSESSMENT OF HANARO AND STATUS OF SAFETY IMPROVEMENT MEASURES

I.C. LIM, C.S. LEE, J.W. SHIN, S.P. YIM, S.G. DOO
Research Reactor Utilization Department, KAERI
111, Daedeok-daero 989beon-gil, Yuseong-gu, Daejeon, 34057 – Korea

S.I. WU, J.S. RYU
Research Reactor Technology Development Department, KAERI
111, Daedeok-daero 989beon-gil, Yuseong-gu, Daejeon, 34057 – Korea

ABSTRACT

The Fukushima Daiichi accident in March 2011 made all the nuclear installations conduct the reassessment of safety and the safety of nuclear facilities in Korea was reviewed as well. A special safety review team composed of civilian experts and regulators conducted the reviews of nuclear installations in Korea and the safety of HANARO was also reviewed. The review was focused on the followings; safety of structure under seismic event and tsunami, stability of systems for electricity supply, firefighting and cooling under flooding, measures against severe accidents, emergency preparedness and prevention of radioactive material release. Several recommendations were made for the improvement of safety of HANARO. The measures were taken for the recommendations and reported to the regulatory body. The seismic assessment of reactor building showed the reactor concrete island(RCI) which accommodates the major reactor systems has enough margin over the design basis earthquake. However, it was found that some part of the confinement building wall need reinforcement and the reinforcement activities are being conducted. This paper will give the summary of measures taken to fulfill the recommendations and the status of building reinforcement activities.

1. Introduction

After the Fukushima Daiichi accident in March 2011, public concern about the safety of domestic nuclear facilities had increased in Korea. Thus, the safety of HANARO was reviewed and the first step was a self-assessment. This safety assessment was to evaluate the response of HANARO for extreme natural events and verifying the prevention and mitigation measures to protect public, property and the environment. The review was made for the following issues which occurred at the Fukushima NPPs;

- Earthquake
- Flooding
- Extreme weather
- Fire
- Loss of electrical power
- Loss of ultimate heat sink
- Combination of above issues
- Emergency preparedness

In addition, Korean government conducted a special safety inspection on nuclear facilities in Korea including nuclear power plants, research reactors, nuclear fuel cycle facilities and the emergency medical organizations. The special review team was composed of regulators, specialists from academia and representatives of residents living near the nuclear installations. The special inspection was to review the plant design and configuration, operation procedures, the accident management procedures and the emergency procedures over design basis accidents considered in the safety analysis and the combination of natural

phenomena [1].

Some improvements were found to be necessary for the safety of HANARO and measures have been taken. This paper gives the summary of recommendations and the status of measures to improve the safety of HANARO.

2. Safety Reassessment and Measure for Improvement

2.1 Amendment of Emergency Plan & Procedure

The major recommendation on the emergency preparedness was to consider the simultaneous occurrences of emergency in KAERI nuclear facilities due to a natural event. Thus, the procedures related to teaming and the operation procedures of emergency response facilities were amended.

In addition, there was a public request to enlarge the EPZ boundaries of nuclear facilities and it was reflected in the amendment of the Act on Physical protection and Radiological Emergency in 2014. This made the approximate EPZ boundary of HANARO change to 1,500 m from 800 m in radius from the reactor.

2.2 Protection of Reactor Operators in Control Room against Earthquake

One of the lessons learned from the FDA is that the operators can be injured by the falling of ceiling, lighting fixtures, or furnishings of the control room in the event of an earthquake and this may make them hard to respond. Thus, the special safety review recommendations were as follow:

- To implement the protective measures for reactor operators in the main control room
- To fix the console and operation desk
- To strengthen the lighting fixture seismically for preventing dropping
- To fix all furniture for preventing sliding and collapsing

As the first step, the non-seismic equipment and furniture in need of reinforcement in the control room were identified. Then, were installed new furniture and supporting structures that should meet the seismic criteria through a seismic design and analysis. The lighting fixtures, access floors, control desks, wall cabinet and CCTV monitors were replaced and seismic reinforcements were installed for the halon fire extinguishing cabinets. These improvements enhanced the seismic capability of a control room to withstand itself during an earthquake up to a peak ground acceleration of 0.3g[2]. Figs 1 and 2 are the view of HANARO control room before improvement and after improvement, respectively.

Fig 1. View of HANARO Control Room before Improvement

Fig 2. View of HANARO Control Room after Improvement

2.3 Installation of an Extra Diesel Generator

The function of the existing diesel generator in HANARO is to supply the electricity to the Class I and II electric supply systems and to the essential equipment such as RMS(Radiation Monitoring System) equipment. As this DG is installed at the basement of HANARO building, there is a possibility that the DG may be in a trouble when there is a heavy rain and a flooding. Thus, an extra DG and oil storage tank were installed at a location outside of reactor building where is free from flooding. Fig. 3 is the view of the extra diesel generator and oil storage.

Fig 3. Extra DG and Fuel Storage Tank

2.4 Re-evaluation of the Site Inundation Depth

The special inspection team recommended the estimation of the probable maximum precipitation(PMP) and the preparation of necessary protective measures considering the change of rainfall intensity according to recent global climate change. The assessment activities were conducted by following the procedures as below[1]:

- Investigation of the site hydrometeorology
- Estimation of PMP
- Estimation of the probable maximum precipitation (PMP) reflecting PMP
- Evaluation of the flood margin(Flood level and inundation depth)

This reassessment showed that the HANARO reactor building would not be inundated.

2.5 Evaluation of the Seismic Margin of HANARO Reactor Building.

One of the recommendations made by the special inspection team was to evaluate the seismic margins of HANARO building, exhaust stack and RCI(Reactor Concrete Island) which accommodates the reactor and major systems. From the seismic margin analysis (SMA), it was found that the RCI and the exhaust stack can sufficiently withstand the seismic conditions stronger than the design basis condition in the safety analysis report. However, it was identified that some part of the outer wall of HANARO building did not withstand the design basis earthquake which is 0.2 g in horizontal direction. The reason for this is from the difference in the analysis models for the original design and for the SMA. For the original design, only major structural frames were represented using a beam-stick model. For the SMA, however, every structural and non-structural component was represented in a 3D modeling. Thus, the reinforcement of the building is on-going to meet the design basis condition and have seismic margin. The reinforcement design work was completed in 2015 and the actual construction work is being carried out from the Feb. of 2016. Fig. 4 shows the process of reinforcement design and Fig. 5 shows the skeleton of reinforcement[3]. The concept the reinforcement is to reinforce some parts of outer wall of the HANARO building with steel beams and tendon wires in order to prevent possible flexural behaviors.

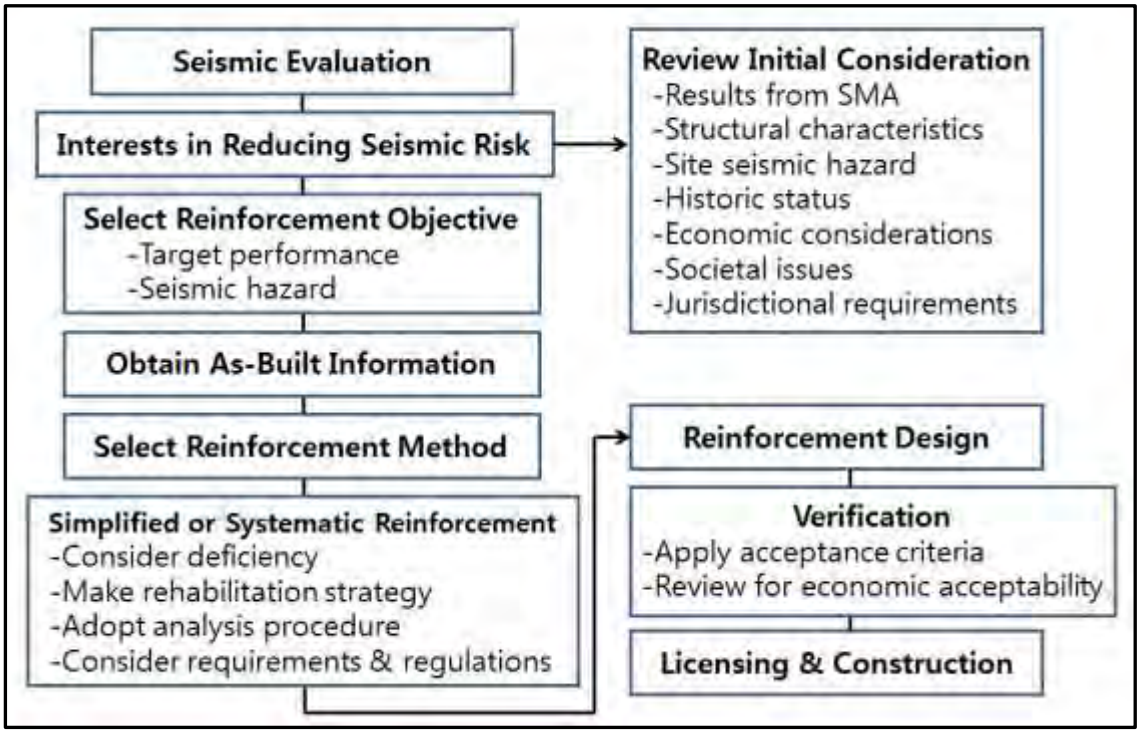

Fig 4. Seismic Reinforcement Design Process

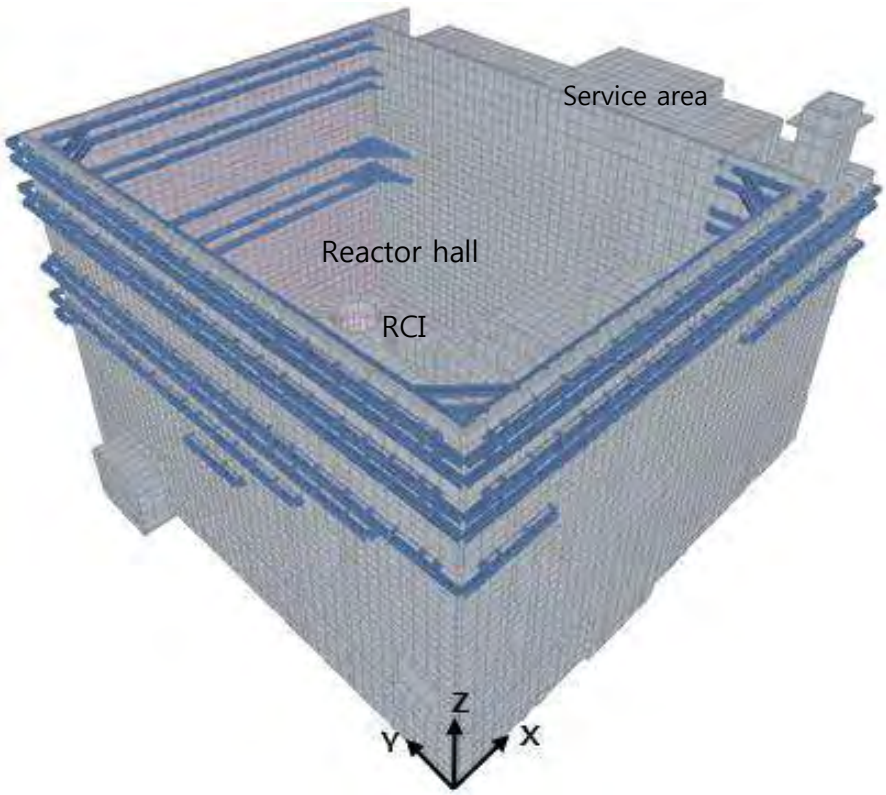

Fig 5. Bird-Eye View of Reinforced HANARO Building

3. Remark

After the Fukushima Daiichi accident in March 2011, the safety of HANARO was reassessed and 5 major recommendations were made. The measures for the 4 items have been already implemented and the reinforcement of reactor building is on-going. The construction activity for the reinforcement will be finished in Aug. 2016 and the reactor will be restarted after the completion. The reassessment was effective for the safety improvement and it is also contributing to the better public acceptance. Following an amendment of Nuclear Safety Act in 2014, a periodic safety review of HANARO has been also conducted from 2015[4] and this will also improve the safety of HANARO.

4. References

[1] H.K. Kim and et al., “Safety Assessment of HANARO Research Reactor in Light of FDA”, presented at the 2014 ANS Annual Meeting, Reno, Nevada, 15-19 June 2014.

[2] J.W. Shin and et al., “Safety Reassessments of HANARO Research Reactor”, presented at the IAEA Regional Workshop on Complementary Safety Assessment of Research Reactors Following the Lessons Learned from the Fukushima Daiichi Accident, Argonne, IL, 9-13 Dec. 2013.

[3] S. Wu and et al., “Seismic Retrofitting Plan of Reactor Building at HANARO”, presented at the IAEA & TRTR Meeting, Bewster, MA, 4-9 Oct. 2015.

[4] M. Kim and C.S. Lee, “Implementation of a Periodic Safety Review of HANARO Research Reactor”, presented at the IGORR 2014, Bariloche, Argentina, 17-21 Nov. 2014.

STATUS OF JRR-3 AFTER GREAT EAST JAPAN EARTHQUAKE

M. ARAI, S. WADA and Y. MURAYAMA
Department of Research Reactors and Tandem Accelerator
Nuclear Science Research Institute, Japan Atomic Energy Agency
2-4, Sirakata-shirane, Tokai-mura, Naka-gun, Ibaraki 319-1195 – Japan

ABSTRACT

JRR-3 at Tokai site of JAEA was in its regular maintenance period, when the Great East Japan Earthquake took place on 11th March 2011. The reactor building with the solid foundations and the equipment important to safety have survived the earthquake without serious damage, and no radioactive leakage has been occurred. Recovery work, check and test of the integrity for all components have been carried out. In response to the accident at Fukushima Daiichi NPS, the new safety standards for research and test reactor facilities came into force on December 18, 2013. The evaluation of natural disasters and prevention of spread of accidents beyond design basis mainly were enhanced in the standards. We have completed the necessary checks and assessments, and submitted an application for reviewing if JRR-3 complies with the new standards to the Nuclear Regulation Authority on September 26, 2014.

1. Introduction

JRR-3 (Japan Research Reactor No.3) is a light water cooled and moderated swimming pool type research reactor with nominal thermal power of 20MW. The reactor building contains reactor facilities such as a reactor pool, cooling system, instrumentation and control system, etc. Neutrons coming from the core are transported to a beam hall and many of neutron beam experiments are carried out in the hall. The secondary cooling tower receives heat generated in the core and emits it to the atmosphere. Air with minor radioactivity in the reactor building is filtered and exhausted to the atmosphere through an exhaust stack.
JRR-3 has suffered the great earth tremor not previously experienced when the Great East Japan Earthquake with the seismic energy of magnitude 9.0 has occurred on March 11, 2011. At that time, JRR-3 was undergoing regular periodical inspection and the reactor was not operated. Although commercial electric supply was stopped, necessary minimum facilities were continuously operated with emergency electric generators. It is very important to confirm immediately whether nuclear fuel materials and reactor containment system are damaged or not. During the aftershocks for a few hours, the reactor pool, nuclear fuels and their storage facilities were checked visually and confirmed to keep their soundness. Although several small cracks were shown on the inside of the walls of the reactor building, they did not result in adverse effect on the integrity of containment and there was no release of radioactive materials to environment.

2. JRR-3 works after the Great East Japan earthquake

2.1 Recovery works

The buildings themselves did not sink since they are built on the bedrock, but ground around the buildings was sunk about 40 cm. According to the ground sinking, an exhaust duct led from the reactor building to a stack was slightly damaged at a connection. A liquid nitrogen storage tank, used for feeding liquid nitrogen to experimental facilities, and electric transformers for secondary cooling system were also damaged and leaned. Some of the ceiling panels in the reactor building were dropped.
Cracks of reinforced concrete were investigated with the installation of a scaffold (see Fig 1).

Although the cracks were mostly less than 1 mm in width, several cracks over 1 mm in width were found. These cracks of concrete were repaired by injecting the epoxy resin. Exfoliation/falling were not found.
All recovery works have already been completed.

Reactor building

Cooling tower

Fig 1. Repair of reactor building and cooling tower.

2.2 Verification of the Integrity

As the Great East Japan earthquake measured larger seismic acceleration than that of seismic design of JRR-3, regulatory body has demanded us to evaluate soundness of reactor facilities and report it for reactor re-operation. Several evaluation have been required such as (1) the impact in the event of station blackout, (2) check and test of all of the SSCs (structure, systems and components), and (3) seismic analysis in the light of the knowledge obtained from the earthquake.

(1) When station blackout occurs, the reactor is shut down automatically. The decay heat of JRR-3 is the thermal power of 1.4 MW that is 1/100 of power rector. The maximum fuel surface temperature after the auto shutdown by station blackout reaches to about 120 °C, and then decreases gradually by natural circulation of the cooling water. This shows that integrity of core is kept if station blackout occurs.
(2) Deformation, buckling or crack of the structure was confirmed by visual observation, and deformation, loosening or the lack of a bolt and a nut was also checked. Soundness of the cooling system, instrumentation and control system etc. needed for reactor re-operation were confirmed by the performance inspection. All of the check and test have been completed.
(3) The earthquake registered 9.0 on the Richter scale, and the intensity was a lower 6 at Tokai. The maximum ground accelerations of 11.83 m/s^2 in horizontal and of 5.12 m/s^2 in vertical were observed at JRR-3. Those are larger seismic acceleration than that of seismic design of JRR-3. Seismic analysis has been carried out in order to confirm the JRR-3 would have been resistant to the earthquake adequately.

The seismic safety for components and their supporting structure were evaluated by the response magnification method. Table 1 shows result of evaluation. The initiation stress is very smaller than the evaluation criterion, because each component is designed with margin. We confirmed that each component had enough strength to be proof against the Great East Japan earthquake.
The results of the integrity were reported to regulatory body on November 2, 2012.

Kind of components	Initiation stress (N/mm^2)	Evaluation criterion (N/mm^2)
Standard Fuel Element	4	54
Follower Fuel Element	18	74
Beryllium Reflector	3	112
Heavy Water Tank	13	58
Neutron Absorber	571	1272
Control Rod Guide Tube	6	123
Horizontal Beam Tube	59	135

Tab 1: Results of evaluation.

2.3 Work in reactor shutdown

Four years from the Great East Japan Earthquake, and the so long reactor shutdown is our first experience. During the shutdown term, main facilities have been kept the integrity by checking operation regularly once in a month. These main facilities are shown in Table 2.
In addition to keeping reactor facilities in a good condition, we feel strongly the importance of keeping motivation and skills of operators. Therefore, we come up with effective management methods such as (1) operating the main facilities and safety protection system and evaluating their integrity monthly, and (2) operating the most of reactor facilities (the cooling system, instrumentation and control system, etc.) for a whole week and confirming the integrity once a year. And we carry out them.

Period of operation	Once a month
Cooling system	Primary cooling system
	Secondary cooling system
	Heavy water cooling system
	Spent fuel cooling system
Safety protection system	Reactor scrum circuit

Tab 2: Main facilities.

3. Work for Re-operation

3.1 New Regulatory Requirements

In response to the accident at Fukushima Daiichi NPS, Japanese government revised the Reactor Regulation Act, for the purpose of introducing new regulation system based on lessons learned from the accident and the latest technical findings. And new regulatory requirements for research and test reactor facilities were enforced on December 18, 2013. In the Act, it is stipulated the introduction of back-fit system that is a system for adopting the latest technological findings and obligating approved nuclear facilities to conform to the new requirements.
The main requirements in new regulatory requirements for research and test reactor are shown Table 3.

Item		Requirement
Basic Design for Earthquake and Tsunami		SSCs with safety functions shall be designed to sufficiently withstand appropriate design basis earthquake and tsunami.
External Events	Natural Phenomena	The evaluations and design to be based on the latest findings related to natural disasters such as volcanic eruptions, tornados, and forest fires, etc.
	Man-Induced Events	The safety of facility will not be impaired by airplane crash, dam break, explosion, fires in neighboring factories, toxic gas, collision ships, electromagnetic interferences, etc.
Fire Protection		The safety will not be impaired by fire considering protective measure for preventing, detecting and extinguishing of fire, and mitigating its effect.
Internal Flooding		The safety of the facilities will not be impaired by postulated internal flooding that may take place within the facilities.
Communication Systems		The communication system can give necessary information and instructions to the person inside and outside the facilities when design basis accident occurs.
Loss of External Power Supply		The facilities shall be so designed that safe shutdown and proper cooling of reactor after shutdown can be ensured in case of the station blackout for a given time.
Radiation Monitoring		The facility shall be designed to enable proper radiation monitoring and surveillance against the release of radioactive materials during design basis accidents.
Prevention of Spread of Accidents		The evaluation against accidents beyond design basis (BDBA) must be conducted.

Tab 3: Main requirements.

3.2 Review to Verify Conformity to New Regulatory Requirements

We have conducted the necessary checks and reassessments of JRR-3, and completed the preparations for the relevant applications. We then submitted the application document to change the current reactor establishment permission to the Nuclear Regulation Authority (NRA) for their review to verify conformity to new regulatory requirements on September 26, 2014.

3.2.1 Basic Design for Earthquake and Tsunami

The standard seismic motions and basis tsunami were newly formulated from the seismological and earthquake engineering point of view on geology, geological structure, seismicity, etc. of the site and its surrounding area based on the latest scientific and technological knowledge and finding. The standard seismic motions and maximum water reaching level are shown in Table 4.

SSCs having important safety functions of JRR-3 can keep their functions for seismic force due to the standard seismic motion, because they are designed with margin. In addition, they will not lose their safety functions even in the face of design basis tsunami. JRR-3 located at the altitude of 19 m prevents basis tsunami from directly reaching and intruding into them through land area.

Standard Seismic Motion	Horizontal	7.96 m/s^2
	Vertical	5.77 m/s^2
Maximum Water Reaching Level		+13 m (sea water level)

Tab 4: Standard seismic motion and basis tsunami.

3.2.2 Evaluation of Beyond Design Basis Accidents (BDBA)

The prevention of fuel damage and the mitigation of the consequences shall be achieved even if BDBA occurs. The postulated events for the BDBA are selected and evaluated as shown in Table 5. Alternative measures or alternative equipment are designed as functions required with sufficient reliability under environmental during postulated BDBA.

Conceivable event		Countermeasure
Loss of shutdown function	2 control rods insert failed	If 2 control rods are not inserted, JRR-3 can be shut down with 4 other control rods.
Loss of cooling function	Loss of commercial and emergency power supply (BLACKOUT)	JRR-3 is shut down automatically and removes its decay heat by the natural cooling circulation.
	Primary cooling water leakage (LOCA)	We can supply the reactor pool with alternative water by using mobile injection pumps, water injection lines or buckets.
Loss of containment function	Loss of emergency exhaust function in case of fuel failure accident	All ventilation equipment is stopped, radioactive materials are locked in the reactor building by the isolation valves.

Tab 5: Evaluation of BDBA.

3.2.3 Other evaluations

(1) Natural Phenomena (tornados and Volcanic eruptions)

Maximum wind speed of most powerful tornado in Japan is 92 m/s. The reactor building of JRR-3 would not be ruined by the tornado or flying objects.

The nearest volcano is located 88km away from JRR-3. Safety functions would not be lost by the falling tephra (volcanic ash).

(2) Man-Induced Events (airplane crash and external fire)

The probability of plane crash on JRR-3 is about 8.8×10^{-8} times/year. It is smaller than 10^{-7} that is reference value to require the design considerations.

Even if forest fires or fires in neighboring factories occur, the temperature of an exterior wall would not be below allowable temperature 200 °C.

(3) Fire Protection

Important cable e.g. signal cable, power supply cable and communication cable are flame resistant as a fire prevention.

(4) Internal Flooding

Internal flooding that may take place within JRR-3 is caused by failure of equipment or piping, the operation of the fire protection system, or sloshing in the spent fuel pool or spent fuel pit. The safety function of shutdown system and cooling system will not be impaired by the internal flooding, even taking into account the secondary impacts. In addition, JRR-3 has a

weir or a barrier to prevent water leakage from radiation controlled area.
(5) Communication Systems
JRR-3 has a communications system that can convey instructions on operation, work, evacuation, etc. to all the people in JRR-3 from the control room or that can convey information of accidents to outside of JRR-3. In addition, the communications system have dedicated and diversified communication lines such as specific cable/wireless lines and satellite telephone, etc.
(6) Loss of External Power Supply
When the power supply from off-site is lost, the reactor can safety be shut down automatically and the cooling after shutdown can be achievable by emergency AC power and natural circulation. If both off-site and on-site AC power are lost, the power for monitoring can be supplied by the emergency DC power of JRR-3.
(7) Radiation Monitoring
The monitoring posts have emergency power to measure and monitor the concentration of radioactive materials and the dose rates during design basis accidents. And the transmission systems of the monitoring posts have diversity so that prompt countermeasures may be taken in case of accidents.

4. Conclusion

Damages by the earthquake have not impaired the safety of the JRR-3. Recovery work mainly for ground sinking has been carried out smoothly. The structure, systems and components needed for reactor operation have been checked to be reusable without major repair. We have confirmed to conform to new regulatory requirements and have submitted an application document for re-operation. The over 10 review meetings were held by the NRA, and that is ongoing.

Innovative Methods

COCONEUT: ENHANCING NEUTRONIC DESIGN FOR RESEARCH REACTORS

J.-G. LACOMBE, C. BOURET, J. KOUBBI, L. MANIFACIER
AREVA TA
CS 50497, 13593 Aix-en-Provence Cedex 3, France
Corresponding author: jeangael.lacombe@areva.com

ABSTRACT

AREVA TA has developed a highly flexible, neutronic calculation tool purposely meant for early stages of Research Reactors (RR) core design. COCONEUT (COre COnception NEUtronic Tool) is based on both multigroup transport (2D) theory and diffusion theory (3D) using APOLLO2 and CRONOS2 deterministic codes. COCONEUT enables one to easily model a wide range of RRs, provided they are based on flat MTR-type fuel plates. Both 2D and 3D models of the core are based on a single geometrical database, included in the pre-processing user interface SILENE. Any type of irradiation device, reactivity control device (single or multiple) or reflector can be modelled (D_2O, H_2O, Be, etc.).
COCONEUT also aims at reducing user-dependency issues and increasing user-friendliness. Being dedicated to early stages of core design, COCONEUT is able to compute large numbers of different core configurations in a short period of time. Both 2D and 3D models are designed to deliver material balance for an equilibrium core within 48h of CPU time and can be used to determine key design parameters (flux maps, k-eff, power peak factors, absorber worths, etc.) for a given set of user-defined shuffling strategies. It is also possible to chain those models with a probabilistic code (MCNP or TRIPOLI4) through properly formatted material balance outputs.
The practical use of 2D and 3D models is to evaluate a large range of core designs using COCONEUT-2D, select the most promising ones, and compute the additional parameters with COCONEUT-3D. First steps of V&V have shown promising results which have been submitted to this conference in other papers.

1. Introduction

In the early stages of core design, many different core configurations have to be tested: several types of fuel elements and control assemblies can be studied, as well as various core layouts and refuelling strategies [1]. Carrying out a detailed study for each core configuration (set of assemblies, core layout, cycle length and refuelling strategy) usually proves to be too time-consuming. Hence, AREVA TA has developed a neutronic calculation line that emphases flexibility and swiftness, named COCONEUT.
It is based on the deterministic lattice code APOLLO2 [2], its pre-processing user interface SILENE [3] and the core code CRONOS2 [4], [5]. These tools are developed and maintained by the CEA. APOLLO2 and CRONOS have successfully been used in the field of RRs in the past ([6], [7]) as well as in the field of light water reactors. However, calculation schemes are usually dedicated to one particular reactor.

The goal of this tool developed by AREVA TA is to be more generic. COCONEUT is also designed to optimize every core concept within a period of time compatible with reactor design phase by producing the main parameters of interest within a few days of CPU-time: reactivity variations, output burnup, burnup swing, and core material balance.
COCONEUT proposes two different calculation approaches, meant to be complementary design tools:

- 2D full core exact geometry,

- 2D assembly calculations (to build cross section libraries) + 3D homogenous calculations.

Determining the most adapted set of assemblies, core layout, cycle length and refuelling strategy is a required step before carrying out more detailed calculations; which can be achieved swiftly and easily with the 2D full core option. Optimised designs can then be evaluated through the 3D approach. Probabilistic calculations (MCNP [8] or TRIPOLI4® [9]) can easily be chained with 2D and 3D versions using material balance.

The present document details the models on which the scheme is based. To illustrate them, results obtained from various cores are presented (including FRG1 [10], [11]).
This document is established in the framework of an AREVA TA and CEA/Direction of Nuclear Energy collaboration.

2. General description of COCONEUT

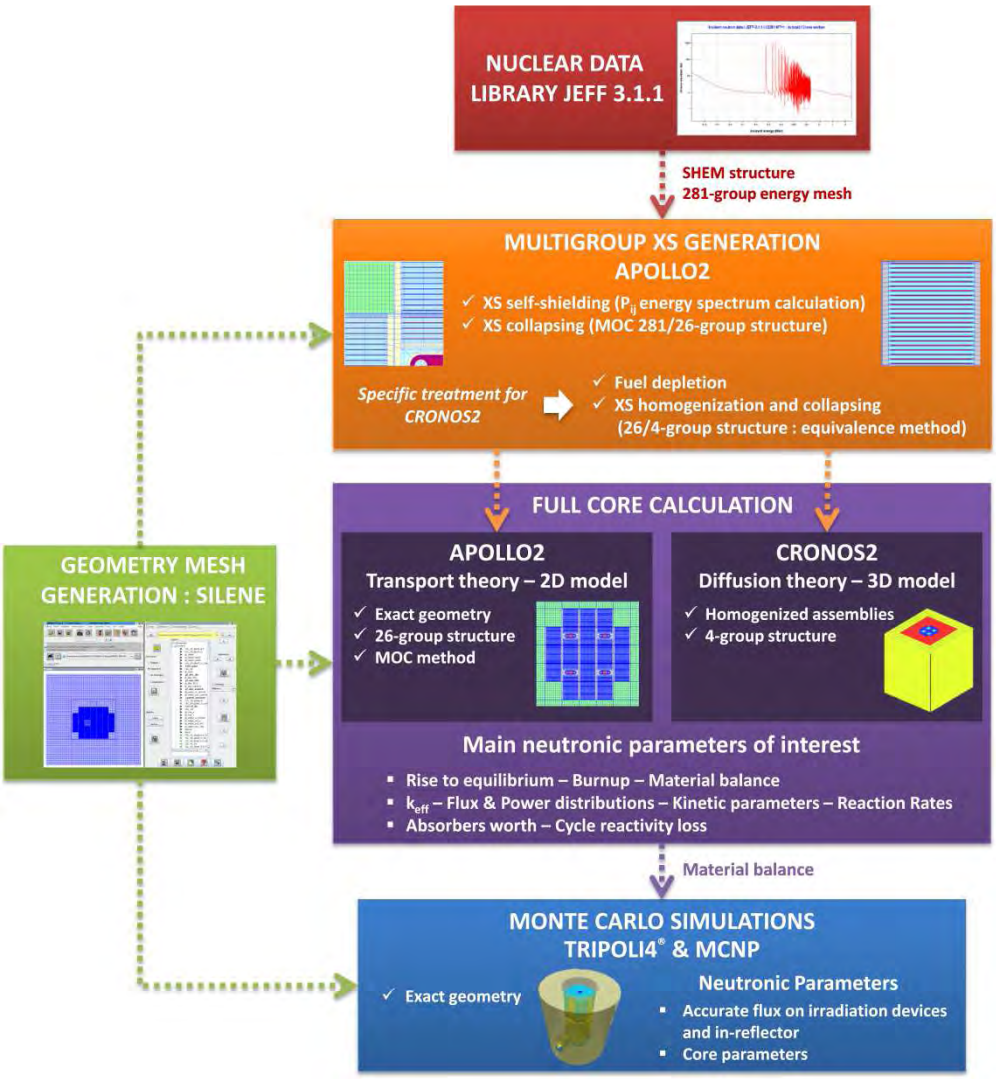

Fig 1 : COCONEUT general overview

The main purpose of COCONEUT (*Fig 1*) is to carry out early stages of core design with maximum flexibility. This implies:

- to swiftly define the nature of fuel and control elements,
- to test various core layouts,
- to optimize cycle lengths according to the shuffling patterns (periodicity and reloaded fraction per cycle) defined.

To do so, it is necessary to test large numbers of core configurations in a short period of time, and select a few of them for more detailed studies. In this scope, the parameters of interest that can be obtained form COCONEUT are:

- output burnup (at plate or assembly level) and average core burnup,
- BU swing,
- flux values in specific parts of the core and its layout *(Fig 2*),
- fuel consumption per cycle,
- k-eff,
- reactivity loss over a cycle.

COCONEUT-3D can complement this set of design parameters with the following data:

- reactivity worth of absorbers,
- shutdown margins (N-1, N-2 criteria),
- axial burnup and power peak factors,
- critical rod positions.

The main focus in the development of COCONEUT was flexibility, low user-dependency and high user-friendliness. As a result of this, a lot of effort has been put into the automation of the most time consuming and hazardous steps of COCONEUT calculation process:

- handling of shuffling patterns (2D and 3D),
- geometry generation (use of a unique data source for APOLLO2, CRONOS2 and TRIPOLI4®),
- material balance edition and conversion between formats (XML, MCNP or TRIPOLI4®).

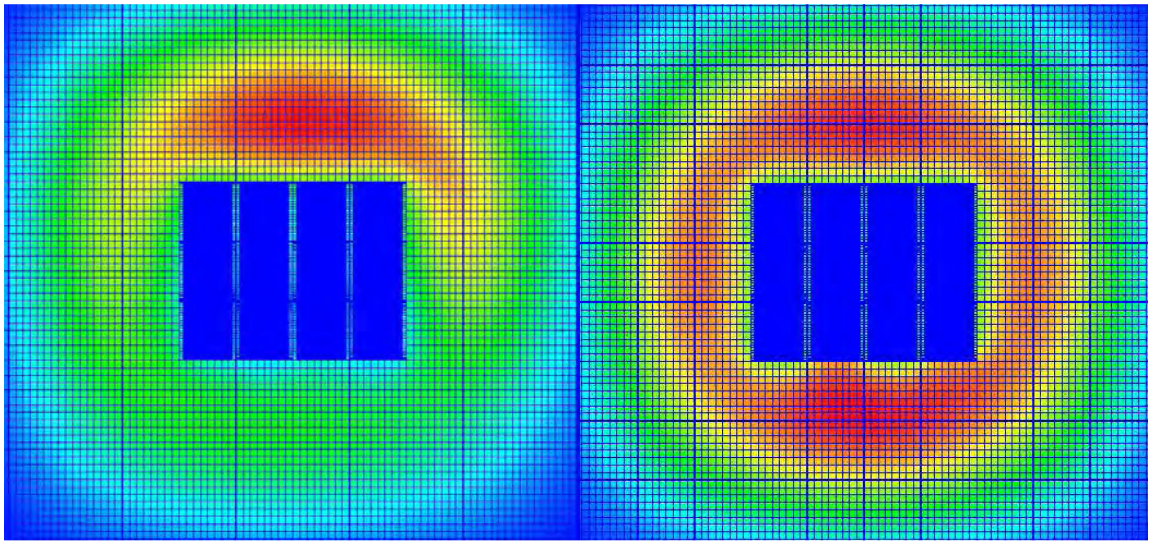

Fig 2: thermal flux map for FRG1 full fresh core obtained with COCONEUT-2D with (right) and without (left) control rods

2.1 Core modelling

All geometries (APOLLO2, CRONOS2 and TRIPOLI4®) are generated from a single mesh database with SILENE.

APOLLO2 calculations always use the MOC solver, and thus, exact 2D geometry. CRONOS2 calculations are based on the MINOS solver with a radially homogenous description of the core (1 cell per assembly). Fuel media definition for COCONEUT-2D & 3D are meant to be complementary. 3D model presents one fuel media for each assembly slab in the core, which provides an axial profile of any parameter of interest (power, burnup, etc.). On the other hand, 2D calculations provide no axial data, but enable one to describe exact geometry. One fuel media is defined for each plate of the core, providing an accurate radial profile.

The nuclear database is JEFF3.1.1 (ref [12]) with 281-group energy mesh, used for cross section preparation and self-shielding in both options (2D full core and 2D assembly calculations). Cross sections are condensed on a 26-group energy mesh for 2D depletion steps and then condensed again into 4-group energy mesh for libraries used as an input for 3D diffusion calculations.

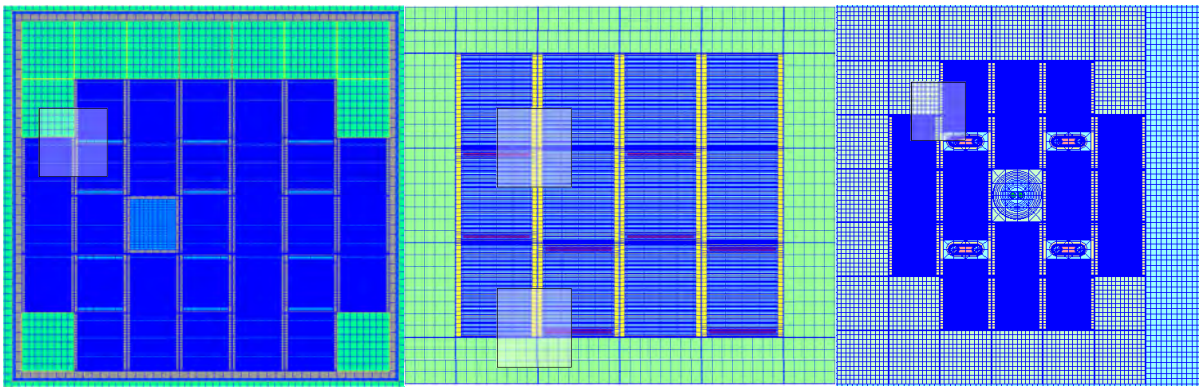

Fig 3: BER2 (left), FRG1 (centre) and HOR (right) reactors as described in COCONEUT. Highlighted boxes present some of the considered lattice patterns for each core

The first calculation step in COCONEUT is cross sections preparation and self-shielding. This step is part of 2D full core calculations as well as cross sections library generation and is carried out using the 2D exact geometry of four adjacent assemblies (actually a quarter of this pattern and periodic boundary conditions) which must be representative of the general core layout (see *Fig 3*). The choice of such a pattern is to be made by the user. It is mandatory to determine an adequate environment, at least for control assemblies. If required, a different pattern can be chosen to compute standard assemblies (if not, cross sections for both types of assemblies will be taken from the same pattern). It is also possible to model follower control assemblies *(Fig 4)*, with an absorbing part above the fuel. Self-shielding is only computed for fresh fuel.

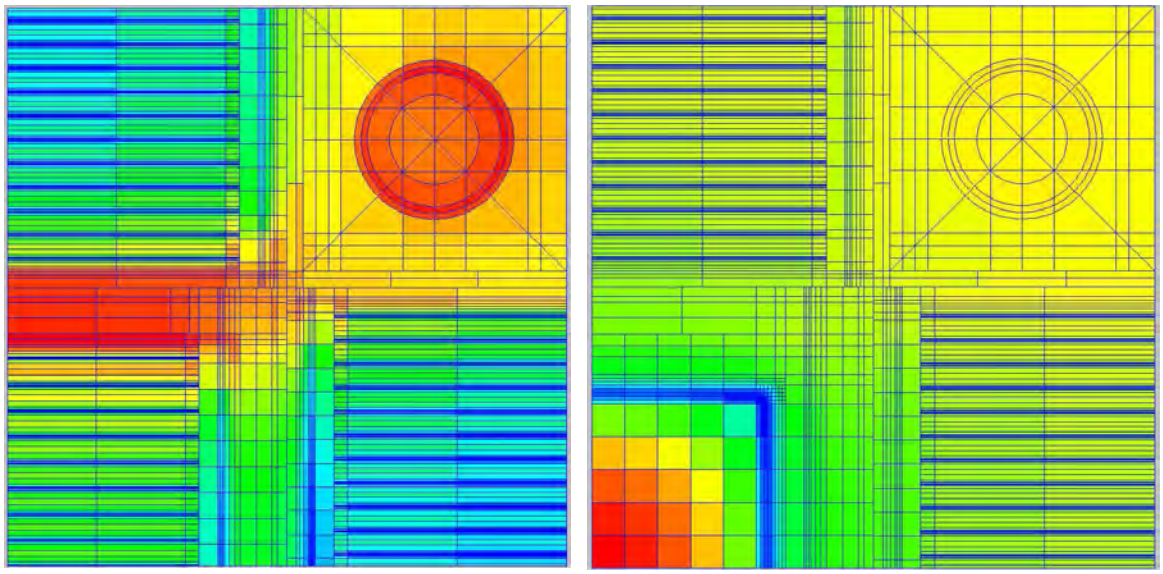

Fig 4: thermal flux maps in a test pattern using follower-type absorber. Flux with extracted control rods is left. The pattern is made of 2 standard assemblies, a follower control and an experimental device

The core is described inside its water pool, which implies to define a 25 to 30 cm layer of water around the core (over and under the core too in 3D) in addition to its probable reflector blocks. In COCONEUT-3D, depending on the core layout, describing each assembly or

reflector block with a single composition (radially homogeneous description of the core) may prove to be inaccurate (including, but not limited to):

- Be bulks and the surrounding waterways (*Fig 5*)
- Follower absorbers. Such devices must not be homogenized with the clad and the inner and surrounding water (*Fig 6*)

These situations can be sorted out by using semi-heterogeneous description of the assemblies.

Fig 5: Illustration of possible CRONOS2 meshes for Be reflector block. Exact geometry is left. Homogeneous 3D mesh is in the centre and semi-homogeneous is right. Calculation biases can be significantly reduced while only increasing CPU-time in a small proportion

Fig 6 : Illustration of possible CRONOS2 meshes for follower-type control element. Exact geometry is left. Homogeneous 3D mesh is in the centre and semi-homogeneous is right. Calculation biases can be significantly reduced while only increasing CPU-time in a small proportion

2.2 Mesh generation with SILENE: the use of a mesh database

SILENE is a pre and post-processing tool used to model geometries and produce various geometric meshes easily and swiftly. This tool developed by CEA [3] is a very strong asset in our scheme. SILENE's component database is a tool that recursively assembles mesh blocks together in order to produce a larger mesh. Each basic block can be declared directly in the component database for regular parts of the mesh. All mesh blocks are saved and can be called in another mesh if required. It is then possible to create a new mesh with pre-existing blocks. This functionality is very interesting especially for early stages of core design.

Practically, a full core mesh (from 25000 to 50000 cells in 2D exact geometry, *Fig 3*) can be produced with only a few hundred lines in the component database.
Another strong asset of SILENE is it handles media instantiation (this functionality is called "mutant") which prevents the user from creating hundreds of fuel media in the dataset. The various fuel media are automatically declared as separate media with the adequate isotopic balance when the mesh file is created.

SILENE is natively able to produce geometry files for:

- APOLLO2-MOC solver, used at assembly and core level,
- TRIPOLI4®, actually used for Verification and Validation process (V&V, ref [13], [14]).

A dedicated script was also developed to build CRONOS2 geometries, with a default axial description or a user defined description (2D geometry defined in the database will be extruded following the given number and size of axial cells).

The use of a single source for material and geometry definition is meant to mitigate user-dependency. Post-processing of APOLLO2 results can also be done with SILENE (e.g. *Fig 2* and *Fig 4*).

2.3 Rise to equilibrium

Determination of the equilibrium state of a RR is the most important feature in COCONEUT. Successive depletion cycles of the core are performed *(Fig 8*) following user-defined shuffling pattern(s). Each cycle follows the steps (2/, 3/ and 4/) described in *Fig 7.*

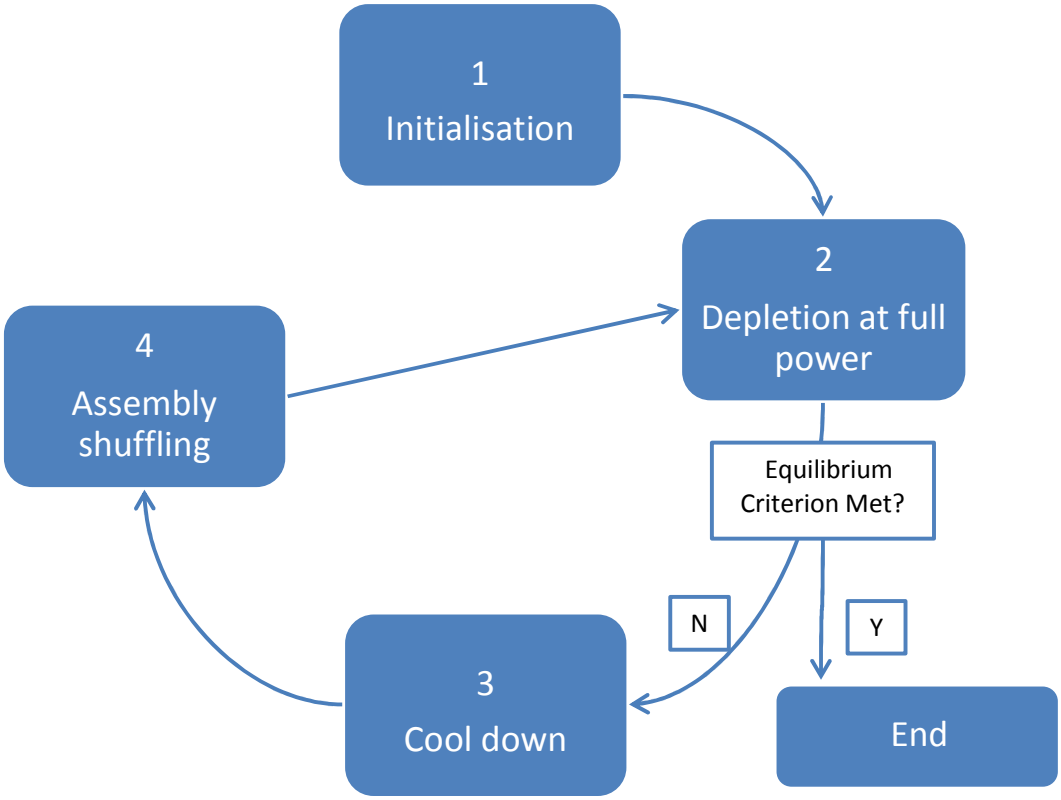

Fig 7: successive steps for rise to equilibrium in COCONEUT-2D and 3D

(1) In COCONEUT-2D, rise to equilibrium starts from a fresh batch core whereas, 3D calculations permit to load the core with a burn up map. Material balance in this case is that stored in the cross section libraries.

(2) Core depletion is carried out with extracted absorbers in 2D which appeared to be the best approximation (ref [15]). In 3D calculations, absorbers can be moved as the users sees fit. Automated research of critical control rod position is also available.
(3) Between each depletion phase, a null power cool down phase is applied in order to simulate the reloading time of the core. Its duration is an input data and can be adjusted by the user. All isotopic balances are calculated during the cool down although its main effect is the decay of neutronic poisons.
(4) The use of refuelling strategies is as flexible as possible in COCONEUT (2D & 3D). Any number of strategies can be used during rise to equilibrium, in any order (be it periodic or not).
Burnup maps at the end of the rises to equilibrium in *Fig 8* are presented in *Fig 9*.

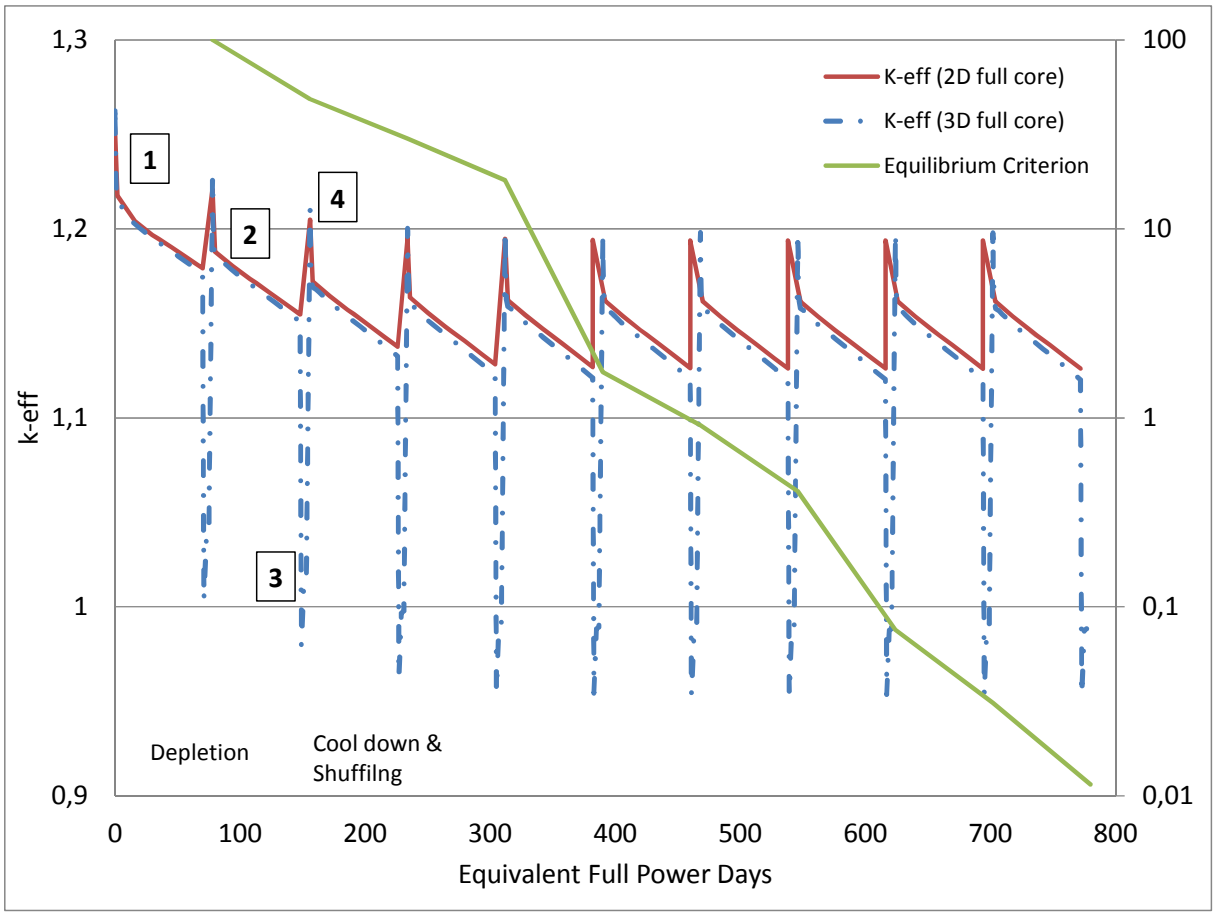

Fig 8: rise to equilibrium for the FRG1 core with COCONEUT-2D (red) & 3D (blue). In 3D calculations depletion cycles are led with extracted absorbers for the sake of comparison with COCONEUT-2D, also, cool down is carried out with inserted control rods, which explains the low values in 3D during the cool down phase

The depletion calculations are based on the variation of extracted energy in MW.days/t_U. This method means that the cycle length in EFPD (Equivalent Full Power Days) is converted to energy using the initial ^{235}U mass and power of the core.

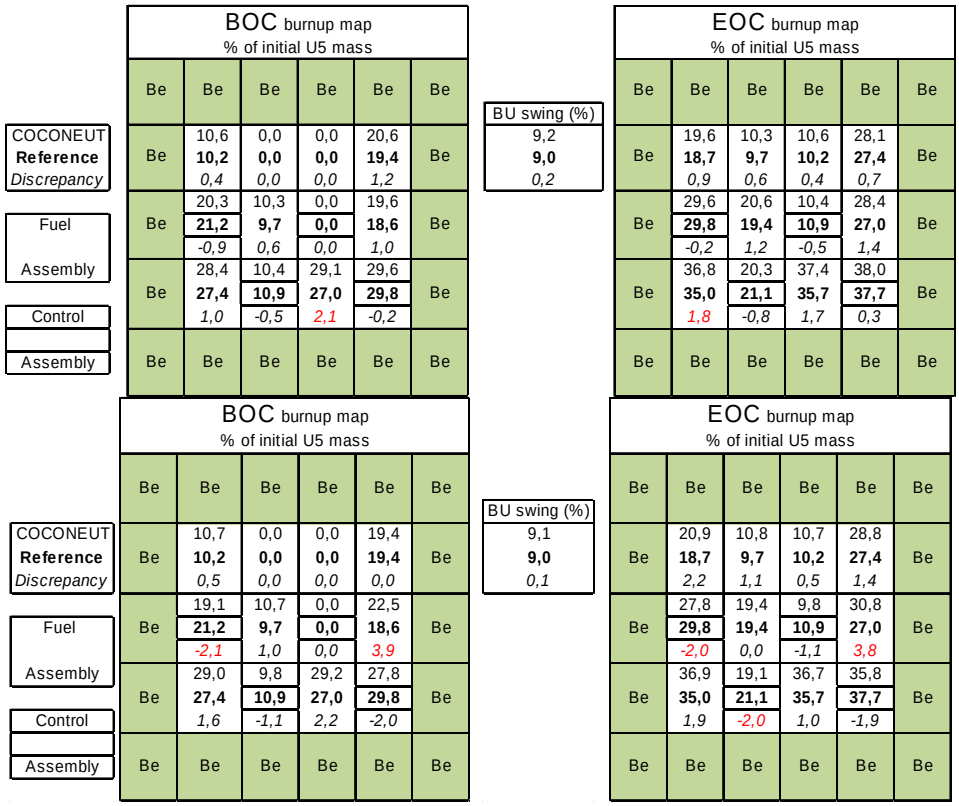

Fig 9: Burnup maps from COCONEUT-2D (top) and 3D (bottom) at equilibrium compared to FRG1 safety report [10], [11]

An equilibrium criterion was implemented to assess whether the core has reached equilibrium or not. This criterion describes the discrepancy between burnup maps at two successive EOCs. The equilibrium is stated when these EOC burnup maps are identical within a user defined tolerance:

$$Eq_{critetion}(cycle\,N) = \sum_{i=1}^{Nass} \Delta(BU_i) = \sum_{i=1}^{Nass} \left[\sqrt{\frac{1}{N_{ass}} \left(BU_{i,N} - BU_{i,N-1} \right)^2} \right] \frac{1}{BU_{eff,N}}$$

Due to controllability considerations, a RR does not usually start its rise to equilibrium phase from a full fresh core. However, when using periodic shuffling strategies, it appears one reaches the same equilibrium state whether the rise starts form a fresh core or not.
The choice to start from a full fresh batch core is a convenient numerical method that does not impact the final equilibrium state for periodic shuffling strategies. This method does not work however for transition cores (for instance: HEU/LEU conversion).

As a part of the validation process, COCONEUT calculations (*Fig 8, Fig 9*) for the FRG1 core have been compared with the Monte-Carlo TRIPOLI4 for a few interesting patterns:

- Assembly patterns with 0,1 or 2 Be blocks around the control assembly (*Fig 10*),
- Full core (2D, exact geometry) with and without absorbers,
- Full core 3D, using the cross section libraries from different assembly patterns.

The parameters of interest for this first V&V step are reactivity and weight of control rods in the case of full core calculation. Only fresh fuel is taken into account at this stage. *Table 1* sums up the results. Discrepancies are found to be below 200 pcm for 2D calculations and around 1500 pcm for 3D calculations. Reactivity biases of such magnitude are considered acceptable for early stages of core design. COCONEUT V&V process is detailed in a specific paper [13].

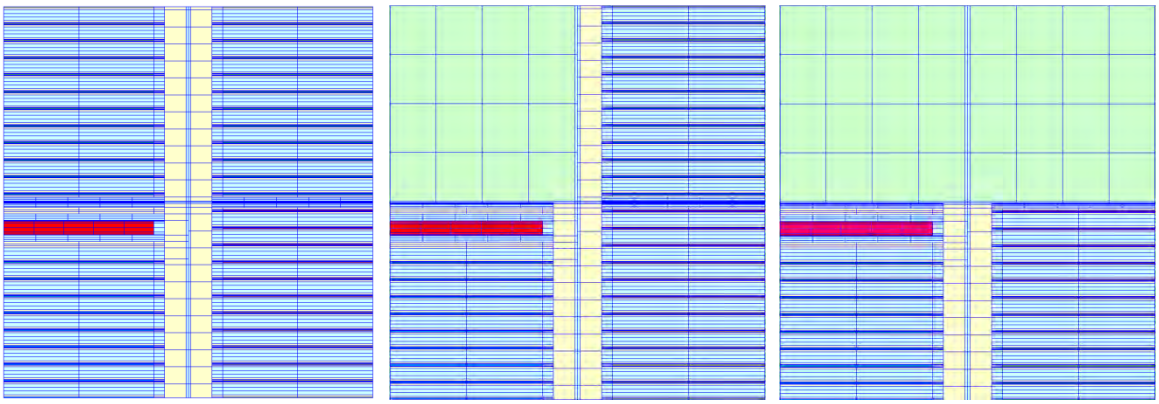

Fig 10: Assembly patterns taken into account for FRG1 modelling and validation with COCONEUT. From left to right: (a), (b) and (c) as referenced in Table 1

Configuration	Description	Scheme	Parameter of interest	Discrepancy
2D assembly	(a) 3 fuel + 1 control (b) 2 fuel + 1 control + 1 reflector block (c) 1 fuel + 1 control + 2 reflector blocks	2D	Assembly reactivity (fresh fuel)	< 210 pcm
2D core	Absorbers withdrawn Absorbers inserted Rod weight	2D	Core Reactivity (fresh fuel)	~ 70 pcm ~ 200 pcm - 130 pcm
3D core	Rod weight, cross sections from (a), (b) & (c)	3D	Rod weight (fresh fuel)	1500 to 2000 pcm

Table 1 : general overview of the reactivity biases observed in COCONEUT for the main calculation steps of the scheme when compared to TRIPOLI4® calculations

3. Conclusion

COCONEUT is AREVA TA's calculation line dedicated to RR design. It is based on the deterministic codes APOLLO2 [2], CRONOS2 [4] and the pre and post-processing user interface SILENE [3].
Its purpose is to enable engineers to have a reliable, accurate and user-friendly tool in order to test very large numbers of possible core definitions with ease and in a short period of time. Therefore, it was designed to compute equilibrium state for any MTR-type RR within 48 hours of CPU-time. Moreover, the use of SILENE and other pre and post-treatment tools ensure great flexibility in calculations so that modelling any core from scratch takes minimum amount of time and efforts for the user.
Although the precision requirements are not as high as for safety studies tools, verification calculations performed show promising results [13], [14]. Precision for burnup maps and k-eff variations from COCONEUT-2D is good enough to carry out early stages of core design:

- assembly definition,
- core layouts tests,
- optimization of cycle length and shuffling patterns.

From such results, optimized designs can be further studied in 3D with COCONEUT or by chaining with probabilistic codes in order to obtain complementary parameters such as weight of absorbers and control margins.

4. References

[1] M. Boyard, P. Péré, L. Chabert, L. Lamoine, T. Bonaccorsi, "Practices for Neutronic Design of RRs: Safety and Performances", International Conference on Research Reactors: Safe Management and Effective Utilization Rabat - Morocco, November 14-18, 2011

[2] R. Sanchez and al. “Apollo2 year 2010”, *Nuclear Engineering and Technology*, 42:474-499 (2010)

[3] Z. Stankovski, “La java de silène : A graphical user interface for 3d pre & post processing”, Joint International Conference on Mathematical Methods and Supercomputing, for Nuclear Applications, Saratoga Springs - USA, October 6-10, 1997

[4] J. Lautard, S. Loubière, C. Fedon-Magnaud. "CRONOS: a modular computational system for neutronic core calculations". IAEA specialist meeting on advanced calculational methods for power reactors. Cadarache, France. 1990

[5] Mengelle, S., A. Nicolas, and E. Richebois. "A new Power Reactor 3D Transport Calculation Scheme using the CRONOS2 and APOLLO2 codes." *International Conference on Mathematical and Computation, Reactor Physics and Environmental Analysis in Nuclear Applications*. 1999

[6] O. Gueton, “The ANUBIS scheme used for safety assessment and operations management of the OSIRIS reactor”, IGORR 12th edition, Beijing - CHINA, October 28-31, 2009

[7] C. Döderlein and al., “The 3D neutronics scheme for the development of the Jules-Horowitz-Reactor”, International Conference on the Physics of Reactors Nuclear Power: A Sustainable Resource, Interlaken - Switzerland, September 14-19, 2008

[8] X-5 Monte Carlo team, “MCNP – A general Monte Carlo N-particle transport code, version 5”, LA-UR-03-1987

[9] C.M. Diop, O. Petit, E. Dumonteil, F.X Hugot ,Y.K. Lee, A. Mazzolo, J.C Trama, “TRIPOLI-4: A 3D continuous-energy Monte Carlo transport code.” PHYTRA1: First International Conference on Physics and Technology of Reactors and Applications. Marrakech, Maroc, 2007

[10] SIEMENS, “Abschlußbericht zur Kernoptimierung des 3x4-Kompaktkems FRG-1”, FRG1 Safety report, November 27, 1998

[11] P. Schreiner, W. Krull, W. Feltes, “*Increasing the neutron flux at the beam tube positions of the FRG-1*”, IGORR 6th edition, Taejon, KOREA, May 1998

[12] A. Santamarina and D. Bernard, “The Recommended JEFF-3.1.1 File and CEA2005v4 Library for Accurate Neutronics Calculations,” JEFF Report, OECD/NEA 2009

[13] C. Bouret, J.-G. Lacombe, C. Bayol, J. Koubbi, L. Manifacier, B. Gastaldi, J.F. Vidal, “COCONEUT: First steps of validation for the new AREVA TA neutronic deterministic scheme for Research Reactor design”, IGORR-2016 Proceedings, *to be published*

[14] J. Koubbi, C. Bayol, J.-G. Lacombe, C. Bouret, L. Manifacier, “Calculation methods for safety assessments of research reactors”, IGORR-2016 Proceedings, *to be published*

[15] J.-G. Lacombe, J. Koubbi, L. Manifacier, “COCONEUT: An Innovative Deterministic Neutronic Calculation Tool for Research Reactors”, IGORR-2014 Proceedings

BEST ESTIMATE PLUS UNCERTAINTY APPROACH IN THE ANALYSIS OF TRANSIENTS IN RESEARCH REACTORS

J.LUPIANO CONTRERAS, A.S. DOVAL

Nuclear Engineering Division, INVAP S.E.
Av. Cmte. Luis Piedrabuena 4950, R8403CPVSan Carlos de Bariloche – Argentina

ABSTRACT

Thermal-hydraulic modelling codes have been historically used to assess the design of nuclear reactors for different purposes, including new reactor and modifications and safety analysis among others. There are many sources of uncertainties in this modelling, such as limitations in the knowledge of the physical phenomena involved, approximations used and hypotheses considered, the use of approximate mathematical methods and empirical correlations to solve the mass, momentum and energy equations and the limitations of the code itself. These uncertainties have led users and regulatory authorities to adopt a conservative approach when it is necessary to prove that safety requirements can be fulfilled.
A best estimate modelling is an alternative approach providing a realistic simulation of the case being studied, with a precision commensurate with the current knowledge of the phenomena involved. If a comparison against limits is needed, an uncertainty analysis is required to supplement the best estimate calculations.
The Best Estimate Plus Uncertainty methodology (BEPU) has been implemented to assess transients in Nuclear Power Plants but its application has not been extended to the analysis of Research Reactors.
This paper considers the BEPU approach to evaluate a Loss of Flow accident in a 30 MW MTR Research Reactor. Supported by users engineering judgement, an uncertainty analysis based on the input error propagation methodology is performed for the relevant parameters involved in the transient. These parameters include those describing the core main characteristics, reactor geometry and thermodynamic local conditions as well as parameters affecting the model correlations for heat transfer and friction.
Finally, a conservative calculation considering initial and boundary conditions and parameters and assumptions leading to a pessimistic estimate of the transient has been included to compare these results with those obtained with the BEPU methodology.

1. Introduction

Thermal-hydraulic codes have been extensively used for the safety analysis, licensing and design of nuclear reactors. While there are variants among the different codes, most of them work by representing the whole system through a series of control volumes and junctions in which the mass, energy and momentum equations are solved for each of the fluid phases involved in that system. Additionally, boundary initial conditions and empirical correlations are required to solve the problem being studied.

The simplifications considered and the numerical methods used to solve the equations, the extensive use of empirical correlations, the limitations in the knowledge of the physical phenomena involved together with the accuracy of the instrumentation, the lack of information on the system being studied and the hypotheses introduced by the user to represent it are all sources of uncertainty which have an influence on the way in which the code predicts the behaviour of the plant.

A conservative approach has been historically implemented to account for these uncertainties as it provides a pessimistic estimate for a physical process in relation to a specified acceptance criterion, thus guaranteeing that all safety margins are satisfied (1).

Even though this approach ensures that the actual plant response to a particular event is enveloped by the conservative response predicted by the code, it has also proved to unnecessarily limit the range of operation of the reactor. The best estimate approach is an alternative which has been implemented together with the development of best estimate computational tools. While a best estimate model is free of the deliberate pessimism involved in the conservative approach, an extensive knowledge of the plant and the physical phenomena involved are required for the analysis to be a realistic estimate of the behaviour of the plant during a particular event. The best estimate approach is usually supplemented by an uncertainty analysis to account for all the unknown parameters and simplifications included in the model. This practice, which has been implemented to analyse the behaviour of Nuclear Power Plants has not been widely implemented for the analysis of Nuclear Research Reactors.

The Loss of Flow Accident (LOFA) is an event to be analysed during the thermal-hydraulic design of a Research Reactor. The present work presents a Best Estimate Plus Uncertainty analysis (BEPU) of this event for a 30 MW Open Pool Research Reactor. The results obtained are later compared with the ones predicted by a conservative model and the margins to the design criteria will be analysed for both models with the aim of evaluating the benefits of using one approach rather than the other.

2. Description of the cooling circuit

The reactor considered for the analysis is a generic 30 MW MTR-Open Pool Research Reactor. The Core Cooling System (CCS) consists of a set of pumps which provide the flow required to remove the heat in a forced convection cooling regime in upward direction. The heat from the core is later transferred to the Secondary System through a set of heat exchangers. Flap valves connected to the inlet pipes allow water to flow from the pool through the core when a natural circulation cooling regime is required. An inertia flywheel in each of the pumps provides the flow required to guarantee a smooth transition from the forced convection to the natural circulation cooling mode.

3. Description of the event

The event under analysis is a LOFA resulting from a main pumps stop. Due to a low flow/low pressure trip, the reactor goes into shutdown and the inertia flywheels provide the coolant required to remove the decay heat during the first period of the transient. As the pressure in the CCS decreases, the flap valves connected to the inlet pipes open, allowing the water in the pool to flow through them and into the reactor core, to establish a natural circulation cooling regime without any flow reversal. This is illustrated in Fig 1.

Fig 1. Forced and natural circulation cooling regimes in an Open Pool Research Reactor

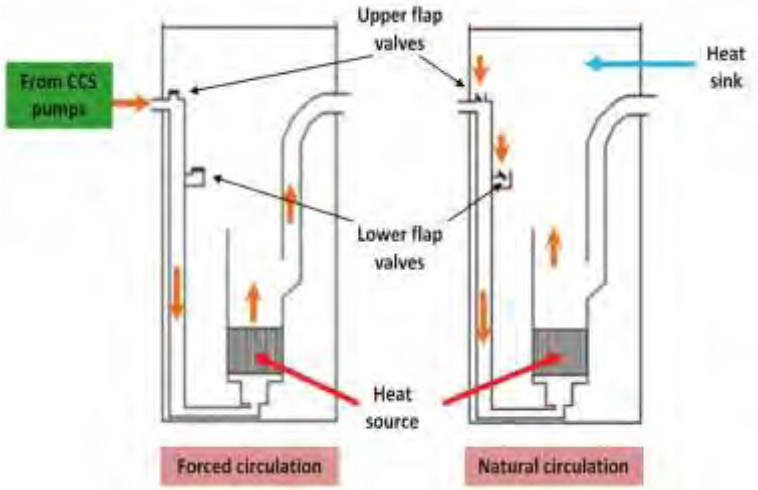

4. Thermal-hydraulic design criteria

The following thermal-hydraulic design criteria have been considered for the analysis of the transient:

***Burn-Out Ratio* (BOR):** is the ratio between the heat flux leading to the Burn-Out (BO) phenomenon (q"$_{BO}$), and the maximum heat flux (q"$_{max}$) in the hot channel.

$$BOR = \frac{q''_{BO}}{q''_{\max}} \geq 1.3$$

The heat flux leading to Burn-Out is calculated by the Fabrega correlation (2):

$$q''_{BO} = D_h \cdot (0.023 \cdot (T_{sat} - T_{inlet}) + 4.26)$$

Being:

D_h : Hydraulic diameter (mm)

T_{sat} : Saturation temperature (°C)

T_{inlet} : Inlet temperature (°C)

q''_{BO} : Heat flux leading to Burn-Out (W/cm^2)

Maximum cladding temperature (T_{clad}): it has also been fixed as a design criterion to avoid blistering.

$$T_{clad} < 450°C$$

5. Analysis

5.1 Calculation model

The analysis has been performed with the best estimate thermal-hydraulic code RELAP 5 MOD 3.2. The whole CCS is modelled by a series of hydrodynamic components (pipes and volumes) connected by junctions. The pumps are represented by the specific component provided by the code while the power generated in the core is represented by the point kinetics model. Heat structures are included to model the heat transfer from the core to the coolant (hot and average channels) and the heat removal from the cooling circuit to the heat sink (Secondary Cooling System). Fig 2. illustrates the nodalization considered for the analysis.

Fig 3. Nodalization in RELAP 5 for the CCS

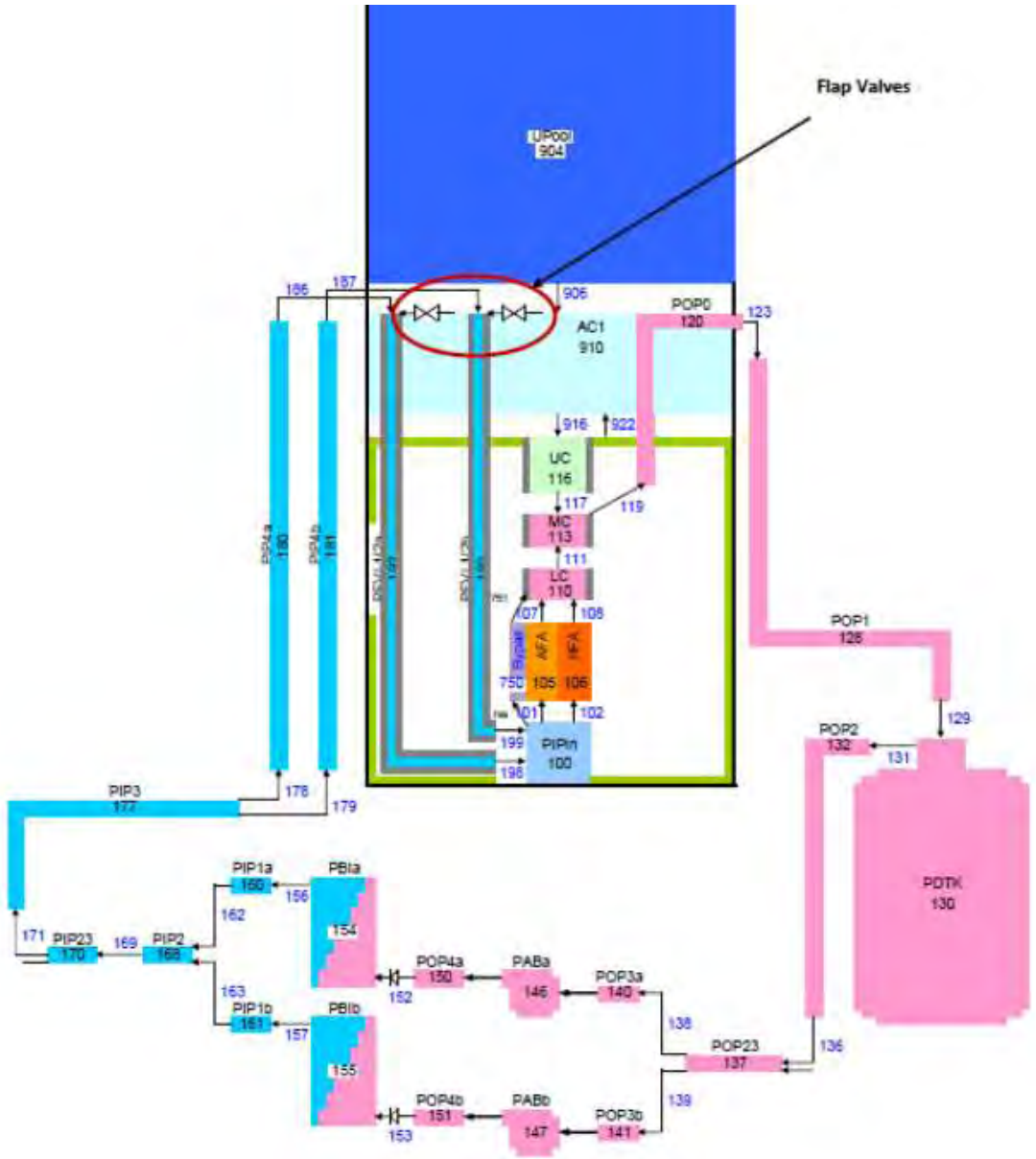

5.2 Methodology

The analysis has been performed considering the input error propagation. Potentially relevant parameters have been identified and their values varied simultaneously within an uncertainty range thus generating different inputs to model the reactor. This results in a distribution of responses which describes different behaviours for the transient being studied. The analysis includes a reference (best estimate) case and leads to the determination of an upper and lower limit for each of the design criteria considered. These upper and lower bounds are the values considered to evaluate the margins to the acceptance criteria.

The number of calculations performed has been determined by considering the Wilks' formula. For a one-sided tolerance limit, a total of 59 runs are required to guarantee a 95% confidence level that the maximum or minimum code result will not be exceeded with a 95% probability of the corresponding output distribution (3).

5.3 Parameters considered and uncertainties

A series of potentially relevant parameters and their range of variation have been identified based on engineering judgment and previous experience. The selected variables include both, reactor parameters and boundary and initial conditions representative of the LOFA event and related to the design criteria, as well. A total of 25 parameters have been considered and grouped according to the operating conditions, the fuel geometry, the set points, the reactivity insertion and to the thermal properties of materials. The convergence criteria and the nodalization adopted are kept fixed and their influence is therefore not included in the analysis.

The selected input parameters and their range of variation have been summarized in Tab **1**. A normal distribution of the values for each parameter has been considered for the analysis. The value adopted for each parameter in each run was randomly selected from this distribution and each of them randomly combined to generate the 59 inputs.

Parameter	Deviation
Operating Conditions	
Total power	+/- 5%
Power Peaking Factor	+/- 15%
Coolant flow through core	+/- 10%
Coolant velocity in Fuel Assemblies	+/- 10%
Coolant inlet temperature	+/- 0.5 °C
Atmospheric Pressure	+/- 4%
Water level in the pool	+/- 1%
Thickness of oxide layer	0 to 36 μm
Pump head	44 to 54 m
Control parameters	
Set point for flap valves opening	+/- 5%
Flow trip set point	+/- 5%
Shutdown System delay time	+/- 0.5 seconds
Reactivity insertion for shutdown	+/- 10% from nominal value
Geometrical parameters	
Gap of cooling channel	+/- 0.2 mm
Cooling channel width	70.2 to 70.7 mm
Plate thickness	+/- 0.05 mm
Meat thickness	+/- 5%
Active length and width	+/- 5%
Moment of inertia in the flywheel	+/- 10%
Thermal properties of materials	
Thermal conductivity and heat capacity	+/- 10%

Tab 1: Input parameters considered in the analysis and their maximum variation

The values of the parameters considered for the *reference case* are summarized in (*) Deviation from nominal reactivity values

Tab **2**. This table also contains the values adopted for a *conservative case*, as the results obtained from the BEPU analysis will be compared with the ones obtained from a conservative calculation.

Parameter	**Value**	
	Reference case	**Conservative case**
Operating Conditions		
Total power (MW)	30	31.5
Power Peaking Factor	3.0	3.5
Coolant flow through core (m^3/h)	3100	3410
Coolant velocity in Fuel Assemblies (m/s)	9.4	8.5
Coolant inlet temperature (°C)	38.0	38.5
Atmospheric Pressure (kPa)	94.4	90.6
Water level in the pool (m)	12.6	12.5
Thickness of oxide layer (μm)	18.0	36.0
Pump head	50.0	44
Control parameters		
Set point for flap valves opening (kPa)	0.6	0.63
Flow trip set point (m^3/h)	2799	2659
Shutdown System delay time (s)	2.0	2.5
Reactivity insertion for shutdown	No deviation (*)	90% (*)
Geometrical parameters		
Gap of cooling channel (mm)	2.45	2.25
Cooling channel width (mm)	70.5	70.2
Plate thickness (mm)	1.35	1.40
Meat thickness (mm)	0.61	0.64
Active width (mm)	65.0	61.8
Active length (mm)	615.0	584.0
Moment of inertia in the flywheel (kg.m^2)	100	90
Thermal properties		
Thermal conductivity of Aluminium (W/m.°C)	167	150
Thermal conductivity of oxide layer (W/m.°C)	2.25	2.03
Thermal conductivity of Stainless Steel (W/m.°C)	16.0	14.4
Heat capacity of oxide layer (MJ/m^3.°C)	3.48	3.83
Heat capacity of Stainless Steel (MJ/m^3.°C)	3.60	3.96

(*) Deviation from nominal reactivity values

Tab 2: Input parameters for the reference case and the conservative model

6. Results

The figures of merit adopted for the comparison of results are the design criteria previously defined, BOR and cladding temperature.

Fig. 3 and Fig.4 show the results for the 59 code runs as a function of time for BOR and maximum clad temperature respectively, and the comparisons with the reference and the conservative cases. As shown in these figures, the 59 results form an uncertainty band around the reference case.

Fig 3: BOR as the flap valves open and the natural convection is established

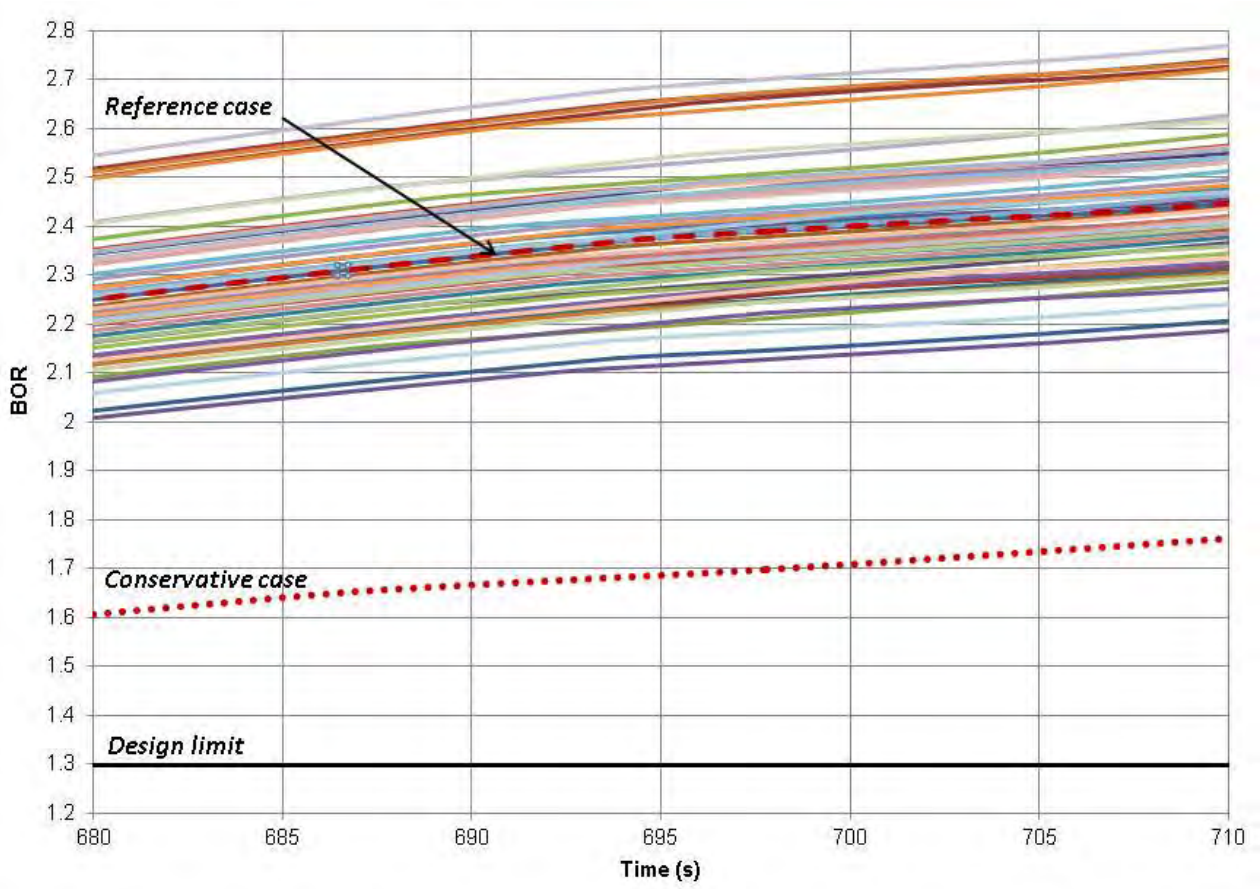

The results obtained show that both, the lower limit of the BEPU analysis and the conservative result, satisfy the design criteria. For the *BEPU* analysis, the lower bound corresponds to a BOR equal to 2.1 when the natural circulation cooling regime is established (at 694 seconds). For the *conservative case*, the BOR is nearly 1.7 at 688 seconds.

Fig 4: Evolution in the clad temperature during the transient

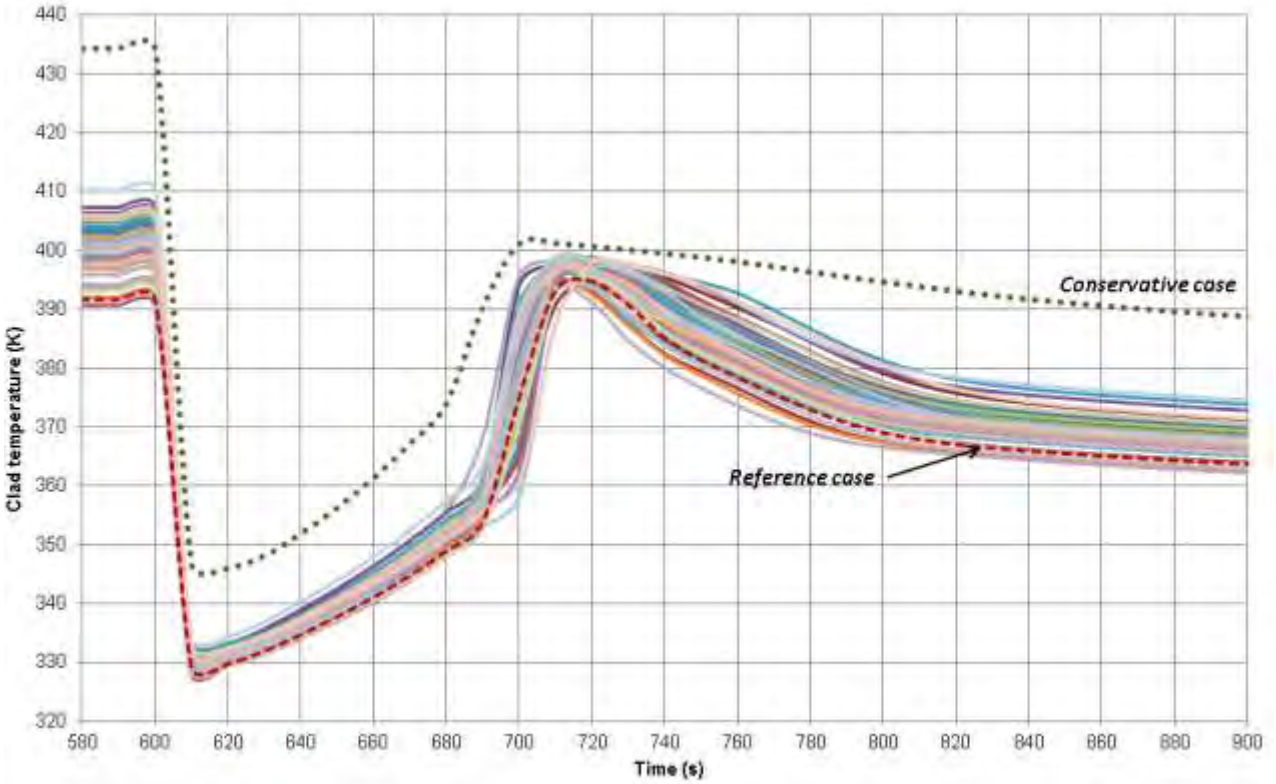

The upper bound for the clad temperature is 137 °C, as the pumps are stopped. This value increases to 167°C for the *conservative case*, showing a difference of 30°C between the upper limit calculated by the *BEPU* analysis and the value predicted by the *conservative* model.

7. Conclusions

The Best Estimate Plus Uncertainty (BEPU) methodology is frequently used to assess the performance of a Nuclear Power Plant during a transient but it has not been widely implemented for the analysis of transients in Research Reactors. Nowadays, with most demanding designs to improve the performance of these reactors, the BEPU methodology becomes a useful and attractive tool.

In this paper a Loss of Flow event was evaluated using the BEPU concept showing that:

- The reference case is bounded by the uncertainty band

- The upper / lower bound calculated by the BEPU methodology gives enough margins to the design criteria.

- The conservative case falls outside the uncertainty band and also fulfills the design criteria.

- The results obtained by the BEPU approach show a greater margin to the design limits when compared to the conservative results. It is therefore expected that a BEPU approach will allow for a more demanding performance of the reactor and a more economic design.

- The range of uncertainty and probability distribution of the values for each of the parameters being considered in the BEPU analysis need to be well supported if trustworthy results are to be obtained.

8. References

1. Safety Analysis for Research Reactors. Safety Reports Series N° 55, IAEA, 2008.
2. S. Fabrega ‘Le calcul thermique des Reacteurs de Recherche refroidis par Eau’, Commissariat a l’energie atomique, CEA-R-4114.
3. Glaeser Horst. GRS Method for Uncertainty and Sensitivity Evaluation of Code. Results and Applications

Advanced small and large core distortions modeling in ZPR to assess core recriticality scenarios of SFR core degradation sequences

M. Margulis[1,2], P. Blaise[2], E. Gilad[1]

1) The Unit of Nuclear Engineering, Ben-Gurion University of the Negev, Beer Sheva 84105, Israel
2) CEA Cadarache, Experimental Physics Service, 13108 Saint Paul-Lez-Durance, France

Corresponding author: maratm@post.bgu.ac.il ; marat.margulis@cea.fr

1. Introduction

Severe core accidents (SCA) in Liquid Metal-cooled Fast Breeder Reactor (LMFBRs) could occur either due to prompt/super-prompt recriticality or serious loss of heat sink [1]. The progression of the SCA in fast reactors (FRs) is strongly affected by the core neutron physics, which is the main focus of the current work. In the current examination of accident progress, SCA due to loss of heat sink is not considered. Since FRs cores are not loaded in their most reactive configuration, relocation of the core materials (fuel, sodium, absorbers and structural materials) have the potential of leading to positive reactivity insertion and unexpected high power excursions. Therefore, this study focuses on the core's neutronic behavior during different stages of a SCA - sodium voiding, material compaction, and molten pool formation, of various sizes.

The mentioned changes to the core configuration can have a pronounced influence on the neutronic characteristics of the core, which could severely damage both normal and emergency operation of the reactor. Therefore, in order to predict the core behavior during such disruptions it is necessary to develop accurate and precise computational and experimental tools and methodologies. Furthermore, there is a need to validate the computational tools against experimental measurements of representative configurations of different severe accident stages in order to evaluate the code performances and quantify any discrepancies between experiment and theory.

This paper presents a new benchmark problem based on the SNEAK-12A critical assembly experiments [2,3]. The SNEAK facility was located at Kernforshungzentrum Karlsruhe (KfK). The experiments in the SNEAK-12A were focused on reactivity differences between an undistorted core and a series of disturbed configurations that simulated the mentioned earlier disruptions. In this paper, a SCA sequence is made from the different experiments that were carried out in the SNEAK-12A facility. The scenario consists of 4 stages:

1. Normal core operation.
2. Small fuel slump in.
3. Large fuel slump in.
4. Molten pool formation.

Several other core disruption experimental programs were carried out around the world (ZEBRA-8G and ZEBRA-12 [4], ZPPR-5 [5], ZPPR-9 [6] and FCA VIII-2 [7]). However, among these programs, SNEAK-12 was the most comprehensive, with a large number of experiments aimed at measuring reactivity changes caused by:

1. Cavities
2. Streaming channels
3. Relocation of structural material
4. Dispersal and fuel recompaction
5. Formation of molten pools at the bottom of the core

The benchmark problem is introduced by the Commissariat a l'Energie Atomique et aux Energies Alternatives (CEA) and Ben-Gurion University of the Negev (BGU). It is calculated using TRIPOLI 4.9 [8] and Serpent [9] neutron transport Monte Carlo codes, with their JEFF3.1.1 based continuous energy libraries, as part of a future experimental program to be implemented in a zero power experimental reactor program, aimed to study recriticality possibilities in both light water reactors (LWR) and fast reactors (FR).

2. Computational tools

2.1. TRIPOLI

TRIPOLI-4 [8], developed by CEA, solves the linear Boltzmann equation for neutrons and photons, using the Monte Carlo (MC) method, in any 3D geometry. The code uses ENDF format continuous energy cross-sections from various international evaluations including JEFF-3.1.1, ENDF/B-VII.0, JENDL4 and FENDL2.1. TRIPOLI-4 solves fixed source as well as eigenvalue problems. It has advanced variance reduction methods to address deep penetration issues. Additional productivity tools, graphical as well as algorithmic, allow the user to efficiently set its input decks. With its large validation and verification data base, TRIPOLI-4 is used as a reference code for industrial purposes (fission/fusion), as well as for R&D and teaching tool, for radiation protection and shielding, core physics, nuclear criticality safety and nuclear instrumentation in France.

2.2. Serpent

Serpent is a continuous energy MC neutron transport code with burnup capabilities [9]. It allows modeling of complicated 2D or 3D geometries. This code was initially developed as an alternative to deterministic lattice physics codes for the generation of homogenized multigroup constants for reactors analyses using nodal codes. Current analyses were performed with cross section libraries based on JEFF-3.11, JEFF-3.1 and ENDF/B-VII.0 evaluated data files. Serpent is utilized in this work as a preliminary calculation tool, due to long calculation time required by TRIPOLI-4. In addition Serpent is utilized as a few-group constant generator for diffusion code.

3. SNEAK-12A – Benchmark specification

The information regarding SNEAK-12A core outline is mainly gathered in the SNEDAX data base [10]. The SNEDAX database contains information on built assemblies and experiments performed in the fast neutron SNEAK (FZK Karlsruhe), MASURCA (CEA Cadarache), ZEBRA (IAEA Winfirth), and the RRR (Rossendorf Ringzinen Reaktor) critical facilities. This section provides a short overview of the SNEAK-12A core geometry outline.

3.1. Core Description

The SNEAK-12A core consists of horizontal fuel plate assemblies and is cooled by air, which flows between the gaps of the fuel assemblies. The total core width, including unused areas (filled with air), is 326.4×326.4 cm^2 and total height of about 240 cm. The active core occupies a region of 130.56×130.56 cm^2 and active height of about 80 cm, surrounded by 30 cm of upper and lower reflectors, which makes a total of 140 cm. The radial blanket fuel assemblies are slightly higher than the fissile fuel assemblies, leading to a total height of about 150 cm. The core consists of three main radial zones: the radial blanket, the fissile active zone and the test zone that changes from a grid of 4×4 to 6×6, as shown in Fig. 1.
The fuel assembly is a 5.44×5.44 cm rectangular filled with horizontal plates of fuel and sodium, with air flowing around as a coolant. A representative fuel assembly is shown in Fig. 2. Most of the fuel assemblies in the core are composed of 35% and 20% enriched uranium metal slabs. The blanket and the axial reflectors consist of depleted uranium dioxide.

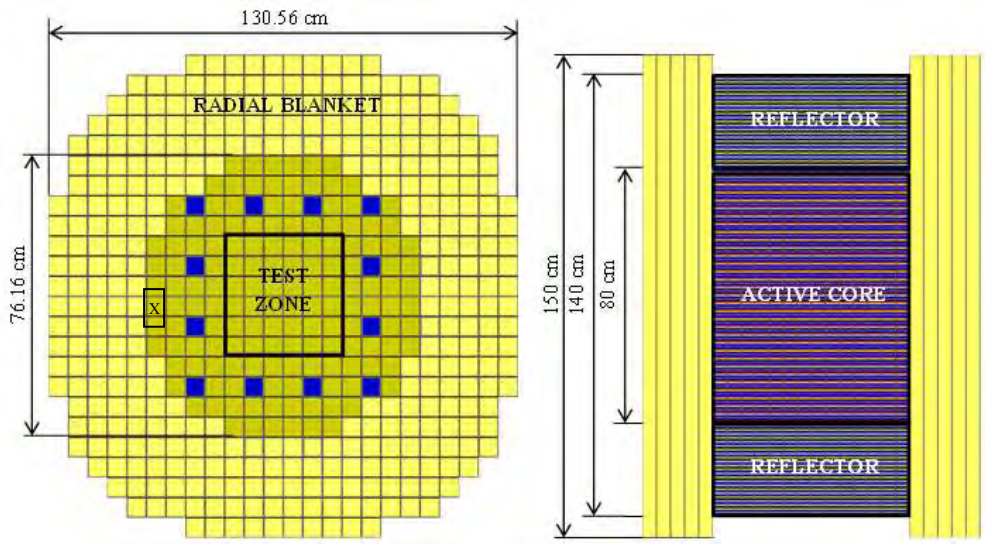

Fig. 1. SNEAK-12A core dimensions: the blue squares indicate the shim rod positions (left – XY cross section, right – XZ cross section) [10].

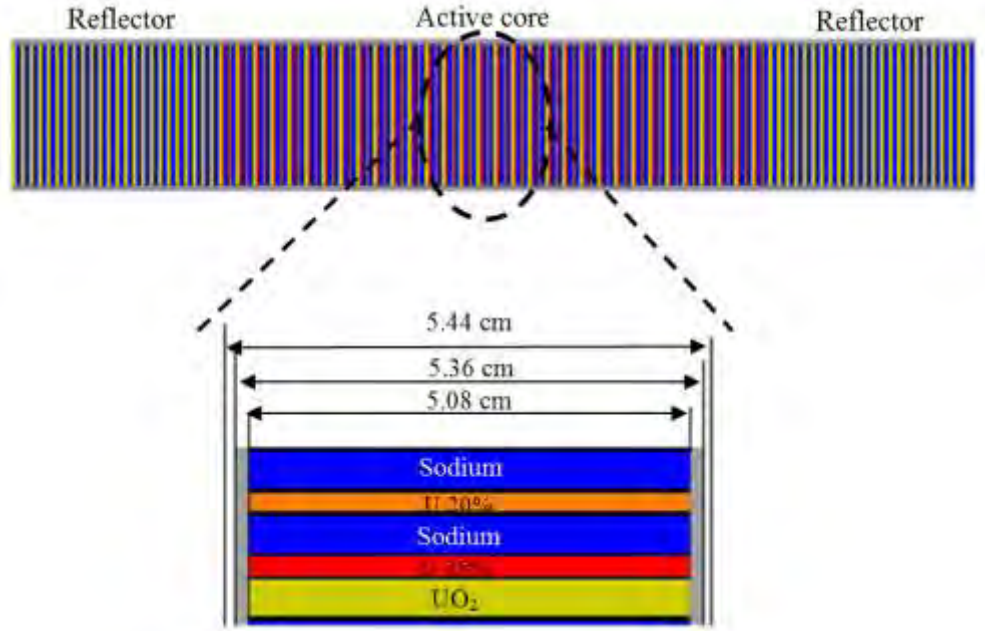

Fig. 2. XZ cross section of a fuel assembly geometry and fuel composition [10].

3.2. Core disruption scenarios

As mentioned earlier in this work, a SCA scenario is considered on two scales – small scale, affecting four central assemblies, and large scale, affecting sixteen central assemblies. The different configurations are shown in Fig. 3 for the small scale scenarios (4 central elements).

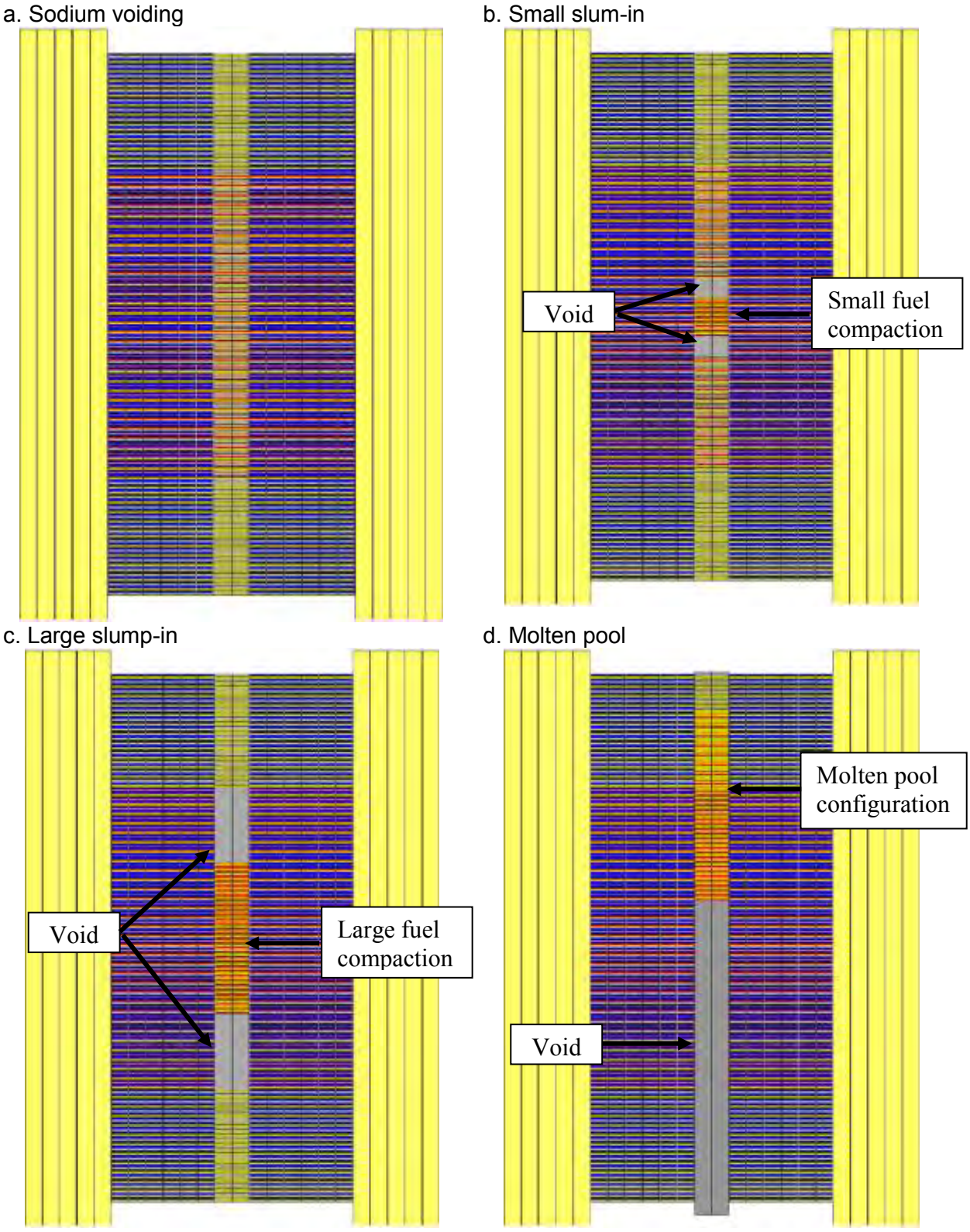

Fig. 3. Small scale (4 elements) representative configuration for core disruption.

4. Results

4.1. Clear criticality comparison

The clear criticality experiment configuration is the one shown in Figure 3.a. The results are summarized in Table 1, where the diagonal entries are the eigenvalue and the off-diagonal are the relative error in pcm between different codes and experiment. The results show an excellent agreement between Serpent, TRIPOLI and the experimental results. Furthermore, there is an excellent agreement between TRIPOLI and Serpent on their capabilities to calculate the flux spectrum and its distribution in 33 energy groups (average 1% difference) and one energy group flux distribution (average 0.5% difference), as shown in Fig. 4. The axial 1g flux distribution is shown in Fig. 5. For the axial flux distribution, the relative error between TRIPOLI and Serpent is remained also low (average of 0.5%).

Source	Experimental	Serpent	TRIPOLI
Experimental	1.00075	-36	-31
Serpent	36	1.00111±7.5E-05	5
TRIPOLI	31	-5	1.00106±7.6E-05

Table 1: Clear criticality results comparison

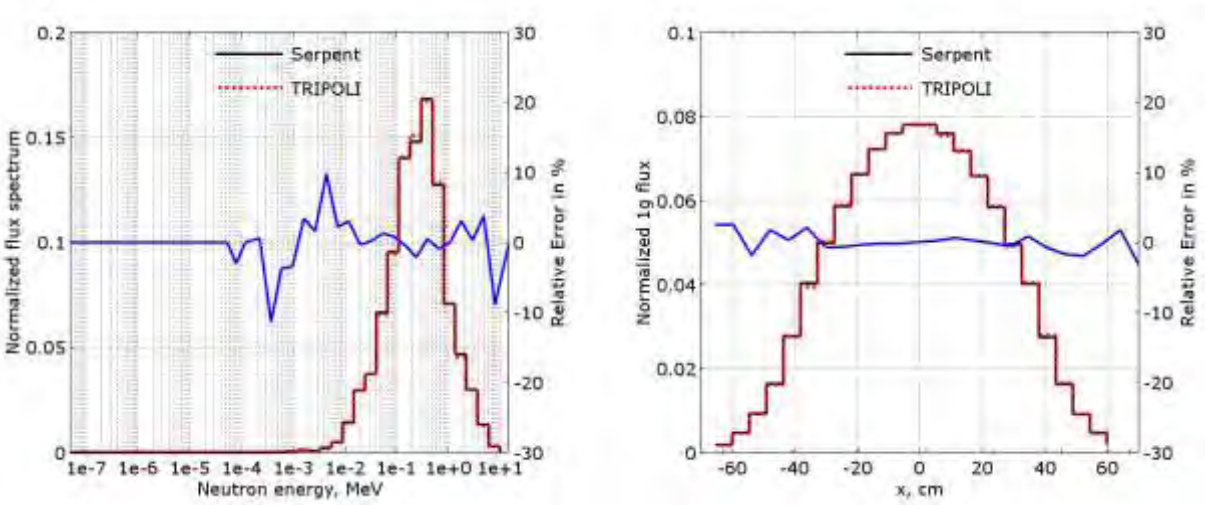

Fig. 4. Flux spectrum in 33 groups (left) and mid plane 1g flux distribution (right) for clean criticality core.

4.2. Accident progression

The reactivity changes due to different stages of fuel relocation, as presented in Fig. 3, are summarized in Tables 2 and 3 for small (4 assemblies) and large (16 assemblies) SCA scenarios, respectively.

As can be seen from Table 2, there is a good agreement between the experiment and the different codes. Furthermore, it can be seen that the initial reactivity change due to sodium voiding is negative due to a leakage increase. As expected, the small slump-in brings a positive reactivity insertion in comparison to the sodium voiding stage. However, the total reactivity remains negative due to the small fuel compaction. On the other hand, the large center core slump-in causes a relatively large reactivity insertion, mainly due to large fuel compaction, which reduces the leakage and creates an area of high neutron importance in the core center. The last stage in the small core distortion is the molten pool formation, where the reactivity insertion is negative due to relatively small fuel removal from the high importance region in the core center.

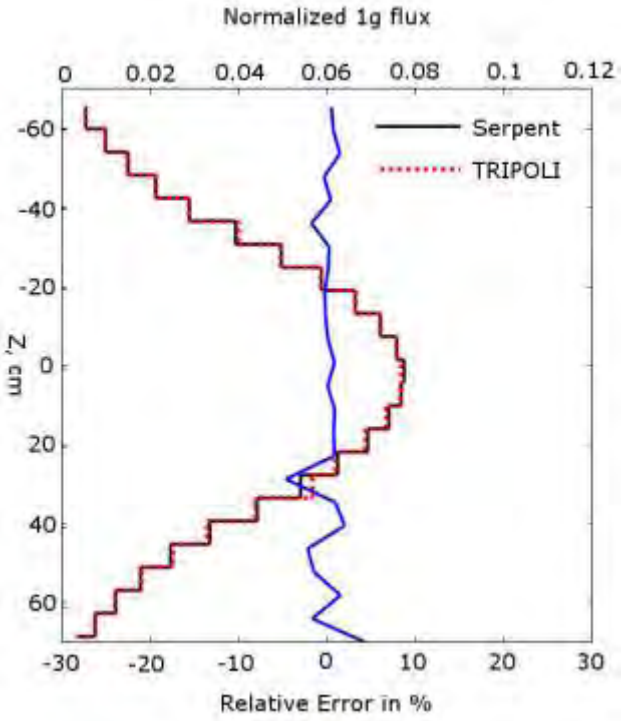

Fig. 5. Center core axial 1g flux distribution for clear criticality experiment.

SCA stage	Experimental	Serpent	TRIPOLI
Clear crit.	0	0	0
Sodium void	-5.9	-8.5	-8.1
Small slump-in	-1.4	-5.8	-4.6
Large slump-in	79.1	77.1	75.9
Molten pool	-72.2	-65.0	-64.5

Table 2: Small scale SCA progression in terms of reactivity worth~~,~~ (values in ¢~~¢~~)

SCA stage	Experimental	Serpent	TRIPOLI
Clear crit.	0	0	0
Sodium void	-25.6	-23.5	-29.8
Small slump-in	-7.4	-13.2	-12.9
Large slump-in	242.3*	349.1	331.0
Molten pool	-120.0	-122.5	-123.0
***** For 12 disturbed elements			

Table 3: Large scale SCA progression in terms of reactivity worth (values in ¢)

The behavior observed in the small scale SCA is repeated in the large scale SCA with larger magnitude, as expected due to larger material relocations. However, large slump-in experiment with 16 elements was not carried out in the SNEAK program. Nevertheless, an experiment with 12 affected elements was performed, and provides a magnitude of the reactivity insertion level.

Regarding the molten pool formation, the greater negative reactivity value is due to the large amount of material that is removed from the center region. However, it is not sufficiently large to create a new importance region in the upper part of the core, as shown in Fig 6. Figure 6 shows that the flux deviation from the clear criticality result is not large in the outer region of the active core (position X in Fig. 1). Therefore, the molten pool formation is followed by a greater negative reactivity insertion [11] due to large leakage factor in this configuration.

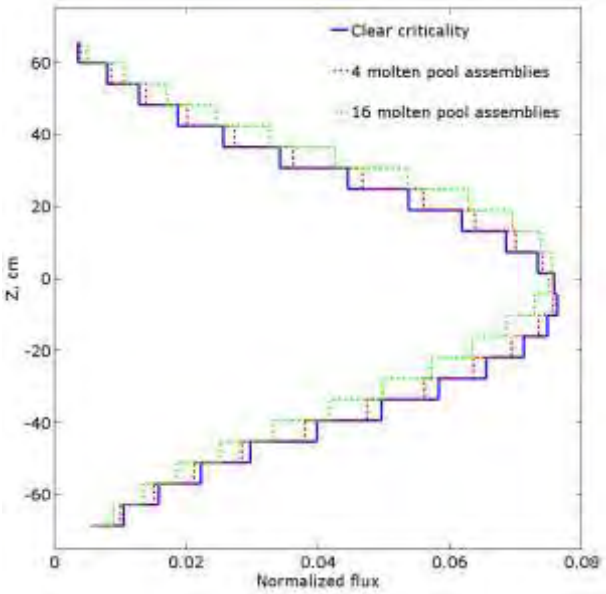

Fig. 6. Local 1g normalized axial flux distribution for different molten pool configuration at detector position X (Fig. 1).

The results shown in Figs. 7 and 8 support the statements made earlier. Figure 7 shows that the change in axial flux distribution is minor when considering the progression from sodium voiding to small slum-in. This is also consistent with the results in Table 2. Furthermore, the flux deviation from the core center is small. Therefore, the removal of material from the core center is followed by negative reactivity response.

On the other hand, Fig. 8 shows that the responses in large SCA are much sharper. The large slump-in into the high importance area is followed by a strong reactivity insertion and a high local power peak. The molten pool formation, following the center core large slump-in, is followed by a negative - but lower - reactivity insertion comparing to the small SCA.

5. Conclusions

In this paper, two SCA scenarios are derived from the SNAEK-12A program. They are readdressed using current state-of-the-art Monte Carlo tools (TRIPOLI, Serpent). The SCA scenario is initiated by a complete channel dry-out, followed by a small fuel compaction in the core center. The small fuel compaction turns into large fuel slump-in into the core center, leading eventually to the formation of a molten pool. The results exhibit good agreement between experimental and calculated data. In addition, the comparison between the two codes indicates an excellent agreement on both reactivity and flux distributions.

Currently, a complete SNEAK-12A benchmark is being prepared for publication in collaboration with KIT. The benchmark includes additional experiments that were carried out during this program. The experiments include small and large slump-in of fuel, in the same plate configuration as presented here. Configuration B of the SNEAK-12 experimental phase (SNEAK-12B) is also of great interest due to utilization of MOX assemblies consisting of fuel rods instead of fuel plates, as in SNEAK-12A. This benchmark will be treated in a separate study due to the completely different behavior of MOX fuel during severe accident progress.

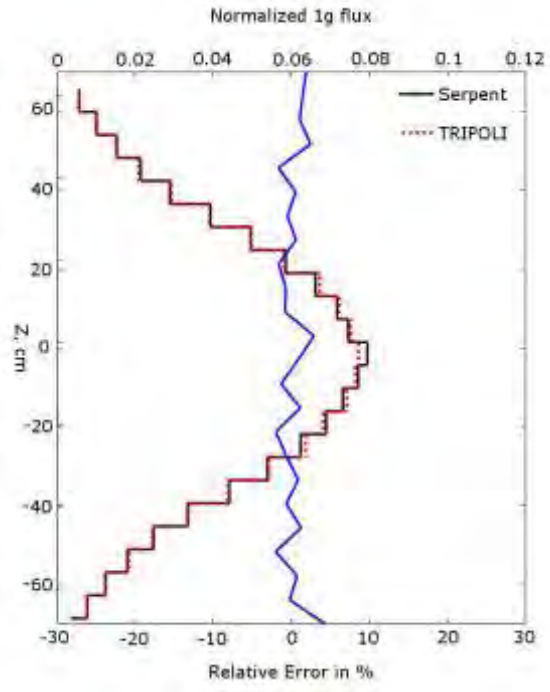

a. Step s1 – Sodium void

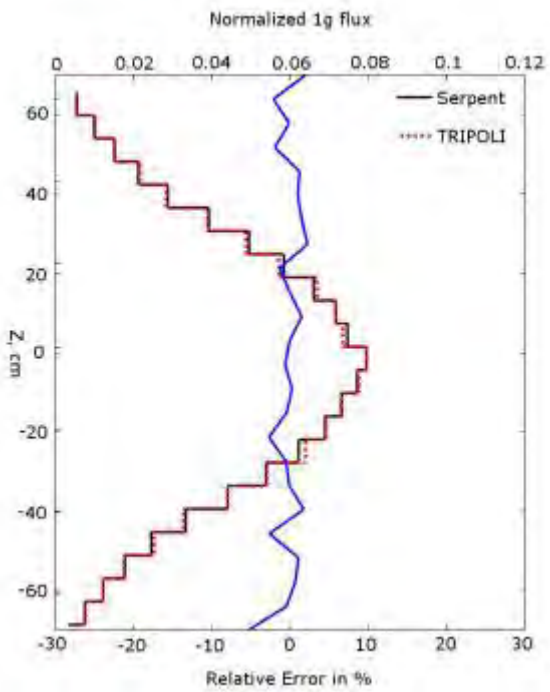

b. Step 2 – Small slump-in

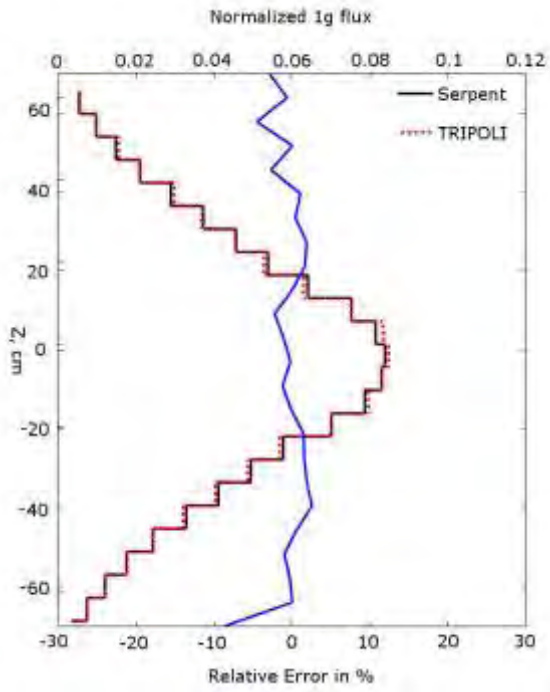

c. Step 3 – Large slump-in

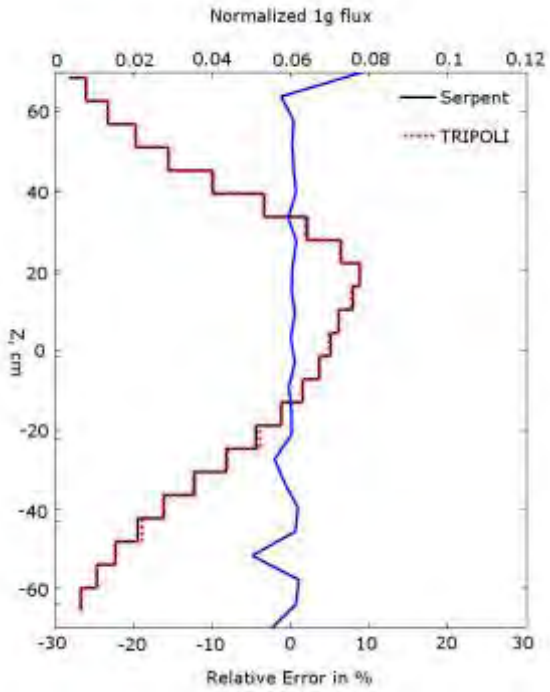

d. Step 4 – Molten pool

Fig. 7. Center core normalized flux distribution for small SCA progression.

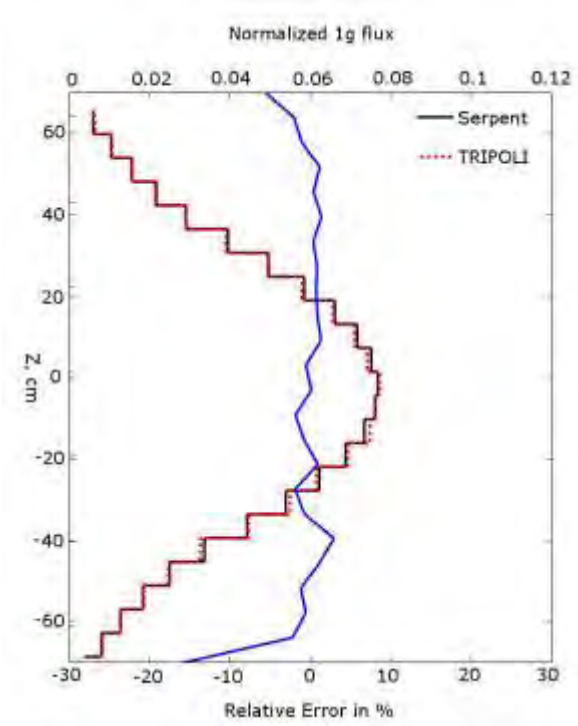

a. Step 1 – Sodium void

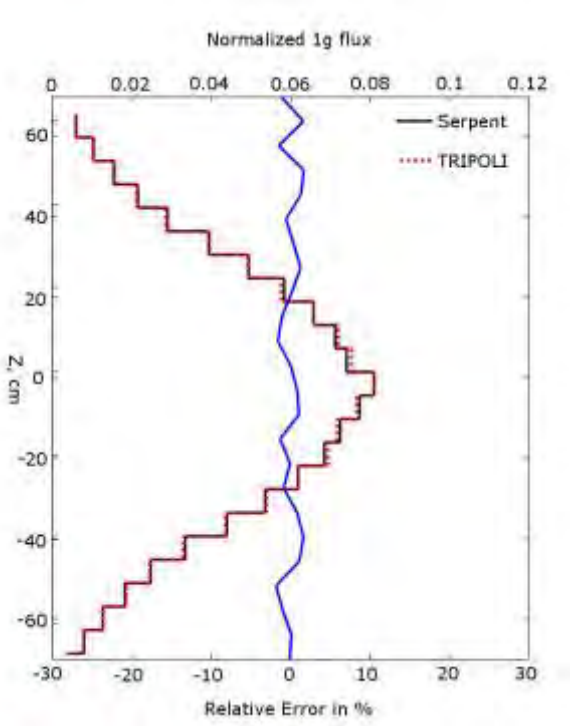

b. Step 2 – Small slump-in

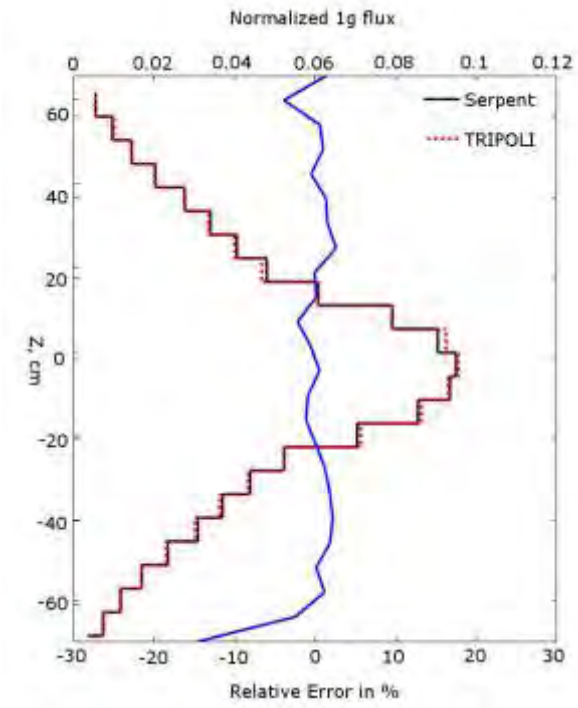

c. Step 3 – Large slump-in

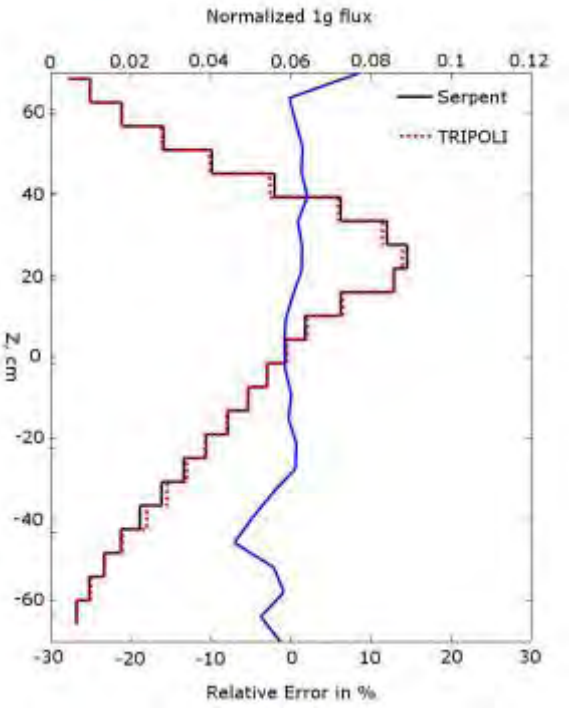

d. Step 4 – Molten pool

Fig. 8. Center core normalized flux distribution for large SCA progression.

6. References

[1] H. Ninokata et al. “A study on recriticality characteristics of fast reactors in pursuit of recriticality accident-free concepts.” Progress in Nuclear Energy, 29: pp. 387–393 (1995).

[2] G. Henneges. “Validation of neutronic codes for distorted core configurations with the SNEAK-12 critical assemblies.” Nuclear Science and Engineering, 100: pp. 314–323 (1988).

[3] F. Helm and G. Henneges. “Measurements and calculations of reactivity effects of material rearrangement in a plutonium-fuelled fast reactor rod lattice.” Nuclear Technology, 71: pp. 68–81 (1985).

[4] P. J. Collins, G. Ingram, and J. Codd. “Simulated meltdown and vapor explosion experiments in ZEBRA 8G and Zebra 12 and their interpretation.” In: Proc. Int. Symp. Physics Fast Reactors. American Nuclear Society, Tokyo, Japan (1973).

[5] R. E. Kaiser, C. L. Beck, and M. J. Lineberry. “Simulation of an HCDA sequence on the ZPPR critical facility.” In: Proc. ANS/ENG Mtg. Fast Reactors Safety and Related Physics. American Nuclear Society, Chicago, IL, USA (1976).

[6] R. Curtis et al. “The use of benchmark criticals in fast reactor code validation.” In: Proc. Int. Symp. Fast Reactor Physics. American Nuclear Society, Aix en Provence, France (1979).

[7] M. Nakano, H. Tsunoda, and J. Hirota. “An experimental study of reactivity changes and flux distortion in simulated LMFBR meltdown cores.” Nuclear Science and Engineering, 294: pp.283–294 (1984).

[8] E. Brun et al. “TRIPOLI-4, CEA, EDF and AREVA reference Monte Carlo code.” Annals of Nuclear Energy, 82: pp. 151–160. ISSN 0306-4549.

[9] Leppanen, J. Development of a New Monte Carlo Reactor Physics Code. Ph.D. thesis (2014).

[10] F. Helm. “The SNEDAX data base - General description and user’s instruction. Technical report”, Forchungszeentrum Karlsruhe, Karlsruhe, Germany (1996).

[11] M. Margulis, E. Gilad and P. Blaise, “Monte Carlo analysis of SNEAK-12A core disruption in liquid-metal fast breeder reactors – The path for innovative severe accident studies in ZPR”, In: Proc. PHYSOR-2016, American Nuclear Society, Sun Valley, ID, USA (2016).

COMPARISON OF MEASURED AND CALCULATED NEUTRONIC AND THERMAL HYDRAULIC REACTOR PARAMETERS OF THE LEU-FUELLED JAMAICAN SLOWPOKE-2 RESEARCH REACTOR

F. PUIG
Nuclear Systems Analysis, Nuclear Engineering Division, Argonne National Laboratory
9700 S. Cass Avenue, Argonne, IL 60439 – USA

H. DENNIS
International Centre for Environmental and Nuclear Sciences, University of the West Indies
2 Anguilla Close, Mona, Kingston 7 – Jamaica

ABSTRACT

The Jamaican SLOWPOKE-2 (JM-1), a 20 kW research reactor manufactured by Atomic Energy of Canada Limited, operated for 30 years at the University of the West Indies, Mona Campus in Kingston, Jamaica, with 93% enriched uranium fuel. As part of the safety analysis for the conversion from HEU to LEU fuel, which was completed in September 2015, full-reactor neutronic and thermal hydraulic analyses were performed and predictions presented for various reactor parameters. Following the successful conversion of the JM-1 reactor, this paper addresses the comparison of the commissioning tests results with the safety analysis work performed in collaboration between the Argonne National Laboratory (ANL) and the International Centre for Environmental and Nuclear Sciences (ICENS) to support the conversion process and provides insight to the observed discrepancies. The comparison includes neutronic parameters, such as the predicted core loading configuration, associated excess reactivity and temperature coefficients, as well as steady state thermal hydraulic parameters, such as the verification of the estimated flow rates through the core as a function of reactor power. The calculated reactor parameters and predicted behaviour are in good general agreement with the available experimental data.

1. Introduction

In September 2015, the JM-1 reactor (SLOWPOKE-2 type) at University of West Indies (UWI) in Kingston, Jamaica, was successfully converted from HEU to LEU fuel, with Argonne National Laboratory (ANL) providing technical coordination and support for the Conversion Program. This accomplishment involved the complete removal of all HEU material from the Caribbean, setting a significant milestone for nuclear non-proliferation efforts, while providing a new core that will allow the reactor to keep operating and contributing to a wide variety of research activities at the International Centre for Environmental and Nuclear Sciences (ICENS) for several decades.

Following the conversion, and partly within the context of the commissioning procedures, a series of tests and measurements were carried out. Despite being somewhat limited in scope at this stage, they provided a good opportunity for a detailed comparative study between the analysis work performed as basis to support the reactor conversion and the experimental results obtained after its completion, which is infrequent. The purpose of this paper is to present a summary of that work, along with its main results and conclusions, as well as a few elements for discussion.

1.1. Reactor description

The SLOWPOKE-2 reactor is a tank-in-pool type, natural convection cooled research reactor designed by Atomic Energy of Canada Limited (AECL) and mainly intended for neutron activation analysis (NAA). It provides a thermal neutron flux at its inner irradiation sites of 10^{12} n/cm^{2}s at a nominal thermal power of 20 kW. The JM-1 reactor was commissioned in 1984 with an HEU core and has been used since for NAA in a variety of applications.

The annular and bottom beryllium reflectors surround the core, minimizing its size (about 22 cm in diameter and 23 cm in height) and the fuel required to achieve criticality, while increasing the thermal neutron flux at the irradiation sites. Additional semi-circular beryllium plates (or shims) can be added on a top tray to periodically compensate for the fuel burnup (see Figure 1). The reactor has intrinsic safety features, with self-limiting power excursion response upon reactivity insertions of moderate magnitude; as a result conventional safety systems are not required. To ensure the safe reactor operation even when unattended (remotely monitored), it is licensed for a maximum of 4 mk of available excess reactivity.

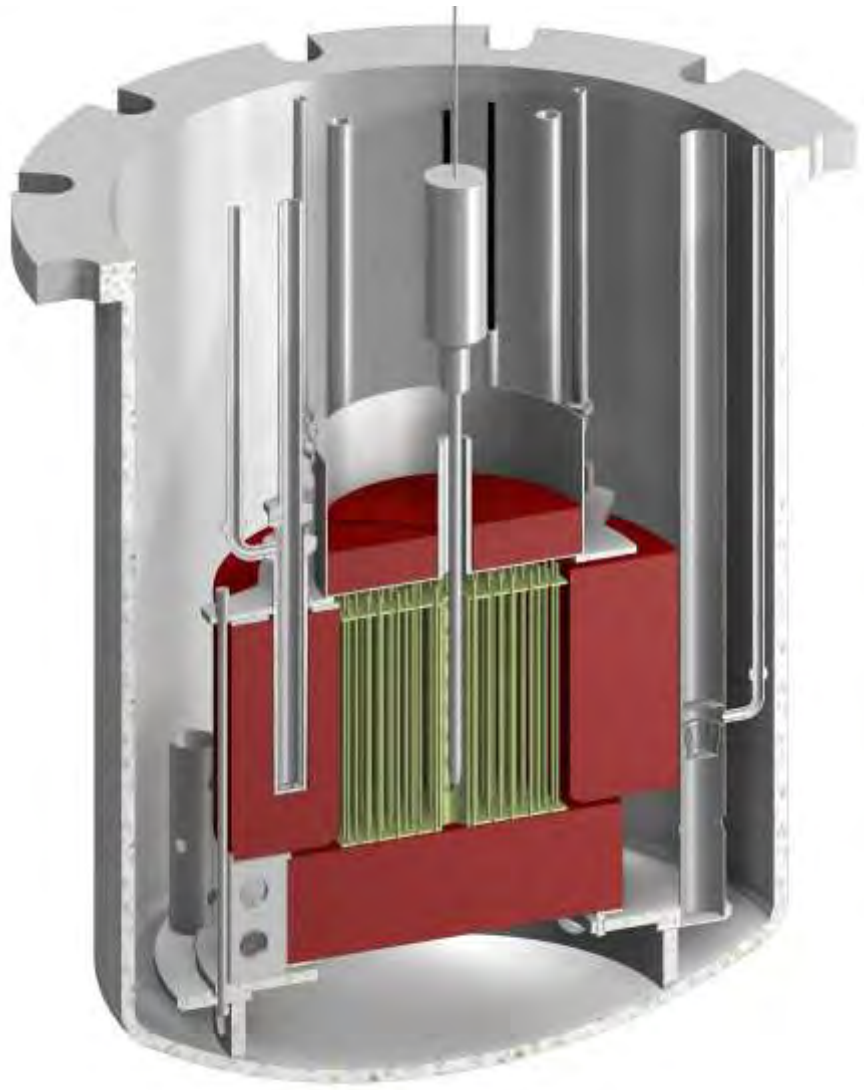

Fig 1. Cross section view of the LEU-fuelled SLOWPOKE-2 critical assembly

A somewhat peculiar trait of the SLOWPOKE-2 reactor, relevant in the later analysis, is that, according to pool heating experiments performed at the LEU-fuelled reactors of the Royal Military College of Canada (RMC) and École Polytechnique de Montréal (EP), it presents a slightly positive temperature coefficient of reactivity below 33°C; in contrast to the ~19°C

threshold for the HEU-fuelled reactor [1]. The unusual behaviour is the result of a positive temperature coefficient of reactivity of the beryllium reflectors and mainly the water reflector (water volume surrounding the beryllium reflectors). The difference between HEU and LEU cores' peak temperatures is the result of a less under-moderated LEU core. This is not a safety issue in terms of operation, since the core coolant temperature coefficient is still strongly negative and, when the reactor power is increased, the core temperature rises far more and far quicker than other regions, ensuring a large effective negative feedback. However, this behaviour should be taken into account to ensure the excess reactivity doesn't exceed 4 mk. Thus, reactivity measurements during commissioning or shim additions are adjusted to a temperature of 33°C.

2. Analysis and results

Thermal hydraulic and neutronics analyses are presented separately in this section. It is worth noting that whenever possible, data from RMC and EP LEU fuelled SLOWPOKE-2 reactors have also been used as reference in addition to that obtained from JM-1.

Two main kinds of experiments, particularly useful for comparative analysis have been carried out in these reactors. Steady state flow experiments involve monitoring of inlet and outlet coolant temperatures at given power levels until they stabilize. The inlet temperature generally keeps increasing slowly over time but conditions can be considered stable for practical purposes. Most of the analysis work presented is related to these experiments.

A second set of experiments, only performed at RMC and EP, involved the heating of the reactor pool by external means up to about 40°C and allowing thermal equilibrium to be achieved. Then, the reactivity was measured with the reactor critical at zero power as the pool heat removal system slowly decreased the temperature. The results were useful to calibrate the total available excess reactivity as a function of the initial reactor temperature. The current unavailability of some equipment at the JM-1 facility, such as the lack of any heating system along with the relatively limited amount of time since the reactor has been converted, have so far prevented the replication of those experiments. Without additional specific experimental data, the reactivity calibration curve obtained at RMC [2] and also consistent with EP results [3] is assumed to be also valid for the JM-1 and used as reference.

2.1. Thermal hydraulic analysis

The bulk of the thermal hydraulic analysis work has been performed using the PLTEMP/ANL code. It provides adequate capabilities for the study of steady state conditions for a natural circulation reactor such as the SLOWPOKE-2.

A few aspects are of particular interest in this analysis. It is important to see whether the simulations can properly predict the observed flow conditions, and whether these are consistent between reactors, as should be expected due the virtually identical geometry. Nominal thermal power is another parameter that has been very difficult to measure directly. Indirect calibration methods, with a significant uncertainty range, are used instead (by means of a neutron source of known power). Even though reactor power cannot be directly determined from these experiments, their analysis could detect inconsistencies in power level estimates if discrepancies were large enough.

2.1.1. PLTEMP/ANL model

The thermal hydraulic model built is fundamentally based on the actual reactor geometry, the laminar flow regime determined to be prevalent during all operation conditions, the friction factor for the coolant flow around the fuel pins, the axial power distribution determined by MCNP5 simulations and the materials thermal properties. However, a reliable theoretical calculation of the pressure losses for the flow through the inlet and outlet orifices intricate

path is not feasible. Instead, a resistance coefficient that determines the pressure drop when multiplied by the flow velocity is calibrated using experimental reactor operation data.

2.1.2. Results and discussion

The specific reactor tests that serve as basis of this analysis include the steady state commissioning tests at RMC, EP and JM-1, as well as three sample irradiation sessions at JM-1. The latter have been key to provide detailed data for a more accurate analysis.

An initial difficulty in the analysis arose from the variety of reactor inlet temperatures at which the tests were carried out. Transforming the input data to differences between inlet and outlet temperatures does not solve the problem, since the effects of temperature on water heat capacity and particularly on its viscosity lead to significantly different reactor behaviour, preventing accurate direct comparison. The resulting situation can be observed in Figure 2, which shows the steady state flow data from the commissioning tests at JM-1, RMC and EP, as well as the irradiation tests at JM-1. Note that the after the 1 hour irradiation session at full nominal power, steady state tests at 5 kW, 10 kW and 15 kW were also performed; full nominal applies to the two 4-hour irradiations.

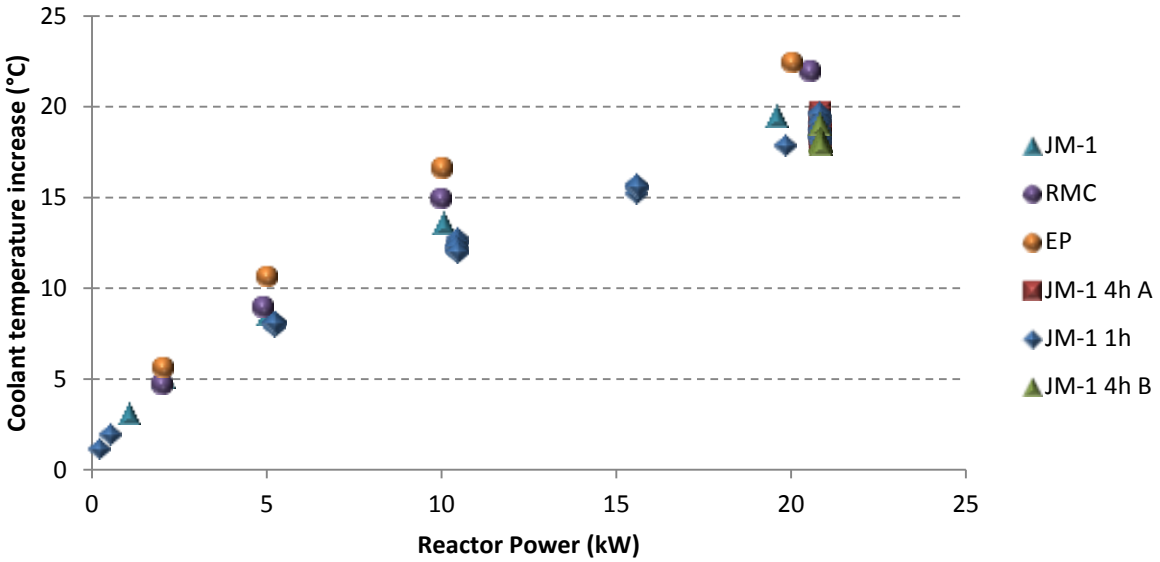

Fig 2. Steady state flow experiments raw data

Steady state flow commissioning tests provided only a single data point at a time when the flow was deemed to have stabilized. It is not completely clear what criteria had been used to determine whether steady state had been reached in each case. Another additional difficulty was the constant undulation of temperature readings, particularly for outlet temperate at high power levels. This behaviour is shown in Figure 3, further increasing the uncertainty about what temperature readings had been taken as reference.

To try to overcome this situation, continuous temperature readings of the three additional irradiation sessions were used, averaging their values over periods from 1 to 6 minutes, so that fairly smooth temperature profiles were obtained. Special care was taken to ensure that no significant changes in power, control rod position or temperature trend occurred during the averaged periods. Each of the averaged periods is shown as a data point in Figure 2.

For each averaged period, the resistance coefficient was calibrated by introducing power and inlet temperature into the PLTEMP/ANL model and requiring the outlet temperature to match the experimental data. Temperature increase for each data point was then recalculated for a common inlet temperature of 26.8°C. The obtained results are plotted in Figure 4.

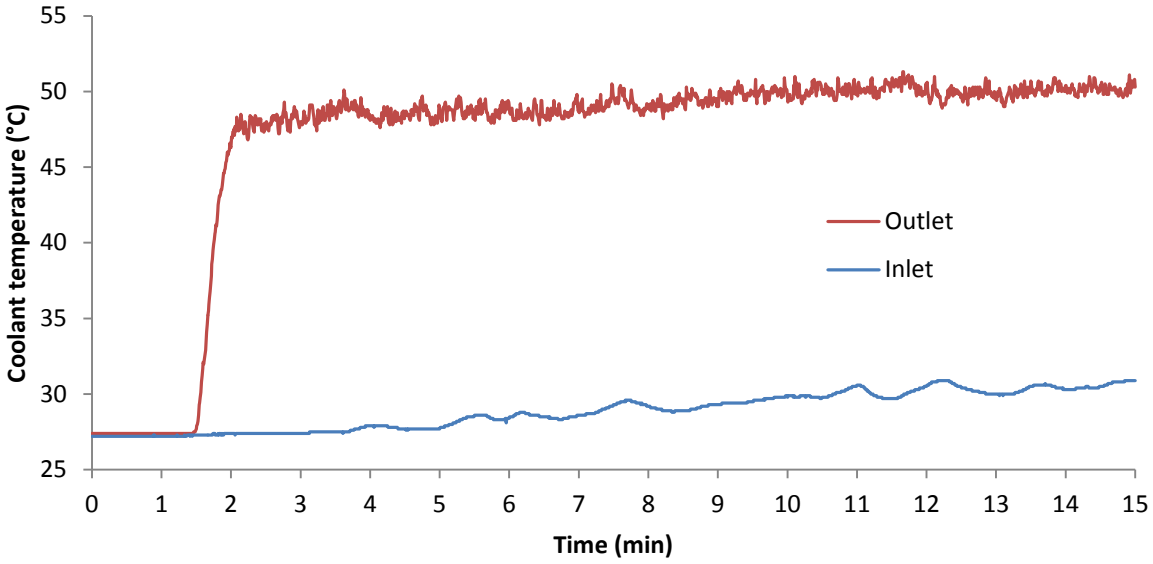

Fig 3. Coolant temperature behaviour during constant 20 kW operation

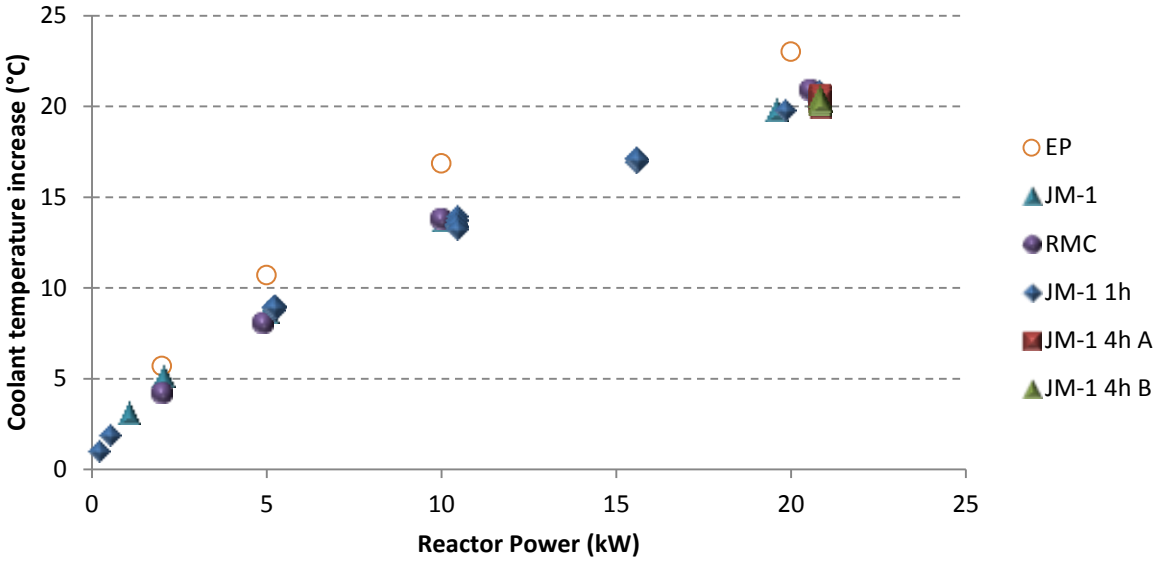

Fig 4. Steady state flow experiments results after calibration

A few relevant conclusions can be extracted from these results. First of all, the reactor flow behaviour as a function of power seems to be consistent and reproducible, obtaining results within the same narrow band of variation in different sets of experiments. Secondly, the model seems capable of accurately capturing the flow and heat transfer phenomena in the reactor, making the experimental results converge when appropriate calibration of the data is applied. Thirdly, the results obtained at RMC apparently match very closely those at JM-1, which is expected for nearly identical reactors. Moreover, it seems to point out that the estimated nominal power of both reactors is also essentially correct, or at least the ratio between them is. The reactor power of the HEU-fuelled JM-1 was originally estimated at 19.08 kW, which would become 20.94 kW after conversion according to MCNP5 calculations, while LEU-fuelled RMC reactor estimated power was 17.7 kW. It is remarkable to confirm that this significant difference in nominal power (providing the same thermal neutron flux at inner irradiation sites) is apparently real. It is likely mainly related to the presence of a D_2O thermal column in the RMC reactor, which may improve moderation and neutron economy. Finally, the EP reactor data seems to diverge substantially from that of the other two reactors, as shown in Figure 4, indicating some anomaly. No reasonable discrepancy in

reactor power or known difference in the facility can explain these results; and they cannot fit any consistent PLTEMP/ANL model. New steady state flow experiments at EP, or updated operation data, may help elucidate this issue. Until then, this EP data set is not considered to be reliable.

The resistance coefficient values resulting from calibration are another interesting aspect to consider. It should be taken into account that the value of this coefficient is very sensitive to small changes in power or temperature, resulting in substantial spread for small uncertainties in the input variables. It should also be noted that the coefficient does not have a direct physical translation, since PLTEMP/ANL code uses the flow velocity through the core as reference instead of the flow through the far smaller inlet and outlet orifice flow areas. Results are plotted in Figure 5. The values obtained from the averaged periods of operation provide the best reactor behaviour reference. The discrete measurements are just relevant to show that their values are roughly within the expected range. What is interesting to notice about the bulk of the data points is the downward trend of the coefficient with the increase of reactor power. Resistance coefficient would be a constant, and the minor pressure drop proportional to flow velocity, if the flow was turbulent at the inlet and outlet orifices. Since the flow is actually laminar, even though the code assumes it to be turbulent at the orifices [4], the pressure drop does not increase linearly with flow velocity, resulting in an apparent decrease of the resistance coefficient. It is worth highlighting that despite the inherent spread of the data, this small predicted effect is also captured in the results.

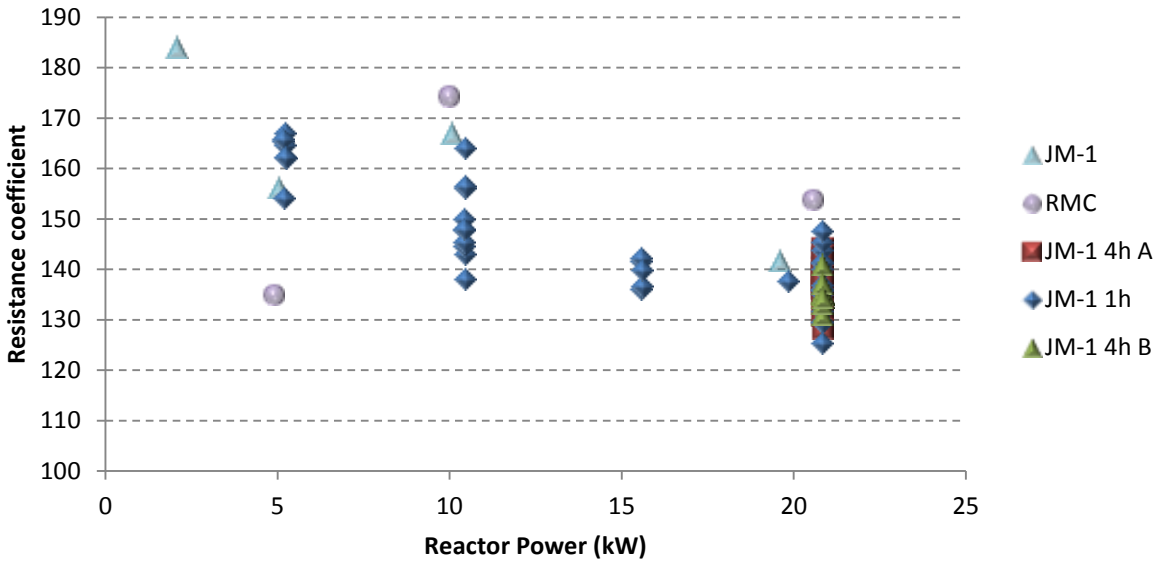

Fig 5. PLTEMP/ANL model calibrated resistance coefficient values

2.2. Neutronics analysis

MCNP5 v1.6 code was the main tool of the neutronics analysis. The accompanying *makxsf* tool for Doppler correction of cross section data libraries according to temperature was also used as required. Additionally, ORIGEN2.2 code was employed to calculate xenon buildup.

2.2.1. Total reactivity and core fuel loading

One of the key parameters considered in the reactor conversion analysis was the total reactivity and the corresponding fuel loading required not to exceed 4 mk at 33°C. The number of LEU fuel pins at both RMC and EP reactors was 198, arranged in the same configuration. Specifically, the excess reactivity at 33°C achieved at EP was 3.69 mk, while at RMC it reached 3.46 mk with a 1.9 mm thick beryllium plate on the shim tray [5].

The fuel design for all three reactors was the same. Aside from some small fabrication differences within specifications, the only known significant change is JM-1's fuel having slightly higher uranium enrichment (19.88% vs. 19.75%). The existence of a D_2O thermal column at RMC or the presence of just one external irradiation site and two neutron detectors at JM-1 are other small differences between the reactors. Reliable information about detailed impurities concentration present in the fuel, beryllium and structural materials for EP and RMC reactors was not available, so an accurate comparative analysis was not possible.

The conversion analysis estimated a fuel loading of 195 fuel pins instead of the typical 198. In addition to the best available reactor geometry data and UO_2 and fuel pins manufacturing tests results, the model also took into account the depletion of self-powered neutron detectors' cadmium emitters and the changes in the beryllium reflector composition due to neutron fluence during the previous 31 years of reactor operation [6], obtained with ORIGEN2.2 and ORIGEN-S codes. The actual JM-1 conversion culminated with 193 fuel pins loaded, plus a 1/16" beryllium shim on the top tray (~1.6 mm thick). The resulting total excess reactivity measured was 3.89 mk at 33°C (using AECL calibration curve based on RMC pool heating experiments for reactivity adjustment). After some small modifications of the MNCP5 model to capture the actual positioning of the irradiation sites air lines (not known until the reactor container was opened for HEU defuelling), the placement of the Be shim and the actual fuel cage orientation in the core, a slightly revised estimate for the total excess reactivity was obtained. The updated value adjusted to 33°C was 2.19 ± 0.04 mk. Total reactivity difference was therefore of just 0.17%. This result is notably accurate and within the reasonable systematic error resulting from uncertainties in the input data, such as limited precision of the impurities concentration in the beryllium reflectors and structural materials, and possible intrinsic code and cross section data limitations. Absolute reactivity estimates tend to have larger error margins than those for reactivity changes. However, a potentially better estimate, using the former HEU core experimental measurements and MCNP5 simulation results as calibration reference, was not possible, since only the enrichment of the original HEU fuel was known, not its precise composition. Therefore, the error margin of HEU core reactivity estimate could easily be larger than that of LEU core prediction.

2.2.2. Temperature coefficients of reactivity

Despite the lack of reactor pool heating experiments being carried out at JM-1 for direct comparison, the reactivity effects of reactor temperature were also analysed. Previous simulations, carried out as part of the conversion analysis (with a 198-fuel pin core and fully extracted control rod), indicated very good agreement between predicted overall reactivity behaviour as a function of temperature and the AECL curve. The new simulations performed with the 193 fuel pin core and only partially extracted control rod, to better simulate reactor operating conditions, are still close to AECL curve. However, the maximum of the curve is somewhat lower and shifted from 33°C to about 32°C (see Figure 6). The effect that temperature increases in the core coolant, beryllium reflector, water reflector, fuel, core (coolant + fuel) and the whole reactor pool have on reactivity has been estimated. The total effect resulting from the addition of all individual contributions is also shown.

Lacking pool heating experiments as reference to validate AECL curve's applicability to JM-1, the prediction of normal operating conditions, exemplified by the three sample irradiation sessions analysed earlier, was attempted instead from the neutronics point of view. This is a far more complex endeavour, mainly because the temperature distribution throughout the reactor is very difficult to estimate based only on the readings of two thermocouples at the core inlet and outlet. The chosen approach considered the beryllium and water reflectors to be at a uniform temperature equal to that of the inlet. On the other hand, given that the core coolant coefficient is significantly non-linear with temperature, a temperature gradient for the core has been estimated according to the axial power distribution calculated with MCNP5. The coolant temperature coefficient is calculated at 11 points along the height of the core and the overall reactivity effect estimated by a weighted average of each segment thickness. For

every selected point in time along the experiments, the reactivity change between current and initial experimental conditions of the beryllium, core coolant and water reflector were calculated. The xenon concentration, and its corresponding reactivity impact, was estimated according to the measured power profile.

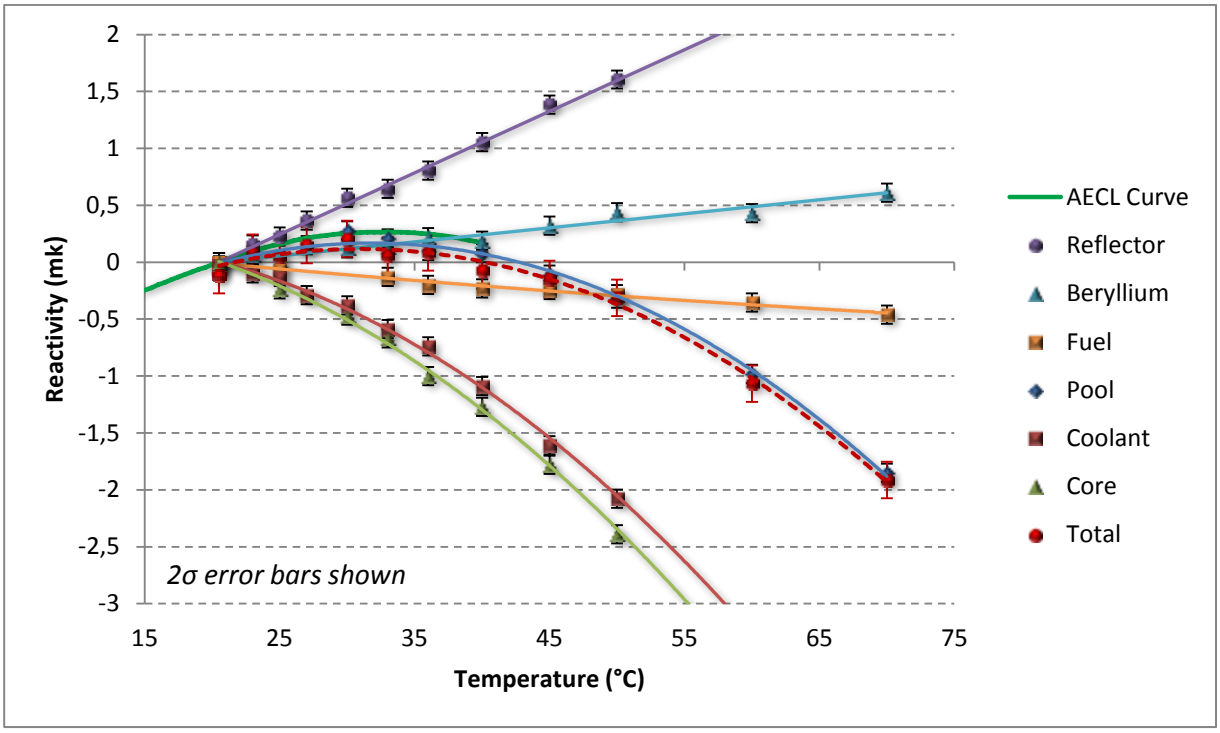

Fig 6. Reactivity feedback effects as a function of temperature

The measured reactivity along the experiments is not directly available either. All that is known is the position of the control rod. With the use of the control rod calibration curve determined during commissioning, the negative reactivity provided by the control rod at any insertion depth could be theoretically determined. However, according to MCNP5 simulations, the worth of the control rod is dependent on core coolant temperature. Total control rod worth would increase by 6% for an average coolant temperature rise from 20.5°C to 70°C. For a measured control rod worth of 5.21 mk at 26°C, the corresponding reactivity change along that range would be of almost 0.3 mk, more than significant enough to be accounted for. The total excess reactivity available also changes slightly between experiments, due to fuel burnup. The actual value is estimated for each test. An additional complication by using actual sample irradiation sessions instead of dedicated tests is the presence of the samples themselves, for which reactivity contribution was estimated according to the control rod position change upon sample extraction from the reactor.

The fuel temperature increase effect on reactivity is calculated according to the fuel temperature predicted by PLTEMP/ANL under those conditions. It should be noted that this temperature is expected to be an upper estimate, since it considers no physical contact between the UO_2 fuel pellets and the zircaloy cladding, forcing all heat transfer through the helium gap. This may be a reasonable assumption, since no pellet swelling is expected in these conditions, though it is still conservative. Therefore, the negative reactivity contribution of the fuel may be slightly overestimated for this reason, resulting in a small overestimation in magnitude of the combined contribution of the reactivity coefficients.

Taking all previous considerations into account, the reactivity results for the three irradiation tests are presented in Figures 7 and 8. The amount of reactivity resulting from the control rod extraction up to its recorded position (and of any irradiation capsules present) is shown in these plots and labelled as “Measured”, though it is actually the estimated value based on previously mentioned calibration and adjustments. Plots also show the combined estimated

magnitude of the negative reactivity resulting from the heating of all reactor components or regions (core coolant, fuel, beryllium and water reflectors) and xenon buildup. This magnitude is plotted in the positive axis to ease the comparison with the positive reactivity inserted. The fuel temperature used as reference is the conservative estimate determined by means of PLTEMP/ANL code. Figure 7 also shows the individual reactivity contributions of the different reactor components. Again, they are shown with opposite sign to ease the comparison.

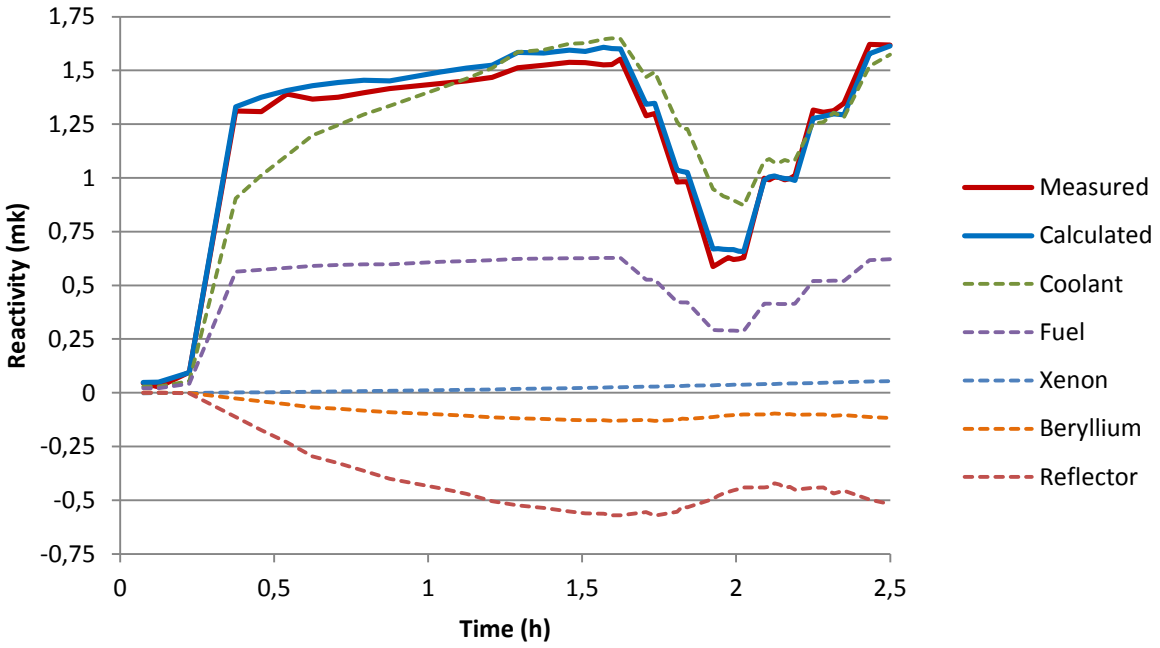

Fig 7. Comparison between measured and calculated reactivity effects (1h irradiation test)

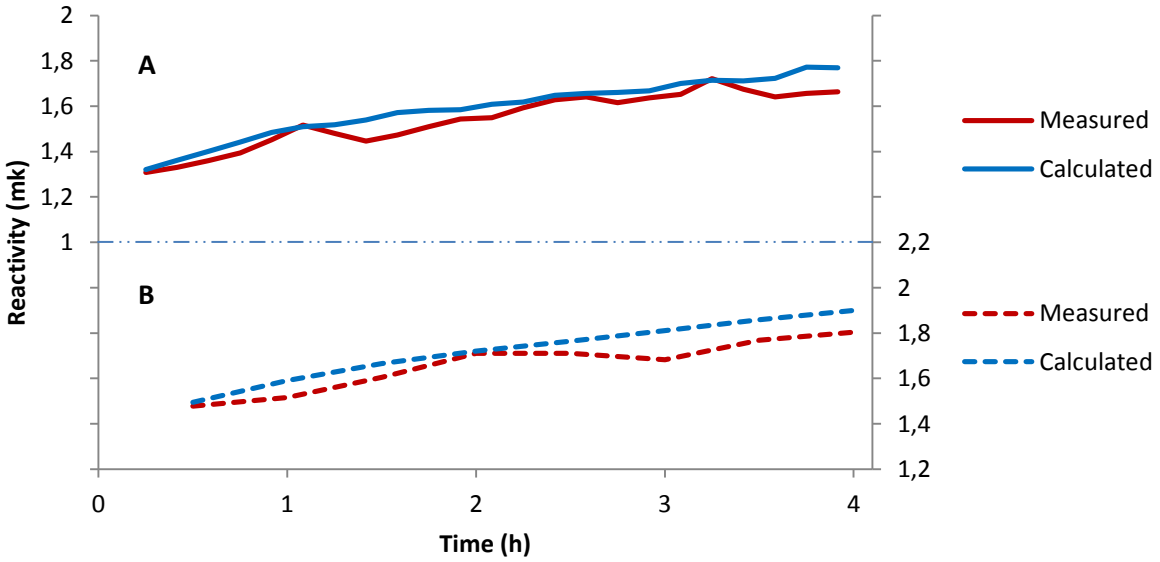

Fig 8. Reactivity evolution comparison (4h irradiation tests A and B)

The agreement of the measured positive reactivity and the estimated negative reactivity magnitude compensating it is quite good in all cases. It should be noted that since the fuel temperature used as reference was conservative, the magnitude of the negative reactivity should be equal or greater than the measured positive reactivity inserted. That is essentially true in all cases except for the last period of Figure 7. It is not clear what may be causing that small divergence. A plausible explanation of some of these discrepancies may be the

existence of complex interactions between reactivity coefficients, in the same way that the worth of the control rod was apparently affected by core coolant temperature. Possible evidence of a variable fuel reactivity coefficient, dependent on both the fuel and core coolant temperatures have been observed in MCNP5 simulation results. The number of available data points in the parameter space and the limitations imposed by the statistical uncertainty of the results prevented a conclusive statement in this regard.

3. Conclusions

A detailed analysis of the available experimental data on the newly converted JM-1 reactor has been performed from both a neutronics and thermal hydraulics point of view. The simulation results obtained using a variety of codes show remarkably good agreement with most measurements. These results provide confidence in the analysis work performed as basis of the reactor conversion and in its conclusions in terms of performance and safety margins of the LEU-fuelled reactor, as well as in the set of tools and methodology used to perform this analysis; valuable for the future conversion of other similar units. At the same, this study provided substantial evidence of the consistent and predictable behaviour of the reactor, while also supporting the soundness of reactor power calibration measurements at JM-1 and RMC. Furthermore, it points out the convenience of examining the suitability of a control rod calibration adjustment as a function of core temperature.

A reactor pool heating experiment and additional reactivity insertion tests at JM-1 are also identified as desirable for future work aimed to precisely measure and predict the reactor reactivity behaviour and its response to transients. Verification of EP steady state data would also be valuable.

4. Acknowledgements

This work is sponsored by the U.S. Department of Energy, National Nuclear Safety Administration (NNSA), Office of Material Management and Minimization (NA-23) Reactor Conversion Program.

5. References

[1] Downs, W.E.; Anderson, M.B.; Smyth, D.L.; McGuire, M.A. “Commissioning of SLOWPOKE-2”, AECL CPSR-326 Rev 1. Ottawa, Canada (May 1973).
[2] Burbidge, G.A.; Jones, R.T.; Townes, B.M. “Commissioning of the SLOWPOKE-2 (RMC) Reactor”, AECL RCC/TR-85-004 Rev 1. Ottawa, Canada (September 1986).
[3] Dennis, H.; Grant, C.; Preston, J.; Puig, F. “JM-1 SLOWPOKE-2 Research Reactor Supporting Analysis Report for the Conversion from HEU to LEU”, International Centre Environmental and Nuclear Sciences, UWI and Nuclear Engineering Division, Argonne National Laboratory, Revision March 30, 2015.
[4] Olson, A.P.; Kalimullah, M. “A User’s Guide to the PLTEMP/ANL Code Version 4.1” ANL/RERTR/TM-11-22, 2011.
[5] Winfield, D.J. “Safety Analysis Report for the École Polytechnique Slowpoke-2 Reactor”, AECL RC-1598, Rev 1. Chalk River, Ontario, Canada (March 1998).
[6] Puig, F.; Dennis, H. “Neutron fluence effects on SLOWPOKE-2 beryllium reflector composition and total reactivity” Nuclear Engineering and Design (under review).

RECENT DEVELOPMENTS IN THE TRIPOLI-4® MONTE-CARLO CODE - APPLICATIONS TO RESEARCH REACTORS

Fadhel MALOUCH(*), Emeric BRUN, Frédéric DAMIAN, François-Xavier HUGOT, Franck LOPEZ, Davide MANCUSI, Odile PETIT, Andrea ZOIA,

Den-Service d'études des réacteurs et de mathématiques appliquées (SERMA), CEA, Université Paris-Saclay, F-91191 Gif-sur-Yvette, France

ABSTRACT

TRIPOLI-4® is a 3D continuous-energy Monte-Carlo particle transport code developed by CEA and devoted to shielding, reactor physics, criticality safety and nuclear instrumentation. The TRIPOLI-4® code includes features useful for research reactors. Additional features are available in the TRIPOLI-4® version 10 released in December 2015. In this paper, we present recent calculations carried out with TRIPOLI-4® for the analysis of two facilities at the CEA-Saclay center: the ORPHEE and OSIRIS research reactors.

1. Introduction

TRIPOLI-4® is a three-dimensional and continuous-energy Monte-Carlo particle transport code developed by the "Service d'Etudes des Réacteurs et de Mathématiques Appliquées" (SERMA), at the CEA-Saclay center. It is devoted to shielding, reactor physics, criticality safety and nuclear instrumentation.

TRIPOLI-4® has been developed starting from the mid of 1990s in C++. A new version of the code is typically released every two years. The TRIPOLI-4® version 9, released in March 2013, included features useful for research reactors. Additional features are available in the TRIPOLI-4® version 10 (released in December 2015).

In this paper, we recall first the key features of the TRIPOLI-4® code. Then, we present an overview of the new capacities of the TRIPOLI-4® version 10 useful for research reactors. Finally, we present recent examples of calculations carried out for the analysis of two facilities at the CEA-Saclay center: the ORPHEE and OSIRIS reactors.

2. TRIPOLI-4® key features [1]

2.1 Tracked particles

TRIPOLI-4® is currently able to simulate four kinds of particles (with coupling):

- Neutrons from 20 MeV down to 10^{-5} eV,
- Photons from 50 MeV down to 1 keV,
- Electrons and positrons from 100 MeV down to 1 keV.

2.2 Nuclear Data

TRIPOLI-4® uses continuous energy cross sections processed with NJOY from any ENDF-6 format evaluation including JEFF-3, ENDF/B-VII, FENDL-2, JENDL-4. TRIPOLI-4® uses also probability tables from CALENDF in the unresolved resonance range.

(*) Corresponding Author (fadhel.malouch@cea.fr)

2.3 Geometry

TRIPOLI-4® has its own geometry module allowing both surface-based and combinatorial representations. TRIPOLI-4® is also directly compatible with a geometry developed in the format of the ROOT software [2]. Thanks to its modularity, the code may be linked with any third party geometry with limited development effort.

2.4 Simulation modes

Three simulation modes are available in the TRIPOLI-4® code:

- "Criticality" mode, used to find the fundamental mode and the associated fundamental eigenvalue of the critical Boltzmann equation.
- "Shielding" mode, fixed-source simulation typically used for radiation protection and shielding analysis.
- "Fixed_Sources_Criticality" mode, fixed source simulation with treatment of fission events, typically used for subcritical fissile instrumentation problems.

2.5 Tallies

A non-exhaustive list of the tallies available in TRIPOLI-4® includes: volume, surface and point fluxes, surface currents, mesh tallies, reaction rates, deposited energy, built-in KERMA response functions, dose equivalent rate, dpa, gamma spectroscopy and effective multiplication factor k_{eff}.

2.6 Variance reduction techniques

Standard variance reduction techniques are available in TRIPOLI-4®, such as implicit capture, particle splitting and Russian roulette. Moreover, TRIPOLI-4® has a special built-in variance reduction module, called INIPOND, based on the Exponential Transform Method, with an automatic pre-calculation of the importance map.

2.7 Doppler broadening of the elastic scattering kernel

For the Doppler broadening of the elastic scattering kernel, the algorithm "Sampling of the Velocity of the Target nucleus" (SVT) is by default used in TRIPOLI-4®. The "Doppler Broadening Rejection Correction" (DBRC) and the "Weight Correction Method" (WCM) have been implemented in TRIPOLI-4® (version 9) to overcome the SVT limitations that affect resonant nuclei (such as ^{238}U) typically in the epithermal region.

2.8 Verification and Validation

The V&V test base is composed of several parts: elementary verification tests, criticality-safety benchmarks, shielding benchmarks, tests concerning parallel operations, tests covering the new features of the code. It includes several ICSBEP and SINBAD benchmarks, as well as proprietary benchmarks concerning CEA experimental facilities from CEA research centers.

3. New features of TRIPOLI-4® version 10 useful for research reactors

3.1 Reactor period calculation [3]

The asymptotic time behavior of neutron transport can be used in reactor start-up analysis or kinetics studies of nuclear systems. In TRIPOLI-4® version 10, the asymptotic reactor period is calculated as the inverse of the dominant eigenvalue (i.e. the fundamental α eigenvalue of the Boltzmann operator). The algorithm is based on a modified α-k power iteration scheme.

3.2 Kinetics parameters computing [4]

Kinetics parameters are key to the study of nuclear reactor dynamics and to safety issues in the context of transient or accidental reactor behavior. The Iterated Fission Probability (IFP) method implemented in TRIPOLI-4® version 10 allows computing the adjoint-weighted

kinetics parameters: the delayed neutron fraction β_{eff}, the mean generation time Λ_{eff}, and the Rossi Alpha $\alpha_{Rossi} = -\beta_{eff}/\Lambda_{eff}$.

3.3 3D core fuel-depletion calculation [5]

TRIPOLI-4® has been recently extended so as to cover depletion calculations by coupling the code to the MENDEL depletion solver developed by SERMA. This coupling allows solving the Boltzmann-Bateman system of equations governing the evolution of materials under neutron irradiation. At a given time step, TRIPOLI-4® computes first the reaction rates in each depleted medium. Then, the MENDEL depletion solver calculates the end-of-step nuclide concentration for each region. TRIPOLI-4® version 10 depletion capability is based on C++ interfaces accessible via CINT (the C++ interpreter of ROOT [2]) that wrap the methods of both TRIPOLI-4® and MENDEL.

3.4 Thick-Target Bremsstrahlung for electromagnetic shower simulation

A simplified simulation mode for the electromagnetic shower, called Thick-Target Bremsstrahlung (TTB), has been implemented in TRIPOLI-4® version 10 to speed up coupled photon-electron-positron calculations. When this option is activated, secondary electrons and positrons produced by photon collisions are not transported, but part of their energy is converted into new bremsstrahlung photons.

3.5 Deposited charge

It is possible to calculate the spectrum of the charge deposited in a given volume by charged particles (electrons and positrons) using the DEPOSITED_CHARGE response recently implemented in TRIPOLI-4® version 10. The charge deposition can be used for nuclear instrumentation in the interpretation of signal of sensors irradiated in nuclear reactors, such as Self-Powered Neutron Detectors (SPNDs).

3.6 Analog neutron or photon transport with analog fission sampling

It is already possible with TRIPOLI-4® to perform a fully analog simulation (concerning both collisions and transport between collisions) for neutron and photon transport. TRIPOLI-4® version 10 enables analog fission simulation by sampling a full fission neutron multiplicity distribution using a coupling between TRIPOLI-4® and an external fission model providing fission sampling data (standard nuclear data libraries provide averaged neutron multiplicities only). It allows addressing time-dependent nuclear instrumentation applications needing detailed correlations between fission chains.

3.7 “Replicate” option upgrading

With TRIPOLI-4®, we can perform a two-step calculation using first a global geometry to store the properties (energy, position, direction, weight) of particles crossing a given surface. Then, we use stored particles as surface sources for simulation on a local geometry. The REPLICATE option activates the particle splitting at the second-step simulation. This technique of variance reduction allows for an improved exploration of the whole phase space, especially when only a limited number of particles has been stored.

4. Recent examples of applications for research reactors

4.1 ORPHEE reactor

ORPHEE is a pool-type research reactor whose main goal is to produce neutron beams for neutron scattering experiments with broad wavelength and energy distributions (Fig 1). The core of ORPHEE is very small in size and highly enriched in ^{235}U, with a heavy water reflector tank (Fig 2).

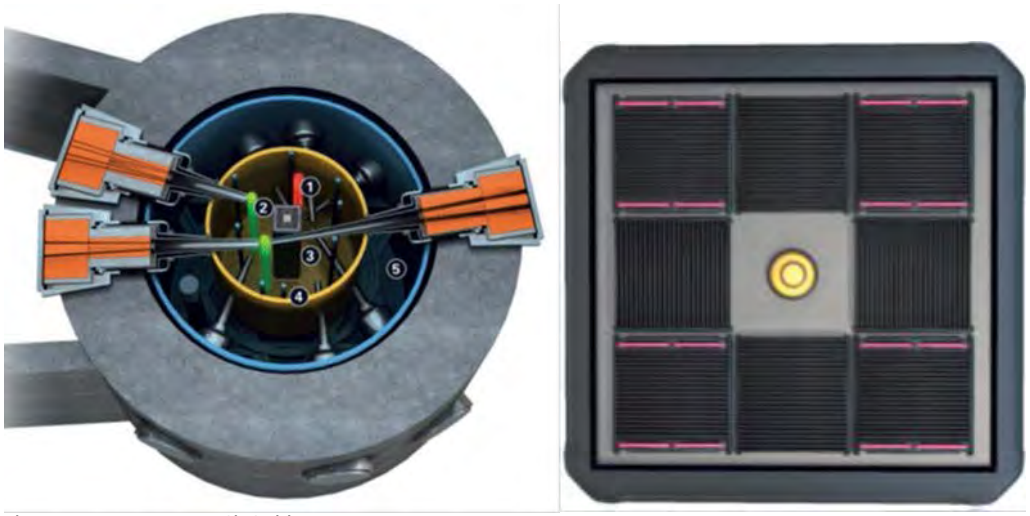

1) Hot neutron source, 2) Cold neutron source,
3) Core, 4) Heavy water vessel, 5) Pool

Fig 1. ORPHEE reactor: Top view (left) and zoom on the core (right)

Monte-Carlo simulations have been recently performed to validate new features of TRIPOLI-4® version 10 against measurements in the case of the ORPHEE reactor [3], [4], [5]. In particular, both prompt and delayed eigenvalues have been computed for a single delayed supercritical configuration of the reactor (Fig 2) with a good agreement with measurements.

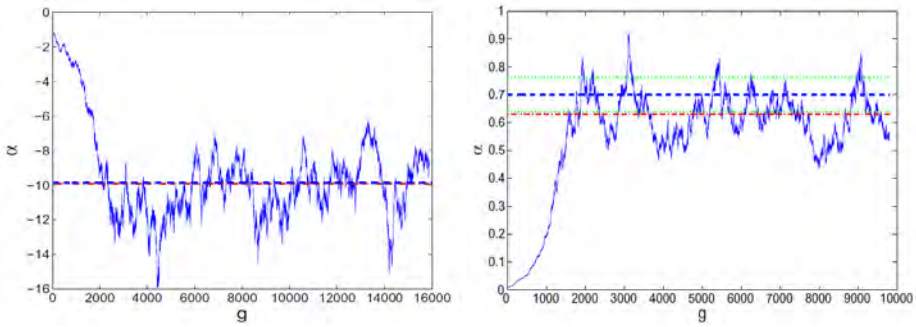

Fig 2. TRIPOLI-4-® simulation convergence of the prompt α eigenvalue (on the left) and the delayed α eigenvalue (on the right) as a function of the number g of generations [3]

The delayed neutron fraction and the Rossi Alpha were calculated using the IFP method for a reactor configuration corresponding to control rod worth calibration [4]. The Monte-Carlo values (β_{eff} = 748 $\pm$ 4 pcm and α_{Rossi} = 41.1 $\pm$ 0.3 s^{-1}) are in agreement with the experimental result for Rossi Alpha and with the deterministic calculation (coming from the APOLLO transport code) for the delayed neutron fraction [4].

In addition, a comprehensive 3D core-depletion analysis has been performed with the TRIPOLI-4® code [5]. Fig 3 and Fig 4 show respectively examples of k_{eff} evolution during irradiation and the radial thermal flux distribution.

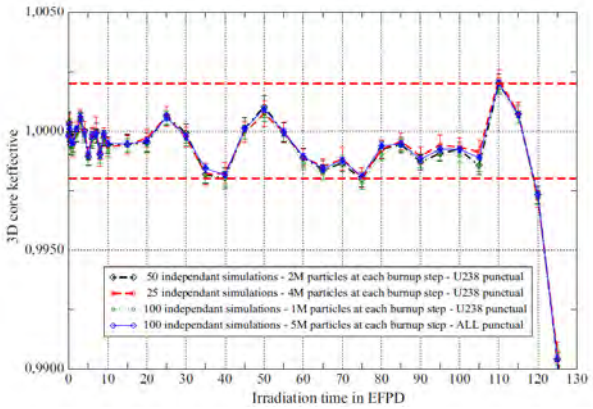

Fig 3. Evolution of the k_{eff} during irradiation. Time is expressed in effective full-power days (EFPD). Controls rods insertion is adjusted during irradiation [5]

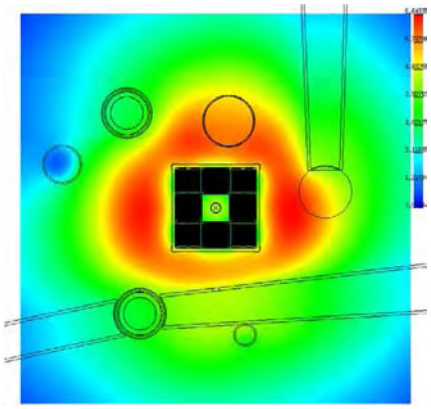

Fig 4. Radial thermal flux distribution of the ORPHEE reactor calculated by TRIPOLI-4-® (3D core-depletion analysis) [5]

4.2 OSIRIS reactor

OSIRIS is a material testing reactor located at CEA-Saclay center and operated from 1966 to 2015. It is a 70 MWth pool type light water reactor with an open and compact core (70×80×90 cm^3). The core tank has a centrally located rack containing 56 cells of 8×8×90 cm^3 each (Fig 5.). These cells are loaded with 38 standard fuel elements, 6 control elements (Hafnium absorber in the upper part and fuel in the lower part) and up to 7 Beryllium elements (south side). The remaining cells are devoted to in-core experiments with high fast neutron flux.

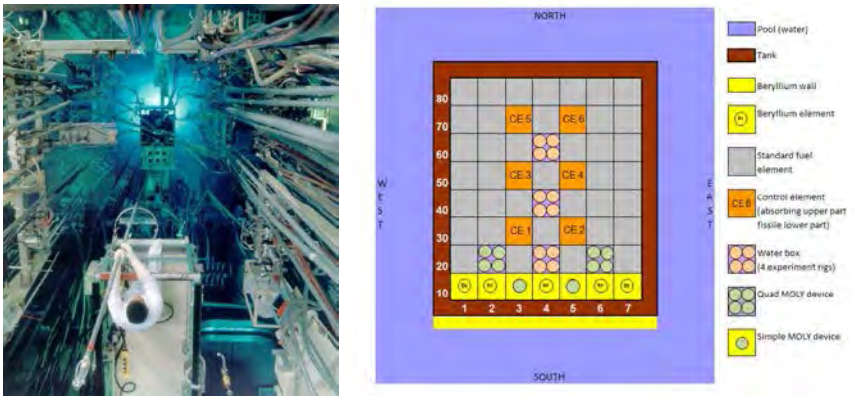

Fig 5. Top view of the OSIRIS reactor and radial cross-section of the core

The first example we show here concerns a nuclear heating calculation using neutron-photon coupled simulation. The goal is to improve the assessment of nuclear heating in reactors [6]. This work consists in developing an innovating and complete coupled neutron-photon calculation scheme for the contribution of neutrons, prompt gamma and decay gamma, based on TRIPOLI-4® (Fig 6 and Fig 7). An experimental validation of the calculation scheme has been performed, based on calorimetry measurements carried out in the OSIRIS reactor.

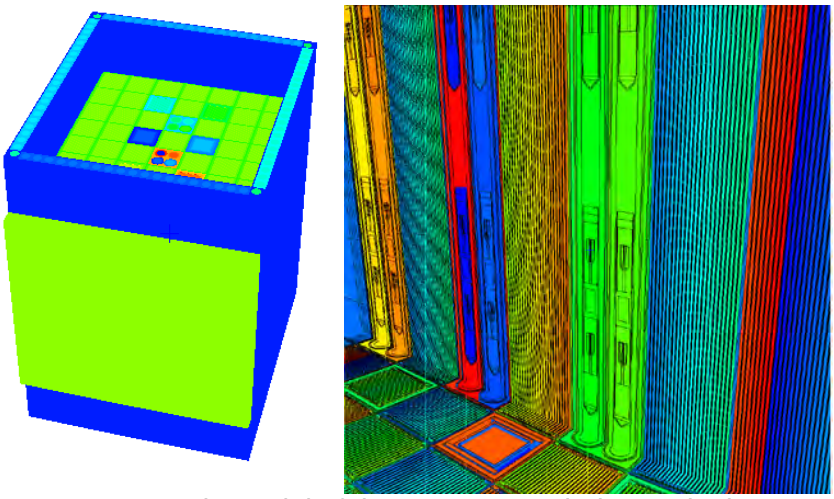

Fig 6. TRIPOLI-4® geometric model of the CALMOS calorimeter in the OSIRIS core [6]

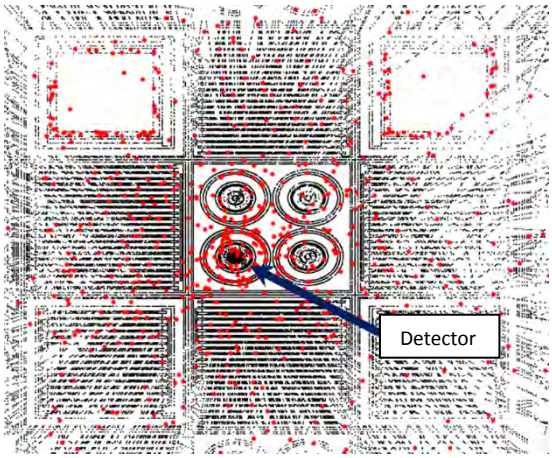

Fig 7. Trajectories of photons from their creation to their interaction in the central water box in the OSIRIS core (representation based on TRIPOLI-4® simulations) [6]

The second example concerns neutron-photon calculations carried out to evaluate neutron and gamma fluxes in the core periphery of the OSIRIS reactor [7]. TRIPOLI-4® Monte-Carlo simulations were performed using a two-step calculation scheme (Fig 8).

In the first step, we use the global geometry to store the characteristics for particles crossing the blue boundary (horizontal cross-section 30 cm x 30 cm) surrounding irradiation locations. In the second step, we use stored particles as surface sources for simulations on a local geometry with particle splitting activated using the “REPLICATE” option (cf. §3.7). In this calculation, each source particle is split in 200 particles (with a statistical weight divided by 200) [7].

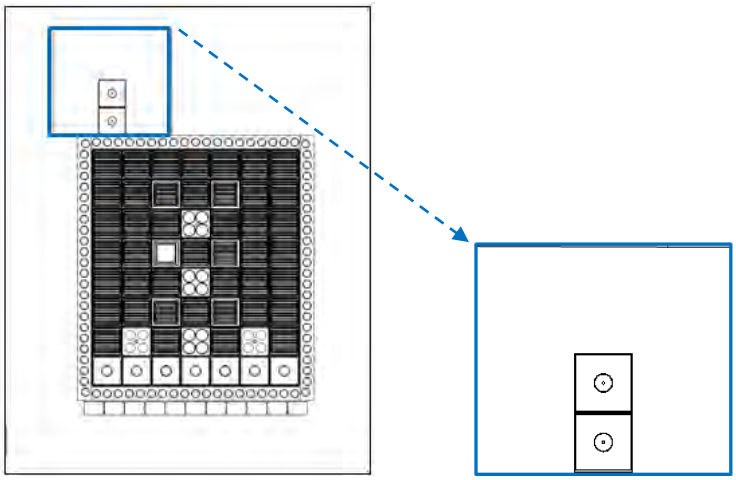

Fig 8. Global and local geometries used in a two-step calculation for the OSIRIS reactor

For the two-step calculation, simulation time was reduced to 1.5 day using 200 processors (20 hours for the first step using the global geometry and 16 hours for the second step using a local geometry). Compter time is then redeuced by a factor of 40 as compared to the one-step calculation (about two months) to reach the same standard deviations ($\sigma < 2\%$).

5. References

[1] E. Brun, F. Damian, C.M. Diop, E. Dumonteil, F.X. Hugot, C. Jouanne, Y.K. Lee, F. Malvagi, A. Mazzolo, O. Petit, J.C. Trama, T. Visonneau, A. Zoia, “TRIPOLI-4®, CEA, EDF and AREVA reference Monte Carlo code”, Annals of Nuclear Energy, Volume 82, August 2015, Pages 151–160

[2] R. Brun, F. Rademakers, “ROOT - An Object Oriented Data Analysis Framework”, Nuclear Instruments and Methods in Physics Research Section A: Accelerators, Spectrometers, Detectors and Associated Equipment, Volume 389, 1997, Pages 81-86. See also http://root.cern.ch

[3] A. Zoia, E. Brun, F. Damian, F. Malvagi, “Monte Carlo methods for period calculations”, Annals of Nuclear Energy, Volume 75, 2015, Pages 627–634

[4] G. Truchet, P. Leconte, A. Santamarina, E. Brun, F. Damian, A. Zoia, ”Computing adjoint-weighted kinetics parameters in TRIPOLI-4® by the Iterated Fission Probability method”, Annals of Nuclear Energy, Volume 85, 2015, Pages 17–26

[5] F. Damian, E. Brun, “ORPHEE research reactor: 3D core depletion calculation using Monte-Carlo code TRIPOLI-4®”, Annals of Nuclear Energy, Volume 82, 2015, Pages 203–216

[6] A. Péron, F. Malouch, C.M. Diop, “Simulation and comparison of the calorimeters measuring the nuclear heating in the OSIRIS reactor, with the TRIPOLI-4® Monte-Carlo code”, IEEE Transactions on Nuclear Science, 2015, Volume 62, Issue 3, Pages 1218–1225

[7] F. Malouch, F. Lopez, L. Barbot, and D. Fourmentel, “Calculation of neutron and gamma fluxes in support to the interpretation of measuring devices irradiated in the core periphery of the OSIRIS Material Testing Reactor” , 4th International Conference ANIMMA 2015 (Advancements in Nuclear Instrumentation Measurement Methods and their Applications), 20-24 April 2015, Lisbon, Portugal

IN-CORE FUEL MANAGEMENT OPTIMISATION OF THE HOR REACTOR USING THE OSCAR-4 CODE SYSTEM

E.B. SCHLÜNZ[a,c,d], A.J.M. WINKELMAN[b], R.H. PRINSLOO[a], P.M. BOKOV[a], J.H. VAN VUUREN[d]

[a] *Radiation and Reactor Theory, The South African Nuclear Energy Corporation SOC Ltd*
PO Box 582, Pretoria, 0001, South Africa

[b] *Reactor Institute Delft, Delft University of Technology*
Building 50, Mekelweg 15, 2629 JB Delft, The Netherlands

[c] *Department of Logistics, Stellenbosch University*
Private Bag X1, Matieland, 7602, South Africa

[d] *Department of Industrial Engineering, Stellenbosch University*
Private Bag X1, Matieland, 7602, South Africa

ABSTRACT

The in-core fuel management optimisation (ICFMO) problem is the problem of finding an optimal fuel reload configuration (or loading pattern) for a nuclear reactor core. ICFMO is known to be a complex optimisation problem. Furthermore, in many cases, multiple (conflicting) objectives are pursued when searching for a best reload configuration. It therefore becomes a difficult task to search manually for reload configurations. Instead, an automated approach is sought which can aid reactor operators with the task of finding good reload configurations. Recently, such an automated approach has been implemented within the OSCAR-4 reactor core calculation system as an optimisation support feature. In this feature, a methodology for single- and multiobjective ICFMO, based on augmented Chebyshev scalarisation and a harmony search algorithm, is used to model and solve an ICFMO problem. In this paper, we apply the OSCAR-4 ICFMO feature to the Hoger Onderwijs Reactor (HOR) located at TU Delft in the Netherlands. Several ICFMO test problems (consisting of different objectives) have been created for the HOR reactor in order to demonstrate the capabilities of the automation tool. A particularly interesting aspect of the ICFMO problem, applied to the HOR reactor, is the stringent shutdown margin constraint which requires the reactor to remain sub-critical when the two most-reactive control rods are fully extracted. The results indicate that the ICFMO feature within OSCAR-4 may be used as an effective decision support tool for finding good-quality reload configurations for the HOR reactor.

1. Introduction

In the in-core fuel management optimisation (ICFMO) problem, an optimal fuel reload configuration for a nuclear reactor core is sought. Problem characteristics for ICFMO include: high dimensionality, discrete variables, nonlinear and non-convex objective functions, and computationally expensive objective function evaluations [1]. In many cases, the problem is also multiobjective in nature, depending on the reactor type and its operational requirements.

The OSCAR (Overall System for the CAlculation of Reactors) code system has been used for several years as the primary calculation tool to support the day-to-day operations of the SAFARI-1 reactor in South Africa [2, 3]. In addition, the OSCAR system has been used to perform core reload and core-follow analyses for two reactors in the Netherlands, namely the High Flux Reactor (HFR) [5] at Petten, and the Hoger Onderwijs Reactor (HOR) [6] at Delft.

The development of an ICFMO module as a new support feature for OSCAR-4 (the latest version of the code system) is motivated by the strong drive towards commercialisation of

research reactors (e.g. via isotope production), as well as the ongoing requirement to service research and development activities. The in-core fuel management strategy becomes a critical component in reactor operations in order to utilise a reactor safely for effective production and research purposes. The use of this ICFMO capability within OSCAR-4, as applied to SAFARI-1, was demonstrated and discussed in [4].

In this paper, the ICFMO feature within OSCAR-4 is applied to the HOR reactor for its core design. HOR is a 2 MW open-pool-type nuclear research reactor. Its core consists of a 6 x 7 lattice which houses sixteen LEU fuel assemblies, four intra-assembly control rods, two in-core irradiation positions, and is surrounded by beryllium reflector assemblies. Furthermore, a number of neutron beams and irradiation facilities surround the core. Of particular interest to fuel reload optimisation in the case of the HOR reactor, is the stringent shutdown margin constraint, which requires that the reactor should remain subcritical with the two most reactive control rods in their fully extracted positions. In meeting this constraint, further optimisation objectives, such as maximising cycle length, optimising beam and in-core fluxes, as well as ensuring good fuel economy, makes for a challenging nuclear engineering task.

In this work we consider several test problem scenarios that have been created for HOR, closely based on an actual core cycle. Each scenario contains different typical reactor utilisation goals. The fuel reload configurations obtained for each of the scenarios are then compared to a typical operational reload strategy.

The paper is organised as follows. Section 2 contains a brief description of the OSCAR-4 code system and the HOR model, followed by Section 3 containing an overview of the ICFMO module. Section 4 starts with a short description of the HOR research reactor, followed by information on the test problem scenarios. The optimisation results are presented in Section 5 and, finally, the conclusions of the paper are reported in Section 6.

2. The OSCAR-4 code system and HOR model

The OSCAR-4 code [2] is a deterministic core calculational system, which utilises response-matrix methods for few-group cross-section generation and multi-group nodal-diffusion methods in search of the three-dimensional global solution. Few-group homogenised cross-sections are generated by the two-dimensional collision-probability-based HEADE code (HEterogeneous Assembly DEpletion) for use in the three-dimensional global diffusion solver. Recently, the Serpent code [7] has also been coupled with OSCAR-4 for large colour-set or full-core-based cross-section generation, as described in [8]. Core calculations are performed with the three-dimensional multi-group nodal-diffusion simulator, called MGRAC (Multi-Group Reactor Analysis Code), which employs the multi-group analytic nodal method.

A new HOR reactor model has been developed using the OSCAR-4/Serpent link, explicitly modelling the in-core and ex-core detail of the reactor in Serpent, and then generating nodal equivalence parameters for each node in the system for use in MGRAC. A node is typically the radial size of a fuel assembly. Axially, an assembly is constructed of 10–12 nodes. In Fig 1, the Serpent model through the axial centre of the reactor is presented on the left, and the nodalisation used in MGRAC on the right. Three such cuts (one axial top, one centre and one bottom) are utilised to generate cross-sections for the full-core nodal diffusion model. In this axially central cut, the R2 beam on the right and the L2 beam on the left are clearly visible. The two in-core irradiation positions, located in the centre and top-left periphery, can also be discerned. The four intra-assembly type control rods diagonally surround the central irradiation position.

The specific cycle of interest applied as test case in this study is cycle 1501 (the first cycle of 2015). In order to generate a reasonable 3D distribution of fuel assembly isotopics, the OSCAR-4 HOR model was used to run a multi-year core-follow history, spanning a time period from 2004 to 2015.

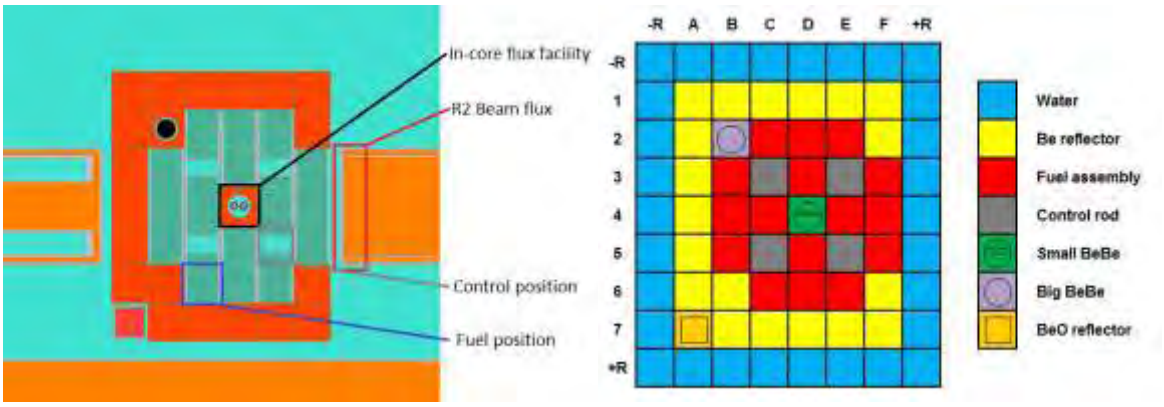

Fig 1. Heterogeneous (left) and nodal (right) central cut through HOR reactor core

3. The optimisation module for ICFMO

The ICFMO module within OSCAR-4 enables decision support in respect of optimising the fuel reload configuration for a reactor core at the beginning of one of its operational cycles. A recently-proposed methodology is employed for the modelling and solution of single- and multiobjective ICFMO problems, for both constrained and unconstrained cases. The reader is referred to [4] for a detailed description of this methodology and only a summary thereof is presented in this paper.

3.1 General working of the module

The optimisation module requires the following data as input: a core layout that indicates the fuel loading positions, a listing of the available fuel assemblies to be loaded into the core, the objective(s) to be pursued along with so-called aspiration levels (see the next section for a description thereof), the constraint(s) that have to be satisfied, and finally, the number of iterations that the optimisation algorithm should perform. The objectives and constraints should be expressible as parameters that may be returned by the OSCAR-4 system.

After the input has been verified as correct, the optimisation algorithm within the module is initialised with random reload configurations (also referred to as solutions hereafter) before iteratively generating new configurations in an attempt to improve the objective functions, as well as satisfy the constraints of the problem. The algorithm may, however, also be initialised with user-defined configuration(s), should this be desired. A newly-generated solution is evaluated by the OSCAR-4 system during each iteration. In the event of a single-objective ICFMO problem, the algorithm yields a single solution, whereas a set of trade-off solutions is yielded for a multiobjective ICFMO problem. In order to accommodate both single-objective and multiobjective problems in the ICFMO module while using the same optimisation algorithm to solve them, a scalarisation approach is adopted for ICFMO problems.

3.2 The augmented Chebyshev scalarising objective function

A reload configuration is represented as a vector $\boldsymbol{x} = [x_1, x_2, \ldots, x_n]$ where $x_i = j$ denotes that fuel assembly j is placed into loading position $i \in \{1,\ldots,n\}$ without repetition. Let $f_k(\boldsymbol{x})$ denote the kth objective function value returned by OSCAR-4 after the evaluation of configuration $\boldsymbol{x}$, for $k = 1,\ldots,q$. These values then form the so-called objective function vector $\boldsymbol{f}(\boldsymbol{x}) = [f_1(\boldsymbol{x}), f_2(\boldsymbol{x}), \ldots, f_k(\boldsymbol{x})]$ corresponding to configuration $\boldsymbol{x}$. The decision maker has to specify, as input to the ICFMO module, an aspiration level α_k for each objective $k = 1,\ldots,q$. An aspiration level is defined here as an objective function value (returned by OSCAR-4) that would satisfy the decision maker. Known target/goal values or unattainable (but realistic) values may therefore be specified.

The scalarising function implemented within the ICFMO module is an augmented Chebyshev function with aspiration levels [9, 10], and is given by

$$\breve{z}_q(\boldsymbol{x}) = \max_{k\in\{1,\ldots q\}} \left| \frac{f_k(\boldsymbol{x}) - \alpha_k}{\alpha_k} \right| + \lambda \sum_{\ell=1}^{q} \left| \frac{f_\ell(\boldsymbol{x}) - \alpha_\ell}{\alpha_\ell} \right|, \quad (1)$$

where λ is a sufficiently small (positive) parameter. The idea behind using this function is to minimise the Chebyshev distance between the objective function vector $\boldsymbol{f}(\boldsymbol{x})$ and the vector formed by the aspiration levels, as seen in the first term of (1). Accordingly, minimisation of $\breve{z}_q(\boldsymbol{x})$ improves the worst deviation between any objective and its corresponding aspiration level at any given time. If the worst deviation cannot be improved, the second term in (1) ensures that improvements in other objectives may still be achieved.

In order to accommodate constraints, an additive penalty function is employed as a constraint handling technique. Accordingly, if a configuration violates any of the constraints, a corresponding penalty is incurred which is related to the magnitude of the violation. The total penalty value of all the constraint violations is then added to the scalarising function to form a composite objective function, to be minimised.

3.3 The harmony search optimisation algorithm

A metaheuristic technique called harmony search (HS) [11] has been adapted for ICFMO and implemented in the module as our optimisation algorithm. The basic HS algorithm consists of the following steps:

1. Initialise a memory structure, referred to as the harmony memory (HM) and fill it with random reload configurations.
2. Improvise (construct) a new configuration according to guidelines that probabilistically consider configurations in the HM, local perturbations and randomisation.
3. Compare this new configuration with the worst-performing one in the HM. Replace the worst-performing configuration with the new configuration if the new one is better.
4. If the stopping criteria are met, terminate the process; otherwise, return to Step 2.

In our implementation of the algorithm, a solution to the ICFMO problem is also represented by the vector $\boldsymbol{x}$, as described earlier. We therefore adapted Step 2 of the algorithm such that non-repeated integer values within the vector are always yielded. Furthermore, we maintain an archive of feasible trade-off solutions obtained during optimisation whenever there are two or more objectives in (1).

4. Optimisation scenarios

In order to demonstrate the capabilities of the ICFMO support feature of OSCAR-4 applied to the HOR reactor, several test problem scenarios have been created. We shall investigate the interrelation of the primary objectives when planning a reload for HOR. First, we have shutdown margin as operational constraint, which requires the reactor to remain sub-critical when the two most-reactive control rods are fully extracted. Then, in order of priority, we have as objectives the maximisation of: cycle length (via excess reactivity as proxy), fuel economy (via single-cycle discharge burn-up as a simplified proxy), beam thermal flux and, central in-core irradiation facility thermal flux. We initially treat each of these four objectives independently, subject to the shutdown margin constraint. Such an analysis provides a good indication of realistic aspiration levels for the individual objectives, when later using them in multiobjective scenarios. Thereafter, we consider various combinations of the objectives, building towards the final scenario where all the objectives are at play simultaneously.

In order to judge the capabilities of the optimisation module, a reference case has been established by loading the fuel assemblies according to a typical operational reload pattern, as extracted from actual historical reload configurations of the HOR reactor. This reference case will hereafter be known as Scenario R.

4.1 Scenario set A: Single-objective optimisation cases

Scenarios A.1–A.4 span the set of single-objective optimisation test cases, addressing respectively, the maximisation of: (A.1) excess reactivity, (A.2) discharge burn-up, (A.3) beam thermal flux, and (A.4) central in-core irradiation facility thermal flux, all subject to the shutdown margin constraint. Since these scenarios each contains only a single objective, the optimisation algorithm yields one reload configuration (the best solution found) as the final result. The objective function value obtained by final reload configuration in each of these scenarios is then compared to the value obtained by the configuration in Scenario R. In scenario A.2, we utilise discharge burn-up at the end of the current cycle as a proxy for long-term fuel economy. Although maximising this proxy this does not guarantee optimal fuel economy in a multi-cycle sense, it serves the purpose of reducing the amount of U-235 discarded at the end of the cycle.

4.2 Scenario set B: Two-objective optimisation cases

Scenarios B.1–B.4 illustrate the benefit of a multiobjective approach, as the outcome of these optimisation calculations is a set of trade-off solutions. We utilise two dimensions for an intermediate analysis, since visualisation of the results become difficult for higher dimensional problems. The obtained set of trade-off solutions allows for post-optimisation selection by the decision maker. In particular, we consider the following scenarios, all subject to the shutdown margin constraint:

- B.1: Maximise excess reactivity and maximise beam thermal flux;
- B.2: Maximise discharge burn-up and maximise beam thermal flux;
- B.3: Maximise excess reactivity and maximise shutdown margin; and
- B.4: Maximise beam thermal flux and maximise central in-core facility thermal flux.

We selected these cases based on the prioritisation proposed by the reload engineer, but we also consider them as building blocks towards understanding of the eventual four-dimensional objective function solution we seek from Scenario C. Note that Scenario B.3 represents an interesting case, as the shutdown margin constraint is simultaneously used as an objective to maximise. This approach yields a set of feasible solutions, thus providing the reload engineer with the option to select from core configurations with varying margins to the safety limit, as a trade-off with the level of excess reactivity.

4.3 Scenario C: Four-objective optimisation case

In this final scenario, the four primary objective functions (cycle length, fuel economy, beam thermal flux and central in-core irradiation facility thermal flux) are combined in a multi-objective maximisation problem, still subject to the shutdown margin constraint. This scenario represents the real day-to-day challenge faced by the HOR reload engineer. For such higher-dimensional cases, a so-called “pay-off” table is presented so as to assist the engineer in selecting a preferred solution from the multi-dimensional trade-off set.

4.4 Summary of scenarios

A summary of all the test problem scenarios is presented in Tab 1. In the table, “shutdown margin measure” represents the level of negative reactivity when the two most reactive control rods are fully extracted, and the remaining two rods are fully inserted. The core is

legal if the sub-criticality level obtained is greater than a predefined safety limit. As such, any shutdown margin measure greater than zero should, in principle, be acceptable.

Objective	Scenario								
	A.1	A.2	A.3	A.4	B.1	B.2	B.3	B.4	C
Excess reactivity	max				max		max		max
Discharge burn-up		max				max			max
Beam thermal flux			max		max	max		max	max
Irradiation facility thermal flux				max				max	max
Shutdown margin							max		
Constraint									
Shutdown margin measure	> safety margin to criticality								

Tab 1: Summary of objectives and constraints within each scenario

5. Results

For all scenarios analysed here, a maximum of 1000 core evaluations were imposed as computational budget limit for placing the 16 available fuel assemblies into 16 possible fuel positions. The control fuel assemblies were loaded in fixed positions according to a typical loading approach and were therefore not considered as part of the optimisation problem.

5.1 Scenario set A: Single-objective optimisation cases

The results obtained for scenario set A are presented in Tab 2 along with that of scenario R. We observe that an improvement in objective function value is achieved in all four scenarios over that of the reference scenario, while adhering to the shutdown margin constraint.

Scenario	Excess reactivity ($)	Cycle burn-up of discharged assembly (%)	Beam thermal flux (n/cm^2/s)	Central facility thermal flux (n/cm^2/s)	Shutdown margin measure (pcm)
R	6.33	2.16	1.57E+13	2.93E+13	50
A.1	6.53	-	-	-	59
A.2	-	2.82	-	-	52
A.3	-	-	1.74E+13	-	1011
A.4	-	-	-	3.08E+13	1484

Tab 2: Results for scenario set A consisting of objective function and constraint values

In terms of percentage, an improvement of 3.20% in excess reactivity is achieved within scenario A.1. Similarly, improvements of 11.3% and 5.12% are achieved in beam thermal flux and central in-core irradiation facility thermal flux, respectively, within scenarios A.3 and A.4 over that of scenario R. In scenario A.2, we consider the amount of within-cycle burn-up of the discharged assembly as the relative quantity (as opposed to absolute discharge burn-up), since the optimisation was only conducted on a single cycle. In this case, an improvement of 30.6% in cycle burn-up of the discharged assembly is achieved over scenario R, as the assembly burned 2.82% in the cycle as opposed to 2.16% in the reference case. In the remainder of this paper, the phrase “discharge burn-up” is used to refer to the amount of burn-up in the cycle experienced by the assembly to be discharged.

In Fig 2, the reload configuration of scenario R and the best configurations found for each of the scenarios in set A are presented visually in terms of the U-235 mass within each fuel assembly. We observe that, in the configuration which improves excess reactivity (A.1), the heaviest assemblies are located near the centre of the core, as expected. Similarly, in the configuration which improves beam thermal flux (A.3), the heaviest assemblies are located in close proximity to the beam tube. Furthermore, in the configuration in which the discharge burn-up is improved (A.2), we observe that the heaviest assemblies are located next to the reflector, with the lightest assembly located, in turn, next to these heavy assemblies and in the central region of the core – all contributing to higher power in the most-burnt assembly.

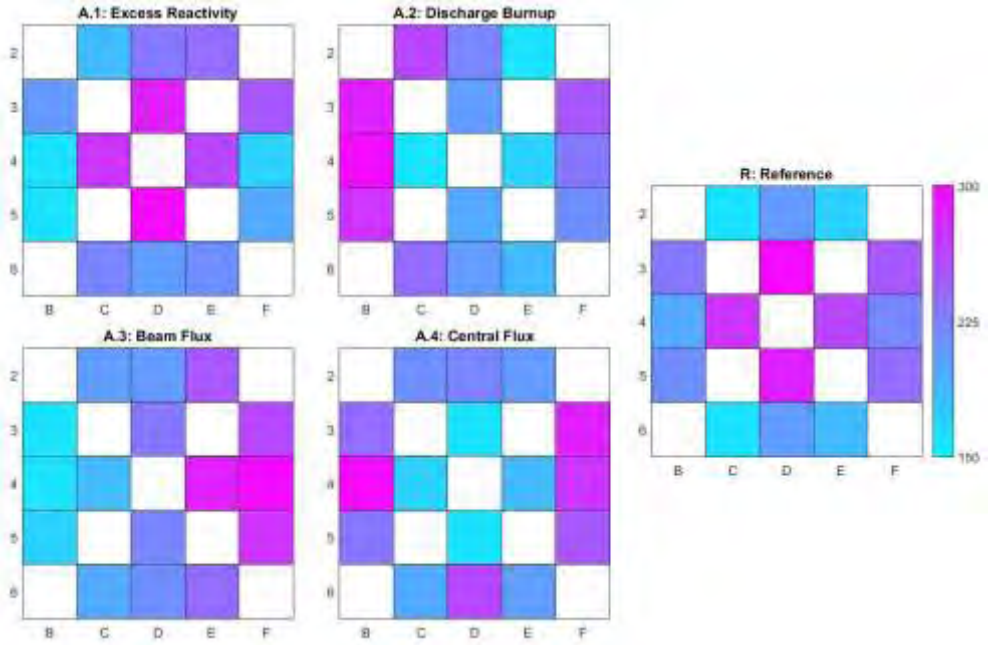

Fig 2. Reload configurations in terms of U-235 mass for the scenarios A.1–A.4 and R

It is, perhaps, less intuitive why the lightest assemblies are located in the centre of the core within the configuration which improves the central in-core irradiation facility thermal flux (A.4). Further analyses of the flux shapes indicate that the reference configuration exhibits an east-west tilt over the core (due to the R2 beam), which is largely flattened by the use of fresh assemblies, as suggested in Scenario A.4. Although the proposed core for A.4 worsens the fast flux in the central facility, the adjustment to the core tilt notably enhances the thermal flux at this position.

5.2 Scenario set B: Two-objective optimisation cases

The results obtained for scenario B.1 are presented in Fig 3 and they consist of the objective function values corresponding to the trade-off set, the best solution found (in terms of scalarising function value) and the reference scenario, as viewed in two-dimensional space. The reload configuration of the best solution found is also presented visually in terms of the U-235 mass within each fuel assembly. We observe that a broad range of configurations are possible at various trade-offs. Furthermore, the optimisation yielded a well-balanced best-found solution in respect of the range of objective values available in the trade-off set. This solution improves the beam thermal flux by approximately 5% to 1.65E+13 n/cm^{2}s over that of the reference solution, at a cost of approximately 2.6% in excess reactivity.

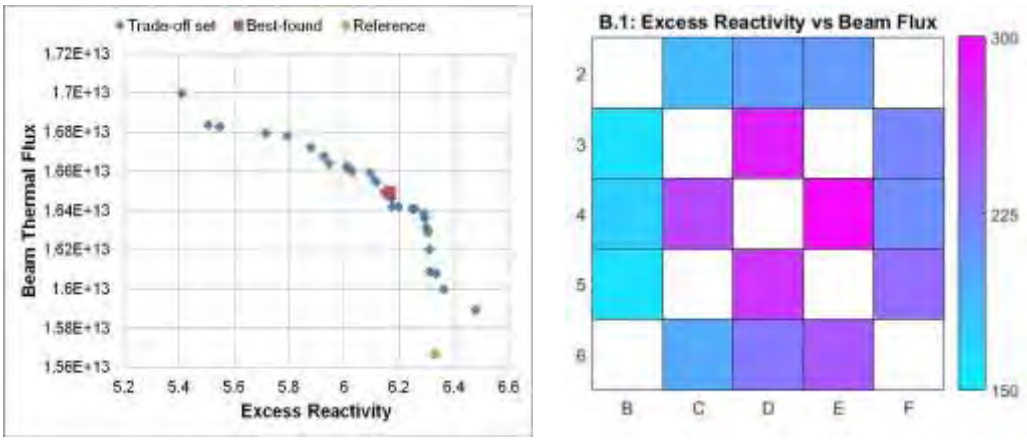

Fig 3. Results for scenario B.1

In Fig 4, the results obtained for scenario B.2 are presented in a similar manner as before. The best solution found in this scenario yields improvements in both the beam thermal flux and the discharge burn-up (i.e. at no trade-off) over that of the reference scenario. We observe in this reload configuration, when compared to the single-objective best-found configurations of scenarios A.2 and A.3, that the heaviest assemblies are located close to the beam tube (as in A.2) whereas the most-burnt assembly is located in position C4 (as in A.3).

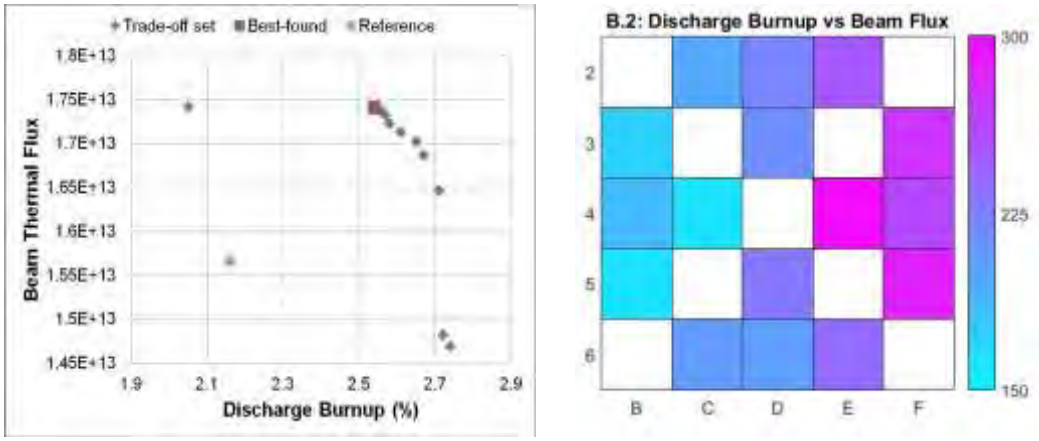

Fig 4. Results for scenario B.2

Finally, the results obtained for scenarios B.3 and B.4 are presented in Fig 5 and consist only of the function values viewed in two-dimensional space. We observe that, for scenario B.3, the reload engineer now has several options to select from with varying shutdown margins to the safety limit, as a trade-off with the level of excess reactivity. Furthermore, in scenario B.4, significant improvements over that of the reference scenario are achievable in the beam and central in-core irradiation facility thermal fluxes, at no trade-off.

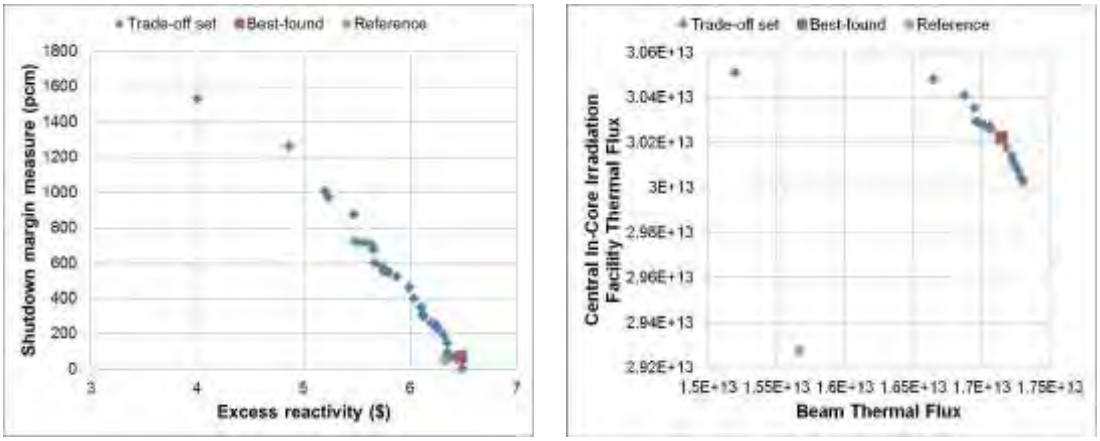

Fig 5. Results for scenarios B.3 and B.4

5.3 Scenario C: Four-objective optimisation case

The results obtained for scenario C consist of a large set of trade-off solutions and are not presented visually due to the four-dimensional nature thereof. Instead, a so-called payoff table is given in Tab 3. Each solution in the trade-off set which yields the best performance in each objective is isolated, and the objective function values corresponding to those solutions constitute the rows in the payoff table. The columns correspond to the different objectives of the problem, and therefore, the shaded entries in the table represent the best value found for each objective. The table represents an approximation of the available ranges obtainable in each objective of the problem instance. This range is visible when observing the data column-wise. Below the objective function values, we also included the corresponding percentage improvement, or deterioration, when compared to the reference scenario R.

	Excess reactivity ($)	Discharge burn-up (%)	Beam thermal flux (n/cm^2/s)	Central facility thermal flux (n/cm^2/s)
Excess reactivity	6.53 (+3.12%)	1.69 (-21.8%)	1.58E+13 (+0.66%)	2.91E+13 (-0.58%)
Discharge burn-up	4.94 (-22.0%)	2.72 (+25.9%)	1.52E+13 (-2.81%)	2.99E+13 (+2.20%)
Beam thermal flux	5.49 (-13.4%)	2.57 (+19.0%)	1.70E+13 (+8.19%)	2.95E+13 (+0.77%)
Central facility thermal flux	4.67 (-26.2%)	2.02 (-6.48%)	1.52E+13 (-2.69%)	3.02E+13 (+3.12%)

Tab 3: Payoff table for the results of scenario C

We observe that the excess reactivity and the discharge burn-up are the most sensitive objectives. Excess reactivity exhibits an approximate range of values from 26.2% worse to 3.12% better, while discharge burn-up varies from 21.8% worse than the reference scenario to 25.9% better. In contrast, the central facility thermal flux is the least sensitive objective, exhibiting a variation from 0.58% worse, to 3.12% better than the reference.

The objective function values corresponding to the best-found solution (in terms of scalarising function value) are presented in Tab 4 along with two other interesting solutions found in the trade-off set. As before, we included the percentage improvement (or deterioration) in objective function value when compared to the reference scenario in brackets below. These three reload configurations are also presented visually in terms of U-235 mass in Fig 6.

	Excess reactivity ($)	Discharge burn-up (%)	Beam thermal flux (n/cm^2/s)	Central facility thermal flux (n/cm^2/s)
Best-found	6.18 (-2.42%)	2.12 (-1.85%)	1.65E+13 (+5.05%)	2.92E+13 (-0.33%)
Alternative 1	6.35 (+0.29%)	2.18 (+0.93%)	1.58E+13 (+1.05%)	2.92E+13 (-0.29%)
Alternative 2	5.49 (-13.34%)	2.59 (+19.91%)	1.68E+13 (+7.21%)	2.96E+13 (+1.03%)

Tab 4: Objective values of selected trade-off solutions for scenario C

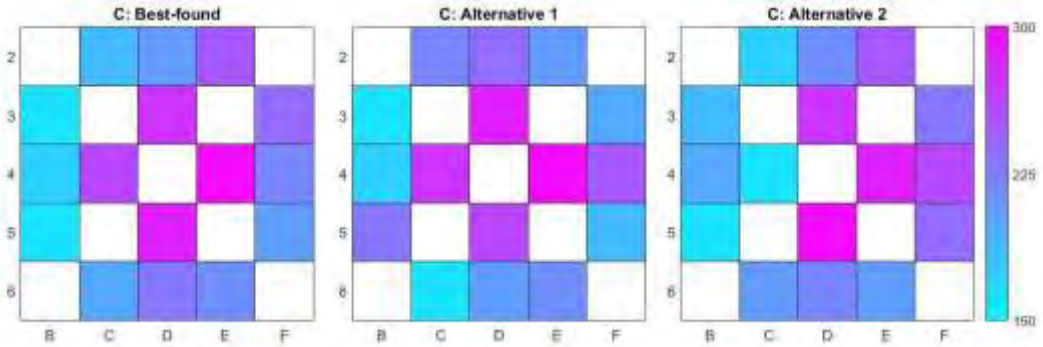

Fig 6. The best-found reload configuration and three alternatives for scenario C

During inspection of Tab 3 and 4, we should note in this analysis, that all objectives were treated largely equally, meaning that the aspiration levels were set to realistically obtainable targets as extracted from the single-objective cases. This is, of course, the intention, so that the resulting set of trade-off solutions could be used for post-optimisation decision making. It would, however, conceivably be possible to "prioritise" the scalarisation process by increasing the aspiration levels of more important objectives. In this case, however, since no bias was introduced in obtaining the best-found solution, an improvement of 5.05% is achieved in the beam thermal flux objective, at the cost of worsening the remaining three objectives (albeit by at most 2.42%, keeping in mind that excess reactivity and discharge

burn-up are sensitive to changes). This may not be acceptable to the reload engineer, hence the need for inspecting the solutions in the trade-off set. For example, alternative 1 yields improvements in the first three objectives, at the cost of the last one. Similarly, alternative 2 yields improvements in the last three objectives, at a cost to the excess reactivity objective (which we observed was sensitive).

These results emphasise the need for the reload engineer to impose his/her specific preferences as decision maker in order to choose the most appropriate reload configuration from the set of mathematically equivalent trade-off solutions yielded by a multiobjective optimisation approach. The ICFMO module within OSCAR-4 should therefore always be viewed as a decision support tool and not a replacement for the reload engineer.

6. Conclusion

In this paper, the application of a new ICFMO support feature within the OSCAR-4 code system to the HOR research reactor has been presented. The case is particularly interesting due to both the stringent shutdown margin criteria applied at HOR, and the multiobjective nature of fuel assembly reload requirements. An augmented Chebyshev scalarising function with aspiration levels has been implemented to model a single or multiple objectives of the ICFMO problem. The solution algorithm employed within the feature is a metaheuristic technique called harmony search, and it has been adapted for our ICFMO purposes.

The ICFMO module yielded improved results on single-objective problem instances when compared to the reference case, as well as a range of good trade-off solutions for the multiobjective problem instances. Of particular interest were some cases which yielded somewhat non-intuitive core loadings (even in the relatively simple single objective cases). This illustrates how such an optimisation method not only assists the reload engineer in obtaining a feasible and near-optimal reload configuration for higher dimensional problems, but may contribute to the understanding of the particular properties of the reactor under consideration.

The approach followed in this paper may also be considered good practice in tackling multi-objective optimisation problems, because single-objective optimisation can supply the aspiration levels needed in multiobjective problems. Solving two-dimensional optimisation problems allow for better understanding of the range and sensitivity of chosen objectives, since these trade-off fronts are simple to visualise. In the four-objective optimisation problem, although the trade-off front is difficult to visualise, a payoff-table can assist with interpreting the range and sensitivities of the objectives, while the scalarising function values can aid in the selection of individual configurations.

Future work may include an investigation of alternatives to the harmony search algorithm as solution scheme. Also of interest is the development of a secondary layer of decision support, via multi-criteria decision analysis techniques, in which, for example, an improved ranking of solutions in the trade-off set is proposed. Lastly, extending the methodology to multi-cycle optimisation may also be investigated.

7. Acknowledgments

The first, fourth and fifth authors (E.B. Schlünz, P.M. Bokov and J.H. van Vuuren) were financially supported in part by the National Research Foundation (NRF) of South Africa (Grants 88003, 96281 and 70593, respectively). Any opinion, finding and conclusion or recommendation expressed in this material is that of the author(s) and the NRF does not accept any liability in this regard.

8. References

[1] J.G. Stevens, K.S. Smith, K.R. Rempe and T.J. Downar, “Optimisation of pressurized water reactor shuffling by simulated annealing with heuristics”, *Nuclear Science and Engineering*, **121**, pp. 67-88, 1995.

[2] G. Stander, R.H. Prinsloo, E. Müller and D.I. Tomašević, “OSCAR-4 code system application to the SAFARI-1 reactor”, *International Conference on the Physics of Reactors (PHYSOR ’08)*, Interlaken, Switzerland, September 14-19, 2008.

[3] G. Ball, “Calculational support provided to SAFARI-1”, *AFRA Regional Conference on Research Reactor Operation, Utilisation and Safety*, Algiers, Algeria, April 10-11, 1999.

[4] E.B. Schlünz, P.M. Bokov, R.H. Prinsloo and J.H. van Vuuren, “A unified methodology for single- and multiobjective in-core fuel management optimisation based on augmented Chebyshev scalarisation and a harmony search algorithm”, *Annals of Nuclear Energy*, **87**, pp. 659-670, 2016.

[5] J.A. Hendriks, C.M. Sciolla, S.C. van der Marck and J. Valkó, “Neutronics validation during conversion to LEU”, *International Conference on the Physics of Reactors (PHYSOR ’06)*, Vancouver, Canada, September 10-14, 2006.

[6] P.F.A. de Leege, H.P.M. Gibcus and F. Reitsma, “Reactivity effects of a research reactor (HOR) during transition of a HEU to LEU core”, *International Conference on the Physics of Reactors (PHYSOR ’02)*, Seoul, South Korea, October 7-10, 2002.

[7] J. Leppänen, PSG2/Serpent – A continuous-energy Monte Carlo reactor physics burn-up calculation code, 2012.

[8] B. Erasmus, R.H. Prinsloo, F.A. van Heerden, S.A. Groenewald, C. Jacobs and M. Mashau, “A full core homogenization approach using Serpent as a cross section generation tool for the OSCAR-4 code system”, *Proceedings of the European Research Reactor Conference (RRFM2015)*, Bucharest, Romania, April 19-23, pp. 305-315, 2015.

[9] T.J. Stewart, “The essential multiobjectivity of linear programming”, *ORiON*, **23**(1), pp. 1-15, 2007.

[10] K. Miettinen, *Nonlinear Multi-objective Optimisation*, Kluwer Academic Publishers, Boston (MA), 1999.

[11] Z.W. Geem, J.H. Kim and G.V. Loganathan, “A new heuristic optimisation algorithm: Harmony search”, *Simulation*, **76**(2), pp. 60-68, 2001.

Operation & Maintenance

FRM II:
NON-DESTRUCTIVE TESTING OF THE PRIMARY COOLING LOOP

A. PICHLMAIER, H. GERSTENBERG, A. KASTENMÜLLER, M. KRESS,
C. KROKOWSKI, M. SCHMIDT

Technische Universität München, Forschungsneutronenquelle Heinz Maier-Leibnitz (FRM II)
Lichtenbergstr. 1, D-85748 Garching, Germany

ABSTRACT

The FRM II is a tank in pool type heavy water moderated multipurpose reactor with 20 MW thermal power. Its 12 beam tubes are mainly used for neutron scattering experiments. However, it also operates a dedicated neutron activation analysis instrument, a tomography facility and a positron source. One beamline is used mainly for medical applications. Furthermore, isotope production and Silicon doping are important activities at the FRM II. The FRM II became critical for the first time on March 2nd, 2004. Since the beginning of routine operation in 2005 it has now completed more than ten years of service.

The applicable regulations require that an extensive test program is in place. All in all, every year almost two thousand scheduled examinations are carried out. Non-destructive testing is an integral part of it. The primary loop, being of utmost importance for safe operation is one of the main focal points of these testing activities. While some examinations are scheduled yearly or before or after every reactor cycle, a major program of non-destructive tests is scheduled to be carried out every five or ten years.

In this paper we discuss the main checks and tests carried out on the FRM II primary cooling loop done both to meet the requirements of operator responsibility and to fulfil the requirements set by the German licensing authorities.

1. Introduction

The FRM II is a tank in pool reactor with 20 MW thermal power. A single fuel element, containing 113 fuel plates with highly enriched Uranium, is cooled by light water and placed in a moderator tank filled with heavy water. This setup yields an unperturbed thermal equivalent flux of 8×10^{14} n/cm²/s over a cycle of 60 days. Generally, the reactor is run for up to four cycles per year. Given its first criticality on Mach 2nd, 2004, the FRM II is the most modern German research reactor.

The main purpose of the FRM II is scientific research in beam tube experiments. However, it also is used for radioisotope production; it operates a Silicon doping facility and an installation for medical treatment. Details can be found in [1].

2. The Primary Cooling Loop

At the FRM II, most components of the primary cooling loop are made of austenitic steel. Only the part that houses the fuel element, the so called central channel, is made of Aluminium (EN AW-5754) in order to be able to get the maximum number of neutrons to experiments and irradiation facilities. Design pressure is 16 bar although in standard operation not more than 8 bar are reached at a temperature of about 50 °C. The total flow of cooling water is about 300 kg/s. The four primary pumps are operating in parallel; each is equipped with a check valve to prevent unwanted backflow. Two more check valves on the high pressure side are to meet the same goal thus creating a comfortable redundancy to

meet the requirements of the applicable design base accident scenarios. An opening in the cooling water loop downstream of the fuel element links the loop to the reactor pool. In case of total loss of power this together with two flapper valves ensures the flow of pool water through the fuel element thus providing a simple and effective removal of residual heat. Normally however, after every shut down of the primary pumps, even when scheduled, e. g. at the end of the operating cycle, three redundant emergency cooling pumps are automatically run for a minimum of three hours for removal of the residual heat. The Fig. 1 shows a schematic overview of the cooling loops at the FRM II, a view into the drained pool with part of the primary cooling loop visible is shown in Fig. *2*.

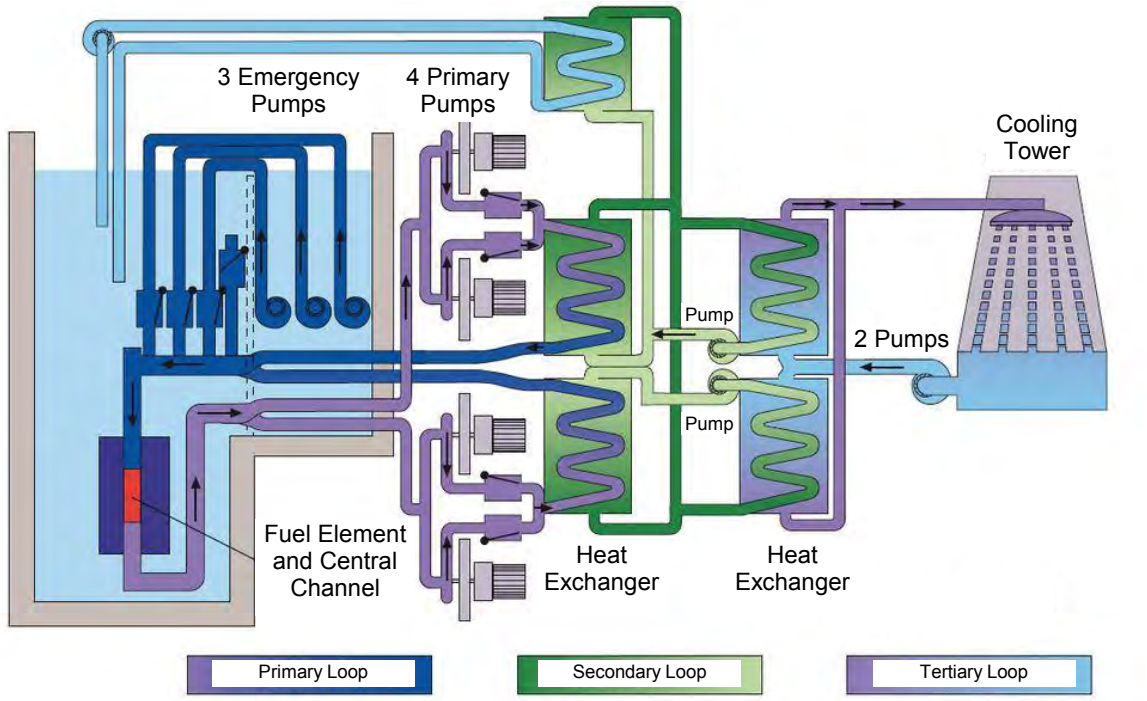

Fig. 1: Schematic layout of the FRM II cooling loops.

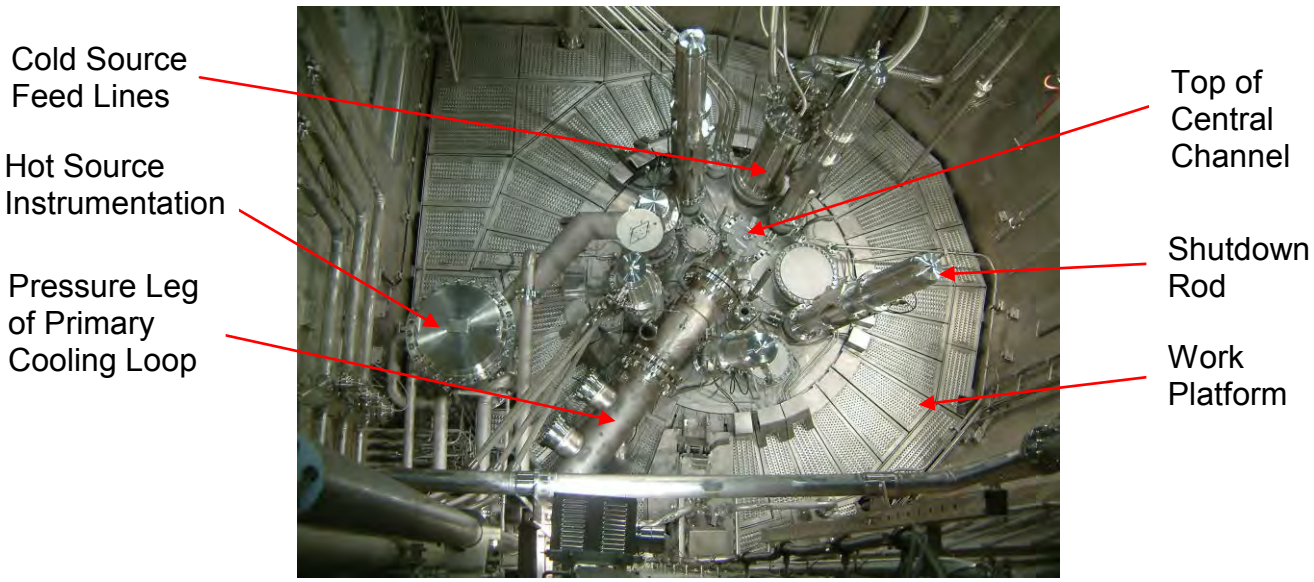

Fig. 2: View into the drained reactor pool. The moderator tank is underneath the work platform and not visible in the picture.

3. The Test Program of the Primary Cooling Loop

Although compared to a nuclear power plant the stress on the primary loop induced by pressure and heat is only marginal (and even less than in some household appliances) an extensive test and monitoring program is in place. Because of the importance of the primary cooling loop for nuclear safety the overwhelming majority of these tests is prescribed in the license and being carried out with external experts present.

While more than one hundred of the most important parameters of the primary loop such as temperature, vibrations, pressure etc. are monitored constantly, on top of these all in all about thirty different scheduled tests are carried out regularly. Goal of these is to guarantee on the one hand the integrity of the primary loop as such and on the other hand the proper functioning of the sensors that monitor the whole system of the primary cooling loop. Some of these are used to trigger emergency measures and therefore are checked with special care in accordance with the licensing requirements. This paper focuses only on the non-destructive tests carried out on the major components of the primary loop itself and does not go into any detail of the ancillary equipment.

The program of non-destructive tests is divided into detailed or more general visual inner and outer inspection, pressure tests, x-ray (RT), ultrasonic (UT) and surface (PT) tests, functional tests and replica tests. As an example, the Fig. 3 shows a robot doing mechanized ultrasonic tests on one of the primary heat exchangers.

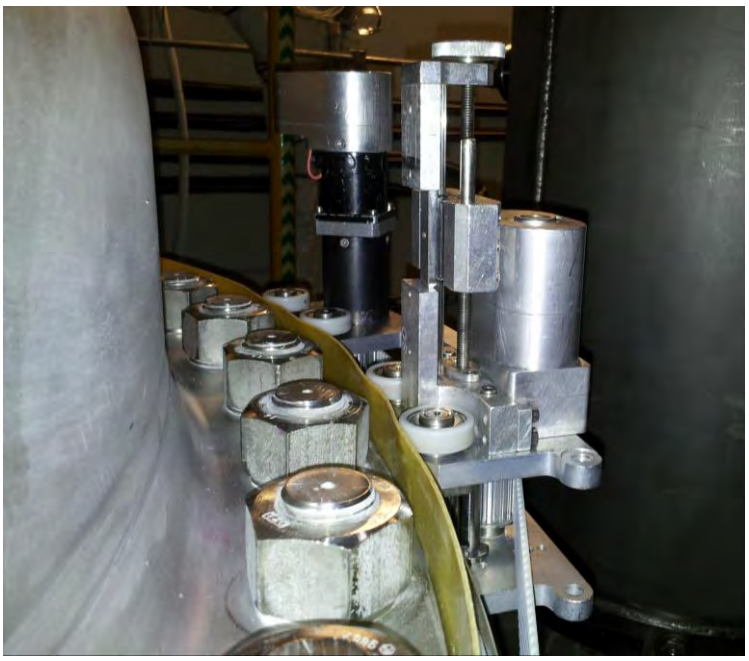

Fig. 3: UT generator and guiding system for mechanized ultrasonic tests (UT) of the primary heat exchanger.

The schedule of all these tests is set by the FRM II operating license according to the classification of the component resulting from the calculated risk associated with its failure. Examples include: replica tests in the central channel surrounding the fuel element after every sixth reactor cycle, UT and RT of the selected components of the whole primary loop every five years in such a way that every component is inspected at least once every ten years. While an integral visual inspection of the whole primary loop is done every year in the form of a scheduled test in accordance with the operating license, selected components undergo VT much more frequently as part of the responsibility of the operator. Pressure tests are done every ten years and are always followed by visual inspection.

The central channel is part of the primary loop and houses the fuel element, cf. Fig. 1. For neutronic reasons it is made from Aluminium EN AW-5754. This material is not typical for nuclear power reactors and the data base on its behaviour under neutron irradiation is slim. The material EN AW-5756 is subject to embrittlement due to changes in the Aluminium matrix under fast neutron irradiation and formation of Silicon due to capture of thermal neutrons on Al-atoms. The first process is relatively benign; the moderate heating during reactor operation turns out to be already an effective remedy. The second, however, is irreversible. At the FRM II we have measured an increase in the Silicon content of the Aluminium from 0.17 % for the fresh material to 0.77 % after an accumulated neutron fluence of about 2.5E22 n/cm², which is equivalent to 3.96 full power years or 26 reactor cycles. This increase in the Silicone content corresponds to a decrease in the yield strain from roughly 22 % to 5.5 % and of the fracture toughness from almost 70 MPa √m to about 27 MPa √m. While the initial concept of aging management foresaw a change of the components made from Aluminium alloys when they had reached a yield strain of less than 5 % recent calculations in combination with these experimental data could show that fracture toughness indeed was the more appropriate parameter to evaluate the component performance. Using this concept an early exchange of the central channel and other components could be avoided thus saving not only cost but also avoiding production of radioactive waste and unnecessary dose for the personnel. The program is ongoing and might even be extended.

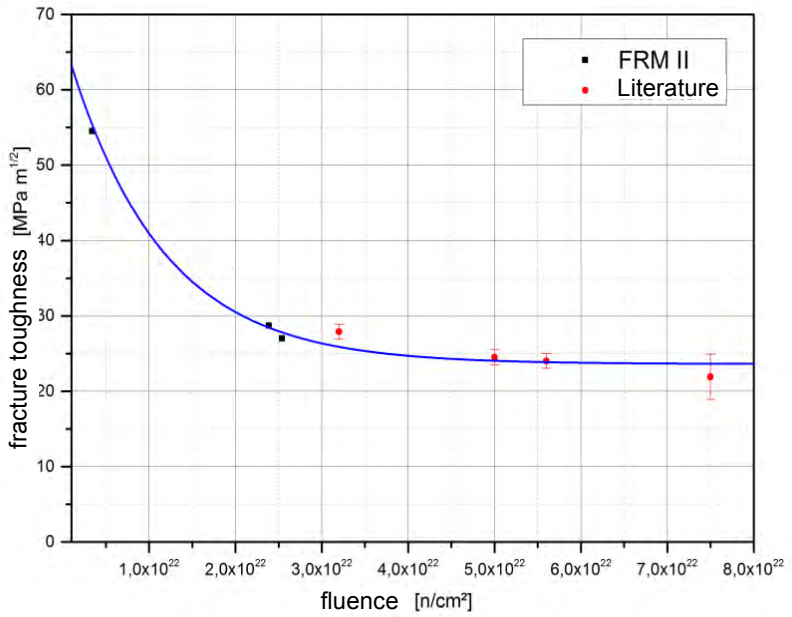

Fig. 4: Extrapolation of K_{Jc}-data measured at FRM II and from literature [2] as a function of neutron fluence. The blue line is an exponential fit to the data meant to guide the eye.

4. Conclusion

In this article, we have given a coarse overview of the main tests and checks carried out on the primary cooling loop of the FRM II. These are an integral part of the concept in place to always guarantee that the parameters specified under the operation license are met. They are also valuable input for constant improvement of the FRM II.

6. References

[1] FRM II description, http://www.frm2.tum.de/die-neutronenquelle/
[2] M. I. de Vries, M. R. Cundy, Results from Post-Mortem Tests with material from the Old Core-Box of the High Flux Reactor (HFR) at Petten, IAEA-SM-310/69P

Nuclide Determination of TRIGA Fuel Elements by Gamma Spectroscopy

D. EICHLEITNER, M. CAGNAZZO, M. VILLA, H. BÖCK
TU Wien
Atominstitut
Stadionallee 2, 1020-Vienna, Austria

ABSTRACT

Fuel elements used at the TRIGA Mark-II reactor located at Atominstitut in Vienna were examined by gamma spectroscopy along the vertical axis. These fuel elements have been used in a TRIGA reactor core in Japan 26 years ago and were transferred through interim storage at Idaho National Lab (INL) to the TRIGA reactor Vienna in October 2012. Therefore only the long lived fission product Cs-137 was expected. For this investigation the fuel elements (FE) were transported from the reactor core with the fuel transfer cask and placed into the fuel scanning device.
The device includes a vertical lifting system to move the fuel in front of a collimator hole for axial gamma scanning using a HP-Ge Gamma detector. Each FE was investigated for peaks and the strongest emission line was detected at 661 keV belonging to Cs-137. Some FE also contained Co-60, Ce-144 and Zr-95. Gamma spectra were recorded every 10 mm along the fuel rod axis resulting in the vertical distribution of the fission products. The activity concentration was calibrated using a standard calibration source of known activity to determine the maximum activity and consequently the burn-up of each fuel element.

1. Introduction

The Vienna TRIGA-Mark II reactor operated by the Atominstitut of the Technical University Vienna is located in Vienna Prater and remains the only operational research reactor in Austria. TRIGA is an abbreviation for "**T**raining, **R**esearch, **I**sotope Production, **G**eneral **A**tomics". This reactor was installed from 1959 to 1962 by the US company "General Atomics" and first went critical on March 7, 1962. Since this date the reactor has been operated without any major problems about 220 days per year. It is a swimming-pool type reactor using standard TRIGA fuel elements. In the past, three different fuel types were used in the core, in November 2012 all these fuel elements were returned to the USA and replaced by low burnt SST clad, 19,8 % enriched TRIGA fuel elements.

On one hand the present work investigates three fuel elements from the current core configuration: The fuel elements were loaded into the Vienna TRIGA core in November 2012, before they were used for a very short period in the Musashi TRIGA reactor in Japan and then they were shipped in 1989 to the Idaho National Lab (INL). Those FE are numbered 9905, 9915 and 9932. These FE were part of the core conversion performed in November 2012 [5] with support of the International Atomic Energy Agency (IAEA) and the United States Department of Energy (DOE).

From August 27 till September 14, 2012, experts from the Atominstitut performed an optical inspection of very low burnt 104-types SST clad LEU elements stored at the INL. Out of a list of one hundred and twenty (120) fuel elements, seventy-seven (77) have been chosen. Seventy-five (75) FE(s) were chosen from the former TRIGA reactor in Musashi, Japan, and two (2) FE(s) from the former TRIGA reactor in Cornell, USA.

- 75 FE came from the reactor in Musashi, Japan
  - This reactor was in operation from January 30, 1963 until March 26, 1985 with Al cladded fuel elements, afterwards the reactor operated from July 25, 1985 till December 21, 1989 with SST cladded fuel elements, the average burn up is in the range below 1%

- 2 FE came from the reactor at Cornell University, USA
  - Initial criticality January 12, 1963, shut down date April 21, 2003,the burn up is slightly above 1%

Furthermore three additional fuel elements from the current core had been measured which belong to the ATI and were installed in the reactor core for several years.

On the other hand eight fuel elements were investigated which had cooled down in the pool storage racks inside the reactor tank for several years. The operational data are shown in Tab 2.

The objective of this work was to gamma-scan some of these fuel rods and to determine the type and amount of individual fission products. For this purpose an existing Fuel Scanning Machine (FSM) developed by the ATI [7] was used in combination with a gamma ray detector to scan the vertical axis of the fuel rods. The raw measurement data of those scans were then transferred to a special application module to display the results in form of gamma spectra. The results were investigated for peaks at certain energies, traceable to certain fission products contained in the fuel elements due to the fuel history.

The detector calibration was done with several different known gamma sources to provide reliable results. From the obtained spectra it is possible to calculate the exact burn-up of each measured fuel element by comparing the data with an available TRIGA fuel sample with exactly know burn-up. This method of fuel burn-up determination has been published previously in /2,5/.

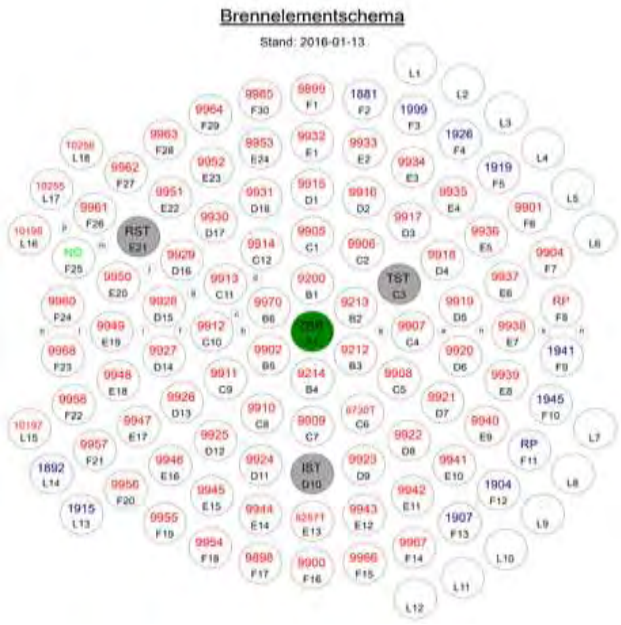

Fig 1: Schematic overview of the fuel element positions

All the investigated fuel elements are of the type 104: their geometrical and material specifications are shown in Table 1.

Fuel element type	Type 104
Fuel moderator material	U-Zr-H1,65
Uranium content (wt. %)	8.5
Enrichment (%)	19,8
Erbium content (%)	0
Diameter x length of fuel meat (cm)	3.63 x 38.1
Graphite reflector length (cm)	8.81
Cladding material	304 SS
Cladding thickness (mm)	0.51

Tab 1: Geometrical and material specifications of the FE Type 104

FE No.	Detetced Nuclides	Date of last Irradiation	Date of measurement	Current position
9972	137-Cs	21/12/1989	12/01/2015	Stored
9973	137-Cs	21/12/1989	13/01/2015	Stored
9974	137-Cs	21/12/1989	14/01/2015	Stored
10255	137-Cs, 60-Co	21/04/2003	15/01/2015	Stored
10256	137-Cs, 60-Co	21/04/2003	21/01/2015	Stored
10197	137-Cs, 60-Co	27/04/2012	26/01/2015	Stored
10198	137-Cs, 60-Co	27/04/2012	28/01/2015	Stored
9959	137-Cs, 60-Co, 95-Zr, 144-Ce	14/04/2014	29/01/2015	Stored
9213	137-Cs, 60-Co, 95-Zr, 144-Ce	25/03/2015	01/12/2015	B2
9214	137-Cs, 60-Co, 95-Zr, 144-Ce	25/03/2015	02/12/2015	B4
9200	137-Cs, 60-Co, 95-Zr, 144-Ce	25/03/2015	02/12/2015	B1
9905	137-Cs, 60-Co, 95-Zr, 144-Ce	25/03/2015	03/12/2015	C1
9915	137-Cs, 60-Co, 95-Zr, 144-Ce	25/03/2015	03/12/2015	D1
9932	137-Cs, 60-Co, 95-Zr, 144-Ce	25/03/2015	03/12/2015	E1

Tab 2: Measured Fuel Elements.

3. Experimental Setup

The fuel elements were transferred from the core with a special lead transfer cask to the “Fuel Scanning Machine” (FSM) by a crane. This machine (Fig.2) allows scanning the elements along the vertical axis and to raise the fuel rods exactly into the desired measurement position. Data were acquired in steps of 10 mm. A collimator concentrates the gamma rays of the element directly to the gamma detector. In the experimental setup a High Purity Germanium (HP-Ge) detector was used. A preamplifier allows to shape the detected decay into an electronic signal that can be further processed. Due to high count rates of the fission product decays a „Multi Channel Analyzer“ (MCA) had to be used, which rejects electronic noise and background radiation and converts the analog signal into a digital signal. The incoming signals are separated into groups with similar energy and are separated into channels. 8192 channels were used for a more detailed result. [1, 3]

However, only one signal at a time can be processed, therefore a gate closes during the conversion process. The closed time is called „Dead Time“ (DT). Incoming signals during DT cannot be processed. To accommodate to this circumstance the measurement time („Real Time“ RT) gets longer to accomplish the planned measurement time („Live Time“ LT)

$$RT = LT + DT$$

With this setup gamma spectra can be transferred to the computer, by plotting the count rates per channel. After calibrating the detector by a source of known activity, each channel can be clearly identified by its energy. The basic equation is given by:

$$\mathrm{E} = \mathrm{S} * \mathrm{Channel} + \mathrm{O}$$

S is referred as the Slope and O is the Offset.

Fig 2: The experimental Fuel Scanning Machine (FSM) set up developed at Atominstitut

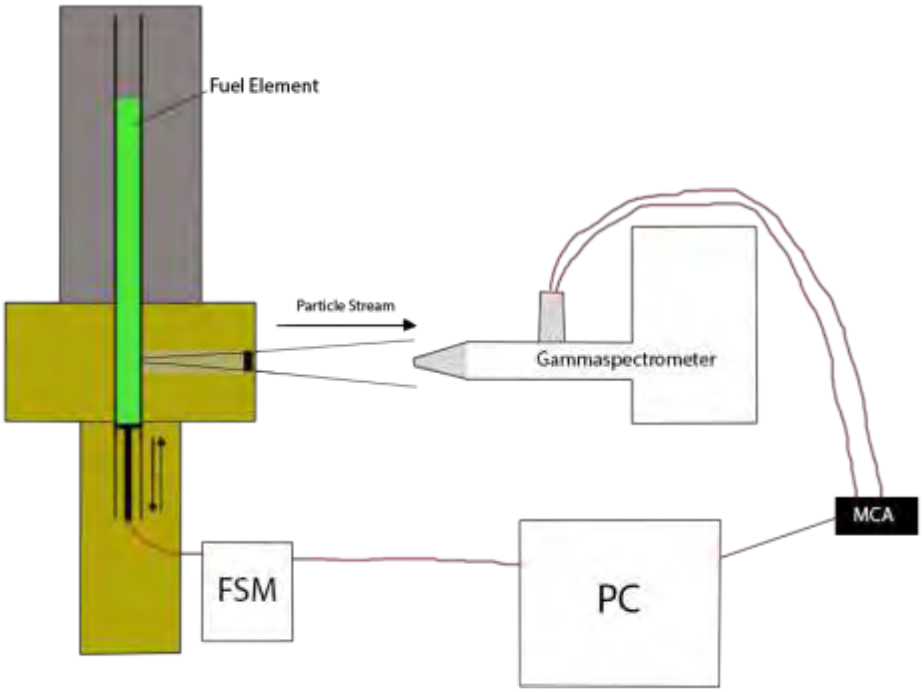

Figure 3 shows a typical measured gamma spectrum which includes peaks of Cs-137, Zr-95 and Co-60, this fuel element was the last time exposed to operation on April 14th 2014 with approx. 8 month of decay time.

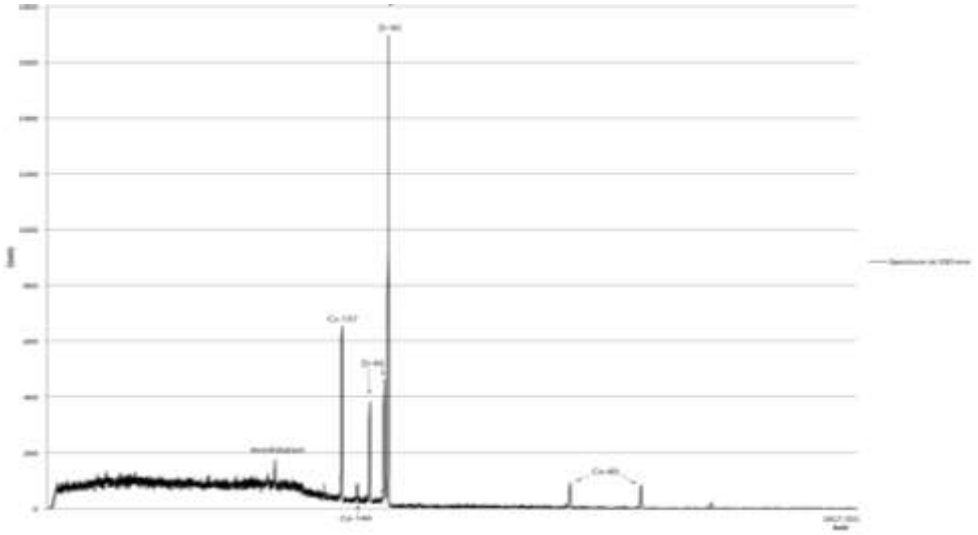

Fig 3: Measured Gamma Spectrum of fuel element 9959

4. Results and Discussions

Due to the fuel cooling time of about 26 years, only Caesium -137 was found in the fuel rods 9972 to 9974 as a fission product. The spectra from the fuel elements 10255, 10256, 10197 and 10198 furthermore contain Co-60, caused from their activated cladding material. All other measured fuel rods contained further nuclides due to a shorter decay time such as Zr-95 and Ce-144. Figure 4 presents the axial distribution of Cs-137 along the length of the measured FE 9200. The axial Cs-137 profile (i.e. maximum in the centre and decreases along the length) follows the axial flux distribution. The two small peaks at the upper and lower end of the FE show the effect of two axial graphite reflectors at both ends of the fuel meat (see Figure 4).

As expected fuel elements with similar history provide similar data. Those fuel rods which were stored inside the reactor tank for almost 26 years emit much lower radiation levels and mostly at 661 keV belonging to Cs-137. Fuel elements with SST cladding material are emitting Co-60 as well originating from cobalt traces in the stainless steel cladding.

Three fuel elements imported from the Musashi Reactor (9905, 9915, 9932) show a decreasing radiation level due to a decreasing flux density at the outer parts of the reactor core, correlating to their position at B1-E1 (Fig 1.). In Table 3 all maxima of Cs-137 activities (at 350 mm measurement position) are given.

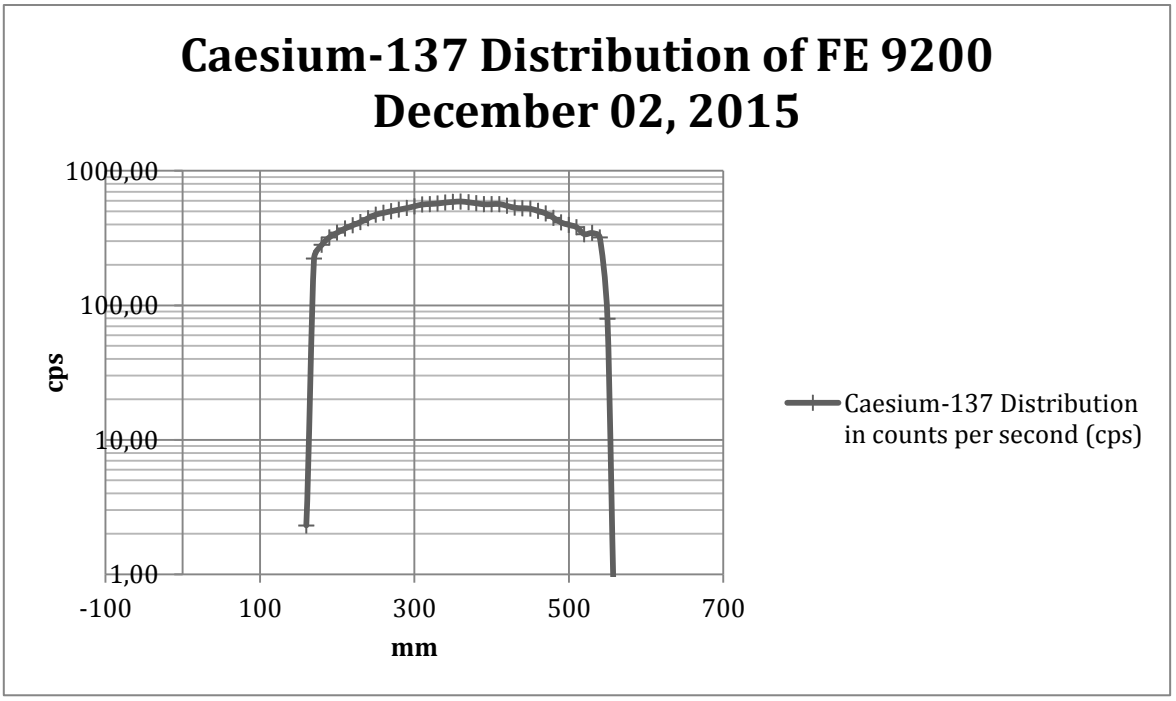

Fig 4: Result-spectrum of FE 9200 - Cs-137 distribution along vertical axis

FE No.	Max. Activity [Bq]	Date Of Measurement
9972	3,84 E+07	12/01/2015
9973	2,11 E+07	13/01/2015
9974	4,83 E+07	14/01/2015
10255	1,75 E+08	15/01/2015
10256	1,70 E+08	21/01/2015
10197	1,03 E+09	26/01/2015
10198	6,48 E+08	28/01/2015
9959	1,56 E+08	29/01/2015
9213	6,01 E+08	01/12/2015
9214	6,54 E+08	02/12/2015
9200	1,93 E+09	02/12/2015
9905	7,53 E+08	03/12/2015
9915	6,95 E+08	03/12/2015
9932	5,17 E+08	03/12/2015

Tab 3: Maxima of Cs-137 Activities

5. Conclusion

During the period from initial start-up in 1962 to April 2012 the TRIGA reactor Vienna operated with a mixed core using three types of fuel elements such as LEU-Al clad type 102, LEU-SST clad 104 and HEU-FLIP-SST clad fuel elements. During this period the FSM helped to verify the fuel burn-up and to optimize the fuel utilization. This results of these experiments were published in [2,6].

After the fuel swap between Atominstitut and Idaho National Lab. in October 2012 /4/ the TRIGA core is now composed of identical type LEU-SST clad type 104 fuel elements. However these fuel elements have different irradiation histories as described in this paper. In order to optimize their lifetime in the reactor core, fuel scanning measurements have been carried out, the results allow to determine the individual TRIGA fuel burn-up and to plan reshuffling of individual fuel elements within the 87 core positions available in the TRIGA core Vienna to achieve a maximum reactor operation lifetime.

6. References

1. Aquino, Benigno. "Determination of Fission Product Distribution in HEU and LEU TRIGA Fuel Elements by Gamma Spectroscopy" Diploma Thesis. Vienna University of Technology. 2013 Vienna; Austria

2. R. Khan, S. Karimzadeh, H. Böck, M. Villa “Triga Fuel Burn-Up Calculations Supported by Gamma Scanning” RRFM Conference 2009 Vienna 22-25.3.2009

3. GBS Elektronik GmbH. "MCA-527 Digital Multi-Channel Analyzer: User Manual". GBS-Elektronik GmbH. Germany

4. M. Villa, R. Bergmann, A. Musilek, J.H. Sterba, H. Böck, C. Messick: "The Core Conversion of the TRIGA Reactor Vienna"; "22nd International Conference Nuclear Energy for New Europe (NENE2013)", Nuclear Society of Slovenia; Nuclear Society of Slovenia, Ljubljana, 2013, ISBN: 978-961-6207-36-2, Paper-Nr. 602

5. R. Khan, S. Karimzadeh, H. Böck, M. Villa, T. Stummer ” Burn Up Calculations and Validation By Gamma Scanning of A Triga HEU Fuel“ RRFM Conference Prague 18-22.3.2012

6. S. Karimzadeh, R. Khan, H. Böck : „Gamma spectrometry inspection of TRIGA Mark II fuel using Caesium isotopes“ Nuclear Engineering and Design. Vol 241 (2011), 118-123

7. H.Böck, G.Allmer:” A combined gamma scanning and optical inspection system for spent TRIGA fuel” 12.US TRIGA Conference, University of Texas, Austin, March 9-11.1990

RADIATION DAMAGE INDUCED IN ZIRCALOY-4 BY 2.6 MEV PROTON: APPLICATION FOR NUCLEAR RESEARCH REACTOR

M. Izerrouken, O. Menchi, H. Medjkoun
Nuclear Research Center of Draria, Bp. 43 Sebbala, Draria, Algiers, Algeria

N. Souami
Nuclear Research Center of Algiers, 2 Bd. Frantz Fanon, BP 399, Alger gare, Algeria

A. Sari
Nuclear Research Center of Birine, BP 108, Ain-Oussera, Djelfa, Algeria

ABSTRACT

The present investigation is devoted to study radiation damage induced in Ziconium alloys (zircaloy-4) by proton irradiation. The structure and morphology modification were investigated using X-ray diffraction (DRX), optical microscopy (OM) and scanning electronic microscopy (SEM). The irradiation has been performed at iThemba LABS, South Africa using Van de Graaff accelerator at energy of 2.6 MeV up to a fluence of 10^{17} p/cm^2. X-ray diffraction analysis reveals that the domain size decreases while the microstrain increases after irradiation to a fluence of 10^{17} p/cm^2. It is found from OM and SEM analysis that the grain size is reduced after irradiation. SEM analysis shows precipitates with cylindrical geometry after irradiation at fluence of 10^{17} p/cm^2 attributed to the hydride precipitates. The experimental data indicates the damage formation during the early stage of irradiation in zircaloy-4.

1. Introduction

Zirconium alloys is well used in nuclear technology as fuel cladding, structural materials and pressurize pipe due to its several properties. It exhibits a good resistance to radiation damage, good corrosion resistance and very low thermal neutron absorption cross section. Recently, several authors have been reported proton irradiation test on the zirconium alloys [1-8]. As well known, the fast neutron generated by the fission reaction with average energy of 2 MeV losses its energy mainly via elastic scattering reactions with hydrogen of coolant water. The recoil protons diffuse in the zirconium cladding material and cause high defect concentration along their path.
In the frame of the ageing management of nuclear research reactor, it is very interesting to evaluate the defect induced in Zirconium alloys by recoil protons. For this purpose, we report in the present communication, a study of the effects of proton irradiation on the morphological and structural properties of the Zircaloy-4.

2. Experimental

The sample investigated in this study is Zircaloy-4 with a thickness of about 2 mm. The chemical composition of the main elements is 1.6 wt% Sn, 0.21 wt% Fe, 0.08 wt% Cr, 0.1 wt% O, 0.29 wt% (Fe+Cr) and 97.7 wt% Zr. Small pieces with size of about 5 mm x 5 mm, were cut from the same zirconium plate by a diamond saw. 2.6 MeV proton beam irradiation was performed at iThemba LABS, South Africa using Van de Graaff accelerator. The irradiations were carried out at room temperature in a vacuum chamber at 5×10^{-6} mbar with proton flux of 10^{13} p/cm^2.s. The displacement damage calculated using SRIM 2003 code with displacement energy of 40 eV and using the “Quick” Kinchin and Peace damage calculation is shown in Fig 1. [9]. The maximum damage (peak damage) is induced at depth of about 43

μm corresponding to the projected range of 2.6 MeV protons in zirconium. The number of displacement per atom (n_{dpa}) was calculated by [10]:

$$n_{dpa} = \frac{\phi.N_d.A}{\rho.d.N_A} \quad (1)$$

where ϕ is the proton fluence, N_d is the number of displacements per ion, A is the molecular mass of the target material, ρ is the density, d is the penetration depth, N_A is Avogadro's number. The n_{dpa} at peak damage corresponding to proton fluences of 10^{16} and 10^{17} p/cm^2 are respectively, 0.0017 and 0.017. After irradiation the microstructure and structural modification are observed using Zeiss, Axio teck 100 optical microscopy (OM), scanning electronic microscope ESEM, XR 30 and X-Ray diffraction, X' PERT PRO MPD Philips diffractometer.

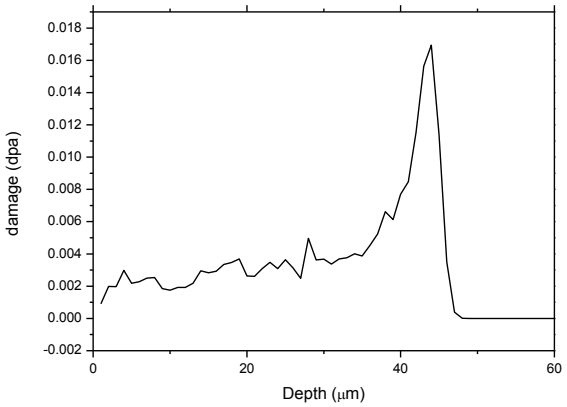

Fig 1. SRIM calculations of n_{dpa} for 2.6 MeV protons at fluence of 10^{17} p/cm^2.

3. Results and discussion

3.1. Structure analysis

X-ray diffraction patterns obtained before and after irradiation at fluences of 10^{16} and 10^{17} p/cm^2 are shown in Fig 2. The main observed diffraction peaks (002), (101), (102), (103) and (004) correspond to the hexagonal Zr-phase. After irradiation one can see that the intensity of (002) peak decreases while that of (101) peak increases (Fig 3.). The same results were observed in pulsed electron beam irradiated zirconium-702 [11]. It was interpreted as a crystallographic texture change.

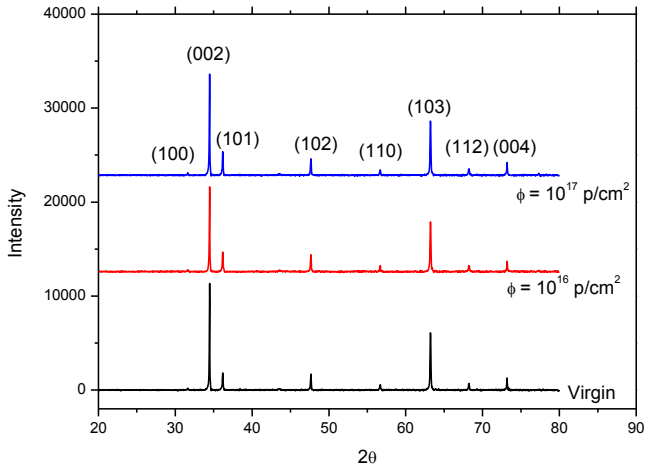

Fig 2. XRD patterns of zircaloy-4 before and after 2.6 MeV proton irradiation at different fluences

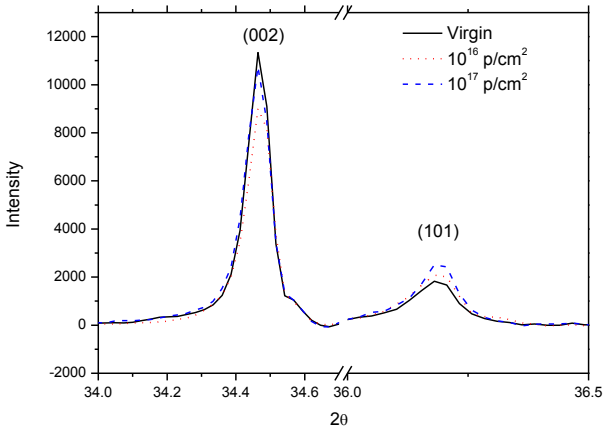

Fig 3. (002) and (101) peaks intensity evolution versus 2.6 MeV proton fluence

According to Williamson-Hall (W-H) technique, the line broadening is due to the contribution of small particle size and microstrain [12]. Using this approach, the integral breath β is related to the domain size D_v and microstrain ε by:

$$\frac{\beta\cos(\theta)}{\lambda} = \frac{1}{D_v} + 4\varepsilon\left(\frac{\sin(\theta)}{\lambda}\right) \qquad (2)$$

where θ is the Bragg angle. A plot of $\left(\frac{\beta\cos(\theta)}{\lambda}\right)$ as a function $4\left(\frac{\sin(\theta)}{\lambda}\right)$ (Fig 4.) gives the domain size and microstrain. The obtained results are reported in table one.

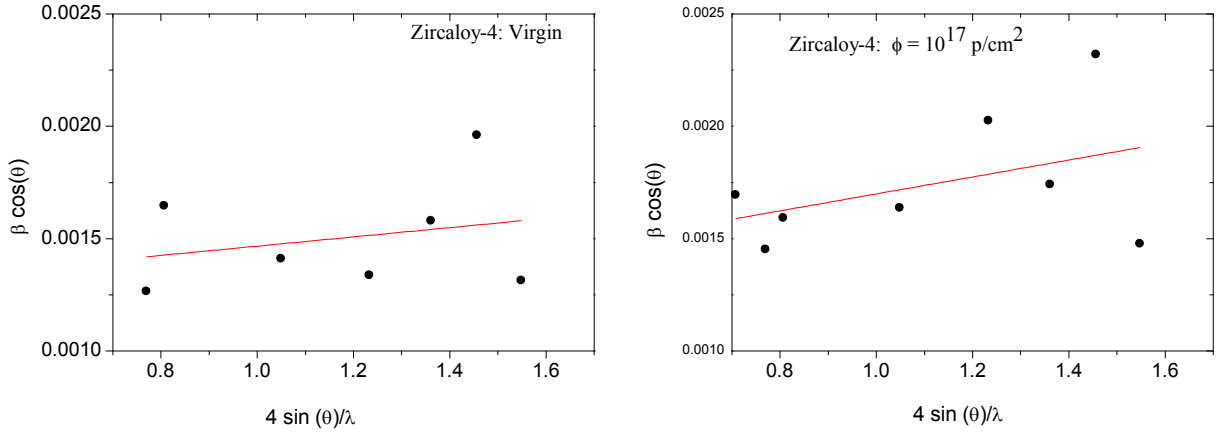

Fig 4. W-H plot for virgin and 2.6 MeV proton irradiated zircaloy-4.

Fluence (p/cm^2)	D_v (Å)	ε (%)
Virgin	793.6	2.1 x10^{-4}
10^{16}	694.4	3.1 x10^{-4}
10^{17}	757.6	3.8 x10^{-4}

Tab 1: Domain size and microstrain values obtained using Williamson-Hall (W-H) plot.

From the table one, one can see that the domain size decreases while the microstrain increases after 2.6 MeV proton irradiation. Similar results were reported by Neogy et al. [13] in the case of Zr-1wt.% Nb irradiated by 5 MeV proton in the same fluence range. The same behavior was also observed in Zr-1.0% Nb-1.0% Sn-0.1% Fe irradiated with 145 MeV Ne^{+6} ions [14]. Taking into account Neogy et al. [13] results, the domain size reduction can be attributed to the dislocation loops formation. However, it is well known from previous studies that loops are formed in zircaloy-4 irradiated by 2 MeV proton at higher doses (> 2 dpa) [15-17].

3.2. Morphology analysis

Fig 5. shows the optical microscopy of zircaloy-4 samples before and after irradiation to 10^{17} p/cm^2. Before analysis, the samples were submitted to fine polishing with alumina slurry and then chemically etched in 10%HF + 45% HNO3 + 45% distilled water in order to reveal grain boundaries. As can be seen, the virgin sample shows a large grain size. After irradiation the grain size is reduced indicating that important damage are produced along the proton path in zircaloy-4. This is well demonstrated by SEM analysis (Fig 6.) where one can see small cavities on the sample surface.

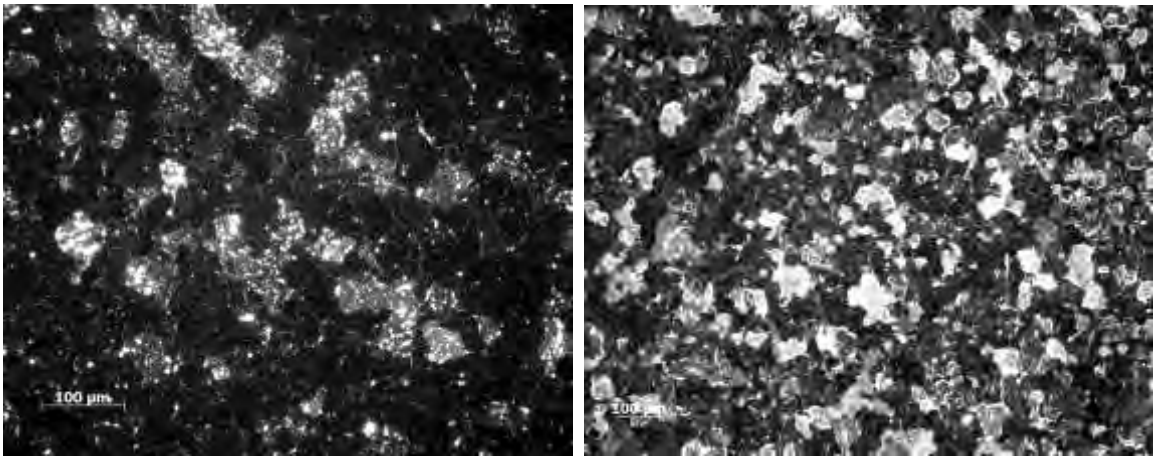

(a) (b)

Fig 5. Optical morphology of zirconium-4 before (a) and after (b) irradiation with 2.6 MeV proton to a fluence of 10^{17} p/cm^2.

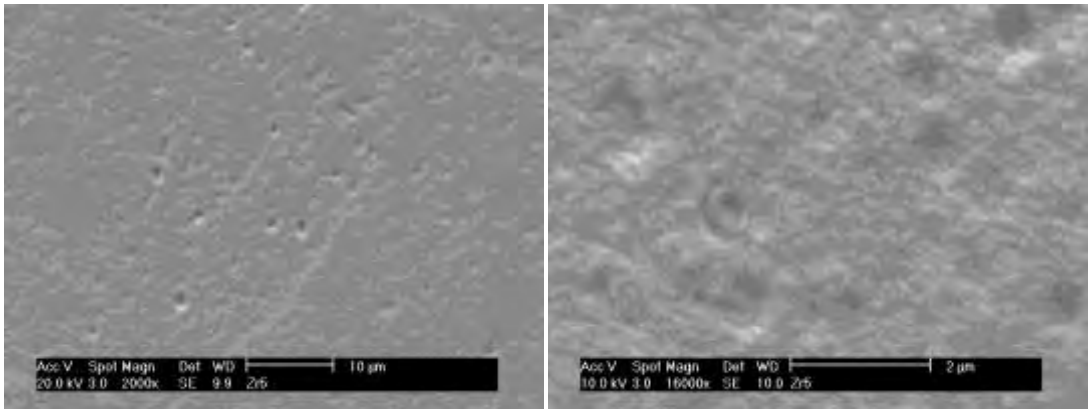

Fig 6. SEM micrographs of 2.6 MeV proton irradiated zirconium-4 to a fluence of 10^{17} p/cm^2 showing cavities on the sample surface

In order to check the damaged induced along the proton depth, a cross sectional of the irradiated sample was performed. Before SEM analysis, the samples were mechanically polished using SiC paper (grits 180 - 600), and then followed by chemical etching in 3%HF +

47% HNO3 + 50% distilled water. The cross-sectional micrographs obtained are presented in Fig 7. The irradiated side shows thin damaged layer with smaller grain (Fig 7b.) compared to the virgin side (Fig 7a). In addition microcacks appear on the surface grain (Fig 7d). However, the analysis of the damaged peak region (located between 35 and 43 µm) shows precipitates with cylindrical geometry (indicated by arrows in Fig 8.) attributed to the hydride precipitates. Though, further studies are needed to confirm this result.

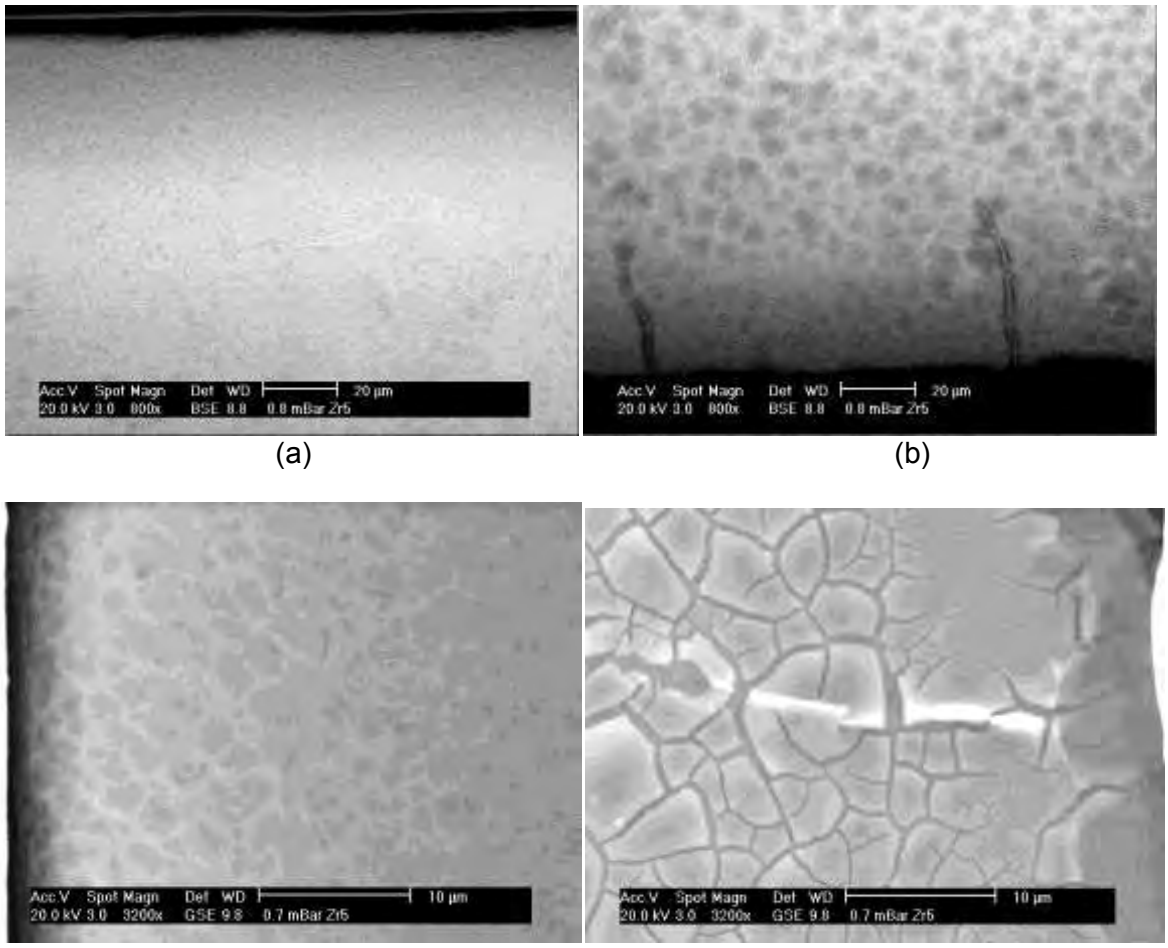

Fig 7. Cross-section SEM micrographs of zircaloy-4. (a) and (c) virgin side. (b) and (d) irradiation side to a fluence of 10^{17} p/cm^2.

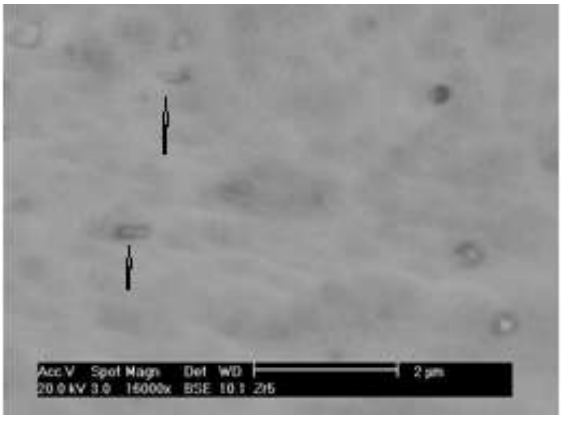

Fig 8. SEM analysis of the damaged peak region (located between 35 and 43 µm) showing precipitates after 2.6 MeV proton irradiation to a fluence of 10^{17} p/cm^2.

4. Conclusion

Zircaloy-4 fuel cladding material was bombarded with 2.6 MeV proton up to a fluence of 10^{17} p/cm^2 at room temperature. According to the experimental data, it is clear that zircaloy-4 properties modification start even at low fluence. It is found:

- 2.6 MeV proton irradiation to fluence of 10^{17} p/cm^2 induces a change in the zircaloy-4 crystallographic texture. The domain size decreases and the microstrain increases after irradiation to a fluence of 10^{17} p/cm^2 indicating the dislocation loops formation.
- Microcracks are shown on the grain surface after irradiation to a fluence of 10^{17} p/cm^2.

This suggests the formation of high defect concentration along the proton depth which affects the zircaloy-4 mechanical properties even at low fluence. This indicates the damage formation during the early stage of irradiation.

Acknowledgements
This work is performed in frame of the CRP project: Establishment of Material Properties Database for Irradiated Core Structural Components for Continued Safe Operation and Lifetime Extension of Ageing Research Reactors. IAEA Research contract N° 17881.

References

[1] G. E. Lucas, M. Surprenant, J. Dimarzo, G. J. Brown, J. Nucl. Mater 101 (1981) 78-91
[2] J. J. Kai, W. I. Huang and H. Y. Chou, J. Nucl. Mater 170 (1990) 193-209
[3] C.D. Cann, C.B. So, R.C. Styles a and C.E. Coleman, J. Nucl. Mater 205 (1993) 267-272.
[4] G.S. Was, T.R. Allen, J.T. Busby, J. Gan, D. Damcott, D. Carter, M. Atzmon, E.A. Kenik, 270 (1999) 96±114
[5] C.K. Chow, R.A. Holt, C.H. Woo, C.B. So, J. of Nucl. Mater. 328 (2004) 1–10.
[6] G. S. Was, J. T. Busby, T. Allen, E. A. Kenik, A. Jensson, S. M. Bruemmer, J. Gan, A. D. Edwards, P. M. Scott, P. L. Anderson, J. Nucl. Mater, 300 (2002)198-216.
[7] H. H. Shen, S. M. Peng, X. Xiang, F. N. Naab, K. Sun, X. T. Zu, J. Nucl. Mater, 452 (2014)335-342.
[8] Chunguang yan, Rongshan Wang, Yanli Wang, Xitao Wang, and Guanghai Bai, Nucl. Eng. Technol 47 (2015) 323-331
[9] F. Ziegler, J.P. Biersack , U. Littmarck, 1985 the stopping and Range of ions in solids (New York: Pergamon) ‘‘http://www.srim.org/’’.
[10] R.M. Hengstler-Eger, P. Baldo, L. Beck, J. Dorner, K. Ertl, P.B. Hoffmann, C. Hugenschmidt, M.A. Kirk, W. Petry, P. Pikart, A. Rempel, j. nucl. Mater. 423 (2012) 170–182.
[11] Shen Yang, Jie Cai, Peng Lv, Conglin Zhang, Wei Huang, Qingfeng Guan, Nucl. Instr. and Meth. B 358 (2015) 151-159.
[12] G. K. Williamson, W. H. Hall, Acta Metall. 1 (1953) 22-31.
[13] S. Neogy, P. Mukherjee, A.P. Srivastava, M.N. Singh, N. Gayathri, A.K. Sinha, D. Srivastava, G.K. Dey, J. Alloy. Compd. 640 (2015) 175–182.
[14] A. Sarkar, P. Muherjee, P. Barat, J. Nucl. Mater. 372 (2008) 285-292.
[15] L. Tournadre, F. Onimus, J.-L. Béchade, D. Gilbon, J.-M. Cloué, J.-P. Mardon, X. Feaugas, O. Toader, C. Bachelet, j. Nucl. Mater. 425 (2012) 76–82
[16] L. Tournadre, F. Onimus, J.-L. Béchade, D. Gilbon, J.-M. Cloué, J.-P. Mardon, X. Feaugas, J. Nucl. Mater 441 (2013) 222–231
[17] E. M. Francis, A. Harte, P. Frankel, S. J. Haigh, D. Jädernäs, J. Romeo, L. Hallstadius, M. Preuss, J. Nucl. Mater. 454 (2014)387-397.

A FACILITY INFRASTRUCTURE MANAGEMENT SYSTEM FOR THE JM-1 SLOWPOKE RESEARCH REACTOR.

J.A. PRESTON, H.T. DENNIS, R.D.CUSHNIE

International Centre for Environmental and Nuclear Sciences,
University of the West Indies Mona Campus,
2 Anguilla Crescent, Kingston 7, Jamaica

ABSTRACT

The JM-1 20kW SLOWPOKE Research Reactor at the International Centre for Environmental and Nuclear Sciences, University of the West Indies Mona Campus in Kingston Jamaica was installed in 1984, and has been successfully used for mainly neutron activation analysis in geochemical, agricultural, environmental and health studies. The facility has also cooperated with the IAEA in the establishment of the Caribbean Research Reactor Coalition (CRRC) with reactors in Colombia and Mexico, to increase regional access to research reactor services and nuclear-related education and training. The HEU core of the reactor has just been replaced with a LEU core under the GTRI programme, and the facility is readying itself for the next 40 years of operation. During the first 30 years, much experience has been gained on the types and frequency of component failures, character of preventative maintenance required, and general data gathering and curation needs to minimize downtime and increase utilization. As it embarks on the next 40 years of operation, the facility is developing a software based facility infrastructure management system (FIMS) to assist its small core technical and operating staff in managing both reactor operation and utilization issues. This paper describes the system, its architecture, features, and implementation plan. As the amount of sensor and utilization data increases, tools to analyse and provide insight on status and trends will guide operation, maintenance and utilization, to ensure maximum efficiency in all areas.

1. Introduction

1.1 Background

The JM-1 SLOWPOKE-2 research reactor at the International Centre for Environmental and Nuclear Sciences (ICENS), University of the West Indies, Mona Campus, Jamaica, was built by Atomic Energy of Canada Limited (AECL), and commissioned in 1984. It has operated safely and reliably for over thirty years, where it has been used for neutron activation analysis (NAA) in geochemical, agricultural, environmental and health studies, and the teaching of nuclear analytical techniques[1,2]. The facility has just completed a replacement of the original high enrichment uranium (HEU) core with a low enrichment uranium (LEU) one under the GTRI programme, and is readying itself for the next 40 years of operation.

During the initial 30+ years of reactor operation there have been relatively few issues, with the majority related to auxiliary systems which comprise: a source of low-pressure service water for the pool water cooling system make up; a 50 litre tank of compressed air to operate components in the NAA irradiation systems, and pool water purification system; a closed loop pool water purification system; a reactor water purification system; and a reactor gas purge system. All these systems have weekly, monthly and yearly checks to ensure that they are functioning. However the tests are mainly qualitative and do not identify the likely hood of imminent system failure. If any of these systems are not available, operation of the reactor is prohibited. It is therefore very important that these systems be maintained in such a way as to minimize their downtime and not inhibit reactor utilization.

The facility operates with a small core complement of staff tasked with operating and maintaining the reactor. To adequately deal with the administrative, operational and maintenance challenges, the facility is developing a software based infrastructure management system (FIMS) to assist its small

core technical and operation staff in managing both reactor operation and utilization issues. It will provide a convenient and effective way to gather data on system operating status and monitor trends to guide operation, maintenance and utilization, by enabling actions to be taken long before system failures, thereby reducing downtime.

2. System Objectives

2.1 System attributes

The FIMS covers all physical structures, equipment, computer systems and their data, and administrative controls related to the operations of the reactor and associated systems. It operates independent of the reactor control systems and its function is to capture and curate data on the status of various systems, provide machine learning tools that will analyse the data streams and fill knowledge gaps on systems performance and levels of operability of sub-systems for operators and managers. It is independent of the reactor control system and does not override any of its control mechanisms. Table 1 lists some of the knowledge objectives that FIMS will meet.

Objective	Knowledge Gap
Auxiliary system status and performance.	Is a particular auxiliary system functioning normally and/or is it on a path to system failure?
System failure diagnosis.	Is the failure of an auxiliary system correlated with other events such as preventative maintenance tasks or the loss of electrical power?
Auxiliary system reliability.	What is the mean time between failure (MTBF) and the mean time to failure (MTTF) for the auxiliary systems, and are they correlated with specific components.
Reactor facility information.	What is the operating history of the reactor required to estimate LEU burn-up, core life, and calculate fission product inventories.

Table 1, Some FIMS knowledge objectives.

2.2 System Architecture

The architecture of the FIMS is shown in Figure 1. It is made up of layers which perform separate and distinct tasks. At the base are producers which provide sensed system parameters and stream events via a transport layer to the archive. The transport layer provides reliable fault tolerant transport mechanisms to guarantee delivery of the producer events to the archive store. It also provides for event streams to be intercepted and streamed to analytic processes as notification of specific events. The archive store comprises a highly scalable and reliable searchable database engine. Analytic processes sit atop the archive and transport layer to perform knowledge discovery and other analytical tasks. The outputs form these processes can be stored in the archive. User visualizations are requested via multiple paths with the analytic layer.

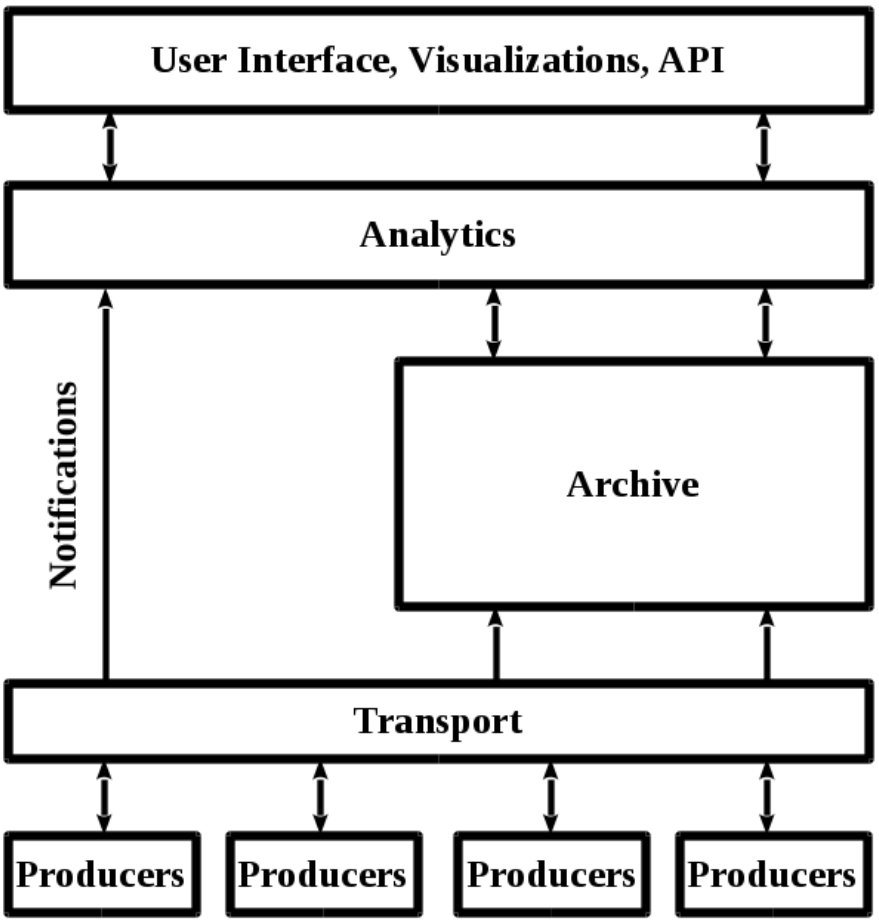

Figure 1, FIMS system architecture

2.3 System Security

The nodes and data streams that comprise the FIMS, though not connected to the reactor control system are however critical to the safe operation of the reactor, and are treated as sensitive. The FIMS system security adopts a graded approach which applies a higher level of security measures to those nodes and data streams with a higher potential consequence from an attack. Security levels are assigned to nodes and data streams to inform the degree of security protection required with each level adopting an appropriate set of protective and corrective measures. Table 2 lists the system security levels and protection.

Level	Protections
1	Highest level of protection applied to those nodes and data streams that provide details of the operating condition of the reactor such neutron flux, core temperature, etc. Encryption of streams and monitoring by autonomous agent processes to ensure data integrity.
2	Medium level of protection applied to those nodes and data streams that provide details of the auxiliary system operations and reactor utilization.
3	Base level of protection applied to all computer nodes and data streams. Administrative controls applied to ensure all updates and changes are authorized. Monitoring by

	autonomous agent processes for infringements and unauthorized communications, and other activities.

Table 2, FIMS security levels

2.4 System Quality Assurance

An important application of the FIMS is the use of autonomous intelligent agents to mine the voluminous datasets and discover knowledge and produce reports. To achieve this, information on the quality of the data streams must be available so that agents can adjust their processes in mining the data. FIMS provides for autonomous agents to intercept data streams and compute multiple metrics that are stored along side the data. These metrics are later used to compute quality factors for all outputs produced.

3 System Implementation

The FIMS is being implemented using a number of open source tools with active development and a large user community. Apache Flume [3] is used for the transport of data from producers to the archive as it provides a reliable and highly available service to consuming and streaming data in near real-time. Elasticsearch [4] is a distributed database system used for the archive that provides data storing, indexing and searching services. Grafana [5] is a web based tool used for visualizing time series data and application analytics.

Currently producer nodes have been implemented that stream data on reactor operating parameters of neutron flux, core temperature, control rod position, and radiation levels in and around the reactor room. These data streams have a resolution between .5s to a few seconds. Figure 2 shows a dashboard used to monitoring the reactor during operation.

Figure 2, FIMS dashboard

One of the planned near term developments is a software tool to automatically compile a reactor operating log. The log will provide for each reactor operating run, graphs showing neutron flux, core temperature, control rod, relevant radiation area monitor readings and tables of operating metrics such as flux hours, and samples irradiated. These logs will be compiled annually and feed into the annual facility report. When this tool is completed it is expected to save in the region of 400 hours of staff time per year.

4 Conclusion

A design for a facility infrastructure management system for the JM-1 SLOWPOKE research reactor has been developed and is currently being implemented. It is expected that as all the various auxiliary systems are brought online it will allow the operators to better understand and predict their behavior and improve routine maintenance programmes and schedules. This will inevitably reduce downtime and improve utilization.

References

[1] C. Grant, G. C. Lalor, J. Preston, R. Rattray and M. K. Vutchkov, Neutron Activation Analysis with the Slowpoke Reactor In Jamaica, Jamaican J. Sci Technol., 9,1998, p.63.

[2] M. Vutchkov, C. Grant, G.C. Lalor, J. Preston, Standardization of the Slowpoke-2 reactor in Jamaica for routine NAA, Journal of Radioanalytical and Nuclear Chemistry, 224 (2), 2000, p. 355-359.

[3] http://apache.flume.org

[4] https://www.elastic.co/products/elasticsearch

[5] http://grafana.org/

THE NEW I&C SYSTEM OF THE TRIGA MARK II REACTOR VIENNA

M. VILLA, R. BERGMANN, H. BÖCK
Vienna University of Technology, Atominstitut
Stadionallee 2, 1020, Vienna, Austria

M. KROC, M. PROKS, V. VALENTA
Skoda Company
Orlik 266, 316 06 Pilsen, Czech Republic

M. KASE, J. HERRMANN, J. MATOUSEK
dataPartner
Senovážné nám. 15, 370 01 České Budějovice, Czech Republic

ABSTRACT

The TRIGA Mark-II reactor was installed by General Atomic (San Diego, California, U.S.A.) in the years 1959 through 1962, and went into operation for the first time on March 7, 1962. The TRIGA Mark II reactor in the Viennese Prater is part of Atominstitut which was founded in 1958 as an inter-university institute for all Austrian universities and started operation in 1962, when the TRIGA Mark II research reactor of the institute was officially opened. As part of the reform of the university system, the Atominstitut was integrated 2002 into the Faculty of Physics at the TU Wien. The operation of the reactor since 1962 has averaged 220 days per year, without any long outages. During the last 50 years 3 different I&C systems were in use to control the reactor power and safety related parameters. From 3 different vendors, Skoda, Invap and GA, the Skoda company located in Pilsen was chosen in November 2013. The main work is done together with the subcontractor dataPartner.

1. Introduction

The TRIGA Mark II research reactor of the Vienna University of technology is in operation since the 7th March 1962. When TRIGA reactors were developed in the mid-fifties, the typical state of the art of I&C systems was based on vacuum tubes. At the Atominstitut this type of I&C systems produced by the company General Atomic (GA) was in use until 1968. Towards the end of the sixties transistors replaced electronic tubes also in I&C systems, and a new type of TRIGA instrumentation based entirely on transistors were marketed. Therefore, during the seventies many TRIGA reactors converted to such types of I&C systems which in a few cases are still in use. At the Atominstitut this replacement took place in 1968. This type of reactor instrumentation produced by the company AEG was easy to maintain and spare parts could easily be replaced for about 20 years until they slowly disappeared form the market. As a result, a new type of digital and modern software based I&C systems were developed and available from the early nineties onward. As software based I&C systems were usually not accepted by the regulatory authorities, a hard-wired back up system for safety related parameters were required and, therefore, a combination of both was the state-of-the-art I&C system in most of TRIGAs world-wide for long time. In 1992 the old transistor

based I&C system was replaced by a new digital software based I&C system produced by the company GA. Nowadays, after use for more than 20 years of software/hardwired digital I&C systems various components of those have again reached their end of life-time. Therefore, the University decided the fourth time to replace the old I&C system by a new one. This new generation 4-digital I&C systems are capable to monitor and control variables and parameters of physical and other processes, component and system statuses, as well as to react on predefined project limits and safety conditions. The details of this new I&C system produced together by the Skoda Company located in Pilsen and dataPartner located in Ceske Budejovice, both Czech Republic, are presented in this paper.

2. System Architecture

Generally, system and equipment architecture follows the existing concepts. The whole system consists of SCRAM logic, neutron flux measurement channels (OPM - Operational Power Measurement, IPM – Independent Power Measurement, and PPM - Pulse Power Measurement), I&C field instrumentation, control system, new operator's console and data acquisition system.

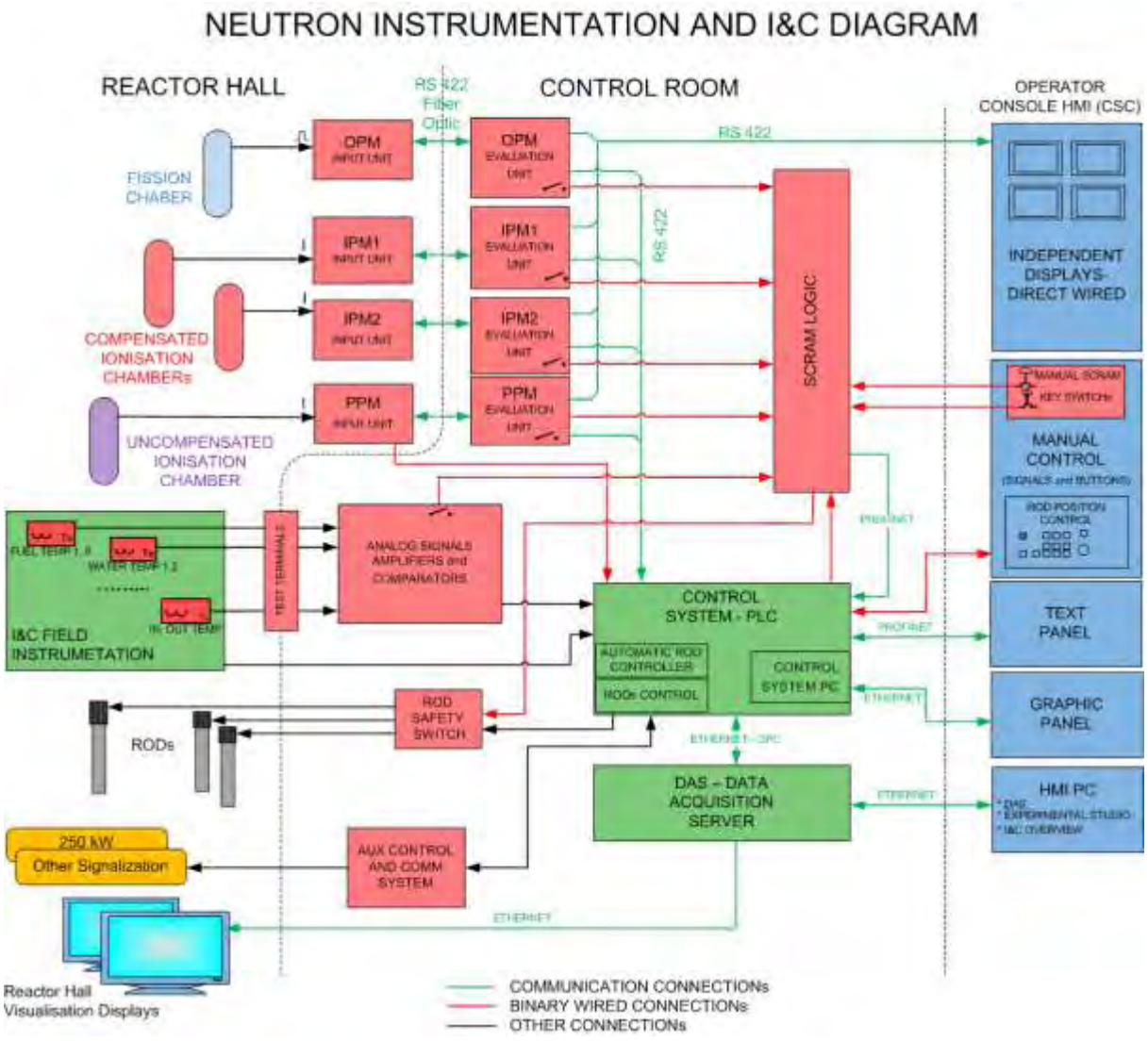

Figure 1: I&C Overview Diagram

3. Neutron Detectors

The following three different types of detectors for neutron flux measurements are used on the TRIGA® reactor:

- 1 pc of fission wide-range chamber for neutron flux measurements and for reactor control from source range (about 5 mW) to nominal power (250 kW). It works in Campbell mode – Photonis type CFUL08.
- 2 pcs of compensated ionization chamber for reactor control and especially for safety functions from source range to nominal power – Centronic type RC6
- 1 pc of non-compensated ionization chamber for measurements in pulse mode (peak till 250 MW, energy till 12 MWs. It measures amplitude, length and shape of pulse) – Centronic type RC7.

4. Neutron Flux Measurement Channels

- 1 pc wide-range operational channel – Operational Power Measurement (OPM)
- 2 pcs wide-range safety channels – Independent Power Measurement (IPM)
- 1 pc wide-range pulsing channel – Pulse Power Measurement (PPM)

Signals read from chambers are directly numerically processed to reactor power value and reactor power change rate – period in wide-range channels. The power value is converted to common units and can be expressed in %, cps, A or W. Actual values are updated every 100 ms and are sent via optical serial line to an independent display and via second optical interface to a control system. These channels open Safety Relay contacts in the Scram Logic loop if measured values exceed the preset protection setpoints or in the case of any system internal failure is indicated.

All channels consist of the two following units:

- Input unit for processing neutron chamber signal and converting the analog signal into digital domain for transmission to the evaluation unit.
- Evaluation unit for comparison of the neutron flux measured values against the safety system setpoints.

The hardware platform is based on Texas Instruments Hercules safety microcontrollers. These microcontrollers are based on ARM Cortex-R dual-lockstep IP cores and are designed specifically for IEC 61508 safety critical applications.

The software is developed in C programming language using Texas Instruments ARM compiler and tools. The software development respects recommended practices and guidelines, e.g. MISRA standard or NUREG CR-6463 guidelines.

Channels are equipped with test signal generators, which allow auto diagnostics and safety function check every time before the reactor is started up.

5. Scram System

The TRIGA type reactor is the only nuclear reactor in this category with worldwide excellent safety record of over 50 years due to inherent features such as the intrinsic characteristic of the standard reactor U-Zr-H fuel. It results in safe and reliable self-shutdown while the temperature coefficient acts independently of any external controls in the event of an accidental reactivity insertion. That offers true "inherent safety," rather than relying on

"engineered safety" features. Nevertheless the new I&C System provides additional external means to assure that the TRIGA reactor safely shuts down in unexpected power or temperature deviations.

Scram Logic Circuit

The entire SCRAM circuitry is hardwired and is not affected by any software based systems or the Control or Data acquisition system.

Automatic SCRAM logic is implemented on relay logic, consisting of certified safety relays. The design allows for 100% testability features and accurate analysis of the safety function reliability. The safety relays are capable to perform self-diagnosis. Power relays are continuously diagnosed at every contact switching. Diagnosis is mainly focused on sticking relay control (checks and evaluates the time till contacts open). The diagnosis consists of two redundant computation branches. If at least one of the branches evaluates the safety condition failure, it opens the output contactor contacts (reactor trip).

Output contactors disconnect power to magnets and pneumatic valve resulting in drop of control rods (reactor trip).

Figure 2: SCRAM Module Example

Specifically SCRAM Logic boards use:

- Safety category relays. These are compact, slim relays conforming to:
  - EN Standards (EN50205 Class A, certified by VDE),
  - EN61810-1 (Electromechanical non-specified time all-or-nothing relays)
  - UL standard UL508 Industrial Control Device,
  - CSA standard CSA C22.2 No. 14 Industrial Control Devices

6. Reactor Control System

The Reactor Control System (RCS) is a modular distributed control system with PLCs in different locations. The fast industrial bus Profinet facilitates interfaces among the PLCs, displays, inverters, and other components. Profinet commands can implement requested rod position including maximum rod motion speed. RCS has the capability to self-diagnose status and failures of inverters and motors. The Siemens Simatic S7 PLC system, a widely used industrial control system in Europe, was selected for TRIGA reactor control.

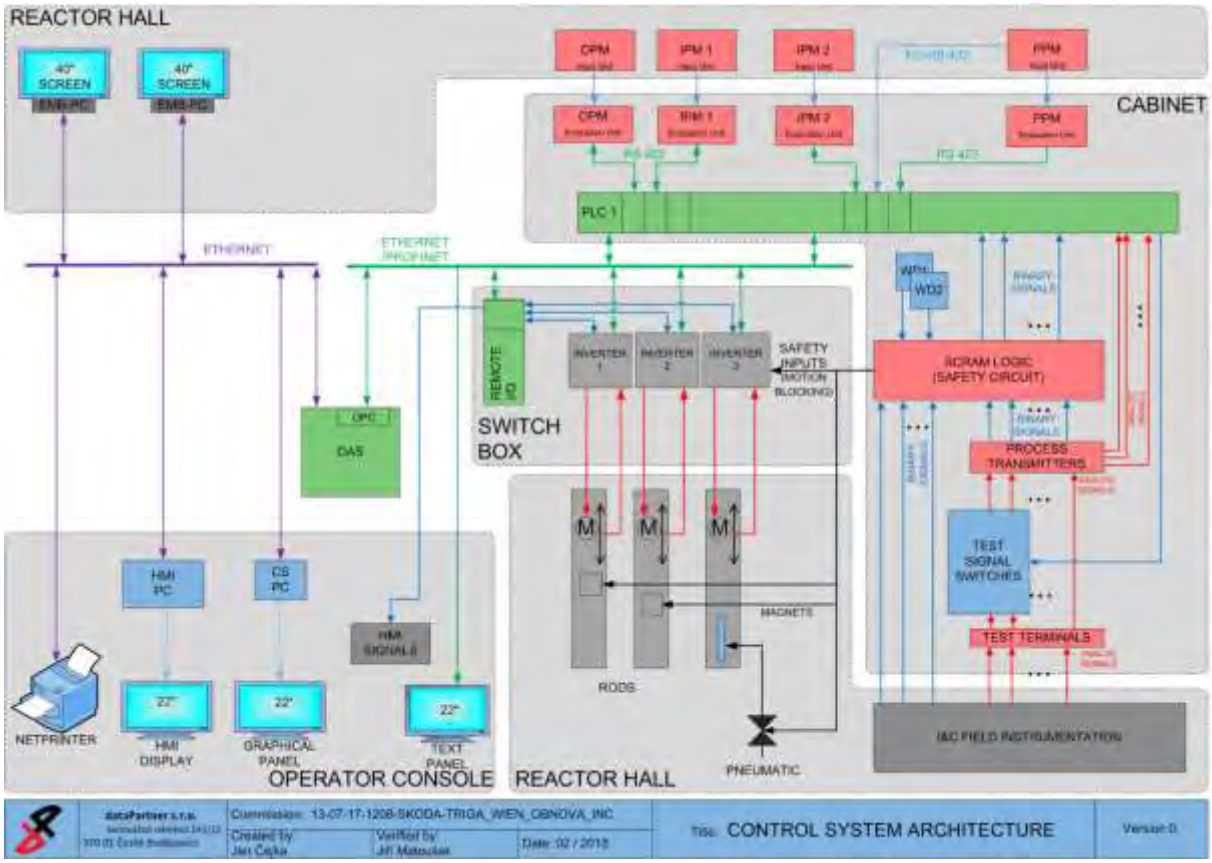

Figure 3: Control System Architecture

Reactor Control System States

At any moment the reactor control system is in one of four possible states: *Standby*, *Shutdown*, *Pre-start Checks* and *Operation.*

Reactor Operation Modes

Manual Mode

In the *Manual* operation mode, the operator controls the drives manually, thus an operator manually controls the power output of the reactor without active automatic intervention of the control system (as long as the reactor power stays below the maximum pre-set levels).

Auto Mode

The reactor control system, when placed in *Auto* operation mode, will automatically control the position of the regulating rod or the safety rod or any combination of the two to maintain a specific power level. The remaining rods including the transient rod are under manual control.

Pulse Mode

The *Pulse* operation mode allows to produce a very high power, short duration pulse from the reactor. This pulse effect is accomplished by firing the transient rod upward with compressed air.

7. Experimental Studio

The Experimental studio is a SW tool for working with data acquired during experiments and training. It is suitable especially for teaching students to work independently when processing and evaluating data and confirming theory. The Experimental studio allows easy and effective creation of mathematical tasks for acquired data analysis – the batch processing of recorded data as well as online streamed incoming data. The Experimental studio can use online reactor operational data or recorded history data.

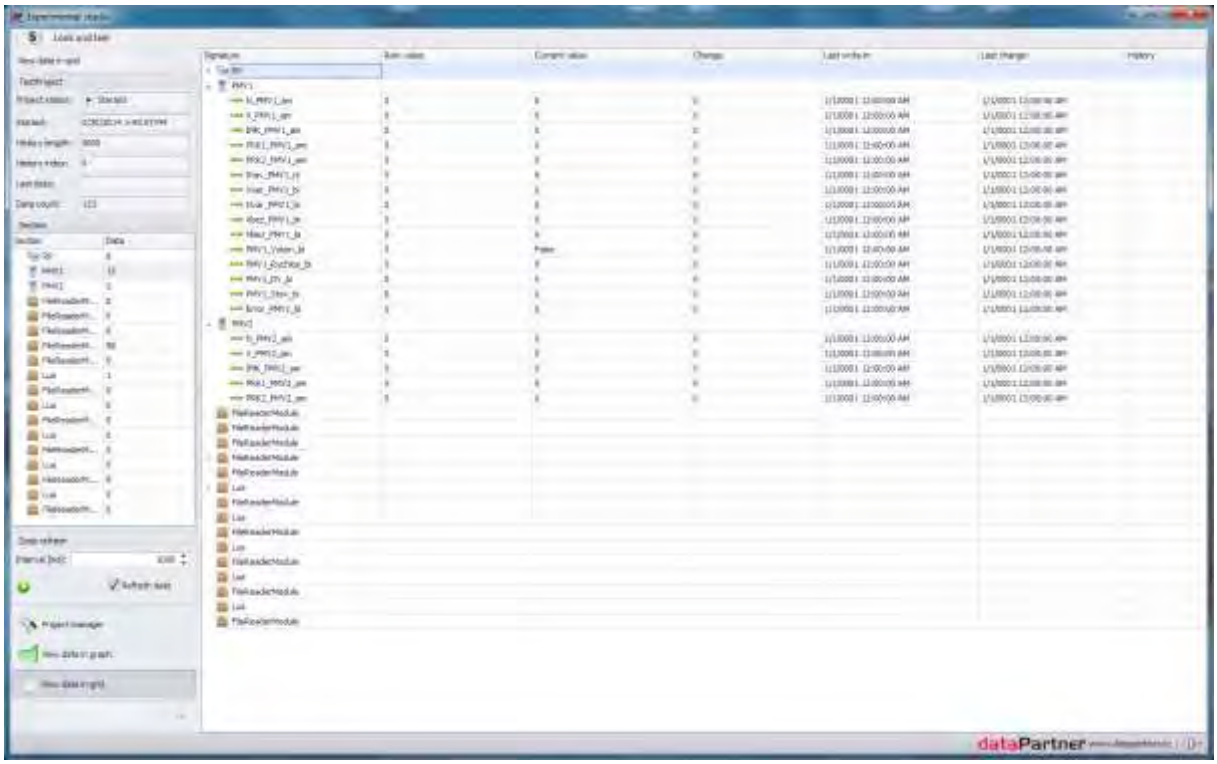

Figure 4: Experimental studio screenshot

8. Data Acquisition System

For storing all measured and computed variables at the operator console, a dedicated data acquisition and logging system (DAS) is used. DAS is based on industrial PC architecture, the data is stored on hard discs. It gathers data from the control system and stores it to the database for later recall, analysis or playback.

9. Safety Systems Qualification

All I&C structures and components are designed so that they can perform reliably their functions under the environmental conditions they will be submitted to during their mission time. The operability of I&C structures and components under the related environmental conditions was demonstrated by tests, analysis, operation experience, etc. The supplier's qualification procedures are established to confirm that the equipment is capable to meet the requirements for performing safety functions while subjected to environmental conditions existing prior to and at the time when it is required throughout operational life.

Qualification includes the following:

- Functional Tests
- EMC Tests
- Accelerated Ageing Tests
- Seismic Tests

Seismicity

The equipment is designed, manufactured, and tested on the basis of the general dataPartner qualification procedures for seismic resistance which should also be valid for the actual realization site per Reference [11].

The tests have been performed according to [11] IEC 980: 1993 with acceptable results. The applied test earthquake intensity exceeds required seismicity criteria in the document ATIB1010 Sicherheitsbericht 2013 [19].

Equipment Lifespan

The reactor site integrated radiation dose is so low that it does not significantly impact ageing of the equipment outside of reactor, thus neutron flux measurement modules and SCRAM relays are tested for at least 15 years qualified lifetime by accelerated ageing methodology.

SW qualification

The system SW is developed and tested by standards, methodology, and QA procedures required by the Czech State Authority for a 10 MW research reactor LVR-15 in the Czech Republic. Safety System SW development follows Reference [14] including Graded Approach. Safety Related System SW development follows Reference [15] as it is documented accordingly.

10. References

[1] Verhandlungsverfahren mit vorheriger Bekanntmachung im Oberschwellenbereich, Ausschreibungsunterlagen für die Erneuerung der gesamten Reaktorinstrumentierung und des Kontrollsystems für den 250 kW TRIGA® Reaktor in Wien, Österreich, Zahl 26300.02/003/2013, 8.7.2013.

[2] Technische Details des 250 kW TRIGA® Mark II Reaktor, Wien, Österreich, M. Villa, Atominstitut 2010.

[3] IAEA Safety Standards Series No. NS-R-4 (2005): *Safety of Research Reactors*.

[4] IAEA Safety Standards No. SSG-24: Safety in the Utilization and Modification of Research Reactors.

[5] ANSI/ANS 15.15-1978: Criteria for Reactor Safety Systems of Research Reactors.

[6] IAEA – TECDOC-973: Research Reactor Instrumentation and Control Technology.

[7] RCC – E, Design and Construction Rules for Electrical Components of Nuclear Island, 2012.

[8] EN 61226:2010: Nuclear power plants – Instrumentation and control important to safety – Classification of Instrumentation and control function.

[9] IEC ISO 9001:2008: *Quality Management System* (QMS).

[10] IEC 60987 2009: Nuclear Power Plants - Instrumentation and Control Important to Safety – Hardware Design Requirements for Computer-based Systems.

[11] IEC 980:1993, Recommended Practices for Seismic Qualification of Electrical Equipment of the Safety System for Generating Stations.

[12] IEC 60780:1998, Nuclear Power Plants – Electrical Equipment of the Safety System-Qualification.
[13] IEC 61513, Ed. 2.0 2011-08: Nuclear Power Plants – Instrumentation and Control Important to Safety – General Requirements for Systems.
[14] IEC 60880, 2006: Nuclear Power Plants – Instrumentation and Control Important to Safety – Software aspect for computer-based systems performing category A functions.
[15] IEC 62138, 2004: Nuclear Power Plants – Instrumentation and Control important to Safety – Software aspect for computer-based systems performing category B or C functions.
[16] IAEA Safety Standards, Specific Safety Guide No. SSG-22 (2012): Use of a Graded Approach in the Application of the Safety Requirements for Research Reactors.
[17] Safety Guide No. DS-436: Instrumentation and Control and Software Important to Safety for Research Reactors, Draft 7, February 2014.
[18] *Sicherheitsbericht des Atominstituts – chapt. 2.4,* M. Villa, A. Musilek, D. Hainz; Atominstitut, ATIB1010, 2013.
[19] Operation and Maintenance Manual Microprocessor Based Instrumentation and Control System for the Atominstitut der Östrereichischen Universitäten Wien, Austria, GENERAL ATOMICS, 1993, E117-1016, Appendix A, revision 4, Operators Manual 1.4.1995.

THE THIRD REFURBISHMENT PROGRAMME OF THE BR2 REACTOR IN MOL, BELGIUM

S. VAN DYCK; J. VERPOORTEN
BR2 reactor, SCK●CEN
200 Boeretang, Mol - Belgium
W. CLAES
Infrastructure operation, SCK●CEN
200 Boeretang, Mol - Belgium
P. LEYSEN
Nuclear Systems Design , SCK●CEN
200 Boeretang, Mol - Belgium

ABSTRACT

The BR2 material test reactor, operated by the Belgian Nuclear Research Centre at Mol, is undergoing its third refurbishment operation. This operation is part of its plant asset management program, which aims at optimizing safety, availability and economy of reactor operation in the long term. The plant asset management program responds also to the requirements for long term operation in the frame of the periodic safety reassessment, due in July 2016.

The core of the refurbishment operation is the replacement of the Beryllium matrix of the reactor. This component has a limited life time and is proactively replaced in order to allow for reliable and flexible operation of the reactor for at least the period covered by the periodic safety reassessment. Other major maintenance and modernization operations are defined from the ageing risk analysis in the plant asset management program, operational feedback and regulatory evolutions.

This paper describes the methodology of the plant asset management program, gives operational feedback on the replacement of main components and reviews the outlook on future operation and experiments of the reactor.

1. General characteristics of the BR2 reactor

The BR2 reactor is the most performant operating material test reactor in Europe in terms of attainable neutron fluxes. The range of neutron flux in the core of the reactor is from 7.10^{13} to 10^{15}n/cm²s for the thermal flux and 10^{13} to 6.10^{14}n/cms for the fast flux (E>0.1MW). The reactor is fueled with cylindrical fuel elements, containing concentric aluminum clad highly enriched uranium dispersed in an aluminum matrix. The reactor is light water cooled and moderated by a combination of water and Beryllium. The primary coolant is pressurised to 1.2MPa and flowing with a linear velocity of 10m/s on the fuel plates. These conditions allow for a maximum heat flux of 470W/cm² on the driver fuel surface, although in experimental irradiations in the primary

coolant, 600W/cm² is allowed. The nominal reactor power is 100MW, but the actual operating power is adjusted in order to meet the requirements of the irradiations both in terms of flux as well as in terms of reactor cycle duration. Typically, the reactor power is fixed in the range of 55 to 70MW for a reactor cycle of 3 to 4 weeks.

The reactor core is consisting of 79 irradiation channels. The reactor configuration is not fixed by design nor license, allowing a unique flexibility to accommodate a large diversity of irradiation experiments in a single core load. These experiments can be loaded in an empty irradiation channel, which has a standard diameter of 84mm. Besides the standard channels, 5 200mm diameter channels are available (of which one is located in the center of the reactor), while also 10 channels of 50mm diameter are available in the periphery of the core. Irradiation experiments can also be loaded in the central cavity of the cylindrical fuel element (15 or 25mm diameter) in order to perform experiments under maximum fast flux. Eventually, special fuel elements can be loaded in order to accommodate larger irradiation experiments in a high fast flux field inside a 200mm channel. As illustration, figure 1 shows different core configurations, optimised for maximum thermal flux in a central flux trap (1a), additional fuel elements for fast reactor simulation in the central irradiation channel (up to 19 fuel pins with average power of 500W/cm in representative sodium fast reactor spectrum) or a large modular driver fuel element, containing a helium cooled fast reactor loop in a peripheral 200mm channel.

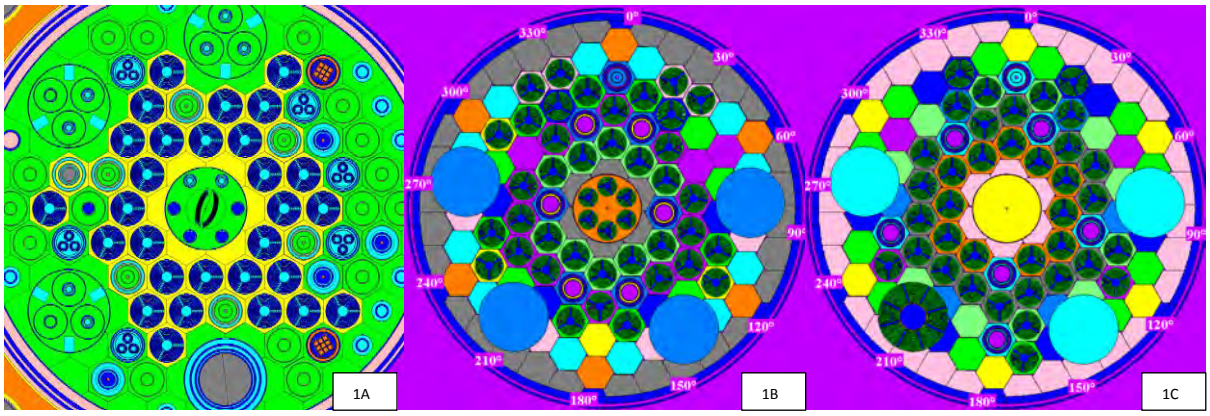

Figure 1: examples of reactor configurations of the BR2

1a (left): symmetrical configuration around central flux trap to maximise the (thermal) flux in the central position

1b (middle): symmetrical configuration with additional driver fuel in the central cavity to maximise (fast flux) around a central sodium loop

1c (right): asymmetric configuration in order to accommodate a gas cooled fast flux test loop in a peripheral 200mm channel with circular booster element.

The reactor core is compact (roughly 1m in diameter with 800mm fueled length), but accessibility to the irradiation channels is facilitated by their geometric arrangement in a hyperboloid of revolution. Consequently, the channels are accessed on the reactor top cover, which has a diameter of 2m, allowing easy loading and connection of instrumentation in irradiation rigs. In 17 of the 79 channels (including the 5 200mm channels) also a lower access

is available through the sub-pile room. This facilitates the installation of through loops in the reactor (figure 2).

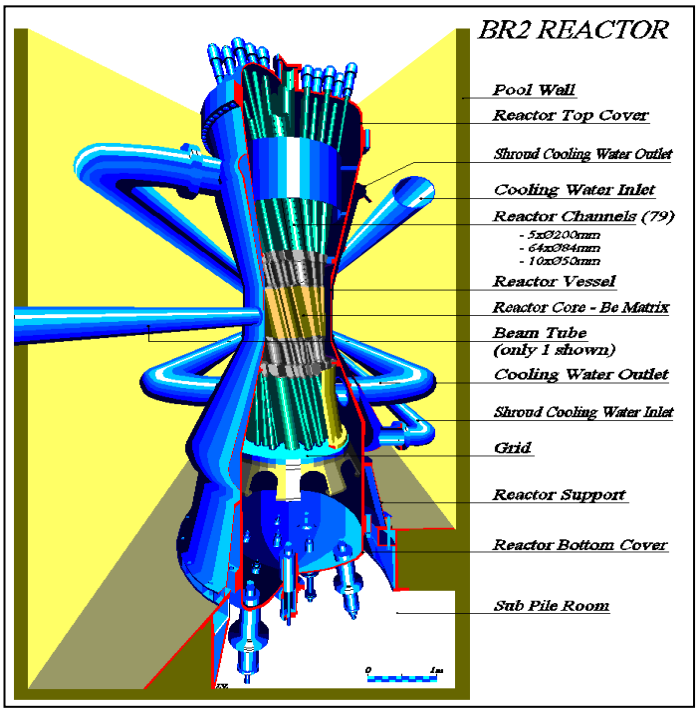

Figure 2: graphic representation of the geometrical lay out of the irradiation channels in the BR2 reactor.

2. The periodic safety reassessment 2016

The BR2 reactor started operation in 1963 with an initial license of 25 years. However, with the introduction of nuclear power generation in Belgium in the early 1980s, the legislation was modified towards a periodic reassessment of the license without end of license date. This legislation is also applied to the operating research reactors in Belgium. Hence, since 1986, the BR2 reactor is subject to periodic safety reassessments, of which the next period is starting in July 2016. The safety reassessment procedure is based on the IAEA guideline SSG-25 and focusses on 15 safety factors [1]. These factors can be grouped along 3 axes, namely the plant, the organisation and the protection of workers, environment and population. Within the safety factors related to the plant, an explicit requirement is defined to present a systematic management programme for achieving the long term operation objectives for the research reactor[2].

Besides the ageing management project, the periodic safety reassessment is centered along the review of the safety analysis report according to modern methods and conformity of the plant design to modern safety standards. In both aspects, the conclusions of the stress test analysis are integrated within the initiating events for safety studies and in the design base [3].

3. Plant asset management

The plant asset management programme for the BR2 reactor was started in 2010. The objective of the programme is to set-up a comprehensive management system for mitigating the ageing risks in the installation and identify potential improvements. This programme not only targets the safety of the installation, which remains the dominating priority, but also the availability and economy of operation.

The programme is set-up in three parts:

- The asset configuration management: this part identifies all relevant assets in the scope of the programme and evaluates the potential impact of failure of these assets on the safety, availability and economy of the installation. The separate scores for the respective severity of the impact of asset failure are multiplied in order to generate a total asset score. The assets are then grouped in 4 categories (A to D), for which a graded approach towards mitigation of the risk associated to the failure of the asset [4].
- The installation concept management: this part contains the actual analysis for the risk of failure of the different assets, with a graded approach in terms of detail of the analysis according to the category of each asset. For most critical assets (class A), an FMECA (failure effect and criticality analysis [5]) is performed to identify the critical failures, according to the relevant failure modes [6] and the likely frequency of occurrence. For the second class of assets, a generic failure analysis is performed and for the third class of assets, good practices are reviewed in order to identify cost saving measures to prolong life of the asset. For the fourth class, failure is tolerated and only curative measures are taken. In order to mitigate the identified risk of failure for the considered assets, a specific maintenance strategy is defined, according to the scheme in figure 3.
- The work order and skills management: in this phase, the selected mitigating measures are defined in inspection and maintenance procedures for preventive maintenance. If failure can be tolerated, (scheduled) replacement procedures are defined and spare parts management is defined in order to limit lead times for scheduled replacement or repair after failure. If no satisfying mitigation measures can be identified, design upgrades can be applied in order to mitigate the impact of failure of the asset or to reduce the risk of failure or its impact. The implementation of upgrades is managed through the process of plant modification.

The conclusions of the plant asset management programme have been implemented in the 2015-2016 refurbishment programme of the BR2 reactor. The refurbishment is a combination of inspections, replacements and upgrades to major components of the BR2 reactor. The core of the refurbishment operation is the replacement of the Beryllium matrix and lower internals of the reactor. This operation defines mostly the critical path of the refurbishment operation, which is planned over 16 months, from March 2016 to July 2016.

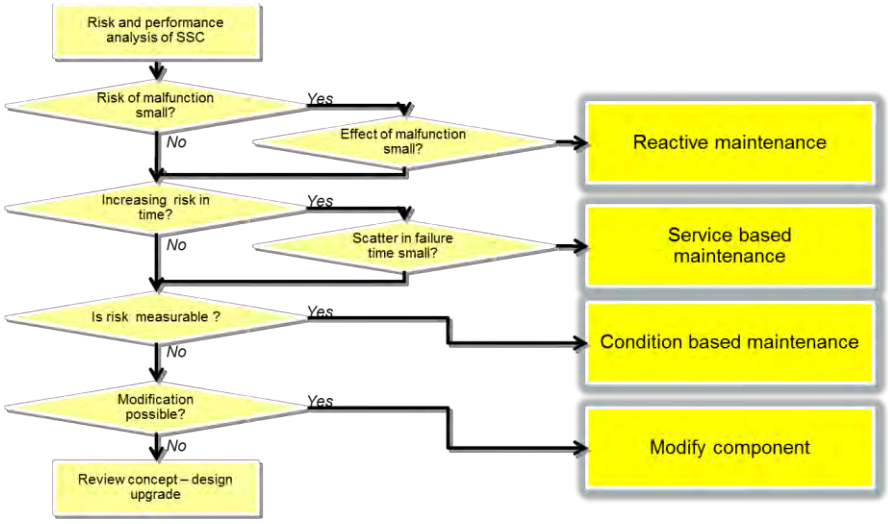

Figure 3: graded approach in maintenance strategy according to the conclusions of the plant asset management analysis.

4. The refurbishment programme

4.1. The beryllium matrix

The beryllium matrix is exposed to intense neutron irradiation as it is surrounding all fuel elements in the BR2 core. The spacing between the channels is limited for optimum neutron moderation, while the radial flux gradient in the reactor causes non uniform exposure of the beryllium elements. The operational experience has shown that the (differential) swelling of the beryllium causes cracking of the beryllium, which may lead to stray particles in the primary coolant and causes increased staff exposure during the replacement operation. Therefor, after the first replacement in 1978-1980, the maximum accumulated fast fluence in the matrix has been set to 6.4 10^{22}n/cm² in the license. Also, the extent of cracking is to be limited in order to exclude blocking of cooling of fuel or motion of control rods. The plant asset management analysis classifies the beryllium matrix in the class A, as its cracking is relevant to safety, unscheduled need for replacement will have large impact on availability of the installation and the cost of unscheduled replacement is high. Therefor, two mitigating measures are defined:

- The irradiation channels are periodically inspected for cracking, in order to monitor the crack evolution as a function of accumulated fluence. In this way, the safety relevant failure mode of fragment release is excluded.
- The failure mode by reaching the fluence limit of the Beryllium would become a certainty within the next period covered by the periodic safety reassessment (2016-2026). As no inspection nor maintenance measure can mitigate this risk, replacement is the only option (as condition based maintenance, cfr figure 3).

The replacement of the beryllium matrix is planned before the limit fluence is reached. The replacement period is determined based on internal and external considerations: on one hand, the replacement requires a long stop of the reactor. This opens a window of opportunity to perform large maintenance operations, which require a long stop. The plant asset management programme contains a number of operations that will require a long stop of the reactor. With the

irradiated matrix, the accumulation of ^3He during outage limits the length of the reactor stops in order to maintain the subsequent reactivity control parameters within the technical specifications. Therefor, it would be difficult, if not impossible, to achieve the objectives of the plant asset management programme within the limited outage periods of the reactor with its irradiated matrix. On the other hand, as the BR2 reactor plays a significant role in the global supply of medical radio-isotopes, the outage for the replacement of the matrix is scheduled between early 2015 and mid-2016. As two major isotope producers were scheduled to stop operation (OSIRIS, end 2015) or production of radio-isotopes (NRU, late 2016), while a new potential producer (JHR, 2020) is only expected later, the selected period is optimal, given the lead time and expected end of life for the BR2 beryllium matrix.

The matrix components have been purchased and assembled, the alignment of the parts per channel verified and the total matrix was validated by loading in a mock up vessel. The irradiated matrix was extracted from the reactor by remote handling and the new matrix is installed. The reactor vessel is inspected when the matrix was unloaded (see below).

4.2. The reactor vessel

The reactor vessel is a class A component in the plant asset management due to its relevance for safety and replacement duration and cost. The failure modes considered are brittle fracture (enhanced by irradiation), swelling, fatigue and corrosion. Literature data show that all these phenomena occur of over a (very) long time period. The analysis of degradation shows that corrosion nor swelling are of concern when the reactor is operated under the nominal conditions. The risk of fatigue is analysed and demonstrated to be small and limited to the non-irradiated parts of the vessel (the inlet nozzles being the most critical parts). However, given the small amplitude and limited number of cycles, fatigue is not an issue. Radiation induced embrittlement reduces the resistance of the reactor vessel to brittle fracture. The embrittlement phenomenon is driven by the transmutation of aluminum into silicon by thermal neutrons. The embrittlement is monitored by a surveillance programme, based on accelerated irradiation of representative base metal and weld specimens in the central channels of the BR2 reactor. This programme yields a high lead factor and allows predicting the material condition at the end of the upcoming period, covered by the periodic safety reassessment (2016-2026). The integrity analysis of the reactor vessel is reviewed according to the findings of the surveillance programme as well as the operational records for the past period and the forecast for the next period. The analysis is supported by an in service inspection, demonstrating the condition of the reactor vessel and its compliance with the minimum required fracture toughness of the material, in combination with the expected operational conditions (including incidental/accidental transients) and the observed (fabrication) flaws in the vessel. The updated inspection and analysis report have been reviewed by the safety authority as a hold point in the refurbishment project in December 2015.

4.3. The reactor pool

The reactor pool acts as radiation shield in normal operation and ultimate heath sink in incident/accident conditions. It is therefor a safety critical component (class A). The integrity of the reactor pool has been reassessed at the occasion of the stress test. It was concluded that,

even in extreme conditions (beyond design), the general resistance of the pool was sufficient to guarantee its structural integrity. Operational records have shown that leakage can occur at the level of the penetration of the beam tubes, having led to replacement of the seals between tubes and pool lining in 1996. The graded approach from figure 3 has led to the installation of a leak detection and measurement system in 2010, allowing for condition based maintenance. However, in order to avoid major outage in case of important leakage and considering the economic obsolescence of the beam tubes, it was decided to remove the beam tubes during the refurbishment of the reactor. This is facilitated by the removal of the irradiated beryllium matrix, reducing the exposure of staff during the operation. The beam tubes were removed by remote machining and the pool walls were plugged and equipped with new seals. Leak monitoring on the new seals is maintained for the future operation of the reactor, although ageing risks are reduced by the removal of the beam tubes (reduced radiation levels on sealing material).

4.4. The cooling loops

The primary cooling loop is the most important loop in terms of availability of the reactor. The schematic lay out of the primary cooling loop is given in figure 4. It is constructed in aluminum for reasons of corrosion and compatibility with the water chemistry which is optimal for the performance of the aluminum clad fuel. The primary circuit is divided in three main parts:

- The in pool part, containing the reactor vessel and the bypass to support cooling by natural convection.
- The in containment part, containing the isolation valves, which are safety critical to isolate the reactor in its pool and containment in order to warrant the residual heat evacuation to the pool by natural convection and the containment of radio-active contaminants in the reactor building.
- The out of containment part, containing the pumps, pressurised and heat exchangers to cool the reactor during normal operation and shut down.

In order to support condition based maintenance of the primary circuit, periodic tests and inspections are performed. Short period tests are functional tests of the safety functions (isolation valves, instrumentation,…) which are performed each reactor cycle or at least once per year. More quantitative inspections are performed for safeguarding the containment function of the primary circuit and its integrity in general. The frequency and scope of these inspections have been set along the principles of the ASME XI standard, although the standard is not directly applicable to the material and operating conditions of the BR2 primary loop. In order to define acceptance criteria for the non-destructive inspections of the primary circuit, the R6 code has been applied to the actual conditions.

As part of the refurbishment operation, all in-pool and in-containment within the scope of the inspection programme have been inspected by superficial (visual and die penetrant test) and volumetric methods (ultrasonic test). Part of the out of containment loop has also been inspected according to the ASME XI guidelines (fraction and period of inspection). When applicable, qualified repair techniques are applied for mitigating the effect of construction defaults. Specific qualification has been performed by exposure of the repair materials to gamma radiation (doses well over the expected dose in 20 years of service) and representative

primary coolant (to assess chemical releases to the coolant, as the repair material is qualified for underwater repairs).

For a number of components, some safety functions could not be tested (such as loss of containment by internal leak). In such case, design upgrades have been defined and implemented in order to render the safety function inspectable.

The pool cooling and filling circuit has as safety function to maintain the pool water level (and quality) for normal and accident conditions. From the stress test analysis and the plant asset management programme several upgrades to this system have been defined and implemented. These include the installation of a back-up refilling duct in case of extreme events, improvement of the containment function of the circuit in case of failure of piping and renewal/upgrade of the buried piping sections in order to render them inspectable (in order to avoid possible soil contamination in case of leaking).

The secondary cooling loop has no safety function, but is essential for availability of the installation. The operational experience has shown several parts of the loop being prone to corrosion induced failure. The loop contains a large amount of buried piping of low alloy steel, protected by an internal bentonite coating and an external tar based wrapping. The coolant is demineralised water at 40°C, optimised for compatibility with the aluminum alloy primary heat exchangers. The produced heat of the reactor is evacuated to the air by direct exchange with the secondary water, drawn through cooling towers by forced convection. After 50 years of service, the coatings are approaching their end of life. The steel piping may be attacked by external corrosion enhanced by the use of salt on roads, at locations where underground piping is crossing under the roads. The piping is replaced by equivalent piping, given the proven life time, with renewed coating technology, qualified for compatibility with demineralised water and use for underground piping.

The secondary pumps and cooling tower ventilators have all been revised and the ventilator fans have been replaced by composite fans. The concrete corrosion in the cooling towers is mitigated by renewal or addition of protective coatings.

4.5. Electrical system

The electrical system has been reviewed and mitigating measures are implemented towards both physical as well as economical ageing. Modifications are implemented in order to comply to modern legislation on safety of electrical systems and replacing components prone to lack of maintenance support in the near future. Specific upgrades are implemented in order to improve the level of defense in depth, the normal and emergency feeds to safety components are physically separated by the installation of additional cabling for the emergency feeds. The emergency generators and battery systems are renewed, with emphasis of physical separation in order to avoid common cause failure by fire or other external events. Also, subsequent to the stress test, a robust system is designed and implemented in order to monitor the installation conditions after extreme external events.

5. Utilisation potential

The BR2 reactor has a proven record of very broad utilisation capabilities in the field of fuel and material irradiation testing, radio-isotope and neutron transmutation doped silicon production and instrument functional testing under irradiation. In order to optimise the utilisation of the reactor, standardised and reusable rigs are made available besides the capability for development and implementation of dedicated experimental rigs. The main types of rigs are reviewed below.

5.1. The RECALL device for supporting ageing management of power plants

The RECALL device is designed to perform irradiation of steel specimens with a cross section up to 10x10mm² (Charpy V or small CT specimens) for the support of ageing management of pressure vessels of water cooled reactors. The challenges for the device is to provide a flexible and reloadable device with stable irradiation temperature control and sufficient space to irradiate at least one full set of Charpy specimens (at least 10) with homogeneous dose and temperature. The solution presented consists of an integrated loop with hot water circulation that can be loaded in a standard irradiation channel of the BR2 reactor. The loop design allows for preheating (range 280-310°C) of the specimens before irradiation starts and keeps the specimen temperature well controlled by gradual switching from electrical to nuclear heating as the reactor comes to power. The flexible loading position of the device allows achieving between 0.05 and 0.2dpa (in steel) per reactor cycle. Up to 20 Charpy specimens can be loaded and the device is reusable, offering very short lead times for experiments.

5.2. The MISTRAL device for database generation at medium flux and temperature

The MISTRAL device is designed to irradiate a large number (87) of miniature specimens (5mm diameter or 3x4mm² cross section and length of 27mm) in stable temperature conditions (160°C-350°C) with medium to high fast flux level (up to 2.5 10^{14} n/cm²s, E>1MeV). This challenge is met by inserting a pressurised water filled capsule in the central cavity of a special (5 plate) driver fuel element. The rig can be reloaded, so lead times for experiments are limited as well as the rig costs. Of the 87 specimens, 26 are located in the zone having over 90% of the maximum flux in the rig. The irradiation temperature is monitored by measurement inside dummy specimens and the irradiation temperature is fixed by setting the saturation pressure in the rig and sustaining boiling by electrical heating if the nuclear heating is insufficient to maintain boiling (during start up and shut down of the reactor).

5.3. The HTHF device for screening irradiations at high flux and temperature

For irradiating materials at maximum fast flux (3 10^{14} n/cm²s, E>1MeV) and controlled temperature up to 1000°C, a gas filled capsule with active temperature control is designed. This capsule is constructed of graphite, allowing high temperature stability and heat evacuation under the highest fluxes available in the BR2 reactor. The design is adjusted according to the experimental needs (specimen number and geometry, temperature range) and the capsules are single use. However, capsule cost and experiment lead time are controlled by the generic design and the reuse of the out of pile control equipment. The availability of several driver fuel

elements with comparable neutronic conditions allows for the simultaneous irradiation of HTHF devices, for example to compare different materials or generate data at different irradiation temperatures.

5.4. The PWC capsule for water reactor fuel pin irradiation

The pressurised water capsule for fuel irradiation is an instrumented capsule that can be used for base irradiation of fuel pins up to 1m long, with on line power monitoring and control of the cladding temperature by setting the water pressure in the capsule. The device can also be used for transient testing, either by loading a mobile absorber in the vicinity (multiple transients with small amplitude) or by varying the overall reactor power (large single transients). The setup of the device is such that fuel pin failure can be tolerated. Eventually, a fuel pin with instrumentation can also be loaded in the device.

5.5. The EVITA loop for MTR fuel element irradiation

The EVITA loop has been designed in order to provide an enhanced flow rate environment for testing of prototype fuel assemblies for material test reactors. The device is a semi open loop, providing enhanced flow in order to extend the thermal hydraulic conditions beyond the characteristics of the BR2 primary circuit, especially to accommodate fuel elements with smaller spacing (and thus higher pressure drop) than the BR2 standard fuel elements. Instrumentation can be added in order to monitor power and flux levels into the experimental fuel element and the flux can be tailored by modifying the environment of the fuel element in order to obtain the desired power level as a function of burn-up. This device was successfully used for the qualification of the Jules Horowitz reactor in France[8].

5.6. The commercial production devices

Besides the experimental irradiation rigs, the BR2 reactor is equipped with a number of devices for producing radio-isotopes and neutron transmutation doped silicon. Radio-isotopes are produced by fission of uranium-235 and activation of stable isotopes. The former is done in 6 devices, allowing on line loading and unloading of material, so supply of irradiated uranium targets to produce ^{99}Mo is possible on a nearly daily basis. The weekly irradiation capacity amounts to 7800Ci ^{99}Mo (6 day calibrated). Activation isotopes can be produced in thimble tubes (on-line loading, thermal flux up to 4 10^{14} n/cm²s) or baskets in the primary coolant flow (thermal flux up to 10^{15} n/cm²s in central flux trap or fast flux up to 6 10^{14} n/cm²s, E>0.1MeV inside a fuel element).

Silicon crystals of diameter between 4 and 8 inch can be irradiated up to an annual capacity of about 30 tons to yield neutron transmutation dopes silicon with specific resistivity ranging from typically 50Ωcm to 1000 Ωcm.

6. Operational perspective

With its third refurbishment programme, the BR2 reactor is prepared for the next operational period of 2016 to 2026. The plant asset management programme aims at optimising the maintenance operations, in order to technically allow for higher availability of the reactor on

annual basis. Pending on the economic feasibility and utilisation needs, the annual availability could be increased from 120 to 196 days at power.

The investments made in the refurbishment operation all provide replacement components and upgrades with life times well over the 10 years of the next licensing period. It is therefor intended to start feasibility studies on operation for the following 10 year period.

7. References

[1] IAEA. Periodic safety review for nuclear power plants. sl : IAEA, 2013. SSG-25.

[2] Coenen, S. Strategienota "Long Term Operation" van de Belgische onderzoeksreactoren. sl : FANC, 20/05/2011. 2011-05-20-SCO-5-4-1-NL.

[3] FANC. Weerstandstesten. Nationaal verslag voor andere inrichtingen van klasse 1 (niet kerncentrales), April 2013.

[4] IAEA. The use of a graded approach in the application of the safety requirements for research reactors. sl : IAEA, 20/11/2009. Safety Standard DS351

[5] IAEA. Application of reliability cebtred maintenance to optimize operation and maintenance in nuclear power plants. sl : IAEA, Mei 2007. IAEA-TECDOC-1590.

[6] IAEA. Ageing management for research reactors. sl : IAEA, 2010. SSG-10.

[7] Koonen, E. "Experience gained from the BR2 beryllium matrix replacement and second matrix surveillance program", IAEA-SM-310/68, Int. Symp. Research Reactor Safety

[8] Gouat, P. Nucl. Eng. & design, March 2011, issue 241 (3), p. 925-941

IAEA ACTIVITIES IN THE OPERATION AND MAINTENANCE OF RESEARCH REACTORS

HYUNG KYOO KIM, CHARLES R MORRIS
Research Reactor Section, Division of Nuclear Fuel Cycle and Waste Technology, Department of Nuclear Energy, International Atomic Energy Agency
1400 Vienna
Austria

Corresponding author: H.K.Kim@iaea.org

ABSTRACT

There are 246 operating research reactors globally, as of 2015, according to the International Atomic Energy Agency (IAEA) Research Reactor Database (RRDB). These reactors have a well-documented history of contributing to peaceful nuclear research and technology development, and have helped in the education and training of generations of scientists, reactor operators, and engineers. They are also used for basic research, radioisotope production, neutron radiography, neutron beam research, material characterization and testing, and other applications.
In fact, more than half of all operating research reactors are over forty years old and face concerns regarding ageing and obsolescence of equipment. The IAEA Research Reactor Section (RRS) works with Member States to optimize RR availability and reliability through shared operating experience as well as the development and implementation of operational and maintenance (O&M) plans, ageing management plans, training programs and international peer reviews. IAEA continues supporting MS, through Coordinated Research Projects and development of publications, development of research reactor ageing database (RRADB) and material property database (MPDB) to share knowledge about material ageing and available equipment and facility upgrades to sustain RR operability.
The RRS offers MS Operations and Maintenance Assessment of Research Reactors (OMARR), a peer-to-peer review to assist with improvement of operational and maintenance practices. Thus far, two facilities have used this opportunity, and another is planned for 2016. IAEA is establishing a specialized activity for conducting non-destructive examinations and in-service inspections at research reactors. Additionally, RRS is currently participating in several projects through the Technical Cooperation organization to assist individual and regional MS on specific projects.

1. Introduction

According to the Research Reactors Database [1], more than 50% of existing operating research reactors have been in operation for more than 40 years, with many of them exceeding their original design life. The majority of these reactors are challenged by ageing facilities and equipment, and obsolescence of equipment. The IAEA is leading several efforts to optimise RR availability and reliability through Coordinated Research Projects and sharing operating experience as well as the development of publication and implementation of operational and maintenance (O&M) plans, ageing management plans, training programs and international peer reviews. Additional O&M issues being addressed by MSs are fuel optimization, equipment modernization, modifications required due to security and safety requirement changes, and modifications aimed at increasing facility

reliability and availability. The Research Reactor Section (RRS) offers MSs Operations and Maintenance Assessment of Research Reactors (OMARR), a peer-to-peer review to assist with improvement of operational and maintenance practices. The IAEA is establishing a specialized activity for conducting non-destructive examination (NDE) and in-service inspection (ISI) at research reactors. Additionally, RRS is currently participating in several projects related to instrumentation upgrades, fuel upgrades, safety infrastructure support, and decommissioning planning through the Technical Cooperation organization to assist individual and regional MSs. This paper presents RRS activities to support MS with RR O&M.

2. Operation and Maintenance Assessment for RRs (OMARR) missions

OMARR stands for Operational and Maintenance Assessment of Research Reactors and its aim is to provide advice and assistance to Member States to improve their operational and maintenance (O&M) practises by peer to peer reviews thereby optimising availability, reliability and the application of human and financial resources throughout their facilities operational life cycle, from commissioning through to decommissioning.

OMARR, to be initiated in 2012, will be available to Operating Organizations in all Member States with research reactors (RRs) under construction, commissioning or in operation. Robust design, careful manufacture and sound construction are all prerequisites for RR sustainable availability and reliability. However, a high quality operational and maintenance programme ultimately depends on effective management, sound policies, procedures and practices, on comprehensive instructions, on adequate resources and on the capability of the O&M personnel. OMARR considers these aspects in assessing the effectiveness of a research reactor's O&M experience feedback programmes. The assessment considers the application of IAEA and international standards and related technical reports. Although these standards establish an essential basis for effective O&M practises, the incorporation of more detailed requirements in accordance with national or international good practices may also be necessary. Moreover, some special aspects might need to be assessed by experts on a case by case basis.

The IAEA Code of Conduct on the Safety of Research Reactors and the Optimization of Research Reactor Availability and Reliability Recommended Practices, IAEA Nuclear Energy Series, No. NP-T-5.4 document [2], cover the baseline for good practises in RR O&M. The OMARR guidelines, based on these two documents, provide overall guidance for the experts to ensure the consistency, and comprehensiveness of the assessment. This could also be used by the facility to prepare a self-assessment report on the effectiveness of its O&M experience feedback processes. It recommends the required expertise of the OMARR team members themselves and forms the bases of the assessment.

OMARR missions are performance oriented in that they accept different approaches to O&M management that represent good practices and may contribute to ensuring a good operational availability and reliability on the part of the operating organization. Recommendations and potential solutions are made on items of direct relevance to O&M with a principal aim to improve performance. While suggestions made could also enhance plant safety, these are considered a secondary, although positive outcome, more directly related to the objective of INSARR Missions. The OMARR service, focusing on O&M improvements, is one of a suite of complementary services offered by the IAEA for the research reactor community. The OMARR will consist of up to three missions: pre-OMARR Mission, main mission and follow up mission if requested by the facility.

It was decided to have two pathfinder missions to kick off the OMARR program, one on a

larger power RR and the second on a smaller facility. Two pathfinder OMARR missions have been completed and the process is now available for member states to take full advantage of this peer to peer assessment. NIST was the first to respond and is a 20MW reactor; LENA 250kW, was the first small facility to express a desire for an OMARR mission.

3. Building Capacity in conducting Non-destructive Examination and In-service at Research Reactors

In-service inspection (ISI), which is performed using non-destructive examination (NDE), is an important measure for assurance of equipment integrity and the avoidance of failure and thus a key tool in the management of research reactor safety and lifetime. The IAEA has consistently supported the operation and maintenance programmes of research reactors, particularly in the formulation and implementation of ageing management and surveillance programmes, which include the regular examination of structures, systems and components of reactor facilities for potential degradation to verify reactor safety and maintain optimal availability.

A Coordinated Research Project "Application of Non-Destructive Testing and In-Service Inspection to Research Reactors" was organized and successfully completed during 1995–2001 and eponymous guideline (TECDOC-1263) for NDE/ISI as part of an ageing management and surveillance programme of research reactors was released in 2001 [3]:

- NDE methodology for use in ISI of research reactor of various types;
- Guidance for the preparation of appropriate programmes/plans/schedule, including documentation, of such ISI and for their implementation;
- Appropriate methods and procedures to be used in ISI of research reactors of various types;
- Guidance on the requirements for qualification and certification of NDE personnel involved in ISI of research reactors.

The IAEA has been preparing to establish and promote a specialized activity for conducting NDE/ISI at applicant reactors. The necessary equipment had been procured and is in storage at the IAEA Seibersdorf Laboratory, to assist member states in the performance of NDE/ISI. Table 1 shows the scope of available equipment from IAEA. The IAEA can assist by providing experts to train local staff, promulgate best practices and improve ageing management and surveillance programmes using procured equipment.

Through training workshop, Member States had the chance to share experiences, lessons learned and good practices, and was provided a practical demonstration using selected IAEA equipment as well as a theoretical training on ISI methods and the performance of ISI activities. The practical trainings, the measurements of the thickness of pipes using ultrasonic tester and a fact-finding inspection with an underwater camera, were given to participants at the TRIGA research reactor at the Atominstitut of Vienna University of Technology.

1. Underwater Camera Systems	**a. <u>Monochrome Camera</u>** • 200 MRAD radiation tolerance • 40.5 mm diameter • Water tight to 50m up until 55°C • High resolution (600 tv-lines) • Wide range of viewing heads for radial viewing • Easy-to-use i.e. mostly used for fuel inspection, pipe inspection • Option of video recording and still images (DVD and USB recording

	provided) **b. <u>HD Colour Camera</u>** • Image Resolution: 800 H-TVL • Format: 1080i / 720p • Light Output: Four 10W LED lights (40W total output) • Zoom: 10:1 Optical; 4x digital • Field of View (horizontal): 5° - 50° • Minimum Focal Distance (wide): Front window • Focus: Auto / manual • Tilt Range: +/- 140° • Pan Range: +/- 180° • Envelope: 3.9" x 11.4" • Weight (in air): 11 lb. • Housing: Stainless steel • Radiation Tolerance: 108 Rads* (103 Rads/hr) • Operating Temperature: 50°F to 113°F
2. Ultrasonic Tester	**<u>USM-36 KRAUTKRAMER</u>** • emersion probe 10 MHz (cable 10m long BNC to COAXIAL) • angled probe 5.0 MHz (1m cable BNC to DOT, wedges 45°, 60°, 70°) • longitudinal probe 5MHz (TR probe, cable 2.0m BNC to LEMO type) • Calibration standards block, stainless steel, IIW block • Stepper blocks for aluminium for calibration not available (to be manufactured for your own application)

Tab 1: Scope of Equipment Available from IAEA

4. Coordinated Research Project (CRP)

4.1. CRP T34003: Condition Monitoring and Incipient Failure Detection of Rotating Equipment in Research Reactors

Online Monitoring (OLM) technologies have been successfully implemented in power reactors for a number of applications such as condition based calibration, performance monitoring of process instrumentation systems, detection of process anomalies, and distinguishing between process problems/effects and instrumentation/sensor issues. In spite of great advances in OLM technologies for power reactors, research reactors are yet to benefit from all that OLM can offer. The experience from these implementations has stimulated an interest in the research reactor community to use OLM for improved maintenance regimes, safety and reliability of research reactors, and to contribute to their life extension and aging management objectives.

This CRP T34003 is the second in a series involving on-line monitoring techniques. The first was CRP T34001 "Improved Instrumentation and Control (I&C) Maintenance Techniques for Research Reactors using the Plant Computer" implemented 2012 to 2015. As research reactors continue to operate, there is increasing pressure for improved asset management programs that involve advanced predictive maintenance technologies to manage equipment degradation and aging. For example, advanced technologies are now available for predictive maintenance of motors, compressors, fans, and turbines and also for on-line condition monitoring of plant instrumentation. These methods have been used successfully for numerous applications in industrial processes such as equipment health and condition monitoring, reliability assessment, aging management, life extension, troubleshooting, safety improvement, and process optimization. Although some research reactors have taken advantage of these developments, significant improvements are still needed toward a

systematic implementation of these technologies at research reactors.

The overall objectives of this CRP are to avoid lengthy and costly shutdowns, and to promote safe and reliable operation and lifetime extension through monitoring the health of key rotating components.

Condition monitoring techniques can provide various types of information that can be used to better plan and schedule maintenance activities. Planned activities can be carried out in a much more efficient, and safe manner than activities carried out in response to an unknown failure event. Unforeseen failures and their unscheduled repair place significant stress on plant staff and have the potential to adversely affect related plant equipment and plant safety. Knowledge of poor equipment condition may be used to reduce the load on that equipment such that the risk of further damage is minimized until the next maintenance opportunity, and the consequent maintenance time, and direct costs are reduced. Condition monitoring techniques are equally important to identify normal conditions. Indications of the proper equipment condition can be combined with other information to plan maintenance activities only when they are necessary.

4.2. CRP T34002: Establishment of a Material Properties Database for Irradiated Core Structural Components

The CRP will provide a forum for the establishment of a material properties database for irradiated core structural components. A structured database is required to understand the material behaviour in core components of research reactors for their continued safe operation and lifetime extension of ageing research reactors. The database can be used by research reactor operators and regulators to help predict ageing related degradation. This would be useful to minimize unpredicted failures of core components and to mitigate lengthy and costly shutdowns.

The database will be a compilation of data on material degradation from research reactors operator input, comprehensive literature reviews and experimental data from research reactor. Moreover, the CRP will specify further activities needed to address the identified gaps of the database for potential follow-on activities required by Member States. The database will be provided by IAEA to interested end-users Member States with controlled access.

Continued safe and efficient operation depends amongst others on the predictability of structural materials behaviour of major components such as reactor vessel and core support structures, many of which are difficult to replace. Management of the ageing process requires predictions of the behaviour of materials subjected to irradiation. Ageing management of research reactors includes a comprehensive effort of engineering, operation and maintenance strategy to ensure reliability and availability of structures, systems and components (SSC) important to safety. Age-related degradation mechanisms can result in unplanned outages as well as lengthy shutdowns and the need for additional regulatory activity, which can be prevented by utilising available data and implementation of appropriate maintenance and surveillance programmes. In many instances data for the radiation-induced changes of research reactor core materials resulting from exposure to very high neutron fluences are not generally available because the materials and operating conditions are diverse and specific. Therefore, effective sharing of experimental results related to the core-structural materials is needed in order to evaluate the reliability of ageing reactor core components. Moreover, safe operation, reliability, and availability of the RR irradiation services has to be assured as older, heavily utilized facilities may be required to extend their operation to provide these services. Consequently, the uncertainties in the core structural materials behaviour need to be reduced for timely action for improvements and/or replacement of components. Furthermore, predicting the lifetime of irreplaceable components will contribute considerably to the

managerial process of decision making on operation schedules.

The overall objective of the CRP is to collect, review and assess existing data of the relevant materials properties and operating experience with research reactors worldwide for inclusion in a Research Reactor Components and Material Properties Database that can be used by research reactor operators to help predict ageing related degradation in order to avoid lengthy and costly shutdowns, and to promote safe and reliable operation and lifetime extension.

5. Conclusions

The activities outlined in this paper represent the current body of work for Operational and Maintenance issues in the Research Reactor Section. In addition to the above there are IAEA organised workshops and technical meetings on a variety of O&M issues such as aging management, continued work on the aging database and support for RR safety work in O&M areas (with the Nuclear Safety Research Reactor Safety Section).

In practice, an ageing management programme is accomplished by coordinating existing programmes, including maintenance, periodic testing and inspection and periodic safety reviews, as well as applying good operational practices, and incorporating lessons learned from operating experience.

The IAEA has consistently supported the operation and maintenance programmes of research reactors, particularly in the formulation and implementation of ageing management and surveillance programmes, which include the regular examination of structures, systems and components of reactor facilities for potential degradation to verify reactor safety and maintain optimal availability.

6. References

[1] International Atomic Energy Agency, Research Reactor Database: https://nucleus.iaea.org/RRDB/RR/ReactorSearch.asp

[2] International Atomic Energy Agency, Optimization of Research Reactor Availability and Reliability: Recommended Practices, Nuclear Energy Series NP-T-5.4, IAEA, 2008

[3] International Atomic Energy Agency, Application of Non-destructive Testing and In-service Inspection to Research Reactors, TECDOC-1262, IAEA, 2001

Exact power evaluation due to introduction of Mo-99-LEU targets for FRM II

A. RÖHRMOSER
Technische Universität München, ZWE FRM II
Lichtenbergstrasse 1, 85748 Garching - Germany

In order to contribute considerably to the security and supply of the medical isotope Mo-99 Germany's high flux research reactor FRM II is foreseen to be equipped with a dedicated facility that allows the simultaneous irradiation of up to 16 LEU plate targets.

The irradiation shall take place within a vertical tube in the heavy water moderator tank. The basis for any cooling concept and thermo-hydraulic layout are heat source determinations through neutronic calculations. They are carried out in this case in in a very detailed full core manner with exact geometrical resolution of all targets in the irradiation device. The production of total and local power is also resolved over the irradiation time span. A detailed balance sheet of all heat contributions in and outside the irradiation device due to the introduction of the targets is given, too. Additionally the influence on the reactor power detection is examined thoroughly. By those means TUM is convinced to be able to predict exactly all extra power contributions introduced with Mo-99-LEU targets at FRM II in total as well as locally.

1 Introduction

The project at FRM II for irradiation of a uranium targets to produce the Mo-99 Isotopes now spans nearly a decade. The first chosen position (2007) at the only free vertical irradiation channel was kept. The tube had to be extended in a reactor stop in 2011 to 74 cm below the core central level to provide sufficient place for a ‚stack' of four to five targets on top of each other. But internally the concept [1] has changed a lot; since several years it is now based on LEU plate targets instead of circular HEU targets, that were very widely used at project start in 2007. As a consequence the cooling channels became now lens shaped to be able to introduce a flat plate assembly (s. Pict. 2 below).

One aim of this work is to give an exact balance sheet fort the total nuclear heat in the channels in the loaded state with this new target geometry (stipulated Dec. 2011) und specification of the target manufacturer of Mai 2012 [2]). The amount of fissile U-235 is unchanged in comparison to the first layout with annular targets with exact 4.0g of U-235/target. A first result was that the produced nuclear power per target will be of 25 kW in average of 4x4 LEU targets and thus only slightly below the former value (27 kW at 3x5=15 annular HEU targets). The totally accumulated heat is of about 400 kW at maximum target load for both cases. So far are the rough estimates. But a layout must provide much more detailed and also local data, which will be gathered together in this paper. And still in the state 'free of targets' there has to be removed a heat power of some kW, what has to be respected.

2 Calculational model

2.1 MCNP

At the studies, described as follows, flux densities for neutrons and fast photons were ascertained, here particularly regarded in the area of the irradiation channel, which reaches down now 74 cm

below core central level. All data were found by using a 3d-MCNP (Monte-Carlo-method of the transport theory [3]) model for the whole reactor FRM II [4] with inclusion of all relevant installations in the heavy water tank.

2.1.1 Model of reactor and surrounding in the direction of the tube

Picture 1 from MCNP model gives a sketch of the geometrical characteristics for the target irradiation at FRM II:

- the down-prolonged thimble of zirkonium material with enough room fort the targets,
- the rather big distance to the core, meaning a pronounced thermal neutron spectrum from the reactor, but still in an area of very high flux to guaranty a high output on fission products as Mo-99.

All calculations are done for a ‚mid of cycle' (MOC)-situation of the reactor cycle (in picture 1 with the central control rod withdrawn to 16 cm above central core plane.

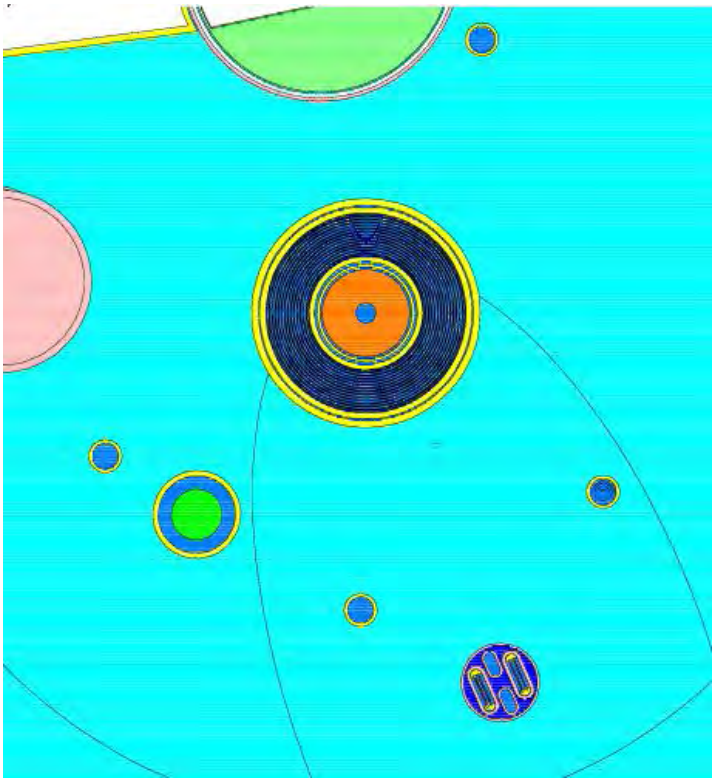

Picture 1:
Horizontal cut at about the core mid plane through the fuel element and its proximity in the heavy water (HW) tank. The Mo99-thimble (in the right downside corner) at distance 45 cm to the axis of the tank and the fuel element is shown here already equipped with the new LEU plate targets in the channels (inert He fills the gaps). The orientation of the plate targets is nearly in the axis to the core.

The pair of coolant channels A and B is directing to the fuel element, so that both target channels see nearly the same neutron flux at the same distance to the core. Only small differences are calculated between A and B due to some asymmetry of the insertions in the heavy water (HW) tank (s. later). Picture 2 presents two identical coolant channel pairs for giving a best possible independence for target insertion.

2.2 Model for target insertion

In both identically designed channel pairs (up and down stream) lie two plate targets lateral parallel. Four targets can be irradiated at every height position. The full (maximal) target load shall be 4 layers à 4 plates (64 g fissile U-235 in the HW tank at the maximum). They will add roughly 400 kW to the pure reactor power, which shall stay at 20 MW thermal.

The channels for the Mo99 target irradiation were designed in 2012, respecting several technical arguments with the channels showing a lens shape (picture 3a+b).

The plate targets will come down in the bigger side channels independently and they are cooled with water streaming from bottom to the top. The two smaller channels will have no inserts and bring the coolant down to the bottom pipe elbow. The pair allows an independent insertion of targets (left or right or both). For determination of the power data both LW channels were regarded as reaching down till the bottom of the thimble.

The coolant channels are thermally isolated in the thimble due to the stagnating He gas inside. A most exact balance sheet for the nuclear heating power in the LW channels was a goal and is shown in this work. All the locally deposited nuclear heat must be removed by the LW coolant channels.

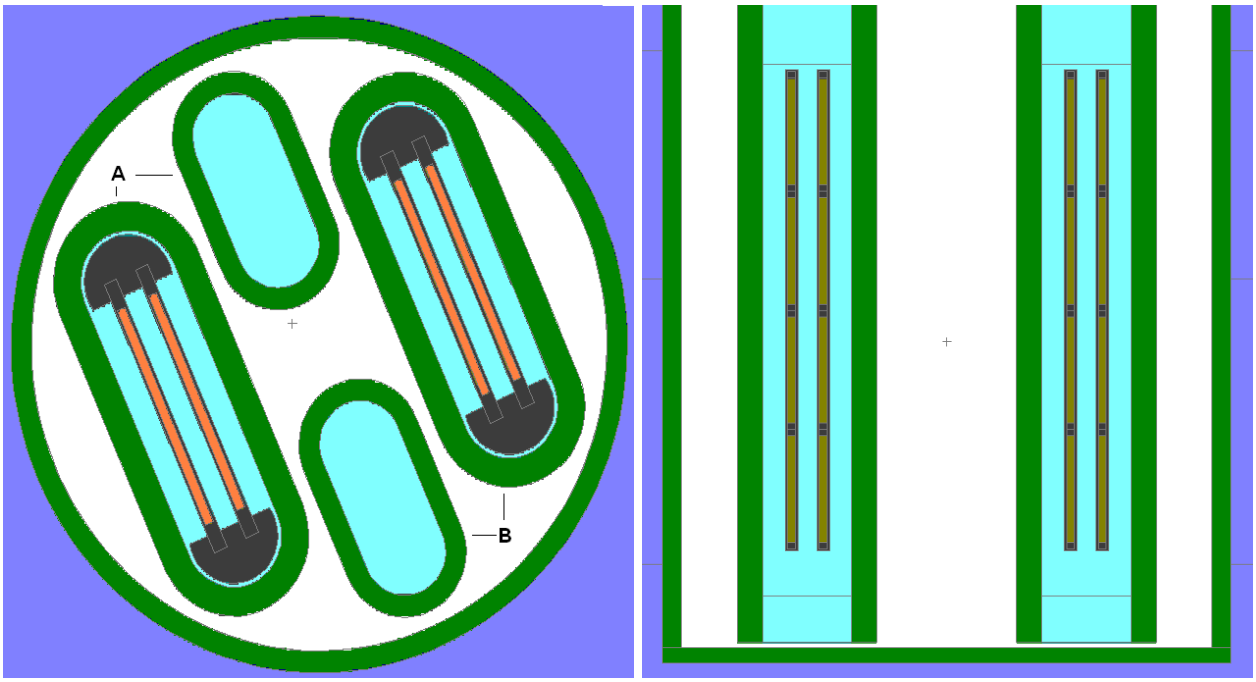

Picture 2 a+b:
Horizontal and vertical cut through the irradiation thimble and the pair of two identical coolant channels (with insertion of 4x4 targets in picture 2b, meaning the maximum load of the design).

2.2.1 Model fort the target and the heating tallies

The plate targets were segmented for MCNP-tallies over the height and the width for determining the specific local nuclear power. Over the width of the fuel a raster of 3/6/14/6/3 mm was sufficient (32 mm total width), meaning that the edges were resolved much finer (s. later Picture 4).

All these MCNP tallies were counted over volumina (zones) and are of type heat tally (F6 bzw. F7 for the fission heat). In addition an extra (F4) tally was introduced for respecting the locally deponated ^{28}Al-β-heat following the ^{27}Al-capture (delayed but quasi steady state; source for more than extra 10 kW power at the targets, s. later).

The decay-γ's following the n-capture of Al to Al-28 (T½ = 2.2 minutes) can be treated here absolutely steady state. This contribution was integrated into a file with an extra γ-source term (13027.52c) for MCNP; without using it one would again ignore some extra kW for the target cooling.

The LEU-load was assumed to be 100% in the area of the fuel. The local power values, given by this work, are thus nominal ones, tolerance factors can be respected on base of these local power data.

c // -- fuel material - targets – LEU (19.75% enriched)

M32	13027.52c	52.43E-03 $// Al
	92235.66c	1.2904E-03 $// U-235, provides exactly 4g U-235 in the targets
	92238.66c	5.1634E-03 $// U-238, nearly 80% of the uranium are U-238
	92234.66c	0.0116E-03 $// U-234
	92236.66c	0.0019E-03 $// U-236

Table 1:
materials specification for the LEU fuel in the MCNP input, used cross section data and density values of the fuel layer of the LEU targets.

2.3 Heat terms in detail

Recoil heat from fission products and fast neutrons is deposited locally as well as heat from fast decay β-s.
In a conservative manner, one could accumulate for local cooling all main contributions of the nuclear power, inclusively the γ-s in the targets, what would equal to the quite good number of 200 MeV/fission. This was supposed at the very start of the project; and it shows up now, that even 190 MeV/f were still on the conservative side, since a big part of the γ-energy, produced in the fuel of the targets, must escape into the HW-cooled surrounding; this is confirmed in the very details by this work.

2.3.1 Target load

Insertion of 4x4 LEU targets means an extra thermal power production of more than 400 kW. Although a part of this heat will be removed by the HW cooling system, there remain about 90% of the heat (s. details in the table below) in the LW channels. The contributions are in detail:

- slow down of fission fragments locally in the fuel
- slow down of penetrating fast neutrons (core contribution very low, s. below)
- β-heating due to decay of isotopes, generated by n-capture reactions (here mainly β-decay of ^{28}Al); attributed to this also
- γ-heat due to the delayed β-decay of ^{28}Al
- γ's due to n-capture in all structures of the thimble and the surrounding
- γ-heat as a consequence of prompt and delayed γ's due to fission and decay of unstable products (core contribution again very low, s. table)

2.3.2 Target free case

The target free case had to be calculated the same way to answer the question for necessary cooling without local fission heat. At full reactor power all nuclear heat contributions sum up to nearly 4.5 kW in the Zr-walls of the coolant channels and 0.9 kW in the LW coolant, what is much more than can be dissipated alone through thermal conduct or radiation.

3 Results for nuclear heat load

The results are given by calculations done for a typical MOC-situation of the reactor cycle and normed to full thermal reactor power (without targets) of 20 MW.

3.1 Balance sheet

At the target load, assumed at the maximum of four layers à 4 plates (4x4), the following heat load contributions can be settled in detail in the different areas in the thimble.

[kW]	n-heat	1σ	γ-heat	1σ	FP core 90% yI	1σ	FP tgt 90% yI	1σ	Al β-heat	sum-heat terms -FP Tgt	+FP Tgt	resp. [MeV/Sp.]
LEU	354,3	6E-04	1,710	0,002	0,068	0,029	1,115	0,028	10,96	356,1	368,2	176,33
Al/plate	0,025	8E-04	0,424	0,002	0,019	0,04	0,215	0,031	0,08	0,6	0,8	0,37
	354,3		2,13		0,09		1,33		11,04	356,6	368,9	176,69
tgt-hoalder	0,019	0,001	0,415	0,002	0,031	0,028	0,146	0,039	0,31	0,8	0,9	0,44
Zr-back-	0,027	6E-04	5,278	0,002	0,429	0,019	1,932	0,026		5,7	7,7	3,67
pro channel	0,009	8E-04	2,007	0,002	0,207	0,025	0,575	0,034		2,2	2,8	1,34
LW-pro	0,450	9E-04	0,364	0,002	0,035	0,035	0,095	0,038		0,8	0,9	0,45
-back stream	1,316	6E-04	0,825	0,002	0,042	0,027	0,365	0,028		2,2	2,5	1,22
	1,82		8,89		0,74		3,11		0,31	11,5	14,9	7,12
Zr thimble	0,013	6E-04	3,25	0,002	0,59	0,011	0,78					
bottom	0,000	6E-04	0,12	0,012	0,008	0,139	0,00					
	0,01		3,37		0,60		0,79				4,8	

Table 2: heat load contributions (in [kW], FP=fission products) of the channels of the Mo99-target facility. The numbers behind the result columns mean the statistical error value in declaration 1σ. The last column provides the value 'specific heat/fission event'.

The nuclear heat load at reactor full power with freshly introduced targets is calculated in total at the 4x4-target-maximum (without/with delayed FP-decay of targets):

$\mathbf{P_{tgt}}$= 356/369 kW	in the targets themselves (to be removed over their surface)
$\mathbf{P_{can}}$= 11.5/14.9 kW	additional heat of the LW-channels and
P_{Zr} = 4.0/4.8 kW	in the Zr wall of the thimble

The maximum heat load, that had to be removed from the target surface is thus $\mathbf{P_{tgt}}$= 369 kW, whereas the LW of the channels attributes an extra heat load of 15 kW.

And the data mean a specific heat load at the channels of:
normP =176.7 MeV/fission, when summing up all contributions of the plate targets (incl. FP Tgt);
normP =183.8 MeV/fission, when adding the contributions in the Zr wall and in the LW of the channels.

The pure γ-heat contribution of the Zr wall of the thimble falls to the HW cooling system, as well as 40 kW further heat load, introduced to the HW as a consequence of the assumed 4x4-target-load. The total power added to the reactor (s. later for power signaling) by the 4x4 targets sums up to 420 kW.

It had to be shown, that the full loading means the maximum local heat load, too. One single stack of 2x4 targets (no stack in the 2nd channel) represents exactly the same power for the hot target row (east side, both channels) than the case of the hot target stack with two parallel stacks (hot row on east side).

3.2 Heat load distribution in the targets over the heigth and width

All calculations so far were done with a fixed reactor source. In order to take also into account the very small influence of the target-source on the neutron source terms in the fuel element, one can calculate directly in coupled mode (but much more CPU-intensive)* .

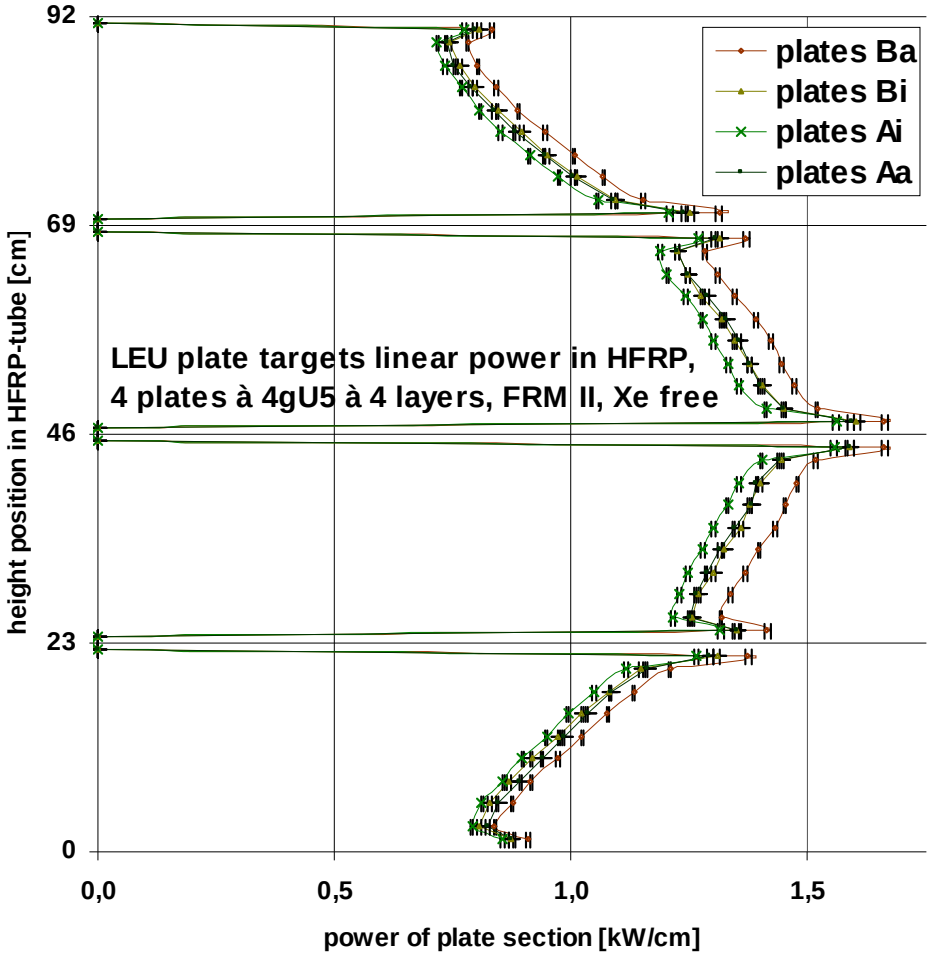

Picture 3: distribution of the nuclear heat load over the height of the 4x4 targets. One stack with 4 targets on top of each other spans over a total height of 92 cm. The target stacks are located at the same height in both lines, with the emphasis some cm below core center line (=52cm in this picture). The hot target row Ba is at the east side.

Picture 3 and 4 show the fission heat distribution (F7- tally) over the height and the width (32 mm) of the targets, here normed with normP =180 MeV/f, what fits quite well to the average heat development value over the full height of the plate targets (s. table 2). One can quote some characteristics of the linear heat load distribution over the height (and width) and explain the small detail differences:

- The target stack is positioned with the emphasis some cm below the core center line in a way, that the nuclear heat load appears in a quite well symmetric manner over the height.
- The targets in the stack center (heights H2 und H3) reach higher fission rates and product amounts than those at the stack ends (H1 und H4); the power data for the targets H2 and H3 are of same size but with reversed profile over the height. The same is true for a comparison of the targets at heights H1 and H4.

* This coupled mode resulted in a maximum reload of the power of the fuel element of about 1% in direction of the side of the element to the target thimble. And this means, that the target power values are also about 1% higher in comparison to the calculations with unperturbed source. A further influence of the ‚target'-source on the reactor is given for the power detection of the reactor.

- There will be a small power peaking at the plate ends. The ends are geometrically resolved with a zone of 5 mm at the edge (nominal = 100% U load) und the values there will be about 12 % above the extrapolated trend curve at each target.
- The plates most left or right (Ba and Aa) have somewhat higher power than the inner ones. And the heat loads in channel B (s. Bild 2a, east side) are some % above those of channel A. The latter effect is more obvious at the height H2, where two beam tubes go by at the side A.
- The profiles over the plates are very the same with some peaking at the sides and the maximum at the side, which views the reactor. The profile over the width is the same for all targets and for any target cross section, with a very small difference (flater) only at the peakings at the target ends.

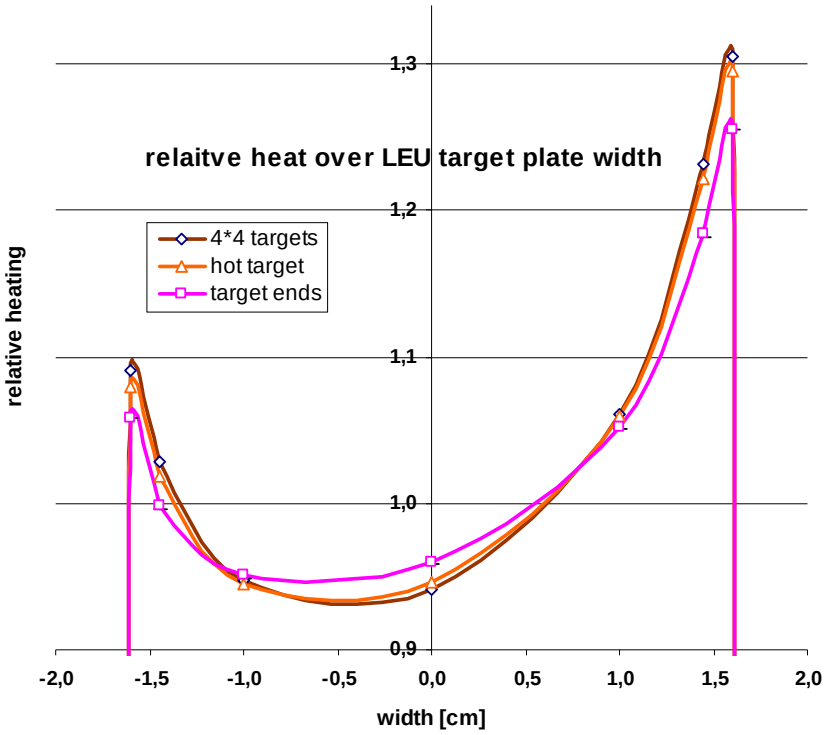

Picture 4: distribution of the nuclear heat load over the width of the targets.

4 Time dependancies

Extra modeling was introduced to be able to predict the timely evolution with the targets. Therefore the actual Monteburns (MB [3]) burn up model of the reactor [4] was extended with the U-platelets (one zone for 4 plates at any height). The platelet stacks were introduced prompt to the reactor in the calculation (‚feed'-mode in MB), so that they got irradiated at 20 MW full power in the mid of FRM II's cycle (here from day 26 to day 33 of the element); after the irradiation time the calculation continued without reactor power to simulate the further course of the nuclide concentration in the platelets.

4.1 Power of the U-targets over a week of irradiation

The typical course of the power production of U-platelets introduced into the reactor FRM II during the irradiation shows Picture 5 and Table 3.

Table 3: relative power of the targets as function of the irradiation time in FRM II; values are taken from the flattened course of the diagram

Irr. days	rel. power
0	100,00%
0,25	98,46%
0,7	97,13%
1,5	96,26%
4,5	94,42%
6,5	93,05%

The flux depression of Xe-135 leads to a lower target power (3%) in the first day. Till the end of the irradiation after a week the fission rate will be reduced by further 4% due to build up of further fission products and some loss on U-235 in the targets. It shall be mentioned that this behaviour is not a preprint for other reactors!

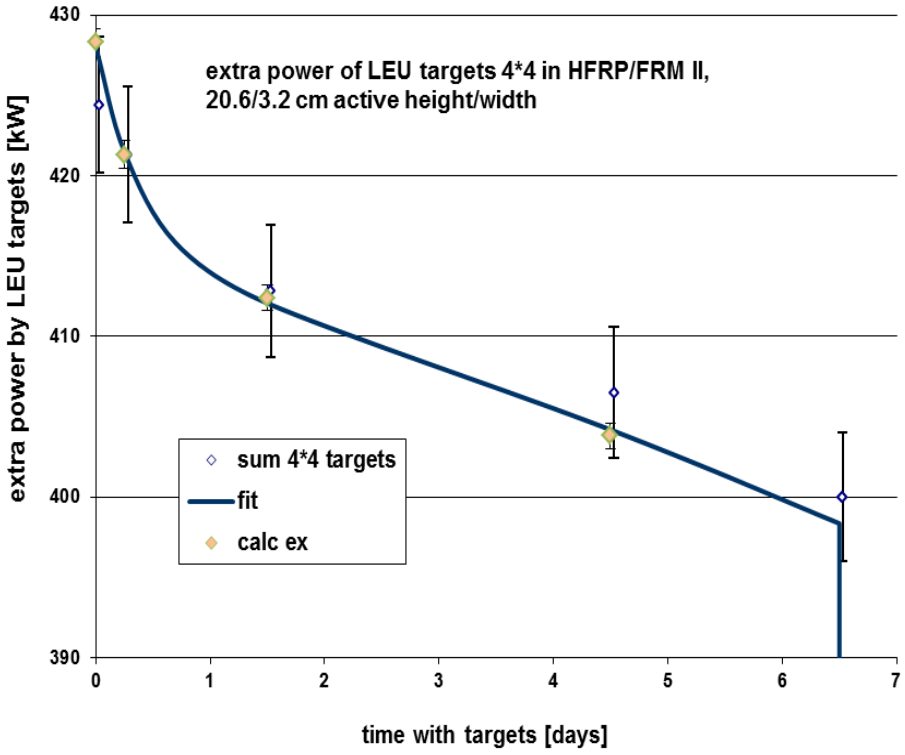

Picture 5: Course of the total power production by 4x4 U-platelets (sum) during the irradiation of here 6,5 full power days. In the targets themselves there will be released 90% as a good number of the extra power. (with 'calc ex' the single time step calculations can be continued after the burn up scenario, leading to much better results)

The calculation tells us, too, that 3.2 g U of originally 63.8 g U-235 in 4x4 targets got fissioned or converted to U-236 during 6.5 full power days.

5 Influence on reactor and installations

5.1 Reactivity

The additional n-multiplication of the uranium targets in the HW tank of the FRM II has an influence on all other neutron physical terms in the reactor in principal.

Introduction of targets must lead to an increase of core reactivity; it is a small effect, but due to the very small reactivity loss per operations day of FRM II, this can be expressed in a difference of 2-3 days of full power operation. A gain, that can't be used 'gross' in reality, since introduction of the cooling channels will take some reactivity permanently away.

5.2 Flux differencies

With respect to other beam tubes, one can clearly state, that there will be no real change for any user (maximum change 1% at one beam tube) during target irradiation. But there must be expected greater changes of the thermal n-flux in the sector area of the tank behind the thimble through the n-multiplication in the uranium targets. This is of significance for the reactor, as there is located a power range detector (LB) for power calibration in this area behind the wall of the HW tank.

5.3 power calibration

The detectors for power range control (LBs) have to follow and signal instantaneously the power changes of the fuel element. They are threefold due to redundancy reasons and located around the HW tank nearly equidistant. Multiplied neutrons from the targets, although amounting only to 2% of the core neutrons, contribute also to the signal of these detectors. And they can also falsify somewhat the display of the differential reactor power at the LBs, as was shown by exra 3d calculations.

A former reactor model with signalling of the three LBs could be folded with the new target model of the reactor. Because of the extremely low possibilities for detection of multiplied neutrons at the LBs and the necessity to prove a very small influence on the detectors in the low % range, one needs not only very long calculation times but also the application of a particular, differential scheme, that was used already for several purposes at TUM.

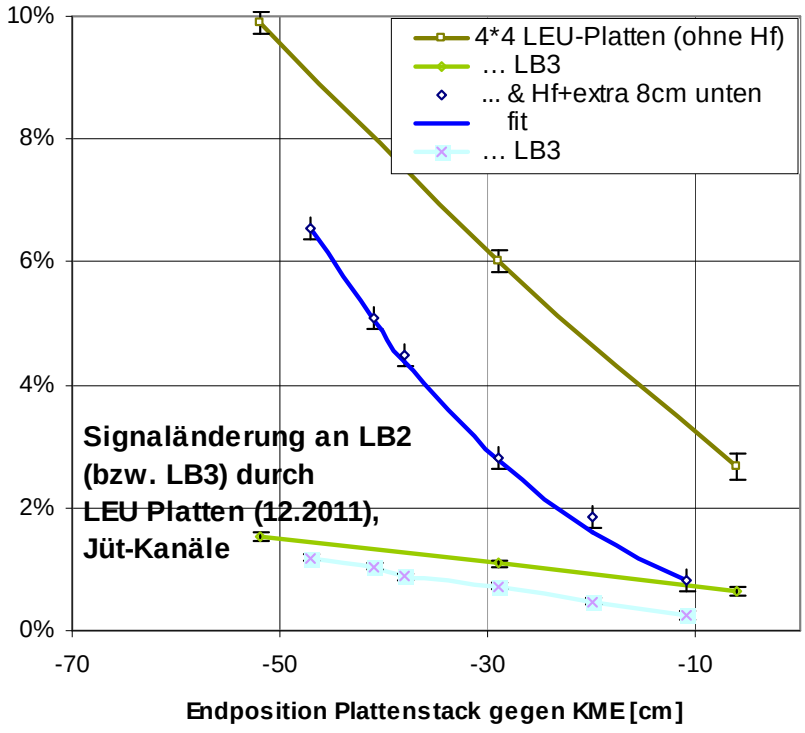

Picture 6:
calculated contribution of the LEU targets on the display of the differential reactor power detection at LB2 und LB3 as function of the position in the thimble and with the complement of Hf platelets below the target stacks. The marks at the ‚4*4'-curves without Hf show a driveway of exactly one target-height in the stack.

LB1 and LB3 lay at quite different azimuth angles in the tank than LB2, which is located behind the target-thimble. Fission neutrons from the targets (especially the low lying ones) have a clearly higher possibility to arrive at LB2 than LB1 or LB3. The specific power of the targets will be reflected much more at LB2 than given with the calibration of the LBs for the specific core power. This will be accepted for the reactor operation only in a rather narrow range.

Some results are shown with Picture 6. At the position of the 4*4-targets for optimal fission product amount, the disturbance reaches nearly 10% at LB2 and less than 2% for LB3 (also LB1). The disturbance by the targets on LB2 is thus 7-fold stronger than at LB3 (LB1). Measures to reduce this strong disturbance on LB2 against the one on the two other LBs were under investigation with these models, since the high importance for the reactor operation.

A technical relative simple solution with absorber (Hf) platelets of the same size than the LEU targets would give indeed a clear reduction of the disturbance (again Picture 6) after the neutronic calculation, when positioned at the lower end of the driven stack. The absorption would compensate somewhat the effect of the targets on the LBs when arriving in the thimble. It is not before the deep position, the last 20cm driveway, that the Hf platelets became clearly weaker.

5.4 Other power influences

The targets imply an extra neutronic and γ- heat source in the direct neighborhood, as already given in some numbers. This means the necessity to calculate the extra heat terms for any sensitive installation in the neighborhood with comparable methods as given here.

For example, there is projected an ultra cold neutron source (UCN), which could be affected very much by introduced targets. With nearly a doubled amount of power, as calculated for the UCN source [6], this can't be accepted for its operation, meaning a local shift of the dedicated UCN kernel position more away from the targets or any other scheduling for the project.

SUMMARY

Heat load values in the channels of the projected facility at FRM II for Mo99-isotope production were determined by ‚best estimate' methods. It can be examined without to much detailing, that with a load of 4x4 fresh LEU platelets about 400 kW of additional heat will be released at reactor full power.

The fine balancing of the heat gave much more insight. The LW cooling streams in both channel pairs must remove then 368 kW (or 384 kW incl. the delayed target contributions), at the 16 platelets there will be released 356 kW (or 369 kW incl. delayed contributions) of heat, only 3 kW will be released directly in the LW and further 9 kW (11 kW) come from further structures (target holder, Zr tubes). The production rate on Mo-99-activity at full power of the reactor will be 20.5 kCi (already reduced value due to Xe build up) with a 4x4 target load.

Besides the additional heat load terms rather small neutronic effects of the targets on the reactor and other user places of the reactor were examined; but the effect on the power signalling was found to be of a pronounced and not negligible size by the calculations.

ACKNOWLEDGEMENT

This work has been supported by a grant from the Bundesministerium für Bildung und Forschung (BMBF).

REFERENCES

[1] „Feasibility Study for a Mo99 Production Facility at the FRM II Research Reactor", A. Röhrmoser, C. Müller, I. Neuhaus, P. Jüttner, H. Gerstenberg, W. Fries, FRM II Projektablage, OPA343, 1.7.2009

[2] „Specification de Produit ‚Cibles IRE LEU/DU'", internal document, 2.5.2012

[3] "MCNP - A General Monte Carlo N-Particle Transport Code, Version 5", LA-UR-03-1978 (4/2003,10/2005), X-5 Monte Carlo Team, Los Alamos National Laboratory

[4] „MCNP-Modell zum ‚as-built'-Zustand der experimentellen Tankeinbauten des FRM II und Vergleich mit früheren Ausführungen", OPA00330, FRM-Projektbericht, A. Röhrmoser

[5] „Nukleare Heizlast der Kanäle (Juet) der geplanten Anlage zur Mo99-Isotopen-Erzeugung des FRM II ohne Target-Beladung", Projektbericht, Mo-99 Projekt / FRM II, interne Id: 8746-BN-1303, A. Röhrmoser, Garching, 28.10.2013

[6] „Ultrakalte n-Quelle (UCN) im Strahlrohr SR-6 des FRM II. Verschiedene Studien zu Flussverhältnissen im Reaktor und nuklearer Wärmedeposition", FRM-Projektbericht, A. Röhrmoser, Garching, 21.8.2008

TU Vienna - Atominstitute, Austria

TRIGA® 250 kW Reactor I&C System Refurbishment

PAVEL RŮŽIČKA

ŠKODA JS A.S., SENIOR TERRITORY SALES MANAGER

ORLÍK 266/15, PLZEŇ, CZECH REPUBLIC

MIROSLAVA KOCHOVÁ, JIŘÍ MATOUŠEK

dataPartner s.r.o., I & C DIVISION

SENOVÁŽNÉ NÁM. 241/15, 370 01 ČESKÝ BUDĚJOVICE, CZECH REPUBLIC

ŠKODA JS JSC

Since 1970, ŠKODA JS has supplied seven research reactors to Nuclear Research Institute Řež (NRI), the Faculty of Nuclear and Physical Engineering at the Czech Technical University in Prague, and finally the research centre of ŠKODA itself.

ŠKODA JS, with reference to its own project, is capable of designing, manufacturing and supplying the research reactors. Moreover, ŠKODA JS can also assist at the design stage and production of custom-made models, or the modernization of old equipment including the I&C system modernization.

Within the framework of a contract concluded with ÚJV Řež with respect to the technological part for the “Scientific and Technical Park and Business Incubator Řež”, ŠKODA JS supplied an experimental supercritical water loop (SCWL) in 2008. This device is unique in the whole world and is used to survey the materials of newly designed Generation IV. supercritical water reactors (SCWR) and to study water radiolysis at supercritical parameters.

After the successful upgrade of the control and protection system of the VR-1 training reactor at the Czech Technical University in Prague, ŠKODA JS also upgraded analogical systems of the LR-0 research reactor in the Nuclear Research Institute in Řež in 2008. A new control system for demineralized water preparation and a special, power-

operated closure of the reactor's experimental horizontal channel were supplied for the VR-1 training reactor.

Current ŠKODA JS´s research reactor projects:

- production and installation of new internals for the Belgian BR2 research reactor
- modernization of the control and management system for the Triga II research reactor and production and installation of new drive mechanisms for Austria's Atominstitute
- production and installation of control rod drives for the WWR-K research reactor operated by the Institute of Nuclear Physics in Almaty, Kazakhstan

dataPartner Ltd.

Company produces and implements Information and Control systems for industrial companies in the specific areas of:

- Production Planning
- Monitoring and Data Acquisition, Device or Order Monitoring
- Maintenance Management
- Machine Control, Critical and Technological Process Control, Instrumentation and Control Systems
- Individual Software or specific Hardware Development
- I&C and Process Automation

dataPartner Ltd. was first established in 1998 to distribute the real-time operating system for embedded applications from Phar Lap Inc., USA. In 2002 started to distribute the RTX real-time product for MS Windows, made by IntervalZero Co. As well as distributing, dataPartner uses the RTX product for development and implementation of its own control systems. The leading product is the PATRIOT® information system, a platform for the implementation of modern functionalities for support of industrial

production, and the DisCO® software product intended for real-time and process control and SCADA systems.

dataPartner has a certified quality control system for customer deliveries according to ISO 9001:2008. The certificate was granted by the NQA association (National Quality Assurance, Great Britain).

I & C System Refurbishment

New fully digital I&C System is capable to control and monitor variables and parameters of physical and other processes, component and system statuses considering project limits and safety conditions. The new I&C systems is able to perform all the functions in both, standard or abnormal conditions, including emergency scenarios. Technical equipment will monitor and record all main parameters, which may have an impact on safety and also gain all information needed for reliable and safety reactor operation. The I&C system is equipped by appropriate control and safety devices to keep critical variables within Technical Specification limits.

The scope delivery includes following systems:

- Neutron Instrumentation System (4 x Neutron detectors, 4 x Neutron measurement channels)
- Reactor Safety Systems (SCRAM and Interlock)
- Control System
- HMI (Operator console with displays, display soft controls, classical indicator and controls panels, display monitors, keyboards and mice, 2x display monitors in the reactor hall)
- Data Acquisition System
- Control Rod Drives

Quality Assurance

Project design and its implementation are in compliance with the high quality requirements according to nuclear equipment standards. The ISO 9001 quality management standards is applied during all production and delivering process stages including technical and quality documentation.

All equipment are designed, manufactured, installed, tested, and verified according to the best engineering practices.

The nuclear industry basic design principles and implementation practices will be used per Customer's scope and safety requirements:

Reliability, SFC (Single Failure Criteria), Redundancy, Independence, Diversity, functional aspects, iterative process of design, Verification and Validation (SW, HW).

Graded Approach

The graded approach (a structured method) is used in review and evaluation of the present TRIGA® reactor design, operation, and maintenance documents/analyses including integration of the new I&C. The extent of nuclear reactor safety requirements is applied according to the TRIGA® reactor characteristics.

Specifically, the TRIGA® reactor safety features (derived from the facility FSAR and reactor supplier documents) result in adequate scope of application of the general nuclear reactor safety requirements.

The TRIGA® reactor inherent safety is based on the TRIGA® Uranium and Zirconium Hydride (U-Zr-H) alloy fuel. The intimate contact between the uranium and the hydrogen of the fuel results in a self-moderated reactor fuel.

The TRIGA® reactor has the greatest inherent safety of any available megawatt level research reactor. The safety of the TRIGA® is due to the large prompt negative temperature coefficient of reactivity, which is an intrinsic characteristic of the standard U-Zr-H fuel. Therefore, the TRIGA® reactor in Vienna can be safely operated in a pulse mode with rapid power rise up to 250 MW and the negative temperature coefficient brings the power level back to approximately 250 kW after the excursion.

The TRIGA® temperature coefficient acts independently of any external controls to assure safe and reliable self-shutdown in the event of an accidental reactivity insertion. This reactor feature meets the definition of inherent (intrinsic) passive safety.

The TRIGA® reactor facility can be categorized as a facility with no radiological hazard potential beyond the research reactor hall or connected experimental facility areas.

Subsequently, verification if the design principles (Defense in Depth, Independence, Redundancy, Common Cause Failure, etc.) are properly applied is based on these TRIGA® reactor features. For example, the TRIGA® reactor safety and reliability requirements result in a lower degree of redundancy and separation in the design.

The Triga 250® kW reactor I&C Refurbishment increases nuclear safety, performance, and operational reliability.

OPAL REACTOR CONTROL SYSTEM UPGRADE AND THE CONVERGENCE OF THE INFORMATION TECHNOLOGY AND CONTROL SYSTEM INDUSTRIES

S. HARRISON
Reactor Operations, Australian Nuclear Science and Technology Organisation
New Illawarra Road, Lucas Heights NSW – Australia

ABSTRACT

The OPAL Reactor (Open Pool Australian Light Water Reactor) has recently upgraded its reactor control system. During the engineering development of the upgrade it was important to recognise and incorporate changes occurring in the control system industry. Ongoing development in the commercial Information Technology industry has created expectations for users of control systems (plant operators, maintainers and engineers) in terms of the usability and flexibility of modern systems. Increased use of commercial Information Technology equipment and practices by the Control System industry has provided this increased user flexibility and other benefits. These include the integration of readily available commercial hardware into control systems helping to decrease system costs and increase maintainability.

In response to industry-driven changes in architecture and design of control systems, a field previously the exclusive domain of instrumentation engineers now requires significant input from Information Technology professionals. This input is necessary throughout the design and maintenance of a modern control system, and to highlight issues relevant to computer based systems – such as cybersecurity and flexible approaches to implementation including computer virtualisation. Balancing this flexibility against the requirement for strict design, maintenance and configuration management becomes an important factor to manage within an operating organisation.

The evolution of the control system from dedicated hardware to include a mix of commercial Information Technology equipment also requires a change in the ageing management approach. Where control system hardware typically has a lifetime of a decade or more with upgrades and replacements planned around this timeframe, the Information Technology industry operates on a much shorter life cycle. Maintaining the support and system flexibility provided by the inclusion of the Information Technology system components requires the life cycle of these components be considered accordingly.

This paper considers the developments in the control system industry and their application to the OPAL control system upgrade. The upgrade design has considered aspects ranging from changes in the network architecture through to moving away from periodic large upgrades to continuous smaller upgrades of individual system components. The paper also considers how conventional plant engineering processes need to be reviewed and revised to reflect the shifting nature of control systems.

1 Introduction

An instrumentation and control system plays a key role in any industrial facility or plant. Not only is it normally the primary operator interface, the degree of flexibility and user interaction available can have a significant impact on the overall utilisation of the facility. Over the last fifteen years, developments in the control system industry have resulted in great changes to the underlying architectures as well as design and maintenance considerations. The research reactor community is not immune to these changes. While the control systems installed may typically be smaller than those in nuclear power plants or other large industrial youplants, the common technology platform and industry direction requires that research reactors are familiar with the resulting challenges, and are also able to benefit from the available opportunities.

While computers have long formed a key component of control systems, technological shifts within the Information Technology (IT) industry are triggering re-evaluations of the fundamental designs of control systems. The OPAL Reactor, operating since 2006, completed a significant upgrade of its control system in 2015. The engineering development of this upgrade forced long standing thinking to be challenged and new technologies to be embraced. It has also resulted in changes to the practices surrounding operation, engineering, maintenance and management of the control system within the operating organisation.

This paper reviews the experience of OPAL and seeks to provide guidance to other facilities; whether they are designing a new or upgraded control system, or are seeking to improve their management of current systems.

2 OPAL Control System

2.1 Overview

The OPAL Reactor Control and Monitoring System (RCMS) integrates the control of the reactor, including reactivity and cooling, electrical and other support systems as well as the reactor utilisation services including irradiation facilities and neutron beam control. Control of neutron beam instruments themselves and the collection of scientific data are performed by different systems from the RCMS.

The RCMS provides the primary reactor operator interface in both the Main and Emergency Control Rooms through multiple workstations in each room. Built on the Schneider Electric/Foxboro I/A distributed control system (DCS) platform, the RCMS integrates over 5000 input/output points, multiple PLCs used on individual plant subsystems and connectivity to more than 50 Modbus devices. The RCMS also provides electrically isolated, one-way read only visibility of the reactor's protection systems. Designed as a heavily instrumented reactor, the RCMS provides nearly complete visibility of the entire facility to operators within the control room. Computer terminals are also located throughout the facility allowing read only access to all of this data for operations, maintenance and engineering purposes.

In 2011, it was identified that the availability of vendor support for the control system would start to become limited within approximately two to three years. The increasing cost and difficulty of acquiring spare parts, as well as the increased rate of failure of the ageing computing equipment meant that the ongoing reliability of the reactor could be challenged. Design of the control system upgrade commenced in approximately 2013, with the upgrade works occurring throughout 2015.

2.2 Previous System Design

The previous RCMS installation was based on a very traditional computer platform design. Each operator or user terminal/workstation comprised a local physical machine connected to the system network. Several server computers also connected to the network provided

administrative and engineering functions. These computers all ultimately connected (though by different physical and software means) to the control network which provided an interface through the 'control processors' to the physical inputs, outputs and control hardware performing plant logic and loop control.

Real time synchronisation between redundant pairs of the control processors provided high reliability of plant control functions and management of data input and output. Ensuring that reactor operator access to the control system was also of high reliability was a combination of industrial grade computers and the provision of multiple terminals in the control rooms.

This system architecture was the original platform installed with the reactor construction and commissioning through 2003 and 2006. Since that time, some minor upgrade works were undertaken to update parts of the system to improve the level of vendor support and hardware availability. Despite this work, the increasing age of key system components (such as the operator workstations and engineering servers) meant that when hardware failures occurred it was increasingly difficult to obtain spare parts. This problem was particularly evident on the engineering and data historian servers whose failure rates increased such that every few months there was some loss of functionality until the computer could be rebuilt and backups restored.

A common aspect of DCS installations is that proper operation is dependent on all elements of the system running compatible versions of the vendor's software and hardware. The age of the OPAL system and the available vendor versions meant that any partial system upgrades would not result in long term risk reductions.

An options study examined the possibilities for improvements, considering aspects ranging from the engineering effort required, technology maturity as well as the human factors elements involved (for operators, engineering and maintenance personnel). This study determined that the most effective work would be to upgrade the control system to the current supported platform version from the vendor, while maintaining software that was familiar to the reactor operators in order to minimise the impact on human factors and retraining.

2.3 Upgraded Design

The resulting system upgrade design evolved out of significant effort between ANSTO and the system vendor. Drawing on the experience of ANSTO engineers and platform developments within the vendor, a novel system was implemented. An important aspect of the upgrade was the shift of the vendor towards the use of more standard computer equipment on which they based their platform – a trend becoming common across the industry driven by the obsolescence rate of commercial IT equipment.

This shift in technology allowed the best practices from the high reliability commercial IT industry to be considered and applied as required. While the applications may be different (internet or email server vs. control system user interface), the drive for reliability and fault tolerance are common. The most significant aspect of this technology exchange in the upgrade design was the extensive implementation of virtualised computers, terminal servers and 'thin clients.'

Virtualised Computers and Thin Clients

Over the past 30 years, the use of 'mainframe' type computers with 'dumb terminals' has completed a full circle. Popular in the 1970s and 1980s when computer infrastructure was both expensive and inefficient to distribute, the use of terminal clients was popular. Providing minimal or no computing functions at the client end, they simply acted as a relay and display agent for the server computer. With the introduction of personal computers in the 1990s this configuration was no longer viewed as the best option and became unpopular.

From the mid-2000s however, the commercial IT industry began to return to the use of server machines and client terminals. Network capacity improvements, a desire to efficiently use available computing power and efforts to minimise total cost of ownership has led to the reintroduction of virtual machines, terminal servers and 'thin clients.' While multiple technology options exist, the common element is that readily available power server machines can be much more efficiently utilised than having many user-facing desktop machines. A single server machine can 'virtualise' many different individual computers but use only one set of common storage, processor, networking and power systems.

With some of the benefits of this technology listed below, as implemented in the upgraded RCMS they provide for improved reliability and availability.

1. Removal of computers containing heat and dust-sensitive parts from around the facility reduces failure rates and decreases maintenance requirements. Thin client terminals are solid state.
2. All computer functions can be centrally managed, improving the ease of system changes, backups and maintenance. All such work can be performed from a central location. If a thin client somewhere in the facility fails, it is a simple 'plug-and-play' swap operation to replace it as it contains no software or configuration itself.
3. Redundancy and fault-tolerant software solutions developed for the commercial IT industry can be readily implemented for control system functions.

Fig 1. Comparison of the old (left) and new (right) equipment cabinets. The shift to the use of conventional IT hardware is very clear.

Fig 2. An operator workstation from the old system (bottom) with a new thin client (top).

Network Design

Consideration of how the control network design could be optimised for reliability also led to significant changes from the point-to-point architecture previously implemented. The 'trunk and patch' architecture was implemented throughout, providing several benefits:

1. Reduction in the number of cables needing to penetrate the reactor containment boundary.
2. Reduction in the number of cables needing to be run, providing spare capacity for expansion or to replace damaged cables.
3. Flexibility to allow relocation or reconfiguration of system components in the future by using re-patchable fibre optic and copper cables.

3 Cybersecurity

A popular topic in all industries which use computer equipment is cybersecurity. Efforts to investigate this topic and mitigation measures are being made by multiple government and industry groups around the world, including nuclear specific approaches by the IAEA [1]. Maintaining perspective in system design and operation must be maintained however. While cybersecurity aspects have not necessarily been well considered in the past, it is important that good engineering practices be maintained.

System design activities have always needed to consider the interaction of functional requirements, human factors, maintainability, nuclear safety and often physical security. Fundamentally, cybersecurity is simply another aspect to be considered in a system's design and operational engineering. Potential impacts on the system's integrity or security through electronic means and the measures needed to mitigate these must be considered in the same way. Integrating this consideration into system documentation and change management processes, operating procedures and architectural design inputs allows for systems to be much more secure.

While cybersecurity is important, its requirements are no more or less important than other system requirements. Just as other system requirements can often conflict and compromises need to be made, appropriate judgement must be used when implementing cybersecurity

measures. Best practice measures from the commercial IT industry are not always directly transferable to control systems, and in some cases are definitely inappropriate.

A typical example is a standard requirement around incorrect password entries. The Australian Signals Directorate requires '*accounts must be locked out after a maximum of five failed log in attempts.*' [2] While this protects corporate computer accounts well, consider a reactor transient event whereby an operator, in a stressed environment, inadvertently makes several incorrect password entries while attempting to access the control system. The potential loss of facility control is likely considered unacceptable and this mandated IT control is inappropriate for direct application.

While there may be differences in the perspectives of control system engineers and IT professionals, this should not be viewed as a conflict between functionality and cybersecurity. If viewed as a conflict, rather than management of system requirements a poor approach to system design, management, and ultimately security can result. While these points have been considered in a distinct section of this paper, it should not convey that either cybersecurity or other system requirements are more or less important.

4 Ongoing System Management

4.1 Change Management

Research reactors, like the rest of the nuclear industry, have a good understanding of the need for proper change management and its documentation [3]. Implementing these concepts is relatively straightforward for physical systems such as piping and cooling pumps or hardware based systems like shutdown relay logic. Nuclear specific efforts have also been made into the management of software [4] to ensure that changes are considered. Computer systems offer a myriad of configuration options which often produce only minor system changes and means to manage or document them are often not straightforward.

Consider the following case at OPAL wherein network switches only have the particular ports in use enabled, while the balance are disabled. This configuration represents a good security practice, reducing the potential for unauthorised computers to be added to the network. The port configuration of the switch is detailed on network drawings and in descriptive documentation. Proper change control processes ensure that changes to the set of enabled ports on the switch are first approved and any associated documentation updated. This process ensures that the documentation always matches the as-built and implemented status, and that any future system changes, security or design audits or investigations can be easily performed.

Similar concerns apply to changes which could be made to the Human Machine Interface software. As with many other safety-focussed and regulated industries, procedural compliance is very important to operation. Consequently, seemingly minor changes which are not first fully considered could have unexpected and undesirable impacts on reactor operation.

This approval and documentation process can often seem burdensome, particularly those with an exclusively IT industry background. As with cybersecurity, development of change management process which balances this documentation need with the ready flexibility offered by modern IT systems is required. While IT change control principles are not dissimilar to those in the nuclear industry, IT focussed processes and software systems are not easy to integrate within a larger nuclear change management system.

Following the control system upgrade, OPAL is developing an improved change management process to reflect the change in operating equipment. Key to this process is

recognising the different types of control system changes which can be made, and appropriately grading the required approval and documentation processes.

4.2 Ageing Management

Traditionally upgrades of control systems occur in the same way as upgrades to other major systems within a reactor. Typically this involves large scale changes to the system involving partial or complete replacement during an extended reactor shutdown period. Extensive planning, installation and commissioning work is involved. Given the role of the control system in a modern reactor design, the degree to which this kind of planning and testing work is required is increased due to the complex interaction with other systems.

This traditional ageing management model is well understood within the engineering and maintenance spheres and works quite well for systems which are operated until either obsolescence or a significant degradation in reliability occurs. Depending on the organisational mindset, challenging this traditional thinking about system upgrades being large yet infrequent can be difficult.

Such a challenge is necessary for IT dependant control systems though, as the traditional approach has several major drawbacks.

1. Different parts of the IT infrastructure become obsolete at different rates (for example, operating systems age must faster than network switches).
2. Software obsolescence is often tied to hardware, potentially requiring the upgrade of both to maintain support.
3. The longer the time between upgrades, the more difficult it is to provide a continuous type of service or continuity of the system data.

A more effective approach is to maintain system support by upgrading different parts of the system as they become obsolete. Smaller upgrades minimise the scope and consequently the extent and rigour of planning, installation and testing activities. Furthermore, upgrades which occur closer to each other in both time and technological generations typically mean the required engineering effort is reduced.

With OPAL implementing ISO 55000 and the principles of asset management to ensure ongoing reactor availability, this control system upgrade strategy is being input to expected capital expenditure plans.

5 Recommendations

5.1 User Expectations

Control systems are increasingly being challenged by users who know what features can be provided by an IT system. The incredible integration of computerised systems within the workplace and at home over the last 15 years has resulted in a very information technology literate workforce. Demands for ease of use, ready availability of data, expected levels of system performance and even the visual appearance of a control interface are all impacted. While not always possible or practical to implement, engaging users about what they desire can yield useful design inputs which may not have been considered by those who engineer or maintain the system.

While an entrenched and often repeated principle, engaging users in the design and implementation of a system is critical. When properly engaged, not only will an upgrade or installation process be much easier to manage (for example, resulting in less confrontation over changes), operators can be the most useful people to identify system deficiencies and possibilities for improvements.

This was very important during the RCMS upgrade where operators were shown that there concerns were valued, understood and work was visibly occurring to rectify problems. This allowed typical commissioning problems to be properly prioritised and addressed accordingly rather than relatively minor technical, but somewhat frustrating issues being improperly highlighted. Close cooperation with operators also had unexpected benefits in that they invested effort themselves to find work-arounds to problems, further easing demands on the commissioning team.

5.2 Engineering and Information Technology

Conflicting Goals?

This paper has discussed how the perspectives of control system engineers and IT professionals can be both complementary and apparently conflicting. Recognising the differences and similarities between a reactor control system and a commercial data centre is important. Changes to control system architectures and the underlying technologies require that both sets of knowledge and expertise are involved in managing a modern control system. This needs to be considered in work force planning to ensure a system can be properly design and managed.

This crossover does not mean there should be, or is, a conflict between control system engineers and IT professionals. It simply means that a common understanding and some compromises need to be reached. The following examples show how the two disciplines need to adjust their thinking to the particular computerised control system application.

1. While movement of control system software via USB data sticks and its development on an engineer's desktop computer is convenient, it is absolutely not good cybersecurity practice.
2. Server computers need to be backed up regularly and efficiently however the size of a control system and the frequency of changes made to the system do not necessarily require fully automatic data tape management equipment as used in a data centre.

A useful experience from OPAL has been the use of reactor specific IT personnel, distinct from the corporate or organisational IT department to ensure that the particular concerns are understood.

Vendor and Operator Proficiency

As noted earlier, control system vendors are embracing the change in available technologies and utilising more commercial IT equipment. Just like control system operators though, the need for understanding of both professions within the vendors is also important. Their skills and understanding may still be developing. It is critical that during an upgrade or new system design a system operator be an active and informed customer to ensure the best design is achieved.

This skills requirement should be considered before embarking on any control system project so that a system design appropriate to the available skill set of its designers and maintainers is produced.

5.3 Architectural Flexibility

Recognising the technology shifts in the industry, some indication of future directions can be drawn from examination of the commercial IT industry. The multi-year lag between the two provides a reasonably good leading indicator. Computer virtualisation and the on-line redundancy benefits it offers is becoming significant in the IT industry and will very likely see much more use in control systems given the great reliability improvements. System architecture designs should consider what flexibility is required to allow future technologies to be integrated without requiring a complete system design.

This was considered in the RCMS upgrade and an example of this was the inclusion of provisions for future installation of online storage networks and redundancy features.

6 Conclusion

This paper has considered the upgrade and architectural changes to the OPAL Reactor Control and Monitoring system. It has been shown that it is critical to understand the changing environment in which both reactors, their control systems and their users exist. A useful control system, capable of being properly maintained and managed can only be properly achieved by ensuring the right personnel with the right sets of skills and experience are available.

While work at OPAL continues to consider and implement new processes to manage the upgraded system, it is hoped that the recommendations within this paper serve useful to other facilities embarking on similar projects.

7 References

[1] International Atomic Energy Agency, “Computer Security at Nuclear Facilities,” 2001. http://www-pub.iaea.org/MTCD/Publications/PDF/Pub1527_web.pdf

[2] Australian Signals Directorate, "Australian Government Information Security Manual Controls", 2015. *Control 1403.* http://www.asd.gov.au/publications/Information_Security_Manual_2015_Controls.pdf

[3] International Atomic Energy Agency, “Managing Change in Nuclear Facilities,” 2001. http://www-pub.iaea.org/MTCD/publications/PDF/te_1226_prn.pdf

[4] International Atomic Energy Agency, “Software Important to Safety in Nuclear Power Plants,” 1994. https://www.iaea.org/NuclearPower/Downloadable/I-and-C/TRS367.pdf


RRFM
EUROPEAN RESEARCH REACTOR CONFERENCE 2016
IGORR
BERLIN
13 - 17 March 2016
GERMANY

Security

MANAGEMENT OF SAFETY AND SECURITY FOR HANARO RESEARCH REACTOR AND NUCLEAR FACILITIES

HOAN-SUNG JUNG, BONG-HWAN KIM, MUN-JA KANG, IN-AH HWANG
Department of Nuclear Safety and Security
Korea Atomic Energy Research Institute
111 Daedeok-daero 989beon-gil, Yuseong-gu, Daejeon, 305-353, Korea

ABSTRACT

KAERI operates HANARO research reactor and other many nuclear facilities in addition to various R&D facilities. Safety and security are important subjects in operation of nuclear installations. Nuclear safety is an ultimate goal of operators to protect workers, the public and the environment from undue radiation hazards by preventing of accidents or by satisfying operating conditions. Nuclear security is another paramount goal to prevent theft, sabotage, unauthorized access, illegal transfer or other malicious acts involving nuclear and radioactive materials. Two goals are similar in the minimization of risks. But they are different in processes and measures. And sometimes they are contradicting in view of their characteristics. Openness, collaboration, access, and external monitoring are major concept for operator to enhance the safety. On the other hand, hiding, separation, barrier, and internal surveillance are basis to increase security of nuclear facilities and radioactive materials. It is necessary to integrate the concept and the basis into a well-organized management system for mutual benefits of safety and security so that actions and measures are implemented in a manner that they do not interfere, but enhance each other. KAERI has developed an integrated management system and a dedicated information system, to implement safety and security concept by integrating safety, health, environment, quality, and security management functions. This paper describes the integrated management system and the activities to conduct the system.

1. Introduction

Radiation protection and nuclear safety are basic principles in nuclear installations. KAERI is operating various nuclear facilities including research reactors since 1959. The operation of HANARO research reactor began at by KAERI in February, 1995. There are many experimental facilities for thermal hydraulic test, LOCA test, severe accidents test, and tests for next generation reactor system in the site of KAERI.

Some areas and building are designated as radiation controlled area and other areas are classified as restricted area. These controlled areas are subject to the limitation of access, entry and exit of things for the security, waste, and contamination. But it is needed to reduce the limitations for the convenience and for the exit in an emergency such as fire. So sometimes it is difficult to apply both rules on a place due to contradictory requirements. Information sharing is also another dilemma. For the safety it is needed to disseminate details of some accidents or events to protect similar case. But for the security some information should not be opened and released.

KAERI made one organization consisting of small teams related to safety and security to control and to coordinate their tasks effectively without conflicting each other. And a business system was developed to support tasks for safety, security, and quality.

2. An advanced nuclear safety information management system

The information system, ANSIM (acronym for Advanced Nuclear Safety Information Management) is a computerized business support system to process documents, data bases, approval, distribution, and storage for the nuclear facilities including HANARO research reactor. ANSIM supports the following activities for the overall nuclear facilities at KAERI and the functions are in figure 1.

- Radiation Safety Management
- Radiation Safety Management of Advanced Radiation Technology Institute
- Management of Radiation and Radioactivity Analysis

- Management of HANARO (High Advanced Nuclear Application ReactOr) Facilities
- Management of IMEF (Irradiated Material Examination Facilities)
- Management of PIPF (Post Irradiation Examination Facilities)
- Management of RWTF (Radioactive Waste Treatment Facilities)
- Document Management of New (Gijang) Research Reactor Design
- Document Management of Jordan Research Reactor Design
- Document Management of SMART (System integrated Modular Advanced ReacTor) Design
- Management of Nuclear Material Control and Accounting
- Management of IAEA Expended Declaration
- Management of Nuclear Emergency Preparedness
- Management of Nuclear Quality Assurance

Figure 1. Functions of ANSIM

With the ANSIM, jobs and tasks for the operation of nuclear facilities are controlled and approved thru reviews by related responsible supporting organizations. For the works involving nuclear materials in a radiation controlled area, overall activities are checked up with the radiation work permit stating details of hazards, resources, and limiting conditions by persons related to the safety and security functions. During the approval of the work permit, reviewers put some comments into the document. Then the applicant and workers listed in the work permit should read the issued permit before entering into the radiation controlled area. Some contradictions can be resolved during this process effectively with the integrated organization of KAERI. Records and experiences accumulated in the ANSIM can be disseminated thru portal screen and some safety culture program among peoples involved for the facilities.

3. An Integrated safety and security management organization

KAERI has a comprehensive organization for safety and security, “Nuclear Safety and Security Department” headed by a vice president responsible for, is shown figure 2. It consists of 6 teams for following functions;

- Radiation protection and health physics
- Nuclear safeguards

- Environmental radiation monitoring and assessment
- Emergency preparedness
- Industrial health and safety
- Physical protection
- Security of personnel
- Waste collection and treatment
- Disaster response and Reserved army training

A vice president for safety and security department reports to the president of KAERI directly. So some managerial settlements between safety and security persons or teams can be reached easily thru internal meetings or by manager's decisions. Efficient and comprehensive coping with any emergency situation is possible due to a simple line of command and fast information sharing by ANSIM and organizational relationship. But the level of information sharing is controlled by duties of each person for the security.

Figure 2. A comprehensive Safety and Security Organization

4. Concluding Remarks

The advanced information system, ANSIM, and the comprehensive safety and security organization are functioning effectively in KAERI. This information and management system was selected as good practice during IAEA IPPAS Mission in 2013. The IPPAS team reported that the nuclear safety and security department controls safety and security related issues, reporting directly to the president of KAERI and, thus, enabling decisions to be made efficiently and in a timely manner.

References

[1] Hoan-sung Jung, et al., Development of Safety Management Portal System for HANARO Research Reactor, Proceedings of IGORR, Argentina, 2014

[2] Jae-min Sohn, et al., Development of the Advanced Nuclear Safety Information Management (ANSIM) System, Proceedings of Korean Nuclear Society Spring Meeting, 2012

Fuel Back-end

NEW DUAL-PURPOSE CASK CASTOR® MTR3 FOR DISPOSAL OF SPENT FUEL FROM GERMAN RESEARCH REACTORS

DR. METEHAN BOZKURT, DR. JÖRN BECKER, DANIEL LANDSIEDEL
GNS Gesellschaft für Nuklear-Service mbH
Frohnhauser Straße 67, 45127 Essen – Germany

ABSTRACT

According to the German Atomic Law, the operators of nuclear facilities have to ensure a safe disposal of their waste streams which are generated during the entire life-time cycle. On this account, TUM, together with Johannes-Gutenberg-Universität Mainz and Helmholtz-Zentrum-Berlin, also operators of research reactors, assigned GNS Gesellschaft für Nuklear-Service mbH (GNS) to design the required dual-purpose cask and to conduct the corresponding licensing procedure. Based on the transport and storage legislation, GNS designed the CASTOR® MTR3 cask as a new member of the well-established CASTOR® series.
The CASTOR® MTR3 features a monolithic body made of ductile cast iron, two trunnions for handling operations and a customized fuel basket for up to five fuel elements from FRM II. To ensure leak-tightness during various scenarios under transport and storage conditions, the cask is equipped with a proven double lid-sealing system. The outer dimensions of the CASTOR® MTR3 are approx. 1.5 m (diameter) by 1.6 m (height). The total weight of a loaded cask is approx. 16 t. The package design of the CASTOR® MTR3 under the transport regime comprises the cask and a set of impact limiters. Because of its compact design, up to three casks can be stacked on top of each other during interim storage.
GNS applied for the certificate of approval for the CASTOR® MTR3 in June 2014 and currently prepares a series of drop tests with a test sample of the cask (scale 1:1) to demonstrate that the cask meets all safety requirements according to the SSR-6 guideline. In a first step the application is limited to the handling of FRM II inventories due to the needs based on its operational schedule. A future extension of the certificate of approval is already planned for further spent fuel assemblies from other research reactors (TRIGA- and MTR-design).
The disposal plan foresees the transport of the casks to an off-site interim storage facility after loading at FRM-II. The upcoming transports under the certificate of approval are planned to be carried out via road.

1. Introduction

1.1 GNS Gesellschaft für Nuklear-Service mbH

GNS Gesellschaft für Nuklear-Service mbH is a German manufacturer of dual-purpose casks and is fully owned by the German utilities E.ON, RWE, Vattenfall and EnBW. GNS is the competence center for the spent fuel and nuclear waste management and is responsible for the entire life-time cycle of nuclear waste streams starting from the design and manufacturing of transport and storage casks, their loading, transport and storage (see Fig. 1).

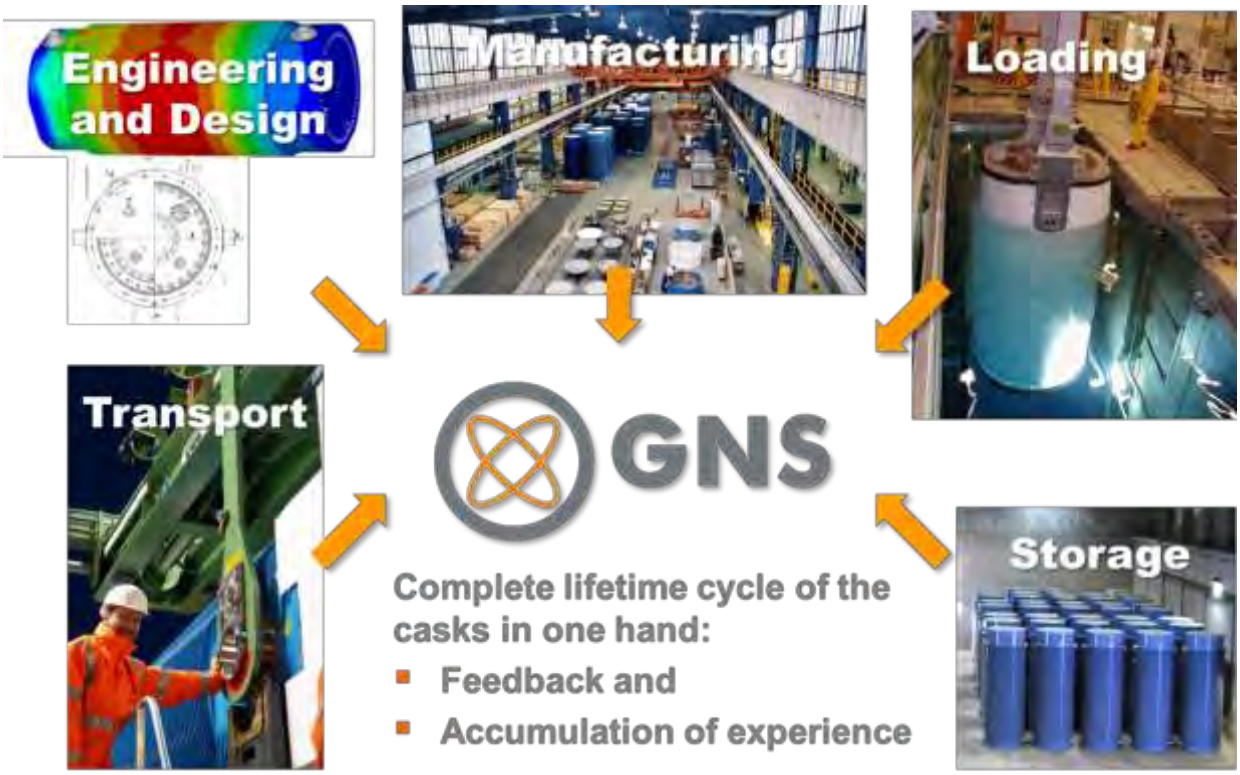

Fig 1 Operating areas of GNS

GNS and its subsidiaries companies offer a full service to its customers comprising:

- Design and manufacturing of spent fuel and waste casks
- Design and manufacturing of transport and handling equipment
- Design and manufacturing of waste treatment facilities for intermediate level wastes
- Engineering services on nuclear topics
- Design of interim storage facilities
- Realization of loading and waste treatment campaigns

1.2 Dual Purpose Casks for Storage and Transport of Spent Nuclear Fuel

The main objectives for the design of dual-purpose casks for storage and transport of irradiated fuel elements are:

- Maintaining the sub-criticality of the inventory under all handling, transport and storage conditions.
- Containment integrity must be maintained in such a way, that the activity release and contamination is limited to the admissible limits for each design condition.
- Integrity of the shielding must be maintained in such a way, that the dose rate is limited to the admissible limits for each design condition.

GNS looks back on more than 30 years of operational experience especially with dual-purpose casks. Following customer demands, GNS developed two different cask series for spent nuclear fuel (SNF); CASTOR® and CONSTOR® cask types (see Fig. 2). CASTOR® type casks are optimized for high thermal load which allows loading with extremely short cooling times and/or high burn-up of the SNF. While CONSTOR® type casks are optimized for a cost-efficient storage of large quantities of SNF.

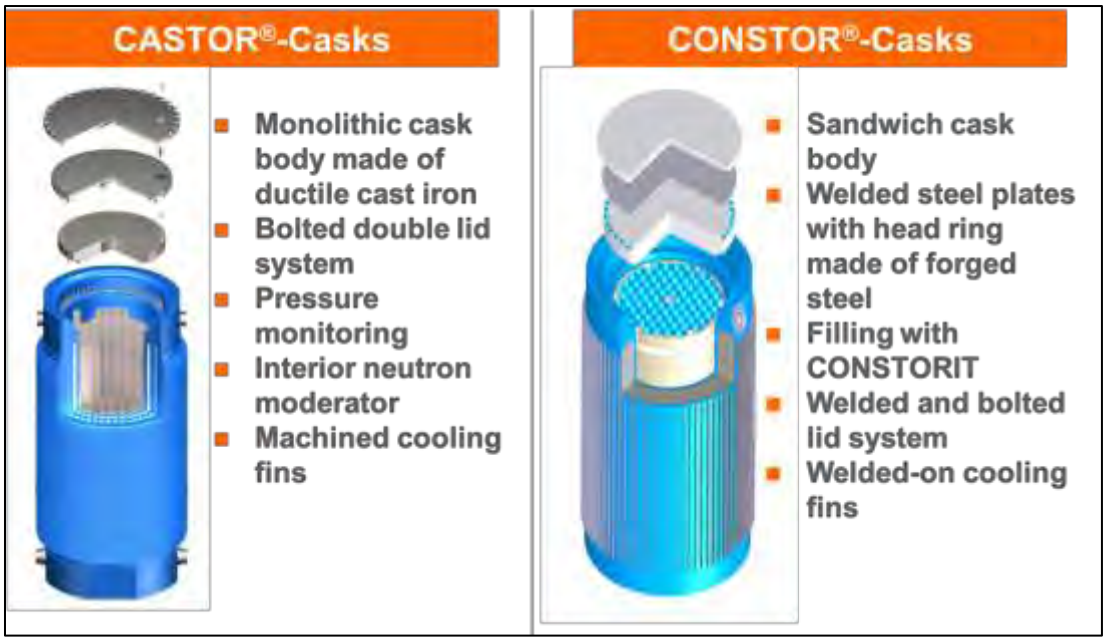

Fig 2 Main Features of CASTOR® and CONSTOR®

The main difference between the various types of casks available is given by the materials used for the cask body. The cask body of CASTOR® casks is made of ductile cast iron (DCI) whereas CONSTOR® cask bodies consist of an inner and outer liner made of steel welded onto a forged head piece where the space between the liners is filled with a specific heavy concrete material denoted as CONSTORIT®. The materials used for the cask body provide the necessary gamma shielding and ensure the integrity of the leak-tight enclosure of the SNF. For a further improvement of the shielding capability different neutron moderator and absorber materials may also be used. The casks normally have a bolted multi-lid sealing system which allows a monitoring of the leak-tightness during the storage period. Optionally a welding of the CONSTOR® lid system is possible.

The loaded casks remain in the same configuration during the complete operational cycle. Directly after loading of the cask in the spent fuel pool, the cavity is closed by the complete lid system. In this configuration the cask is ready either for storage or for transport. During a transport, only shock absorbers have to be assembled to the cask body.

The GNS casks are stored with or without a storage building depending on the national regulations. For the heat removal from the storage building, a passive cooling system by natural convection is sufficient. The storage building provides additional protection from environmental influences and reduces radiation exposure.

By now worldwide over 1,200 casks are in operation with individual storage periods of up to 30 years; and the accumulated storage time of all CASTOR® casks amounts to more than 10,000 years. Operational experiences gained by numerous loadings mainly carried out by GNS staff, are consequently considered in the cask design. The result is a cask design which offers easy handling and guarantees minimum turnaround times within the reactor unit.

According to the customer demand and the transport planning, GNS successfully obtained specific Certificate of Approvals, validations and storage licenses in various countries (a. g. Switzerland, Czech Republic, Bulgaria, Netherlands, Belgium, France, United States of America).

2. CASTOR® MTR3

Operators of nuclear facilities in Germany are responsible by the German Atomic Law, to ensure the safe disposal of the waste streams of their facility. Due to that fact, Technische Universität München (TUM) has to prepare for the future disposal of the spent fuel assemblies from their research reactor FRM II, which is in operation since 2004. In order to ensure the safe disposal of the waste generated during the entire life-time cycle of this reactor, TUM, together with Johannes-Gutenberg-Universität Mainz and Helmholtz-Zentrum-Berlin, also operators of research reactors, assigned Gesellschaft für Nuklear-Service mbH (GNS) to design a dual-purpose cask. Based on the existing regulations for transport and storage, GNS designed the CASTOR® MTR3 as a new cask in the CASTOR®-cask-series (s. Fig 3). The cask will be transported via road, rail or inland waterways. It is planned to transport the casks via road to the off-site interim storage facility in Germany after the loading at FRM II.

Fig 3 CASTOR® MTR3

2.1 Main features

The CASTOR® MTR3 features a monolithic body made of ductile cast iron and a customized aluminum fuel basket, which can be loaded with up to five fuel assemblies from FRM II. It is designed to endure a maximum of 272 W of decay heat power. To ensure leak-tightness during various transport and storage scenarios, the cask is equipped with a double-lid sealing system including metallic seals.

The under-water loading and long-term corrosion protection is ensured by a nickel coating of the lid seating area and the cavity. Handling operations can be done by a set of two trunnions, made of stainless steel which are located in the upper part of the cask body. The trunnions and the load attachment points are designed according to the German safety standard KTA 3905 with increased requirements. This design standard eliminates potential

drop scenarios of the cask or the lid-system during the handling in case of using corresponding lifting equipment.

The CASTOR® MTR3 has an outer diameter of approx. 1.5 m, a height of 1.6 m and a total loaded weight of approx. 16 t. The cavity has a diameter of 721 mm and a height of 920 mm which gives the flexibility to implement various fuel basket designs for different research reactor fuel assemblies. The main dimensions complies with the former CASTOR® MTR 2 which is already in use as transport cask for high-enriched MTR fuel assemblies from the High Flux Reactor (HFR) in Petten, Netherlands or which is in use as dual-purpose cask for WWR-M, WWR-M2 and EK-10 fuel assemblies from the Rossendorfer Forschungsreaktor (RFR) in Dresden.

In transport configuration, the package consists of the cask and a set of impact limiters. The outer dimensions for this configuration are approx. 2.4 m (diameter) and 3 m (height), and it has a total weight of approx. 24 t. The various features are summarized in Tab 1.

CASTOR® MTR3 for FRM II	
Dimensions	1.5 m (diameter) x 1.6 m (height) (Storage configuration) 2.4 m (diameter) x 3 m (height) (Transport configuration)
Heat load	max. 272 W
Weight	16 t (Storage configuration) 24 t (Transport configuration)
Cask body	Monolithic; ductile cast iron
Trunnions	2 pieces; Stainless steel
Fuel basket	Aluminum; Capacity of 5 fuel elements from FRM-II
Lid system	2 stainless steel lids with metallic seals; Nickel coated ductile cast iron as part of the monolithic casting

Tab 1 Features of the CASTOR® MTR3

During interim storage, up to three casks can be stacked on top of each other.

2.2 Design

The design of the CASTOR® MTR3 is founded based on the long-term experience with the well-established CASTOR® series. The mechanical components of the cask are designed and checked on basis of state-of-the-art dynamic numerical analyses methods. All relevant drop orientations were simulated. To further verify these numerical analyses, GNS will conduct a series of drop tests with a test sample of the cask in a 1:1-scale.

For this purpose, drop tests onto an unyielding target in different orientations are planned. An exemplary drop test is shown in Fig. 4. These drop tests will verify that the cask meets all safety requirements according to the SSR-6 guideline and the numerical simulations have adequate conservatism.

Fig 4 Exemplary drop test of a MOSAIK® Cask

As a final test before utilization of the cask, cold trials will be performed at FRM-II site and at the off-site storage facility, to verify the handling operations.

2.3 Inventory

After completion of the first licensing process, the CASTOR® MTR3 will be loaded with highly enriched (HEU) fuel assemblies from FRM II with an enrichment of up to 93 % and a burn-up of 1,300 MWd.
In future application processes it is planned to extend the potential inventories for the CASTOR® MTR3 covering fuel assemblies from TRIGA- and MTR-research reactors.

2.4 Handling of the cask

The equipment, which is necessary to handle the cask for the drop tests as well as for the loading and storage operations, will be part of the scope of supply of GNS. It consists, among others, of:

- Multi-equipment (e. g. for dewatering and vacuum-drying)
- Lifting yoke for cask and lids
- Working-platform, pedestals, transport-frame

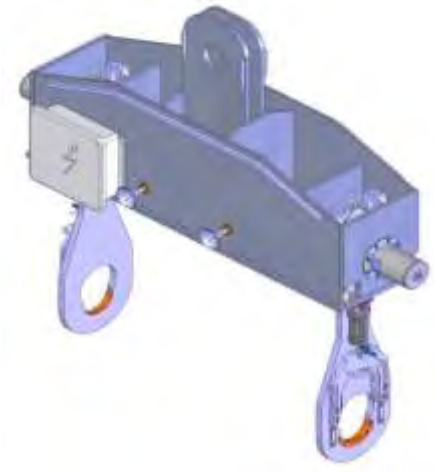

Fig 5 Cask lifting yoke

Fig 6 Equipment for vacuum drying

2.5 Licensing process

The licensing procedure for the new cask type CASTOR® MTR3 is currently running under transport regime as well as under storage regime. GNS applied for the certificate of approval at the German Competent Authority Bundesamt für Strahlenschutz (BfS) in June 2014. On basis of the operating schedule of the facility it is expected to complete the licensing process in 2018.

3. Outlook

The use of the CASTOR® MTR3 is at first limited to inventories from FRM-II. In the future, it is planned to extend the certificate of approval and therefore the use of the cask for spent fuel elements from TRIGA- and MTR-research reactors, to accommodate the needs of the other two stakeholders, Johannes-Gutenberg-Universität Mainz and Helmholtz-Zentrum-Berlin.
The certificate of approval will allow a transport via road, rail or inland waterways. The transports from FRM II to the interim storage facility are planned to be carried out via road exclusively.

AUSTRALIAN RESEARCH REACTORS SPENT FUEL MANAGEMENT: THE PATH TO SUSTAINABILITY

R. FINLAY, R. MILLER, L. DIMITROVSKI
Australian Nuclear Science and Technology Organisation (ANSTO)
New Illawarra Road, Lucas Heights, NSW 2234 - Australia

X. DOMINGO, P. LANDAU, J. VALERY
AREVA NC
1 place Jean Millier, 92400, Courbevoie – France

V. LALOY
AREVA TN
1 rue de Hérons, 78180, Montigny le Bretonneux - France

ABSTRACT

Since the late 1950's, ANSTO has successfully operated three research reactors in Australia: HIFAR (1958-2007), MOATA (1961-1995) and OPAL (2006-).

Specific strategies were developed and implemented for the management and disposition of spent fuel from HIFAR and MOATA. They included strategic considerations, technical options, fuel characteristics, storage capacity, operational constraints and associated implications. In addition, the operating licenses of the Australian reactors have required the identification of spent fuel disposition arrangements, i.e. the "deferment" strategy of storage indefinitely is not acceptable. Disposition then employed three routes with direct disposal in the USA under the US-DOE FRRSNFA Program and reprocessing in France by AREVA, and in the UK by the UKAEA. Both reprocessing routes included return of vitrified waste.

ANSTO and AREVA have worked together since the late 1990's on the disposition of uranium aluminide (UAlx) spent fuel from HIFAR. Today, ANSTO is committed to develop a lifetime strategy for management and disposition of uranium silicide (U_3Si_2) spent fuel from OPAL.

AREVA's ability to offer an integrated solution for storage, transport, reprocessing, waste return and long-term management, including addressing individual customer needs (type of fuel, timelines, quantities, final waste management strategy,…), has provided ANSTO with a viable spent fuel management strategy, for OPAL's lifetime.

1. Introduction

Australia has been operating research reactors since late 1950's and is responsible for the safe, secure and sustainable management of associated radioactive waste, including the corresponding spent fuel. During this time ANSTO gained invaluable experience in the storage, transport, reprocessing, and disposition of spent fuel through the development and implementation of strategies developed with international service providers such as France (AREVA), USA (US-DOE), and the UK (UKAEA). More recently, that experience has been used to assess available options for spent fuel

management of OPAL fuel. This paper reflects on the Australian experience and outlines that strategy for managing spent fuel from OPAL.

2. Australian research reactors and spent fuel inventories

2.1. HIFAR reactor

The 10 MW, DIDO class, HIFAR reactor operated from 1958 to 2007. It was originally designed for materials testing to support Australia's planned use of nuclear power. A decision in the early 1970s not to adopt nuclear power saw the mission of the reactor change to nuclear science and nuclear medicine and production of NTD Silicon. During nearly 50 years of operation 2281 spent fuel assemblies were generated.

Having commenced operation with HEU fuel assemblies enriched to 93% ^{235}U, for most of its operating life HIFAR used aluminium clad fuel assemblies enriched to 80% ^{235}U. HIFAR eventually converted to LEU with enrichment of ^{235}U less than 20%. Almost all HIFAR elements were manufactured in the UK, with a small number manufactured in France while the enriched uranium was supplied by both the UK and the USA.

The design of HIFAR fuel underwent a number of changes which in broad terms were associated with a reduction in enrichment to meet the goals of the RERTR program, and an increase in U-235 loadings which were the result of improvements in fabrication technology and design. The enrichment dropped from 80% to 60% before the goals of the RERTR program were fulfilled with a conversion to LEU in 2006. The geometrical design of HIFAR fuel changed from parallel curved plates (Mk II), to an involute design (Mk III) with the bulk of HIFAR fuel being concentric tubes (Mk IV).

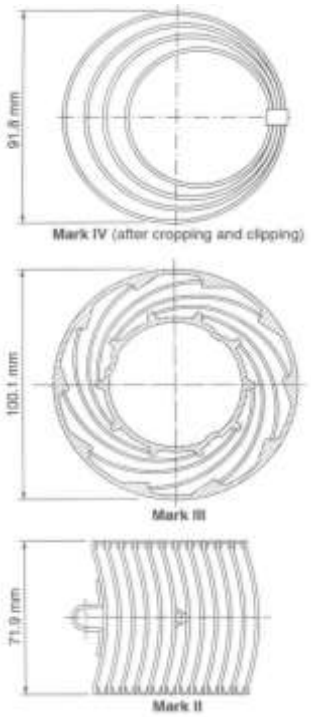

Figure 1. A photograph of HIFAR and a sketch of the cross sections of the different designs of the fuelled section of a HIFAR fuel element.

2.2. MOATA reactor

ANSTO operated a 100kW Argonaut reactor, MOATA from 1961 to 1995 using HEU.

2.3. OPAL reactor

The OPAL reactor at ANSTO is a 20MW multi-purpose research reactor that conducts commercial production of medical and industrial radioisotopes and also provides high flux neutron beams for scientific experiments.

In 2016, ANSTO will celebrate 10 years successful operation of OPAL which reached first criticality on August 12, 2006. OPAL has become known for its high reliability and availability for its stakeholders in areas of nuclear science, nuclear medicine and industry. In 2015 OPAL operated for 300 days at significant power (>10MW). The major by-product from the successful operation and utilisation of OPAL is a significant inventory of spent fuel assemblies. In accordance with the OPAL spent fuel strategy, plans are now being implemented to ensure the disposition of this fuel in a timely manner.

OPAL fuel is 1045mm long and 80.5mm square in cross section. It uses low enriched uranium silicide (U_3Si_2) clad in aluminium 6061. The fuel was initially manufactured by INVAP (Argentina) but since the resolution of the fuel fault in 2008 has been manufactured by AREVA-CERCA (France).

Figure 2. Photograph of the entry to the OPAL reactor building and the top end of an OPAL fuel assembly.

3. Previous spent fuel management – strategy and implementation

3.1. Australian approach

Long term disposition strategies for research reactor spent fuel are required because aluminium clad spent research reactor fuel inevitably degrades over extended periods of time and consequently, spent fuel is unsuitable for very-long time periods of storage or ultimate disposal. Historically, ANSTO and its precursor, the Australian Atomic Energy Commission (AAEC) has considered a number of disposition options that are compatible with the physical constraints presented by the radioactivity and aluminium cladding. The plans and arrangements changed to reflect internal and external factors over the operating life of HIFAR.

3.2. History of HIFAR reactor spent fuel management

When HIFAR commenced operation the strategy was for spent fuel to be sent to the UK, or the US, for reprocessing, recovering and recycling of the residual high enriched uranium (HEU). One shipment of 150 fuel elements was sent to the UK in 1963. This practice did not continue as a decision was made to store fuel on site which continued until the mid-1980s. The major influence was the prospect of establishing a domestic reprocessing capability in Australia. This was in line with Australia's (then) plans for the introduction of nuclear power.

This decision necessitated the expansion of the storage facilities. A combination of increased wet storage, a new dry store (for 1100 spent fuel elements), and the use of transport containers as storage containers provided the necessary storage capacity. Onsite storage continued until it became obvious in the late 1970s that the likelihood of nuclear power being introduced in Australia was very low. As a result the AAEC began to explore other options for spent fuel disposition. In the short term re-racking of wet storage facilities provided further capacity while overseas options were evaluated.

3.2.1. Direct disposal in the USA under the US FRRSNFA Program

Enriched uranium for HIFAR fuel was obtained from the UK and the USA which had a strong bearing on the disposition arrangements for the fuel. In 1985 the Australian Government approved the transport of 450 spent fuel elements to the US for reprocessing at a US-DOE facility. Contracts were signed but before the transport could be performed in 1989 the US DOE announced that no further deliveries of spent fuel would be accepted pending a review of its policy on return of foreign research reactor spent fuel. In 1993, the US DOE announced a resumption of the program to accept foreign research reactor spent fuel containing US origin HEU subject to completion of an Environmental Impact Statement (EIS). It was completed in 1996 and the first shipment of 240 spent fuel assemblies from HIFAR was conducted in 1998. An extension of the program from 2006 until 2016 permitted the remaining inventory of US origin spent fuel including the LEU used in 2006 and 2007 and all MOATA fuel plates to be sent to the US-DOE in 2006 and 2009 after being allowed to cool sufficiently to be transported and accepted. In total, 729 fuel assemblies containing U.S. origin uranium were repatriated to the U.S.A. under the Foreign Research Reactor Spent Nuclear Fuel Acceptance (FRRSNFA) Program where the U.S. Government took ownership and is responsible for safe storage and disposition. No waste arising from the storage or handling of this spent fuel is returned to Australia.

3.2.2. Reprocessing in the UK and France

In 1997, the Australian Government formally announced a decision to build a replacement reactor for HIFAR and committed funding. It also included funding for the disposition of all HIFAR fuel fabricated with UK origin uranium as a consequence of the formal decision not to establish a domestic reprocessing facility and therefore to pursue offshore reprocessing. In the year prior, a second shipment of 114 fuel assemblies was made to Dounreay and plans were underway for a further four shipments. However, in 1998 the UK government decided to cease all commercial reprocessing. This decision prompted the Australian Government to enter into contracts with the French organisation COGEMA (currently known as AREVA-NC) for the transport, reprocessing and return of waste residues. Four shipments of HIFAR spent fuel totalling 1288 elements were made to La Hague in France between 1999 and 2004. The contract also made provision for the reprocessing of the spent fuel from the OPAL reactor.

Figure 3. TN-MTR cask – loaded and awaiting departure from ANSTO.

Year	Destination	No. of FA
1963	Dounreay (UK)	150
1996	Dounreay (UK)	114
1998	Savannah River (USA)	240
1999	La Hague (France)	308
2001	La Hague (France)	360
2003	La Hague (France)	344
2004	La Hague (France)	276
2006	Savannah River (USA)	330
2009	Savannah River (USA)	159

Table 1. Summary of all HIFAR spent fuel shipments

3.2.3. Status of spent fuel/waste inventories and legacy

In December 2015 the ILW residues that were allocated from the reprocessing of HIFAR spent fuel in France were returned to Australia in a number of CSD-U containers housed within a single TN-81 transport/storage cask. Australia has not established a national radioactive waste repository yet and therefore the TN-81 cask is currently stored at ANSTO in a dedicated facility. The return of the residues has been an excellent exercise in demonstrating to the Australian public that the wastes arising from the long term operation of a reactor can be managed in a safe, secure and effective manner.

Figure 4. TN-81 cask during unloading at Port Kembla, Australia and standing in the ILW store on the ANSTO site at Lucas Heights.

The ILW return from the UK is expected to be completed by 2020. A change to UK legislation in 2012 has permitted vitrified waste to be substituted for the originally proposed cemented waste. A significant reduction in the volume of ILW to be transported and stored has been achieved.

ANSTO has gained considerable experience in the management and disposition of spent fuel from the successful programs implemented for HIFAR. This experience has been invaluable in the development of the strategy for OPAL spent fuel disposition.

4. OPAL reactor spent fuel management strategy

The OPAL reactor was designed and licensed with a strong focus on the plans and arrangements for spent fuel and radioactive waste. From the beginning of the OPAL project there was a firm commitment on ANSTO's and the then Government's part to continue the strategy employed for management of HIFAR spent fuel. This was communicated in the Environmental Impact Statement [1] which proposed reprocessing spent fuel overseas where the wastes would be conditioned into a long–lived intermediate level waste form and the return of the wastes for storage. Licensing permits for the preparation of the site, construction, and operation of OPAL assessed and approved of ANSTO's strategy.

Therefore the management of spent fuel has been under active consideration from the design phase of the OPAL project and initial plans have been actively monitored and updated through the 10 years of operation of OPAL.

A significant consideration when assessing potential options for the disposition of OPAL spent fuel is the impact on operations. ANSTO aims for high availability of OPAL with a target of 300 days at power each year and derives a significant portion of the operating budget from income achieved from its commercial operations, largely comprised of Mo-99 production and NTD silicon. The neutron scattering community require high availability and certainty for the large number of external users who often commute large distances to make use of their allocated beam time. Therefore, spent fuel loading needs to be conducted with minimal impact on OPAL availability and utilisation.

OPAL spent fuel is stored in the Service Pool (SPO) which is adjacent to the Reactor Pool (RPO). It has a storage capacity for approximately 10 years of OPAL spent fuel and would be full by 2020 without action. OPAL would be shut down as a consequence. As a result ANSTO has been working with service providers to assess all available options.

To minimise the impact on operations during cask loading, it is planned to bring multiple transport casks into the reactor hall via a floor hatch which can only be opened during a shutdown. They will be set on the floor of the reactor hall and then transferred, one at time, into the SPO for loading. Once loaded the cask would be returned to its position on the reactor hall floor and prepared for shipment and the next cask transferred to the SPO. At the next shutdown the loaded casks would be removed through the floor hatch and any further casks would be brought into the hall to repeat the process.

Figure 5. The OPAL reactor hall showing the RPO (circular) in the foreground and the SPO (rectangular) in the background of the photograph.

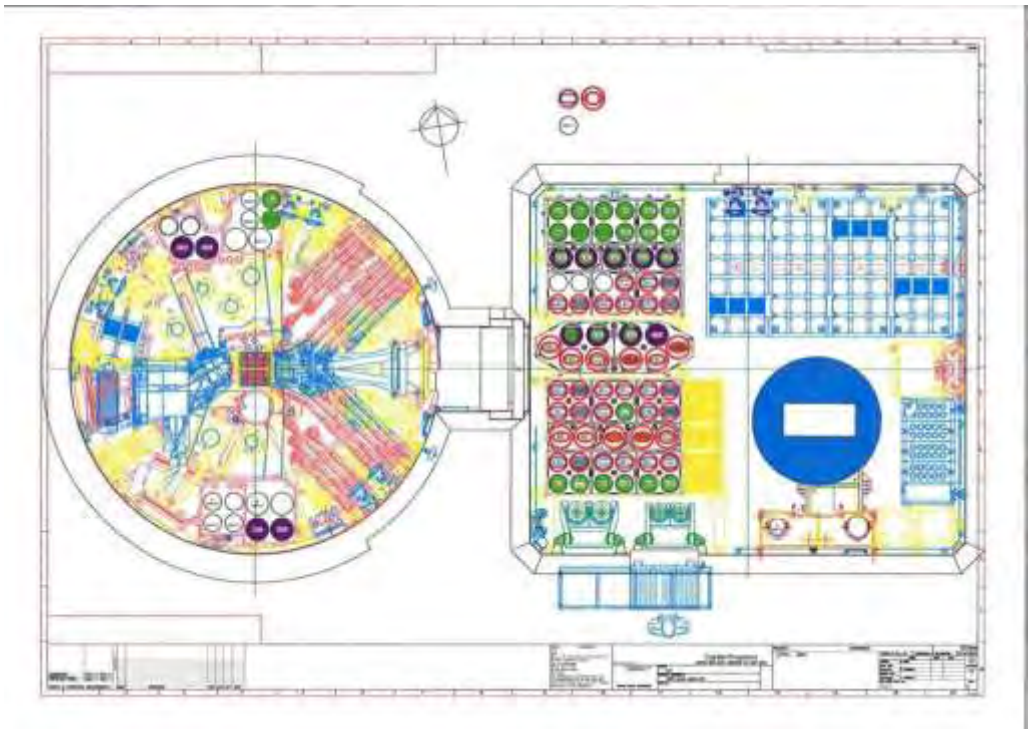

Figure 6. Schematic (plan view) of the RPO and the SPO. The location for the spent fuel cask is shown as a large blue circle in the SPO.

4.1. Direct disposal in the USA under the US FRRSNFA Program

The OPAL spent fuel generated before May 12th 2016 is eligible for return under the FRRSNFA Program. When the FRRSNFA Program was extended in 2004 for a further 10 years from 2006 to 2016, ANSTO was given special consideration and OPAL was included. The program was originally only open to reactors commencing operation by 1996, but OPAL was assessed to be a replacement for the eligible HIFAR reactor. The extension was based

on the US-DOE recovering a small fraction of the eligible HEU and delays to the qualification of new LEU fuels to allow the users of HEU to convert.

The option to send OPAL spent fuel to the US for a fee and have no returned waste is very attractive and ANSTO did plan to dispose of eligible OPAL spent fuel under the FRRSNFA Program. After careful evaluation ANSTO has elected not to pursue this option. The FRRSNFA Program has a finite end date of May 2016 which requires ANSTO to develop another disposition route beyond this date. The US-DOE have been consistent in their message that there will not be an extension of the program. Therefore ANSTO would have had to develop plans and arrangements for a second route. Planning for disposition to a single destination, using a single cask type, with a single provider provides numerous advantages in terms of simplicity, risk minimisation, and cost. The returned residue requirement does not pose a significant burden on ANSTO because it has been implemented for HIFAR.

4.2. Reprocessing in France

AREVA NC has offered an integrated solution for the transport, reprocessing and waste return of UAlx spent fuel from research reactors for many years, with HIFAR spent fuel management being one of the examples. After consultation and analysis, AREVA and ANSTO have developed and are working to implement a similar solution for spent OPAL uranium silicide fuel that is consistent with ANSTO's spent fuel management strategy.

The reprocessing of U_3Si_2 fuel has presented some technical challenges because of the high concentration of silicon which is not compatible with the PUREX process. AREVA has developed the capability for the silicon to be separated from the dissolution solution through the use of centrifuge and managed through a dedicated process. In 2015 AREVA-NC submitted an application to the French Safety Authority (ASN) to commence reprocessing of uranium silicide fuel and expects to have permission from the ASN in 2016 [2]. A more detailed submission specifically to cover the industrial reprocessing of OPAL uranium silicide fuel will be made to the ASN that aims for approval in 2017.

An intergovernmental agreement between France and Australia is also required. The agreement facilitates the framework for the transport of spent fuel to France, reprocessing, use of recovered material and return of the residues to Australia of appropriately packaged intermediate level waste. Although France and Australia have entered into a similar agreement previously the time scale to complete a new agreement spans a number of years. Contractual negotiations and planning may proceed in parallel and can be concluded before the IGA is ratified. The IGA is to be ratified before OPAL spent fuel is transported to France

The shipment of HIFAR spent fuel to France for reprocessing and the return of the residues is a well-established practice as described in Section 3.2.3. It is recognised however, that a number of tasks are yet to be completed and as a risk mitigation measure ANSTO has signed a contract with AREVA to purchase a TN-MTR transport cask in the event that the necessary agreements are delayed. The cask provides for an increase in the number of spent fuel assemblies per transport, a reduction in cask rental fees and an increase in the time interval between transports.

5. Conclusions

ANSTO has drawn on more than 50 years' experience in research reactor spent fuel management to evaluate all available options for the management of OPAL spent fuel.

Consistent with the planning and design philosophy of OPAL, offshore reprocessing has been selected.

ANSTO is working closely with AREVA to implement technical, regulatory, industrial, intergovernmental and financial aspects of this strategy, including at-reactor site management, transportation, reprocessing and waste storage activities. Securing long-term disposition arrangements for OPAL spent fuel provides confidence to ANSTO's stakeholders on this important topic.

6. References

1 PPK Environment and Infrastructure and Australian Nuclear Science and Technology Organisation (July 1998), *Draft Environmental Impact Statement on the Replacement Nuclear Research Reactor Volume 1 - Main Report*, PPK Environment and Infrastructure.

2. J.F. Valery et. al. 'Status on Silicide Fuel Reprocessing at AREVA La Hague (2015)', Transactions of RRFM2015, p 453-463, Bucharest, 19-23 April, 2015.

OPTIMIZING APPROACHES TO SPENT NUCLEAR FUEL TRANSPORT

J.N. DEWES
Savannah River National Laboratory
Aiken South Carolina 29808 - USA

I. BOLSHINSKY
Idaho National Laboratory
Idaho Falls, Idaho - USA

S. M. TOZSER
International Atomic Energy Agency
Vienna International Centre, PO Box 100, 1400 Vienna - Austria

ABSTRACT

The security risk associated with transport of HEU spent nuclear fuel is, among other factors, proportional to the duration of the transport process. Many other factors such as distance, access to airports, railheads, and docks also impact options available for transport. Economic also play a large role in the selection of transport mode. For the past ten years the approach for spent nuclear fuel transport in Europe and Asia has been modified based upon changes in technology and careful exploration of options. This paper will summarize the historical evolution of transport mechanisms utilized for the Russian Research Reactor Fuel Return Program. It will also explore the factors utilized in determining the appropriate approach to fuel transport for particular situations and provide a basis for comparison in support of future transport projects.

I. Introduction

The Atoms for Peace program was initiated in 1953 by then U.S. President Eisenhower as a means of developing peaceful uses for the atom. The aim of the program was to establish the infrastructure necessary for development of nuclear power in foreign countries allied with the United States. One key aspect of the program was the provision of research reactors and low enriched uranium (LEU) fuel. These reactors could be utilized to foster research in nuclear technology as well as for production of isotopes for medical and industrial purposes. In addition, they could support the education and training of personnel needed to support the nuclear industry. The Soviet Union established a similar program in the same time period.

Over time, the original LEU fuel was limiting the performance of the reactors, and high enriched uranium (HEU) fuel was developed as a means of increasing the neutron flux and thus increasing the efficacy of the reactor facilities in countries all around the world. In subsequent years, the threat associated with utilization of HEU fuel became evident, and substitution of HEU fuel was initiated by both governments in 1978 under programs such as the US Reduced Enrichment for Research and Test Reactors program. Progress was slow, however, due to funding constraints and economic difficulties.

II. History of the Russian Research Reactor Fuel Return Program

In 1999 the IAEA, the United States, and the Russian Federation established an agreement in concept to repatriate Soviet origin fuel to the Russian Federation with the assistance of the United States and the IAEA. In October 2000, the Director General of the IAEA sent a letter regarding the management of research reactors of Soviet-/Russian-origin to the relevant Ministers in various countries, offering participation in a program to repatriate HEU fuel back to the Russian Federation. Over the next few years the Russian Federation developed legislation necessary to support the program.

Following the events of September 11, 2001, efforts to convert reactors and repatriate HEU became a priority. Concern over 80% enriched uranium fuel at the Vinca facility in Serbia led to the three parties to launch a recovery effort for the HEU in 2002. This was a critical breakthrough in cooperation on repatriation of Russian origin fuel. A formal agreement between the U.S.A. and the Russian Federation establishing the Russian Research Reactor Fuel Return (RRRFR) program was signed in 2004. The two countries established a Joint Coordinating Committee to manage the effort.

Since 2004, the RRRFR program has successfully returned more than 2000kg of fresh and spent HEU to the Russian Federation. After the first urgent HEU removal operations from Serbia and Romania (in 2003), several more shipments of fresh HEU fuel were repatriated over the next three years. In 2006 the first shipment of spent nuclear fuel was completed from Uzbekistan. Since then over 60 shipments of fresh and spent HEU have been completed from 15 countries.

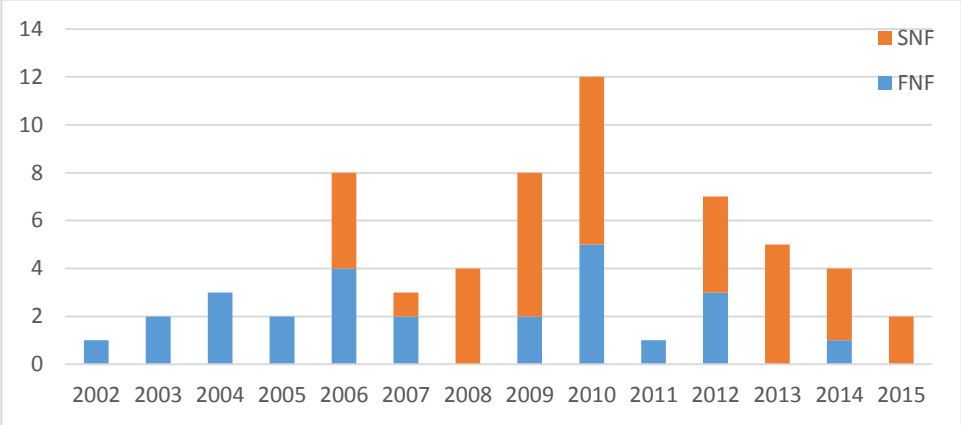

FIGURE 1. RRRFR SHIPMENTS

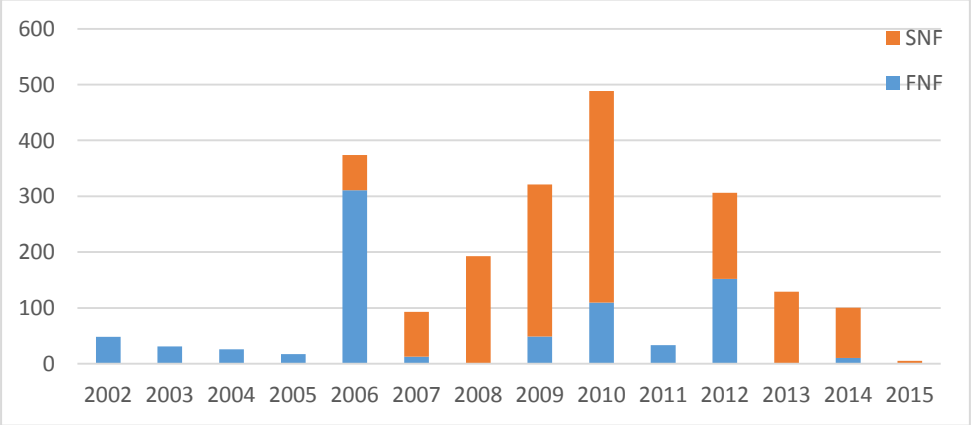

FIGURE 2. HEU MASS SHIPPED

As can be seen from Figure 1 and 2, shipments were limited to fresh HEU during the initial phases of the program. This was largely due to difficulties in developing the legislation and process for licensing of spent fuel shipments. This was overcome by 2005 and the first spent fuel shipment licensed under these new regulations occurred in 2006.

III. Security of Spent Nuclear Fuel Shipments

The threat of HEU is the ease with which it can be used to build a nuclear device. Given sufficient fissile materials, application of simple machining technology along with rudimentary experience with explosives can produce a device with significant explosive power. The design and methods for construction of such a nuclear device, although currently kept out of the public eye by most governments, has been disseminated to a fair extent in the past. Construction of a crude nuclear device can be accomplished by a competent team of scientists without significant prior experience. Terrorists seeking to fabricate a nuclear device are therefore largely limited by the availability of fissile materials.

Sources of fissile materials for non-State actors are extremely limited, as measures to secure existing stockpiles are substantially complete and scrutiny of possible black market transactions is intense. Assuming that a terrorist organization seeks to steal materials, factors in target selection would include the quantity of material, the form of the material, and the security of the facility in question. HEU fuel in research reactors have sufficient material in an easily transportable form, and historically did not have security measures as rigorous as other facilities containing fissile materials. Although security measures have been greatly improved over the years, no security posture is completely effective at preventing theft.

Given the improved security posture at research reactors and the intention to repatriate the HEU materials to the country of fuel origin as the publicized ultimate solution, theft during shipment has now become a much more significant risk. With the material removed from the reactor and packaged in a suitable shipping container, diversion of a shipment becomes a strictly force-on-force effort requiring far less time to accomplish than theft from a facility. It is for this reason that the NNSA has sought to minimize the number of transport modes, the duration each mode of transport, and the number of mode transfers, which eventually results in minimization of the transit time for HEU fuel shipments.

Another significant factor in the risk of transport is the number of shipments. Although the reactor fuels in Soviet-designed research reactors came in different shapes and sizes, the bulk of the fuel to be shipped were VV-R or IRT type assemblies, which are “sticks” of roughly 0.8 m in length. For fresh fuel, casks of sufficient capacity of Soviet design such as the TUK-14/16 have been available as to avoid multiple shipments.

Most Soviet research reactor facilities were designed to utilize the TUK-19 shipping cask system for shipment of spent nuclear fuel. The TUK-19 weighs 5 tons, which is the capability of the cranes in most facilities, and rail cars specifically designed for transport of these casks were also developed. The capacity of the TUK-19 is 4 assemblies. With 20 TUK-19 casks in existence, and roughly 15,000 assemblies to ship under the RRRFR program, the number of shipments approached 200. As a result, reducing the number of shipments was also made an NNSA priority.

IV. Evolution of Transport Modes

Development of the Škoda VPVR/M Cask

After assessment of available spent fuel shipping casks, it was determined early on that a higher capacity cask was needed to reduce the number of shipments required to complete the program, as well as expansion of transport modes available. The IAEA conducted a

procurement to design and build a high capacity cask, which was awarded to the Škoda company. The Škoda VPVR/M cask[1] holds 9 times as much fuel as the TUK-19, holding 36 assemblies, and was certified for vehicle, rail, and sea transport. Sixteen casks were manufactured, ten of which were procured by the IAEA and six of which were procured by the Nuclear Research Institute (NRI) in Řež, Czech Republic[2].

Although the higher capacity Škoda VPVR/M cask seemed the logical choice to use, the program took an "all of the above" approach to shipments and assessed the best method of shipment for each facility. Cask selection for a particular facility has been a function of the quantity of fuel to be shipped, the time frame during which fuel is ready to be shipped, modes of transportation available, facility infrastructure, and the proximity of the facility to its destination.

Most facilities undergoing conversion of their reactors had at least two shipments, with the fuel available for shipment taken out as soon as possible, and the remainder shipped following conversion to LEU fuel and sufficient cooling time. For this reason, the higher capacity Škoda VPVR/M cask was not required in some cases. In other situations, involving large quantities of fuel to be shipped, a combination of all Škoda VPVR/M casks and all TUK-19 casks were utilized.

The original design of the Škoda VPVR/M cask included a companion ISO sea land container specifically modified to hold either one or two Škoda VPVR/M casks, allowing easy inter-modal transfers during shipment. This allowed for an expansion in the modes of transport from the vehicle or rail shipment modes allowed for the TUK-19 cask by allowing sea transport. In order to utilize the TUK-19 cask in modes other than by truck and rail, a similar ISO container was developed[3], opening the door to sea shipment of the TUK-19[4].

Where suitable for other reasons, utilization of the Škoda VPVR/M cask required the additional task of modifying the facility to accommodate the greater weight of the cask (13T vs 5T). In some of these cases, facilities were extensively modified by constructing a new structure with a higher capacity crane around the existing fuel storage facilities. The cost of construction of these facilities was a small fraction of the cost of a typical shipment, and therefore cost effective. Where modification of the facility was not feasible or desired, special transfer casks were developed to load fuel from the facility spent fuel pool into the Škoda VPVR/M cask.

The development of the Škoda VPVR/M cask dropped the number of shipments required substantially, allowing transport of all stored SNF in a single shipment for most facilities. Overall, utilization of the Škoda VPVR/M cask was the greatest single factor in reducing the security risk of spent HEU fuel shipments.

Program Acceleration

Following the Bratislava meeting between the United States and the Russian Federation, as well as the subsequent Nuclear Security Summits, acceleration of the RRRFR program became a priority. Assessment of the factors limiting the pace of shipments resulted in the conclusion that other means of transport needed to be developed. This included development of a means to ship HEU spent nuclear fuel by air. Packaging for shipment of spent nuclear fuel by air did not exist at that time. Shipments of spent fuel by air had been done under emergency situations in the past, utilizing Type (B) packaging, but it was apparent that development of suitable Type (C) packaging was necessary.

SOSNY corporation was awarded a contract to develop Type (C) packaging. Rather than starting from scratch, the SOSNY approach was to develop an over pack for the existing Škoda cask. The simple design of the TUK-145C package[5] utilized an over pack that surrounds the Škoda cask with hollow titanium spheres that absorb the momentum of the cask by crushing upon impact. Trailers were also developed to transport the TUK-145C,

allowing for a complete transportation system. Following quarter scale testing of the TUK-145C, it was certified by the Russian Federation for land, sea, and air shipment. Two TUK-145C over packs were constructed, allowing for shipment of up to 72 assemblies by air.

Only two over packs were constructed based on the weight of the TUK-145C system, which is 47 tons. Simultaneous shipment of both over packs approaches the cargo capacity limit of commercial airplanes. The Antonov-124 cargo plane, with a capacity of 150 tons, has been utilized for all shipments of the TUK-145C to date. Since the weight of aircraft fuel is also a factor, long shipments of both over packs can involve multiple refueling stops.

Another significant factor in the time required for shipment of spent nuclear fuel was the requirement in the safety analysis of the Škoda VPVR/M cask for multi-year cooling of spent fuel removed from the reactor prior to shipment. Time frames ranging from 36 months to 20 years were imposed[6], restricting how soon fuel could be shipped. The cask analysis included three limits on the contents of the cask; thermal power, radioactivity, and weight. The thermal power and radioactivity are calculated using standard industry codes that assume a certain set of radioisotopes. The cooling limitations allowed for simplification of the analysis by neglecting many short-lived radioisotopes associated with fission products. Re-evaluation of the limits allowed for elimination of the spent fuel cooling time limit, allowing for assessment against only the thermal and radioactive limits[7]. Elimination of the fuel storage time limit therefore reduced the time to shipment by two years in most cases.

Reducing the time required for conversion of a reactor core from HEU to LEU was also a factor that warranted consideration. During operation, research reactor operators periodically substitute a small portion of the most highly irradiated fuel with fresh fuel, and then re-distribute the remaining fuel so as to evenly distribute the neutron flux within the core. This allows for optimum utilization of the fissile content of the fuel. Conversion of a reactor historically involved introduction of LEU fuel as part of this normal refueling cycle, a process that resulted in a three-year conversion timeframe.

In order to accelerate this process, some reactors developed an approach that discharged the entire HEU core and substituted an LEU core. This involved a reduction in capacity for a period of time, however, as it required startup with a smaller core due to the higher reactivity of fresh fuel, allowing for addition of fresh fuel as the core exposure increased.

V. Cost Impacts of Transport Modes

Over the history of the RRRFR Program, shipping modes have evolved from land to sea to air. This has, in most cases, involved higher costs for the actual transport vehicles associated with each mode. The total impact of the cost for shipment by various modes is not, however, dependent upon the actual transport vehicle cost. Several other factors can impact the overall cost, such as licensing, security, and support costs.

At the time preparations began for the second Hungarian SNF shipment, and prior to the initial use of air transport, an analysis of relative costs associated with various transport routes were compared in some depth[8]. The results of the cost comparison were somewhat surprising, as the costs associated with utilizing multiple modes and transiting multiple countries were significant factors.

Table 1 is a simplified table illustrating the costs of each option studied. Given the significant reduction in time-at-risk for the shipment, the incremental costs of air transport were funds well spent. It should also be noted that the cost of licensing the initial air shipment was higher than that in subsequent shipments.

One factor that should be noted is how the political situation can impact selection of routes, costs, and security. Note that the Land option in Table 1 is by far the most cost effective

option, and given the physical distance between the country of shipment and its destination, an expedient rail shipment might seem the logical choice. This option was not feasible, however, due to a lack of current agreements on transport of such materials between the governments involved.

TABLE 1. COST COMPARISON FOR MULTIPLE ROUTES

COST	INITIAL SHIPMENT	PORT A	PORT B	LAND	AIR
LICENSING	$800,000	$800,000	$700,000	$470,000	$1,100,000
INSURANCE	$22,000	$86,000	$86,000	$86,000	$86,000
TRUCK TRANSPORT	$240,000	$925,000	$750,000	$240,000	$140,000
RUSSIAN TRANSPORT	$900,000	$900,000	$900,000	$800,000	$400,000
RAIL TRANSPORT	$200,000	$480,000	$200,000	$200,000	
SECURITY	$67,907	$200,000	$200,000	$100,000	$100,000
SEA TRANSPORT	$1,500,000	$560,000	$860,000		
AIR TRANSPORT					$3,000,000
TOTAL	$3,729,907	$3,951,000	$3,696,000	$1,896,000	$4,826,000

VI. Future Transport Approaches

Over the course of the RRRFR program, transit times, and the commensurate risk of transport, have been significantly reduced. The average air shipment requires no more than 3 days, with the only significant vulnerability being the transport between the facility and the airport. In comparison, some shipments have taken as much as a month to complete.

Every mode of transport has positive and negative aspects. Proximity to rail heads, airports of sufficient length, availability of suitable trucks, and the political situation between governments involved will always be factors to consider. Future shipments will be assessed on a case-by-case basis to determine the most cost effective and secure solution.

VII. References

1. M. Tayack et al: *Development of new transportation/storage cask system for use by DOE Russian Research Reactor Fuel Return Program*. PATRAM 2007, 21-26 Oct, 2007 Miami, Florida, USA.
2. F. Sviták: *Experience Gained from Skoda VPVR/M Cask Use for RRRFR programme*. Regional Workshop on RRRFR Program Lessons Learned. 7-10 June 2011, Jackson Hole, Wyoming US.
3. O.P.Barinkov, B.A.Kanashov, K.V.Golubkin, V.M.Ipatov, *Transport Overpack for TUK-19 Packages*, Nuclear & Environmental Safety, №1, 2009.
4. S. V. Komarov et al: *Serbian SNF Repatriation Operation: Issues, Solving, Lessons Learned*. PATRAM 2013, 18-23 Aug, 2013, San Francisco, CA USA

5. M.E. Budu, D.V. Derganov, O.A. Savina, S.V. Komarov, S.D. Moses, *Developing a Spent Fuel Cask For Air Transport*, Nuclear Engineering International magazine, February 2014 Edition.
6. Czech Republic State Office for Nuclear Safety, *Decision 6943/2005*, CZ/048/B(U)F–96, March 23, 2005.
7. Czech Republic State Office for Nuclear Safety, *Decision 2827/2007*, CZ/048/B(U)F–96, February 16, 2007.
8. J. Dewes, I. Vidovszky: *Task 1 Shipment Initiation, Subtask 1.2 Project Authorization and Transport Concept*, RRRFR Internal Report, Budapest 2012.


RRFM
EUROPEAN RESEARCH REACTOR CONFERENCE 2016
IGORR
BERLIN
13 - 17 March 2016
GERMANY

CNS

DEVELOPMENT OF A COLD NEUTRON SOURCE AND NEUTRON BEAM FACILITIES AT THE PENN STATE BREAZEALE REACTOR

K. ÜNLÜ
Radiation Science and Engineering Center, Pennsylvania State University
University Park, PA 16802 - USA

ABSTRACT

Most of the neutron beam applications can be enhanced by using subthermal, "cold," neutrons. Only two cold neutron beam facilities were developed at the U.S. university research reactors, namely at Cornell University and the University of Texas at Austin. The mesitylene moderator in the Cornell Cold Neutron Beam Facility (CNBF) was cooled by a helium cryorefrigerator via copper cold fingers to maintain the moderator below 30 K at full power reactor operation. Texas Cold Neutron Source (TCNS) also uses mesitylene moderator that is cooled by a cryorefrigerator via a neon thermosyphon. The thermosyphon cools and maintains mesitylene moderator at about 30 K in a chamber. A third generation of mesitylene moderated university cold neutron source (CNS) is being built at the Penn State Breazeale Reactor (PSBR). The operation of the PSBR CNS is based on a helium cryorefrigerator and circulating liquid helium line. Liquid helium cools and maintains a cold neutron moderating material (mesitylene) at about 15-20 K in a 10 cm diameter aluminum chamber located inside the D_2O tank of the PSBR. The cold neutrons coming from the mesitylene chamber will be transported out of the biological shield of the reactor with three super-mirror neutron guides. The PSBR is a 1 MW, TRIGA with moveable core in a large pool and with pulsing capabilities. In steady-state operation at 1 MW, the thermal neutron flux is $1x10^{13}$ n/cm^{2}sec at the edge of the core and $3x10^{13}$ n/cm^{2}sec at the central thimble. The PSBR can also pulse with the peak flux for maximum pulse ~ $6x10^{16}$ n/cm^{2}sec with pulse half width of ~10 msec. The RSEC facilities are heavily used for nuclear science and engineering research and education. A description of the PSBR cold neutron source and planned new neutron beam facilities will be presented.

1. Introduction

The research applications at university research reactors can be enhanced by using subthermal neutrons--"cold neutrons." The "temperature" of a neutron beam can be reduced by passing it through a cold moderator. Cold neutrons will have lower energies and higher wavelength than thermal neutrons. Neutrons sufficiently long wavelengths (cold neutrons) can be reflected from some surfaces and they can be transported using neutron guides without the normal $1/r^2$ attenuation and can be bent out of the line-of-sight paths followed by other radiation. Past two decades only two cold neutron beam facilities were developed at the U.S. university research reactors, namely at Cornell University and the University of Texas at Austin. The Cornell Cold Neutron Beam Facility (CNBF) included a moderator, a cryorefrigerator, copper cold fingers, a neutron guide system, vacuum jackets, shielding, and various connecting and control lines [1-4]. The mesitylene moderator in the CNBF was cooled by a helium cryorefrigerator via copper cold fingers to maintain the moderator below 30 K at full power (500 KW) reactor operation. Cold neutrons from the mesitylene moderator were transported to an

experimental facility using thirteen 1-m long natural Ni coated neutron guide elements. Texas Cold Neutron Source (TCNS) uses mesitylene moderator that is cooled by a cryorefrigerator via a neon thermosyphon [5-10]. The operation of the TCNS is based on a helium cryorefrigerator, which liquefies neon gas in a 3-m long thermosyphon. The thermo siphon cools and maintains mesitylene moderator at about 30 K in a chamber. Neutrons streaming through the mesitylene chamber are moderated and thus reduce their energy to produce a cold neutron distribution. The cold neutrons are transported out of the biological shield of the reactor and to a sample chamber location by a 6-m long curved neutron guide and an 80-cm long converging neutron guide. The design features, cooling and warm-up characteristics, and the performance of both CNBF and TCNS will be briefly discussed below. The investigation of thermal and thermal-hydraulic characteristics of the cooling systems of both CNBF and TCNS carried out in order to design and build a mesitlylene based cold neutron source at the Penn State University, Breazeale Nuclear Reactor (PSBR) [11-16]. A third generation of mesitylene moderated university cold neutron source (CNS) is being built at the Penn State Breazeale Reactor (PSBR). The operation of the PSBR CNS is based on a helium cryorefrigerator and circulating helium line. Circulating liquid helium cools and maintains a cold neutron moderating material (mesitylene) at about 15-20 K in a 10 cm diameter aluminum chamber located inside the D_2O tank of the PSBR. The cold neutrons coming from the mesitylene chamber are transported out of the biological shield of the reactor with three super-mirror neutron guides. New core-moderator assembly and new beam ports and design features of the PSBR CNS will be presented.

2. University Research Reactor Cold Neutron Beam Facilities in the USA

2.1 Cornell Cold Neutron Beam Facility

Cornell Cold Neutron Beam Facility (CNBF) was located at one of the radial beam port of the 500 kW TRIGA research reactor and adjacent beam floor area (Fig. 1a) [1-4]. (Cornell University administration decided to close the Ward Center for Nuclear Sciences on June 2002 hence Cornell reactor and Ward Center for Nuclear Sciences are no longer available for scientific community). The CNBF consisted of a cooled moderator, a cryorefrigerator, a copper rod (cold finger), and neutron guide elements (Fig. 1b). The moderator placed in a neutron beam port close to the reactor core. The moderator used in the Cornell cold neutron source is mesitylene, a 1,3,5-trimethyl benzene. Because mesitylene freezes at 228K and boils at 437K, it is safer and much simpler to use than liquid hydrogen, D_2O ice, or solid methane, the more traditional cold-neutron-source moderators. The handling system for mesitylene does not need to withstand large or abrupt changes in pressure, but must be a closed system to avoid contaminating the mesitylene or releasing it since it is slightly carcinogenic and toxic.

The CNBF moderator was contained in a thin-walled aluminum right-circular cylinder 7.5 cm diameter by 2.5 cm deep position inside a beam tube at the graphite reflector of the reactor. The moderator was cooled by conduction through a 5-9's purity (99.999+%) 1.8 cm diameter, 216 cm long copper rod. The copper rod was connected to the second stage of a cryogenic refrigerator located outside the biological shield of the reactor. A Gifford-McMahon cycle Cryomech model GB04 helium cryorefrigerator was used for cooling. The moderator chamber temperature varied from 11K at 0.0 kW reactor power with an evacuated chamber to a 28.5K at 500 kW reactor power with a mesitylene filled

chamber. The neutron guide of Cornell CNBF contained thirteen 1-meter long elements. Each element was comprised of two parallel side plates of dimension: 8 cm high by 100 cm long by 1 cm thickness, separated top and bottom by epoxied, ground glass strips of dimensions 2 cm wide by 100 cm long by 1 cm thickness. The cross sectional view resembled a "double bar H", with internal dimensions of 2 cm wide by 5 cm high. The four interior surfaces were coated with a 5 Å thick evaporated layer of natural nickel. The predicted thermal equivalent flux at the exit of the neutron guides at 480 kW reactor power was about 4 x 10^6 n/cm^2 sec.

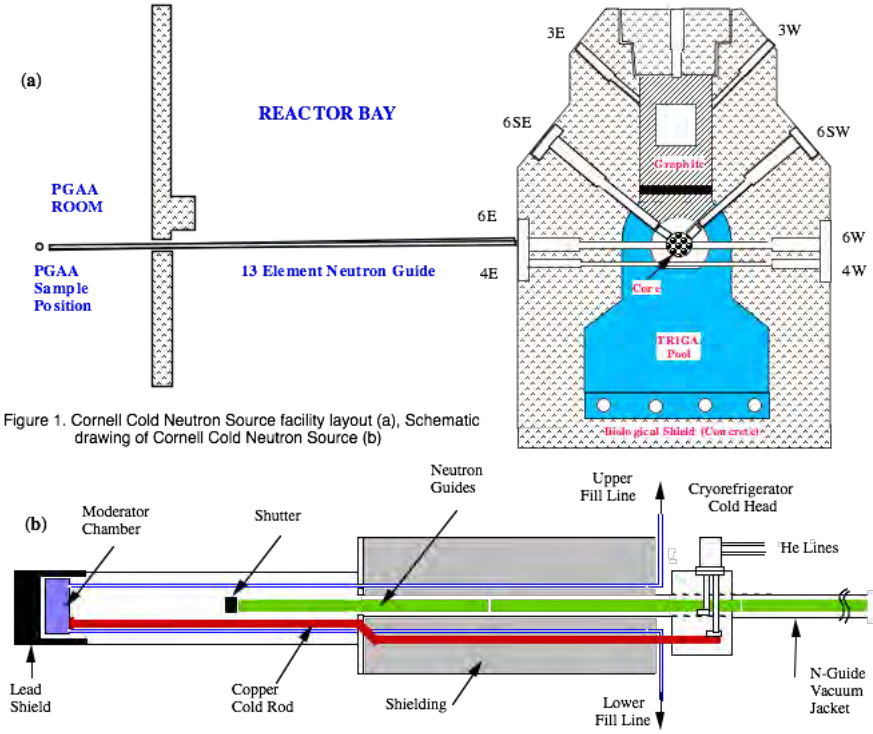

Figure 1. Cornell Cold Neutron Source facility layout (a), Schematic drawing of Cornell Cold Neutron Source (b)

Fig. 1. Schematic drawing of the Cornell Cold Neutron Beam Facility

2.2 Texas Cold Neutron Source (TCNS)

The operation of the TCNS is based on a helium cryorefrigerator, which liquefies neon gas in a 3-m long thermosyphon [5-10]. The thermosyphon cools and maintains a cold neutron moderating material (mesitylene) at about 30 K in an aluminum chamber located inside the graphite reflector of the University of Texas at Austin (UT-Austin) 1000-kW research reactor. The cooling down and warming up trends of the TCNS is similar to Cornell Cold Neutron Source. Neutrons streaming through the mesitylene chamber are moderated and thus reduce their energy to produce a cold neutron distribution. The cold neutrons coming from the mesitylene chamber are transported out of the biological shield of the reactor and to the PGAA sample chamber location by a 6-m long curved neutron guide and an 80-cm long converging neutron guide. Fig. 2 is a cross sectional view of the external components of the TCNS, curved guides and the UT-PGAA facility. The curved neutron guide is made up by three 2-m long sections, curved to a 300-m radius and divided into three vertical channels (5 x 0.45-cm) by 0.1-cm-thick walls. This

array provides blocking of the straight-path background components streaming through the guide. The TCNS curved neutron guide, with all reflecting surfaces coated by a 1000-Å ^{58}Ni layer, utilizes total reflection to transport neutrons without the normal $1/r^2$ intensity loss. The critical angle for total reflection of neutrons from ^{58}Ni is 0.12° per Å. The characteristic wavelength of the curved neutron guide is 2.7 Å, which corresponds to neutron energy of 11 meV.

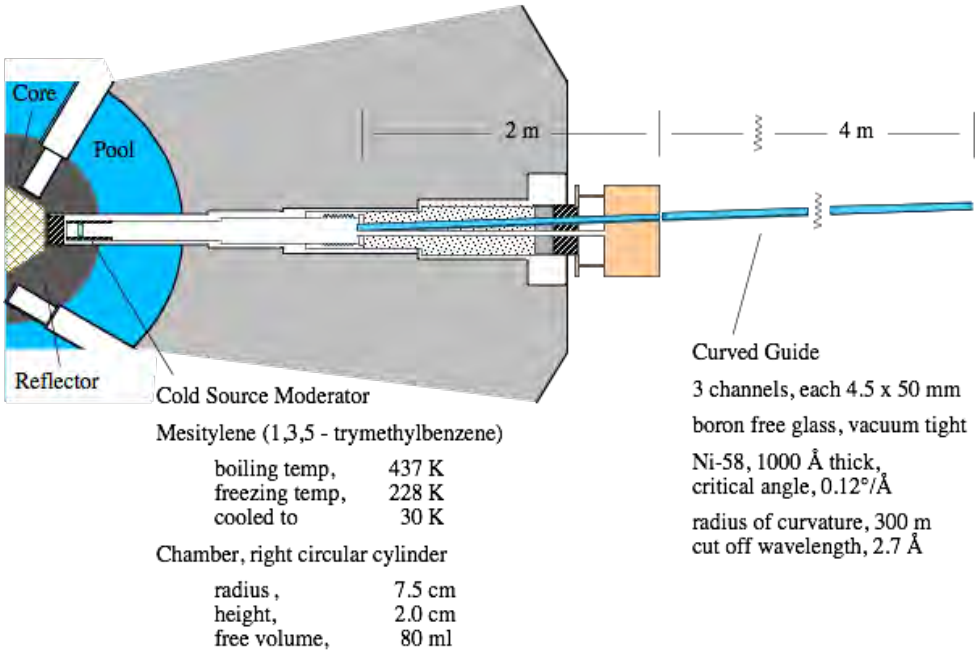

Fig. 2. Cross-sectional view of the Texas Cold Neutron Source in the piercing beam port of the UT-TRIGA research reactor, showing the location of the 6 m long curved neutron guide.

3. Penn State Breazeale Nuclear Reactor (PSBR)

The Penn State Breazeale Reactor (PSBR) at the Radiation Science and Engineering Center (RSEC) is a 1 MW TRIGA Mark III reactor with pulsing capabilities. The moveable core at PSBR has no fixed reflector and is located in a 24 ft deep pool with ~71,000 gallons of demineralized water. A variety of dry tubes and fixtures are available in or near the core for irradiations. When the reactor core is placed next to the D_2O tank and graphite reflector assembly near the beam port locations, thermal neutron beams become available. In steady state operation at 1 MW, the thermal neutron flux is $1x10^{13}$ n/cm^2sec at the edge of the core and $3x10^{13}$ n/cm^2sec at the central thimble. The peak flux during a maximum pulse is ~ $6x10^{16}$ n/cm^2sec with a pulse half width of ~10 msec.

3.1 Inherent design Issues with PSBR

The PSBR, the centerpiece of the RSEC, first went critical in 1955 and is the longest continuously operating university research reactor in the United States. The initial reactor design utilized plate-type MTR fuel elements with a 61-cm active fuel length and up to 93% enrichment. Seven beam ports were built into the facility design for analyzing the nuclear properties of materials, determining reactor dynamics and examining the

effects of radiation on materials. After ten years of service, the reactor core design was changed to a TRIGA Mark III. The design conversion to a TRIGA core produced three major advantages for the reactor: (1) the reactor power was increased from 200 kW to 1 MW; (2) the reactor was moved to the low-enriched safeguards category since 20% enriched fuel elements are used in the TRIGA core and (3) pulsing capability was added to the core due to the inherent prompt negative feedback characteristics of the TRIGA fuel elements, which are a matrix of uranium and $ZrH_{1.6}$ moderators. Unfortunately, the design conversion also resulted in a partial loss of experimental capability for the facility, such that six of the seven beam ports are limited in neutron beam utilization. This is mainly due to the physical differences between MTR and TRIGA fuel element designs. Since the active length of a TRIGA fuel element (38.1 cm) is considerably smaller than the active length of an MTR fuel element (~61 cm), six beam ports, which were aligned with the MTR fuel, are now directed 12.7 or 27.9 cm below the core center. In this existing beam port configuration, only beam port (BP) 4 is located at the core center. In addition, five of the seven existing beam ports could not be properly aligned to the core-moderator assembly after the design change. A schematic drawing of the existing reactor core, D_2O tank, graphite and seven beam ports extended toward the reactor core are given in Fig. 3. Therefore, the PSBR is not capable of simultaneously utilizing all the available beam ports with the current configuration of the beam ports and the core-moderator assembly.

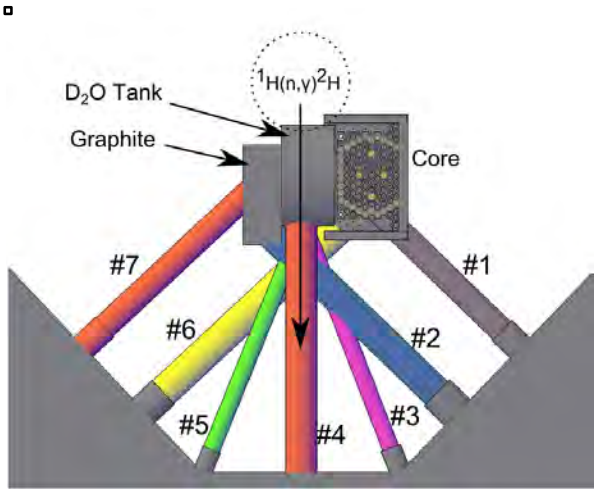

Figure 3. PSBR 3D AutoCAD® drawing of the existing core-moderator assembly layout with extended views of existing beam ports (top view).

3.2 New Core-Moderator Assembly Design at PSBR

A significant redesign of the core-moderator assembly and beam port was complete to make full use of the PSBR's capabilities and to establish state-of-the-art neutron beam facilities. A new PSBR core-moderator assembly design and five new beam ports were completed. This design eliminates all the limitations of the existing design by increasing the number of simultaneously utilized beam ports from two to five and by mitigating the amount of prompt gamma-rays in the beam port facilities. The major constraints of the PSBR are mainly geometric factors such as available infrastructure in the beam hall, the tower design, geometrical arrangement of the beam ports and the core and moderator

designs. Furthermore, thermal-hydraulics safety of the core was taken into account in the design process. The optimal design parameters and the neutronic performance of the new design were calculated [11-16].

The existing core-moderator assembly design is the main cause of the geometric mismatch of the beam port configuration. The key parameter in the design process is the calculation of the optimal size and shape of the moderator tank. A crescent-shaped moderator tank was chosen since it allows for the simultaneous utilization of five new beam ports. After the selection of the moderator tank shape, the second design step was the proper coupling of the moderator tank with the reactor core in order to eliminate the prompt-gamma contamination problem by minimizing pool water at the interface of the core-moderator assembly. This was achieved by keeping the faces of the top and bottom grid plates and the crescent-shaped moderator tank as close as possible (0.62 cm between the core and the moderator tank). The final step in the design process was how to support a new core design with a new reactor tower. The existing reactor core is supported by a tower through the bottom grid plate. The top grid plate is connected to the bottom grid plate. In the new design, the top and bottom grid plates are equal in size and smaller than the existing grid plates. As a result, the tower design will be changed by installing four new support bars and two supports plates on top of the core. Fig. 4 shows the core-moderator assembly and tower design for the PSBR after the design changes.

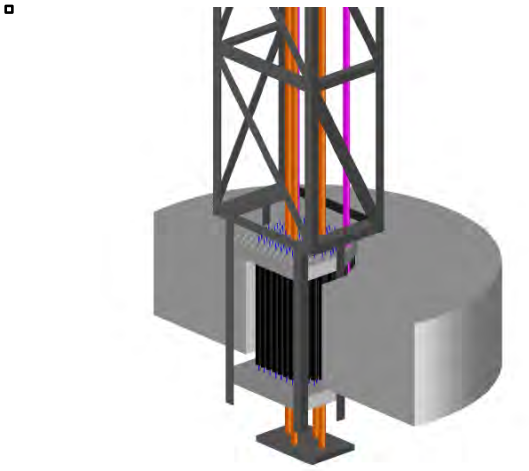

Fig. 4. PSBR 3D AutoCAD® drawing of the new core-moderator assembly and tower design.

3.3 New Beam Port Design at PSBR

The neutronic performance of the new beam ports is not only affected by the core-moderator assembly design but also the beam divergence, collimator system, filter material and other geometric factors like physical dimensions. In the optimization study, the neutronic design of the new reactor was explored with five beam port models without considering these factors. However, the final design features of each neutron beam port will be based on the experimental facility to be used. Five neutron beam ports are designed for the new reactor. A cold neutron beam port which utilizes cold neutrons

from three super-mirror neutron guide is considered. Therefore, there will be seven neutron beams available in the new facility. The design features of the new beam ports with the new core-moderator assembly are shown in Fig. 5. Three neutron guide tubes will be available to utilize the cold neutrons in the cold neutron beam facilities.

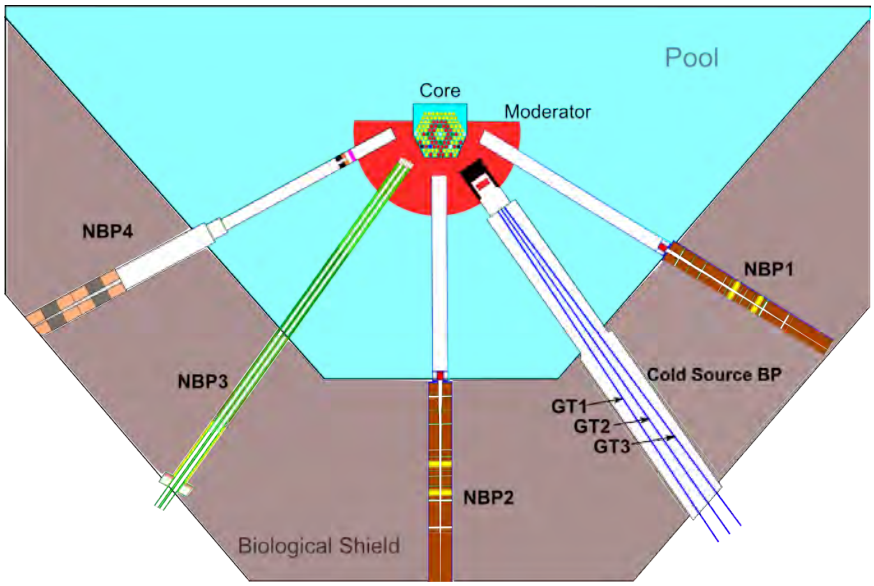

Fig. 5. A schematic layout of the final PSBR design with four thermal neutron beam ports and one cold neutron beam port with three neutron guides.

3.4 Penn State Cold Neutron Source (PSU-CNS)

A schematic drawing of the PSU-CNS is shown in Fig. 6. The PSU-CNS is located inside a piercing beam port that is in the D_2O tank. The front end of the beam port is 15 cm away from the face of the reactor core. There will be a lead shield in front of the beam port that the mesitlyene moderator is located. The beam port is heat shielded and evacuated. A 10 cm diameter and 2.5 cm thick mesitylene moderator chamber is cooled with circulating line of liquid helium from a cryorefrigerator located outside of the biological shield. Both designs of Cornell and Texas Cold Neutron Source were initially considered. A thermodynamic analysis of two phase-closed thermosyphon with vapor reservoir for cooling of moderator of cold neutron source was carried out to investigate the operational characteristics and performance limit [17]. For this analysis, experimental results of a previous cooling system installed at University of Texas – Austin was considered. The data showed a limitation of the cooling capacity (only up to 4W), due to lack of liquid (dryout) in the evaporator section of the thermosyphon. An analytic model was developed based on basic thermodynamic analysis that determines the dryout point for such TPCTR. The model prediction of the dryout point for the TCNS cooling system was within 5% of the experimental data. Using this model various parametric analysis were performed to investigate the effects of initial pressure, reservoir temperature, volume ratio (ratio of the volume of reservoir to that of thermosyphon) and working fluids.

The results show that the dryout temperature varies the most when the volume ratio varies. In general, increase in volume ratio will increase the dryout temperature and hence the operational temperatures range of the TPCTR cooling system. Increase in initial pressure increases the dryout temperature under any volume ratio conditions. Decrease in reservoir temperature will increase the dryout temperature for lower volume ratio TPCTR systems. However the effect of reservoir temperature decreases at higher volume ratios. From the parametric study of the fluids considered in this study it is concluded that usage of a two phase closed thermosyphon will be sufficient for the PSU-CNS. However, a circulating line of liquid helium from a Cryomech cryorefrigerator design will absorb much more heat load and will be more effective cooling system. Therefore, a Cryomech cryorefrigerator (PT815) with circulating liquid helium line was chosen for the PSU-CNS cooling system.

Both neutronic and thermal hydraulic performances of new core moderator assembly and neutron beam port were modeled. Neutron flux spectrum at the surface of the mesitylene moderator chamber toward the neutron guide side is shown in Fig. 7. Three supermirror neutron guides will be placed as close as possible to moderator chamber. A super-mirror neutron guide system with beam bender and focusing sections will be used. The guide system selection is continuing at the time of this study.

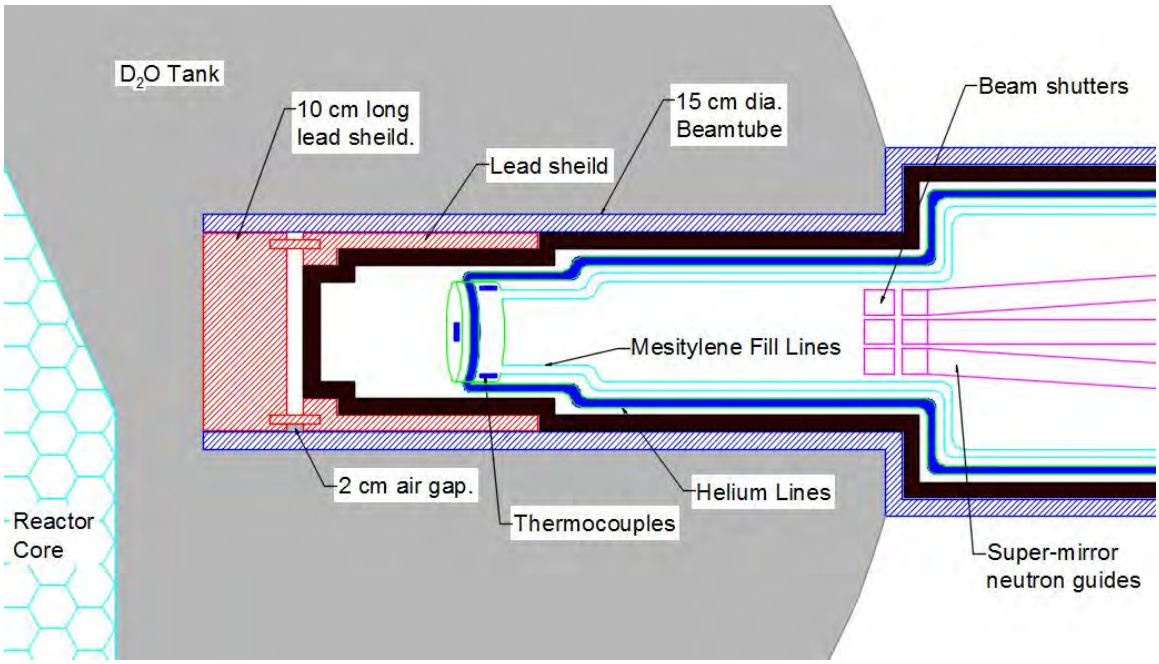

Fig. 6. Schematic drawings of the PSBR-CNS showing front sections of the beam port embedded into D_2O tank.

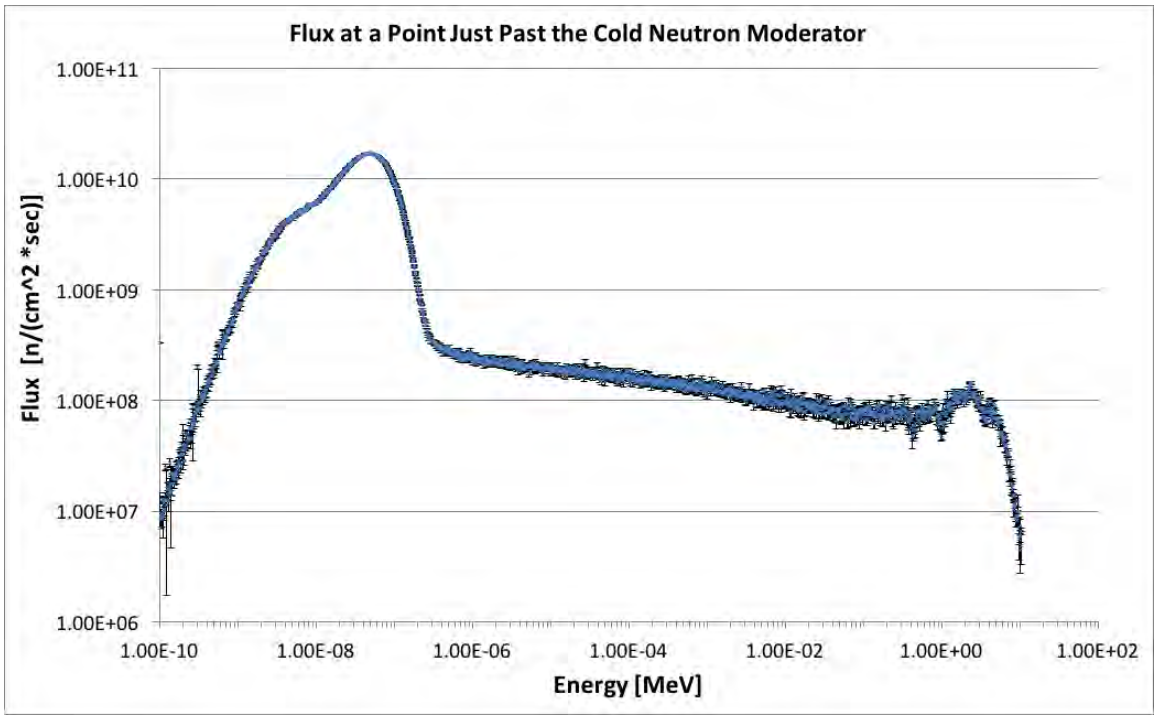

Fig. 7. Neutron flux spectrum at a point at the surface of the mesitylene moderator chamber of PSBR-CNS toward the neutron guide side.

4. Summary and Conclusions

Five new neutron beam ports were designed for the PSBR facility. This new arrangement would require cutting and removing a section of the existing biological shield and placing five new beam ports with various diameters depending on the intended neutron beam technique to be applied. A mesitylene-based cold neutron source and three neutron guides will be installed in one of the beam ports. Four new experimental techniques (triple-axis spectrometer, conventional and TOF-NDP, neutron powder diffraction, and prompt gamma activation analysis) will be added to the existing neutron imaging and neutron transmission facilities. The geometrical configurations along with the filter and collimator system designs of each neutron beam port were selected based on the requirements of the experimental facilities. MCNP5 simulation results predicted that the thermal neutron flux would be increased by a factor of between 1.23 and 2.68 in the new beam ports compared to the existing design. In addition, the total gamma dose will be decreased by a factor of 100 in the new PSBR facilities.

The areas envisioned for the RSEC's new neutron beam port/beam laboratory are for mostly cutting-edge nuclear and materials science research. Some examples include: a NDP facility for depth vs. concentration measurements, impurity determination of He-3 and B-10 in semiconductors, metals, and alloys; a mesitylene-based Cold Neutron Source and Cold Neutron Prompt Gamma Activation Analysis for neutron focusing research, materials characterization, and determination of impurities in historically or technologically important materials; a Neutron Powder Diffractometer for structural determination of materials; and a Triple Axis Diffractometer to train students on neutron

diffraction and perform preliminary structural determinations of materials. Brief descriptions of some these techniques are given below. The majority of funds to develop and implement these techniques are already available at the RSEC. Most of the required equipment (e.g., neutron imaging systems, neutron activation analysis systems, NDP chamber and the related data acquisition and processing equipment, and the prompt gamma activation analysis system) has already been purchased, and some of these techniques are already available at the RSEC with limited capacity. With the new and expanded laboratory, the techniques and associated research projects will be improved and new research projects will be available for the development of cold neutron beam and neutron guides.

The new and expanded laboratory will add new beam ports that are geometrically aligned with the core-moderator assembly for optimum neutron output at experimental positions. With state-of-the-art neutron beam facilities, coupled with the existing PSBR and RSEC capabilities will offer unparalleled research opportunities for Penn State faculty and graduate students in many disciplines and will provide an excellent test-bed for development of instruments and experiments for researchers at Penn State, as well as other regional and national university researchers, industry, and national laboratories.

5. References

[1]. D. D. Clark, C. G. Ouellet, J. S. Berg, “On the Design of a Cold Neutron Source,” Nucl. Sci. Engr. Vol. 110, No. 4, 445 (1992).

[2]. S. A. Spern, Ph.D. dissertation, “Initial Characterization of Cornell Cold Neutron Source,” Cornell University, (1998)

[3]. L. J. Young, Ph.D. dissertation, “The Design and Construction of a Cold Neutron Source for use in the Cornell TRIGA Reactor,” Cornell University, (1983)

[4]. K. Ünlü, D. D. Clark, “Development of Cold-Neutron Prompt Gamma Activation Analysis Facility at Cornell University”, MTAA-10, Tenth International Conference on Modern Trends in Activation Analysis, April 19-23, 1999, Bethesda, Maryland.

[5]. K. Ünlü, C. Rios-Martinez, B.W. Wehring, “The University of Texas Cold Neutron Source,” Nucl. Instr. and Meth. in Phys. Res. A 353 (1994) 397.

[6]. C. Rios-Martinez, "Prompt Gamma Activation Analysis using the Texas Cold Neutron Source" Ph.D. Thesis, The University of Texas at Austin, (1995).

[7]. K. Ünlü, C. Rios-Martinez, B. W. Wehring, “Prompt Gamma Activation Analysis with Texas Cold Neutron Source,”J. of Radioanal. Nucl. Chem., Articles, 193, No.1, (1995) 145.

[8]. B.W. Wehring, K. Ünlü, C. Rios-Martinez, “Application of Cold-neutron Prompt Gamma Activation Analysis at the University of Texas,” Appl. Radiat. Isot. Vol. 48, No.10-12. pp. 1343-1348, (1997).

[9]. C. Rios-Martinez, K. Ünlü, B. W. Wehring, “Performance of the University of Texas Cold-neutron Prompt Gamma Activation Analysis Facility,” J. of Radioanal. Nucl. Chem., Articles, 234, No.1-2 , 119-123 (1998).

[10]. B.W. Wehring, J.Y. Kim, K. Ünlü, “Neutron Focusing System for Texas Cold Neutron Source,” Nucl. Instr. and Meth. in Phys. Res. A 353 (1994) 137

[11] D. Ucar, “Modeling And Design Of A New Core-Moderator Assembly And Neutron Beam Ports For The Penn State Breazeale Nuclear Reactor (PSBR)”, PhD Dissertation, The Pennsylvania State University, Department of Mechanical and Nuclear Engineering, (2013).

[12] D. Ucar, K. Ünlü, B. J. Heidrich K. N. Ivanov, M. N. Avramova, "Neutronic Designs and Analysis of a new Core-Moderator Assembly and Neutron Beam Ports for the Penn State Breazeale Reactor", PHYSOR 2014 - The Role of Reactor Physics Toward a Sustainable Future, Kyoto, Japan, Japanese Atomic Energy Agency, Special Issue of PHYSOR 2014 (JAEA-Conf-2014-003)

[13]. F. Alim, K. Bekar, K. Ivanov, K. Ünlü, J. Brenizer, Y. Azmy, Modeling and Optimization of Existing Beam Port Facility at PSBR, Annals of Nuclear Energy, Vol. 33, Issues 17-18, p1391-1395, (2006).

[14]. K. B. Bekar, Y. Azmy, K. Ünlü, J. Brenizer, “A Case Study to Bound the Search Space of the Optimization Problem for the PSBR Beam Tube”, PHYSOR 2006 – Advances in Nuclear Analysis and Simulation, September 10-14, 2006 Vancouver, BC, Canada (2006).

[15]. J.S. Butler, “Instrument Selection and Layout for the Penn State Neutron Beam Hall Expansion,” MSc. Thesis, The Pennsylvania State University, Department of Mechanical and Nuclear Engineering, (2006).

[16]. B. Sarikaya, F. Alim, K. Ivanov, K. Ünlü, J. Brenizer, Y. Azmy, “Modeling of Existing Beam Port Facility at PSU Breazeale Reactor by Using MCNP”, PHYSOR 2004 -The Physics of Fuel Cycles and Advanced Nuclear Systems: Global Developments (2004).

[17]. M. Habte, “Thermal Hydraulic Analysis of Two-Phase Closed Thermosyphon Cooling System for New Cold Neutron Source Moderator of Breazeale Research Reactor at Penn State,” PhD Dissertation, The Pennsylvania State University, Department of Mechanical and Nuclear Engineering, (2008).

12 Years of Experience from Running a Cold Neutron Source at FRM II Research Reactor

DIETMAR PÄTHE [1]), ANDREAS WIRTZ [1]), HEIKO GERSTENBERG [1]), ANTON KASTENMÜLLER [1])
[1] *Technische Universität München, ZWE FRM-II, Lichtenbergstraße 1, 85747 Garching – Germany*

ABSTRACT

FRM II is a 20 MW multipurpose high flux research reactor operated by the Technische Universität München in Germany. The probably most important scientific installation is a Cold Neutron Source (CNS) based on the moderation of thermal neutrons by liquid deuterium at a temperature of about 24 K. As compared to other installations the CNS is the only one which necessarily must be in cold operation mode to allow the operation of the reactor itself.
The task of this contribution is to review the experiences from 12 years of CNS operation including maintenance.
A short description of the process technology will be given to characterize the type of CNS used at FRM II. Additionally a number of items will be pointed out that distinguishes this facility from differently designed cold neutron sources used in other research reactors. A particular focus will be laid on the deuterium storage using solid hydride materials and the treatment of H-3.
After running the source for several years and after performing an extensive maintenance and test program in 2014 an overall view on the performance of the CNS is available. Positive and negative experiences will be presented and discussed. The root cause of some of the few interferences that occurred during CNS operation will be presented along with the changes that had been taken to avoid them in future.

1. Introduction

On March 2nd 2004 the first criticality of the new research reactor FRM II of the Technische Universität München was achieved and the nuclear commissioning started. The Cold Neutron Source (CNS) was part of the original experimental equipment of FRM II and consequently it was commissioned along with the reactor itself. The routine operation started in April 2005.

FRM II is a heavy-water moderated and light-water cooled tank in pool reactor. Highly enriched uranium is used to allow a very compact design of the core being made up by a single fuel assembly. By means of this concept a maximum undisturbed thermal neutron flux density of 8 * E14 n/(cm^2*s) in a distance of about 30 cm from the core is provided at a thermal power of only 20 MW (see Fig. 1). Each reactor cycle takes 60 full power days and ends after a burn-up of 1200 MWd, the targeted lifetime of a fuel assembly.

The FRM II is equipped with 11 beam tubes, 5 irradiation facilities and a cold and a hot neutron source. The latter two installations are secondary sources that shift the thermal neutron energy spectrum in the D_2O moderator to lower and higher energies respectively and make a broad range of neutron velocities available for many different experiments (see Fig. 2).

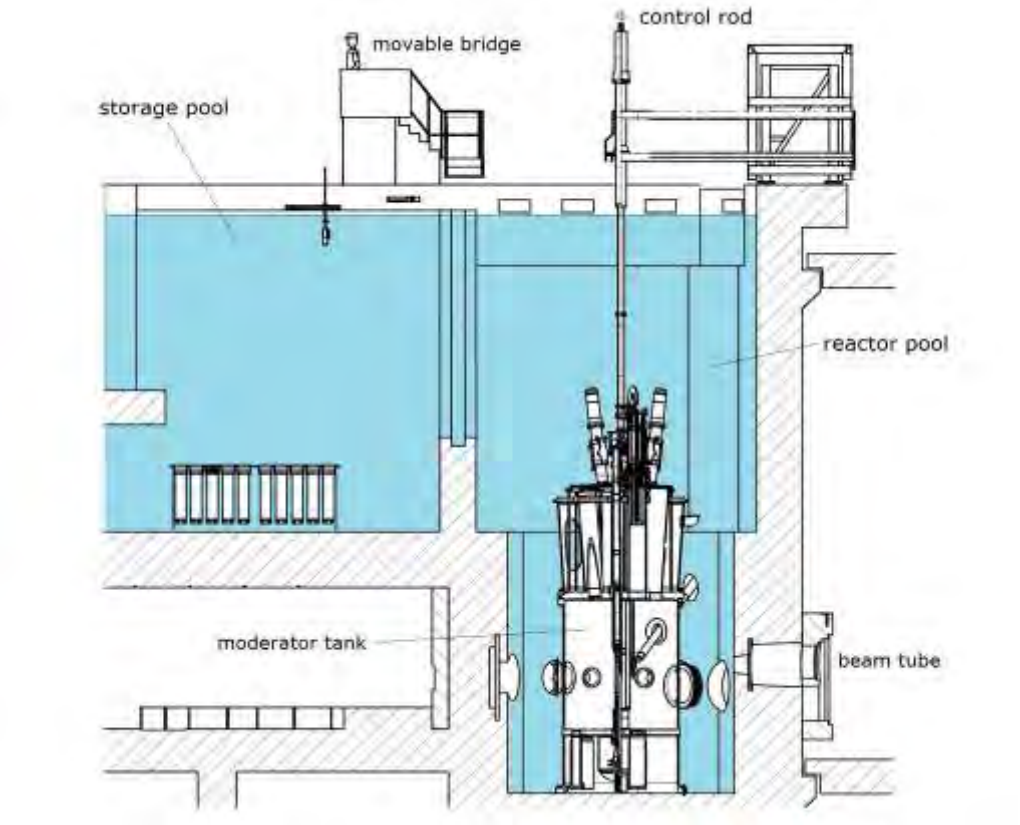

Figure 1: Vertical cross-section through the reactor pool

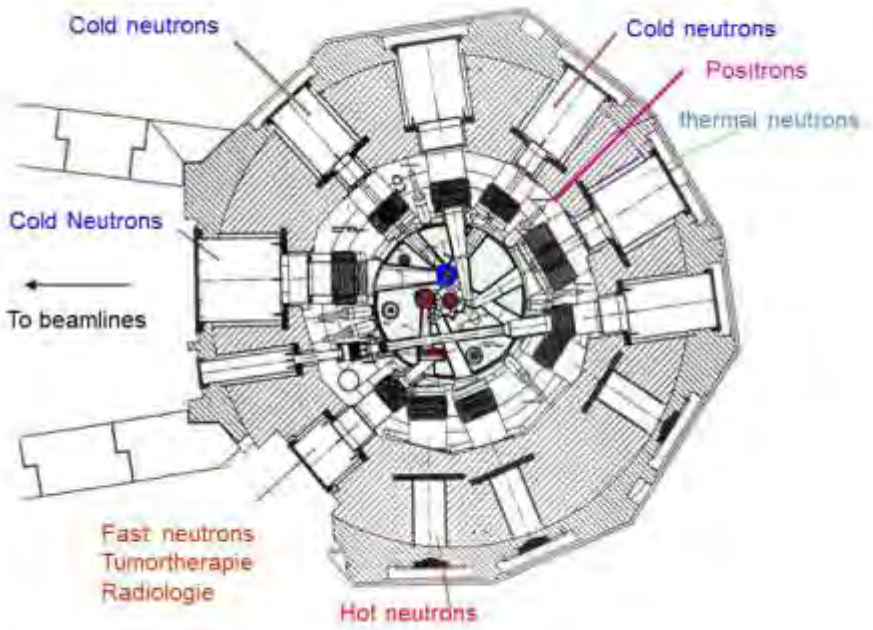

Figure 2: Horizontal cross-section through the reactor at beamtube-level

2. The Type of CNS at FRM II: A Short Description of the Used Technology

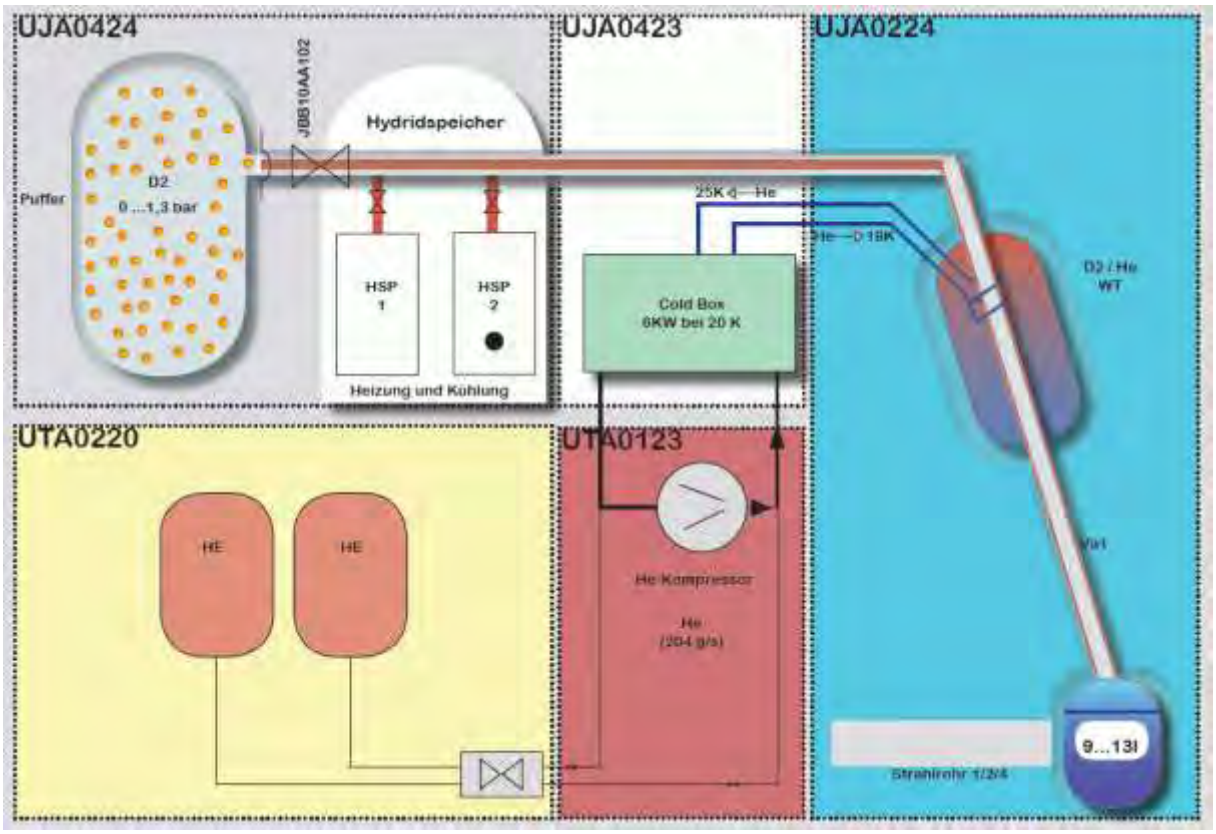

Figure 3: General overview of the CNS

The CNS at FRM II is installed inside the heavy water moderator tank. It is operated using liquid Deuterium at approximately 24 K as moderator. Because the space on top of the reflector tank is extremely narrow, the CNS-inpile construction is tilt by an angle of 10° as compared to vertical. This design guarantees a position of the moderator vessel close to the reactor core in the area of maximum thermal neutron flux density. Vertically the moderator vessel is located in the core mid-plane.

In cold operation mode the deuterium gas is condensed in a heat exchanger located in the upper part of the inpile. The liquid deuterium rinses down to the moderator vessel. In the moderator vessel the liquid Deuterium is evaporated and the vapour ascends in the same pipe the liquid descends. In summary the system of liquefaction and evaporation is a two phase thermosiphon cycle. The moderation is run at approximately 24 K corresponding to a pressure of 145 kPa. The filling level is typically 12 l (2.7 kg) and the evaporation rate is estimated to be 23 g/s at full reactor power of 20 MW.

.

The moderator vessel is made from Al 6061 T6. It is housed in a surrounding vacuum vessel made from zircaloy.

The cooling power is provided by a Helium cryogenic refrigerator delivering about 200 g/s He-gas at 19 K. The needed cooling power is estimated to be almost 7 kW.

3. Special Items of this CNS

The CNS at FRM II exhibits some properties and components that may be unique.

The noses of 3 beam tubes being supplied by the CNS are in immediate contact to the outer wall of the insulation vacuum container surrounding the moderator vessel of the CNS. Inside the moderator vessel a dispenser is installed in a position closest to the beam tubes. This bucket with an open bottom and a volume of 5.8 l is filled with deuterium vapour dispensing liquid deuterium. By this measure the cold neutron flux is increased by about 10 % while saving deuterium and a bit of cryogenic cooling power.

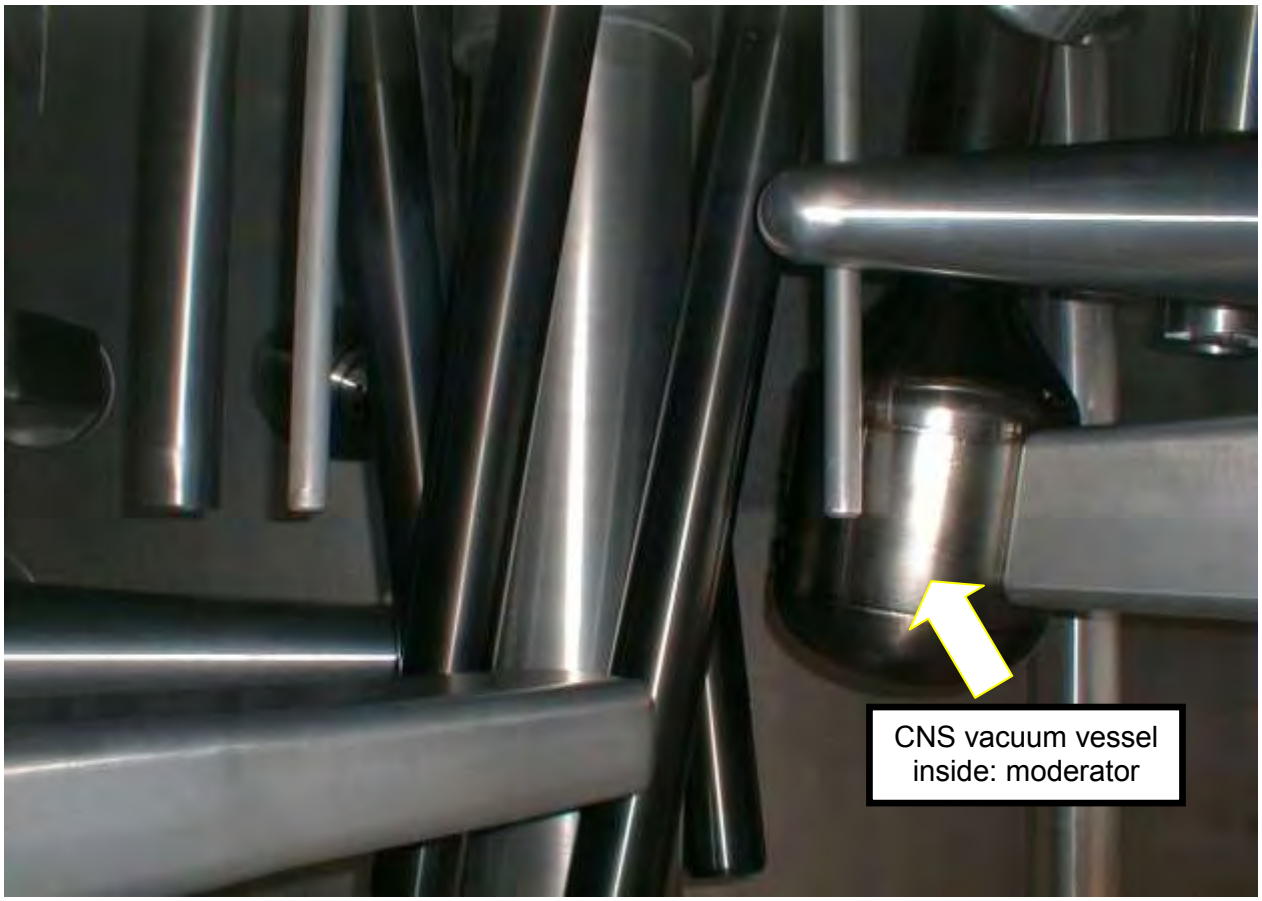

Figure 4: Inner installations of the moderator vessel with CNS

During neutron irradiation deuterium is activated to produce radioactive tritium (H-3). Consequently special attention has to be paid to enclose and store the deuterium in a safe manner while the CNS is warmed up (“warm state”). For this purpose two metallic hydride storages are available in addition to a conventional buffer-vessel. Hence, within limits, alternative storage places are available.

While the CNS is warm, the reactor may be run only at a power of 200 kW (1 % of nominal power) in maximum. This limit has been set in order to prevent the damage of the CNS due to overheating. Consequently, the CNS has to be cooled down to operational temperature of 24 K before the reactor power may be increased to its nominal value of 20 MW. In addition, in case the CNS fails during reactor operation, the reactor is scrammed automatically in order to protect the CNS from serious damage.

While cooling down the CNS the supply temperature out of the cryogenic refrigerator to the helium/deuterium heat exchanger is chosen below 19 K to condense the deuterium at a pressure of about 30 kPa. After this procedure buffer and hydride storages are shut off and the pressure is increased to its nominal operational value of 145 kPa at about 24 K. So most of the inventory of deuterium can be liquefied and used for moderation. This method limits the required volume of deuterium but on the other hand it required the use of hydride storages.

While the CNS is not in operation, i.e. the system is at ambient temperature, the deuterium is stored in a buffer-vessel or in metal hydride storages. The buffer is double-walled with a volume of 14 m³. Upon evaporation of the deuterium there is a pressure of about 140 kPa (1.4 bar abs) present in the buffer without using the hydride storages. The entire inventory of deuterium may be sucked into to hydride storages.

There are two hydride storages: HSP1 and HSP2.
HSP1:
Material: 150 kg of ZrCoNi-Alloy as granulate material and powder (as bulk fill)
Operable pressure range: 50kPa … 10Pa
Operating temperatures: 20 °C … max.400 °C

HSP2:
Material: 250 kg of LaCoNi-Alloy as granulate material and powder (as bulk fill)
Operable pressure range: 300 … 10kPa
Operating temperatures: 20 °C … max.200 °C

Each of the storages is able to adsorb the entire inventory of deuterium.
While HSP2 is the main storage, adsorbing the deuterium down to a pressure of < 10 kPa, HSP1 works as a vacuum getter pump, adsorbing the gas down to 100 Pa or below.

The adsorption of hydrogen or deuterium in hydride materials is exotherm, desorption is endotherm. In consequence the storage needs to be heated for desorption to remove the deuterium from the storage and it needs to be cooled for adsorption to load the storage. This turned out to be a difficult task in cases when loading and unloading in short time and at low pressures is required. Under high pressure the hydrogen/deuterium itself conducts the thermal energy between the getter material and the heat exchanging surfaces. At low pressures the thermal conduction is drastically reduced and the above mechanism fails. Because of the poor heating and cooling it takes much longer as expected from the original concept to load and unload the storages.

4. Advantages and Disadvantages

The CNS is in operation since 2004. Some experiences will here be summarised.

Advantages:
1. Relatively low inventory of deuterium:
   - Advantage in handling and once it will to be dispose.

2. Use of hydride storages:
   - The inpile of the CNS (moderator vessel, heat exchanger) can be emptied to very low pressures (< 500 Pa).
   - Allows the use of a smaller lot of deuterium (see 1.).
   - Hydride storages are part of the disposal concept for the tritium contaminated deuterium.

3. Provision of high neutron flux values:
    - Using deuterium as moderator.
    - Using a dispenser.
    - Placing the moderator vessel near the core in the area of maximum thermal flux.

Disadvantages:

1. Operation of the reactor only possible when CNS is in cold operation:
    - There is not enough natural ventilation to prevent overheating the moderator vessel.
    - The CNS is leading in time schedule when starting a reactor cycle.

2. Using hydride storages:
    - It is a new technology, not approved for those applications (low pressures).
    - Very unique application, no other experiences.

3. Using deuterium as moderator:
    - The deuterium will become contaminated by tritium.
      Beside explosion prevention the radioactivity is to consider.
      There is a need to arrange a special handling.

5. The 10-Year Periodic Safety Review in 2014

After 10 years of nuclear operation a big Periodic Safety Review of the entire facility is mandatory for the FRM II. The first 10 years periodic inspection of FRM II started in spring 2014 and took several months.

Figure 5: CNS inside moderator vessel after 10 years of operation in May 2014

Nevertheless for the CNS many of the demanded proofs are covered by our normal periodic inspections, like tightness of vacuum and deuterium rooms, functionality of safety mechanisms and so on. An exception was the pressure test of the moderator tank, which is

also an external pressure test of the CNS, and the visual examination of the moderator tank and its inner components.
All the tests were passed without any critical comments by the supervisors.

Figure 5 shows a picture of the CNS taken during inspection inside the moderator vessel.
It shows a clean vacuum vessel and the noses of the 3 beam tubes facing the CNS. (During the inspection the moderator vessel was filled with light water. The radioactivity in that area causes the flickering pixels. The camera was working at its limit.)

6. Some Performance Data

In 2004 the FRM II received the permission to start the nuclear commissioning.
The regular operation began in 2005.
Meanwhile almost all places for experiments at neutron beam tubes are taken and about 2/3 of these experiments use cold neutrons.

Year	Reactor cycles (52 or 60d)	Hours of operation of CNS (with liquified D_2)	Outage caused by CNS Reason
2005	3 á 52d	3963 h	0
2006	5 á 52d	6448 h	0
2007	4,5 á 52d	5945 h	1 : Defective oil level-sensor at He-compressor
2008	4 á 60d	6415 h	0
2009	4 á 60d	6179 h	0
2010	3,5 á 60d	4550 h	1: crashed bearing at He-compressor motor; 2: suspicious noises: stop of operation and check of He-compressor motor
2011	1 á 60d	1731 h	0
2012	3,5 á 60d	5414 h	2 times: SCRAM by power grid blackout (thunderstorms)
2013	4 á 60d	5924 h	1: broken fan wheel at He-compressor motor
2014	2 á 60d	2989 h	0
2015	2,5 á 60d	4535 h	1: Frequency converter fault of He-compr.mot. 2: He-compressor motor: interwinding fault 3: He-compressor motor: interwinding fault

Table 1: Operating times of CNS at FRM II

Table 1 shows the number of reactor periods per year along with the hours of yearly CNS operation. Additionally it indicates the unplanned downs caused be the CNS.

This table leads to a surprising observation:
Neither the CNS itself nor the deuterium-storages or the He-refrigerator caused the faults, but the conventional electric motor with its frequency converter.

Besides some weak points in engineering, i.e. the hydride storages, the manufacturer provided us with a reliable device to work with. Nevertheless it needs an open eye and proper maintenance to keep the equipment in good condition.

Meanwhile we also realised and implemented various improvements regarding the He-cleaning within the cooling circuit, heating and cooling of the hydride storages in order to accelerate their loading/unloading and the electrical stability of the He-compressor. The changes to the gas cleaning and hydride storages turned already out to be successful whereas the changes to the power supply of the compressor cannot finally be evaluated before additional experience will be available.

7. Conclusion

The CNS at FRM II runs from an overall point of view very reliable.
Most of the unexpected downs were caused by the He-compressor electric: motor, frequency converter, power grid faults.

The metal hydride storages are still components to learn about.
We use these storages not the way it was intended originally.
The construction of hydride storages for low pressures has to be quite different from those known for instance from automotive applications.
It was a long way to learn how to use them anyway. Now we know what we want, but we are still busy to learn how to get it. There is still a lot of engineering to do.

The used deuterium is contaminated with tritium. The disposal of this deuterium could become an increasing problem because of changing political and legal circumstances.

Operational Experience on the Cold Neutron Source at the OPAL Reactor

Ashok Sah, Paul Walsh, Anthony Tobin, Simon Breslin, Ravi Abraham, Weijian Lu*

Australian Nuclear Science and Technology Organisation, Lucas Heights, NSW 2234, Australia

* Corresponding author: wjl@ansto.gov.au

ABSTRACT

The Cold Neutron Source (CNS) at ANSTO's OPAL Reactor has operated with near perfect reliability since July 2013, supplying cold neutrons to neutron scattering instruments for more than 300 days a year. This recent highly productive and reliable operational period had come after a 16-month rectification program in 2012-2013 that resolved major compressor and turbine faults in the helium cryogenic system. It has been underpinned by a more focussed approach by a team of analysts, engineers and technicians, fully supported by senior management in the organisation. Drawn from the in-house knowledge base developed over the major-fault-affected years, the CNS team has been able to quickly identify the root cause of minor faults and process anomalies and carry out rectification in a timely fashion to ensure the CNS and reactor's availability. A comprehensive Reliability Centred Maintenance (RCM) strategy has been developed, based on Failure Mode, Effects and Criticality Analysis (FMECA) methodology as part of the asset management program of the entire reactor facility. In this paper, we will share our experience with some examples of operational events. A successful project of upgrading the helium cryogenic system's PLC in 2014 will also be discussed.

1. Introduction

The OPAL Reactor at Australia Nuclear Science and Technology Organisation (ANSTO) is a 20 MW multi-purpose research reactor that carries out a range of commercial and scientific activities as its mission [1, 2]. The OPAL Reactor targets 300 days of operation per year and has reached the target in 2015. Each reactor cycle is about 30 days on average. The Cold Neutron Source (CNS) at the OPAL Reactor employs 20 L of liquid deuterium as the cold moderator, which is cooled and maintained in single phase by a helium refrigerator in a vertical thermosiphon [3]. The CNS is required to have availability over 98% in each reactor cycle to supply cold neutrons to seven neutron scattering instruments [4, 5], all of which are open to international users and have been substantially over-subscribed.

The OPAL CNS was fully commissioned in 2006. Between 2006 and 2012, it operated with availability less than 80% due to some major faults in the helium refrigerator [6, 7]. Those major faults were fully rectified in 2013 [8]. Since then, the CNS operated with near 100% availability. The rectification efforts in 2012/2013 included not only modifications to the helium refrigeration plant, but also re-structuring of the CNS team. The CNS team currently consists of a specialist adviser, two system engineers, a technician and a trainer who also specialises in PLC code. This is a "virtual" team because those individuals come from different units of the Reactor Operation organisation and report to their respective line managers. The CNS team meets regularly and discusses all the CNS issues.

The functioning of such a team is fully supported by senior management. A direct line from the specialist adviser to the Division General Manager and the Reactor Manager ensures matters of critical importance are communicated promptly. Although the CNS operated with near perfect availability since 2013, it has not been without faults. This team structure has ensured the best consensus decision was made on those occasions. Furthermore, the CNS team is now best positioned to do some strategic thinking on the important issue of ensuring long term health and reliability of the CNS.

2. Reliability Centred Maintenance

The Reliability Centred Maintenance (RCM) methodology was first developed for the Aviation industry in the early 1960s, in order to increase the reliability and availability of the aircraft fleets of the US armed forces and later, the commercial airline operators. In the 1980s it became more universally recognised in other industries utilising complex systems as a methodology to ensure that performance to company targets were maximised through the structured analysis of components functions and their previous failure history. The methodology has, in recent times, been implemented by several major global manufacturers and operators as the industry has moved to more structured Reliability, Availability, Maintainability and Safety (RAMS) programs.

The OPAL Reactor organisation adopts the RCM methodology and provides a performance focus to the operation and maintenance aspects of the CNS. CNS maintenance strategy is derived from its ability to efficiently maintain the system, to maximise availability and reliability. OPAL has incorporated the RCM methodology into its Failure Modes Effects and Criticality Analysis (FMECA), in order to underpin this requirement for the CNS.

The RCM process acknowledges the basic premises that each component of the CNS exists to provide a function. While the user or operator may not notice the failure of a component, they will notice that the CNS no longer performs the function that it was intended to undertake. Consequently, RCM attempts to plan maintenance not around the failure of any one component, but around the loss of the functionality required by the CNS. In order to achieve this, seven key questions are asked of the CNS asset in order to determine the best maintenance strategy.

1. What are the functions and associated performance standards of the CNS operation in its present operating context?
2. In what ways can it fail to fulfil its functions?
3. What causes each functional failure?
4. What happens when each failure occurs?
5. In what way does each failure matter?
6. What can be done to predict or prevent each failure?
7. What should be done if a suitable pro-active task cannot found?

The answers to the first four questions were developed by FMECA, assessing what are considered to be the critical components from reliability-prediction's perspective. Having identified all of the failure modes and consequences in the FMECA stage, the CNS team conducts cross-functional reviews of the suggested maintenance activities. As such, engineering, maintenance and operation are actively engaged in a joint workshop environment to answer the final three questions in the RCM process and complete the associated FMECA worksheets. This RCM / FMECA approach has proven successful in ensuring that all parties understand the constraints that apply to the design and maintenance of the CNS and its sub-systems.

In the final development stage of the RCM / FMECA process, failure modes are analysed to determine whether the failure is evident, will affect safety, will impact the conformance to environmental

regulations, or is operational or non-operational. Maintenance tasks such as condition monitoring, scheduled service or scheduled replacement are specified, depending on the operational effect of the failure.

OPAL has undertaken an extensive RCM analysis on the CNS and used this information to continuously develop a more efficient and effective maintenance strategy. OPAL has ensured that Original Equipment Manufacturers (OEM) provide extensive maintenance information on their equipment.

There are six main failure patterns usually exhibited by components in complex system like CNS, known as bathtub, end of life, wear out, wear in, random failures and infantile failure. A critical aspect of the maintenance development process is an understanding that not all components fail in the same manner. As such the maintenance strategy for each component of the CNS has been assessed on the basis of its failure pattern. As well as the failure pattern, another critical element of determining the best maintenance strategy for a component is an understanding of the key indicators to failure. If an impending failure is identifiable, it is possible to monitor such indications and conduct preventative maintenance prior to failure. This approach has been extensively taken at OPAL.

3. Helium Refrigerator PLC Upgrade

The original PLC in the helium refrigerator was a Eurotherm PC3000. Process control and logic was programmed using the GRAFCET structure. Although the PC3000 was highly reliable as well as flexible during ten years of operation, Eurotherm ceased production of this controller and we could no longer find a reliable supplier for a spare. To ensure long term guarantee of supply, we decided to replace the PC3000 with a new PLC that was more widely used in the industry thus more easily accessible in the market. The package of work was contracted to an experienced local firm who specialised in supplying PLC hardware and software for industrial process control. The contractor offered Siemens S7 as the replacement PLC. The primary goal of the contract was to make a carbon-copy translation of the process program from PC3000 to S7. It was understood that although the contractor would be responsible for installing the new PLC and translating the software, the actual process tests would be conducted under the guidance and control of the ANSTO CNS team.

To minimise the plant's downtime, as much software-checking as possible was done prior to installation. The actual reactor shutdown time requested for commissioning was three weeks. The commissioning program consisted of multiple stages of verification of instrumentation I/O's (all field sensors), active control (e.g. all valves, heater controllers and a variable frequency drive), all normal process and maintenance subroutines and select fault subroutines. In the OPAL CNS, liquid deuterium is sub-cooled. The operation of the helium refrigerator is therefore by and large detached from the liquid deuterium condition. This allowed the refrigerator to be almost fully tested before it was necessary to raise the reactor to power for the full-heat-load test and the sudden-loss-of-heat-load test (i.e. reactor trip). The fault subroutines were selected to cover turbine protection functions and several known abnormal process conditions such as power outage to the compressors and power outage to the PLC itself. Some fault conditions were physically produced such as power outage. Others, such as low turbine bearing pressure or high turbine brake temperature, were produced by digitally forcing the sensor input to the PLC to avoid any mechanical risk to the turbine. However the protective action as a result of the fault signal was allowed to be executed in full by the new program for verification.

Another critical job during commissioning was to tune all the PID controllers in the program, including the compressor high/low (or discharge/suction) pressure controller, the turbine speed controller, the turbine bearing temperature controller, the turbine outlet pressure controller and the CNS helium inlet temperature controller. The controllers' configurations were initially copied from PC3000. Each of them was closely monitored during the tests and re-tuned when necessary (e.g. when excessive overshoots or oscillations took place). As a result, at the completion of commissioning, the new

program was more than just a carbon copy of the old program in terms of functionality and equipment safety protection, but an improved version that could handle some transient conditions more smoothly.

The PLC upgrade project was completed on budget and on time. It signified the transfer of PLC ownership from the refrigerator OEM to ANSTO. The easy accessibility of a local firm has brought tangible benefits that should not be under-estimated. At the present time, there are continuing efforts by the CNS team in collaboration with the contractor to fix legacy bugs and make improvements in process control logic.

4. Helium Purity Control

It is conventional wisdom within the industry that gas purity control is paramount in a cryogenic plant such as an expansion-turbine-based helium refrigerator like ours. High levels of impurity can be a major cause of process faults such as heat exchanger degradation or even clogging and turbine failure. In the history of the OPAL CNS helium refrigerator, impurities such as nitrogen (from two different sources which are air and the purging gas), alcohol (from compressor oil degradation by oxidation or shear by the screws) and hydrogen (from compressor oil degradation) have been identified. We know with certainty that excessive amount of nitrogen can cause mechanical damage to the turbine wheel during warm-up when nitrogen “ice balls” can be blown off from the cold box adsorber. We also know with certainty that alcohol, so volatile that it cannot be trapped by the charcoal adsorber in the compressor oil removal skid, finds its way into the cold end of the turbine bearing and condenses there, causing shaft seizure. Hydrogen, due to its low condensation temperature, poses no direct risk to the refrigerator as a free gas, but it is a strong indicator of failures elsewhere in the process. The experience of failures, mostly due to OEM design faults which have all been identified and rectified, nevertheless has taught us a lot about the plant’s functionality and characteristics.

The purity of helium in the refrigerator used to be monitored by taking a sample and have it analysed in an external gas chromatograph instrument. In June 2015, there was an incident where 3000 ppm of nitrogen was measured to be in the helium due to inadequate purging after charcoal replacement in the oil removal skid. Our helium refrigerator does not have a secondary purifier such as a liquid-nitrogen pre-cooler. The only way to cool the helium is to run the turbine. One option was to completely replace the helium inventory by fresh gas bottles, which would be costly and time consuming. Under time constraint to start the refrigerator to allow the reactor to return to power on schedule, we decided to use the refrigerator to “clean itself” instead, that is, to run the turbine down to about 80 K knowing that nitrogen does not pose a direct risk to the turbine as long as the refrigerator is not permitted to warm up (to avoid the nitrogen ice ball scenario), stop the turbine shortly after 80 K is reached and perform a regeneration of the cold box charcoal adsorber to remove the nitrogen. The method took about 10 hours and worked. Nitrogen level dropped from 3000 ppm to 100 ppm, which was acceptable for *entering* normal operation. Note the actual nitrogen level during normal operation is below the detection level of 1 ppm. The reason for the residue 100 ppm after the *quick regeneration* was that not the entire buffer volume of the helium inventory had the time to circulate through the cold box.

Since the incident, a flame-spectroscopy-based multi-channel gas detector has been installed in the helium refrigerator which can give us in-situ reading of nitrogen and moisture levels in real time. We have used it to verify the self-cleaning method with a small amount of residue nitrogen in the system. The data consistently shows that nitrogen is in fact completely adsorbed in our cold box charcoal at 150 K, as shown in Figure 1, much higher than the 77 K condensation temperature. The self-cleaning method based on quick regeneration is a very effective way to purify the helium after maintenance should an abnormal high level of nitrogen be present. It poses no risk to the turbine.

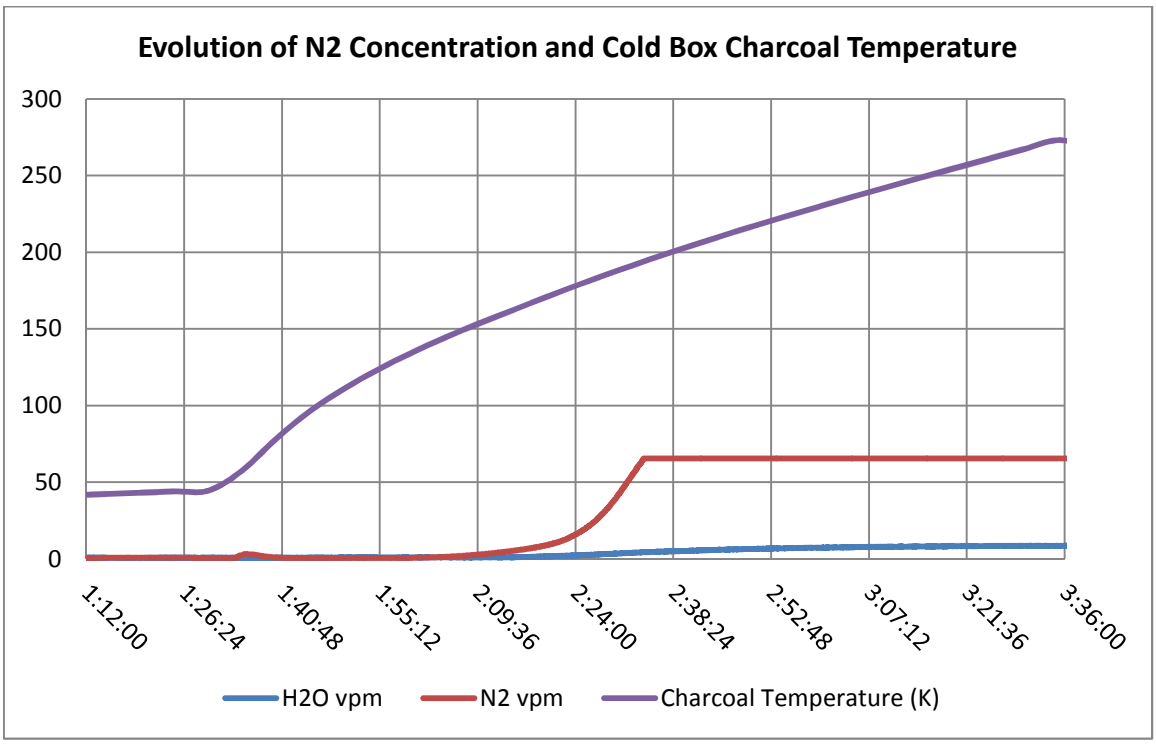

Figure 1 Nitrogen adsorption by charcoal to below 1 ppm level at temperature < 150 K. The instrument reading saturates at 60 ppm.

5. Helium Refrigerator Heater Controller Fault

In a study published in 2009 [9], accurate measurements of the OPAL CNS nuclear heat load as well as the non-nuclear heat load were reported. The nuclear heat load is around 3.6 kW at reactor full power of 20 MW. The same study also demonstrated that liquid deuterium was in sub-cooled state in the thermosiphon. The non-nuclear heat load was measured to be 388 W at the time, but we have observed an increase since then, most likely due to neutron activation of the structural material in the CNS over many years of full power reactor operation. By thermal balance during routine operation, the total CNS heat load is estimated to be about 4.5 kW at present. In April 2015, two years after the full rectification of the helium refrigerator, we ran a series of tests to determine its maxmum cryogenic power. By forcing the turbine to work at full speed, the helium temperature set point was incrementally lowered until both compressors were running at full speed. At that point, the refrigerator was “full”. The measured cryogenic power was 6.2 kW at 19 K, 37% (1.7 kW) more than the CNS requirement. The margin is quite substantial.

Because liquid deuterium is sub-cooled in the OPAL CNS, the helium inlet temperature to the CNS is fixed and does not depend on deuterium pressure. The helium inlet temperature’s set point is ensured by an in-line heater which has a fast response. Heat load change typically happens during liquefaction, evaporation or reactor power change. Normally the helium inlet temperature can be maintained well within 0.1 K of the set point of 20.5 K. In February 2014, it was observed that the helium inlet temperature was unusually noisy with an oscillation magnitude over 0.5 K. It was also observed that the CNS heat balance was off by more than 1 kW, although we were confident that deuterium remained in liquid state. It was first thought that the CNS thermosiphon might have reversed its flow direction which caused heat transfer instability. That possibility was ruled out after we raised the helium temperature to boil off some liquid deuterium and re-liquefied, only to see the temperature instability remained. It was also speculated that there might be a leak in the turbine by-pass valve (6290-PV-698 in Figure 2), letting through a warm flow of helium which brought extra heat load. Calculations revealed that for this scenario to happen the turbine by-pass valve would have to

be wide open, which was extremely unlikely given that the very same valve seemed to be controlling certain transients as accurately and precisely as expected.

The root cause of the problem was finally determined to be a faulty heater controller. Measurements of its output voltage and current revealed that there was a discrepancy of 1 kW between the controller's indication and the actual power output to the heating elements. By replacing the heater controller, the fault was then completely cleared. Even though this fault was due to unpredictable electronic failure, it is important to note that the margin in the refrigerator cryogenic power was adequate to overcome the extra heat load from the faulty heater controller and keep the CNS functional, i.e. keep deuterium in liquid state, and save the neutron instrument scientists from disappointment for a whole reactor cycle.

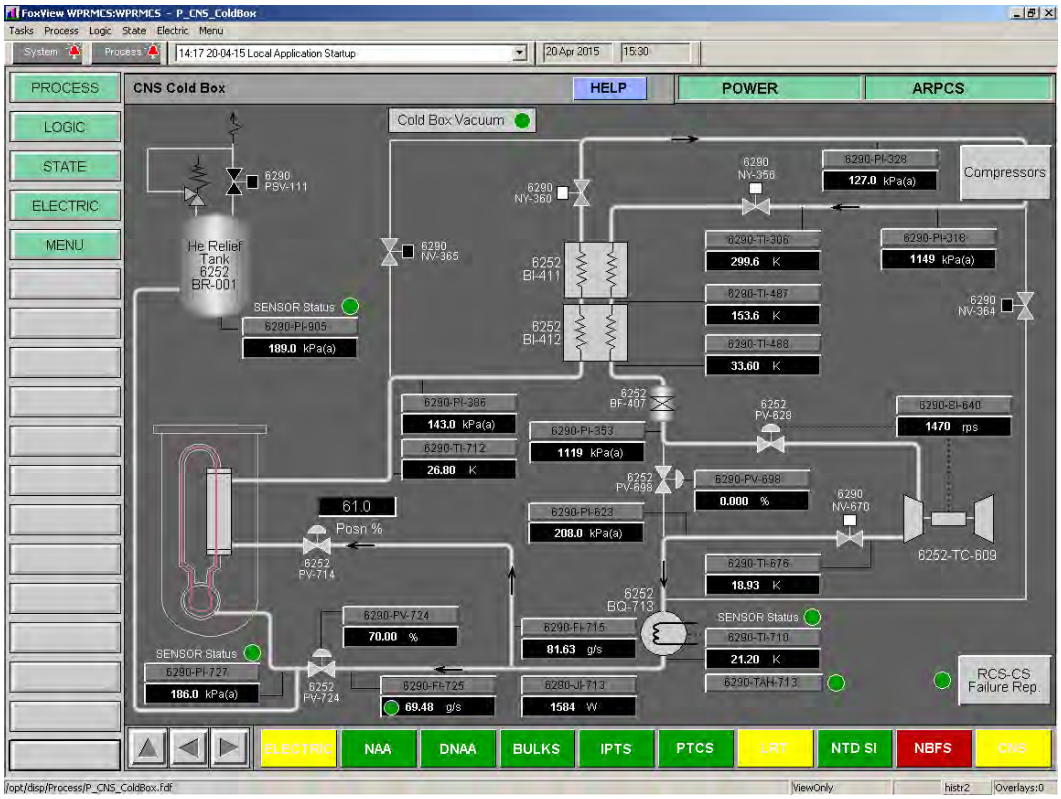

Figure 2 A simplied cold box P&ID showing the helium refrigerator operating at full capacity of 6.2 kW

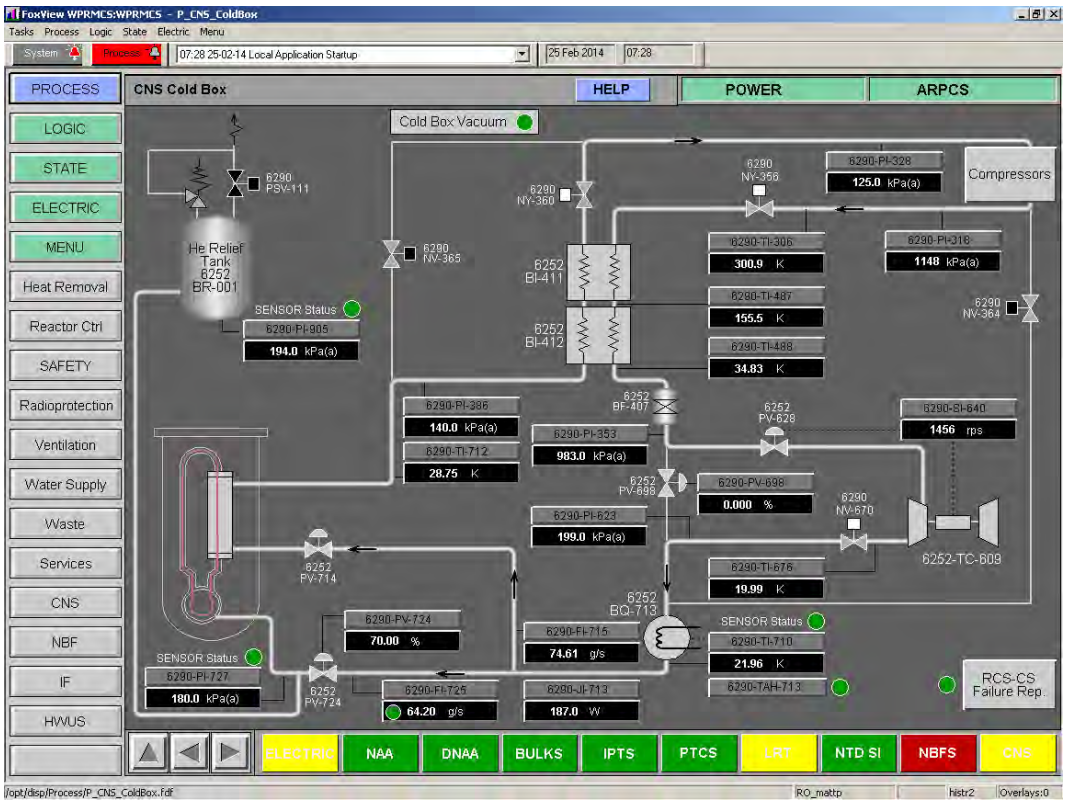

Figure 3 A simplified cold box P&ID showing the status of the helium refrigerator when the heater controller output (6290-JI-713) was off by over 1 kW

6. Summary

The OPAL CNS has operated reliably since its major rectification in 2013. In order to build up the knowledge base and ensure the best informed decisions are made during routine operation and maintenance, we have taken a team approach in the OPAL organisation. We described a RCM based maintenance strategy that has been adopted. Some of the operational events were discussed, including minor faults and their rectification.

7. References

[1] Miller, R. and Abbate, P.M., "Australia's New High Performance Research Reactor," IGORR 9 Conference Proceedings, Sydney, Australia, 2003.

[2] Hergenreder, D.F., Lecot, C.A., Lovotti, O.P., Villarino, E.A., Braoudakis G., Ersez, T., "Contract performance demonstration tests in the OPAL," IAEA-CN-156, Proceedings of the International Conference on Research Reactor: Safe Management and Effective Utilization, Sydney, 2007, IAEA, Vienna (2008)

[3] Bonneton, M., Lovotti, O., Mityukhlyaev, V. and Thiering, R., "Installation and testing of the OPAL (ANSTO) Cold Neutron Source," IGORR 10 Conference Proceedings, Gaithersburg, DC, USA, 2005.

[4] S. J. Kennedy, "Construction of the Neutron Beam Facility at Australia's OPAL Research Reactor," Physica B 385-386, 949-954 (2006)

[5] Close, F., Constantine P., Kennedy, S. J. and Robinson, R. A., "The Neutron Beam Expansion Program at the Bragg Institute", Journal of Physics: Conference Series 528 (2014) 012026

[6] Lu, W. and Thiering, R., “Using a Multi-Parameter Monitoring Methodology to Predict Failures in the Cryogenic Plant of the Cold Neutron Source at Australia’s OPAL Reactor,” Advances in Cryogenic Engineering, AIP Conf. Proc. 1434, 1537-1542 (2012)
[7] Thiering, R., Taylor, D. and Lu, W., “Helium Refrigerator Maintenance and Reliability at the OPAL Cold Neutron Source,” Advances in Cryogenic Engineering, AIP Conf. Proc. 1434, 1543-1550 (2012)
[8] Lu, W., “Rectification of the OPAL Cold Neutron Source Cryogenic System,” IGORR 15 Conference Proceedings, Daejeon, South Korea, 2013
[9] Lu, W. and Thiering, R., “The OPAL Cold Neutron Source Heat Load Measurements,” IGORR 12 Conference Proceedings, Beijing, China, 2009

COLD NEUTRON SOURCES
AN INTERNATIONAL TECHNICAL MEETING IN AIX-EN-PROVENCE

L. MANIFACIER, J. KOUBBI, M. BOYARD
AREVA TA, CS 50497, 13593 Aix-en-Provence Cedex 3, France
Corresponding author: laurent.manifacier@areva.com

ABSTRACT

Cold Neutron Sources (CNS) have an on growing importance in the world of Research Reactors. Standing at the crossroads between core design, reflector layout, neutronic performances and overall facility safety, these unique devices need to be thought, designed and optimized together with the whole reactor in which they are to be placed. Such a challenging global approach is the ideal work for a reactor design engineering company.

Novelty arising from discussion and confronting different views and designs, AREVA TA decided to organise an international technical meeting on CNSs in March 2015. This modest two day event took place in France, in two AREVA TA sites: Aix en Provence and the JHR construction site in Cadarache. The aim of this meeting was to gather world experts in the field of these highly specific experimental devices. Participants came from Australia (ANSTO), France (CEA, ORPHEE, AREVA TA), Germany (FRM2, BER2), Hungary (BRR), Netherlands (HOR), RSA (NECSA) and USA (NIST).

The first day was dedicated to CNS technical presentations from operator participants and was followed by a working session on the topic: design, operating and end-using vs moderator type and cell geometry. Discussed disciplines covered neutronics, hydraulics, safety, I&C and mechanics. The second day also saw the opportunity to discover the future JHR, under construction in Cadarache. After a detailed presentation of the project (technical, organisational aspects and ins & outs were presented), a visit of the construction site took place, from basement to roof. Guests were to discover all the features of the reactor and see the correspondence between the size of the building with the performances of such a small core. Even though the JHR has no CNS, issues related to reactor design vs specific experimental devices remain identical.

This extremely fruitful meeting was concluded by a free discussion out of which arouse the importance of having such a kind of recurrent event for the CNS community. The interest might not be restricted just to operators and designers and could reach circles far beyond: material providers, physicists, research centres.
Regular meetings could be organized, not necessarily in a dedicated event, but jointly during existing conferences in the form of a dedicated session, in order to continue valuable sharing around CNSs. This kind of event could be supported by IAEA.

The paper presents:
- How essential CNSs are for science,
- Material and mechanical issues,
- The importance of the cryogenic system,
- Diversity of CNS designs,
- The main conclusions of this first meeting

1. The meeting itself

In the spring of 2015, AREVA TA took the opportunity to organise a technical meeting on Cold Neutron Sources (CNS). Operators around the world having kindly opened their facility in the past for us to visit, we decided to give everyone the chance, in return, to meet together

and discuss the many topics in and around CNS in Aix-en-Provence (France), headquarters of AREVA TA. What initially started as a friendly and unofficial event ended up by word of mouth as a small 2 day international meeting.
Twelve external scientists gathered from CNS and reactor operators as well as institutions: ORPHEE (CEA Saclay, France), FRM-II (TUM Münich, Germany), BER-II (HZB Berlin, Germany), HOR (TU Delft, Netherlands), OPAL (ANSTO Lucas Heights, Australia), NBSR (NIST Gaithersburg, USA), BRR (Budapest, Hungary) and also CEA, CERCA and NECSA (South Africa) members.
Of all the facilities represented, six operate at least one CNS: ORPHEE, FRM-II, BER-II, OPAL, NBSR and BRR.

During the first day, participants had the chance to freely present their facility, its operation and all related issues. Extremely interesting discussions followed between everyone, confronting ideas and existing solutions to identified problems. Topics spread from neutronics to mechanics, also including hydraulics, I&C and safety.
The second day enabled to carry on with the discussions. In the morning, advantage was taken of the nearby JHR construction site in Cadarache to organize a visit.

Photo with all the participants, on the first day.

2. Cold Neutron Sources in science

One of the many uses of a research reactor is the production of neutrons through neutron beams. The complementary nature of neutron and X-ray scattering on materials characterisation has led from the beginning to developing intense neutron beams along with all the associated highly sophisticated instruments. Throughout the years, combined needs of more intense and higher wavelengths have grown. Indeed, neutrons being used for diffraction, their wavelength should be compatible with the lattice parameters of the sample which is studied in the experiment.

X-Rays are today available in extremely intense beams and have a rather wide wavelength range from infrared down to fractions of an Angström. Neutrons, on the other hand, can be slowed down to energies of approximately 1 meV, which corresponds to cryogenic temperatures (10-20K) or wavelengths between 5 and 10 Å or greater. In this range, scientists can then study molecules, polymers, proteins or other large organic structures. There is a worldwide strong demand for such experiments among the community.

neutrons:		Hot	Thermal	Cold	Ultra cold
Energies	(meV)	500	100	10	0.04	1E-04
Wavelengths	Å	0.4	0.9	3	50	900
Temperature	K	5800	1160	110	0.5	0.001

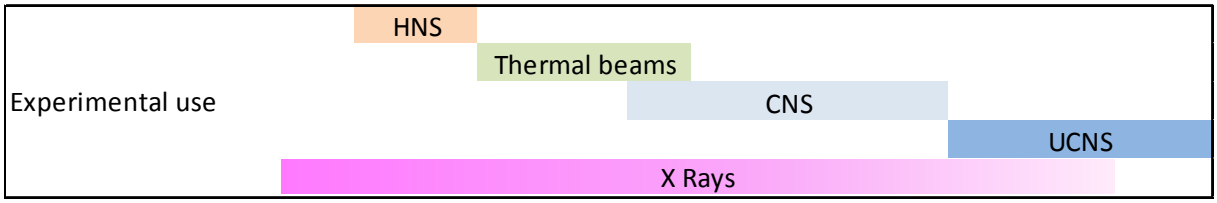

Table 1: Usual neutron energy scale versus experimental devices:
from Hot Neutron Sources to Ultra-Cold Neutron Sources (X-rays are given for comparison)

Furthermore, neutrons provide a much better contrast between elements, particularly light atoms which are dominant in organic molecules and can be difficult to distinguish in X-Ray diffraction experiments involving other elements, especially heavy ones since X-Ray diffraction is proportional to the number of electrons. Neutrons interact with the nucleus, thus, cross sections are very different, making neutron diffraction such a unique technique and so preciously complementary.
In addition to their use in the study of molecules and large structures, cold neutrons are also useful in finding traces of absorbing elements (boron, cadmium, lithium etc.) since their capture rises with the neutron wavelength. Finally, they are also used for specific industrial applications in neutronography, some artefacts being only visible with cold neutrons.
In the end, in facilities equipped with a CNS, it turns out that a large part of experiments are conducted on cold neutron beams (and even sometimes the majority), thus making cold neutrons a key source of information in modern science, as well as making the facility greatly attractive.

Slowing down the neutrons exiting from a core reactor (or a spallation source: ESS, ISIS, PSI…) is achieved by the use of a proper moderator cell, filled with a moderating medium which is cooled down to cryogenic temperatures. The cell is located in the core reflector and this points out the complexity of the proper design of the core+reflector+CNS system. Each of these three components has to be properly chosen, designed and jointly optimised along with the other two, depending on the end-use of the neutron beams.

The aim of this paper, however, is not to present detailed description of CNS, which is abundantly found elsewhere in literature. Instead, we address specific issues that arouse from the discussions that took place during this first technical meeting. We do not discuss either the topic of spallation sources, even though some subjects mentioned in this overview are also applicable to these facilities.

3. Design issues

Due to significant diversity in reactor designs because of the different applications they are optimised for, cold neutron sources, when present, also show very distinct features. However, in the past 40 years, two main families of CNS have emerged: liquid hydrogen or deuterium moderators, even though some exotic moderators are encountered, like ice or methane. In this section, we discuss issues related to the design (and consequently the operation) of these highly sophisticated devices. We will at first address the complexity of materials and mechanics before focusing on cryogenics and moderator-related issues.

Figure 1 below summarizes the complexity of a CNS design approach. An initial need expressed by experimentalists' requirements has consequences on the operation of the

global facility as well as implications in all the fields commonly encountered in nuclear engineering: neutronics, thermal hydraulics, mechanics, cryogenics, I&C, operation, manufacturing, safety and overall core+reflector design.

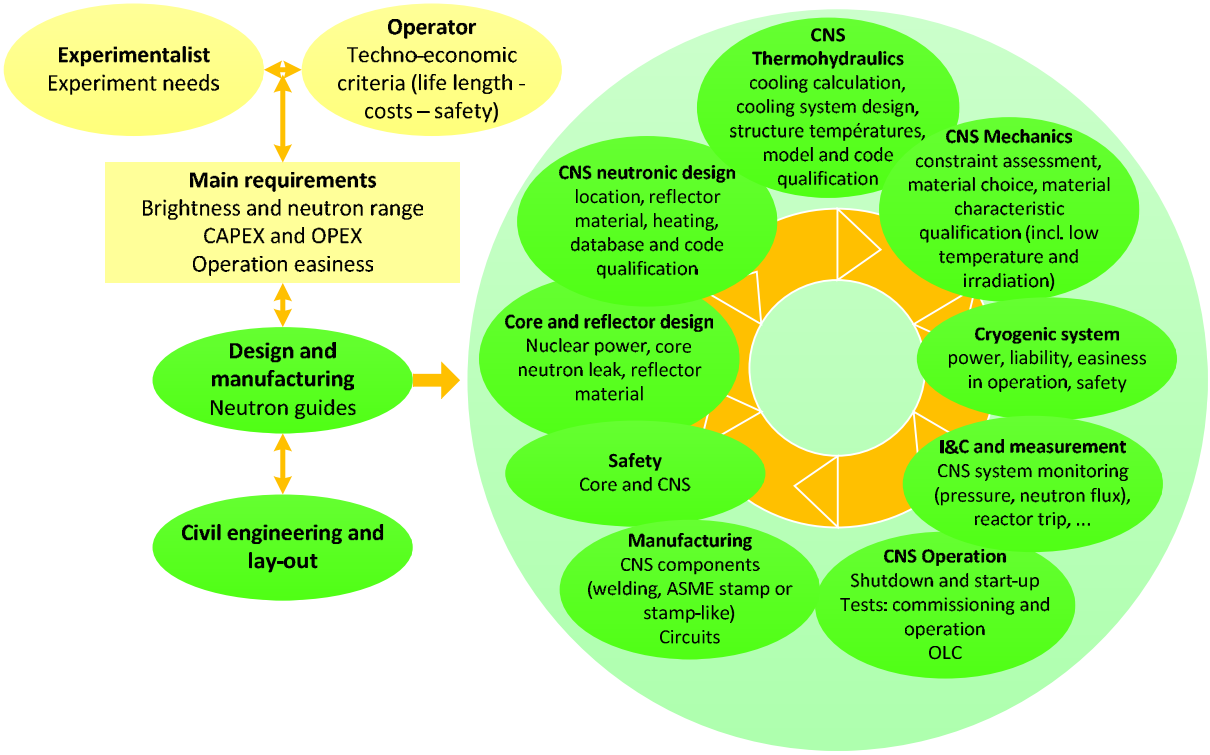

Figure 1: Key technical domains involved in the design phase of a CNS

3.1 Materials and mechanics

Evidently, the main engineering challenges related to a Cold Neutron Source originate from the presence of a cryogenic vessel being placed inside a reactor tank and thus under constant and generally intense nuclear flux (neutron and gamma) with the corresponding extreme heating. This technological paradox is the source of all the difficulties encountered, which spread into all the concerned disciplines: mechanics, hydraulics, neutronics and I&C.

From an overall point of view, the efficiency of the complete system lays inside the following key-points (from experimenter to the core):

- Optimization of the transmission rate of the cold neutrons between the experiments and the CNS,
- High efficiency of the cell shape and chosen moderator to feed the neutron guide,
- Best compromise between high neutron flux and low material heating for the location,
- Qualification of the structural material to allow an extended lifetime,
- Stability of the CNS neutron feeding by the core,
- Easiness of use in operation of the cryogenic system (including the exchanger).

The first step is to consider neutronic performances of the source. Low neutron absorption materials are necessary if great fluxes are expected. This narrows the choices down to zircalloy or aluminium. The latter is cheaper and many different aluminium grades are possible: AlMg3, AlMg5, AG3NET, Al-6061.

But neutronics do not drive the whole design process. The second step is to restrict nuclear heating in the CNS. A thermal insulation is necessary of course and achieved through void and/or helium flow separating several (generally two or three) containment vessels. The main source of heating comes from gamma radiation and neutron activation. If aluminium walls are

selected, whatever the grade, the most significant contribution of activation comes from Al-28 decay. Generated silicon then induces weakening of the material and its general ageing.

The main idea remains that, the smaller the source, the less it heats. This, however, is more easily proclaimed than done for some deuterium sources require huge volumes to be efficient. Then, a way to minimize the heat load within the vessel is to use light elements which are preferred in order to minimise gamma absorption. This, again, generally leads to aluminium. Attempts to use magnesium in the past have proven to be very difficult.

Pressure considerations might then require certain grades, wall thicknesses or even certain specific materials. For instance, the first ORPHEE moderator cells were made of stainless steel. Neutron absorption was high but so was the resistance of the cells. Heating was then not an issue and the reactor could operate with the sources in stand-by mode, which is no longer the case today with the new aluminium cells. That characteristic isn't an issue for ORPHEE: the production of cold neutron beam is the main objective.

Manufacturing is crucial. Among all the issues in this topic, welding is also strongly present. A rule of thumb is that it is preferable to minimize welded zones, particularly those under neutron flux. The first NBSR moderator cell (made in a Mg alloy) revealed very challenging welding techniques. Engineers later switched to Al-6061-T6. It turns out that welding and junctions are generally more critical than the component itself. As a consequence, many designs around the world now try to reach for welding-free cells, as much as technologically achievable.

Many operators and designers point out the difficulty to obtain materials for the CNS and moderator cell walls which are compliant with technical requirements related to the composition of alloys and impurities contents. Composition discrepancies seem common and a particular attention should be given to this issue through traceability and Quality Assurance.

Choice of a given material is then not necessarily due to neutronic requirements, but is the result of a compromise between neutronic efficiency (transparency), heat load reduction, reactor operability and ageing.
Behaviour of the components under extreme nuclear flux and the evolution of their mechanical characteristics on a wide range of temperature is an essential topic (fatigue, allowable stress and fast fracture). Much effort is undertaken within the community to enhance the design lifetime of the CNS components, particularly the moderator cell. Samples are constantly irradiated within the reactors in order to monitor ageing and innovative approaches are explored to properly assess the lifetime of the source [1].

Although a wide variety of aluminium grades is found in moderator cells, 6061-T6 generally seems to have the longer lifetimes [2] [3].

3.2 Cryogenics and moderators

Cryogenic issues are related to the moderator which is selected for the CNS, and to the corresponding volume which has to be cooled, leading to powerful compressors, due to the low cryogenic system efficiency, especially in the case of D_2. In this sense, hydrogen and deuterium cryogenic systems behave quite differently.

Liquid H_2 cells usually require less than 1 litre because of the combined effect of its high scattering power and also its significant absorption which increases with wavelength. D_2, on the other hand, because of its weaker scattering power, requires high volumes greater than 10l and up to 30l or more. D_2 can be preferred because of its very low absorption which enables to reach high cold fluxes in the great wavelengths range.
In both cases, CNS moderator flow is often vertical, which enables the use of a thermosiphon. This solution is relatively easy to set up, but in some cases, such as a vertical

source, or supercritical hydrogen for instance, pumping the moderator through the circuit is necessary in order to maintain a liquid phase in the moderator chamber.

Inside the cell, various thermodynamic states of the moderator are found. It can either be fully liquid, boiling or supercritical. The reasons can be technological, safety or performance related. For instance, the choice of the OPAL single phase liquid deuterium cell [4] is driven by neutron performances.

D_2 and H_2 both have close boiling points. H_2 however, at 20K, is slightly lower than D_2 at 23K. As a result, the spectrum of a hydrogen moderator should be colder than that of deuterium. But because of a smaller cell volume, outcoming cold flux from a hydrogen cell can actually be slightly warmer than that of deuterium. In addition, absorption is much higher in hydrogen, resulting in brighter fluxes obtained from a deuterium CNS, despite the 20 ratio on volume levels.

Another issue related to moderators is contamination. On a general aspect, one of the main difficulties with the use of deuterium, other than its operational cost, is the production of tritium under neutron flux. However, depending on the design of the source, the storage tanks and the moderator volume, this might not be determining. But attention should be given and eventual decontamination procedures should be considered.
A different and specific contamination issue is found at the source in Münich at FRM-II. It uses a rather unique feature of metal-hydride storage to empty the circuits of the moderator by adsorption. The D_2 moderator is “contaminated” by approximately 5% in hydrogen which could actually enhance the neutron flux [3].

CNSs, just like many other devices, are designed for running constantly. The material qualification is a key point and two main issues are considered in qualification reports: material characteristics at cryogenic temperature with neutron irradiation and effects of temperature cycling between this state and ambient temperature.

Another key-point is the easiness of operation for cryogenic system. The whole cryogenic circuit is usually managed with huge helium compressors that cool the moderator through heat exchangers. These compressors are not specific to RR but the whole system is fitted for the nuclear safety requirements of the CNS (for example ORPHEE reactor has a spare of 20 sec of HP He in case of electrical failure).

4. Technical main conclusions of the meeting

This first of a kind meeting triggered many valuable discussions among specialists worldwide. Main conclusions are summarised in Table 1 below. The variety of CNSs and reactor designs represented though the participants was sufficient to draw a few rules of thumb.

The first question a future operator asks himself is the end-use of the reactor. There are obviously no general rules for this since the process is driven by specific needs and constraints. However, it is noticeable that the trend nowadays in the research reactor field seems to be the multipurpose facility since no one can foresee what the future will be like in the next 40 years. It can be considered wiser to design a flexible reactor which can then easily adapt to evolutions in the scientific community needs as well as in the industrial and medical fields. Today, silicon doping and molybdenum production may be a valuable source of income that sustain otherwise “open source” reactors for on-growing academic research demands. But what will the future be like?

The second main question is related to core-CNS interaction. There is no question about the core-CNS system which has to be jointly designed and optimized to reach the higher fluxes

possible. But despite neutronic interactions, one of the most fundamental steps in the safety analysis of the global facility is to exclude the CNS from the reactor and consider it auxiliary equipment. This dramatically facilitates the safety demonstration. CNS containment walls, should they withstand an internal hydrogen explosion, enables one to consider the CNS as being outside the reactor.
Hydrogen explosion is not the only issue. Generally speaking, the CNS should ideally not have an effect on the reactor core physics, especially for safety reasons. However, this is extremely difficult to achieve, if not impossible, and for the vast majority of reactors, a CNS shutdown usually triggers a reactor scram through I&C. Even though one can easily demonstrate that a CNS failure resulting in emptying the hydrogen (or D_2) and filling the cell in water (light or heavy) has a minimal impact on reactivity, there remains the heating issues. Massive use of aluminium alloys (whatever the grade) usually requires that the reactor stops because the CNS cannot withstand the heat load without the intrinsic moderator cooling.

Some reactors do however have the possibility to operate with the CNS not operating. This was the case in mark-I ORPHEE, with its stainless steel sources that could withstand nuclear heating. It is the case today in OPAL and BRR with its “stand-by mode”. The source had to be slightly pushed away from the thermal flux optimum in the D_2O tank, though, in order to decrease the intense heat load. This compromise enables the reactor to remain functional and in particular guarantees joint production of doped silicon and molybdenum not to be impeded. This feature proved to be highly valuable during the first years of operation for OPAL [4] [5].
The question of a stand-by mode or not is irrelevant in the case of a reactor that would be dedicated to neutron beams since there would evidently be no point in burning fuel for no reason if the CNS is not operating (ORPHEE, FRM-II, NBSR, BER-II)

Once end-use and consequently moderator type and materials involved are chosen, proper geometry of the moderator cell should then be defined. When in a wide D_2O tank, neutron population is rather disconnected from the core. This results in an isotropic and Maxwellian population. Consequently, global performances of the source are little affected by geometry optimisation of the moderator cell. The latter usually ends up in a basic cylinder (or sphere) and the dominant parameter is the volume (and thickness in the case of hydrogen rather than deuterium). A remarkable exception though is the NBSR source, with its spherical hydrogen cell [2]. It should be noted however that in the case of deuterium cells, cold flux is often enhanced with the proper use of a displacer which illuminates the beam noses with cold neutrons originating from the centre of the moderator cell.
On the other hand, in a light water reactor, whether there is a presence of a dedicated beryllium reflector or not (which, of course, is preferable), neutron flux gradients are high and the geometry of the source is of first importance. Several studies on the subject can be found and lead to optimum focusing shapes which can be very different depending on the core and reflector layout (ellipse [6], hemispheres [6] [7] or cone [7], as well as extensive studies in [8]).

In the case of a refurbishing, however, adding a CNS in an existing reactor (such as in BRR) only leaves the choice of a hydrogen moderator, due to size issues.

The main conclusion is that there is no perfect CNS. Depending on the end-use, reactor history, budget and space available from the operator, very different but satisfying solutions will arise from the design phase in the end. It should be noted however that D_2, despite being probably the best option for a new-build, severely constraints the design since it requires a heavy water tank to give the best cold fluxes. Any future modification of the core layout or of experimental devices is thus compromised. H_2 may, on the other hand, have slightly weaker fluxes but provides the best flexibility.

Table 2 below summarises the main design conclusion through a matrix of the major characteristics for CNS performances. Conclusions are limited though to either hydrogen or

deuterium moderators, which happen to be dominant in the world of research reactors. It should however be noted that there can be considerable overlap in the performances and operation between H_2 and D_2 sources causing inevitable exceptions to the otherwise general conclusions compiled in the matrix below.

	Two dominant moderator types	
	H_2	**D_2**
Advantages	- Cheaper - Cheaper installation - Low moderator volume - Overall installation is more compact - Gain factors greater than 1 in the 1-2Å range (thermal experiments remain possible on a cold neutron beam)	- High gain factors above 4Å - Easier to optimise the geometry
Disadvantages	- Complex ortho-para ratio issues - Lower gain factors than D_2 above 4Å - Complex geometry optimisation	- Expensive - High moderator volume - High heat load and consequently powerful heat exchangers - Tritium production - consequent need for a heavy water tank severely impedes future flexibility in the core layout
Related requirements	- Performances are enhanced with a dedicated reflector, typically beryllium (BER2) or heavy water (ORPHEE) - In the absence of a D_2O reflector, the CNS should be as close to the core as possible, near the thermal flux peak (which causes heating issues)	- A heavy water tank seems compulsory, considering the size of the moderator cell, in order to get the best cold flux possible - Important volumes are necessary outside the pool for deuterium tanks
Ideal for	- Refurbishments and adding a CNS within an existing reactor with little available space - Facilities wishing to remain flexible	New builds (only for a beam-dedicated facility)
End-use	Hybrid experiments requiring a broad range of wavelengths from 1 to 10 Å	Experiments exclusively within the cold range: $\lambda > 4$ Å

Table 2: Matrix of main characteristics for CNS performances

The scientists present during this workshop wish that such a concept of a dedicated CNS related meeting goes on. We are currently studying a way to perpetuate this means of exchanging among specialists in a non-formal way.

5. Acknowledgements

The authors wish to thank all the participants in this most interesting meeting, particularly Mr G. Campioni, T. Grosz, L. Moloko, A. Menelle, D. Päthe, L. Rosta, W. Lu, S. Welzel, R. Williams and A. Winkelman, and also those who couldn't make it at the last minute (ILL, ESS).

They are also grateful to Mr C. Pascal, J. Estrade and G. Bignan for advice, sometimes help and, always, valuable discussions.

6. References

[1] J. Kohler, B. Lecarpentier, “Design life evaluation of a Cold Neutron Source – a methodological approach complementing ASME classical rules with RCC-MRx design rules”, IGORR-RRFM 2016, Berlin, *to be published*

[2] R. Williams, M. Rowe, “Developments in neutron beam devices and an advanced cold source for the NIST research reactor”, Physica B 311 (2002) 117–122

[3] K. Gobrecht, “Status report on the cold neutron source of the Garching neutron research facility FRM-II”, IGORR 1999, Bariloche

[4] S. Kennedy, “Construction of the neutron beam facility at Australia’s OPAL research reactor”, Physica B 385–386 (2006) 949–954

[5] W. Lu, “Rectification of the OPAL cold neutron source cryogenic system”, IGORR 2013, Daejeon

[6] P. Schreiner, W. Knop, D. Coors, D. Vanvor, “New moderator chamber of the FRG1 Cold Neutron Source for the increase of cold neutron flux”, RRFM-IGORR 2007 transactions session II, p 10-14

[7] L. Manifacier, J. Koubbi, B. Beauvais, D. Grémeaux, M. Boyard, “Creativity in Cold Neutron Sources Design”, IGORR 2014, Bariloche

[8] J. A. Bucholz, “Physics Analyses in the Design of the HFIR Cold Neutron Source”, pp 29-40, BgNS Transactions, Vol 5, No. 1, July 2000

The ORNL High Flux Isotope Reactor Supercritical Hydrogen Cold Source

D. L. SELBY
Oak Ridge National Laboratory
708 Andover Blvd. Knoxville, Tennessee 37934

C. A. CHRISTIAN
Oak Ridge National Laboratory
PO Box 2008 Oak Ridge, Tennessee 37831-6255

ABSTRACT

This paper will address the design and operational history of the ORNL High Flux Isotope Reactor (HFIR) cold source. The HFIR cold source began operation in the spring of 2007 after a multi-year design and testing program. This cold source has successfully operated for 54 reactor cycles without a single reactor scram associated with it. The HFIR cold source is a supercritical hydrogen system that operates with a temperature of around 20 to 22 degrees Kelvin. The aluminum moderator vessel has a reentrant cavity that provides about a 30% increase in the cold neutrons delivered to experiments. The cold source is located in the HB-4 beam tube and the cold neutrons produced by the cold moderator feed 4 cold neutron guides. A modular design concept is used for the cold source system to enhance maintenance and component replacement capability. Subjects covered by the paper will include the design issues and justifications for certain design decisions, safety requirements and features, neutronics performance, and operational history.

1. Introduction

In the late eighties and early nineties a project was in place at Oak Ridge National Laboratory (ORNL) to replace the HFIR with a new high power research reactor designated as the Advanced Neutron Source. In 1994, the US Department of Energy made the decision to cancel this project and replace it with a neutron spallation source facility project. However, even in canceling the project, DOE understood the need to maintain a state-of-the-art continuous neutron source capability at ORNL. Thus, in parallel with the design and construction of the Spallation Neutron Source, a project was initiated in 1995 to upgrade the existing High Flux Isotope Reactor (HFIR) at ORNL. This project included increasing the size of the neutron beam tubes, construction of new neutron instruments, and the design and installation of a cold neutron moderator for neutron spectrum modification.

2. HFIR Cold Neutron Source Feasibility Study

The addition of the cold neutron source to the HFIR reactor was considered the most critical aspect of the upgrades and in 1995 a feasibility study was performed to determine the most practical concept for a cold source in the HFIR reactor.

The use of beryllium as the reflector in the HFIR presented some special problems in designing a cold source. Beryllium is such a good reflector that the neutron flux drops rapidly with distance from the reactor core. This meant that the cold moderator needed to be

close to the reactor core boundary and its extension into the reflector region needed to be minimized. This eliminated the use of deuterium as a moderator material. In addition, the high heat flux associated with being close to the core eliminated the thermal siphon option. It was determined that hydrogen was the most practical moderator material. In addition, for safety considerations a decision was made to go with a supercritical rather than liquid hydrogen state. This hydrogen state was much more stable under accident conditions than the liquid state and the higher pressure involved with the supercritical condition had very little impact on the design. This is the concept that was carried forward for the detailed design.

3. HFIR Cold Source Design Requirements

There were three major design requirements for the cold source concept:

a) The purpose of the HFIR cold source is to increase the available neutron flux delivered to instruments at wavelengths from 4 to 12 Å. Optimization is to be based on the neutron brightness (/s/cm2/steradian/Å). The gain factor on brightness, as measured on HB-4, for these wavelengths should be comparable to existing hydrogen cold sources.

b) The HFIR cold neutron source facility will be designed such that there is low probability (less than 1×10^{-6}/yr best estimate frequency) that neither the reactor nor the public will be endangered by accidents that occur within the cold source or as a result of the cold source facility interacting with the reactor or its safety systems.

c) The design and operation of the HFIR cold source will follow National Aeronautics and Space Administration (NASA) guidelines and the US Department of Labor Occupational Safety & Health Administration (OSHA) standard 29 CFR 1910.103 for the use of hydrogen in either a gas or liquid sate.

These four requirements established the basis for the final design and fabrication of the cold moderator system.

4. HFIR Cold Source Characteristics

The HFIR cold source system is composed of a number of modules. The moderator vessel located just outside the core is the container for the low temperature supercritical hydrogen in the high flux field. The purpose of the remaining modules is to keep the hydrogen in the moderator vessel cold and to provide safety functions. These two aspects of the cold source system are described below.

4.1. The moderator vessel requires design considerations that take into account the harsh environment of its location close to the reactor core and the need to maximize the cold neutron flux delivered to the experiments. An extensive evaluation of materials was performed to determine the material for the moderator vessel. The detailed evaluations are reported in an ORNL report[1]. The results indicated that aluminum 6061-T6 was the best material for the new HFIR cold source. It had good strength for the supercritical hydrogen pressure, it had good thermal properties, the material was relatively transparent to neutrons, and it had no significant irradiation

creep. Figure 1 is a picture of the HFIR cold source moderator vessel. It is fabricated in two pieces from solid aluminum and then welded together with one electron beam weld. Two identical moderator vessels were fabricated using the same process. One of the vessels was then pressurized and tested to failure. The vessel failed at slightly over 5 times the normal system pressure and failed in the base material rather than the weld material. Radiographs of the weld were also performed to confirm that there were no significant flaws. Another potential issue with the moderator vessel was the irradiation damage to the vessel at cold temperature, due to the intense neutron and gamma fields close to the reactor core. It was determined that by returning the moderator vessel to room temperature between each reactor cycle, close to 95% of the damage could be annealed. Finally, the vessel was designed with a cavity which gave about a 30% increase in cold neutron flux delivered down the beam tube.

Figure 1: HFIR Cold Source Moderator Vessel

4.2. The remaining modules consisted of pumps, transfer lines, heat exchanger, refrigerator and other support systems that were optimized for reliability.

a) The refrigerator system uses expansion engines rather than a turbine system for increased flexibility.

b) There are 4 expansion engines when only 3 are required and a transfer to the spare engine can be performed while the system is in operation if a problem with an engine is discovered.

c) There is a similar spare compressor for the same reason.

d) The hydrogen lines and components have a vacuum boundary and a helium cover gas boundary which is monitored for leaks at all times.

e) The refrigeration system is designed to provide the cooling power needed to remove approximately 3 kw of heating and maintain the hydrogen in the moderator vessel at a temperature of approximately 20 K.

5. HFIR Cold Source Neutronic Performance

The purpose of the cold moderator system is to shift the spectrum delivered to the neutron instruments to longer wavelengths. As previously mentioned, the cold source was designed to optimize the neutrons with wavelength between 4 and 12 angstrom. This optimization was accomplished by varying the thickness of the supercritical hydrogen shell in the moderator vessel. The gain factors (ratio of neutron flux with cold source divided by the flux without cold source as determined by MCNP modeling) is shown in Figure 2 for several cold sources including the HFIR cold source design.

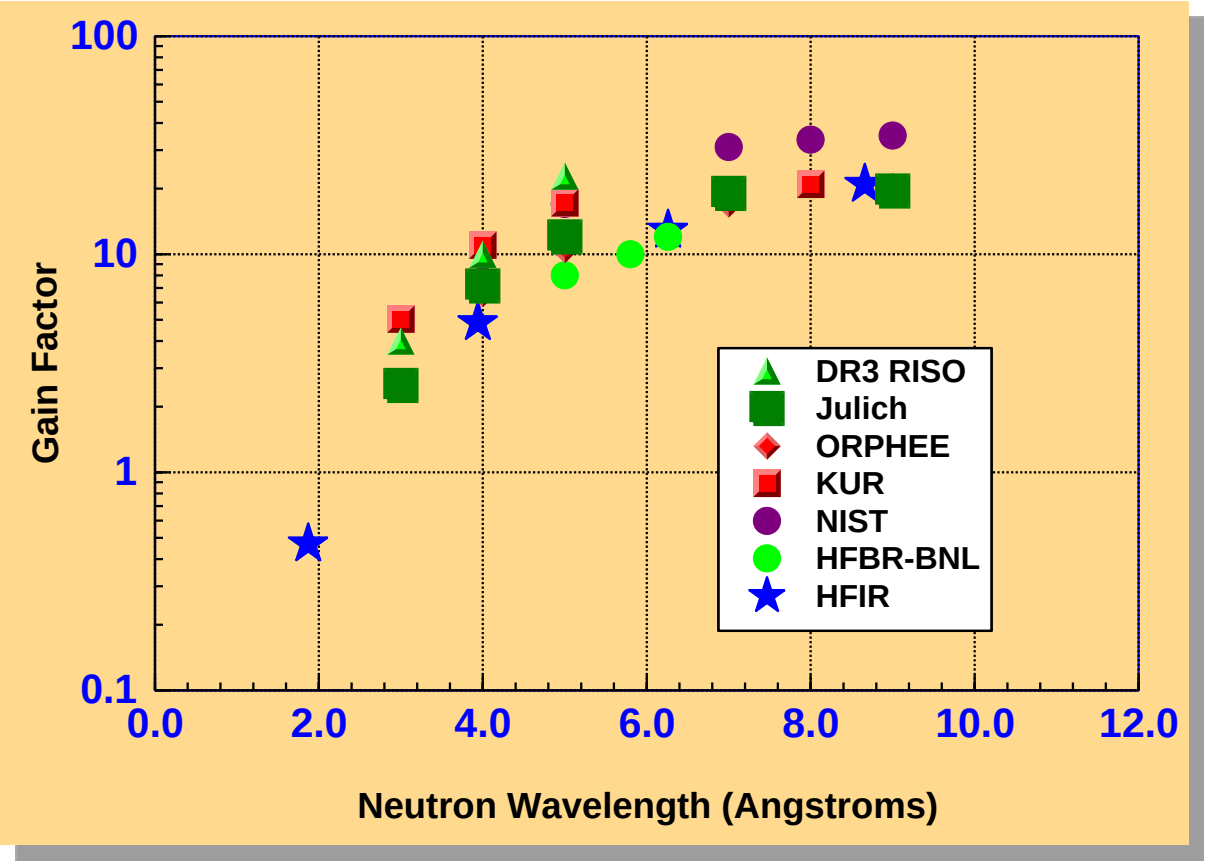

Figure 2: Gain Factors As a Function of Wavelength for Different Cold Souces

As seen from Figure 2, the gain factors for the HFIR cold source is around 20 for the 8 to 10 angstrom range. The small size of the HFIR cold source limited by the size of the beam tube keeps the gain factor in the low range, as compared to other facilities. Time of flight measurements performed at the end of the beam tube after the cold source was installed indicated that the MCNP model underpredicted the source brightness and gain factors by about 30%. A comparison of the measured and MCNP model calculation of the neutron source brightness is shown in Figure 3.

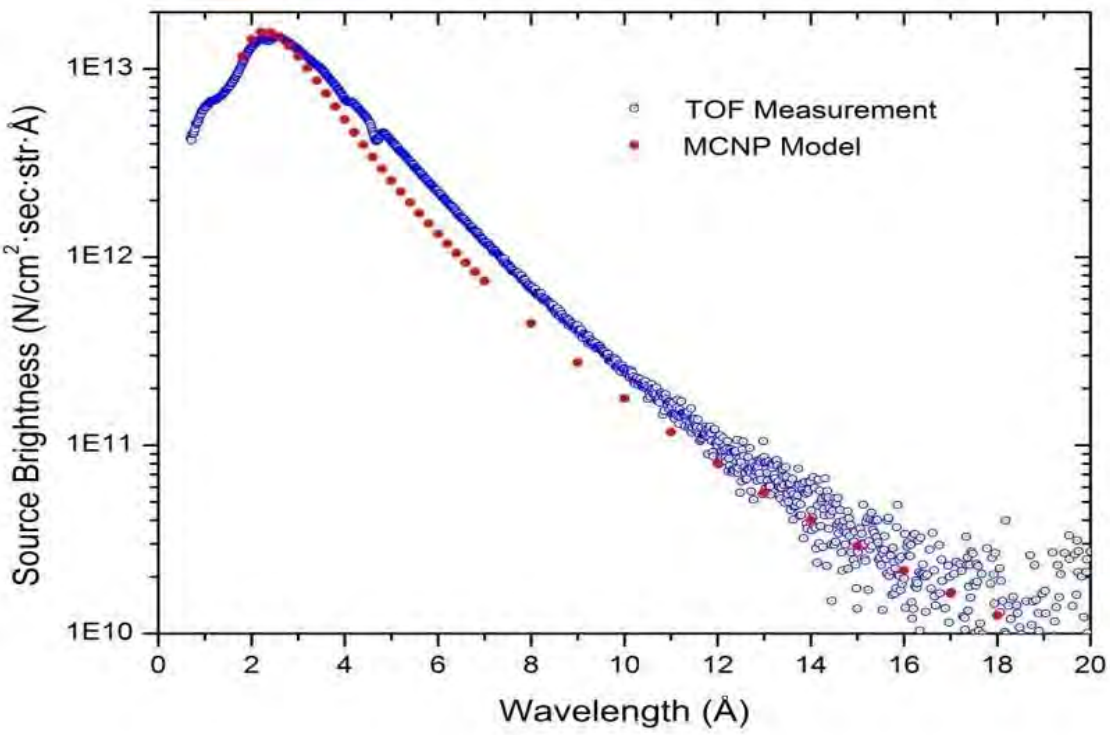

Figure 3: Comparison of the Measured and Calculated Neutron Brightness[2]

6. Cold Source Safety Considerations

The general safety policy for the HFIR cold source was that safety must be considered in all aspects of the life cycle of the cold source. The primary hazard associated with the HFIR cold source was the inadvertent production of a flammable or detonable mixture, leading to a fire or detonation. An analysis of the industrial, research, and aerospace accidents from the use of hydrogen were evaluated; as part of the cold source project. The results indicated that following factors were the primary causes leading to hydrogen accidents:

a) Mechanical failure of a containment vessel, piping, auxiliary components
b) Reaction of the hydrogen with a contaminant such as air
c) Failure of a safety device to operate properly
d) Operational error

The safety objective of the cold source project was to design the cold source system in such a manner that the probability of occurrence of these types of events be made as low as practical. In addition, a detailed hazard analysis and accident analysis was performed for those component failures that could not be excluded from the design basis probability space. This analysis included multi-failures within the probability space and thus this was more than just a single failure analysis.

It should be noted that there is always a potential hazard when hydrogen is present. However, design considerations can be made to greatly decrease the probability of such

events. The risks associated with these hazards can be minimized by having limited controlled access to areas where hydrogen leaks are most likely, by minimizing the potential for a leak (e.g. multiple barriers), and by early detection of a hydrogen leak, if it were to occur. All three of these hazard reduction techniques have been incorporated into the HFIR cold source design.

7. HFIR Cold Source Operations

The HFIR cold source system has operated since the spring of 2007 with very little impact on the reactor operation. There have been no reactor scrams or loss of scheduled reactor operating time tied to the cold source. Thus the system has experienced high reliability. One of the reasons for this high availability is the preventive maintenance and inspection program that has been in place. Every outage we perform inspections on the expansion engines including cleaning, checking of belt tension and alignment, and measurement of the main shaft/fly wheel coupling torque and the bold torque. At 5000 hours or approximately one year of operation, there are a number of preventative maintenance activies:

a) We perform a complete rebuild of the expansion engines which includes replacing the bearings and all belts.

b) The pistons are removed and baked in a vacuum oven and then the O-rings and felts are replaced.

c) The intake and exhaust valves are rebuilt.

d) We have four spare engines that are rebuilt and ready to install, during this scheduled preventive maintenance activity.

Every two years the filters and coalescers in the helium compressors are replaced. During the same time period, the hydrogen circulator is replaced with a rebuilt spare.

It should be noted that the original cold source had only one vacuum station in the beam room and one in the hydrogen equipment area. We have changed this and added a second station in both locations to eliminate single point failures and to increase the run time before we need to do preventive maintenance on the stations. When we only had one at each location the decision was made to rebuild each station annually. Now that we have spare stations and upgraded components, the rebuild is now performed on a four year schedule with inspections every two years.

Over the nearly 9 years of operation, we have had one significant release of hydrogen which occurred outside at a fill station. Surprisingly the hydrogen did not ignite which contrary to our safety assumption that a release of any significance would ignite because of the very low energy level required for ignition.

Other equipment failures over the years include some power supplies, the hydrogen compressor, as well as bearing and starter motor failures on the refrigerator expansion engines.

Finally, over the years the decision was made to increase the operating temperature from 20 K to 23-25 K. This provided increased stability in the operation of the system with very little impact on the cold source neutronic performance.

8. Summary of the HFIR Cold Source and Future Plans

In summary, the HFIR cold source has had nine years of successful operation with little impact on reactor operation and no reactor scrams tied to the cold source. As a minimum, for the future, plans are to replace the moderator vessel and all other cold source components within the beam tube (including the beam tube) when the beryllium reflector is replaced in about 6 years. Work on this activity is expected to begin this year with the intention of fabricating the components well before they are needed so that they can serve as spare parts, if needed in the short term. It should also be noted that a second cold source for HFIR which would potentially double the number of user instruments is still a possibility.

9. References

[1]J. L. Ken Farrell, Materials Selection for the HFIR Cold Neutron Source, ORNL/TM-99-208, August 2001.

[2]J. L. Robertson, Measurement of the Neutron Spectrum of the HB-4 Cold Source at the High Flux Isotope Reactor at Oak Ridge National Laboratory, Reactor Dosimetry State of the Art 2008, Proceedings of the 13th Internationl Symposium on Reactor Dosimetry, Editors: Vim Voorbraak, Luigi Debarberis, Pierre D'Hondt and Jan Wageman, World Scientific, Singapore, ISBN 981-4271- 10-1

STATUS OF THE LIQUID DEUTERIUM COLD NEUTRON SOURCE FOR THE NIST RESEARCH REACTOR

R.E. WILLIAMS, M. MIDDLETON, P. KOPETKA, J.M. ROWE and P.C. BRAND
NIST Center for Neutron Research
100 Bureau Drive, Mail Stop 6101
Gaithersburg, MD 20899 USA

ABSTRACT

The NBSR is a 20 MW research reactor operated by the NIST Center for Neutron Research (NCNR) as a neutron source providing beams of thermal and cold neutrons for research in materials science, fundamental physics and nuclear chemistry. A large, 55 cm diameter beam port was included in the design for the installation of a cold neutron source, and the NCNR has been steadily improving its cold neutron facilities for more than 25 years. Monte Carlo simulations have shown that a liquid deuterium (LD_2) source will provide an average gain of 1.5 between 4 Å and 9 Å with respect to the existing liquid hydrogen cold source, and a gain of 2 at the longest wavelengths. The conceptual design for the LD_2 source will be presented along with the current status of the project.

To achieve these gains, a large volume (35 litres) of LD_2 is required. The expected nuclear heat load in this moderator and vessel is 4 kW. A new, 7 kW helium refrigerator is being installed to provide the necessary cooling capacity. It is expected that acceptance testing will be completed later this year. The source will operate as a naturally circulating thermosiphon, very similar to the horizontal cold source in the high flux reactor at the Institut Laue-Langevin in Grenoble. A condenser will be mounted on the reactor face about 2 m above the source providing the gravitational head to supply the source with LD_2. The system will always be open to a 16 m^3 ballast tank to store the deuterium at 4 – 5 bar when the refrigerator is not operating; this provides a passively safe response to a refrigerator trip. It is expected the source will operate at 23 K, the boiling point of LD_2 at 1 bar. All components will be surrounded by a blanket of helium to prevent the possibility of creating a mixture of deuterium and air. A preliminary design for the cryostat assembly, consisting of the moderator chamber, vacuum jacket, helium containment and a heavy water cooling water jacket, has been completed. The ballast tank and a pair of condensers (one spare) have been procured. Initial bids for the cryostat assembly were way over budget, however, and NCNR is seeking additional funding. It is now expected that installation of the LD_2 source will be delayed until at least 2021.

Funding for the refrigerator and the cold source upgrade has been granted by the National Nuclear Security Administration of the Department of Energy as a mitigation strategy to offset the anticipated 10% loss in neutron flux when the NBSR is converted to low-enriched uranium (LEU) fuel.

1. Introduction

The NBSR is a 20 MW research reactor operated by the National Institute of Standards and Technology (NIST) Center for Neutron Research (NCNR), primarily for neutron scattering instruments to study the properties of materials, but also for research in fundamental physics and nuclear chemistry. With completion of the first guide hall in 1990, and the installation of

the first liquid hydrogen (LH_2) cold neutron source (CNS) in 1995, the NCNR has become one of the world's premier centres for cold neutron research. In 2012, the NCNR completed another major expansion project with the addition of a new guide hall and 5 new guides. As shown in Figure 1, about 20 instruments will be using cold neutrons when the entire suite of instrumentation is completed. Along with the expansion of the facility, the cold neutron sources have been improved and expanded. The original LH_2 source was replaced with the Advanced LH_2 Cold Source (Unit 2) in 2002, doubling the flux of cold neutrons to all the instruments [1,2]. In addition, a second LH_2 source was installed in the thermal neutron beam port, BT-9, solely for the Multi-Axis Crystal Spectrometer (MACS II) which was relocated to BT-9 to accommodate the 5 new guides [3]. The only way to improve upon the highly optimized Unit 2 is to replace it with a large volume, liquid deuterium (LD_2) source.

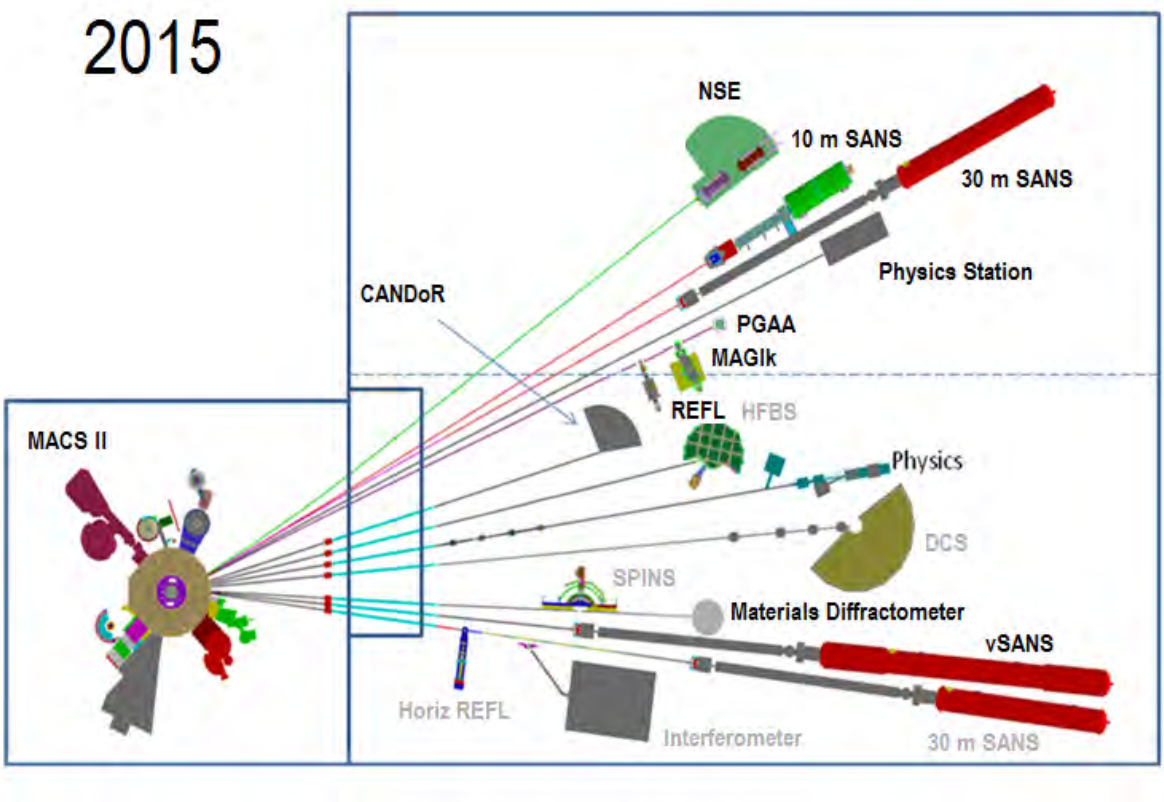

Figure 1. Anticipated layout of cold neutron instruments at the NCNR upon completion of the Expansion Project funded by the national American Competitiveness Initiative. The new guide hall, above the dotted line, nearly doubles the area of the cold neutron facility, and increases the number of guides from 7 to 12.

2. LD_2 Cold Source Performance Calculations

Monte Carlo Simulations using MCNP were performed to optimize the gain in cold neutron brightness of the LD_2 with respect to Unit 2, and to calculate the anticipated heat load of the LD_2 source. Reference 1 provides a description of the methods used for these calculations, which will be briefly summarized here. The NCNR maintains a very detailed MCNP model of the NBSR that has been used for relicensing of the reactor, LEU conversion studies, and cold source development. A powerful variance reduction tool of MCNP, the DXTRAN feature, is used to achieve good statistics for rare events, namely the tallies of cold neutron

currents into narrow energy and cosine bins at the entrance of neutron guides, far from the source. (At every collision, a pseudo particle is generated and directed toward the DXTRAN sphere [4] around the tally surface. The probability that it will be scattered and transported to the DXTRAN sphere is calculated, and its weight adjusted accordingly. Inside the sphere, pseudo particles are transported normally, contributing to the tallies. If the neutron actually reaches the sphere it is killed so as not to be counted twice.)

A two-step process is used, starting with the generation of a surface source file around the region of the cold source from a criticality calculation. The surface source provides the starting particles for subsequent calculations to study the effects of ***minor changes*** in the source geometry, LD_2 density, ortho-para fraction, etc. using the DXTRAN sphere. A minor change is one that does not affect the NBSR power distribution; major changes require separate surface source calculations. Recently, MCNP6.1 was released [4], so the gain and heat load calculations have been repeated using the latest version of the code and the ENDF/B-VII.1 cross section data [5] released with it.

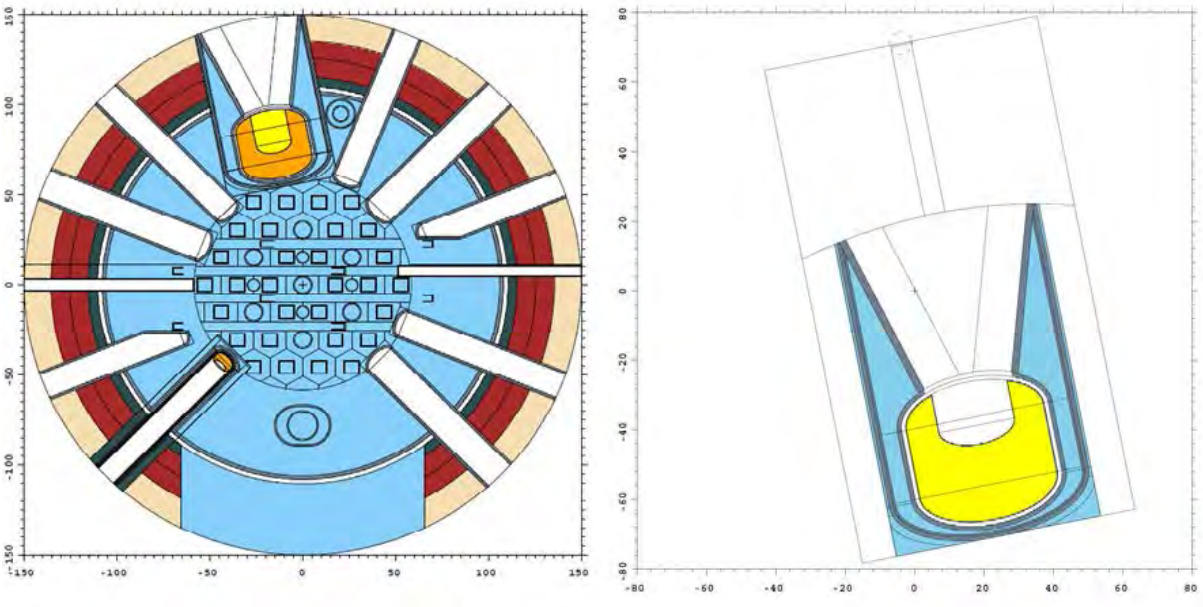

Figure 2. MCNP models of the NBSR core (left) and the LD_2 cold source (right). The surface source generated from the core calculation provides the starting neutrons for the CNS performance calculations (note the DXTRAN sphere, top right in the center).

2.1 Gain Calculations

The gain is defined as the ratio of the brightness of the LD_2 source to that of Unit 2 at a particular wavelength, or in general, for neutrons with wavelengths greater than 4 Å. The brightness in units of n/cm^2-s-ster-Å is obtained from the current tallies across a surface within the DXTRAN sphere. Simulations of cold neutron production and transport depend heavily on the scattering kernels (cross sections for low energy neutrons, or S(α,β) data) of the cold moderators. Kernels for ortho and para liquid hydrogen and liquid deuterium, and for liquid and solid methane are provided in the nuclear data released by the Los Alamos National Laboratory (LANL) with MCNP. The recently released ENDF/B-VII.1 data include continuous energy and angle S(α,β) data [6] and MCNP6.1 has improved interpolation

routines that eliminate non-physical peaks and valleys in the current tallies with small energy and cosine bins.

Because the LANL kernels for LD_2 were evaluated at 19 K but its boiling point at 100 kPa is 23.6 K, an alternate set of S(α,β) data was obtained [7]. These data, prepared by the Institut fur Kernenergetik und Energiesysteme (IKE), University of Stuttgart, included kernels for ortho and para LH_2 and LD_2 at a few temperatures. Introducing the IKE kernels for LH_2, however, resulted in quite a difference (15% to 35%) from the Unit 2 performance with the LANL kernels. The IKE ortho-LH_2 kernel has lower final energies than the LANL kernel for the same initial energies, so an "IKE model" of Unit 2 has substantially higher brightness than a "LANL model", all other parameters being equal. The actual ortho-LH_2 content of Unit 2 is unknown, but the shape of the spectrum indicates that the scattering is dominated by ortho, which has a much higher cross section.

The modeling discrepancy led to a series of time of flight measurements on one of the new guides, NG-Bu, to benchmark the MCNP model of Unit 2 against the brightness inferred from the measurements. The LH_2 average void fraction for the Unit 2 benchmark came directly from data collected from the original mockup tests conducted at NIST Boulder [8], but there is considerable uncertainty regarding the spatial distribution of the voids. Using the ENDF/B-VII.1 kernels from LANL, the best agreement with the measurements was obtained with an ortho-LH_2 content of 17%, considerably lower than previously thought [9]. Using the brightness measurements, the gains for LD_2 are calculated with respect to the best possible TOF data available. The IKE kernels were used only to obtain an average correction factor to account for the flux decrease at 23.6 K versus 19 K, a factor of 0.88 over the range of 4 Å to 10 Å.

There are many other factors that affect the performance of the LD_2 source, such as the size of the vessel, the depth and diameter of the reentrant hole, the void fraction, and the ortho/para fraction. In general, the performance increases with the volume of the source, but not as fast as the heat load increases. We chose a 400 mm diameter, 400 mm long cylinder with a 220 mm diameter reentrant hole, 180 mm deep (see Figure 2). The resulting volume is 35 liters, nearly twice the size of any other LD_2 source. Our choice was a vessel that is as big as possible, but allowing ample room for the required vacuum, helium containment and heavy water cooling jackets. The cryostat assembly will be installed horizontally into a 550 mm ID thimble. The diameter of the reentrant hole was fixed by the requirement that the neutron guides extending ± 16° from the axis be fully illuminated to at least 10 Å. The reentrant hole depth represents a compromise between the highest gains at the longest wavelengths (~2) versus the losses at 2.5 Å (0.6). Most of the instruments in the guide hall use wavelengths between 4 Å and 9 Å.

To estimate the void fraction, the Kazimi/Chen Correlation for pool boiling [10] was compared to measured values for three cold source thermal-hydraulic mockups, the LH_2 mockup at NIST-Boulder [8], the R-134 mockup of the small BT-9 source at NIST [3], and the mockup of the horizontal LD_2 source [11] in the High Flux Reactor at the Institut Laue-Langevin (ILL) in Grenoble. In all cases the correlation over-estimates the void fraction by about a factor of two. These mockups (and all three cold sources) vary significantly from pool boiling in that (1) there is no liquid/vapor interface (they are all flooded with a two phase mixture return flow) and (2) there is a continuous supply of subcooled liquid from the condenser. Therefore, for these situations the correlation is multiplied by 0.5:

$$\alpha' = 0.5 * \{ 1 + [0.645*(V_s/V_\infty)^{0.35}] / \ln (1 - 0.645*(V_s/V_\infty)^{0.35}) \}$$

where,

α' = CNS void fraction
V_s = superficial gas velocity = (volume of gas per second) /(flow area)
$V_\infty = [\sigma*g*(\rho_L-\rho_V)/ \rho_L^2]^{0.25}$
σ = surface tension
g = acceleration due to gravity
ρ_L = density of liquid, and
ρ_V = density of gas.

Applying the modified correlation the estimated average void fraction is 13%.

Deuterium, like hydrogen, exists in two states, ortho and para, owing to the nuclear exchange symmetry of the deuterons in the molecule. Unlike hydrogen, however, there is just a small difference in the scattering cross section between ortho and para, with the ortho state favoring the production of lower energy neutrons. At room temperature the ortho-LD_2 fraction, governed by quantum statistics, is 2/3. The liquid will reach an equilibrium ortho concentration of 0.955 at 25 K in the absence of radiation. In a cold neutron source, the molecular dissociation favors recombination in the 2/3 quantum ratio, so the ortho fraction will equilibrate at some point between those two limits. Raman spectroscopy measurements of the LD_2 source at SINQ (the spallation neutron source at the Paul Scherrer Institut in Switzerland) determined that the ortho content is 0.762 at a power density of 220 mW/g [12]. As seen in Section 2.2 below, the direct heat deposition in the NIST LD_2 source is calculated to be 290 mW/g, so the ortho fraction is expected to be about 75%. Using all the parameters above in the MCNP6 model, and using current tallies at the entrance of guide NG-B, the ratio of the calculated brightness of the LD_2 source to the measured brightness of Unit 2 is plotted in Figure 3. The average gain for cold neutrons, with wavelengths greater than 4 Å, is 1.5, with a gain of a factor of 2 at the longest wavelengths.

2.2 Nuclear Heat Load

MCNP6 was also used to calculate the expected heat deposition rate in the LD_2 and the moderator vessel. Aluminum alloy 6061 will be used for the vessel; the wall thickness will be 3.2 mm. The LD_2 source is much more massive than Unit 2 and the nuclear heat load will be about 3600 W (see Table 1). Because the heat load will triple with respect to Unit 2, and because the boiling and freezing points of LD_2 are about 3 K higher than those of LH_2, a new 7 kW cryogenic helium refrigerator is being installed. The apparent overcapacity is needed for the LH_2 cold source in BT-9 (operating at 200k Pa) and a contingency against unavoidable heat leaks and for future expansion. Installation of the refrigerator was delayed by the default of the vendor, but is now scheduled to be fully operational at the end of 2016. The cryostat assembly, with a total mass of about 150 kg, is cooled by the D_2O Experimental Cooling System; its nuclear heat load is estimated to be 15 kW.

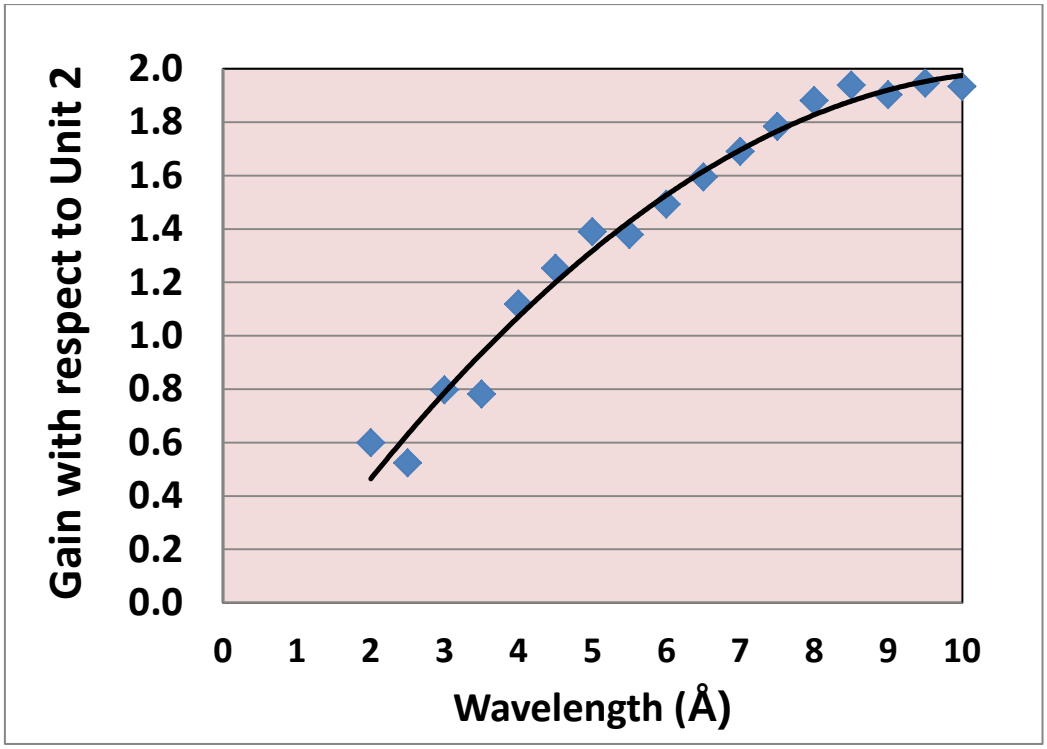

Figure 3. Anticipated gains of the LD_2 cold source with respect to TOF measurements of the existing LH_2 source.

	Deuterium 5160 g		Aluminum 7155 g	
Radiation Source	**Rate (W/g)**	**Heat (W)**	**Rate (W/g)**	**Heat (W)**
Neutrons	0.0851	440	0.0008	6
Beta Particles	-	-	0.0793	567
Gamma Rays	0.204	1053	0.215	1538
Subtotal		1493		2111
TOTAL Cryogenic Heat Load = 3604 W				

Table 1. Heat Load in the LD_2 Moderator and Vessel.

3. Thermal-Hydraulics of the LD_2 Thermosiphon

The NIST LD_2 cold source must be installed horizontally into the cryogenic beam port, and the condenser installed no more than 2 m above the beam port (its height is limited by a radial crane). A naturally circulating thermosiphon is the simplest way to operate the source, as is now done with Unit 2. Liquid from the condenser flows by gravity to the moderator vessel and the vapor produced rises back to the condenser with no need for a pump. There are two other horizontal LD_2 sources in operation, one in the High Flux Reactor at ILL since 1988, and the second at the SINQ spallation neutron source at the Paul Scherrer Institut since 1996. Extensive tests of a mockup of the ILL source were conducted to measure its thermal-hydraulic parameters to ensure that the thermosiphon would operate at the expected heat load, 3 kW, with an acceptable void fraction at 150 kPa [11]. The data from

Reference 11 have been analyzed and scaled to model the NIST source, and this model was used to determine the size of the of the LD_2 supply line and the vapor/liquid return line for operation at 1 bar and a heat load of 4 kW [13]. The internal diameters of the supply and return lines will be 22 mm and 31 mm, respectively. The flow areas need to be greater than the ILL lines because that source has 3 m of head available, and operates at a higher pressure. To ensure the vessel remains completely filled with liquid, the portion of the return line extending into the moderator vessel will have two rows of small holes in the top, replicating the "piccolo" in the ILL source (and in the small LH_2 source at NIST).

4. The Deuterium System

The existing LH_2 sources at NIST are connected to ballast tanks providing a low pressure (less than 500 kPa) expansion volume in the event of a refrigerator failure. A very large 16 m^3 ballast tank has been fabricated and installed for the LD_2 source to store the entire inventory at a pressure not to exceed 500 kPa. It is expected that the tank will be charged to an initial pressure of 400 kPa and the source operated at 100 kPa, but it is sized to operate at a higher pressure if desired. The tank has a helium containment surrounding it and all of the connecting valves and pipes. It will be located outdoors along the west wall of the new guide hall, and a small enclosure will be built to house instrumentation and the charging manifold, and to allow the cold source team to pump out the system and load it with deuterium.

Another consequence of the added heat load of the LD_2 source is the need to replace the existing LH_2 condenser. Two 6 kW, brazed aluminum, plate-and-fin type deuterium condensers (one spare) have been fabricated and one will be installed on the reactor face above the beam port. New LD_2 supply and return lines are required also. Vacuum jackets and helium containments will surround these components, as they do on the LH_2 sources.

A vacuum pump skid will be located on top of the guide shields to provide the insulating vacuums for all of the cold components. The vacuum system will be securely fixed to the shields and the vacuum lines protected, precluding a guillotine break in the lines and uncontrolled air ingress. The pumps will operate in a sealed, helium containment, so in the event of a leak into the vacuum, the D_2 will mix with an inert gas. The LH_2 source in BT-9 has its own vacuum pump skid (under construction) completely isolated from the LD_2 vacuum system.

A conceptual design of the cryostat assembly, consisting of the moderator vessel, vacuum jacket, helium containment, and D_2O cooling water jacket, was completed in 2014. NIST issued a request for proposals to fabricate the entire assembly and provide a complete quality assurance program to document the materials used (Al-6061), radiographs of all the welds, and the results of all leak and pressure tests. Bids were far over budget, however, and work on the cryostat was suspended for about 2 years. Recently, additional funding was secured and it is now expected the cryostat will be completed in 2020 and installed in 2021.

5. Safety

Many of the safety features of the LD_2 source have been described above. The underlying philosophy at NIST is that the cold source be simple, reliable and safe. This is assured by

providing at least two barriers between the deuterium and air, minimizing gas handling, rigorous quality assurance standards, protecting components from physical hazards and by a passively safe design. All deuterium-filled components are surrounded by monitored helium containments maintained above one atmosphere to signal if a barrier is compromised. The system is loaded with D_2 and then sealed, hopefully for many years. The D_2 system is completely welded and checked for leaks via helium mass spectrometry so that the leak rate is less than 10^{-9} STP cm^3/s (no detectable leaks). System components are also surrounded by protective shields, preventing an accident with the crane or a fork truck. Inside the confinement building, the piping to the ballast tank is located in a totally inaccessible floor trench. Thus a massive release of deuterium into the building with the reactor operating is not credible. In the event of a refrigerator failure, the LD_2 boils and the gas flows back to the ballast tank where it was loaded initially, requiring no active components or relief valves in the D_2 system. The reactor must be shutdown, however, until the refrigerator recovers to avoid overheating the moderator vessel.

An accident analysis is being prepared for the Engineering Change Notice, the standard internal review process required by the Nuclear Regulatory Commission to ensure compliance with 10 CFR 50.59 (the chapter in the Code of Federal Regulations concerning nuclear facility changes). The helium containment vessel surrounding the moderator chamber is designed to withstand the maximum pressure generated in the cryostat assembly by any credible leak of LD_2 into the vacuum system, or leak of air into the vacuum system. The Maximum Hypothetical Accident (MHA) assumes that the vacuum pump containment is inadvertently left filled with air instead of helium, followed by a pump failure allowing the air to flow into the vacuum and freeze on the surface of the moderator vessel. It further assumes that as the mass of oxygen reaches its maximum, the vessel fails and there is a LD_2 – solid O_2 detonation. Pressure measurements of such detonations were made by Ward et al [14] and the results can be scaled to predict the pressure in a different size vessel. The peak pressure generated in the MHA would be 2.2 MPa, well below the design pressure of the helium containment which is greater than 6 MPa. There are already five other LD_2 cold moderators at other nuclear facilities, incorporating similar safety standards, accumulating decades of accident free operation.

6. Conclusion

The NCNR, continuing its commitment to expand its cold neutron research capabilities, is planning to replace the existing cold source with a LD_2 source that will provide an average gain of 1.5 for cold neutrons, and a factor of 2 for the longest wavelengths. The source is scheduled to be installed by the end of 2021.

7. Acknowledgements

The authors gratefully acknowledge Jeremy Cook and John Barker for planning, executing and analyzing the time of flight spectrum measurements on NG-B. We also wish to thank the National Nuclear Security Administration of DOE for its support of the entire project to upgrade the cold source and neutron guide network.

8. References

1. Kopetka, P., Williams, R. E. and Rowe, J. M., “NIST Liquid Hydrogen Cold Source”, NIST Internal Report, NISTIR-7352 (2008).

2. Williams, R. E., Kopetka, P. and Rowe, J. M., “An Advanced Liquid Hydrogen Cold Source for the NIST Research Reactor”, Proceedings of the Seventh Meeting of the International Group on Research Reactors, IGORR-7, San Carlos de Bariloche, Patagonia, Argentina (October, 1999).

3. Kopetka, P., Middleton, M., Williams, R. E. and Rowe, J. M., “A Second Liquid Hydrogen Cold Source for the NIST Research Reactor”, Proceedings of the 12th Meeting of the International Group on Research Reactors, IGORR-12, Beijing, China, (October, 2009).

4. Goorley, John T. et al, “Initial MCNP6 Release Overview – MCNP6 version 1.0”, LA-UR-13-22934 (June, 2013).

5. Chadwick, M. B. et al, “ENDF/B-VII.1: Nuclear Data for Science and Technology: Cross Sections, Covariances, Fission Product Yields and Decay Data”, Nuclear Data Sheets, 112, 2887-2996 (2013).

6. Conlin, Jeremy Lloyd, “Continuous-S(α,β) Capability in MCNP”, (LA-UR-12-00155) 2012 ANS Annual Meeting, Chicago, IL (June, 2012).

7. Mattes, M. and Keinert, J, “Present Status of Evaluated Thermal Neutron Scattering Data in the Temperature Range 20 K < T < 300 K for solid and liquid moderators important for the design of cold neutron sources”, IKE – University of Stuttgart, JEFF Meeting (November, 2005). (RSICC Order Number: NEA 1787 ZZ-CRYO-S(A,B)-ACE1).

8. Siegwarth, J. D. et al, “Thermal Hydraulic Tests of a Liquid Hydrogen Cold Neutron Source,” National Institute of Standards and Technology Internal Report, NISTIR 5026, Boulder, Colorado (1994).

9. Cook, J. C. et al, “Experimental characterization of the Advanced Liquid Hydrogen Cold Neutron Source spectrum of the NBSR reactor at the NIST Center for Neutron Research”, NIMA, **792**, 15-27 (2015).

10. Kazimi, M.S. and Chen, J.C., “Void Distribution in Boiling Pools with Internal Heat Generation”, Nuc. Sci. & Eng., **65**, 17-27 (1978).

11. Hoffman, H., “Natural Convection Cooling of a Cold Neutron Source with Vaporizing Deuterium at Temperatures of 25 K”, from: Natural Convection Fundamentals and Applications, S. Kakac, W. Aung and R. Viskanta, Editors, Hemisphere Publishing Corporation (1985).

12. Atchison, F. et al, “Ortho-para equilibrium in a liquid D_2 neutron moderator under irradiation”, Phys. Rev. B, **68**, 094114 (2003).

13. Rowe, J. M., “Scaling Analysis of Proposed Deuterium Source”, Private Communication (July, 2012).

14. Ward, D. L. et al, “Liquid-Hydrogen Explosions in Closed Vessels”, Adv. Cry. Eng., **9**, 390 -400 (1964).

New Projects

JULES HOROWITZ REACTOR: PREPARATION OF THE COMMISSIONING PHASE AND NORMAL OPERATION

J. ESTRADE, X. BRAVO, G. BIGNAN, J.L. FABRE, O. MARCILLE
French Atomic Energy and Alternatives Energies Commission - Nuclear Energy Directorate
Cadarache and Saclay Research Centres- France

Contact author: jerome.estrade@cea.fr

ABSTRACT

The Jules Horowitz Reactor (JHR) is a new modern Material Testing Reactor (MTR) currently under construction at CEA Cadarache research centre in the south of France. It will be a major research facility in support to the development and the qualification of material and fuel under irradiation with sizes and environment conditions relevant for nuclear power plants in order to optimise and demonstrate safe operations of existing power reactors as well as to support future reactors design. It will represent also an important research infrastructure for scientific studies dealing with material and fuel behaviour under irradiation. The JHR will as well contribute to secure the production of radioisotope for medical application. This is a key public health stake.
The construction of JHR is going-on and shall be operational by the beginning of the next decade. Once in operation, the reactor will provide modern experimental capacity in support to R&D programs for the nuclear energy for the next 50 years.
In parallel to the facility construction, the preparation of the future staff and of the organisation to operate the reactor safely, reliably and efficiently is an important issue. CEA must also design and implement the first experimental devices for the start-up of the reactor. In this framework, many actions are in progress to elaborate:

- the staffing and the organisational structure for the commissioning test phases and also for normal operation,
- the documentation in support to the reactor operation (safety analysis report, general operating rules, procedures, instructions, …),
- the maintenance, in service and periodic test programs,
- the staff training programs by using dedicated facilities (simulator,…),
- the commissioning test programs for ensuring that the layout of systems and subcomponents is completed in accordance with the design requirements, the specification performances and the safety criteria,
- the design and implementation of the first fleet of experimental devices in support to the commissioning test program and the future experimental programs.

These commissioning tests will also be helpful for transferring the knowledge on the installed systems to the operating team.
This paper gives an up-to-date status of the construction and schedule plan of the reactor and of the organisation for commissioning tests activities to prepare the future operation.

1. Introduction

This paper gives an up-to-date status of the construction and a description of the organizational structure, responsibilities and main actions for the Jules Horowitz (JHR) Material Testing Reactor (MTR) commissioning and routine operation.
Its construction is going-on and the reactor shall be operational by the beginning of the next decade. It will be operated by CEA, as an international user's facility on the CEA Cadarache site. The design of the reactor will provide modern experimental capacity in support to R&D

programs for the nuclear energy for the next 50 years. It will also supply radio-isotopes used for medical applications.
JHR will be a modern MTR. It is a pool-type reactor; the maximum power will be 100 MWth. Its design allows a large experimental capability inside and outside the reactor core. Due to the high power density, the core primary circuit is slightly pressurized. Several equipments will be implemented in the reactor building and be used in support to the experimental programs (3 small cells attached to the main 4 hot cells will allow the preparation and examination of test devices before and after irradiation, non-destructive examination benches (gamma spectrometry, X tomography, neutron imaging system) and specific laboratories (fission product lab, chemistry lab and dosimetry lab)).
In parallel to the construction of the reactor, the future staff training and the preparation of the organization, to operate the reactor safely, reliably and efficiently is a key item. In this framework, many actions are on-going to elaborate:

- the staffing and the organizational structure for the commissioning test phases and also for normal operation,
- the documentation in support to the reactor operation (safety analysis report, general operating rules, procedures, instructions, …),
- the maintenance, in service and periodic test programs,
- the staff training programs by using dedicated facilities (simulator,…),
- the commissioning test programs for ensuring that the layout of systems and subcomponents is completed in accordance with the design requirements, the specification performances and the safety criteria,
- the design and implementation of the first fleet of experimental devices in support to the commissioning test program and the future experimental programs.

2. JHR general description

As a short description, the JHR layout is as follows:

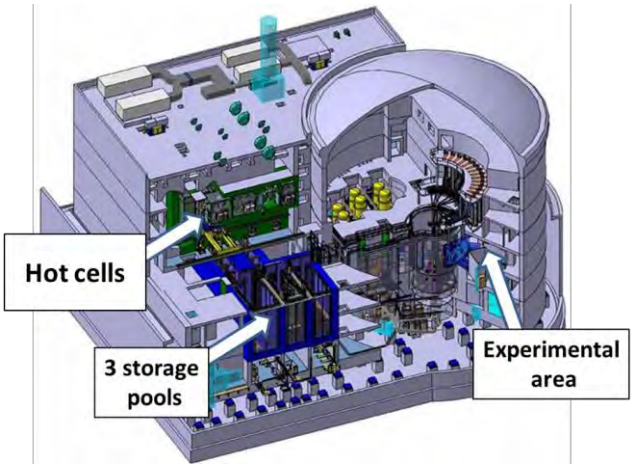

Fig.1 JHR Facility

The nuclear unit of JHR consists in a reactor building and a nuclear auxiliary building.
The reactor building is made in pre-constraint concrete with a diameter of 37 m. The nuclear auxiliary building consists in 3 storage pools for spent fuels, irradiated experimental devices and 4 main hot cells for irradiated fuel and waste management but also preparation, conditioning of experiments and non-destructive examinations on irradiated samples. A transfer channel between the reactor building and the nuclear auxiliary building allows the underwater transfer of spent fuels and experimental devices between the two buildings.

3. JHR update status

Construction is currently under progress at CEA Cadarache Centre. Engineering studies were devoted to AREVA group subsidiary AREVA-TA, which now ensures the supervision of the construction site, and is also in charge of providing key reactor components. More than twenty other suppliers in the fields of civil works, mechanics, heating, ventilation, air-conditioning, electric components… contribute to the construction of the facility.

General view of Reactor Building and Auxiliary unit building (Fall-2015)
Fig. 2: some views of the building site

Regarding the construction work currently underway, apart from anticipated work (civil works, cranes, manufacturing of the main reactor pumps), the main electro-mechanical contracts were started from year 2011 on. Current status on construction site is more than 90% progress of civil works and increasing contribution of electro-mechanical tasks is going-on (recent highlights: polar crane tests, installation of the support structure for the pools liner and installation of the first electrical cabinets and batteries).

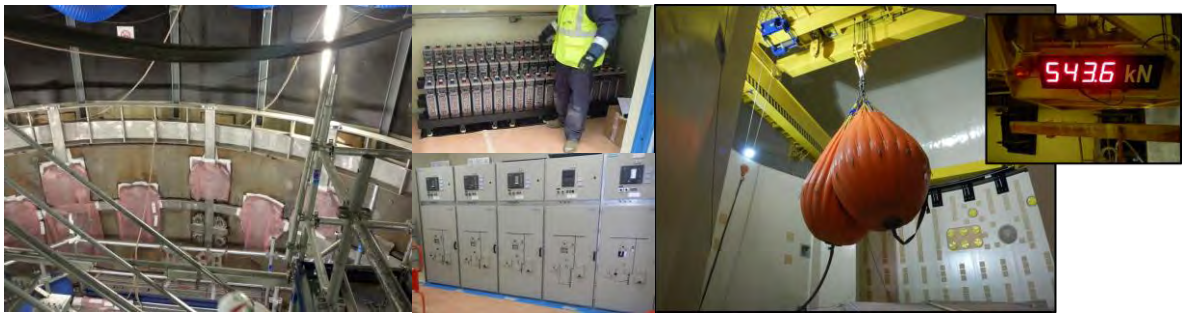

Support structures for the pool liner, electrical cabinets and batteries, Polar crane Test
Fig. 3: some views of equipments

Next important milestones will be the installation of main circuits components (for the reactor building), and the completion of the hot cells complex structure (for the nuclear auxiliaries building). In parallel, several components are in phase of realization or qualification (pumps, valves, diesel generator, equipments of the block core…).

Fig. 4: hot cells complex structure

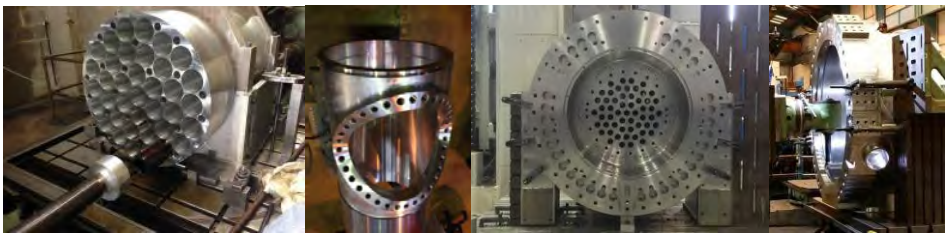

Fig. 5: realization of equipments of the Block core

4. Organization of the JHR project

The organization of the JHR project, the complexity of the design and its associated challenges and the modern safety requirements lead to a specific organization to prepare the facility commissioning. Concerning the organization of JHR project:

- the primary contractor, AREVA [12], has to design and to construct the future unit except the different equipments or systems in support to the experimental programs,
- CEA has :
    - to install and commission the experimental devices and equipments,
    - to operate the reactor and the different systems during the commissioning test phases and after, during routine operation.

In 2010, a specific JHR section was set-up with 5 mains missions:

- Human Resources management to prepare the future operator,
- Setting-up of the operating referential (Safety Analysis Report, General Operating Rules…),
- Training and qualification of control room operator,
- Setting-up of the major contracts linked to the JHR operation (fuel assemblies, equipments, sub-contractors…),
- Design, manufacturing follow up, implementation and commissioning of the first fleet of experimental devices and associated equipments (non-destructive examination benches, laboratories…).

The future reactor operation and experimental systems operation staffs belong to this section to prepare the operation of the reactor and the nuclear auxiliaries as well as the integration of the test devices. These “mixed” staffs will contribute to enhance efficiency during this commissioning period but also for the future normal operation (existence of means shared between the operation and the experimental staffs to create a unique culture around the JHR).

5. Mains topics in preparation to start and operate JHR

5.1. Proposal of staffing and organizational structure

Based on the others research reactors feedback, the project of organization is also adapted to the reactor mission (neutrons for industry and medical application). This structure takes into account the future schedule of the reactor in operation and the maintenance and periodic test programs. The objective is to define clearly the responsibilities and the technical skills of each staff member (reactor manager, operation manager, shift manager and reactor operator) from the commissioning test phase to the normal operation.
JHR section and JHR project are also preparing the organization that will take place for the commissioning test program phase. The aim is to define the liability of each actor (main contractor, JHR project, future operator, contractors and sub-contractors).

For the future, an organization structure has been proposed and consists in two specific units: one to operate the reactor, the other one to conduct the experimental program.

5.2 Elaboration of the licensing and the operating documentation

5.2.1 Elaboration of the licensing documentation

Regarding the licensing documentation, CEA has to complete the project of Safety Analysis Report, provided by the primary contractor, with the test devices specifications (specific licensing document for each of them) and also with some complements on the core configurations (eg: first core and the associated safety studies).

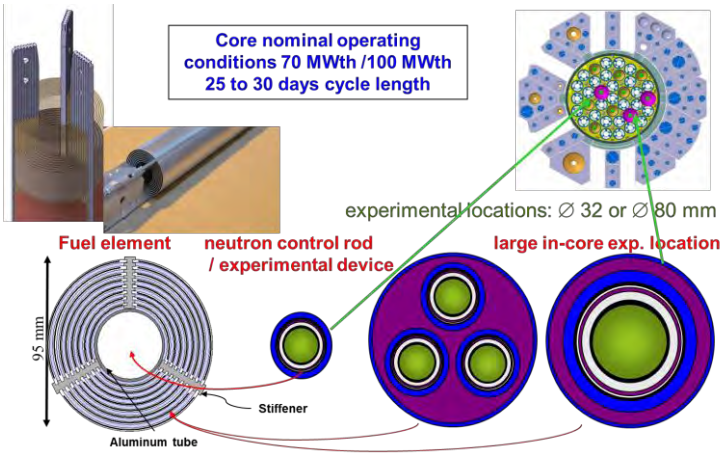

Fig 6. JHR core

This Safety Analysis Report is completed by General Operating Rules (description of reactor operations, strategy in case of incidental or accidental situations, periodic tests and maintenance programs…).

5.2.2 Elaboration of the operating documentation

To elaborate the different documents in support to the commissioning test program and the future operation (routine operation), CEA has defined the operating documents structure based on the feedback of nuclear power plants, taking into account the specificities of experimental reactors. Three types of documents will be established:

- management and JHR safety and security referential documents (licensing),
- operating procedures (reactor and test devices),
- others activities (waste and nuclear materials management, transportation…).

JHR section is in support to the JHR project to follow the construction studies or the tests of the main utility equipments (primary pumps, the fuel handling machine, the hot cells equipments…) mainly for the operation and maintenance items. Through the documentation and the studies on going, the JHR section analyses the systems and the equipments to establish the maintenance and periodic test program but also starts elaborating the reactor operating rules. Approximately, 6000 documents will be used to operate the reactor and the experimental hosting systems. Most of them will be validated during the commissioning test program, others by using the simulator (most of the incidental and accidental situations). Operational procedures must provide direction and guidance to the reactor staff in the performance of operational activities, including the conduct of test devices but also for the technical and administrative support activities (training, waste management, human resources, nuclear materials management…). They are in accordance with the safety requirements.

Concerning the operating procedures, we have rules and instructions:

- the rules: these documents identify the requirements, the conditions to operate close to the limits, the strategy to conduct the operation,

- the instructions: these documents are associated to the rules ; they provide step-by-step actions for accomplishing a specific task within that activity.

A specific item concerns the definition of the strategy of conduct in incidental and accidental situations. The conduct strategy proposal, in incidental and/or accidental situations, is based on the feedback of the strategies applied in nuclear power plants, taking into account the specificities of experimental reactors and the specific design of the command control of JHR. More than 200 Postulated Initiating Events (PIE), will be taken into account. The proposed strategy consists in separating the complex situations from the simple ones. For the complex situations, a document of «entrance to instruction » will allow:

- to confirm the expected automatic actions,
- to check the safety functions parameters,
- to realize a diagnosis with the aim of an orientation towards the adapted instruction.

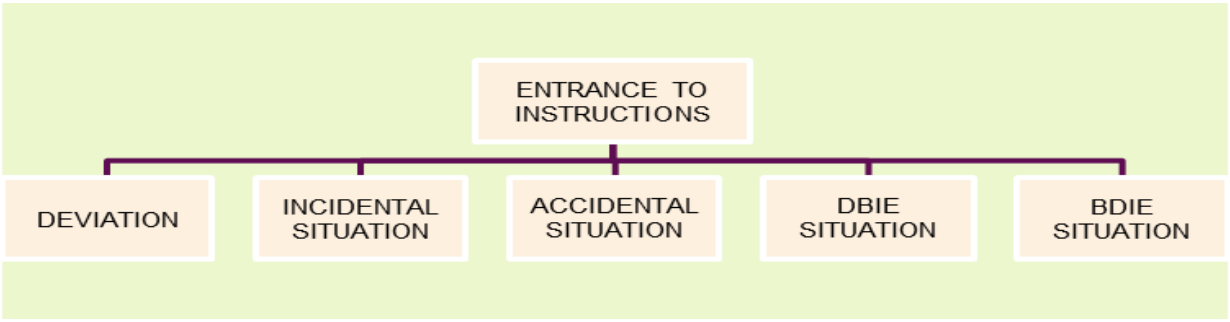

Fig 7. Strategy of conduct in incidental and accidental situations

The orientation will be only a Deviation situation (D), or an Incidental (I) or an Accidental (A) situation or a Design and Beyond Design Basis Accident (H and U) situations.

The sequence of events includes the actuation of the Safety Category 1 systems that control the process initiated by the Design Basis Initiating Events (DBIE). Where prompt reliable action is required to deal with DBIE, the reactor design includes the means to automatically initiate the operation of the necessary safety systems. This ensures that the three main safety functions, namely: reactor shutdown, core cooling, and radionuclides confinement remain fulfilled with a high degree of reliability. The design reduces operator actions as far as feasible, particularly for the period during and following an accident condition with actuation of a protection/safeguard system (within 30 minutes). This period is devoted to use «entrance to instructions».

Considering this first action to define the conduct strategy in incidental and accidental situations, the next step will be to elaborate the first procedure and perform the study to identify the best strategy. The final step will consist in validation by using a simulator.

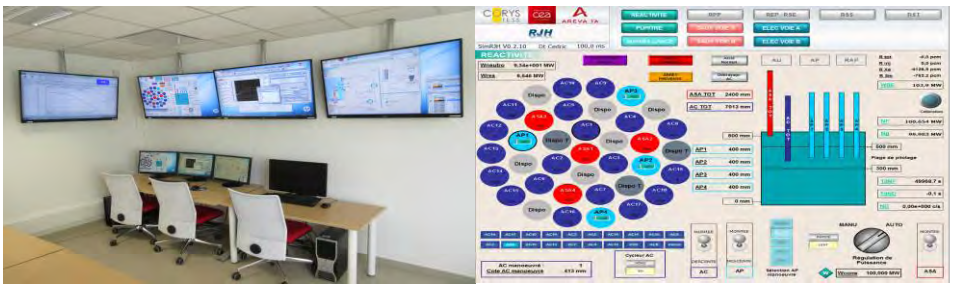

Fig 8. First version of the Simulator

5.3 Elaboration of the maintenance, in-service and periodic test programs

After identifying the main Systems, Structures and Components (SSC), important to safety, a first inventory of maintenance, surveillance, inspection and testing activities has been performed. Taking into account the project of organization of the operator staff (number of operator and competences), an optimization of the maintenance plan has been proposed in three categories:

- the maintenance program is done by the operator,
- the maintenance program is done by a specific sub-contractor,
- the maintenance program is done by general sub-contractors managed by the Cadarache research center.

The objective of this categorization is also to optimize the maintenance subcontracting of a limited number of SSCs.
This maintenance program should be reviewed since each contractor will send its own maintenance program strategy to confirm or modify the current project of maintenance plan. This part of activities can have a significant impact on the reactor operation cost.

The in-service inspection and periodic test program will be in compliance with the requirements associated to the SSCs and depends on the different categories of classification (safety category 1 to 3). This program is adapted and optimized also with the schedule of the reactor in operation.

5.4 Elaboration of staff training program

As a basis of the future organizational structure, this training program for the future operators has been elaborated taking into account the feedback of similar worldwide nuclear facilities and the project of JHR organization structure. The strategy to establish this training plan was:

- to identify the different requirements for working in a nuclear unit (occupational health and safety, radiation protection, nuclear safety culture, waste management, nuclear materials management…),
- to identify the needs of competences for operating the reactor and the different circuits and establish the corresponding training program.

The training program preliminary inventory has identified approximately 130 different training courses. This program includes the JHR specificities. For the different phases of the project (commissioning test program, first start-up...) a schedule of the training sessions will be established in agreement with the actual annual recruitment of the reactor operation staff.

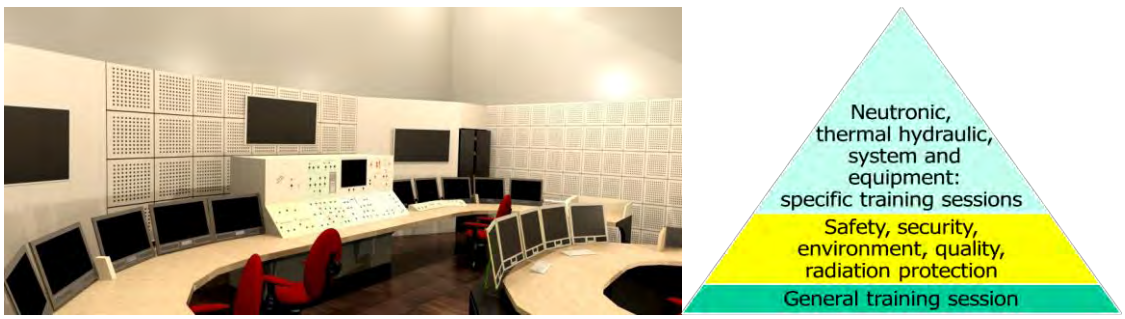

Fig 9. JHR Control room and training program

5.5 Elaboration of commissioning test programs

The elaboration of the Commissioning Test Program consists to identify the needs of tests,

instrumentation and/or calculations to verify the safety criteria and the performance of each Systems, Structure and Component (SSC) during the commissioning phases. The approach is a “step by step” one:

- Step 1: test assembly for each SSC,
- Step 2: functional test,
- Step 3: individual integration test,
- Step 4: global integration test.

Following some on-going studies (neutronic and thermal hydraulic calculations) specific devices/instrumentation, in support to the first core loading and the first start-up, will be developed. The aim is to check the JHR nominal performances and safety criteria (neutron and gamma detectors, temperature or flow sensors…).
The commissioning phases have been divided into stages:

- Stage A: test of the required SSC before fuel loading
- Stage B: fuel loading and approach to criticality tests
- Stage C: step by step power increase, and power tests.

These commissioning tests will also be helpful for transferring to the operating staff the knowledge on the installed systems.

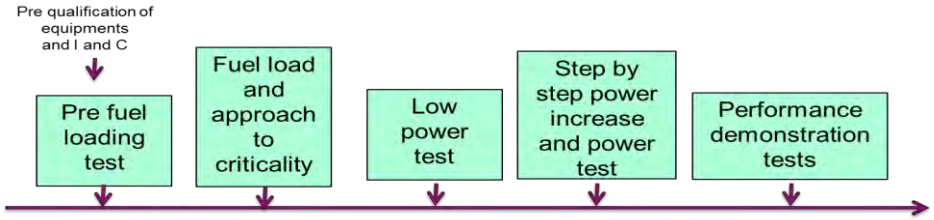

Fig 10. Different steps of the commissioning program

5.6 Design and implementation of the experimental device

CEA is developing a set of test devices that will be operational for the startup of the reactor or few years later. These experimental hosting systems will have to fulfil experimental needs concerning current NPP technologies (GEN II-III) and possible support to future reactor concepts as well.
Experimental programs could be related to either fuel basis properties acquisition, mastering of margins or improvement of fuel products (clad and pellet), in term of performance, safety, maximum burn up, innovative materials or extension of validation domain of fuel performance codes.
The main experimental hosting systems currently under design are:

- MADISON test device which will be available at the JHR start up, and will allow testing the comparative behavior of several instrumented fuel rods (between 1 to 8 rods of up to 60 cm fissile stack height) under NPP normal operating conditions (no clad failure expected).
- ADELINE test device which will be available for the JHR start up, and will allow testing a single experimental rod up to its operating limits. The fuel rod will be tested under conditions that correspond to off-normal situations with possible occurrence of a clad failure. The first version so called ADELINE “power ramps” will focus on the clad failure occurrence during one of these abnormal situations.
- LORELEI test device which will be available right after the JHR start up and will allow testing a single rod under accidental situation that may lead to fuel damage. It will be able to reproduce all sequences of a LOCA-type transient, including the re-irradiation, the loss of coolant and the quenching phases, on a separate effect approach.

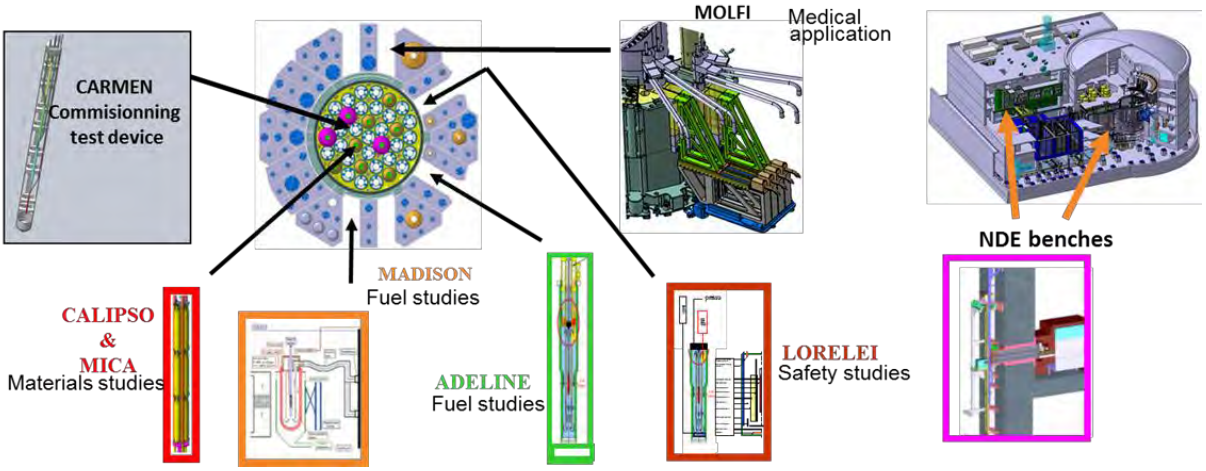

Fig 11. Set of test devices that will be operational for the startup of the reactor or few years later

These experimental devices dedicated to the fuel studies are completed by in-core and in reflector material test devices, corresponding to large ranges of irradiation conditions, in terms of temperature, neutron flux and neutron spectra. A special attention focuses on the improvement of the thermal stability and gradients in the interest zones of irradiated samples. Some specific devices will be described such as equipments designed to the qualification of reactor pressure vessel steels (OCCITANE test device), to the studies of creep-swelling of structural materials (MICA test device) or to the study of the stress corrosion cracking assisted by irradiation phenomena-IASCC(CLOE test device: a corrosion loop with an accurate water chemistry monitoring for PWR or BWR requirements).

CEA , in some cases with partners, is designing a first fleet of test devices expected at the reactor start-up or in the first operation years. JHR safety requirements are used also to design these experimental hosting systems. An important issue is the implementation of these test devices in the reactor: for each device, the implementation in the reactor building is studied to identify, for example, the power supply and instrumentation and control cabinet needs and also the impact on the venting and effluents facility networks. The equipments in each experimental cubicle and the implementation of electrical cabinets are defined. The studies include also the use of hot cells, handling systems and temporary storage area. The JHR section uses the same “integrated system” (the CATIA software) as the primary contractor.

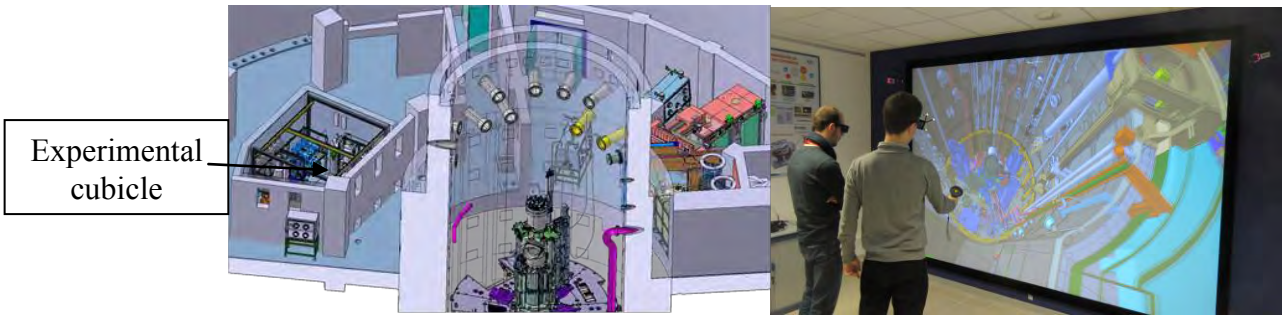

Fig 12. Layout of the experimental device in an experimental cubicle and 3D simulator

6. Conclusion

The construction of JHR is going-on and the reactor shall be operational by the beginning of the next decade. In parallel to the construction of the reactor, the preparation of the future staff and of the organization to operate the reactor safely, reliably and efficiently but also the design and realization of the first set of hosting device are important issues. This paper gave an overview of these actions to prepare the commissioning phases, the routine operation and the future experimental programs.

7. References

[1] The Green Paper, “Towards a European Energy Security Strategy”, published by the European Commission in November 2000

[2] FEUNMARR, Future European Union Needs in Material Research Reactors. 5th FP thematic network, Nov. 2001 – Oct 2002

[3] S. Gaillot and al.: “The Jules Horowitz Reactor Project - Experimental capabilities”. 10th IGORR conference, September 2005 – Gaithersburg Maryland, USA

[4] M. Boyard and al.: “The Jules Horowitz Reactor Project: JHR core and cooling design”. 10th IGORR conference, September 2005 – Gaithersburg Maryland, USA

[5] G. Bignan, D.Iracane, “The Jules Horowitz Reactor Project: A new High Performances European and International Material Testing Reactor for the 21st century”. Nuclear Energy International publication (NEI-Dec 2008)

[6] G. Bignan, D. Iracane, S. Loubière, C. Blandin, “Sustaining Material Testing Capacity in France: From OSIRIS to JHR”. 12th IGORR conference, October 2009 Beijing, China

[7] G.Bignan, P. Lemoine. X. Bravo, “The Jules Horowitz Reactor: A new European MTR (Material Testing Reactor) open to International collaboration: Description and Status”. RRFM 2011 Roma, Italy

[8] G. Bignan et al., “The Jules Horowitz Reactor: A new European MTR open to International collaboration”.13rd IGORR conference,September 2010, Knoxville ,TN –USA)

[9] G. Bignan et al.,”The Jules Horowitz Reactor: A new European MTR (Material Testing Reactor) open to International collaboration: Update Description and focus on the modern safety approach”. IAEA International Conference on Research Reactors: Safe Management and Effective Utilization, November 2011, Rabat, Morocco)

[10] J. Estrade and al., “The Jules Horowitz Reactor: a new high performances European MTR (Material Testing Reactor) with modern experimental capacities – Building an international user facility”. Research Reactor Fuel Management 2013, 21-25 April, 2013, St-Petersburg, Russia.

[11] C. Blandin and al., “LWR Fuel irradiation hosting systems in the Jules Horowitz Reactor”. LWR Fuel Performance Meeting 2013, 15-19 September 2013, Charlotte, NC, USA.

[12] H. Beaumont and al.:”The Jules Horowitz Reactor: Engineering Procurement Construction Management missions and Construction status”. 13th IGORR conference, October 2013, Daejeon - Corea.

[13] “The Jules Horowitz Reactor: A new high performance MTR (Material Testing Reactor) working as an International User Facility in support to Nuclear Industry, Public Bodies and Research Institutes”, X. Bravo, G. Bignan Journal of Nuclear Energy International-December 2014

TREAT TRANSIENT TEST REACTOR RESTART STATUS

JOHN BUMGARDNER
Transient Testing Director
Idaho National Laboratory
PO Box 1625
Idaho Falls, ID 83415 USA
john.bumgardner@inl.gov

Abstract:

The United States Department of Energy has authorized resumption of transient testing and the restart of the Idaho National Laboratory TREAT reactor. The TREAT reactor was used from 1959 to 1994 to conduct more than 2,500 nuclear fuel transient tests, and was placed in standby in 1994. The plant was extensively upgraded shortly before it was placed in standby. Present day assessments revealed that a sound infrastructure remains at the plant; testing has revealed that all major reactor plant systems can be re-used; the previous procedures, drawings, and other documentation were preserved; and some personnel who were involved in historical operations are available. Some issues must be resolved, such as control rod actuator shock absorbers and some portions of the fire protection system must be replaced. Efforts are now under way to renew reactor systems and infrastructure as required, update procedures and configuration management documents, and to fully qualify the new operating organization. Reactor startup is anticipated no later than 2018. The infrastructure for preparation and conduct of experiments is being evaluated, and progress has been made with the design and fabrication of new test vehicles with modern instrumentation.

1. Transient testing is needed for nuclear fuel development and qualification

Transient testing involves placing nuclear fuel or material into the core of a nuclear reactor designed to operate at high power for a short time, and subjecting the nuclear fuel or material to short bursts of intense, high-power radiation. After the experiment is completed, the fuel or material is analyzed to determine the effects of the radiation. The results are then used in fuel or material design and/or qualification.

Transient testing is required for essentially all nuclear fuel design and qualification efforts to learn how nuclear fuel will respond during accidents involving transient overpower and/or under cooling events. For example, nuclear fuel may fragment when exposed to higher than normal power. This fragmentation can cause unacceptable performance. Transient testing is also needed to validate performance models for nuclear fuel and materials. These models, when validated, will dramatically shorten the development and qualification life cycle for nuclear fuels, supporting rapid development of low emissions, reliable power generation.

In the past, transient testing was primarily done in facilities that no longer exist. The U.S. Department of Energy evaluated how to provide the required transient testing capability and, following completion of the National Environmental Policy Act process, they selected the Transient Reactor Test (TREAT) facility to resume transient testing.[1] TREAT is located at Idaho National Laboratory (INL).

2. Overview of TREAT

Operating from February 1959 until April 1994, TREAT was specifically constructed to conduct transient reactor tests, where the test material was subjected to neutron pulses that can simulate conditions ranging from mild upsets to severe reactor accidents. The reactor primarily was used to test fast reactor fuels, but it has also been used for light water reactor fuel testing and testing of other unique special purpose fuels (e.g., space reactors).

TREAT is an air-cooled, thermal spectrum test facility designed to evaluate reactor fuels and structural materials. TREAT was designed to do the following:

- Induce intense fission heating in the nuclear fuel being tested
- Test nuclear reactor fuels under severe reactor-accident conditions
- Test prototypic-sized reactor fuel pins and bundles
- Provide nondestructive test data through neutron radiography of fuel samples.

TREAT historically was used to study fuel meltdown, metal-water reactions, interactions between overheated fuel and coolant, and the transient behavior of fuels for high-temperature systems. The open core design of TREAT also allows for detailed monitoring of the experiments during the test. In steady-state operation, TREAT can be used as a large neutron radiography facility that can nondestructively examine assemblies up to 15 feet long.

3. Status of reactor restart

The reactor and support systems were significantly upgraded shortly before the reactor was placed in standby. The reactor remained fueled during the time it was in standby and many of the facility's preventative maintenance activities have continued to be performed. As a result, the facility's material condition is very good. A summary of the infrastructure, personnel, and required documentation status is provided in the following sections.

3.1 Infrastructure

Automatic Reactor Control System (ARCS): The ARCS is based on INTEL Multibus architecture. Parts and vendor support are readily available. The ARCS has been energized and initial testing of hardware and legacy software completed. Power supplies were found to be degraded, and were replaced.

Reactor Trip System: The Reactor Trip System been successfully energized, with only 2 of the 28 modules tested being inoperable following initial system startup. The system requires some repairs and, subsequently, testing and calibration to be performed by INL staff. Power supplies were found to be degraded, and were replaced.

Electrical System: The electrical system was significantly upgraded in the 1980s. It has remained energized, preventative maintenance has been completed, and spare parts are available if needed. The system can be used as is.

Control Rod Drives: Maintenance and testing of control/shutdown, compensation/shutdown, and transient rod drives are in progress. Preliminary results indicate the systems' storage conditions were excellent. Functional testing revealed that SCRAM times were within specification, and the only significant deficiency found was the several hydraulic shock absorbers were found to have lost fluid, and were replaced. This action required full removal of the associated control rods and actuators. All hydraulic shock absorbers will be replaced prior to reactor operation.

Reactor Fuel: Previous fuel inspection documents have been evaluated. It is anticipated the original fuel can be used for long-term operations. Confirmatory inspections were initiated in 2015.

In preparation for inspection activities, a non-fueled assembly (identical to a fueled assembly, except for the uranium content) was removed from its storage location, inspected, and returned to storage. The non-fueled assembly was in good condition, with no noted storage-related degradation. Subsequently inspections were conducted of over 100 fuel elements in the core, with no significant deficiencies found. Some foreign material was found, primarily yellow plastic. Cleanup of the foreign material has been completed. Reactor core conversion to low-enriched uranium fuel is being pursued in parallel with reactor restart. A lead test assembly will be inserted after reactor restart.

Experiment Infrastructure: The existing comprehensive nuclear experiment preparation and analysis infrastructure at INL is being evaluated for updates and enhancements to reflect the current needs of fuel and material testing.

3.2 Personnel

A dedicated team for reactor restart and operations has been assembled and is supported by the broader INL scientific and engineering staff. Personnel who previously operated the facility have been identified. Several are under subcontract to support the restart effort. Training is under way, and the first Reactor Operators and Senior Reactor Operators have achieved certification for shutdown operations.

3.3 Documentation

Over 300 boxes of stored records have been retrieved. Procedures, training material, drawings, system descriptions, and other documents are being updated to current standards. The Safety Analysis Report written to the requirements of Regulatory Guide 1.70 is acceptable to the U.S. Department of Energy regulator and is being used for current facility operations. An update to the Safety Analysis Report has been drafted and will be submitted by March 31, 2016.

4. Conclusions

The Transient Testing Program is making positive progress toward TREAT restart and resumption of transient testing. The remaining inspections on the reactor control system, control rod drives, and reactor fuel will determine the final work scope required to restart the reactor. At this point, the program is on track for resuming transient testing operations during or before 2018.

REFERENCES

1. U.S. Department of Energy, *DOE/EA-1954, Environmental Assessment for the Resumption of Transient Testing of Nuclear Fuels and Materials*, (February 2014).

MANAGING CONCURRENT DESIGNS OF NEW RESEARCH REACTORS

N.P. DE LORENZO
Nuclear Projects Division, INVAP
Luis Piedrabuena 4950, R8403CPV, Bariloche – Argentina
delorenzo@invap.com.ar

ABSTRACT

Diverse Research Reactor (RR) projects, involving INVAP as a design organisation, are being presently developed around the world. Currently, the following range of projects coexists at INVAP, each at a different development stage and with different requirements stated by the future Operating Organization:

- One 30 kW pool type training reactor
- Two 30 MW multipurpose research reactors
- One Mo-99 production oriented facility

This variety of designs, along with the periodic review of older designs, poses a demanding workload over the design and management teams. Moreover, all these projects, while maintaining an independent course, as per the commitments made with each Operating Organisation, should provide opportunities for a synergetic integration that benefits all, by the possibility of sharing the lessons learnt, the development costs of new technologies, the retrofitting of proven designs and other issues.

This paper deals with the strategies, procedures and practices implemented at design and managerial levels in order to proceed with the projects while maintaining a close control of the variety of designs each with its specific and unique characteristics, thus ensuring full compliance with safety requirements and with final user specifications.

Among the management tools implemented for every project and integrated at organizational levels, the following are described in this paper:

- Project Management tools: including Work Breakdown Structure, Master Schedule and Risk Assessments.
- Design Management tools: including Design Plans development, Design Review and Integration Process, Innovation Control and others.
- Configuration Management tools: including Design, Procurement, Construction and Operational Configurations control.
- Life Cycle Assessments / Integrated Logistics Support: including development of operation and utilisation documentation (manuals, procedures, etc), staff training, spare parts assessments and other issues.
- Safety Assessments: probabilistic and deterministic evaluations, safety analysis, dose calculations, siting assessments, etc.
- Quality Management tools: integration, at project level, of Operating Organization and Design Organization Quality Management Plans.
- Project Documentation Management tools: including Documentation tracking, reviewing and control; secure hosting and file transfer protocols; managing multiple languages platforms and other issues.

1 Introduction

Simultaneous design of facilities ranging from a “zero power” research reactor up to multipurpose reactors with power exceeding some tens of megawatts confront the design organisations with a demanding challenge, which requires the use of managerial and design techniques in an efficient manner.

Project Management (PM) techniques applied by INVAP are oriented at ensuring that each facility is unique and constitutes a state of the art design fulfilling the final user specifications as well as guaranteeing that new developments, design improvements and lessons learnt are being shared among the projects.

The following sections detail the techniques applied and the benefits of their application both in managerial and technical aspects. It is acknowledge that a graded approach in the application of these techniques is always required as depicted in Figure 1.

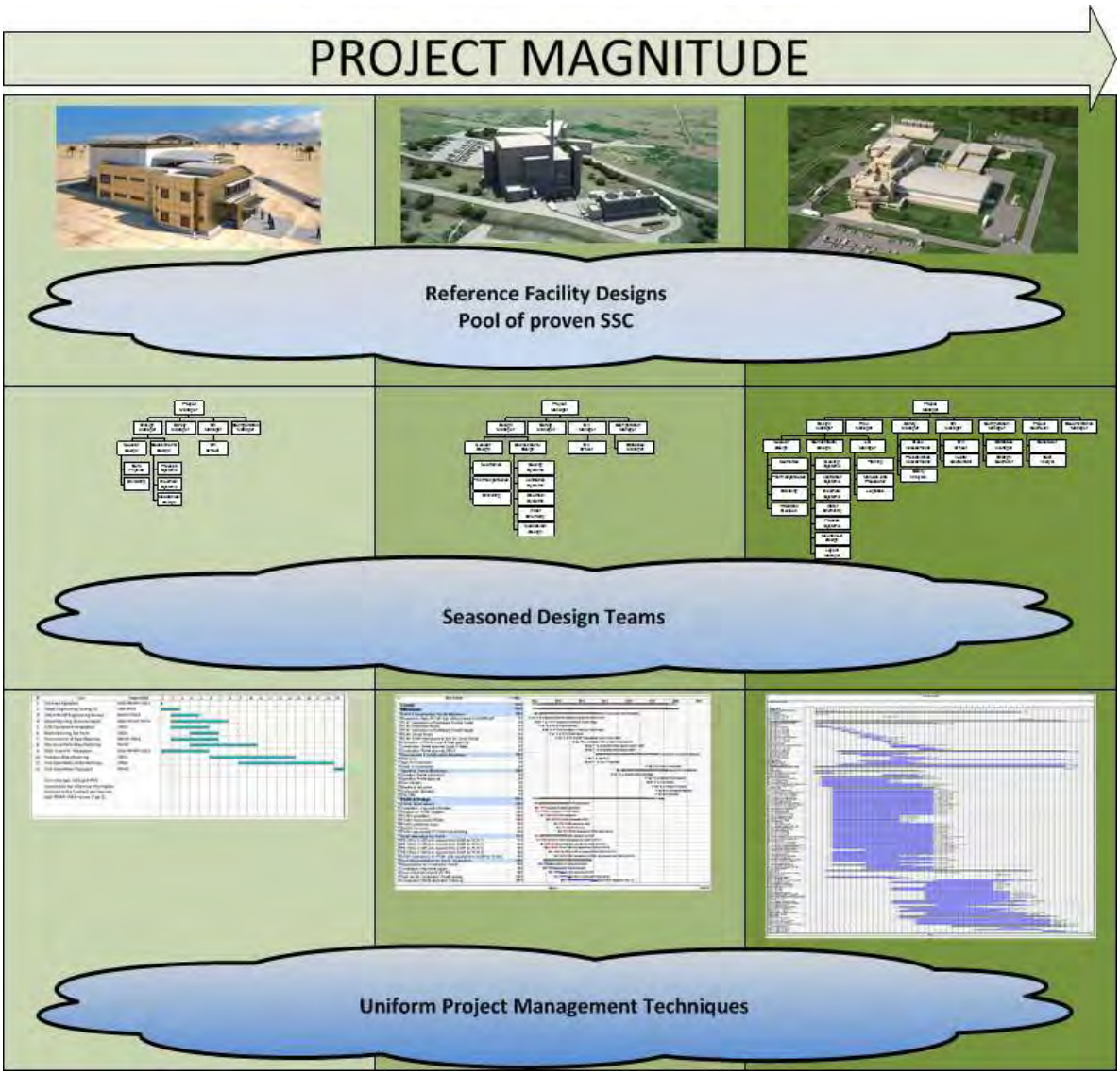

Figure 1: Graded approach followed in different projects

2 Management tools

2.1 Project Management

An efficient utilization of the resources, both technical and managerial, by the concurrent designs being engineered is required. A dedicated Project Management Plan (PMP), based on a general model available at company level is developed for each project and is tailored in accordance with each commercial agreement established with the final users.

The PMP for each project shall define:

- Project scope and objectives
- Master Organisation Chart and appointed staff
- Work Package (WP) structure
- Project Master Schedule (PMS)
- Official communication channels
- Outline of Risk Management (RM) policy
- Outline of Configuration Management (CM) policy
- Outline of Quality Assurance (QA) policy

A Master Organisation Chart is included in the PMP, defining the responsibilities of each position and the corresponding counterpart within the final user organisation structure.

The WPs are organised in a logical scheme by main activity (such as: nuclear design, mechanical design, prototypes and mock ups) and by design stage (namely, conceptual, basic and detailed). Each WP describes the scope and the products to be generated.

A Work Breakdown Structure (WBS) that includes the WPs of a single project is actually a subset of a General WBS applicable to all the RR projects. Empty spaces in the General WBS are available for including special activities required only by certain projects while not applicable activities are deleted. Thus, the WBS of each particular project is generated representing the unique set of activities required to develop the design requested by the Operating Organisation.

Figure 2 shows a typical WBS including WPs classified by main activity and design stage. Dependences along the evolution of the design are clearly deduced by the coding system adopted.

A compatible WBS among the different projects provides for the optimisation in the allocation of the resources (by flattening the resource demand curve by design area) and improves the interrelation between the different design teams (by a consistent utilisation of the same design workflow).

The outline of the RM, CM and QA policies define the top level elements while three specific plans identify actions, responsibility and procedures.

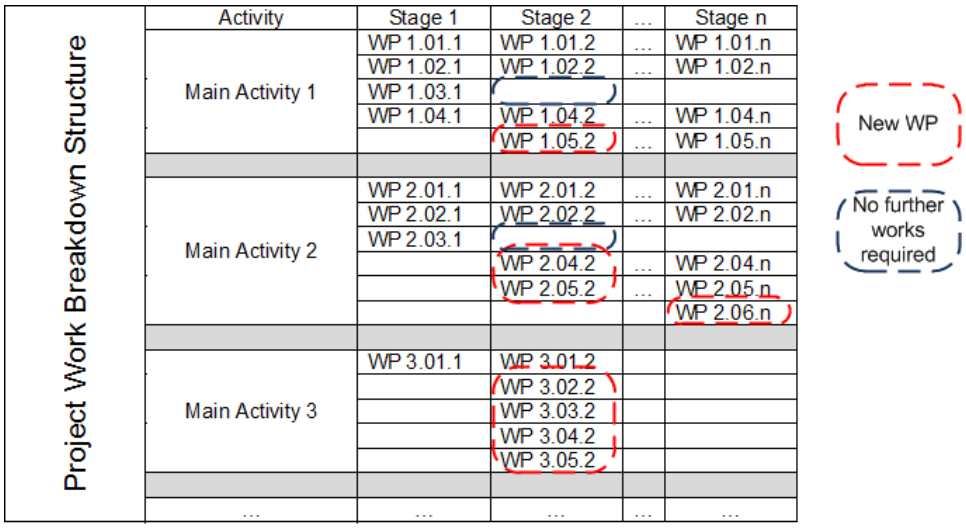

Figure 2: Typical WBS

2.2 Design Management

Each design project at INVAP is developed following a specifically defined Project Design Plan based on a general INVAP Design Plan and tailored to the scope of INVAP participation within the overall project.

INVAP Design Plan depicts the general procedures to conduct the design activities throughout the project phases, including the guidelines to develop individual WP Design Plans for each of the WPs identified in the WBS.

The Project Design Plan includes the following topics:

- Definition of the facility general requirements (functional, performance, etc.).
- Definition of project parameters (seismic loads, applicable standards, etc.)
- List of SSC defined for the reactor
- The safety, seismic and quality classification corresponding to each SSC
- Implementation of Project Preliminary and Critical Design Reviews
- Design audits
- Design documentation
- Independent review scheme and requirements
- Prototyping and Testing
- Design validation and verification process

Based on the umbrella defined by the Project Design Plan, specifically developed for each particular project, WP Design Plans are developed for each WP to deal with:

- SSCs included in the WP
- Specific requirements for the SSCs associated with the WP
- Disciplines required for the design of these SSCs
- Interphases with other WP Design Plans (inputs and outputs)
- Applicable Validation and Verification (V&V) processes

Using a common structure for the Project Design Plan and WP Design Plans along the different projects ensures an optimum integration of the different design groups by using standard engineering tools with common interphases.

Innovative designs are project cross cutting activities developed using specific Design Plans generated at company level and generally involving extensive prototyping and testing campaigns.

2.3 Configuration Management

A Configuration Management System is individually implemented for each project defining appropriate Configuration Items (CIs) according to the evolution of the design. The procedures to define the configuration items and to control them along the evolution of the design are common to all the projects.

Typical lists of CIs are available to be used as starting point by the different projects, which require periodic reviews along the design progress. As a general rule during design stages, the information shared among the different design areas is considered a potential CI.

A procedure to handle modifications in the list of CIs or in a particular CI based on the company procedures is available. The procedure includes the possibility to inform other projects of relevant changes, thus providing for a synergetic development of concurrent designs.

The CIs are managed by an in-house database application, able to handle the whole structure, to maintain interlinks and to track modifications and resulting impacts.

The Facility Configuration developed during the design stage will be re-evaluated at the end of the detail design, and its deliverable version may be later used in procuring, construction, commissioning and operational phases.

2.4 Life Cycle Assessments/ Integrated Logistics Support

Depending on the scope of the project (i.e. development of engineering services for a portion of the facility or turnkey schemes), different Life Cycle Assessments are developed. In the most encompassing scheme, these assessments include:

- Development of manuals, procedures and instructions for the future operation and maintenance of the facility.
- Performing Level of Repair Analysis (LORA) to determine the workshop equipment and trade staff skills required during routine operation and maintenance.
- Analysing Spare Parts needs to define optimum stock levels and procurement strategies.
- Developing training needs analysis.

These activities are part of the Integrated Logistics Support (ILS) approach followed at INVAP in order to ensure the elements required to operate the facility in the future in a safe and efficient manner are being timely considered and developed.

Guidelines to develop state of the art manuals and procedures are available to be used in a consistent manner throughout the different projects, thus ensuring that high quality levels are achieved even in small projects. These guidelines include material ranging from electronic templates and list of adequate terms and jargon, up to predefined texts in different languages.

Training needs are addressed based on previous experience. These analyses allow an early definition and specification of the training tools needed such as mockups or simulators.

2.5 Safety Assessments

Safety is of foremost importance in the design process within INVAP. A dedicated group of experts mastering the required techniques to perform both deterministic and probabilistic assessments in accordance with different regulatory frameworks (e.g.: NRC, ARPANSA, ARN) is available for all the projects.

In house and commercial off the shelf software to calculate the impact (doses) of routine and abnormal releases are available for all the projects, allowing for verification of the obtained results calculated under different regulatory frameworks.

Similarly, reliability databases, which merge reference failure rates and commercial suppliers' information, are available to run safety calculations using suitable computer codes.

Data for the potential sites of the facilities being designed are made available to all the projects as a set of reference values obtained from previous experience or by analysis of real data provided by the future Operating Organisation.

In addition, the group running these assessments is continuously supporting the designers by providing advice on issues such as systems availability and reliability in order to achieve the required performance.

2.6 Quality Assurance

The company is ISO qualified, and plans and procedures to be applied during the development of the works are available and mandatory. Moreover, Quality Assessment (QA) schemes required by the future Operating Organisation or the National Organizations of the local country are also considered.

Therefore, a Project QA Plan and its Procedures are individually developed for each project as per the following actions depicted in Figure 3:

- Identify the INVAP procedures applicable to the QA established for the specific project.
- Develop those additional procedures required only for this specific project.
- In case that any one of INVAP procedures is not in line with these additional procedures newly developed, then the actions required by this INVAP procedure shall be adequately merged into the new procedures.
- Demonstrate the completeness of the resulting set of procedures against the future Operating Organisation or its National Organisations requirements.
- Request an independent Audit in order to demonstrate the Project QA Plan and its Procedures are aligned with the future Operating Organisation and its National Organisations requirements.

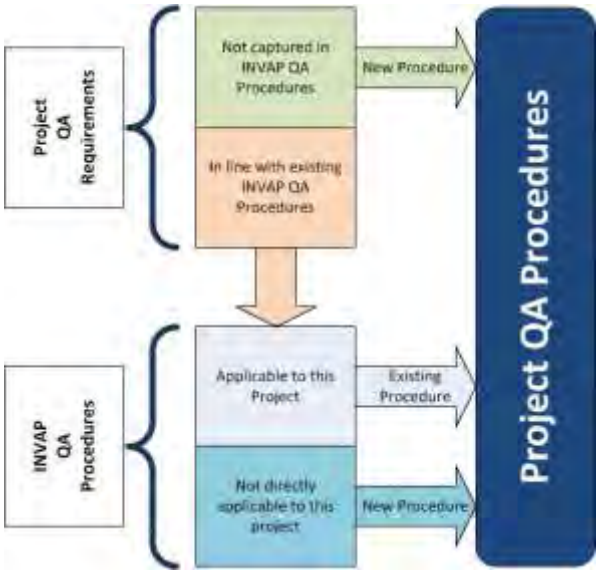

Figure 3: development of the project QA procedures

A QA Officer is appointed for each project, with responsibility for ensuring the quality of the design being developed as per the Plan and procedures defined.

2.7 Documentation Management

Thousands of documents are drafted during the development of the engineering of a research reactor by all the parties involved, such as designers, user representatives, auditors, consultants, regulatory authority representatives, subcontrators, etc.

Documentation produced in different formats and languages, with different status (draft, valid, superseded, etc) are adequately managed including their review process and their transference under secure protocols.

An in-house software developed at company level is applied to each project with the adequate tailoring including:

- Encoding procedure
- Review and approval scheme
- Digital signature
- Secure file document transfer protocol
- Secure access (with passwords and profiles)

The application of software packages during the design process featuring direct 3D modelling or intelligent process and instrumentation diagrams is incorporated at the extent agreed with by the Final User. This methodology reduces the amount of documents in a considerable manner, but it requires that the Final User has installed a similar or compatible design package in its servers. If this were not the case, documents delivered to the final users are outputs of these software packages such as isometric drawings or views exported into “pdf” or other suitable formats.

The following Figure 4 shows a typical workflow followed during the preparation, review and release of documents during project design stages.

3 Conclusions

The application of these PM tools allows the simultaneous design of diverse facilities in an independent manner thus preserving the interest of the future users while maintaining a suitable interchange of information aimed at ensuring high quality and efficient designs throughout all the projects.

This approach also encourages the development of standard designs for some SSC to be lately used in different projects with minimum adaptations, thus reducing the design efforts and associated costs.

Since the gradual implementation of these PM tools, the company has developed a Project Manager Toolbox containing the infrastructure required to launch new projects, starting from a common baseline, which ensures compatibility among simultaneous execution of various projects.

Periodic meetings, where the results of the application of these tools are measured against predefined indicators, will be implemented in the short term in order to retrofit the approach, if required.

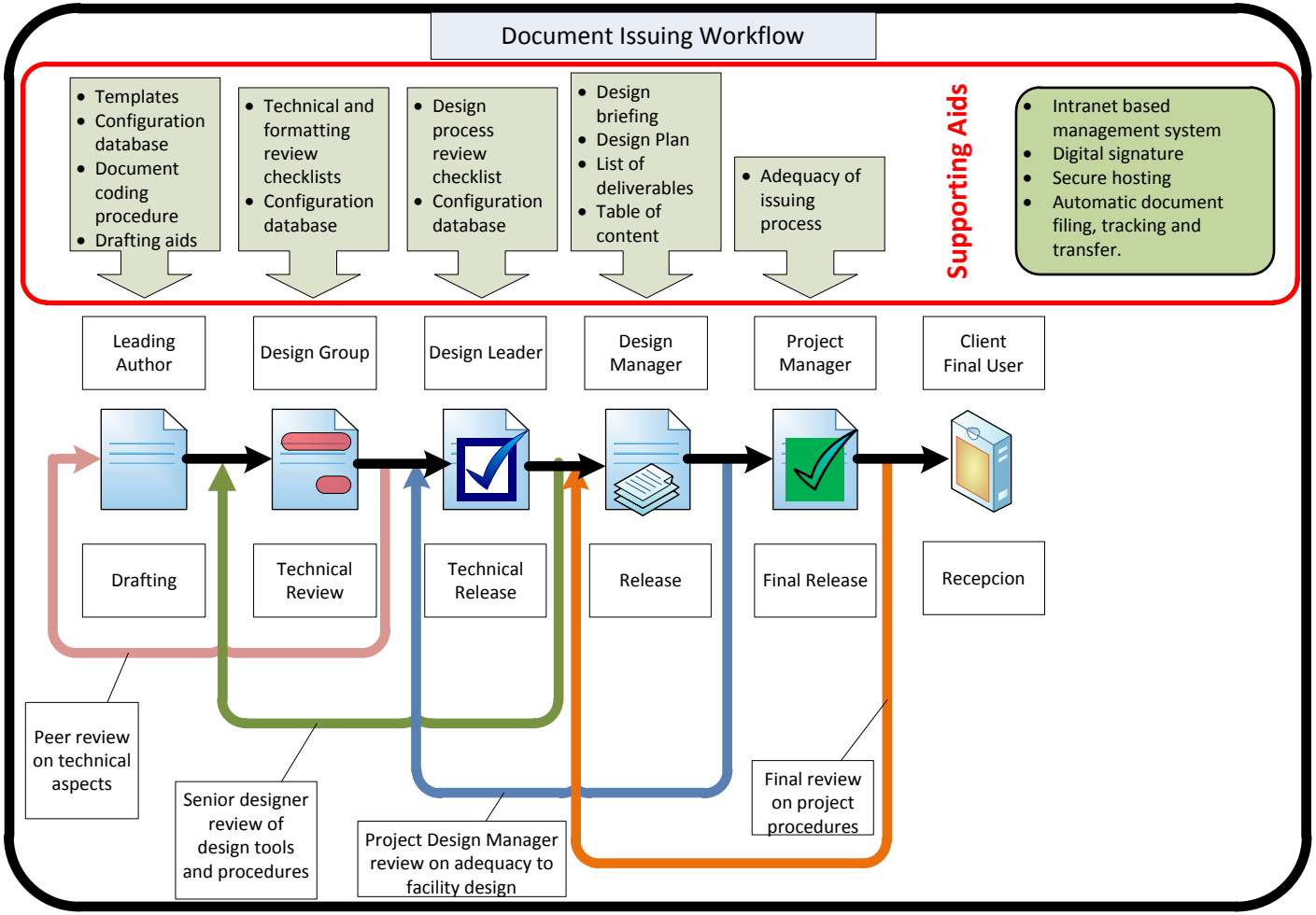

Figure 4: Typical workflow

PROGRESS OF KIJANG RESEARCH REACTOR PROJECT

T.H. KWON, K.H. LEE, JUN.Y. KIM, JEE.Y. KIM, J.K. KIM
KIJNAG Research Reactor Design and Construction Agency, Korea Atomic Energy Research Institute
989-111 Daedeok-daero, Yuseong-gu, Daejeon, 305-353 Korea

ABSTRACT

As a major national project for nuclear science and engineering in Korea, Kijang research reactor (KJRR) project was officially launched on April 2012, 1) to meet the domestic and global needs of medical and industrial radioisotopes, 2) to enlarge the supply of NTD silicon doping, and 3) to validate advanced technologies related to the research reactor. The Korean Ministry of Science, ICT and Future Planning (MSIP) is responsible for coordinating this project by providing its support for stable government financial subsidies, and the local governments is responsible for land preparations including the purchase of land for this project and setting up infrastructures for utilities including the electric power and industrial water line. The Korea Atomic Energy Research Institute (KAERI) is responsible for all the procedures such as development, design, licensing, installation, and commissioning to complete the KJRR research reactor project.

The reactor is be composed of low enriched uranium (LEU) U-Mo plate fuel, which is the first-of-a-kind application in the world and characterized by an average 60% high burn-up pertinently. The burn-up test for a fuel assembly is now being carried out at the Idaho National Laboratory (INL) to test and qualify the LEU-Mo fuel. Also it is designed to produce fission Mo 2,000 curies/week as requirement.

Currently, the conceptual and basic design of the facilities has been completed and the detail design of architectural engineering is near the end. Contracts for the manufacturing major equipment, such as a reactor assembly package and man-machine interface system, have been made as scheduled. KAERI is planning to order the construction for next year as soon as the construction specification will be prepared. The preliminary safety analysis report (PSAR) has been submitted to apply for the construction permit (CP) in November 2014 and the licensing review is expected to be completed by the end of 2016.

Then, the application of the operation license would be scheduled in September 2017 and the initial criticality will be achieved in March 2019.

1. Introduction

KAERI is utilizing the 30MW of High-flux Advanced Neutron Application Reactor (HANARO), which is the first multi-purpose research reactor in Korea. It is being utilized for neutron scattering experiments, material and fuel tests for nuclear power plants, RI productions, silicon doping, neutron activation analysis, and neutron radiography. However, in medical applications, HANARO is only supplying I-131 and Ir-192 on a small scale and many radio-isotopes including Mo-99 are coming from imports. In 2009, the importing amount of the open radioisotope (RI) source was about 25,000 Curie (Ci) and that of the sealed RI was about 71,000 Ci respectively. The self-sufficiency of RI demand becomes an important issue for the public health service in Korea. Also, in industrial applications, there is a growing demand of neutron transportation doping (NTD) Silicon in the power market where semiconductor devices require high precision and uniformity of the phosphor dopant in the silicon lattice. For example, a study showed that the demand of NTD silicon from the hybrid car will reach to 157~510 tons in 2020 and 786~2550 tons in 2030 [1].

In response to such demands, a new research reactor called Kijang research reactor (KJRR) was decided to be built as a major national project for nuclear science and engineering in

Korea. It aims 1) to meet the domestic and global needs of medical and industrial radioisotopes, 2) to enlarge the supply of NTD silicon doping, and 3) to validate advanced technologies related to the research reactor.

The Korean Ministry of Science, ICT and Future Planning (MSIP) is responsible for coordinating this project by providing its support for stable government financial subsidies, and the local governments is responsible for land preparations including the purchase of land for this project and setting up infrastructures for utilities including the electric power and industrial water line. The Korea Atomic Energy Research Institute (KAERI) is responsible for all the procedures such as development, design, licensing, installation, and commissioning to complete the KJRR project. In this paper, the progress of the KJRR project is presented.

2. Status of KJRR

2.1 Design requirements

The KJRR project was officially launched on the first of April 2012 and is scheduled to take seven years for its construction and commissioning. The KJRR project is intended for filling the self-sufficiency of RI demand including Mo-99, increasing the NTD capacity and developing technologies related to the research reactor. The project includes not only a reactor facility for its operation, but also its utilization facilities such as a fission molybdenum production facility (FMPF), an RI production facility (PIPF) and a radioactive waste treatment facility (RWTF).

The reactor is be composed of low enriched uranium (LEU) U-Mo plate fuel, which is the first-of-a-kind application in the world and characterized by an average 60% high burn-up pertinently. The burn-up test for a fuel assembly is now being carried out at the Idaho National Laboratory (INL) to test and qualify the LEU-Mo fuel. Also, it is designed to produce fission molybdenum 2,000 curies/week as requirement. The main design requirements of KJRR are summarized in Table 1.

Thermal Power	~15 MW (optimized in conceptual design)
Reactor Type	Open Tank in Pool type
Neutron Flux (Max)	> 3.0x1014 n/cm2s (Central Trap)
Operation day	~300 day/year
Life Time	50 year
Fuel Type & Material	Plate Type, LEU U-Mo in Al matrix (U loading: ~8.0 g/cc)
Reflector	Beryllium
Coolant /Moderator	H2O, Downward Forced Convection
Utilization	RI Production including Mo-99 NTD & fast neutron for silicon wafer

Tab 1: Design requirements of the KJRR

2.2 Site development

Site investigation

The site is located in the county called KIJANG in Korea. There are already several nuclear power plants in operation near the site and there has been growing acceptance for nuclear facilities. In addition, the site is very close to Busan which is the second largest city in Korea. Busan has an international airport and harbors which can provide good accessibility for people as well as easy transportation of products.

The geological and seismological investigation was carried out from October in 2012 through January in 2014 in order to obtain a geological and seismic data to determine site suitability. The site investigation was planned in two stages; the first stage is to find an estimate for the elevation of site and the second stage is to obtain geotechnical engineering data. Also, the location of the reactor core was determined by reviewing not only geological information but also a collection of information from architects engineering.

Meteorological tower (Figure 1) was constructed as the first physical structure in the site in August 2014. The location of the tower was selected at a distance of 10 times the height of reactor building considering topography, plant grade, power and communication issues, tower engineering based soil conditions, and accessibility during construction as well as maintenance later. It is collecting basic meteorological data to develop atmospheric transport and diffusion parameters so that potential radiation doses to the public can be evaluated with appropriate atmospheric dispersion models. Also, regulatory body requires 12 month period meteorological data before applying a construction permit (CP).

Site grading work

The local government is responsible for land preparations including the purchase of land for this project and setting up infrastructures for utilities including the electric power and industrial water line. The local government had purchased all lands for the site and KAERI took the ownership from the local government in April 2014. The licensing of the nuclear installations requires the ownership of the site before the CP application.

The site is located in the medical industrial complex. The final design of the complex was approved in January 2014. Then, site grading work was started and completed in October 2015 as shown in Figure 2.

Fig 1. Meteorological tower in the site

Fig 2. Completion of site grading work

2.3 Architectural engineering

Site layout

The site is created in elevations of EL+67m and EL+61m. Figure 3 shows the elevated view of the site.

Fig 3. Elevated view of the site; 1) FMPF, 2) reactor facility, 3), utility facility, 4) RWTF, 5) RIPF, 6) electric building, 7) diesel generator building, 8) stack, 9) cooling tower, 10) demi water system and pump house, 11) natural evaporation building, 12) guard house

In the elevation of EL+67m, a reactor building, RWTF, RIPF, a power receiving facility, a diesel generator building, a stack are located. The reactor building is divided into a reactor section, a FM production section, and a utility section. The building has been designed as a nuclear safety class and seismic category I structure with confinement to satisfy functional requirements. In the elevation of El+61m, a cooling tower, a demi-water system, a pump building, and a natural evaporation building are located.

The Exclusion Area Boundary (EAB) is defined within 160 m radius of the reactor core considering the nuclear source term and the ground release condition regarding the design basis accident. In addition, a double fence is designed around the radius of 200m for the physical protection.

General arrangement

Architectural engineering (AE) company was selected though the tendering system in April 2014. The work scope of AE includes 1) basic and detail design of reactor facilities and related auxiliary facilities, 2) site suitability evaluation, 3) licensing support, and 4) engineering support to procurement, construction, installation, and commissioning. The figure 4 shows the current development of general arrangement.

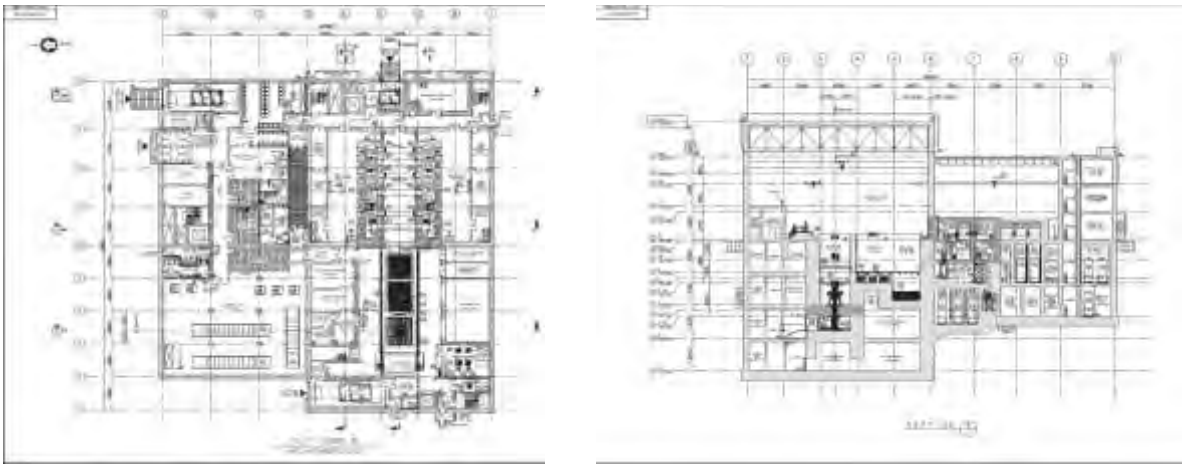

(a) (b)

Fig 4. General arrangement for KJRR, (a) plan view at the first floor and (b) section view in the middle

Operation pool water level is 12m. FM target is designed to be transferred through the service pool to FM processing hot cells. AE is currently working on detail design for supplying

technical documents and preparation of complete sets of the project drawings that at sufficient for construction. KAERI is planning to order the construction by the end of 2016 when the production library for construction work will be prepared.

2.4 Procurement

Contracts for the manufacturing major equipment, such as a reactor assembly package and man-machine interface system, have been made. The manufacturing a reactor assembly is one of critical activities that affect the end date in the project schedule. The term of the contract is 38 months for design, manufacturing, and delivery. Manufacturing items also includes the bottom-mounted control rod drive mechanism (CRDM) that can provide the advantage of easy access for the loading and unloading of RI targets.

Fig 5. Partial cross sectional view of reactor assembly

2.5 Project Schedule

The arranged project schedule is shown in Figure 6. The Preliminary Safety Analysis Report (PSAR) was completed and an application of CP was filed to the Nuclear Safety and Security Commission (NSSC) in November 2014. The PSAR is being carefully reviewed by the NSSC. It is expected to take one year for reviews and a physical construction will proceed when the CP will be issued. Then, the application of the operation license would be scheduled in September 2017 and the initial criticality will be achieved in March 2019.

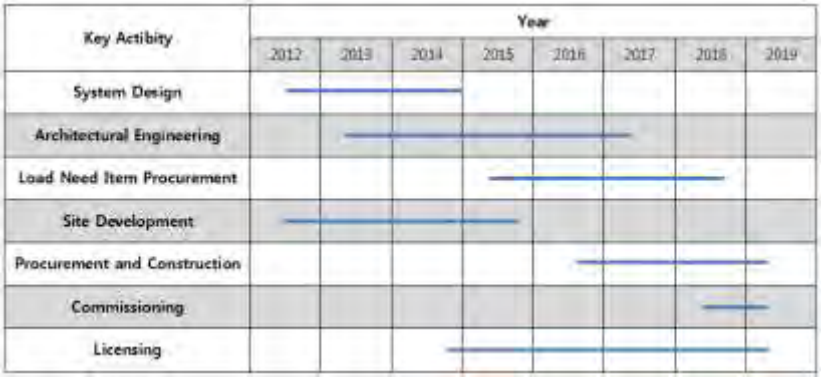

Fig 6. Arranged KJRR project schedule

3. Concluding remarks

Domestically, the KJRR project will provide self-sufficiency in terms of medical and industrial RI supply. It will greatly enlarge the RI industry in Korea as well as the power device industry though NTD service. Internationally, KJRR will be the first application of U-Mo plate type fuel for research reactors in the world. It will be sharing the knowledge and experience from the project. After the completion of construction, it will serve as a regional reactor whose benefit can be shared by increasing medical RI supply in world.

4. References

[1] M.S. KIM and et al., “Estimation of Future Demand for Neutron Transmutation Doped Silicon caused by Development of Hybrid Electric Vehicle and its Supply from Research Reactors”, presented at the 13th Int. European Power Electronics Conference, Spain (2009).

[2] OECD/NEA, “The Supply of Medical Radioisotopes”, The Path to Reliability, NEA No. 6985 (2011).

[3] I.C. LIM, “Plan of New Research Reactor Construction in Korea”, ICRR-2011 (2011).

[4] S.I. Wu, T.H. Kwon, I.C. Lim, J.J. Ha, “Korean New Project for the Jijang Reseach Reactor”, SMiRt-22, San Francisco, USA (2013).

REVIEW OF POOL-TYPE RESEARCH REACTORS DESIGN AND UTILIZATION-RELATED FEATURES IN LIGHT OF UP TO DATE PRACTICES

Claude PASCAL
Research Reactors & Installation Department, AREVA TA
PO Box 50497, 13593 Aix en Provence Cedex 3 - France
Jerome ESTRADE
Nuclear Energy Directorate, French Alternative Energies and Atomic Energy Commission - Cadarache Research Centre- PO Box 789, 13108 Saint Paul Lez Durance - France

ABSTRACT

Among the population of high performances multipurpose and MTRs research reactors that can perform the same applications with similar flux performances, there are various pool-type designs. Some have open core designs; others have tank-in-pool designs with various grades of primary cooling circuit enclosure and leak tightness.

This paper presents from user, operator and designer perspectives the main outcomes of the overall reactor architecture, mainly on the basis of French MTR lessons learned. After an introduction and presentation of the stakes, the main topics which will be described in the paper will cover:

- A reminder of the main possible overall architectures of pool-type reactors highlighting the pool contribution as regards the core cooling system and the containment of radioactive products under normal and accidental conditions,
- A discussion of differentiating outcomes of the overall reactor architecture including:
  - Utilization-related considerations regarding experimental irradiations and radioisotope production: flux performances, versatility of use
  - Operational considerations: availability-related concerns including refuelling outage and periodic inspection and testing, water chemistry control, radiation protection of operating personnel especially during normal operation and anticipated operational occurrences (e.g. activity increase in the primary circuit and radiolysis phenomena)
  - Safety considerations focused on the main safety functions, namely the cooling and containment functions

As concluding remarks, the possible designs according to the user needs are defined including an overview of the discriminating topics.

1 INTRODUCTION

Among the population of high performances multipurpose and MTRs research reactors that can perform the same applications with similar flux performances, there are various pool-type designs. Some have open core designs, others have tank-in-pool designs with various grades of primary cooling circuit enclosure and leak tightness. The purpose of this paper is to discuss different design features in light of current context considering more demanding radiological doses constraints and safety requirements such as extended design conditions in the safety assessment.

The paper is mainly illustrated with French research reactors and is focused on Material Testing Reactors utilized for material testing (material and fuel) and radioisotopes production since the design of neutron sources with neutron beams is more clearly driven by flux performances.

The main characteristics of pool-type research reactors are the direct view and access to the reactor block, the efficient shielding and the huge thermal inertia of the pool water.

In terms of requirements for a new built RR, the current trend could be characterized by:

- the continuation or increase in the stringency of utilization and operational requirements:
  - irradiation capabilities (irradiation location number and high thermal fluxes),
  - operating time at full power,
- decrease in the radiation doses to operating personnel and users,
- increasing importance given to the 4th line of defense–in-depth (ref <1.> considering design extension conditions such as extended loss of electrical power and design extension hazards (natural and human induced hazard from higher intensity than those considered in the design conditions),
- an increase of the cost pressure constraints.

This set of requirements is so called “modern requirement” in the paper.

2 REACTOR TYPES

Among the different overall research reactors designs, the following types ranked according to increasing potential neutron flux performances and/or power are encountered:

- **Open-core downward flow (fig.1)**: in this design the fuel assemblies are plugged into a grid and the pool water is sucked downwards for core cooling. SILOE and FRG1 reactors (both decommissioned) belong to this class. The reference pressure of the primary circuit is the hydrostatic pressure of the pool at core inlet. At shutdown, the core is cooled by natural convection of the pool water thanks to passive opening of flap valves located under the core and flow reversal once the primary pump flywheels inertia effect has been exhausted.

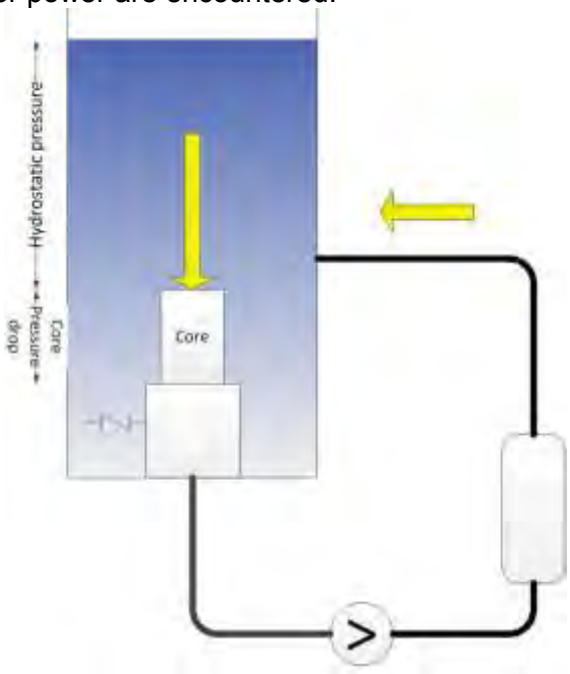

- Figure 1: Open core downward flow

- **Open-core upward flow**: in this design, the core is housed in a box having a chimney opened to the pool at core outlet fixing the pressure reference of the primary cooling circuit. In terms of water flow, the design is such that a continuous ingress of pool water inside the primary circuit is ensured; the global water mass balance in the circuit is obtained thanks to the continuous extraction towards the purification circuit or bypass in case of unavailability of the purification circuit, eventually going back to the pool. OSIRIS, OPAL and HANARO belong to this class. At shutdown, the core is cooled by natural convection of pool water once the primary pumps flywheel effect is exhausted and the natural convection flap valves located at the inlet of the primary circuit are passively opened.

- Figure 2: Open core upward flow :

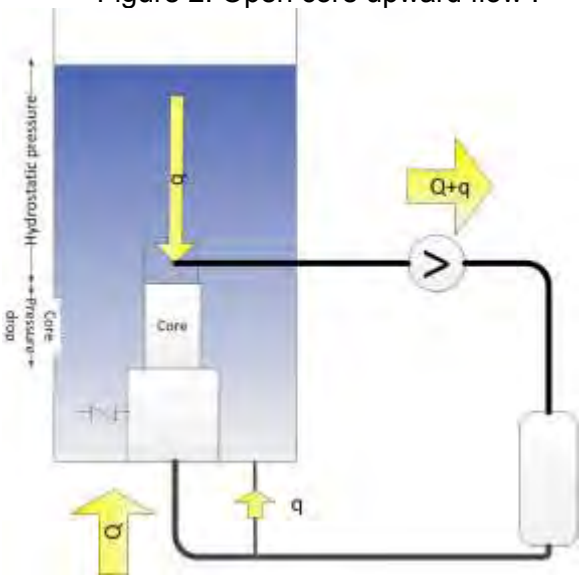

- **Tank-in-pool open primary circuit with pressure reference from the pool**: in this design the core is housed within an enclosed tank. The primary circuit is enclosed as well except for a piping linking the primary circuit (e.g. pump inlet) to the pool thus allowing mass change within the primary circuit and setting the pressure reference of the primary circuit (depending on the design it could be the pool hydrostatic pressure or a higher pressure when a pressurising system has been implemented on this pipe). This class of design can be applied to the 2 possible core cooling flow directions: ORPHEE, FRM II downward flow and JHR upward flow. At shutdown, the core is cooled by forced convection for a couple of hours depending on the core power density before the primary circuit can be opened to the pool and cooled by natural convection.

Figure 3: Tank in pool open primary circuit with pressure reference from the pool

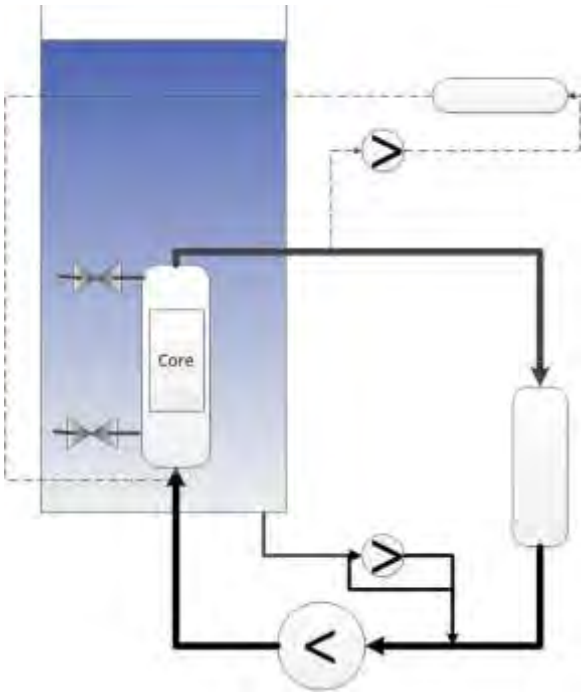

- The last design type consists in **tank-in-pool with an enclosed leak tight primary circuit**. In this design, the primary water is totally segregated from the pool water. Typically, the tank-in-pool research reactors cooled with heavy water belong to this class (e.g. HFR/ILL Grenoble). At shutdown, the core cooling is generally ensured by forced convection. Natural convection cooling capability could be implemented but its use has to be limited to the highest level of defense-in-depth because of the heavy water (tritium activities). It is interesting to notice, as shown on figure 4, that some research reactors in this class (e.g. sister reactors SAFARI and HFR/Petten), presenting neutron fluxes accessible with other types of design, do exist as well. In these cases, the design seems to have been driven by the confinement of radioactive release in the primary circuit.

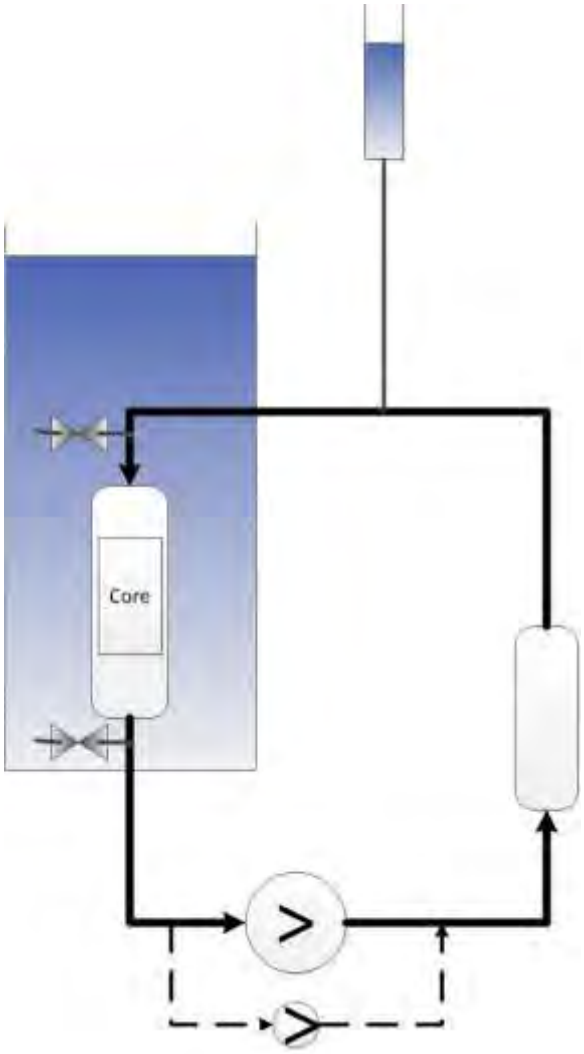

Figure 4: tank in pool leaktight

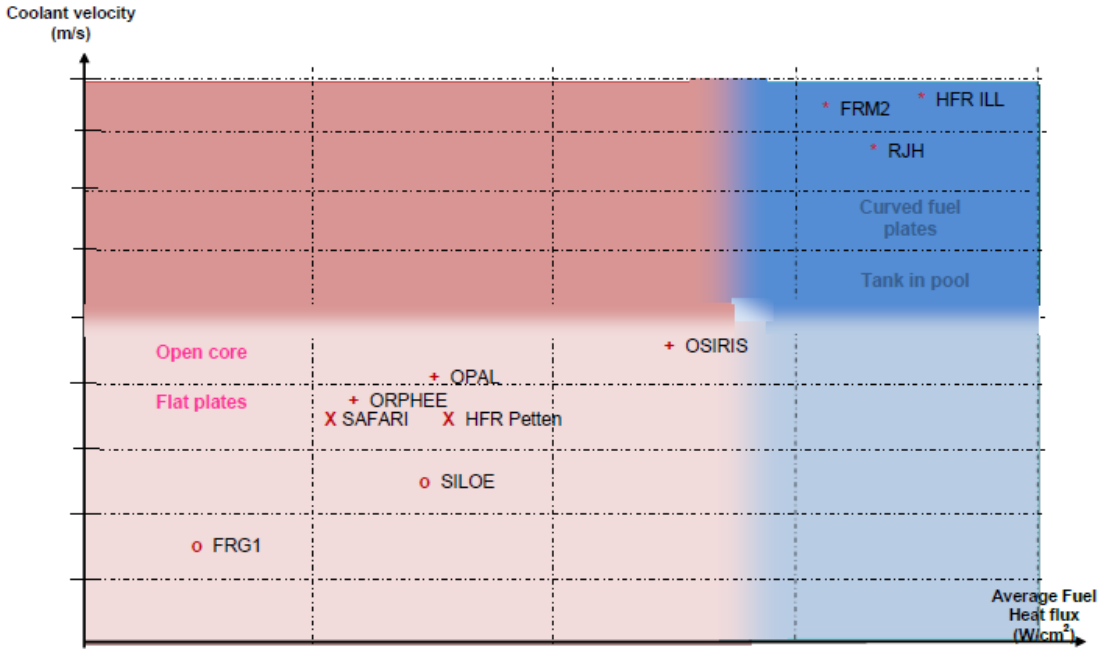

Figure 5: Design type versus cooling *

* *showing the maximal heat flux changes the ranking of the JHR: highest heat flux*

3 DESIGN AND CONSTRUCTION

3.1 Confinement of radioactive materials

Research reactors usually implement the concept of the 3 confinement barriers:

- the confinement first barrier is ensured by the reactor fuel clad,
- in the case of an open core design, the second confinement barrier is the pool water, the pool liner and the primary circuit outside the pool. This definition might be subject to criticism especially for people familiar with PWRs.
- the 3rd confinement barrier is ensured by the containment i.e. the means of containment: building and associated ventilation according to IAEA definition (see ref <1.>).

Except for the noble gases, the pool water is very efficient to ensure confinement of fuel fission products. Having the same efficiency with a containment enclosure would lead to meet a leaktightness requirement significantly lower than specified value for the most stringent confinement class according to the ISO standard ref <2.>.

The genuine concern for research reactors is to prevent the dewatering of the core and therefore to maintain a sufficient water level above the core. For French research reactors, the practical elimination of the core dewatering event is ensured by the water retention within a water block and the amount of pool water compared to the decay energy from the core. This water block concept has been implemented on French RRs for a long time (e.g. today decommissioned research reactor SILOE already had this feature). Regarding the retention of water to provide a long grace period before having heat sink issue, it is obvious that due the respective values of thermal power and water inventory, this type of feature can generally not be met by NPPs.

For open core downward flow design type, the delay time of circulation within the primary circuit induces a decay time of radioactive elements in the pool water, mainly for N16.
For the other isotopes, the transit time is too short to have a significant decay impact. The barrier efficiency and characteristics rely on the pool water and hot water layer. However, in the event of clad failure or even fuel melting, the kinetics of fission products release from the core to the hall is slow enough to allow egress of the operating personnel from the reactor hall (cf <3.> SILOE nov 1967).

For the open core upward flow, the primary circuit works under dynamic confinement (see fig 2) since there is a permanent pool water ingress in the primary circuit at core outlet and since the corresponding flow of primary water (required to maintain the mass balance) returning to the pool is purified before being exhausted to the pool. In this design, an efficient protection of the operating personnel is ensured as proved by the lessons learned from OSIRIS: when operated before using silicide fuel, OSIRIS experienced several clad failures; however it was never required for the operating personnel to evacuate the reactor hall since the radiological consequences in the hall were very limited.

For a tank-in-pool, as soon as there is a communication between the primary circuit and the pool, even if the core tank is maintained enclosed when the reactor is shut down, it is really difficult to credit the primary circuit as an efficient barrier in the safety analysis without defining an operating condition leak-tightness of the primary circuit boundary. If it were to be the case, monitoring the leak-tightness of the primary circuit boundary would be quite challenging (e.g. there are necessary water ingress/egress to accommodate changes due to temperature variations). There is a risk, to be forced to introduce a lot of complexity for a very limited benefit in terms of limitation of radioactive products dissemination out of the primary circuit.
In any case, the tank-in-pool design requires an off-gas system collecting and managing the gases coming from the primary coolant (radiolysis gas for example…) in the reactor block.

Crediting the primary circuit boundary as confinement barrier is only for the last type of design i.e. when the primary circuit is totally enclosed, leak tight and independent from the pool.

3.2 Chemistry of primary coolant

Usually, the required primary coolant chemistry is obtained by controlling the resistivity of the demineralized pool and primary circuit water and the natural acidification of demineralized water leading to a pH stabilization in the range of 5-7. This pH value is fortunately convenient in most of cases including open core RRs. More stringent pH control is required for especially high flux reactors requiring special care concerning the prevention of fuel cladding corrosion. In these cases, the primary circuit has to be enclosed for cooling capability reasons facilitating adequate water chemistry control.
Chemistry of the primary coolant does not seem to be a driver regarding the open core vs tank-in-pool design.

3.3 Cooling

The fuel cooling capability directly drives the reactor neutron flux performances. Depending on the required flux performances, different designs (cooling, fuel plate, pressure…) are possible. Their limits depend on the implemented safety analysis approach (accidental transients and combination of biases, uncertainties and tolerances).
Of course, the coolant velocity between the fuel plates is the first main driver of the cooling capability.

3.3.1 Normal operation and anticipated operational occurrences

The main comments regarding the different design types are as follows:

- Open core downward flow
  - This concept can be implemented as long as for all design basis conditions for which forced cooling is required, the net pressure suction head at pump inlet is compatible with the pump efficiency. This is the main limiting factor of flux performances.
  - At shutdown state, the flow reversal induced by the establishment of a natural convection cooling (when the primary pump flywheel effect is finished) is challenging for the computer codes qualification. Despite this difficulty, this configuration works very well on a lot of research reactors.
  - Regarding the transition towards cooling at shutdown in the event of loss of flow, everything is passive and does not require any operator action, nor any automatic action.
  - The "Achilles tendon" (especially for high flux reactors) of this design is the fuel cooling blockage. The preventive measures are usually administrative measures. Engineered features could be implemented to decrease the occurrence likelihood of such event but they limit the access to the core which is the essential benefit of this design.
- Open core upward flow
  - This design provides a higher cooling capability than open core downward flow. The limiting factors are the coolant velocity inside the core and the margin against reactivity injection (command control rod ejection or experimental device ejection). The first limiting factor is not actually an issue since the second one is the driving parameter. The coolant velocity may induce curving of the fuel plate, limiting the vibration risk (impacting the fuel assembly cost) or in extreme cases difficulties of passive dropping of the neutron absorbers when they are subject to core cooling conditions.
  - The transition towards core cooling at shutdown is totally passive and the heat sink is the pool which may provide a huge grace period before any action is necessary. In a modern safety approach, this design is especially interesting because of its robustness when adequately sized.
- Tank-in-pool open primary circuit with pressure reference from the pool
  - Basically, this design allows, compared to open core, for higher performances thanks to the increase of the cooling capability due to the pressure increase in the core. Both coolant circulation directions can be found on existing designs.
  - Above a certain performance level, it is required to force the cooling at shutdown during a very limited period of time (up to a couple of hours for the most performing research reactors). The pumps are usually powered by an UPS (Uninterruptible Power Supply) as backup.
  - One important question is the cooling at shutdown. In particular, is it allowed or not to open the primary circuit to the pool at shutdown? When an enclosure is not required, passive transition to natural convection is possible and the huge thermal inertia of the reactor pool can be used, thus providing a long grace period.
  - In the modern safety approach, additional independent means of forced cooling including power supply would be implemented to cope with design extension conditions; this has been done for the JHR.
- Tank-in-pool with totally enclosed primary circuit
  - In terms of cooling capability, there is no difference among the various candidate architectures of tank-in-pool reactors. For this design, up to now there is no identified example of long term passive cooling of the core at shutdown state maintaining the primary circuit enclosed.

- The usual solution regarding long-term passive cooling consists in opening the primary circuit to the pool allowing natural convection cooling of the core and involvement of the reactor pool huge inventory providing long grace period. Human action or automatic action could be required to open the primary circuit to the pool.

3.3.2 Behaviour in the event of accidents

- Loss of flow
  - The transition towards core cooling at shutdown is usually ensured with flywheels on the primary pump shaft allowing natural convection initiation or time for starting the shutdown cooling pumps. When high neutron fluxes performances are required, maintaining forced cooling in the core is required during a limited period of time (up to a couple of hours).
- Loss of coolant
  - The large pipe breakdown is unlikely for research reactors whatever their design. Since the loads are minimal, the likelihood of occurrence of such an event is lower for an open core design than a tank in pool design type.
  - The characteristic of loss of coolant is the fact that the pressure is imposed at the pipe breakdown location. Therefore the primary circuit pressurization which characterizes the initial state of the transient is from a second order compared to the location and geometry of the primary piping which drive the cooling capability during the accidental sequence.
- Reactivity injection
  - To cope with reactivity injection transients when required neutron fluxes increase, once the coolant velocity has been increased, it could be required to also increase the second cooling capability driver i.e. pressure in the core as shown on fig 5.

3.4 Complexity of the system

The complexity of the reactor design increases because of the core performances and the closure of the primary system which makes the total number of functions and SSCs increase and because the functions are being ensured by active features instead of passive features.
The ranking is the same as shown in §2

Table 1: required systems according reactor designs

		Open core downward flow	Open core upward flow	Tank in pool	Tank in pool enclosed primary circuit
Reactor block	Inlet plenum				
	Outlet plenum	x	x	x	x
	Chimney				
	Core box				
	Natural convection valves	X flap valves	X flap valves	X valve if any	X valve if any
Cooling systems	Flywheels	x	x	x	x
	Shutdown pumps	-	-	x	x
	Emergency cooling system		lines	x	x
	Irradiation devices cooling system	Ensured by primary cooling system	Ensured by primary or reflector cooling system	x	x
	Primary circuit pressurization system	-	-	x	x
	Reflector cooling system	-	x	x	x
	Extended design conditions core cooling systems	To be discussed	To be discussed	x	x
	Extended design conditions pool cooling systems	-	Depending on the power and pool size	Depending on the power and pool size	Depending on the power and pool size

Table 1 outlines the specific systems to be integrated in the design for the different architectures. Most of them are safety or safety related systems. It reflects the increase in the complexity according to the design type. As a consequence, there are significant impacts on the engineering and construction costs of the reactor

3.5 Regulatory requirements

Among the regulatory requirements, the pressure equipment regulation could have a significant impact on the design of the reactor block components since the open core design types are not concerned. Currently, the JHR experiences significant impact on the project resulting from the French nuclear pressure equipment regulation since it requires specific design features and regulation conformity assessment under notified body surveillance.

3.6 Radiation protection

The protection of operators against radiation and radioactive products issued from the reactor are ensured on French research reactors by the following features:

- The shielding against external exposure is ensured by 2 different water layers:
  - location of the reactor core deep in the pool as usual for all the pool-type research reactors, the pool water activity being controlled by the purification circuit (mainly limitation of Na24 activity). The most significant radiation sources of the pool water are the activated products (Na24, Co60) issued from the aluminium (e.g. fuel cladding, reactor block or stainless steel components issued from reactor block components or primary circuit

- a hot water layer made of purified and heated pool water in order to establish a stable and clean water layer providing efficient shielding against radiations issued from the rest of the pool. This design feature is widely used but some research reactors do not have it (alternatives are a lid with an opening or nothing).

- protection of operators against radioactive gases issued in the pool water (and the reactor) is ensured by the collection and extraction at pool surface towards the HVAC system preventing the dissemination of radioactive products into the reactor hall. This design feature consisting in a sweeping of pool surface with clean air has been implemented on all French RRs for a long time no matter the RR design.

The operators and users external radiation doses records of French RRs (see ref <4.>) demonstrate the suitability of this design features and their sizing. At OSIRIS, among 150 concerned operators and users, the so-called critical group of personnel is made of the 60 people ensuring in-pool handling or working on the reactor, fuel and isotopes. A typical figure of annual collective dose is in the order of 15 man.mSv and the average annual dose of the critical group members is in the order of 0.2 mSv. None of them has received annual doses greater than 3 mSv for a long time (>15 years).

Records lead to the conclusion that the theoretical potential advantage of tank-in-pool is not decisive. Hence, any type of design when adequately sized and operated can achieve the current and future radiation doses targets.
For the new generation JHR, since the shielding sizing has targeted lower radiation rates at the pool border, it should be even lower.
In this regards, the presumed advantage of a tank-in-pool reactor is actually not significant.

3.7 Flux performances

The neutron flux performances drive the cooling capability which drives the selection of the design type. Above a certain threshold, each type of design reaches its limits and it is required to select a design allowing for higher cooling capacity as shown on fig.5.

4 OPERATION

4.1 Refuelling operation

Open core designs, since they require less operation before accessing to the fuel assemblies to be handled during core outages, would be more suitable.
The analysis of lessons learned from existing reactors shows that the impact of the design is generally from a second order of magnitude on the outage duration. The shortest outages are achieved by tank-in-pool research reactors demonstrating the existence of other driving parameters.

4.2 Maintenance, In-service inspection and testing

The in-service inspection programme results on one hand from the reliability and ageing considerations of SSCs for nuclear safety purpose and on the other hand from regulatory requirements such as pressure equipment regulation. Globally, the trend is an increase in their stringency. Tank-in-pool designs have more components subject to pressure equipment regulation. Within the modern safety approach, this induces more components to be inspected and periodically tested as outlined in table 1. At least, the difference between open core and tank-in-pool in terms of perimeter concerns the core vessel and core inlet and outlet pipelines for regulatory reasons as well as the SSCs ensuring the forced core cooling at shutdown including the support systems.
Even moderated, the impact on the in-service inspection and testing programme is significant. Tank-in-pool reactors have more SSCs as outlined in table 1. The workload and

potential impact on the reactor availability directly depend on their number. Tank in pool reactors would require more work than open core reactors.

4.3 Operation time at full power

The current target of new designs is generally over 250 FPDY and up to 300 FPDY.
Basically, the operation time at full power results from:

- Core cycle duration: not concerned since independent from considerations addressed in this paper
- Refueling outage duration: as discussed in §4.1, this parameter is only slightly impacted by the reactor design. Once special reactor designs have been excluded, it could be considered as not significant regarding the concern addressed in this paper
- Unplanned shutdown: for existing French research reactors, the records show that they are limited to 3 % (see ref. **Erreur ! Source du renvoi introuvable.**) i.e. in the order of magnitude of a week per year including irradiation devices contribution for half the total for OSIRIS.
- Shutdown for maintenance, inspection and testing: as discussed in §4.2, this contribution could be considered as significant especially when the target is over 250 FPDY. The regulatory requirements and outcomes of the licensing process seem also sensitive. The replacement of the core box or reactor vessel for ageing reason has a significant impact on this parameter even if not frequent (once or a couple of replacements during the plant lifetime).

Common sense presumes that the more complex the reactor is, the less favourable regarding its operation time at full power it is. Actually, the records don't always reflect this correlation. It seems that the way to operate and maintain the reactor to meet the needs of the utilization programmes is still the dominant driving parameter of the existing fleet.

4.4 In core measurements

An additional interesting characteristic of an open core is the easiness of access facilitating neutron flux mapping by measurements. Despite the progress made in the accuracy of neutronic computer codes, this capability remains especially suitable for material testing reactors having to accommodate during their lifetime very different irradiation programmes using a wide diversity of irradiation devices (capsules and loops).

For tank-in-pool design, having this function is more complex and expensive since it requires a specific configuration in terms of hardware and safety documentation.

5 UTILIZATION

5.1 Irradiation location configuration

To meet the target of irradiation and radioisotopes production which will necessarily be evolving during the lifetime of the reactor, the reactor has to offer irradiation locations with a wide diversity in terms of neutron fluxes and spectra. In this regards, the most flexible design is the open core as shown e.g. by SILOE and OSIRIS.
In open core downward flow, there is actually no limitation in terms of geometry as long as the core configuration remains within the validity domain of the safety analysis. In addition, the flux performances on irradiation locations are very good compared to the reactor power density since the irradiation could be located close to the fuel and there is no reactor block structure absorbing neutrons between the fuel and irradiation locations.

In open core upward flow, the core box introduces a slight limitation since the geometry usually remains rectangular-shaped. The regular pitch of the core is very suitable as regards the irradiation location.

In open core designs, the in-core irradiation location could benefit from core cooling and primary circuit activity monitoring (and clad failure detection system) and does not require any dedicated cooling system, nor any coolant activity monitoring.

For high performance reactors, due to the pressure increase in the core, the core vessel geometry is more constrained. For the highest primary pressure, the only convenient option in terms of core vessel shape seems to be revolution geometry. The pressure vessel shape imposes geometrical constraints on the irradiation locations.

5.2 Access to irradiation devices

Open core designs are the most favourable regarding the access to in-core irradiation locations at any time, as soon as the bypass when the in core device being handled has been considered in the safety analysis.

For access to in-core irradiation positions within tank-in-pool reactors, the reactor vessel lid leads to awaiting a reactor shutdown to access the in-core irradiations or to having a thimble in the lid and a dedicated cooling system.

6 CONCLUDING REMARKS

The selection of the design is mainly driven by performance considerations.
The introduction of so called modern requirements does not significantly affect the conclusion.
Open cores are simpler; the main advantage with regards to design extension conditions and hazards is the simplistic design and the purely passive transition towards natural convection cooling during a long grace period provided by the huge pool volume. It can be implemented as long as the flux performances to be achieved are compatible with cooling capabilities. When suitably designed and operated, the radiological doses to operators and users can be very low even in the event of anticipated operational occurrence such as clad failure. The versatility and flexibility of use are especially interesting for isotope production and material testing market evolutions.
Tank-in-pool designs are required to achieve higher flux performances. Having benefits from the core boundary as a confinement barrier is clearly in competition with passive core cooling. There is no known example of any proven design meeting all the requirements at the same time. The physical barrier of the tank and the active components ensuring core cooling at shutdown induce constraints on the utilization and operation of the reactor. The respective advantages and disadvantages of each design type are amplified by the modern context.

7 REFERENCES

<1.> NS R 4 Safety of research reactors
<2.> ISO 10682 Containment enclosures – classification according leak tightness and according checking methods
<3.> SILOE – Nov 1967
<4.> OSIRIS – operation records -

CONCEPTUAL DESIGN OF A LOW-POWER HYBRID RESEARCH REACTOR FOR EDUCATION AND TRAINING

I.C. LIM, S.T. HONG
Research Reactor Utilization Department, KAERI
111, Daedeok-daero 989beon-gil, Yuseong-gu, Daejeon, 34057 – Korea

ABSTRACT

Since the birth of first nuclear reactor in 1942, the low-power research reactor(LPRR) has been considered as a good tool for the education on nuclear engineering and the training of engineers. In addition, the number of newcomers who wish to introduce LPRR for education and training as well as for infrastructure building is increasing. Even though the demands for LPRR exist, the revolution of LPRR design is not fast. It is believed that the important elements of revolution are intrinsic safety and innovative design. The intrinsic safety includes a large negative power coefficient and passive decay heat cooling. The innovative design includes the provision of versatile experiments and utilizations which will make the contents of education and training deeper and wider. The reduction of fuel cost and ensured availability will be also necessary for the economy and sustainability in facility management. KAERI is developing a new concept LPRR, i.e., a hybrid core LPRR. This can be operated in critical mode for nuclear experiments, NAA and the production of RI for research purpose. If a slant beam tube is installed with super mirrors, neutron imaging can be performed as well. The unique feature of this concept is the split core concept which allows an empty space at the center of core structure by moving the half of core in horizontal direction. This area can be used for the experiments in sub-critical condition such as the neutron flux distribution in a selected cell arrangement, kinetic experiments and detector response experiments which will make the students or trainee experience more physical phenomena. The fuel is UO_2 in Zr-4 cladding which has been used for many years in NPP and are safe enough in low temperature and low pressure condition. In addition, the availability of fuel will be not a problem.

1. Introduction

Many countries have used LPRRs as tools for educating and training students or engineers and for scientific services such as neutron activation analysis[1]. The constructions of LPRRs were very active in 1950s and 1960s. In the 1950s, following the birth of the first nuclear reactor in 1942, the main objective of nuclear technology shifted from experimental demonstrations of theory to the development of application technology. Professional education for nuclear technology was disseminated to universities and many LPRR models such as ARGONAUT[2], AGN[3] and TRIGA[4] reactors were developed in this period. The 1960s were the period for the developed models to be constructed in many countries. In 1970s, AECL developed the SLOWPOKE for isotope production and neutron activation analysis at universities, hospitals, and research institutes[5]. In the 1980s, China remodeled SLOWPOKE as MNSR and it was built in several developing countries[4]. Table 1 shows the status of low-power research reactors constructed under brand names. AGN and ARGONAUT were developed for universities with a consideration of their financial burden, and were thus limited in terms of design changes or power upgrades to accommodate varieties in utilization. This has made 70 to 80% of them be decommissioned or in a prolonged shutdown. 60% of TRIGAs are still in operation. However, the TRIGAs in universities in the USA are believed to be faced with some difficulties in utilization[6].

Name	Decommi-ssioned	Prolonged Shutdown	In Operation or Temporary Shutdown	Total
TRIGA	19(8)	7(1)	37(12)	63(21)
AGN	16(16)	1(0)	7(7)	24(23)
ARGONAUT	19(5)	5(0)	5(3)	29(8)
SLOWPOKE or MNSR	7(2)	9(0)	12(1)	19(3)

※ No. in parenthesis : No. of RRs in universities

Tab 1. Status of Brand-Name Low-Power Research Reactors

As the introduction of a research reactor is considered as a stepping stone for a nuclear power development program, many newcomers are considering implementing an LPRR. Considering that a research reactor is a long-lasting and costly scientific tool, one should be very cautious in defining its user requirement and the selection of the design[6].

The key elements of the design of an LPRR should be safety and innovative design. In view of safety, the followings are key factors mentioned in the IAEA guideline for the research reactor bidding process[7]. In view of safety, the followings are essential[6]:

- A negative power coefficient as large as possible
- Adoption of passive decay heat cooling
- No fuel failure during a transient

In view of an innovative design, the followings should be considered[6]:

- Design to bring balance between a computer analysis and experiment in a nuclear education program by providing
  - Something more than conventional reactor experiments such as a criticality approach and rod-worth measurement,
  - Experiments to simulate typical fuel arrangements and
  - Training on the use of in-core instruments
- Adoption of technologies used in high-power beam reactors to maximize the neutron flux level for utilization
- Reduction of fuel cost
- Design of reactor and labs for neutron activation analysis(NAA), which will be helpful for revenue generation

KAERI is developing a new concept LPRR, i.e., a hybrid core LPRR which will provide the safety and design characteristics as above. This LPRR can be operated in critical mode for nuclear experiments, NAA and the production of RI for research purpose or in sub-critical mode in which an empty space available at the center of core structure by moving the half of core in horizontal direction allows the experiments such as the neutron flux distribution in a selected fuel arrangement, kinetic experiments and detector response experiments. If a slant beam tube is installed with super mirrors, neutron imaging can be performed as well. This paper describes the characteristic of this hybrid LPRR in design as well as utilization.

2. Characteristics of the Hybrid LPRR

2.1 Design

The core parameters of the hybrid LPRR in Table 2 show the design characteristics. It is a 70 kW pool type research reactor using water as coolant and 5% enriched UO_2 fuel in Zr-4 clad. The core shape is almost cubic, 32.4x32.4x32 cm, which minimizes the neutron leakage. The reflector material is graphite and the fuel burn-up is compensated by increasing the amount of graphite reflector. The reactor has one control rod and two shut-down rods which are inconel tubes having B4C powder inside. The use of two shut-down rods satisfies n-1 criteria and the shut-down margin is evaluated to be 12 mk. By using the UO_2 fuel, the amount of negative power feedback from shut-down to full power stage can be maximized and it is -1.54 mk. The UO_2 fuel with Zr-4 clad has been used so widely in nuclear power

reactors which operate in high pressure and high temperature conditions that the application in atmospheric pressure and low temperature condition has no safety concern. In addition, it can be obtained easily in a relatively lower price. The proposed reactor can operate more than 20 years without refueling if the reactor operates 40 hours per week at its full power. Figure 1 shows a plan view of core and the concept of graphite reflector for fuel burn-up compensation.

Component	Parameter	Value
Core	Power (kW)	70
	Average thermal neutron flux (n/cm^{2}s)	0.5x1011
	Size (WxLxH in cm)	32.4x32.4x32
Fuel Rod	Fuel material	UO_2
	Clad material	Zr-4
	Fuel radius (mm)	4.096
	No of rod	321
Reflector Material		Graphite
Structure Material		Al 6061T6
NAA Irradiation Holes	Location	Out of core
	No of holes	2
	Inside Diameter(cm)	3

Tab 2. Values of Major Characteristic Parameters of Hybrid

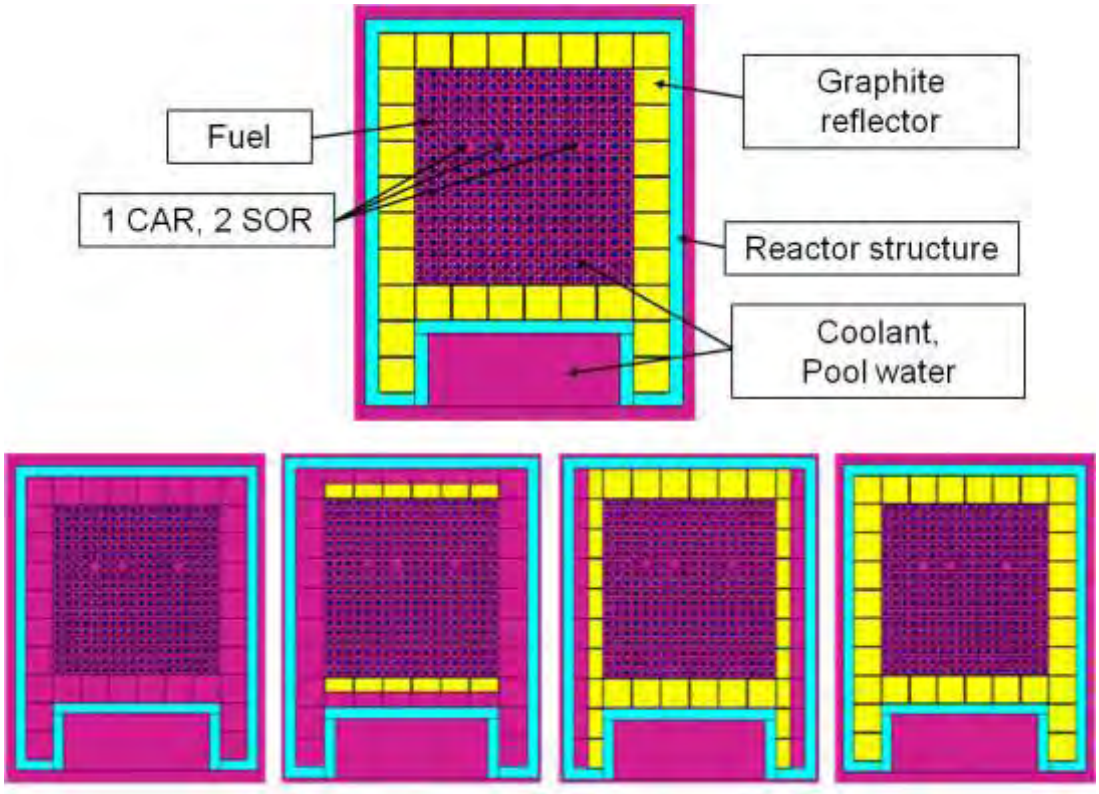

Fig 1. Plan View of Hybrid LPRR core and Concept of Burn-up Compensation

Figure 2 is a bird eye view of the reactor structure and a plan view of reactor pool. In the reactor shown at the left hand side of this figure, the central empty space is provided by moving the half of the core in a horizontal direction by using a mechanical system.

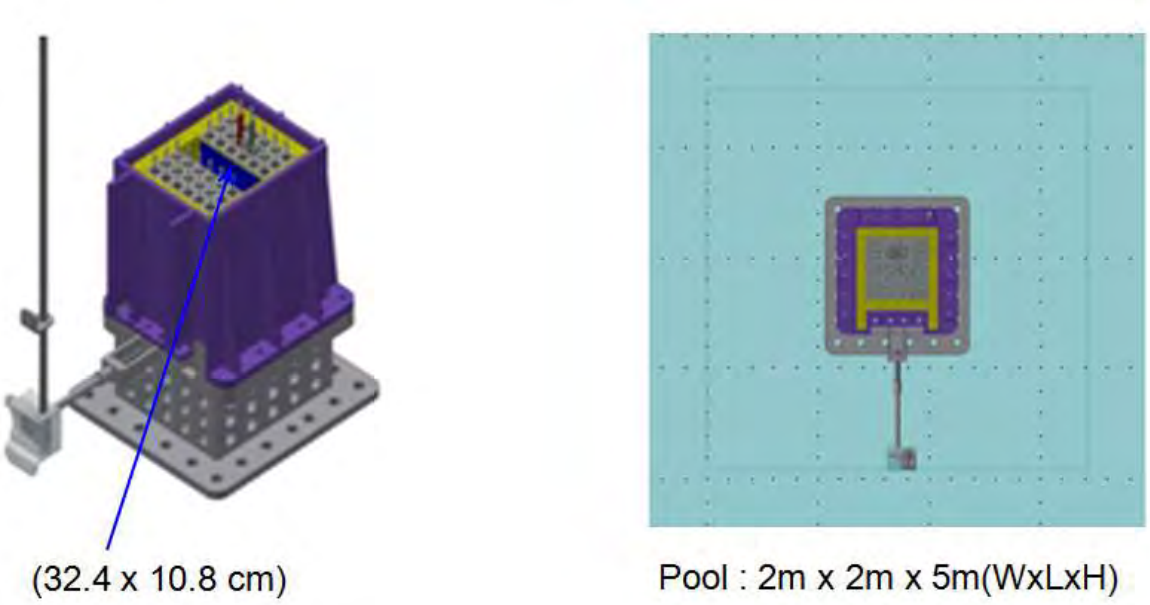

Fig 2. View of Reactor Structure and Reactor Pool

The schematic diagram of pool cooling and purification system is depicted in Figure 3. As in this figure, the purification system is incorporated into the pooling cooling system.

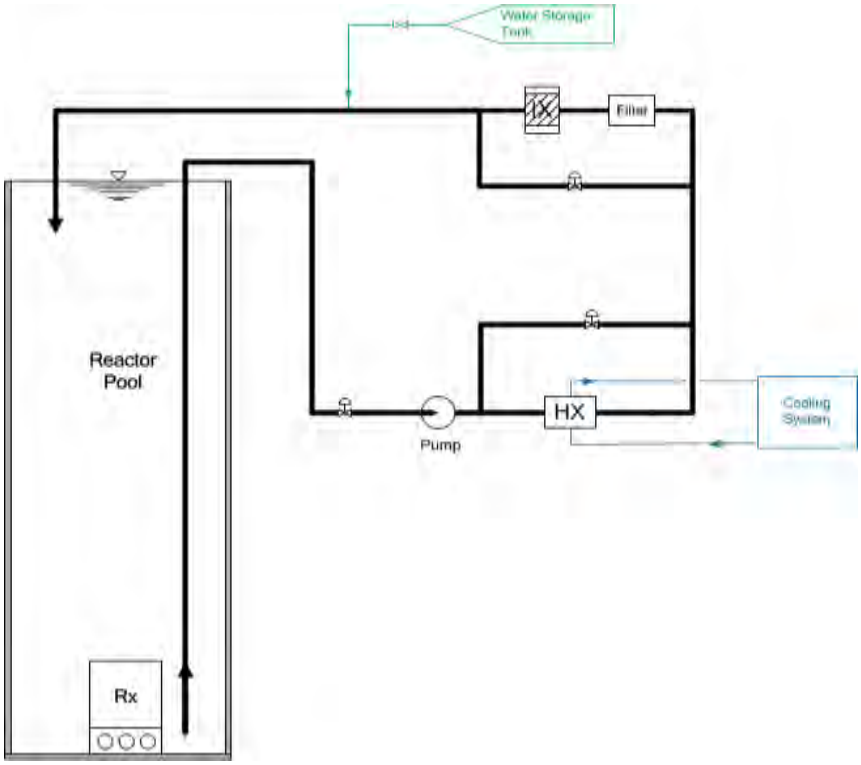

Fig 3. Schematic Diagram of Pool Cooling and Purification System

Figure 4 is a typical general arrangement of major facility spaces such as reactor pool, control room, pool cooling equipment room, ventilation equipment room and NAA room. For this arrangement, the size of reactor room is 8mx8m which is believed to be large enough to

accommodate the students performing reactor experiment. Arranging a NAA room as a part of reactor facility makes the sample transfer time short and makes the ventilation system compact. As there is no horizontal beam tube, the pool structure is buried into ground.

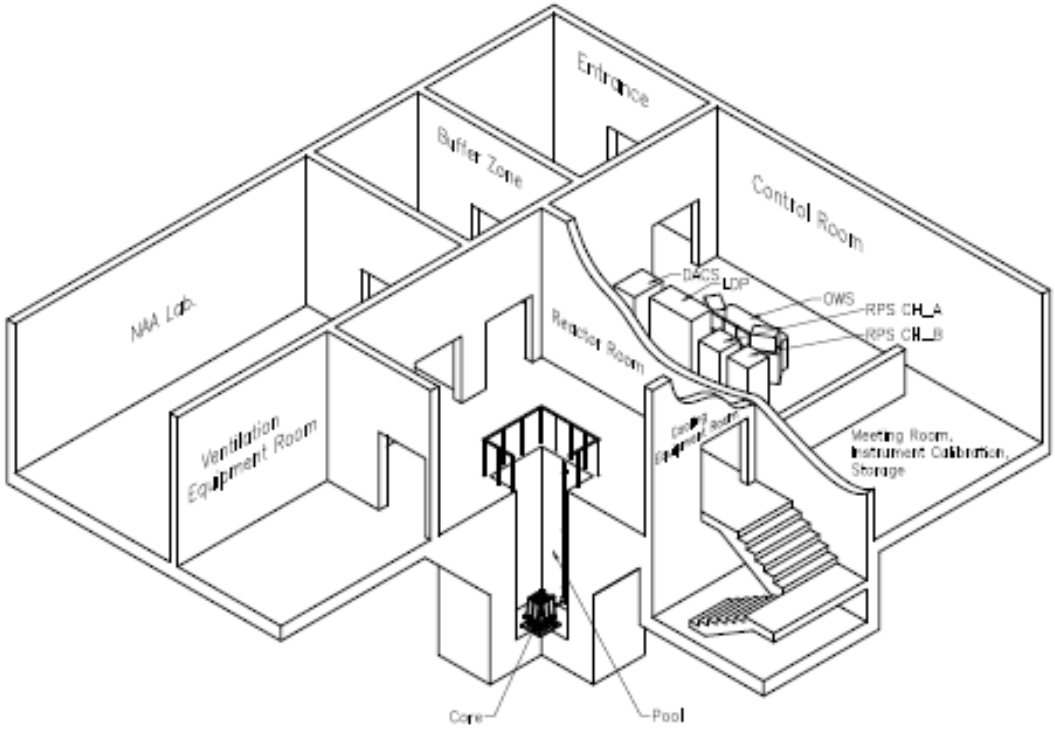

Fig 4. Arrangement of Major Spaces

2.2 Utilization

The reactor is equipped with two irradiation holes of 3 cm in diameter for NAA. The thermal neutron flux at the holes is 10^{11} n/cm^{2}s and the Cd ratio is between 10 and 20. The rabbit can be transferred manually or automatically depending on the user requirement.

The irradiations holes for RIs can be easily prepared by replacing some reactor fuels with irradiation tubes

If a slant beam tube having super mirrors is inserted at the side of core, the thermal neutron flux in the range of 10^5 n/cm^{2}s can be obtained at a typical sample table location which is about 5 m far from the side of reactor structure. This neutron flux is high enough for the imaging experiments for education purpose.

The conventional reactor experiments available from this LPRR will be as follows.

- Reactor period measurement
- Critical mass measurement
- Control rod worth measurement
- Neutron flux measurement
- Temperature coefficient measurement
- Measurement of the effect of reflector on reactivity

In addition, the following experiments will be typical experiments which can be performed if the core is in the split mode:

- Neutron spectrum measurement in arrays designed for education
- Measurement of the reactivity effect of inserted materials
- Measurement of neutron detector characteristics

3. Conclusion

The contribution of LPRR is well recognized for the phase 1 of NPP program milestones when a country is developing a general understanding of the implication of a nuclear power program before taking the decision. In addition, there is no substitute of research reactors for RI production, NAA, and neutron radiography. Also, there should be replacements of LPRRs built in 1950s and 1960s for education and training. The coming LPRR to satisfy these demands should be safer than the previous ones and must include some innovation. A conceptual design of LPRR described in this paper is believed to cope with safety requirements and to be better utilized for the education of students in nuclear engineering.

4. Acknowledgement

This work was supported by the Advanced Research Center for Nuclear Excellence (ARCNEX) program by the Ministry of Science, ICT and Future Planning of the Republic of Korea.

5. References

[1] IAEA Nuclear Energy Series, NG-T-6.1, “Status and Trends in Nuclear Education”, IAEA, Vienna, 2011.

[2] http://www.ne.anl.gov/about/reactors/training.shtml.

[3] The University of New Mexico AGN-201M Reactor Operation and Training Manual, Dept. of Chemical and Nuclear Engineering, Univ. Of New Mexico, Albuquerque, NM, USA, 2011.

[4] H. Bock and M. Villa, “Survey of Research Reactors, http://www.reak.bme.hu/Wigner_Course/WignerManuals/Bratislava/Research_Reactors_I.htm“

[5] E,K. Ronald and et al., SLOWPOKE: A New Low-Cost Laboratory Reactor, Int. J. of Applied Radiation and Isotopes, Vol.24, pp.509-518, 1973.

[6] I.C. Lim and et al., “Review of Low-Power Research Reactor Development for Education and Training”, presented at the IGORR 2014, Bariloche, Argentina, 17-21 Nov. 2014.

[7] IAEA Nuclear Energy Series No. NP-T-5.6, Technical Requirements in the Bidding Process for a New Research reactor, Vienna, IAEA, Draft, 2013.

The investigation of the new multipurpose research reactor succeeding to JRR-3

K. TAKINO, M. ARAI and Y. MURAYAMA
Department of Research Reactors and Tandem Accelerator
Nuclear Science Research Institute, Japan Atomic Energy Agency
2-4, Sirakata-shirane, Tokai-mura, Naka-gun, Ibaraki 319-1195 - Japan

ABSTRACT

We have started to investigate basic concepts of the new research reactor that will be accepted twenty years later. The aim of this project is to build up the design of the new multipurpose research reactor which is constructed instead of JRR-3 for utilization of the neutron beam, irradiation, training and so on. The new reactor is desired to be able to see the reactor core from the top of the reactor vessel and utilize various energy neutrons. And these neutron fluxes shall reach much higher than JRR-3.
As the first stage in design study of the new reactor, the thermal power, the basic shape of the reactor core, the fuel element design and the reflector component are proposed to gain high neutron flux and satisfy the safety levels.
As a result of the core arrangement study in this paper, the maximum horizontal power peaking factor of the new reactor became less than 90% of JRR-3. The thermal and fast neutron flux also became over 1.5 and 2.9 times than JRR-3 respectively.

1. Introduction

Japan Research Reactor No.3 (JRR-3), which is one of the largest multipurpose research reactors in Japan, is a light water cooled and moderated pool type reactor with thermal power of 20MW at Japan Atomic Energy Agency (JAEA). JRR-3 is utilized from the research to industrial use as neutron beam experiments; irradiation tests of the reactor material, manufacturing radio isotopes for medicine use, and the silicon semiconductor by neutron transmutation doping (NTD).
On the other hand, the use of Japan-Proton Accelerator Research Complex (J-PARC) which is one of the highest intensity proton accelerators in the world was started from 2008 by JAEA and High Energy Accelerator Research Organization (KEK). J-PARC is suitable for extensive experiments utilizing high intensity pulse neutron beam. JRR-3 is suitable for high accuracy experiments utilizing continuous neutron beam. Both neutron experimental facilities are complementarily indispensable for science and technology utilizing neutron.
However, the operation of JRR-3 was begun from 1990 and the aging problems are becoming apparent. Moreover, taking the neutron utilization after the stop of JRR-3 into account, the basic design of the new multipurpose research reactor should be investigated.
This paper shows the status of study: the new multipurpose research reactor is analysed focusing on its performance.

2. Reactor concept

2.1 Utilization purpose

The research reactor is categorized as the following depending on the purpose of utilization;

(1) The beam experimental reactor which utilize neutrons for the research of physics, chemistry, and several subjects,
(2) The material testing reactor utilized for irradiation of the reactor fuel or component,
(3) The reactor which produces radioisotopes,

(4) The reactor utilized for education or training,
(5) The experimental or prototype reactor for developing the next generation reactor.

JRR-3 is the reactor utilized mainly for the neutron beam experiment, but it can produce radioisotopes and silicon semiconductors by neutron transmutation doping. The aim of the new multipurpose research reactor is to contribute widely from the fundamental research to life-science and industry. In addition, it can irradiate any material in order to investigate the durability of reactor components. That is, the new reactor will have the capability of providing selectively cold, thermal and fast neutrons for various purposes.

2.2 Excellent design in economy

The economic performance must be improved by saving the expense of construction, operation and maintenance. Generally speaking, the cost of the fuel is expensive among the operation/maintenance expenses. For example, improving burn-up of the fuel is one of the effective ways to saving expenses. Similarly, the laboursaving for maintenance is also effective. The number of equipment should be reduced and the material that is hard to be activated needs to be chosen for easy access to reactor components on that account. The reduction of the exchange frequency is also effective for laboursaving like as the automation of the maintenance system.

2.3 Operation rate improvement

The improvement of operation rate requires operating the reactor continuously for a long time per a cycle. The continuous long time operation will be achieved by the core design of being aggregated, flattening power density and by several factors like improving the burn-up. To make the enrichment of fuels higher is also effective, but research reactor fuels are required to be made of less than 20% enriched Uranium. Moreover, the increase of the Uranium load is also effective. However that is equal to make the neutron flux low. The Uranium load should be determined studiously to satisfy the needs of users in that kind of meaning.

3. Reactor design study

3.1 Fuel element outline

The fuel of the research reactor is generally the plate type fuel because of its high heat removal. Since the new multipurpose research reactor is assumed to be operated under high thermal power density, the plate type fuel is suitable.
Moreover, the fuel core plate is assumed to be made of Uranium and Molybdenum, which is being investigated in each country. Since Uranium-Molybdenum (U-Mo) fuel is able to contain more Uranium than Silicide fuel per a fuel plate, U-Mo fuel can be burned longer in the reactor. U-Mo fuel is also superior to Silicide fuel from the point of view of reprocessing.

3.2 Perspective of reactor core

The new multipurpose research reactor is desirable to be the pool type reactor because irradiation samples can be handled easily and the reactor facility system is simplified. The thermal power of existing pool type reactor is limited less than or equal to almost 20 MW. Generally speaking, in the case of the thermal power density is raised for high neutron flux, the reactor type needs to be the tank type for pressurizing the reactor pool to prevent water around the core from boiling locally.
JRR-3 is the pool type reactor of 20MW, but the pool type reactors more than 20MW exist like HANARO (Korea) and CARR (China). The new reactor is assumed to be able to increase thermal power by flattening power density and improving cooling performance. Thus its temporary power is set to 30MW and reactor type is defined as the pool type.
The major parameters of the new multipurpose research reactor are expressed as Table 1.

		JRR-3	New reactor
Thermal power [MW]		20	30～35
Reactor type		Pool type	Pool type
Neutron flux [n/cm^2/s]	Core	2×10^{14} (Fast) 3×10^{14} (Thermal)	5×10^{14} (Fast) 5×10^{14} (Thermal)
	Experimental facility	1×10^8 (Thermal)	1×10^9 (Thermal)
Coolant		Light water	Light water
Moderator		Light water	Light water
Reflector		Heavy water Beryllium	Heavy water Beryllium Aluminium

Tab 1: Major parameters of new multipurpose research reactor.

The maximum thermal neutron flux of JRR-3 is about 2×10^{14}n/cm^2/s at around the core and 1×10^{8}n/cm^2/s at the point of the experimental facility. On the other hand, the aim of the maximum thermal neutron flux about the new reactor is about 5×10^{14} n/cm^2/s at around the core and 1×10^{9}n/cm^2/s at the point of the experimental facility. The neutron flux of the new reactor will become high by the arrangement of core shape, improvement of transportation method and various different ways instead of by a large increase of thermal power. The neutron flux should be high, but its stability and continuity are more important. Therefore the core should be designed considering a local change of neutron flux and the operation rate.
Furthermore, the high fast neutron flux would be needed to irradiate materials. In order to accommodate the new reactor to the experiment of light water reactor components, the neutron flux of the new reactor must become as high as that of existing light water reactor at least. Hence the aim of the maximum fast neutron flux is about 5×10^{14} n/cm^2/s in the core. By the way, the fast neutron is not able to be utilized efficiently at the region of the heavy water reflector. Therefore aluminium blocks are put around the core longitudinally, seen from directly above the core, to irradiate much more materials by fast neutrons.

4. Core neutronics

The aim of neutron flux and thermal power about the new multipurpose research reactor were discussed in Chapter 3. In this Chapter, the core characteristics focusing on horizontal power peaking factor (PPF) which is the ratio of local power versus average one are analysed to improve the performance of the new reactor.

4.1 Basic theory for the multipurpose research reactor

The core shape is proposed to make the neutron flux high so as to reach the aim of the new reactor. Generally, the relationship between neutron flux and thermal power is expressed by the following equation.

$$\phi = \frac{P_{th}}{\sum_i \kappa_i N_i \ \sigma_{f,i} V} \qquad (4.1.1)$$

ϕ : Neutron flux
P_{th} : Thermal power
κ_i : Energy release per fission of the *i*-th nuclide
N_i : Number density of the *i*-th nuclide
$\sigma_{f,i}$: Microscopic fission cross section of the *i*-th nuclide
V : Volume of fuel

The reactor must maintain chain reactions. The balance of neutrons in the multiplying system is expressed by the following equation using the one-group diffusion theory.

$$-D\nabla^2\phi + \Sigma_a\phi = \frac{1}{k_{eff}}\upsilon\Sigma_f\phi \qquad (4.1.2)$$

Generally, the following equation about the geometric buckling holds.

$$\nabla^2\phi + B_g{}^2\phi = 0 \qquad (4.1.3)$$

Eq.4.1.2 can be modified as the following equation by using Eq.4.1.3 for the effective multiplication factor that is the indicator of chain reaction.

$$k_{eff} = \frac{\upsilon\Sigma_f}{\Sigma_a + DB_g^2} \qquad (4.1.4)$$

k_{eff} : Multiplication factor
v : Number of neutrons produced per fission
Σ_f : Macroscopic fission cross section ($\Sigma_f = N\sigma_f$)
Σ_a : Macroscopic absorption cross section
D : Diffusion coefficient
B_g : Geometric buckling

According to above equations, a neutron flux becomes higher as power density grows. Hence it is desirable that the power density is grown as long as the fuel soundness can be kept. However, if the power density grew locally, neutrons would concentrate on a certain point and the power density of whole core would become smaller unless a heterogeneous fuel element is invented. It causes the problem that neutrons of high flux cannot utilize widely. Furthermore, a neutron flux varies locally as burn-up progresses, and a constant high neutron flux is not obtained. That is also one of the reasons that the operation rate becomes low. Thus the core shape should be decided so that the maximum PPF becomes smaller in the situation of assembling the core with the fuel element whose Uranium is uniformly distributed. Moreover, a small absorption rate of neutrons makes a neutron flux high by a small fission rate. That is to say, it should be minimized that the large absorption cross section materials are put in the core.

4.2 Fuel element design

The temporary fuel element and neutron absorber are designed in the motif of JRR-3. Those of the new multipurpose reactor are expressed as Table 2.

Outline [mm]		77.7×77.7×820
U235 enrichment [wt%]		20
Uranium density [g/cm^3]		7.0
Fuel meat	Thickness [mm]	0.51
	Width [mm]	63.5
	Length [mm]	800
Cladding	Thickness [mm]	0.38
Fuel plate	Thickness [mm]	1.27
	Width [mm]	73.0
	Length [mm]	820
Number of fuel plate		17
Coolant flow path [mm]		3.3
Fuel meat material		Uranium Molybdenum dispersion alloy
Cladding material		Aluminium alloy
Neutron absorber	Outline [mm]	77.7×77.7×820
	Thickness [mm]	5.0
	Material	Hafnium

Tab 2: Standard fuel element and neutron absorber specification.

The Uranium density is provisionally defined as 7.0g/cm^3 in this paper. The thickness of the fuel meat and plate are same as JRR-3. If the life of the fuel element is simply combined with JRR-3, the number of the fuel plates must be increased. However, considering the increase of the thermal power, the number of the fuel plates must be decreased or the width of the coolant flow path must be broadened to satisfy the soundness of cooling function. Therefore the outline and length of the fuel element are slightly stretched.
The control rod is composed of the standard fuel element and neutron absorber; the upper is the neutron absorber whose shape is square-tube type, the lower is the fuel element. The reactivity of the reactor is controlled by the control rods moving up and down.

4.3 Analytical models

The relationship between power density and neutron flux was discussed above and it is assumed that the load of Uranium should be minimized to make neutron flux high. Hence in this paper, several sets of the fuel elements are prepared and these core shapes are proposed to minimize the maximum horizontal PPFs. The sets of the fuel elements, which are now considered, are shown as Table 3.

Number of fuel elements	24	26	28	30	32
Uranium load [kg]	74.0	80.2	86.3	92.5	98.7

Tab 3: Considered sets of fuel elements.

The maximum neutron flux is crucial to the new multipurpose research reactor. Additionally, the PPF should be evaluated in each burn-up step to investigate a change of the maximum

that. From these points of view, Monte Carlo method is suitable for neutron transport calculation and MVP-BURN[1] is utilized to carry out alternately neutron transport and burn-up calculation. The major parameters of these calculations are summarized as Table 4.

Calculation code	MVP-BURN
Nuclear data library	JENDL-4.0[2]
Total number of histories (MVP)	10,000,000
The number of Burn-up steps	15 steps/year

Tab 4: Major parameters of neutronics calculation.

4.4 Analysis results

The core shapes whose maximum horizontal PPFs were minimized are expressed as Figure 1 and these maximum horizontal PPFs change as Figure 2 in each burn-up step.

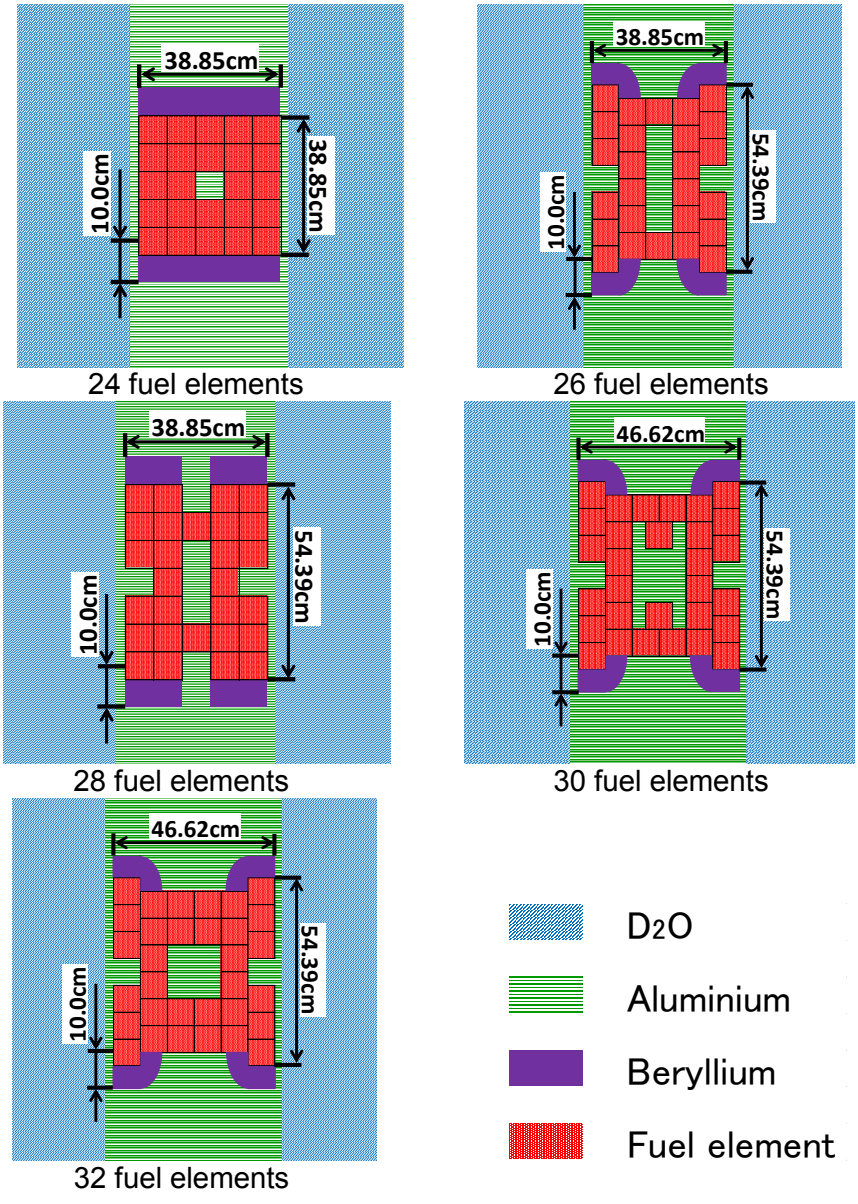

Fig 1. Core shapes whose maximum horizontal PPFs were minimized.
(view from directly above)

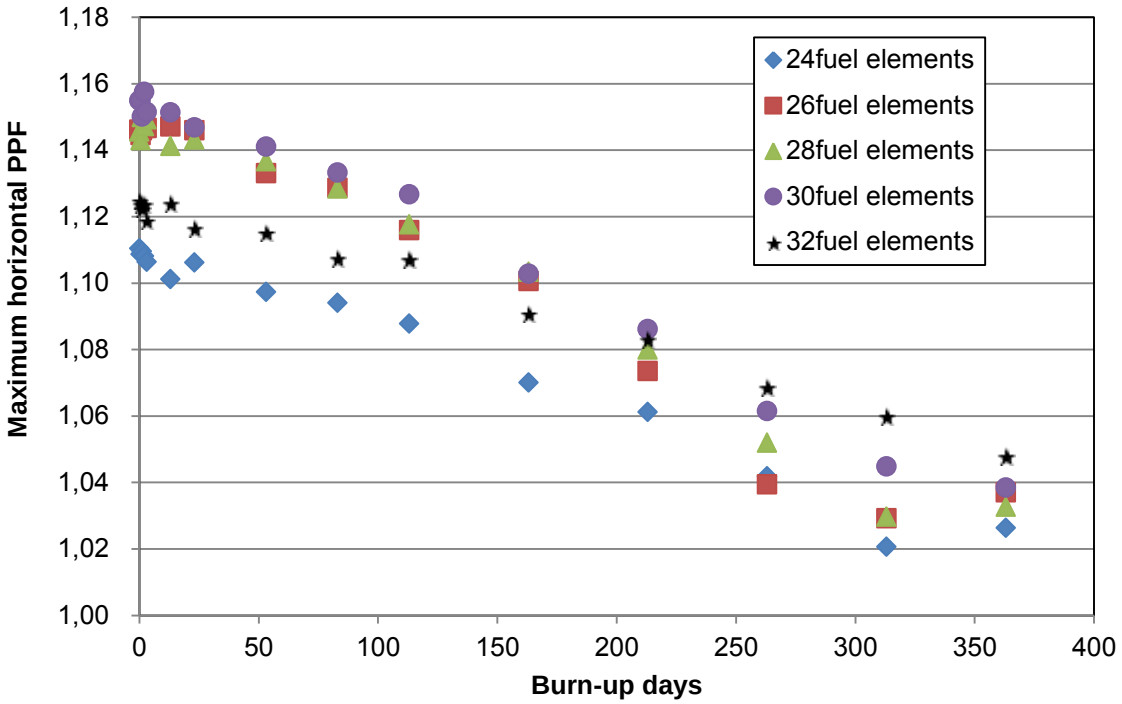

Fig 2. Changes of the maximum horizontal PPFs in each burn-up step.

The core shapes were designed to be aggregated for the improvement of the operation rate as well.
Figure 2 shows changes of the maximum horizontal PPFs in the case of averaging thermal power by a fuel element. It is now postulated that control rods are not in the core and burnable poisons are not used for high neutron flux. Beryllium blocks are also put around the core beside the aluminium frame to compensate fission reactions for the local place of small horizontal PPF. A beryllium is generally used for the reactor component as the reflector. It contributes the multiplication of neutrons because it decelerates neutrons efficiently and initiates (n, 2n) reactions for fast neutrons.
It was found that the highest maximum horizontal PPF was observed at first step of burn-up from Figure 2. Hence the core shape should be designed so that the maximum horizontal PPF becomes as small as possible at first step of burn-up. The core shapes that control rods are put at large PPF locations or around there are shown in Figure 3.
The control rods were distributed to make the core sub-critical when those are wholly inserted. Some core shapes were also arranged to make the maximum PPFs smaller based on the shapes not considering control rods. The maximum horizontal PPFs and power densities of the core shapes shown in Figure 3 are summarized as Table 5.

Fuel elements	24	26	28	30	32
Maximum horizontal PPF	1.15	1.14	1.20	1.16	1.47
Maximum power density [kW/cc]	3.57	3.10	2.99	2.76	3.36

Tab 5: Maximum horizontal power peaking factor and power density.

The control rods of each core shapes are now adjusted to make the effective multiplication factor 1 and drawn uniformly. The maximum horizontal PPFs of all shapes became less than 1.2 and shrank to less than 90 percent of JRR-3 except for the 32-fuel-elements core. In addition, as a matter of course, the fewer the number of fuel elements is, the higher power density becomes. Consequently, the maximum permissible level of power density must be

analysed and the appropriate number of fuel elements should be determined through the fuel element design.

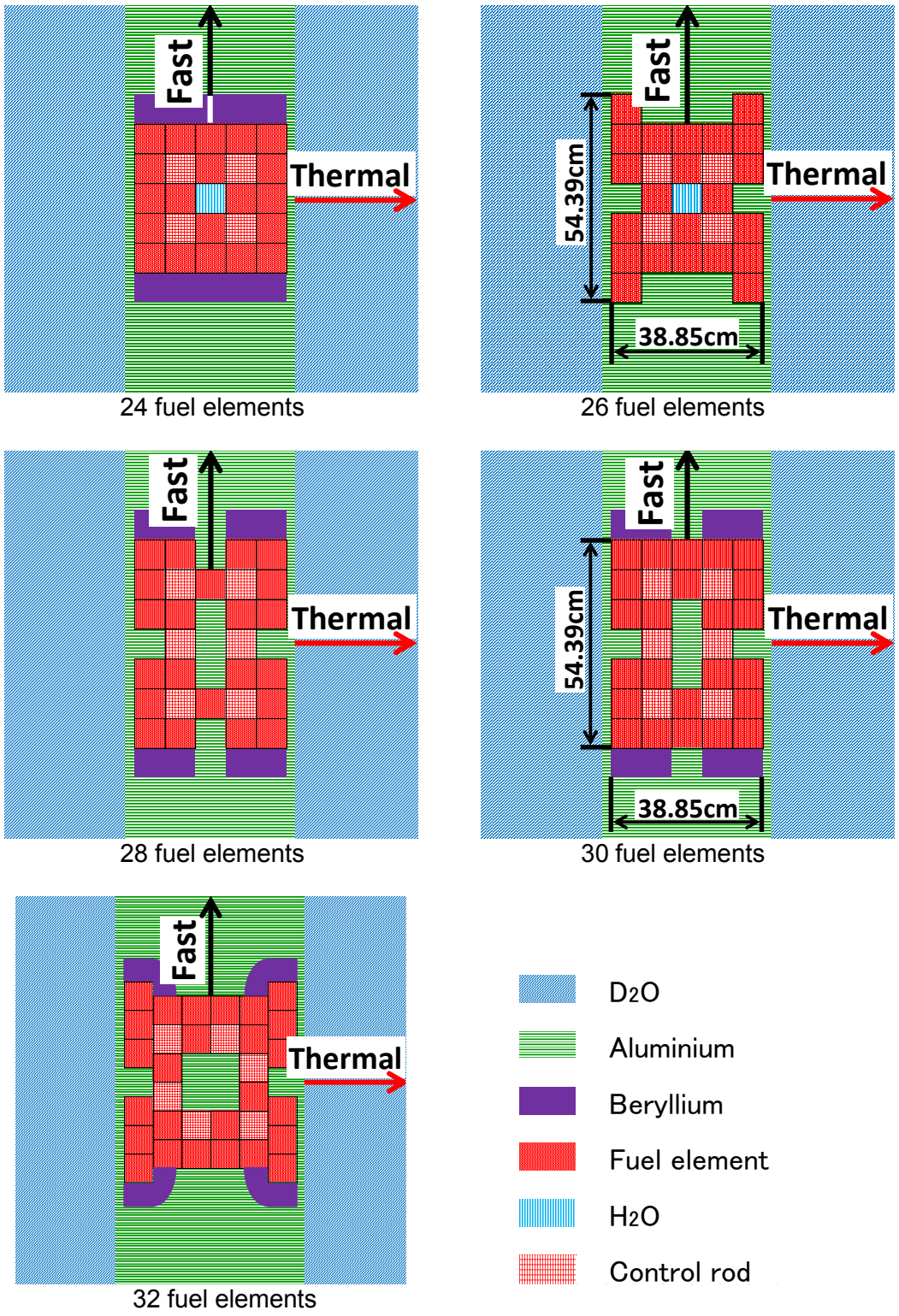

Fig 3. Core shapes with the control rods.
(view from directly above)

The start-up core neutron fluxes of each core shape are described as Figure 4.

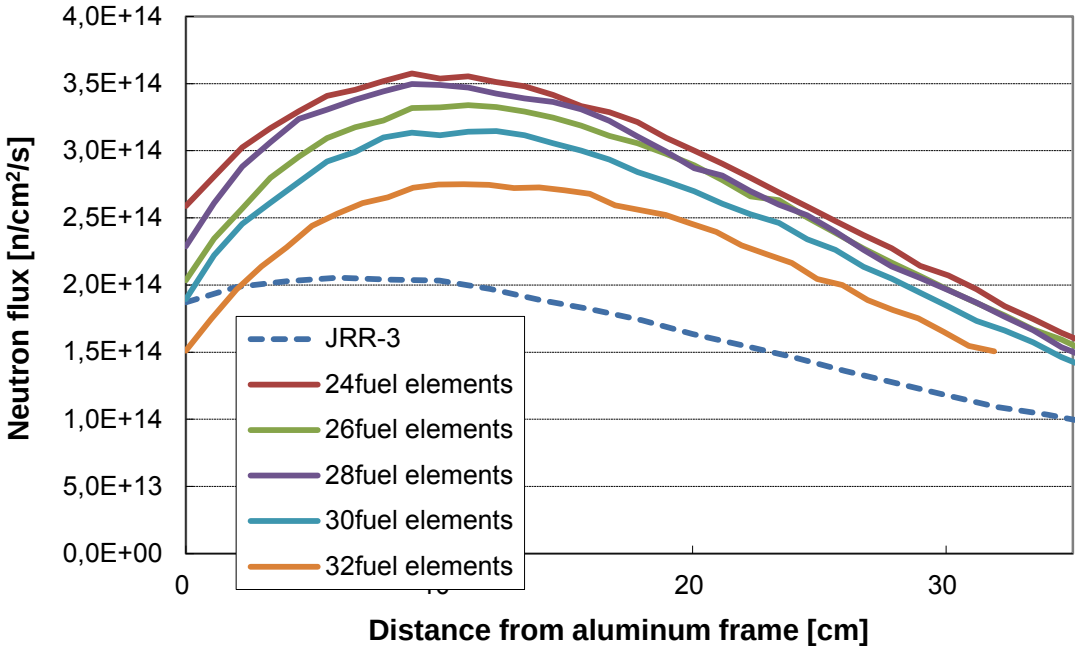

Thermal neutron flux (0 degree direction)

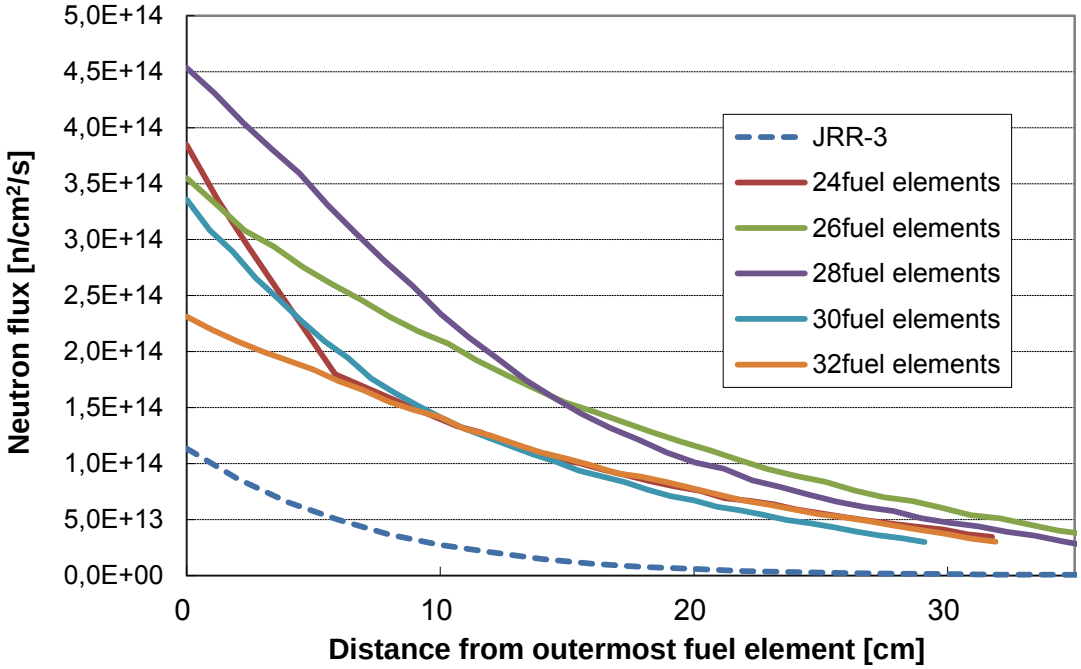

Fast neutron flux (90 degree direction)

Fig 4. Neutron flux of each core shapes adjusted to k_{eff}=1.

Those are now expressed as the following by using Figure 3; thermal neutron flux (< 0.6eV) of 0 degree direction which is set initial point on the aluminium outer frame, fast neutron flux (> 100keV) of 90 degree direction which is set initial point on the outer frame of the outermost fuel element.

The thermal neutron fluxes of each number of fuel elements became over 1.5 times higher than JRR-3 except for the 32-fuel-elements core. Similarly, the fast neutron fluxes became over 2.9 times higher. A neutron flux becomes much higher as fuel burns, therefore the neutron fluxes will achieve the aim or get closer to it.
Generally, a neutron flux becomes higher as power density grows, however the neutron fluxes of the 28-fuel-elements core were higher than those of the 26-fuel-elements core; the thermal flux of the 28-fuel-elements core became high by its high horizontal PPF and PPF being higher toward the centre, the fast flux became high because the certain point of observation area surrounded by the core. The core shapes of the 28 and 30-fuel-elements core, whose centre is made from aluminium, are effective in the case of much higher fast neutron flux is required.

5. Conclusion

The concept of the new multipurpose research reactor was investigated and the nuclear characteristics of the reactors were analysed with changing the load of Uranium focused on the number of the fuel elements.
As a result of it, the horizontal power peaking factor of the new reactors became less than 90% of JRR-3 except for the 32-fuel-elements core. The neutron flux of the new reactor became much higher than JRR-3 as well; the thermal neutron flux was over 1.5 times, the fast neutron flux was over 2.9 times.
After this, the design of fuel element and the detail design of core shape must be carried out to satisfy safety limits through thermal-hydraulic and neutronics analyses. In addition, the neutron flux of the experimental equipment will be improved and the design of the coolant system is to be carried out.

Reference

[1] Okumura K., Mori T., Nakagawa M. and Kaneko K. "Validation of a Continuous-Energy Monte Carlo Burn-up Code MVP-BURN and Its Application to Analysis of Post Irradiation Experiment", J. Nucl. Sci. Technol., 37, 128 (2000).
[2] K. Shibata, O. Iwamoto, T. Nakagawa, N. Iwamoto, A. Ichihara, S. Kunieda, S. Chiba, K. Furutaka, N. Otuka, T. Ohsawa, T. Murata, H. Matsunobu, A. Zukeran, S. Kamada, and J. Katakura: "JENDL-4.0: A New Library for Nuclear Science and Engineering," J. Nucl. Sci. Technol. 48(1), 1-30 (2011).

KEY TECHNICAL CHARACTERISTICS RELATED TO THE DESIGN OF THE RA-10 MULTIPURPOSE REACTOR

P. CANTERO, P. RAMIREZ, F. BROLLO, G. MARINSEK, H BLAUMANN

Nuclear Engineer Division – Nuclear Energy Department – National Atomic Energy Commission (CNEA)
Centro Atómico Bariloche, POB 9, Exequiel Bustillo Avenue 9500, R8402AGP, S. C. de Bariloche, Prov. de Río Negro – Argentina

J. ZALCMAN, M. MILBERG, L. GIULIODORI, L. MARZANO, G. QUESADA, D. ESTRYK, G. RIOS, J. ALARCON, G. RODRIGUEZ, J. LEE, D. GARCIA, C. VERRASTRO, C. HOFER

I&C Division– Nuclear Energy Department – National Atomic Energy Commission (CNEA)
Centro Atómico Ezeiza, Pbro. Juan Gonzalez y Aragon Nº 15, B1802AYA, Ezeiza
Prov. de Buenos Aires – Argentina

ABSTRACT

Since 2010, the National Atomic Energy Commission of Argentina is carrying out the RA-10 project. The project includes the design, construction, licensing and start-up of a new research and radioisotopes production reactor, the “Argentine Multipurpose Reactor RA-10”.

In this paper we present technical characteristics of systems relevant to safety and availability focusing on the design philosophy.

We discuss details of systems performing innovative solutions to specific functions addressed on the design of a research and production reactors, considering design bases, defence in depth, safety qualification and safety requirements.

We present the Reactor Protection System, designed based on FPGA technology, and the architecture for the system, which includes redundancy and internal diversity for each of the redundancies. We also present details of the Nuclear Instrumentation System, which includes redundancy, diversity and implements a new statistic pulse-processing algorithm that allows safety settings that increments both, safety and availability. Both systems are designed, constructed and will be installed by the I&C department of the CNEA, located at the Ezeiza Atomic Centre.

Related to control rod movement, we present a new autonomous system devoted specifically detect and stop reactivity insertion events that may be caused by the improper movement of control rods, specifically focusing on the Reactor Control and Monitoring System malfunction when implementing the reactivity control function.

The Argentinian regulation requires to analyse the radiological risk figure, both for public and workers, and to demonstrate that this risk is acceptable given specific rules. We present two systems that increase the engineering safety features related to minimize this risk. Those systems are the “Autonomous Area Radiation Monitors” focused on minimizing the workers dose and the “Ventilation Reconfiguration System” focused on minimizing public dose.

Finally, we briefly present the project status, planned advance and general schedule of next activities related to the project.

Introduction

On 23 August 2006 the Argentinian government announced the re-bumping of the Argentinian Nuclear Plan, which was recognized particularly relevant for nuclear applications related to public health, science and technology.

In this framework Argentina is carrying out the RA-10 project with the participation of INVAP S.E. as the main contractor.

The RA-10 project is supported by national funding and is conducted by CNEA. It started on 2010 and will be finished with the reactor commissioning on 2019.

The RA-10 project represents a great opportunity to keep the country, and particularly to the community related to nuclear technology, at the forefront as Multipurpose Nuclear Reactors supplier.

The strategic objectives of the project are:

- To consolidate and expand the production of radioisotopes.
- To provide for the future installation of a device for testing nuclear power plants and experimental reactors fuel elements.
- Offering, the scientific and technological system based on new capabilities, neutron techniques for use in basic research and advanced technological applications.

The main specific objectives are:

- To consolidate and increase the radioisotope production in order to assure the future needs.
    - Reach a production of 2000 Ci/week of Molybdenum-99.
    - Achieve an increase in the production of Lutetium-177 and Iridium-192.
- To provide fuel and material testing irradiation facilities for supporting the development of national technology in this field
    - Provide for the future devices for testing new developments on fuel elements including mini plates.
    - Provide for the future facilities for material tests and studies on radiation damage and corrosion assessment.
- To offer new applications in the field of science and technology based on neutron techniques.
    - Provide facilities of cold and thermal neutrons for the implementation of materials science and biology techniques and areas of interest.

Design Basis

After consolidating the user's requirements, the following facilities have been specified for the RA-10 reactor design:

- Intermediate thermal flux positions for bulk radioisotope production (Mo, ORI)
- High thermal flux positions for sealed cans radioisotope production (Ir/Lu)
- Sealed capsules irradiation positions with neumatic devices
- Silicon irradiation positions (6", 8"and 10" diameter lingots)
- High fast flux irradiation positions for material testing irradiation rigs
- Intermediate fast flux irradiation positions for material testing irradiation rig
- MTR plates and fuel irradiation position
- NPP fuel test irradiation loop
- D2 cold neutron source
- Cold neutron beams
- Thermal neutron beams
- In pool neutron radiography

Main features related to the design basis of the RA-10 are shown in Table 1.

Type	Open pool
Power	30 MW
Fuel elements	MTR, uranium silicides, 19.7% enrichment, 4.8 gU/cm3, with burnable poisons
Control rods	Hafnium plates, external to the fuel elements
Moderator and coolant	Light water
Flow direction in core	Upward
Reflector	Heavy water
Operation cycle	26 days
Extraction burnup	Higher than 45%
Shutdown systems	Control rods and reflector tank emptying

Utilization

CNEA expects to maximize the RA-10 utilization. So a program for the reactor applications development is under being carried out in order to assure fully utilization for the RA-10, including human resources development and the update/construction of related installations.

Site

The RA-10 reactor will be located at the Ezeiza Atomic Center. It covers an area of 840 hectares and is located in Ezeiza, province of Buenos Aires, approximately 33 km southwest of the city of Buenos Aires.

The RA-10 reactor project includes the following buildings:

- Reactor Building.
- Auxiliary Building.
- Neutron Guide Building.
- Services Building.

Figure 1 shows the buildings and layout for the RA-10

Figure 1: RA-10 Reactor, Site and Buildings

Framework of the paper

In this paper we present technical characteristics of systems relevant to safety and availability. The design of these systems respond to the safety analysis and design methods that the RA-10 project has set for the reactor design.

We present the approach utilized in the application of basic principles for the RA-10 design, and then we present specifically the technical characteristics of the systems described.

Defence in Depth

The principle of defence in depth shall be applied in the design of the RA-10 Reactor in order to obtain a scaled protection against various identified events such as equipment failure or human errors. The principle of defence in depth shall be implemented in the design utilizing a scheme of five levels.

1. The purpose of the first level of defence is to prevent deviations from the normal operation and prevent system failures or human error operation. Hence requirements emerge the Reactor RA-10 design in the application of appropriate design techniques, such as the application of redundancy, independence and diversity.
2. The purpose of the second level of defence is to control (by detection and intervention) deviations from operational states in order to avoid anticipated operational events (AOE) degenerate into events that may affect the safety of the installation. This level requires the existence of specific systems, provided by the design and analysed in the safety evaluation of the installation, to prevent or minimize the consequences resulting from these initiating events.
3. For the third level of defence is assumed that there is a possibility, although very remote, that the previous levels of defence cannot stop the evolutions of some AOE and that serious consequences can occur. These unlikely events, called Design Basis Events (DBE), are included in the design basis of the RA-10. In order to limit the evolution of these events, the design includes inherent safety elements, intrinsic safety mechanisms, additional equipment and procedures to control their consequences and achieve stable and acceptable states of the nuclear installation after these events. Hence the requirement of providing Engineering Safety Features (ESF) that allow get the reactor to a safe shutdown state maintaining at least one confinement barrier of radioactive material.
4. The purpose of the fourth level of defence is to deal with cases of Beyond Design Basis Events (BDBE) including Severe Accident (SA) in which the limits considered in Design Basis (DB) are exceeded, and ensure that radioactive emissions remain at the lowest level possible. The most important objective of this level is the protection of the confinement function. This can be achieved by complementary measures and procedures to prevent progression of the accident and by alleviating the consequences of certain BDBE and SA, called Extended Design Basis Event, EDBE, for which ESF are provided, in addition to emergency procedures and intervention measures.
5. The fifth and final level of defence aims to mitigate the radiological consequences of potential releases of radioactive materials that may occur as a result of accidents. This requires the existence of a place properly equipped from where the emergency management and emergency response plans, on-site and off-site, can be performed.

The principle of defence in depth is mainly applied by safety assessment and the use of reliable methods for the design and operation based on international recommendations and the CNEA experience operating experimental reactors and other nuclear installations. This analysis is performed in the design stage to ensure the fulfilment of safety objectives.

Engineering Safety Features and event classification

The design of the RA-10 Reactor includes as an essential part of it safety, in addition to the inherent characteristics of the design, the provision of technical elements of safety, that is, Structures, Systems or Components (SSC) whose function is to implement the basic safety functions in order to limit the evolution and mitigate consequences of abnormal conditions or derived from the occurrence of initiating events.

According to the categorization of events adopted for the RA-10 project, abnormal conditions are categorized in relation to their frequency of occurrence. In connection to this event classification, ESF elements are classified on Design Basis ESF, DB-ESF and Beyond Design Basis ESF, BDB-ESF.

The DB-ESF are

- Reactor Protection System - RPS
- First Shutdown System - FSS
- Natural convection core cooling
- Natural convection cooling of experimental devices, external to the core.
- Analog Autonomous Area Monitors

The EDB-ESF are:

- Second Shutdown System - SSS
- Emergency Water Injection System.
- Long-term pool cooling.
- Confinement.
- Post Accident Monitoring System.
- Alternative Control Room.
- Uninterrupted and Secured Power Supply System.
- Evacuation Alarm

We will focus this paper in four systems designed to implement their function in level two, level three and level four of defence in depth.

The system in level two of defence in depth is the Control rod abnormal movement detection system (DeMA). It is designed to face the control rod movement failure, specifically focusing on the Reactor Control and Monitoring System malfunction when implementing the reactivity control function. It is an autonomous system devoted specifically detect and stop reactivity insertion events that may be caused by the improper movement of control rods.

The systems described in this paper and located in level three of defence in depth are the RPS and Nuclear Instrumentation System (NIS). Both together are designed to face an event that causes reactivity insertion beyond the acceptable limits. The Reactor Protection System is designed based on FPGA technology. The architecture for the system includes redundancy and internal diversity for each of the redundancies. The Nuclear Instrumentation System includes redundancy, diversity and implements a new statistic pulse-processing algorithm that allows safety settings that increments both, safety and availability.

The System that performs its function in level four of defence in depth is the “Autonomous Area Radiation Monitors”. The Argentinian regulation requires to analyse the radiological risk figure, both for public and workers, and to demonstrate that this risk is acceptable given specific rules. This system is devoted to minimize the workers dose after a human error manipulating experimental devices or facilities.

Control rod abnormal movement detection system (DeMA)

This system is related to control rod movement. It is included in the FSS instrumentation design. The system is devoted specifically to detect and stop reactivity insertion events that may be caused by the improper movement of control rods, specifically focusing on the Reactor Control and Monitoring System malfunction when implementing the reactivity control function.

The system is fed for three quadrature encoders on each control rod mechanism that informs the direction and velocity of the control rod movement. When the system detects abnormal movement, it de-energises the electromagnets limiting the abnormal movement. The response time of the system guarantees that the reactivity insertion is less than 40 pcm, a limit that the national regulatory authority allows to mobile experiments.

Figure 2 shows the system architecture.

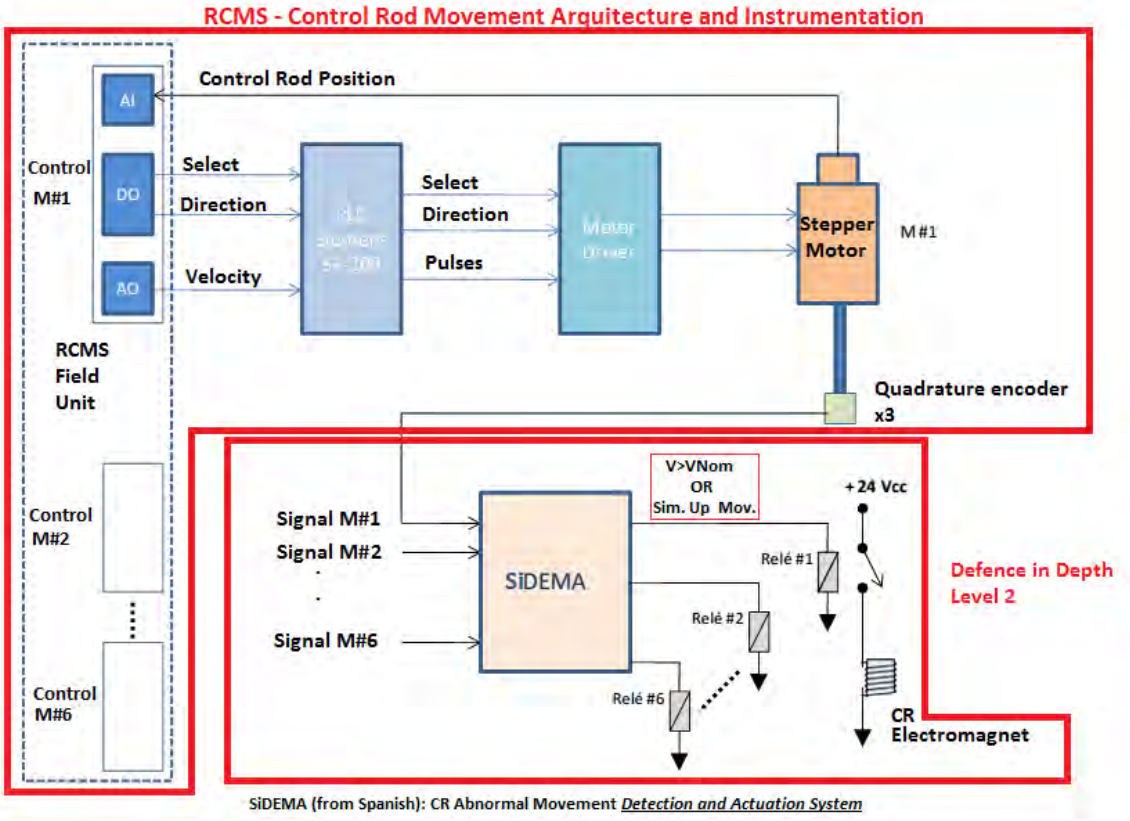

Figure 2: DeMA architecture

Reactor Protection System

The Reactor Protection System (RPS) is the security system that demands the protective actions related to reactivity control and the confinement of radionuclides, in the case of system failure, misoperation or external threats.

To do so, the RPS:

- Monitors the evolution of variables and detects if they surpasses the trigger thresholds.
- Implements the trigger logic that demands the start of protective actions necessary to get the plant to a safe state.
- Provides the operator the means for manually triggering the starting of protective actions.

- Indicates the system safety settings on the desk of the control rooms to the operators.
- Monitors itself for safe operation.

The RPS can demand the start of four protective actions:

- Trigger First Shutdown System (FSS). The action of the FSS is the rapid insertion of all absorber plates. The completion of this action is diversified in two actions 1) the disconnection of the power to the motor driving the control rod mechanisms releasing the mechanism to the action of gravity, and 2) the injection of compressed air into a pneumatic cylinder that forces the introduction of the plates into the core.
- Trigger the Second Shutdown System (SSS). The action of the SSS is the partial drain of the heavy water from the reflector tank. The action is performed by opening six valves that connect the reflector tank to the heavy water storage tan.
- Trigger reconfiguration of the ventilation system to implement reactor confinement.
- Activates the evacuation alarm.

The design criteria applied in the RPS engineering arise from the applicable regulations, international recommendations and the rules of good art of engineering. The most important criteria are safe fail, manual operation, simple fault tolerant, simplicity in design, proven technology, redundancy, independence, diversity, self-verification, availability, ease of testing and maintenance, resistance to extreme environmental conditions, etc. The SPR consists of three trains that each one implements measurement, voting and triggering. Each train includes its own sensors to measure safety variables, comparators, voting systems and independent drivers, thus forming a triple redundant system. The safety signals are digitized and compared against tripping thresholds that define whether the safety signal is in the range of safe operation giving the initiation signals. Figure 3 shows this concept.
The initiation signals are exchanged between the three trains, so that each train has the information to implement the voting logic and its own triggering signals in a redundant trains architecture. The initiation signals then are processed in a 2oo3 voting logic to give the redundant protection signals, which then are resolved in the final actuation logic. This final voting system generate signals TRIP 1, TRIP 2, TRIP 3 TRIP 4 demanding the initiation of the systems that performs the safety functions.
The main components of RPS are designed based on configurable FPGA devices. The design proposed for the implementation of the RA-10 Reactor RPS incorporates beyond traditional concepts of redundancy, fail safe, self-test, etc; *the internal diversity concept*. This concept consists of the execution of the safety functions inside each train by the means of two different security units in parallel: Diversity # 1 and Diversity # 2.

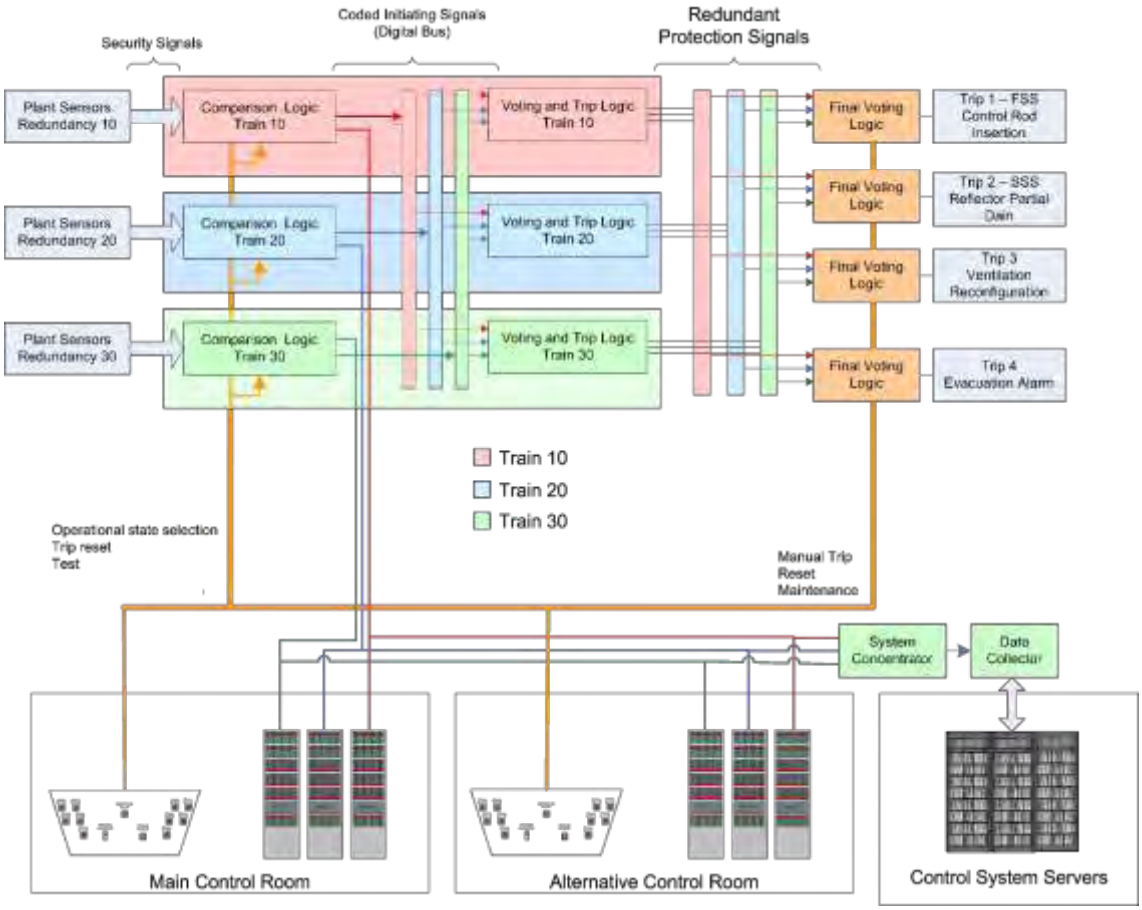

Figure 3: RPS Architecture

This feature is incorporated to meet the requirements of self-verification and to mitigate common mode failures in complex electronic device configuration. The internal diversity of each train is then resolved in the drivers module in a 1oo2 logic.The components that implement each diversity are provided for different manufacturer and the development is carried out by different teams. Each diversity has different internal configuration. Figure 4 shows this concept.

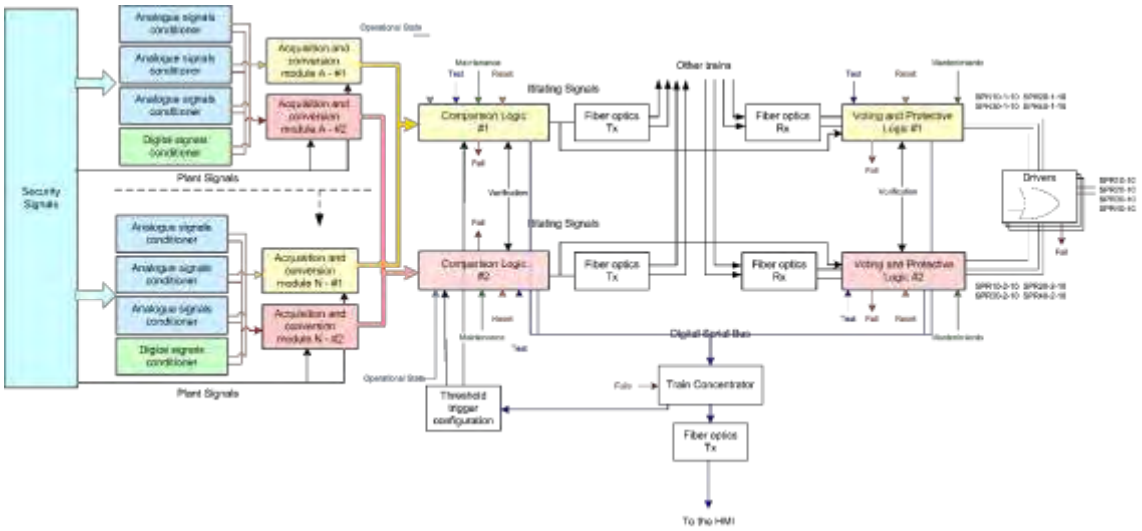

Figure 4: Internal diversity in a train.

Nuclear Instrumentation System

The Nuclear Instrumentation System (NIS) comprises all the instrumentation responsible for neutron flow measurements. The detectors used are located in the vicinity of the reflector tank. The preamplifiers are located in cabinets in the top of the pool, in the outer side. The associated signal processing electronic is located in cabinets housed in shared rooms with RPS.
The NIS is composed of the following instrumentation channels:

- Wide Range Channels used to cold start-up
- Wide Range Channels used for normal operation
- Current Channels used for normal operation
- Auto range linear Channel used for the automatic power control
- Gamma ionization channel - N16 used for the automatic power control
- Self-Powered neutron detectors, to map the neutron flux in the experimental devices

Figure 5 shows the NIS architecture.

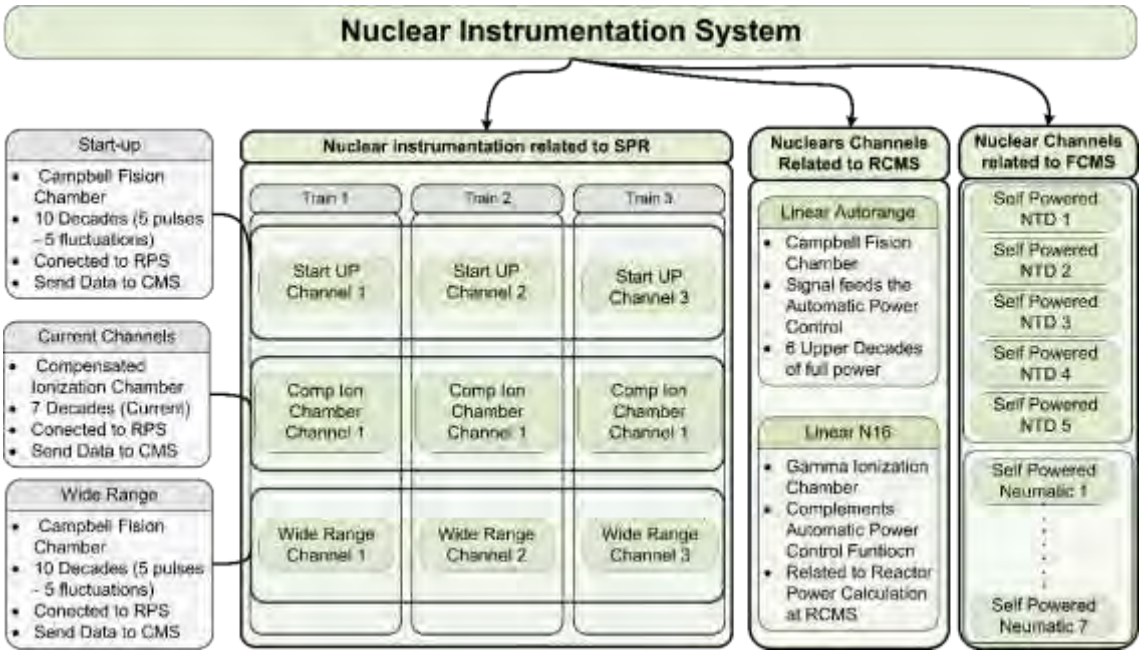

Figure 5: Nuclear Instrumentation System architecture

The cold start up channels are used in the commissioning of the reactor or after the reactor has been without power operation for long periods. Wide range channel used for normal operation and cover the full operation range, from start-up to full power. The lower six decades in pulse mode and the upper 5 decades in fluctuation mode, thus giving more than one decade of overlap between the two modes. The current channels are also used for normal operation. They cover the las five decades of the power.
This three families of channels feed the RPS.
The wide range channels, typically, are not used in pulse mode to trigger safety functions (as the FSS) based on the flow rate variation due to the intrinsic noise of the signal. Traditionally analogue signals are generated proportional to the flow rate and variation, then compared to trigger levels to detect TRIP condition or inhibition of control rod rising. The fast and accurate estimation of these parameters, with the instruments currently available: analogue impulse-meter and digital scaler, is not an easy task. In the first decades of start-up mode, the statistical fluctuation measuring the

rate of change in pulse mode is so important that requires to remove it from the safety logic, relegating it to inhibit the rising of control rod.
CNEA has developed a new digital neutron instrumentation system. Currently it has two instruments, one for estimating the average neutron flux and one for estimating the average value of the rate of change of neutron flux. Both instruments use configurable logic (FPGA) to implement its algorithm. Unlike the traditional method, that normally uses a preset time, this method works on the basis of a preset number of pulses counted, allowing better adaptation to flow variations, which in turn results in variable response time adjusted with dimensional statistical errors. The method automatically resolves the relation between accuracy and response time and automatically determines the parameter changes.
Values and criteria used to adjust the parameters of the algorithm to achieve adequate performance in estimating the logarithmic flow, are different from those required to achieve minimum fluctuations in the estimation of the rate change. Therefore, two separate instruments, one for each estimation was developed.
To use this technology to comply with the requirements of diversity and mitigate the effects of common mode failure, CNEA proposes to use for each channel measuring neutron flux in pulse mode, three comparators:
a) High level in the Neutron Flow logarithmic signal (normally used)
b) High level in the Neutron Flow variation rate signal, calculated on fix count number basis.
c) Sliding triggering level in the neutron flux logarithmic signal.
The NIS of the RA-10 Reactor, incorporates as activation channels at the RPS, besides the traditional trigger described in a), the two signals described on points b) and c) in the previous paragraph.
This signals provide adequate protection against rapid changes during the pulse regime at reactor start-up. The trigger of safety function based on these signals can anticipate several decades the trigger obtained in current or fluctuation modes.
These triggers do not need to be inhibited when the channel passes from pulses to fluctuation. Finally the use of two different methods can mitigate common mode failures.

Autonomous area radiation monitoring

The Argentinian regulation requires to analyse the radiological risk figure, both for public and workers, and to demonstrate that this risk is acceptable given specific rules.
The RA-10 design includes several channels of area radiation monitors. One redundant channel is fed to the RPS and triggers the FSS actuation.
The area radiation monitoring system also includes channels disseminated in de the plant that feeds the Reactor Control and Monitoring System (RCMS) and triggers alarm. Those channel are safety category B, and are devoted to monitor normal operation of the plant.
The system also includes extended range monitoring channel used in accident condition for the Post Accident Monitoring System (PAM).
Focusing on facing human errors manipulating irradiation facilities or production facilities, and in events that shutting down the reactor does not decreases the dose rate in certain areas, the RA-10 design includes channels in the radiation area monitoring systems, whose function is to alert the operators or experimenters that they are in an area of high unacceptable dose rate. The systems increases the engineering safety features related to minimize this radiation risk to workers at the facility. Those systems

are the "*Autonomous Area Radiation Monitors"* focused on minimizing the workers dose.
These channel implement local audible and visible alarms and area safety category A.
Figure 6 shows the architecture of the Radiation Monitoring System (RMS).

Figure 6: Radiation Monitoring System architecture

Project status

The RA-10 project initiated its activities in 2010. The conceptual engineering was finished for the first semester of 2011. The basic engineering was finished for the last quarter of 2013. Nowadays we have almost finished the detailed engineering with a percentage of advance of 90% with only four work packages still running. We plan to close the design engineering stage in July 2016. The main contracts for the civil works and manufacturing and assembly are already signed. The main contract is the manufacturing and assembly ans is being carried out ofr INVAP S.E., our main partner and contractor.
We plan to finish the construction activities in 2019 and release the RA-10 to operation in 2020. Figure 7 shows the time line for the RA-10 Project.

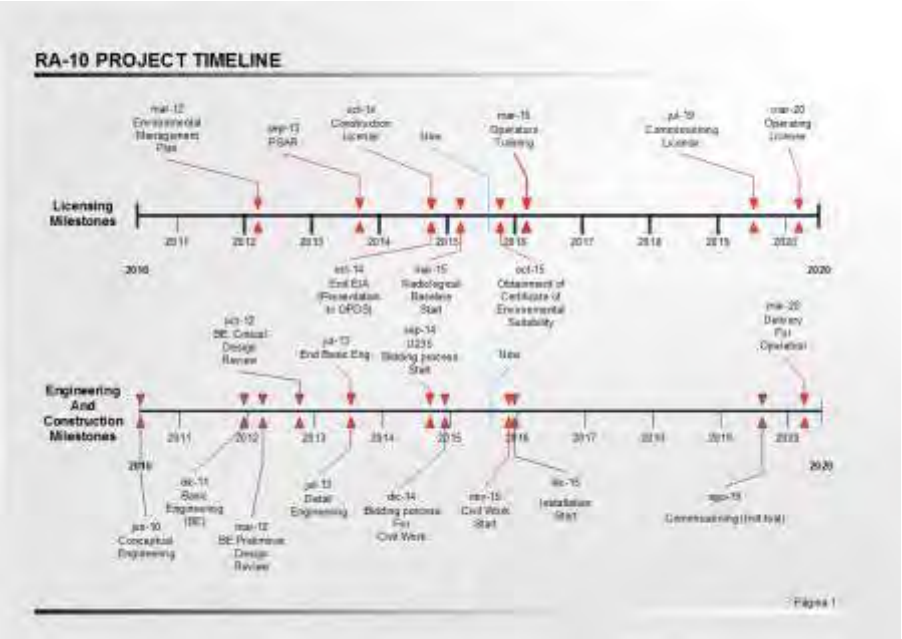

Figure 7: Time line for the RA-10 Project

Decommissioning

DISMANTLING OF THE SVAFO RESEARCH REACTOR R2 & R2-0 IN SWEDEN

Hans-Uwe ARNOLD
Dirk SCHNEIDER
AREVA GmbH, Paul-Gossen-Str. 100
91001 Erlangen - Germany

Gilles Clement
AREVA NP, 1 Place Jean MILLIER
92084 Paris - France

1 Introduction

AB Atomenergi in Sweden, ordered the facility through Allis-Chalmers. Time of operation was 1960 to 2005. Three sister facilities were built; Safari (RSA) and Petten (NL) are still operating. R2 and R2-0 reactors are installed in a three-part pond.

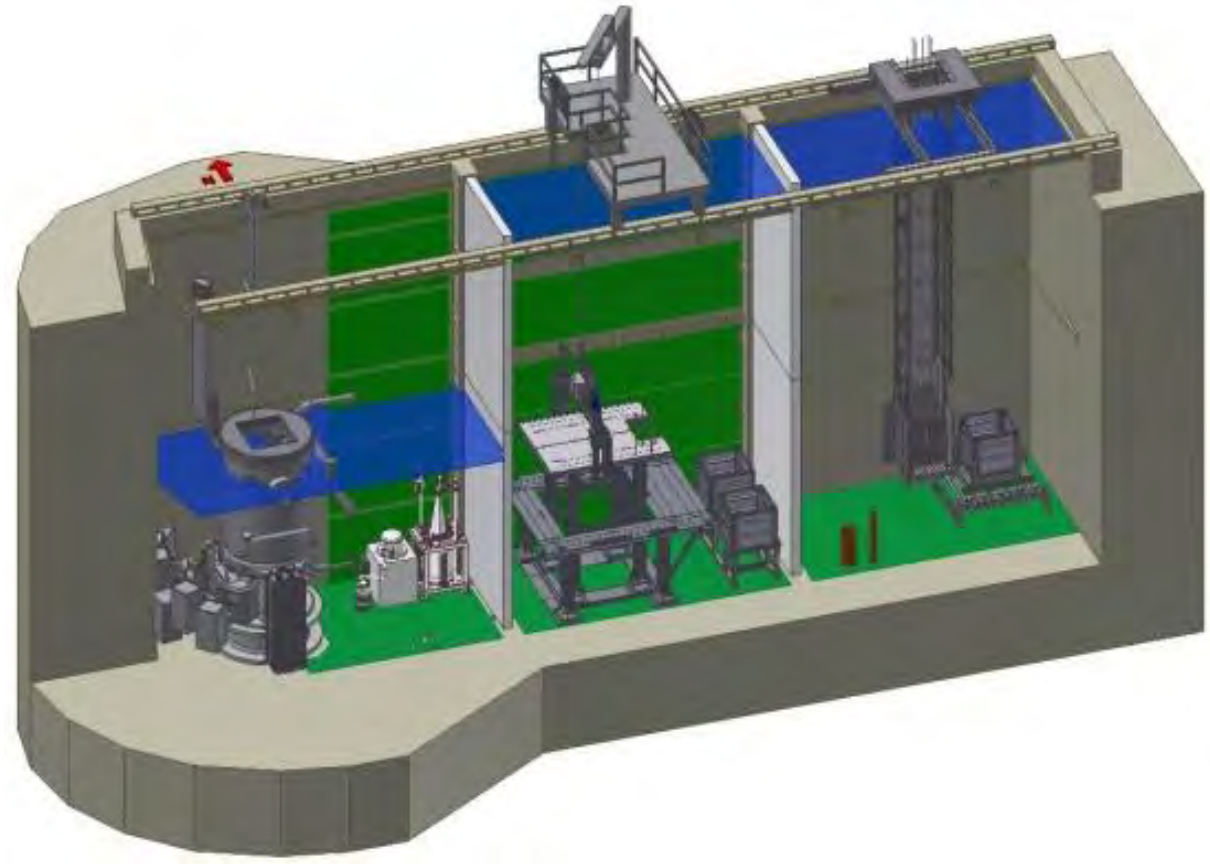

Fig 1. R2 & R2-0 reactors, D&D preparation phase

Each pool is approx. 6m x 3m x 9m and takes about 150m³ of water.
R2 had a performance of 30MW, upgraded in 1969 to 50MW and is placed in pool 1. Pool 2 was a storage place for spent fuel or test equipment. R2-0 was of convection cooled type

and ASEA's first reactor, loaded with MTR fuel elements (19.75% U235) and a power rating of 1MW. It was hooked up in a different area on the pool 3 wall.
Main points during operation were radiotherapy, attempts to examine the material behavior, test of fuel elements under BWR/PWR-conditions in special test loops, isotopes production for medical and industrial applications.
Dismantling project R2 began in year 2005. At the end of 2010 the dismantling-decision was finalized and the nuclear license by Studsvik was transferred to SVAFO.
The "Decommissioning plan" developed under Swedish "SSMFS 2008:1 directives", adjusted "Safety Assessment Report" and other documents up to "Radiological Mapping" were developed by SVAFO.
Phase 1 dismantling project was awarded to AREVA on 06/2014 and the work was finished in 2015 to the full satisfaction of the parties.

2 Scope of work

The decommissioning project is split into 3 phases. The target for phase 1 was:

- Dismantling R2-0 in Fig. 1 to the right
- Dismantling of equipment and peripheral systems of R2 in Fig. 2 to the left
- Dismantling R2
- Treatment of the disassembled components
- Emptying the ponds

The reactors consist of aluminium and stainless steel restraint structures and connection elements of the mostly flanged components.

R2-0 & R2	masses
Aluminium	5400kg
Stainless steel	6000kg
Peripheral equipment	1000kg
total	12400kg

Tab 1. R2 & R2-0 reactors, masses

The paper describes the steps, starting with the team building, then the dismantling operations with challenges encountered and lessons learned.

3 Challenges

While the most demanding on a radiological point of view was the R2-0 reactor, it was limited to approx. 1m³ construction volume but with an extremely heterogeneous activation profile. Based on the calculated radiological entrance data and later sampling nuclide vectors for both reactors depending on the real placement of the single component and on the material (aluminium and stainless steel) were created.
The 10 experimental channels (Fig. 2, right cut) and the extended reinforced constructions, the so-called restraint structures (Fig. 2, left cut) were the biggest challenges of the R2 reactor on a radiological and dismantling point of view. The highest activated component came from R2 reactor with 85Sv/h.

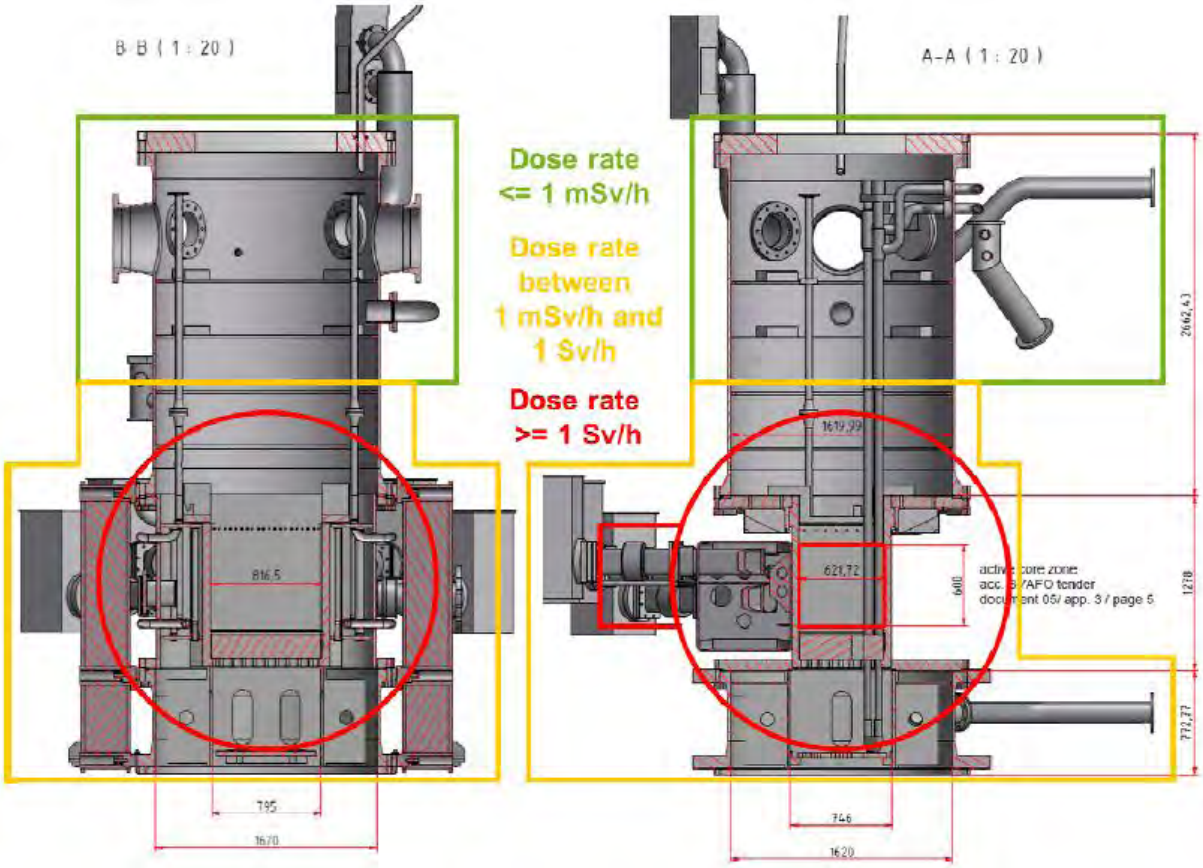

Fig 2. R2 reactor, radiological characterization

4 Preparation

The dismantling principles adopted on a safety point of view were the following: The always protected base area of the ponds served as a flexible buffer area for waste components and packaging. Specific protections were also installed on the walls to protect them from mechanical stress which may occur during dismantling work (Fig. 1, green areas).
A specific work platform was installed for the dismantling and sawing works closer to the water surface. This was the main working place used for the cutting of disassembled components under sufficient water cover (Fig. 1, pool in the middle).
Further safety related equipment was a special developed pneumatically balancer for a sensitive handling of components – mainly the two highly activated restraint structures - under confined dismounting conditions close to the pool liner.
A water cleaning system was used to collect the generated saw chips and fine particles mobilized during cutting (Fig. 1, left pool, right corner).

5 Performance

Nearly all the reactor components were flanged (Fig. 3). For dismounting a remote handled hydraulic impact wrench was used. In some cases some special cardanic prolongations were necessary to reach all nuts and screws. For intervention reasons an contact arc metal cutting (CAMC) tool was prepared, but all screws could be opened finally and the CAMC tool was not required to apply.

Fig 3. R2 reactor components

The cutting of the reactor components for packing according to the measured dose rate was performed on the cutting table in the middle pool by circumferential sawing technique with saw blades up to 1m in diameter.
The measured dose rates of the cut components were compared with the expectations and in case of significant deviations recalculated for new cutting layout and respectively packing plan. To use the time window we installed a very tight collaboration between the involved parties supported by WLAN access in the reactor hall. 84 pieces (1125kg) required special treatment after measurement because of conservative entrance data which had to be used for preliminary planning. Finally 24 cassettes for intermediate and 7 small cylindrical casks for high active waste were filled.

6 Results

No accidents, no pool leakages and a lower than estimated collective dose.

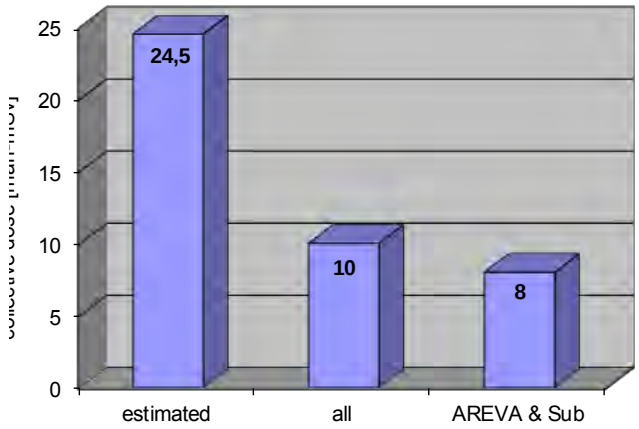

Tab 2. R2 & R2-0 reactor dismantling, collective dose

AN OPTIMIZED CASK TECHNOLOGY FOR CONDITIONING, TRANSPORTATION AND LONG TERM INTERIM STORAGE OF « END OF LIFE » NUCLEAR WASTE

F. LEFORT-MARY, C. LAMOUROUX, X. DOMINGO
AREVA NC
1 place Jean Millier, 92400, Courbevoie – France

B. DUMONT, B. KERR, V. LALOY
AREVA TN
1 rue de Hérons, 78180, Montigny le Bretonneux - France

ABSTRACT

During operational phase or when preparing the decommissioning of a nuclear facility, one has to consider a large diversity of nuclear waste and material in term of types, volumes and activities. This ranges from High Level Waste to Low Level Waste with different nature such as activated fuel structures, control rods, thimble plugs, in-core instrumentation, contaminated equipment, sludge, resins, liquids, standardized residues issued from the reprocessing,…

As of today, when the waste is ready for conditioning, the operator frequently faces the obligation to undertake multiple and costly waste management operations including handling, reconditioning or re-transferring from one package to another, for example when moving from on-site storage to transportation mode. Casks or packages available today are often limited to one waste type or to one step of the management process.

Multiplicity of packages for the management of several waste and material types induces significant administrative and operational complexity.

The optimization of waste streams from conditioning to long term interim storage is a key factor for reducing waste/material management costs.

To address this issue, AREVA developed an optimized cask technology for conditioning, transportation, and long term interim storage of nuclear waste, the TN® MW. This cask is answering to 2012 AIEA regulations with a total weight of 10T.

This cask is developed on a flexible concept, adapted to the various nuclear needs resulting in a family: from IP2 to B(U)/ B(U)F on-site/ international transport, long term interim storage. Licensing and manufacturing of several items of this TN® MW is already underway. A specific TN® MW cask will be dedicated to transportation and long term interim storage of low quantities of HLW / ILW waste issued from Research Reactor Spent Fuel reprocessing.

This paper aims at presenting the range of application of this technology taking into account the operational concerns.

1. Introduction

The purpose of this paper is to present a new dual purpose cask system dedicated to waste packaging, transportation and long term interim storage.

When preparing for the decommissioning of a nuclear facility, during its “end of life” management and while performing the actual dismantling operations, one has to consider a large diversity of nuclear waste in term of types, volumes and activities. It ranges from High Level Waste to Low Level Waste with different natures such as: spent resins, sludge, activated fuel structures, control rods, thimble plugs, in-core instrumentation, contaminated equipment…

As of today, when waste is segmented and ready for conditioning, the operator faces the challenge to package, transport, and long term interim store. Solutions available today are often limited to one single waste type or to a single step of the overall management route.

Operators in charge of waste management are frequently faced with the obligation to undertake multiple and costly handling, reconditioning or re-transferring operations from one package to another, for example when moving from on-site storage to transportation or from transportation to storage. More than often, they also have no choice but to select different packaging solutions for each different type of waste type, or even more constraining: to develop a new packaging solution when waste characteristics are not compatible with the specifications of existing designs. This is also induced by the variety of regulatory requirements that can be very different from one waste type to another and from one country to another.

Following such observations and recent feedback from operators, AREVA initiated the development of a new dual purpose cask – named TN® MW (MW for multi waste) - which main features are developed in the following sections.

2. OPERATIONS FEEDBACK

Operators in charge of waste management are expressing more and more concerns about the complexity, cost and sub-optimization of their waste management strategies.

Too often, each waste type has its own processing route and packaging solution (and some of them don’t even have any). This leads to a multiplicity of different packaging models, increasing volume to be stored and sub-optimized usage of the storage space. It can also lead to an additional multiplicity of operations to perform during the waste management life cycle. For example when a packaging model is adapted only to local storage of the waste and cannot be used for the next steps which are transportation and long term interim storage.

Most complex situation is encountered with HLW (High Level Waste) / ILLW (Intermediate Long Life Waste). Nuclear operators worldwide are looking for the best solution - technically and economically - to condition their HLW/ ILLW, keeping in mind that the waste generated today shall be conditioned for interim storage for a period of about 40 to 50 years nominally (or more if the final disposal is not available).

Following production of waste, operators could face a dilemma: either to define a strategy for the waste conditioning and packaging up to the long term interim storage period, or to containerize it temporarily, waiting for disposition conditions to be better defined before finalizing the waste management and packaging approaches. In some countries however, authorities allow only the first approach to be followed.

In the first case, one takes into account the available information and future trends relative to acceptability of the packages in order to define a robust solution. The benefit is to minimize costs for future package development and manufacturing, as well as to reduce the amount of multiple handling to transfer the waste package further down the road. Moreover it pushes for forward looking and standardization of packages as a far as possible, which is also another source of cost savings.

Pros and Cons of the second approach are inverted. It has the advantage of leaving the options opened, (and reducing the initial investments in solutions that would come to use in the future). However the main drawback is that it is exchanging uncertainties and unknowns related to future waste management criteria with uncertainties and unknowns related to the costs and risks of future retrieving and re-packaging operations. In addition, potential evolutions/degradations of the initial waste form in the meantime, would lead to extra costs and to the production of additional secondary waste.

It is however possible today to provide high integrity waste packaging solutions at a competitive price, such as the AREVA's TN® MW design. This system avoids multiple handling and reconditioning operations, while minimizing the risks of non-compliance with future WAC (Waste Acceptance Criteria).

3. FUNCTIONAL DEFINITION of the TN® MW dual purpose cask

The main drivers for the definition of the TN® MW dual purpose cask were the following:

- Cask is built-up from a generic cask design, with well integrated options providing flexibility and adaptability to different configurations, such as:
    - Standardized design of the key elements (with respect to licensing) including: the closure system, external dimensions of the package, penetrations, construction material, shock absorbers…
    - Additional shielding options inside the shell
    - Adaptable baskets to provide for waste retention

- Weight
    - Operators expressed the strong desire to handle casks with existing means available in their facilities (especially legacy plants under D&D). This avoids the need for extensive and costly refurbishment of existing devices or installing new and large equipment which usually have significant impact on the facility structure.
    - 10 metric Tons was found to be the appropriate limit. This also allows using standard forklifts to move the package, which provides additional handling flexibility

- Dimension
    - The cask is to be used in cluttered environment such as those encountered in decommissioning projects. For example in reactors facilities or research labs

there is limited available space to transfer casks and to stage them, before and after filling them with segmented waste. Sometimes waste packages have even to be interim stored in corridors because there are no other options.
    - Consequently it is of utmost importance to limit the outer height and width of the package in order to fit with the majority of existing limitations.
    - Our analysis of typical operators environment led to choose an overall volume limit of 1.5 m^3 with an outside diameter of 1080 mm (42,52 inches). The height is not critical but limited by the overall mass constraint. The standard height of 1475 mm (58,07 inches) was adopted, corresponding to a total mass of 10 metric Tons.

- Design life objectives
    - Operators target for interim storage duration range between 40/50 up to 70/100 years. The limiting factors are: long term demonstration for the resistance to corrosion, and the cask closure tightness. TN® MW technology can easily meet the corrosion resistance criteria. Concerning closure tightness, one can hardly reach more than 40 years without replacement of the gaskets or perform periodic monitoring and confirmation of its tightness.
    - Simplified maintenance
    - Transportation by road, rail or boat, inside ISO 20' container,
    - Wet and dry loading / unloading

4. FIRST TN® MW TYPE B(U) MODEL

4.1. Description of the cask – design presentation

The first model considered - in the TN® MW family - is a Type B(U) package (compliant with 2012 IAEA regulation) to be licensed for transportation and interim storage for at least 40 years.

The TN® MW cask is designed to provide most cost effective solutions in terms of capital as well as operating costs, using common fabrication material and standard procedures. It is intended to be used for packaging, transportation and storage of HLW (High Level Waste), ILLW (Intermediate Long Life Waste) and ILW (Intermediate Level Waste).

The design basis includes the following requirements:

- Ensure containment of the radioactive contents in any conditions (normal conditions, transportation conditions, accidental and storage conditions)
- Ensure occupational exposure protection of workers and public, with the following transportation limits:
    - 2 mSv/h at any point of the surface of the cask in normal conditions,
    - 0.1 mSv/h at any point, 2 m from the external surface of the cask in normal conditions
    - 10 mSv/h at any point, 1 meter from the external surface of the cask in accident conditions

An overview of the TN®MW cask is provided in the following figures:

Fig. 1. TN® MW cask in storage configuration

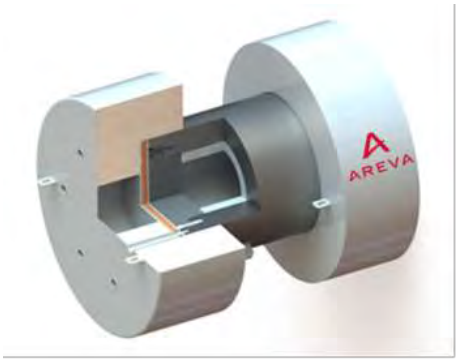

Fig. 2. TN® MW cask with shock absorbers for transportation configuration

Fig. 3. TN® MW cask in storage configuration positioned on its forklift frame

Fig. 4. Stripped down view of the TN® MW cask equipped with additional internal shielding

The waste types taken into account in the design basis include maintenance and operation waste as well as waste coming from dismantling operations. The TN® MW cask can be transported by road, rail or boat, inside an ISO 20' container with the following features:

- Underwater Loading / Unloading capabilities
- Dispositions to facilitate draining/drying of the package cavity
- On-site transfer and interim storage of the package without shock absorbers in vertical position
- Interim storage for up to 40 years on-site without maintenance (no gasket replacement nor leak-tightness monitoring required)

The TN® MW cask is composed of the following parts:

- A thick forged body with the following features
  - Bottom and top vents (on the lid) to perform draining / drying operations
  - 4 lifting lugs (welded or screwed on the container depending on client's preferences) or special gripping and handling interfaces
  - A closure system consisting of a lid secured by screws and two concentric gaskets (elastomer or metallic)
  - A test plug used for tightness monitoring
- Optional shielding shells
- Baskets to adapt the cavity and to maintain waste inside the cask
- Two shock absorbers (top and bottom) installed in transportation configuration.

4.2. Special characteristics

The cask design is based upon standard and proven models and technologies already developed and in use at AREVA's for other B(U) models. The body and lid are made of the same material and use same technology as used for other successful design packages, well approved by safety authorities. An important design constraint for the main structure is the brittle fracture at low temperatures. For this reason TN®MW is made of forged steel (instead of cast iron) which also provides for cost savings in the manufacturing process.

The shock absorbers are also derived from AREVA standard type B(U) existing design, well-known and accepted by safety authorities.

Metallic gaskets are used to ensure long term interim storage without maintenance for at least 40 years period, as already licensed for another series of AREVA casks.

4.3. Baskets characteristics

Different types of baskets can be used depending on the activity and shape of the waste.

The main requirements for the basket design are the following:

- they are made of non-corrosive material,
- the contents are mechanically wedged in the basket to fulfil to the transportation license requirements
- the baskets are drilled at their bottom if draining of the cavity is needed

	Dimensions (mm)	**Max Weight (including basket) (kg)**	**Max. Activity (TBq eq. Co-60)**
Basket Type 1 High volume / Intermediate activity	Diameter : 680 Height : 920	2 000	2
Basket Type 2 Low volume / High activity	Diameter : 515 Height : 820	650	300

Table 1. Basket types and characteristics

The TN® MW is designed to be leak-tight. For that purpose each penetration of the cask is designed to be able to maintain a total leak rate that does not exceed 1.10-8 Pa.m3.s-1 SLR.

The only penetrations of the TN®MW cask are:
- the primary lid,
- the draining and drying openings.

5. TN® MW Cask characteristics

Overall diameter (without shock absorbers)	1080 mm
Overall height (without shock absorbers)	1475 mm
Mass with type 1 basket (without shock absorbers)	8.5 T
Mass with type 2 basket (without shock absorbers)	9.6 T
Mass with type 1 basket (with shock absorbers)	10.4 T
Mass with type 2 basket (with shock absorbers)	11.5 T

Table 2. TN® MW Cask characteristics
NB: given masses and dimensions are nominal values

To satisfy tightness specifications, each penetration is equipped with a metallic gasket and machined stainless steel contact surfaces. The metallic gaskets are designed for long-term stability and have high corrosion resistance over the entire storage period.

These high performance gaskets are composed of two metal linings formed around a helical spring. The sealing principle is based on plastically deforming the gasket outer linings. Permanent contact of the lining against the sealing surface is ensured by the outward force exerted by the helically-wound spring. Additionally, all metallic gasket seating areas are stainless steel overlaid for improved surface control.

This type of metallic gaskets is fully qualified for a lifetime of at least 40 years, and has high temperature resistance (at least 280°C in normal operation and 370°C in accident conditions). Therefore, the containment analysis is performed so as to demonstrate the compliance with IAEA TSR-1 regulatory criteria:
- 10^{-6} A2 per hour in normal transport conditions,
- 1 A2 per week for other radionuclide under accident conditions.

A specific containment analysis is performed for each type of waste contents taking into account its distinctive characteristics (source distribution, isotopes, mass…).

6. NEXT TN® MW MODELS

The next models currently in development to expand the TN® MW family are the following:

- a “dry” version with no penetrations and reduced package cost when only dry loading/unloading is required
- a “transportation only” version with elastomer gaskets to reduce costs when no storage is anticipated
- an “IP-2 version” for LSA or SCO material with no shock absorbers and elastomer gaskets
- an “on-site transfer” specific version adapted to 400L drums with or without shock absorbers
- a “large version” adapted to special waste or equipment (such as dismantling parts that cannot be segmented on site) with the objective to stay below 60 T
- a “fissile” version for the transportation of waste with fissile material contents (ex: research reactor PIE samples or ^{99}Mo production residues)
- a “CSD” version for the transport and the interim storage of residues issued from the Research Reactor Spent Fuel reprocessing which are under the form of CSD-V, CSD-B, CSD-U and CSD-C (Universal canisters containing vitrified or compacted residues). This version will addressed to residues a thermal power up to 500 W and could also be adapted to residues up to 2 kW.

7. Conclusion

Optimization of the “End of Life” waste streams management - from conditioning, up to long term interim storage - is a key factor to monitor and reduce life cycle dismantling costs in a predictable way. The comprehensive and forward looking approach brought by the TN® MW technology provide operators in charge of waste management with reduction of equipment costs, types of different casks to procure, amount of operations to perform, and secondary wastes production.

Thanks to the flexibility of its design, the “CSD” version which is currently under consideration will help to find a solution in terms of transportation and interim storage of final waste for Research Reactors operators considering reprocessing in their spent fuel management strategy.

The fabrication, licensing and delivery of the first TN® MW items are to be achieved by 2017.

8. References

[1] C. Lamouroux, A. Rodrigues, E. Bossé, F. Cochin – Proceedings of Global 2015 “Innovative solutions for waste management: Optimization of waste packages for the long term disposal”

PREPARATION OF OSIRIS REACTOR SHUTDOWN AND DECOMMISSIONING

J.S. ZAMPA* ①, G. LASOU ②, M. AUCLAIR ③

① *OSIRIS reactor, DRSN/SEROS*

② *DPAD/CPSA*

③ *DRSN/SIREN*

CEA Centre de Saclay,
91191 Gif-sur-Yvette – France

* Corresponding author: jean-sebastien.zampa@cea.fr

ABSTRACT

OSIRIS is a French Material Testing Reactor (MTR) operated by the Alternative Energies and Atomic Energy Commission (CEA) since 1966. This reactor is designed to realize technological irradiations. It can also perform neutron transmutation doping of silicon and produce industrial and medical radioisotopes. The decision to shut down OSIRIS at the end of 2015 was announced by the French government in 2014.

Since this decision, OSIRIS had to face an increase of its activities. Many new irradiations were requested by its clients and partners to finalize the conclusions to the research programs before the shutdown. OSIRIS had also to increase significantly its production of technetium-99 to avoid a shortage of this medical radioelement in Europe in 2015 when two major research reactors were temporarily and simultaneously stopped.

The human resources and skills necessary after shutdown were analyzed and determined by OSIRIS management. These needs were confronted with the wishes of the workers in terms of professional evolutions. A part of the personal decided to participate to the dismantlement of OSIRIS and another part was helped to find opportunities in other CEA services, like in the JHR in Cadarache where their skills and knowledge will benefit to the successor of OSIRIS reactor. However some transfer could not been postponed after 2015. That is why, since 2014, OSIRIS has been faced to an important turnover of its personnel.

The preparation of pre-decommissioning activities was another challenge. In France, a certain number of operations are possible before the issuing of the decommissioning decree like the evacuation of dangerous and radioactive materials, the disassembling of experimental devices, the clean-up of the facility, the simplification and or revamping of utilities, the development of new areas for interim storage and waste management and the installation of new tools… An evolution of the organization chart of OSIRIS was decided. An operational team was created to determine and program these operations. The adaptation of the safety referential and of the operating and maintenance procedures to shutdown was launched. The new activities after shutdown were studied, prepared and scheduled.

A dedicated project team was also set up to evaluate different decommissioning scenarios. Different kinds of studies will help doing the job: complete history of the reactor events, inventories, characterizations of materials, waste management preparation, and eventually construction of new specific equipment. Most of these studies were launched before OSIRIS shutdown. The decommissioning report will be submitted to the French regulatory body for approval by December 2016.

1. INTRODUCTION

OSIRIS is a French Material Testing Reactor (MTR), located in SACLAY, near PARIS. It is operated by the Alternative Energies and Atomic Energy Commission (CEA). It was built from 1964 until 1966 and diverged the 8th of September 1966. The creation decree of OSIRIS was signed the 8th of June 1965.
The initial nominal power of OSIRIS reactor was 50 MW. After two years of operation, it was increased to 70 MW. A high enriched Uranium-Aluminum fuel was initially used. In 1980, OSIRIS was converted to a low enrichment fuel uranium oxide fuel (UO_2). Since 1995, OSIRIS reactor has used a silicide fuel with a 19.75 % enrichment.
OSIRIS was designed to realize technological irradiations of nuclear fuel and of structure material. However OSIRIS has also capabilities to perform neutron transmutation doping of silicon and to produce industrial and medical radioisotopes.
More than a hundred persons are employed by the CEA to operate the reactor, one quarter for the shift crew, one third for the design of irradiation devices and for the follow up of experimental programs, the rest for other operational and support activities.

Fig 1: CEA employee in charge of the operation of OSIRIS, one week before reactor shutdown

In 2011, the CEA asked the French regulatory body ASN to prorogate the shutdown of OSIRIS from 2015 until 2018. No answer was given to this request. The decision to shut down OSIRIS by the end of 2015 was announced by the French government during the summer 2014.
OSIRIS reactor was definitively stopped on the 16th of December 2015.

2. THE OPERATION OF OSIRIS REACTOR BEFORE ITS SHUTDOWN

During its last years of operation, and especially in 2015, OSIRIS was faced to a very strong increase of its irradiation activities.

This phenomenon can mostly be explained by the announcement of the shutdown of the reactor. Indeed, some clients and partners had delayed the decision to launch important irradiation programs until the very last moment. Other clients requested additional irradiations to extend or strengthen the conclusions of their experimental programs or just needed their samples to accumulate as much neutron fluency as possible.

The irradiations realized in 2015 were not only numerous, many of them were particularly innovative and have necessitated important evolutions of the existing irradiation devices. Some of then have permitted to study accidental nuclear physics and more precisely fission products release after clad rupture. Others tested innovative sensors measuring the evolution of creep under irradiation. Others brought important contribution to the CEA Am-recycling program [1]…

To answer this irradiation demand, the number of days of operation of OSIRIS was extended in 2015. The summer outage could be shortened and summer maintenance program reduced to the strict necessary. OSIRIS also benefited from an excellent availability coefficient. As a result, 9 reactor cycles corresponding to 195 days of operation could be realized in 2015 instead of 8 cycles usually (157 days of operation in 2014).

During the year 2015, the irradiation capacities of OSIRIS were exploited close to their maximum. A record was reached during the cycle F283, in October and November 2015 when 17 experiments were simultaneously irradiated in the reactor, 8 in the core and 9 in its close periphery (deflector). OSIRIS was also intensively used during its last cycle. 16 experiments were being irradiated when the reactor was shut down. The number of experiments irradiated in 2015 was 125, almost twice as much as in 2014 (67 experiments irradiated).

Fig 2: The core of OSIRIS reactor during cycle F283

The production of medical radioisotopes like ^{99}Mo/^{99}Tc used for scintigraphy also reached a peak in 2015. During the same cycle (F283), as two important European reactors were stopped, 78 MOLLY targets were irradiated in OSIRIS. A shortage in the European technetium production was thus avoided. During the same cycle, 33 MOLLY targets were simultaneously irradiated in the reactor (a simultaneous irradiation of 30 targets was the previous record). Such a massive MOLLY production had been made possible thanks to the creation of new MOLLY irradiation locations in the core of OSIRIS. The total amount of irradiated targets of MOLLY in 2015 was 303. It represents more than a million scintigraphy (mainly bone scanning). It is not a record for OSIRIS but it is a significant contribution to public health and a great pride for OSIRIS staff that have realize this task simultaneously as a huge experimental program.

It must be noted than an increase of irradiation activities such as the one encountered at OSIRIS before reactor shutdown is not a unique case. SILOE Reactor in CEA Grenoble was also faced to a similar phenomenon before it was shut down in 1997.

3. IMPACT OF SHUTDOWN ON HUMAN RESOURCES

The evolutions of the nature of the activities, of the skills needed and of the number of employees needed for OSIRIS operation were carefully analyzed by OSIRIS management before the reactor shutdown. The goals of this analysis were:

- to keep the reactor fully operation and staffed during its last years of operation,
- to prepare the reduction of staff related to shutdown,
- to maintain sufficient well trained staff after shutdown.

Six shift crews ensure a continuous follow-up of OSIRIS reactor. Each team consists of five members: a supervisor, a reactor conductor, a mechanic, an electrician and an experimenter. Having OSIRIS shift crews fully staffed is always a challenge and an important investment, the duration of the training and tutorship programs necessary to be habilitated to join a shift crew being more than a year. In 2015, the number of transfers from OSIRIS was unusually high. In addition, the number of departures for retirements was important. That is why every transfer was carefully studied. Sometimes, the transfer could be delayed. Thanks to these efforts, most of the movements could be anticipated, and fully trained and habilitated new operators were available to replace the missing persons when needed. Permutations within shift teams and contributions of former members of shift teams have also contributed to temporary solutions in some difficult cases. An agreement was also found to treat the financial and statutory evolution of employees quitting shift crew after OSIRIS shutdown. The existence of such an agreement was a very positive point to maintain the shift crew fully staffed and operational in 2015.

Irradiations and experimental activities were identified as the first activities impacted by OSIRIS shutdown. The activities of conception of new irradiation devices stopped around one year before shutdown. Even if irradiation follow-up was important during the last year of operation, experimental activity came to a complete stop immediately after shutdown. That is why, many measures have been take since the beginning of 2015 to facilitate the transfer of the experimenters: preliminary information of new vacant positions, priority to apply for a vacant position, favorable conditions if an experimenter needs to move for his professional reconversion etc.

Projections of the needs of workers for reactor operation after shutdown had been established longtime before the shutdown. These projection were not only done in terms of number of workers but also in terms of skills needed. To match these projections to individual cases, each employee of OSIRIS passed two individual interviews in 2015. During these interviews the possible perspectives of work in OSIRIS for each worker were discussed. Each-one was then required to express its projects or wishes, keeping on working for OSIRIS or searching for a professional opportunity in another service of the CEA after the reactor shutdown. According to his needs, several actions could be initiated after the interviews to help each worker for the realization of its professional project: training program, coaching… The results of these interviews gave precious information to manage staff evolution after shutdown.

Specific measures were also taken to facilitate transfers of OSIRIS workers to CADARACHE where they can make the JHR reactor benefit from their knowledge and experience of OSIRIS.

It must be noted that even if OSIRIS shutdown will globally lead to a decrease of activity, some activities remains very important: recruitments have even been necessary in some fields like nuclear waste management, project management or safety.

4. THE OPMAD: OSIRIS AFTER SHUTDOWN AND BEFORE THE DISMANTLEMENT DECREE

In France, dismantling operations properly speaking cannot be started immediately after shutdown. A dismantlement decree must first be obtained. However, some operations, called OPMAD (OPérations Préliminaires à la Mise à l'Arrêt Définitif) can be achieved before the dismantlement decree. They are limited to the following:

- last operations to operate the facility,
- setting the facility in order (disassembling of experimental devices…),
- preparation of decommissioning operations (project preparation, staff training, installation of equipment necessary for dismantlement, development of new areas for interim storage and waste management, installation of new tools…)
- characterization of the facility (production of radiological maps, including destructive tests or sampling of elements relevant for decommissioning),
- simplification, revamping, adaptation or renovation of utilities networks (electricity, fluids, ventilation, etc.),
- evacuation of hazardous or radioactive substances (radioactive materials, chemicals, fluids, waste, etc.).

Irreversible operations are generally prohibited except some limited irreversible operations necessary for the evacuation of radioactive and hazardous substances that can be allowed on a case-by-case basis.

A project group was created to supervise the OPMAD. In 2015, the OPMAD group realized a list of the OPMAD to be realized before dismantlement. Each operation was described, shortly studied and justified. This list was submitted to the Regulatory Body (ASN) for approval.
At the same time, the general operating rules of the reactor and the control and maintenance procedures were adapted to better fit to post shutdown conditions.

The first OPMAD to realize in 2016 were studied in details in 2015 and already scheduled before shutdown. Most of them consist in the evacuations of fuel, or in the disassembly and evacuation of irradiated or contaminated items and experimental equipment.

A pilot projects consisting of underwater cutting of the former aluminum vessel fuel rack was carried out during the summer outage in 2015. When OSIRIS was in operation, fuel elements control rods were placed in an aluminum fuel rack, placed in the reactor vessel. OSIRIS vessel fuel rack as well as the reactor vessel had been replaced in the year 2001 and stored underwater, in the water channel of the facility, to benefit from their activity decay. In order to realize the cutting of the former fuel rack, a new underwater cutting machine, more precisely a nibbler, was ordered. The machine was first tested and adapted underwater, in a non nuclear environment. The limitation of the production of metal filings was an important objective. The cutting was a success. It was completed in less than two weeks. Only few metal filings were produced. These filings could be easily retrieved thanks to an underwater suction device.

Other OPMAD planned to be launched in 2016 are the following:
<u>Adaptation of electric emergency-electrical supply inverters:</u>
After OSIRIS shutdown, the electrical inverters are too powerful for the electric emergency-electrical supply used in case of SBO (Station Black Out). The CEA will take advantage of the maintenance program of some of these inverter to size down their capacities.

Isolation and draining of the secondary circuit,
After reactor shutdown, the cooling of the reactor by the secondary circuit is no longer necessary. However the refrigeration units of the facility will still need external cooling. Emptying the main lines of the secondary circuit, and proceeding to appropriate permanent isolations of these lines will permit an improvement of the robustness of the first and the second containment barriers. At the same time, some optimizations on the line that will remain in service for the refrigeration units will be realized to reduce the consumption of cooling water.
Safe isolation of unused parts of the primary circuits,
This operation consists in safe isolations of portions of the primary circuit (primary pump, Heat exchangers…) as well as of auxiliary circuits (clad failure detection lines, emergency filtration etc…) that are no longer necessary after shutdown. This reduction of the size of circuits containing contaminated water will lead to a simplification of the operations and controls realized and have a positive impact on the risks of incident. The isolation of the main circuit underwater could be realized thanks to the intervention of divers [2].

Some OPMAD to perform during the following years are already being carefully studied like the complete revamping of the electrical distribution of the facility including the replacement of some of the Diesel generators, the disassembly of reactor vessel (even if this operation was included in OSIRIS initial design and already realized twice, the Safety Authority addressed strong objection against its realization during the first phase of the OPMAD), the disassembly of primary pumps and heat exchangers.

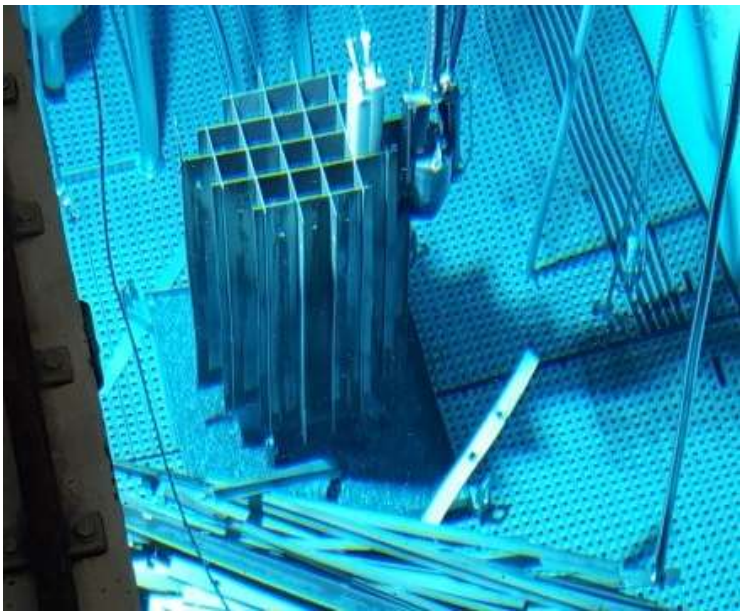

Fig 3: underwater cutting of vessel internal rack during summer 2015

5. DECOMMISSIONING PROJECT

5.1 Preliminary studies

The first task of the decommissioning project is to provide the CEA hierarchy with the most realistic view of the duration, costs and risks of the project. This task will be continued during the entire new life of the facility.

In order to evaluate the different scenarios for Osiris's dismantling, it is necessary to know precisely the status of the facility. Various studies and investigations have been launched since several years to achieve this goal. These preliminary studies concern:

- Conducting an inventory of all the waste that will be generated during decommissioning, comprising Long Lived Intermediate Level Waste, Low and Very Low Level Waste and conventional waste, and also some exotic and difficult to manage components and waste (like beryllium rods for example),
- Compiling a history of the operations of the facility that will permit identification of all significant events and possible or proven contamination of surfaces,
- Recovering and digitizing the blueprints of the facility (> 16000) and identifying points of interest, for example pipes sunk in concrete,
- Realizing a 3D laser scan and modeling the different parts of the building and equipment,
- Simulating and calculating the level of activation of the pool's walls,
- Measuring different spectrums and dose rates, particularly for the most irradiating waste in order to evaluate the waste routes.

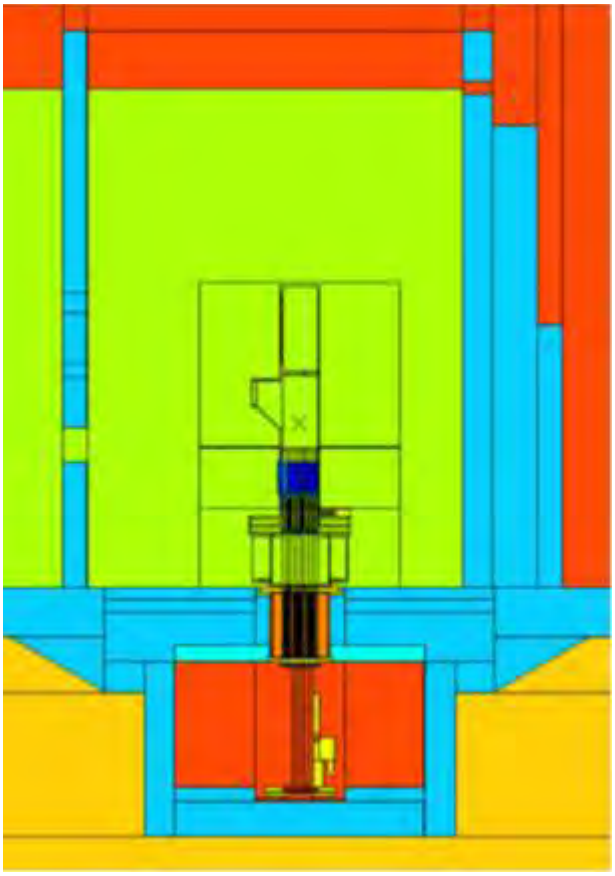

Fig 4: Tripoli model of OSIRIS bloc pile and pool used for the activation calculation (courtesy CEA/DEN/DM2S/SERMA)

More intrusive actions are ongoing since the reactor shutdown: civil engineering studies, identification of the quality of concrete and reinforcements, resistance of slabs, a complete asbestos diagnosis of the processes and an investigation of the pollution of surrounding soil. Detection of hot spots will also be carried out by a gamma camera scanning of the facility.
All these elements will serve as an entry to the safety report that will submitted to the Nuclear Safety Authority in December 2016.

5.2 SACLAY Strategy

It is also necessary to know the environment of OSIRIS. In our case, the Saclay Solid Waste Treatment facility will be definitely closed in 2017 before the beginning of OSIRIS dismantling thus meaning the end of the ILW route at SACLAY center.
The role of the project team is then to trace new ways to treat the waste. Construction of a shielded cell for packaging mid and highly irradiating waste is being investigated. ECODI

(Enceinte de COnditionnement des Déchets Irradiants) will be built in a new building next to the rear of OSIRIS hot cells.

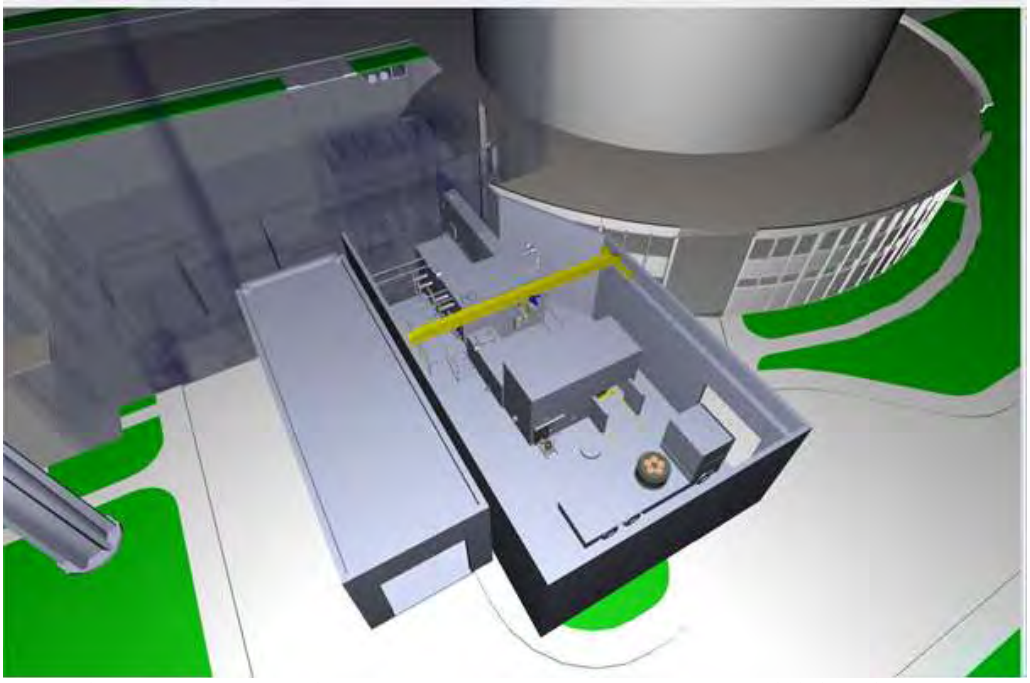

Fig: Schematic view of the shielded cell in the rear zone of OSIRIS hot cells

Irradiating waste will be cut in small pieces in the water canals, then transferred in the hot cells, dried, and sent in baskets to ECODI, where it will be characterized and sorted. The interest of the characterization and sorting at source is flow's optimization. Aluminum waste will further be melted in order to drastically reduce the surface in contact when cementing.
The waste will be put in 50 liters leak-free bins, using a patented technique that guarantees the absence of external contamination. Finally, the bins will be send to intermediate storage facilities in Cadarache for mid irradiating waste and in MARCOULE for highly irradiating waste.

OSIRIS facility, if ECODI project succeeds, would also be able to treat the irradiating waste flow coming from the other SACLAY reactor ORPHEE; if technically possible, once this facility comes into the decommissioning phase.

Another problem that will have to be addressed by the project team is the liquid waste management. This liquid waste (water in the pool and the canals) is low activity, the principal isotope being tritium. But the liquid waste treatment facility in SACLAY now has different priorities and may not be able to take care of the 2000 cubic meters of liquid waste.

5.3 Dismantling Scenario

OSIRIS dismantling scenario is typical for a reactor pool. The main steps are:

- Evacuation of the irradiated fuel elements, radioactive sources and other dangerous materials (sodium potassium alloy)
- Underwater disassembly and cutting operations for irradiating waste
- Emptying of the pool and the canals
- Disassembly and evacuation operations of other equipment
- Disassembly and evacuation of hot cells
    - Casing removal
    - Structure's decontamination and remediation

At each step, it is necessary to identify methods and equipment that will optimize costs and duration while providing the maximum level of safety and security. ALARA (As Low As

Reasonably Achievable) approach is integrated at every step of the project. When necessary, alternative solutions are proposed in addition to the nominal solution.

6. CONCLUSION

After its cessation of activities last December, the reactor is now in the preparatory phase for final shutdown, OPMAD in French.
The decommissioning safety report will be submitted to the French regulatory body in December 2016, will be analyzed by the French Technical Safety Organization IRSN and will also be subject of a public inquiry. The dismantling decree is awaited between 2019 and 2021. This decision will mark the official entry into the decommissioning project, a second life for the facility, which is planned over a period of 20 years.
Full dialogue between the different teams responsible for the project, the preparatory phase and the maintenance of the facility is essential for the success of the whole project. A delicate and crucial phase is the evacuation of irradiating waste which is planned over 8 to 10 years, a bit more if ORPHEE waste is included.
Beyond the legal obligation of immediate dismantling for the Alternative Energies and Atomic Energy Commission (CEA), every decommissioning project is a challenge for the future of nuclear energy.

7. REFERENCES

[1] Design and first operation of the DIAMINO ($U^{241}AmO_2$) experiment in OSIRIS MTR for Am-recycling program - IGORR 2014 - S. BENDOTTI, C. NEYROUD, S. BEJAOUI, T. LAMBERT (CEA)

[2] Diving in the pool of a Research Reactor - Inspection of the natural convection valves of the primary circuit of OSIRIS reactor during summer outage - IGORR 2014 - J.S. ZAMPA, G. BARRACHIN (CEA)

ANALYSIS OF THE ACTIVATION AT THE END OF OPERATION OF THE BERLIN EXPERIMENTAL REACTOR II

JANIS LAPINS, NICOLE GUILLIARD, WOLFGANG BERNNAT
Institute for Nuclear Technology and Energy Systems, University of Stuttgart
Pfaffenwaldring 31, D-70569 Stuttgart

STEPHAN WELZEL, MICHAEL ROSE
Helmholtz-Zentrum Berlin GmbH,
Hahn-Meitner-Platz1, D-14109 Berlin

ABSTRACT

For the Research Reactor BER II, for which operation is planned until end 2019 (start 1973), an analysis of the activation of the main structure is done to support the decommissioning planning at the "Helmholtz-Zentrum Berlin für Materialien und Energie GmbH". The whole geometry is modelled with MCNP6 where all (major) details can be accounted for (plate fuel elements, irradiation tubes, cold neutron source etc.) without discretisation. MCNP6 offers an automatic export of the geometry for a regular 3-d mesh grid to PARTISN. In both codes, the neutron transport equation can be solved for identical material compositions. MCNP6 uses continuous energy microscopic cross sections (XS), for PARTISN macroscopic multi-group XS were generated with the ORNL code SCALE6.1. As irradiation history a lumped period (1974 - 85) and a detailed period (1991 – 2019) was defined with a large number of irradiation and decay steps. The activation calculation is done using the FISPACT programme. For the environment of the complex irradiation tubes, an alternative approach for the flux calculation is used based on MCNP6. To check the validity of the computational model and the results, activation measurements for specific components at the beam tube of the cold neutron source are used and compared with calculated values.

1. Introduction

The Berlin Experimental Reactor-II (BER-II) started operation in 1974 with 5 MW. In 1985 it underwent retrofitting where power was increased to 10 MW, a beryllium reflector was added, and the thermal column made of graphite was replaced by a conical irradiation tube with a supercritical hydrogen container that is to generate cold neutrons. It is planned to operate until end of 2019. In order to prepare the decommissioning, it is necessary to have activity maps of the distribution of important radionuclides such as Co-60, Fe-55, Eu-152, H-3 and C-14.

With its numerous irradiation tubes and a cold neutron source, a full 3-d geometry model must be regarded. Therefore use is made of a combination of stochastic (MCNP6 [1]) and deterministic discrete ordinate (PARTISN [2]) methods to determine the neutron flux for the whole reactor geometry including the entire concrete structure on a detailed 3-d grid. With the neutron flux together with the time history provided by the Helmholtz-Zentrum Berlin is used to determine the activity distribution for each cell of the geometry with the help of the programme FISPACT [3].

2. The BER-II and its Main Components

The BER-II is a research reactor with fuel elements that are made up by UAl-alloy plate pins encapsulated in aluminium. Each fuel element contains 23 plate pins. 30 fuel elements make a core of 60 cm height. The core consists of a rectangular grid with 6 x 7 positions. Of the 42 positions, only 30 are filled with fuel elements. There are six control rods to control the neutron flux. A control rod contains B_4C together with some fuel plates. Additionally, there are some positions in the outer core that are filled with beryllium reflector elements and one position for irradiation (C3), see Figure 1. The core is surrounded by a 20 cm thick beryllium reflector layer in which the ends of the 9 irradiation tubes are located. There is also a conical irradiation tube that houses a cold neutron source with supercritical hydrogen. This cone contains two types of neutron guides which reach the experimental hall in the next building. The core support is made of AlMg3. The core is located in a 12 m deep pool with 3.5 metres in diameter and cooled by light water. Next to the reactor pool there is a pool (3.5 m) for the spent fuel elements. Both pools are arranged side by side and are interconnected to enable fuel changes. The pool is surrounded by an AlMg3 liner followed by a concrete structure for radiation shielding. In the core region, barite concrete with a density of 3.4 t/m^3 is used. Surrounding the cold neutron source, ferrite concrete with a density of 4.3 t/m^3 is used. All other concrete structures are normal concrete with a density of 2.3 t/m^3.

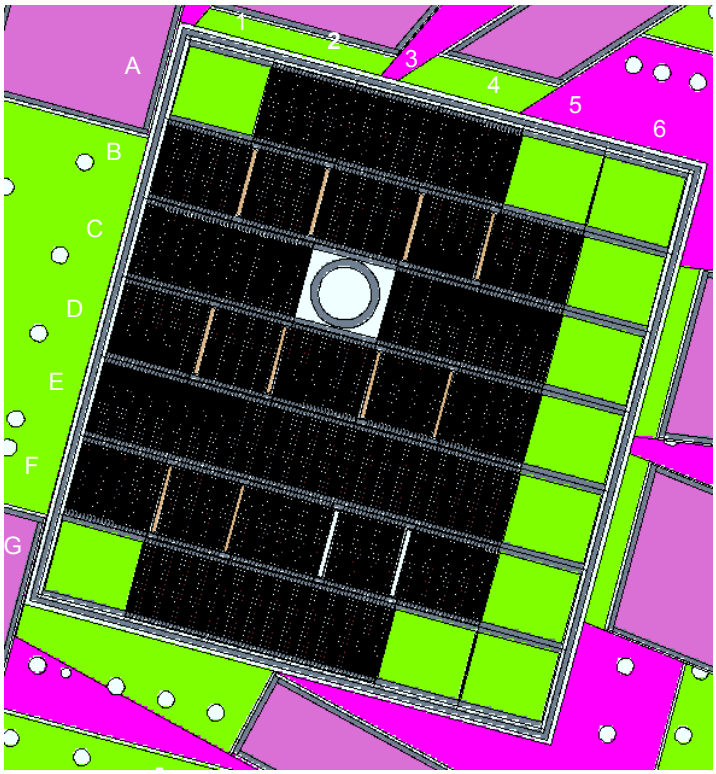

Figure 1: Horizontal section: Subdivision of the BER-II core with 10 MW, there are 42 positions, 24 positions (black) are filled with regular MTR fuel elements, 6 positions allow insertion of the control rods (B2, B4, D2, D4, F2, F4, black & brown), position C3 is for irradiation; corner elements are filled with beryllium reflector elements. The part surrounding the core (green and pink) is the beryllium reflector with drilling holes; light pink parts are the ends of the irradiation tubes.

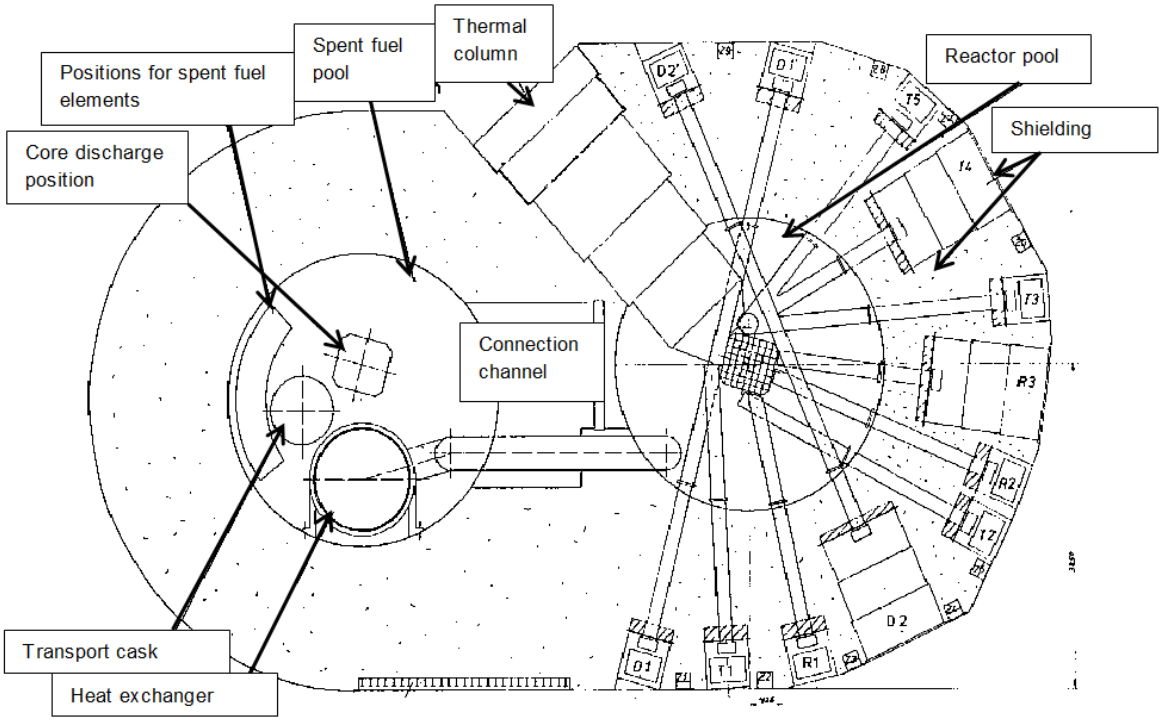

Figure 2: Horizontal section of the spent fuel pool and the reactor pool in a side-by-side arrangement with its irradiation tubes. The thermal column was replaced by a conical irradiation tube with a cold neutron source. The diagonal irradiation channel D2 and D2' and the tangential irradiation channel T3 were closed during retrofitting from 1985 - 1991 [5]

3. Method of Calculation

In order to have an accurate description of all the components with their real geometric complexity, MCNP6 is used to create the geometry model. With MCNP6, all components can be input explicitly without discretisation. However, for MCNP6 it is rather time consuming, if not impossible, to calculate the neutron flux distribution for the most remote parts of the concrete. Given that, a different approach was applied. MCNP6 has an automatic geometry export option which can be used for the discrete ordinates transport code PARTISN. Since PARTISN does need a discretisation, a mesh grid subdivision in x,y,z-direction has to be provided within the MCNP6 input before applying the export option. When using the export function, the reactor geometry is subdivided into volumes according to the subdivision done by the user with up to 6 different materials from MCNP6 being mixed together with their respective volume fractions. For all different materials appropriate macroscopic cross sections (XS) have to be generated for PARTISN and subsequently used for determination of the neutron flux distribution. To create these XS, use was made of the SCALE6 package [7]. Here, the ENDF/B-VII.1 library is available in the typical 238 energy group structure and was used to account for self-shielding of the fuel the unresolved resonance range which was treated with the BONAMI module applying the Bondarenko method of background XS. The 238 energy group cross sections were then used for 1-d spectrum calculations with ANISN [7] to account for the anisotropy of both the neutron scattering and the neutron flux.

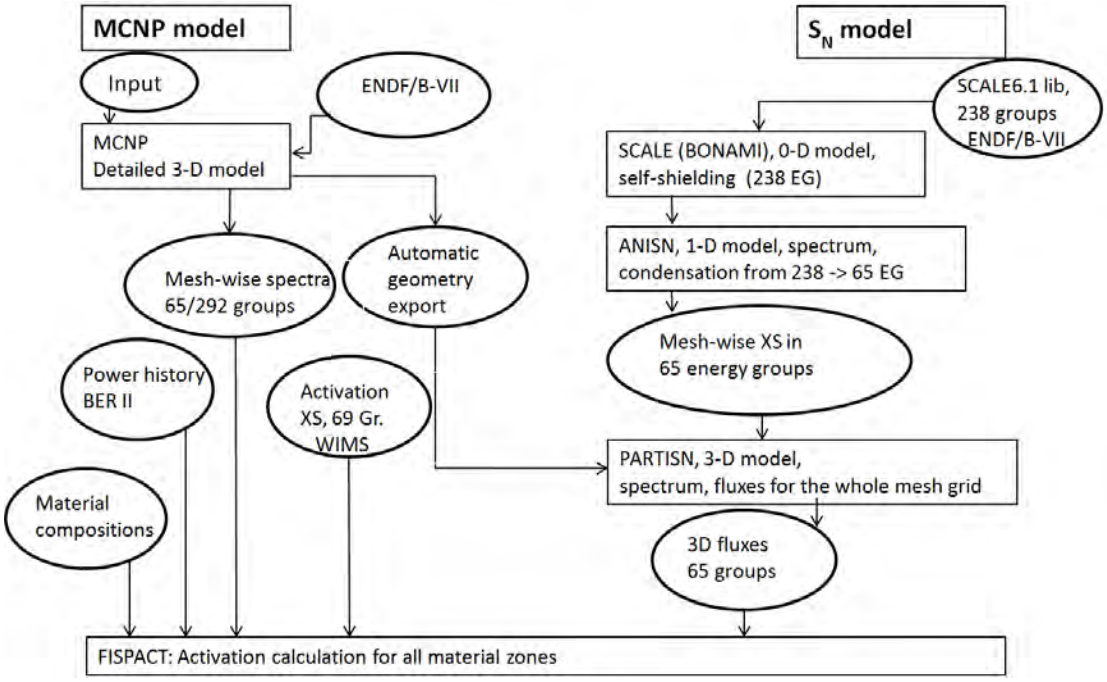

Figure 3: Method of computation with both MCNP6 and discrete ordinates, the mesh-wise spectra of MCNP6 (left side) are only used for calculation of details, i.e. the neutron flux distribution for certain areas applying mesh tallies

This is done using a S_N order of 16 with a Legendre expansion of P_5. The energy groups are condensed from 238 to 65 groups. With the spectrum weighted macroscopic XS, the neutron transport equation is solved for the whole reactor geometry with PARTISN. The solution is a detailed flux distribution in 65 groups for a fine mesh grid. For the activation analysis, more data have to be available, e.g. the power history over the whole lifetime has to be accounted for; also the detailed compositions of all materials for which activation has to be determined. This comprises not only the main nuclides necessary to compute the neutron flux, but also the traces of manufacturing impurities such as uranium, cobalt, caesium, europium or gadolinium etc. Lastly, activation XS have to be generated. The energy bin structures of the spectra of the transport calculation have to be adapted to the FISPACT structure.

This whole procedure is depicted in Figure 3. On the left side of this figure, there is also one step included that is only performed if certain details have to be calculated more accurately, e.g. the activity of certain screw nuts. To get a more detailed activation distribution around the beam tubes, special MCNP6 transport calculations were performed for fine mesh grids (mesh tallies). For these calculations, weight windows generated derived from adjoint fluxes calculated with PARTISN.

4. MCNP6 Model of the BER-II and Materials

The geometry of the BER-II was modelled with MCNP6. From a previous project that concerned the optimisation of the geometry of the cold neutron source container, the model of the core up to the aluminium liner was already available. In this work, the components surrounding the reactor pool were complemented. This includes the spent fuel pool, the concrete shielding, and the irradiation tubes with their respective penetrations within the concrete to coincide with the irradiation tubes within the reactor pool. The model comprises 17 different materials: the fuel elements, $AlMg_3$, water, beryllium, helium, CO_2, air, stainless steel, steel, grey cast iron, boron carbide, bismuth pellets, lead shot, normal concrete, magnetite concrete, barite concrete, and

concrete bricks with a steel coating. However, the barite concrete also contains steel reinforcements which are denser in the region close to the reactor pool and the region next to the reactor hall (see Figure 4, three subdivision of the barite concrete). All, materials are assumed at 300 K, except the hydrogen chamber in the conical irradiation tube which is at 25 K.

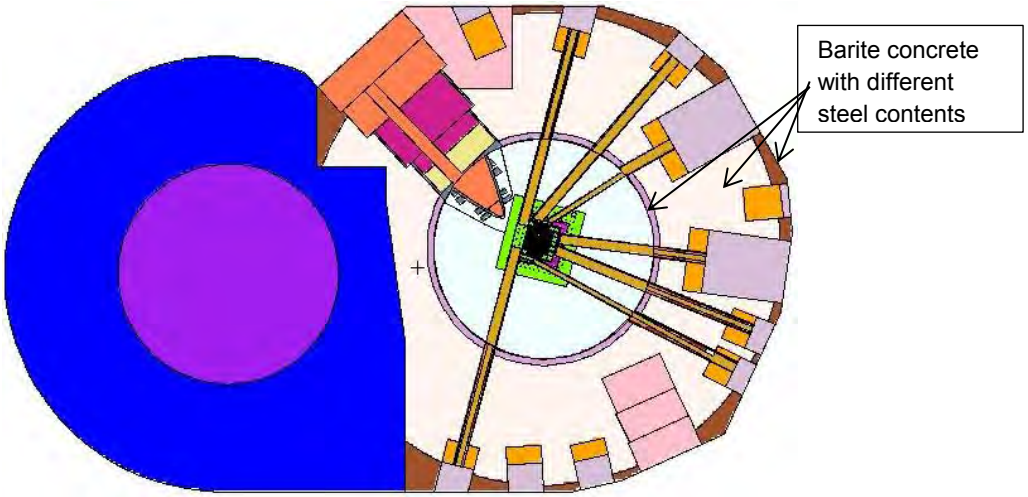

Figure 4: Horizontal section at the plane with 7 out of 9 irradiation tubes. The blue part is the spent fuel pool, normal concrete and the water within. The right side shows the core (black), the beryllium reflector (green), and 7 irradiation tubes (light brown).

Using the export option from MCNP6 to PARTISN the geometry is discretised according to the user-provided subdivisions. While the mesh grid is finer in the core region (approx. 3.5 cm), the mesh size increases towards the periphery (5+ cm). The coarsest mesh size is 11 cm. The overall number of computational cells for the whole geometry in PARTISN is 2,790,000 (155 x 120 x 158).

Material specifications are provided by the Helmholtz-Zentrum Berlin (HZB). However, for some components there are only material specifications, e.g. Co < 10 ppm which are not measured afterwards. Since cobalt is not an alloy element, the respective content is estimated according to either values from literature or from other reactor activation analysis. Here, measured values for impurities of uranium, caesium, gadolinium, cobalt, and europium content could be used for this analysis.

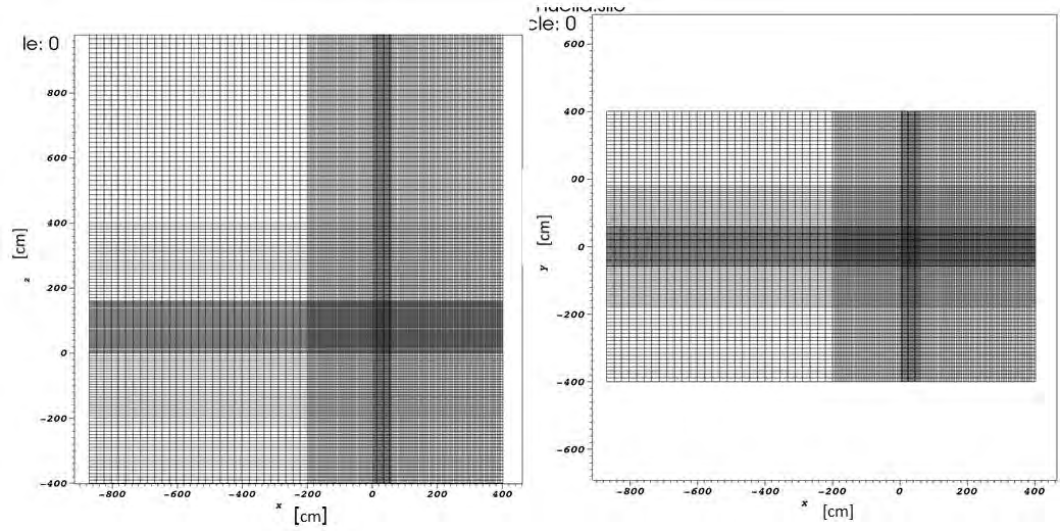

Figure 5: Mesh size distribution in the x,z-plane (left) and in the x,y-plane (right), the region with the densest mesh grid is the core region

5. Results of the Neutron Flux Calculation

The neutron flux distribution of the BER-II produced with PARTISN for the whole geometry is shown for a section of major interest, i.e. the height of the irradiation tubes. The neutron flux ranges over 59 (!) orders of magnitude (2.8e+14 – 7e-45), but for reasons of visibility the minimum is set to 1.e-4. In Figure 6 and Figure 7, it is shown that there is still neutrons going over the concrete structure next to the cold neutron source and even find their way to the leftmost side by travelling through the concrete structure.

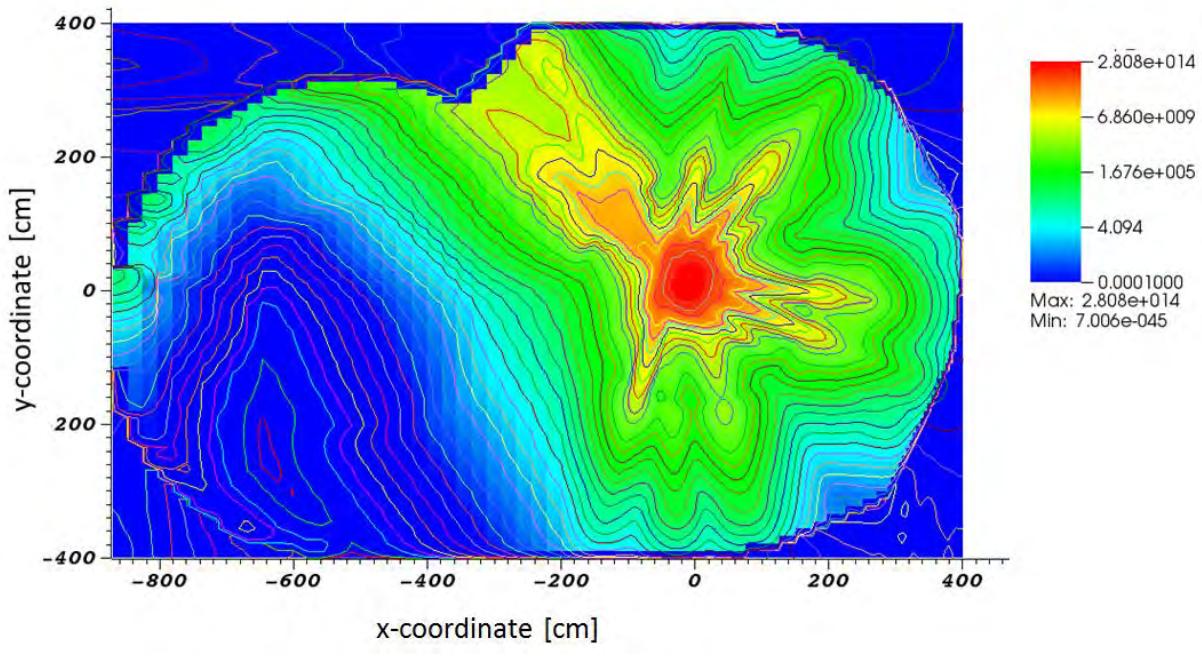

Figure 6: Fast neutron flux distribution in the x,y-plane with 7 irradiation tubes, section see Figure 4

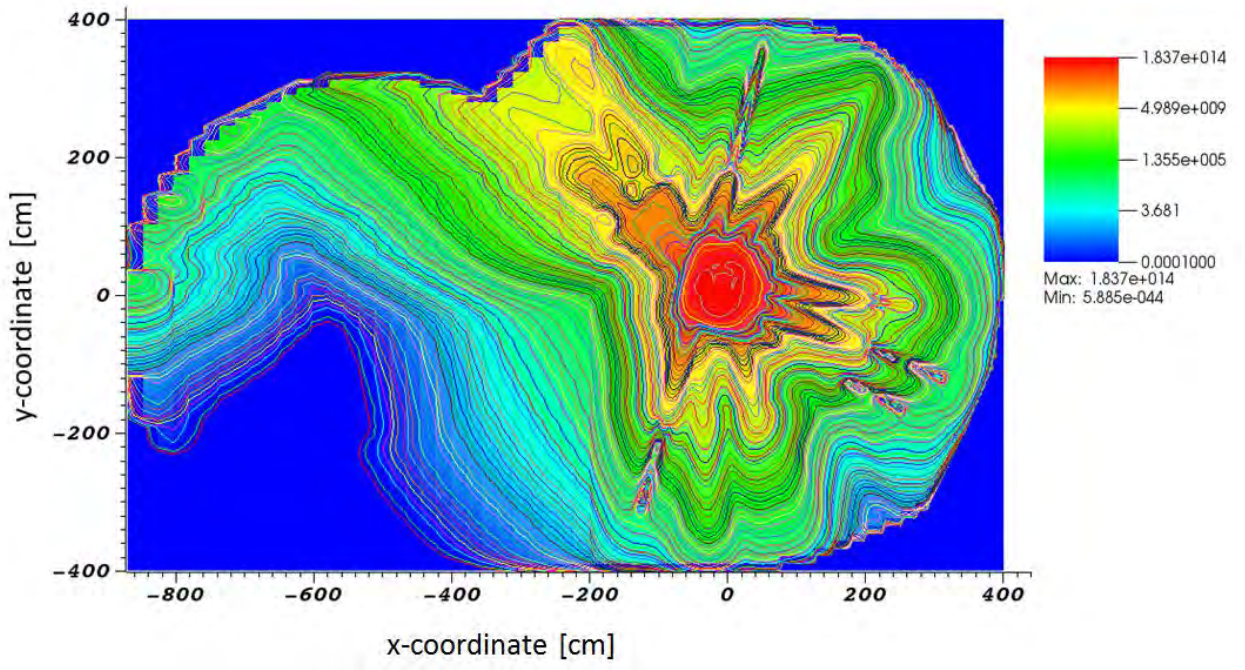

Figure 7: Distribution of the thermal neutron flux on the plane with 7 irradiation tubes, compare Figure 4

6. Power History

For the activation, it is important to know the neutron flux distribution throughout the whole operational life-time. In this analysis, it is assumed that the neutron flux distribution throughout the whole operation time keeps the shape, but the amplitude is adjusted with respect to the increase in burn-up in a certain time interval. For the years 1974 – 1985, the increase of burn-up is only given for a whole year. Starting from 1991, the increase in burn-up is given in weeks. From there on, the power level is adjusted such that the power produced matches the burn-up increase. This is done for the 1991 – 2015. For the years 2016 – 2019 there are only prognoses of the planned power production. As only the planning for the year 2016 is available, the years 2017 – 2019 are assumed to have the same load periods. However, for activation, this time is most important as most nuclides that cause dose rates are built up within this period. For this analysis there are 274 time intervals considered over the whole life-time, see Figure 9. Some components were removed during operation. For the activation of these components the appropriate history was used and the decay periods from the time of removal until the time of measurement are accounted for, e.g. some screw nuts of the flange of the cold neutron source tube were exchanged and the activity was measured, see Figure 8.

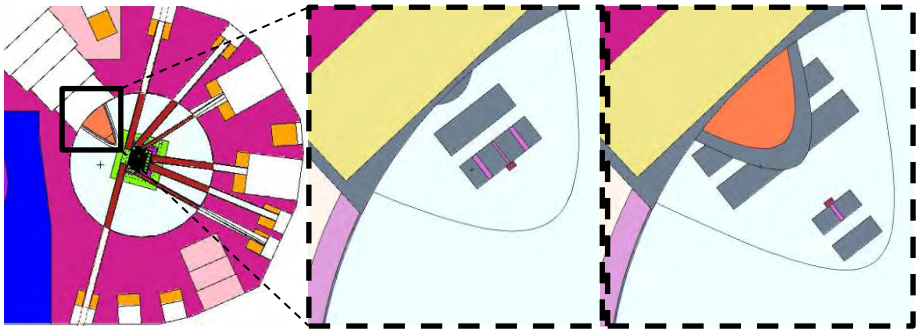

Figure 8: Leftmost: position of the flanges in the reactor, middle: back flange with modelled bolt and nut (9.9E+06 Bq/g), rightmost: front flange with modelled bolt and screw nut (5.84E+07 Bq/g)

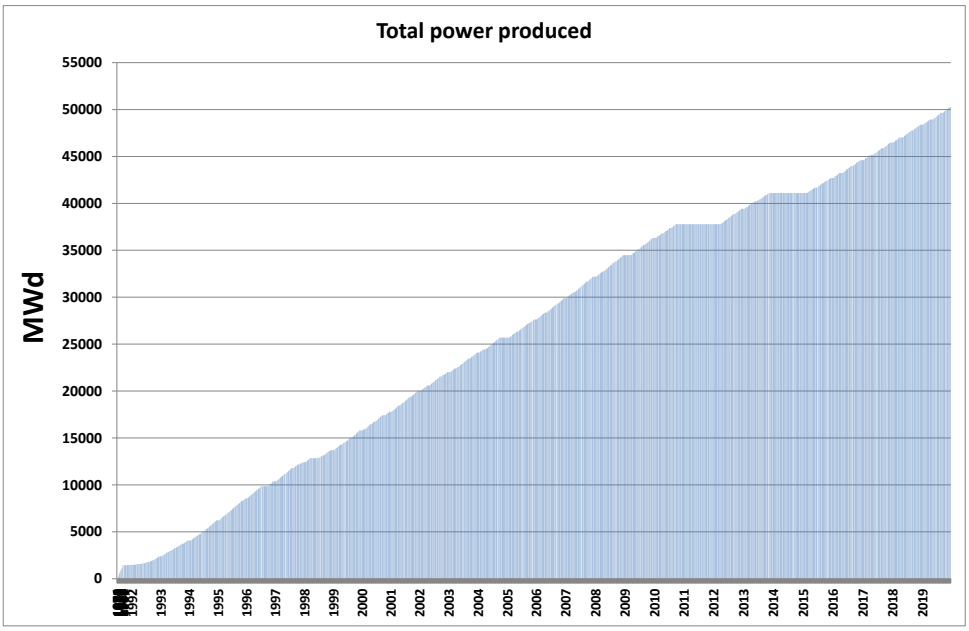

Figure 9: Total power production of the BER-II during operational lifetime including planned power production until 2019 (the year of 2016 is used for extrapolation). The years 1974 – 1985 are shown in a distorted manner as only annual power production was provided.

7. Results of the Activation Calculation and Calibration Points

With the neutron flux presented in the previous chapter, the activation calculations were performed with the burn-up and activation code FISPACT. The typical permitted limits for the most important nuclides in decommissioning are presented in Table 1 below. These values are also used for the iso-surfaces of the isotopes within the computational area (Figure 11).

The power history of the BER-II is taken as shown in chapter 6. The flux shape remains the same, only the amplitude varies with respect to the power produced. Effects of burn-up or moving of control rods are not accounted for. The resulting Co-60 distribution within the reactor geometry is presented in Figure 10 for the x,y-section at the height of the seven irradiation tubes. Figure 11 represents the distribution of Co-60 beyond the unrestricted limit and also for the restricted release limit.

Table 1: Unrestricted release limits for different isotopes from the "Strahlenschutzverordnung"(German Radiation Protection Ordinance) [1]

Isotope	Unrestricted	Restricted	Unit
Co-60	1E-01	6E-01	Bq/g
Fe-55	2E+02	1E+04	Bq/g
Eu-152	2E-01	1E+01	Bq/g
H-3	1E+03	6E+04	Bq/g
C-14	8E+01	4E+03	Bq/g
Cs-137	5E-01	1E+01	Bq/g

For the verification of the activation calculation, some measurements of components are provided by HZB. These are measurements of the irradiation channel inside the core (Figure 1) and the screw nuts on the flange of the conical irradiation tube (Figure 8). The nuts were in the reactor from 1991 until week 40 of 2011. They were measured Nov 23rd 2015. Another calibration point was the AlMg3 from the in-core irradiation channel, see Figure 1.

Table 2 shows that the activities calculated sufficiently agree with the measurements. Only the first value close to the core is somewhat underestimated. However, it has to be mentioned that cobalt is only specified in the manufacturing specification. Here, measurements to determine

the exact content would be very helpful. Other isotopes contents and activities should be measured.

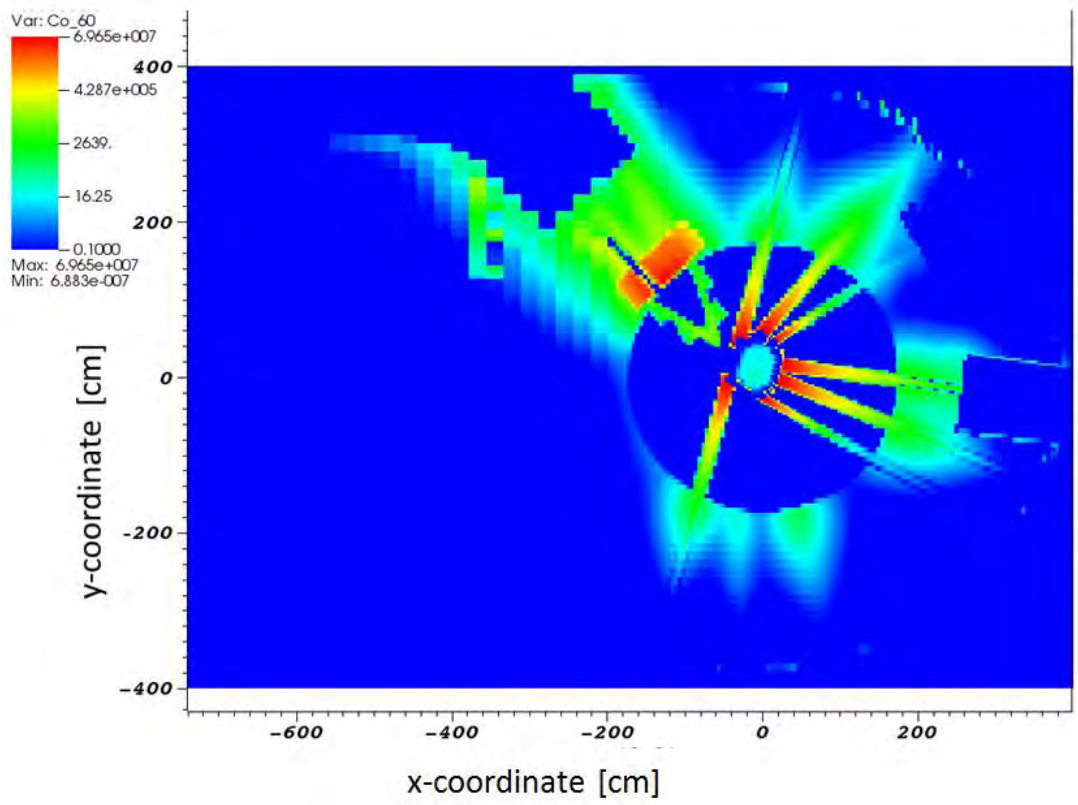

Figure 10: Distribution of Co-60 in Bq/g per gram of material mixture within a cell, x,y-section of the plane with 7 irradiation tubes at the end of operation

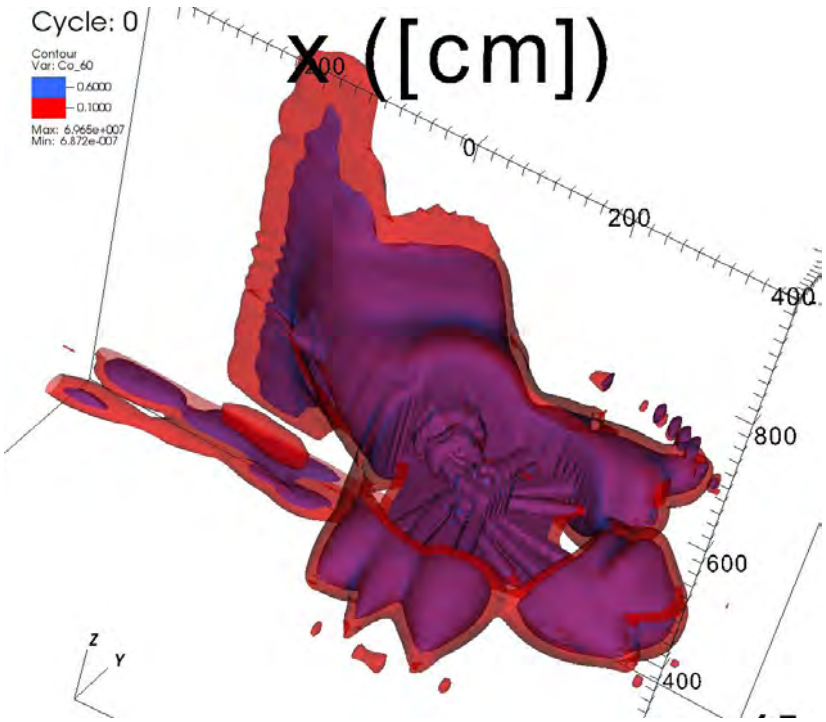

Figure 11: 3-D distribution of Co-60 within the reactor geometry, unrestricted release limit in red, restricted release limit in blue (seems purple).

Table 2: Comparison of the specific Co-60 activity, measured and calculated

Component	Position	Measured [Bq/g]	Calculated [Bq/g]
Screw nut (stainless steel)	front flange	5.84E+07	3.81E+07
Screw nut (stainless steel)	back flange	9.9E+06	1.12E+07
Irradiation channel (AlMg3)	inside the core	2.4E+06	4.12E+06

8. Conclusion

In this paper, a full procedure for an activation calculation including the concrete shielding is presented. With the combination of the options offered by MCNP6 and PARTISN, an effective method to compute the neutron flux for a reactor geometry model with 2,790,000 cells could be achieved. The fact that for calculations with PARTISN some extra effort to generate the XS is needed is more than compensated by the fact that for all volumes of the model neutron fluxes are produced that can be subsequently used for the activation calculation. With the power history provided together with the material compositions an activation map was created for the whole structure, even for the most remote parts. The results for the activation at calibration points give an example that the use of detailed calculation methods allows reliable estimation of the activity of relevant nuclides, here Co-60. Especially the mean and the maximum activity can be determined. For a more detailed analysis, it is desirable to provide more calibration points, where the results of the activation can be validated.

9. References

[1] D.B. Pelowitz (Ed.), "MCNP6^{TM} User's Manual Version 1.0," LA-CP-13-00634, Rev. 0 (2013).

[2] R. E. Alcouffe, R. S. Baker, J. A. Dahl, S. A. Turner, R. C. Ward: "PARTISN: A time dependent, Parallel Neutral Particle Transport Code System", LA-UR-08-07258, (November 2008).

[3] R. A. Forest: "FISPACT-2007: User manual", UKAEA FUS 534, (March 2007).

[4] Verordnung über den Schutz vor Schäden durch ionisierende Strahlen §29 Anhang 3, (German Radiation Protection Ordinance §28 appendix 3), (Stand 11.12.2014).

[5] H. Buchholz, C. O. Fischer, K. Waßerroth & INTERATOM, „Sicherheitsbericht für den Reaktor BER-II" (engl.: Safety report for the BER-II reactor), (June 1972).

[6] SCALE: A Comprehensive Modelling and Simulation Suite for Nuclear Safety Analysis and Design," ORNL/TM-2005/39, Version 6.1 (2011).

[7] "W. W. Engle, Jr., "A USER MANUAL FOR ANISN, A One Dimensional Discrete Ordinates Transport Code with Anisotropic Scattering", K-1693, ORNL, (March 1967).


RRFM
EUROPEAN RESEARCH REACTOR CONFERENCE 2016
IGORR
BERLIN
13 - 17 March 2016
GERMANY

Poster


RRFM
EUROPEAN RESEARCH REACTOR CONFERENCE 2016
IGORR
BERLIN
13 - 17 March 2016
GERMANY

Poster CNS

A MCNPX TRIGA RC-1 EXPERIMENTAL CHANNELS MODEL FOR THE DESIGN OF A NEW NEUTRONIC DIFFRACTION FACILITY

L.FALCONI[1], N.BURGIO[1], M.PALOMBA[1], E.SANTORO[1],M.CARTA[1]
M.PRATA[2], A.SALVINI[2],P.GHIGNA[3],S.ALTIERI[4,5],S.BORTOLUSSI[5],L.REVERSI[6]

[1]ENEA CR Casaccia - via Anguillarese 301 00123 Santa Maria di Galeria, Italy
[2]L.E.N.A. - Laboratorio Energia Nucleare Applicata - Università degli Studi di Pavia - Via Aselli 41 - 27100 Pavia - Italy
[3]Dipartimento di Chimica - Università degli Studi di Pavia - Via Taramelli 12 - 27100 Pavia - Italy
[4]Dipartimento di Fisica- Università degli Studi di Pavia - Via A. Bassi 6 - 27100 Pavia - Italy
[5]INFN - Istituto Nazionale di Fisica Nucleare - Via A. Bassi 6 - 27100 Pavia - Italy
[6]Università degli Studi di Firenze - P.zza S.Marco, 4 - 50121 Firenze - Italy

ABSTRACT

TRIGA RC-1 Mark II reactor of ENEA Casaccia Research Center reached its first criticality in 1960, with a maximum thermal power of 100 kW. In 1967 it was upgraded at the thermal power of 1 MW.A MCNPX model of the facility has been developed to support experimental measurements and devices installations. The present study is part of an ongoing feasibility study focused on the installation of a new neutron diffractometer. It is focused on the neutronic characterization of two horizontal experimental channels selected as the most suitable to be coupled with the diffraction facility. The channels have been implemented into the TRIGA-RC1 MCNPX model and preliminary results have been obtained about the characteristics of neutron fluxes entering the device. Experimental data regarding flux measurement available at different positions in all channels have been compared with simulated data. The measured and simulated data are in relative agreement with measurements and further work must be addressed in the calibration of the model. However, the results indicates that channel A and TPC fulfill the requirements to host a neutron powder diffraction facility.

1. Introduction

Nowadays, neutron beam techniques represent a well established and very useful tool for a detailed material characterization [1]. In particular, neutron diffraction techniques are invaluable tools for the study of the structure of the matter and it is used in various fields such as materials science, structural chemistry and physics [2]. As reported in [1] the minimum neutron flux intensity at the sample required to performs powder diffraction and residual stress analysis is of 10^5 n cm^{-2} s^{-1}. Aim of this paper is to preliminary investigate the potentiality of two horizontal channels namely, radial channel A and the Tangential Piercing Channel (TPC), of the TRIGA-RC1 facility of Casaccia. The first stage of such investigation is the implementation and execution of a set of Monte Carlo simulation calculations on the TRIGA MCNPX model to ascertain and compare the neutron performance of both channels. The outcomes from this preliminary investigation have been compared with experimental results that confirm that, potentially, both channels could host the facility. However, further experimental work and model implementation should be executed in future to improve the Monte Carlo model and to couple it with the MCStas [11] [12] code to evaluate the possible layouts, and their performances, on both channels.

2. TRIGA RC-1 Research reactor

RC-1 is a thermal pool reactor, based on the General Atomic TRIGA Mark II reactor design, operating at the thermal power of 1MW [3]. The core, in the current configuration, is loaded with 111 standard TRIGA fuel elements, it is contained in an aluminium vessel, seven meters deep, filled with demineralised water. A cylindrical graphite structure around the core is the lateral reflector of the reactor. The biological shield is provided by concrete with an average thickness of 2.2 meters. The water inside the vessel provides the first biological shield, neutron moderation and core cooling. Thermal power is removed from the core by natural convection, and exchanged with the environment through two thermohydraulic loops, coupled by two heat exchangers and two cooling towers. In Fig 1 the horizontal and vertical section of the reactor are shown, together with a 3D section of the reactor with neutron channels.

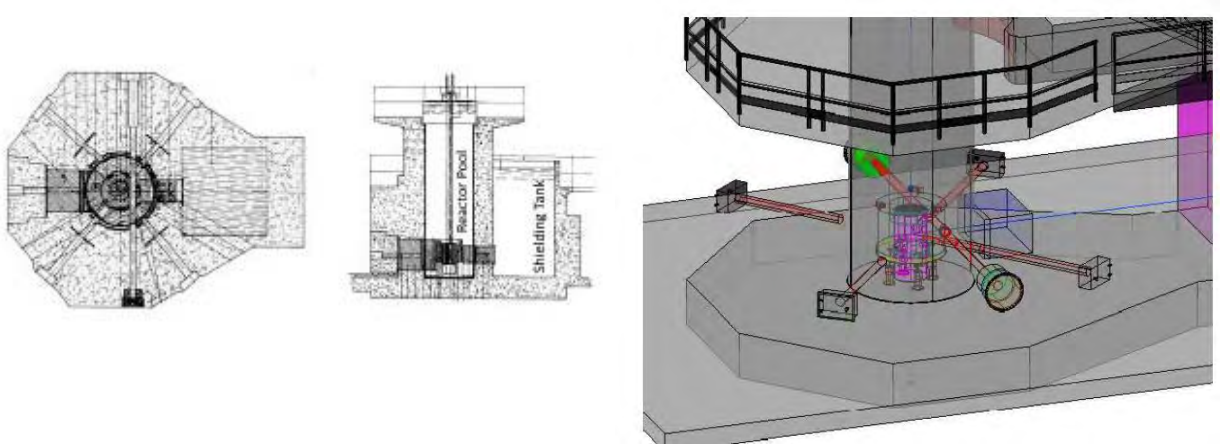

Fig 1 Horizontal and vertical sections of RC-1 research reactor and neutron channels

The RC-1 core, surrounded by a graphite reflector, consists of a lattice of TRIGA standard fuel elements, graphite dummies elements, control and regulating rods. There are 127 channels on the upper grid plate available for these core components and the grid itself is divided into seven concentric rings. One channel houses the start up source (Am-Be) while two fixed channels are available for irradiation (central channel and *rabbit*).
The TRIGA fuel elements, cylindrical shaped and stainless steel cladded (AISI 304 - thickness 0.5 mm) consist of a ternary alloy of H-Zr-U. The Uranium is 20% enriched in ^{235}U, and represents the 8.5% of the total fuel weight. Two graphite cylinders at the top and at the bottom of the fuel rod ensure upper and lower neutron reflection. The fuel element is provided externally with two fittings in order to allow the remote movements and the correct placements into the grid plates. The metallurgic alloy's stability is related to a variation of the total number of atoms less than 1% [4]. Another feature regards the prescription that forces the removal of elements from the core if their burn up is higher than 35%: this is a condition linked to the U-ZR-H lattice properties. From the point of view of the utilization, the reactor is mainly utilized for training, flux measurements and irradiation of neutron detectors.
The reactor is controlled by four boron carbide rods: three, stainless steel cladded, are *fuel follower* type (two shims and the safety rods) whereas the last, aluminium cladded, is the regulation rod [5].

2.1. TRIGA RC-1 neutron flux measurement at the horizontal channels

The TRIGA RC-1 is equipped with many experimental channels designed for the extraction of neutron and gamma beams from the biological shield. Tab 1 reports thermal neutron fluxes(Φ_{th}),Cadmium ratio (R_{CD}), diameter and shape of the 5 experimental channels that are considered in this work.

Channel type	Φ_{th}(ncm^{-2}s^{-1})	R_{CD}	Shape	Diameter(mm)
A-Radial (Piercing)	4.8 10^{12}	~2	Cylinder	Φ_{INT}=152
B- Radial	4.3 10^{10}	~3	Cylinder	Φ_{INT}=152
C- Radial	4.3 10^{10}	~3	Cylinder	Φ_{INT}=152
D- Tangential	5.4 10^{10}	~10	Cylinder	Φ_{INT}=152
Tangential Piercing Channel (TPC with collimator)	1.1 10^{6}	~2	Cylinder	Φ_{INT}=180
Tangential Piercing Channel (TPC-without collimator)	2.0 10^{8}	--	Cylinder	Φ_{INT}=200

Tab 1 Neutron flux and Cadmium Ratio (R_{CD}) for the selected horizontal channels of TRIGA-RC-1 (see also Fig 1 for positions)

The thermal flux has been measured by means of activation of bare gold foils located in the inner part of A (yellow point in Fig 2), B (blue point in Fig 2),C (violet in Fig 2) and D (grey point in Fig 2) channels, while the flux value for the TPC is measured at the beam port (the green point in Fig 2). Corresponding Cadmium ratios have been obtained using gold foils under Cadmium. In the TPC the Φ_{th} level depends on the channel actual design, which includes a neutron collimator installed in the channel inner part [6]. Flux measurements at the same position, without the neutron collimator, are available from previous research activities and show a value of about 2.0 10^{8}n cm^{-2} s^{-1} [7]. All experimental data are affected by relative error ≤ 5%.
Some other experimental data can be considered for the complete neutron characterization of the channels even if not directly related to a possible location for utilization coupled to a neutron diffraction facility, but having an important role in the validation of the MCNPX model of the reactor. The first set of data is a complete ensemble of measurements executed in the available core positions, located between the grid plates and, in some cases, near an experimental channel (Fig 2).

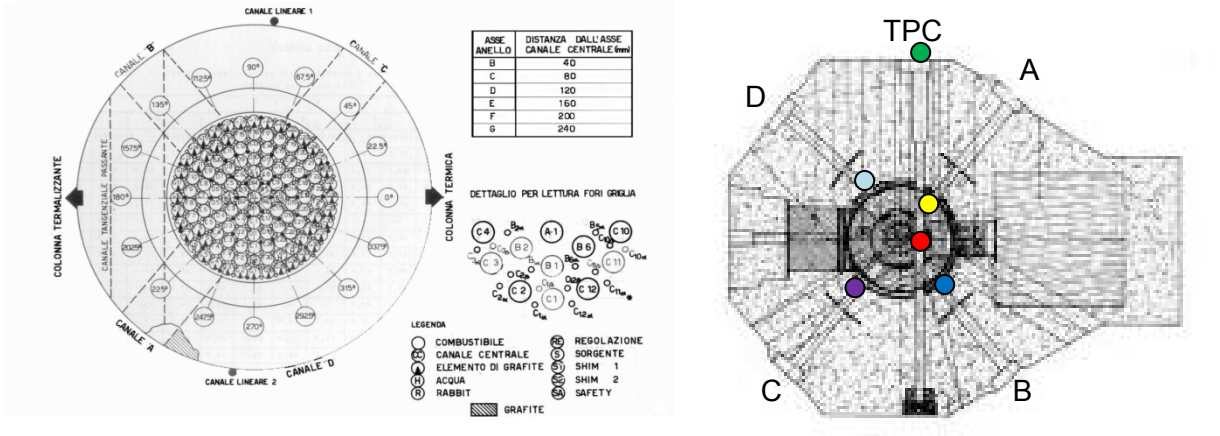

Fig 2 In-core irradiation positions map and horizontal section

Moreover, some experiments [8] carried out before the installation of the neutron collimator on the TPC show a thermal neutron flux value equal to 2.0 10^{12} cm^{-2} s^{-1}(uncertainty 5%) corresponding to the position in the TPC inside the reflector (red point in Fig 2).

3. TRIGA RC-1 MCNPX model

The MCNPX [9] model described in this paper is based on detailed material compositions retrieved from plant documentation and schemes [2]. The aim is to put particular attention to the horizontal channels. Fig 3 shows two sections of the model: the first focuses on the radial channels, while the second on the TPC.

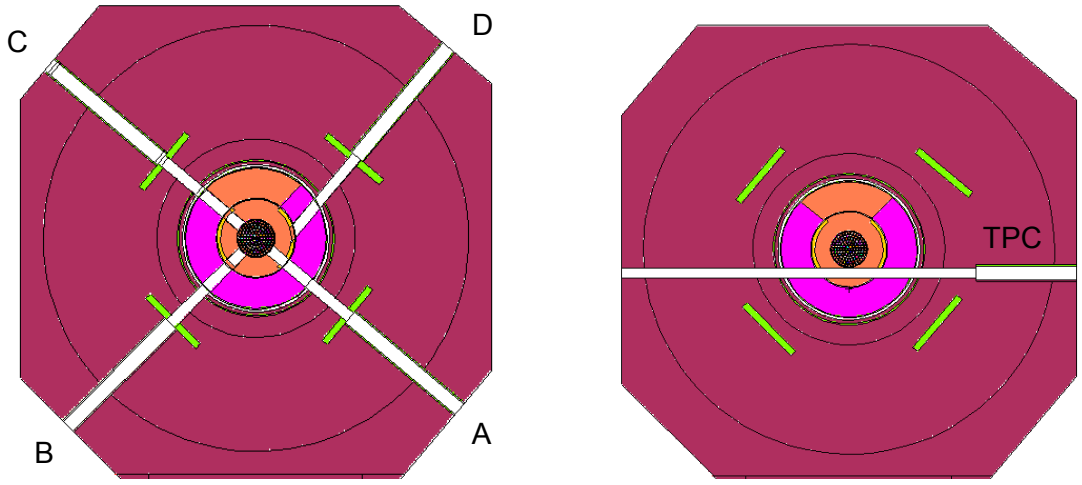

Fig 3 Horizontal sections of the TRIGA RC-1 MCNPX model

The considered reactor core consists of 76 fuel elements at nominal zero burn up corresponding to the first historical core configuration at 1 MW [2]. This choice is related to the necessity of validating the MCNPX model by means of criticality calculation, flux calculation and control rod calibration curves [10]. Furthermore, experimental measurements, as shown in Tab 1, have been performed on this core configuration. As nuclear data the model uses ENDF/B-VI cross sections evaluated at 20 °C (together with the corresponding S(α,β) matrices for light nuclei),neglecting in this way the fuel temperature coefficient (experimental value not less than -10 pcm/°C) for the steady operative condition at 1 MW. On the other hand, the validation process can considered correct because some experimental data are evaluated at the thermal power of 20 W, corresponding to all core components in equilibrium at room temperature, 20 °C (isothermal condition). The last consideration is about the current geometrical model adopted in the calculations which does not include the thermalizing column and the outer part of the thermal column. This design choice is justified by the corresponding mean free path of neutrons in the graphite of the thermal and thermalizing columns: neutrons scattered out of this two zones are not able to influence the neutron population inside the horizontal channel. The TPC is modelled as it was in the original configuration without any collimator inside (as in the current design). Finally, in order to minimize the variance of MCNPX results, a geometry splitting of the horizontal channel is adopted.

3.1. MCNPX characterization of horizontal and tangential piercing channels

MNCPX [9] flux and current estimations have been made by means of F1 (neutron current) tally and F5 (point detector) tally in various positions inside each experimental channel with the aim to:

- to compare calculated thermal fluxes with the experimental data in Tab 1.
- obtain an estimation of the flux divergence respect to the channel axis in each chosen position. The aim is to investigate the flux divergence as a general property of each channel to evaluate their performance as a suitable source for a neutron guide.

Preliminary calculations show that for the present work, the use of F5 tally has higher efficiency than F4 tally to achieve convergence at the same level of precision. The energy binning adopted for the above estimations is based on 4 groups subdivision shown in Tab 2

	Energy intervals (MeV)
Cold and thermal neutron	10^{-7}
Epithermal	$10^{-7} \div 5.010^{-3}$
Fast	$5.0\ 10^{-3} \div 1$
High Energy	$1 \div 20$

Tab 2 Energy intervals used in MCNPX evaluation

The (F1) current divergence has been estimated considering the cosine of the angle between the neutron direction of flight at the surface crossing and the normal of the surface itself. The normal has been selected to be coincident with the channel axis and with the neutron leakage direction from the core. The cosine (angular) binning starts from a minimum of 9 bins for some coarse estimations up to 20 bins for more detailed cases. All the divergence results have been normalized to the total current score of the maximum cosine bin. It is noteworthy to mention that the thermal component estimated by F1 tally with a divergence up to 2° is considered as a fraction of inherently collimated neutrons that can be used directly for the diffraction activities and can be considered as a figure of merit measuring the performance of the channel under consideration. Experimental results (see Tab 1) and general design considerations suggest to consider, among the others, radial channel A and the TPC as suitable for a neutron diffraction experiment. The first, being a piercing channel, is characterized by high neutron flux but it has the major drawbacks of an intense γ field and relatively high fast neutron population. The second, as tangential channels, minimizes the γ field and shows a relatively high thermal neutron flux with a lower fraction of fast neutron flux. MCNPX simulations have been performed for each position inside all the experimental channels corresponding to the results shown in Tab 1. For the radial channel A, current, flux and point detector estimators have been located in positions 1, 2 and 3 of Fig 4a. The same estimators have been located at TPC in positions 1 and 2 of Fig. 4b. The geometry splitting method has been adopted to reduce the MCNPX variance.

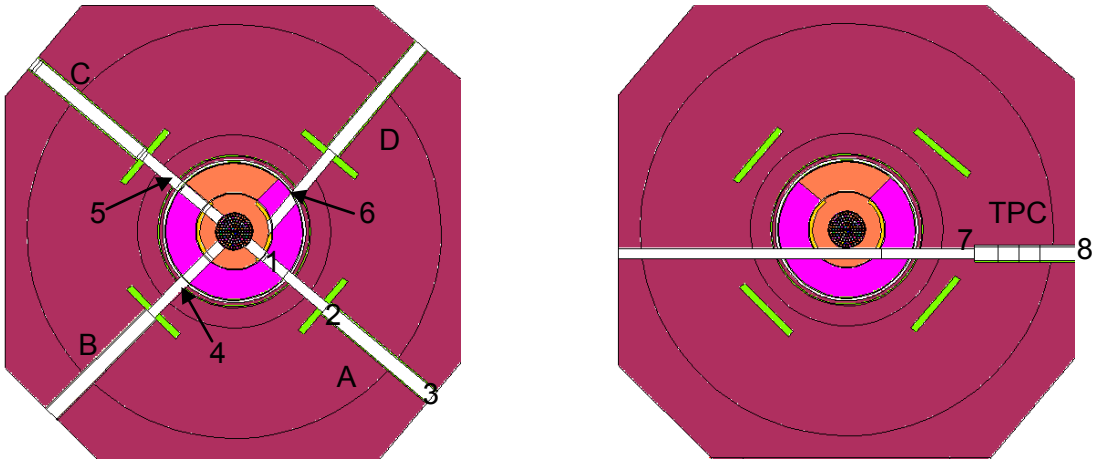

Fig 4a and 4b Schematic representation of MCNPX tally evaluation points

In order to compare the simulation calculations outcomes with the experimental results, estimations have been also performed in correspondence of the useful end points (e.g. as closest as possible to the reflector) of each channel (see Figs 4a and4b– Points 1 to 8).

3.2. Results and Discussion

Tabs from 4 to 6 show the simulation outcomes for F5 neutron flux estimators for channels A,B, C, D and TPC, only for the thermal energy bin (i.e. up to 0.1 eV).

Channel A Thermal Neutron flux [n cm^{-2} s^{-1}]			
Type of estimator	**Point 1**	**Point 2**	**Point 3**
Tally F5	(1.61± 0.02) 10^{12}	(9.13 ± 0.7) 10^{9}	(1.44±0.03)10^{7}

Tab 4 MCNPX results for channel A

Thermal Neutron flux [n cm^{-2} s^{-1}]			
Type of estimator	**Channel B**	**Channel C**	**Channel D**
	Point 4	**Point 5**	**Point 6**
Tally F5	(5.56 ± 0.1) 10^{10}	(3.65 ± 0.06) 10^{10}	(1.96 ± 0.07) 10^{10}

Table 5 MCNPX results for the channel B,C and D

Channel TPC Thermal Neutron [n cm^{-2} s^{-1}]		
Type of estimator	**Point 7**	**Point 8**
Tally F5	(2.33±0.13)10^{9}	(9.03±0.25) 10^{7}

Tab 6 MCNPX results for Tangential Piercing Channel

Comparing the innermost points of estimation (Points 1,4,5,6 and 7) the higher thermal flux was found in channel A. However, the results at the outermost points of channels A and TPC (Points 3 and 8) show that the thermal neutron flux of the TPC channel is higher by a factor four with respect to the one in channel A.

Comparison of prompt γ fluxes [p cm^{-2} s^{-1}]		
Type of estimator	**Channel A (point 1)**	**TPC (point 7)**
Tally F5	(1.450±0.002)10^{12}	(3.490±0.023) 10^{9}

Tab 7 MCNPX results for Channel A and TPC prompt γ fluxes

Table 7 reports the estimation of the prompt γ fluxes in channel A and TPC: the channel A has a photon flux that is a factor 415 higher than the TPC one. Assuming that the level of γ generated by the material activation is negligible, the design indication of a lower level of γ flux in TPC with respect to channel A is confirmed by calculations. Table 8 shows the comparisons of the experimental data with calculated results for the neutron fluxes in the selected points of the various channels.

Experimental Channel	Experimental measure	Evaluated Data	Ratio experimental to evaluated
Channel A	$4.8\ 10^{12}$	$1.61\ 10^{12}$	2.98
Channel B	$4.3\ 10^{10}$	$5.56\ 10^{10}$	0.78
Channel C	$4.3\ 10^{10}$	$3.65\ 10^{10}$	1.18
Channel D	$5.4\ 10^{10}$	$1.96\ 10^{10}$	2.76
Channel TPC	$2.0\ 10^{8}$	$9.03\ 10^{7}$	2.21

Tab 8 Comparison between experimental value of neutron flux in the different horizontal channels and the corresponding evaluated data

Measured data are affected by a relative error of about 5% whereas the evaluated relative errors are comprised between 6% in the case of the channel C and 1.2% in the case of channel A. The high discrepancies among measured and simulated data is originated by several uncertainties concerning material compositions, measurement positions and nuclear data. An accurate uncertainties analysis is beyond the scope of the present paper. Since the simulated and measured data agree on the order of magnitude of the neutron fluxes a meaningful comparative analysis is still possible. Tab 9 shows the comparison of the calculated neutron energy distribution for TPC and A channels at the respective innermost points (see Point 7, Fig 4b – Point 1 Fig 4a). These points are candidates to be considered for using neutron guides necessary to transport thermal neutrons up to the sample.

Energy interval	% of population	
	Channel A	**TPC Channel**
Thermal (up to 0.1 eV)	56.95%	32.80%
Epithermal ($0.1eV<E_n<1KeV$)	23.72%	36.24%
Fast ($1KeV<E_n<1MeV$)	14%	25.38%
High ($1MeV<E_n<20MeV$)	5.34%	5.59%

Tab 9 Comparison of Neutron energy components at the innermost estimation points in channels A and TPC (point 1 and 7 respectively) as estimated by F5 tallies

The two spectra highlight that Channel A has an higher thermal neutron population in comparison with the TPC channel and lower epithermal, fast and high energy populations. The spectral characteristics of channel A allow a more effective filtering of the non-thermal neutron fractions. Finally, Tab 10 shows the fraction of estimated forward current on plane surfaces that include, respectively, point 7 (TPC channel) and point 1 (Channel A) having divergence compatible with an inherently optimal neutron collimation (from 0° to 2° with respect to the channel axis).

	TCP Channel	Channel A
Type of estimator	**Point 7**	**Point 1**
Tally F1	3.24%	8.82%

Tab 10 Comparison of the estimated fraction of the forward thermal neutron currents having a divergence between 0 and 2 degrees with respect to the channel axis.

Channel A shows approximately a 3 times greater fraction of thermal neutrons in the forward direction respect to the TPC channel. More quantitatively, it is possible to estimate the useful thermal neutron flux intensity Φ_{us} of the two neutron source related to point 1 (channel A) and point 7 (TPC channel) using the following relation:

$$\Phi_{us} = F_s \Phi_{Tot} F_{Therm} F_{\theta} \quad \text{(Eq. 1)}$$

Where

Φ_{Tot}= Total neutron flux intensity at the given estimation point;
F_{term}= Fraction of the thermal neutron population;
F_{θ}= Fraction of thermal neutron with divergence between 0 and 2 degrees.
F_S= 0.5: Conservative factor taking into account statistical uncertainties in calculated results.

The useful flux Φ_{us} is 3.7 10^{10}n cm^{-2} $s^{-1}$for channel A at point 1 and 1.2 10^{7}n cm^{-2} s^{-1} for TPC channel at point 7.

4. Conclusions

MCNPX results are in the same order of magnitude of experimental data, further work, both on experimental and simulation sides, will be addressed to improve the facility model. The current results provide a first approximation source term for the neutron guide component of both channels A and TPC. The greater γ flux present in channel A is the main drawback for the selection of this channel to host the facility. However, with a more accurate calibration of the model, a favourable trade-off between γ filtering and neutron thermal flux intensity can be investigated for such channel. Finally, an interface with McStas code [11] [12] will be necessary to evaluate the neutron flux at the sample position for all the possible layouts considered for the neutron diffraction facility.

5. References

[1] IAEA - Technical Report No. NP-T-5.3 Application of Research Reactors
[2] S.C. Vogel A review of Neutron Scattering Applications to Nuclear Materials, Hindawi Publishing Corporation
[3] L. DI PALO, RC-1 Reattore 1MW – Progetto definitivo e rapporto di sicurezza, CNEN Centro Studi Nucleari Casaccia, 1966 (Italian)
[4] Gruppo Esercizio TRIGA RC-1, Prescrizioni tecniche per l'esercizio, 1985 (Italian)
[5] Dipartimento FPN, ENEA, Manuale di Operazione del reattore RC-1 1 MW, C.R. Casaccia (Italian)
[6] F.Andreoli, M.Mattoni, M.Palomba, R.Rosa Neutron collimator for neutron radiography application at the tangential port of the TRIGA RC-1 reactor ITMNR-6 (2008) Kobe, Japan
[7] R.Rosa, N.Burgio, A.Santagata, R.Bedogni, G.Gualdrini, D.Tortorella, Neutron and photon experimental characterization for and improved neutron radiography facility at ENEA Casaccia TRIGA reactor - preliminary results (2002)
[8] LFNA - Laboratorio Fisica Nucleare Applicata, Prove nucleari eseguite con il reattore RC-1 1MW, CNEN, 1967 (Italian)
[9] D. B. Pelowitz editor, “MCNPX 2.7.0. Users Manual”, April 2011- LA-CP-11-00438
[10] L.Falconi, C.Innarella, M.Palomba, M.Carta, M.Sepielli Activities at TRIGA RC-1 Research Reactor, RRFM 2015 Bucharest
[11] MCStas www.mcstas.org
[12] L.Reversi"Studio Computazionale per la realizzazione di un fascio di diffrattometria neutronica presso il reattore TRIGA di Pavia", Master Thesis, (italian)

DESIGN LIFETIME ESTIMATION OF A COLD NEUTRON SOURCE

A METHODOLOGICAL APPROACH USING RCC-MRX DESIGN RULES IN ADDITION TO ASME CLASSICAL RULES

B. LECARPENTIER, J. KOHLER
AREVA TA, CS 50497, 13593 Aix-en-Provence Cedex 3, France
Corresponding author: jerome.kohler@areva.com

ABSTRACT

Lifetime of a Cold Neutron Source (or other pressure vessel irradiated components) could be estimated with simple analysis based on materials ductility decrease under irradiation. A lower boundary of ductility is fixed, it gives the allowable neutron fluence and therefore the lifetime of the material.

Nevertheless this approach does not take into consideration the specific mechanical damages under irradiation, such as described and codified in the RCC-MRx code ref. [1]. The goal of this article is to explain how to use the RCC-MRx to covers specific damage under irradiation in addition to a usual design code (for example ASME VIII ref [2]). It provides a more precise lifetime estimation for mechanical components subject to ageing due to neutron embrittlement.

This methodology could be applied in Cold Neutron Source design, for irradiated areas, and thus provide a better assessment of the lifetime. Using standard codes ensures an efficient process from design to manufacturing.
RCC-MRx includes specific design rules for significantly irradiated components. Those rules are based on elastic analysis adapted to materials with a limited ductility. Those mechanical components could be more sensitive to local damages (such as peak stress), because of the significant decrease of plasticity (and toughness) under irradiation. Those rules also codify the effect of irradiations as complementally load (for example, thermal load in structure as a result of neutronic or gamma heating).

The mechanical damages driving the lifetime of the Cold Neutron Source happened to be justified through a combination of the two design codes:
- Fatigue such as codified in ASME analysis,
- Allowable stress under irradiation (“type P” analysis) such as described in RCC-MRx,
- Fast fracture (considering the loss of toughness under irradiation) as prescribed in RCC-MRx.

1. Mechanical sizing methodology for a Cold Neutron Source

The Mechanical sizing of a Cold Neutron Source (CNS) (or other pressure vessel irradiated components) is performed on the basis of ASME VIII criteria ref. [2] (using Div2 Part5) as the CNS has a specifical geometry. The estimation of the lifetime performed according to this method is very accurate.

This methodology differs from classical approaches because it includes an additional analysis of irradiated (or low ductility such as Al 6061T6) components according to RCC-MRx 2012 criteria ref. [1].

The following table illustrates the mechanical damages covered by a classical code and by RCC-MRx, and their overall consistency.

	Mechanical damages	ASME [2] VIII Div2 Part5	RCC-MRx 2012 [1] Section III VolB
Negligible irraidation	Defect susceptibility		covered
	Elastic or elastoplastic instability & excessive deformation (immediate or time-dependent)	covered	covered
	Local failure	covered	
	Buckling	covered	covered
	Fatigue (progressive cracking)	covered	covered
	Progressive deformation & thermal stress ratchet	covered	covered
	Fast fracture	Covered (if required)	covered (if required)
Significant irradiation	Defect susceptibility		covered
	Plastic instability and excessive deformation		covered
	Buckling		covered by negligible irradiation analysis
	Fatigue (progressive cracking)		
	Progressive deformation & thermal ratcheting		
	Fast fracture		covered (if required)

In the table above, the bolded boxes highlight main damages regarding lifetime.

Lifetime estimation of the CNS, depends on some of the listed damages, such as :

- Fatigue (with negligible irradiation),
- Defect susceptibility (with significant irradiation),
- Plastic instability and excessive deformation (with significant irradiation),
- Fast fracture analysis (with significant irradiation).

Hence it could be interesting to complete classical approach (ASME for negligible irradiation conditions) with RCC-MRx criteria for significant irradiation conditions. It is important to notice that, for negligible irradiation, the two codes are similar. The exposed methodology is therefore consistent.

Transition between negligible and significant irradiated rules is defined by data curves of negligible irradiation conditions. For aluminum, this transition is defined by criterion on ductility (A% irradiated = Agt% unirradiated for Al 6061T6).

It is hereafter reminded the different steps to evaluate mechanical sizing, including lifetime of the Cold Neutron Source:

- **ASME VIII Division 2 Part 5 ref. [2] - Justification in negligible irradiation conditions**:
    - Safety margins considering plastic instability and excessive deformation damages,
    - Safety margins considering local failure damage,
    - Safety margins considering buckling damage,
    - Safety margins considering fatigue damage (progressive cracking) → this specific analysis could provide a maximum number of cyclic loading in normal and incidents situations during the lifetime,
    - Safety margins considering progressive deformation (and thermal ratchet),
    - Safety margins considering fast fracture damage (if required by a low material toughness without irradiation),

- **RCC-MRx Section 3 volume B ref. [1] - Justification in significant irradiation conditions** :
    - Safety margins considering defect susceptibility (simplified approach to evaluate the material ability with this damage, which could require an exhaustive fast fracture analysis) → this specific analysis could provide a lifetime limit, with minimal irradied toughness material required, depending on fluence,
    - Safety margins considering plastic instability and excessive deformation → this specific analysis could provide a lifetime limit, with material ductility depending on fluence,
    - Safety margins considering buckling (should be covered by negligible irradiation analysis, since yield limit material increase with irradiation)
    - Safety margins considering fatigue damage (should be covered by negligible irradiation analysis),
    - Safety margins considering progressive deformation and thermal ratchet (should be covered by negligible irradiation analysis),
    - In addition to standard RCC-MRx analysis : safety margins considering fast fracture analysis (this specific analysis could provide a lifetime limit, with minimal irradied toughness material required, depending on fluence).

Hence lifetime of a CNS could be eventually limited by 3 damages:

- In negligible irradiation conditions : Fatigue, driven by the number of operating cycles considered,
- In significant irradiation conditions : Plastic instability and excessive deformation, since the allowable stress is driven by ductility (decreasing with fluence),
- In significant irradiation conditions: Fast fracture, since criteria are directly linked with toughness material (decreasing with fluence).

Other limiting factors on the design life could be expected, such as:

- Irradiation swelling stress and irradiation creep: lifetime can be limiting by swelling stress or functional aspect (gap, pinching refrigeration, maintenance…),
- Material knowledge in irradiation (such as a lower boundary for ductility in joints), or maximum allowable irradiation condition (validity of material data or maximum allowable fluence),
- Thermal creep,
- Other effects not quantified by stress analysis.

2. RCC-MRx criteria in significant irradiation conditions

Such as other Design Codes (Ramsès II or SDC-IC “ITER Structural Design Criteria for In-Vessel Components”), RCC-MRx provides specific rules for structural sizing with low ductility materials. Two cases of materials could be identified: those with a very low initial ductility, and those for which ductility is deeply affected by irradiation effects. These specific rules are coming in addition to the classical limitation for primary stress and primary + secondary stress, as defined in classical “pressure vessel” codes such as ASME or RCC-M.

RCC-MRx includes specific design rules for significantly irradiated components. Those rules are based on elastic analysis adapted to materials with a limited ductility. Those mechanical components could be more sensitive to local damages (such as peak stress), because of the significant decrease of plasticity (and toughness) under irradiation. Those rules also codify the effect of irradiations as complementally load (for example, thermal load in structure as a result of neutronic or gamma heating).
A set of criteria have therefore to be verified, comparison of the elastic stress versus the allowable limitation Sem and Set (define below).

These specific rules also codify as complementary load the effect of irradiations (for example, thermal load in structure as a result of neutronic or gamma heating).

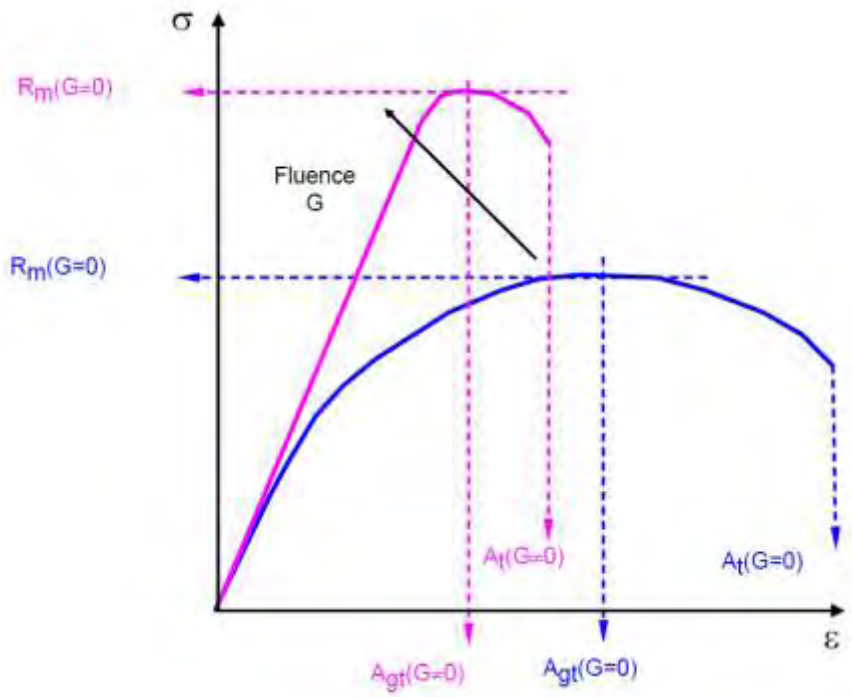

Fig1. Influence of irradiation on typical stress / strain curve (from the blue curve to the pink curve)

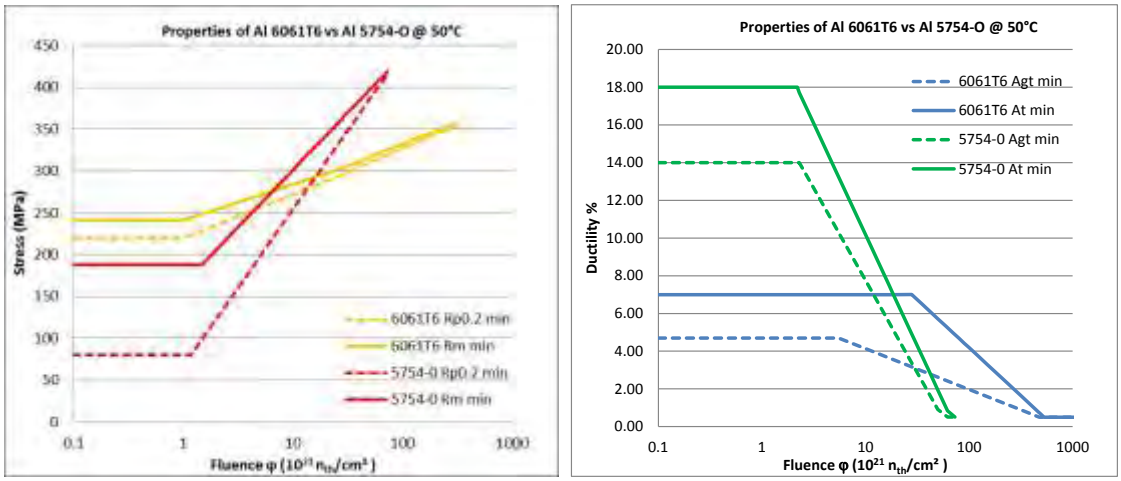

Fig2. Influence of irradiation on properties of Al 6061T6 vs Al 5754-O at 50°C from ref. [1]

	Al 6061T6 @ 50°C				Al 5754-0 @ 50°C			
$\Phi_{th\ conv}$ *10^{21} (nth/cm²)	$R_{p0.2\ min}$ (Mpa)	$R_{m\ min}$ (Mpa)	Agt min (%)	At min (%)	$R_{p0.2\ min}$ (Mpa)	$R_{m\ min}$ (Mpa)	Agt min (%)	At min (%)
0	219	241	4.7	7.0	80	188	14.0	18.0
1.18	219	241	4.7	7.0	80	188	14.0	18.0
2.2	234	245	4.7	7.0	131	211	14.0	18.0
2.3	235	246	4.7	7.0	134	214	14.0	17.7
5.5	256	266	4.7	7.0	205	266	10.3	13.2
28	296	303	3.2	7.0	338	362	3.4	4.9
62	314	321	2.5	5.3	403	409	0.5	0.8
73	318	324	2.3	5.0	416	419	0.5	0.5
100	327	332	2.0	4.2	maximum allowable irradiation			
200	344	348	1.3	2.6				
300	354	357	0.9	1.7				
481	-	-	0.5	0.7				
532	-	-	0.5	0.5				
670	-	-	0.5	0.5				
1000	maximum allowable irradiation							

Tab1. Influence of irradiation on properties of Al 6061T6 vs Al 5754-O at 50°C, partial data from ref. [1]

3. Principles of Sem and Set rules

When material ductility is reduced, RCC-MRx provide complementary limitation of the stress (elastic analysis), for primary, secondary and peak stress. These complementary rules are applied to membrane and total stress.

- Equivalent primary + secondary membrane stress should meet the following criteria :

$$\overline{P_m + Q_m} \leq S_{em}{}^{i}(\theta_m, G_m)$$

With ;
$S_{em}{}^{i}$ the maximal allowable membrane stress, depending on criteria level (i= A, C or D), for average temperature through thickness θ_m and for average fluence through thickness G_m.

- Equivalent primary + secondary total stress should meet the following criteria :

$$\overline{P_l + P_b + Q + F} \leq S_{et}^{\,i}(\theta, G)$$

With ;
$S_{et}^{\,i}$ the maximal allowable total stress, depending on criteria level (i= A, C or D), for temperature θ and for fluence G.

3. Evaluation of allowable stress Sem and Set

In the figure below is illustrated how are evaluated allowable stress Sem and Set, starting from minimal tensile properties of the material.

- Sem is evaluated as the elastic stress when limiting stress at Rm and ductility at $A_{gt}(\theta_m, G_m) - \varepsilon_{pl}(S_m^{\,i})$, and taking into account elastic follow-up with r factor, r = 3 (this value is considered to cover all structural analysis other than pipes and nozzles).

- Set is evaluated as the elastic stress when limiting stress at Rm and ductility at $\frac{A_{gt}(\theta,G) + A_t(\theta,G)}{2} - \varepsilon_{pl}(S_m^{\,i})$, and taking into account elastic follow-up with the same r factor.
The ductility limitation used to evaluate Set considers the plastic deformation obtained with the assumption that the primary stress equal to $S_m^{\,i}$ (there is no plastic deformation with criteria A level).

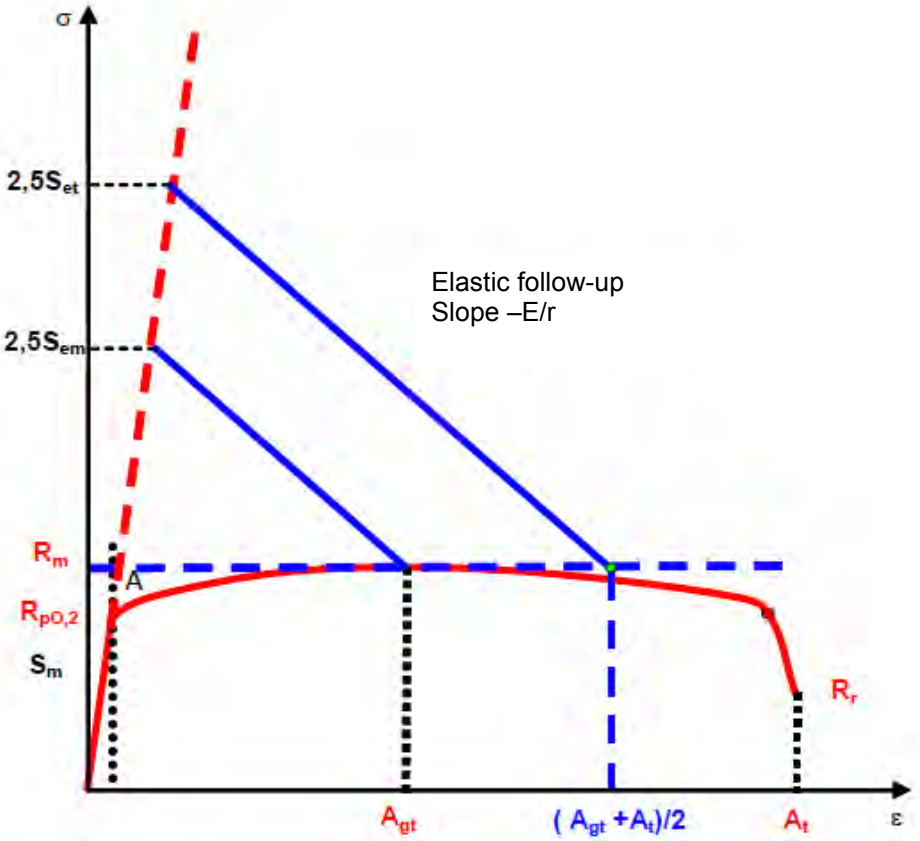

Fig3. Evaluation of allowable stress with significant irradiation Sem and Set on typical stress / strain curve

Allowable stress limitation of membrane stress and total stress (given by elastic analysis) are thus given in the following formulas. It results from the graphical construction and takes into account regulatory safety factors of 2,5 - 2 and 1,35 for respectively criteria of A, C and D level :

- $S_{em}{}^{A}(\theta_m, G_m) = \left\{ \frac{r}{r+1}.R_m(\theta_m, G_m) + \frac{E}{r+1}.\frac{1}{100}\left[A_{gt}(\theta_m, G_m)\right] \right\} / 2.5$
- $S_{em}{}^{C}(\theta_m, G_m) = \left\{ \frac{r}{r+1}.R_m(\theta_m, G_m) + \frac{E}{r+1}.\frac{1}{100}\left[A_{gt}(\theta_m, G_m) - \varepsilon_{Pl}\left(S_m^C\right)\right] \right\} / 2$
- $S_{em}{}^{D}(\theta_m, G_m) = \left\{ \frac{r}{r+1}.R_m(\theta_m, G_m) + \frac{E}{r+1}.\frac{1}{100}\left[A_{gt}(\theta_m, G_m) - \varepsilon_{Pl}\left(S_m^D\right)\right] \right\} / 1.35$
- $S_{et}{}^{A}(\theta, G) = k_b.\left\{ \frac{r}{r+1}.R_m(\theta, G) + \frac{E}{r+1}.\frac{1}{100}\left[\frac{1}{2}\left\{A_{gt}(\theta, G) + A_t(\theta, G)\right\}\right] \right\} / 2.5$
- $S_{em}{}^{C}(\theta, G) = k_b.\left\{ \frac{r}{r+1}.R_m(\theta\ , G) + \frac{E}{r+1}.\frac{1}{100}\left[\frac{1}{2}\left\{A_{gt}(\theta\ , G) + A_t(\theta\ , G)\right\} - \varepsilon_{Pl}\left(S_m^C\right)\right] \right\} / 2$
- $S_{em}{}^{D}(\theta, G) = k_b.\left\{ \frac{r}{r+1}.R_m(\theta\ , G) + \frac{E}{r+1}.\frac{1}{100}\left[\frac{1}{2}\left\{A_{gt}(\theta, G) + A_t(\theta, G)\right\} - \varepsilon_{Pl}\left(S_m^D\right)\right] \right\} / 1.35$

With :

$R_m(\theta_m, G_m)$: Minimum tensile strength for temperature Θ and fluence G, “m” is referred to the average in the thickness.

$A_{gt}(\theta_m, G_m)$: Percentage total elongation at maximum force elastic + plastic) in %, for temperature Θ and fluence G

$A_t(\theta_m, G_m)$: Percentage total elongation at fracture (elastic + plastic) in %, for temperature Θ and fluence G

E : Young modulus

$S_m{}^C$: Allowable stress with C level criteria $S_m^C = \min\left[1{,}35.S_m\ ;\ R^t_{p0,2min}\right]$

$S_m{}^D$: Allowable stress with D level criteria $S_m^D = \min\left[2{,}4.S_m\ ;\ 0{,}7.R^t_{m\,min}\right]$

S_m : Allowable stress with A level criteria

$$S_m = \min\left[\frac{2}{3}R_{p0,2\,min}\ ;\ \frac{2}{3}R^t_{p0,2min}\ ;\ \frac{1}{3}R_{m\,min}\ \ ;\ \frac{1}{2{,}7}R^t_{m\,min}\right]$$

$\varepsilon_{pl}\left(S_m^C\right)$: Plastic deformation due to stress S_m^C on the minimum monotonic curve of irradiated materials.

$\varepsilon_{pl}\left(S_m^D\right)$: Plastic deformation due to stress S_m^D on the minimum monotonic curve of irradiated materials.

k_b Parameter giving the margin between allowable bending and membrane stress in a shell $k_b = \frac{3}{2}\left[1 - \frac{1}{3}\left(\frac{100.R_m(\theta,G)}{E.A_{gt(}\theta,G)}\right)^2\right]$, $k_b \geq 1$

r : parameter quantifying elastic follow-up on secondary stress. This parameter evaluates the difference between σ_{el} and ε_{el} in a strictly elastic behavior, and the correct values σ and ε related by the monotonous traction curve. $r = -\frac{E(\varepsilon-\varepsilon_{el})}{\sigma-\sigma_{el}}$

This parameter comes to 0 when spring effect disappears, and when stress is completely secondary $(\varepsilon \to \varepsilon_{el})$. The parameter becomes very high when stress is completely primary $\sigma \to \sigma_{el}$).

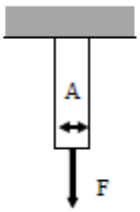

Fig4. « a case »
Load applied

$\sigma = \frac{F}{A}$

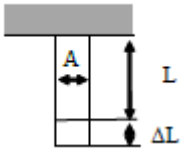

Fig5. « b case »
Displacement applied

$\sigma = E.\varepsilon = E.\frac{\Delta L}{L}$

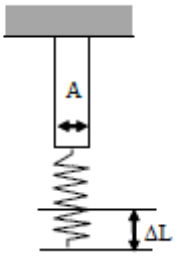

Fig6. « c case »
Displacement applied at the end of a spring, stiffness k

$\sigma = \frac{F}{A} = k.\frac{\Delta L}{L}$

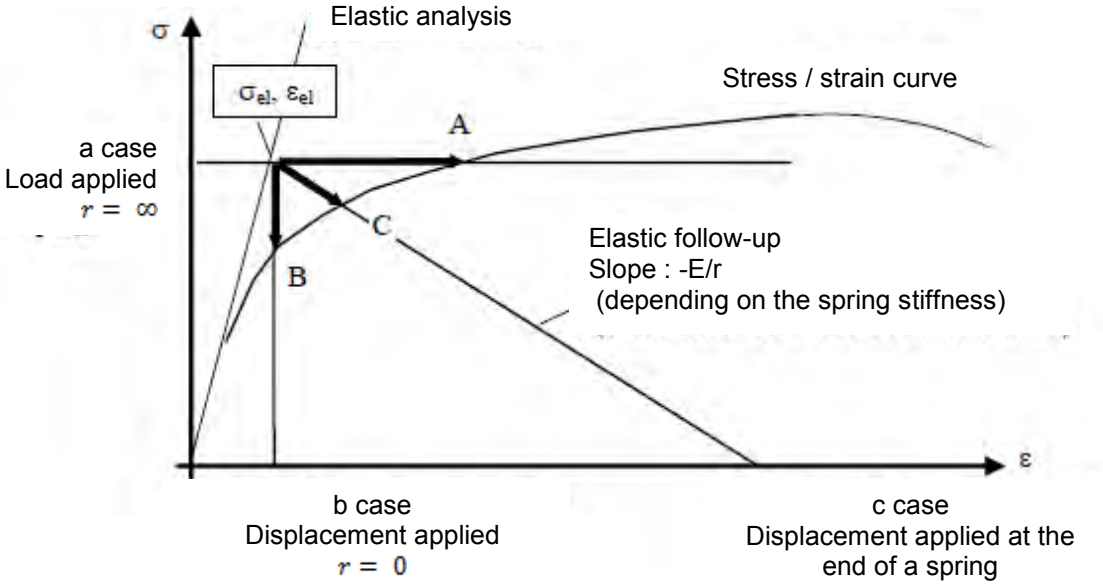

Fig7. Illustration of elastic follow-up “r”

6. References

[1] RCC-MRx Edition 2012
Design and Construction Rules for Mechanical Components in high-temperature structures, experimental reactors and fusion reactors.

[2] ASME Section VIII
The American Society of Mechanical Engineers - Rules for Construction of Pressure Vessels

Poster Safety

EFFECT OF REACTOR REGULATING SYSTEM ON A FLOW BLOCKAGE EVENT OF A RESEARCH REACTOR

SOO-BEEN YUM, SU-KI PARK
Safety Analysis Group, Korea Atomic Energy Research Institute,
989-111 Daedeokdaero, Yuseong, Daejeon, 305-353, Republic of Korea

ABSTRACT

The effects of reactor regulating system (RRS) on a flow blockage-induced event for an open-pool type research reactor are investigated. Since a research reactor with plate type fuels has isolated narrow rectangular cooling channels, a flow blockage causes a loss of cooling capability of the blocked channel. The overheated fuel plates result in an increase of void fraction in the blocked channel, therefore, the reactor power decreases by the void reactivity feedback. The void reactivity feedback plays an important role in an inherent safety feature, which decreases the reactor power. However, the RRS behaves against the inherent power decrease since it regulates the power to meet the power demand initially set by an operator. RELAP5/MOD3 is modified to properly simulate the behavior of fuel plate temperature up to and beyond the critical heat flux (CHF) condition by implementing the CHF correlation developed for narrow rectangular channels. The control mechanism of RRS is implemented in the inputs for RELAP5/MOD3. Using the modified RELAP5/MOD3 with the RRS modeling, the overall reactor behaviors as well as the safety parameters are analyzed. Then, the effects of RRS are discussed in terms of the safety assessment.

1. Introduction

The safety analysis of the research reactors usually neglects the behavior of reactor regulating system (RRS) because it decreases the reactor power while a reactivity-induced event increases the reactor power.

The RRS considered in this study is a computer-based system which regulates the reactor power by moving up and down the control absorber rods (CARs) and by controlling their speed [1]. The RRS controls the reactor power to regulate neutron power within a predetermined level in the range between 10^{-8}%Full Power (FP) to 100%FP. Since the RRS tends to regulate the power in Reactivity Induced Accidents (RIAs) with positive reactivity insertion, it is a more conservative assumption not to implement the RRS control during these events. However, the RRS can affect the transient in a different way during the power decreasing events, such as a flow blockage event.

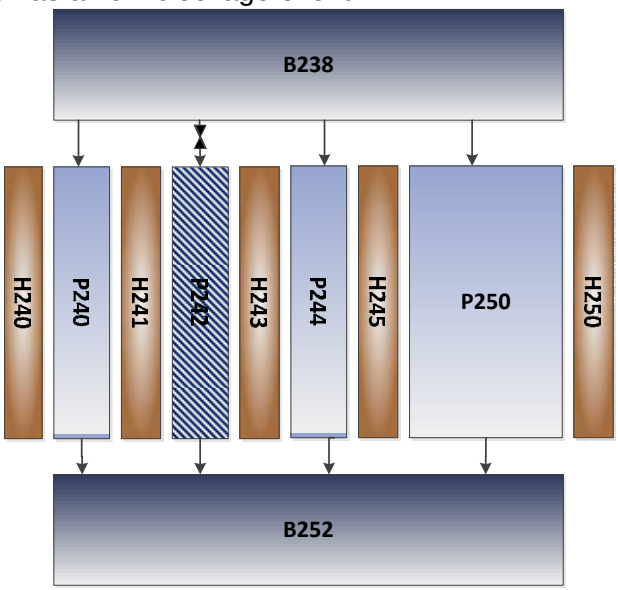

Fig 1. Nodalization for steady-state for flow blockage event

Variable	Value
Core Power	15MW
Core Inlet Temperature	36℃
Power Peaking Factor	3.0
Fuel Temperature Coefficient	-3.45E-2 mk/℃
Moderator Temperature Coefficient	-2.15E-2 mk/℃

Tab 1: Main initial conditions for the analysis

A flow blockage event may occur when the reactor is operated with miscellaneous materials or debris in the core [2]. Such foreign materials can be introduced into the core during the refueling and maintenance period. No alarm or indication might be available for the operator to take proper action to prevent fuel failures by the flow blockage event. Once a flow blockage in a fuel channel occurs, the coolant flow in the blocked channel decreases suddenly resulting in the increase of voids fraction in the channel. At the same time, the temperature of the fuel plates at the blocked channel increases by the decrease of the heat transfer coefficient due to the flow reduction. Therefore, the core power decreases by the negative reactivity feedback owing to both void and fuel temperature. Meanwhile, the RRS notices the discrepancy between the current core power level and power demand (PDM) and regulates the power by compensating the feedback effects.

In this paper, a complete blockage of a single fuel channel either with or without RRS control is analyzed to examine the reactor behavior and the fuel integrity. Then the effects of RRS on the event are discussed in terms of the reactor safety.

2. Analysis Methods

2.1 Heat Structure Modeling in RELAP5/MOD3 input

Figure 1 shows the core model for the analysis of a flow blockage event. There are 22 Fuel Assemblies (FAs) in the core. Each FA consists of 21 Fuel Plates (FPs) with 20 internal flow channels and 2 outer channels. For the single channel blockage analysis, 4 fuel plates among 462 fuel plates of FAs are classified as hot fuel plates and the rest are classified as average fuel plates. In addition, the three fuel channels between 4 hot fuel plates are named as hot fuel channels. The hot fuel channel at the center (P242) is modeled as a blocked channel. A motor valve was modeled at the top of the blocked channel to simulate flow blockage phenomena. The main initial conditions considered in this analysis are listed in Table 1. The temperature coefficient in the table is converted into density reactivity to be used for RELAP5/MOD3.

The fuel temperature as well as core power are considered as a safety parameter to determine the fuel integrity during the flow blockage event. The fuel temperature is estimated by considering the engineering hot channel factors on the value calculated from RELAP5/MOD3.

The engineering hot channel factors are evaluated from the manufacturing uncertainties of the fuel plates and coolant channels, core power calculation and heat transfer correlations in the coolant channels. The blockage of a flow channel leads to a deterioration of the heat transfer between the fuel and coolant, causing a failure of the fuel plates.

The transient analysis on the flow blockage of the hot channel in 15-MW pool-type research reactor is performed. Since the RELAP5/MOD3 does not equip a proper correlation set for narrow rectangular channel, Kaminaga CHF correlation is implemented in the code as a new subroutine. The implementation of the correlation facilitates the realistic heat transfer behavior at the fuel surface near the CHF condition [3].

To simulate the temperature behavior of fuel plates at melting point, the heat capacity of the fuel plates are modeled to have a large arbitrary value (10^{20} J/m^{3}K) at the fuel melting temperature of 843.2K.

2.2 Implementation of RRS into RELAP5/MOD3 Input

To consider the RRS in safety analyses, the control logic of RRS is implemented in the

RELAP5/MOD3 using control variable inputs [4].

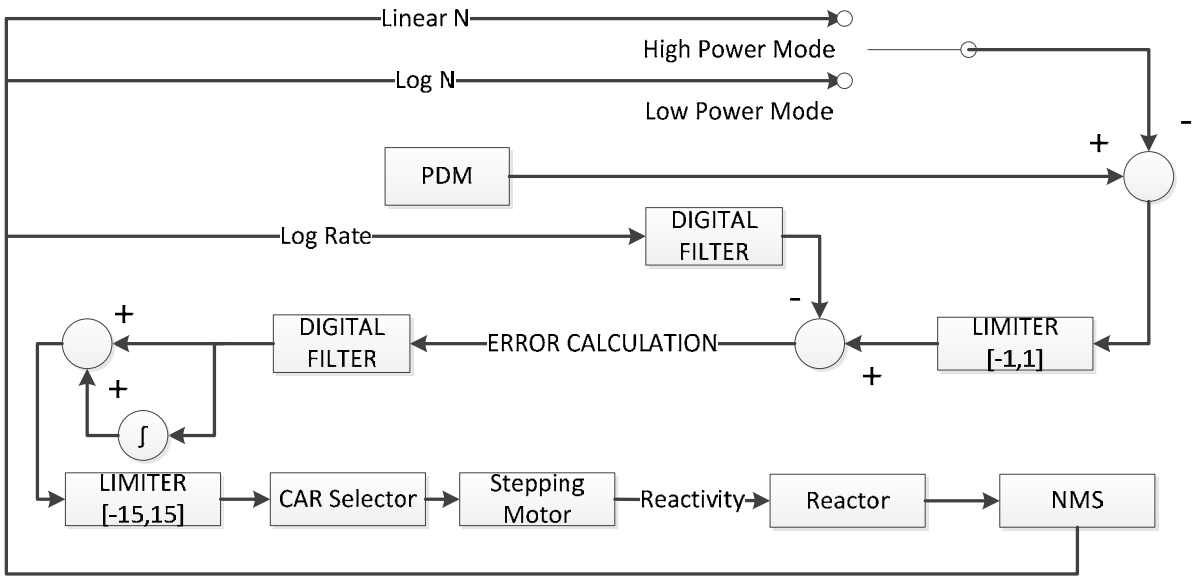

Fig 2. Reactor power control algorithm of RRS

Figure 2 shows the feedback power control algorithm of RRS. The RRS builds the error structure which consists of the PDM to power ratio and the power log rate as below.

$$\mathrm{ERROR} = \langle (G1) Log(\frac{PDM}{N}) \rangle_{[-1,1]} - (G2) \frac{1}{N} \frac{dN}{dt}, \qquad (1)$$

where G1 and G2 are the controller gains regarding the characteristics of RRS. The first term, the ratio of PDM to the neutron power N, is for a proportional control according to the difference between PDM and the current power. The second term which is the power log rate is added to limit a fast power change during the control. The error balances the power and power log rate to limit the CAR movements during power transients. Once the error term in Equation (1) is calculated, it passes several filters and is converted into the step number of a CAR to move. After the step number is determined, the RRS selects a CAR and controls the position through a hard wire connected to the step motor of each CAR within a cycle of 200ms.

3. Implementation of RRS on Flow Blockage

3.1 Flow blockage without RRS

To check the influence of RRS behavior on the fuel integrity as well as core power, the following analysis are performed without considering RRS. These analyses include two different cases: with or without considering feedback effects.

(1) Without Feedback Effects

Figure 3 shows the void fraction, fuel temperature and core power respectively. Since the void fraction directly affects the heat transfer at the fuel surface, the fuel temperature in the blocked channel increases up to the melting point with the event initiation and maintains its value. However, since there is no feedback effect considered in this analysis, the void as well as fuel temperature do not affect the core power. Therefore, the core power maintains the initial value during the transient. The fuel plates next to the blocked channel fuel are intact by the accident and their maximum temperatures are far below the melting point.

(2) With Feedback Effects

The void fraction in the blocked channel shows similar behavior with that in the case without RRS. Figure 4 shows the behavior of the main parameters during the transients.

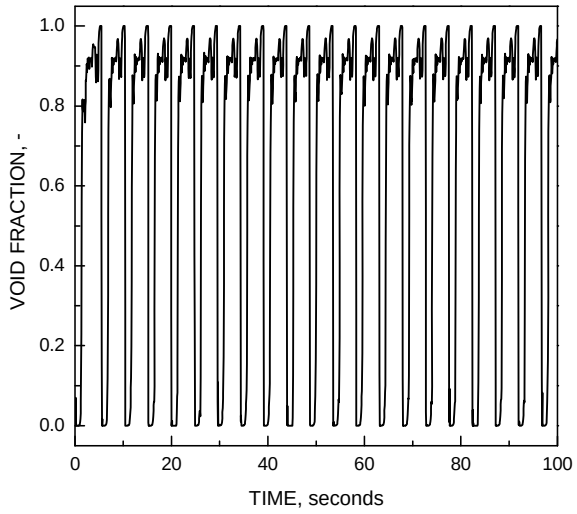

(a) Void fraction in the blocked channel (P242)

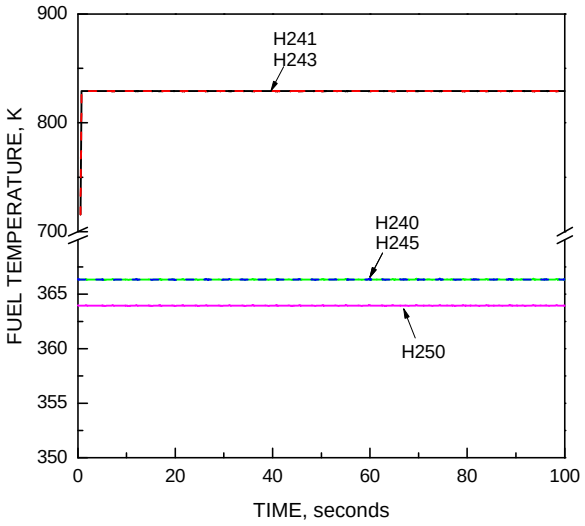

(b) Fuel temperatures

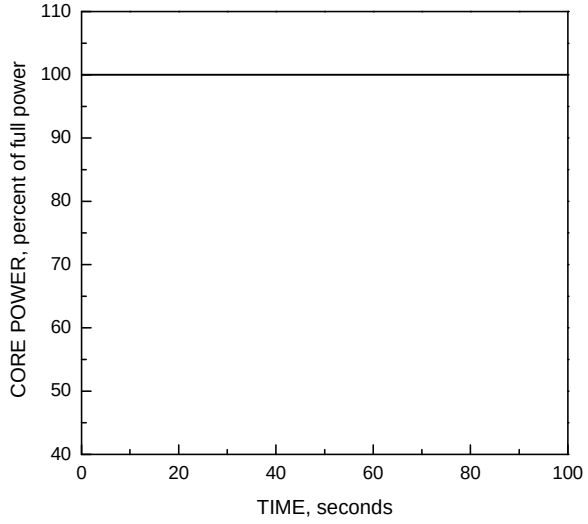

(c) Core power

Fig 3. Thermal hydraulic parameters in the case without feedback effects and RRS control

The reactivity feedback owing to void and fuel temperature starts to lower the core power level gradually because the RRS control is not considered in this analysis. Also, the power fluctuates by the void profile in the blocked channel. The fuel temperature of the fuel plates in the blocked channel reaches the melting temperature and maintains the value (Figure 4-(b)). The maximum temperatures of the fuel plates next to the blocked channel fuel decrease following the core power. The temperatures fluctuate more than those in the case without reactivity feedbacks, because the power itself fluctuates. The net feedback reactivity are governed by the void rather than the fuel temperature, it decreases as the core power decreases (Figure 4-(c)) since the feedback by the fuel temperature is determined by the average fuel temperatures. The oscillating periods of power and void fraction are determined by the energy balance between the coolant and the fuel plates at the blocked channel: the coolant in the blocked channel dries out, the accumulated voids escapes the blocked channel and the coolant refloods into the blocked channel again (Figure 4-(d)). Therefore, the oscillating periods are determined as follows:

$$\mathrm{Q} \times \mathrm{period} = \rho_f V C_P \left(T_{sat} - T_f\right) + h_{fg} V \qquad (2)$$

The period changes with respect to the core power. In this case, the period increases over time, since the core power decreases by the negative reactivity.

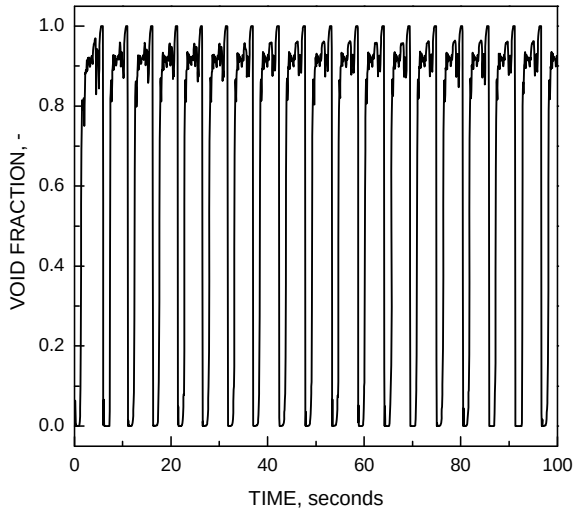

(a) Void fraction in the blocked channel (P242)

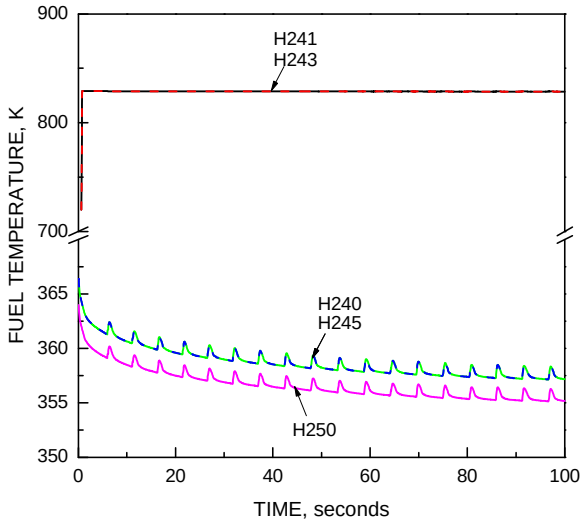

(b) Fuel temperatures

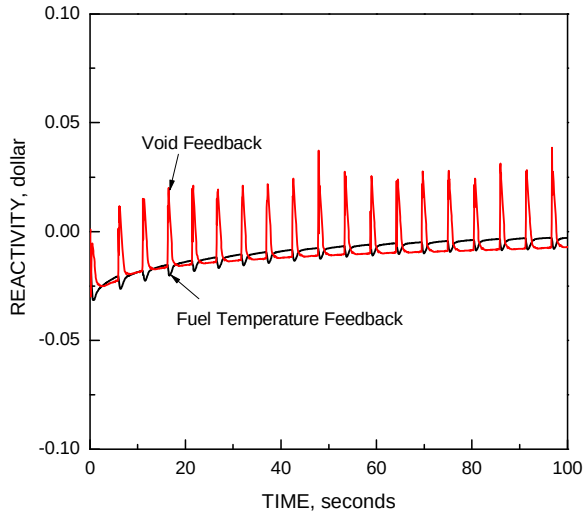

(c) Reactivity by feedback effects

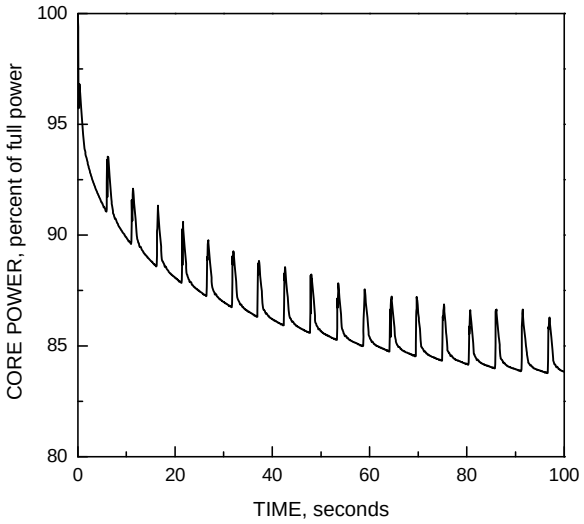

(d) Core power

Fig 4. Thermal hydraulic parameters in the case with feedback effects and without RRS control

3.2 Flow blockage with RRS

To check the effect of RRS on the core power during the flow blockage event, the RRS is modeled to be activated during the transient. Figure 5 shows the behavior of the main thermal-hydraulic parameters during the transients. Figure 5-(a) and Figure 5-(b) show the void fraction and fuel temperature, respectively. The void fraction of blocked channel oscillates from 0.0 to 1.0 showing a similar behavior as the event without RRS. Figure 5-(c) shows the reactivity by the feedback effects and RRS control. By the effects of void and fuel temperature, negative reactivity is inserted into the core. A difference from the case without RRS is that the maximum temperatures of the fuel plates next to the blocked channel oscillate around constant values. The reactivity feedback by fuel temperature shows the negative value during the whole transient while void feedback fluctuates between positive and negative values because of a strong oscillation. Since these feedback effects lower the core power, RRS detects the discrepancy between the current core power level and PDM and starts to withdraw CARs to recover the PDM. Therefore, the positive reactivity by RRS control is inserted to compensate for the power decrement. Since the core power oscillates around the initial value of 100%FP (Figure 5-(d)), the oscillation periods of power and void fraction maintain the initial value during the transient.

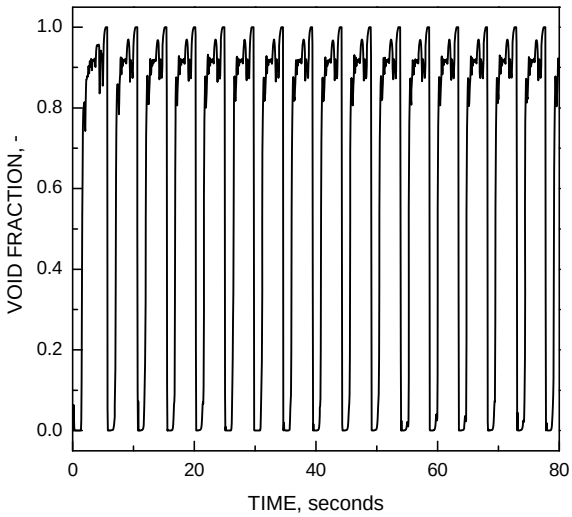

(a) Void fraction in the blocked channel (P242)

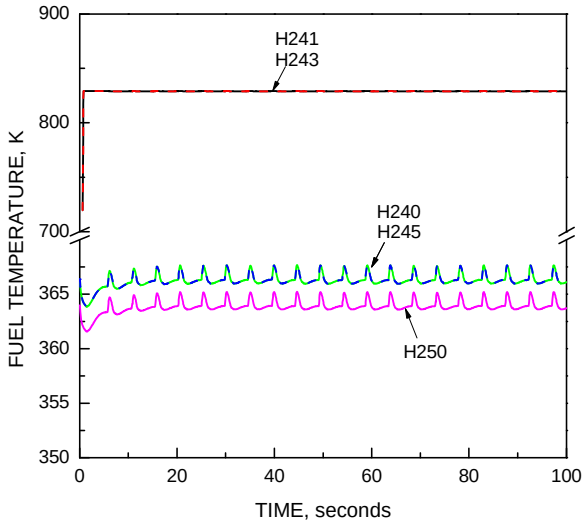

(b) Fuel temperatures

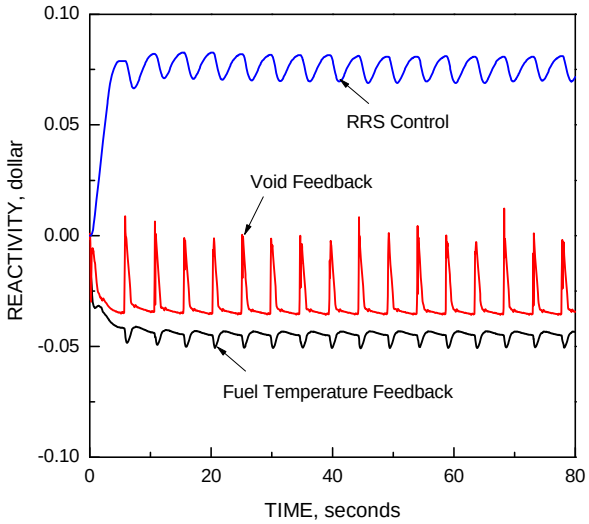

(c) Reactivity by feedbacks and RRS

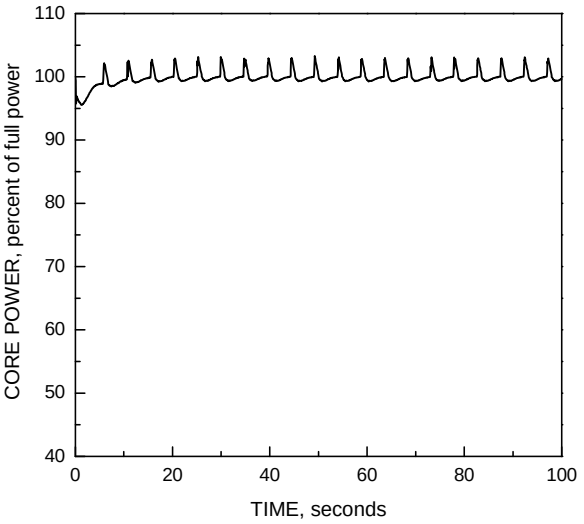

(d) Core power

Fig 5. Thermal hydraulic parameters in the case with feedback effects and RRS control

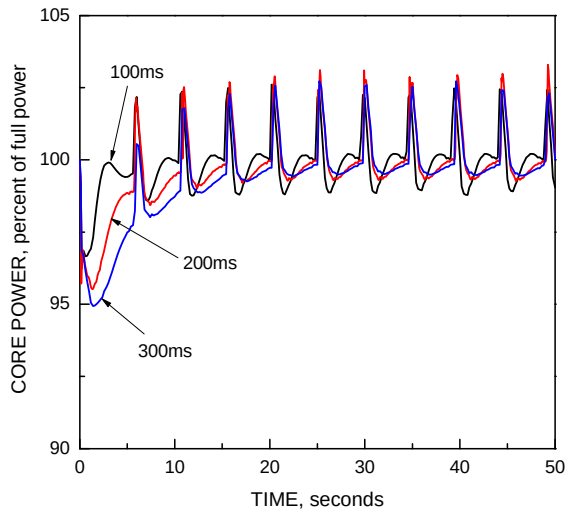

(a) Various control periods

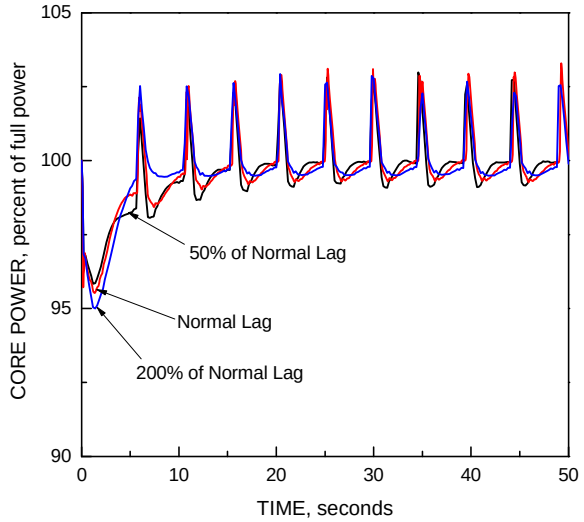

(b) Various lag time

Fig 6. Sensitivity tests in various control periods and lag times

Figure 6 shows the core power behavior resulted from the additional sensitivity studies. The overall reactor behavior in the cases is not sensitive to the control parameters of RRS such as the control period or lag, because the transient is generally slow except the local peaks by

void fluctuation.

3.3 Summary

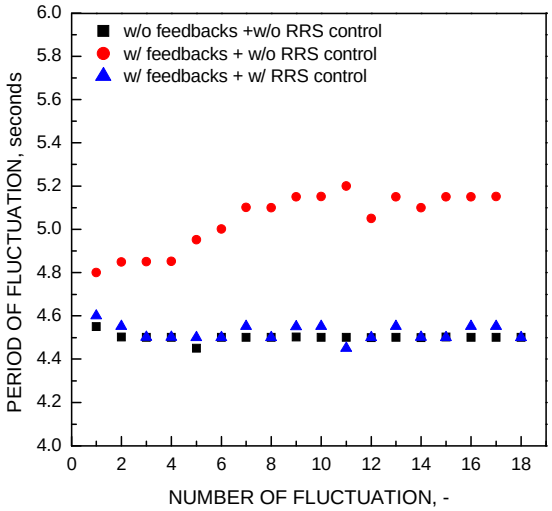

Fig 7. Comparison of oscillating periods

Figure 7 shows a comparison of the oscillating periods of power and void fraction from three different cases. Since the period changes with respect to the core power, the case with feedback effects and without RRS control shows the increase of oscillating periods, whereas the others are almost constant over time.

Table 2 summarizes the main results regarding the fuel integrity from three different cases: the maximum core power, maximum fuel temperature at the blocked channel and those next to the blocked channel. In case with RRS, the core power reaches its maximum value of 103%FP during its oscillation and it results in the oscillation of fuel temperature next to the blocked channel. The local peak of the fuel temperatures and the power even exceeds those constant values in the case without the RRS and reactivity feedbacks. On the other hand, the core power as well as fuel temperature decreases in the case without the RRS behavior and with reactivity feedback. Therefore, the consideration of RRS control on the flow blockage event results in the most conservative consequences in terms of the reactor safety.

Condition		Core power	Fuel temperature next to the blocked channel
RRS Control	Feedbacks		
X	X	Constant	Constant
X	O	Gradually decreases with oscillation	Gradually decreases with oscillation
O	O	Oscillation	Oscillation

Tab 2: Comparison of main results

4. Conclusions

In this study, the effects of the reactor regulating system (RRS) on a flow blockage-induced event for an open-pool type research reactor are investigated. Since the RRS regulates the core power to achieve the PDM which is initially determined by an operator, it tends to deteriorate the inherent reactor safety by the reactivity feedbacks of void and fuel temperature. Therefore in a flow blockage event, the modeling including the RRS showed the most conservative results in terms of the fuel temperature since it increases the fuel temperatures of the fuel plates next to the blocked channel fuels and affects the core power. The RRS implementation results in a higher local peak in the fuel temperatures and reactor power than those from without RRS control.

Acknowledgement

This work was supported by the National Research Foundation of Korea (NRF) grant funded by the Korea government (NRF-2012M2C1A1026916).

References

[1] Kim, H.I., Park, S.K. and Park, C., 2014. Simulation of Power Maneuvering Using Coupled Analysis of Kinetics and Thermal-Hydraulics in a Research Reactor, International Group Operating Research Reactors, Bariloche, Argentina, November, 17-21.
[2] W, Fan, et al., 2015. CFD study on inlet flow blockage accidents in rectangular fuel assembly, Nuclear Engineering and Design 292, 177-186.
[3] Lee, B.H. and Park, S.K., 2015, Propagation of Fuel Damage by Flow Blockage of a Channel for Plate Type Fuels. KAERI/TR-6043/2015, September.
[4] Yum, S.B., Lee, B.H. and Park, S.K., 2015, Implementation of Reactor Regulating System in Safety Analysis of Research Reactor. In: 36th International Meeting on Reduced Enrichment for Research and Test Reactors, Seoul, Korea, October 11-14.

A SELF-CONTROLLED LOW POWER REACTOR

F. BOSCHETTI, A.S. DOVAL, D.F: HERGENREDER, J.LUPIANO CONTRERAS, F.D: SARDELLA

Nuclear Engineering Division, INVAP S.E.
Av. Cmte. Luis Piedrabuena 4950, R8403CPV San Carlos de Bariloche – Argentina

ABSTRACT

The universe of research reactors encompasses a wide variety of reactor and fuel assemblies designs, optimised out of the utilization goals. Low power reactors of some tens of kWatts provide an opportunity to develop nuclear expertise while maximising safety through fault tolerance capabilities. One of the outstanding characteristics of this type of reactors is the response to a positive reactivity insertion event. This paper presents the analysis of the uncontrolled withdrawal of a control rod, and compares the results from analytical calculations with those obtained using a RELAP5 model. The latter considers point kinetics for the core and a few control volumes representing the different regions of the pool to simulate the thermal response of water in order to calculate the core feedback coefficients. The self-control of these reactors, together with some design features of the fuel and the pool producing ample safety margins allow to manage a much broader set of initiating events including multiple failures without core damage. This eases not only the operation requirements, but also the safety analysis, and provides a smooth way through the licensing process, which is an attractive starting point for newcomers of nuclear activities.

1. Introduction

Low power reactors constitute a useful tool for student training purposes, human resources development and represent for several countries the access door to the nuclear development.

Taking into account the multipurpose characteristics of the reactor and its use for beginners at nuclear activities, several design aspects shall be considered in order to improve the safety characteristics.

We can mention the following design characteristics of a generic reactor that enhance the safety:

- Power limited to 100 KW
- Fuel rods with the same characteristics as the one used in Nuclear Power Plants (UO_2 pellets with Zirconium alloy cladding) provide large margins form the operation condition point of view. The fuel integrity is ensured at power levels up to 5.5 MW.
- Low Uranium enrichment (few percentage)
- Reactivity Excess lower than one dollar and large shutdown margin values. If only one of six control rods is inserted, the reactor is subcritical.
- Negative feedback coefficients
- Natural convection cooling regime and large volume of the reactor pool providing large heat capacity

The solid safety characteristics will also lead to a more simple licensing process.

To evaluate the response of a 100 kW low power reactor to a reactivity insertion accident, two different approaches were done:

- Analytical calculations with a simple model

- Analysis with a thermal-hydraulic system code

2. Description of the Analytical Model

The neutronic behaviour of the core was modelled by the Point Reactor Kinetics equations, including a module to represent the dynamics of the Xenon concentration and its influence in the reactivity. Temperature reactivity effects were considered through a model that represents the heating of the fuel plates and the delays in the transmission of the heat to the coolant. The control rods were also modelled in detail considering their reactivity insertion characteristics.

The computational tool used to implement the models was the software package MATLAB/Simulink, which is especially suited for this purpose.

The model consists of three parts: Reactor Kinetics Model, Thermohydraulic Model and Xenon Dynamics Model

Fig 1 shows a block diagram of the global reactor model. The different physical processes are separated in subsystems that execute specific computations. The following sections describe each of these subsystems.

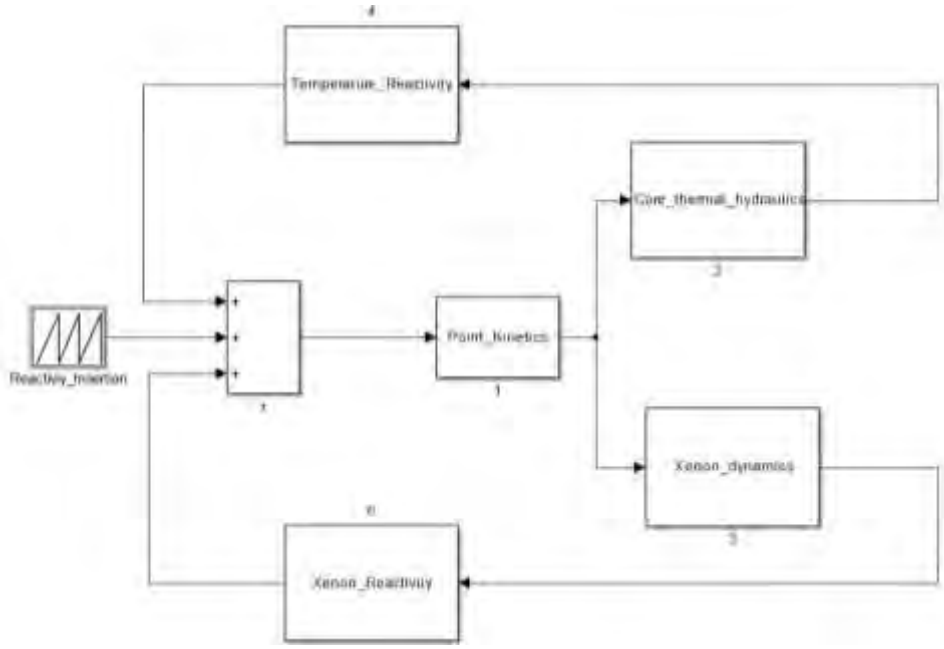

Fig 1. Block diagram of the reactor model

2.1 Reactor Kinetics Model

This model represents the dynamics of the neutron population in the reactor core, as a function of the total reactivity. The equations implemented are those of the point kinetics, with one delayed neutron group:

$$\frac{dn}{dt} = \frac{\rho - \beta}{\Lambda} n + \lambda C \qquad \text{neutron population}$$

$$\frac{dC}{dt} = \frac{\beta}{\Lambda} n - \lambda C \qquad \text{precursor concentration}$$

Where:

n: neutron population,

ρ: total reactivity,

β: effective delayed neutron fraction,

Λ: prompt neutron generation time,

λ: delayed neutron decay constant,

C: group i precursor concentration,

Typical values of kinetic parameters are:

β = 770 pcm

Λ = 4.5E-5 seg

λ = 7.6E-2 seg^{-1}

2.2 Core Thermal-Hydraulics

This model evaluates the fuel and coolant temperatures as a function of the total reactor power. The output is the average temperature of Fuel, Cladding and Coolant. The equations used for these calculations are the following:

$$m_f c_f \frac{dT_f}{dt} = P_T - h_1 A_1 (T_f - T_{clad}) \quad \text{fuel}$$

$$m_{clad} c_{clad} \frac{dT_{clad}}{dt} = h_1 A_1 (T_f - T_{clad}) - h_2 A_2 (T_{clad} - T_w) \quad \text{cladding}$$

$$m_w c_w \frac{dT_w}{dt} = h_2 A_2 (T_{clad} - T_w) - q_w c_w (T_i - T_o) \quad \text{coolant}$$

$$T_w = \frac{T_i + T_o}{2} \quad \text{average coolant temperature}$$

Taking into account the previous definition it is possible to rewrite the equation in the coolant as:

$$m_w c_w \frac{dT_w}{dt} = h_2 A_2 (T_{clad} - T_w) - 2 q_w c_w (T_i - T_w)$$

where

m_f: fuel mass of a Fuel Rod.

c_f: fuel specific heat

T_f: fuel temperature

P_T: total power

h1: global heat transfer coefficient between fuel and clad.

A1: heat transfer area between fuel and cladding

T_{clad}: cladding average temperature

m_{clad}: cladding mass of a Fuel Rod.

c_{clad}: cladding specific heat

h2: global heat transfer coefficient between cladding and water

A2: heat transfer area between cladding and water

Tw: coolant average temperature

m_w: coolant mass inside the subchannel

c_w: coolant specific heat

q_w: coolant mass flow rate

To: coolant outlet temperature

Ti: coolant inlet temperature

Although the model is simple, it adequately represents the dynamics of reactor core's thermal-hydraulic behaviour. It is pointed out here that fuel and coolant temperatures only influence power through reactivity feedback, so their variations are important, rather than their absolute values.

The formulas used to calculate the temperature reactivity are the following ones:

$\rho_f = \alpha_f (T_f - T_{fref})$ fuel

$\rho_w = \alpha_w (T_w - T_{wref})$ coolant

Where:

ρ_f: fuel temperature feedback reactivity

α_f: fuel temperature reactivity coefficient for Beginning of Cycle (BOC) and Cold Zero Power (CZP) condition.

T_{fref}: fuel reference temperature

ρ_w: coolant temperature feedback reactivity

α_w: coolant temperature (and void) reactivity coefficient for BOC and CZP condition.

T_{wref}: coolant reference temperature

Following are typical values for this type of designs

α_f = -2.6 pcm/ºC

T_{fref} = 20ºC

α_w = -14.9 pcm/ºC

T_{wref} = 20ºC

2.3 Xenon Dynamics Model

Only ^{135}Xe was included in the model, as it is by far the most important isotope with respect to reactivity contribution. The equations used to calculate the Xenon concentration, and its corresponding reactivity are the following:

$$\frac{dI}{dt} = \gamma_I \Sigma_f \phi_T - \lambda_I I \quad \text{Iodine}$$

$$\frac{dX}{dt} = \lambda_I I + \gamma_X \Sigma_f \phi_T - \lambda_X X - \sigma_{aX} \phi_T X \quad \text{Xenon}$$

Where:

I: iodine concentration

γ_I: effective fission yield of ^{135}I

Σ_f: macroscopic thermal fission cross section

ϕ_T: thermal neutron flux

λ_I: decay constant of ^{135}I

X: xenon concentration

γ_X: effective fission yield of ^{135}Xe

λ_X: decay constant ^{135Xe}

σ_{aX}: microscopic thermal absorption cross section of ^{135}Xe

ρ_X: Xenon reactivity

ϕ_{T0}: steady-state thermal flux (corresponding to 1 W)

γ_I = 0.0560

Σ_f = Correlated with Power

λ_I = 2.9E-05 s^{-1}

γ_X = 0.0030

λ_X = 2.1E-18 s^{-1}

σ_{aX} = 3.5E-18 cm^2

In the following table the relevant information for correlating thermal flux and power, and Xenon worth and concentration is presented.

Power[kW]	Thermal Flux [n/cm^{2}s]	Xe worth
1E-3	5.32E+06	1E-5
30	1.61E+11	65E-5
100	5.41E+11	200E-5
280	1.53E+12	530E-5

Tab 1. Correlation between thermal flux, power and Xe reactivity worth

$$\phi^{th} = \phi^{th}(Pot[W])$$

$$\phi^{th} = 5.31263 * 10^6 Pot^{1.00168}$$

It is important to remark that the initial steady condition was set to 1W. Because of this, the Xenon concentration set as reference is the one computed at this power.

$$Rho([Xe(t)]) = 7.68533 * 10^{-18}([Xe(t)] - [Xe(1W)])$$

The only input variable is the normalised power (obtained from the point kinetics model), and the output is the Xenon reactivity contribution and concentration.

3. Verification against CONDOR-CITVAP Calculation Line

The model was verified against CONDOR-CITVAP Calculation Line. For this, reactivity steps were simulated in order to obtain a specific Power. The Xenon was not modelled for this experience. Fig. 2 shows the reactivity excess as function of the reactor power.

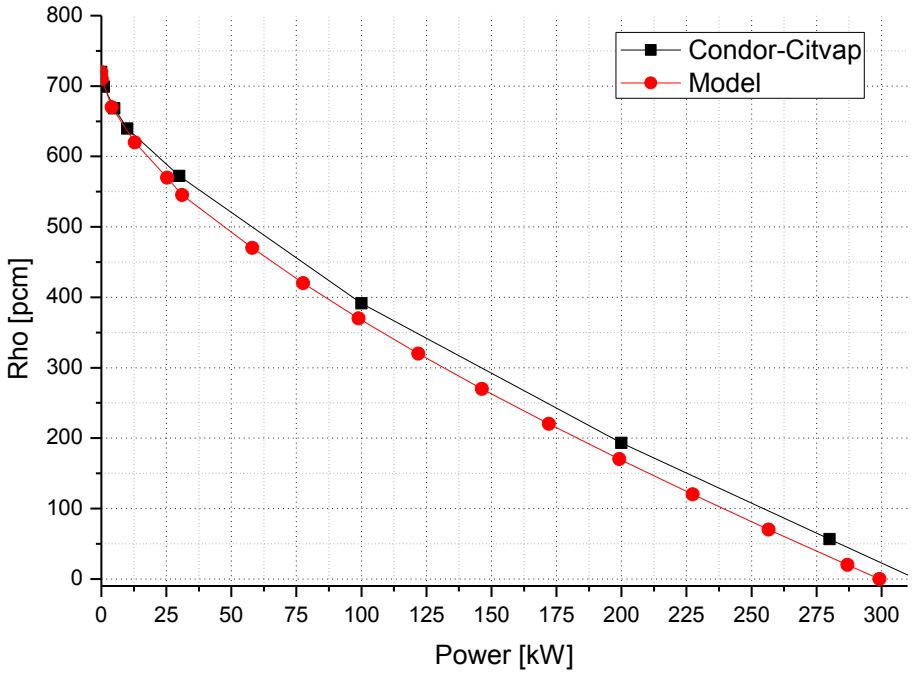

Fig 2. Reactivity Excess as function of the reactor Power.

4. Transient analysis

The starting point for the power transient is the critical reactor at a power of 1W, where all temperatures are assumed at 20°C. In this configuration all control rods are withdrawn from the core, except the one used to maintain the reactor critical with a position of 44% of withdrawal. The core reactivity excess is 720 pcm, that is lower than 1 dollar.

The transient starts with the withdrawal of this control rod at the maximum velocity of 3 mm/s.

The time required to fully withdraw the control rod is 95.2 seconds.

Fig 3 shows the positive reactivity introduced by the control rod as function of time.

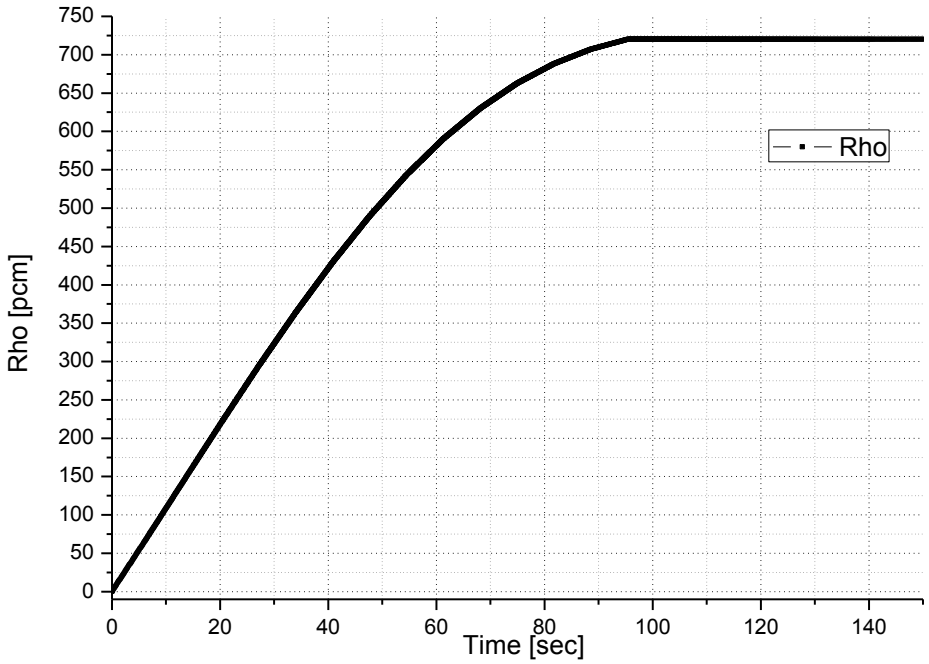

Fig 3. Reactivity introduced by the control rod

4.1 Results

The analysis for the reactivity insertion was done considering two time scales. The first one, from 0 to 1000 seconds where the influence of the Xenon cannot be seen.

The second time scale from 1000 to 250000 seconds shows the importance of Xenon from a long-term point of view. As the Temperature of the pool was conservatively fixed in 20ºC; the reactor reaches the steady state at a power level of 135 kW.

A best estimate model that takes into account the heating of the pool water and its effect on coolant/moderator coefficients will reduce significantly the steady state power level. Due to the complexity of the natural convection in a reactor pool, the best estimate model with and without the pool cooling system on will be analysed in the future.

Fig. 4 and 5 show the power evolution for the two time scales.

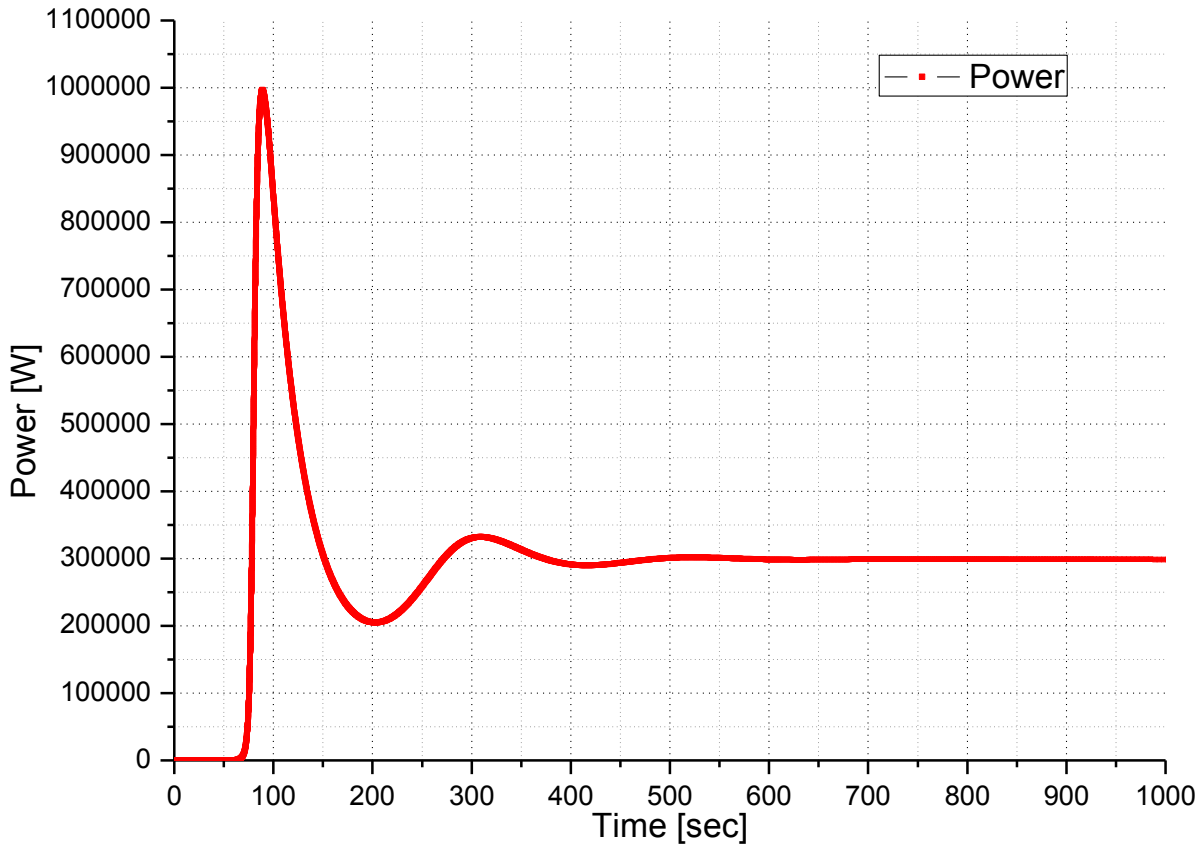

Fig 4. Power Transient after Reactivity Insertion accident (all control rods out of the core) - 0 to 1000 seconds.

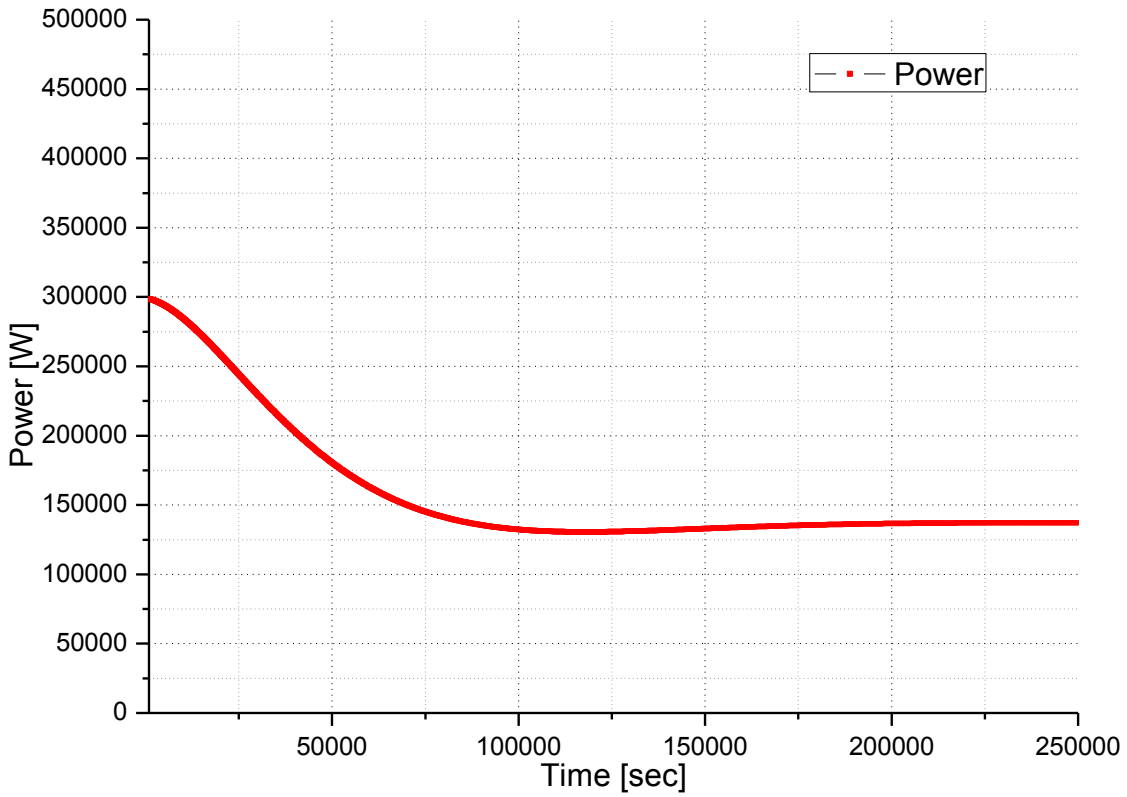

Fig 5. Power Transient after Reactivity Insertion accident (all control rods out of the core) - 1000 to 250000 seconds.

5. Analysis with a thermal-hydraulic system code

The objective of this section is to compare the evolution in the reactor power with a positive reactivity insertion as calculated from the analytical model presented with the response obtained through the thermal-hydraulic system code RELAP 5 MOD 3.2.

5.1 Calculation model

The cooling circuit is modelled by a series of hydrodynamic components (pipes and volumes) connected by junctions in which the mass, energy and momentum equations are solved. The power in the core is introduced into the model through the “Reactor kinetics” cards which consider the power at Steady State, the changes in reactivity as a function of time due to the control rod withdrawal, and the effect of feedback coefficients both, the doppler and moderator density reactivity coefficients. The core is modelled by two pipes, representing a hot and an average channel. The heat transferred to the coolant is included by coupling each of the channels to a heat structure. The natural convection cooling loop is closed by introducing a pipe which represents the reactor pool as the cold leg. This pipe is also coupled to a heat structure which removes the heat generated in the core with the objective of adjusting the coolant inlet temperature.

The natural circulation loop was modelled as a closed loop neglecting the cross flow to the pool as it is an open array of rods. This assumption leads to lower moderator/fuel temperatures, which results in lower feedback coefficients.

Only the first time part of the transient was calculated as the Xe reactivity is not included in RELAP calculations.

The nodalization adopted for the study is illustrated in Fig 6 while Tab. 2 summarizes the input parameters considered in the model. They have been adjusted to reproduce the conditions considered in the analytical calculation.

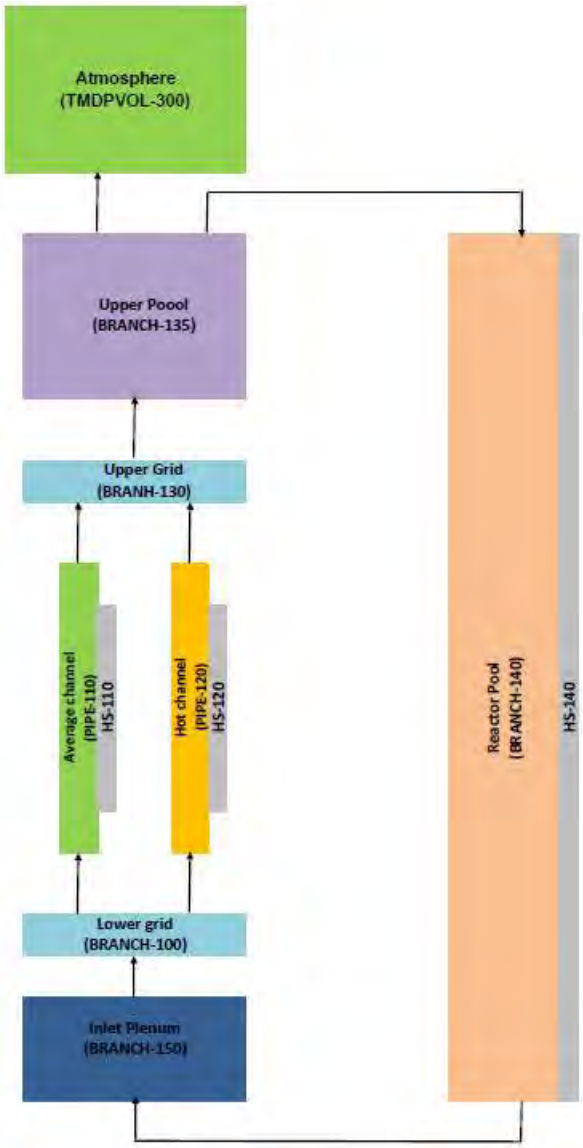

Fig 6. Nodalization in RELAP 5

Parameter	Value
Initial power (W)	1.0
Power Peaking Factor	1.9
Coolant Inlet temperature (°C)	20.0
Operating pressure (kPa)	160.0
Beta (pcm)	770
Doppler reactivity coefficient (pcm/°C)	-2.6
Coolant temperature (and void) reactivity coefficient (pcm/°C)	-14.9

Tab 2: Input parameters

5.2 Results

Fig. 7 shows the changes in power as the rod is withdrawn.

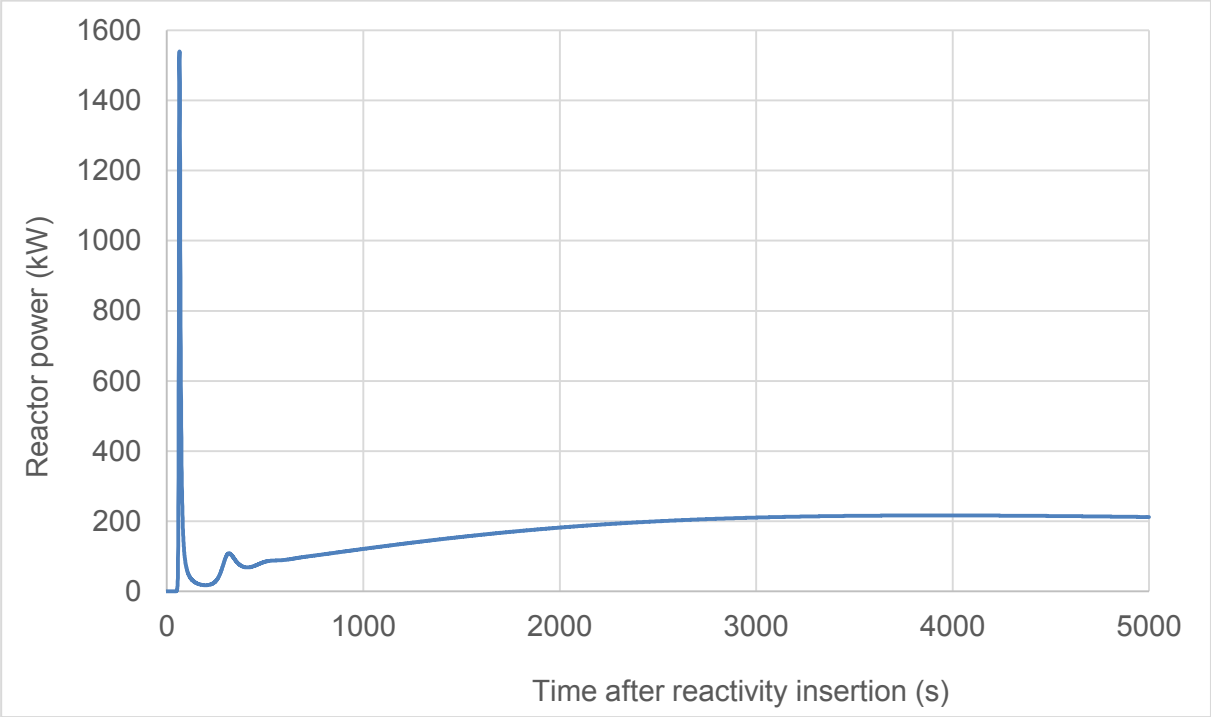

Fig 7: Reactor power after the reactivity insertion

A maximum value of 1.54 MW is achieved at 65 seconds from the beginning of the rod withdrawal. The reactor power later falls achieving a steady state value of 215 kW.

Both, the maximum power and the steady state power achieved, are in good agreement with the analyticial results.

6. Conclusions

The simulations shows that due to the reactivity insertion accident, the reactor has a short time power peak of about 1 MW for the analytical model (1.54 MW in case of the RELAP5 model). Despite of the differences between models, the values obtained (lower than 5.5 MW) ensure the fuel integrity

After the initial peak, the reactor power stabilizes at 300 kW for less than one hour and then slowly decreases to reach the steady state at 135 kW. The same behaviour is reproduced with the computational model, 215 kW at a longer time (more than one hour)

Since this model conservatively does not take into account the heating of the pool water and its effect on coolant/moderator coefficients, a more detailed model including this heating will reduce the steady state power to a level similar or lower than the nominal power.

Regarding the computational model, the natural circulation loop was modelled as a closed loop leading to lower moderator/fuel temperatures, it means that most probably the feedback coefficients will reduce the final steady state value of the reactor power.

Influence of critical heat flux correlations on safety analysis of research reactors with narrow rectangular fuel channels

A. Rawashdeh[1*], M. Albati[1], K. AbuSaleem[1, 2], A. AbuShqair[1], M. Omari[1], M. Alrwashdeh[1], B. Lee[3], Y.J. Chung[3]

[1]*Jordan Atomic Energy Commission, Jordan Research and Training Reactor, 70 Amman (11934) Jordan*

[2] *The University of Jordan, Amman (11942) Jordan*

[3]*Korea Atomic Energy Research Institute, 1045 Daeduk-Daero, Dukjin-Dong, Yuseong-Gu, Daejeon, 305-353, Republic of Korea*

*Corresponding author: Abdullah.rawashdeh@jaec.gov.jo

ABSTRACT

The influence of different critical heat flux correlations on the minimum critical heat flux ratio (MCHFR) during a typical accident of a 5 MW research reactor is investigated. The reactor uses plate type fuel, where the cooling channels have a narrow rectangular shape. RELAP5/MOD 3.3 uses critical heat flux (CHF) Look-up table to find CHF at the power reactor and the high power research reactor. Using default tables (Look-up-table) in RELAP5/MOD 3.3 does not show CHF values in this small research reactor, because the subroutines in REALP5/MOD 3.3 do not run when the coolant temperature lower than the saturation temperature. All-primary coolant system-pump failure event applied in this work, and some experimental CHF correlations are applied and implemented using RELAP5/MOD3.3. Mirshak and other CHF correlations tend to over-predict the CHF at this low coolant velocity event (<2.5 m/s), compared to that by Kaminaga, and therefore the correlation set is implemented in RELAP5/MOD 3.3 to be used instead of Look-up table.

1. Introduction

In research reactors, there are some applicable CHF (Critical Heat Flux) correlations are used widely in fuel channels, where there are many CHF correlations cannot be used for some research reactors, especially those have high heat flux range applicability. Selecting CHF correlations to be applicable in reactors are governed by channel geometry (i.e. rectangular channel), pressure, flow direction, coolant temperature, hydraulic diameter, global or local type conditions and others.

However the scientists and researchers of research reactors have developed many CHF correlations that have applicability to be used for the proper reactor channels. Thus safety analysis studies try to select the most suitable CHF correlation depending on the current conditions; also conservatism can give advantage for CHF correlations in some cases.

The CHF prediction methods are empirical correlations, table look-up method and theoretical or mechanistic models. Empirical correlations can be divided to global (inlet or outlet) condition type and local condition hypothesis. Inlet and outlet condition types both are function of hydraulic diameter, heated length, pressure and mass velocity/flux (G), in addition, the inlet type is function of inlet subcooling , and the exit type is function of quality. Also the local condition hypothesis is function of the same parameters of the exit type except the heat length in which it is not considered in the local condition hypothesis. In this reactor, experimental correlations are implemented in RELAP5 code to find CHF instead of Look-up-tables which used by default to find CHF [1].

In this reactor, all primary coolant system (PCS) pump-failure event which classified in loss of flow accident is simulated using RELAP5/MOD 3.3 to find the most suitable correlation among the implanted correlations which described in next section.

2. Implemented experimental CHF correlations in REALP5 code

The channel of this research reactor is narrow rectangular channels. Thus, this study concentrates on

the experimental correlations which developed for the rectangular channel. Table-1 shows the reactor channel conditions.

Table 1: the reactor channel conditions and description at loss of flow accident

Channel hydraulic diameter [mm]	4.53
Heated length of the channel [mm]	680
Channel length/gap [mm]	1.16 e+3/2.35
Coolant type	Water
Flow direction	Downward
Flow type	Forced convective
Channel pressure [kPa]	1.7
Mass flow rate [kg/s]	7.6
Initial inlet temperature [K]	298
Inlet/outlet subcooling [K]	78/0
Outlet quality	0
Mass velocity [kg/s.m^2]	Downward flow of 2,400

Kaminaga-1998 CHF correlation used 596 data for water from different sources to cover all previous conditions, and they found a RMS (root-mean-square) of +-33 %. Thus MCHFR (Minimum critical heat flux ratio; a ratio of critical heat flux to maximum heat flux) should be larger than 1.5; 1/(1-0.33) due to an error of -33% as it is recommended by Kaminaga [2]. The correlation is Inlet and outlet type condition. Table-2 shows Kaminaga correlation conditions. The correlation is developed for narrow rectangular channel.

Table 2: Experimental Kaminaga CHF correlation conditions

	From	**To**
Channel gap [mm]	2.25	5.0
Heated length/ hydraulic diameter	8	240
System pressure [MPa]	0.1	4
Mass velocity [$\frac{kg}{m^2.s}$]	Downward flow of 25,800 to stagnant	Upward flow of 6,250
Inlet subcooling [K]	1	213
Outlet subcooling [K]	0	74
Outlet quality [-]	0	1

Mirshak_Towell CHF correlation is based on rectangular cross section channel and annular in 65 tests. The minimum velocity of correlation is 1.52 m/s. Thus, the comparison will be over larger velocity than 1.52 m/s. However Mirshak_Towell correlation has ±16% Fitting error and 8% of standard deviation [3].

Other correlation conditions ranges are in Table 3.

Table 3: Experimental Mirshak_Towell CHF correlation conditions

	From	To
System pressure [bar]	1.7	5.8
Coolant velocity [$\frac{m}{s}$]	1.52	13.72
Coolant subcooling at the axial location [K]	5	75
Flow direction	Downward	-

Bernath CHF correlation can be used to calculate CHF in water, ammonia, and diphenyl. It is based on CHF data from 13 sources for water, ammonia and diphenyl [4]. Table 4 shows the correlation conditions.

Table 4: Experimental Bernath, CHF correlation conditions

	From	To
System pressure [bar]	1.6	207
Coolant velocity [$\frac{m}{s}$]	1.2	16.5
Coolant subcooling at the axial location [K]	0	182

Labunstov CHF correaltion is originally for the subcooled water, and it is developed for circular channels. It is based from 9 data sources. It shows $\pm 17\%$ of fitting error and it is within high velocity range relatively, high pressure and subcooling temperature range [5]. Table 5 shows the conditions range of Labunstov. The correlation is developed for **circular** channels.

Table 5: Experimental Labunstov CHF correlation conditions

	From	To
System pressure [bar]	1	204
Coolant velocity [$\frac{m}{s}$]	0.7	45
Coolant subcooling at the axial location [K]	1	213

3. Result and discussion

Figure 1 shows critical heat fluxes of the different correlations, which are applied at the middle of the channel using REALP5/MOD3.3. The compared velocity range starts above 1.7 m/s or 1.8 m/s because Mirshak is applicable on the velocity range higher than 1.5 m/s or 1.85 (in order to avoid occurring negative subcooling).

However, all are used in local conditions type except Kaminaga, and the ranges are within forced downward flow. Bernath and Mirshak over-predict critical heat flux, compared that by Kaminaga correlation. These correlations cannot be dependent in this research reactor, because the correlations have different conditions, compared that for JRTR and Bernath correlation is developed for circular channels. In addition the correlations show low conservatism, compared that by Kaminaga. Labunstov is nearer to Kaminaga compared with the last two correlations. But it is two times higher than CHF of Kaminaga and it has different conditions compared with that for JRTR.

For more conservative, critical heat flux ration (CHFR) is calculated by Kaminaga. For acceptance criterion, minimum CHFR should be larger than 1.5 in Kaminaga and for the other correlations is around 1.5. In all PCS pump-failure event, minimum CHFR for the correlations except Kaminaga is more than two times of the accepted criterion of CHFR. However, Figure 2 shows minimum CHFR in Kaminaga, where it is within accepted criteria.

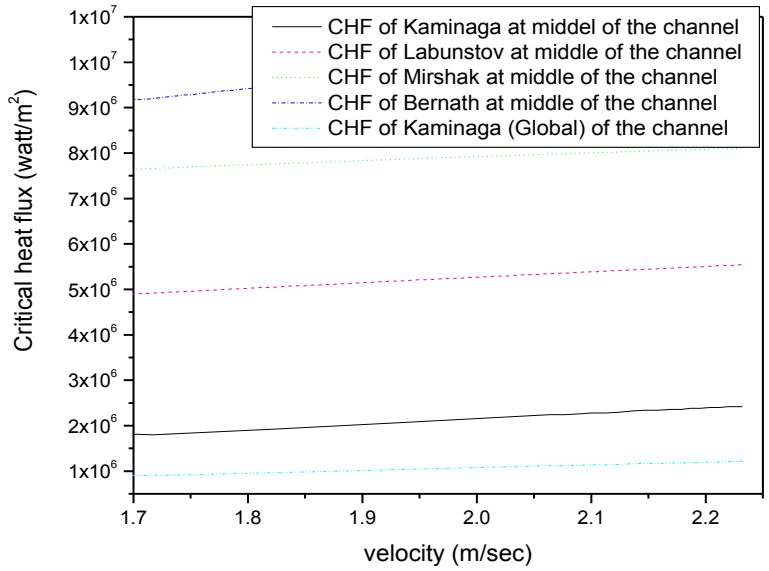

Figure 1: Comparable CHF Correlations at all PCS pump-failure event

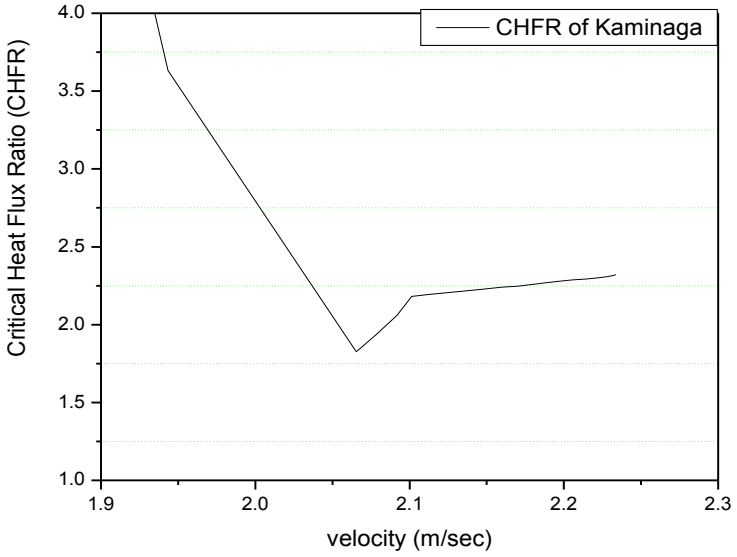

Figure 2: CHFR of Kaminaga at all PCS pump-failure event

4 Conclusion

In this research reactor, Look-Up-Table cannot be applied to find CHF. There are correlations which cover conditions in the reactor, Kaminaga is the most suitable correlation to estimate CHF in the heated channel of the since the correlation is developed for JRR3, the research reactor has similar channel geometry and operating condition with the applied research reactor. The correlations are implemented in RELAP5 code and compared each other. The other correlations could be used in different conditions.

Acknowledgement

This work has been carried out under the auspices of the Jordan Research and Training Reactor and Training Reactor Project being operated by Korean Atomic Energy Research Institute.

References

[1] NUREG/CR-5535, "RELAP5/MOD3.3 CODE MANUAL, VOLUME IV: MODELS AND CORRELATIONS", December 2001.

[2] Kaminaga, M, K Yamamoto, and Y Sudo. "Improvement of critical heat flux correlation for research reactors using plate-type fuel." *Nuclear Science and Technology* 35 (1998): 943-951.

[3] Mirshak S., Durant W. S., and Towell R. H., "Heat Flux at Burnout," E. I. du pont de Nemours & Co., DP-355, Available from Office of Tech. Services, U. S. Dept. Commerce, Washington, D. C., 1959

[4] Bernath L., "A Theory of Local Boiling Burnout and Its Apllicatio to Existing Data," Chem. Eng. Prog. Symp. Series, 56 (30), 95, 1960.

[5] Labunstov D. A., "Critical Thermal Loads in Forced Motion of Water Which is Heated to a Temperature Below the Saturation Temperature," Soviet J. of Atomic Energy (English Translation) Vol. 10, No. 5, pp. 516-518, 1961.

A Comparison of THERMO-T System Code with Experimental Data from the SPERT-IV D12/15 Series

M. Margulis and E. Gilad

The Unit of Nuclear Engineering, Ben-Gurion University of the Negev
Beer-Sheva 84105, Israel

Corresponding author: gilade@bgu.ac.il

1. Introduction

Research reactors (RRs) are mainly constructed as test facilities and neutron generators for broad range of scientific, industrial, and medical purposes. Due to the special designations of RRs, they are characterized by small core size with low total thermal power (usually not exceeding 100 MW_{th}), which lead to high power density and low operating temperature and pressure. Furthermore, a vast range of fuel compositions, geometric configuration, and different range of relevant operational parameters constitute different neutronic and thermal-hydraulic design [1-4].

The unique characteristics of RR designs must meet different safety requirements and unique safety features to ensure their safe utilization in nominal and off-nominal operation conditions and safe shutdown in case of an emergency or an accident. The SPERT-IV experiment aimed to study the unique dynamic behavior of the nuclear reactor system by the performance and analysis of reactor kinetic experiments [5].

This paper presents the further evaluation of the THERMO-T model [6], which is currently under development at Ben-Gurion University of the Negev. In previous studies the THERMO-T was compered [6] to state of the art codes such as – RELAP5, PARET, RETRAC-PC and CPBRA-EN, in the frame of the IAEA 10 MW_{th} MTR benchmark [7]. The result showed good agreement between the different codes. However, in order to provide a more realistic and quantitative validation for THERMO-T code, the code was compared with experimental data.

Such experimental data is available in [5] and was part of the IAEA coordinated research project (CRP) 1496 – “Innovative Methods in Research Reactor Analysis: Benchmark Against Experimental Data on Neutronics and Thermal Hydraulic Computational Methods and Tools for Operation and Safety Analysis of Research Reactors”. The SPERT-IV transients present a unique overview of self-limited reactivity insertion transients with different hydraulic conditions and reactivity insertion steps.

2. Computational tools

2.1. Serpent

Serpent is a continuous energy MC neutron transport code with burnup capabilities [8]. It allows modeling of complicated 2D or 3D geometries. This code was initially developed as an alternative to deterministic lattice codes for the generation of homogenized multigroup constants for reactors analyses using nodal codes. Current analyses were performed with cross section libraries based on JEFF-3.11, JEFF-3.1 and ENDF/B-VII.0 evaluated data files. Serpent utilized in this work as a steady state solver in order to obtain the three-dimensional (3D) power distribution of the SPERT-IV core.

2.2. THERMO-T

THERMO-T is a coupled thermal-hydraulic (TH) – neutronic point kinetics (PK) code. The code solves the three TH conservation equations (mass, momentum, and energy) in time and space, allows for the core to be divided into any number of TH channels, and solves the

seven equation of the PK model with one prompt and six delayed groups of neutrons, where the axial and radial power distributions are calculated using Serpent.
The main challenge in such self-limiting transients is the proper prediction of the departure from nucleate boiling (DNB). In previous studies [9] the most suitable correlation for this type of experiment was found to be Tong et. al. DNB correlation [10], which is shown in Eq. 1. This correlation was implemented in THERMO-T and is the one utilized during this study.

$$q''_{DNB} = (0.23 \times 10^6 + 0.094G) \cdot (3.0 + 0.01\Delta T_{sub}) \cdot \left(0.435 + 1.23e^{\frac{0.0093L}{D_e}}\right) \cdot (1.7 - 1.4e^{-a})$$
$$a = \left[\frac{0.532\left(H_f - H_{in}\right)}{H_{fg}}\right]^{\frac{3}{4}} \left(\frac{\rho_g}{\rho_f}\right)^{-\frac{1}{3}} \quad (1)$$

THERMO-T adopts the approach presented in Todreas and Kazim [11]. This approach locates the point at which the local heat flux supports the bubble nucleation and the onset of significant void. The formulas presented in Eq. 2 and 3.

$$\frac{(T_w - T_{sat})_i^2}{(T_w - T_{bulk})_i} = \frac{1}{\Gamma} \qquad \Gamma = \frac{k_l h_{fg}}{8\sigma T_{sat} v_{fg} h_c} \quad (2)$$

$$T_{sat} - T_{bulk} = 0.0022\left(\frac{q'' D_H}{k_l}\right) \qquad Pe < 7E4$$
$$T_{sat} - T_{bulk} = 154\left(\frac{q''}{G \cdot C_{P,l}}\right) \qquad Pe > 7E4 \quad (3)$$

3. SPERT IV – Benchmark specification

SPERT-IV was a light water cooled and moderated pool type reactor, with upward forced and natural convection cooling. The SPERT-IV D-12/25 core was the final aluminum plate-type core studied as part of the Special Power Excursion Reactor Test (SPERT) project. The core was composed of 25 fuel assemblies, 20 standard and 5 control fuel assemblies. The different fuel assemblies are placed in a 5×5 section of the 9×9 support grid, as show in Fig. 1. The reactors fuel plates were highly enriched uranium (HEU) with aluminum cladding, UAl_x-Al. Each standard fuel assembly contained 12 fuel plates, housed in an aluminum assembly can. The four control assemblies and the single transient rod are made of double-blade control rods of the same style, but with a different operational direction. The control rod is operated downward, while the transient rod has an opposite operation direction. The control assembly contains 6 fuel plates [5, 12-18]. The SPERT-IV experiments consist of a series of non-destructive self-limiting tests for a variety of coolant flow conditions, initiated by step insertion of positive reactivity by quick withdraw of the transient rod. A summary of all the step insertion tests appears in [17]. For most of the transients the initial power was ~1W and the thermal-hydraulic condition correspond to this power level. The experiments were executed in the sequence shown in Fig. 2. Reactivity insertion values for the tests were varied in the range between 0.8 and 2.14 $, resulting in transients with initial periods of between 980 and 7 *ms*. The initial bulk temperature was at ambient room temperature (~20^{o}C), the total core coolant flow rate was controlled at 0, 500, 1000, 2500 and 5000 *gpm* (corresponding to coolant velocities of 0, 0.387, 0.771, 1.929 and 3.87 *m/s*). The reactivity coefficients are summarized in Table 1. The reduced prompt neutron life is discussed later in subsection 4.1.

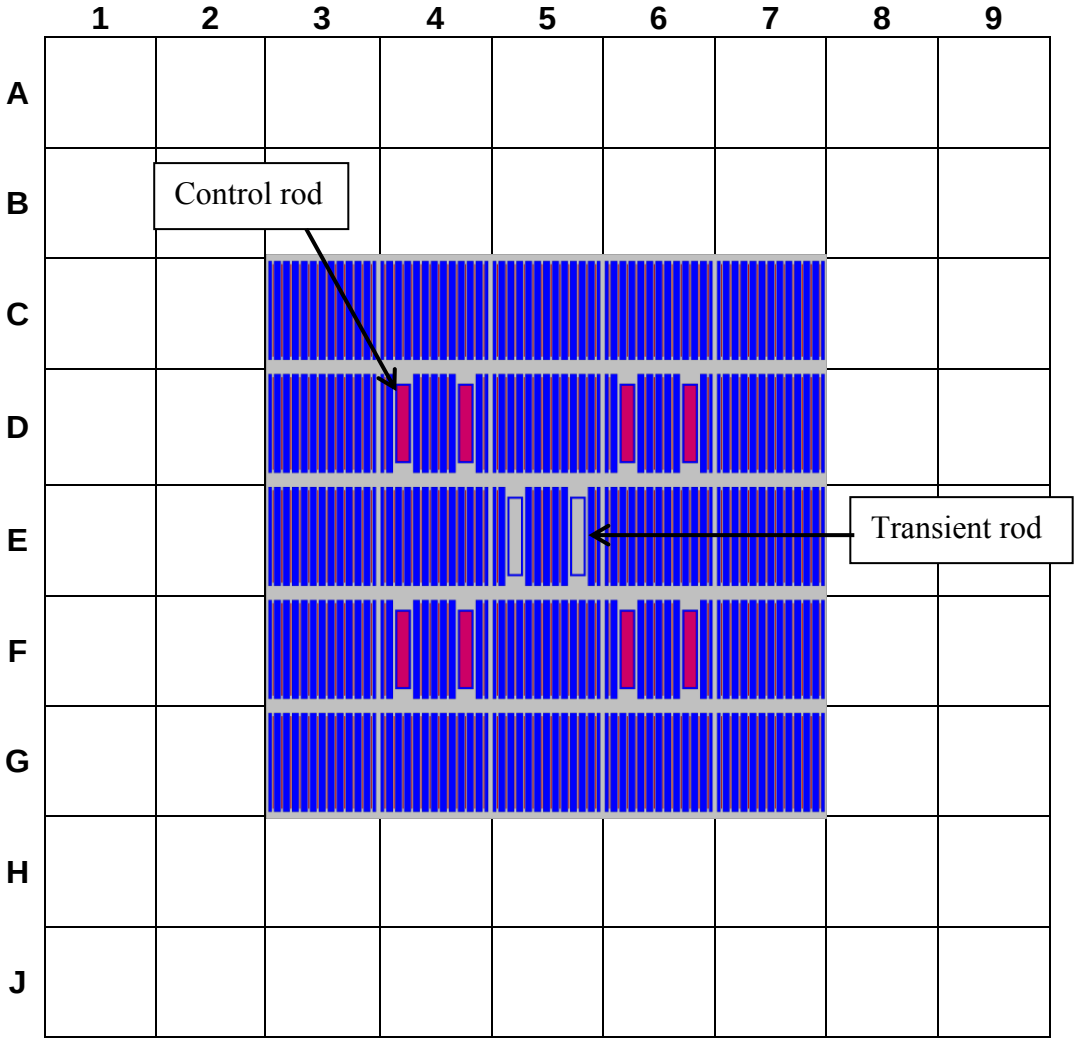

Fig. 1. SPERT IV D-12/25 core configuration.

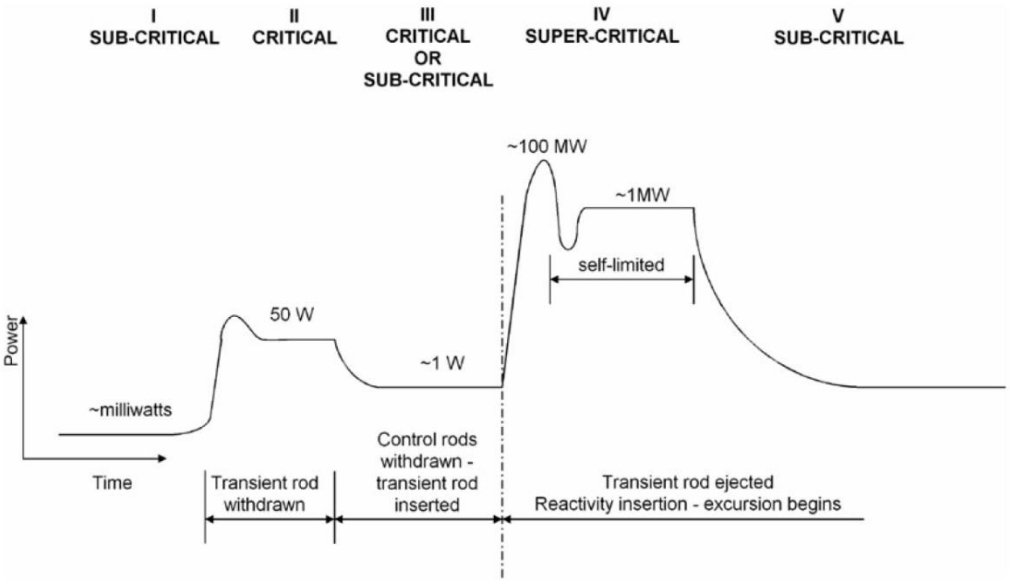

Fig. 2. SPERT IV Reactivity insertion transient sequence [9].

Parameter	Value
Average coolant temperature feedback at 20°C	-0.7 ¢/°C
Average coolant temperature feedback at 35°C	-1.2 ¢/°C
Average density/void feedback coefficient	-41.5 ¢/% decrease in moderator density
Doppler feedback coefficient	N/A[a]
Reduced prompt neutron lifetime $\Lambda/\beta_{\text{eff}}$	8.1×10^{-3} s

[a] Not applicable since HEU fuel contains minimal amount of ^{238}U

Table 1. Model Input Parameter Summary

4. Results

The result section is twofold, i.e., static and transient calculations. The static comparison deals with Serpent calculation and the available static results from the SPERT-IV reactor [18]. The transient section present the results for a constant reactivity insertion at different coolant velocities.

4.1. Static comparison

The thermal flux distribution has been measured in SPERT IV by means of cobalt wires located at the core positions shown in Fig. 3. In order to validate the Serpent results, the measured and calculated thermal fluxes were compared in several core positions, where the energy cutoff for thermal flux was set to 0.5 eV [5]. The selected positions for comparison were D4, D5, E4, E5, F5 and G7. The results are shown in Fig. 4. The results show good agreement between the calculated and the measured fluxes. The main difference is in the reflector region. However, since this region is of little importance for the transient analysis, this difference was neglected.

The calculated values of the reduced prompt neutron life ($\Lambda/\beta_{\text{eff}}$) are summarized in Table 2. The comparison between Serpent and TRIPOLI4 are very good. However, there is a slight deviation from the experimental data. This in turn could affect the transient calculations.

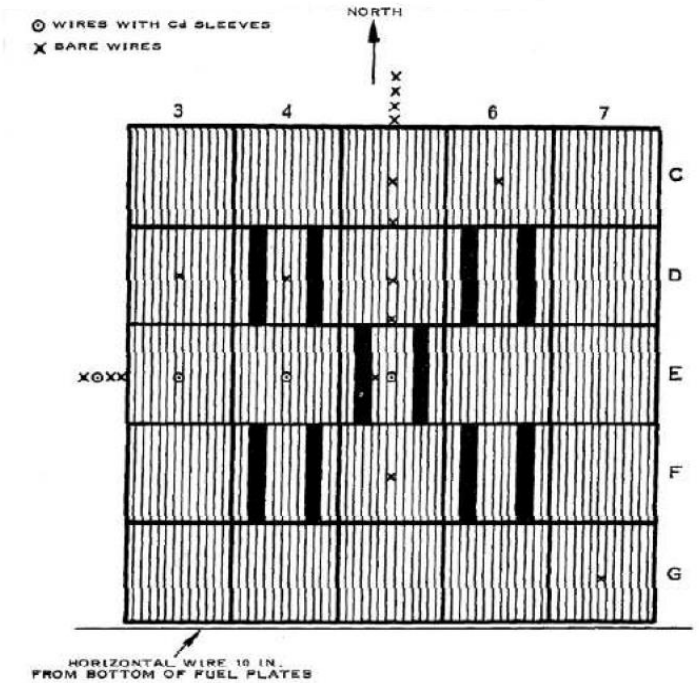

Fig.3. Radial positions of the cobalt wires for thermal flux measures [5]

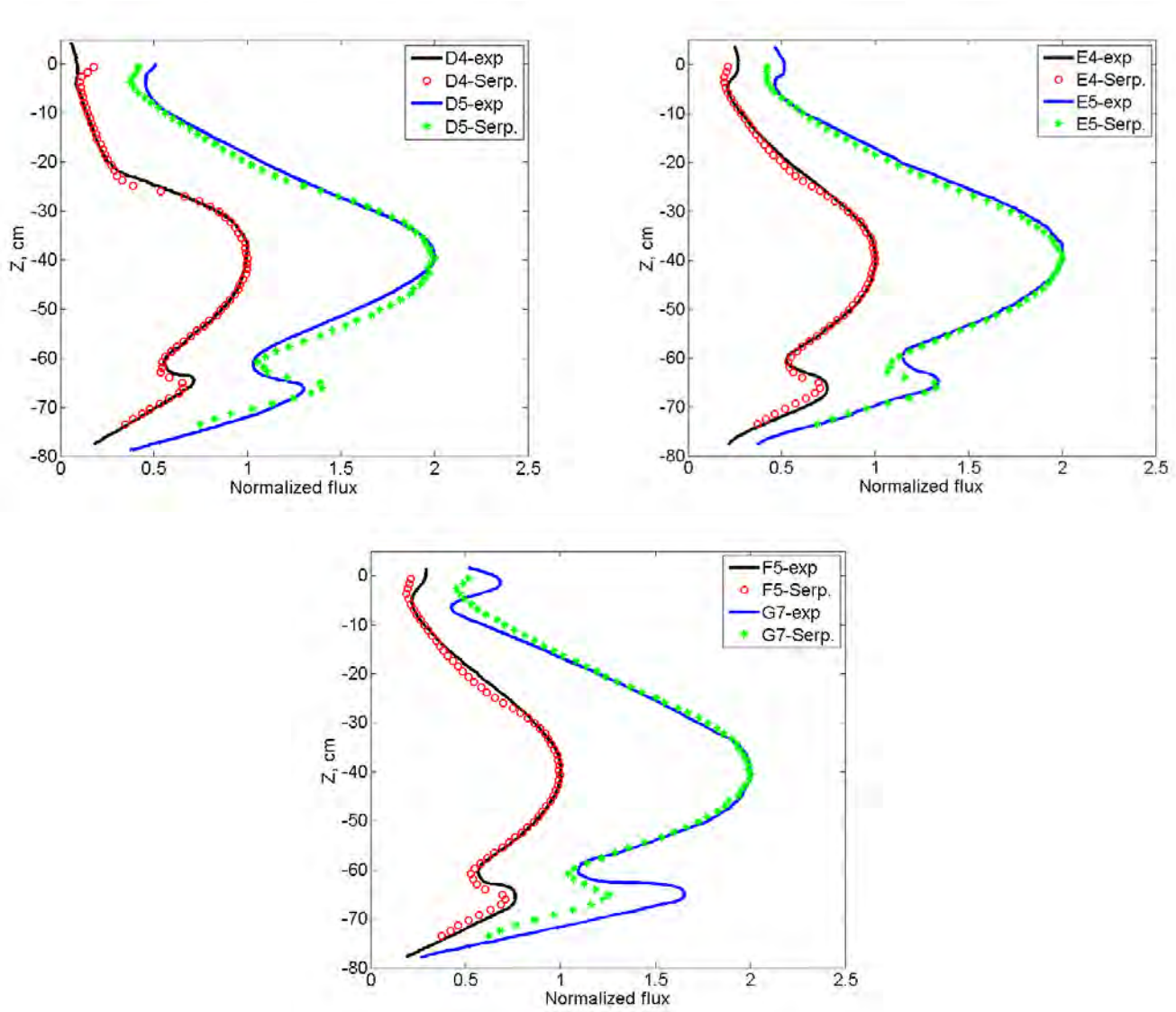

Fig. 4. Comparison of several thermal flux detectors, experiment vs. Serpent.

	β_{eff}	Prompt neutron life time [s]	$\Lambda/\beta_{\text{eff}}$
Serpent	(748±2) pcm	(6.25±0.01)×10^{-5}	8.36×10^{-3}
TRIPOLI4*	(768±9) pcm	(6.40±0.02)×10^{-5}	8.30×10^{-3}
Experiment	N/A	N/A	7.94×10^{-3}

* Source CPR 1496

Table 2. Kinetic parameters

4.2. Reactivity insertion results

The results of reactivity insertion of 1.14$ for different mass flow rates are summarized in Fig. 5 and 6 for peak cladding temperature at the point of interest and the peak power in the core as function of mass flow rate. Figure 7 shows the temperature and power change as a function of time for volumetric flow of 500 *gpm*. The additional point in Fig. 5, denoted as "unclear point", is found in table B-I in the original benchmark [5] for that experiment but with lacking information.

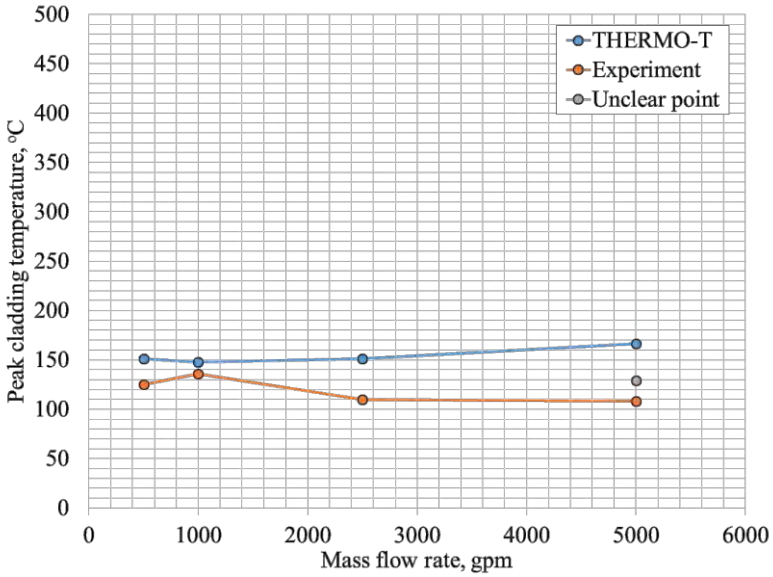

Figure 5 – Peak cladding temperature as function of mass flow rate

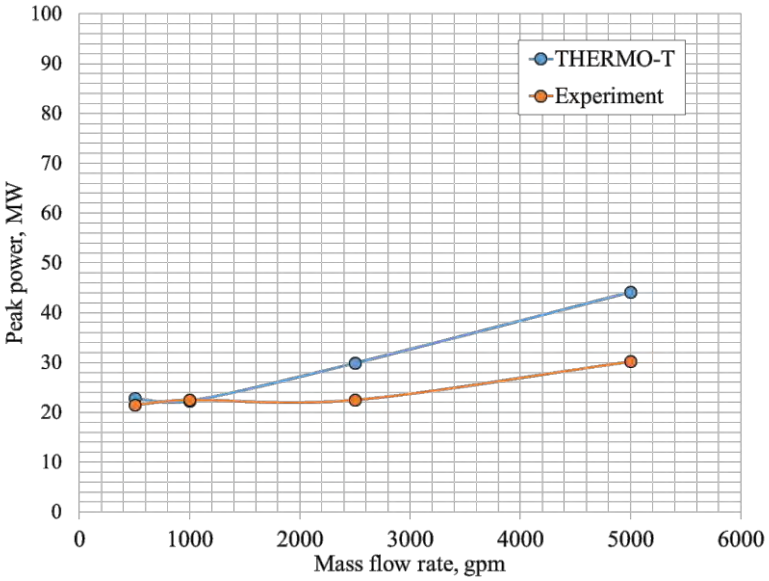

Figure 6 – Peak power as function of mass flow rate

The results obtained by THERMO-T are consistently higher in comparison to the experimental results. This is true not only for peak values, as shown in Fig. 7, where the time dependence of these parameters is shown. This over-estimation of both cladding temperature and power level is self-consistent since the higher cladding temperature results from the higher power level. The over-estimation of power and temperature is probably due to three-dimensional coupled neutronics and thermal-hydraulic effects, which need to be further examined. Furthermore, additional examination of the boiling prediction model is required as well as the utilization of appropriate correlations for highly voided core conditions.

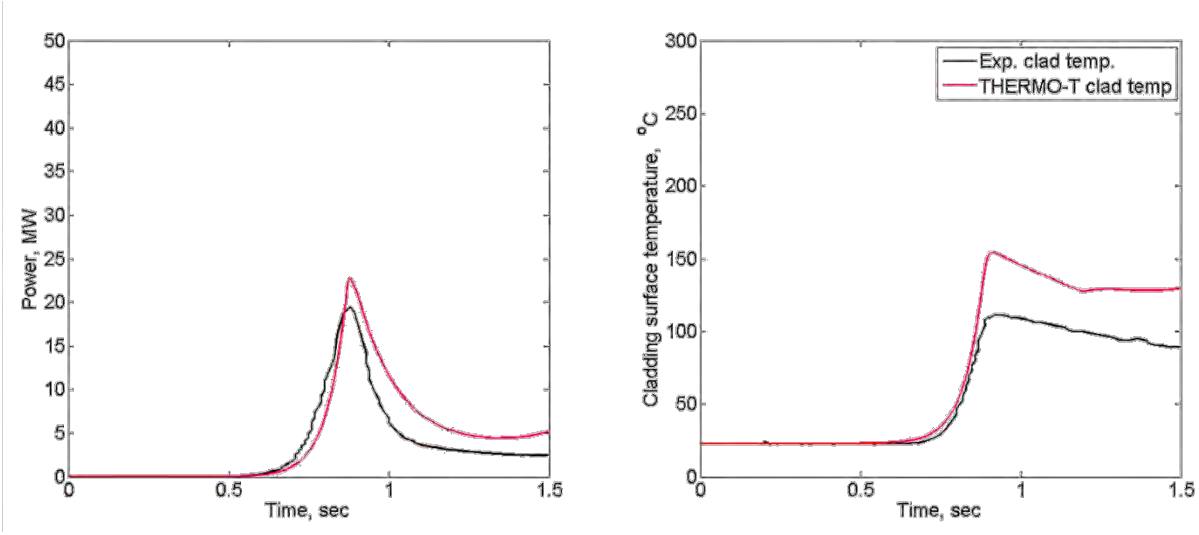

Figure 7 – Power and cladding temperature as a function of time for 500 gpm

5. Conclusions

This work presents the first evaluation of the system code THERMO-T versus experimental data available from SPERT-IV D-12/25 core. The paper presents an initial evaluation of the static behavior of the SPERT-IV experiment using Serpent, as well as transient behavior of the experiment calculated by THERMO-T.
The results obtained from THERMO-T are consistent with previous modeling of this reactor with well-established tools as RELAP5 and PARET [9,19], which are consistently over estimating the power and cladding temperature.
Future work includes a revisit of the two phase flow model in THERMO-T, which is expected to significantly improve the code performances, as well as studying three-dimensional effects due to the large differences in the reactivity coefficients.

6. References

[1] F. D'AURIA and A. BOUSBIA-SALAH, "Accident analysis in research reactors," in "15th Pacific basin nuclear conference, Sydney, Australia, Oct 15-20 2006," (2006), pp. 88–93.
[2] T. HAMIDOUCHE, A. BOUSBIA-SALAH, E. K. SI-AHMED, and F. D'AURIA, "Overview of accident analysis in nuclear research reactors", Progress in Nuclear Energy, 50, 1, 7–14 (2008).
[3] M. ADORNI, A. BOUSBIA-SALAH, F. D'AURIA, and T. HAMIDOUCHE, "Application of Best Estimate thermalhydraulic codes for the safety analysis of research reactors," in "International Conference on Nuclear Energy for New Europe 2006, Portoroz, Slovenia, Sep 18-21, 2006," (2006).
[4] M. ADORNI, A. BOUSBIA-SALAH, F. D'AURIA and T. HAMIDOUCHE, "Accident analysis in research reactors," in "International Conference on Nuclear Energy for New Europe 2007, Portoroz, Slovenia, Sep 10-13 2007", (2007).
[5] J. G. CROCKER and L. A. STEPHAN, "Reactor power excursion test in the SPERT IV facility", IDO-17000, Phillips Petroleum Company, (1964).
[6] M. MARGULIS and E. GILAD, "Analysis of protected RIA and LOFA in plate type research reactor using coupled neutronics thermal-hydraulics system code, in "The 16th International Topical Meeting on Nuclear Reactor Thermal-Hydraulics (NURETH-16). Chicago, Illinois Aug. 30 – Sep. 4, 2015", (2015).
[7] IAEA, "Research reactor core conversion guidebook", TECDOC 643, IAEA (1992).
[8] J. LEPPANEN, "Development of a new Monte Carlo reactor physics code, Ph.D thesis, Helsinki University of Technology, (2007).

[9] S. CHATZIDAKIS, A. IKONOMOPOLUS and S.E. DAY, “PARET-ANL modeling of a SPERT-IV experiment under different departure from nucleate boiling correlation”, Nuclear Technology, 177, 119-131 (2012).
[10] L.S. TONG, H.B. CURRIN and A.G. THORP, “New correlation predict DNB conditions”, Nucleonics, 21, 5 (1963).
[11] N.E. TODREAS and M.S. KAZIMI, “Nuclear Systems Volume I: Thermal Hydraulic Fundamentals”, CRC Press (1989).
[12] R. E. HEFFNER, E. L. MORRIS, D. T. JONES, D. R. SEAMAN, and M. K. SHANE, “SPERT IV Facility,” U.S. AEC Technical Report IDO-16745, Phillips Petroleum Co. (1962)
[13] F. SCHROEDER, “Quarterly Technical Report, SPERT Project: July, August, September, 1962”, U.S. AEC Technical Report IDO-16829, Phillips Petroleum Co. (1963).
[14] J. R. HUFFMAN, W. E. NYER, and F. SCHROEDER, “Quarterly Technical Report, SPERT Project: January, February, March, 1963”, U.S. AEC Technical Report IDO-16893, Phillips Petroleum Co. (1963).
[15] J.G. CROCKER, J.E. KOCH, Z.R. MARTINSON, A.M. McGLINSKY and L.A. STEPHAN, “Nuclear Start-Up of the SPERT IV Reactor”, U.S. AEC Technical Report IDO-16905, Phillips Petroleum Co. (1963).
[16] S. E. DAY, “SPERT-IV Reactor Specification”, IAEA Coordinated Research Project 1496: Innovative Methods in Research Reactor Analysis (2009).
[17] S. E. DAY, “SPERT-IV Benchmark Specification”, IAEA Coordinated Research Project 1496: Innovative Methods in Research Reactor Analysis (2009).
[18] S. E. DAY, “The Use of Experimental Data in an MTR Type Nuclear Reactor Safety Analysis”, PhD Thesis, McMaster University, Hamilton, Ontario, Canada (2006).
[19] W. L. WOODRUFF. N. A. HANAN and J. E. MATES, “A Comparison of the RELAP5/MOD3 and PARET/ANL Codes with the Experimental Transient Data from the SPERT-IV D-12/25 Series”, International Meeting on Reduced Enrichment for Research and Test Reactors, Jackson, Wyoming, USA (1997).

DETECTION OF BOILING OCCURRENCE BY SENSING PRESSURE WAVE OF COLLAPSING BUBBLES IN SUBCOOLED WATER

DAESEONG JO, HONGRAE JO

School of Mechanical Engineering, Kyungpook National University,

80 Daehak-ro, Buk-gu, Daegu 702-701, Republic of Korea

ABSTRACT

In thermal hydraulic point of view, boiling occurrence on fuel in a core is the starting point for all possible normal and abnormal events: during normal operation, operational range of a research reactor is limited to the Onset of Nucleate Boiling (ONB). In accidents, the Critical Heat Flux (CHF) should be avoided to maintain the fuel integrity. Because of the reasons, detection of boiling occurrence is important for reactor operation and safety. Since most of research reactors are submerged under the water, boiling occurred in the core is difficult to detect because it condenses in subcooled pool water. In the present study, boiling occurrence is detected by sensing pressure wave of collapsing bubbles while it condenses in subcooled water. To detect pressure wave of collapsing bubble, a hydrophone is used. The condensing phenomena is also investigated with wide range of subcooled temperature difference and various sizes of bubbles.

1 Introduction

For reactor safety, the fuel integrity should be maintained under accident events. In thermal hydraulic point of view, boiling occurrence on fuel in a core is the starting point for all possible normal and abnormal events: during normal operation, operational range of a research reactor is limited to the Onset of Nucleate Boiling (ONB). In accidents, the Critical Heat Flux (CHF) should be avoided to maintain the fuel integrity. Because of the reasons, detection of boiling occurrence is important for reactor operation and safety. Since most of research reactors are submerged under the water, boiling occurred in the core is difficult to detect by convectional measurement tools such as conductivity probe, optic fiber, or thermocouples because it condenses in subcooled pool water. The convectional measurement tools should have direct contact to vapor bubbles, and they should be installed

on the top of the fuel for an accurate reading. It may cause unfavorable accidents such as partial or complete channel blockage accident. Previous studies done by Ajbar et al. (2009), Osterman et al. (2009), Tinguely (2013), and Tang et al. (2015) showed that the collapsing bubbles during condensation and cavitation generate acoustic oscillation or pressure waves. Therefore, in the present study, boiling occurrence is indirectly detected far away from the fuel by sensing pressure wave of collapsing bubbles while it condenses in subcooled water. To detect pressure wave of collapsing bubble, a miniature hydrophone is used. The condensing phenomena is also investigated with wide range of subcooled temperature difference and various sizes of bubbles.

2 Experimental setup

To detect and sense the pressure wave of collapsing bubbles while it condenses in subcooled water, the test facility consists of steam generator, needle injectors, water reservoir, syringe pump, pre-heater, needle valves, and measurement tools (hydrophone, thermocouple, pressure transducer, and high-speed camera) as shown in Figure 1. Steam as the condensable gas is generated by the steam generator, and ejected through various sizes of injectors (ASME standard tubes with outer diameter and tube thickness of 1/16" x 0.015", 1/8" x 0.028", and 1/4" x 0.035"). While it ejects, departs, and condenses in subcooled water, its dynamic behaviors are recorded by a high-speed camera and hydrophone. Air as the non-condensable gas is supplied by the syringe pump (10 ~ 100 ml/h) with a syringe of 50 ml. Images by the high-speed camera are recorded at the rate of 4,000 ~ 20,000 FPS. To clearly observe the dynamic behaviors of the bubbles departing from the injectors, the water reservoir is designed as a rectangular channel, 0.59 inches thick and 11.81 inches wide, 59.06 inches long. To study the effect of the subcooled temperature, the demineralized water in the water reservoir is heated up by the pre-heater. The signal taken by the hydrophone is simultaneously recorded with the images taken by the high-speed camera in order to detect the pressure wave of the collapse bubble when it completely condenses.

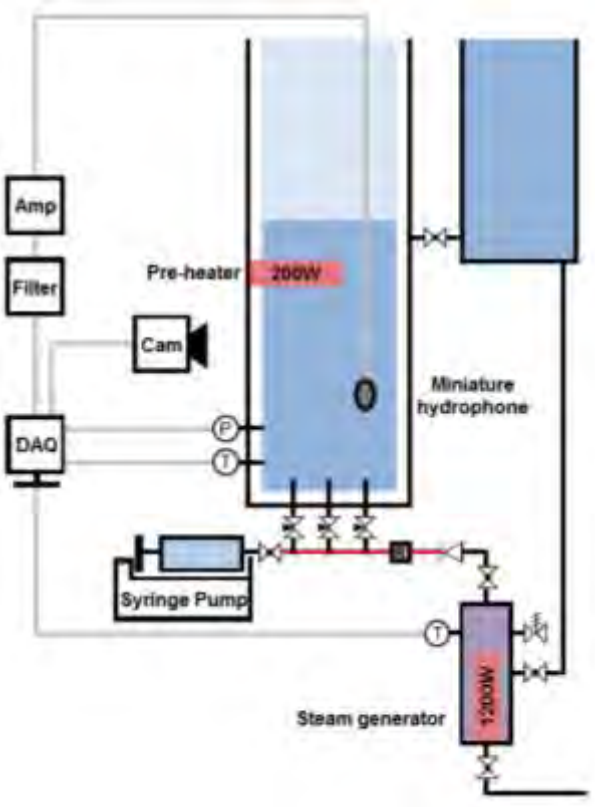

Fig 1. Schematic drawing of test facility

3 Results

During the experiments, bubble images are recorded by a high-speed camera, and the acoustic signals are measured by a hydrophone. Figure 2 shows the dynamic behaviors of the non-condensable gas with various sizes of injectors. As seen, there are oscillations of the bubble shape after it depart from the injector. The oscillation seems more significant if the departure bubble size is larger. With the injector size of 1/4 inches, the tail of the departure bubble penetrates into the departure bubble right after break. During the oscillation, the tiny bubble horns and tails are observed at the top and bottom of the departure bubble periodically. With the injector size of 1/16 inches, the oscillation becomes weak, and the shape approaches spherical. Figure 3 shows the dynamic behaviors of the condensable gas with various subcooled temperatures. With the subcooled temperature of 1 ^{o}C, there is oscillation, which is seen from non-condensable gas. Based on the complete condensing time, the condensing rate is lower with lower subcooled temperature, which means steam vapor exposed to lower subcooled water takes longer to condense completely: (1) with the subcooled temperature of 1 ^{o}C, it takes 77 ms, (2) with the subcooled temperature of 12 ^{o}C, it takes 62 ms, and (3) with the subcooled water temperature of 31 ^{o}C,

it takes 39 ms.

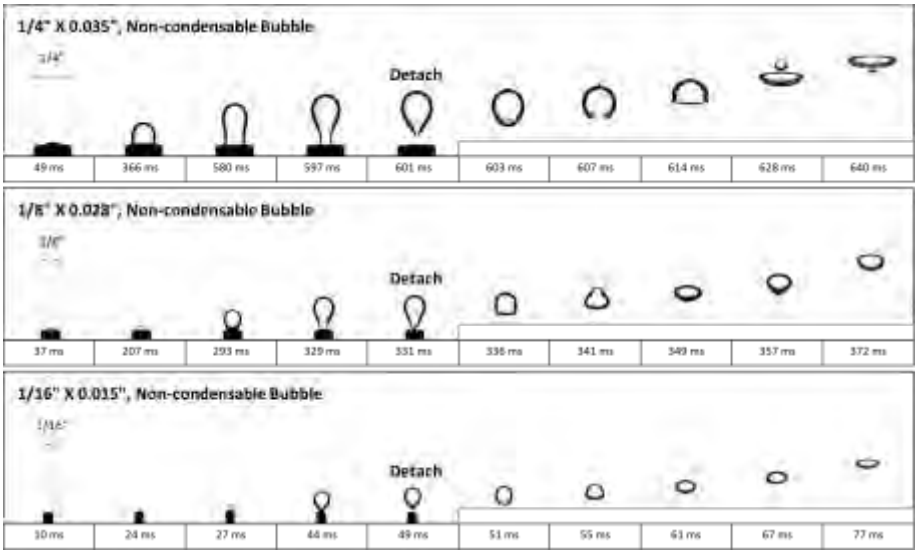

Fig 2. Non-condensable gas departure behaviors with various sizes of injectors

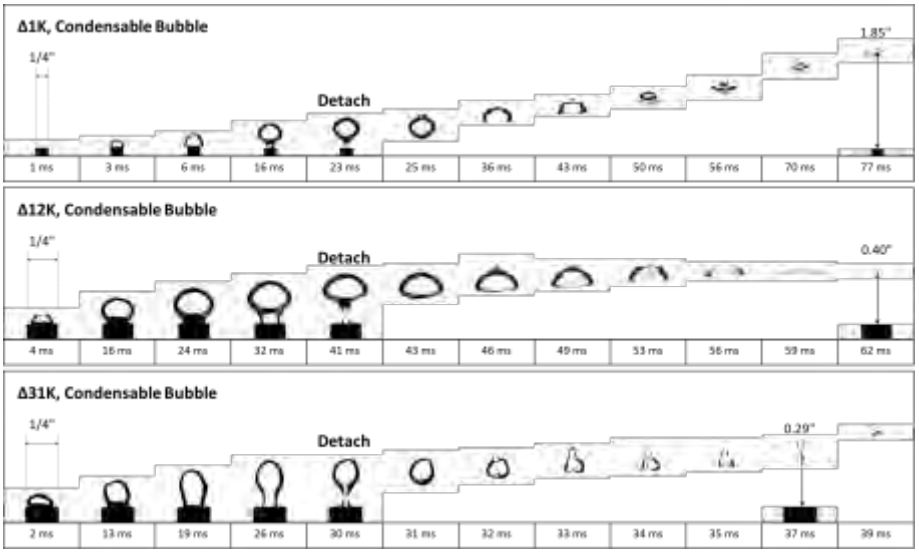

Fig 3. Condensable gas departure behaviors with various subcooled temperatures

Figure 4 shows the signal taken by the hydrophone when the steam vapor completely condenses. From the original signal, the peak value is not significantly higher than the background value, but it is distinguishable. The signal can further analyzed using Daubechies Discrete Wavelet Transform (DWT), and the results are shown in Figure 5. DWT analysis allows us to see the original signal separately into several frequency ranges specified as shown in Figure 5. As seen, frequency ranges from 1,600 to 12,800 Hz have better resolutions of the wavelet while the steam vapor condenses in subcooled water. As a

result of the present study, boiling occurrence in the reactor core can be detected far away using a hydrophone.

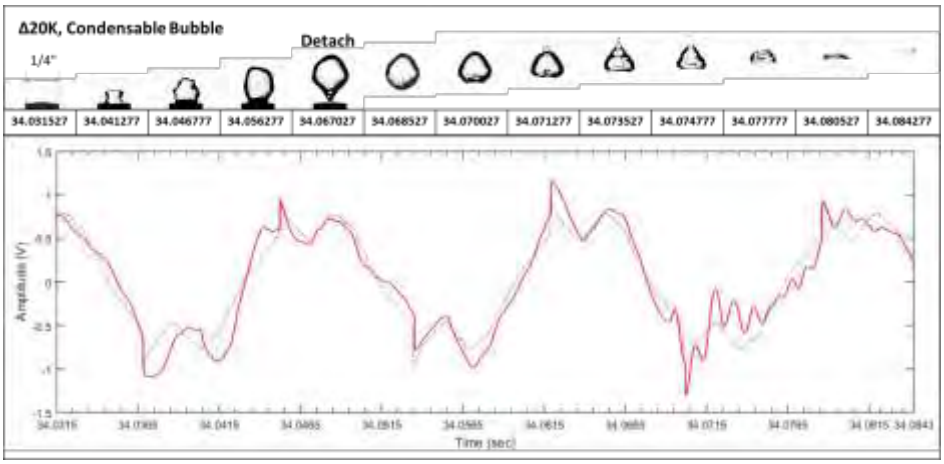

Fig 4. Hydrophone signal of collapsing bubble

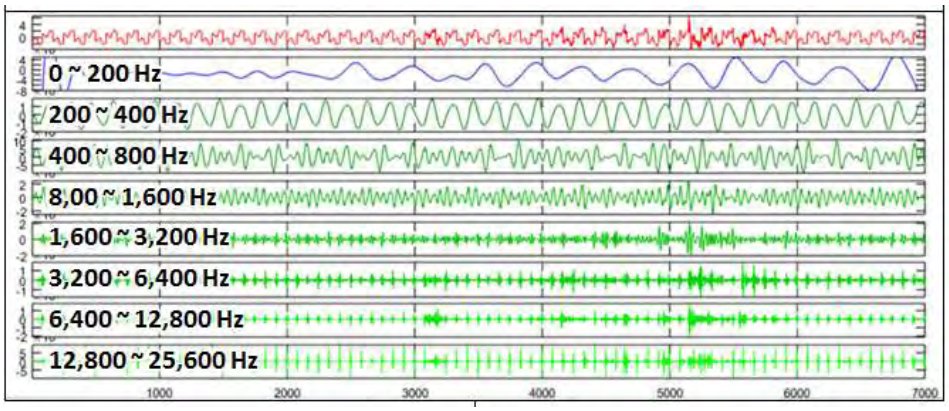

Fig 5. Discrete Wavelet Transform analysis results

4 Discussions

In the present study, boiling occurrence, which may occur in a reactor core, is detected by sensing the pressure wave of the collapsing steam vapor with a hydrophone. A reactor core submerged in a reactor pool is simulated as a steam generator with a rectangular water reservoir. To investigate the dynamic behaviors of non-condensable and condensable gases, a high-speed camera is used to capture the images at the rate of 4,000 ~ 20,000 FPS. Oscillation over the departure bubble is observed when the bubble size is larger, and the condensing rate is qualitatively determined. When the condensable bubble departing from the injector condenses completely, it generates the pressure wave. This pressure wave is detected by a miniature hydrophone, and the signal is analyzed with Discrete Wavelet

Transform (DWT) method. DWT analysis gives a better resolution of the pressure wave. As a result of the present study, boiling occurrence can be detected using a hydrophone. It could provide advantages during commissioning tests and thermal hydraulic experiments. To be more precisely, we plan to carry out the following items:

- Analyze the intensity of the pressure wave with various subcooled temperatures and vapor sizes
- Investigate the dynamic behaviors of non-condensable and condensable gases using image processing technique
- Capture the pressure wave of the collapsing vapor using a Schlieren photography

5 References

[1] Ajbar, A., Al-Masry, W., Ali, E., 2009. Prediction of flow regime transitions in bubble columns using passive acoustic measurements. Chemical Engineering and Processing: Process Intensification 45, 101-110.

[2] Osterman, A., Hocevar, M., Sirok, B., Dular, M., 2009. Characterization of incipient cavitation in axial valve by hydrophone and visualization. Experimental Thermal and Fluid Science 33, 620-629.

[3] Tinguely, M., 2013, The effect of pressure gradient on the collapse of cavitation bubbles in normal and reduced gravity. Ph.D thesis, Lausanne.

[4] Tang, J., Yan, C., Sun, L., 2015. Feature of acoustic sound signals involved in vapor bubble condensation and its application in identification of condensation regimes. Chemical Engineering Science 137, 384-397.

A REVIEW OF THE DESIGN FEATURES OF RESEARCH REACTOR AIR VENTILATION AND CLEANING SYSTEM

MINJIN KIM, CHUNG SUNG LEE
HANARO Operation Department, Korea Atomic Energy Research Institute
989-11 Daedeok-daero, Yuseong-gu, Daejeon, 34057, Korea

ABSTRACT

The Korea Atomic Energy Institute (KAERI) exported a research reactor, the JRTR (Jordan Research and Training Reactor), to Jordan, which is in the stage of commissioning. In addition, KAERI is operating HANARO, a research reactor and going to build a new research reactor, KJRR (KiJang Research Reactor) in Korea. In this paper, the design features of the reactor building air ventilation and cleaning system (hereafter air ventilation system) of HANARO, JRTR and KJRR are reviewed and discussed. The reactor building air ventilation system of HANARO was designed in the late 1980s and constructed according to the effective code and standards at that time. In HANARO, there is a normal ventilation system which is designed to clean the air of the reactor building during normal operation. To clean the air inside the reactor concrete island (RCI), the RCI normal ventilation system is provided. When the high radiation in the reactor hall is detected, the RCI emergency ventilation system comes into operation as an engineered safety feature. The safety grade isolation dampers will be closed if the reactor building is deemed to require complete isolation and further decay. In the JRTR, the air ventilation system is composed of the normal air ventilation of the reactor building and the normal air ventilation of the RCI. During normal operation of the reactor, normal air ventilation of the RCI is continuously running to clean and exhaust the air from the RCI to the atmosphere through the filter unit and the stack into the environment. When the high radiation in the reactor hall is detected, the reactor building air ventilation is stopped and the RCI air ventilation system is put into recirculation mode while the safety grade isolation dampers mounted on the inlet and outlet duct of the reactor building are closed. When the isolated air in the reactor building is decayed, a small air cleaning system equipped with an activated carbon filter will be running to discharge the decayed air through the stack into the atmosphere. The KJRR is a new research reactor that will produce Fission Molybdenum and NTD (Neutron Transmutation Doping) Silicon. It is now in the completion stage of its design and the construction permit to the regulatory body has been submitted. We adopted the advantages of the design features of the HANARO and JRTR air ventilation system to improve the safety. The details will be discussed in this paper.

1 Introduction

The importance of the reactor building air ventilation system cannot be emphasized enough no matter how hard we try. It maintains not only adequate environmental condition such as temperature, humidity and cleanliness for human comfort, prevention of overheating of the equipment and control panel, but also negative pressure to prevent the release of contaminated air into the atmosphere. The design of the reactor building air ventilation system varies according to the characteristics of the reactor design, utilization, siting, population, etc. Usually, a power reactor calls for an emergency ventilation system as an engineered safety feature; however, a research reactor does not. By applying the graded approach, some confinement isolation dampers (hereafter CIDs) and non-safety grade emergency ventilation system were implemented instead.

2. Overview of HANARO Design Characteristics

HANARO is an Open Tank-in Pool type reactor, and its coolant is light water. It is cooled by forced cooling using two primary cooling pumps. The reactor building is a confinement type and consists of a steel frame and reinforced concrete. It has 7 horizontal beam ports and 36 vertical holes. Other major reactor characteristics are shown below.

Item	Design Features
Type	Open Tank-in-Pool
Thermal Power	30 MW
Max Thermal Flux	$4.5 \times 10^{-14} \mathrm{n/cm^2 s}$
Fuel	LEU(19.75 w/o ^{235} U) U_3Si-Al Meat, Al Clad
Coolant/Moderator/Reflector	H_2O/[H_2O, D_2O]/D_2O
Absorber	Hafnium

Tab 1: Reactor Characteristics of HANARO

2.1 System Description of Reactor Building Air Ventilation System

The reactor hall maintains negative pressure compared to the atmosphere. Air flow is made from the less contaminated area to the higher contaminated area using a once-through system. The reactor building air ventilation system maintains adequate temperature, humidity and cleanliness for human comfort and prevents overheating of the equipment and control panels. Under radiation emergency, the CIDs are closed to isolate the confinement from the environment. The CIDs (one for inlet and the other for outlet of reactor building) are designed as Non-Safety grade, Seismic category I. The air ventilation system of the reactor building is designed as Non-Safety grade and Non-Seismic category. Temperature and humidity are maintained as 20-27°C, 50±10% RH. The air change rate of the reactor building is once per hour.

2.2 Confinement of HANARO

The concept of confinement is applied in HANARO as an engineered safety feature because it is operating at low temperature and low pressure even in the design basis accident. The confinement is to protect the equipment and systems of the reactor building from external events. The confinement comprises the reactor building together with CIDs that will fail open upon a loss of control signal or power. The CIDs are open when the emergency ventilation system is activated by a high radiation signal from one of the pool surface radiation detectors, reactor ventilation exhaust duct radiation detectors, and failed fuel detectors. The allowable leakage rate of the confinement of HANARO is 600 m^3/hr at 25 mmWg of DP, and is defined to limit the radiation doze within the acceptable limit in the EAB (Exclusion Area Boundary) and LPZ (Low Population Zone) for all design basis accidents.

2.3 Code and Standards for ESF Cleanup System

In Korea, according to the Presidential Decree [1] of the National Nuclear Safety Act, Article 4.3.6 prescribes that the Preliminary Safety Analysis Report of the Power Reactor as well as Research Reactor should address the Engineered Safety Features including containment. In addition, the Safety Review Guidelines for Light Water Reactors [2] issued by the Korea Institute of Nuclear Safety prescribes the ESF cleanup system, but the one for a research reactor does not. In U.S., the General Design Criteria 41, 42, and 43 in Appendix A to 10CFR Part 50 [3] require that containment atmosphere cleanup systems be provided as necessary to reduce the amount of radioactive material released into the environment following a postulated DBA.

A graded approach was applied in the ESF cleanup system for a research reactor with the consideration of the above guidelines and criteria.

2.4 System Description of Emergency Ventilation System (RCI Abnormal Air Ventilation System)

The internal pressure of the confinement building is maintained as 25 mmWg below atmospheric pressure. When the high radiation is detected by one of the three radiation detectors mentioned above, one (1) of two (2) 100% exhaust fans is actuated. The air inside the confinement is then filtered and exhausted through the filter bank equipped with a HEPA filter, an adsorber system using the impregnated activated carbon and an air heater that are designed, constructed, and tested in accordance with ASME AG-1. Redundancy is provided to the exhaust fan and its actuation signal of the emergency ventilation system. When the radiation detected at the stack exceeds the predetermined value, the emergency ventilation system can be manually stopped by the operator's judgment, and the air inside the reactor building is isolated by the CIDs. In this stage, leakage from the confinement building to the atmosphere begins within the predefined allowable leakage rate. Electric power of the emergency ventilation system is backed up by the emergency diesel generator.

2.5 Operation of Reactor & RCI Air Ventilation system

In normal operation mode, both the reactor ventilation system and RCI normal ventilation system are in operation. In the case of radiation emergency, the reactor ventilation system and RCI normal ventilation system will stop, and the abnormal RCI ventilation (emergency ventilation) system then comes into operation to filter the contaminated air by the adsorber system and to exhaust them through the stack into atmosphere. When the stack radiation monitor detects the high radiation exceeding the established dose limit, RCI abnormal ventilation system stops and CIDs are closed to isolate the contaminated air inside the confinement.

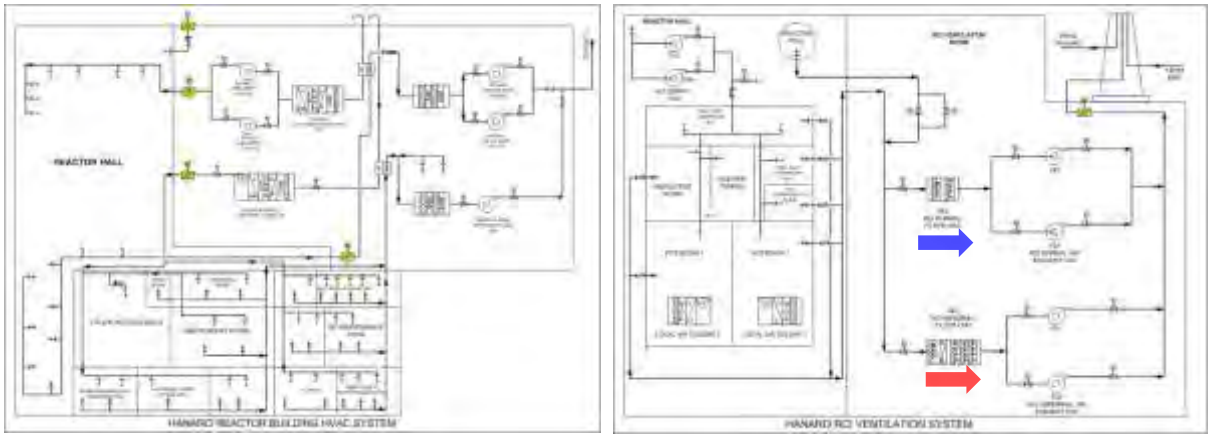

Fig 1. HANARO Reactor Ventilation & RCI Ventilation System

3. Overview of JRTR Design Characteristics

JRTR is an Open Tank-in Pool type reactor and its coolant is light water. It is cooled by forced cooling using two primary cooling pumps. The reactor building is a confinement type and consists of a steel frame and reinforced concrete. It has four beam tubes and 35 irradiation facilities. Other major reactor characteristics are shown below.

Item	Design Features
Type	Open Tank-in-Pool
Thermal Power	5 MW

Max Thermal Flux	$1.45 \times 10^{-14} \mathrm{n/cm^2 s}$
Fuel	Plate Type, LEU(19.75 w/o ^{235} U) U_3Si_2-Al
Coolant/Reflector	H_2O/D_2O,Be
Absorber	Hafnium

Tab 3: Reactor Characteristics of JRTR

3.1 System Description of JRTR Reactor Building HVAC System

The JRTR Reactor Building HVAC System is quite similar to that of HANARO. It requires a negative pressure control system that enables the contaminated air to flow from the less contaminated area to a higher contaminated area using a once-through system. It does not allow a recirculation of air. The HVAC system of the reactor building maintains adequate temperature, humidity and cleanliness for human comfort and prevents an overheating of the equipment and control panels. The HVAC system of the reactor building is designed as non-safety grade and non-seismic category.

3.2 System Description of JRTR RCI Ventilation System

The RCI ventilation system maintains a negative pressure that enables the air to flow from the reactor hall to the RCI area. The filter train consists of a medium filter, electric heater, HEPA filter, carbon adsorber and shut-off damper. The RCI ventilation system is a once-through system in normal operation mode.

3.3 System Description of Air Discharge System

The Air Discharge System (ADS) will be operated manually for controlled and monitored release of the reactor building air into the environment, while the CIDs are closed in the event of radiation emergency. It was designed to minimize the public dose with respect to the ALARA when a DBA such as a flow channel blockage accident occurs, to improve the accident management by providing a path for the gaseous release, and to depressurize the reactor building atmosphere when the reactor building HVAC system is not available for a long period of time. The ADS consists of two (2) manually operated confinement isolation valves (CIVs), one (1) electric duct heater, one (1) filter train, one (1) exhaust fan, and one (1) set of stack radiation monitor. Two (2) CIVs are classified as Safety Class III, and Seismic Category I and installed inside and outside of the reactor confinement wall with the consideration of a single failure criterion. The filter train consists of a moderate filter, HEPA filter, and carbon adsorber. Except for CIVs, the remaining equipment is designed as Non-nuclear safety and Seismic Category II.

3.4 The Confinement of JRTR

The confinement comprises the reactor building, CIDs, and CIVs of ADS. The confinement of the JRTR was designed to protect the equipment and systems from external events and is a part of Engineered Safety Feature. The reactor building, CIDs, and CIVs were designed as Safety Class III and Seismic Category I and shall fail close upon loss of the control signal or power. Three (3) sets of CIDs are installed in the duct penetrating reactor wall to isolate the confinement from the environment during a design basis accident and will be closed automatically upon a high radiation signal from the Reactor Protection System. They are manually operable by an operator.

3.5 Operation of Reactor/RCI Ventilation and ADS system

All of the CIDs are open during normal operation and fail close upon a loss of power or actuation signal. The CIDs for RCI ventilation system are installed on a RCI exhaust duct line

to the stack and open to allow filtrated exhaust air flow to stack during normal operation. When the high radiation is detected at the stack monitor, CIDs for RCI ventilation can be closed manually to allow the recirculation mode of RCI ventilation. The CIDs are installed in a reactor hall exhaust duct line to the stack, and the remaining CIDs are installed in a supply air duct line to the reactor hall. These CIDs are open while the reactor building ventilation system is running. When the high radiation is detected on the stack monitor, these CIDs are closed manually and the reactor building ventilation system is stopped. The CIVs are installed in the reactor hall exhaust duct line to the ADS. The CIVs are kept closed during normal operation and manually opened when the operation of ADS is deemed necessary.

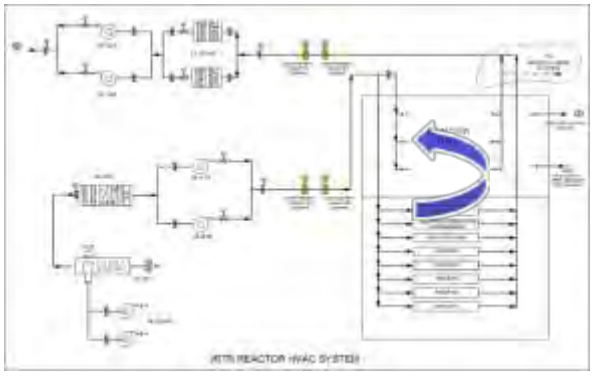

Fig 2. JRTR Reactor HVAC System

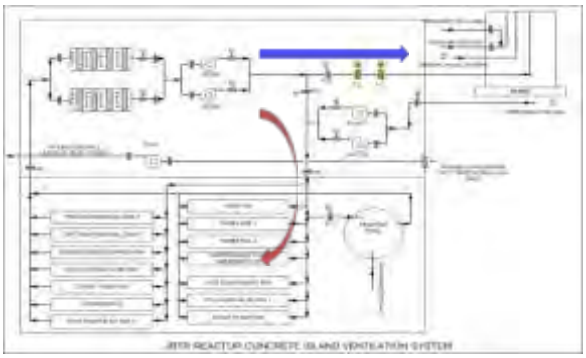

Fig 3. JRTR RCI Ventilation System

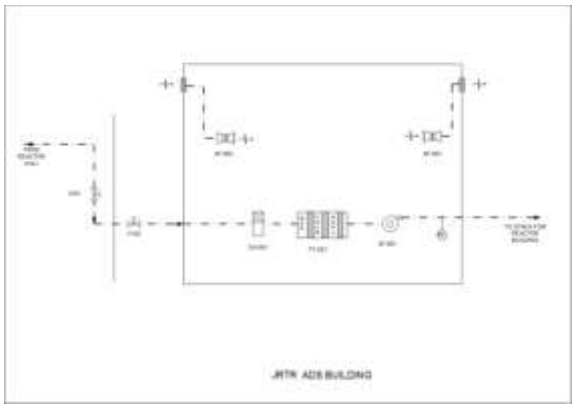

Fig 4. JRTR ADS System

4. Overview of KJRR Design Characteristics

KJRR is an Open Tank-in Pool type reactor and its coolant is light water. It is cooled by forced cooling using three (3) 50% capacity primary cooling pumps. Two pumps are in operation and one is in standby. The reactor building is a confinement type and consists of a steel frame and reinforced concrete. It has forty (40) irradiation facilities. Other major reactor characteristics are shown below.

Item	Design Features
Type	Open Tank-in-Pool
Thermal Power	15 MW
Max Thermal Flux	$3.2 \times 10^{-14} \mathrm{n/cm^2 s}$
Fuel	Plate Type, LEU(19.75 w/o ^{235} U), U-Mo
Coolant/Reflector	H_2O/Be
Absorber	Hafnium

Tab 3: Reactor Characteristics of KJRR

4.1 System Description of KJRR Reactor Building HVAC System

The HVAC system of the KJRR reactor building maintains a negative pressure control system that enables the contaminated air to flow from the less contaminated area to higher contaminated area by a once-through system. The HVAC system of the reactor building maintains the adequate temperature, humidity, and cleanliness for human comfort and prevents an overheating of the equipment and control panels. It was designed as non-safety grade and a non-seismic category.

4.2 System Description of KJRR RCI Ventilation System

One of the two (2) 100% RCI supply fans enables the air to flow from the reactor hall into the RCI area. The RCI ventilation system is a once-through system. In normal operation mode, the air from the RCI area flows through the filter train consisting of moderate filter and HEPA filter by one of the two 100% exhaust fans. When a DBA such as a flow channel blockage accident occurs, CIDs are automatically closed by the RPS signal and all the ventilation fans are stopped. When the purification and release of the contaminated air in the reactor hall is deemed necessary, the operator can operate the Contaminated Air Purification System (CAPS) equipped with a moderate filter, HEPA filter, activated carbon filter, and moderate filter to release the air from the RCI area into the atmosphere through the stack.

4.3 System Description of Contaminate Air Purification System.

All CIDs are closed by an RPS signal when the design basis accident such as one fuel channel blockage occurs. The HVAC and RCI ventilation systems of the reactor building are also stopped. When the confinement is completely isolated, if it is deemed necessary, the operator can operate the CAPS manually by opening the CIDs on its exhaust duct and operating one of two exhaust fans. By doing this, the contaminated air in the reactor can be purified and released with the rate derived from the radiation dose within the acceptable limit in EAB and LPZ for all design basis accidents. The CAPS consists of two (2) manually operated confinement isolation dampers (CIDs) in series with the consideration of a single failure criterion, two (2) 100% filter trains, and two (2) 100% exhaust fans. Two (2) CIDs are classified as Safety Class III, and Seismic Category I and installed on the exhaust duct of the reactor confinement wall. Each filter train consists of a moderate filter, HEPA filter, and carbon adsorber. Except for CIDs, the remaining equipment is designed as Non-nuclear safety and Seismic Category II.

4.4 The confinement of KJRR

The confinement comprises the reactor building and CIDs. The confinement of the KJRR was designed to protect the equipment and systems from external events and is a part of the Engineered Safety Feature. The reactor building and CIDs were designed as Safety Class III and Seismic Category I. CIDs shall fail close upon a loss of control signal or power. Three (3) sets of CIDs (two are in series) are installed in the duct penetrating reactor wall to isolate the confinement from the environment during a design basis accident and will be closed automatically upon a high radiation signal from the Reactor Protection System. They are manually operable by an operator.

4.5 Operation of Reactor/RCI Ventilation System and CAPS

All of the CIDs are open during normal operation and will fail close upon a loss of power or actuation signal. The CIDs for the RCI ventilation system are installed on a RCI exhaust duct line to the stack and open to allow filtrated exhaust air flow to stack during normal operation. When the high radiation is detected at the stack monitor, CIDs for the Reactor ventilation system and RCI ventilation system of the reactor building are closed by the RPS signal. The

CIDs are installed in a reactor hall exhaust duct line to the stack and the remaining CIDs are installed in a supply air duct line to the reactor hall. CIDs are open while the reactor building ventilation system is running. When the high radiation is detected by the RPS, all CIDs are closed automatically and the reactor building ventilation system and RCI ventilation system are stopped. When it is deemed necessary to operate the CAPS, the operator can open the related CIDs and operate one of the two exhaust fans.

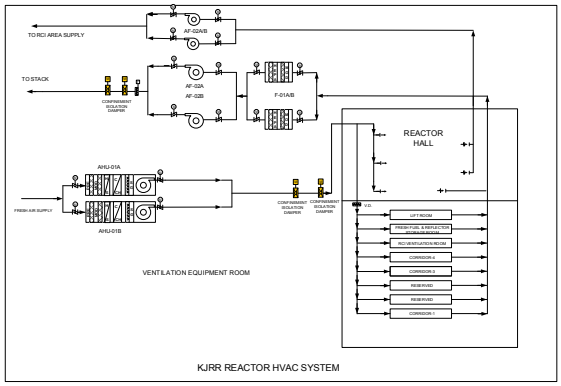

Fig 5. KJRR Reactor Building HVAC System

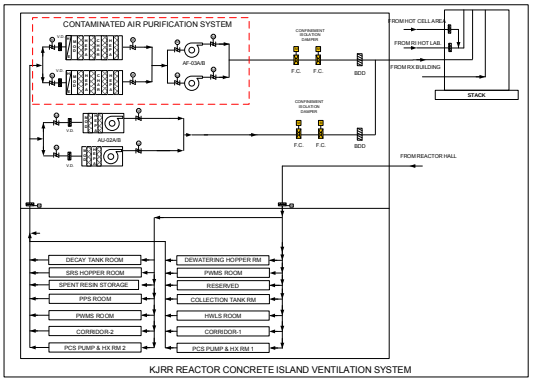

Fig 6. KJRR RCI Ventilation System

5.0 Conclusion

An ESF cleanup system is not a mandatory requirement for a research reactor as we see in the code and standards of Korea and the U.S. However, three research reactors designed by the Korea Atomic Energy Research Institute have implemented an air cleaning system in view of the ESF cleanup system with the consideration of a graded approach.

- In HANARO, confinement, CIDs, and RCI abnormal ventilation system constitute ESF.
- In JRTR, the confinement and CIDs constitute ESF. CIDs are closed and the whole ventilation system stops to isolate the confinement upon radiation emergency. RCI ventilation will be switched to recirculation mode upon radiation emergency. By the operator judgment, CIVs can be manually open and ADS can be operated to release the reactor air with the predetermined rate through filter train equipped with an activated carbon filter into the atmosphere.
- In the KJRR, confinement and CIDs constitute the ESF. CIDs are closed and the whole ventilation system stops to isolate the confinement upon radiation emergency. Based on operator judgment, CIDs in the exhaust duct of CAPS will be open to release the reactor air with the predetermined rate through the filter train equipped with activated carbon filter.

6. References

[1] Presidential Decree No. 26426 of National Safety Act 2015.7.21

[2] KINS/GE-N001 Safety Review Guidelines for Light Water Reactors Rev.3

[3] General Design Criteria 41, 42, and 43 in Appendix A, “General Design Criteria for Nuclear Power Plants,” to 10CFR Part 50, “Domestic Licensing of Production and Utilization Facilities,”

DYNAMIC ANALYSIS OF A TRIGA REACTOR

PAWEL DOMITR,
National Atomic Energy Agency (PAA)
Warsaw, Poland - E-mail: domitr@paa.gov.pl

JOHN RAMSEY
US Nuclear Regulatory Commission, Office of International Programs
Rockville, Maryland, USA - E-mail: jack.ramsey@nrc.gov

PETER KOHUT
Brookhaven National Laboratory, Nuclear Science and Technology Department
Upton, New York, USA - E-mail: kohut@bnl.gov

ABSTRACT

Nuclear energy offers long-term economic and environmental benefits providing a reliable energy source with significant environmental advantages in reducing the effect of human activities on global warming. National governments in countries operating or planning to establish nuclear facilities have instituted regulatory regimes on the use of nuclear materials and facilities to insure a high level of operational safety. Research and Test Reactors (RTRs) play a significant role as research, training, and development facilities providing scientific bases and expertise for nuclear power programs. TRIGA-type reactors play a significant role as one of the most widely used research and training reactors in the world utilized for many diverse fields of applications. TRIGA installations have a unique, pulsing capability allowing the thermal power to reach very high levels for a very short period of time. The paper presents the results of a dynamic analysis of a TRIGA reactor using the coupled PARCS/TRACE code system. A pin-wise PARCS neutronic model was developed coupled to a simplified TRACE thermal-hydraulic representation of the reactor pool. Power pulse analysis from low and operating power level and the consequent peak power and temperature behavior suggest that present Technical Specification limits on fuel temperatures for pulsing is adequate to insure the safe operation of the TRIGA reactors. The study validates presently accepted methodologies and provides further assurances that TRIGA reactors can safely be pulsed and operated as research and training reactors.

1. Introduction

Research and Test Reactors (RTRs) play a significant role as research, training, and development facilities providing scientific bases and expertise for nuclear power programs. One of the most important functions of RTRs is the training of generations of nuclear scientist and engineers ensuring the safe and reliable use of nuclear energy that offers long-term economic and environmental benefits with significant environmental advantages. TRIGA-type reactors designed/built by General Atomics, play a significant role as one of the most widely used research and training reactors in the world (66 worldwide installations) utilized for many diverse field of applications.

TRIGA reactors operate at steady-state thermal power levels as high as 14 MW and many installations have a unique, pulsing capability allowing the thermal power to reach high levels for a short period of time. Safe pulsing capability is due to the strong feedback characteristics of uranium-zirconium hydride fuel. In the 1970s some fuel elements were found damaged at a TRIGA reactor operating 1 MW with a pulsing program that had reactivity insertions up to $2.7. The analysis attributed the fuel damage to hydrogen gas migration under high pulsing temperatures and the subsequent pressure generated in the fuel matrix causing fuel porosity and swelling. The safe operation and pulsing of TRIGA reactors over many years suggest that technical specification requirements limiting fuel temperatures for both steady-state and pulsing operations are adequate. As a consequence, the appropriate prediction of maximum fuel element powers and temperatures

near the transient rod ejected during pulsing is an important part of the safety analysis demonstrating the safety of the TRIGA reactor both in normal operating conditions and during pulsing operation.

A number of neutronics and thermal-hydraulic codes are used to demonstrate that TRIGA reactors can safely be operated both in the steady-state and pulse mode of operation. Most of these codes generally incorporate conservative physical models and assumptions and/or the use of simplified neutronics models. The present work concentrated on utilizing a three-dimensional neutronic representation of the reactor core with the PARCS code (Purdue Advanced Reactor Core Simulator) [1] coupled to the best-estimate Thermal-Hydraulic system code TRACE [2] to perform a dynamic analysis of a TRIGA reactor.

The main purpose of the analysis was to demonstrate the use of the coupled code systems for pulsing analysis and validate the existing Technical Specification limits on fuel temperatures and reactivity insertions insuring safe operation of the TRIGA reactors. The safety limit for TRIGA reactors is the maximum fuel temperature 1150°C based on the properties of the U-ZrH alloy fuel [3] and is a long standing recommendation of the fuel vendor. The limit has been verified through a vigorous testing program that tested fuel that safely reached even higher temperatures. The 1150°C fuel temperature limit prevents cladding failure when the clad temperature is below 500°C, while the limit is reduced to 950°C when the cladding temperature may reach the fuel temperature.

After the Texas A&M fuel damage experience [4], GA recommended an additional safety margin for pulsing by reducing the maximum fuel temperature limit during pulsing to 830°C. After long steady-state operation the hydrogen in the U-ZrH alloy fuel redistributes to the cooler, outside region. During pulsing the temperature is higher at the outside region resulting in a higher hydrogen pressure. By reducing the maximum pulsing fuel temperature to 830°C, it was calculated that the internal hydrogen pressure is reduced by a factor 2 allowing pulsing under any conditions. Most TRIGA installations in the US establish a general fuel temperature safety limit based on the 1150°C with the added safety margin of limiting maximum reactivity insertion to such value that the peak fuel temperature in any fuel rod during pulsing cannot exceed the 830°C.

In the present work SCALE/TRITON code package was used to develop a detailed core model generating beginning-of-life cross section set as a function of fuel temperature. It was further verified by two independent models using Monte-Carlo methods. The cross section set was used to develop a PARCS pin-wise neutronic model that was coupled to a simplified TRACE thermal-hydraulic representation of the reactor pool. The TRACE model included two flow channels, one representing the fuel element with the peak power near the ejected, transient absorber rod and another representing the average fuel rod.

2. Reactor Neutronics/Thermal-Hydraulic Model

The reactor model was based on a TRIGA research reactor that originally was designed as a Material Test Reactor (MTR) and was converted to contain TRIGA fuel elements. The reactor geometry is an x-y grid with typical TRIGA fuel assemblies containing Low Enriched Uranium (LEU) fuel in a four-rod cluster configuration. The reference reactor for this analysis is routinely operated at 1 MW in an irregular core arrangement that contains in addition to fuel rods, a number of water regions inside the reactor core, reflected by both water and graphite regions. The core contains one regulating, a number of safety control rods, and one transient rod that can be pneumatically ejected providing the pulsing capability. The control rods have fuel followers, while the regulating rod is water, and the transient rod is air followed. For this analysis, the core is assumed to be at clean, cold conditions, without any Xenon and Samarium buildup at the beginning of life.

In the PARCS core model each fuel rod is represented as one homogeneous region in x-y directions and axially divided to 10 fueled and 5 water and graphite reflector cells on the top and bottom of the core. The core is modeled with 6 different, unrodded fuel rods compositions, which were grouped, based on the surrounding fuel or control rod types, three different control rods, and two reflector types representing the water and graphite regions respectively. Figure 1 shows a representative region near a control rod with two different fuel types.

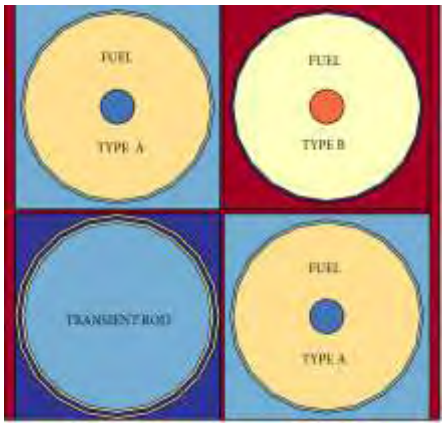

Figure 1: Representative Fuel Types

The control rods were modeled as unrodded and rodded regions depending on the follower types. Each fuel composition represented the effect of fuel design, burnup history, and the fuel temperature dependency. The cross section data was generated using the SCALE/TRITON lattice physics code (using the NEWT 2-dimensional lattice method) by developing a detailed core model generating beginning-of-life cross section set as a function of fuel temperature and verified by two independent models using Monte-Carlo methods. Nuclear cross sections were based on ENDF/B-VII data. Data presented in Table 1 indicates a good agreement between the SCALE/TRITON core model and similar 2 – dimensional Monte-Carlo methods:

Method	TRITON/NEWT	MCNP	SERPENT
Full core $k_{effective}$	1.08717	1.08212	1.09010

Table 1: Two-Dimensional Reactor Core Analysis

PARCS was used for the analysis of the typical TRIGA core by making use of an interpolation scheme for obtaining macroscopic cross section data in two energy groups at various fuel temperatures, moderator densities for the fuel rods of at a specified composition and location. The data at BOC is generated for seven different values of fuel temperatures as the most significant dependency during the reactor pulsing.

PARCS is a three-dimensional, two-group diffusion model using nodal methods. PARCS was coupled with TRACE to simulate both the steady-state and transient reactor behavior of the TRIGA core. The neutronic and thermal-hydraulic nodes are coupled through a mapping scheme that determines the power in the thermal-hydraulic and heat structure components in TRACE and allows the calculation of the thermal-hydraulic feedback.

The representative TRIGA core is a heterogeneous, pool-type reactor cooled by natural convection of water at all power levels and in all operational modes. The reactor core contains TRIGA fuel assemblies containing four fuel and/or control/transient rods at specific locations. Heat is removed by natural convection, with water rising up through the fuel rod channels. The TRIGA fuel assemblies have two different hydraulic channels, one between four fuel rods and another at the reactor periphery between a fuel rod and the reflector

regions. The fuel rod channels are the most limiting, since at the periphery only a partial side of the flow channel is heated.

The TRACE model calculates the steady-state natural convection flow through the vertical water coolant channel adjacent to the fuel rods providing the heat source. The code calculates the heat flux from the fuel rods and determines the axial temperature distribution of the natural convection flow. The TRACE TRIGA reactor model consists of several hydraulic components coupled to heat structures as shown on Figure 2.

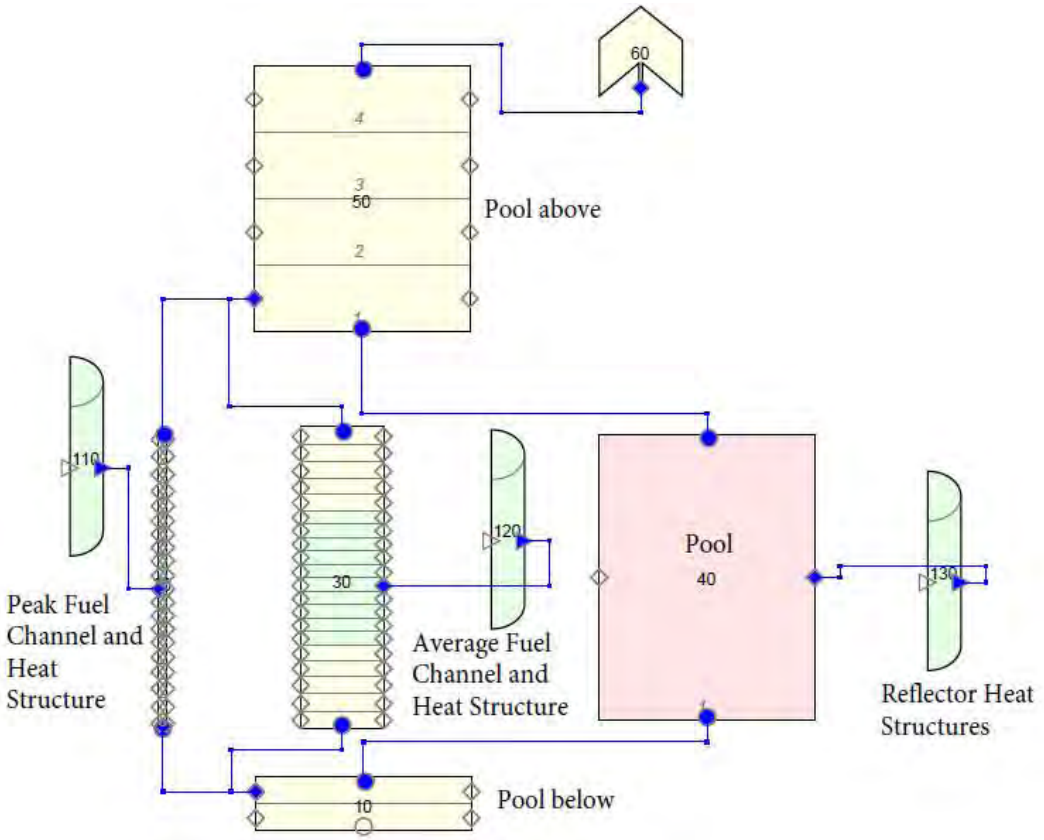

Figure 2: TRACE TRIGA Model and Nodalization

The model contains a “hot or peak channel” coupled to a heat structure representing the fuel rod with the peak power in the reactor core. The full power distribution of the reactor core including the location of the peak power is calculated by the coupled PARCS code. Another channel represents the lumped “average” coolant channel of all the remaining fuel rods in the reactor core. The two hydraulic channels are physically separated and vertically parallel to each other. For simplicity, conservatism and better comparison with TRIGA operator analysis both average and hot channel are modeled as channels between four rods cluster. The reactor pool is represented by three large hydraulic volumes at the bottom, the top, and alongside the core flow channels that is coupled to the reflector regions. The pressure of the core outlet flow equals the pressure of the cold water column outside of the core at this elevation. The power generated in the core results in fluid density difference between the core and the pool next to the core providing the buoyancy head for the core natural circulation.

3. Steady-State Results

Steady state calculations were carried out to validate the coupled PARCS-TRACE model by comparing with results as calculated by the facility and also with measurement data that was performed at the facility after reloading the core with LEU 30/20 fuel. The primary data

available included calculated and measured control rod worths both, site calculated excess and shutdown reactivity values. The steady-state reactor core analyses performed by the facility were completed with a 3-D MCNP model and provided the basis for the PARCS model validation.

The individual and total control rod worth values are shown in Table 2 including both calculated and measured data. The PARCS model over predicts the total worth of the control rod that is probably due to the difficulties in generating average fuel rod cross sections near control rods where the neutron flux varies rapidly. Any deviation in predicting the control rod worths highly influence the measured excess reactivity and shutdown margin, which are derived by using the individual and total control rod worths values. Since the uncertainty in the rod worth may lead to significant uncertainties in the peak fuel enthalpy increase, further analysis may be required to reduce the uncertainties in the control rod worth.

Control Rod worth	Calculated		Measured
	PARCS	Facility, MCNP	$
k_{eff}, all control rods withdrawn	1.04747	1.04553	
k_{eff}, all control rods inserted	0.94278	0.94314	--
Control rod #1 [$]	3.56	--	3.17
Control rod #2	1.74	--	2.03
Control rod #3	2.48	--	2.90
Control rod #4	5.55	--	4.61
Regulating rod	3.02	--	3.46
Transient rod	1.58	--	1.02
Total control rod worth	$17.93	$16.34	$17.19
Excess reactivity	6.47	6.22	7.48
Shutdown margin [$]	-9.02	-8.61	-9.70

Table 2: Control Rod Worths, Excess Reactivity and Shutdown Margin, Cold Clean Reactor Core

Table 3 shows some of the thermal-hydraulic parameters as calculated by the coupled analysis and compared to the analysis done by the facility using the computer code TAC2D. In general, there is a reasonable agreement and the slight deviation in the predicted coolant temperature is probably due to the differences in the code models, simplification of TRACE model and its capabilities to reproduce natural convection flow, and also not having all data used for the TAC2D analysis.

Parameter	Steady-State Value	
	TRACE	TAC2D
Peak Fuel temperature in hot-rod, ºC	360	368
Peak fuel temperature, average rod, ºC	278	282
Exit maximum coolant outlet temperature, ºC	85	77
Exit average coolant temperature, ºC	73	65

Table 3: TRIGA Thermal-Hydraulic Parameters for 1 MW Operation

4. Transient Results

Two pulsing scenarios were analyzed: Scenario a) full ejection of the transient rod with reactor power below the 1 kW pulsing limit and Scenario b) accidental insertion of a positive reactivity at full, 100% operating power level due to either inadvertent ejection of the transient rod or rapid withdrawal of an experiment. The reactor power trip set point is set at

125% nominal power that initiates a reactor scram by inserting all safety control rods in 1.2 sec with a delay time of 0.1 sec, which has no effect on the maximum power, however, reduces the energy release in the tail end of the pulse.

A pulsing transient is usually initiated first adjusting the control/regulating rods to reach criticality at low power level and then by ejecting the transient rod in about 0.1 sec from its inserted position with the capability of adjusting the total positive reactivity insertion that is limited by a mechanical stop.

For a $2 reactivity insertion at low power (Scenario a) Figure 3a-c indicates the reactivity, power, and fuel temperature behavior of the pulse. The pulse is entirely controlled by the fuel temperature feedback (rhotf) while the scram (rhocr after ~.3 sec) ensures that the temperature rise and energy release is limited in the tail end.

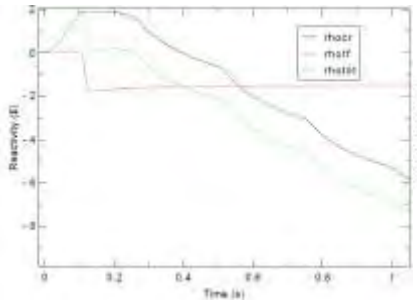

Figure 3a: Reactivity

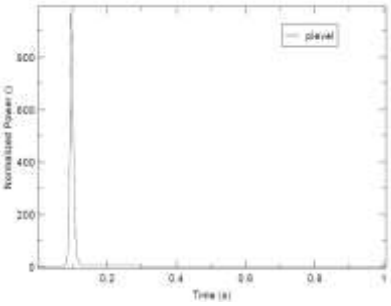

Figure 3b: Power Pulse

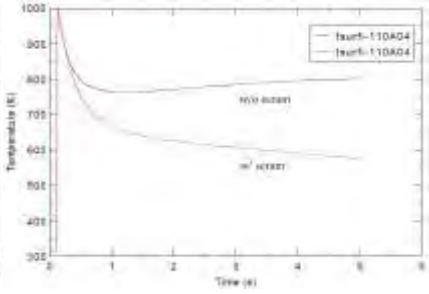

Figure 3c: Fuel Temperature

A series of calculations were done comparing the PARCS/TRACE pulse performance results with the facility analysis done by the space-independent kinetics BLOOST code as shown in Table 4. In addition, the TRIGA facility also performed a number of pulse measurements to validate the BLOOST predictions, which are also included in Table 4.

Reactivity $	Peak Pulse Power [MW]			Peak Fuel Temperature [ºC]		
	PARCS	BLOOST	Measured	PARCS	BLOOST	Measured
1.15	12		33	100		297
1.24	59		64	330		393
1.42	160		222	450		476
1.45		227			455	
1.56	360	399	423	523	525	616
1.95	896	1008		716	755	
2.10	1100			790	830	
2.30	1520	1873		862	921	

Table 4: Pulse Performance from 1 kW Power

The agreement between the measured and BLOOST data is within the experimental error that arise from thermocouples and power channel indications and also form the value assigned to the prompt reactivity insertion values. In addition, the transient rod calibration also have a few cents error that itself can easily account for the deviation seen between the BLOOST predicted and measured values.

The PARCS/TRACE analytical results predict ~5-10% lower peak power than BLOOST, but still within the measurement uncertainty. For lower reactivity insertions (<$1.5), the coupled model slightly over predicts BLOOST, but under predicts for >$1.5 insertions. The peak fuel temperature is also lower by ~5 that primarily is due to the different fuel rod thermal models.

Moderator effects only influence the total energy release in the tail end and have no impact on the peak power and fuel temperatures.

Scenario b, pulsing from full 100% power, is a hypothetical accident requiring the violation of administrative procedures including the full insertion of the transient rod and bypassing of the pulse limit interlock. Various amount of positive reactivity insertion may be simulated by partial ejection of the transient rod. The 125% power scram initiates the insertion of all control rods even before the peak pulse power is reached.

The analytical results are compared to values reported by the facility that consisted of combination of BLOOST analysis, a separate diffusion-theory power peaking, and hand calculations. The PARCS calculated power peak is substantially higher 40-50%, but the predicted pulse width much narrower and the energy release is lower resulting in lower predicted peak fuel temperatures in every reactivity insertion level. Still the peak fuel temperatures obtained from PARCS calculations and facility operator analysis are predicted to be below safety limit. Both PARCS and BLOOST/hand calculation results may have significant uncertainties, and would require further analysis, but it still presents a reasonable approach to evaluate the effects of an unexpected accident.

Reactivity $	Peak Pulse Power [MW]		Peak Fuel Temperature [ºC]	
	PARCS	BLOOST/Calculation	PARCS	BLOOST/Calculation
2.1	630	471	572	740
2.95	1125	827	650	864
3.1	1280	830	670	866

Table 5: Pulse Performance from 1 MW Power

5. Conclusion

The objective of the work was to develop a coupled neutronics thermal-hydraulic model to study TRIGA rod pulsing events. The study will provide a basis for understanding the sources of uncertainties in calculating fuel rod behavior in pulsing events. The coupled PARCS-TRACE code was used for the three-dimensional simulation of the TRIGA pulses for a typical 1 MW TRIGA reactor at the beginning of life with initial conditions at cold, clean, critical reactor.

The model was used to calculate the reactor core power and fuel temperatures with different reactivity insertion in the prompt-critical region up to $2.30 insertion initiated at 1 kW and up to $3.1 from 1 MW power level. The initial results were primarily limited to peak fuel temperature and maximum reactivity addition conditions, since these are used in technical specifications as limiting conditions. The analysis validates the values predicted by the BLOOST computer code that is widely used to predict pulsing behavior. The study indicate the capabilities of the coupled TRACE-PARCS codes package providing reasonable results for reactor cores with irregular geometries, typical for research reactors and validates its ability using code for additional confirmatory analysis of TRIGA reactors.

6. References

[1] T. Downar., et al., “PARCS v3.0 U.S. NRC Core Neutronics Simulator User Manual,” Department of Nuclear Engineering and Radiological Sciences, University of Michigan, Ann Arbor, MI, October 2010

[2] “TRACE V5.0 User’s Manual,” Volume 1-5, Division of Risk Assessment and Special Projects, Office of Nuclear Regulatory Research U. S. Nuclear Regulatory Commission, Washington, DC.

[3] M.T. Simnad, “The U-ZrH_x: Its Properties and Use in TRIGA Fuel,” *Nuclear Engineering and Design* 64 (1981) 403-422

[4] “Interpretation of Damage to the FLIP Fuel during Operation of the Nuclear Science Center Reactor at Texas A&M University,” GA-A16613, December 1981.

HYPOTHETICAL ACCIDENT ANALYSES OF THE PROPOSED SPLIT CORE AT NIST USING ANL-PARET CODE

ZEYUN WU*, ROBERT E. WILLIAMS, and J. MICHAEL ROWE
NIST Center for Neutron Research
100 Bureau Drive, Mail Stop 6101, Gaithersburg, MD 20899 USA
**Corresponding author: zeyun.wu@nist.gov*

ABSTRACT

Preliminary design basis accident analyses have been performed on the proposed split core to examine the thermal-hydraulics (T/H) safety characteristics of the new design. The multi-channel T/H safety analysis code PARET, developed by Argonne National Laboratory, is employed to perform the transient analyses with the power and kinetics parameters provided by neutronics calculations. Two important transient overpower phenomena, control rod withdrawal accident during the core start-up and maximum reactivity insertion accident at the full power operation condition, are investigated in the paper. The accident scenarios are investigated at both the start-up (SU) and end-of-cycle (EOC) core status in an equilibrium cycle to examine the T/H performance characteristics at different stages of the cycle. The postulated accidental transients are simulated in PARET with real-time monitoring of the fuel cladding temperature, power rate and mass flow rate. Reasonable T/H safety margins of the new design are achieved by comparing the minimum critical heat flux ratio and the peak clad temperature to the safety criteria specified for typical low enriched uranium (LEU) test reactors.

1. Introduction

In anticipation of the eventual retirement of the research reactor (NBSR) at the National Institute of Standards and Technology (NIST), research efforts are ongoing at NIST Center for Neutron Research (NCNR) to design a new research reactor. The primary purpose of the new reactor is to optimize cold neutron production for scientific neutron scattering experiments. The new design has two high quality cold neutron sources (CNS). The thermal power of the new reactor is 20 MW and the operating cycle of the equilibrium core is set to be around 30 days. Low enriched uranium (LEU) fuel - U_3Si_2/Al fuel – with U-235 enrichment less than 20% is used to comply with nuclear non-proliferation agreements.

Neutronics studies have been performed to demonstrate the viability of the design. A full core model has been developed using MCNP6 [1]. The core consists of 18 MTR-type fuel elements, which are arranged in a compact pattern and are horizontally split into two halves. The core is cooled and moderated by light water but reflected by heavy water to create a large thermal neutron flux trap in the reflector region between the core halves. To maximize the scientific utilization of neutrons, the reactor vessel in the current design is equipped with two horizontal cold neutron source beams and four tangential thermal neutron beams. The CNS were positioned to keep the heat load of each below 4 kW and to optimize cold neutron brightness performance. The neutronics feasibility of the new design is justified by the effective multiplication factor of the system and the maximum thermal flux performance. The superiority of the new design is demonstrated by the cold neutron spectrum brightness in the CNS per unit reactor power [2, 3].

In this paper, the preliminary design basis accident analyses are performed on the split core to examine the thermal-hydraulics safety characteristics of the new design. Hypothetical transient overpower accidents are analyzed using the system safety analysis code PARET [4, 5], which was developed by Argonne National Laboratory. The accidental scenarios in both the start-up (SU) and end-of-cycle (EOC) core status for an equilibrium cycle are examined to compare the T/H performance characteristics at different status. In the PARET model, the active core is simplified as a two-channel model with kinetics and feedback parameters provided by neutronics calculations. The overpower transients are simulated with the real-time monitoring of the fuel cladding temperature, power rate and mass flow rate. The thermal-hydraulics (T/H) safety margins of the new design are verified by the minimum critical heat flux ratio and the peak clad temperature.

2. Overview of the Split Core Design

The proposed NIST reactor employs the standard 'tank-in-pool' design pattern, in which a cylindrical heavy water tank 2.5 m diameter and 2.5 m height is placed in the center of a large light water pool that functions as the thermal and biological shields. The core design embraces the compact core concept and creates a thermal flux trap in an easily accessible location in the reflector tank to maximize the flux. The reactor core is enclosed by two zirconium core boxes to separate heavy water and light water. To maximize useful flux trap volume in the reflector, an innovative horizontally split core is employed in the design such that the thermal flux trap between the core halves would provide ideal locations to place cold neutron sources (CNS). Two vertical liquid deuterium CNS are placed in the flux trap located in the north and south sides of the core. Two CNS beam tubes are connected to the CNSs with guides pointing in the north and south directions. Four thermal beam tubes are placed in the east and west sides of the core at different elevations (20 cm above and below core mid-plane) with the pointing direction tangential to the core face. A schematic view of the reactor components and the fuel element radial layout in the split core is illustrated in Fig. 1.

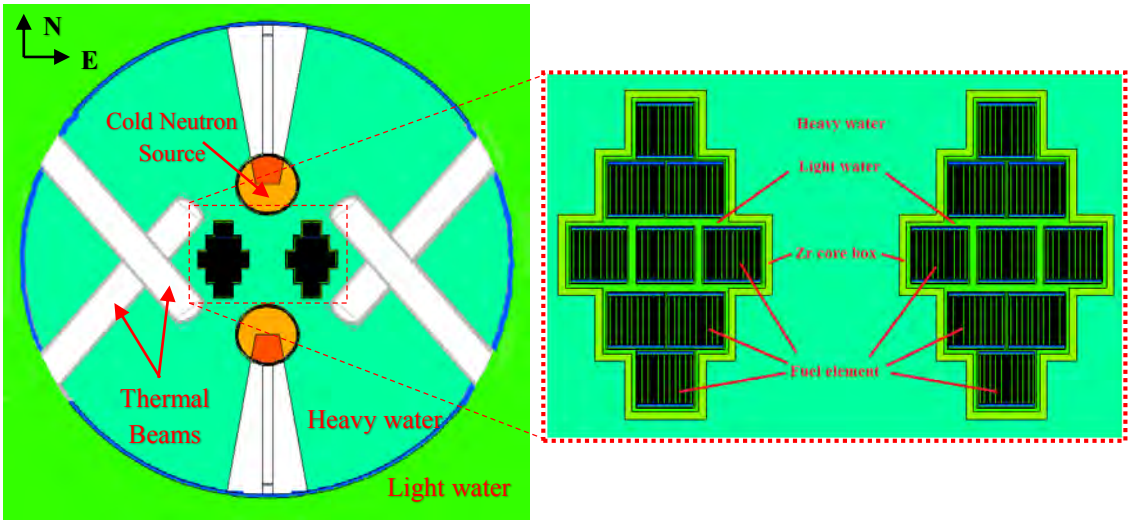

Fig. 1. A schematic view of the mid-plane of the reactor with horizontally split cores [3].

The power distribution in the fuel is required for reactor safety analyses to specify the initial heat source profile for the heat structure in the T/H model. In this study, the power density for a given position in a core is calculated by MCNP6, in which we conservatively assume that all the recoverable fission energy is deposited at the point of fission, and the power density is proportional to fission density. In order to obtain a detailed power distribution for the core, the fuel plate (really

the fuel meat inside the plate) is evenly divided into 3 stripes, and each stripe is evenly divided into 30 axial pieces. Fig. 2 depicts the axial power distributions along the hottest and average coolant flow channel in SU and EOC core, respectively.

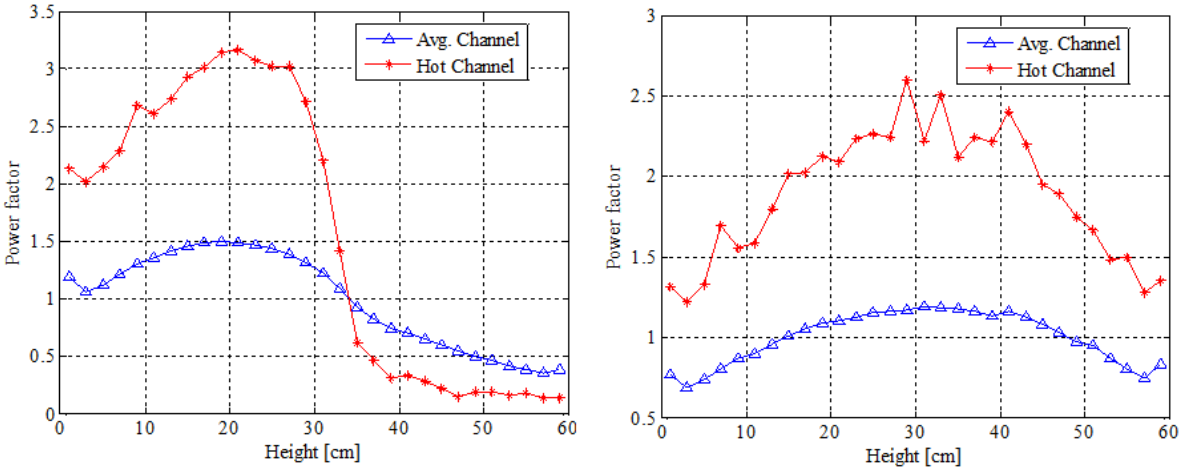

Fig. 2. Steady-state axial power distribution in the SU (left) and EOC (right) core.

The results shown in Fig. 2 represent the steady-state axial power distributions that have been normalized to the total reactor power, and serve as initial power profiles for all point kinetics reactor model based transient analyses. The hot channel refers to a fuel plate that produces the largest amount of power, whereas the average channel represents the core average power effects. Since the control elements are partially inserted from the top of the core to compensate the large excess reactivity at SU, the peak power is significantly skewed to the bottom region of the core at SU (see the left figure in Fig. 2). This asymmetry vanishes in EOC case as the controls are fully withdrawn out the core at this status (see the right figure in Fig. 2).

The necessary kinetics parameters required for safety analysis, the prompt neutron generation time and the effective delayed neutron fraction, in SU and EOC are summarized in Table 1. They are calculated with MCNP6 using the adjoint-weighted tally methodology that is newly developed in the code [1].

Table 1. Kinetics parameters calculated by MCNP6

Kinetics Parameter	SU	EOC
Prompt neutron generation time - Λ (μs)	202.61 ± 4.60	203.82 ± 4.42
Effective delayed neutron fraction (β_{eff})	0.00740 ± 0.00047	0.00717 ± 0.00041

Four sets of H-shaped hafnium control blades are utilized as both criticality and safety control elements for the reactor. Due to the limited space in the core, all control blades are about 0.5 cm thick and 60 cm long (the same length as the active fuel length). The blades are controlled by a mechanical driver located at the bottom of the core but with the fully withdrawn positions at the top of the core. Reactivity worths of the control rods are needed by the safety analysis code to determine the correct negative reactivity inserted to the core after scram. Fig. 3 shows the reactivity worths of the control rods in the split core at SU and EOC. Due to different excess reactivity existing at different stages of the cycle, the critical control rod position at SU and EOC are different. As indicated in Fig. 3, the differential reactivity worth at the critical position for SU is

higher than the one for EOC. This will result in a greater reactivity insertion rate for SU than EOC at the time of scram, if the control rod insertion speed is assumed to be constant and the reactor is assumed to be operating at critical status. Therefore a faster power reduction after scram is expected for the SU case, and this fact is verified by the PARET simulation results discussed in the result section.

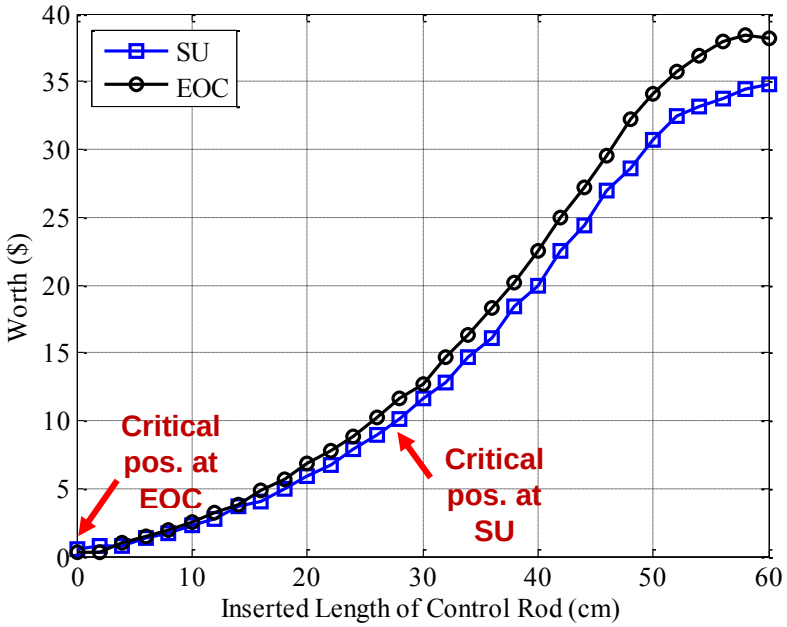

Fig. 3. Reactivity worths of the control rods at SU and EOC.

3. The PARET Model and Safety Analysis Criteria

The ANL-PARET code is intended primarily for safety analysis of research and test reactors that use plate-type fuel elements, or round fuel pins. The code employs 1-D hydrodynamics, 1-D heat transfer and point kinetics model with considerations of proper reactivity feedback. The hydrodynamics equations and heat transfer equations are numerically solved simultaneously to obtain the temperature distributions for fuel, clad and coolant along the axial direction. The solutions to these equations also yield the pressure drop across the core, as well as point-wise fluid enthalpies, pressures, and mass flow rates in the coolant channels. PARET was initially written for nondestructive reactivity accident analyses (i.e., overpower transient analyses) [4], and was recently extended to provide an ability to follow a loss-of-flow (LOF) transient with down flow initially, through flow reversal and finally through the establishment of natural convection cooling [5]. All the features perfectly meet the requirements of the safety analysis on the split core. The work presented here is mainly focused on transient overpower analyses, and the LOF analyses will be investigated in future research.

For simplicity, a two-channel PARET model is developed in this study to account for physical conditions in the hot and average channel, respectively. Each channel includes a 1-D slab geometry of fuel plate, extending from the plate centerline to the coolant centerline on both sides of the plate. Appropriate volume fractions are weighted for each channel to account for proper heat source transferred in the channel. A diagram to illustrate a T/H channel is shown in Fig. 4 with the corresponding dimensions provided in Table 2.

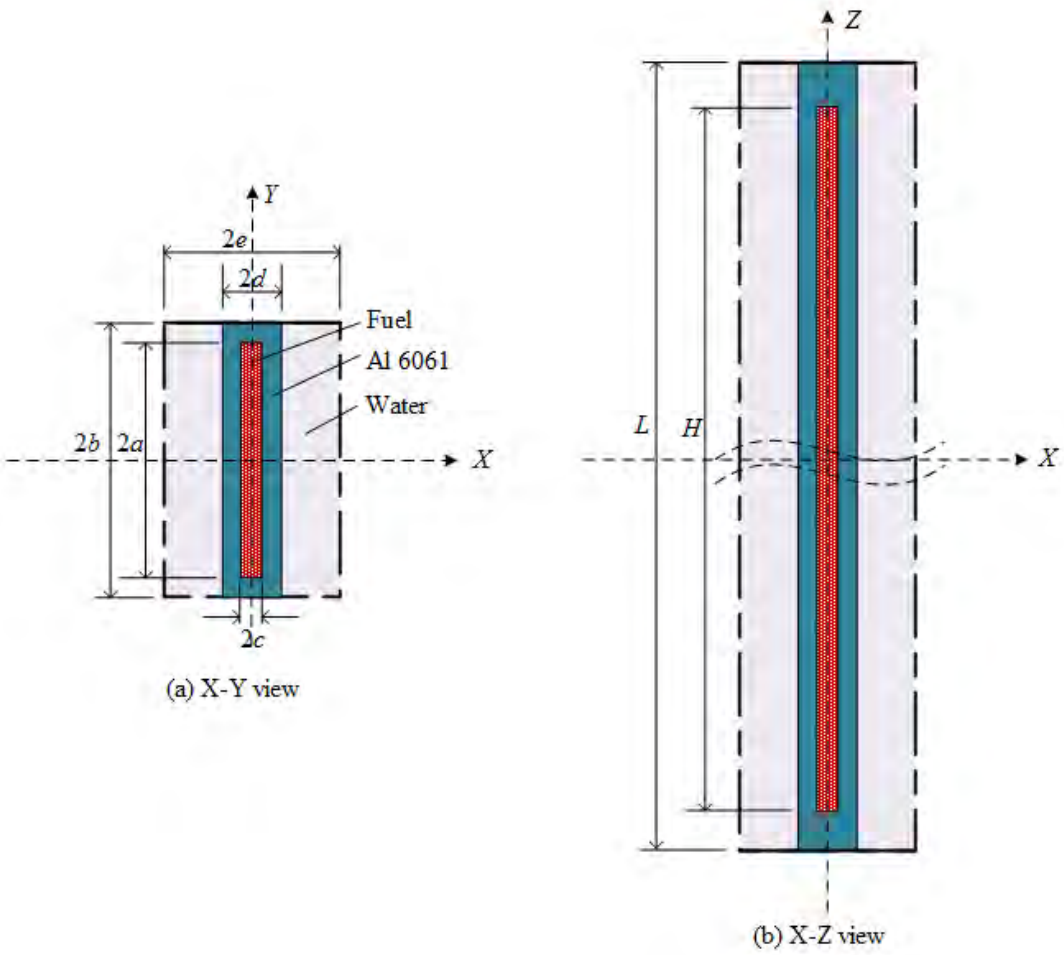

Fig. 4. Diagram of the flow channel model in the plate-type core.

Table 2. The dimensions of the channel model in Fig. 4.

Parameter	Size (cm)
Half width of the fuel meat (*a*)	3.067
Half width of the fuel plate (*b*)	3.3325
Half thickness of the fuel meat (*c*)	0.033
Half thickness of the fuel plate (*d*)	0.0635
Half pitch of the fuel plates (*e*)	0.211
Length of the fuel meat (*H*)	60
Length of the channel (*L*)	67.28

PARET is not able to model the entire primary coolant system of the reactor, but rather develops equivalent T/H characteristics of a flow channel in the core region by providing proper boundary conditions. For the split core design, a downward flow with a total flow rate 8000 gal/min or 1817 m^3/hour was assumed and the inlet coolant temperature was set at 37 °C. With these conditions, the temperature rise along the average channel was about 10 K based on energy conservation. The core was assumed to be operated at atmospheric pressure and the outlet pressure was assumed to be 135 kPa. All these T/H conditions were designated with the intention to achieve T/H performance similar to the existing reactor at NIST [6]. A summary of the required T/H boundary conditions and parameters based on the channel dimensions is outlined in Table 3.

Table 3. T/H Conditions and parameters used in the PARET model.

Conditions and Parameters	Values
Outlet pressure (kPa)	135
Inlet temperature (°C)	37
Inlet volumetric flow rate (gpm)	8000
Flow area of the channel (cm^2)	1.9662
Heated surface area of the channel (cm^2)	736
Rectangular channel width (cm)	6.67
Wetted perimeter of the channel (cm)	13.63
Hydraulic diameter (cm)	0.58

To satisfy safety concerns, two thermal constraints are examined during the course of the transients. The first one is the peak clad temperature (PCT), which is a direct indicator of the physical damage to the fuel plate. For reactor designs, it requires the PCT must not reach the fuel blister temperature, which is taken as **515 - 575 °C** for silicide LEU fuel [7]. Another constraint is on the critical heat flux (CHF), which characterizes the departure of nucleate boiling (DNB) occurring to coolant flow at the surface of the fuel cladding. The DNB may significantly reduce the heat transfer coefficient and subsequently cause the flow burnout phenomena. An indicator for the CHF constraint is known as the minimum critical heat flux ratio (MCHFR) defined as the DNB heat flux estimated from an appropriate correlation divided by the expected heat flux. The limit of MCHFR is set **1.32**, which is also obtained from the safety report of the existing NIST reactor [5]. To conform to current existing options in PARET, the Mirshak DNB correlation [8] is used to estimate the DNB critical heat flux in the model.

4. Transient Overpower Accident Analyses

4.1 Steady-State Conditions

The PARET inputs have been run to establish the steady-state conditions for the core at full power (20 MW). Table 4 shows the respective results for SU and EOC. It can be seen that the PCT and MCHFR at steady-state conditions for both SU and EOC satisfy the thermal constraints specified above very well.

Table 4. T/H performance characteristics at steady-state conditions

Core Status	SU	EOC
Coolant outlet temperature [°C]	52.96	56.09
Peak clad temperature [°C]	107.05	95.51
Peak fuel temperature [°C]	120.46	106.18
MCHFR	2.21	2.77

4.2 Control Rod Withdrawal Start-up Accident

The control rod withdrawal start-up accident is modeled with a slow ramp reactivity insertion to a critical core from a very low power with selected assumptions made to examine the severity of the event. The core condition is considered at both the start-up (SU) and the end-of-cycle (EOC) of an equilibrium cycle to show the different power transient behaviors under the accidental scenarios. The reactor is initially critical and operating at a power of 2 Watts (0.01% of the full power). The ramp reactivity is assumed to be inserted with a rate \$0.1/s to mimic the slow reactor start-up procedure. The reactor scram occurs with a power trip at 24 MW (120% of the full power). A time

delay constant 25 ms is defined in the model to account for the finite time required for the safety rods to start the movement after scram. The control rods are assumed to move with a constant rate 1.2 m/s for scram. At this moment, all reactivity feedback coefficients (including fuel, coolant density, and moderator void) and the period trip are neglected in the analyses.

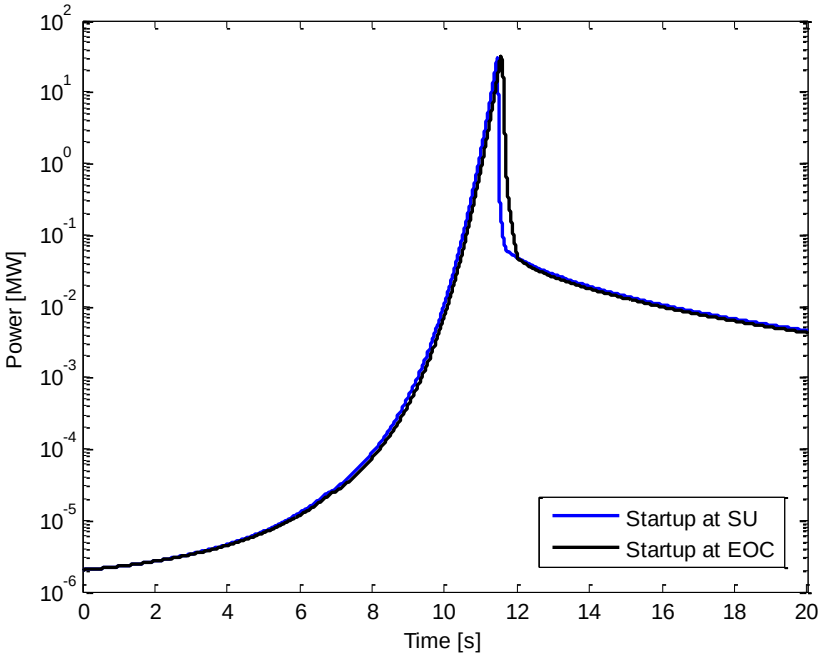

Fig. 5. Reactor power in start-up accidents.

Fig. 5 shows the reactor power transient behavior of first 20 seconds in the start-up accidents. Because the kinetics parameters for SU and EOC have only slight differences (see Table 1), the power increases with identical rates in start-up transients for SU and EOC, and both reach the maximum power around 30 MW at about 12 seconds into the accidents. They then both quickly drop off to the decay heat power level after the scram. The power reduction curve for the SU, however, exhibits a shorter time constant, this is due to the higher differential reactivity worth of control rods at the critical position in SU (see Fig. 3). Since the core is initially operating at critical and the control rods are assumed to move with a constant rate, the SU core thereby obtains larger negative reactivity than the EOC core in a period following the scram. As a result, the power at the SU case decreases faster at that time period.

The corresponding PCT and MCHFR behavior are shown in Fig. 6 and 7, respectively. The specified thermal limits for these two parameters are also shown as red dashed lines in the figures. It can be clearly seen that the safety criteria are satisfied during the entire transient. In fact, large safety margins are observable in the PCT figure (Fig. 6). The extreme quantities of the power, PCT and MCHFR and the corresponding time of occurrence in the accidents are summarized in Table 5.

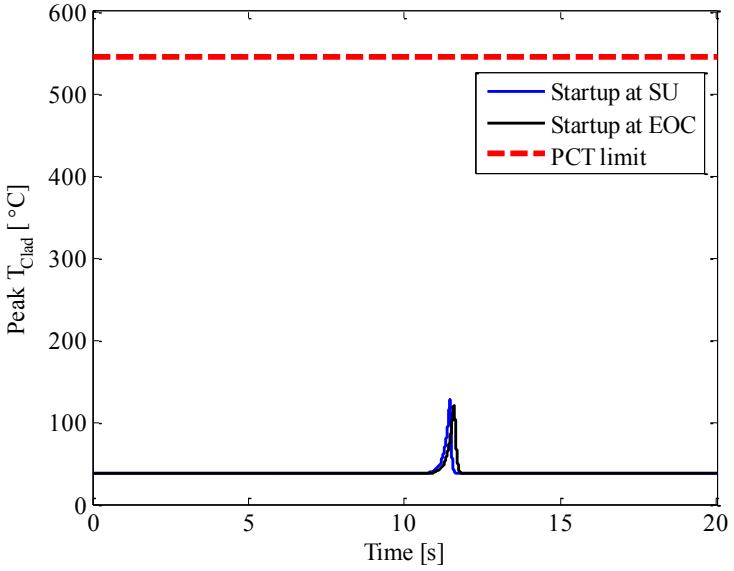

Fig. 6. Peak clad temperature in start-up accidents.

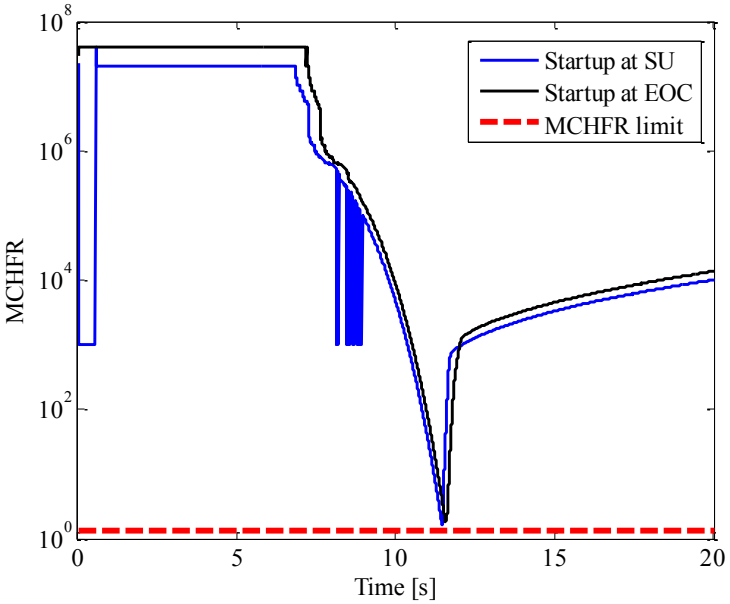

Fig. 7. Minimum critical heat flux ratio in start-up accidents.

Table 5. Peak quantities and their occurring time in start-up accidents

Core Status	SU	EOC
Peak Power [MW]	29.12	31.05
Peak power time [s]	11.45	11.56
Power trip time [s]	11.42	11.51
Peak clad temperature [°C]	127.38	119.49
PCT time [s]	11.46	11.57
MCHFR	1.66	1.86
MCHFR time [s]	11.46	11.57

4.3 Maximum Reactivity Insertion Accident (MRIA)

The maximum reactivity insertion accident models the power excursion with a large positive reactivity inserted in the core that may be caused by experiments removed from the core. Both SU and EOC core are considered for the accident. The reactor is assumed to be initially operated at a full power of 20 MW. A large positive reactivity 1.5$ was inserted to the core in a time range 0.5 s. The scram set point, time delay constant for the scram and the constant control rod movement speed are all assumed to be the same as the start-up accident case. For conservatism, all reactivity feedback coefficients are assumed to be zero. As shown in Fig. 8, the power, for both SU and EOC, increases to a maximum power about 26 MW in in about 120 ms in MRIA. The PCT and MCHFR, however, remain well below the thermal limits as shown in Fig. 9 and 10, respectively. The extreme quantities of the related parameters and the corresponding time of occurrence in the transients are summarized in Table 6.

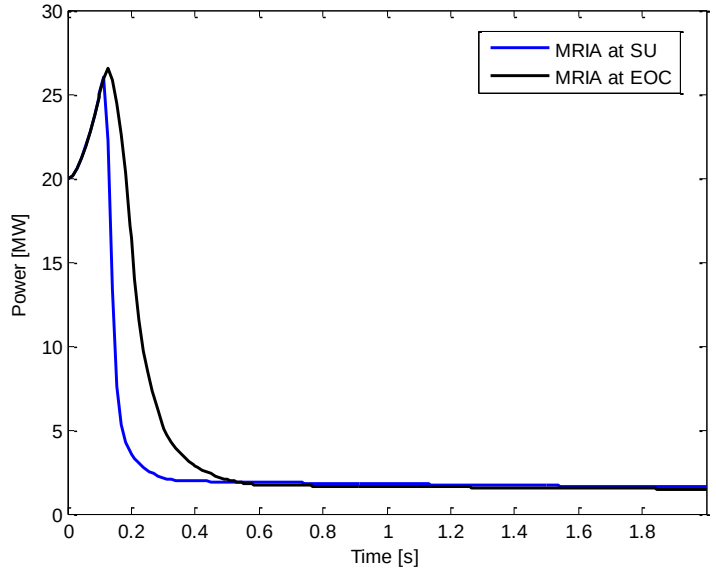

Fig. 8. Reactor power in maximum reactivity insertion accidents.

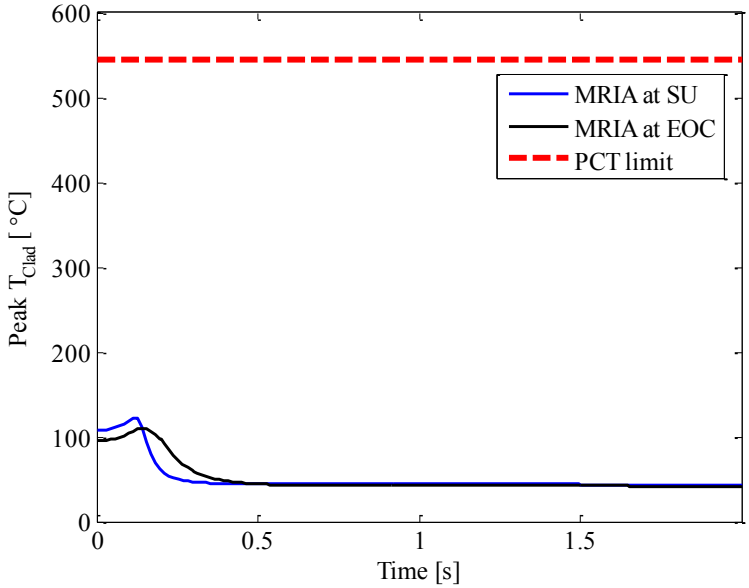

Fig. 9. Peak clad temperature in maximum reactivity insertion accidents.

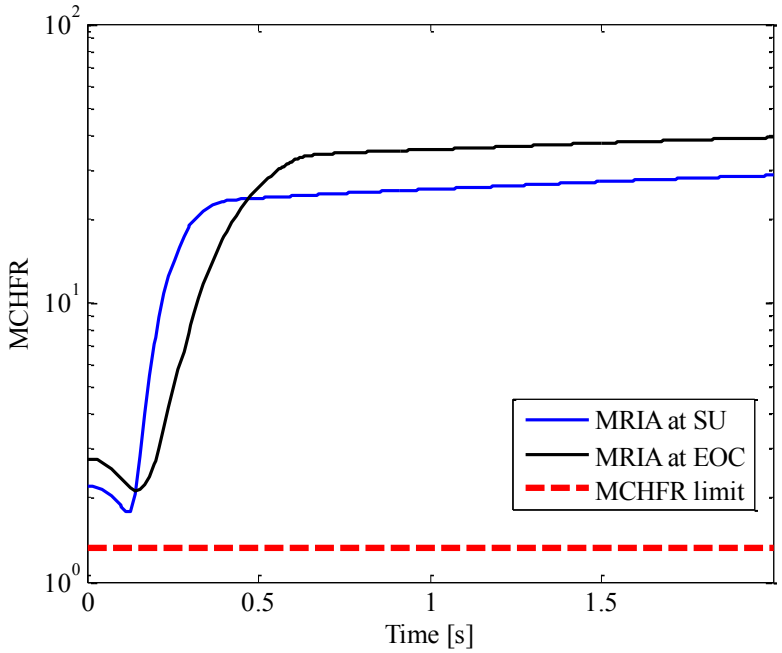

Fig.10. Minimum critical heat flux ratio in maximum reactivity insertion accidents.

Table 6. Peak quantities and their occurring time in maximum reactivity insertion accidents

Core Status	SU	EOC
Peak Power [MW]	26.03	26.51
Peak power time [s]	0.1126	0.1266
Power trip time [s]	0.0985	0.0985
Peak clad temperature [°C]	121.99	109.99
PCT time [s]	0.1267	0.1406
MCHFR	1.78	2.12
MCHFR time [s]	0.1267	0.1406

5. Summary and Conclusions

Preliminary design basis protected transient overpower accident analyses on the NIST's proposed LEU fueled split core reactor are performed using the ANL-PARET safety analysis code. The control rod withdrawal start-up accident and the maximum reactivity insertion accident are modeled with selected assumptions to maximize the severity of the event. The accidents are analyzed at respective SU and EOC conditions of an equilibrium cycle. The peak clad temperature and minimum critical heat flux ratio are examined during the transients to ensure the safety criteria are fully satisfied. The DNB critical heat flux is estimated by the Mirshak correlation in this study. The safety analysis results indicate reasonably sufficient safety margins were achievable in both start-up and MRIA accidents.

In the near future, the loss-of-flow (LOF) accidents will be investigated also using the PARET code to assess the safety margins as well as the natural circulation heat removal capability for the design under these conditions. The loss-of-coolant accident (LOCA) will also be analyzed with a more comprehensive model including the entire primary system of the reactor. A more systematic T/H system analysis code such as RELAP5 [9] will be used for such studies.

6. References

[1]. D. B. Pelowitz Ed., "MCNP6™ User's Manual," LA-CP-11-01708, Los Alamos National Laboratory, (December 2012).

[2]. Z. Wu, M. Carlson, R. E. Williams, S. O'Kelly, and J. M. Rowe, "A Novel Compact Core Design for Beam Tube Research Reactors", Transactions of the American Nuclear Society, 112, 795-798 (2015).

[3]. Z. Wu and R. E. Williams, "Core Design Studies for A Low-Enriched Uranium Reactor for Cold Neutron Source at NIST," *the Joint International Conference on Reactor Physics PHYSOR 2016 - Unifying Theory and Experiments in the 21st Century*, Sun Valley, ID, USA, May 1-5 (2016).

[4]. C. F. Obenchain, "PARET—A Program for the Analysis of Reactor Transients," U.S. AEC Technical Report IDO-17282, Phillips Petroleum Co. (1969).

[5]. W. L. Woodruff and R.S. Smith, "A User's Guide for the ANL Version of the PARET Code, PARET/ANL (2001 Rev.)," ANL0RERTR0TM-16 (2001).

[6]. "Safety Analysis Report (SAR) for License Renewal of the National Institute of Standards and Technology Reactor – NBSR; NBSR-14, Rev 4," National Institute of Standards and Technology (NIST), Gaithersburg, MD (2010).

[7]. "Safety Evaluation Report Related to the Evaluation of Low-Enriched Uranium Silicide-Aluminum Dispersion Fuel for Use in Non-Power Reactors," NRC/NUC-NUREG-1313 (July 1988).

[8]. S. Mirshak, W. S. Durant, and R. H. Towell, "Heat Flux at Burnout," DP-355 (1959).

[9]. "RELAP5/MOD3.3 Code Manual," Information Systems Laboratory, Nuclear Safety Analysis Division (2002).

Poster new projects

DESIGN AND QUALIFICATION OF JULES HOROWITZ REACTOR CONTROL ROD DRIVE MECHANISMS

C.DUMANOIS, F.DONNIER, R.VALY, P.ROPKE, L.RANC
Mechanical & Electromechanical Department, AREVA TA
BP9, 13115 St Paul Lez Durance – France

ABSTRACT

The Jules Horowitz Reactor Control Rod Drive Mechanisms (CRDMs) are subject to stringent requirements such as: safety, operation, environment and geometry. Therefore the development of two different types of CRDMs demanded a huge effort in terms of design and qualification. AREVA TA successfully led the project to meet the specifications. A major milestone, the drop times of the rods qualification, has recently been achieved.

The 27 control rods located in the center of the fuel assemblies are actuated by 27 CRDMs from 2 types ensuring respectively the emergency shutdown response time and the control of the reactor and maintain at shutdown. Specific design features have been developed and qualified to address the following very challenging issues: the short passive drop time of the control rods despite the significant countercurrent flow, the leak tightness at the pool interface, 2 lines of defense against the neutron absorber ejection, narrow space, high reliability.

The paper presents the context, the requirements, the design features and the development and qualification process of the 2 CRDM types.

The paper details:
- JHR mechanisms general design features by means of functional diagrams and CAD pictures focusing on:
The different sub-assemblies and how they are loaded in the reactor
The 2 different ways to prevent absorber ejection under upwards flow
The implemented features to prevent vibration under high velocity flows
The 2 diverse CRDMS designs actuating respectively the safety rods and the other control rods
- The main qualification tests that are being led on an ASA and an APAC prototype mechanism with a specific hydraulic loop

1 INTRODUCTION

The Jules Horowitz Reactor Control Rod Drive Mechanisms (CRDMs) are subject to stringent requirements such as: safety, operation, environment and geometry. The development of two different types of CRDMs demanded a huge effort in terms of design and qualification. AREVA TA successfully led the project to meet the specifications. A major milestone, the drop times of the rods qualification, has recently been achieved.

The paper presents the context, requirements, the design features and the development and qualification program of the 2 CRDM types.

2 SPECIFIC MECHANISMS FOR A SPECIFIC CORE

Like other material testing reactors, JHR CRDMs are located below the reactor pool and fulfil permanent water tightness during normal operation and maintenance. The core being quite specific, specific mechanisms have had to be designed.

As illustrated on Figure 1, JHR core is made of 34 cylindrical fuel elements (FE), arranged as a daisy pattern of 102 mm pitch, and integrated to the core barrel of 700 mm diameter. The barrel has a total of 37 cells, one central, 6 on the first crown, 12 on the second and 18 on the third. Three cells are dedicated to load a big size experiment.

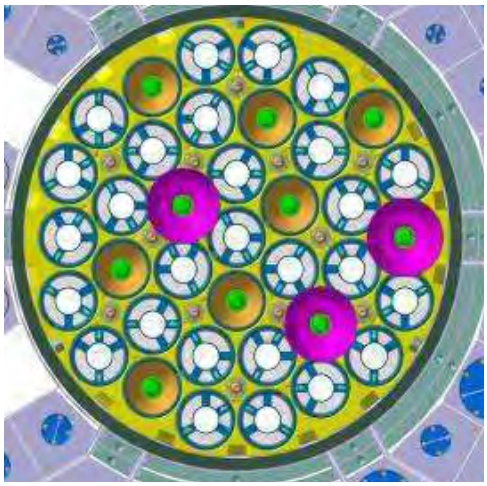

Figure 1 : cross section of JHR core barrel with 3 big size experiments (colored purple), 7 small size experiments (colored orange), 27 mobile rods locations (colored white)

Neutronic absorbers are located inside fuel elements, the room inside each fuel element being limited to a cylinder of 41 mm diameter.

Therefore, to ensure the criteria of the shutdown systems, it has been defined that a total of 27 absorbers are required, distributed as following:

- 4 absorbers dedicated to the emergency shutdown, labelled ASA (for “Absorbant de Sauvegarde Arrêt), one located in the central cell, and 3 in cells of the second crown of the barrel,

- 4 absorbers which main function is the neutron flux monitoring, labelled AP (for “Absorbant de pilotage”), two located in cells of the second crown, and two in cells of the third crown of the barrel.
- 19 absorbers which main function is to compensate slow loss of reactivity during an irradiation cycle, labelled AC (for “Absorbant de Compensation), and located in cells of the first, second and third crown of the barrel.

A fixed tube between the absorber and the fuel element makes a physical separation and enables to load and unload fuel element with no action on the absorber. Being the internal interface of the fuel element, this tube delimits the first gap of water of the fuel element. This tube guides the mobile absorber and is called the guide tube.

When the absorber is extracted from the core, it must be replaced by an aluminum structure called the rod follower, to limit the quantity of water inside the fuel element and limit thermalizing neutrons.

The guide tube, the mobile absorber and its follower are integrated to the mechanism. All 27 mechanisms are loaded in the reactor and must not require any intervention for several years.

To fulfill neutron flux performances, gap of water thickness along fuel elements is limited to 2 mm. Nominal thermal power of the core is 100 MW, and nominal flow rate is 7400m^3/h. The consequence is an important drop of pressure along the core, and high speed coolant flux. The speed can reach 15 m/s inside the fuel elements, and radial speed can reach 6 m/s in lower and upper plenum. The mechanism and the internal structures of the reactor have to be designed taking into account fluid induced efforts and vibrations.

3 INSERTION OF THE ABSORBER OPPOSITE TO THE FLOW AND NON EJECTION ENSURED BY TWO DEFENSE LINES

Early in the RJH project, it has been decided to have an upward cooling flow.

Two solutions were then conceivable for the CRDM: an insertion upward helped by the flow but opposite to gravity or an insertion downward helped by gravity but opposite to the flow. The second solution (insertion downward) has been selected because of the two main following reasons:

- Considering that the absorber is mechanically linked to a rod that crosses the bottom plug of the pool and gaskets, this rod is subjected to the upward drop of pressure of the core, but as well to the downward drop of pressure of the reactor. The downward drop of pressure of the reactor produces an additional force on the rod opposite to the flow.
- In some cases, the reactor is operated with no significant flow, but gravity is permanent.

The postulate ejection at high speed of an absorber at full power under the upward flow can potentially lead to the BORAX accident. It is a severe accident event following the safety methodology, the highest level below excluded events. This

requires to guaranty non ejection by means of two different ways called defense lines.

This accident does not concern emergency shutdown absorbers as they are already extracted from the core (to the upper position) when the core is diverged.

A schematic representation of the two defense lines is given on figure 2.

The first line is the rod with its mechanical connection to the absorber, down to the outside of the reactor, which is submitted to the core upward drop of pressure and to the reactor downward drop of pressure. As long as this assembly has no failure, the resulting force considering the hydraulic forces and gravity is oriented downward, to the direction of insertion.

The second defense line consists in limiting the upward hydraulic force applied to the rod by limiting the flow inside the guide tube of the mechanism. The flow must be limited enough so that the absorber do not eject even in case of a rod failure.
The water flow inside the guide tube is limited by means of:

- The core drop of pressure monitoring,
- The guide tube itself, at the end of which is fixed a hydraulic diaphragm.

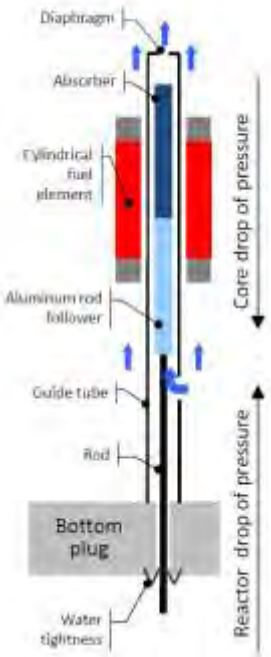

Figure 2 : schematic representation of the two defense lines to guaranty non ejection of the neutron absorber

The second defense line for non-ejection, as it limits the flow inside the guide tube, penalizes the refrigeration of the absorber and of its follower. The design is optimized for the efficiency of refrigeration.

As illustrated on Fig.3, the absorber is made of two concentric hafnium tubes (metallic material that benefits of a high and steady absorbtion cross section) around a central aluminum rod, and the follower is made of an aluminum tube around the same central aluminum rod. Thus the absorber has 3 gaps of water and its follower has 2 gaps of water inside the guide tube. All pieces are linked by sectors so that all

gaps are properly water fed. The assembly integrates a lower and upper rollers equipped carriages to guide the mobile rod inside the tube.

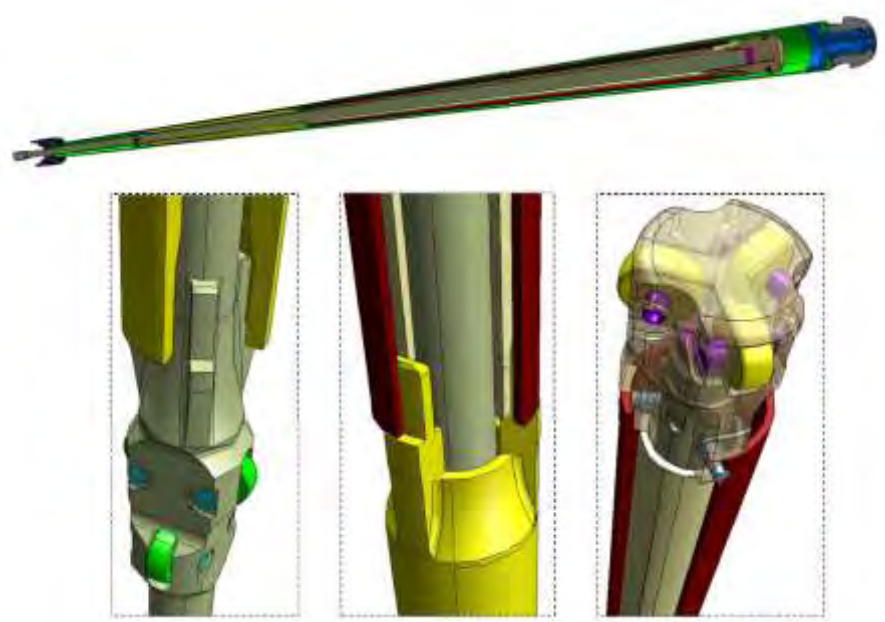

Fig.3 : illustration of the upper rod assembly; lower and upper carriages and connections between central rod, aluminum tube of the follower and hafnium tubes of the absorber

4 JHR CRDMS MAIN SPECIFICATIONS

JHR CRMDs main specifications are the followings:

- The stroke is 600 mm.
- ASA type mechanism (dedicated to emergency shutdown) must have a diverse design from AP and AC type mechanisms.
- Absorber insertion must be passive (applicable for ASA, AP and AC type mechanisms).
- Drop times of the rod (the reference instant is the electric cut off ; these values are technical target values ; safety values are higher):
  - ASA : 80% of the stroke < 0,4 second and 100% of the stroke < 0,8 second,
  - AP : 80% of the stroke < 1,4 second and 100% of the stroke < 1,8 second,
  - AC : 100% of the stroke < 5 seconds.
- Speed generated by the driving motor must be between 4 to 5 mm/s; a speed upper than 6 mm/s must not be possible.
- The 4 CRDMs dedicated to flux monitoring, must be able to produce repeated short stroke displacements of about 2 mm, with short time answer; frequency of short stroke displacements can reach one displacement per second.
- Drop times and driving speeds must be satisfied whereas the reactor is pressurized (nominal flow in the pressure vessel) or not (operating mode with the pressure limited to the height of the pool).
- Life time of parts located inside or near the core must be 3 years. Life time of other parts must be same as reactor life time (50 years) considering a reasonable periodic maintenance is acceptable.
- High reliability is required.
- Short time maintenance is required.

5 JHR CRDMS GENERAL PRESENTATION

Each of the 27 JHR CRDMs is made of:
- A guide tube and driveline assembly vertically loaded from the pool inside the reactor vessel, threw one of the core barrel cells;
- A water tightness system and an actuator below the pool plug; these components are of two types depending if it is an ASA or APAC type mechanism.

5.1 GUIDE TUBE AND DRIVELINE ASSEMBLY

The guide tube and the driveline assembly have had to be designed in two pieces each, because of the two main following reasons:
- Mechanism section that is in or near the core is exposed to high flux and has a limited life time.
- To avoid specific radiologic protection when components are handled above the top point of the pressure vessel, components length must be limited so that there is enough water above the component. Handling tools length is adapted to make sure that the minimum required water height is always guaranteed.

The two pieces are (see figure 4 for a representation of the subassemblies in the pressure vessel):
- Lower subassembly made of a lower guide tube in which takes place a lower driveline assembly;
- Upper subassembly made of an upper guide tube at the top of which is the diaphragm and in which takes place an upper driveline assembly, at the top of which are the absorber and the neutronic rod.

The lower guide tube is centered in the reactor at its two ends:
- Bottom end is centered in the locking plate (upper plate of the pool plug),
- Top end is centered in the bottom grid of the core barrel.

Once the lower guide tube loaded, the bottom end of the lower drive line assembly crosses the plug and reaches the maintenance water tightening housing fixed on the lower plate of the pool plug. This allows to obtain the maintenance tightness required for future mounting of the actuator.

The upper guide tube is connected to the lower guide tube by means of a self-locking bayonet energized by a spring. At this stage the bottom end of the upper driveline assembly is centered in the top end of the lower driveline assembly, the locking between the two drivelines being guarantied during future mounting of the actuator below (when the driveline assembly is lifted from its maintenance position to its bottom normal operation position).

A hydraulic dash-pot is integrated in the bottom end of the guide tube, to obtain a smooth deceleration of the rod at the end of drop, and such that the impact speed is minimized.

ASA and APAC type mechanisms have the same upper subassembly but specific lower subassemblies. Each type of mechanism has a specific drop speed and requires a specific dash-pot. ASA type mechanism includes a propulsion spring.

Each subassembly has a total length of about 3.3 meters during handling operation (drive assembly being then at its downstop position in the guide tube). The two pieces are loaded threw the core barrel cells, and must have a diameter limited to about 80 mm, limit that applies also to the handling tool. The upper part of the upper guide tube, on which the fuel element is loaded, has a diameter limited to 40 mm.

The weight of the lower subassembly is about 50 kg and the weight of the upper subassembly is about 10 kg.

The lower subassembly is made of stainless steel. The upper driveline assembly is made of aluminum 6061T6 except the absorber made of hafnium and the top carriage made of zircaloy. Upper guide tube is made of aluminum except the diaphragm made of zircaloy. The bottom end parts of the upper guide tube and of the upper drive assembly are made of zircaloy and iron so that there is no aluminum in the mechanical connections with the lower assembly.

The upper driveline and the upper guide tube have required a huge effort in terms of design and manufacturing studies to meet the RCCMX level 1 standards and dimensional and metallurgical specifications. Here are given examples of some technical challenges that have been achieved:

- External diameter of the aluminum guide tube is machined on its all length to obtain thin local keys which are the mechanical interfaces with the fuel element stiffeners.
- Each end of the thin aluminum guide tube is welded by electron beam.
- Lower carriage is machined straightly in the middle of the aluminum rod so that there is no mechanical junction along the rod; a specific industrial process allows to keep a good rectitude of the rod.

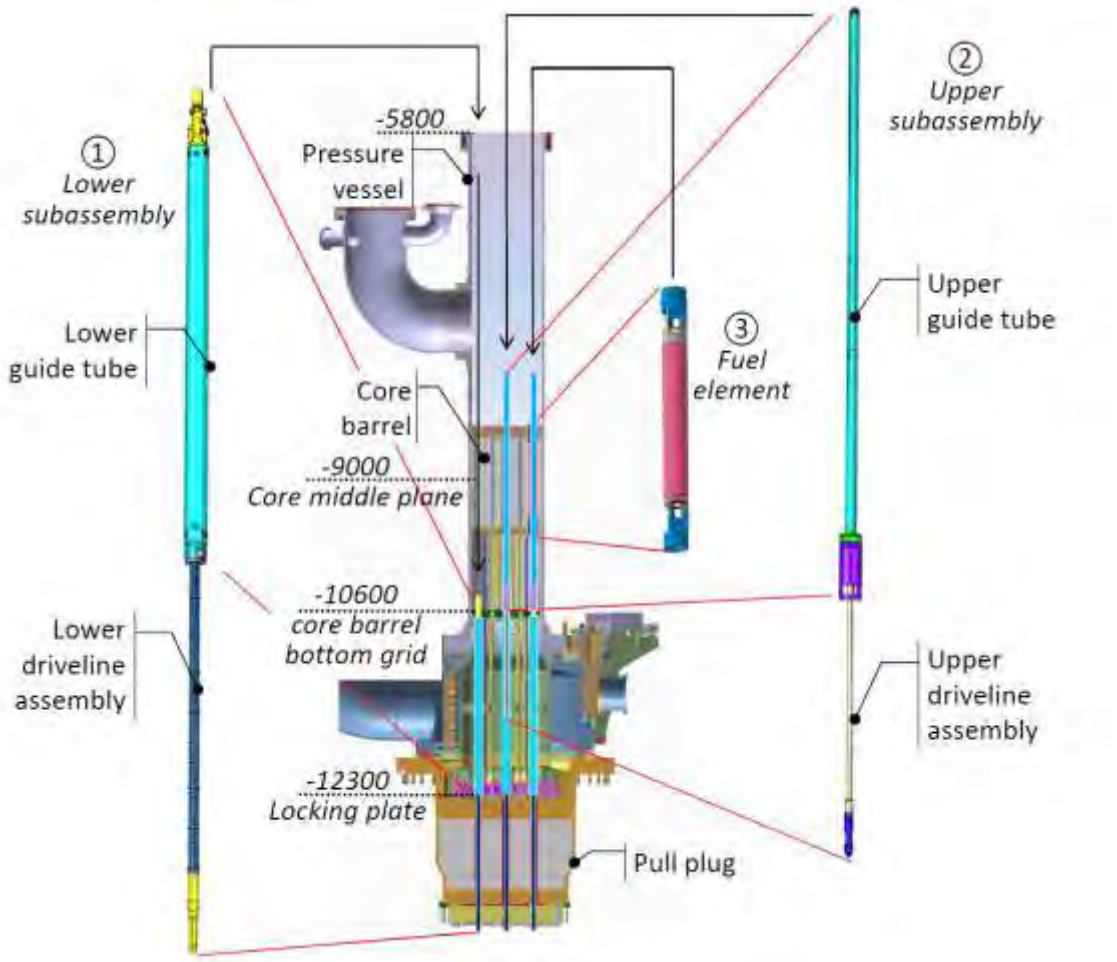

Figure 4 : upper and lower CRDMs subassemblies in the pressure vessel

Because of the high speed of the flow inside the reactor, specific disposals have been implemented to avoid fluid induced vibrations on the mechanisms:

- The driveline assembly is protected from high speed transverse flow by means of the guide tube. Water feeding of the guide tube is made by radial holes located below the core barrel bottom grid, where the flow is mainly axial.
- The lower guide tube is rigid. Specific elastic blades are integrated on each end of the tube to develop radial blocking forces once the tube is properly locked in the grids. Specific experiments have been led to determine the minimum radial force required.
- The connections inside the self-locking bayonet are made by means of conical junctions to eliminate mechanical clearances between the two parts of the bayonet.
- Along the fuel element and its three stiffeners, there are local thickenings on the guide tube to reduce mechanical clearance.
- Above the fuel element, the guide tube is covered by a thicker tube called the cap tube, which protects the guide tube from the flow outlet.

5.2 ACTUATORS

Actuators enable to drive the driveline assembly. The actuators are very different depending if it is an ASA type mechanism or an APAC type mechanism. An illustration of the actuators is given on figure 5.

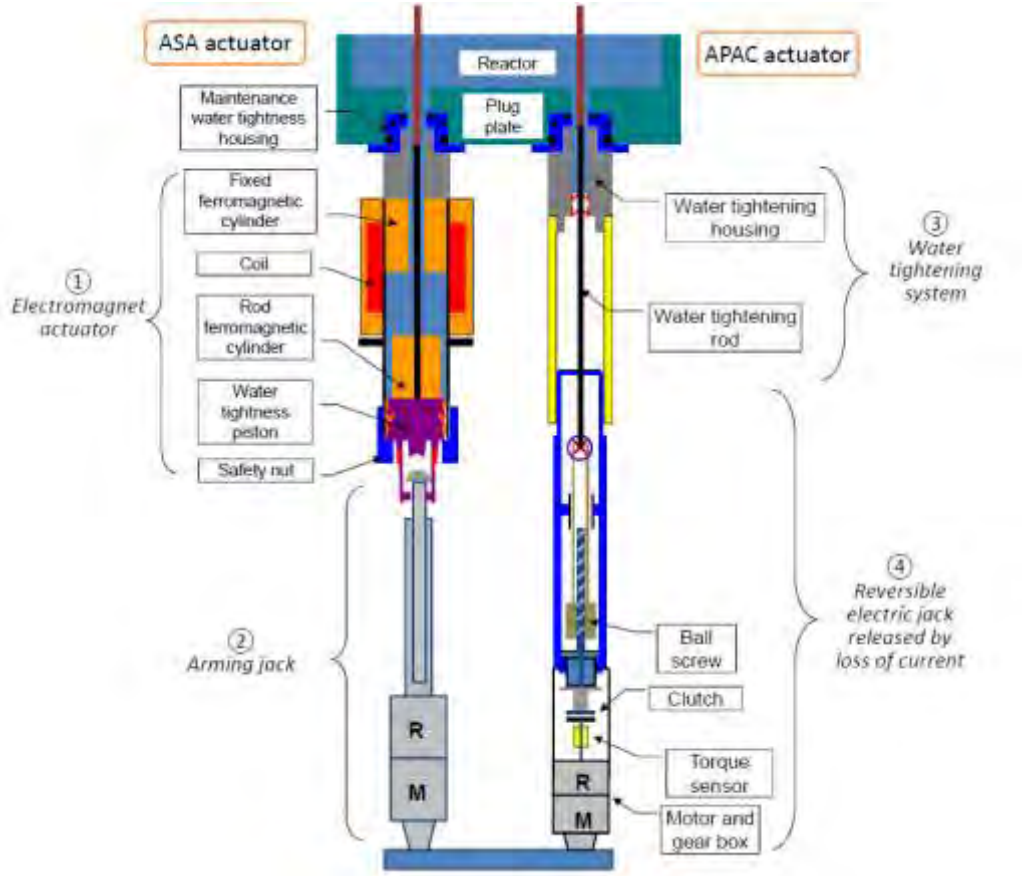

Figure 5 : illustration of ASA and APAC actuators

5.2.1 ASA type actuator

The ASA type mechanism operation is as follow:
- The ASA is armed before the core is diverged.
- Once the electric power is cut off, the ASA mechanism rod must drop as quickly as possible.
- Status of the mechanism (armed or inserted) is monitored with a high reliability level.

The main design features are:
- No water tightness along the driveline assembly, water tightness being made by separate parts.
- The driveline assembly is maintained in the upper position 100% magnetically by means of a specific magnetic actuator.
- An electric jack enables to arm the mechanism in the upper position.

The electromagnet actuator consists in a long cylindrical housing screwed in the bottom plate of the pool plug. A water tightness piston can be translated inside the housing by means of the electric jack located below. A safety nut at the bottom end of

the housing ensures that the piston cannot be disengaged. The bottom end of the rod inside the housing is equipped with a ferromagnetic cylinder.

By means of the jack, the piston and the mechanism rod that is laid down on the piston are translated upward, energizing the propulsion spring of the rod, up to the upper position where the ferromagnetic cylinder of the rod is stopped by a fixed ferromagnetic cylinder. The electromagnet coil is energized and the magnetic force holds the absorber in the upper position while the jack and the piston are translated back to the lower position. Electric cut off of the electromagnet triggers the drop of the rod.

A specific sensor detects the rod in its upper position and another specific sensor detects the piston in its lower position, which are the 2 conditions required to attest that the mechanism is loaded (ready to drop). A specific sensor detects the rod in the lower position to check the full insertion of the rod. Being safety functions, each type of sensor is repeated three times. Additional sensors are integrated to check the drop times of the mechanism during drop tests.

The jack integrates a stroke sensor and a force sensor to check the effort produced during the loading phase.

5.2.2 APAC type actuator

The APAC type actuator is made of a water tightening system and of a specific jack actuator. The jack is connected to the mechanism's driveling assembly, runs the translation of the driveline assembly, and must retract rapidly and passively on an electrical power cut off to allow the drop of the driveline assembly.

The water tightening system is made of a housing screwed in the bottom plate of the pool plug and equipped with two gaskets in which translates a rod of the driveline assembly.

From the bottom up, the jack consists in a motor, a reducing gear, a torque sensor, a clutch, a ball screw unit, the translating rod.

Once the clutch is energized, the electric motor operates the jack to translate the driveline assembly. At any time, because of the reversible ball screw, the electric cut off of the clutch triggers the drop of the mechanism, with the screw being put in rotation by the driveline assembly.

A specific sensor detects the rod in the lower position to check the full insertion of the absorber. Being a safety function the sensor is repeated three times. A cogwheel linked to the screw and a pair of detectors fixed on the frame, enable to monitor the rotation of the screw and the corresponding translation of the driveline assembly. Incremental detectors are used to check the stroke of driveline assembly during normal operation and to check the drop times of the mechanism during drop tests.

5.2.3 A challenging actuators arrangement

Actuators arrangement has to fit with the daisy pattern of the core which means 27 actuators fitted inside a cylindrical area of 700 mm diameter, with a 102 mm pitch between actuators, and a large number of electric components and sensors to wire.

It must be possible to mount or unmount an actuator safely, without risking loosing water tightness during operations. It must be possible to make maintenance on one system (typically gaskets replacement) with no action on the other systems that are fixed on the plug plate.

This has been made possible by designing specific actuators and specific tools for mounting assistance. The tools mainly consist in an articulated arm, mounted on a vertical beam, the vertical beam being mounted on a rotary crown. The operator rotates the vertical beam in the direction where he wants to operate. Different tools can be set on the arm, depending on the part to be mounted or unmounted. Here after is given a picture of the tool used on the hydraulic testing loop. This tool is similar to the one that will be used in the reactor except it is not fixed on a crown as only one mechanism is mounted in this case.

Figure 6 : articulated arm for actuators mounting on the hydraulic testing loop

6 DEVELOPMENT AND QUALIFICATION OF JULES HOROWITZ REACTOR CRDMS

A huge effort in terms of design and qualification process has been led by AREVA TA to meet JHR mechanisms specifications. Here after are given few milestones of the project.

Choice of a downward insertion of the absorber rather than an upward insertion, based on extensive studies of different solutions, taking into account neutronic, thermoydraulic, mechanical and safety aspects.

Development of a global numerical model of the two types of mechanisms to calculate important characteristics such as: efforts produced by the flow on the rod, location of the failure that could lead to an ejection, cooling performances, drop

performances. This model enabled to set the drop time values (technical target values and safety values).

Hydraulic tests on a mock-up to check drop of pressure along the absorber and the neutronic rod, flow speeds in the different gaps, the flow leading to the ejection of a broken part. These tests have been carried out at AREVA Technical Center at Le Creusot.

Development of specific components with selected suppliers and manufacturing of prototypes:
- ASA type mechanisms : electromagnet, propulsion spring, arming jack,
- APAC type mechanisms : electric motor, reversible screw nut,
- Both types of mechanisms : high safety level sensors (up and low positions detections), specific elastic blade for radial locking of the lower guide tube, under water internal connections.

Design and manufacturing of different mock-ups and benches for tests :
- Gaskets tests to determine friction, water tightness efficiency, and service life.
- APAC mock up tests: choice of a reversible screw/nut technology, selection of the pitch screw value, ratio of the gear box and motor technology; test of the ability to operate a load with no additional break on the motor and with repetitive small displacements; drop time measurement ; efficiency of the dash-pot deceleration.
- ASA mock up tests: piston tightness efficiency; electromagnet efficiency and water gaps required for the drop speed.

These tests have been carried out by AREVA TA in Cadarache testing facility.

Detail designed has been optimized all along the development and qualification process, taking advantage of all tests results and using many of AREVA TA's areas of competence such as geometrical functional analysis, thermo-mechanical calculations, safety and reliability, I&C, integrated logistic support. Also an exhaustive industrial study has been led with the main manufacturer of JHR CRDMs that is Technoplus Industries located near Cadarache.

All these steps enabled to manufacture one mechanism of each type and a specific hydraulic loop to start functional tests by the year 2014.

7 FUNCTIONAL AND ENDURANCE TESTS ON A DEDICATED HYDRAULIC LOOP

Being a major safety component of JHR reactor, control rod drive mechanisms have to fulfill an exhaustive qualification process among which functional and endurance tests on a dedicated hydraulic loop. Test conditions in the loop must be the most representative possible as reactor conditions. Below is given a short description of the hydraulic loop, and presented main drop tests results.

7.1 JHR MECHANISMS HYDRAULIC LOOP

The loop is designed to test one mechanism at once, either an ASA or APAC type mechanism.

The loop is made of a hydraulic section about 6.5 m long above a pit where can be mounted the actuators, the total length being 10 meters. An external circuit allows monitoring the flow inside the mechanisms, the inlet pressure and the fluid temperature. The inlet pressure is made constant during mechanism drop transitory by means of a hydraulic accumulator. The outlet pressure results of the diaphragm being used on the mechanism.

The loop has the same mechanical interfaces as the reactor's (material and dimensions). Vertical alignment between mechanical interfaces can be adjusted to fit to the possible misalignments calculated for the reactor. The referential alignment in the loop is checked by tracker laser. The fuel element interfaces are made by 3 cells, which are mounted around the guide tube and can be misaligned also. The upper hydraulic section can be opened and swiveled on the side to make it easier to load mechanism's lower subassembly. Dedicated tools are used to load mechanical subassemblies. An articulated arm is settled in the pit, similar to the one that will be used in the reactor, to mount or put down the the watertightness system and the actuator.

Few adaptations have been made on CRDMs prototype to benefit of specific measurements very useful for functioning analyses, such as:

- Dash-pot room pressure measurement,
- Speed and displacement measurement by a cable displacement sensor ; this sensor is very useful for ASA type tests made at atmospheric pressure with the hydraulic section opened at the top, the cable of the sensor being connected straightly to the top of the rod,
- Multi-intermediate positions detection for ASA prototype mechanism (whereas only one intermediate position is detected on reactor),
- APAC actuator thrust force in addition to screw torque measurement to check screw nut efficiency.
- Electric actuators temperature measurments.

A dedicated monitoring system enables a manual and an automatic drive of each type of mechanism during tests. Electric components have been chosen to be the most representative as the ones defined for the reactor electric boards. Some electric parameters are measured, such as the drop of current that ignites the drop of the mechanism.

Here after are pictures of the test facility and of an ASA type actuator mounted on the loop.

Figure 7 : overview of the test facility with the hydraulic loop and the pit

Figure 8 : ASA type actuator mounted on the loop

7.2 MAIN DROP TESTS RESULTS

Here after are given the main drop tests results of ASA and APAC type mechanisms (drop trajectory measurement compared to drop time target values).

- ASA type mechanism (Figure 9): drop trajectory is measured by means of 26 intermediate position detections; tests are made with no flow and with different levels of flow; the flow increases slightly the drop times ; target values are respected in all cases.
- APAC type mechanism (Figure 10): drop trajectory is measured by means of the incremental detector of the actuator (300 points for the total stroke); tests are made with no flow and pressure, and with flow and pressure; the pressure significantly reduces the drop times ; target values are respected in all cases.

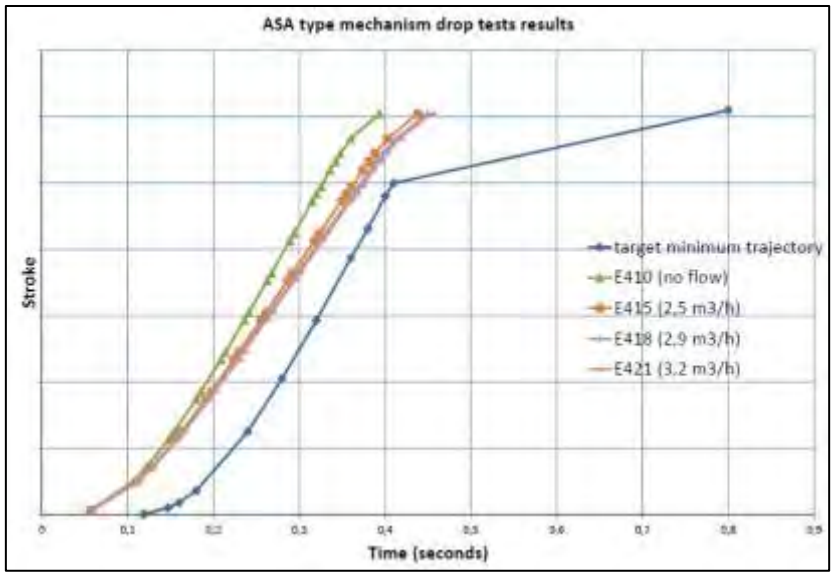

Figure 9 : ASA mechanisms drop tests results

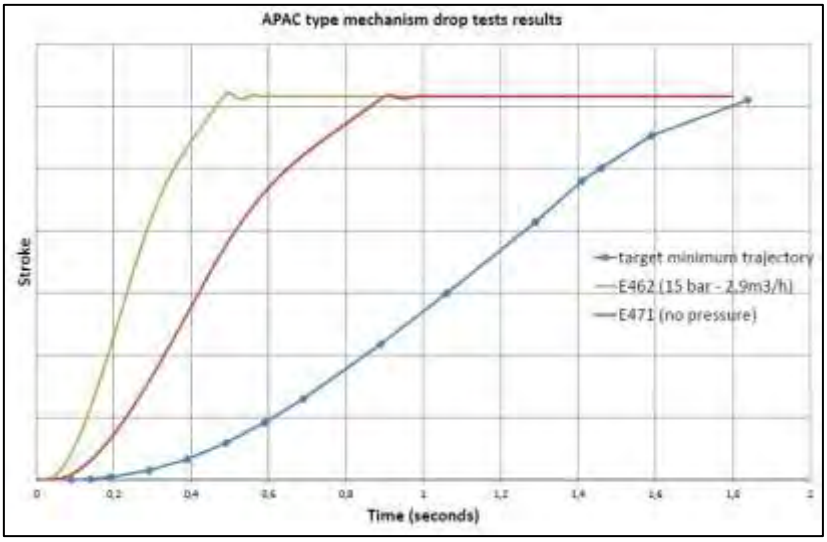

Figure 10 : APAC mechanism drop tests results

8 CONCLUSION

JHR CRDMs have required a huge effort in terms of design and qualification process led by AREVA TA, and still require an important effort up to the commissioning of the CRDMs on the reactor.

Endurance tests are actually being led on the hydraulic loop with good first results. Some other important tests still have to be done such as reliability tests and should be achieved by the year 2016.

The actual level of qualification has been considered high enough to authorize AREVA TA to start manufacturing of the 27 mechanisms for the reactor, the mounting on reactor being planned by the year 2017.

Poster decommissioning

Safety and regulatory aspects of shutdown operations and decommissioning of Phénix Reactor

X. Masseau[1], Stanislas Massieux[1]

[1]Institut de Radioprotection et de Sûreté Nucléaire (IRSN), Fontenay-aux-Roses, France

E-mail of the corresponding author: xavier.masseau@irsn.fr

Abstract. Phénix NPP is a sodium-cooled fast breeder reactor dedicated to research purposes as well as electricity production. Phénix NPP was shut down in 2009. This paper describes the regulatory and technical process related to the transition between the reactor shutdown and the beginning of the decommissioning operations, in the context of a periodic safety review.

Key words: Decommissioning, Licensing process, Permanent shutdown, Phénix NPP.

1. Introduction

This paper aims to describe the transition between operation and decommissioning in France with the example of the Phénix NPP sodium-cooled fast breeder reactor. A focus will be made on the authorization process as well as the safety reviews for the operations that will be conducted as from the shutdown of the facility. This paper will address the particular situation of the Phénix NPP facing at the same time the regulatory review process for decommissioning and the regulatory requirements to conduct periodic safety review for nuclear facilities.

The *Commissariat à l'énergie atomique et aux énergies alternatives* (CEA) was commissioned by decree of 31st December 1969 to create and operate a sodium-cooled fast breeder reactor called Phénix.

The Phénix NPP is located at the Marcoule nuclear site in southern France and was connected to the grid in 1973 with an electric output power of 250 MW. After a refurbishment in 1999-2003, which improved seismic stability and fire protection of the nuclear premises, the Phénix authorized thermal power was decreased by one third for safety reasons. Phénix was disconnected from the grid in 2009. In addition to electricity producing, Phénix prototype has played a role as a research reactor.

The CEA has been proceeding to preliminary operations in order to prepare Phénix dismantling. These operations mainly consist in nuclear fuel and internal heavy equipment removal. As they are conducted during the transition between cessation of operation and the beginning of the dismantling actions, the paper describes them and focus on their safety assessment, including the management of the remaining risks after the end of these operations.

2. Phénix NPP presentation

Phénix NPP is designed as a pool-type sodium-cooled fast breeder reactor. Its conception principles are similar to any sodium fast reactor (see *FIG.1.*).

The Phénix NPP is designed as an integrated reactor block except for a few auxiliary circuits such as the primary sodium purification circuit. The entire primary sodium system contains about 800 tons of sodium and is enclosed in the 11.8 m diameter main reactor vessel.

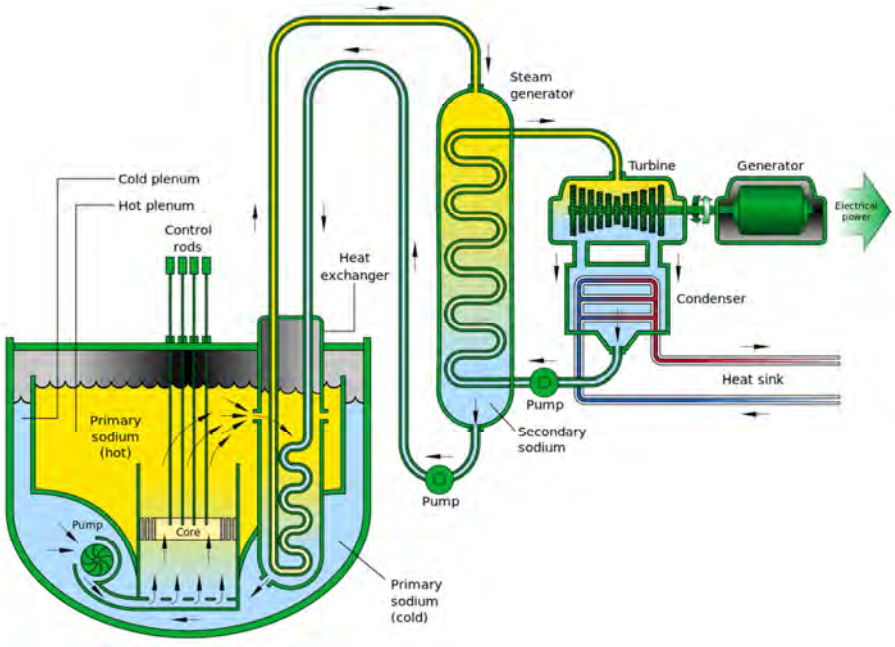

FIG. 1. A pool-type sodium-cooled fast reactor
Credits: http://www.gen-4.org/

3. Phénix NPP dismantling strategy and scenario

In compliance with the IAEA recommendation, the CEA has chosen an immediate dismantling strategy for the Phénix NPP. This strategy allows the CEA to benefit from analogue projects in France or abroad, especially on other sodium-cooled fast breeder reactors (Superphénix, Rapsodie, KNK II…). The dismantling strategy aims to reach an end state which is (in the case of Phénix) the decontamination and clean-up of every building after the removal of all equipment.

Several phases are needed to achieve a full decommissioning. Five main phases are identified by the CEA:

- preliminary operations (condenser and turbine removal, fuel core removal, control rods removal, heat exchanger and primary pumps dismantling),
- liquid sodium hydrolysis with a dedicated new installation (called NOAH, stands for NaOH – *sodium hydroxide*),
- sodium-contaminated waste treatment with a dedicated new installation (called ELA – stands for *Enceinte de Lavage en Actif - Active Washing Chamber*), and radioactive waste temporary storage,
- reactor block dismantling,
- facility final clean-up and decontamination.

At the end of these operations, which are planned to be completed before 2045, the CEA will demolish the NOAH and ELA new installations but will keep the existing buildings. The CEA may apply for the administrative decommissioning (i.e. release of the facility from regulatory controls or de-licensing) once the decontamination is achieved.

4. Regulatory aspects

4.1. Commissioning and decommissioning decrees

The life cycle of a nuclear facility is regulated by several decrees throughout its life.

At first, a commissioning decree allows the licensee to create and operate a nuclear facility. At the end of the operating period of the facility, once the reactor is shut down, a decommissioning decree is issued so the licensee can perform dismantling actions. However, this decree is issued after a transition period which starts at the permanent shutdown of the facility (see *FIG.2.*).

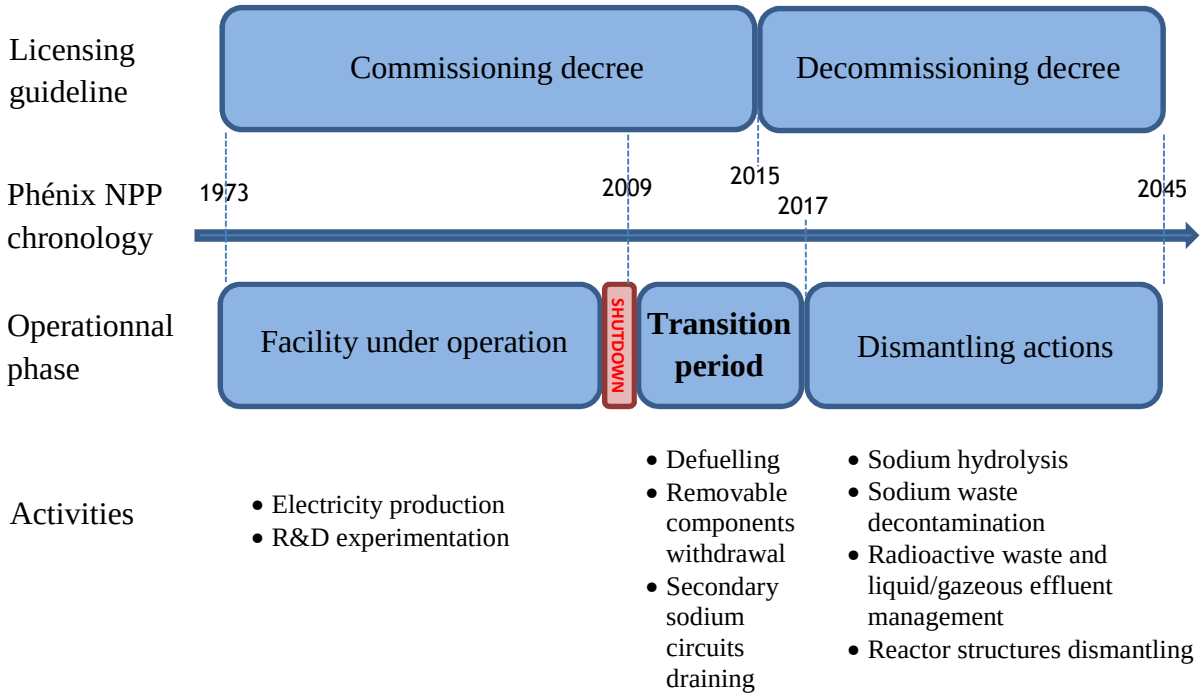

FIG. 2. The Phénix NPP life cycle and regulatory milestones.

Once the targeted end state is achieved, a ministerial order ratifies the de-licensing of the nuclear facility so the facility is not considered as a nuclear installation anymore.

In France there is however no "*back to the greenfield*" status. Even after decommissioning, a public servitude is imposed to the existing location to retain the memory and to possibly limit further use of the location if there were to be left some significant residual radioactive contamination. This is not generally a problem for the nuclear licensees since the decommissioned location is generally intended to be reused for industrial purposes.

4.2. Authorisations for discharges of radioactive and chemical effluents

The existing authorisation for liquid and gaseous effluents discharges remains valid during the transition period, since the operations performed during the transition are covered by the commissioning decree. In the case of Phénix NPP, some dismantling actions will, in a few years, lead to a significant increase of the volumes and activities due to the chemical effluents release produced by the primary sodium disposal. Radioactive and chemical effluents discharge generated by the dismantling actions will be updated accordingly and addressed under the decommissioning license (or decree).

4.3. Periodic safety review

Besides the commissioning decree, the licensee must demonstrate the ability of the facility to be safely operated, using an extensive safety review, throughout the next decade.

In France the licensing of a nuclear facility is given once and for all for an unlimited period of time. The regulatory requirements however stipulate that a safety review must be conducted every 10 years at least. This audit have to take into account feedback from safety and radiation protection (i.e. dosimetry), effluents discharges, radioactive waste, anomalies, incidents, as well as the feedback from events or accidents that happened on similar installations in France or abroad. The periodic safety review aims to assess the safety of a nuclear facility situation under the applicable rules, and to update the appreciation of the risks and inconveniences against interests[1] listed in the L. 593-1 article from the *Code de l'Environnement.*

A safety review case consists in two parts:

- a conformity review aiming to assess the facility evolutions (ageing, modifications, material obsolescence...),
- a safety reassessment, taking into account the conformity review and aiming to review and improve the facility safety level, using best available techniques and latest safety and radiation protection standards.

5. The transition period

5.1. Objectives

The transition period takes place between the permanent shutdown (the term "permanent shutdown", as used in this publication, means that the facility has definitively ceased operation and operation will not be recommenced, accordingly to IAEA General Safety Guide Part 6) of the reactor and the beginning of the dismantling operations.

The transition period typically include defuelling and removal of minor components as well as some operational waste management. These operations are covered by the facility applicable safety report. For the Phénix NPP, these operations are:

- the continuation of sodium heating and purification,
- the nuclear fuel removal from the core,
- the removable equipment withdrawal (primary pumps, intermediate heat exchangers).

[1] *public security, health and safety, protection of nature and the environment*

There are two main goals for the transition period. In one hand, they aim to put the facility in a stable condition and to reduce hazards related to the operation length. On the other hand, the licensee intends to reorganize the facility management. In this concern, the Phénix NPP has changed its organization and management system in order to be able to conduct future dismantling operations: some organizational aspects, such as feedback and subcontractors management, need to be updated to match the new needs.

The remaining risks after the transition period will be similar to any nuclear facility undergoing decommissioning (fire hazard, exposure of workers to ionizing radiation, radioactive material dissemination...) in addition to the sodium specifically related risks.

The operating license remains valid during the transition period. Operations to be performed in this period, must already be authorized by the commissioning decree (see TABLE.I.).

TABLE I: THE SAFETY DEMONSTRATION APPROACH TO COVER TRANSITION PERIOD AND DISMANTLING ACTIONS

Operations	**Covering safety demonstration**	
	Safety reassessment	**Dismantling operations safety assessment**
Sodium heating and purification	✔	
Nuclear fuel and small core components removal	✔	
Fresh fuel storage	✔	
Sodium disposal preliminary operations		✔
Sodium disposal (NOAH facility)		✔
Sodium-contaminated waste disposal (ELA facility)		✔
Reactor block dismantling		✔
Dismantling mutual operations (waste storage, sodium draining…)		✔

5.2. Phénix NPP transition period in the context of a periodic safety reassessment

Each licensee must conduct a safety reassessment every 10 years at least. In the case of Phénix NPP, the licensee chose to anticipate the safety reassessment date (which was required to be performed in 2017) and to align it with transition period and dismantling needs.

The objective of the safety reassessment was to demonstrate the safety of the transition period operations. In this concern, the safety reassessment ensures the facility will match the specifications required by the future dismantling actions. For instance, temperatures and thermal cycling of sodium circuits are likely to be different between operation and

dismantling, so their specifications needed to be reassessed. This shall also apply to handling and lifting devices, as well as ventilation and containment systems.

6. The IRSN assessment

As a technical support organization for the Nuclear Safety Authority (ASN), the IRSN reviewed:

- the safety report of dismantling actions in support of the final decommissioning plan, including radioactive waste and effluent management,
- the safety reassessment in the spotlight of the transition period operations which are planned to take several years.

In particular, the conformity assessment of the Phénix NPP performed by the licensee highlighted that some equipment will be used throughout both the transition and dismantling periods, especially containment systems, sodium pipes/capacities and lifting/handling devices. The foreseeable operating range of the sodium pipes and capacities for the transition period operations (sodium draining and transfer) has also been reassessed.

The IRSN also reviewed the safety assessment of the future workshops (NOAH and ELA) that will be built in the purpose of sodium and sodium-contaminated waste chemical treatment.

IRSN experts on human and organizational aspects considered that the technical and organizational provisions implemented by the licensee to limit the risks and inconveniences of the Phénix NPP, first in its current configuration, second in future sodium treatment and dismantling operations, are overall satisfying.

In conclusion, the IRSN review of the safety reassessment concluded to the ability of Phénix NPP to match the requirements of the transition period operations and to safely prepare the upcoming dismantling actions.

The IRSN underlines the innovative nature of the Phénix NPP safety assessment review process, as it was conducted in the light of future dismantling actions requirements. This process allowed the licensee to anticipate the required human and organizational aspects, as well as the expected behaviour of existing equipment.

The IRSN finally emphasizes the need for milestones before each main dismantling phase in the upcoming decommission decree. Considering the technical description and safety assessment of some long-term dismantling actions, such as the reactor block dismantling, cannot be precisely defined today, these milestones will be an opportunity for the safety authority to ask for a precise safety assessment prior to the beginning of each phase.

Poster innovative methods

DESIGN OF A DRY BEAM RADIATION SHIELDING PLUG FOR RESEARCH REACTORS

H. G. MEIER, D. F. HERGENREDER

INVAP S.E.
Comandante Luis Piedra Buena 4950, CP: 8400, San Carlos de Bariloche, Río Negro - Argentina
hgmeier@invap.com.ar - dhergenreder@invap.com.ar
http://www.invap.com.ar/

ABSTRACT

Multi-purpose research reactors are commonly designed and constructed with radiation extraction beam tubes. These tubes are used to transport photons and neutrons to irradiation facilities far away from the reactor core. A normal procedure when no irradiation experiment is conducted, it is to disable the beams filling the beam tube with water. Water is used because it is a good radiation shielding material, but it can also corrode the tube material increasing the probability of having a loss of coolant accident (LOCA)
The aim of this work is to design a dry beam radiation shielding plug that replaces the water inside not used beams. A dry plug decreases the corrosion tube risk, but has also to ensure the radiation shielding efficiency. The modularity of the shielding plug is a very important requirement in order to ease the manoeuvre of installation and un-installation inside the beam tube.
Radiation shielding efficiency can be measured by dose rates minimization criteria. Dose rates at the end of the plug are produced by neutron and photon fluxes. Some photons are transported from the core but others are created by neutron capture during the neutron flux attenuation. Neutrons and photons are not equally shielded, thus a combined radiation shielding strategy with different modular materials has to be used.
The design verification is carried out using a stochastic transport method code which calculates the neutron and photon flux profiles and spectrums through the different materials modules and then the dose rates at the end of the plug. The optimum design of a dry beam radiation shielding plug is the result of combining the modularity requirement with the transport calculations.

1 Introduction

This study is focused on pool type multi-purpose research reactors which are commonly designed and constructed with radiation extraction beam tubes. These tubes are used to transport photons and neutrons to irradiation facilities far away from the reactor core.

In order to transport photons and neutrons without significant flux decrease, extraction beams tubes lay inside the pool close to the core and penetrates the reactor tank and the reactor heavy concrete block till the irradiation facilities. This direct path from the core means that beam tubes have to be appropriately shielded in order to protect operators and public in the experimental halls. Also, every core tank penetration, like extraction beams tubes, have to be designed, constructed and maintained with the criteria of reducing the loss of coolant accident (LOCA) risk.

A normal procedure when no irradiation experiment is conducted, it is to disable the beams filling the beam tube with water. Water is used because it is a good radiation shielding material, but it can also corrode the tube material increasing the probability of having a loss of coolant accident (LOCA)

2 Development

The aim of this work is to design a dry beam radiation shielding plug that replaces the water inside not used beams. A dry beam plug decreases the corrosion tube risk and also has to ensure radiation shielding efficiency.

A second order goal is to achieve a modular design in order to ease the manoeuvre of installation and un-installation inside the beam tube.

2.1 Reactor and Extraction Beam Characteristics

The adopted pool type multi-purpose research reactor for the study has a Material Testing Reactor (MTR) fuel core of 3.5 MW_{th} power. The core is inside a 150 cm radius light water pool which is also in a 200 cm width heavy concrete block.

The extraction beam has two tubes, one of 8 in. and other of 10 in. diameter each. In the tube intersection there is a 1 in. lead jacket. Finally, the extraction beam is closed at reactor face by a 30 cm lead block.

A schematic lay-out of the reactor and the extraction beam is shown in Fig. 1.

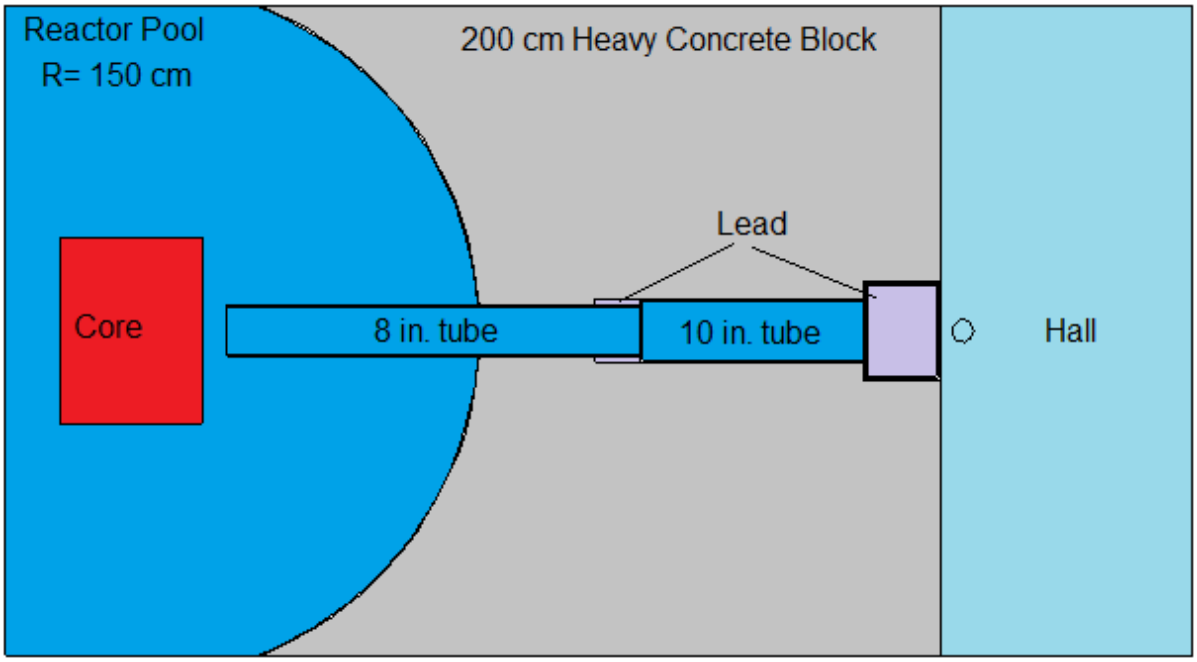

Fig 1. Lay out of the pool type multi-purpose reactor and extraction beam tube when is disabled and filled with water.

2.2 Design Criteria

Radiation shielding efficiency can be measured by dose rates minimization criteria. Dose rates at the end of the plug are produced by neutron and photons fluxes.

The adopted shielding criterion is to achieve the same shielding efficiency that has the beam filled with water. Due to neutrons and photons are not equally shielded, a combined radiation shielding strategy with different modular materials has to be used.

These modular materials have to be enough light to allows an easy handling and a quick back to service of the beam, the adopted criteria is to have modular block that weight less than 50 kg.

2.3 Dose Rate Calculation

Equivalent ambient dose rate, from now on simply dose rate, is calculated using a stochastic transport method code, MCNP5 v1.6 [0], which calculates the neutron and photons flux profiles and spectrums through the different materials modules and at the end of the plug.

To convert to dose rate, neutron and photon fluxes are multiplied by conversion coefficients from ICRP-74 [2].

2.4 Dry Shielding Plug Design

The plug has to shield from the neutron and photon fluxes coming from the core, and photons created by neutron capture during the neutron flux attenuation.

Typical neutron shielding scheme first uses a light Z material that lower the neutron energy to take advantage of a larger absorption cross section at low energy. Then, to complete the task a good neutron absorbing material is used.

Conversely, for photon shielding is better to use large Z materials. In our situation due the generation of photons via neutron captures is better to allocate the photon shielding after the neutron shielding modules. The adopted modular shielding scheme consists of:

a. 140 cm of Graphite inside the first 8 in. tube divided in two cartridge of 70 cm length of approximately 40 kg each.
b. Two 30 cm length concrete blocks inside the 10 in. tube. With 2.3 g/cm^3 density each one weights approximately 35 kg.
c. A 1 cm cadmium plate after the concrete blocks, approximately weight 5 kg.
d. A 5 cm lead plate after the cadmium plate, approximately weight 25 kg.

The graphite cartridges are for neutron moderation, the concrete blocks and cadmium plate for neutron absorption. Finally, the lead plate and block are used to shield photons. The described lay-out is shown in Fig.2.

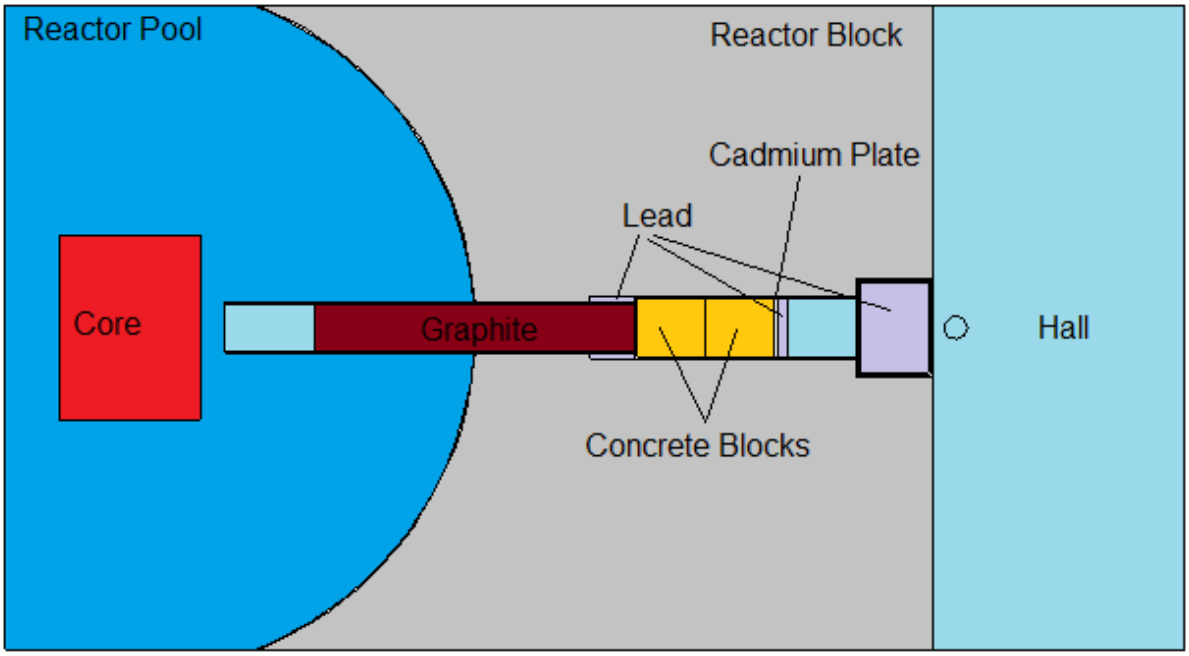

Fig 2. Lay-out of the proposed dry shielding plug design.

2.5 Modelling

The MCNP 5.1.6 general used model includes a box that represents the core, the light water pool, the heavy concrete block, both beams tubes and the lead jacket and rear lead block.

Then two specific models are used:

a. Water filled model: is the general model but with both beam tubes filled with water
b. Dry shielding plug model, is the general model but with the shielding modules inside the tubes.

The neutron and photon source is obtained with a previous calculation where an all control rod out 3.5 MW_{th} power core is modelled and all particles that cross core box surfaces are saved.

Then the saved superficial core source is taken to transport neutron and photons across the extraction beam. To obtain better statistic of transported particles through shielding material far away from the core, the importance scheme technic [1] is used.

3 Results and Discussion

Considering the weights of the different parts of the plug it can be seen that the proposed design fulfils the easy handling criteria.

The radiation shielding efficiency criteria is evaluated comparing dose rate calculation for the water filled model against the dry shielding plug model. Furthermore, detailed neutron and photon flux maps and figures will be shown in order to achieve a better understanding of the shielding process.

All the calculations here presented have results with relative statistical error of less than 10.0 % at 1σ.

3.1 Water Filled Results

Fig. 3 shows the neutron and photon dose rate maps for the water filled beam model. The calculations show, as it is expected, that water shields better neutrons than photons.
Neutron dose rate at the end of the extraction beam is less than 1 μSv/h while for photons is less than 30 μSv/h. The aim of this work is to obtain a dry shielding beam plug that have equivalent shielding performance.

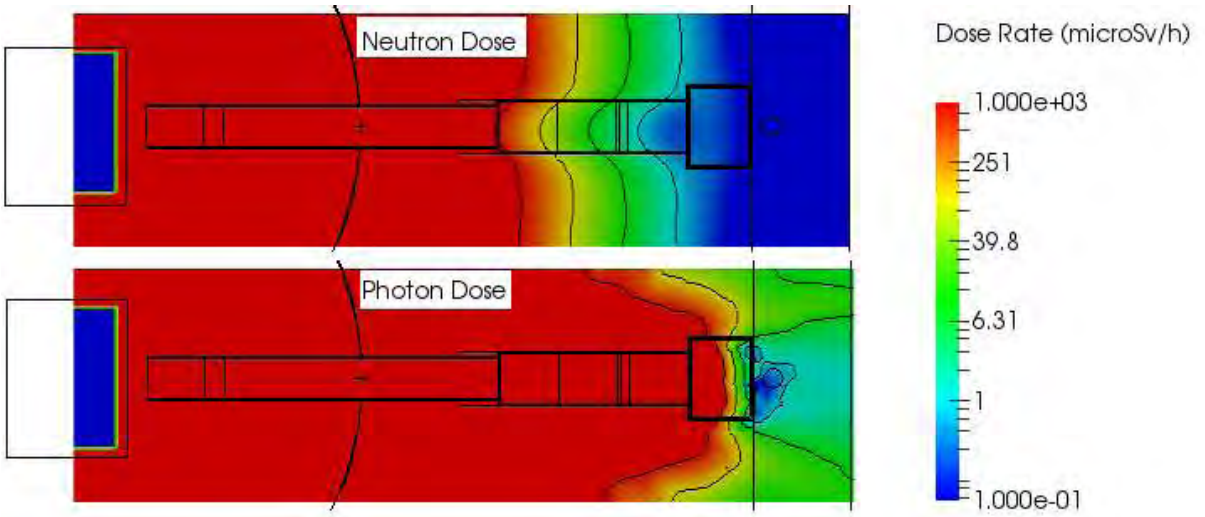

Fig 3. Neutron and photon dose rate maps in water filled beam model.
Each map shows iso-surfaces at 1000, 100, 10 and 1 μSv/h.

3.2 Dry Shielding Plug Results

Fig. 4 shows the neutron and photon dose rate maps for the dry shielding beam plug model. In this case neutron dose rate is larger than photon dose rate.

Neutron dose rate at the end of the extraction beam is lower than 10 μSv/h while for photons only directly behind the lead block is under 1 μSv/h but outside the lead block shadow it reaches 10 μSv/h.

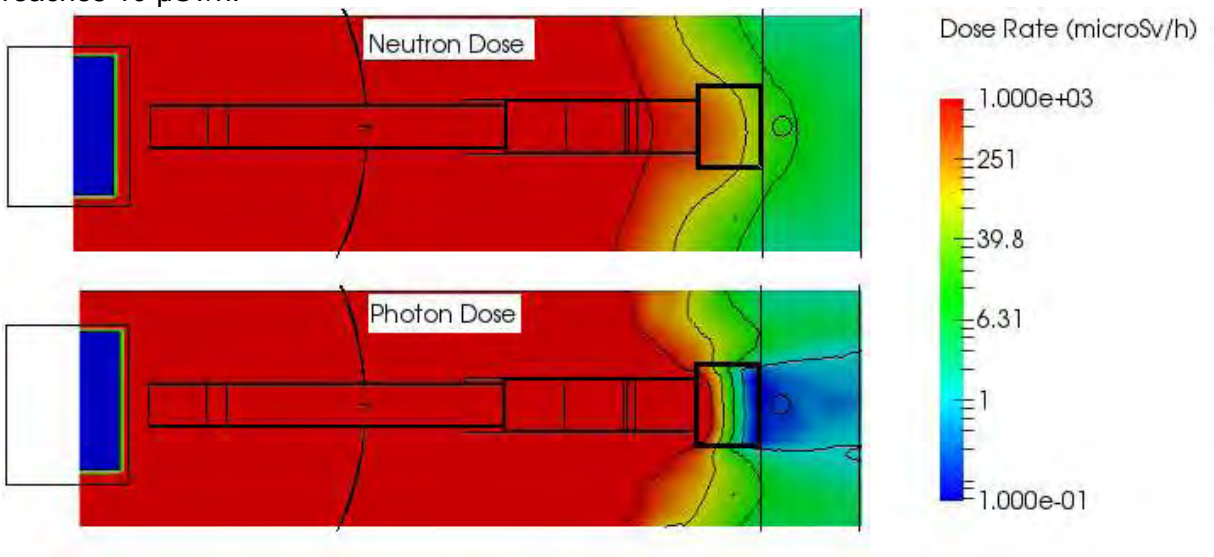

Fig 4. Neutron and photon dose rate maps in dry shielding beam plug model. Each map shows iso-surfaces at 1000, 100, 10 and 1 μSv/h.

3.3 Material Shielding Behaviour

Fig. 5 presents the neutron and photon fluxes at different distances from the core. The slopes of the curves shows how neutron and photons are attenuated for the different materials, water better shields neutrons while lead better shields photons.

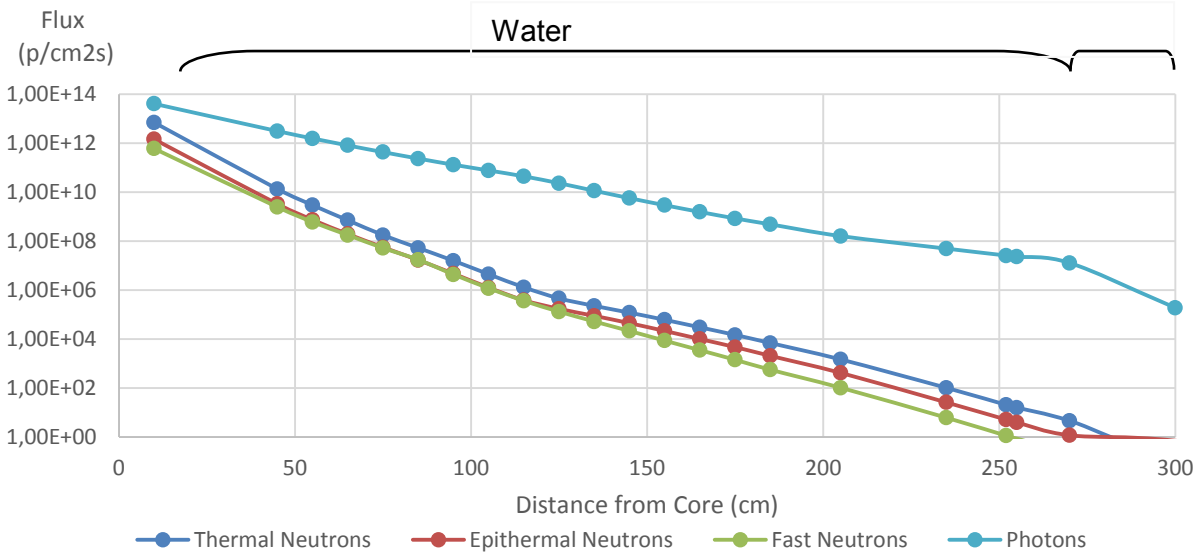

Fig 5. Neutron and photon fluxes vs core distance in water filled beam model.

Fig. 6 shows the same as Fig.5 but for dry shielding beam plug case.

For neutrons, it is seen how at the end of the graphite modules the thermal neutron flux increases due to the moderation of the fast and epithermal flux. The increased thermal flux then at 250 cm from the core it is absorbed by the cadmium plate due to its large thermal neutron abortion cross section.

For photons, it is seen that most flux attenuation shows up at the end of the beam where the lead modules are positioned.

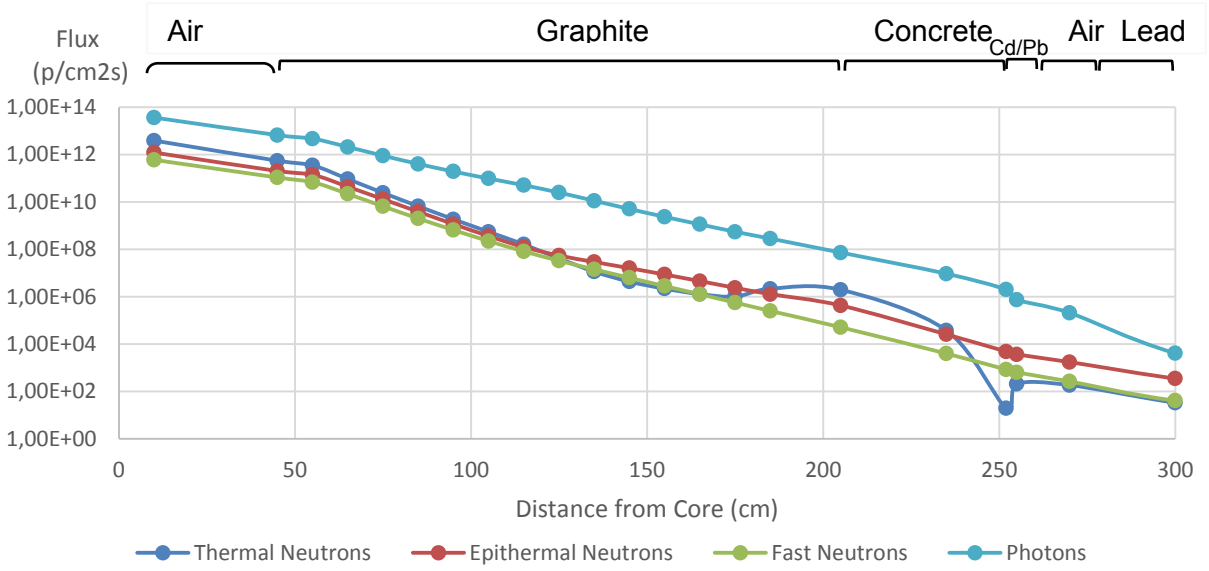

Fig 6. Neutron and photon fluxes vs core distance in dry shielding beam plug model.

In Fig. 7 there are neutron fluxes maps at different energies. The iso-surfaces shows how fast and epithermal flux decrease while thermal flux increases until it reaches the cadmium plate and it is absorbed.

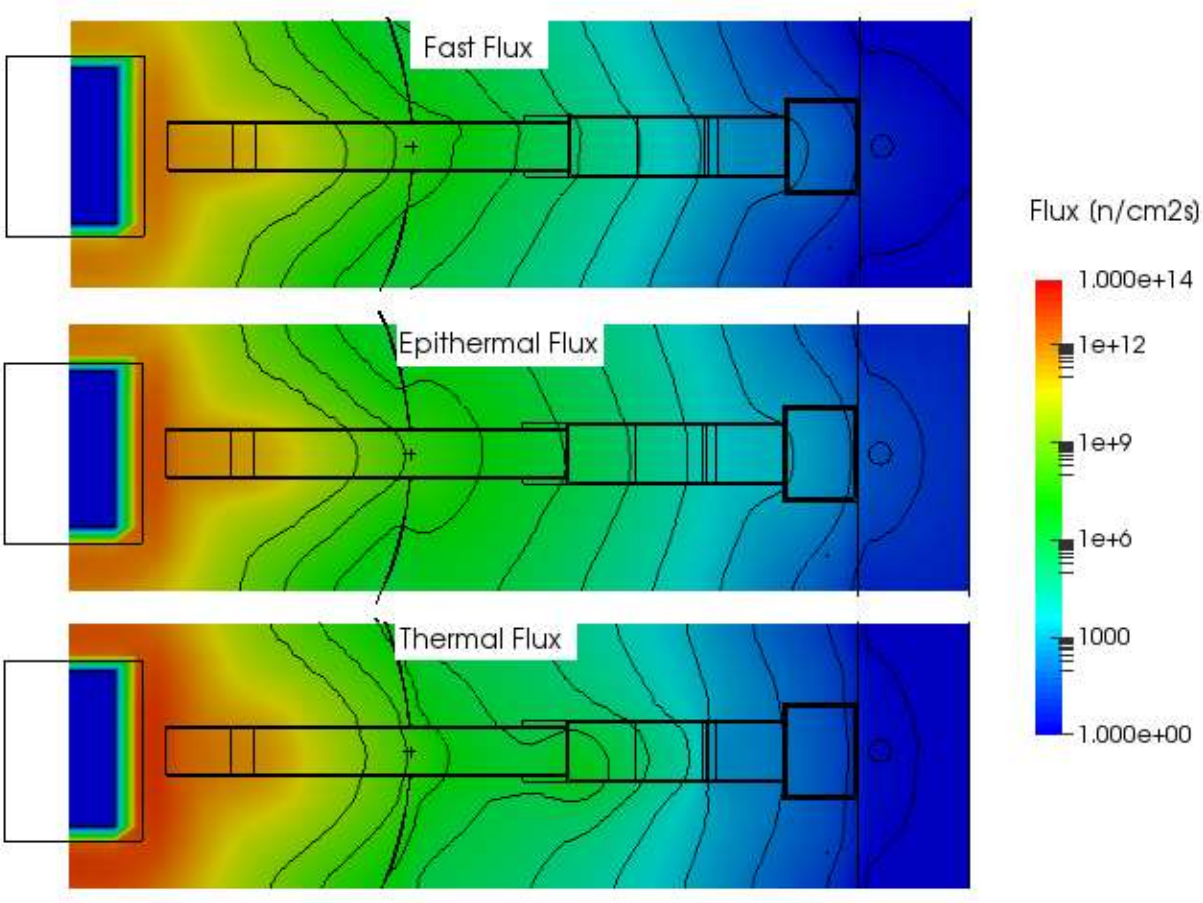

Fig 7. Neutron fluxes maps for dry shielding beam plug.
Each map shows iso-surfaces at 10^9, 10^8, 10^7, 10^6, 10^5, 10^4, 10^3, 10^2, 10 and 1 n/cm^{2}s.

Fig. 8 has a photon flux map. The iso-surfaces shows also how the maximum attenuation occurs at the end of the beam where the lead blocks are positioned.

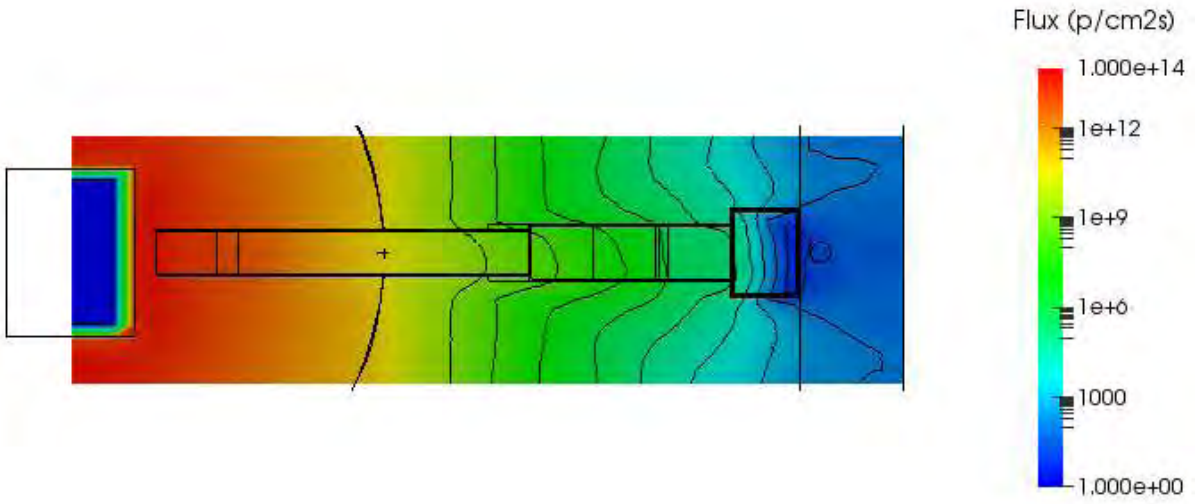

Fig 8. Photon flux map for dry shielding beam plug.
The map shows iso-surfaces at 10^9, 10^8, 10^7, 10^6, 10^5, 10^4, 10^3, 10^2, 10 and 1 p/cm^{2}s.

4 Conclusions

A modular design of a dry shielding beam plug is presented. The design fulfils both proposed design criteria.

Dose rates maps in Fig.3 and Fig.4 shows that the dry shielding beam plug has a shielding efficiency equivalent than water filled beam case, both dose rate of less than 30 μSv/h. Furthermore, the ease of handling criteria is fulfilled by the modular components which are enough light in weight as proposed.

The proposed dry shielding beam plug case shows a larger neutron than photon dose rate. This results is well explained due to the different material shielding behaviour seen in the flux maps and graphs from Fig. 5, 6, 7 and 8.

5 Acknowledgement

This work have been done with the support of the Nuclear Energy Department (DIN) of INVAP S.E.

6 References

[1] **MCNP – A General N-Particle Transport Code, Version 5 – Volume I**: Overview and Theory, X-5 Monte Carlo Team, LA-UR-03-1987, Los Alamos National Laboratory (April, 2003, revised February 2008).

[2] **ICRP Publication 74**. Conversion Coefficients for use in Radiological Protection against External Radiation, 1st Edition. Annals of the ICRP, Volume 26/3, 1996.

CALCULATION METHODS FOR SAFETY ASSESSMENTS OF RESEARCH REACTORS

J. KOUBBI, C. BAYOL, J.-G. LACOMBE, C. BOURET, L. MANIFACIER
AREVA TA
CS 50497, 13593 Aix-en-Provence Cedex 3, France
Corresponding author: jeremy.koubbi@areva.com

H. KROHN, S. WELZEL
Helmholtz-Zentrum Berlin für Materialien und Energie
Hahn-Meitner-Platz 1, D-14109 Berlin, Germany

ABSTRACT

The BER II (Berliner Experimental Reactor) is an open pool type reactor located in Berlin (Germany), primarily used for neutron scattering experiments. It has been in operation since 1973. After each core refuelling, the German safety authority imposes to perform a large amount of low power measurements in order to demonstrate that the new core fulfils the limits allowed by the SAR (Safety Analysis Report). Absorbers reactivity worth and fluxes measurements are systematically carried out to check the compliance of the new core. In order to reproduce these measurements, AREVA TA and BER II have decided to perform a set of neutronic calculations with COCONEUT (COre COnception NEUtronic Tool). This scheme is based on both multigroup transport (2D) theory and diffusion theory (3D) using APOLLO2 and CRONOS2 deterministic codes. It allows one to evaluate the main performances and safety parameters for any types of MTR-type fuel core with a minimal amount of time and effort. The aims of this study are to evaluate the compliance of COCONEUT calculations to safety assessments. Results of the calculations are benchmarked with experimental data from Kern #117 core's BOC (Begin Of Cycle). This paper presents the first comparisons between the experimental data from BER II and the results of COCONEUT calculations on the reactivity worth of the absorbers.

1. Introduction

After the commissioning phase, safety assessments are achieved along the reactor life. The aim is to regularly demonstrate the compliance between the core and the SAR (Safety Analysis Report). Safety parameters can be either calculated by numeric tools dedicated to the reactor, or experimentally measured. The first method is the less restrictive. However, a large number of old reactors in the world don't follow this methodology because they do not have suitable calculation means.
BER II (Berliner Experimental Reactor) is among them. After each core refuelling, the German safety authority imposes to perform a large amount of low power measurements to check the new core is within the limits allowed by the SAR. Consequently, AREVA TA and BER II have decided to perform a set of neutronic calculation tests with COCONEUT (AREVA TA's neutronic scheme dedicated to research reactors). The objective is to demonstrate such experiments can be replaced with dedicated calculations.

First, the BER II research reactor and the neutronic measurements achieved in it are presented. Second, the main aspects of the neutronic simulation with COCONEUT are described.

Finally, results of those two methodologies are benchmarked and analysed. This study allows evaluating the compliance of COCONEUT calculations to safety assessment predictions.

2. General overview of BER II research reactor

BER II research reactor is an open pool type reactor located in Berlin (Germany), primarily used for neutron scattering experiments. BER II has been operating since 1973, and was upgraded from 1985 to 1991 to increase the neutron flux. Consequently, the power was increased from 5 to 10 MW_{th}. In addition the core was compacted and was then encompassed by a beryllium reflector. Finally, a Cold Neutron Source was installed. The conversion from HEU (High Enriched Uranium) to LEU (Low Enriched Uranium) fuel elements began in 1997 and finished in 2000 [1]. Per year, three cores are commissioned and twelve cycles are achieved (three weeks in operation and one for maintenance), corresponding to approximately 250 operation days.

Actually, the core has a 6x7 core lattice, housing 30 fuel elements of which 6 receive hafnium control rods (forks), 11 beryllium reflector elements and one “DBVK” dummy element (Fig 1). The core lattice is surrounded by a beryllium reflector block where beam tubes and the Cold Neutron Source are located (Tab 1).

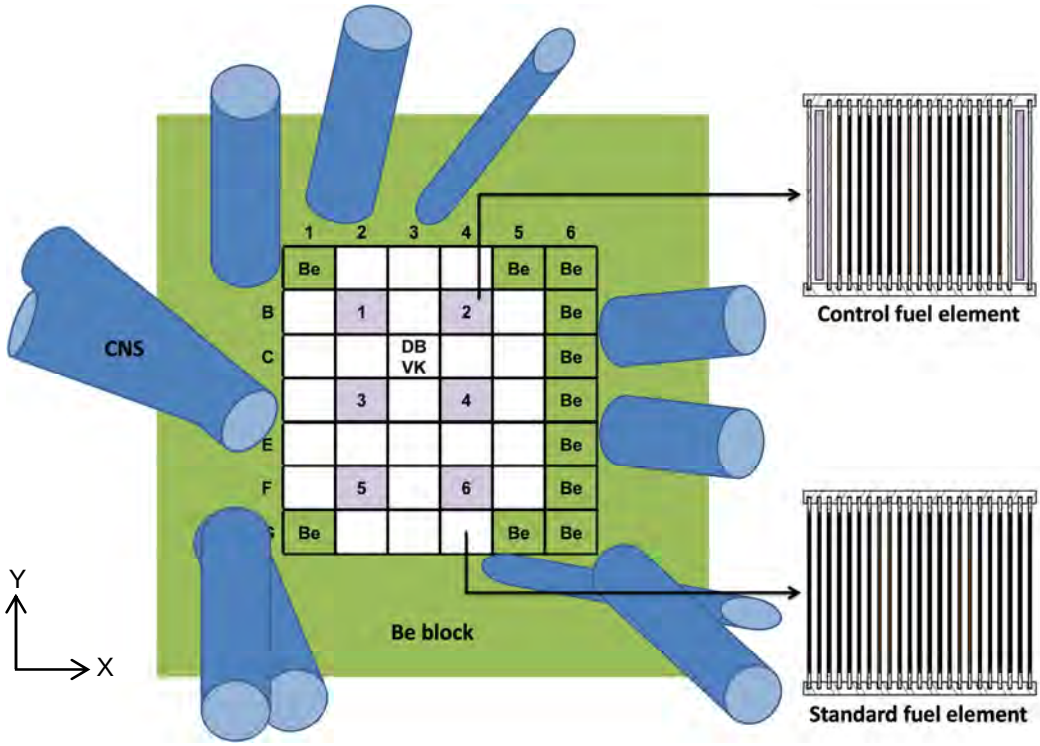

Fig 1. BER II reactor core layout

The reactor is currently operating with a 19.75% enriched U_3Si_2-Al (4.8 $g.cm^{-3}$ of Uranium) material [2]. The core is fuelled with MTR-type fuel elements (23 plates in fuel assembly and 17 in control assembly), detailed in Tab 2.

3. Measurements for safety assessments

As explained in the introductory section, BER II staff must verify the compliance of every new core to be loaded with SAR limits by performing several measurements at low power which are used to determine a set of key parameters. With this specific method, it is possible to demonstrate the core can be operated safely at its nominal power (10 MW_{th}).

Description	Value
Power (MW_{th})	10
Core Grid (X x Y)	6 x 7
Fuel element	24
Grid pitch (X x Y) (cm)	8.1 x 7.7
Active height (cm)	60
Control element	6
Beryllium reflector positions	11
Dummy element (DBVK)	1
Beam tubes	9
Cold Neutron Source	1
Fuel Design	MTR-type
Control Design	Hafnium forks

Tab 1. Main characteristics of the BER II core

Parameters	Control Assembly	Fuel Assembly
Fuel type	U_3Si_2-Al	U_3Si_2-Al
^{235}U enrichment wt %	19.75	19.75
Uranium density ($g.cm^{-3}$)	4.8	4.8
Number of fuel plates per assembly	17	23
Total Uranium in alloy (masse %)	73 – 74	73 – 74
^{235}U per fuel plate (g)	14	14
Fuel meat thickness (mm)	0.408	0.408
Fuel cladding thickness (mm)	0.431	0.431 – 0.546

Tab 2. Standard fuel and Control fuel assembly data

Concerning the neutronic framework, the main parameters examined are explained below:

- Shut-down margin and reactivity worth of the absorbers: The main parameter needed to be checked is the Shut-Down Margin (SDM). BER II operating licence imposes that the SDM with the most effective control completely withdrawn (SDM with single failure criterion) shall be at least of 1% $\Delta k/k$ [3]. This criterion is verified through the calibration of absorbers. For each absorber, the calibration is done by a compensation mechanism of two given absorbers (determination of the differential efficiency). The calibrated absorber is withdrawn about 30 mm from the critical position and the positive reactor period is measured. Then, the released reactivity is compensated by insertion of the second absorber. The total reactivity worth of absorbers is calculated as the sum of the total efficiency of each absorber.
- Excess of reactivity: BOC (Beginning Of Cycle) and EOC (End Of Cycle) potential of reactivity are determined by a simplified analytical method based on the weight of uranium and plutonium isotopes in each plate taking into account the fuel consumption per cycle.
- Critical position of absorbers: Critical position of absorbers is determined experimentally by a classical sub-critical approach. The kinetics used is the following: First, 5 absorbers are withdrawn to a sub-critical position. The piloting rod is then gently moved until a critical state of the core is reached.
- Burn-up swing: Burn-up swing is calculated from the input burn-up, the cycle length (defined in advance) and an estimate of the fuel consumption during the cycle.
- Flux maps: Flux maps are measured by irradiation of copper wires attached to aluminium blades as shown on Fig 2. 26 blades (3 blades maximum per assembly, no blade in control elements) per semi-core are manually introduced in selected fuel assembly water channels. After one hour of irradiation, blades are extracted from the core and Copper decay is measured in the reactor lab from the 511 keV gamma-rays emitted (12 axial measures per copper

Fig 2. Copper wire on an aluminium blade

wire). Two flux measurements are performed for a critical state per semi-core: 2 irradiations at a symmetric position (all 6 absorbers are equally drawn out), and 2 others with a maximum asymmetric position (one is fully inserted, while another is extracted 100 mm above the 4 remaining) in order to simulate the maximum flux shift in the core. These measurements only permit to obtain the 3D flux maps (no absolute flux available with this methodology) because the activity of Copper is proportional to the neutron flux. For normalization considerations, the 4 central assemblies are instrumented for each semi-core.

- Power peak factors: Power peak factors are derived from flux distributions and uranium contents distribution within the core for each fuel plate. They are used to prove the burn-out safety margin. This parameter is important for thermal hydraulic calculations (issue not discussed in this paper).

Globally, for each new core, this experimental process increases significantly the intercycle period by about three days and requires heavy maintenance. Furthermore, these operations reduce the operational days available for experiments (almost 25% [3]).

All the measurements performed for the safety assessments compliance of each new core are reported in a specific document [4] which is sent to the TÜV Nord (German Regulatory Body) in order for BER II to obtain the authorization for operating the reactor at 10 MW_{th}.

4. COCONEUT: AREVA TA Neutronic Calculation system

AREVA TA's neutronic calculation system, named COCONEUT (COre COnception NEUtronic Tool), is dedicated to MTR-type reactor calculation. COCONEUT is based on both multigroup transport theory (APOLLO2 lattice code [5], 2D model – 26-group energy mesh) and diffusion theory (CRONOS2 core code [6], 3D model – 4-group energy mesh) to compute equilibrium states of the reactor [7]. Both codes are developed and maintained by CEA, French Atomic Energy and Alternative Energies Commission.
Two main steps are required to estimate main neutronic parameters of interest with COCONEUT (Fig 3):

- The first step is dedicated to cross section preparation. Multi-group cross sections library is based on the Joint European File JEFF3.1.1 [8]. Self-shielding calculations are performed using the Sanchez-Coste method with collision probability method (P_{ij}) calculated in 2D in the 281-group SHEM energy mesh [9]. The energy spectrum is calculated for several 2D patterns. Such cross section treatment needs to be computed for each element type in the core (standard and control assemblies, reflector blocks, others components).

  Cross sections are then collapsed into a 26-group energy mesh, optimized for MTR type research reactor energy spectrum. The 281/26-group energy condensation is carried out using the Method of Characteristics (MOC) [10], [11] that enables a treatment of the scattering anisotropy (P3).

  To perform 3D diffusion calculations, an additional treatment consists in homogenization and condensation of cross sections into 4-group energy mesh as a function of burn-up (cross section libraries creation). First, fuel depletion 26-group calculations with the MOC solver are achieved to get an optimal energy spectrum for cross sections collapsing. Then the 26/4-group energy condensation is carried out through an equivalence procedure that preserves the reference reaction rates.

- The second step is full core calculations and the core equilibrium states assessment. Main neutronic design parameters are evaluated both in transport with MOC method and a 2D exact description of the core and in diffusion on a 3D model with a homogenized assembly description.

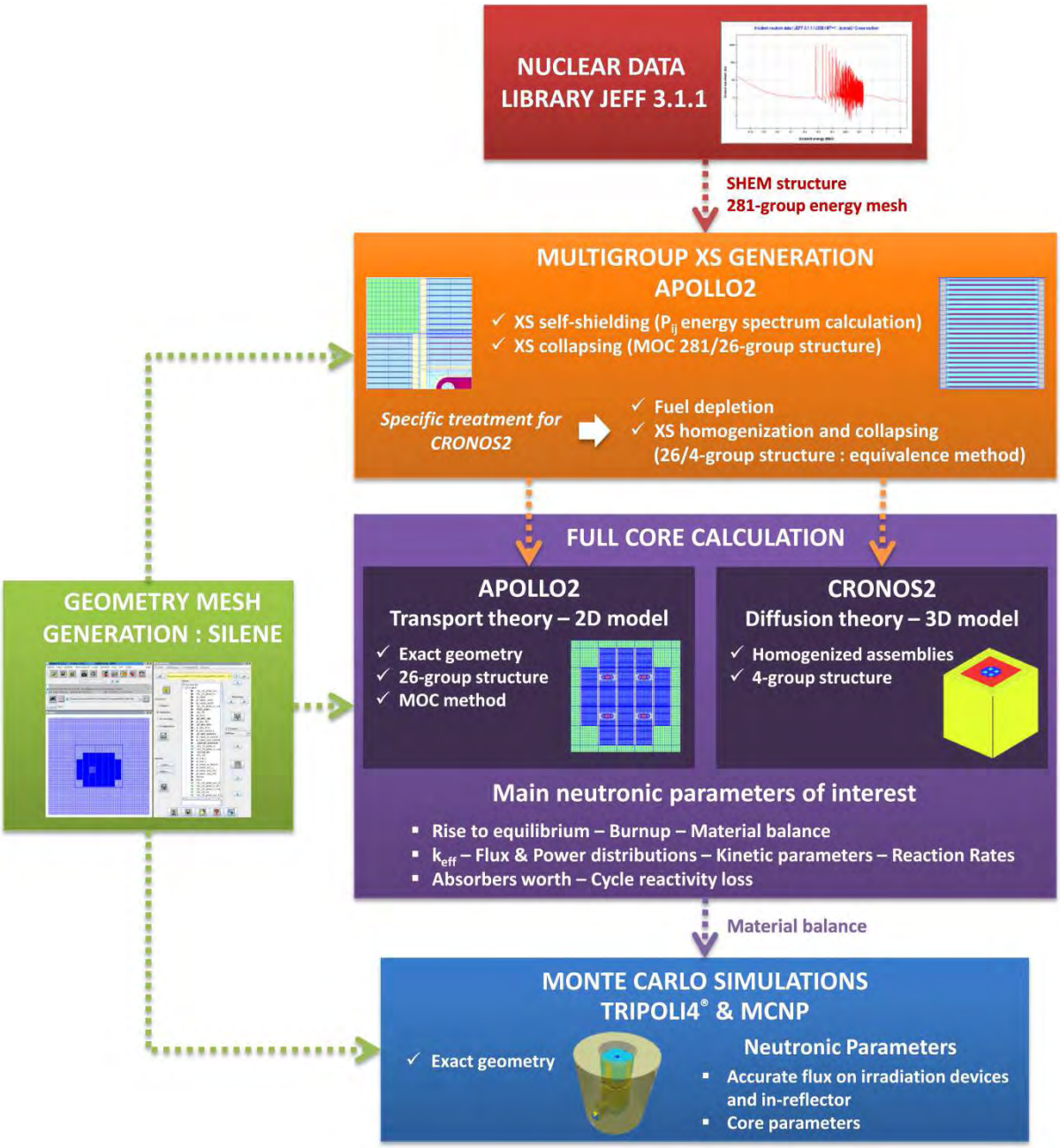

Fig 3. COCONEUT general overview

Biases regarding this calculation scheme have been evaluated [12] using the TRIPOLI4® [13] and MCNP [14] Monte Carlo codes.

These probabilistic codes are also linked to COCONEUT scheme via formatted material balance outputs. Stochastic models are used to evaluate accurately neutronic performance of the reactor such as neutronic flux in reflector, gamma heating. Therefore, COCONEUT system allows one the evaluation of main reactor performances and safety parameters.

5. COCONEUT BER II Model and calculations performed

In this section, the calculations performed to reproduce the experimental core #117's data are described. Overall neutronic calculations are carried out using only deterministic models. The geometry of BER II core is created without the CNS and neutron beam tubes.

Besides the geometrical data and material description, input data is burn-up per assembly at BOC (Begin of Cycle) for the studied core. The burn-up map considered is presented on Fig

4. Burn-up is expressed in MWatt.days per ton of initial Uranium (*i.e. Uranium loaded for the Core #117 – BOC*) (MWd/t_U). The burn-up is determined from the extracted energy and the estimated mass of Uranium per each assembly. These data were provided by BER II.

	1	2	3	4	5	6
A	Be	33,942	0	18,885	Be	Be
B	16,828	0	99,110	46,519	18,160	Be
C	35,741	88,173	DB VK	81,640	53,391	Be
D	68,467	84,929	117,922	89,787	69,811	Be
E	0	90,559	100,785	80,760	53,813	Be
F	72,684	48,963	96,764	0	34,202	Be
G	Be	34,904	0	49,716	Be	Be

Fig 4. Burn-up map for Kern #117 – BOC

The refuelling strategy employed for this core is an OUT-IN type. The studied core has 5 fresh fuel assemblies, 2 control elements and 3 standard elements. The average burn-up of this core is 52,882 MWd/t_U. In the deterministic core calculation, data according to specific burn-up are allocated for each assembly as described in the section above. A stationary calculation is performed to obtain physical parameters (for instance burn-up or reactivity).
The modelled absorber increment is the centimetre. Positions of the absorbers are rounded to the closest centimetre. The different calculations are mentioned below:

- The first parameter evaluated with COCONEUT is the core excess of reactivity at BOC. We performed a calculation with all absorbers completely withdrawn (*i.e. all the absorbers at 60cm from the bottom of the core*). Then the critical state of the core is determined by positioning the absorbers at positions described in BER II manual [4].
- The next calculations are dedicated to characterise the reactivity worth of each absorber. We have reproduced by calculation the differential efficiency experiments (around 200 calculations performed). The total reactivity worth of 6 absorbers is the sum of the individual ones.

All these calculations allow us to determine the SDM-1 criterion, defined as follows: Reactivity worth of all absorbers minus the reactivity worth from the most effective control rod (experimentally Rod #4) minus the excess of reactivity [3].

6. Benchmark results

In this section, results obtained with the COCONEUT scheme are presented and compared to experimental measurements performed in BER II. All the values presented hereafter are best estimate.

As the reactor's core control is the most important parameter, the first comparisons focus on the reactivity worth of absorbers and the excess of reactivity of the core. The excess of reactivity obtained by COCONEUT is 8,734 pcm. In comparison, the excess of reactivity determined by the BER II methodology is 9,278 pcm. For this core configuration COCONEUT underestimates the excess of reactivity by 5.9%. This result is quite acceptable, as burn-ups used for the calculations are axially homogeneous. In addition, the method used for determining the excess of reactivity only gives a rough estimate.

The critical position of the absorbers (Rod #1 to Rod #5 at 27.3 cm and Rod #6 at 27.4 cm from the bottom [4]) is reproduced in the COCONEUT calculation (all rods at 27 cm from the

bottom). The result of computation is: keff = 1.01393, and corresponds to a reactivity of 1,374 pcm. It means critical state of the core is overestimated by calculation. The automated procedure for reaching the critical positon of the rods implemented in COCONEUT gives a calculated critical position at 25 cm.

The following figures show the differential efficiency (in pcm/cm) for control rod obtained by measurements and calculation. For each absorber, the integral worth of absorbers is also drawn on each graph.

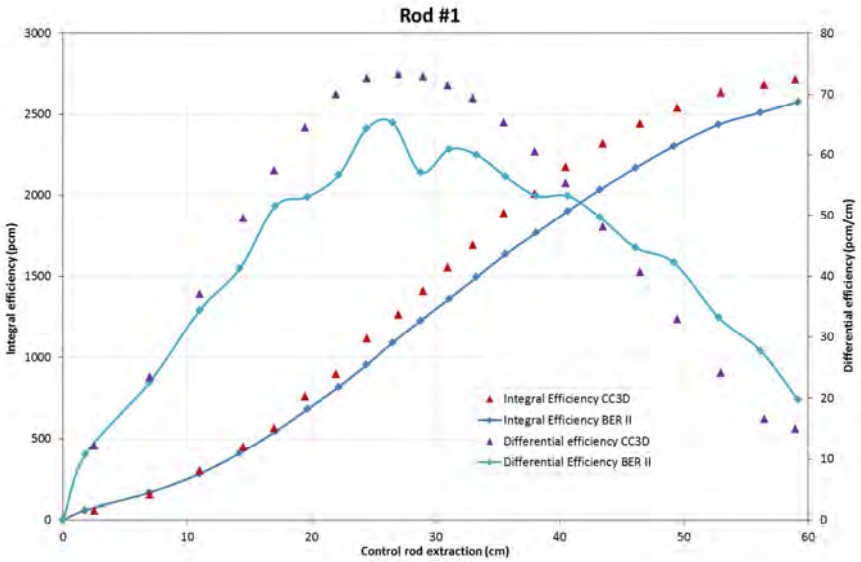

Fig 5. Efficiencies for control Rod #1 obtained by experimental measurements (BER II) and COCONEUT 3D calculations (CC3D)

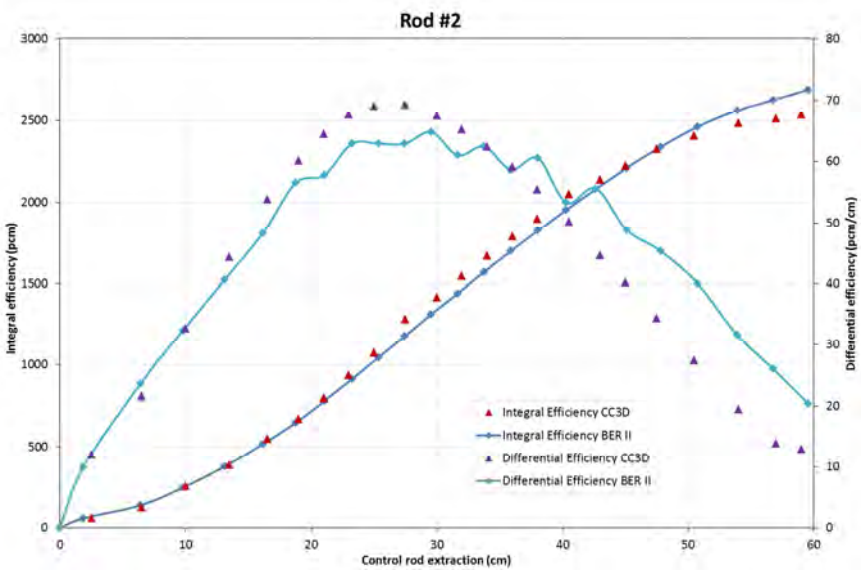

Fig 6. Efficiencies for control Rod #2 obtained by experimental measurements (BER II) and COCONEUT 3D calculations (CC3D)

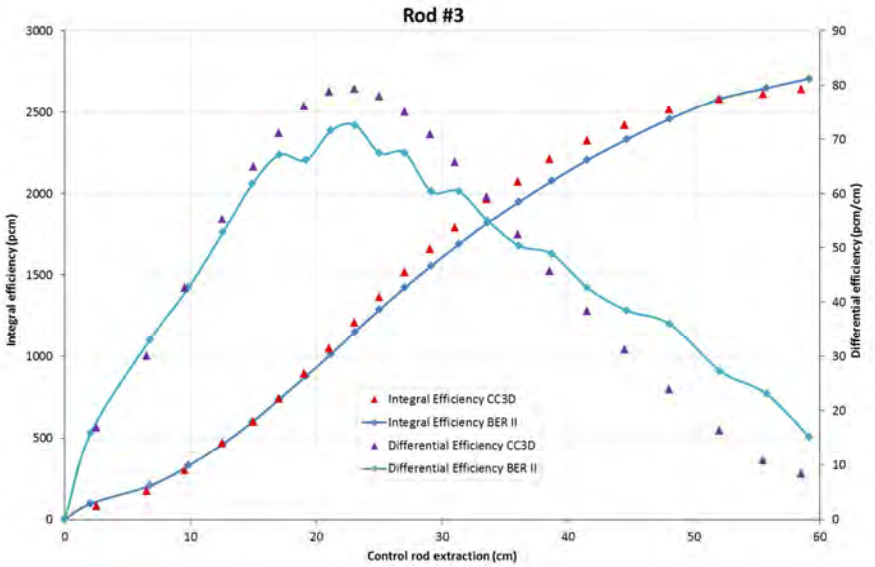

Fig 7. Efficiencies for control Rod #3 obtained by experimental measurements (BER II) and COCONEUT 3D calculations (CC3D)

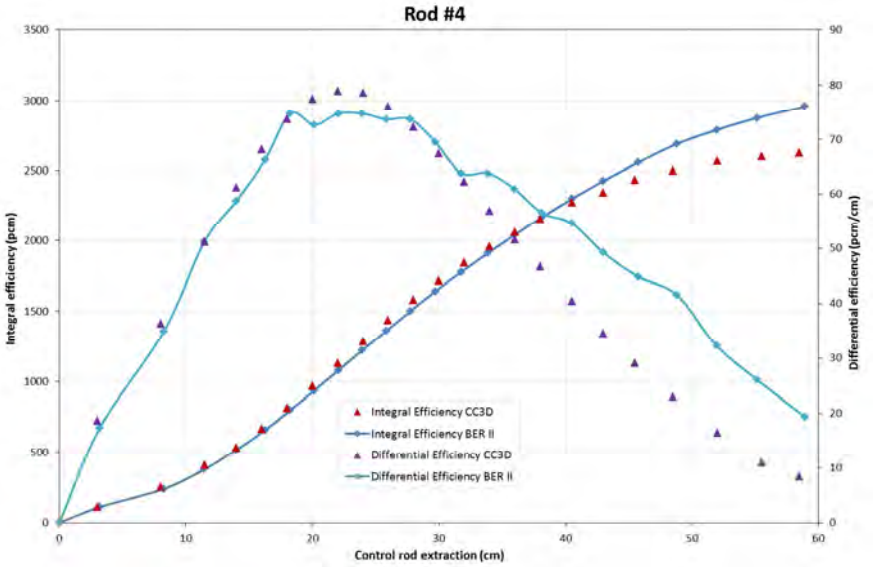

Fig 8. Efficiencies for control Rod #4 obtained by experimental measurements (BER II) and COCONEUT 3D calculations (CC3D)

Figures 5 to 8 show a good evaluation of the differential efficiency by COCONEUT. Integral efficiencies are compliant to measurements results. For all absorbers, a discrepancy between experimental measurements and calculations occurs above mid-core plane. The lack of axial burn-up profiles per assembly and the approximated position of control rod in calculations could impact the results provided by COCONEUT.

Tab 3 reports the reactivity worth in pcm of each absorber determined by COCONEUT and experimental measurements.

Reactivity worth of absorbers	**Rod #1**	**Rod #2**	**Rod #3**	**Rod #4**	**Rod #5**	**Rod #6**	**TOTAL**
BER II (pcm)	2,578	2,689	2,707	2,958	2,733	2,954	**16,619**
COCONEUT (pcm)	2,719	2,540	2,642	2,627	2,557	2,793	**15,877**
Discrepancies (%)	*5.5*	*-5.6*	*-2.4*	*-11.2*	*-6.4*	*-5.5*	***-4.5***

Tab 3. Reactivity worth of absorbers

Results obtained for the estimation of reactivity worth of absorbers from COCONEUT 3D calculation show a rather good agreement with experimental data. Integral efficiency is underestimated by 4.3% in average based on Tab 3. The maximum error observed concerns Rod #4 and is less than -12%. The particular position of this absorber in the core, near the DBVK and in front of Be block, can explain this significant discrepancy.

The most effective control rod is #6 and weighs 2,793 pcm, experimentally, it is #4. As Tab 3 shows, their reactivity worths are very close. In these conditions, it is not abnormal to find the one or the other as the most effective one by calculation. The total efficiency calculated for all 6 absorbers is 15,877 pcm. COCONEUT underestimates this efficiency by only 4.5%. These results then allow us to determine the SDM-1 criterion.

	BER II (pcm)	**COCONEUT (pcm)**	***Discrepancies (%)***
Total reactivity worth of absorbers	16,619	15,877	*-4.5*
Most effective rod	2,958	2,793	*-5.6*
Excess of reactivity of core	9,278	8.734	*-5.9*
insertion of DBVK	300	300	--
TOTAL	**4,083**	**4,051**	***-0.8***

Tab 4. Shut-Down Margin-1 criterions

As Tab 4 shows, calculated SDM-1 criterion is underestimated only by 0.8%. In these conditions, the calculations achieved with COCONEUT enable to determine the SDM-1 of the core with a very good confidence.

7. Conclusions and prospects

This paper presents the benchmark of AREVA TA's neutronic deterministic scheme dedicated to the Research Reactors design. These first results are focussed on reactivity effects related to safety issues. In particular, the SDM-1 was recalculated by COCONEUT with a very good agreement with experiments. All the parameters taken into account in the determination of SDM-1 are underestimated by an average 5.2%. These results are very satisfactory and allow COCONEUT to be used for safety assessments. Besides, COCONEUT enables one to compute a large number of core configurations with a limited dataset input and a single launch command. A complete Control Rod calibration method requires several dozens of absorbers positions to be assessed. Such a study, for a single absorber, can be led in less than an hour.

COCONEUT is currently still under development, especially for its 3D deterministic part. Results presented in this paper could significantly contribute to ongoing developments. Results confirm the importance of the axial profile of the burn-up map. The latter influences the excess of reactivity and the control rods efficiencies. In this way, it could be convenient to develop a specific methodology taking into account the axial profile of the core.
Furthermore, in order to complete this benchmark, 3D flux distributions and power peak factors (BOC and EOC) remain to be assessed with COCONEUT.

This kind of benchmark will be conducted on a large amount of research reactors throughout the world (mainly due to specific safety requirements per country) in order to take into account different core designs (number of fuel plates, uranium density, pitch, absorber design, experimental devices, reflector material and position…).

8. References

[1] A. Axmann, H. Buchholz. C.-O. Fischer and H. Krohn*, "Status of the BER II", Proceedings of the 1992 International Meeting on Reduced Enrichment for Research and Test Reactor,* Roskilde, Denmark, 1992

[2] K. Haas, C.-O. Fischer, H. Krohn, "HEU/LEU-Conversion of BER II successfully finished", *2000 International Meeting on Reduced Enrichment for Research and Test Reactors*, Las Vegas, Nevada, 2000

[3] H. Krohn, C.-O. Fischer, K. Haas, "Conversion of the BER II", *22nd International Meeting Reduced Enrichment for Research and Test Reactors (RERTR)*, Budapest, Hungary, 1999

[4] Helmholtz-Zentrum Berlin [Private Communication], "Neue Kernaufbauten und Kernumladungen", Betriebshandbuch, 2013

[5] R. Sanchez and al. "Apollo2 year 2010", Nuclear Engineering and Technology, 42:474-499, 2010

[6] J. Lautard, S. Loubière, C. Fedon-Magnaud. "CRONOS: a modular computational system for neutronic core calculations". IAEA specialist meeting on advanced calculational methods for power reactors. Cadarache, France. 1990

[7] J.-G. Lacombe, C.Bouret, J. Koubbi, L. Manifacier, "COCONEUT: Enhancing Neutronic Design for Research Reactors", IGORR-2016 Proceedings, *to be published*

[8] A. Santamarina and D. Bernard, "The Recommended JEFF-3.1.1 File and CEA2005v4 Library for Accurate Neutronics Calculations," JEFF Report, OECD/NEA 2009

[9] N. Hfaiedh, A. Santamarina, "Determination of the optimized SHEM mesh for transport calculation." International topical meeting on Mathematics and Computation, Supercomputing, Reactor Physics and Nuclear and Biological Applications. Avignon, France, 2005

[10] S. Santandrea, R. Sanchez, "Acceleration techniques for the characteristic method in unstructured meshes", *Annals of Nuclear Energy* 29, 323-352, 2002

[11] S. Santandrea, R. Sanchez, P. Mosca, "A Linear Surface characteristic approximation for neutron transport in unstructured meshes", *Nucl. Sci. Eng.* Vol. 160, no.1, Elsevier, pp. 23-40, 2008

[12] C. Bouret, J.-G. Lacombe, C. Bayol, J. Koubbi, L. Manifacier, B. Gastaldi, J.F. Vidal, "COCONEUT: First steps of validation for the new AREVA TA neutronic deterministic scheme for Research Reactor design", IGORR-2016 Proceedings, *to be published*

[13] C.M. Diop, O. Petit, E. Dumonteil, F.X. Hugot, Y.K. Lee, A. Mazzolo, J.C. Trama, "TRIPOLI-4: A 3D continuous-energy Monte Carlo transport code." PHYTRA1: First International Conference on Physics and Technology of Reactors and Applications. Marrakech, Maroc, 2007

[14] X-5 Monte Carlo team, "MCNP – A general Monte Carlo N-particle transport code, version 5", LA-UR-03-1987

COCONEUT: FIRST VALIDATION STEPS OF THE AREVA TA NEUTRONIC SCHEME FOR RESEARCH REACTOR DESIGN

C. BOURET, J.G. LACOMBE, J. KOUBBI, L. MANIFACIER
AREVA TA
CS 50497,13593 Aix-en-Provence Cedex 3, France
Corresponding author: cyrille.bouret@areva.com

B. GASTALDI, J.F VIDAL
CEA/DEN/DER/SPRC
F-13118 Saint-Paul-lez-Durance, France

ABSTRACT

AREVA TA has developed a highly flexible, neutronic calculation tool for Research Reactors core design and optimization. This calculation scheme, named COCONEUT (COre COnception NEUtronic Tool), allows performing neutronic calculations on complex geometries using automated generic models and accurate numerical methods. COCONEUT is based on both multigroup transport (2D) theory and diffusion theory (3D) using APOLLO2 and CRONOS2 deterministic codes. This paper describes the Verification & Validation methodology applied to assess COCONEUT performances and associated computational biases. Validation has been performed by comparisons to reference calculations using TRIPOLI4® and MCNP Monte Carlo codes. First results highlight the ability of COCONEUT to calculate material testing reactor within 400 pcm accuracy on multiplication factor in 2D and 3D models. Discrepancies on fission reaction rate distributions are less than 3 % with 2D model.

1 Introduction

AREVA TA's neutronic scheme COCONEUT (COre COnception NEUtronic Tool) is dedicated to MTR-type reactor design and allows performing neutronic calculations on complex geometries using automated generic models and accurate numerical methods.

COCONEUT [1], [2] is based on both multigroup transport theory (APOLLO2 [3], [4], 2D) and diffusion theory (CRONOS2 [5], 3D) to compute equilibrium states of the reactor. Both codes are developed and maintained by CEA, French Atomic Energy and Alternative Energies Commission. The parameters of interest calculated with COCONEUT are equilibrium material balance, fluxes, Burn-Up distributions, power maps and reactivity worth of absorbers.

Currently, COCONEUT is undergoing a large verification, validation [6] and uncertainty quantification program (V&V) in order to determine and optimize its accuracy in evaluating key parameters for research reactors. The validation process consists in comparison of COCONEUT results against reference Monte Carlo continuous-energy calculations (MCNP [7] and TRIPOLI4® [8] codes). The main parameters analysed are:

- Reactivity of the whole core and of its elementary components (cell level),
- Absorption and fission rates,
- Neutronic weight of absorbers (individual and global),
- Reactivity loss over a depletion cycle,
- Neutronic balance via a six-factor formula
- Xenon poisoning at equilibrium and peaks concentration.

The validation process is carried out on several reactor designs to extend the validity domain of the calculation scheme and is divided in several steps:

- Validation of the entire calculation process to determine biases on key neutronic parameters,
- Elementary validation for each step of the calculation process in order to evaluate separately each source of discrepancy and to assess compensation mechanisms within the scheme.

This paper describes the methodology applied to determine COCONEUT's biases and the preliminary results of this process. The outcomes highlight the remarkable capability of COCONEUT to perform accurate calculations with limited CPU-time consumption.

2 COCONEUT: V&V process

2.1 COCONEUT general description

COCONEUT is designed to assess main neutronic design parameters for a given core concept within a short period of time. Two main steps are required to estimate such parameters with COCONEUT:

- The first step is dedicated to cross section preparation. Multi-group cross sections library is based on the Joint European File JEFF3.1.1 [9].Self-shielding calculations are performed using the Sanchez-Coste method with collision probability method (P_{ij}) calculated in 2D in the 281-group SHEM energy mesh [10]. The energy spectrum is calculated for several 2D patterns (standard assembly geometry, control assembly surrounded by standard assembly). Such cross section treatment needs to be computed for each element type in the core (standard and control assemblies, reflector blocks, others components).

  Cross sections are then collapsed into a 26-group energy mesh, optimized for MTR type research reactor energy spectrum. The 281/26-group energy condensation is carried out using the Method of Characteristics (MOC) [11], [12] that enables a treatment of the scattering anisotropy (P3).

  To perform 3D diffusion calculations, an additional treatment consists in homogenization and condensation of cross sections into 4-group energy mesh as a function of burn-up (cross section libraries creation). First, fuel depletion 26-group calculations with the MOC solver are achieved to get an optimal energy spectrum for cross sections collapsing. Then the 26/4-group energy condensation is carried out through an equivalence procedure that preserves the reference reaction rates.

- The second step is full core calculations and the core equilibrium states assessment. Main neutronic design parameters are evaluated both in transport with MOC method and a 2D exact description of the core and in diffusion on a 3D model with a homogenized assembly description.

Probabilistic codes (TRIPOLI4® and MCNP) are also linked to COCONEUT scheme via formatted material balance outputs. Stochastic models are used to evaluate accurately neutronic performances of the reactor such as neutronic flux in reflector or gamma heating). Therefore, COCONEUT line enables the evaluation of all main reactor performances and safety parameters.

An overview of the COCONEUT different calculation steps is shown in Fig 1.

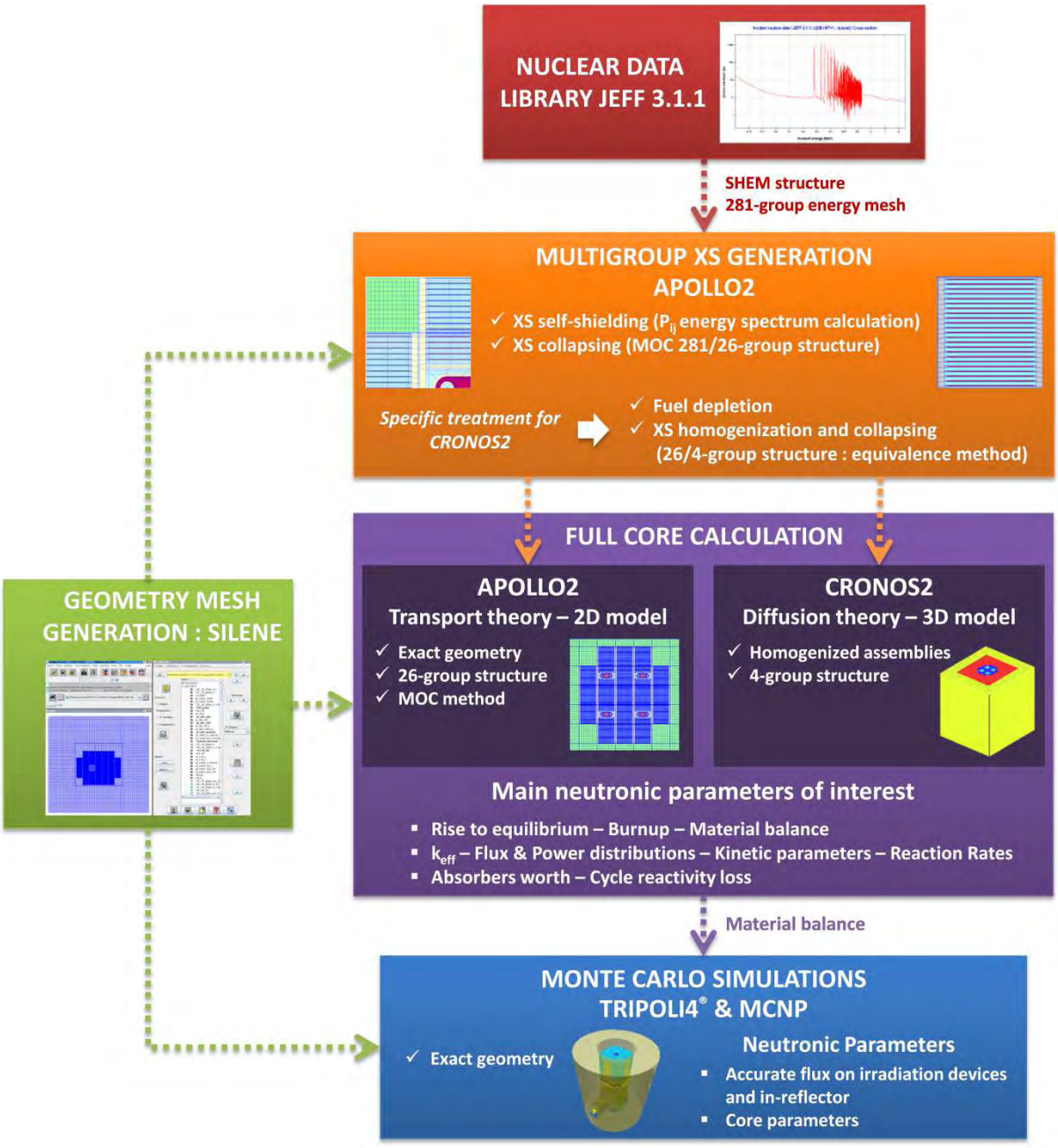

Fig 1. COCONEUT general overview

2.2 V&V: parameters of interest

In the neutronic field, the Monte Carlo method (reference method) makes possible code vs. code comparisons (numerical validation) and thus enable the evaluation of deterministic computational scheme biases (model, methods assumptions...).The purpose of COCONEUT validation is to characterize the complete calculation line (cross sections preparation step, 2D and 3D whole core calculation) for a representative panel of research reactor designs.

The main neutronic parameters studied in this first validation step are:

- Infinite and effective multiplication factors k_{∞}, k_{eff},
- Fission reaction rates,
- Neutronic balance via a six-factor formula [13],
- Absorber worths.

Neutronic balance via six-factor formula

The six-factor formula is an alternative formulation of the four-factor formula. It is used to determine the neutronic balance of a nuclear chain reaction in an infinite geometry model. These factors give spatial and energetic[1] information and highlight neutronic compensation effects.

$$k_{\infty} = \chi_{\mathrm{n\to xn}} * \varepsilon_{\mathrm{even}} * \varepsilon_{\mathrm{odd}} * p * f * \eta \quad (1)$$

- "n → xn" factor $\chi_{\mathrm{n\to xn}}$: It corresponds to the neutrons excess produced by (n → xn) reactions:

$$\chi_{\mathrm{n\to xn}} = \frac{Absorption}{Absorption - (\mathrm{n} \to \mathrm{xn})} \quad (2)$$

- Fast fission factor $\varepsilon = \varepsilon_{\mathrm{even}} * \varepsilon_{\mathrm{odd}}$ with:
  - $\varepsilon_{\mathrm{even}}$: This factor characterizes the fission of even actinides (^{234}U, ^{236}U, ^{238}U, ^{238}Pu...) in fast energies:

$$\varepsilon_{\mathrm{even}} = \frac{\frac{Production}{Absorption}}{\frac{Production_{fast}(odd) + Production_{\ thermal}}{Absorption - \ Fission_{fast}(even)}} \quad (3)$$

  - $\varepsilon_{\mathrm{odd}}$: This factor represents the fission of odd actinides (^{235}U, ^{239}Pu, ^{241}Pu, ^{241}Am...) in fast energies:

$$\varepsilon_{\mathrm{odd}} = \frac{\frac{Production_{fast}(odd) + Production_{\ thermal}}{Absorption}}{\frac{Production_{fast}(odd) + Production_{\ thermal}}{Absorption - \ Fission_{fast}(even)}} \quad (4)$$

- Resonance escape probability p: This factor is the probability that a neutron reaches the thermal energies without being absorbed into the capture resonances of heavy isotopes:

$$p = \frac{Absorption_{thermal}}{Absorption - Fission_{fast}} \quad (5)$$

- Thermal utilization factor f: This factor characterizes the probability that a thermal neutron absorption takes place in the fuel:

$$f = \frac{Absorption_{thermal}\ (fuel\ zone\ )}{Absorption_{thermal}} \quad (6)$$

- Reproduction factor η: This factor is equal to the neutron multiplication factor for thermal neutrons:

$$\eta = \frac{Production_{thermal}}{Absorption_{thermal}\ (fuel\ zone)} \quad (7)$$

2.3 TRIPOLI4® and MCNP codes

The reference calculations were performed with TRIPOLI4® and MCNP Monte Carlo codes using pointwise cross sections. The SILENE GUI [14] has been used to generate the 2D and 3D TRIPOLI4® input geometries. Media definitions and isotopic concentrations were obtained from COCONEUT by means of an embedded data export tool. A total number of up to one hundred million neutron histories were used to reach a good statistical convergence (1σ always < 20 pcm in reactivity and between 0.5% and 0.05% in fission reaction rates).

[1] Thermal range: below 0.625 eV

3 MTR BENCHMARK: COCONEUT validation case

MTR fictitious core is a 2 MW (thermal) open pool validation benchmark reactor. It is composed of a compact core surrounded by three rings of reflector blocks (Beryllium) inside a light water pool. The reactor core contains 25 Fuel Assemblies (FA) of which 20 standard FA and 4 control FA.

Fuel meat is composed of uranium silicide. Each FA has two aluminium side plates with 19 slots. These slots are used to hold the 19 fuel plates of standard FA while 2 slots are used to hold Hf fork in case of control FA.

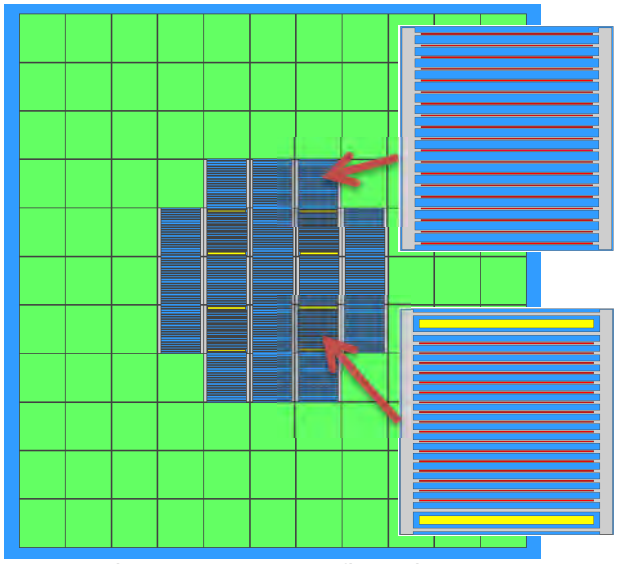

Fig 2. MTR core configuration (Hf: yellow ; Be: green)

Main parameters	Value
Number of standard FA	17
Number of plates per assembly (standard FA)	19
Number of control FA	4
Number of plates per assembly (control FA)	17
Neutron absorber material	Hf
Total Uranium mass (kg)	31.45
Uranium density ($g.cm^{-3}$)	4.3
^{235}U enrichment (%)	19.75
Cycle length (days)	70
Fuel temperature (°C)	50
Clad temperature (°C)	35
Moderator temperature (°C)	20
Reflector temperature (°C)	20

Tab 1. Main parameters of MTR core

4 First step: cross sections preparation

Self-shielded and collapsed cross sections are obtained at the first calculation step of COCONEUT. The energy spectrum required for cross section processing is calculated in several 2D geometries (standard assembly geometry, control rod assembly surrounded by standard assembly).

Two pattern types are defined for this MTR core configuration. “FA” and “CFA” acronyms identify them in the following figure for respectively the standard fuel assembly and the control fuel assembly pattern. First comparisons are made on these models to determine the calculation bias due to this first calculation step.

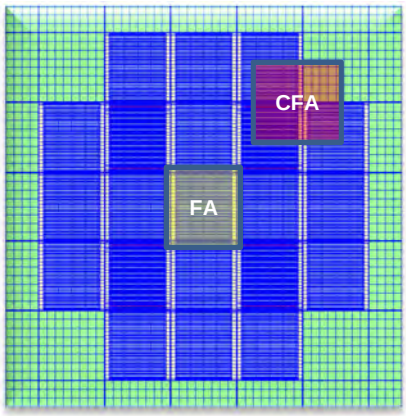

Fig 3. Patterns for cross sections calculation

4.1 Standard fuel assembly: FA cross sections self-shielding

The results presented in this section are obtained with:

- COCONEUT after cross sections self-shielding and 281/26-group condensation on FA pattern. Axial neutron leakages are imposed to null value in validation calculations to represent the TRIPOLI4® boundary condition,
- TRIPOLI4® 2D model with reflection boundary conditions.

The following formula is used for comparisons of neutronic factors:

$$\partial X = \ln \frac{X_{\text{COCONEUT}}}{X_{\text{TRIPOLI4®}}} . 10^5 \quad (8)$$

Parameter	COCONEUT	TRIPOLI4®	$\partial X = \ln \frac{X_{\text{COCONEUT}}}{X_{\text{TRIPOLI4®}}} . 10^5$
$\chi_{n \to xn}$	1.00019	1.00019	**0**
ε_{even}	1.00233	1.00237	**-4**
ε_{odd}	1.03019	1.03027	**-8**
p	0.89439	0.89531	**-103**
f	0.87235	0.87039	**225**
η	2.03636	2.03651	**-7**
k_∞	**1.64092**	**1.63922** ± 6 pcm	**103**

Tab 2. Six-factor formula – Standard fuel assembly

Discrepancies in six-factor between COCONEUT and TRIPOLI4® do not show significant compensations. An underestimation of about 100 pcm by COCONEUT in the resonance escape probability p can be assigned to the treatment of ^{238}U capture resonances. Discrepancy in *p* is offsetting by an overestimation in the utilisation factor f. Negligible differences are observed on other parameters.

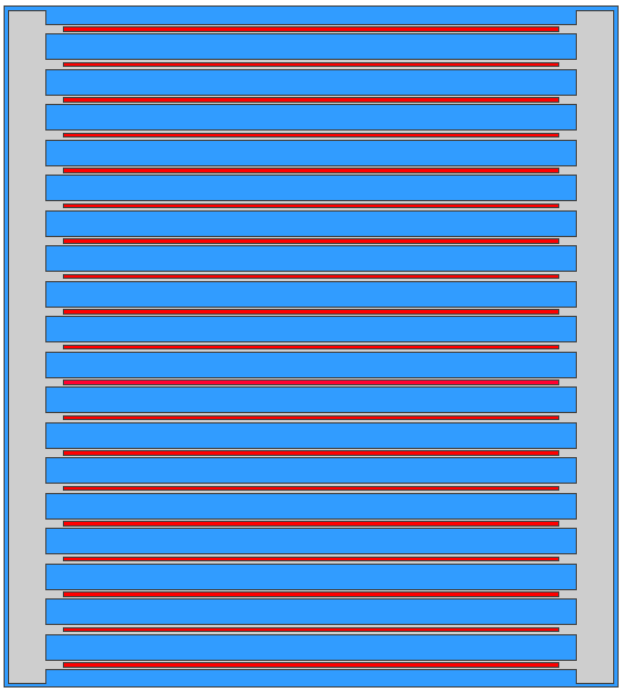

Fuel plate	COCONEUT	$\frac{\text{COCONEUT} - \text{TRIPOLI4®}}{\text{TRIPOLI4®}}$ (%)
1	5.436E-02	**-0.23**
2	5.350E-02	0.01
3	5.294E-02	0.01
4	5.262E-02	0.07
5	5.235E-02	0.00
6	5.221E-02	0.07
7	5.206E-02	-0.01
8	5.202E-02	**0.08**
9	5.195E-02	0.02
10	5.197E-02	0.06
11	5.195E-02	-0.04
12	5.202E-02	0.00
13	5.206E-02	-0.01
14	5.221E-02	0.07
15	5.235E-02	0.01
16	5.262E-02	**0.08**
17	5.294E-02	0.04
18	5.350E-02	0.03
19	5.436E-02	**-0.24**

Tab 3. Comparison of normalized fission rates

The comparison of fission reaction rates shows good agreement with TRIPOLI4®. The maximum discrepancy is obtained for the most outer plates with an underestimation by COCONEUT less than 0.25% (1σ < 0.05%). COCONEUT's ability to predict fission rates is very accurate with respect to the objectives set for this scheme (early stages of core design).

4.2 Control rod fuel assembly: CF cross sections self-shielding

A similar analysis is achieved for CFA pattern. The geometry used is a combination of four quarter of assemblies that represent common surroundings for an absorber element. Two

types of models are compared, one with the absorber inserted and the other one with the absorber fully extracted.

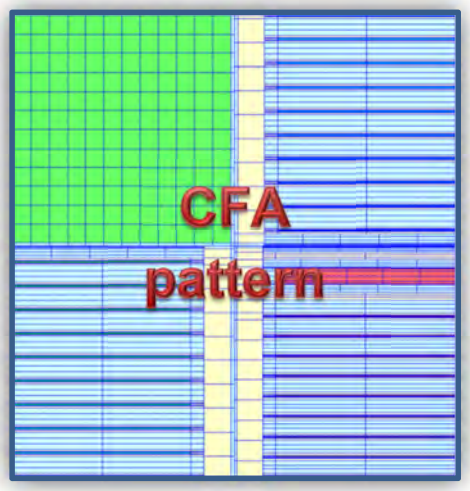

Fig 4. Pattern used for CFA cross section calculation (in red: Hf or water)

The comparisons of six-factor breakdown for both configurations are shown in the following tables [Tab 4, Tab 5].

Parameter	COCONEUT	TRIPOLI4®	$\partial X = \ln \frac{X_{\text{COCONEUT}}}{X_{\text{TRIPOLI4®}}} . 10^5$
$\chi_{n \to xn}$	1.02645	1.02758	**-107**
ε_{even}	1.00327	1.00325	**0**
ε_{odd}	1.05271	1.05275	**-9**
p	0.79134	0.79028	**126**
f	0.73311	0.73213	**137**
η	2.03605	2.03612	**0**
k_∞	**1.28048**	**1.27844** ± 19 pcm	**146**

Tab 4. Pattern with control rods fully inserted

Parameter	COCONEUT	TRIPOLI4®	$\partial X = \ln \frac{X_{\text{COCONEUT}}}{X_{\text{TRIPOLI4®}}} . 10^5$
$\chi_{n \to xn}$	1.02618	1.02715	**-97**
ε_{even}	1.00194	1.00192	**0**
ε_{odd}	1.02847	1.02860	**-10**
p	0.89641	0.89683	**-45**
f	0.85654	0.85425	**257**
η	2.03674	2.03673	**0**
k_∞	**1.65368**	**1.65165** ± 23 pcm	**105**

Tab 5. Pattern with control rods removed

As for the standard FA, neutronic factors comparisons put forward limited compensations between p and f factors. Analysis of $\chi_{n \to xn}$ factor highlights a bias of approximately 100 pcm between COCONEUT and TRIPOLI4®. Error on this factor is the result of the Beryllium block modelling. Indeed, a significant proportion of "$n \to xn$" reactions contribute to neutronic balance for both configurations.

Finally, discrepancies with reference calculations are satisfactory with respect to the objectives set for COCONEUT-for early stages of core design.

5 2D & 3D full core calculation

5.1 2D-model: MOC method

The 2D whole core modelling with COCONEUT comprises a pool of 30 cm. In this case, the neutron radial leakage is taken into account in the calculations while no axial leakage is represented (null value imposed for buckling). The same geometry and boundary conditions are used with TRIPOLI4®.

Main parameters	$\mathrm{COCONEUT_{2D}}$	TRIPOLI4® (± 1σ)	$\partial\rho$ (pcm)
k_{eff} (Control rods removed)	1.41545	1.41414 ± 3 pcm	**-65**
k_{eff} (Control rods inserted fully)	1.23077	1.22775 ± 3 pcm	**-203**
Control rods worth (pcm)	10 601	10 738 ± 4 pcm	**138**
β_{eff} (pcm)	697	698	**1**

Tab 6. Discrepancies in main neutronic parameters

Discrepancies in main neutronic parameters studied in this first validation step highlight very good agreements between $\mathrm{COCONEUT_{2D}}$ and Monte Carlo reference calculations. Biases in effective multiplication factors are less than 200 pcm. $\mathrm{COCONEUT_{2D}}$ calculates control rod worth with less than 1.5 % error. There is no bias on β_{eff} parameter.

Six-factor formula

Parameter	$\mathrm{COCONEUT_{2D}}$	TRIPOLI4®	$\partial \mathrm{X} = \ln\frac{X_{\mathrm{COCONEUT}}}{X_{\mathrm{TRIPOLI4®}}}.10^5$
$\chi_{n\to xn}$	1.03058	1.03115	**-55**
ε_{even}	1.00250	1.00259	**-9**
ε_{odd}	1.03588	1.03638	**-48**
p	0.91042	0.90971	**78**
f	0.71329	0.71231	**137**
η	2.03697	2.03714	**-8**
k_∞	**1.41545**	**1.41414** ± 3 pcm	**95**

Tab 7. Six-factor formula - Core with control rods removed

Parameter	$\mathrm{COCONEUT_{2D}}$	TRIPOLI4®	$\partial \mathrm{X} = \ln\frac{X_{\mathrm{COCONEUT}}}{X_{\mathrm{TRIPOLI4®}}}.10^5$
$\chi_{n\to xn}$	1.03229	1.03300	**-69**
ε_{even}	1.00324	1.00332	**-8**
ε_{odd}	1.04719	1.04792	**-70**
p	0.86319	0.86078	**280**
f	0.64564	0.64500	**99**
η	2.03672	2.03667	**2**
k_∞	**1.23102**	**1.22775** ± 3 pcm	**235**

Tab 8. Six-factor formula - Core with control rods fully inserted

The decomposition of the neutronic balance on six-factor does not highlight significant compensation effects. This confirms the good performance of $\mathrm{COCONEUT_{2D}}$ from both energy and spatial point of views. To check the good agreement at spatial level, a comparison of normalized fission rates calculated with $\mathrm{COCONEUT_{2D}}$ and TRIPOLI4® is shown in Fig 5.

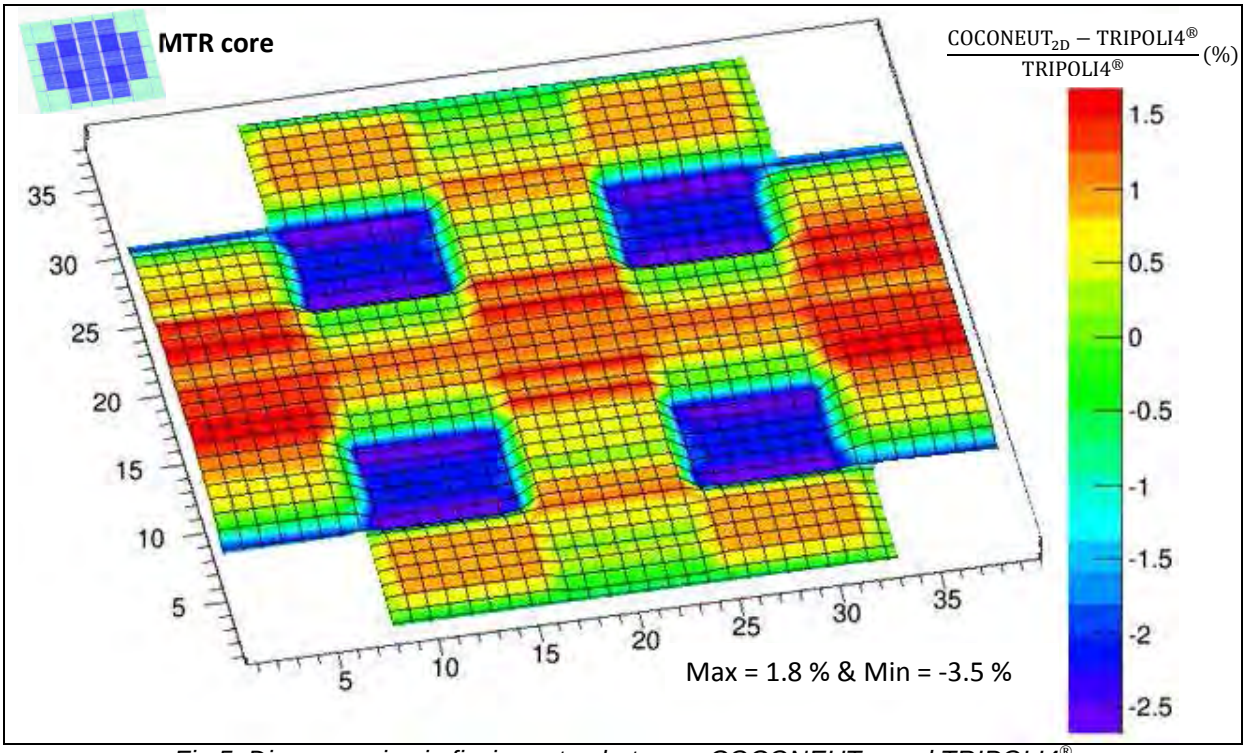

Fig 5. Discrepancies in fission rates between COCONEUT$_{2D}$ and TRIPOLI4®

Fission rates distribution obtained with COCONEUT$_{2D}$ attests of the scheme's accuracy. Discrepancies are within 3 % of error. The maximum error is located in the control assembly.

5.2 3D-model

First comparisons of results obtained with COCONEUT$_{3D}$ and MCNP calculations are presented in the following table. COCONEUT_{3D} calculations are achieved in diffusion theory in 3D "homogenised model".

Main parameters	COCONEUT_{3D}	$\text{MCNP}_{(\pm 1\sigma)}$	$\text{COCONEUT}_{3D} - \text{MCNP}_{\ pcm}$
k_{eff} (Control rods removed)	1.29726	1.29195 ± 15 pcm	**317**
k_{eff} (Control rods fully inserted)	1.14076	1.12019 ± 16 pcm	**1610**
Control rods worth (pcm)	10 575	11 868 ± 22 pcm	**-1293**

Tab 9. Discrepancies in main neutronic parameters

The difference between the 3D homogenized model and a Monte Carlo reference calculation on effective multiplication factor is less than 350 pcm with an overestimation by COCONEUT. The discrepancy on control rod worth is somewhat larger than the 2D model and about 11 % due to diffusion theory assumption and homogenised model.

6 Conclusion and prospective improvements

AREVA TA's neutronic scheme COCONEUT is currently submitted to a large verification, validation and uncertainty quantification program in order to determine and optimize its accuracy in evaluating key parameters for research reactors. The first steps of validation highlight the remarkable ability of COCONEUT to perform accurate calculations with limited CPU-time consumption. COCONEUT performances were numerically validated in comparison with Monte Carlo reference simulations. COCONEUT predicts reactivity within 300 pcm accuracy in 2D and 3D models. Discrepancies on fission reaction rates distribution are less than 3 % with 2D model.

In future works, this validation process will be carried on several reactor designs in order to extend the validity domain of the calculation scheme and distributed in several steps:

- Validation of the entire calculation process to determine biases on key neutronic parameters on equilibrium core,
- Validation of the fuel depletion,
- Elementary validation for each step of the calculation process in order to evaluate, separately, each source of discrepancy and assess compensation mechanisms within the scheme (e.g. Monte Carlo simulation based on COCONEUT multi-group cross sections).

7 References

[1] J.G. Lacombe, J. Koubbi, L. Manifacier, “COCONEUT: An Innovative Deterministic Neutronic Calculation Tool for Research Reactors”, IGORR-2014 Proceedings

[2] J.G. Lacombe, C. Bouret, J. Koubbi, L. Manifacier, “COCONEUT: Enhancing Neutronic Design for Research Reactors”, IGORR-2016 Proceedings, *to be published*

[3] R. Sanchez and al. “Apollo2 year 2010”, *Nuclear Engineering and Technology*, 42:474-499 (2010)

[4] J.F. Vidal, O. Litaize, D. Bernard, A. Santamarina, C. Vaglio, “New Modelling of LWR Assemblies using the APOLLO2 Code Package”, Proc. Int. Conf. on Math. and Comp. M&C2007, Monterey (USA), April 15-17, 2007.

[5] J. Lautard, S. Loubière, C. Fedon-Magnaud. "CRONOS: a modular computational system for neutronic core calculations". IAEA specialist meeting on advanced calculational methods for power reactors. Cadarache, France. 1990.

[6] J. Koubbi, C. Bayol, J.G. Lacombe, C. Bouret, L. Manifacier, H. Krohn, S. Welze “Calculation methods for safety assessments of Research Reactors”, IGORR-2016 Proceedings, *to be published*

[7] X-5 Monte Carlo team, “MCNP – A general Monte Carlo N-particle transport code, version 5”, LA-UR-03-1987

[8] C.M. Diop, O. Petit, E. Dumonteil, F.X Hugot ,Y.K. Lee, A. Mazzolo, J.C Trama, “TRIPOLI-4: A 3D continuous-energy Monte Carlo transport code.” *PHYTRA1: First International Conference on Physics and Technology of Reactors and Applications.* Marrakech, Maroc, 2007

[9] A. Santamarina and D. Bernard, “The Recommended JEFF-3.1.1 File and CEA2005v4 Library for Accurate Neutronics Calculations,” JEFF Report, OECD/NEA 2009.

[10] N. Hfaiedh, A. Santamarina, “Determination of the optimized SHEM mesh for transport calculation.” *International topical meeting on Mathematics and Computation, Supercomputing, Reactor Physics and Nuclear and Biological Applications.* Avignon, France, 2005

[11] S. Santandrea, R. Sanchez, “Acceleration techniques for the characteristic method in unstructured meshes”, *Annals of Nuclear Energy* **29**, 323-352 (2002)

[12] S. Santandrea, R. Sanchez, P. Mosca, “A Linear Surface characteristic approximation for neutron transport in unstructured meshes”, *Nucl. Sci. Eng.* Vol. 160, no.1, Elsevier, pp. 23-40 (2008)

[13] N. Hfaiedh, “Nouvelle méthodologie de calcul de l'absorption résonante“. PHD-2006, Institut de Recherches Subatomiques, Université Louis Pasteur Strasbourg.

[14] Z. Stankovski, “La java de silène: A graphical user interface for 3d pre & post processing”, Joint International Conference on Mathematical Methods and Supercomputing, for Nuclear Applications, Saratoga Springs - USA, October 6-10, 1997

Heat Transfer Analysis of Microscale UO_2 Particle-Graphite System in TREAT Fuel

K. Mo, Y. Miao, A.E. Wright, H.M. Connaway, A.M. Yacout
Argonne National Laboratory
9700 South Cass Ave, Argonne, IL 60439 USA

ABSTRACT

The Transient Reactor Test Facility (TREAT) at Idaho National Laboratory in the United States is now being prepared to restart its operation and perform transient testing to assist with advanced fuel development. In parallel with TREAT restart preparations, a program is underway to develop a low-enriched uranium core to replace the current highly-enriched uranium core. In this study, heat transfer simulation of UO_2 particle-graphite systems in highly-enriched and low-enriched fuels for TREAT was performed using the finite element method (FEM). The irradiation degradation of both UO_2 particles and graphite was taken into account in the simulation. The UO_2 particle size limits for both HEU and LEU fuels were discussed based on the FEM simulation. In addition, a prototypical particle-distribution model was developed to evaluate the effect of size and spatial distribution of UO_2 particles within the graphite.

1. Introduction

The Transient Reactor Test Facility (TREAT) at Idaho National Laboratory in the United States is now undergoing preparations to resume performing transient testing to assist advanced fuel development efforts. In parallel with TREAT restart preparations, a program is underway to develop a low-enriched uranium core to replace the previously used highly-enriched uranium core. Compared to the original HEU TREAT fuel, the prospective LEU TREAT fuel will contain a much higher volume of UO_2 particles, and the particle size may also differ due to the difference in fuel design and advances in manufacturing techniques. The particle size might impact the fuel and reactor performance: (1) For large particles, overheating of the fuel particles during a sharp pulse (reactivity-step) transient is a concern, as it could cause partial melting of the UO_2 particles. In addition, a sufficiently large particle can induce a high thermal resistance in the microscale fuel-matrix system [1], and thus produce a time-lag (defined as the displacement in time between the time-temperature curve for the oxide particle and the time-temperature curve for its surrounding moderator), which may lead to an increase in the integrated power due to the delay in operation of temperature coefficient [2]. (2) Small particles have greater number density in the fuel, leading to larger fission-fragment damaged regions. As a result, the radiation-induced thermal conductivity degradation can be significant when the average particle size in the fuel is sufficiently small. The present study focused on evaluation of the upper size limit of UO_2 particles in TREAT fuels.

2. Basic FEM model

The basic model of the micro-scale UO_2-graphite system was developed and is shown in Fig. 1. This model is also known as the “cell calculation”: consistent with the overall volume ratio of

UO_2-to-graphite, the “cell” model is composed of a fuel particle (as the core) and a graphite matrix (as the shell). Accordingly, the fuel in TREAT was simplified to be a micro-scale UO_2 particle-graphite system based on the assumption that all UO_2 particles are uniformly dispersed within the graphite matrix. Both the graphite matrix and the UO_2 particle embedded in the matrix are modeled to be spherical, with a radial ratio of 1/13.7 for HEU and an assumed ratio of 1/8.2 for LEU. The decrease in thermal conduction due to radiation damage to the graphite at the particle-matrix interface, with its corresponding effect on particle-to-matrix heat transfer, was taken into account. As the design of LEU is not finalized, the thermal properties measured from HEU were also used in the LEU analysis. Detailed description of the model and the thermal properties of both UO_2 and graphite were given in ref. [1]. The UO_2 particle-graphite model developed in this work utilizes the commercial finite-element code COMSOL Multiphysics® [3]. The simulation employed the “heat transfer” module to solve for the time-dependent heat transfer in the UO_2 particle-graphite system.

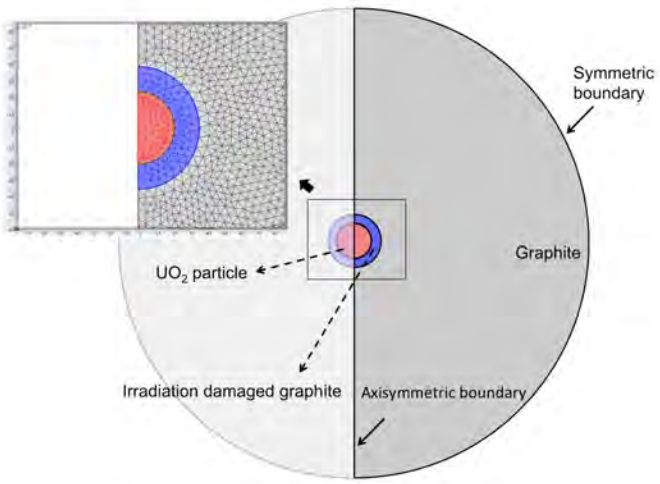

Fig 1. Schematic of the UO_2 particle-graphite model; the UO_2 particle (red) was embedded in the graphite matrix (grey). A fission fragment irradiated zone (blue) was built between the two phases.

A 4.63% reactivity step transient of a HEU core (Fig. 2), the highest power transient generated in TREAT using the HEU fuel [4], was used as the input for the computation. In order to account for the possible higher power needed in a LEU core to achieve similar performance to the HEU core, and to include the consideration of a hot spot in the core, different peaking factors (PFs) were taken into account in the simulation.

- *TREAT HEU Core Temperature-limited Natural Burst Transients*

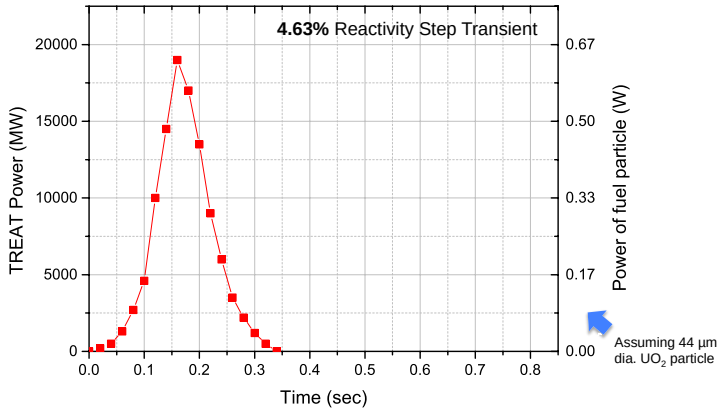

Fig 2. TREAT core temperature-limited natural burst transient power (left y-axis) and the scaled power inputs of a UO_2 particle with a 44 μm diameter (right y-axis) in HEU fuel as functions of time; the transient was measured in a HEU core.

3. Critical particle size

Fig 3 shows the temperatures at the UO_2 particle center as a function of UO_2 particle diameter. Here, we define the critical particle size as the maximum size of the UO_2 particle that maintained a high temperature below the UO_2 melting point of ~2,865°C during the transient. In other words, the particle center would melt if the particle size exceeded the critical size. Tab 1 provides a summary of the critical particle size in HEU and LEU for different PFs. As the volume fraction of UO_2 in LEU fuel is much higher than that in HEU fuel, each particle in LEU fuel produces less power than a particle in HEU fuel. If an identical transient was applied, the temperature of LEU fuel particles would be much lower. Accordingly, the acceptable range of particle size for LEU fuel is much broader. Even with the extreme case of PF = 2.0, the temperature of UO_2 fuel particles of size 105 μm in LEU fuel would not exceed the UO_2 melting point (~2,865°C) during the transient.

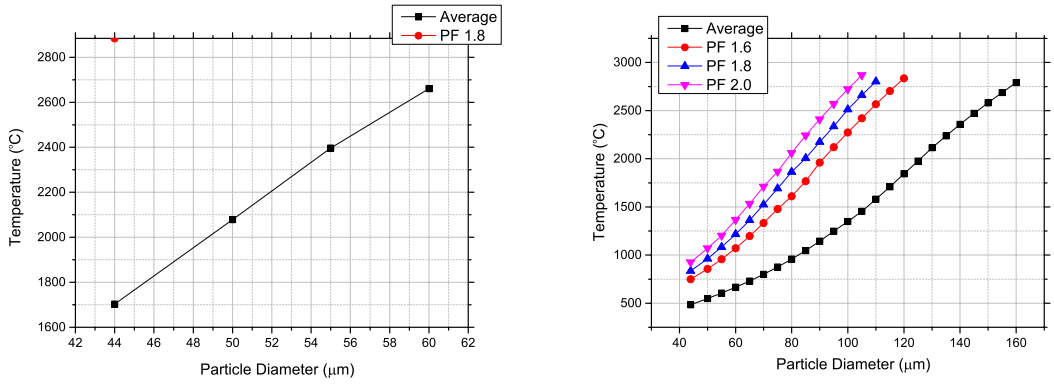

(a) (b)

Fig 3. The maximum temperature of differently-sized particles in the (a) HEU and (b) LEU UO_2 particle-graphite systems.

Fuel Type	PF=1 (core average)	PF=1.6	PF=1.8	PF=2.0
HEU	60	-	44	<44
LEU	160	120	110	105

Tab 1: Critical particle size for HEU and LEU fuels (unit: μm); Note: the PF of HEU fuel was evaluated to be ~1.8. Therefore, the cases with PF values below 1.8 were not calculated for HEU fuel.

4. Prototypical UO_2 particle-distribution model

Previous HEU fuel used U_3O_8 as powders for fuel fabrications because U_3O_8 appears to have a more discrete particle size than UO_2, and UO_2 has a strong tendency to agglomerate [5]. The U_3O_8 powders were reduced to UO_2 during thermal annealing. To study the effect of the agglomeration, we not only built the simple cell model as shown in Fig. 1, but also developed a more complicated prototypical model that includes hundreds of UO_2 particles within a graphite cube. This model can also be used to evaluate the performance of the simplified cell model which assumes all UO_2 particles are uniformly dispersed within the graphite matrix. An example of the modeling is shown in Fig. 4: 1 mm × 1 mm × 1mm graphite cube with ~150 UO_2 particles of various sizes (<44 μm) in a random spatial distribution. The particle size is also randomly distributed, and the average size is ~20 μm. The volume ratio of UO_2 particle to graphite is ~550, a similar value to that in the LEU fuel. We allowed some particles to connect to mimic agglomeration of UO_2. (Fig. 5)

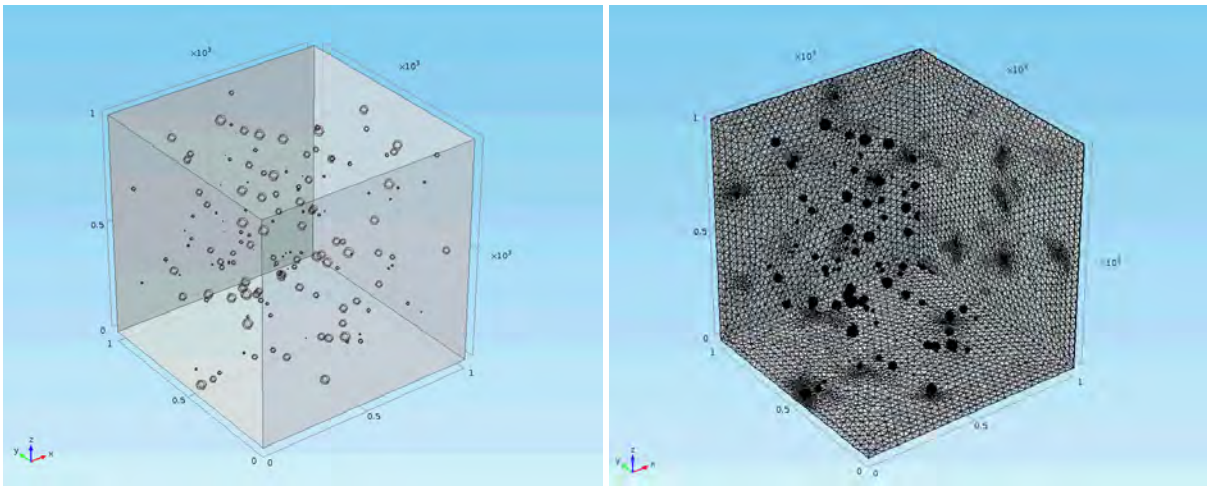

(a) (b)

Fig 4. UO_2-graphite system with 150 UO_2 particles embedded in a 1mm × 1mm × 1mm graphite cube: (a) random distribution of UO_2 particles in the prototypical model; and (b) the model after meshing.

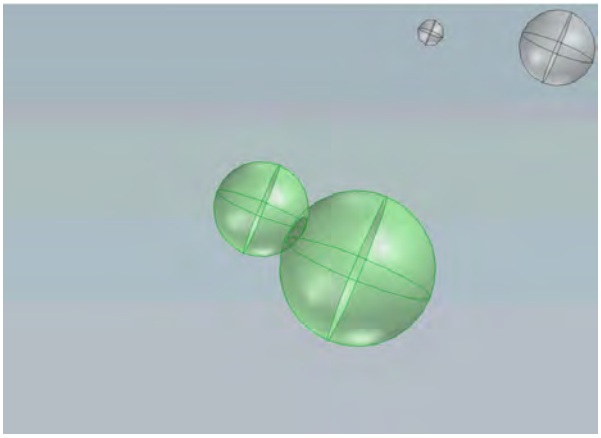

Fig 5. Two connected UO_2 particles sampled from the model in Fig. 4.

The results of the simulation based on the prototypical model are given in Fig. 6 and 7. The temperature gradients are clearly seen in Fig. 6 as a function of particle size and spatial distribution. The average temperature of the particles and graphite are given in Fig. 7. This result can be further processed to compute the time-lag in the LEU fuel.

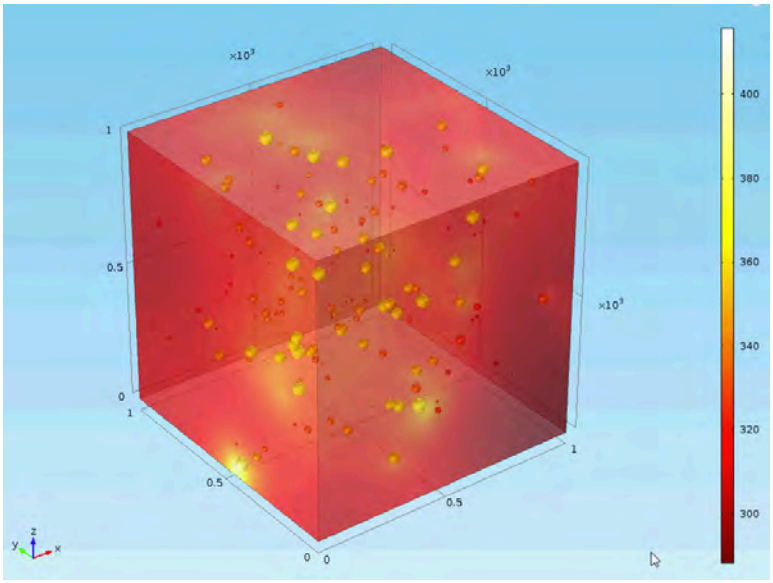

Fig 6. 3D temperature distribution of the model in Fig. 4. The snapshot was taken at 0.172s of the transient given in Fig. 2.

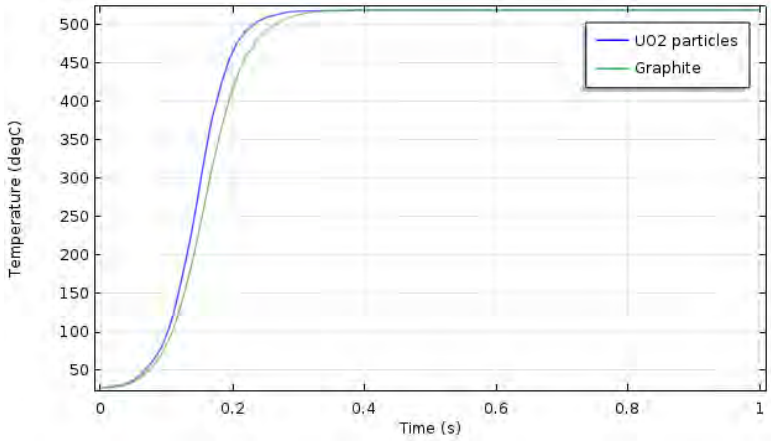

Fig 7. Temperatures of UO_2 particles and graphite in the model given in Fig. 4. The temperature of the UO_2 particles is the volume average of all UO_2 particles within the system. The temperature of the graphite is volume averaged over all the graphite matrix within the system.

5. Conclusion

In this study, the heat transfer in a UO_2 particle-graphite system in TREAT fuel was simulated with the finite element method. After analyzing the temperature development of the fuel particle during the highest power transient able to be generated in TREAT using the HEU fuel, the critical particle size of both HEU and LEU fuels was determined. The critical particle size of LEU fuel was found to be much larger than that of HEU fuel. Even with a radiation damaged layer and a large PF applied, particles of 105 μm in size would not melt in LEU fuel.

The effect of UO_2 agglomeration can be better studied using the more complicated prototypical model. When high-resolution microscopic or radiographic images of “simulated LEU fuel” are available, a more practical and realistic simulation can be conducted using the prototypical model. The cracks and other defects can also be taken into account in the model. When the particle size and spatial distributions are available, we can also perform a systematic study to evaluate the temperature distribution and possible time-lag in the LEU fuel.

Acknowledgements

This work is sponsored by the U.S. Department of Energy, National Nuclear Security Administration (NNSA), Office of Material Management and Minimization (NA-23) Reactor Conversion Program, under Contract No. DE-AC-02-06CH11357 between UChicago Argonne, LLC and the Department of Energy.

Reference

[1] K. Mo, D. Yun, A.M. Yacout, A.E. Wright, Heat transfer simulations of the UO_2 particle–graphite system in TREAT fuel, Nucl Eng Des, 293 (2015) 313-322.
[2] G.A. Freund, P. Elias, D.R. MacFarlane, J.D. Geier, J.F. Boland, Design Summary Report on The Transient Reactor Test Facility (TREAT), ANL-6034, Argonne National Laboratory, 1960.
[3] COMSOL, COMSOL Multiphysics® 5.1, User’s Guide. , COMSOL Inc., 2015.

[4] J.P. Tylka, A.B. Rothman, P.H. Froehle, G.J. Pokorny, M.E. Stephenson, A.J. Ulrich, EOS Series of Experiments in TREAT, Trans. Am. Nucl. Soc., 27 (1977) 508.
[5] J.H. Handwerk, R.C. Lied, The manufacture of the graphite-urania fuel matrix for TREAT, ANL-5963, Argonne National Laboratory, 1960.

FIRST STEPS TOWARDS A COUPLED CODE SYSTEM FOR TRANSIENT CALCULATIONS

C. REITER, H. BREITKREUTZ, A. RÖHRMOSER, W. PETRY
Forschungs-Neutronenquelle Heinz Maier-Leibnitz (FRM II), Technische Universität München
Lichtenbergstraße 1, 85748 Garching bei München, Germany

ABSTRACT

The Forschungs-Neutronenquelle Heinz Maier-Leibnitz (FRM II) is Germany's most powerful neutron source and has the highest flux-to-power ratio in the world. With a thermal power of only 20 MW the compact core provides an undisturbed maximum thermal neutron flux of 8.0 * 10^{14} n/(s cm²). To support the global non-proliferation efforts, FRM II is actively working towards the conversion of its fuel element to a uranium enrichment which is significantly lower than the current 93%. Changes in fuel type and core geometry require a re-evaluation of neutronic and thermal-hydraulical behavior of the FRM II, in normal operation as well as in off-normal transients.

A coupling of the neutronic code TORT-TD and the thermal-hydraulic system code ATHLET was identified as most promising solution for transient evaluation, as most standard-code systems are not applicable for the challenging conditions of the FRM II core. Models for these codes are derived from the validated MCNP6 and CFX models. As intermediate step and to calculate the homogenized group cross sections, a Serpent 2 model was created from a simplified MCNP6 model.

The simplified MCNP6 model uses a vertical stack of plates instead of involutes. The total core material inventory and the general assembly design are retained. It correctly reproduces the power deposition profile with less than 3% deviations, up to 2.5% of which are statistical fluctuations. Only near the top and the bottom very small areas exceeding these values can be found.

Reactivities for MCNP6 and SERPENT 2 match within $\Delta\rho < 0.0003$, i.e. one standard deviation. One particular item in the comparison of the models was the influence of the (n, 2n) reaction in the Beryllium follower of the FRM II control rod. With a $\Delta\rho \sim 0.002$, this effect contributes nearly two days of total cycle length. Again, both codes Serpent 2 and MCNP show a good agreement.

In a next step, the TORT-TD model will be created and CFX and ATHLET results have to be compared.

1. Introduction

The Forschungs-Neutronenquelle Heinz Maier-Leibnitz (FRM II) is Germany's most powerful neutron source and has the highest flux-to-power ratio in the world. With a thermal power of only 20 MW the compact core provides an undisturbed maximum thermal neutron flux of $8.0 \cdot 10^{14}$ n/(s cm²).

To support the global non-proliferation efforts, FRM II is actively working towards the conversion of its fuel element to a uranium enrichment which is significantly lower than the current 93%. In an international collaboration with other research reactor operators, a new high density fuel based on uranium-molybdenum (UMo) alloys is being developed to replace the currently used fuels which cannot provide a sufficiently high chemical Uranium density to lower the enrichment as intended. Slight changes to the core geometry and the different absorption behavior of the UMo alloys require a re-evaluation of both the neutronical and

thermo-hydraulical behavior of the FRM II, in normal operation as well as in off-normal transients. While steady state operation behavior has already been demonstrated to a large extent [1, 2, 4]) and is still ongoing, this project focuses on the adaption of a complete code system for transient calculations.

2. Project Description

In a first step, different codes have been analyzed regarding their applicability to the very constraint conditions found within the compact core of FRM II. As the most promising solution, a coupling of the neutronic code TORT-TD and the thermal-hydraulic system code ATHLET was identified. Both codes were developed at the Gesellschaft für Anlagen- und Reaktorsicherheit (GRS). TORT-TD is a time-dependent, three dimensional multi group code used to calculate the neutronics of reactor transients. TORT-TD is based on TORT of the ORNL code system DOORS [6].

The basis for the development process is the well-established full core MCNP model of FRM II. After a simplification of the model, an equivalent model in Serpent 2 was developed and verified against the results of MCNP 6. With a fully functional Serpent 2 model, the homogenized group cross sections, which are needed for TORT-TD, can be calculated. In the end of this process, all results, especially reactivity, flux and fission power distribution obtained from TORT-TD will be validated against the MCNP 6 calculations.

A similar proceeding was chosen for the thermal-hydraulic calculations. A CFD core model already exists for Ansys CFX steady state which has previously been analyzed in depth. After modeling the FRM II in ATHLET, the results will then be validated using the CFX results [1] and NBK results. NBK is a multi-channel thermal-hydraulic code developed by TUM during FRM II's design phase to calculate thermal conditions like temperature, pressure or coolant flow in flat or curved fuel element cooling channels [3, 4].

Following the validation of the neutronic and thermal-hydraulic models, TORT-TD and ATHLET will be used in coupled mode in order to calculate the respective transients.

This paper discusses the first steps of the neutronic model construction and validation of the FRM II, starting from the well-established full-core MCNP6 model.

3. The FRM II Fuel Element

Yet, the complex geometry of the very compact core and installations in the moderator tank of the FRM II cannot be modeled as-built in deterministic codes with acceptable solution time: FRM II is a light water cooled and heavy water reflected reactor. The heavy water is situated in a separated tank outside the central channel and contains numerous installations, e.g. a cold and a hot source, safety shut down rods, irradiation positions, etc. As a compact core reactor, FRM II has only a single fuel element consisting of 113 involute shaped fuel plates.

Such a complex geometry cannot be reproduced in TORT-TD. Hence, a simplified geometry needs to be found that still delivers the same values for the neutronic key-parameters such as fresh core excess reactivity, thermal neutron flux and power deposition in the plates.

4. Substitutional geometry

As first simplification steps for the MCNP6 model with involute plates (Figure left), already existing models [1] using concentric tubular plates or using vertically stacked plates (Figure right) have been analyzed regarding reactivity and energy deposition.

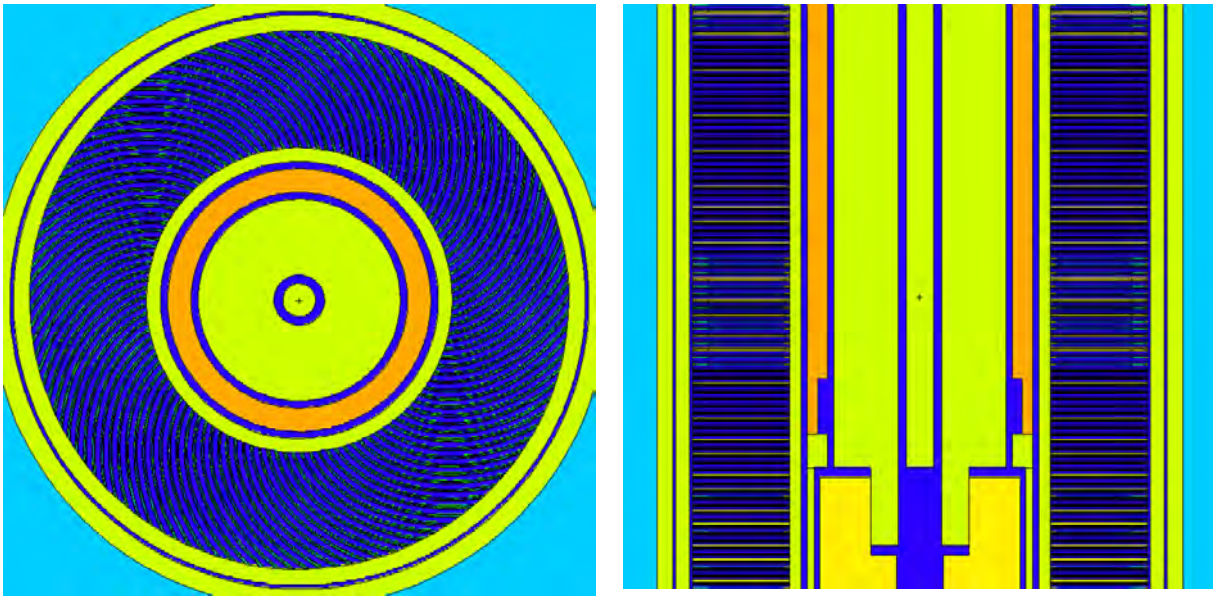

Figure 1. Top view of the involute MCNP6 model (left). Side view of the substitutional vertical stack MCNP6 model (right).

Based on this evaluation, a modified version of the vertical stack model was selected. It uses 196 stacked plates resembling the geometry of the original plates. Two plates with 31% of the original thickness have been placed at the top and bottom of the fuel zone in order to fill the remaining space as well as to correctly reproduce the power deposition profile vertically. Total core material inventory and the general assembly design are therefore retained. The stacked design particularly allows for high resolution, in the vertical direction of the power deposition profile and also reproduces that radial distribution correctly, even near the density step. This sharp decrease in the uranium density between the inner and outer fuel zones of the fuel plates is one of the key elements in order to reduce the heat load near the heavy water.

Fresh core excess reactivity for both models matches perfectly (Table 1).

Table 1: Comparison of the fresh core excess reactivity for the involute plate and the vertical stack model.

	Involute plate model	**Vertical stack model**
Plates	113 original involute plates	192.62 virtual vertical discs
k_{eff}	0.99772 ± 0.00009	0.99772 ± 0.00009

The comparability of the power deposition of both models has been assessed using tmesh tally type 3 (Figure). The size of the mesh was chosen so that it covers one complete fuel plate, whereat near material borders the radial frequency of mesh cells gets bigger, ranging from 0.08 cm near the control rod over 0.125 cm in the plate center to 0.01 cm near the density decrease and the outer edge.

The power distribution between both models differs less than 3%, with a statistical fluctuation of only 2.5%. The power distribution results of both models match well. Only near the lower and upper border of the active zone, where the two reduced plates were introduced into the vertical stack model, does the deviation increases to approximately 3 to 7%. The impact of those small areas is negligible on the macroscopic key core parameters.

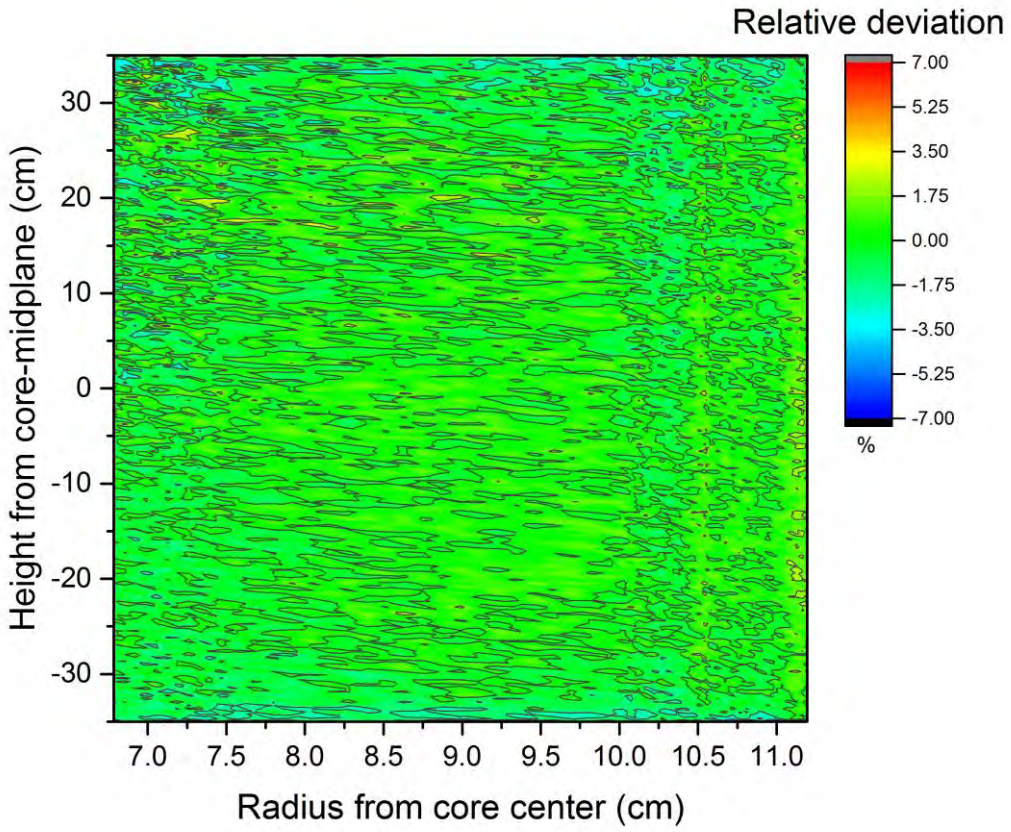

Figure 2. Relative deviation of the power deposition of the involute model and the vertical stack model in percent.

5. COMPARISON OF MCNP6 AND SERPENT 2

In the next step, the MCNP 6 stack model described in the previous paragraph was translated into a geometrically equivalent model for Serpent 2.

The calculations in MCNP 6 and Serpent 2 were performed using 50,000 particles per cycle, 50 inactive and 250 active cycles on. Results for the fresh core excess reactivity are presented in Table 2. The results of both codes match well within one standard deviation.

Table 2: Comparison of the fresh core excess reactivity for the MCNP 6 and Serpent 2 model.

	MCNP 6	**Serpent 2**
$\mathbf{k_{eff}}$	0.99794 ± 0.00029	0.99832 ± 0.00031

6. IMPACT OF THE (N, 2N) REACTION IN THE BERYLLIUM FOLLOWER

One particular issue in the comparison of the MCNP6 and Serpent 2 models was the influence of the (n, 2n) reaction in Beryllium, this reaction was not supported by Serpent 2 in the ENDF/B V libraries. This reaction turned out to be the cause of a notable mismatch in excess reactivity that was observed in our calculations.

The control rod of FRM II consists of a hafnium absorber at top and a beryllium reflector at the bottom. By adjusting the cross section libraries accordingly, the influence of this single reaction on total reactor performance can be isolated. In Serpent 2, this was achieved by directly turning off the reaction. In MCNP 6, the same was achieved using first order perturbation theory with the kpert card.

Table 3: Comparison of the Influence of the (n, 2n) reaction gained with different codes

	MCNP 6 (standard)	**MCNP 6 (kpert, no n,2n)**	**Serpent 2 (without n,2n)**
$\mathbf{k_{eff}}$	0.99794 ± 0.00029	0.99538	0.99551 ± 0.00031

Table 3Table 3 shows the impact of the (n, 2n) reaction in beryllium for a fresh fuel element. The delta of ca. 0.002 in reactivity is within statistical error scope and, contributes nearly two days of cycle length. Again, both codes, Serpent 2 and MCNP6 are in agreement within statistical error scope.

7. SUMMARY AND PERSPECTIVES

The modified vertical stack model provides a suitable substitutional geometry that allows for a TORT-TD model to be created and validated. The results found by this model for reactivity, power deposition, as well as thermal flux distribution, match with the full involute model.

Following this comparison a Serpent 2 model was created to provide a tool allowing for the calculation of the multi group cross sections which are needed for the deterministic transient calculations in TORT-TD. MCNP6 and Serpent 2 deliver matching results for reactivity. During these studies it was found that the (n, 2n) reaction in the beryllium follower of the control rod contributes nearly two days of operation.

In further studies the results for the thermal and fast neutron flux distribution obtained with MCNP6 and Serpent 2 as well as the fission energy deposition in the fuel plates will be compared. For transient calculations a cross-section database for multiple temperatures will be created with Serpent 2. The results for reactivity and flux distribution obtained with the new TORT-TD model will be compared to the data obtained with MCNP6 and Serpent 2. Afterwards the thermo-hydraulical development will be performed in a similar way.

As last step full Transients will be calculated using TORT-TD and ATHLET in coupled mode.

REFERENCES

[1] A. Röhrmoser, "Core model of new German neutron source FRM II," *Nuclear Engineering and Design,* pp. 1417-1432, 2010.

[2] A. Röhrmoser, Neutronenphysikalische Optimierung und Auslegung eines Forschungsreaktors mittlerer Leistung mit Zielrichtung auf einen hohen Fluss für Strahlrohrexperimente, Technische Universität München: PhD Thesis, 1991.

[3] A. Röhrmoser, Untersuchungen zur Kühlbarkeit eines neuartigen Kompaktkerns für Forschungsreaktoren, Technische Universität München: Diplomarbeit, 1984.

[4] H. Breitkreutz, "Coupled Neutronic and Thermal Hydraulics of High Density Cores for FRM II," PhD Thesis, Technische Universität München, 2011.

[5] C. Döderlein, Untersuchungen zur Kühlbarkeit eines kompakten Reaktorkerns mit evolventenförmigen Brennstoffplatten, Technische Universität München: Diplomarbeit, 1989.

[6] "GRS Website," 29 Dezember 2015. Available online: http://www.grs.de/content/tort-td/.

IMPROVEMENTS IN NEUTRON AND GAMMA MEASUREMENTS FOR MATERIAL TESTING REACTORS

J-F. VILLARD, C. DESTOUCHES, L. BARBOT, D. FOURMENTEL, V. RADULOVIC
CEA, DEN, DER, Instrumentation Sensors and Dosimetry Laboratory
Cadarache, Bat 238, F-13108 St Paul Lez Durance, France

ABSTRACT

In order to ensure quality and relevance of irradiation programs in the future Jules Horowitz Reactor (JHR), the French Alternative Energies and Atomic Energy Commission (CEA) has significantly increased its R&D efforts in the field of in-pile instrumentation during the last decade. Major progresses have thus been achieved in capability to perform accurate in-pile measurements using reliable and updated techniques.
Benefits of this enhanced measurement potential, illustrated with some improvements achieved in neutron and gamma flux detection, are described in this paper.

The CEA has recently developed and validated a numerical toolbox which predicts the output signal of Self-Powered Neutron Detectors (SPNDs) in various irradiation conditions. This original simulation toolbox named 'MATiSSe', based on Monte Carlo calculations and a comprehensive SPND model, is particularly useful to design, implement and operate SPNDs. These neutron detectors are already identified among the most relevant sensors for thermal neutron flux measurements in the JHR, due to their robust construction, simple use and relatively low cost. The 'MATiSSe' toolbox will contribute to a better knowledge of irradiation conditions in JHR.
In addition, the CEA has also improved its measurement techniques for neutron and gamma flux assessment. A unique system for online measurement of fast neutron flux has been developed and qualified in-pile in 2015. The Fast-Neutron-Detection-System (FNDS) has been designed to monitor accurately high-energy neutrons flux (E > 1 MeV) in Material Testing Reactors. FNDS system is based on a Pu242 fission chamber and dedicated hardware and software that allow a large measurement range, an efficient gamma rejection and an online correction of the sensor sensitivity change during irradiation. FNDS system will be used to perform spectral neutron characterization of JHR channels as well as more accurate monitoring of the fast neutron dose in tested materials.
New sensors, specifically designed for MTR irradiation conditions, have also been released. As an example, a miniature gas ionization chamber has been developed and manufactured by the CEA. Tests performed in different research reactors demonstrate the reliability and the accuracy of this instrumentation dedicated to in-pile and real-time measurement of gamma flux over a large range of radiation level from residual power to nominal power, including estimation of delayed gamma flux.

1. Introduction

Over 50 years of fuel and material irradiation tests has led to many countries developing significant improvements in instrumentation to monitor physical parameters and to control the test conditions in material testing reactors (MTRs). Various types of instruments have been developed and used in MTRs, and many of these sensors have been gradually upgraded and refined since their initial development [1].
Recently, there is increased interest to improve the existing in-pile instrumentation and to enlarge measurement capabilities in MTRs, particularly in France where the Alternative Energies and Atomic Energy Commission (CEA) is currently building the future Jules Horowitz Reactor (JHR). Operated at 100 MW_{th}, the JHR will generate radiation levels that are expected to be significantly higher than the previous French MTR OSIRIS definitively shutdown at the end of 2015. In JHR's irradiation locations, thermal neutron flux is expected to reach $5.5 \cdot 10^{14}$ $n.cm^{-2}.s^{-1}$ in the reflector while fast neutron (E > 1MeV) flux will reach the same level in the core, allowing material ageing up to 16 $dpa.y^{-1}$. At the same time, nuclear heating will range as high as 20 W/g, bringing new challenges to design experimental devices.

In these harsh conditions, highly-instrumented experiments will be required to evaluate the performance of fuels and materials for advanced pressurized water reactors (PWR) and Generation IV (Gen-IV) reactor systems, but also the performance of radiation-resistant materials for fusion reactors. Hence, new sensors are needed that can provide “real-time” measurements of key irradiation characteristics.
To illustrate CEA’s research and development effort and progresses that have been achieved in the capability to perform accurate in-pile measurements, some improvements obtained in neutron and gamma flux detection using reliable and updated techniques are described below.

2. Improvements in neutron and gamma flux detection

2.1 Progress in Self-Powered Neutron Detector simulation

The JHR will host a large variety of irradiation experiments, which will require several diverse neutron detectors. Self-Powered Neutron Detectors (SPND) are already identified as major contributors to neutron level qualification in JHR irradiation experiments, due to their robust construction, simple use and relatively low cost. Nevertheless SPND response calibrations need to be adapted to diverse irradiation conditions, requiring numerous and fastidious SPND calibration tests. In this perspective, the Instrumentation Sensors and Dosimetry Laboratory (LDCI) of CEA Cadarache has been developing, since 2010, a numerical toolbox based on Monte Carlo calculations for self-powered neutron detector design, simulation and operation. This CEA SPND simulation toolbox was named ‘MATiSSe’ for ‘Monte cArlo Tool for SPND Simulations’ [2].

Generally, SPND have a coaxial geometry with a central electrode, called emitter, surrounded by an insulator and an external concentric electrode, called sheath or collector (see Figure 1). This sensitive part is connected to the measuring system by an integrated mineral insulated cable. Self-powered neutron detector principle is based on the collection of electrons mainly created in the emitter, coming from neutron interactions with the detector materials. These moving electrons are generating an electric signal which is measurable.

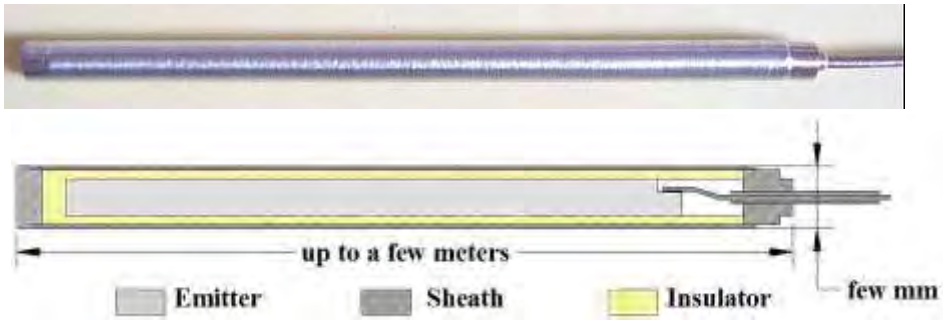

Figure 1. Picture and drawing of a typical self-powered neutron detector

When a SPND is irradiated in a mixed neutron and gamma field, numerous nuclear interactions are taking place in the three components of the detector. For neutron measurements, two different types of SPNDs are considered. First, detectors with dominant (n, β^-) reaction are called ‘delayed SPND’ because their time response is driven by the decay constant of the created beta emitter. Second type SPND are called ‘prompt’ because of their instantaneous response due to the predominant $(n,\gamma)(\gamma,e)$ reaction. External gamma (fission, activation…) interactions also create some free electrons in detectors, (γ,e) reaction.

All created electrons, while moving between the electrodes, are giving rise to a direct electric current between the emitter and the sheath, which is proportional to the mixed neutron and gamma field where the SPND is irradiated. The SPND total output current, when irradiated in

a mixed field, is always a sum of partial currents coming from the three mentioned reactions in all involved materials: emitter, insulator, sheath and close detector surroundings.

The SPND model relies on two fundamental points: the exhaustive study of all possible free electron creation sources within SPND materials and the transport calculation of these electrons in the different SPND components and their corresponding charge depositions.

In the model implemented in LDCI's MATiSSe toolbox (see Figure 2), the SPND signal is determined as a combination of the net electron currents at the emitter/insulator and insulator/sheath boundaries and an analytical expression of the fractions of electrons currents being reflected by the electric field created in the insulator, originating from electric charges being deposited in the material [3]. Using close neutron and gamma fields (levels and spectra) accurately established beforehand, a fine model of the SPND and its immediate environment and different steps of Monte Carlo and analytical calculations, the three main reaction contributions are calculated [2].

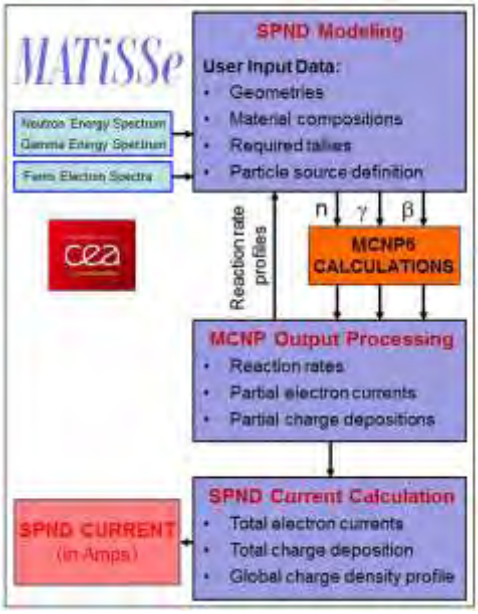

Figure 2. Block diagram of LDCI's MATiSSe toolbox for self-powered detector simulation

Between 2011 and 2014, successive dedicated experiments have been performed to validate MATiSSe numerical tool. Different types of SPNDs, including Rhodium, Cobalt and Silver emitter materials and various geometries, have been tested first at the Slovenian TRIGA Mark II reactor operated by the Jožef Stefan Institute (JSI), then at the French OSIRIS reactor operated by CEA, and at the Polish MARIA reactor operated by the National Centre for Nuclear Research (NCBJ). Details about these programs are given in [4].

Results show the good agreement between the SPND currents evaluated by MATiSSe and the measurements. Detailed results are given in [2].

The MATiSSe toolbox is now available for SPND design, simulation and data analysis. It is particularly relevant for the study of neutron detection systems that are expected to be implemented in future reactors. This tool will be part of the instrumentation suite to be used for the commissioning tests of the Jules Horowitz Reactor. It will participate in the quality of the neutron flux assessment for the future material and fuel irradiation tests.

2.2 Qualification of Fast-Neutron-Detection-System

Real-time neutron flux measurements can also be performed using fission chambers. The choice of the fissile deposit in a fission chamber depends on the neutron energy range of interest. The resulting online spectral information is valuable for neutronics studies at zero-power reactors and for flux monitoring in experimental devices in MTRs.
A fission chamber is typically composed of two coaxial cylindrical electrodes, one of which is covered with fissile material. The inter-electrode gap is filled with gas, often argon. After a neutron-induced fission in the deposit, one of the fission products is ejected into the gas, creating a large number of charge pairs. These charges are collected by a polarization voltage applied between the electrodes, leading to a current pulse.

CEA has developed and can manufacture thermal and fast fission chambers having an outer diameter as small as 3 mm for miniature chambers, or even 1.5 mm for subminiature chambers. While most fission chambers are primarily used for thermal neutron detection, the Joint Instrumentation Laboratory between CEA and the Belgian Nuclear Research Centre (SCK•CEN) has developed an instrumentation suite based on fission chambers for online in-core measurement of the fast neutron flux (E > 1MeV) [5].

This Fast Neutron Detection System (FNDS) has been designed to measure fast neutron flux in typical Material Testing Reactor conditions, where overall neutron flux level can be as high as 10^{15} n.cm^{-2}.s^{-1} and is generally dominated by thermal neutrons. Moreover, the neutron flux is accompanied by a high gamma flux of typically a few 10^{15} γ.cm^{-2}.s^{-1}, which can be highly disturbing for the online measurement of neutron fluxes.
The patented FNDS system is based on two miniature fission chambers allowing the simultaneous detection of both thermal and fast neutron flux. Thermal neutrons can be measured using SPND or U235 fission chamber, while fast neutron detection requires a special fissile material presenting an energy threshold near 1 MeV. This fissile material is usually Pu242 for MTR conditions [6]. The fission chambers are operated in Campbelling mode for an efficient gamma rejection [7]. FNDS also includes a specific software that processes measurements to compensate online the fissile material depletion and to adjust the sensitivity of the detectors, in order to produce a precise evaluation of both thermal and fast neutron flux even after long term irradiation.

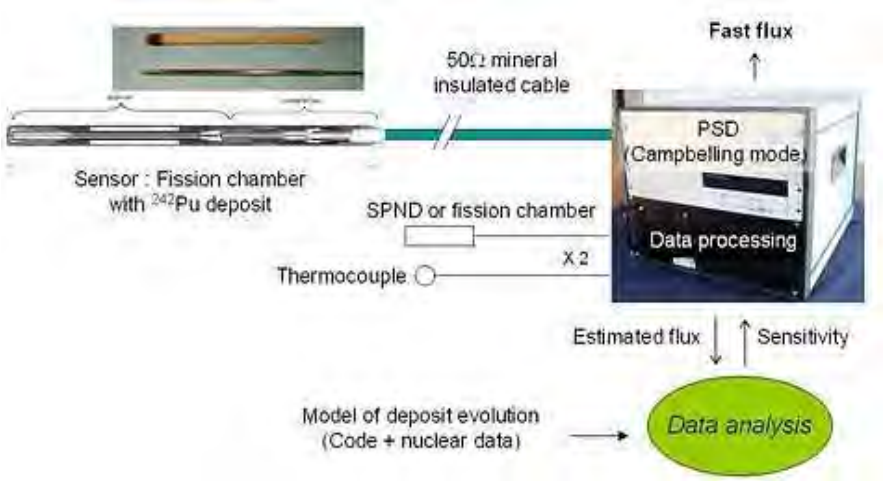

Figure 3. Fast Neutron Detection System developed by CEA and SCK•CEN

FNDS has been validated through a two-step experimental program. A first set of tests was performed in 2009 at BR2 reactor operated by SCK•CEN in Belgium. Two FNDS prototypes were operated in-pile during nearly 1000 hours. These tests exhibited the consistency of the measurement of thermal to fast neutron flux ratio with MCNP calculations, as well as the right compensation of fissile material depletion [8]. Then a second test was completed in 2015 at ISIS reactor operated by CEA in France. For this irradiation, FNDS signal was compared to reference thermal and fast neutron flux measurements using activation dosimeters analyzed under COFRAC® Quality Certification. During this latter test, FNDS proved its ability to measure online both thermal and fast neutron flux with an overall accuracy better than 10%.

FNDS is now operational and is assumed to be the first and unique acquisition system able to provide an online measurement of the fast neutron flux in MTR conditions. This system will of course be used to perform spectral neutron characterization of JHR channels, but it may also be implemented in future irradiation experiments, for a better and real-time evaluation of the fast neutron flux received by material and fuel samples.

2.3 Development of miniature gas ionization chambers

In nuclear reactors, including MTRs, photon flux is commonly calculated by Monte Carlo simulations but rarely measured. However, photon flux is assumed to be the main contributor to energy deposition in materials, and thus to nuclear heating which is of first importance to design and operate irradiation experiments. In this context, CEA recently developed a miniature gas ionization chamber (MIC) designed to be operated on a large range of photon flux levels covering MTR conditions, up to a few 10^{14} $\gamma.cm^{-2}.s^{-1}$. This sensor is based on a 3 mm fission chamber design (see Figure 4).

Figure 4. Picture and drawing of a 3 mm miniature gas ionization chamber manufactured by CEA

A first test of this sensor has been performed in 2012 at OSIRIS reactor. The MIC was irradiated along a suite of sensors including fission chamber, SPND, Self-powered gamma detector (SPGD), gamma thermometer and differential calorimeter [9]. This test proved the consistency of the MIC signal with other evaluations of gamma flux.
A second test was achieved in 2014 at the Slovenian TRIGA Mark II reactor. Measured MIC signal was compared with calculated currents based on simulations with the MCNP6 code. This irradiation confirmed the relevance of MIC sensor for online and real-time evaluation of gamma flux over a wide range of flux level. As illustrated in Figure 5, MIC has proven to be particularly appropriate to follow reactor SCRAMs (reactor shutdown with rapid insertions of control rods). These measurements demonstrated the importance of the delayed contribution to the photon field in nuclear reactors, providing evidence that over 30% of the total measured gamma signal is due to the delayed photon field, originating from fission and activation products (which are often untreated in calculations) [10].

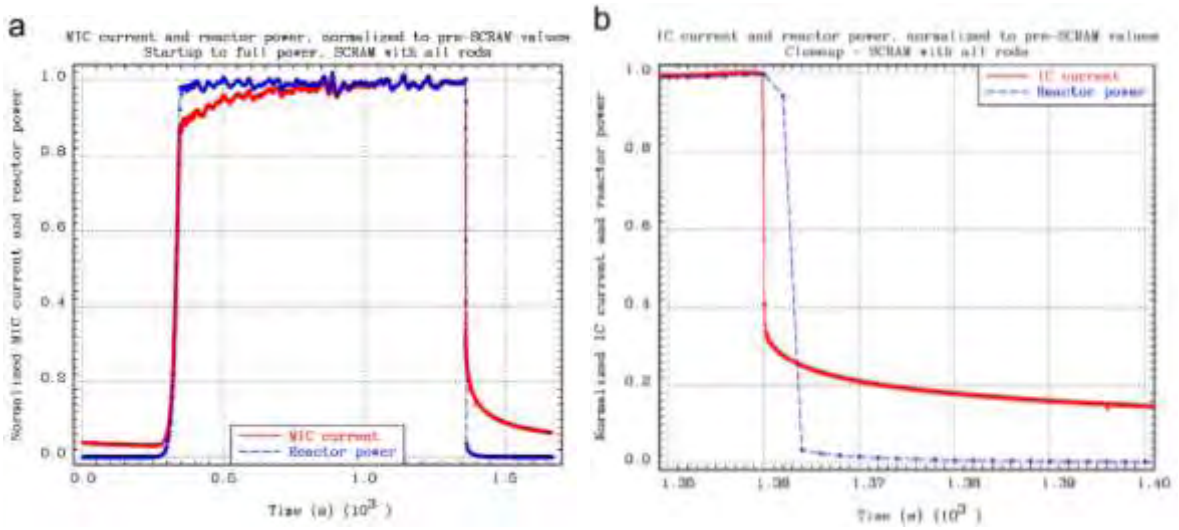

Figure 5. Measured MIC current (normalized to maximum value) at the Slovenian TRIGA Mark II. Figure a: reactor start-up from zero to full power, followed by a reactor SCRAM ; Figure b: reactor SCRAM close-up

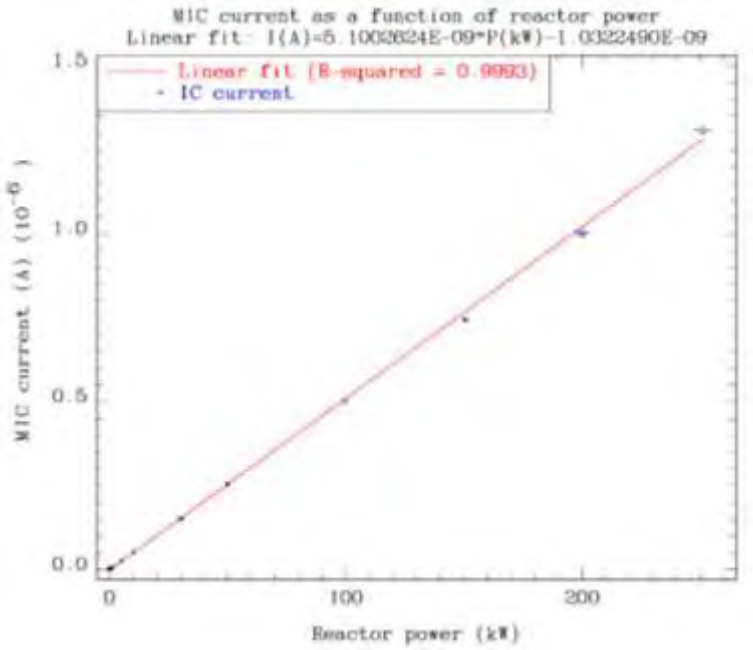

Figure **6**. Measured MIC current as a function of Slovenian TRIGA Mark II reactor power at steady power levels [11]

As shown in Figure 6, MIC measurements at different stable reactor powers exhibited the linearity of the MIC current with reactor power (the R^2 value of the linear fit being 0.9993). This demonstrates that MICs are good real-time monitors of the reactor power.

Finally, miniature gas ionization chambers are versatile sensors with a large dynamic measuring range. They are excellent candidates for gamma flux characterization, as well as real-time monitoring of reactor power. MIC will of course be part of the instrumentation suite that may be installed for the commissioning tests of the future Jules Horowitz Reactor.

3. Conclusion

Significant advances in the capability to monitor online and real-time neutron and gamma flux in Material Testing Reactors have recently been achieved by French Alternative Energies and Atomic Energy Commission (CEA), in the framework of fruitful collaborative programs conducted with Belgian Nuclear Research Centre (SCK•CEN), Slovenian Jožef Stefan Institute (JSI) and Polish National Centre for Nuclear Research (NCBJ).

In particular, calibration processes have been improved using combination of modelling and comparison with dosimetry measurements, leading also to substantial reductions to the uncertainty budget. In addition, these calibration processes extend the operating range of sensors from relative to absolute neutron or gamma flux evaluation.

As illustrated in this paper, development and qualification of Self-Powered Neutron Detector simulation, Fast-Neutron-Detection-System and miniature gas ionization chambers will be especially beneficial for the characterization of the future Jules Horowitz Reactor currently under construction in Cadarache. Furthermore, their interest covers also a large range of potential applications in other research and power reactors.

4. References

1. B. G. Kim et al., “Review of Instrumentation for Irradiation Testing of Fuels and Materials,” *Nuclear Technology,* 176, pp 155-187, Nov 2011

2. L. Barbot et al., ‘Experimental Validation of a Monte Carlo based Toolbox for Self-Powered Neutron and Gamma detectors in the OSIRIS MTR’, to be presented at the *PHYSOR conference*, Sun Valley, Idaho, USA, May 1 – 5, 2016

3. L. Vermeeren et al., ‘Theoretical study of radiation induced electromotive force effects on mineral insulated cables’, American Institute of Physics, *Review of Scientific Instruments* volume 74 - number 11, 2003

4. L. Barbot et al., ‘Calculation to experiment comparison of SPND signals in various nuclear reactor environments’, *4th International Conference ANIMMA 2015*, Lisbon, Portugal, April 20-24, 2015

5. J.-F. Villard et al., “Advanced In-pile Measurements of Fast Flux, Dimensions and Fission Gas Release,” *Nuclear Technology*, 173, pp 89-97, January 2011

6. P. Filliatre et al., “Reasons why Plutonium 242 is the best fission chamber deposit to monitor the fast component of a high neutron flux”, *Nuclear Instruments and Methods in Physics Research A* 593 (2008) 510– 518

7. L. Vermeeren et al., “Experimental Verification of the Fission Chamber Gamma Signal Suppression by the Campbelling Mode”, *IEEE Transactions on Nuclear Science*, Vol. 58, N°2, April 2011

8. B. Geslot et al.,” New measurement system for on line in core high-energy neutron flux monitoring in materials testing reactor conditions”, *Review of Scientific Instruments* 82, 033504 (2011)

9. D. Fourmentel et al., “Measurement of photon flux with a miniature gas ionization chamber in a Material Testing Reactor”, *Nuclear Instruments and Methods in Physics Research A* 724 (2013) 76–82

10. D. Fourmentel et al., “Delayed Gamma Measurements in Different Nuclear Research Reactors Bringing Out the Importance of the Delayed Contribution in Gamma Flux Calculations”, *4th International Conference ANIMMA 2015*, Lisbon, Portugal, April 20-24, 2015

11. V. Radulovic et al.,” Measurements of miniature ionization chamber currents in the JSI TRIGA Mark II reactor demonstrate the importance of the delayed contribution to the photon field in nuclear reactors”, *Nuclear Instruments and Methods in Physics Research A* 804 (2015) 149–154

Flat reactivity operation course when converting FRM II

A. Röhrmoser
Forschungsneutronenquelle Heinz Maier-Leibnitz *(FRM II),*
Technische Universität München, D-85747 Garching , Germany

ABSTRACT

FRM II has an obligation in its nuclear license for conversion of the reactor to lower enrichment. Any realistic study must at first search for some measures as with the core and fuel volume to regain reactivity lost due to the much higher U-238 content and absorption with lower enrichment and to avoid higher local heat loads.

Nevertheless one can also search for possible general improvements in the concept with the compact core. One actual characteristic is the very high reactivity grasp of the central control rod (CR), what results in higher heat loads in the outside region of the core bottom side. The idea is now to flatten out the reactivity course at operation by introducing much more burnable poison in the outer fuel element tube to compensate the less absorbing CR. This reduces also heat loads for the outer hot coolant stripes. Other advantages with such a solution can be seen in the general lower reactivity grasp of the CR, so that this safety issue is graded down.

A published element design based on high density UMo7 fuel (8gU/cc) at 30% enrichment was taken as example for comparison to show the advantages, thanks to better balanced power and burn up distribution. The gained margin can be used in principal to further reduce the enrichment without extra geometry extensions of the fuel element (here with 76cm active height).

The study was based on a conservative basis without changes to major reactor systems like pumps or the control drive system respectively the shutdown rods. The technical feasibility to introduce a thin boron layer coat at the outer core tube has to be examined sincerely.

1 Introduction

FRM II has an obligation in its nuclear license for conversion of the reactor to lower enrichment. Principal as well as more realistic studies were performed for the conversion of the very compact core. The studies are based on high uranium density U_3Si_2 and UMo fuel and are kept on a conservative basis without changes to major reactor systems like pumps and control or shut down rods. A main constraint at any conversion study is to fulfil the cycle time of the current reactor in order to avoid major penalties beside unavoidable losses in neutron flux levels.

The principal studies have shown that with an 8gU/cc UMo fuel an enrichment level of 50% is still a big challenge for FRM II unless some change to the outer geometry. Thus any realistic study must search for some gain in core volume to regain reactivity lost due to the much higher U-238 content. The first option is a somewhat prolonged fuel element and the most favorable measure would be an increase in the outer fuel radius, even if only in the mm range. This helps also very much to overcome higher heat loads for hot coolant stripes and could be achieved if the central channel (CC) tube could be replaced by zircaloy material. This would enable to reach 30% enrichment with U7Mo fuel at density of 8gU/cc through some optimizing at the plates with thicker fuel meat (RRFM 2012) at moderate loss in n-flux for the user locations.

In comparison to this UMo solution [Frm12] in 2012 a geometrically identical conversion option will be discussed in this work, but thanks to burnable poison as coat of the outer fuel tube several advantages would arise.

2 Core reactivities during operation cycle

Knowledge of a series of reactivity values, necessary for operation of FRM II, was gathered by a huge amount of calculations from the scratch. All main operational conditions, experienced since becoming critical at 2.3.2004 could be pre-estimated in a very reliable manner. A critical experiment was avoided for this absolute new compact core design thanks to good expectations for 2d- and 3d-neutron transport and core burnup methods as well as cross section data, but a reactivity reserve of 2% was settled ad hoc in the '80s. FRM II is running since 2005 in official user operation mode with now maximal four cycles per year à 60 days of full nuclear power of 20MW. The core cooling goes from top to bottom, having about 8 bars at the core entrance and 2-3 bars at the end.

2.1 Thick Hf control rod (small boron ring)

A consequence of the thick Hf control rod is the very high reactivity grasp of the CR.
The final layout for controlling the FRM II is a rather thick (10mm) Hf control rod (CR), it moves motor driven inside the current HEU single element up and down with two allowed slow speeds.

2.1.1 Reactivity grasp of the CR / HEU case

Figure 1 shows the differential reactivity grasp of the central rod, calculated for the fresh fuel element with the maximum driveway of the CR (-41 to +41cm). At reactor start the HF CR has to be driven nearly till the core center (-6 cm) for reaching criticality at full power (hot state). Hence The first day of operation the CR is rather at the maximum of $\Delta\rho$=0,005 per cm driveway of the CR (s. diagram).

This leads to the situation, that at BOC about 2%3 of the power are produced in the lower halve of the core with lower water pressure. A more flat top to bottom power profile would be advantageous for reaching the safety values at any conversion scenario and can be reached with a reduced reactivity grasp of the central rod.

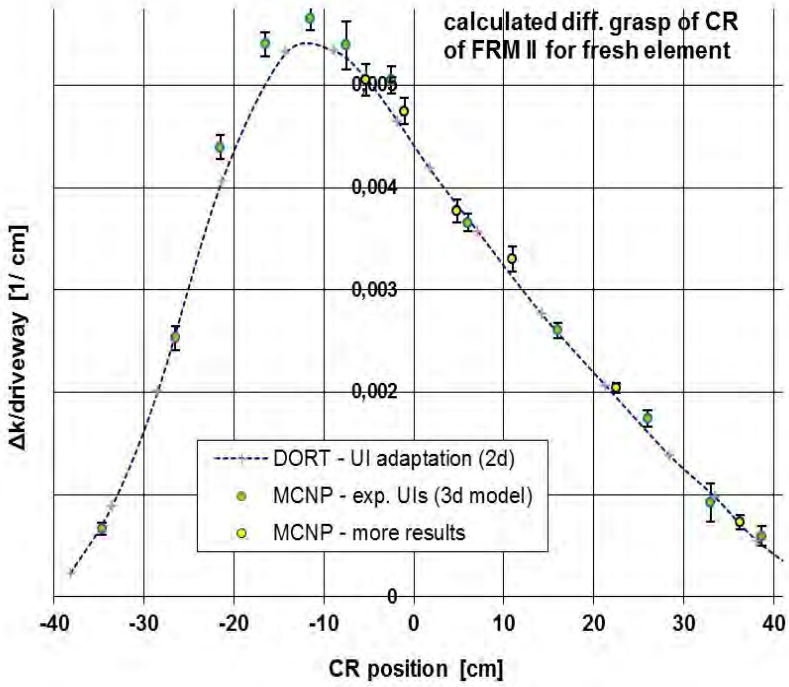

Fig. 1:
Calculated differential reactivity grasp of the central rod of FRM II for a fresh fuel element.

2.1.2 Worst case safety scenario

Some critics of FRM II found some obstacles in the approving phase for the reactor at about year 2000.

A main objection argument was the prompt insertion of reactivity into the core with an abrupt rise of the control rod of exactly 4cm during full power operation. Although regarded not possible technically and physically (of course, the CR has no free driveway), it was assumed, that the CR got this clearance in a worst case scenario. This would insert abrupt $\Delta\rho=4*0{,}005=0{,}02$ or nearly 3$ of reactivity into the core at the maximum differential reactivity grasp of the CR; this was supposed and meant extra work for discussion and assertion of the general safety and some delay in licensing. And it underlines that a smaller reactivity grasp should be favourable in general (for any conversion study).

2.1.3 Driveway of the control rod

During one full operations cycle of full nuclear power of 20MW the CR will move upwards inside the element and compensate the loss of fissile uranium and the build-up of absorbing fission products, especially Xe-135 at the first 2-3 days of reactor start. For the HEU case there are shown the real and the calculated driveway curves, that fit quite well together, when assuming no extra poisoning effect through secondary n-capture reactions in Be (He-3 and Li-6), what must be fairly true for the first through running cycle with 52 FPdays (cycle_6, no stop).

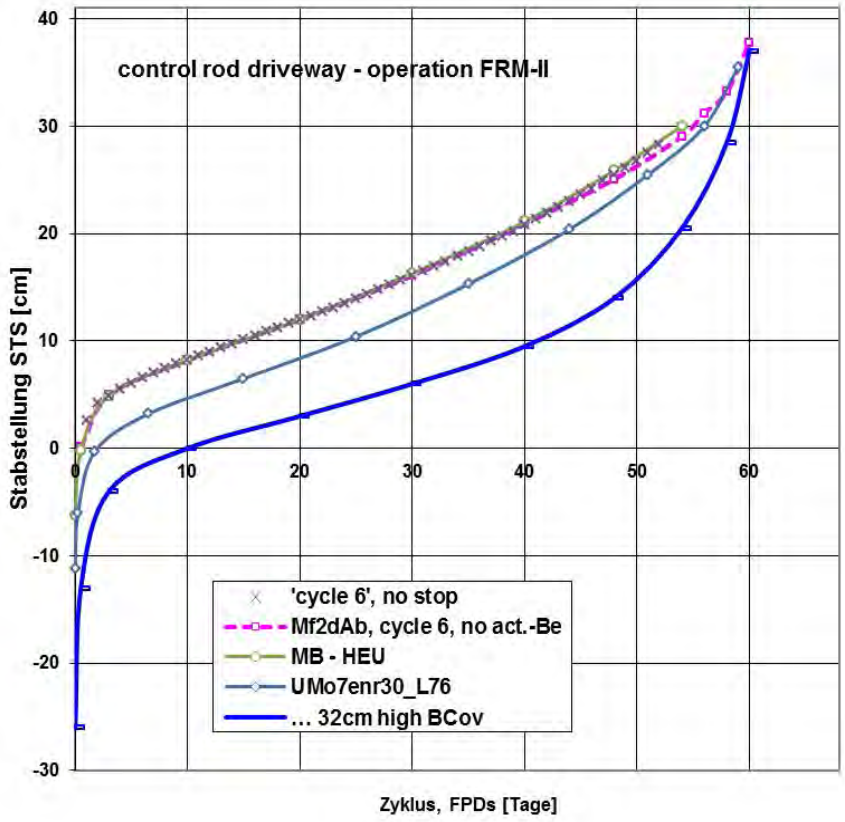

Fig. 2:
Driveway of the central control rod of FRM II during one full operations cycle of full nuclear power of 20MW. It is shown the actual case with an HEU fuel element (real and calculated) and the 30% (25%) enriched UMo fuel case with a boron ring as now (and also a boron coat/cover as alternative, here H_Bor= 32cm).

All driveway curves (for calculations with lower enrichment see below) approach the upper end state of the CR (upper driveway end, CRP = +41cm) after 60 FPDs.

A secondary effect of the different CR driveway is less n-capture of the inner Be reflector (He-3 and Li-6) over the cycle with the BCov solution, what will lead to a small but real regain of reactivity in general!

2.1.4 UMo fuel conversion case UMo30_L76 (30% enriched)

In 2012 it was published an element design based on 30% enriched high density UMo7 fuel of uranium density of 8gU/cc in the meat (UMo30_L76). In Fig. 2 it is also shown the calculated driveway of the central control for this 30% enriched (MEU) case. It is rather comparable to the HEU case, although the differential reactivity grasp of the central rod is slightly lower with MEU than with the HEU case, meanly because of the 6cm enlarged height of the core. But the main characteristic is the same. There remains still a very huge shut down overcapacity when moving the CR fully down to (low driveway end, CRP = -41cm).

2.2 Thin control rod, outer boron cover

This case UMo30_L76 will be taken now for comparison to show principal advantages when introducing a very small amount of boron in a thin coat at the down side of the outer element tube (the technical aspects are discussed with the fuel element producer CERCA). Surely, a boron ring as actual would then be surplus.

2.2.1 UMo25_L76_DCoat fuel case

The exactly same outer element geometry will now receive a boron coat in the lower region (DCoat='downside coat') of the outer element tube. The driveway gets now a quite different characteristic (again Fig. 2).

Burning of the absorbing boron in the coat will compensate partly the longer living fission product absorber buildup the first weeks of the cycle. This means, that the reactivity grasp of the CR may become clearly lower since the boron coat fills the gap (compare also start values of k_{eff}). And that's why the CR could be changed to a lower absorbing material (here Ni, like at the French-British-German research reactor HFR at F-Grenoble, but also other materials are thinkable).

And thanks to better balanced power and burn up distributions (s. Fig. 3), the gained margin can be used to change some parameters in order to further reduce the enrichment, while the outer radii of the fuel element with be kept as well as the active height of 76cm!

One could introduce more uranium with really thicker fuel meat at a reduced number of plates. This type of parameter studies showed, that the enrichment level could be reduced consequently down to at least 26% while introducing 94 fuel element plates with a thicker fuel layer of 1.15 mm. The core would then incorporate an increased value of fissile U-235 (10.4 kg and 40 kg U total), what can't be the aim; and of really highest importance must be fabrication arguments with economy and production yields always on the table. And they tell us to be careful with supposing too thick fuel layers.

A much better way to use the gained margin must go a quite different direction, keeping also the plate parameters or the whole core geometry:
The quite better power density form factor can be used to avoid the density step (which had the same purpose), thus gaining much in core reactivity, especially at EOC, what further allows lowering the enrichment and the fissile mass footprint of the element; all arguments that are higly favourable. The parameters and main results of this study for the same outer and inner fuel element geometry (Ha=76cm) are presented now.

It must be stated, that the supposed 0.76 mm thick meat layer at a thinner cladding of 0.30 mm is still a very ambitious aim for the high density 8gU/cc fuel (2012 study and this comparison case). This could be clearly too optimistic. With current plate thickness values comparable studies would result in clearly higher enrichment values.

2.2.2 Flat reactivity course

Fig. 3:
Flat reactivity course with high boron coat H_Bor= 48cm and a less grasping central control at FRM II during one full operations cycle of full nuclear power of 20MW. Comparable calculations (both with constant poisoning in the inner Be moderator) for the actual case with an HEU fuel element and the 25% enriched UMo fuel case with a boron coat/cover as alternative.

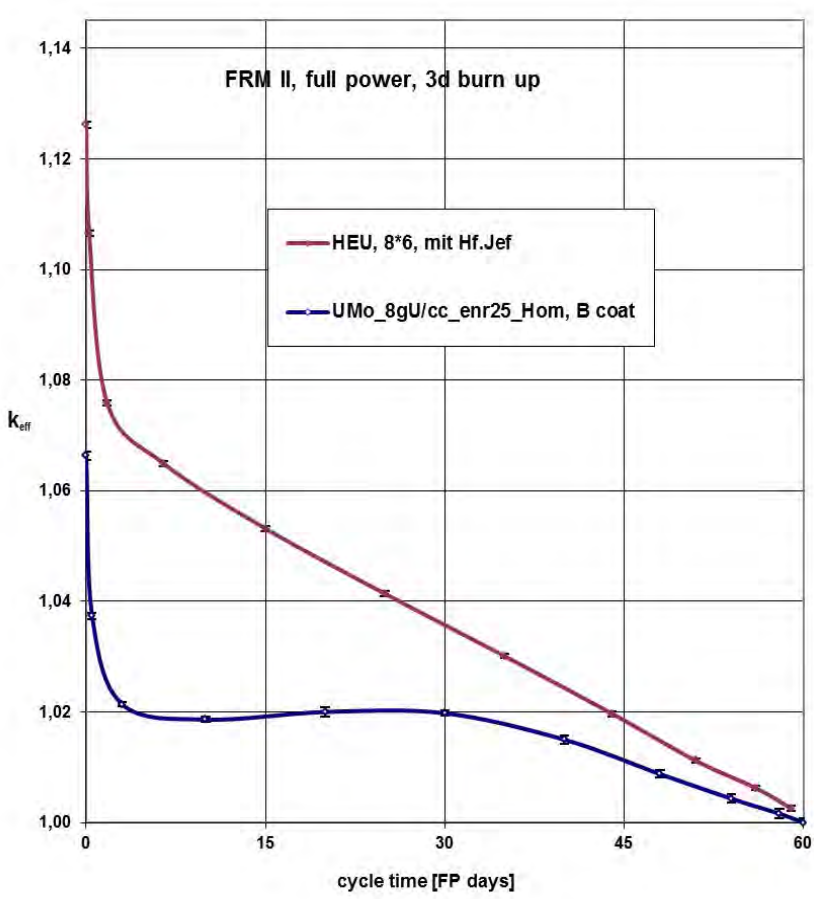

Picture 3 makes the rather flat reactivity course with a boron coat covering the lower halve of the element most obvious. After saturation of the Xe-135 poisoning after about 3 days there will be a very low change in reactivity of the element with burn up over the cycle till about 40 days of FP operation. The starting reactivity of the element is only half of the HEU element, what could be very advantageous with respect to necessary shut down margins (another wording for the thin=<less absorbing> control rod).

Due to several reasons the reactivity decline at the cycle end (when the boron is burnt) will be always lower with a 20-30% enriched core than with the HEU core (which shows still a rather flat course with the high fission mass).

3 Core comparison

All results were found by using a threeedimensional MCNP (Monte-Carlo-method of the transport theory [MCNP]) model for the whole reactor FRM II [ModFrm2] with inclusion of all relevant installations in the HW tank. The fuel and boron burn up were coupled with MonteBurns [MB2.2].

Geometry	**HEU / real, (boron ring)**		**30% enr., boron ring**	**gain in volume**	**25% enr., boron coat, 48 cm high**
fuel material	U_3Si_2		UMo		UMo
Enrichment	**93%**		**30%**		**25%**
uranium density [gU/cc]	3.0 and 1.5		8.0 and 4.0		only 8.0!
Inner radius of CC	6.5 cm		6.5 cm		=
Outer radius of CC	11.45 cm		11.65cm	5.7%	=
fuel free gap inside/outside	0.25 cm		0.25 cm		=
radius of reduced density	10.56 cm		10.8 cm		no
active element height	70 cm		76 cm	8.6%	=
meat thickness	0.6 mm		0.76 mm	26.7%	=
cladding thickness	0.38 mm		0.30 mm		=
Cooling channel (CC) thickness	2.2 mm		2.2 mm		=
number of plates	113		113		=
Outer radius outer core tube	12.15 cm		12.35 cm		=
CCT inner radius	12.3 cm		12.45 cm		=
CCT outer radius	13.1 cm		13.1 cm		=
CCT material in calculation	AlMg3		Zirkaloy		=
Volume ‘meat’	2.960 l		4.302 l	45%	=
Mass U-235	7.54 kg		9.51 kg		8.6 kg
Mass uranium total	8.11 kg		31.7 kg		34.4 kg
Neutronics, all results by coupled MCNP					
cycle length at 20 MW thermal power	60 days		60 days		60 days
Critical control rod position, BOC-EOC, hot core	-6.2↔40cm		-11↔40cm		-26↔40cm
k_{eff} BOC,	1.133		1.117		1.067
k_{eff} EOC, 3*5(*3) radial/axial(/az.) burn up zones core, dynamic CR and totally withdrawn at end	1.0076 ±0.0002		1.0070 ±0.0002		very com-parable
Fission density maximum (plate of 5mm*5mm),	1.8 10^{21}		<1.3 10^{21}		
Thermal hydraulics, calculation NBK, case BOC					
flow area inside fuel element	172.5 cm^2		181.5 cm^2		=
pressure drop over element	5.3 bar		=		=
flow velocity of LW between plates	16 m/s		15.4 m/s		=
water temperature, fuel element inlet	38 °C		=		=
water temperature, fuel element outlet	54.3 °C		54.0 °C		54.0 °C
mass flow of LW through fuel element	274 kg/s		277½ kg/s		277½ kg/s
max. heat flux at plate surface (hot point)	370 W/cm^2		336 W/cm^2		401 W/cm^2
hot point at plate surface, **cnsvtv heat transfer**	96.0°C		95.4°C		97.3°C
voiding safety value, S_{onb} at minimum	2.48		2.575		2.63

3.1 General data

The last column of the table assumes the same outer and inner fuel element geometry (Ha=76cm) as presented for a split density and 30% enriched element of UMo7 at 8gU/cc in a 0.76 mm thick fuel layer at 0.3mm clad thickness. Hence the number and thickness of plates and coolant could be kept as it is today, but now with only one fuel layer in the plates (better plate fabrication economy) and a thin boron coat around the lower part of the element. At only 25% enrichment level the core incorporates now only 8.6 kg of fissile U-235 (34,4 kg U total), a quite well value below that for the 30% enriched case (9.5 kg and 32 kg U total)!

The reactivity grasp of the CR is only $\Delta\rho$=0.066 when running 66 cm (now $\Delta\rho$=0.133 when running 46 cm), meaning that a differential reactivity grasp of about 40% of the current value is already sufficient!

3.2 Power density comparison

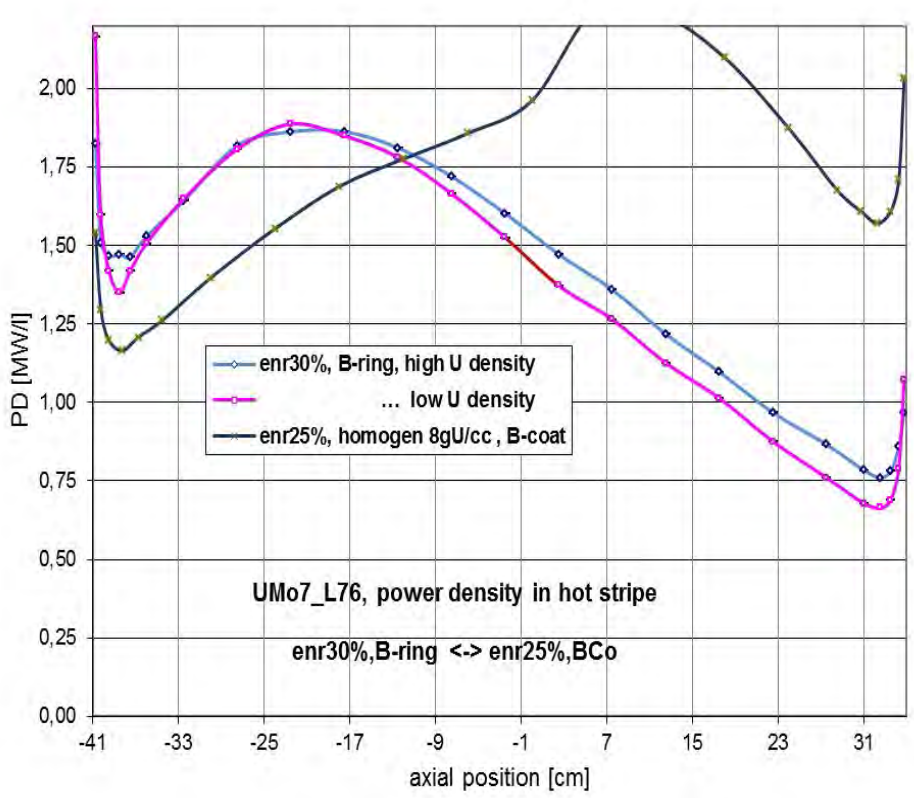

Fig. 4:
power density at the hot coolant stripes at BOC for both MEU fuel element cases of same outer size:
a) 30% enr., B- ring, split meat
b) 25% enr., B-coat, homogen meat

With respect to the minimum value S_{onb} (onset of nucleate boiling) during the cycle at full power, the starting point BOC is usually the most demanding time point, as the PD at the hot coolant stripe is there most remarkably shifted to the <low pressure/warm water> region. This pronounced point BOC was the case in any study up to now and demonstrated for the actual fuel element at [RRFM09].

But with the boron coat in the lower element part, one receives a very remarkable shift of the PD towards the <high pressure/cold water> region. Thanks to the extreme advantage of the much better PD distribution, the hot coolant stripe can receive much more heat without arriving at a lower minimum value S_{onb} (s. table). And this allowed having only one (homogeneous) high U density in the meat and only this opened the field to come down from 30% to 25% enrichment level at unchanged outer and inner fuel element dimensions!

With burn up of the fuel and the boron coat the distribution will change somewhat; the change is comparably softer than without boron coat (s. Pict. 4). The overall heat load of the hot stripe at the outer element side will be lowered only somewhat in the first halve of operations cycle (then again

more pronounced, when the burn up of the fuel dominates as it is always the case without boron coat). There will be seen a slight backshift of the emphasis of the PD distribution from top to bottom with the boron burn up in the lower element in the first half of the cycle. But the minimum ONB-value at 'nominal cooling conditions' is not lowered, it will be comparably slightly better at 30 operation days with $S_{onb} = 2.66$ (lying higher) instead of lower positioned $S_{onb} = 2.63$ at BOC (2.44 now) with the same calculation method. Then till the cycle end the minimum safety values will again rise clearly (lower heat loads for hot stripes, s. curve for '48d'), so that instead of having the focus mainly on the BOC state, it will now be more spread over the first halve of the cycle to guaranty a full time coverage and to confirm, that the BOC situation further on describes the lowest ONB-situation quite well (as done here for full power 'nominal cooling conditions').

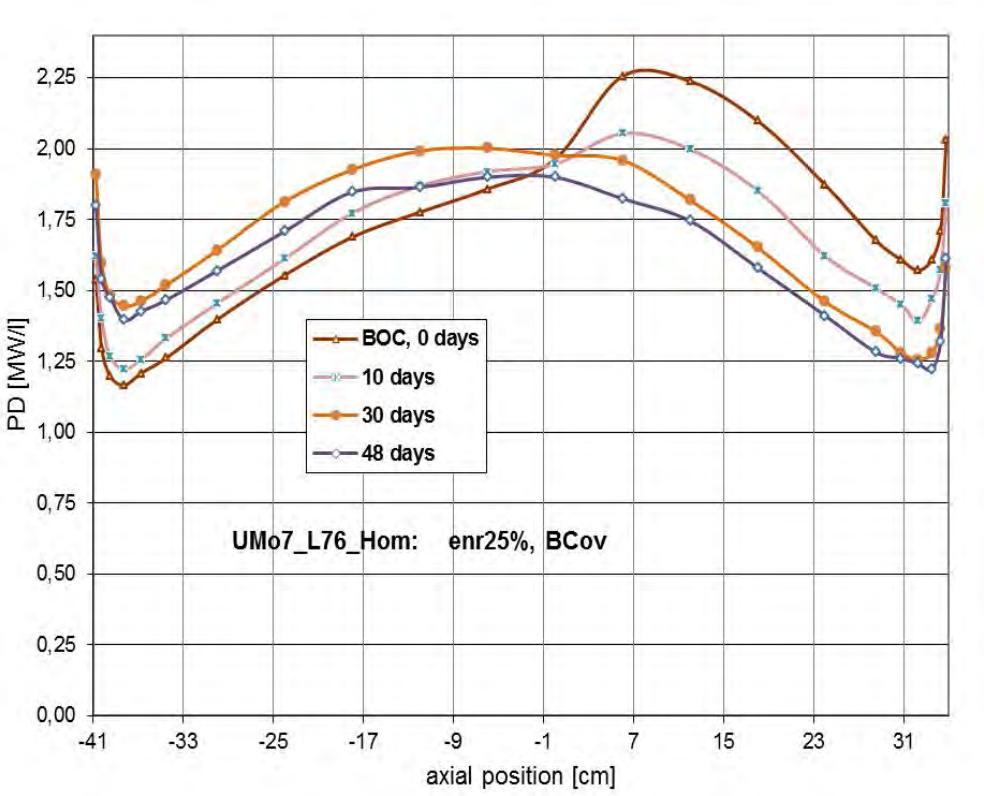

Fig. 5: power density at the hot coolant stripe at BOC and at later operation time points for the L=76cm case, now with B-coat (25% enriched uranium)

4 Results for the users

When we compare to the 30% enriched core with split density (as now and no boron coat, 2012) the thermal neutron flux cloud in the HW tank will be slightly different with the solution of a boron coat and the homogenous UMo7 fuel (8gU/cc) of reduced enrichment (25%).

The calculations show an average loss of extra 1½% at the radius of the thermal beam tube noses, 1% at the cold source (CNS) and less than 1% more core distant. But through the better balanced neutron source in the element, the flux cloud is also shifted a little bit up into the core central plane, where the emphasis of the beam tubes are located (and also the CNS). That helps to regain nearly 1% in the beam tube nose average, so that there can be stated no real extra neutron flux loss for the users (in comparison to the 30% enriched element case of same geometry, 2012).

And the argument of regain potential in cold flux of several % through pronounced reduction of heating for the cold source at full power is the same way (even better) valid as for the 30% enriched element (2012).

SUMMARY

Studies for conversion of FRM II have to respect the current physical situation of the reactor and they must deal on a conservative manner with major operational systems like (primary) pump and control (CR) and shut down (SR) systems.

One actual characteristic is the very high reactivity grasp of the central control rod (CR), what results in higher heat loads in the outside region of the core bottom side. The idea is now to flatten out the reactivity course at operation by introducing much more burnable poison in the outer fuel element tube to compensate the less absorbing CR. This reduces also heat loads for the outer hot coolant stripes. Other advantages with such a solution can be seen in the general lower reactivity grasp of the CR, so that this safety issue is graded down.

The case for comparison is a conversion solution with 30% enriched UMo fuel at density 8gU/cc, presented in 2012. The fuel element was extended 6 cm to the bottom and the inner diameter of the element and the outer diameter of the central channel tube were kept in the study. Inner parameters as there are the thickness of the plates and the cooling channels were unchanged, too (keep in mind: 'the thicker meat at somewhat thinner cladding in this comparison study is the same way optimistic as formerly'). For the same geometry it was introduced a boron coat in the lower part outside at the fuel element and a less bold control rod material. Thanks to this a much better power density distribution could be achieved, what allowed to have one (homogeneous) high U density in the meat. And only this opened the field to come down now from 30% to 25% enrichment level at unchanged outer and inner fuel element dimensions, whereas all safety values of the reactor and criteria for the coolant flow are met at a very comparable level to the current HEU fuel element.

The relative flux output at different beam tubes was calculated. Because of the flux cloud located now more to the core central plane the flux losses will now be less dependent on the location of the beam or irradiation tube of regard, in the average at 8.5% at thermal beam tube noses and less at the irradiation channels (e.g., 6% for the remote silicium doping or the fast converter facility). The cold beam tubes would be hardly affected at all with lower flux through regain due to pronounced reduction of heating for the cold source at full power.

As with the 2012 study there remain major questions with fabrication and licensing issues, now with the extra subject 'boron-coat'.

ACKNOWLEDGEMENT

This work has been supported by a combined grant (FRM0911) from the Bundesministerium für Bildung und Forschung (BMBF) and the Bayerisches Staatsministerium für Wissenschaft, Forschung und Kunst (StMWFK).

REFERENCES

[Frm12] "Extended studies of FRM II core conversion with UMo dispersive fuel at a prolonged fuel element", International Topical Meeting on Research Reactor Fuel Management, RRFM 2012, Prag, A. Röhrmoser, W. Petry, H. Breitkreutz

[MCNP] "MCNP - A General Monte Carlo N-Particle Transport Code, Version 5", LA-UR-03-1978 (4/2003,10/2005), X-5 Monte Carlo Team, Los Alamos National Laboratory

[ModFrm2] „MCNP-Modell zum ‚as-built'-Zustand der experimentellen Tankeinbauten des FRM II und Vergleich mit früheren Ausführungen", OPA00330, FRM-Projektbericht, A. Röhrmoser

[MB2.2] "MonteBurns (2), an Automated Multi Step Monte Carlo Burnup Code System", LA-UR-99-4999, Los Alamos National Laboratory, distributed by RSICC or NEA

[RRFM09] "Fuel plate temperatures during operation of FRM II" , 14th International Topical Meeting on Research Reactor Fuel Management, A. Röhrmoser, RRFM 2009, Vienna

[RERTR10] "FRM II, New burn up calculations", Lisboa, Portugal, RERTR meeting 2010, A. Röhrmoser

[FrmMdl] "Core Model of new German Neutron source FRM II", Nuclear Engineering and Design, June 2010, A. Röhrmoser

[THnbk] "Fuel plate temperatures during operation of FRM II" , 14th International Topical Meeting on Research Reactor Fuel Management, A. Röhrmoser, RRFM 2009, Vienna

THE ANET CODE: FROM HIGH ENERGY PHYSICS TO STOCHASTIC DYNAMIC NEUTRONICS WITH THERMAL HYDRAULIC FEEDBACK

T. XENOFONTOS[1], A.G. MYLONAKIS, P. SAVVA, M. VARVAYANNI, N. CATSAROS
Institute of Nuclear & Radiological Sciences & Technology, Energy & Safety
NCSR Demokritos
Neapoleos 27, 15341 Aghia Paraskevi – Greece

J. MAILLARD
Institut du Développement et des Ressources en Informatique Scientifique, CNRS
John Von Neumann, 91403 Orsay Cedex, France

J. SILVA
Université Pierre et Marie Curie, Campus Jussieu
75252 Paris Cedex 05, France

ABSTRACT

ANET is being developed targeting to a multiple capabilities code which can inherently, dynamically and accurately simulate GEN II/III reactors as well as Accelerator Driven Systems (ADSs). ANET is oriented towards an open-source pure Monte-Carlo transient code with Thermal-Hydraulics (T-H) feedback. It incorporates the treatment of all types of particles' creations and collisions as existing in the High Energy Physics code GEANT while its capabilities have been extended to energies below 20 MeV so as to cope with fission neutrons and their possible reactions in a reactor core (transport, elastic and inelastic scattering, capture and fission). The developed code aims to account for core evolution in both short and long time-scales, allowing for T-H feedback and assessment of the fuel isotopic composition variations, including neutron poisons' evolution. In order to analyze ADSs, ANET can incorporate specific codes (such as FLUKA and INCL/ABLA) for the treatment of spallation targets of various materials and geometries. Regarding verification and validation (V&V) studies ANET has been successfully tested against measurements and/or independent numerical results with respect to its capability to compute criticality, neutron fluence and reaction rates. Also ANET neutron yield computations for three of the most popular spallation target materials (Pb, W and U) hit by accelerated protons of various energies are satisfactorily compared with independent simulations and experimental results. Moreover, preliminary ANET applications for the prediction of changes in the fuel isotopic composition show encouraging results compared with measurements as well as corresponding simulations.

1. Introduction

The necessity for precise simulations of a nuclear reactor especially in case of complex core and fuel configurations has imposed the increasing use of Monte Carlo (MC) neutronics codes. Besides, a demand of additional stochastic codes' inherent capabilities has emerged regarding mainly the simulation of the temporal variations in the core isotopic composition as well as the incorporation of the T-H feedback [1]. In addition to the above, the design of

[1] *Also: Department of Electrical & Computer Engineering, Aristotle University of Thessaloniki, Egnatia Str.-University Campus, 54124 Thessaloniki, Greece*

innovative nuclear reactor concepts, such as the Accelerator Driven System (ADSs), imposed extra requirements of simulation capabilities. More specifically, the combination of an accelerator and a nuclear reactor in the ADS requires the simulation of both subsystems for an integrated system analysis. Therefore a need arises for more advanced simulation tools, able to cover the broad neutrons energy spectrum involved in these systems.

Among the most widespread MC neutronics codes are MCNP [2], KENO [3] and TRIPOLI [4]. Steady state neutronics calculations are inherently performed by these codes, while time dependent results can be provided through their coupling with an external module making use of the neutron diffusion theory. Burnup assessment by MCNP and KENO is usually performed via coupling with ORIGEN [5], REBUS [6], and MCB [7]; typical examples are given in [8], [9], [10], [11]. Capability of TRIPOLI burnup calculations has been reported in [12] where the code is integrated in the CRISTAL V1 package, the latter containing (among others) the CESAR computer code capable of performing depletion calculations [13]. Regarding the ADS analysis, the common procedure is to separate the spallation target from the sub-critical core through the utilization of two different codes, i.e. a High Energy Physics (HEP) code for the accelerator (e.g. FLUKA or MCNPX [14], [15]) and a neutronics code for the nuclear reactor. Efforts to analyze ADSs using a single code are found in [16], [17]. Apart from the aforementioned, well documented MC neutronics codes, one should also cite those being under development in various Institutes such as the OpenMC [18], the MCU [19] and the Serpent [20], the latter including also burnup calculation capabilities.

This work presents the main features and capabilities of the new MC neutronics code ANET (**A**dvanced **N**eutronics with **E**volution and **T**hermal hydraulic feedback), being developed in NCSR Demokritos (Greece) in cooperation with CNRS/IDRIS and UPMC (France) and intending to meet as effectively as possible the above described modelling requirements.

2. The ANET code

ANET is based on the open-source version of the HEP code GEANT3.21 [21] and is targeting to the creation of an enhanced computational tool in the field of reactor analysis, capable of simulating both GEN II/III reactors and ADSs. ANET is structured with inherent capability of (a) performing burnup calculations and (b) simulating the spallation process in the ADS analysis, while taking T-H feedback into account. The basis for ANET code was established following a fundamental GEANT3.21 modification, i.e. its applicability extension for neutron energies below 20 MeV that is in the region of the neutron energy spectrum involved in nuclear reactors' analysis. Preliminary ANET runs were carried out to demonstrate the code performances in simulating elastic collision, capture and fission [22], [23], [24]. In these preliminary applications criticality was derived indirectly through dividing the neutrons produced from two successive generations of fissions, while an assumption of a special yield for a tungsten spallation source (without including inherent spallation process) was adopted. Subsequently the ANET structure was further developed and improved; the evolved code attributes are briefly discussed in the following paragraph.

The current ANET version utilizes the three standard Monte Carlo estimators for the neutron multiplication factor (k_{eff}) calculation, i.e. the collision estimator, the absorption estimator and the track-length estimator. Regarding the simulation of neutron fluence and reaction rates, the collision and the track-length estimators are implemented in ANET following the standard Monte Carlo procedure (e.g. as in [2], [4], [18]). For the burnup calculations ANET attempts to apply a pure Monte Carlo approach, adopting the typical procedure followed in stochastic codes. The latter (either burnup is provided inherently or through coupling with a deterministic module) includes two computational steps, i.e. calculation of the neutron density distribution and assessment of the nuclide concentrations changes, assuming that these parameters can be estimated sequentially in a cyclic manner by alternating the two computational steps, each time using results from the previous steps. In the above procedure the steady state neutron flux (and therefore the reaction rates) for given materials

composition are computed during the first step, while during the second step the changes in the nuclide composition are calculated assuming constant reaction rates. In ANET the above methodology is applied with the difference that reactions rates are computed and utilized directly. The real life time-step and the relevant computational time-step are assigned to two variables defined in the input file of ANET. It is in the user's discretion to decide the correspondence between the real life time-step and the number of cycles (computational time-step) that will be used by the code so as to calculate the reaction rates and subsequently the material evolution. The number of cycles that will be chosen for the computation of the reaction rates is a compromise between computational cost and minimization of reaction rates' statistical error. In the current code version approximately 150 nuclides are included and can be treated for the transmutation reactions and the radioactive decays. More details on the code structure for burnup assessment are given in [25]. With respect to code improvements for the ADS analysis, so far ANET has incorporated the INCL/ABLA code [26] so that the spallation process can be inherently simulated. The ANET reliability in typical computations was tested using observational data and parallel simulations by different codes as described in the following chapters.

3. Steady state ANET calculations for GEN II/III reactors

In representative applications on current reactor types, ANET results are compared with measurements performed in critical and subcritical installations as well as with corresponding simulations from stochastic and deterministic (XSDRN/CITATION [26], [28]) neutronics codes. To validate ANET simulations of critical reactors, measurements performed in the Portuguese Research Reactor (RPI) and the VENUS facility at SCK CEN, Belgium, are utilized. For the ANET tests in subcritical installations, data from the Training Nuclear Reactor of the Aristotle University of Thessaloniki (TNR-AUTh) have been exploited.

The RPI is a 1MW pool-type reactor (Fig. 1) using Low Enrichment in Uranium (LEU, 19.75% nominal U-235) fuel. The analyzed core consists of seven standard (SA) and five control (CA) fuel assemblies (FAs) of MTR (Materials Test Reactor) type. SA and CA contain respectively 10 and 18 flat fuel plates while meat in each fuel plate contains an U_3Si_2 (silicide) powder dispersed in pure Al and clad by AG3NE Al alloy. RPI uses four shim-safety rods and one regulation rod, placed in the central channels of the CAs. The shim-safety rods consist of a 1 mm-thick cadmium layer supported and covered by 1.5 mm-thick stainless steel, while the regulating rod (RR) is a hollow 2.2 mm-thick stainless steel tube. The control rods (CR) have oval cross-sectional shape. The RPI core is reflected by graphite (in the thermal column), beryllium and light water, while four dummy assemblies (DAs) are placed in the core periphery. The DA looks like the FA but instead of fuel plates it contains a central aluminum tube. The FAs, the DAs and the beryllium reflectors are mounted on a grid plate in a 9x6 pattern. More details about RPI are given in [29]. The ANET V&V studies based on RPI data combine also comparisons with corresponding results by MCNP5, TRIPOLI (version 4.4. or 4.8) and XSDRN/CITATION, and concern criticality and neutron fluence rate.

The VENUS facility is a zero power critical reactor with a core consisting of 12 "15×15" subassemblies. The central core part (four 15×15 assemblies) consists of fuel pins enriched by 3.3 wt % in U-235 (UO_2 pins) while forty pyrex pins also exist. In the core periphery eight rows of the most external fuel pins (initially containing 4.0 wt.% enriched in U-235) are replaced by mixed oxide fuel pins (UO_2-PuO_2) enriched 2.0 wt.% in U-235 and 2.7 wt.% in high-grade plutonium (2/2.7 MOX pins). Details on the isotopic composition of the three fuel types and the core geometry are given in [30]. The ANET V&V studies which exploit VENUS data, in combination with corresponding computations by MCNP5 and TRIPOLI-4.8, concern fission reaction rates (FR) and are based on the benchmark described in [30].

The (TNR-AUTh) is a subcritical assembly consisting of a cylindrical reactor tank with 150 cm height and 123.4 cm diameter. It contains 270 fuel tubes with 3.605 cm radius, arranged in a hexagonal lattice. The fuel tube at the lattice center is substituted by the ^{241}Am-^{9}Be (α,n)

neutron source. The fuel tube contains five fuel rings of 21.08 cm height separated by aluminum disks of 0.11 cm thickness. The fuel is natural U-metal with internal and external radius 0.73 cm and 1.41 cm respectively, cladded in both edges by aluminum, 0.12 cm thick. Light water is used as moderator and reflector. Details of the TNR-AUTh features are given in [31]. The ANET verification studies based on TNR-AUTh are about criticality and exploit comparisons with corresponding results by MCNP5, TRIPOLI-4.4 and XSDRN/CITATION.

	k_{eff} (RPI)	k_{eff} (TNR-AUTh)
Observation	~1.00000	-
ANET	1.00094 ± 0.00054	0.80104 ± 0.00029
TRIPOLI-4.4	1.00584 ± 0.00019	0.80137 ± 0.00023
MCNP5	1.00786 ± 0.00028	0.80133 ± 0.00017
XSDRN/CITATION	1.00593	0.80060

Tab 1: comparison of ANET k_{eff} computations

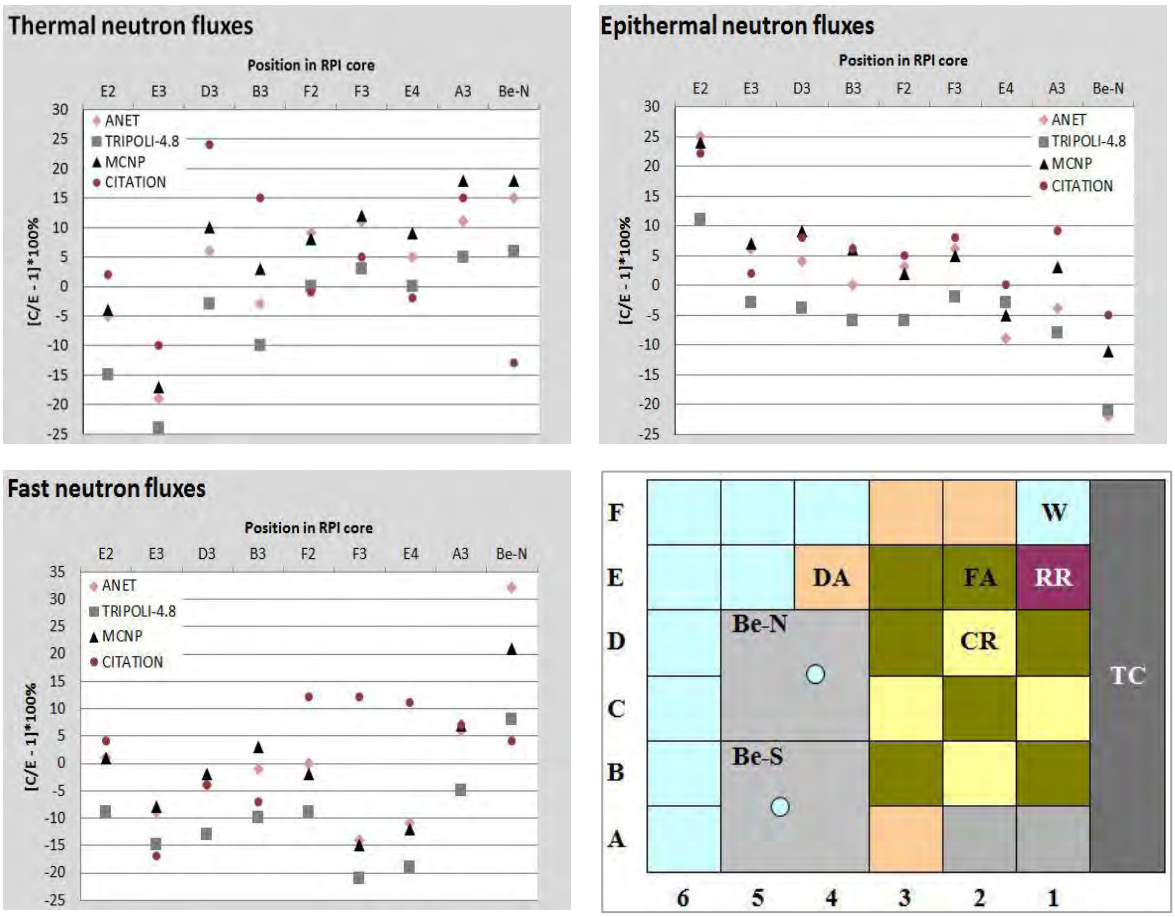

Fig. 1: Discrepancies (%) from measurements for thermal (up-left), epithermal (up-right) and fast (down-left) neutron fluxes in different positions of RPI core (down right; W: water, TC: thermal column, Be-N and Be-S: north and south beryllium blocks, respectively)

ANET is applied on the above setups using the JEFF3.1.2 neutron cross section library, also used by MCNP5, while TRIPOLI-4.8 uses the CEAV5.1.1 library based on JEFF3.1.1. TRIPOLI-4.4 is applied with the ENDF/B-VI while the XSDRN/CITATION is applied with the 238-group ENDF/B-V. The ANET V&V results for criticality and fluence rates are respectively shown in Table 1 and Fig. 1. Concerning k_{eff} estimation, ANET shows a satisfactory agreement with the different code results, with maximum discrepancy (found vs MCNP) of

692 pcm in the RPI case. Moreover, ANET fluence rates computations are in compliance with simulations performed by well-established stochastic and deterministic codes. For the reaction rates, the results for two MOX fuel rods are indicatively presented (Fig. 2) and adequately demonstrate that ANET successfully performs reaction rate computations in large critical systems containing both standard and MOX fuel. For the UO_2 pins it is noted that the ANET results compare well with MCNP5 and TRIPOLI-4.8 as well as with measurements giving absolute discrepancies ([C/E-1] % where "C" stands for "Computation" and "E" for "Experiment") lower than 6% [32]. The above results show the ANET capability in providing reliable simulations as regards to basic parameters for GEN II/III reactors.

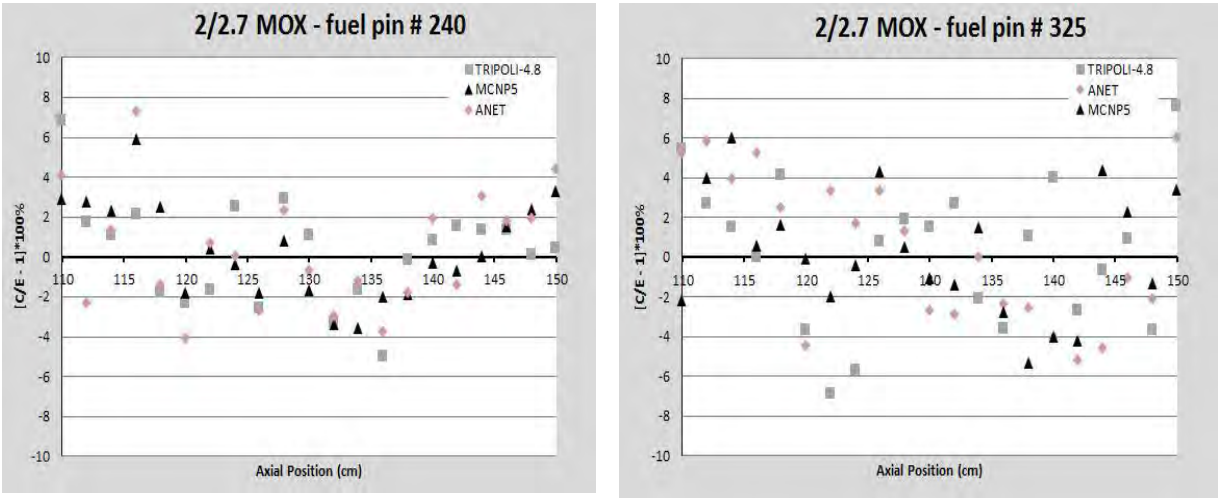

Fig. 2: Discrepancies (%) from experiment for the axial FR distribution of two MOX fuel rods

4. Time dependent ANET calculations

At this stage ANET is tested for its capability to simulate time dependent phenomena with time scales relevant to the core inventory evolution. The first verification study of the dynamic ANET is performed for 306 days operating time using the setup described in [33]. ANET results are examined in comparison with representative measurements for a fuel pin irradiated within a reactor core. Since in the present simulations the fuel pin is not treated for in-core exposure but it is modelled independently as a stand-alone setup, the test against measured values is exploited only to indicate tendencies; it is not claimed that it accurately reproduces the experiment. Therefore, the ANET results are also compared with deterministic ones provided by XSDRNPM/CITATION. The latter simulate the fuel pin as homogenous and zone-averaged cross-sections for each contained material are utilized for the burnup calculations. CITATION standard chains are used while for the fission products generation cumulative yields for four fissionable nuclides, i.e. U-235, U-238, Pu-239 and Pu-241 are taken from [34]. Representative results are presented in Table 2.

The preliminary ANET application for dynamic analysis is encouraging since it indicates the code capability to inherently provide a reasonable prediction for the core inventory evolution. It is worth underlining that uncertainties of the order of 20% and even higher are traditionally expected in core inventory evolution calculations since besides the uncertainty introduced by the algorithms of the simulation code, the nuclear data of the various fission products such as decay, half-life, yield and cross section data constitute additional, major sources of uncertainty [35]. In view of the above and also taking into account the differences between experimental and modelling conditions (assumption of a stand-alone setup) as well as between the simulation methods, it may be concluded that the ANET results compare favourably with the indicative measurements and the deterministic simulation. Incorporation in ANET of several methods utilized for the numerical solution of the system of differential

equations that describe the changes of the fuel composition is being realized whereas extensive verification and validation effort is planned for the near future.

Nuclide	Indicative measurement	ANET	CITATION
U-234	4.1361E-06	5.5899E-06	5.5823E-06
U-235	2.1802E-04	3.9979E-04	5.2972E-04
U-236	8.0484E-05	1.5934E-04	3.0828E-05
U-238	2.1413E-02	2.1603E-02	2.1621E-02
Pu-239	1.0792E-04	4.6658E-05	4.9946E-05
Pu-240	4.3327E-05	2.2707E-05	5.4316E-05
Pu-241	1.7098E-05	4.1993E-06	1.9616E-05
Pu-242	7.2139E-06	1.2316E-06	1.3530E-06
Np-237	6.8403E-06	2.0478E-06	5.6488E-07
Pu-238	2.5721E-06	8.2263E-08	3.1612E-08
Cs-133	3.8660E-05	1.0385E-05	2.6366E-05
Cs-135	1.6131E-05	1.0348E-05	1.6243E-05
Sm-149	1.1773E-07	2.0794E-07	1.4607E-07
Sm-152	3.4623E-06	5.7899E-06	1.0930E-06

Tab. 2: Compared ANET results for irradiated fuel composition (nuclei/b-cm)

5. ANET coupling with Thermal-Hydraulic calculations

Since in problems of reactor physics the neutronic nature is strongly bonded with the T-H one, the development of a thermal-hydraulic feedback capability and its integration into ANET is considered important. At this stage an investigation is made concerning the main features which such a T-H feedback capability should have, the main constraints that limit its action and, finally, the main algorithmic parameters that could be improved in order to achieve higher accuracy and lower computational cost. For T-H coupling with ANET, the COBRA-EN [36] T-H solver was selected. However, in order to test and further develop various techniques and procedures before the final implementation into ANET, a preparatory coupling was performed with OpenMC which is an open-source, fully operational MC code. Initially, OpenMC was coupled with COBRA-EN in a sequential (Block Gauss-Seidel) numerical concept. In this work a one-to-one mapping between the axial and radial nodalization of the two codes being involved in the coupling is implemented [37].

For handling the material cross-sections evolution within this coupling scheme, the method of pseudo-materials was adopted. According to this, each material in the neutronic side of the coupling scheme is defined as a mixture of two pseudo-materials. The temperatures of the two pseudo-materials which compose the actual one correspond to the upper and lower bounds of the particular interval in which the actual temperature obtained from T-H is lying. In order to test the performance and the accuracy of the methodologies under development, suitable benchmark problems are needed. At the first stage the single pin Boiling Water Reactor (BWR) benchmark for coupled MC/T-H analysis was adopted [38]. As a second slightly larger benchmark case, a model of a Pressurized Water Reactor (PWR) fuel assembly [39] was adopted after it was suitably equipped with T-H parameters.

As the convergence of an algorithm is always an important issue, an improvement of the convergence behaviour by adopting a new numerical technique (Approximate Block Newton method) and developing an innovative neutronic-MC/T-H coupling scheme, was attempted. It was found that the proposed coupling methodology outperforms the traditional sequential one as shown in [40]. The improvement seems to be more significant in the BWR cases, however further investigation especially in larger scale problems is needed in order to exploit in more detail the features, the advantages and disadvantages of this innovative coupling scheme.

After defining the strategy that will be used in the coupling of ANET with T-H, the T-H code COBRA-EN was coupled with ANET, starting with the simpler sequential coupling algorithm. Coupling was done in both an internal and an external way. The term “internal” means that coupling subroutines were inserted within ANET and as a result the information exchange with T-H is done via computer memory, whereas in the “external” case the information is transmitted via input files. The procedure of the extensive verification and validation is on-going aiming mainly to verify that the accuracy of the results meets the expectancies of the reactor scientific community. As regards further research and development, coupled analysis of problems of larger scale is the next step, since they will probably introduce new questions related mainly to data exchange and constraints inserted by the involved solvers.

6. Simulation of spallation process for ADS analysis

The V&V study of the ANET-INCL/ABLA coupling was based on experimental results and MCNPX 2.6.0 calculations of neutron yields [41]. Three of the most popular spallation target materials, i.e., Pb, W and U were examined using ANET-INCL/ABLA and ANET-FLUKA along with the standalone FLUKA [42].

Target material	Target diameter / height (cm)	ANET-INCL/ABLA	ANET-FLUKA	FLUKA	Experimental
U-238	61 / 10.2	36.22 [-10.57]	27.17 [-32.91]	31.86 [-21.33]	40.50
Pb-nat	61 / 20.4	18.91 [-7.58]	19.61 [-4.15]	24.89 [21.65]	20.46
Pb-nat	61 / 10.2	16.58 [0.73]	15.87 [-3.58]	19.78 [20.17]	16.46

Tab. 3: Compared neutron yield results for proton energy 960 MeV

Energy (GeV)	ANET-INCL/ABLA	ANET-FLUKA	FLUKA	Experimental
0.8	13.56 [0.44]	12.84 [-4.89]	16.14 [19.56]	13.5
1.0	17.35 [-0.86]	16.74 [-4.34]	20.74 [18.51]	17.5
1.2	20.75 [-6.95]	20.58 [-7.71]	25.31 [13.50]	22.3
1.4	23.23 [-11.67]	24.19 [-8.02]	29.54 [12.32]	26.3

Tab. 4: Compared neutron yield results for a 10.2cm × 61cm, Pb target

Energy (GeV)	ANET-INCL/ABLA	ANET-FLUKA	FLUKA	Experimental
0.8	13.80 [-8.00]	13.89 [-7.40]	17.96 [19.73]	15.0
1.0	17.84 [-12.98]	18.65 [-9.02]	23.86 [16.39]	20.5
1.4	24.07 [-15.54]	27.50 [-3.51]	34.40 [20.70]	28.5

Tab. 5: Compared neutron yield results for a 10.2cm × 40cm, W target

For the comparison with calculated neutron yields, three of the most popular spallation target materials, i.e., Pb, W and U were examined using ANET-INCL/ABLA and ANET-FLUKA along with the standalone FLUKA [42]. The simulations were performed using a proton beam of energy E=1GeV and include (a) targets with diameter 5 cm and depth 5, 10, 15, 20, 25, 30 cm, and (b) targets with diameter 5, 10, 15, 20 cm and depth 30 cm. For the comparison with experimental results, the neutron yield for different target materials and dimensions as well as for different proton beam energies was calculated. The code performance was found very satisfactory in all tested cases. The obtained results are indicatively presented in Tables 3-5; the relative discrepancy with experiment (C/E-1(%)) is also given in brackets below the calculations.

7. Conclusions

ANET is being developed in NCSR Demokritos (Greece) in cooperation with CNRS/IDRIS and UPMC (France) and targets to the creation of an enhanced computational tool capable of simulating both GEN II/III reactors and ADSs. V&V studies based on experimental data and/or corresponding simulations independently performed by other codes show that ANET can accomplish reliable core analysis comprising criticality as well as fluence and reaction rate assessment, while it provides promising preliminary results regarding the dynamic reactor core evolution. Meanwhile a significant work that has been performed up to this stage has paved the way for a satisfactory coupling of ANET with T-H calculations. At the same time, ANET incorporating INCL/ABLA shows a very satisfactory performance in predicting neutron yields for spallation targets of various materials and dimensions, demonstrating thus inherent capability of analyzing ADSs.

Acknowledgements

This research has been co-financed by the European Union (European Social Fund-ESF) and Greek national funds through the Operational Program "Education and Lifelong Learning" of the National Strategic Reference Framework (NSRF) - Research Funding Program: Thales- Investing in knowledge society through the European Social Fund. Authors would also like to thank Ms E. Adamidi PhD candidate of the Technical University of Athens and her supervising Professor E. Gazis for their contribution regarding the stand-alone FLUKA calculations.

References

[1] SNE-TP, 5.1.3, Strategic Research Agenda of “Modelling, simulation and methods” (2009).
[2] J.F. Briesmeister, “MCNP-A general Monte Carlo N-Particle Transport Code System”, Version 4C. LA-13709-M, Los Alamos National Laboratory (2000).
[3] T. Sumner and S. Goluoglu, "Verification of KENO V.A and KENO-VI Using Analytical Benchmarks," p. 361-363 Proc. of the 8th International Conference on Nuclear Criticality Safety (ICNC 2007), Vol. 1, St. Petersburg, Russia, May 28-June 1, (2007).

[4] O. Petit, F.X. Hugot, Y.K. Lee, C. Jouanne, A. Mazzolo, “TRIPOLI -4 User Guide. Report” CEA-R-6169. Code available from OECD/NEA Data Bank, (2008).
[5] C. V. Parks, “Overview of ORIGEN2 and ORIGEN-S: Capabilities and limitations”, p. 57-63 Proc. of the 3rd International Conference on High-Level Radioactive Waste Management, Vol.1, Las Vegas, Nevada, April 12-16, (1992).
[6] B. J. Toppel, "A User's Guide for the REBUS -3 Fuel-Cycle-Analysis Capability," ANL-83-2, Argonne National Laboratory (1983).
[7] Jerzy Cetnar, W. Gudowski, J. Wallenius, “User Manual for Monte Carlo Continuous Energy Burnup (MCB) Code – Version 1C”, NEA-1643/01, August, (2002).
[8] M. Zheng, W. Tian, H. Wei, D. Zhang, Y. Wu, S. Qiu, G. Su, “Development of a MCNP–ORIGEN burn-up calculation code system and its accuracy assessment”, Annals of Nuclear Energy, Vol. 63, p. 491-498 (2014).
[9] S. M. Bowman, M. D. DeHart, and L. M. Petrie, “Integrated KENO Monte Carlo Transport for 3-D Depletion with SCALE” Proc. of The Monte Carlo 2005 Topical Meeting, The Monte Carlo Method: Versatility Unbounded in a Dynamic Computing World, Chattanooga, Tennessee, April 17-21, 2005, on CD-ROM, American Nuclear Society, La Grange Park, Illinois (2005).
[10] N. A. Hanan, A. P. Olson, R. B. Pond, J. E. Matos, “A Monte Carlo burnup code linking MCNP and REBUS”, ANL-TD-CP-97492, also Proc. of the 21st RERTR Meeting, October 18 - 23, 1998, Sao Paolo, Brazil (1998).
[11] Z. Zhong, Y. Gohar, A. Talamo, “MCNPX and MCB Coupled Methodology for the Burnup Calculation of the KIPT Accelerator Driven Subcritical System”, Proc. of “International Conference on Mathematics, Computational Methods & Reactor Physics (M&C 2009), Saratoga Springs, New York, May 3-7, 2009, on CD-ROM, American Nuclear Society, LaGrange Park, IL (2009)
[12] J.M Gomit, P. Cousinou, C. Diop, G. Fernandez de Grado, F. Gantenbein, J.P. Grouiller, A. Marc, D. Mijuin, H. Toubon, “CRISTAL V1: Criticality package for burn up credit calculations”, Proc. of the 7th International conference on nuclear safety safety- Challenges in the pursuit of global nuclear criticality safety (ICNC2003), Tokai, Ibaraki (Japan), October 20-24, 2003, Report JAERI-CONF--2003-019-PT2 (2003).
[13] M. Samson, J. P. Grouiller, J. Pavageau, P. Marimbeau, “Cesar: a simplified evolution code for reprocessing applications”, Proc. of the 5th International Conference on recycling, conditioning and disposal (RECOD 98), Nice (France), October 25-28, (1998).
[14] G. Ren, W. Li, Y. Li, M. Zeng, “Simulation for Radiation Field caused by beam loss of C-ADS INJECTOR II”, p. 489-491, Proc. of International Beam Instrumentation Conference, Oxford’s University, Oxford, UK, 16-19 Sept., Vol. 1, (2013).
[15] H. Louis, E. Amin, M. Aziz, I.Bashter, “Studies on Production of Neutrons in the Spallation Reactions Using the Monte Carlo Code MCNPX”, Nuclear Science and Engineering, Vol. 170 (1), p. 61-65, (2012)
[16] Y. Kadi and F. Carminati, “Simulation of Accelerator-Driven Systems”, Workshop on Hy-brid Nuclear Systems for Energy Production, Utilisation of Actinides & Transmutation of Long-Lived Radioactive Waste, European Organization for Nuclear Research: CERN, Trieste, September 3-7, (2001).
[17] C. Bungau, R. Barlow, A. Bungau, R.Cywinski, “Neutron Spallation Studies for an Accelerator Driven Subcritical Reactor”, Proc.of 23rdParticle Accelerator Conference PAC09, Vancouver, BC, Canada, May 4–8, (2009).
[18] P. K. Romano, B. Forget, “The OpenMC Monte Carlo particle transport code”, Nucl. Technol., 51, p. 274-81, (2013).
[19] E. A. Gomin, L. V. Maiorov “The MCU Monte Carlo Code for 3D Depletion Calculation”, p.997-1006, Proc. of International Conference on Mathematics and Computations, Reactor Physics, and Environmental Analyses in Nuclear Applications (M&C 1999), Vol. 2, Madrid, Spain, Sept. 27−30, (1999).
[20] M. Aufiero, A. Cammi, C. Fiorina, J. Leppänen, L. Luzzi, M. Ricotti, "An extended version of the Serpent-2 code to investigate fuel burn-up and core material evolution of the molten salt fast reactor", J. Nucl. Mat., Vol. 441, p. 473-486, (2013).
[21] R. Brun, M. Hansroul, J. C. Lassalle, “GEANT3 User’s Guide”, CERN DD/EE/84- 1. Computing and Networks Division, CERN (1994)
[22] N. Catsaros, B. Gaveau, M. Jaekel, J. Maillard, G., Maurel, P. Savva, J. Silva, M. Varvayanni, Th. Zisis, “Criticality qualification of a new Monte Carlo code for reactor core

analysis", Annals of Nuclear Energy, 36, pp. 1689-1693, (2009)
[23] N. Catsaros, B. Gaveau, M.-T. Jaekel, J. Maillard, G. Maurel, P. Savva, J. Silva, M. Varvayanni, "Building a Dynamic Code to Simulate New Reactor Concepts", Nuclear Eng. & Design, 246, pp. 41-48 (2012)
[24] N. Catsaros, B. Gaveau, M.-T. Jaekel, A. Jejcic, J. Maillard, G. Maurel, P. Savva, J. Silva, M. Varvayanni, T. Xenofontos, "Investigating the breeding capabilities of Hybrid Soliton Reactors", 20th Int. Conf. "Nuclear Energy for a New Europe", Bovec, Slovenia, September 5-7, (2011)
[25] T. Xenofontos A. G. Mylonakis, P. Savva, M. Varvayanni, N. Catsaros, "Development of a Stochastic Dynamic Neutronics Code ANET" Technical Report in the framework of LENSER project, Research Reactor Laboratory, N.C.S.R. 'Demokritos', (2015)
[26] A.R. Junghans, et al., Nuclear Physics A, 629 p. 635-655, (1998)
[27] N.M. Greene, and L.M. Petrie, "XSDRNPM A One-Dimensional Discrete-Ordinates Code for Transport Analysis", Oak Ridge National Laboratory, NUREG/CR-0200, Revision 6, V. 2, Section F3, ORNL/NUREG/CSD-2/V2/R6 (2000)
[28] T.B. Fowler, D.R. Vondy, G.W. Guningham, "Nuclear reactor core analysis code: CITATION". Oak Ridge National Laboratory, ORNL-TM-2496, Rev. 2 (1971)
[29] J.E. Matos, J.G. Stevens, E.E. Feldman, J.A. Stillman, F.E. Dunn, K. Kalimullah, J.G. Marques, N.P. Barradas, A.R. Ramos, A. Kling, "Core conversion analyses for the Portuguese Research Reactor", Proc. of 28th International Meeting on Reduced Enrichment for Research and Test Reactors, Cape Town, Republic of South Africa, 29 Oct. – 2 Nov., (2006)
[30] B.-C. Na, N. Messaoudi, Benchmark on the Three-dimensional VENUS-2 MOX Core Measurements, Final Report, NEA/NSC/DOC, 2003, ISBN 92-64r-r02160-4
[31] N. Chrysanthopoulou, T. Xenofontos, "Technical report on the Thessaloniki student training nuclear reactor model 9000", Research Reactor Laboratory, N.C.S.R. 'Demokritos', (2012)
[32] T. Xenofontos, G.-K. Delipei, P. Savva, M. Varvayanni, J. Maillard, J. Silva, N. Catsaros, "ANET reaction rates validation based on the Venus-2 MOX core benchmark analysis", Int. Conf. Nuclear Energy for New Europe '15, Portoroz, Slovenia, September 14-17, Nuclear Society of Slovenia, 2015
[33] DeHart M. D., Brady M. C., Parks C. V., "OECD/NEA, Burnup Credit Calcunational Criticality Benchmark Phase I-B Results", NEA/NSC/DOC(96)-06, ORNL-6901
[34] Chart of the nuclides 2014 http://wwwndc.jaea.go.jp/CN10/index.html (2014)
[35] Cabellos O., García-Herranz N., Diez de la Obra C.J., Alvarez-Cascos R., Sanz J., Ogando F., Sauvan P. "Propagation of Nuclear Data Uncertainties in Transmutation Calculations Using ACAB Code", Int. Conf. on Nuclear Data for Science and Technology, Jeju Island, Korea (2010).
[36] D. Basile, M. Beghi, R. Chierici, E. Salina, E. Brega, "COBRA-EN: an upgraded version of the COBRA-3C/MIT code for thermal hydraulic transient analysis of light water reactor fuel assemblies and cores". Report 1010/1, ENEL-CRTN, Milano (1999)
[37] A.G. Mylonakis, M. Varvayanni, D.G.E. Grigoriadis, P. Savva, N. Catrsaros, "Optimization of an Integrated Neutronic/Thermal-Hydraulic reactor core analysis model", 23rd International Conference Nuclear Energy for New Europe, Portoroz, Slovenia, September 8-11, (2014)
[38] NURISP project's website: www.nuresim.com
[39] J.E. Hoogenboom, W.R. Martin, B. Petrovic,"The Monte-Carlo performance benchmark test-aims specifications and first results", In: International Conference on Mathematics and Computational Methods Applied to Nuclear Science and Engineering. Rio de Janeiro, Brazil, (2011)
[40] A.G. Mylonakis, M. Varvayanni, N. Catsaros, "Investigating a Matrix-free, Newton-based, Neutronic-Monte Carlo/Thermal-Hydraulic coupling scheme", Awarded paper, Proc. Int. Conf. Nuclear Energy for New Europe '15, Portoroz, Slovenia, September 14-17, Nuclear Society of Slovenia, (2015)
[41] Böhlen T.T., Cerutti F., Chin M.P.W., Fassò A., Ferrari A., Ortega P.G., Mairani A., Sala P.R., Smirnov G. and Vlachoudis V., "The FLUKA Code: Developments and Challenges for High Energy and Medical Applications", Nuclear Data Sheets 120, 211-214 (2014).
[42] Piénkowski L.P., Gawlikowicz W., Hilscher D., "FLUKA simulation for NESSI experiments", EURISOL-05-25-2006-0014

ENHANCED COMPUTATIONAL MODELS OF THE UNIVERSITY OF FLORIDA TRAINING REACTOR (UFTR)

D. Springfels[1], K.A. Jordan[1]

[1]Nuclear Engineering Program, Materials Science and Engineering, University of Florida
100 Rhines Hall, P.O. Box 116400 Gainesville FL 32611-6400
dspringfels@ufl.edu, kjordan@mse.ufl.edu

ABSTRACT

The University of Florida Training Reactor (UFTR) is a 100 kW ARGONAUT type research reactor, and serves as a resource for education on reactor physics, control, operations, nuclear regulations, and safety culture. The scope of the present work was to build a database of computational models, methods, experimental results, measurements, and associated facility specifications that is useful for supporting the UFTR utilization program. Additionally, the high fidelity models and specifications provide a benchmarking database that can be used for verification and validation of additional computer codes. A detailed reactor description was presented along with experimental data to establish a calculation benchmark for the UFTR that can be used to validate neutronic and thermal-hydraulic codes. High-fidelity computation was employed to provide accurate computational results that matched experimental observation to within 5%. These models will be used to support the utilization, training, and teaching programs at both the UFTR facility and the University of Florida Nuclear Engineering Program.

KEYWORDS

Reactor benchmarking, Monte-Carlo, UFTR, MCNP, SERPENT, PLTEMP/ANL

1. Introduction

The University of Florida Training Reactor (UFTR) is a 100 kW ARGONAUT type research reactor, and serves as a resource for education on reactor physics, control, operations, nuclear regulations, and safety culture. Over its nearly six decades of existence, the reactor has been used for applications such as nuclear medicine isotope production, reactor design benchmarking, nuclear data measurements, and neutron activation analysis supporting research in agriculture, biology, and geology.

In 2006 the UFTR completed a conversion to low enriched uranium (LEU) based fuel. The new fuel design coupled with a redesigned primary coolant system has presented the UFTR with new, unanalyzed physical components and operating conditions. While the gross operating conditions were analyzed in the scope of the fuel conversion analysis, no true validation and characterization work has been completed for the new systems.

As part of the Nuclear Regulatory Commission (NRC) mandated 20-year operating license renewal, a comprehensive safety analysis was conducted using state-of-the-art methodologies to demonstrate that the UFTR has inherently negligible risk. This new safety analysis replaces the previous analysis (from 1982), which was based on the more primitive computational methods available at that time.

Scope of Present Work

As part of past analysis, crude models were developed to analyze steady state and transient operating conditions for the UFTR. These models were insufficient to fully analyze the capabilities and intricacies present in the highly heterogeneous reactor. New, highly detailed models were created to help characterize the reactor to both validate the codes, and help the facility understand the full experimental capabilities available.

The scope of the present work is to build a database of computational models, methods, experimental results, measurements, and associated facility specifications that is useful for supporting the UFTR utilization program. Additionally, the high fidelity models and specifications will provide a benchmarking database that can be used for verification and validation of additional computer codes.

2. General Description of Facility

ARGONAUT type reactors, such as the UFTR, are especially effective training tools due their similarity to a pressurized water reactor (PWR). In both designs, primary coolant flows up through and around cladded fuel assemblies. Further, the ARGONAUT design, like a PWR, uses forced convection coolant; in contrast, most other research reactors use a standing pool design (free convection). The main difference is in the operating pressure.

The UFTR licensed rated thermal power level is 100kW giving a power density of 17.88 $kW \cdot L^{-1}$. The thermal flux at the Central Vertical Port (CVP) is approximately 1.5×10^{12} $n \cdot cm^{-2} \cdot s^{-1}$. (1)

The core is divided into six fuel boxes and each box is subdivided into four fuel bundle locations. Each fuel bundle consists of 14 plates of U_3Si_2-Al LEU enriched to 19.75%. Water serves as the both the coolant and partial moderator. Graphite blocks surrounding the fuel boxes provide further moderation and neutron reflection. Dummy plates and dummy bundles are loaded as necessary to limit the installed excess reactivity. Figure 1 shows a cutaway of the reactor core highlighting key components.

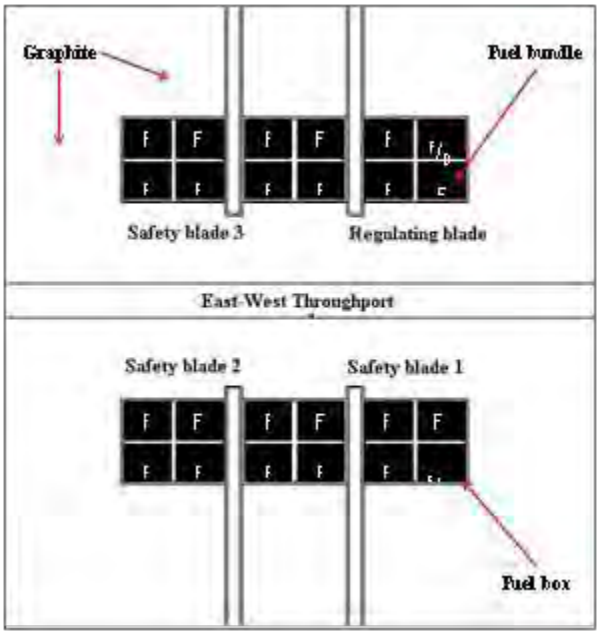

Figure 1) Schematic horizontal cut of the UFTR

The primary coolant (demineralized water) is pumped upward past the fuel plates at slightly above atmospheric pressure. The exiting warm coolant (approximately 40 °C at 100 kW) is gravity-fed to a heat exchanger. This secondary coolant is pumped in from a well and returned to the storm sewer.

Reactor control is provided by four swing-arm, cadmium-tipped control blades. Three blades are for safety and the fourth is for regulating reactor power. Using mechanical drives, the control blades are moved in a vertical arc within the spaces between the fuel boxes. The drives are located outside of the reactor for ease of accessibility and maintenance. These drives can be disconnected from the blades by means of an electromagnetic clutch, which allows the blades to fall by gravity into the reactor for SCRAM. Table 1 shows general properties of the UFTR.

Table 1) General Description of the UFTR Facility

Type of reactor	ARGONAUT-MTR
Nominal Power	100 kW thermal
Maximum neutron flux	$\sim 1.5 \times 10^{12}$ n·cm^{-2}·s^{-1}
Fuel type	Flat plate U_3Si_2-Al Dispersion Al clad parallel plates
Enrichment	19.75wt%
Coolant	Light water, forced convection
Moderator	Light water, Graphite
Nominal flow rate	43 gpm
Experimental Facilities	6 beam tubes Pneumatic Rabbit System Thermal Column

3. Reactor Specifications

Reactor Geometry

The arrangement of fuel bundles, boxes, control elements and housing, as well as the graphite moderator are shown in Figure 1. Letters designating fuel (F) and dummy bundles (D) are shown in the figure to indicate the different possible loading patterns.

Reactor control is provided by four swing-arm, cadmium-tipped control blades. Two different types of control blades, Safety and Regulating, are located between the fuel boxes in magnesium shrouds. There are also three vertical experimental ports that are centrally located with respect to the fuel elements. The East-West Throughport is used by the pneumatic rabbit transfer system. Figure 2 shows an isometric view of the UFTR highlighting the core, thermal column, and control blade control mechanisms.

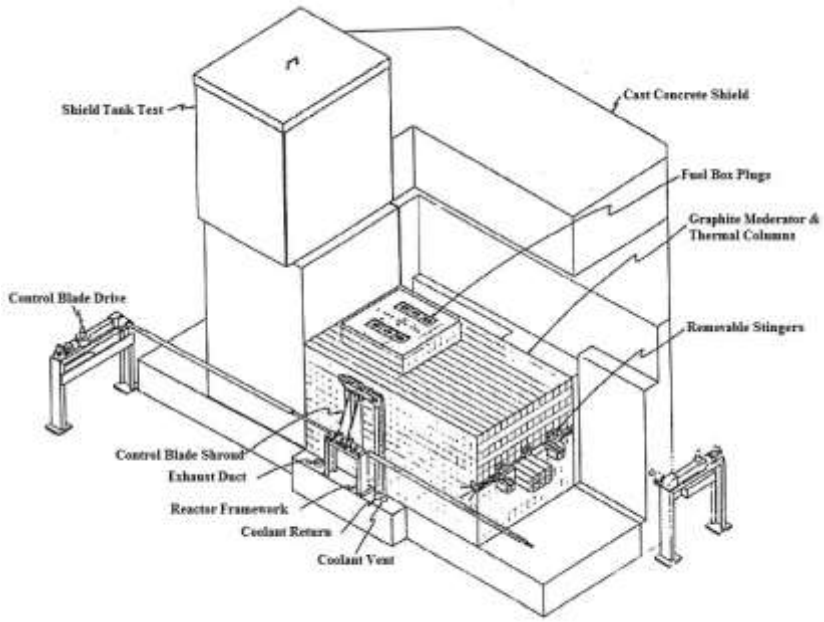

Figure 2) Schematic Isometric View of the UFTR

Fuel Bundle Description

Each full fuel bundle contains 14 fuel plates with a nominal overall width of 7.2263 cm and a nominal water gap of 0.282 cm between the plates. The ends of the plates are separated by aluminum spacers and are bolted together. Aluminum spacers are welded onto the edges of the plates on alternating sides. To eliminate variations in water channel spacing, aluminum combs are installed to physically separate the fuel plates at the nominal quarter-points locations along the fuel plate length. The tolerance on the minimum water channel spacing is a maximum of 20 mils. The nominal water channel spacing at the bolted ends of the fuel assembly on the manufacturing drawings is 110-112 mils (1), giving a minimum water channel spacing of 90 mils. Table 2 gives the nominal fuel bundle design parameters.

Table 2) Fuel Bundle Parameters [cm]

Fuel Meat Dimensions	X	5.9563
	Y	0.0508
	Z	60.0075
Cladding Dimensions	X	7.2263
	Y	0.127
	Z	65.0875
Unit Cell/Water Channel	t	0.28194
Bundle Dimensions	Y-extent	5.72516
	X-axis spacing	0.7874
	Y-axis spacing	0.40132

Table 3) General Fuel Design Data

No. of fuel bundles	22-24
No. of fuel boxes	6
Bundles per box	4
Fuel type	U_3Si_2-Al
Fuel density	5.547 g/cc
Cladding	Al 6061
Cladding Thickness	0.0381 cm
Enrichment	19.75wt%
Fuel meat wt%/U	62.98
Mass ^{235}U per plate	12.5 g
No. Plates per bundle	14
Mass ^{235}U per bundle	175 g

Fuel Box Description

In the UFTR, fuel is loaded into six fuel boxes, each containing three to four fuel assemblies. The fuel region is vertically centered in the fuel box. The arrangement of four fuel assemblies

inside a fuel box is shown in Figure 3. Figure 1 provides a schematic of their locations in the core structure.

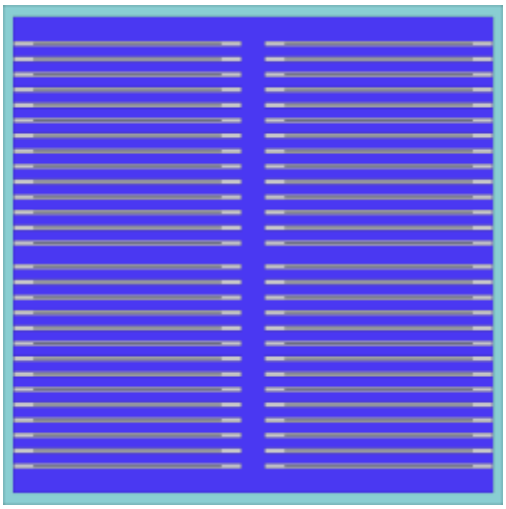

Figure 3) Arrangement of the Fuel Bundles in a Fuel Box

The fuel box design uses two wedge pins to position the fuel assemblies in each fuel box. The two-pin configuration with the smallest assemblies in the largest box produces two wide East-West channels of width 0.7874 cm and a 0.40132 cm central North-South channel. Table 4 provides dimensions of a fuel box; these dimensions are based on the current fuel size.

Table 4) Fuel Box Parameters [cm]

Inner Fuel Box	along X-axis	15.24
	along Y-axis	12.7
	along Z-axis	121.9
Wall thickness		0.3180
Inter-Fuel Box Spacing	along X-axis	2.54
	along Y-axis	30.48
Fuel Bundle Water Gaps	X-axis	0.7874
	Y-axis	0.40132

The water level is at approximately 13.97 cm below the top of the fuel box, i.e., at half the outlet pipe. This is confirmed by measurement of the water column height in the reactor building (measured at an average of 166 cm).

Control Blades

The blades are of the swing-arm type consisting of four cadmium vanes protected by magnesium

shrouds; they operate by moving in a vertical arc within the spaces between the fuel boxes. The shroud is made of magnesium and the blades are made of aluminum tipped with cadmium.

The control blade drive system consists of a motor that operates through a reduction gear train, and an electrically energized magnetic clutch that transmits a motor torque through the control blade shaft, allowing motion of the control blades. The basic control blade drive system is illustrated in Figure 4.

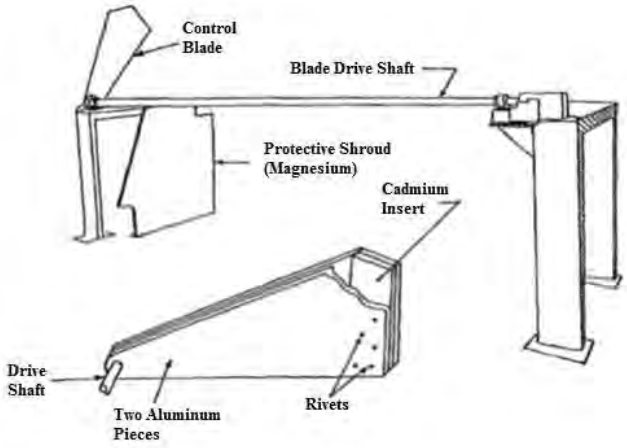

Figure 4) UFTR Control Blade and Drive System

The blades are sustained in a raised position by means of the motor, acting through the electromagnetic clutch. Interruption of the magnet current results in a decoupling of the motor drive from the blade drive shaft, causing the blades to fall back into the core. Figure 5 illustrates the control blades and their operations within the core.

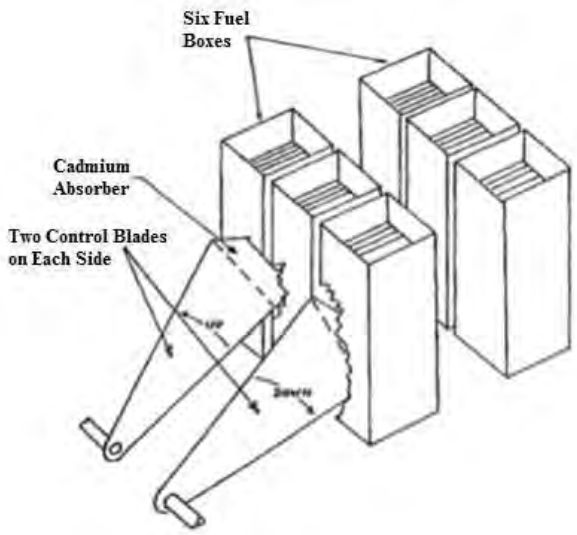

Figure 5) UFTR Core Sketch Showing Operation of the Control Blades

The control blades are tipped with cadmium inserts. The cadmium tip of the Regulating Blade is smaller in size than the tips of the other control blades. Magnesium shrouds protect the blades. The blades have a fully-inserted nominal position of 2.5° above the XY center plane and are moved out of the core by rotating them 45°. The top of the shroud is located 10 cm above the top of the fuel box. Figure 6 shows the fully inserted and fully withdrawn locations of the control blade with respect to one of the shrouds and the centerline of the core; Figure 7 and 8 show the dimensions of the blades and the cadmium inserts.

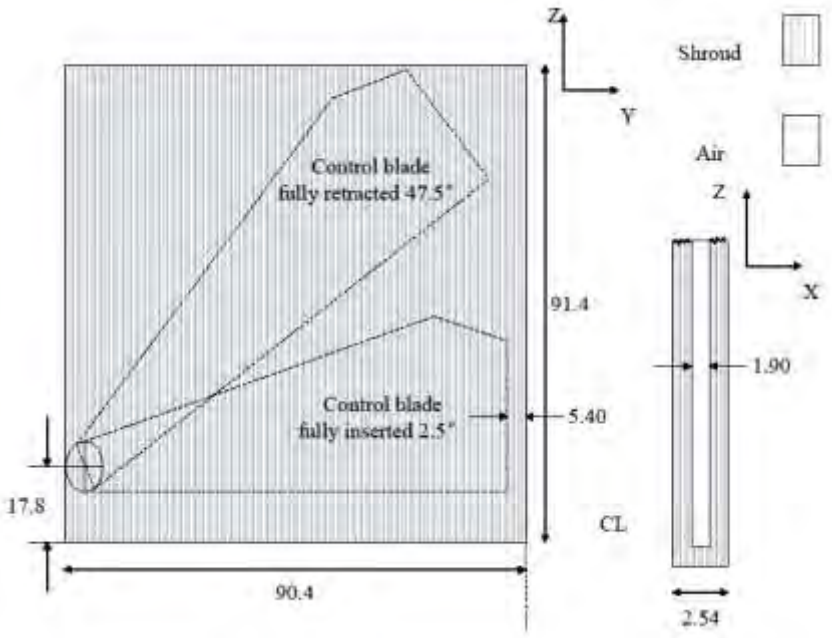

Figure 6) UFTR Control Blade Movement and Spacing [cm]

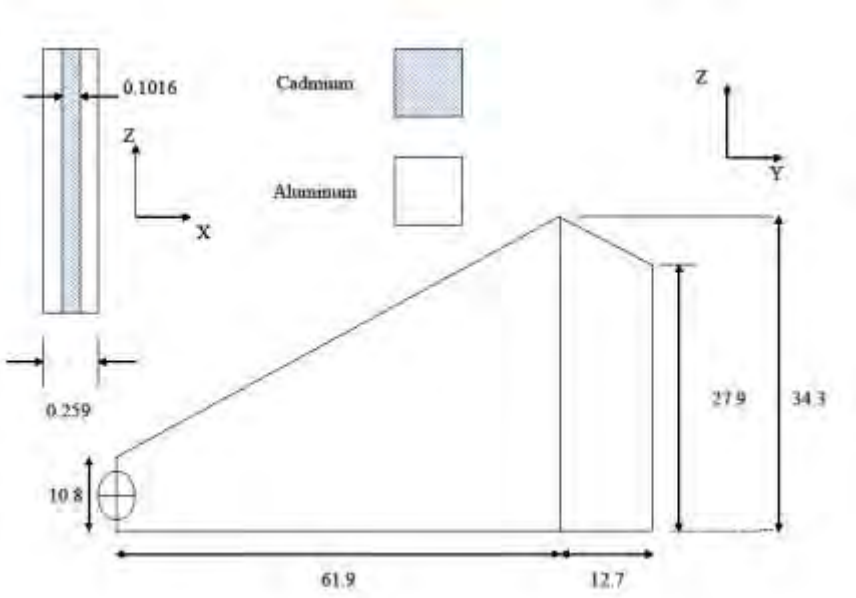

Figure 7) UFTR Control Blade Dimensions [cm]

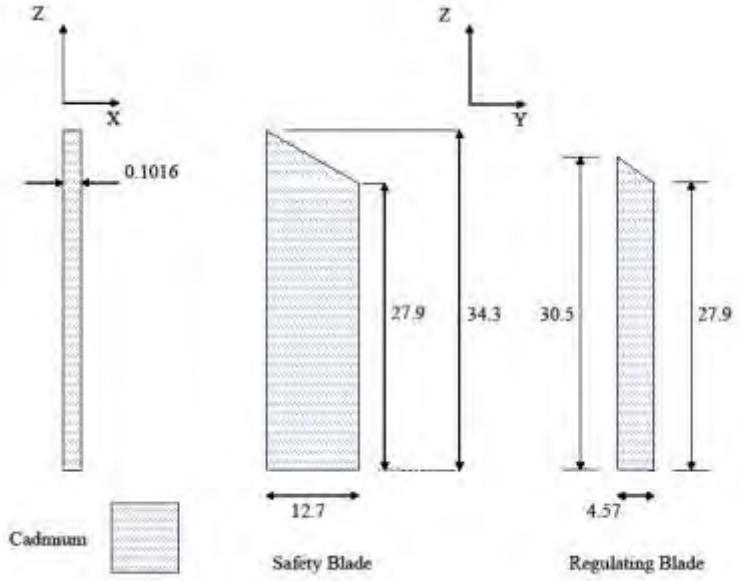

Figure 8) UFTR Control Blade Cadmium Insert Dimensions [cm]

Experimental Facilities

The UFTR provides a range of irradiation ports for experimental capabilities. There are three vertical experimental holes that are centrally located with respect to the fuel elements, allowing for maximum neutron flux. These ports are 3.8 cm long and have diameters of 5.08, 4.45, and 3.81 cm (2.0, 1.75, and 1.5 in) allowing for samples to be inserted for neutron activation

analysis. Figure 9 shows the vertical port's dimensions relative to the centerline and fuel boxes. The horizontal thermal column is 1.52 m x 1.52 m x 1.42 m (60 in x 60 in x 56 in) and extends from the east side of the core reflector. Samples are placed in the center of the thermal column, while surrounding graphite stringers provide high thermalization for experiments. Additionally, there are six other horizontal ports positioned around the reactor central plane. With 10 cm (4 in) diameters, these experimental ports can be fitted with collimators to form neutron beams external to the reactor shielding.

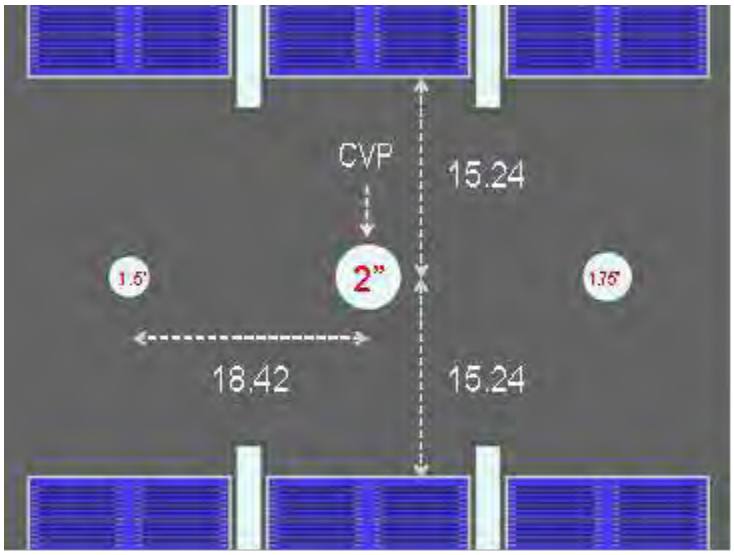

Figure 9) Vertical Experimental Ports locations and Dimensions [cm]

The reactor shield water tank also provides multiple experimental capabilities. The water tank measures 1.52 m x 1.52 m x 4.27 m (5 ft x 5 ft x 14 ft) and is located on the back (west) side, surrounded on three sides by concrete. Additional shielding can be placed above the water tank to minimize the effects of sky shining radiation. The tank can be used to perform shielding analyses or to irradiate large samples. If the fast neutron flux at the sample is insufficient, thermal neutrons from the core can be converted to fast neutrons through the installation of a converter plate inside the tank. An aluminum pipe can also be installed in order to allow for the extraction of a neutron beam from the core.

Finally, the UFTR offers a pneumatic sample transfer system, which can quickly transfer small samples to and from the core for activation analysis. The sample is transferred inside of a small polyethylene capsule (the rabbit). The sample moves through installed piping, through the shield tank, to the reactor center line. The rabbit then returns along the same path back to the receiving station. Directional nitrogen gas flow is used to control the motion of the sample, and the system is designed such that the sample is pulled rather than pushed, in order to minimize chances of damaging or lodging a sample inside of the core.

Materials Specifications

The U_3Si_2-Al fuel composition at beginning of life (BOL) was obtained by averaging six sets of

concentrations obtained from the manufacturer BWXT (2). The fuel matrix aluminum alloy and aluminum cladding compositions were obtained from the same package. Further, it is important to note that in case the impurity concentration is not exact, but bounded, the maximum value is used.

Other materials used in the core are aluminum for fuel clad and other structures, graphite for moderator and reflector, cadmium tips for the control blades, and magnesium for the control blade shrouds. Table 5 presents the properties of these various materials. Specific concentrations of impurities in the fuel silicide matrix and aluminum are given in Table 6 and Table 7.

Table 5) Materials Specifications

Material	Composition	Density
Aluminum - cladding	Al 6061	2.70 g/cc
Aluminum - other structures	Al + 10 ppm of natural boron	2.70 g/cc
Graphite -nuclear-grade	C + 5 ppm of natural boron	1.60 g/cc
Cadmium (abundance in %) - natural cadmium	^{106}Cd (1.25) ^{108Cd} (0.89) ^{110}Cd (12.49) ^{111}Cd (12.80) ^{112}Cd (24.13) ^{113}Cd (12.22) ^{114}Cd (28.73) ^{116}Cd (7.49)	8.75 g/cc
Magnesium	Mg	1.74 g/cc

Table 6) Impurities in U_3Si_2 Powder

Isotope	Concentration (ppm)	Mass[1]
Al	131.67	8.95E-05
Ba	2.00	1.36E-06
Be	0.50	3.40E-07
B	1.33	1.82E-07
Cd	0.50	3.40E-07
Ca	20.00	1.36E-05
C	244.00	1.66E-04
Cr	18.33	1.25E-05
Co	5.00	3.40E-06
Cu	100.83	6.85E-05
Eu	0.20	1.36E-07
Gd	0.20	1.36E-07
Fe	608.50	4.13E-04
Pb	0.50	3.3974E-07
Li	0.10	6.80E-08
Mg	10.00	6.80E-06
Mn	8.67	5.89E-06
Mo	3.00	2.04E-06
Ni	43.33	2.94E-05
N	55.00	3.74E-05
P	20.00	1.36E-05
Sm	0.20	1.36E-07
Ag	1.00	6.79E-07
Na	10.00	6.79E-06
Sn	1.00	6.79E-07
W	21.67	1.47E-05
V	4.50	3.06E-06
Zn	20.00	1.36E-05
Zr	3.83	2.60E-06

[1] per gram fuel

Table 7) Impurities in Aluminum Powder

Isotope	Concentration (ppm)	Mass[2]
Zn	0.02	6.41E-05
Cu	0.001	3.21E-06
Cd	0.001	3.21E-06
Li	0.001	3.21E-06
B	0.001	3.21E-06
Fe	0.167	5.35E-04
O	0.097	3.11E-04

[2] per gram fuel

4. Neutronic Models and Methods

Detailed three-dimensional, continuous-energy MCNP (3) and SERPENT (4) models of the UFTR have been developed for the analysis of whole-reactor characteristics such as critical conditions and reactivity parameters. These models have been applied to the determination of the critical core configuration, reactivity worth for the regulating and three safety control blades, reactivity coefficients, and kinetics parameters.

The Monte Carlo models employed for the UFTR represented the core region in detail, from fuel meat within fuel plates to individual beam ports and air gaps around control blades. The thermal column, air gaps between graphite and the concrete structure, as well as the structure itself are not modeled. The models follow the description of the core layout given in Section 3.

Sections 4 and 5 describe the modeling techniques and a description of the measurement and analysis techniques used to validate the predicted values respectively.

In addition to critical core configuration calculations, the neutronic models have also been used to:

- Estimate the control blade position at BOL and end of life (EOL)
- Perform whole-core depletion calculation to predict fission product inventory
- Calculate power distributions for thermal hydraulics calculations
- Estimate the neutron fluxes in-core and at experimental ports

Detailed Neutronic Model Description

A full-core MCNP and SERPENT model was created to perform calculations of core physics parameters using the ENDF/B-VII.1 (5) cross-section library. Core physics parameters evaluated

include reactivity coefficients, the delayed neutron fraction, and generation time.

Both the MCNP and SERPENT models have the same geometry and materials (see below). This model contains 22 fully fueled bundles, 0 partially fueled bundles, and 2 dummy bundles. The core is loaded with fresh and the composition is the same in each bundle. The models include the contribution due to both prompt and delayed neutrons as well as fission products where applicable.

Figure 10 shows a modeled fuel box and the full core SERPENT model. The dimensions and bundle spacing for the MCNP and SERPENT models are equal.

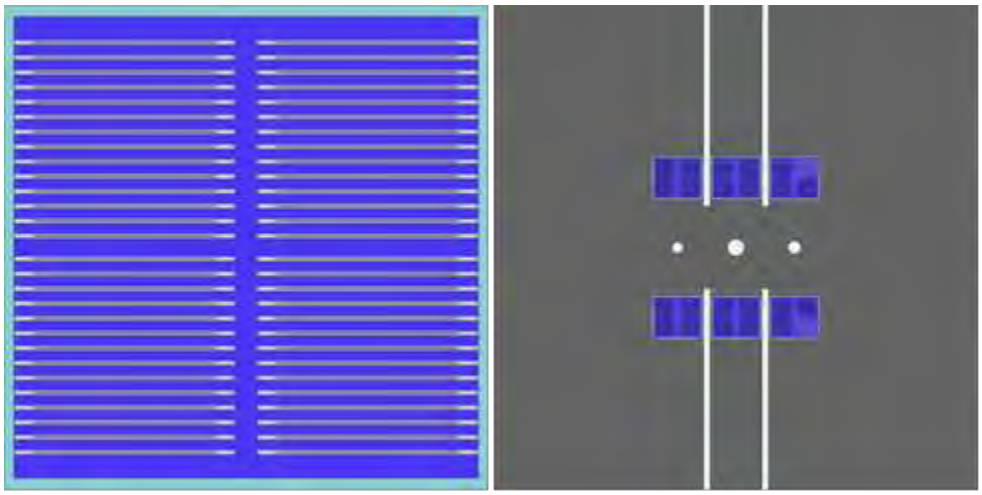

Figure 10) SERPENT Model Highlight Showing the Fuel Box with Four Assemblies (left) and the Core and Graphite Reflector (right)

Temperatures for cross-section treatment are described for each material as follows;

- Water - Linear average of nominal inlet temperature (30 °C) and mixed mean coolant outlet temperature (40.5 °C)
- Al (structure) - Assumed to be the same temperature as water (see above)
- Al (clad) - Linear average of max clad temperature and water temperature calculated above
- Fuel - Linear average of max fuel temperature and water temperature calculated above

Each fuel bundle is filled with unit cells based on core configuration and translated into the appropriate position within fuel box 5. Therefore, all bundle cells (regardless of which box they belong to) have the same sequence of translation thereby reducing complexity.

Modeling of experimental ports was accomplished by taking into account the dimensions of the rabbit system, vertical ports, and the south beam port and incorporating air gaps within the graphite.

Each control blade is constructed from planes specified in the same location, and the cell groupings that create a complete control blade structure are translated into the correct position. The default (reference) angle for each blade is 0° with respect to the horizontal (x-axis). This

corresponds to a “latched” condition. Control blades can be modeled to fit any condition the reactor may be in, however, physical blade restrictions limit positioning between 0° (latched) and 47.5° (fully withdrawn) degrees.

SERPENT and MCNP Model Comparison

Structural differences in the geometric modeling abilities exist between MCNP and SERPENT. Complex and arbitrary shapes cannot be modeled in SERPENT (4). Thus the control blades have to be modeled in such a way as to have the same neutronic characteristics as the complex trapezoidal tips in MCNP as shown in Figure 11. Dimensions for the Cd were replicated and the density reduced until the critical configurations of both models were within 15 pcm (3σ). The two models were then considered equivalent. Table 8 shows the results of the calculations and an 83 pcm difference can be seen in the core excess reactivity between the two models.

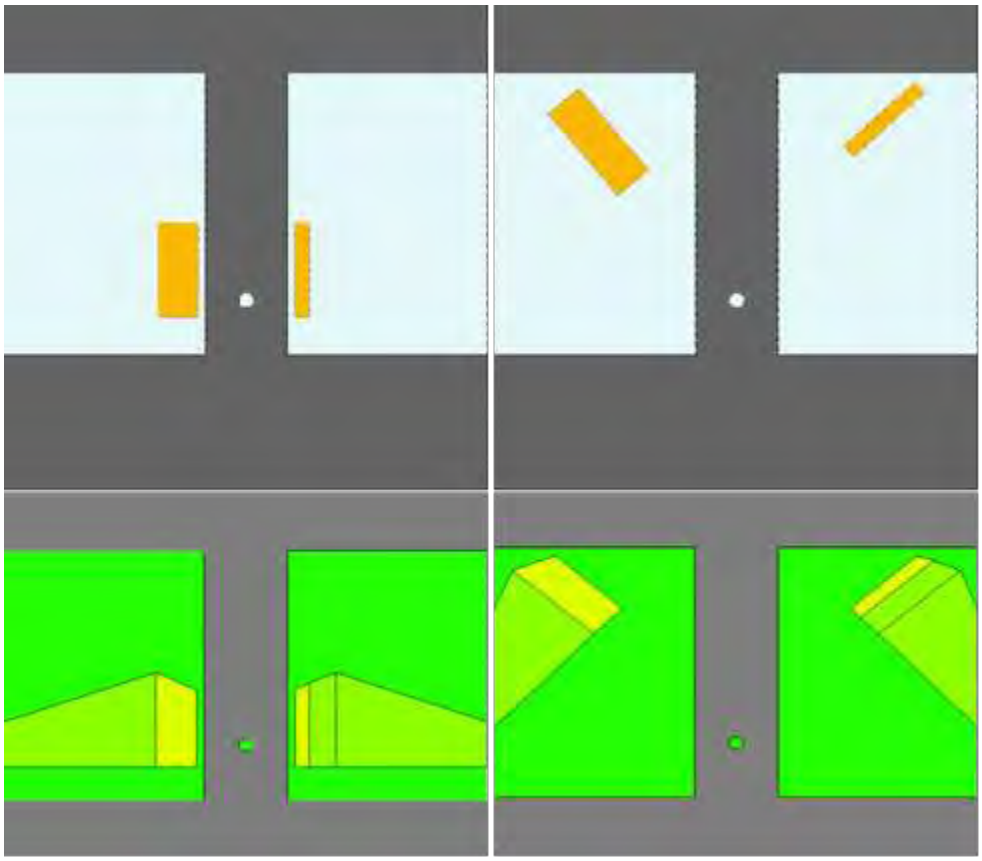

Figure 11) SERPENT Model (top) and MCNP Model (bottom) Highlighting the Differences in Control Blade Modeling

Table 8) Calculated Infinite Multiplication Factor - k_∞

	MCNP	SERPENT	Δ
Bundle (reflected)	1.56661 ± 5 pcm	1.56666 ± 5 pcm	5 pcm
Fuel Box (reflected)	1.42654 ± 9 pcm	1.42641 ± 2 pcm	13 pcm
Core (Blades at 0°)	0.93616 ± 4 pcm	0.93610 ± 7 pcm	6 pcm
Core (Blades at 47.5°)	1.00391 ± 10 pcm	1.00474 ± 20 pcm	83 pcm
Core (Critical Position)	RB at 25°	RB at 29°	

Calculated Core Parameters

The models were used to calculate the core reactivity coefficients for the BOL and EOL conditions. As shown in Table 9, the UFTR design has negative coefficients for fuel temperature, coolant temperature, and void.

Table 9) UFTR Reactivity Coefficients for BOL and EOL

Coefficient	Range	BOL	EOL
α_{void} (pcm/%void)	0-5% Void	-125 ± 4	-94 ± 4
α_{void} (pcm/%void)	5-10% Void	-140 ± 4	-106 ± 4
α_{water} (pcm/°C)	21-99 °C	-6.7 ± 0.3	-4.8 ± 0.3
α_{fuel} (pcm/°C)	21-127 °C	-1.9 ± 0.2	-1.7 ± 0.2
α_{fuel} (pcm/°C)	21-127 °C	-1.7 ± 0.1	-1.6 ± 0.1

Table 10 shows the MCNP- and SERPENT-calculated reactivity parameters for the UFTR. Fair agreement is shown between the two models. Agreement between the two codes for β_{eff} and neutron lifetime is within 3% and shut- down margin is within 10%. Figure 12 shows the calculated and measured integral control blade worth (IBW) for the four control blades. The largest deviation for measured IBW was seen at the upper limit of control blade movement where the relative worth of each blade is the smallest. Large deviations between the SERPENT and MCNP models for IBW can be seen. This is most likely attributed to the modeling differences discussed earlier. Further investigations are underway to correct the discrepancy.

Table 10) Calculated Reactivity Parameters

Parameter	MCNP	SERPENT
Excess Reactivity	391 ± 10 pcm	474 ± 15 pcm
Shutdown Margin	3503 ± 21 pcm	3774 ± 40 pcm
Regulating Blade Worth	775 pcm ± 21 pcm	555 ± 40 pcm
Safety Blade 1 Worth	1409 pcm ± 21 pcm	1335 ± 40 pcm
Safety Blade 2 Worth	1763 pcm ± 21 pcm	1698 ± 40 pcm
Safety Blade 3 Worth	1782 pcm ± 21pcm	1681 ± 40 pcm
Delayed Neutron Fraction (β)	741 ± 10 pcm	734 ± 10 pcm
Neutron Lifetime (μSec)	195.6 ± 0.1	196.2 ± 0.8

Experimental Results

Comparisons of the calculated and measured critical core configuration are shown in Table 11. The measured blade height in Safety Blades 1, 2, and 3 is based on the analog indicator on the console. The three safety blades were withdrawn to their physical limits during the critical core measurement. The critical core configuration for the regulating blade was within 5% of the predicted value.

Table 11) Calculated and Measured UFTR Critical Condition

Parameter	Calculated (Units[3])	Measured (Units)	% Deviation
Safety Blade 1 Height	1000	1015	1.5
Safety Blade 2 Height	1000	1002	0.2
Safety Blade 3 Height	1000	990	-1.0
Regulating Blade	168	160	4.8
α_T (pcm/°C)	-8.4 ± 0.3	-8.2 ± 3.1	2.1

[3]As seen on the analog console indicator. Range is 0 – 1000 Units

Blade worth measurements were obtained using the positive period method. The procedure is based upon making the reactor supercritical by withdrawing the blade to be calibrated a small amount and measuring the resulting period. Figure 12 show the results for the measured integral blade worth experiments. Table 12 provides the experimental data.

Temperature coefficient of reactivity was measured for 2-10°CΔT. Results are shown in Figure 13.

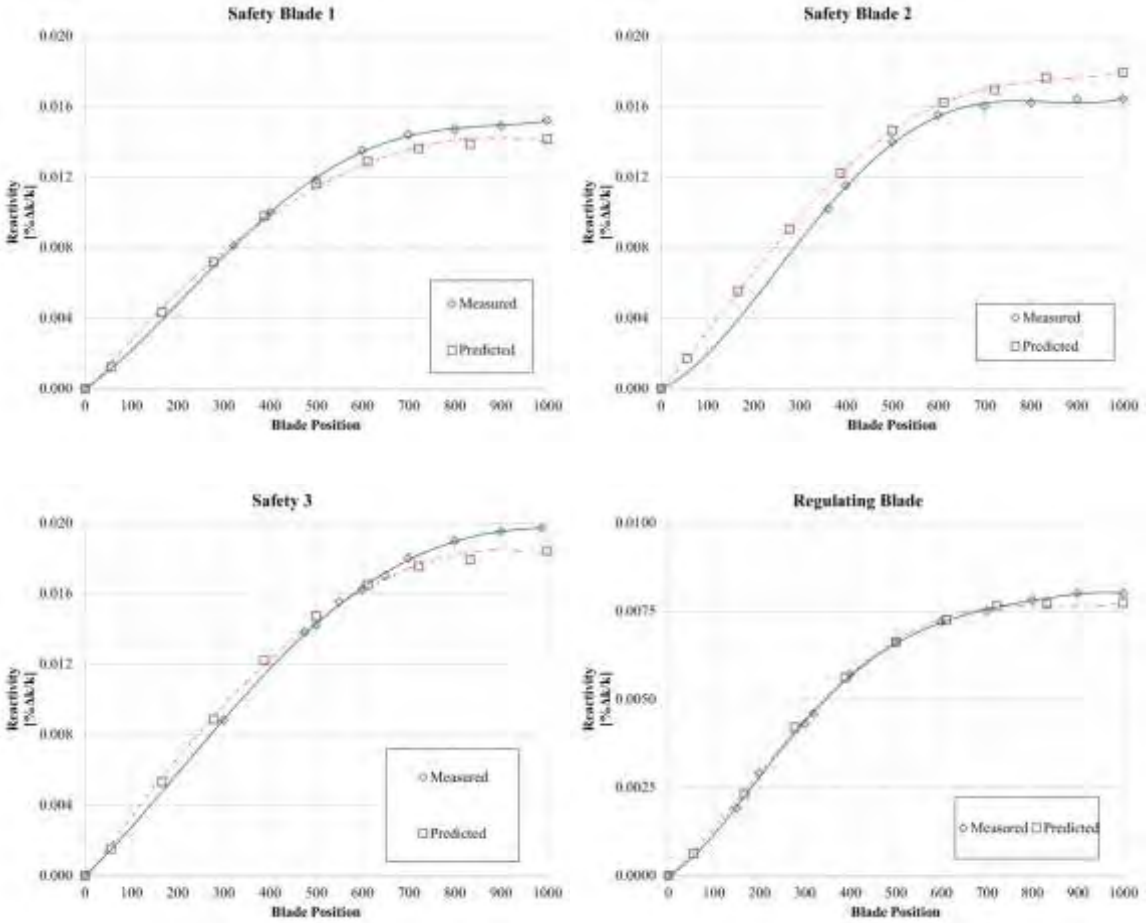

Figure 12) Measured and MCNP-Predicted Integral Control Blade Worth Curves

Table 12) Measured reactivities for the UFTR control blade worths

S1		S2		S3		RB	
Position (units)	Reactivity	Position (units)	Reactivity	Position (units)	Reactivity	Position (units)	Reactivity
0	0	0	0	0	0	0	0
322	0.0081	322	0.0102	300	0.0088	150	0.0019
400	0.01	400	0.0115	475	0.0138	200	0.0029
500	0.0118	500	0.014	500	0.0142	300	0.0043
600	0.0135	600	0.0155	550	0.0155	320	0.0046
700	0.0144	700	0.016	600	0.0162	400	0.0057
800	0.0147	800	0.0162	650	0.017	500	0.0066
900	0.0149	900	0.0164	700	0.018	600	0.0072
1000	0.0152	1000	0.0164	800	0.019	700	0.0075
				900	0.0195	800	0.0078
				990	0.0197	900	0.008
						1000	0.008

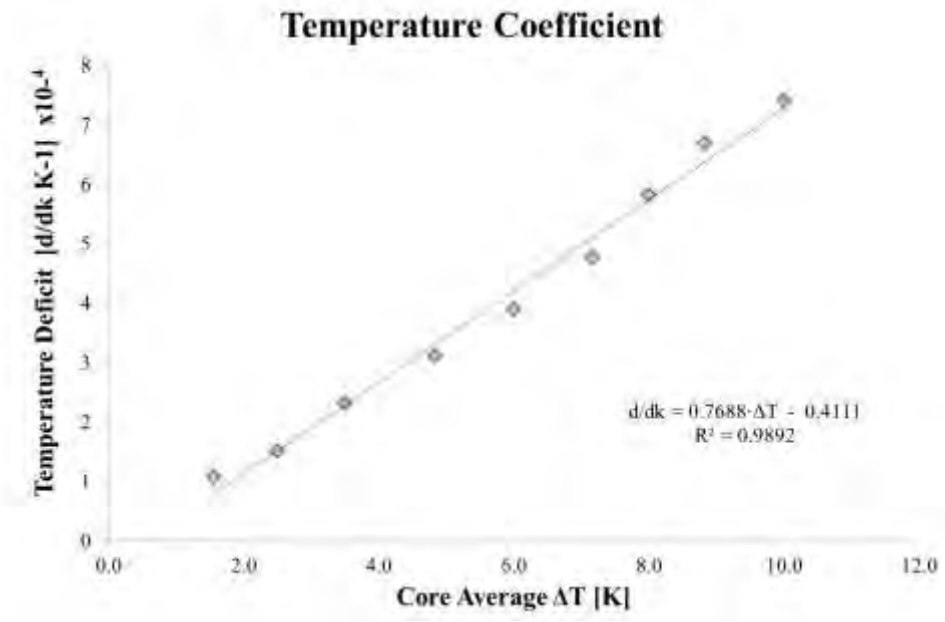

Figure 13) Measured Total Temperature Coefficient of Reactivity

Flux mapping of the CVP was conducted at 200 W to measure thermal flux. Experimental data and results are shown in Table 13. Figure 14 shows the calculated vs experimental data for the CVP foil measurements. Calculations agree within experimental data uncertainty for the in-core thermal flux and have a maximum deviation of 25% at 40 cm.

Table 13) CVP Foil Irradiation Experimental Data and Results

Foil ID	Bare/Cd	Meas. Wt. (g)	Position (cm)	Irradiation Time (sec)	Wait Time (sec)	Meas. Duration (sec)	Activity (CPS)
1	Bare	0.1239	1	1200.000	511516	60	634.167
2	Bare	0.1173	11	1200.000	511371	60	588.767
3	Bare	0.1177	21	1200.000	511232	60	512.383
4	Bare	0.1237	31	1200.000	511093	60	390.900
5	Bare	0.1222	41	1200.000	181528	60	714.967
6	Bare	0.1239	51	1200.000	181370	60	476.083
7	Cd	0.1231	1	1200.000	90693	60	623.267
8	Cd	0.1233	11	1200.000	90548	60	568.783
9	Cd	0.1241	21	1200.000	90437	60	432.933
10	Cd	0.1241	31	1200.000	90302	60	235.633
11	Cd	0.1236	41	1200.000	90031	60	158.500

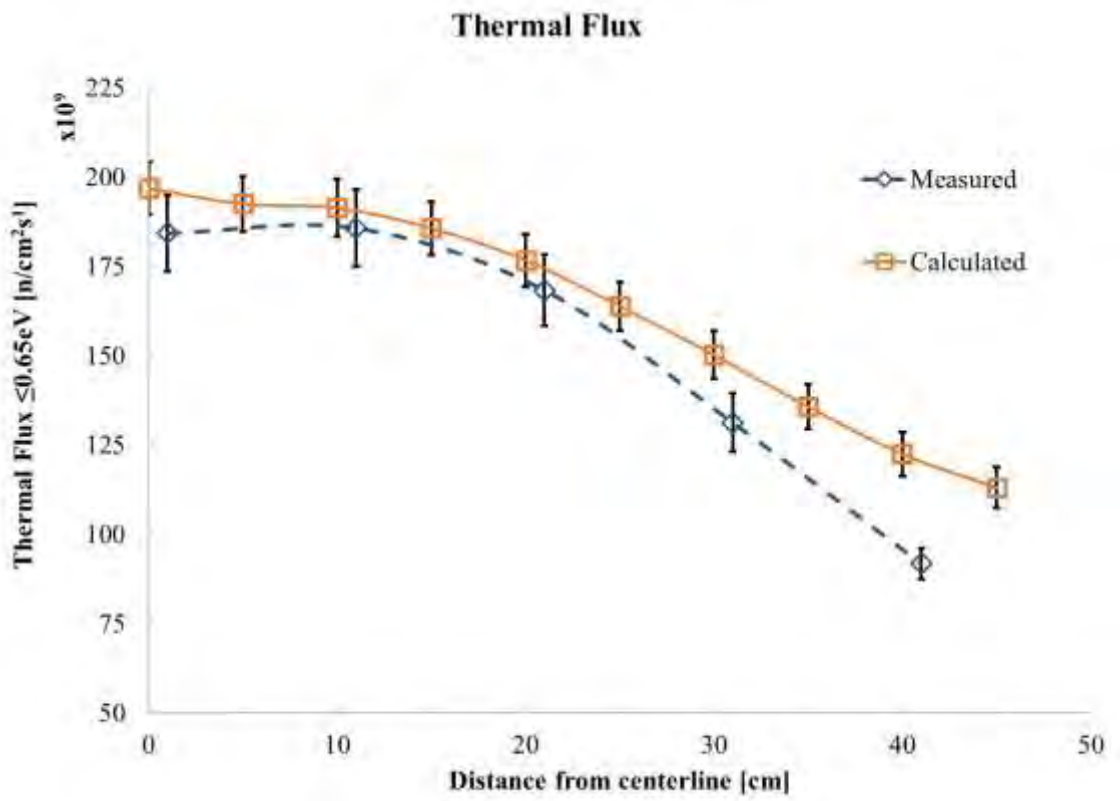

Figure 14) Thermal Flux (<0.625 eV) in the CVP of the UFTR

5. Thermal-Hydraulic Models and Methods

Steady State Model

PLTEMP/ANL (6) & RELAP5-3D (7) were used to determine the thermal-hydraulic conditions of UFTR at full power of 100 kW. Full power and over power conditions were modeled at several inlet flow conditions. The axial power distribution for the hottest plate was obtained from the results of the criticality calculations and applied to all fuel plates in an assembly.

The grid plate, which supports the four fuel assemblies in each fuel box, is included in the hydraulic analysis because it makes the velocity distribution in each fuel box more uniform. The hydraulic model in the code assumes that the hydraulic resistance for each coolant path, from the bottom of the grid plate to the region above the fuel plates, has two components, a form or K-loss and a frictional loss.

The K value includes the form losses at the inlet and exit to the fuel plates and hydraulic resistance due to the grid plate. The total flow area in the grid plate is smaller than the total flow area in the fuel region. A value of 5.0 was assumed for the K-loss value (8).

The ends of the side edges of the fuel plates are open where they contact the side channel. Lateral flow is expected to be small since the local pressure is expected to be essentially uniform

at each axial level. For modelling purposes it was assumed that no cross flow was present. The higher vertical flow velocities in the bigger channels, which have the larger hydraulic diameters, tend to keep the axial pressure drops through each of the parallel paths equal and the pressures uniform at each axial level. The hot channel factors include a 20% uncertainty in channel flow distribution.

Nominal conditions for the UFTR are average inlet temperature to the core is 30 °C at a flow rate of 43 gpm (2.69 kg/s) (1). Inlet coolant flow rate and temperatures were selected based on the nominal steady state reactor conditions. The steady state conditions that were evaluated using PLTEMP/ANL and RELAP5-3D are shown in Table 14.

Table 14) UFTR Modeled Steady State Conditions (All temperatures in °C)

Power [kW]	Inlet Temp. [°C]	Flow Rate [gpm]	$T_{clad,max}$	$T_{coolant,max}$	$ONBR_{min}$	$CHFR_{min}$	$T_{clad,max}$	$T_{coolant,max}$
100	30	30	70.7	67.2	1.687	479.5	69.41	63.20
100	30	43	58.5	54.8	2.407	563.3	60.64	54.35
100	45	30	83.7	80.2	1.387	392.4	83.21	77.12
100	45	43	72.4	68.8	1.954	476.6	75.02	68.86
125	30	30	78.5	74.3	1.418	377.7	72.20	64.46
125	30	43	64.8	60.3	1.972	457.0	67.50	59.71
125	45	30	91.5	87.4	1.155	303.5	86.34	78.75
125	45	43	77.9	73.4	1.634	382.8	81.78	74.14

Transient Analysis Models

The PARET-ANL (9) and RELAP5 codes were used for this analysis. Previous work has validated PARET/ANL using experimental data and quantified the resulting uncertainties (10). Combined with the uncertainties associated with the core input parameters, a total uncertainty of 70% on temperature differences (increase during the accident) must be included when analyzing the final temperature results.

The UFTR model for PARET/ANL was constructed by using the hottest channel and nominal initial conditions of maximum 100 kW power operation with the minimum coolant flow rate of 43 gpm. PARET is limited in its prediction of a thermal crisis by the fact that it employs a steady state DNB correlation. Thus, PARET is limited in its accuracy in the description of hydrodynamic instabilities.

The RELAP nodalization was modeled as two fuel plate channels. One channel represented the

fuel plate and associated coolant for the plate with peak power in the core, and the other channel represented the average of the remainder of the core. The fuel power densities for the peak and average channels were taken from MCNP results for the core operating at 100 kW under steady state conditions. Given the hydraulically separated nature of the RELAP model, the PARET/ANL and RELAP hot channel models are equivalent (11).

6. Discussion

The principal goal of the present research is the validation of the computational tools utilized by the UFTR. The approach is a systematic analysis of pertinent nuclear and thermal-hydraulic parameters and comparing to the expected/calculated values. Additionally, the extension of the analysis using reactor noise and transient techniques will provide benchmarking and validation data for academic and research purposes.

The testing regime is split into two distinct areas, neutronics and thermal-hydraulics. The neutronic verification will include traditional measurement methods and novel experimental setups to measure key reactor parameters. The thermal-hydraulic testing regime will include both steady-state and transient work, however the transient conditions are low power (i.e. below Limiting Safety System Settings). Some of the experiments/studies include:

Flux Mapping

The UFTR has several experimental beam ports that are used for irradiating and activating samples. Characterization of these ports will be performed using foil activation and spectral unfolding to determine flux spectra and intensity.

Knowledge of the flux distribution throughout the core and experimental ports of the UFTR is critical to the design of experiments and future utilization of the reactor. The flux distributions are functions of position in the reactor and neutron energy. These distributions are complex functions of core geometry, materials, and control blade position. Experimental measurements represent the only way of determining the actual flux distributions in the reactor.

To validate these models, a spectral analysis of the neutron field via foil irradiation will be used. A sample containing foils of several elements will be activated in each position in the reactor. Each isotope of each element has different threshold activation energies. High purity germanium detectors (HPGe) will be used to determine total activity and thus the reaction rate. Cadmium covers will be used on the foils with high activation energies to reduce activation of impurities.

Data Library and Model Sensitivity Studies

Nuclear Data Libraries such as ENDF, JENDL, and JEFF contain evaluated nuclear data that varies from isotope to isotope. The effect of utilizing different nuclear libraries on the calculated core parameters must be quantified to continue the benchmarking process of the UFTR.

Additionally, the UFTR neutronics and thermal-hydraulics models are based on nominal dimensions for reactor components. Using engineering drawings and as-fabricated schematics for tolerances, a sensitivity study will be conducted to evaluate the effects of dimensional,

material, and construction uncertainties on the overall uncertainty on the system as whole.

Reactor Kinetics Parameters via Noise Analysis

Reactor or neutron noise is a well-established field within nuclear science and has shown many applications in the field of nuclear reactor physics. The final goal of these analyses is measuring time constants and dynamic characteristics of the UFTR, i.e. the kinetics parameters. These measurements will verify design data produced via the Monte Carlo methods described previously.

7. Conclusions

The University of Florida Training Reactor (UFTR) is a 100 kW ARGONAUT type research reactor, and serves as a resource for education on reactor physics, control, operations, nuclear regulations, and safety culture. A detailed reactor description was presented along with experimental data to establish a calculation benchmark for the UFTR that can be used to validate neutronic and thermal-hydraulic codes. Additional work is now being performed to provide additional experimental data to the research reactor community.

New UFTR safety analysis tools and models, based on modern codes and methods, leverage the advantages of more than three decades of progress in computational reactor analysis. High-fidelity computation was employed to provide accurate computational results that matched experimental observation to within 5%. These models will be used in the utilization, training, and teaching programs at both the UFTR facility and the University of Florida Nuclear Engineering Program.

8. Bibliography

1. **University of Florida Training Reactor.** *Safety Analysis Report University of Florida Training Reactor.* Gainesville, Florida : Department of Nuclear Engineering Sciences, College of Engineering, University of Florida, 2013.
2. **BWX Technologies Inc.** UFTR Fuel Specification.
3. *2004. MCNP. A General Monte Carlo N-Particle Transport Code, Version 5. LA-UR-03-1987, LA-CP-03-0245.* **X-5 Monte Carlo Team.**
4. **Leppänen.** Serpent Monte Carlo Reactor Physics Code. *a three-dimensional continuous-energy Monte Carlo reactor physics burnup calculation code.* [Online] 2010. http://montecarlo.vtt.fi/index.htm.
5. **Chadwick, M.B. and et. al.** *Nuclear Data for Science and Technology: Cross Sections, Covariances, Fission Product Yields and Decay Data.* 2011.
6. **Olson, A.P. and Kalimullah, M.** *ANL/RERTR/TM-11- 22, A User's Guide to the PLTEMP/ANL Code, Version 4.1.* 2011.
7. **Idaho National Engineering.** *RELAP5/MOD3 Code Manual, Volume 1: Code Structure, System Models, and Solution Methods.* s.l. : INL, 1995.
8. **Todreas, N.E. and Kazimi, M.S.** *Nuclear systems II: Elements of thermal hydraulic design. Vol. 2.* s.l. : Taylor & Francis, 1990.
9. **Obenchain, C.F.** *PARET, A Program for the Analysis of Reactor Transients.* s.l. : Atomic Energy Commission Research and Development Report, Reactor Technology, 1969.
10. *PARET-ANL Modeling of a SPERT-IV Experiment Under Different Departure from Nucleate Boiling Correlations.* **Chatzidakis, S, Ikonomopoulos, A and Day, S.E.** 2012, Nuclear Technology, Vol. 177, pp. 119-131.
11. *Modern design and safety analysis of the University of Florida Training Reactor.* **Jordan, K.A., Springfels, D. and Schubring, D.** 2016, Nuclear Engineering and Design, Vol. 286, pp. 89-93.
12. **Woodruff, W L.** *ANL/RERTR/TM-4, The PARET Code and the Analysis of the SPERT I Transients.* s.l. : Argonne National Labs, 1982.
13. **Kalimullah, M.** *Verification and Validation of theANL/RERTR/TM-11-37, PLTEMP/ANL Code for Thermal-Hydraulic Analysis of Experimental and Test Reactors.* s.l. : Argonne National Lab, 2011.
14. **Dionne, B, et al., et al.** *ANL/GTRI/TM-14-3, Summary of RELAP5 Assessments Performed in Relation to Conversion Analysis of Research Reactors.* s.l. : Argonne National Lab, 2014.
15. *Absolute measurement of B eff based on Feynman-alpha experiments and the two-region model in the IPEN/MB-01 research reactor.* **Kuramoto, Renato YR and dos Santos, Adimir and Jerez, Rogerio and Diniz, Ricardo.** 6, 2007, Annals of Nuclear Energy, Vol. 34, pp. 433-442.
16. *Validation of an MCNP4B whole-reactor model for LWR-PROTEUS using ENDF/BV, ENDF/B-VI and JEF-2.2 cross-section libraries.* **Joneja, OP, et al., et al.** 2001, Annals of Nuclear Energy, pp. 701--713.
17. *Validation of absolute axial neutron flux distribution calculations with MCNP with 197 Au.* **Radulovic, V, et al., et al.** 2014, Applied Radiation and Isotopes, pp. 57--65.
18. *On normalization of fluxes and reaction rates in MCNP criticality calculations.* **Žerovnik, Podvratnik and Snoj.** 2014, Annals of Nuclear Energy, pp. 126-128.

Neutron shielding calculation for neutron imaging facility at Maâmora Triga Reactor

A.Ouardi

Centre National de l'Energie des Sciences et des techniques nucléaires*(CNESTEN)*

Cement and concrete has been widely used as shielding material in reactor nuclear in order to minimize exposure to individuals. The biological protection around the future neutron imaging facility at Maâmora Triga Reactor will be housed on the tangential beam port floor outside the biological shielding of the neutron source. It is necessary to design shielding enclosures to prevent neutrons from causing unacceptable activation of the environment.
GEANT4 simulation toolkit is being used to study neutron attenuation, and optimizing the layers of shielding material to minimize thickness. Materials being studied include different types of concrete such as Hormirad mixed with the borax with different boron and iron compositions. Initial studies indicate that optimized shielding material is the Hormirad mixed with Borax (1.19%). A total thickness of 0.7 meters produces the required attenuation factor. Further studies may allow optimizing the shielding enclosures. Because of the low load floor (2500Kg/m2), one solution that could be adopted is the substitution one bloc shielding by two blocks (with a half thickness) with air gap between them. The model allows studying the performance of the shielding materials in this particular space arrangement.

1. Introduction

The shielding consists of concrete walls to moderate and attenuate particles. Cement and concrete has been widely used as shielding material for gamma and neutron shielding in nuclear facilities in order to minimize exposure to individuals. While in case of gamma rays an increase in density is usually efficient enough, protection against neutrons is more complex. In fact, the best materials for shielding neutrons must be able to: First slow down neutrons by material containing light atoms (e.g. hydrogen atoms). Then absorb this slow neutron (thermal neutrons) by capture in materials with high neutrons capture cross sections (e.g. boron, lithium or cadmium) and at last to shield the accompanying radiation. The choice of the material should be done with the condition to avoid any additional shield to attenuate the gamma rays. Since, the shielding design depends upon the location, the intensity, and the energy distribution of the radiation sources, and the permissible radiation levels at positions away from these sources. The development of the newly built of neutron Imaging facility (NERA)of the 2 MW TRIGA MARK-II reactor at Maâmora Nuclear research center (CENM), has to take into account all of the shielding design parameters cited above. Especially, the space available for the size of, and to the amount weight of the biological shield that forms the barrier, according to very severs limitation of load floor (2500Kg/m^2).

Hence here is need for development of advanced shield systems which can minimize or overcome some of the short comings. The new advanced materials should make the shield compact, lighter, more effective as radiation attenuator and probably less costly. This aspect was examined by few neutrons imaging facilities worldwide such as: ANTARES facility at the FRMII in Germany and the SANRAD facility at the SAFARI-1 nuclear research reactor in South Africa. According to the classification limit for the area outside of both ANTARES and NRAD facilities and beam port floor of 25 Sv/h [1,2]. The composition of concrete mix main constituents selected in built are in common approximately the same percent in weight: hydrogen (2-3.5%), boron (5%), Hematite (55-60%), Steel shot and (26-36%). Notice that, the performance of advanced materials composition was defined according to MCNP5 calculations results [3].

In our case, to overcome the sever limitation of load floor, an advanced radiation shields is expected. It was imperative to conduct numerical calculation using fluka and Geant4 to achieve better radiation shielding with no increase in weight and to evaluation and optimizing of the concrete mix to reach better neutrons shielding.

2. Shielding radiation calculation

The Geant4 and FLUKA Monte-Carlo particle transport codes [3, 4] were used for the determination of materials with a high fast neutron attenuation property are mandatory for the construction of customized shielding, such as local neutron shielding surrounding the "beam impact locations" of a neutron imaging facility.
It is noted worthy that the attenuation efficacy of a shielding depends on the neutronic properties of the shielding material as well as the energy spectrum of the incident neutron field. High density iron (ρ=7.8 g.cm^{-3}) has a high inelastic scattering cross section for high energy neutrons. On the other hand, low density polyethylene (ρ=0.93 g.cm^{-3}) possesses a high elastic scattering as well as a large capture cross section for low energy neutrons. Hence, a composite material with a suitable mixture of iron and polyethylene could provide a high (optimised) attenuation efficacy for neutrons with a broad energy distribution.

2 -1 Physical Model

A simple model simulation adopted here was used in previous studies cited below:

- Composition shielding for Upgrade ANTARES facility at FRMII [4];
- Upgrading the Neutron Radiography Facility in South Africa (NRAD) [5];
- The novel composite shielding for German Proton therapy Essen at WPE [6].

We note that the shielding calculation for Upgrade ANTARES and German Proton therapy Essen uses the MCNP [3].
In this model, the neutron source is a point source and the neutron energy distribution is that of the NERA facility. The source is located in the centre of a ball (with radius R=80cm) with isotropic angular distribution of emission. The ball is filled with the shielding material. The shielding effectiveness of Iron/borate polyethylene (5%) combination was tested with the calculation model described below (Fig. 1.) The inner part of the ball is filled by an iron layer of thickness d. The outer part consists of a borate polyethylene (5%) layer of thickness R-d [4].For comparison of different shielding materials, the neutron dose and the dose of generated gamma radiation per source neutron on the surface of the ball is considered [2,5]. This physical model has been adopted in all simulation calculation in this paper.

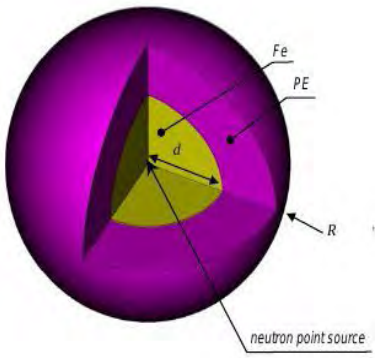

Fig1. Schematic diagram showing the 80 cm radius spheres filled with iron/borate polyethylene composite (5%).

3- Simulation of Shielding Materials

3-1 Boron effect on the neutron dose reduction

Greater reductions in both neutron and gamma ray dose can be obtained by incorporating hydrogen and boron into Shielding material. To examine the boron effect on the neutron

dose reduction, simulations are performed for two polyethylene spheres with different composition : polyethylene (ρ=0.95 g.cm^{-3}) and 5% borated polyethylene(ρ=1.087g/g.cm^{-3}). The neutron source is assumed punctual placed in the centre of each sphere. The neutrons are generated isotropically with energies varying from 0.3eV to 1MeV.
Figure 2 shows normalized count rate N/N0 as energy function. N and N0 count rate of neutrons at the outer surface of 40 cm balls corresponding respectively to polyethylene and % borate polyethylene.

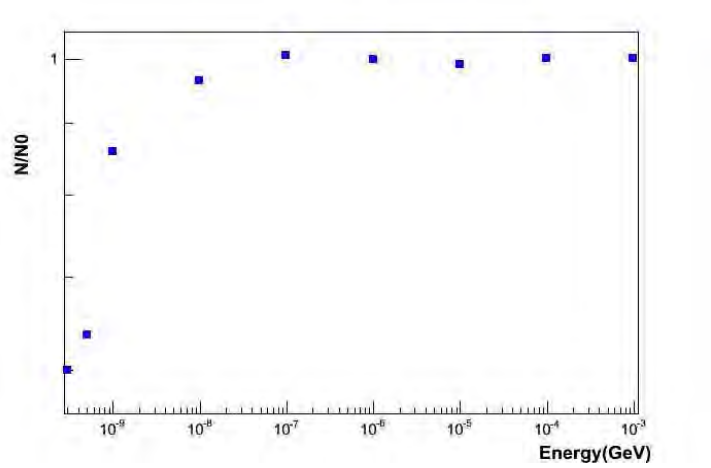

Fig2. N/N0 normalized count rate into on the surface of the ball as function of neutrons energy.

As shown in Fig2. a lower count rate is obtained for thermal neutron energy ranging from 0.3 to 0.5eV for borate polyethylene (5%) and the reduction in normalized (N/N0) is of 0.64% .This energy range is corresponding to thermal neutrons that are absorbed by capture in boron. For higher energies, Although, the little fluctuation of normalized count rate corresponding to energy ranging from 0.5eV to 1eV are obtained, N/N0 still constant for higher energies(Higher than 1eV). These fluctuations are resulting from the slow down neutrons by hydrogen and then captured by boron atoms. As conclusion, the borated polyethylene (5%) can reduce 34 % of the energies deposit by thermal neutron, comparing to ordinary polyethylene.

3-1 Geant4 and fluka Simulations to optimize composition shielding.

3-1-1 Shielding material: iron/borate polyethylene composite (5%)

This part of study is dedicated to model the source of radiation and determine the efficiency of the shielding material in attenuating radiation as the radioactive particles travels through the shield.

Inputs to the simulation model

fluka gives options to choose desired input cards (the type of interaction and transport thresholds can be set in the physics and transport section of the cards). EM- CASCA, and LOW –MAT neutron card is used as a default . Number of primary photons for this study was set at 1 × 107 for 4 MV histories in 5 cycles. Electromagnetic intersection input file was carried out in electromagnetic FLUKA cascade mode [new]. The initial photon direction is assumed to have isotropic. The Method used for the collection of information about events transportation, was done by a simple activation of application such COMSCW and MGDRAW. The Subroutine COMSCW was adopted during the calculations to score the dose deposition according to the local density and energy deposition. But, To get the correct average dose in bins at boundary between two different media The subroutine BXDRAW in MGDRAW. The Subroutine MGDRAW, was activated by option USERDUMP, to writes a "collision tape", i.e. a file where all or selected transport events are recorded [6].

Monte Carlo (fluka) simulations were carried out for the neutron transmission through spherical shielding of various materials. We have simulated the neutron dose at outer surfaces of 40 cm radius spherical spaces filled with iron/borate polyethylene composite (5%)(PE) of selected volume fractions. Fig3. Illustrate the volume fractions cited below:
(a) 100% PE, (b) 2% of iron et 98% PE, (c) 12.5% of iron et 87.5% PE, (d) 20% of iron et 80% PE, (e) 40% of iron et 60% PE, (f) 55% of iron et 45% PE, (g) 95%of iron et 5% PE et (h) 97.5% of iron et 2.5% PE.
A radiation source with isotopic emission is located at the center of spheres and the neutron energies are varying from 0.5eV to 1MeV.

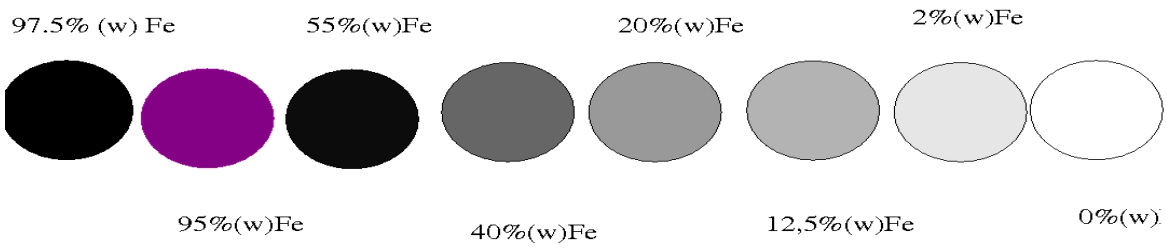

Fig3. Schematic diagram showing the 40 cm radius spheres filled with iron/borate polyethylene composite(5%). The weights of iron are shown explicitly.

Fluka simulations Results

Fig4-a and Fig4-b illustrate, the evaluated neutron dose are plotted as a function of weight fractions of iron additive in the composite and the energies considered are ranging from 1MeV to 0.5eV.

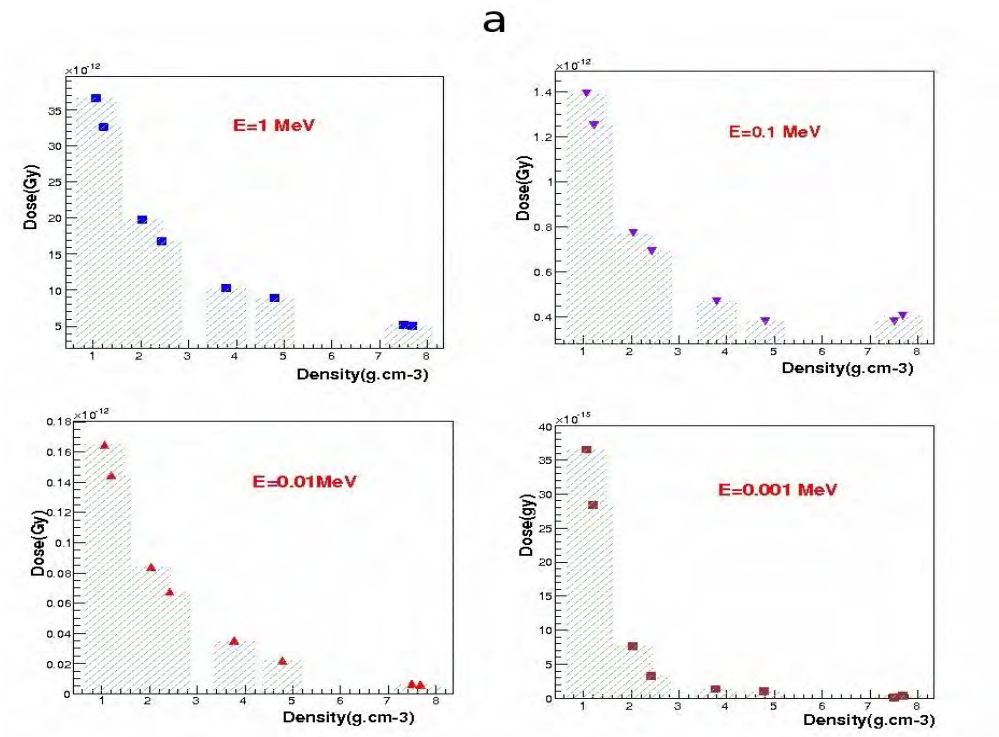

Fig 4-a: Neutron dose deposition corresponding to energies varying from10^{-3} to 1MeV at outer surface of spheres filled with a, b, c, d, e, f; g and h iron/borate polyethylene (5%) composite.

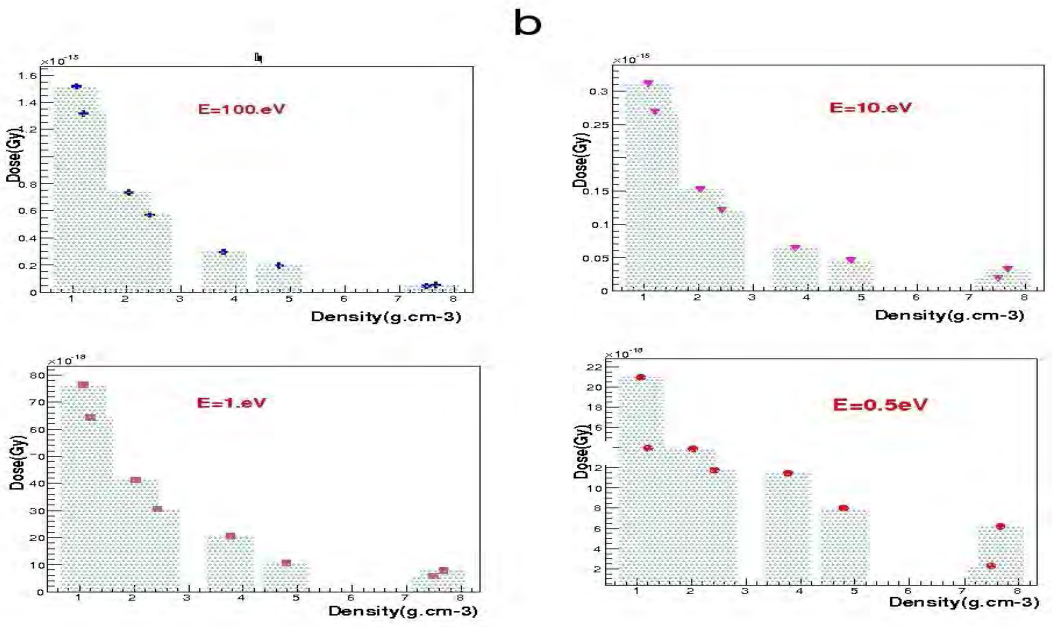

Fig 4-b: Neutron dose deposition corresponding to energies varying from 0.5 to 10^2eV at outer surface of spheres filled with a, b, c, d, e, f, g and h iron/borate polyethylene (5%) composite.

Globally, for the neutrons energies varying from 0.5eV to 1 MeV, the dose on the outer surface spheres decrease as function of partial mass densities of : a, b,c, d, e, e,f g, h iron/borate polyethylene (5%) mixture. A little dose variation is observed for iron/borate polyethylene (5%) mixture with iron volume fraction higher than 55%. Hence, these materials tend to stop fast neutrons and generate a low dose rate deposition. This effect is more accentuated for energies ranging from 10^{-3} to 1 MeV. we can say that the optimum mixture is corresponding to volume fractions of 55% iron 40% polyethylene and 5% boron. This result was confirmed by other studies done in the same context [2,3] .

3-1-2 Shielding material: optimized concrete

Generally concrete can be qualified as ordinary concrete or heavy concrete. The Heavy concrete uses heavy natural aggregates such as barytes (barium sulfate) or magnetite or manufactured aggregates such as iron, steel balls, steel punch or other additives [7].

Here, a four different concrete are selected in this work, mainly:

- High-density concrete commercially available under the name Hormirad mixed with different ratio of the borax respectively, 15%, 5% and 1.19%.
- Hematite is used generally used as the natural source of iron.

In this work, the objective was to characterize the material behavior against neutrons, as well as to define the optimal rate mixings including hydrogen and boron compounds in an effort to improve neutron shielding efficiency. With that purpose, Hematite and Hormirad mixed with borax spheres of different radius were simulated.

The components of these shielding materials and their mass fractions are listed in Table 1.

Shielding material	Hematite	Hormirad mixed with Borax (15%).	Hormirad mixed with Borax (5%).	Hormirad mixed with Borax (1.19%).
Density (g/cm)	3.2	3.94	3.62	3.94
Composition	**Fe2O3 71.2%**	**Fe 58.977%**	**Fe 57.O6%**	**Fe 44.992%**
	SiO2 7.62%	O 33.0 %	O 31.95 %	O 41.95 %
	CaO 7.47%	Ca 4.307%	Ca 4.019%	Ca 3.2257%
	Al2O3 0.56%	Si 1.82%	Si 1.754%	Si 1.383%
	H2O 9.9%	H 0.5675 %	H 0.804%	H 1.75%
		Mg 0.384%	Mg 0.3695%	Mg 0.2913%
		P 0.283 %	P 0.2726 %	P 0.2149 %
		Ti 0.189%	Ti 0.182%	Ti 0.1438%
		Al 0.163%	Al 0.156%	Al 0.1235%
		K 0.062%	K 0.0598%	K 0.04718%
		Mn 0.0612%	Mn 0.0589%	Mn 0.0464%
		V 0.049%	V 0.0475%	V 0.0374%
		C 0.035%	C 0.0342%	C 0.0269%
		S 0.007%	S 0.066%	S 0.0052%
		Na 0.014%	Na 0.603%	Na 3.027%
		Borax 1.19%	Borax 5%	Borax 25.1%

Inputs to the simulation model

GEANT4 tool kit supports various hadronic models. Here the simulations are made with model G4HPmodel. This model has four physical processes for neutrons; elastic, inelastic, fission and capture. The HP model is based on the data formats of ENDF/B-VI. This model includes cross sections and final state information for elastic, inelastic scattering, capture, fission and isotope production [8].

In this part of works, the same physical model described above is adopted. A neutrons and gamma source are initialy generated according to the energy spectra shown in respectively in Fig5-a and Fig-b. These spectrums are corresponding to energies spectrum for Triga reactor at 2MW. The initial events are emitted isotropic directions, and the source radiation is placed in the center of 80 cm spheres filled by the selected shielding material (shielding material samples were chosen from iron/borated polyethylene mixtures with iron weight fractions respectively of 40% and 87%, and the four heavy concrete cited in table 1).

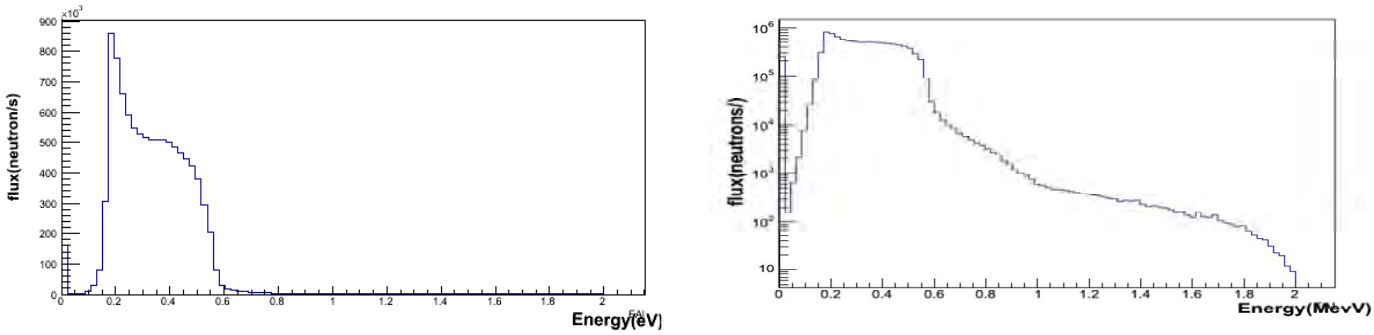

Fig 4-b: Neutron dose deposition corresponding to energies varying from 0.5 to 10^2eV at outer surface of spheres filled with a, b, c, d, e, f, g and h iron/borate polyethylene (5%) composite.

Geant4 simulations Results

The Fig6-a and Fig6-b illustrates, the doses deposition corresponding respectively to

thermal- epithermal neutrons and fast neutrons at the outer surface spheres filled with the selected shielding material. The lowest dose deposition is corresponding to Hormirad mixed with borax (1.19%) and iron/borate polyethylene (5%) mixtures. The shielding capabilities of shielding materials are enhanced with the ratio of about 55 % iron (Fig6-a).

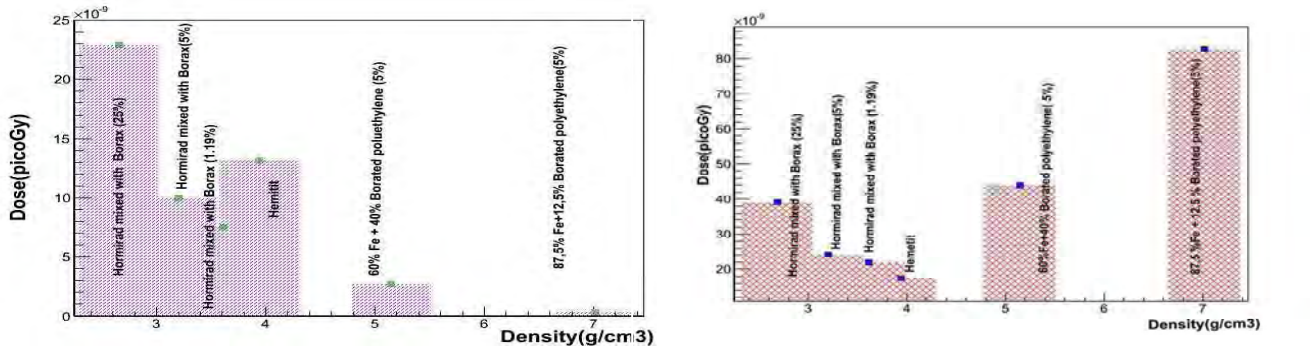

Fig 6: left , the dose deposition at outer surface of spheres filled with concretes and iron/borate polyethylene (5%) composite, left for energies varying from 0.5 to 10^2eV and right, for energies ranging between1 0^2eV and 2MeV.

For neutrons energies larger than 102eV, Although, the iron rate are much higher than 55%in the iron/borate polyethylene (5%) mixture, the lowest dose deposition are recorded for the material shielding with the largest ratio of hydrogen. In fact, this is an expected result because, the fast neutrons lost energies by inelastic interactions with iron atoms and then they are thermalized by hydrogen atoms before the boron capture happen. As conclusion, the combining hydrogen rich materials with iron would provide with more effective fast neutron shields as well as thermal an epithermal neutron.
By adopting the same physical model, Geant4 simulations were carried out to examine the contribution of gamma rays on the total dose deposition in the outer surface of the concrete spheres surfaces. As initial gamma spectrum energies, we adopted the spectrum presented in Fig4-b. Again,The lower gamma dose deposition are corresponding to the shielding material: Hormirax mixed with borax (1.19%) and for the iron/borated polyethylene mixtures (see Fig7).

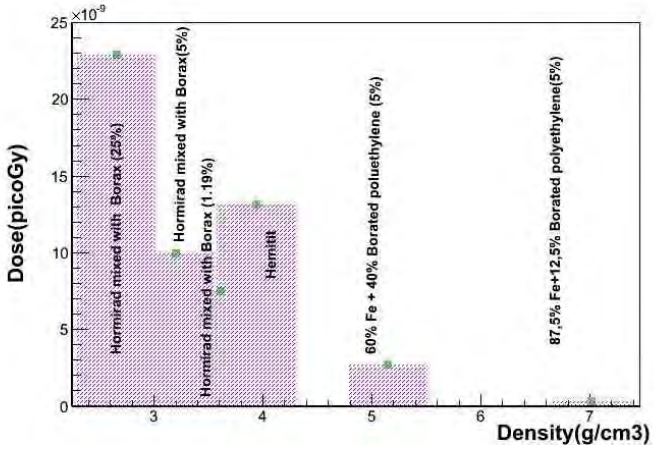

Fig 7: The gammas doses deposition at outer surface of spheres filled with concretes and iron/borate polyethylene (5%) composite as function of the material shielding density

As conclusion and referring to simulations results presented in Fig8, taking account into different contribution dose deposition of neutrons and gamma radiation, the heavy concrete Hormirax mixed with borax (1.19%) with density 3.6 g/cm^3 was defined as optimum material shielding.

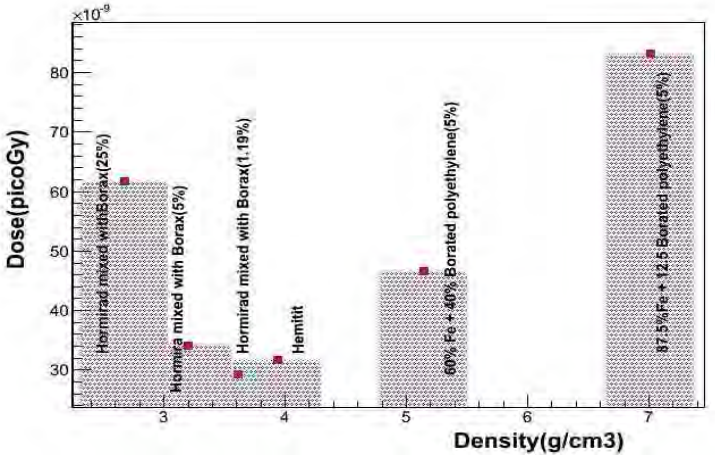

Fig8: The neutrons and gammas doses deposition at outer surface of spheres filled with concretes and iron/borate polyethylene (5%) composite as function of the material shielding density

3-2 Geant4 Simulations to optimize thickness shielding.

In this part of work, we examine effect of sample thickness on shielding capacities As the Hormirad mixed with borax (1.19%) is the optimum composition shielding, this concrete was selected to investigate the effect of material thickness on radiation shielding. The simulation calculations are done with spectrum neutron with energies varying 0.5eV to 2MeV, and for the concrete thicknesses varying from 40 cm to 100 cm. The results are shown in Fig9.

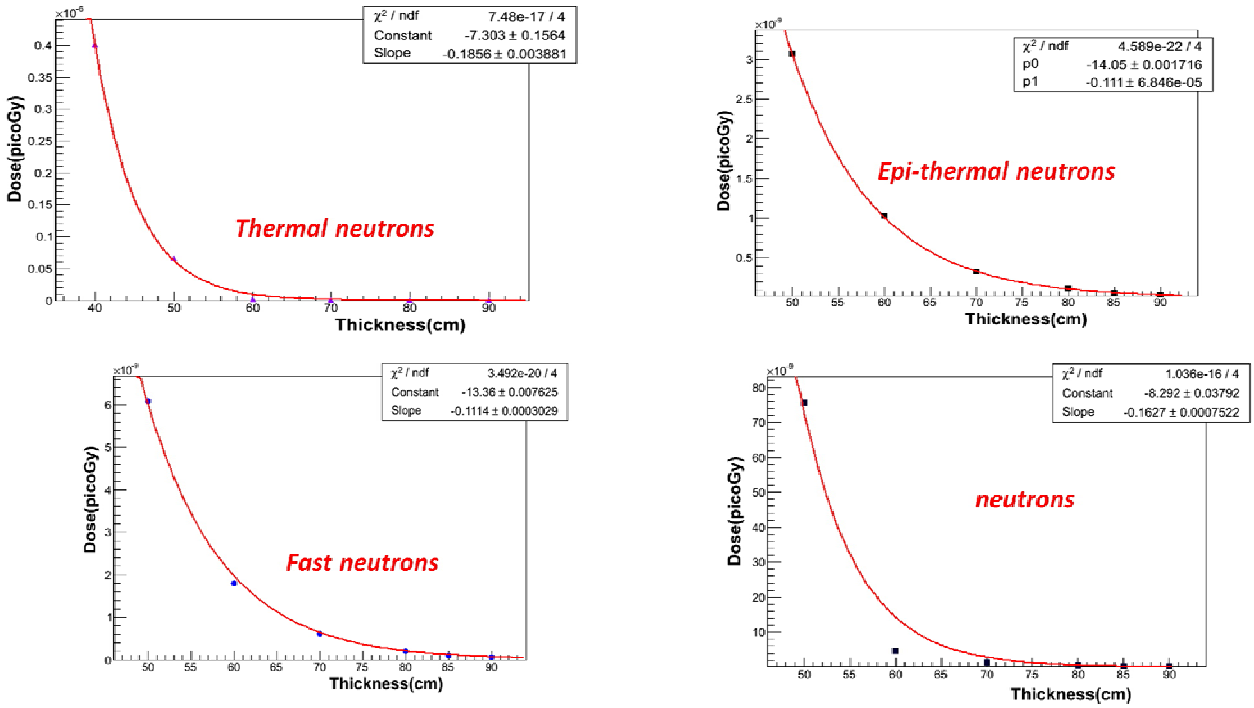

Fig9: Figure 10: Neutron dose as function of shield thickness for Hormirad mixed with borax (1.19%). The data points are fitted with the following exponential functions: -8.292exp(-0.1627x).

We present in Fig 9, the curve of total dose deposition, as well as the dose deposition curves respectively of thermal, epithermal and fast neutrons, as function of the concrete thickness. These curves are well fit by an exponential functionThe dose deposition decrease considerably for the concrete thickness varying ranging from 50 to 70 cm, while the variation of dose is less important for thickness higher than 70cm. This is related to the effect of the material thickness on the penetrating power of neutrons. This effect is quantified here according to the exponential function [9].

$$D(x) = D \exp(-\sum X)$$

Where,

- D(x) is dose deposition in the outer surface of sphere for the concrete thicknesses varying from 40 to 90 cm
- X shielding thickness
- D and ∑ are the specific values of constant -8.29 and 0.1627.

The ∑ value is generally, corresponding to absorption and diffusion (cm^{-1}) specific concrete material, here this coefficient is equal 0.16 which corresponding to iron. This can be explained by the iron rate of 60% in the selected concrete.

As indicated in the beginning of this study, the floor load about (2500Kg/m2), is very low in the hall reactor. However, low density materials such as standard concrete (ρ=2.4 g/cm3) can emit gamma rays when blocking neutrons, neither the use of heavy concrete could be possible because of limitation of the load floor. One solution that could be adopted is the substitution one bloc shielding (70cm) by two blocks (with a half thickness of 35cm) with air gap of 55 cm between them. Fig11 show the geometric arrangement adopted during the simulation by GEANT4. For both geometries arrangement a detector filled with Helium, is positioned at the outlet of the bloc shield.

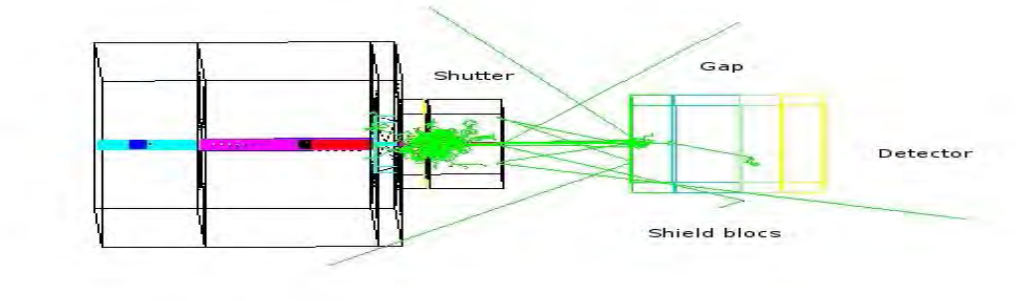

Fig11. Show the geometric arrangement adopted during the simulation by GEANT4

The energies spectra for surviving neutrons in the detector for the two arrangements: one bloc with a thickness of 70 cm and two blocks of 35cm with air gap of 55 cm between them are plotted in Fig12.

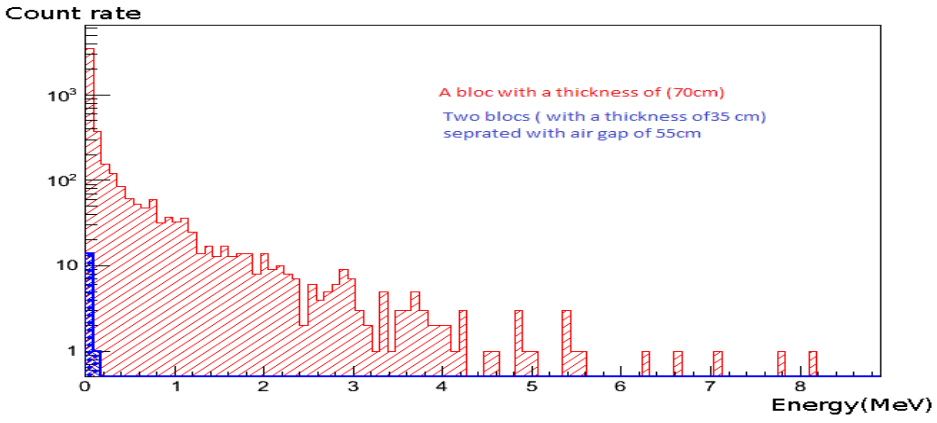

Fig12. Spectra for surviving neutrons in the He detector: for one bloc (red) and two blocs(bleu)

The energy deposition of the surviving neutron after crossing the two shielding bloc with air gap of 55cm is much lower compared to those of a unique bloc with the same thickness (70cm). This effect can be related to a neutrons multiple inelastic scattering in the gap area. The neutrons loss a big part of their the energies before to reach a second bloc.

4. Conclusion

The radiation environment is an important consideration for the design of shield house of the neutron Imaging facility at Moroccan Triga. In this study a various shielding materials has been studies.
It was proved that, the efficiency of shielding material is related on the concentration hydrogen, iron and boron atoms. An optimal mixing of these materials can form a good shield against neutron. For this purpose an iron/borate polyethylene (5%) mixture with different volume fraction has been simulated. The simulation results show that the optimal is corresponding to mixture with volumes fractions higher than: 55% iron 40% polyethylene and 5% boron.
This result was considered as guide line to select the heavy concrete to be investigated. Because of high concentration of iron, Hematit and Hormirad mixed with the borax have been selected. These heavy concrete, were chosen because they can be produced locally.
Referring to the simulations results presented in this study, The optimal concrete composition is corresponding to Hormirad mixed with borax (1.19%), and bloc thickness of 70cm of this concrete is deduced as optimal.

To overcome the problem of low floor load, one solution could be adopted is the substitution one bloc shielding of 70cm with by two blocks (with a half thickness about 35cm) with air gap between them of 55cm. This particular space arrangement was approved, since the shielding capacities are enhanced.

References

[1] Calzada, E., Schillinger, B., Grünauer, F.,2005. "*Construction and assembly of the neutron radiography and tomography facility ANTARES at FRM II*", NIM-A, Volume 542, Issues 1–3, 38–44.

[2] Calzada, E., et.al., 2009. "*New design of the ANTARES-II facility for neutron imaging at FRM-II*", NIM-A, 605, P50

[3] F.C. de Beer, M.J.Radebea, B Schillingerb, R Nshimirimanaa, M. A. Ramushuc, T. Modisea,
"Upgrading the Neutron Radiography Facility in South Africa (SANRAD): Concrete Shielding Design Characteristics," 10th WCNR Physics Procedia 69 (2015) 115 – 123.

10[4] Briesmeister, J., 1996. MCNP – A General Monte Carlo N-Particle Transport Code, Version 4B, Los Alamos National Lab, Los Alamos,

[5] Grünauer, F."Design, optimization, and implementation of the new neutron radiography facility at FRM-II," 2005. PhD Thesis, http://mediatum.ub.tum.de/doc/603112/603112.pdf

[6] A. Fassò, A. Ferrari, J. Ranft, and P.R. Sala, "FLUKA: a multi-particle transport code," CERN- 2005-10(2005), INFN/TC_05/11, SLAC-R-773.

[7] Callan E.J., "Concrete radiation shielding: nuclear physics, concrete properties, design and construction," 2nd edition. United States of America: American concrete institute.

[8] S.Agostinelli & al, **"**Geant4—a simulation toolkit**,"** Nuclear Instruments and Methods in Physics Research Section A: Accelerators, Spectrometers, Detectors and Associated Equipment,Volume 506, Issue3, 1 July 2003, P 250-303.

[9] Gary. S. Was, "Calculation *of Radiation Attenuation Coefficients for Shielding Concretes,* Fundamentals of Radiation Materials Science Springer-Verlag Berlin, 2007, Bashter, I.

NDT TECHNIQUE APPLIED TO DIRECT MEASURING OF THERMAL CONDUCTIVITY IN UMo FUEL MINIPLATES

Olivares L. (1); Lisboa, J. (1); Marin J. (1); Barrera M. (1); Gutierrez C. (1); Salinas P. (2)
1 - Chilean Commission for Nuclear Energy - CCHEN – Chile
2 – Universidad de Santiago de Chile – USACH - Chile

ABSTRACT

Thermal conductivity is one of the most important physical properties of nuclear fuel for research reactors. For high-density fuel, based on U-Mo alloys, the thermal properties are necessary to simulate and to design the reactor cooling system. Current measurements involve, generally, destructive analysis methodologies and the results depend strongly on the characteristics of the samples.

This paper describes a technique to measure, directly, the thermal conductivity of dispersion type UMo miniplates, which corresponding to a three-layer system, comprised of AA 6061 cladding and a core, consisting in a foil or a distribution of particles of UMo alloy, not necessarily isolated from each other, dispersed in a continuous and homogeneous aluminum matrix. The miniplate to be tested is clamped in contact with two surfaces at different temperatures, ice block on top face and steam waterchamber at the bottom side. In steady-state condition (the temperature of the plate does not change with time), the amount of heat per time unit and area transferred through miniplate is proportional to the temperature difference and inversely proportional to plate thickness. Fourier's Law that describes this process can be expressed by an equation that defines a constant, directly related to thermal conductivity coefficient of the test plate.

The values of thermal conductivity from this work tend to be approximately ten times lower, compared to literature values. To overcome this uncertainty, the goal proposed was to evaluate the variation, in percent, of thermal conductivity as function of the volume increasing in miniplates subjected to out-of pile swelling test (350 °C annealing). Measurements reveal that thermal conductivity decreased 24.92% for an UMo miniplate with density of 6 gU/cm^3 and 28.7% for a miniplate of 8 gU/cm^3 after 23 and 28 hours of annealing, respectively. These values are in good agreement with previous studies of thermal conductivity degradation as a function of the burn up level (fission density) [1]. To conclude was possible to evaluate, experimentally, the evolution of thermal conductivity as function of volume increasing of miniplates, through a non-destructive and direct methodology.

1. Introduction

The thermal conductivity is a physical property fundamental for nuclear fuel, although for the fissionable compound uranium silicide, U_3Si_2, the influence of the burn-up over the thermal conductivity is less significant due to the limited density of the silicide fuel. Nevertheless, for UMo alloys, considered as an alternative for high-density fuel, to know exactly the thermal conductivity values allow modeling, design and operate cooling systems for the new fuel. Besides, these values determine the fuel plate's operation temperature, which in turn defines the confidence limits for the safe and efficient performance of the fuel into the reactor core [2].

The qualification of the new fuel based on UMo alloys requires demonstrating its good behavior under irradiation, but it also must to exhibit reliable values of thermal conductivity in function of burn-up level in order to predict safe performance of fuel during its lifetime. Due to the thermal conductivity depends strongly of crystalline structure; it is also very important to know the micro structural changes of the fuel during its irradiation [3].

In agreement with the heat transfer principles, the existence of temperature gradients between the layers that comprises the fuel plates will generate heat transference from the hot zone, which is the fuel meat o fuel zone, towards the coldest zone, which is the aluminium cladding.

Compared with the meat, the aluminium cladding has very high thermal conductivity, which is caused by the great number of free electrons and also due to the efficiency of the electrons to transport the thermal energy. The meat of dispersion type fuel usually is comprises by metallic matrix with a dispersion of an alloy, ceramic or intermetallic compound in which the free electrons concentration is low and the thermal conduction by phonons is predominant [4]. While metals have high values of thermal conductivity, between 20 y 400 W/m*K, the nuclear fuels exhibit values of 15 W/m*K for silicides and 11 W/m*K approximately for UMo alloys [5]. The Table 1 summarizes thermal conductivity values for some nuclear materials [6].

Table 1. Thermal Conductivity values for some nuclear materials

Materials	Thermal Conductivity (W/m*K)
Uranium α (at 20°C)	24
Aluminium (at 20°C)	204
Molybdenum (at 20°C)	138
UAl_3	8 - 15
UAl_4	4-8
U_3O_8	18-23
U_3Si	15
U_3Si_2	15
UMo	11

The methodologies available so far allow evaluating with precision several thermal properties and/or its degradation in function of the burn-up level of fuel. Based on non-steady or dinamic state, its fundamental principle is the generation of minor temperature during short time intervals, modifying, by this way, the temperature of the sample. High sensibility temperature monitor detects these changes. This state is characterized by the fast results and its minor heat losses, which improves the precision of the results. Nevertheless, these are destructive methodologies, whose results depends, strongly, of the density, crystal structure, composition, phase transformations and geometry of the samples, as well as the area chosen to draw the specimen and the temperature at which the test is performed. The biggest difficulty is that, with these techniques, is not possible to evaluate, directly, the thermal conductivity of the entire fuel plate. These plates presents integrated configuration, comprises by a distribution of UMo particles, not always isolated from each other, dispersed in a continuous an homogeneus aluminium matrix, with residual porosity and a significant portion of heat released in every direction of the plate. Additionally, UMo fuel interaction layer formation (mainly UAl_4), also exhibits less thermal conductivity than UMo particles and the Al matrix. In consequence, the thermal conductivity of fuel meat decreases during the irradiation and it causes the gradual increasing of the temperature of fuel. The temperature of fuel plate affects the growing of the interaction layer because it is a thermal activated process. The determination of the temperature profile into a fuel plate during irradiation is very difficult due to the interdependence of the fuel temperature and its thermal conductivity, both parameters continuosly modified by the interaction [7]. All these

factors, besides that the meat/cladding interfase also present opposition to the heat transfer, difficultes the direct characterisation of thermal properties in fuel plates.

This study describes a simple technique for measuring directly the thermal conductivity of dispersion type miniplates. The experimental measurement consists in to place a miniplate, clamped, between two thermal sources at different temperatures, frozen water (ice block) on top face and water steam on below surface.

The steady-state condition is characterized by a temperature difference between the upper and lower surfaces of the plate that is not time-dependent. The Fourier's Law that describes this process can be expressed by means of an equation that defines proportionality constant, related directly with the thermal conductivity of the tested material. The heat transferred is measured by collecting the water from the melting ice. The ice melts at rate of 1 gram per 0.093 Watt of heat flow (the latent heat of melting for ice).

The thermal conductivity, k, is therefore calculated using the following equation:

$$k\ (Watt/m*K) = M \times (0.093\ Watt) \times e / A \times t \times \Delta T$$

Where thickness of plate, e is measured in meters; Mass of melted ice, M in Kg; Area of ice, A in square meters; Time during which ice is melted, t in hours and temperature differential, ΔT in Kelvin.

Among other techniques based in this steady-state, the best know are the Heat Flow Meter and Guarded Hot Plate methods [8].

The results given in this study reveals numeric values with significant deviation (about ten times) less than the values reported in bibliography, Nevertheless, was possible to obtain thermal conductivity values and evaluate its behavior in relation to the annealing time applied to induce out-of-pile swelling effect. Other studies related to the detriment of thermal conductivity in function of burn-up level (fission density) are agreed with the experimental measurements reported in this study.

2. Experimental Methodolgy

2.1 Miniplates manufacturing

Fuel miniplates were fabricated at CCHEN's Fuel Facility using the standard picture frame plate production methodology with nominal uranium loading of 6, 7 and 8 gU/cm^3.

2.2 Out of Pile swelling test

The thermal treatment for out-of-pile swelling test were done in air, at 350°C, during periods of 0 and 50 hours. In order to evaluate the detriment of thermal conductivity of miniplates related to the volume increasing, after each annealing step, the fuel miniplates were subjected to density measurements by Arquimedes immersion methodology.

2.3 Thermal conductivity measurements

The tests for thermal conductivity determination based in Fourier Law's principles were conducted using a heat flow meter system, manufactured by PASCO, model TD-8561, which allows to evaluate the thermal conductivity constant in structural materials. The values of thermal conductivity of metals are very higher than structural materials and the limited range of measurement of the equipment (up to 2 W/m*K), not allow to measure thermal conductivity values reported in the bibliography for metals, probably because in this kind of system an

important fraction of heat is loosed and is not transfer to the ice. For that reason was necessary to modify the system in order to minimize the heat losses by radiation and convection during the measurement.

In order to prepare the system for miniplates measurement, was fabricated a special sample holder of Lexan. In order to improve the isolation of the experiment, was modified the size of ice block (100 x 100 x 50 mm), the same size of hot zone (window of steam chamber). During the test, the ice was placed into high-density polystyrene shield. Even with these modifications, the system continues to given low values of conductivity, but is important to note that for the measurements taken in function of time, the melt ice mass were very similar, which verifies the steady-state of system, although with very high heat losses.

The measurements were conducted according to the directions of system's manufacturer. The methodology consider the following sequence:

- Measurement of plate thickness

- Measurement dimensions and mass of ice at the beginning and the end of each test, with the purpose of to have an average value of contact area between the ice block and upper face of plate.

- Before connect the steam generator to the steam chamber, the ice block is placed over the plate ant the time count start when the ice start to melt. For the measurement, the melt ice (water) is collected into a glass, by two minutes and by this way, the rate of melting for water, at room temperature, is obtained.

- After connect the steam generator to the steam chamber, the melting rate for water is measured, under thermal flow (steam water), for times between 5 to 7 minutes, taking values each one minute. With these values is possible to have an average value for thermal conductivity corresponding to each time of test.

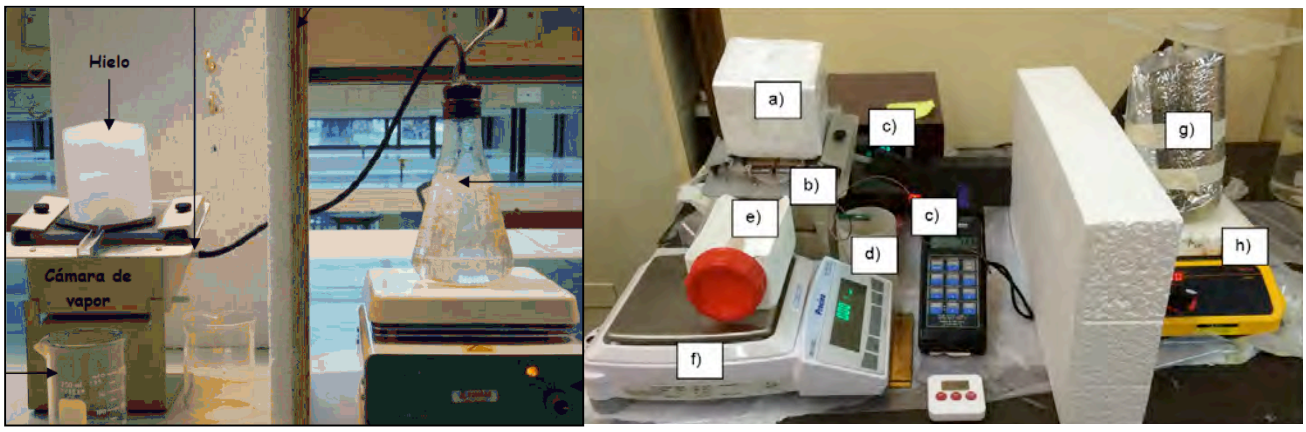

Figure 1. Assembly of the system applied to thermal conductivity measurement system. Left: original system and right: system modified for miniplates evaluation: a) Ice at 0°C, isolated from the environment, b) PASCO modified system for miniplate sizes, c) thermocouples type J, d) collector of condensed water, e) collector of melt ice, f) digital scale, g) Kitasato vacuum flask, h) Electric heater.

3. Experimental Results

The UMo particles used for miniplates manufacturing subjected to this study were obtained by centrifugal atomisation of rotating electrode pin, conducted under argon or nitrogen atmosphere, whose characteristics and details has been reported in a previous paper [9].

3.1 Manufacturing parameters of miniplates

The Table 2 summarize the manufacturing details of dispersion type UMo fuel miniplates applied to this study, where the main differences are the uranium density and the atmosphere used for atomisation of UMo particles.

Table 2. Manufacturing parameters for miniplates used for thermal conductivity measurements

Miniplate Identification		UMo-97	UMo-102	UMo-103	UMo-105	UMo-107
UMo Atomisation atmosphere		Argon	Argon	Nitrogen	Nitrogen	Nitrogen
Uranium density [gU/cm^3]		6.0	8.0	6.0	7.0	8.0
UMo mass [g]		5.93	6.4	5.93	6.18	6.40
Al matrix mass (Al+4% Si) [g]		1.52	1.05	1.52	1.27	1.05
Compact Metrology	Length [mm]	22.41	22.41	22.40	22.40	22.40
	Wide [mm]	18.0	18.0	18.0	18.0	18.0
	Thickness [mm]	2.47	2.47	2.8	2.5	2.46
Fuel Meat Metrology	Length [mm]	86.2	86.2	86.7	83.3	81.9
	Wide [mm]	18.8	18.8	18.0	18.0	18.0
	Thickness [mm]	0.65	0.65	0.69	0.67	0.64
Meat Volume (cm^3)		1.0374	1.0534	1.0768	1.0046	0.9435
Matrix volume fraction		0.50	0.39	0.50	0.45	0.39
Miniplates Metrology	Length [mm]	130.17	130.21	130.42	130.40	130.36
	Wide [mm]	51.32	50.64	50.92	50.69	50.55
	Thickness [mm]	1.44	1.44	1.43	1.43	1.43
Starting thickness (mm)		5.80	5.48	5.80	5.63	5.42
Total Reduction (%)		75.1	73.8	75.3	74.7	73.7
Reduction Rate		1 : 4.01	1 : 3.82	1 : 4.05	1 : 3.95	1 : 3.80

Analyzing the values of Table 2 is possible to note the minor differences between the reduction rates of miniplates manufactured with 6 and 8 gU/cm^3.

3.2 Swelling test of dispersion type UMo miniplates

Dispersion type UMo miniplates, manufactured with UMo particles atomised in argon and nitrogen atmosphere, was subjected to annealing in air and its volume changes controlled by density measurement by immersion technique. The Figure 2 shown the evolution of volume in function of annealing time for the miniplates identified as UMo-102, UMo-103, UMo-105 and UMo-107, fabricated with nominal densities of 6, 7 and 8 gU/cm^3.

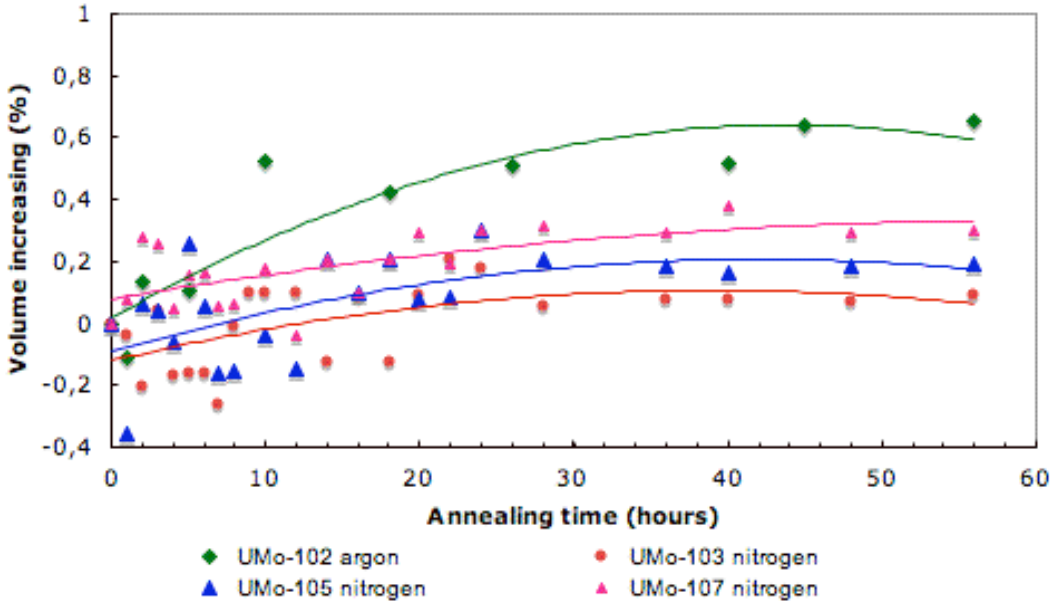

Figure 2. Volume variation in function of annealing time for dispersion type miniplates manufactured with UMo particles atomised under argon and nitrogen

The Figure 2 verified the bibliographic information [1] - [2], regarding to that swelling effect is more evident for those plates manufactured with higher density, for the same annealing time. In other hand, the miniplate manufactured with particles atomized in argon (green line) exhibits higher volume increasing compared with the miniplate manufactured with the same density but using particles atomised under nitrogen atmosphere (pink line).

The UMo-103 miniplate, insofar as the annealing time increased, its behaviour began erratically. Shrinking its volume in the first 8 hours and then increasing its volume until a maximum value of 0.202%, after 22 hours of annealing.

The same behaviour was observed for the UMo-105 and UMo-107 miniplates, shrinking its volume in the first 10 hours and then increasing its volume until a maximum value of 0.299%, both, after 22 hours of annealing.

Regarding to the UMo-102 miniplate, it showed shrinking only at first hour of annealing. After that, its volume was increasing until a maximum value of 0.654%, after 56 hours of annealing.

3.3 Evaluation of thermal conductivity in dispersion type UMo miniplates

The next section summarizes the results of thermal conductivity evolution, as consequence of swelling annealing applied to dispersion type UMo miniplates.

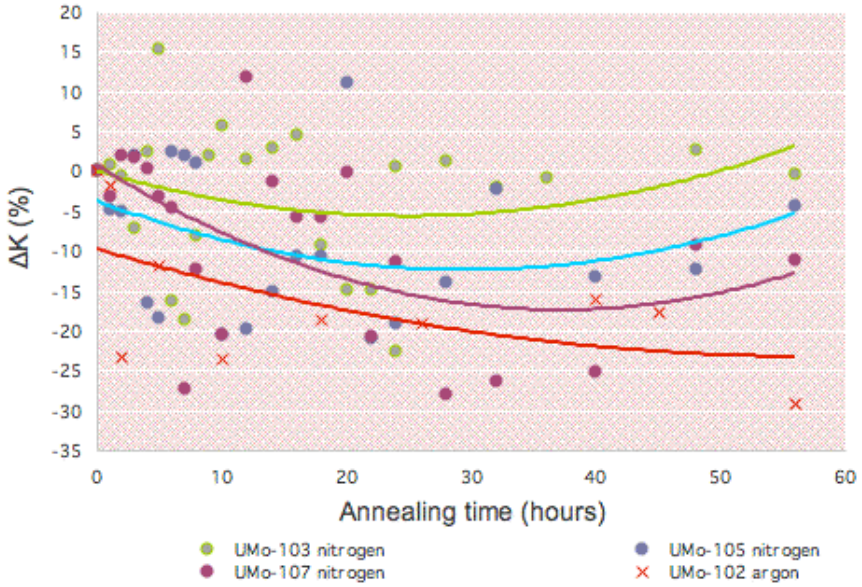

Figure 3. Evolution of the thermal conductivity value in function of annealing time applied to induce out-of-pile swelling in dispersion type UMo miniplates

By means the graph in Figure 3, is possible to observe the decreasing trend of thermal conductivity, in relation to the value taken before annealing, in all miniplates subjected to out-of-pile swelling test. Also this figure shown that, meanwhile the uranium density is increased, the value of the thermal conductivity is more affected by volume increment. It can be noted also in the figure 2, where miniplate UMo-107 (purple line), which has a density of uranium 8 gU/cm^3, exhibits more swelling than others and, therefore in figure 3, this miniplate shown great reduction in thermal conductivity (purple line).

The miniplate UMo-103, according to progress in swelling test, shown great dispersion in its variation of thermal conductivity (green line), obtaining its maximum value of 15% at 5 hours and minimum value of thermal conductivity variation of -24.92% at 23 hours of thermal swelling. After that, this miniplate exhibits fluctuating values until 56 hours of swelling, where it seems to recover its original value of thermal conductivity (variation near to 0%). This behaviour is different. Compared with UMo-105 and UMo-107 miniplates and can be related with the lower uranium density of this miniplate.

UMo-105 miniplate also shown important dispersion in thermal conductivity variation values (violet line), the minimum value of thermal conductivity was about -20% registered after 12 hours of swelling test. Such as happened with the UMo-103 miniplate, at 56 hours of annealing, the thermal conductivity trend to recover its value, but just up to -5% approximately of its starting value.

In the case of UMo-107 miniplate, the thermal conductivity decreased up to a minimum of 28 7% after 28 hours of annealing. Such as the others miniplates, the thermal conductivity shown a trend to recover its original value, but for this case just was possible to obtain a value of -12% approximately after 56 hours of thermal treatment.

The miniplate UMo-102, manufactured as the UMo-107 with uranium density of 8 gU/cm^3, but using UMo particles atomised in argon instead of nitrogen, was the most affected by annealing for thermal swelling. The variation of thermal conductivity shown a decreasing trend almost linear (red line), with a minimum value around -30% at 56 hours of annealing and, contrary to what happened with the others miniplates, the measurements doesn't reveals any sign of recovery its original values, taken prior to thermal treatment.

3.4 Scanning Electron Microscopy of UMo miniplates.

The miniplates UMo-102 and UMo-107, both manufactured with 8 gU/cm^3 but using UMo particles atomised in different atmospheres (argon and nitrogen) were analyzed by Scanning Electron Microscopy. Pictures at low magnification were obtained (40X) and some thickness values were taken from these images.

3.4.1 SEM of miniplate UMo-102

Figure 4 shows a cross section of the UMo-102 miniplate subjected to 56 hours of thermal swelling. This image was obtained from a collage of SEM images taken into 7 zones along the miniplate.

Figure 4. Cross section of miniplate UMo-102, manufactured with UMo particles atomised in argon. After 56 hours of annealing at 350 °C.

The thickness of miniplate and fuel meat registered in as-fabricated condition and before annealing were 1.44 and 0.65 mm respectively. The plate thickness was measured with linear comparator and meat thickness was calculated from the percent reduction obtained after cold rolling.

The UMo-102 miniplate, subjected to thermal swelling for 56 hours, has an average thickness of 1.523 mm and 0.7 mm for miniplate and fuel meat, respectively. The fuel meat exhibit thickness more irregular than UMo-107, showed in Figure 5.

3.4.2 SEM of miniplate UMo-107

The Figure 5 shows a cross section of the UMo-107 miniplate, after 56 hours of thermal treatment at 350 °C.

The values obtained for plate and fuel meat thickness in as-fabricated condition and before annealing were 1.43 and 0.64 mm respectively. The plate thickness was measured with linear comparator and meat thickness was calculated from the percent reduction obtained after cold rolling.

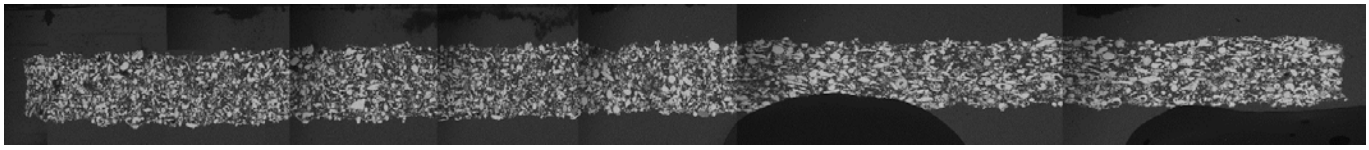

Figure 5. Cross-section of UMo-107 miniplate, manufactured with UMo particles atomised in nitrogen, after 56 hours of annealing at 350°C

After 56 hours of annealing, the miniplate UMo-107 has an average thickness of 1.593 mm and 0.712 mm for miniplate and fuel meat. Respectively. The fuel meat exhibits thickness more regular than UMo-102 miniplate.

The SEM micrograph of both miniplates doesn't exhibit presence of fuel meat fracture or meat-cladding non-bonded areas.

4. Discussions and Conclusions

The application of thermal swelling induced to miniplates by means annealing produces changes in the structure of this composite material. From macro point of view, these annealing generate volume increasing and in terms of microstructure, occurs interdiffusion, atomic diffusion and formation of new phases and compounds with different densities.

The thermal conductivity of miniplates was evaluated subjects them to thermal treatment. During these test, were detected several changes in this property, according to the volume variations of the miniplate. According to the experimental values, interesting trends were discovered and it possible to conclude the following:

The thickness values measured by SEM for miniplate and fuel meat after the heat treatment were higher than the values measured or calculated in as-fabricated condition. This increasing can be related to formation of low density new phases in the interaction layer and/or increasing of fuel meat porosity.

The behavior of the miniplate UMo-102, made with UMo particles atomised under argon verifies a progressive trend to volume increasing in function of annealing time. A behavior very different from that observed in miniplates made of particles atomised under hydrogen, in which occurs negative and positive volume changes along annealing time.

The increment in the uranium density of miniplates from 6 to 8 gU/cm^3, causes increment in the thickness of miniplates and detriment in its thermal conductivity, as happened with UMo-103 and UMo-107 miniplates, which reveals values of thermal conductivity decreased up to -24% and -28.7%, respectively.

Has been verified an inverse relationship between thermal conductivity and swelling, which was observed in all miniplates. The shrinking produced in the miniplate was matched with the increase in the value of thermal conductivity and conversely.

When comparing the UMo-102 and UMo-107 miniplates, both manufactured with the same uranium densitiy, but using UMo particles atomised in different atmosphere, can be concluded that the atomisation in nitrogen allow to obtain greater resistance to volume increase and also to the detriment of the thermal conductivity, which is promising for the proper behavior of these UMo particles as nuclear fuel.

Regarding to the controlling variables for thermal conductivity was possible to verify, experimentally, that the total density and uranium density of each miniplate are parameters that affect this physic property.

Completed the experimental development and after the analysis of results, is possible to conclude that a non destructive methodology has been developed in order to evaluate the thermal conductivity of dispersion type UMo miniplates. The obtained values, although are not numerically exact, are useful to express the detriment of this property in function of volume increasing in these fuel miniplates.

5. References

[1] T. K. Huber, M. K. Fig, D. Garrett, J. R. Kennedy, A. B. Robinson, D. M. Wachs. First results of scanning thermal diffusivity microscopy (STDM). Measurements on irradiated monolithic and dispersion fuel. INL/EXT 12-26708, Idaho National Laboratory, Idaho Falls, Idaho, 2012.

[2] Douglas E. Burkes, Andrew M. Casella, Amanda J. Casella, Edgar C. Buck, Karl N. Pool, Paul J. Macfarlan, Matthew K. Edward, Frances N. Smith - Thermal properties of U-Mo alloys at moderated burnup and power, Journal of Nuclear Materials (494) (2015) 331–341.

[3] R. M. Hengslter, L. Beck, H. Breitkreutz, C. Jarousse, R. Jungwirth, W. Petry, E. Schmid, J. Schneider, N. Wieschalla – Physical properties of monolithic U-8 wt%Mo, Journal of Nuclear Materials (402) (2010) 74-80.

[4] W. D. Callister. “Introducción a la Ciencia e Ingeniería de los Materiales”. Editorial Reverté, (1995).

[5] John Thomas Creasy. “Thermal properties of uranium-molybdenum alloys: Phase of decomposition effects of heat treatments”. Master of Science Thesis - Office of Graduate Studies of Texas A&M University. December 2011.

[6] Ved Prakash Sinha “Development of LEU based plate type targets for Mo99 production: Indian perspective” TM on Global Capabilities for the production and manufacture of Mo-99 Targets, October 20-21, 2015 - Vienna, Austria.

[7] Ho Jin Ryu, Yeon Soo Kim, Jong Man Park, Hee Taek Chae and Chang Kyu Kim, Performance evaluation of U-Mo/Al dispersión fuel by considering a fuel-matrix interaction – Nuclear Engineering and Technology, Volume 40, Issue 5, 409-418, 2008.

[8] Applicable thermal conductivity range (Netzsch, 2014)
Jin-Sung Lee, Kyung-Su Kim, Yooil Kim, Suck-Min Woo ans Seungjin Yun - Experimental Study on Correction of Thermal Conductivity Obtained by Heat Flow Method using Commercial Guarded Hot Plate Method Apparatus, Journal of Ocean Engineering and Technology. 2015. Apr, 29 (2): 169-174.

[9] Luis Olivares, Jaime Lisboa, Jorge Marin, Mario Barrera, Alberto Navarrete – Atomization of UMo particles under nitrogen atmosphere. World Journal of Nuclear Science and Technology. WJNST, Vol 6, January 2016.

VALIDATION OF THE NEUTRON CALCULATION TOOL ANUBIS V3 FOR THE OSIRIS MATERIAL REACTOR

Fadhel MALOUCH(*), Franck LOPEZ
Den-Service d'études des réacteurs et de mathématiques appliquées (SERMA), CEA, Université Paris-Saclay, F-91191 Gif-sur-Yvette, France

ABSTRACT

ANUBIS is a deterministic calculation scheme, based on the 2D transport code APOLLO2 and the 3D-diffusion code CRONOS2, developed for the simulation of the OSIRIS Material Testing Reactor (CEA-Saclay Center). To enhance the tool performances, several improvements have been implemented in the version 3 ANUBIS V3, in particular for the cross sections library generation using a 2D full core transport computation to feed the 3D diffusion calculation. ANUBIS V3 has been validated against TRIPOLI-4® Monte Carlo calculations and experimental results.

1. Introduction

OSIRIS is a material testing reactor located at the CEA-Saclay center and operated from 1966 to 2015. A specific neutron simulation tool, called ANUBIS, was developed for the reactor operation-safety calculations. ANUBIS is a deterministic calculation scheme based on the 2D-transport code APOLLO2 and the 3D-diffusion code CRONOS2 (developed by CEA).

The OSIRIS core contains different types of elements: 38 standard fuel elements, 6 control elements (hafnium absorber in upper part and fuel "follower" in lower part), up to 7 beryllium elements (reflector), MOLY devices, water boxes for in-core experiments, etc. The wide variety of core configurations and their relative heterogeneity make the core difficult to simulate with traditional methods (transport-diffusion calculation scheme). Indeed, the classical approach used to generate the homogenized cross-sections library that are needed in the 3D diffusion core calculation is based on a fuel assemblies modeling in 2D infinite lattice, the depletion calculation being performed with a 281-group transport calculation. Although this assumption appears justified in large PWR where a major proportion of assemblies are surrounded by similar ones (fundamental mode approximation), this is not the case in the OSIRIS reactor where each assembly is always surrounded by different element.

Therefore, we intend to improve the diffusion core calculation by taking into account the neighborhood of each fuel element in the cross section generation. Several improvements have been implemented in the version 3 of ANUBIS (ANUBIS V3), in particular for the generation of the cross sections library within a 2D full-core configuration (at the neutron transport stage using APOLLO2).

ANUBIS V3 has been validated using the TRIPOLI-4® Monte Carlo code (developed by CEA) and experimental results issued from OSIRIS operation. The reactivity and the power distributions obtained with ANUBIS V3 and TRIPOLI-4® were compared for a set of realistic configuration of OSIRIS reactor. Measurements of control rods efficiency, neutron flux in fuel and neutron flux in experimental locations were performed in the ISIS reactor which is the

(*) Corresponding Author (fadhel.malouch@cea.fr)

mock-up of OSIRIS. The method of cross sections library generation within full core configurations gives satisfactory results on both reactivity and power map comparisons.

In this paper, we present first the OSIRIS reactor and the ANUBIS V3 calculation scheme. Then, we detailed the recent improvement of the cross sections library generation within a 2D full-core configuration (neutron transport stage). Finally, we present the main results of the Monte-Carlo and the experimental validation.

2. OSIRIS MTR reactor

OSIRIS is a material testing reactor located at the CEA-Saclay site and operated from 1966 to 2015. It is a 70 MWth pool type light water reactor with an open core (Fig. 1.).

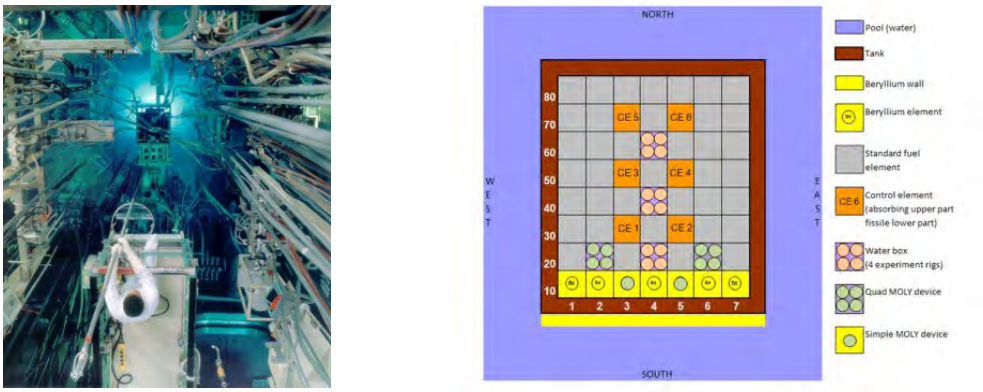

Fig 1. View of the OSIRIS reactor (left) and radial cross-section of the OSIRIS core (right)

The core is a compact unit (70×80×90 cm^3). The core tank contains a centrally located rack containing 56 cells of 8×8×90 cm^3 each one. These cells are loaded with 38 standard fuel elements, 6 control elements (hafnium absorber in upper part and fuel "follower" in lower part) and up to 7 beryllium elements (in row 10, south side). The remaining cells (in particular 24, 44 and 64) are dedicated to in-core experiments with high fast neutron flux (about 2×10^{14} $n.cm^{-2}.s^{-1}$).

3. Neutron calculation scheme

The OSIRIS reactor is constituted of a large amount of different elements (core, reflector, experimental setup…) which can be present or not in normal operation. This wide variety of core configurations and their relative heterogeneity make the core difficult to simulate with traditional methods (transport-diffusion calculation scheme). Indeed, the classical approach used to generate the homogenized cross-sections library that are needed in the 3D diffusion core calculation is based on a fuel assemblies modeling in 2D infinite lattice, the depletion calculation being performed with a 281-group transport calculation. Although this assumption appears justified in large PWR where a major proportion of assemblies are surrounded by similar ones (fundamental mode approximation), this is not the case in the OSIRIS reactor where each assembly is always surrounded by different element. Therefore, we intend to improve the diffusion core calculation by taking into account the neighborhood of each fuel element in the cross section generation. The ANUBIS V3 computation scheme can be divided into three distinct phases.

3.1 Phase 1: Depletion calculation of fuel assemblies at nominal temperature

First we calculate the depletion of fuel assemblies (standard and follower) in 2D infinite lattice and save the composition of fuel medium for each depletion step. The transport calculation is performed with the MOC linear solver of APOLLO2-8.4 with 281 energy groups, with critical leaks, and a degree 1 of cross-sections anisotropy.

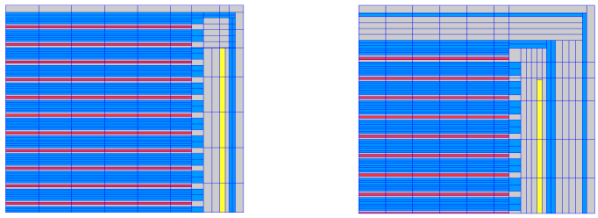

Fig 2. Quarter geometry (generated by SILENE) of standard fuel assembly (left) and follower fuel assembly (right): fuel in red, water in blue, boron in yellow, aluminium in grey

3.2 Phase 2: Media recovery for core calculation with chosen temperatures

For each assembly present in the actual core being studied, the fuel media composition is read as a function of the burnup in the database generated in Phase 1. A 2D infinite lattice transport calculation is performed for each assembly with the actual fuel and moderator temperatures. The computed flux (281 energy group) is then used to spatially homogenize each assembly into four macro media.

In a second step, a 2D transport calculation is performed on a 2D core geometry in which each fuel assembly is modeled by four macro media. The flux computed is used to generate a 6-group cross-section library with different cross-section values for elements in different location. The transport calculation is performed with the MOC linear solver of APOLLO2-8.4 with 281 energy groups, with axial leaks, and a degree 3 of anisotropy. An equivalence Transport-Diffusion is performed at the end of transport calculation in order to generate a set of equivalence coefficients for each calculation configuration.

3.3 Phase 3: Core calculation in 3D Diffusion

The 6 energy groups cross sections library is read by CRONOS2.12 and used to calculate the core (both static and depletion calculation) in 3D diffusion with a dual finite mixed element method. The description of fuel assemblies is similar to macro-regions used in APOLLO2 transport 2D calculation. The choice of the right cross-section library to use for a given rod configuration is performed vertically. For instance, if rod 3 is down, rod 4 is half extracted and rod 6 is ¾ extracted, we'll use a set of 3 cross-section library to describe each area (configuration rod 3 down for first area, rod 3 and 4 down for next area and rod 3, 4 and 6 down for last area).

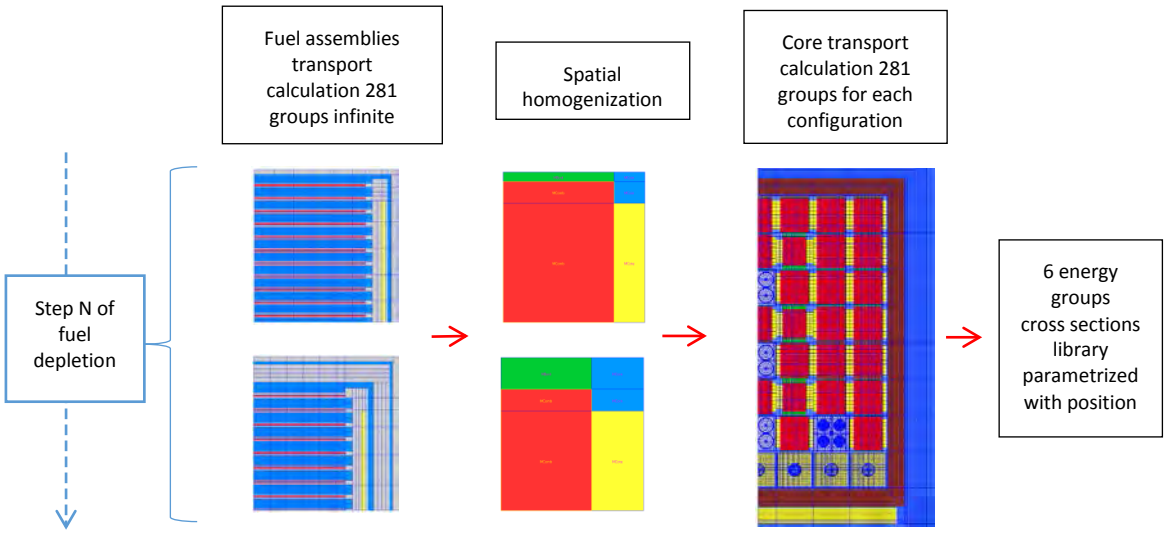

Fig 3. Schematic layout for assemblies recovering within the full core geometry for cross section library generation

4. Monte Carlo Validation with TRIPOLI-4®

The reactivity and 2D power distributions obtained with ANUBIS V3 (3D, 6 groups diffusion) and TRIPOLI-4® [3] (3D continuous-energy Monte-Carlo code) were compared for a set of realistic configuration of OSIRIS reactor. Two effective cycle were chosen for this depletion comparison (F192 2T and F185 3T). A large amount of realistic rod configurations were modeled starting from three control rods down to all control rods up (for a total of 20 configurations calculated). In the following, "34d6h" means that control rods 3 and 4 are down and 6 is halfway up, other rods being up by default.

4.1 Reactivity

Two effective cycle were chosen for this comparison (F192 2T and F185 3T). A large amount of realistic rod configurations were modeled starting from three control rods down to all control rods up (for a total of 20 configurations calculated).

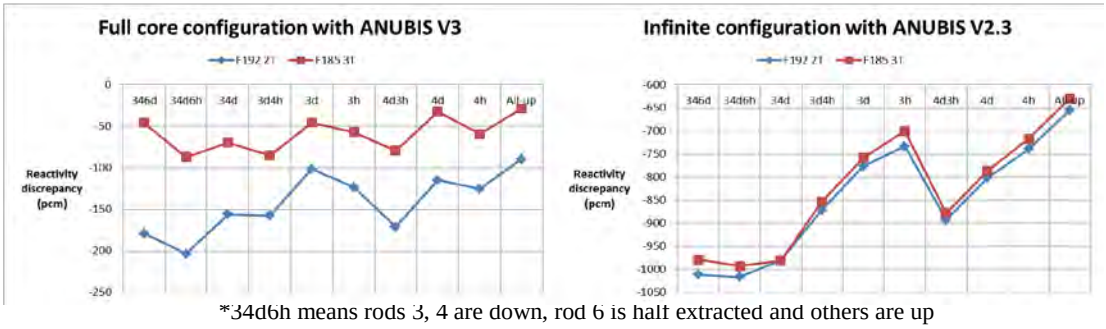

*34d6h means rods 3, 4 are down, rod 6 is half extracted and others are up

Fig 4. Reactivity discrepancies between ANUBIS V3 (and V2.3) and TRIPOLI-4® reference calculations (statistical uncertainties 1σ around 6 pcm) for a wide variety of realistic control rods configurations for two representative cycles

We obtain a good agreement between ANUBIS V3 calculations and TRIPOLI-4® reference calculations (Fig 4). Indeed all the discrepancies lay between -200 and -25 pcm for all realistic core configurations (2T and 3T) which is very satisfactory (the initial goal for the scheme was +/- 1000 pcm). In comparison, calculations with infinite configuration generation of cross-section libraries (with ANUBIS V2.3) were conducted for both cycles and show reactivity discrepancies between -1016 pcm and -629 pcm.

4.2 2D power map per assembly

The power per assembly relative discrepancies are below 4.0% for all realistic core configurations with a standard deviation around 1.6% (Fig 5). In comparison, calculations with infinite configuration generation of cross-section libraries (with ANUBIS V2.3) show discrepancies below 6.3% with a standard deviation around 2.3%.

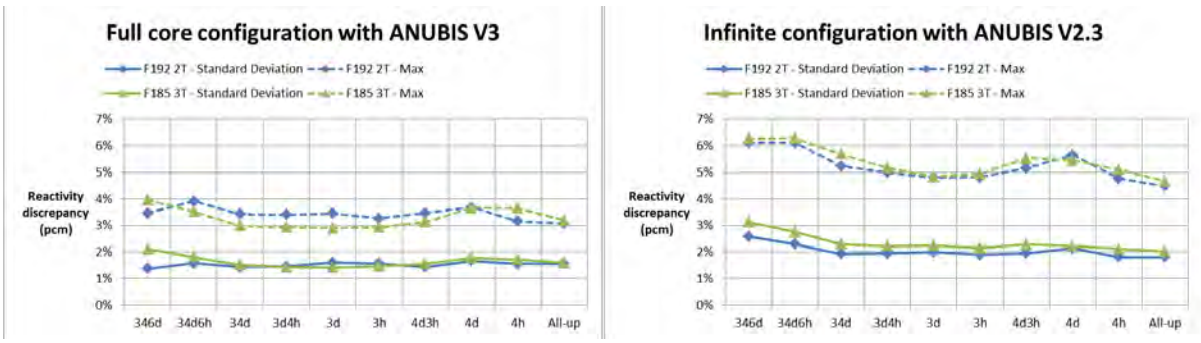

*34d6h means rods 3, 4 are down, rod 6 is half extracted and others are up

Fig 5. Power per assembly relative discrepancies between ANUBIS V3 (and V2.3) and reference

4.3 2D power map per plate

CRONOS2 yields the power in each mesh cell as a second order polynomial function in directions X and Y. Although the fuel plates are not explicitly described in CRONOS2, we can compute the power distribution within an assembly by interpolating the polynomial function. We calculate a map of 22 plates x 4 subdivisions power values per standard assembly and 17 plates x 4 subdivisions power values per follower assembly for a total of 3752 power values. We present here the “All-rods-up” configuration for F192 cycle.

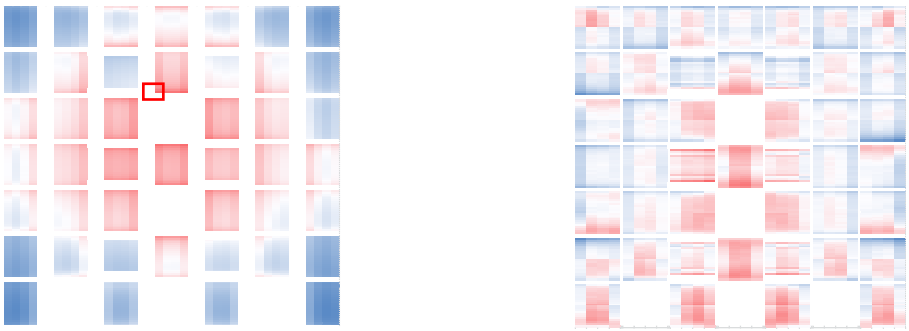

Fig 6. 2D power map plate per plate (left) and map of relative discrepancies between ANUBIS V3 and TRIPOLI-4® (right)

The power peaking factor is located in the bottom left corner of assembly 74 in both ANUBIS V3 and TRIPOLI4 calculations. It is materialized by a red square in Fig 6. The relative discrepancy at the power peaking factor between the 3D diffusion calculation and the Monte Carlo reference calculation is +3.4%. The relative discrepancies lay between -10% and +7% with a standard deviation of 2.2%. The largest discrepancies are obtained in low power area.

5. Experimental Validation

5.1 Control Rods Efficiencies

We present here the validation of the control rods efficiency. These rods are the two central rods which are used in reactor operation (3 and 4) and the North-West rod (6) used for reactor divergence. The calculation shows a good agreement with the measurements with relative discrepancies on the integral efficiency of +3% and -2% for control rod 3 and 4 respectively (Tab 1). The relative discrepancy for the end of control rod 6 is -26% but represents only -122 pcm. The measure uncertainties have been evaluated to 6% at 1 sigma. Moreover the calculation shows a very good agreement with the reference TRIPOLI-4® calculation for all control rods with relative discrepancies below 2%.

Control Rod	Measured Intregral Efficiency (pcm)	TRIPOLI-4 Calculated Integral Efficiency (pcm)	C-T4/M	ANUBIS-V3 Calculated Integral Efficiency (pcm)	C-A3/M	C-T4/C-A3
end of BC6	475	354	0.74	353	0.74	1.00
BC3	3420	3543	1.04	3537	1.03	1.00
BC4	3530	3501	0.99	3445	0.98	0.98
Total	7425	7398	1.00	7335	0.99	0.99

Tab 1. Control rods efficiency measured and calculated in ISIS reactor.

The Fig 7 shows the axial efficiencies profiles of rods 3 and 4 measured and calculated with ANUBIS V3. The profiles in “S” are well reproduced by calculation and stay in the margin of 1 sigma of measurement uncertainty.

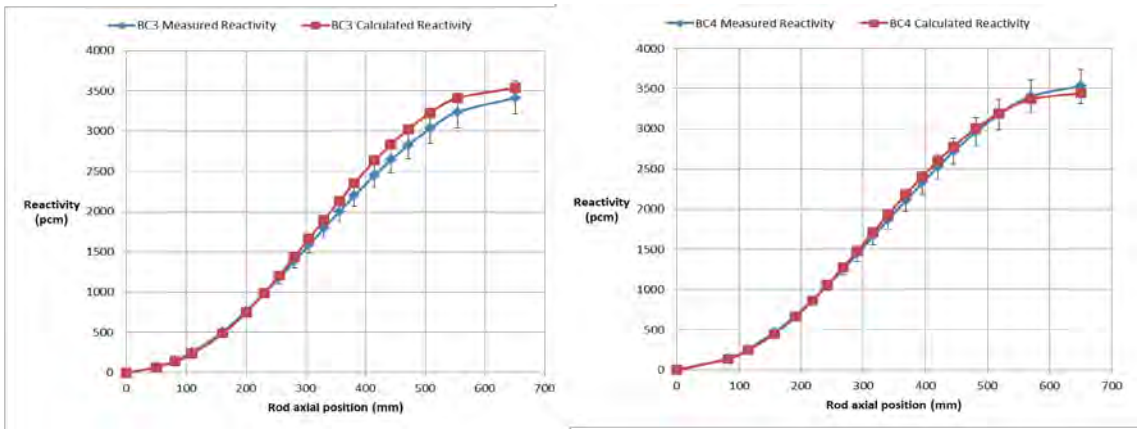

Fig 7. Control rods efficiency measured and calculated with ANUBIS-V3 with axial position around criticality

5.2 Gap to criticality in exploitation

For most of the cycles conducted in OSIRIS reactor, the historic of control rods position was recorded and could be used to simulate a major part of the reactor life.

We decided to simulate several cycles which represent a wide variety of reactor configurations. By fixing the control rods positions, we can verify that the computed reactivity is closed to criticality. The calculation of 37 cycles (more than 4 years of exploitation) is obtain with 426 calculated points and is presented in Fig 8. It shows gaps to criticality between -632 pcm and +549 pcm which is satisfactory and consistent with the objective of calculation scheme (+/- 1000 pcm). The average value is -34 pcm with a standard deviation of 298 pcm (99% are below 2 sigma). We have to remind that sources of uncertainty are plenty, due to the large amount of input data necessary to simulate more than 4 years of exploitation (loading maps, control rods positions, power levels, experimental loads, etc).

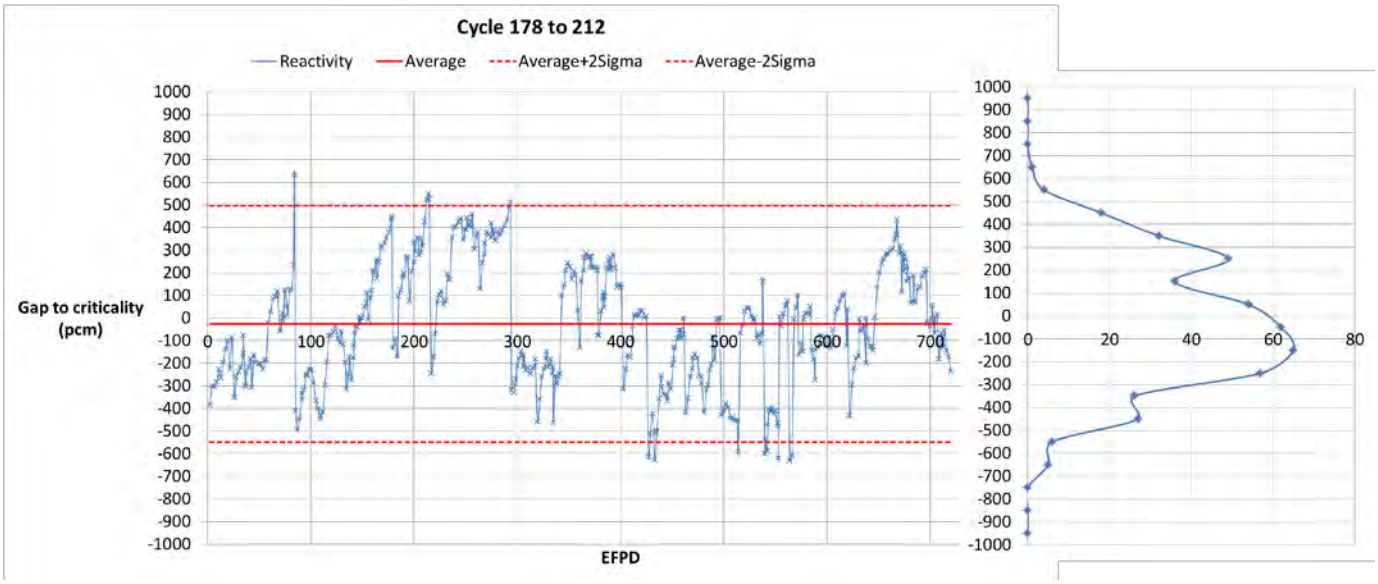

Fig 8. Gap to criticality during irradiation for 4.4 years of exploitation and its distribution around criticality

6. Conclusion

The method of cross sections library generation within full core configurations gives satisfactory results on reactivity, power map distribution, thermal flux in fuel assembly, and thermal and fast flux in experimental locations for both verification and validation (flux comparisons not shown on this paper). Moreover the comparison with traditional infinite lattice calculation method shows major improvements on reactivity and power map distribution. Further flux comparisons in experimental locations should be conducted with OSIRIS reactor in order to reduce the uncertainty on power level which is not well known in ISIS reactor.

7. References

[1] R. Sanchez et al., “APOLLO2 year 2010,” Nucl. Eng. Technol., Vol. 42, No. 5, 2010, pp. 474-499.

[2] Lautard et al., 1990, Lautard J.J., Loubière S., Fedon-Magnaud C., “1990. CRONOS2, a modular computational system for neutronic core calculations”, IAEA Specialist Meeting on Advanced Calculational Methods for Power Reactors, Cadarache, France.

[3] E. Brun, F. Damian, C.M. Diop, E. Dumonteil, F.X. Hugot, C. Jouanne, Y.K. Lee, F. Malvagi, A. Mazzolo, O. Petit, J.C. Trama, T. Visonneau, A. Zoia, “TRIPOLI-4®, CEA, EDF and AREVA reference Monte Carlo code”, Annals of Nuclear Energy, Volume 82, August 2015, Pages 151–160

DEVELOPMENT OF AN ADVANCED RELAP/SCDAPSIM/MOD4.0 U-AL FUEL PLATE COMPONENT MODEL FOR THE ANALYSIS OF DESIGN BASIS AND SEVERE ACCIDENTS IN RESEARCH REACTORS

S. SHUMSKI
Warsaw University of Technology
Nowowiejska 21/25,
00-665 Warsaw, Poland

D. DELBIANCO
INVAP-SE
Av. Cmte. Luis Piedrabuena 4950
S.C. de Bariloche. (8400)
Río Negro. Argentina

R. PERICAS
Universitat Politècnica de Catalunya Av
Diagonal, 647 08028 Barcelona, Spain

C. M. ALLISON
Innovative Systems Software
3585 Briar Creek, Ammon
Idaho 83406, USA

J. K. HOHORST
Innovative Systems Software
3585 Briar Creek, Ammon
Idaho 83406, USA

Keywords: thermal-hydraulic code, RELAP/SCDAPSIM, research reactor, U-Al_x fuel plate

ABSTRACT

RELAP/SCDAPSIM/MOD4.0 is being developed as part of the international SCDAP Development and Training Program (SDTP). MOD4.0 and earlier versions of RELAP/SCDAPSIM have been used to support design basis analysis (excluding fuel damage) for a variety of research reactor designs including those using U-Al_x plate type fuel elements. However, since the accident at Fukushima Daiichi, there has been an increasing demand to extend the modelling options for research reactors to include transients where the fuel elements can be damaged and melting of the fuel elements can be described. As a result, an advanced U-Al fuel plate SCDAP component has been developed and added to a specialized version of RELAP/SCDAPSIM/MOD4.0. This component model is a derivative of a SCDAP component model that was originally developed to support the analysis of the Advanced Test Reactor

(ATR) located near Idaho Falls, Idaho`. However this ATR component model was never released to the general SCDAP/RELAP5 user community.

This paper describes the unique features of the new model including a brief description of the specific models and correlations used in the model. The U-Al_x-specific material property correlations are embedded within the RELAP/SCDAPSIM "MATPRO" materials property library so they can easily be replaced with appropriate correlations for other metallic fuel element materials. The paper also describes the application of the new model to a generic representative research reactor test problem for a loss of coolant transient that results in the uncovery of the core and the melting of fuel elements.

1. INTRODUCTION

The RELAP/SCDAPSIM code, designed to predict the behaviour of reactor systems during normal and accident conditions, is being developed as part of the international SCDAP Development and Training Program (SDTP) [1-3]. SDTP consists of more than 90 organizations in 30 countries supporting the development of technology, software, and training materials for the nuclear industry. The program members and licensed software users include universities, research organizations, regulatory organizations, vendors, and utilities located in Europe, Asia, Latin America, Africa, and the United States. Innovative Systems Software (ISS) is the administrator for the program.

As described in Section 2, RELAP/SCDAPSIM/MOD4.0, is one of the most advanced versions of RELAP/SCDAPSIM, and the first version of RELAP5 or RELAP/SCDAPSIM completely rewritten to FORTRAN 90/95/2000 standards. Section 3, provides a brief overview of a representative research reactor thermal hydraulic model that was used to test the new component model. Section 4, describes the setup of the new component model. Section 5 describes the application of the new model to a generic representative research reactor test problem for a loss of coolant transient that results in the uncovery of the core and the melting of fuel.

2. RELAP/SCDAPSIM/MOD4.0

RELAP/SCDAPSIM/MOD4.0 uses publicly available RELAP/MOD3.3[4] and SCDAP/RELAP5/MOD3.2[5] models and correlations, originally developed for the US Nuclear Regulatory Commission, in combination with proprietary (a) advanced programming and numerical methods, (b) user options, and (c) models developed by ISS and other members of the SDTP. These enhancements allow the code to run faster and more reliably than the original US NRC codes. MOD4.0 can also run a much wider variety of advanced fluids and transients.

A summary and a brief description of RELAP/SCDAPSIM analysis for a variety of research reactors can be found in references [6-7]. RELAP/SCDAPSIM is also used in proprietary design and analysis of research reactors such as the "MTR-type" research reactors designed by INVAP-SE. However, the results of such calculations are not normally available in the open literature.

RELAP/SCDAPSIM/MOD4.0 [8-10], is the first version of RELAP or SCDAP/RELAP5 completely rewritten to FORTRAN 90/95/2000 standards. This is a significant benefit for the development of advanced models and user options. MOD4.0 also includes advanced numerical options such as improved time advancement algorithms, improved water property tables, and improved model coding. As a result the code can reliably run complex multi-dimensional problems faster than real time on inexpensive personal computers. MOD4.0 includes many enhanced user options including an integrated uncertainty analysis capability [11].

3. DEVELOPMENT OF A GENERIC RESEARCH REACTOR INPUT MODEL FOR TESTING AND ASSESSMENT

A generic research reactor input model was developed to test the new component model. It should be noted that this model does not represent any specific research reactor design nor was it intended to serve as a guideline for the development of “best estimate” input for research reactor analysis for loss of coolant transients that may result in core uncovery, heat up, and fuel damage.

Figure 3-1 shows the thermal hydraulic nodalization used in this generic reactor design analysis. The core nodalization consists of three channels using the RELAP/SCDAPSIM pipe component. One channel represents the “Hot Channel”. The fraction of power allotted to the hot fuel channel is selected to produce a maximum heat flux at the central volume equal to the maximum allowable heat flux of the core. The average channel represents the remaining fuel channels and the by-pass channel represents the flow rate difference between the total pumped flow rate minus the flow rates in the fuel channels. Both the average and hot fuel channels are divided axially into volumes, with a cosine power distribution in the axial direction. The power fractions for this cosine distribution include an extrapolated length of 8 cm on each end of the active length because of the assumed light water moderator.

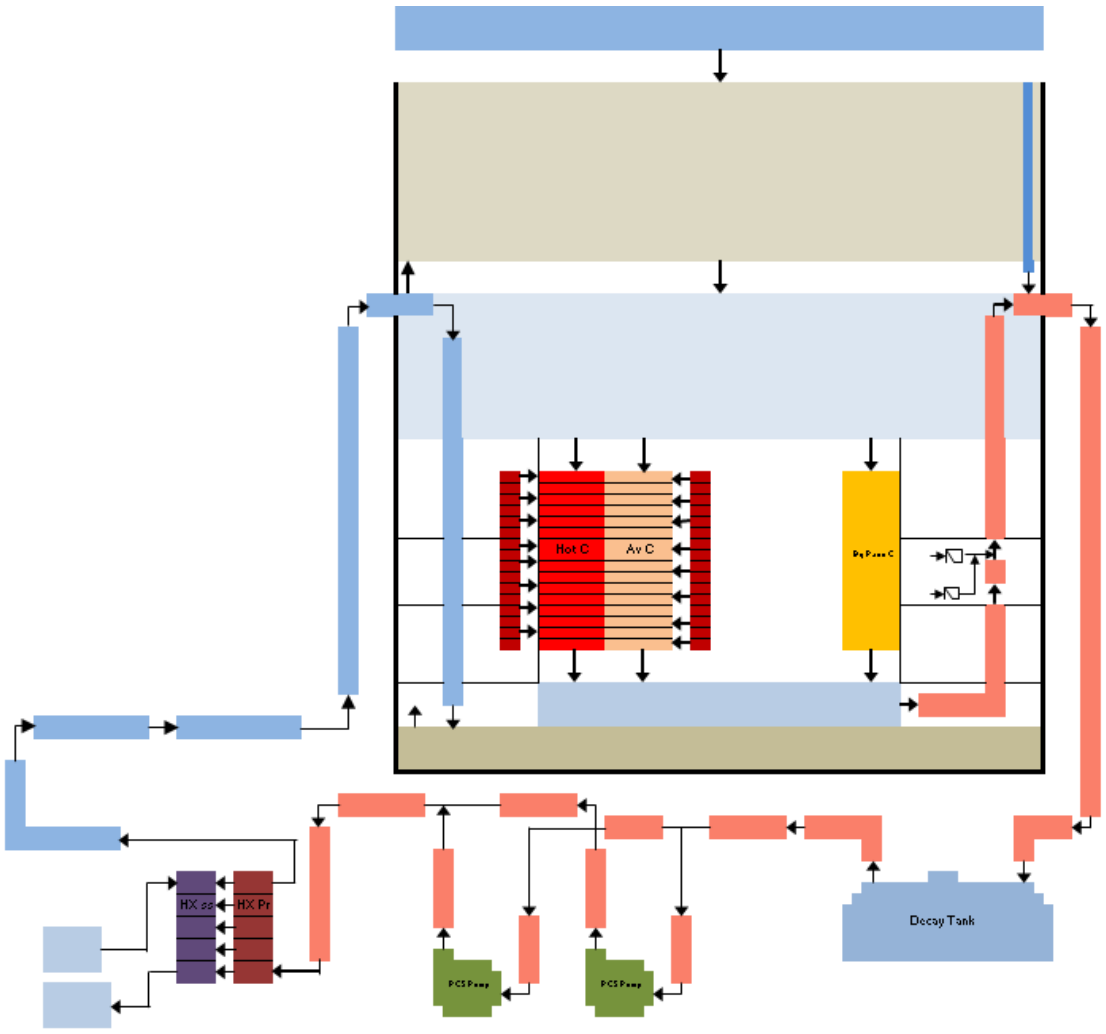

Figure 3-1. Thermal hydraulic nodalization of a generic research reactor.

The lower plenum of the pool is modelled as a single volume component, with a flow area and a hydraulic diameter corresponding to its actual rectangular cross-section. Flap Valve

Lines are usually modelled as motor valves. Their opening and closing trips depend on the pressure difference between the pipe to which they are attached and the volume representing the reactor pool at the valves' position. The flap valve lines and primary cooling system (PCS) pipes are modeled as adiabatic. The two valves can be opened independently of one another. This makes it possible to simulate the opening (or not opening) of any valve when the pumps stop. The two PCS pumps are modelled. The pump motor torque is controlled in the model by a trip signal, allowing the simulation of an electric power outage. After the electric power is removed from the motor, the pump coasts down according to its torque and moment of inertia (which includes the flywheel).

The heat exchanger of the PCS is modelled as the boundary condition of the secondary cooling system (SCS) mass flow rate and water inlet temperature of the SCS. The reactor pool is modelled in using five volumes. The uppermost volume extends from the pool surface level to the reactor pool process penetration level at which the core inlet and outlet lines are located. Subsequent lower fluid volumes describe the fluid conditions between (a) the levels of the pool inlet and outlet lines to the top of the core, (b) the top of the core position to the flap valve lines level, (c) the flap valve lines level to the diffuser level, and (d) the diffuser level to the bottom of the pool.

The flow area and volume of all pool sectors were calculated considering an appropriate reduction due to submerged equipment (this value is relevant only for LOCA simulations). The condition above the upper reactor pool volume is considered as an atmospheric boundary condition.

4. PLATE-TYPE FUEL COMPONENT MODEL INPUT

This section briefly describes the modelling of a plate-type fuel component. The general core input contains information about the general characteristics of the core including its dimensions, the number of applied components, and power source (reactor point kinetics or general power table. It also contains information about bypass channels and slumping of the fuel elements.

The reactor environment for this problem is set to the new research reactor. In this problem only one new component was used. One of the specific characteristics of this component, which must be entered in the input, is the average fuel element perimeter. By using this perimeter the number of fuel assemblies can be defined. For one assembly the fuel element perimeter is equal to the perimeter of one fuel plate multiplied by number of the plates in assembly. If modelling the full size core, it is equal to the perimeter of one fuel assembly multiplied by the number of fuel assemblies.

The material properties correlations are embedded in the RELAPS/CDAPSIM MATPRO library and can easily be expanded through the addition of reactor specific materials. For research reactor applications, the current embedded correlations include aluminium, aluminium oxide, uranium-aluminium alloy, and lithium. For the verification problem, the cladding was defined to be aluminium. The fuel was defined to be metallic uranium.

5. APPLICATION TO A LOSS OF COOLANT TRANSIENT

As a verification problem, it was decided to run the code using LBLOCA (Large Break Loss of Coolant Accident) conditions. LBLOCA is defined as an accident in the primary reactor coolant system (RCS), which results in a hole in the system with a diameter more than 6 inches. This definition also includes full stoppage of the circulation of the primary coolant. In the case of a LBLOCA leakage of the coolant occurs quickly, which leads to an abrupt pressure drop in reactor core.

When the coolant circulation terminates the core is full of water, which starts heating up and later boiling and evaporating. The heated surface of the fuel element, which is normally cooled by a liquid film, starts to overheat due to film dryout.

After dryout of the aluminium cladding, the chemical reactions between the steam and aluminium can become significant factor in the continued heating of the fuel elements. Oxidation of the aluminium by water starts at temperatures of around 370 K and the reaction rate increases with increasing temperature. This results in a highly exothermic aluminium water reaction with an enthalpy of about 280 kJ/mol. Hydrogen is also produced. The following reactions between aluminium and water with hydrogen production are possible:

$$2Al + 6\,H_2O \rightarrow 2Al(OH)_3 + 3H_2 \quad (1)$$

$$2Al + 4H_2O = 2AlO(OH) + 3H_2 \quad (2)$$

$$2Al + 3H_2O = Al_2O_3 + 3H_2 \quad (3)$$

The first reaction forms the aluminum hydroxide, gibbsite, $Al(OH)_3$ and hydrogen, the second reaction forms the aluminum hydroxide, boehmite, AlO(OH) and hydrogen, and the third reaction forms aluminum oxide and hydrogen. All three reactions are thermodynamically favorable from room temperature to past the melting point of aluminum at 933 K. All are also highly exothermic [12].

Figure 5-1 below presents the maximum core temperature growth in comparison with the coolant mass flow decrease through the core. Slow oxidation of the aluminium cladding begins around 11 seconds when the coolant mass flow drops to less than 20% of initial value and continues to decrease. From 11 seconds to 31 seconds the temperature is slowly rising with a significant jump to the melting point of the aluminium cladding observed after 31 seconds. A temperature plateau is observed up to 40 seconds when cladding melt starts taking place and continues until all the cladding has melted. A strong reaction between the molten cladding and fuel results in the next temperature jump up to the fuel melting point around 1137 K and lasts till the total fuel melt has occurred.

It can be easily observed from this figure that the temperature escalation is connected to the liquid level in the core. The core liquid level starts decreasing after the inlet mass flow drops almost to 0.0 kg/s. At 40 seconds, after the full melting of the fuel elements, a large jump in the collapsed liquid level up to its maximum value is observed.

It is believed that when the temperature exceeds 570 K the reaction becomes unstoppable due to very intensive heat generation. This results in the total oxidation of the aluminium cladding.

Figure 5-2 shows a good correlation between the collapsed liquid level and the total hydrogen generation rate in the core. It is shown in the figure that oxidation begins when the collapsed liquid level in the core begins to decrease, and attains its maximum value, when the core has a void fraction of 70%. As the void fraction of liquid increases, the heated surface, which is normally cooled by liquid film, overheats due to dryout.

Figure 5-3 presents an example of some facility parameters near the cladding melt point. It shows a temperature of about 932 K at the hottest axial node 4. Here the melting of the core starts from the middle of the fuel elements due to cosine power shape.

Figure 5-4 presents output from the cladding oxidation model. At this section of the output, parameters such as cladding thickness (Al), cladding oxide thickness, oxide weight gained in Al_2O_3, hydrogen generation rate, steam removal rate and other parameters can be found. This output section is divided to inner and outer cladding parameters.

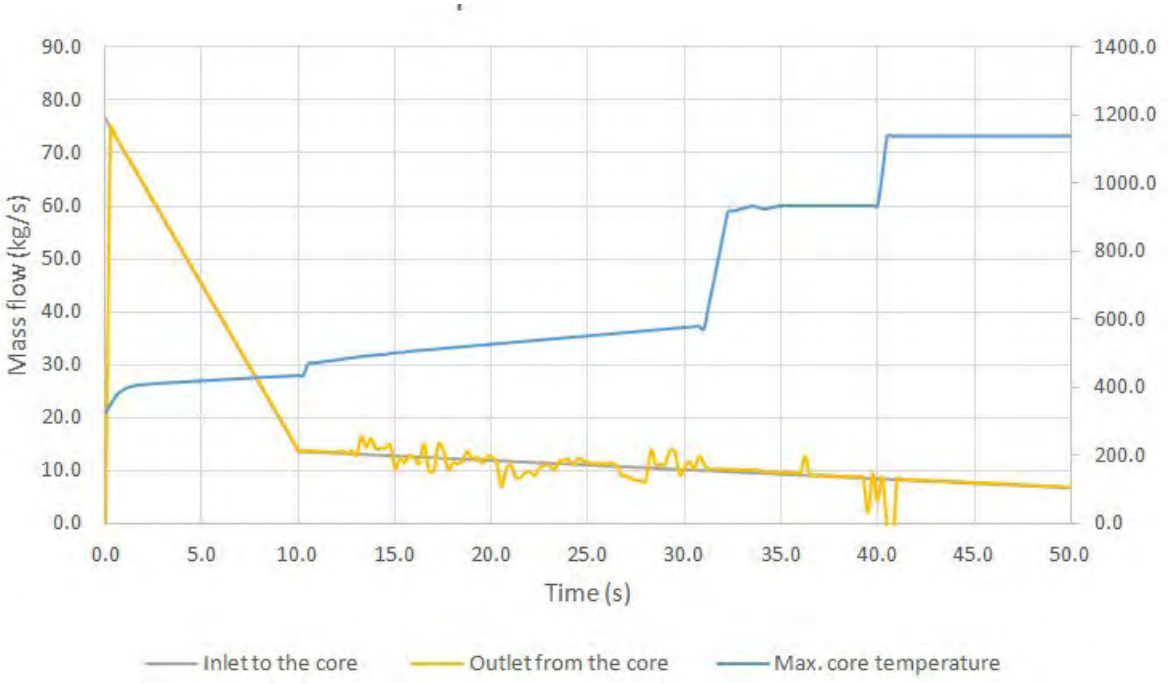

Figure 5-1. Maximum core temperature vs. collapsed liquid level.

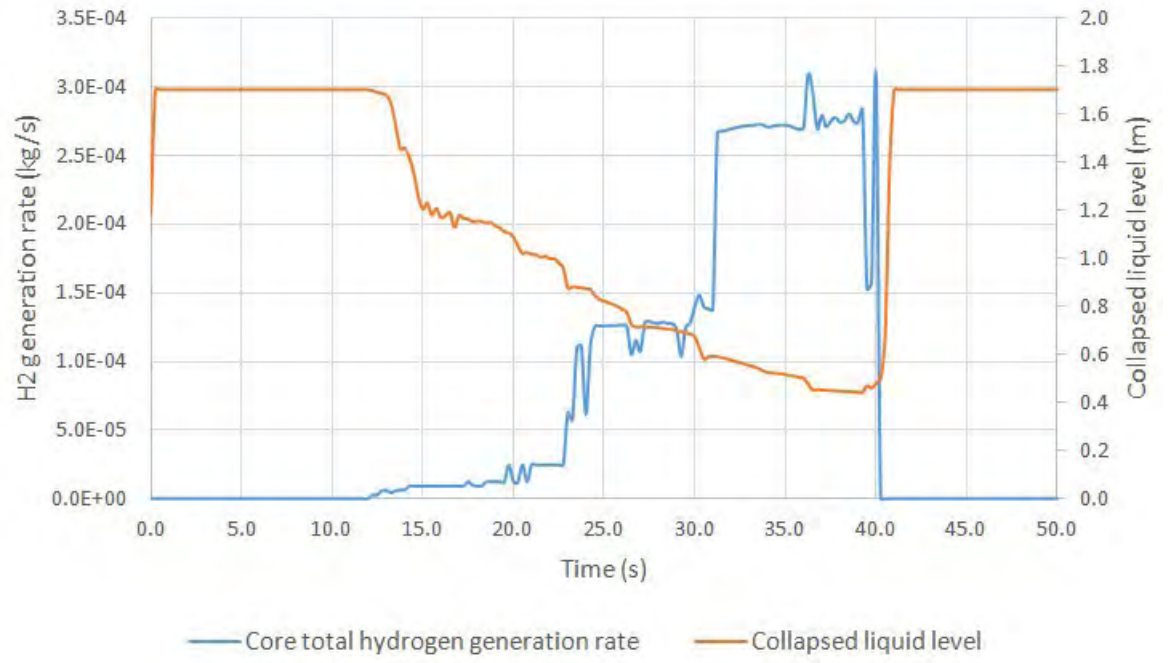

Figure 5-2. Hydrogen generation rate vs. collapsed liquid level.

```
1......... CONFIGURATION OF FACILITY ...................
 maximum temperature in reactor core =  931.94 K
 component no.  1 axial node =  4
 nuclear heat generation=  3.8728E+03 W
 total reactor power =  9.8650E+07 W
 total fission product and actinide decay =  9.8650E+07 W
 total oxidation heat generation=  3.3728E+03 W
 debris oxidation=  0.0000E+00 W
 total hydrogen production from intact rod=  2.2789E-05  kg/s
 total hydrogen production rate=  2.2789E-05  kg/s
```

Figure 5-3. Configuration of the reactor core near the cladding melting point.

```
  output from cladding oxidation model
0 --- inner cladding ---
0cladding al thickness (m)
  3.7846E-04  3.7846E-04  3.7846E-04  3.7846E-04  3.7846E-04  3.7846E-04
0cladding oxide thickness (m)
  8.9726E-11  3.9821E-08  8.1449E-08  6.4570E-08  3.2894E-08  1.1853E-07
0oxide weight gain in al2o3 (kg/m2)
  3.2210E-04  0.3707      0.7582      0.6011      0.3062      4.0748E-03
0hydrogen generation rate (kg/s)
  1.2416E-06  6.9982E-14  6.5711E-14  1.9713E-13   0.000      1.0750E-05
0cladding oxidation heat generation (w/m)
   571.9      2.4514E-05  2.4514E-05  7.3543E-05   0.000       4951.
0steam removal rate (kg/s)
  1.1176E-05  6.2990E-13  5.9146E-13  1.7744E-12   0.000      9.6761E-05
0 --- outer cladding ---
0cladding al thickness (m)
  3.2187E-04  6.5346E-04  1.3137E-04  4.1402E-04  1.3161E-04  3.2106E-04
0cladding oxide thickness (m)
  2.3284E-11  6.2173E-08  1.5077E-08  9.4274E-08  4.4503E-08  1.1853E-07
0oxide weight gain in al2o3 (kg/m2)
  8.3970E-06  0.5787      0.1403      0.8776      0.4143      4.0748E-03
0hydrogen generation rate (kg/s)
  4.7050E-08  1.3996E-13  8.2139E-14  1.9713E-13   0.000      1.0750E-05
0cladding oxidation heat generation (w/m)
   21.67      4.9028E-05  3.0643E-05  7.3543E-05   0.000       4951.
0steam removal rate (kg/s)
  4.2350E-07  1.2598E-12  7.3932E-13  1.7744E-12   0.000      9.6761E-05
```

Figure 5-4. Output from cladding oxidation model.

6. SUMMARY

1. The RELAP/SCDAPSIM/MOD4.0 code, which was originally developed to support the analysis of advanced fluid systems and accident analysis of advanced reactor designs, was extended to include a detailed U-Al research reactor fuel element component for transients where fuel damage may occur.
2. A representative verification test problem was developed to test the model under transient conditions, specifically a LBLOCA where the loss of the coolant results in the boiloff and melting of the fuel elements.

7. REFERENCES

[1] www.relap.com

[2] C. M. Allison and J. K. Hohorst, “SDTP – Development Technology for the Nuclear Industry”, Proceeding of ICONE-13, 13th International Conference on Nuclear Engineering, Beijing – China, (May 16-20, 2005).

[3] C. M. Allison and J. K. Hohorst, “Role of RELAP/SCDAPSIM in Nuclear Safety”, Science and Technology of Nuclear Installations, Volume 2010.

[4] RELAP5 Code Development Team, “RELAP5/MOD 3.3 Code Manual, Vol 1-8”, NUREG/CR-5535/Rev1 (December, 2001).

[5] SCDAP/RELAP5 Development Team, “SCDAP/RELAP5/MOD3.2 Code Manual, Vol. 1-5”, NUREG/CR-6150, INEL-96/0422, (July, 1998).

[6] C. M. Allison, J. K. Hohorst, A. J. D’Arcy, “Role of RELAP/SCDAPSIM in Research Reactor Safety”, Proceedings of RRFM 2009, 13th International Topical Meeting on Research Reactor Fuel Management, Vienna, Austria, (March 2009).

[7] A. R. Antariksawan, Md. Q. Huda, T. Liu, J. Zmitkova, C. M. Allison, J. K. Hohorst, “Validation of RELAP/SCDAPSIM/MOD3.4 for Research Reactor Applications”, Proceedings

of ICONE 13, 13th International Conference on Nuclear Engineering, Beijing, China, (May 16-20, 2005).

[8] M. Perez, et. al., “The Development of RELAP/SCDAPSIM/MOD4.0 for Advanced Fluid Systems Design Analysis”, Proceedings of ICONE-23, 23th International Conference on Nuclear Engineering, Chiba, Japan (May 17-21, 2015).

[9] M. Perez, et. al., “RELAP/SCDAPSIM/MOD4.0 Modification for Transient Accident Scenario of Test Blanket Modules in ITER involving Helium Flows into Heavy Liquid Metal”, Proceedings of NURETH-16, Chicago, USA, (September 2015).

[10] C. M. Allison, R. J. Wagner, L. J. Siefken, J. K. Hohorst, “The Development of RELAP5/SCDAPSIM/MOD4.0 for Reactor System Analysis and Simulation”, Proceedings of the 7th International Conference on Nuclear Option in Countries with Small and Medium Electricity Grids, Dubrovnik, Croatia, (May 2008).

[11] M. Perez, F. Reventos, C. M. Allison, J. K. Hohorst, “Integrated Uncertainty Analysis using RELAP/SCDAPSIM/MOD4.0”, Proceedings of the 13th International Topical Meeting on Nuclear Reactor Thermal Hydraulics (NURETH-13), Kanazawa City, Ishikawa Prefecture, Japan, (September 27-October 2, 2009).

[12] U.S. Department of Energy, “Reaction of Aluminium with Water to Produce Hydrogen”, (Version 2 – 2010).

EXPERIMENTAL DATA ON CRITICALITY OF URANIUM-ZIRCONIUM HYDRIDE SYSTEMS WITH 21 AND 36% ENRICHED URANIUM-235

S.SIKORIN, S.POLAZAU, T.HRYHAROVICH
Joint Institute for Power and Nuclear Research - Sosny,
National Academy of Sciences of Belarus, PO BOX 119, Minsk 220109, Republic of Belarus

The critical facility "Crystal" of the Joint Institute for Power and Nuclear Research-Sosny of the National Academy of Science of Belarus was used investigate the characteristics of four critical assemblies configurations, representing non-uniform multiple zones heterogeneous uranium-zirconium hydride lattices comprising hexagonal fuel assemblies with cylindrical fuel rods, boron absorbing plates, boron and europium absorbing rods, zirconium hydride and steel side and end reflectors. The critical assemblies represented the cores collected from three types of fuel assemblies with different structure, surrounded by assemblies and units of a side reflector. The core included channels for the regulating, compensating and emergency protection rods. The moderator – $ZrH_{1.89}$. The fuel composition – UO_2 with 21 and 36 % uranium-235 enrichment. The absorber in plates – B with 85 % boron-10 enrichment. The absorber in rods – B_4C and Eu_2O_3. We measured the critical configurations, the reactivity margin, the efficiency of the absorber rods and the dependence of the efficiency of the absorber rods on their depth of insertion in a core. Different methods for measuring the reactivity, the reactivity margin and the efficiency of the absorber rods we used. The presentation provides the description of the structure and the composition of the investigated critical assembly configurations and the associated experimental results.

1. Introduction

The Joint Institute for Power and Nuclear Research - Sosny of National Academy of Sciences of Belarus has developed several critical facilities to study various reactor configurations with a zirconium hydride moderator and different nuclear fuels, absorber and reflector materials.

This paper presents experimental data for four non-uniform multiple zones heterogeneous uranium-zirconium hydride configurations with 21 and 36 % uranium-235 enrichment, produced at the criticality facility “Crystal”.

2. Critical assemblies

The structural base of the investigated critical assemblies is a cylindrical casing from stainless steel, housing fuel cassettes, shroud tubes (channels) of the control rods, and side reflector cassettes. The casing has an outer diameter of 692 mm and a height of 720 mm. The internal surface of the casing has the configuration of the side reflector periphery. The effective thickness of the casing side wall is 45 mm. The bottom of the casing is a spacer grid (tube plate), 40-mm thick. The spacer grid has 151 sleeves with a 17 mm diameter hole for installing the fuel cassettes and the reflector cassettes in the hexagonal grid with a 45 mm pitch, as well as twelve (12) 50-mm diameter holes for installing the shroud tubes of the control rods. The critical assembly casing rests, by its outer collar, on the support flange representing a steel ring 50-mm high, with the outer and inner diameters of 814 mm and 693 mm, respectively. The supporting flange is fastened to four steel supporting channels, fastened to the 25-mm thick steel plates of the critical assembly support structure.

Four stainless steel rings are placed between the critical assembly casing bottom and the support structure steel plates; these rings are 140 mm high, with the outer and inner diameters of 780 mm and 700 mm, respectively, and three stainless steel plates of the total thickness 105 mm and the diameter 880 mm. The plates include 12 holes, 47 mm in diameter, through which the shroud tubes of the control rods pass. The lower plate rests on the supporting plate of the critical assembly support structure.
Forty eight (48) steel cylinders, 44 mm in diameter and 1100 mm in height, are installed around the critical assembly casing.

3. Elements of the active core and reflector in the experimental configurations

Four critical assembly configurations were studied: nonuniform heterogenic hexagonal lattices with multiple zones containing fuel assemblies (45 mm pitch) with zirconium hydride moderator, shroud tubes (channels) for absorbing rods, cassettes for zirconium hydride reflector. These elements of the critical assemblies are placed in the cylindrical casing on the stainless steel spacer grid. The neutron detectors are attached on special poles from organic glass around the critical assemblies.

The experiments used three types of fuel assemblies (*see FIG.1*). The claddings of all fuel assemblies represent a thin-wall hexagonal stainless steel tube for the 44 mm wrench (the wall 0.4 mm).

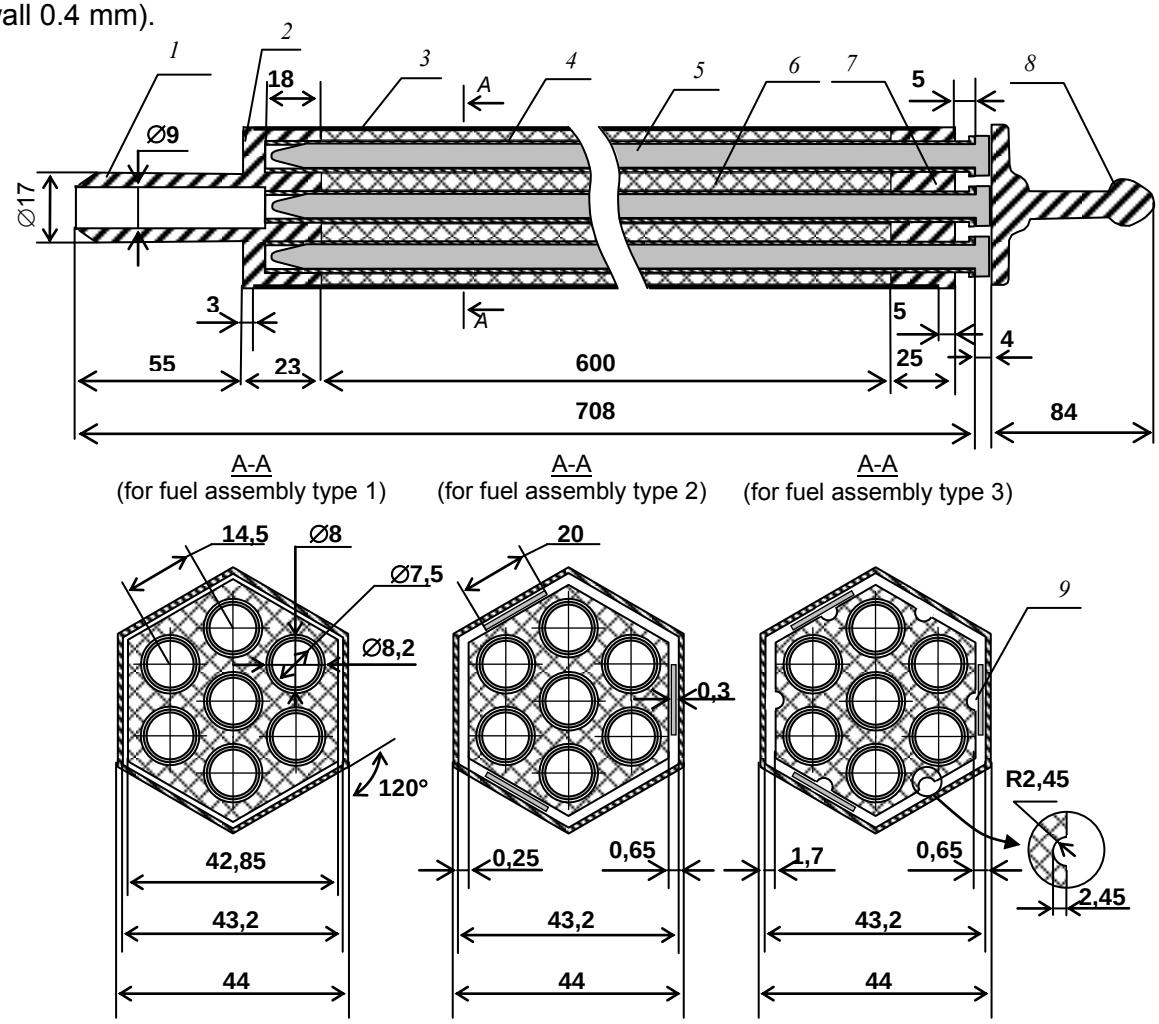

FIG. 1. Fuel assemblies:
1 — shank; 2 — lower tube plate; 3 — cladding; 4 — casing tube; 5 — fuel rod; 6 — zirconium hydride units; 7 – upper tube plate; 8 – upper part; 9 — tape with boron absorbe

The type 1 fuel assemblies have 12 hexagonal moderator units (inserted into the hexagonal tube) from zirconium hydride $ZrH_{1.89}$ (the height 50 mm, 42.85 mm wrench). The moderator units include seven 8.2 mm holes (pitch 14.5 mm), housing channel stainless steel tunes with the outer diameter 8 mm and the wall thickness 0.25 mm. All fuel assemblies have seven fuel rods. In central tube of the fuel assembly is placed one fuel rod with 36 % enriched uranium-235 (fuel rod type 1), in peripheral - six fuel rods with 21 % enriched uranium-235 (fuel rod type 2).

Unlike type 1 fuel assemblies, fuel assemblies of types 2 and 3 include three tapes with boron absorber; the tapes are located alternatively on 3 of 6 planes in central section at a height of 300 mm inside the clearance between the hexagonal tube and the zirconium hydride units. This tape is made from stainless steel alloyed with boron (85 % boron-10 enrichment). The tape is 20 mm wide and 0.3 mm thick. The type 3 fuel cassette differs from

the type 2 cassette in that the zirconium hydride units, located in the central sections of the cassettes (at a height of 300 mm) have recesses, ensuring the moderator content in this section of the moderator equivalent to the zirconium hydride $ZrH_{1.50}$.

Cassette of the reflector consists from a hexagonal tube made of stainless steel, 640 mm long, fit for a 44 mm wrench, and 0.4 mm wall, containing hexagonal zirconium hydride $ZrH_{1.89}$ units, for a 42.85 mm wrench, and a central cylindrical block from organic glass 27.0 mm dia.

The fuel rod type 1 (*see FIG.2*) represents a stainless steel tube in outer diameter 7 mm, wall thickness 0.35 mm and length 600 mm, filled on the length 500 mm by an powdered uranium dioxide UO_2 density 5.25 g/cm^3, with stainless steel caps in the length 60 mm. The common length of fuel rod is 620 mm. The core of fuel rod consists of UO_2 with average enrichment 36.3 %. Average weight UO_2 of fuel rod is 81.88 g. The mass of uranium-235 in the fuel rod 26.08 g. Clad and caps of fuel rods were made from stainless steel.

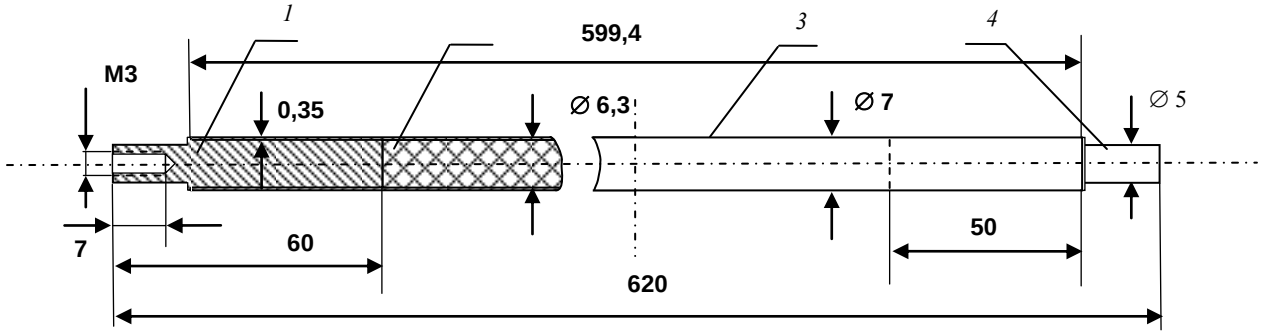

FIG. 2. Fuel rod type 1:
1 – upper plug; 2 – fuel core; 3 – cladding; 4 – lower plug

The fuel rod type 2 (*see FIG.3*) consists of a fuel core, cladding, two fixing devices, a spring and end parts, i.e., the upper and the lower plugs. The fuel rod cladding is made from stainless steel with the outer diameter 6.2 mm and the wall thickness 0.4 mm. The fuel core consists of tablets with the diameter 5.2-5.3 mm and the height 5-7 mm, made from uranium dioxide density 10.2 g/cm^3. The uranium-235 enrichment is 21.2 %. The total height of the core is 500 mm. Average weight UO_2 of fuel rod is 109.83 g. The mass of uranium-235 in the fuel rod is 20.47 g. The total length of the fuel rod is 651 mm. The fuel rod cladding has a 0.55-mm stainless steel wire coiled around the shell with the 100 mm pitch.

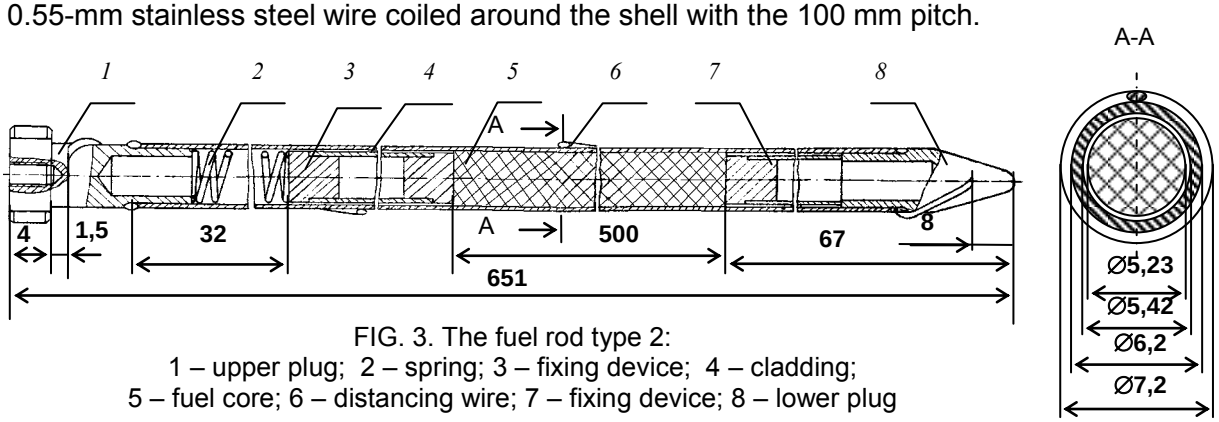

FIG. 3. The fuel rod type 2:
1 – upper plug; 2 – spring; 3 – fixing device; 4 – cladding;
5 – fuel core; 6 – distancing wire; 7 – fixing device; 8 – lower plug

The reactor core of the critical assemblies included 12 channels of control rods; six of them were located at the 119 mm radius (the inner zone) and six on the 206 mm radius (the outer zone). The control rod channel was a stainless steel tube, with the diameter 42 mm, 3 mm wall and the length 1350 mm. The control rod channels housed 2 rods of critical emergency protection (the inner zone), 2 rods of manual regulation (the outer zone) and 8 reactivity compensation rods (4 in the inner zone and 4 in the outer zone). The absorbing part of the emergency protection rods (configurations 1 and 2) was a stainless steel tube, 30 mm in diameter and 1 mm wall, filled with 1.4 g/cm^3 boron carbide B_4C for the length of 500 mm. The emergency protection rods (configurations 3 and 4), regulation rods and the reactivity

compensation rods comprised absorbing and dissipating links. The upper absorbing link represented two concentric tubes, with 33x1.0 and 17x0.5 mm diameters, respectively; the gap between them was filled with europium oxide Eu_2O_3 with the fill density of, at least, 5.3 g/cm^3 for the length of 400 mm. The inner tube, 17x0.5 mm, was filled with aluminum oxide Al_2O_3 with the density of 2.1 g/cm^3. The lower dissipating link represented a stainless steel tube, 33x1.0 mm, filled with the powdered Al_2O_3 with the density of 2.1 g/cm^3. When removed, the absorbing part of the rods was outside the reactor core and the dissipating part in the core.

4. Neutron physical parameters of the critical assemblies

Figures 4 – 7 represent loading charts of uranium-zirconium hydride critical assemblies.

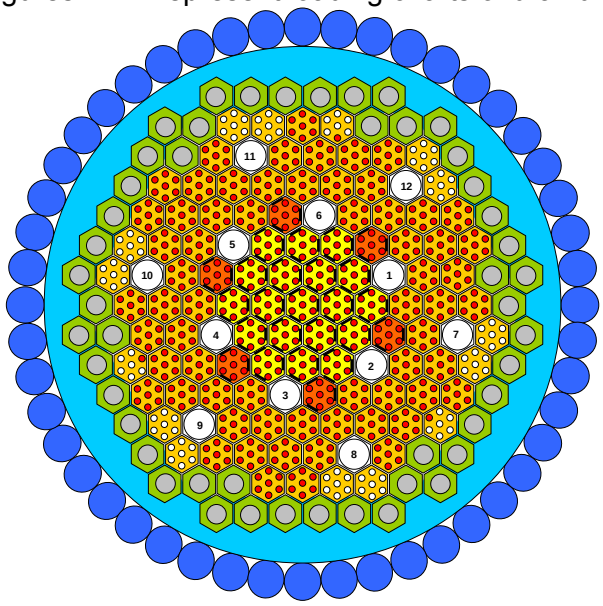

FIG. 4. Loading chart of the critical assembly configuration 1

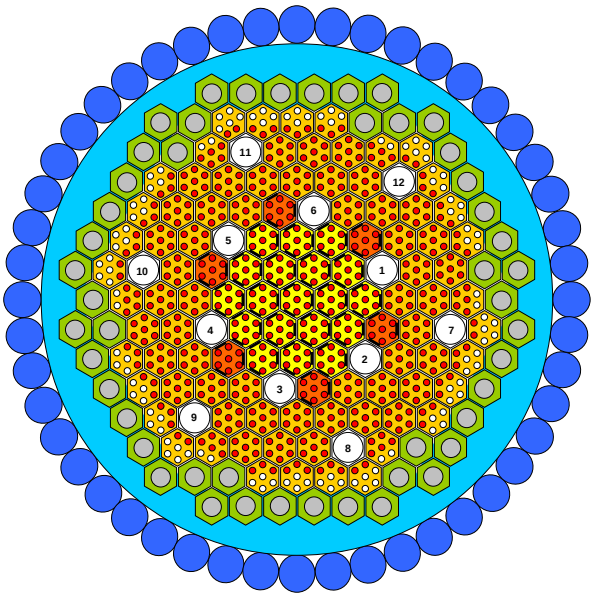

FIG. 5. Loading chart of the critical assembly configuration 2

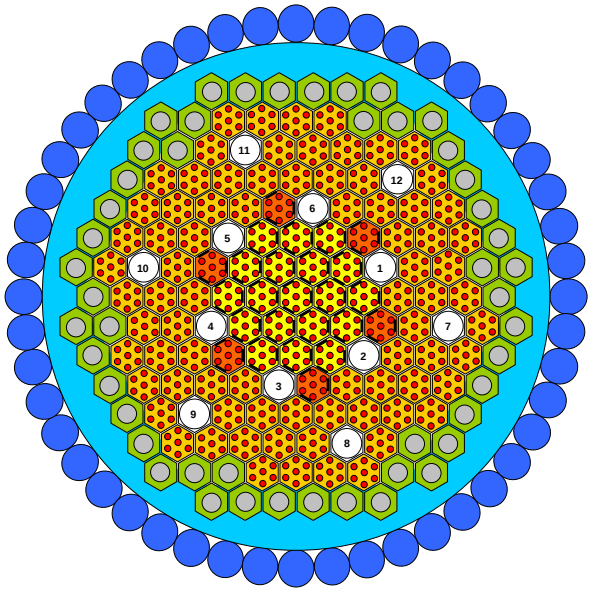

FIG. 6. Loading chart of the critical assembly configuration 3

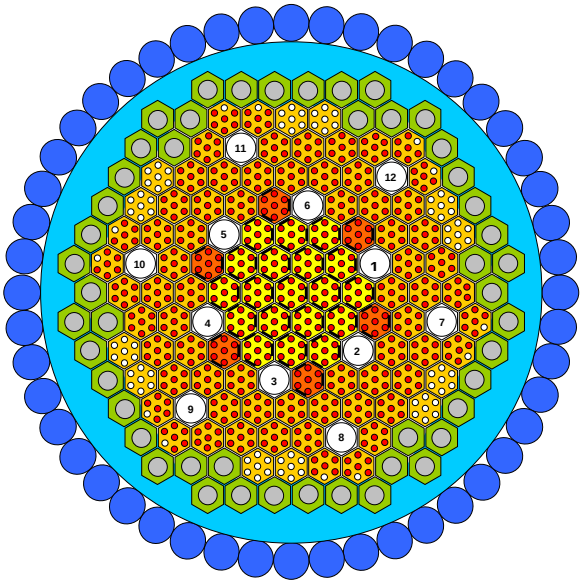

FIG. 7. Loading chart of the critical assembly configuration 4

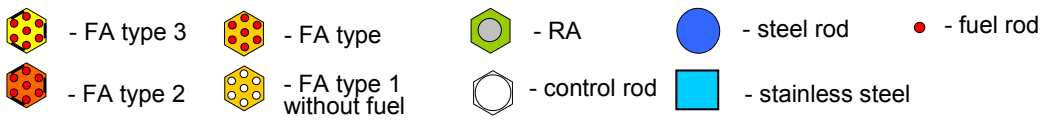

The reactivity of the critical assemblies are measured by the experimental unit “Reactivity Meter”, using the inverse kinetics method [1, 2]. In order to exclude spatial effects of reactivity, the measurements were made using six ionization chambers, arranged at every 60° behind the side reflector of the critical assembly. In addition, in order to compare the obtained results, the supercriticality of the critical assemblies was measured sometimes by the asymptotic period method, while the subcriticality by the methods of the source multiplication and analysis of neutron fluctuations in the frequency region. Also, the power ratio in critical states before and after a reactivity perturbation method was used to measure the efficiency of control rods [3]. The experimental results, obtained by these methods, coincided within measurement errors with the results obtained by the method of reverse solution of the kinetics equation.

The margin reactivity of the critical assembly configuration 3 was defined by the methods: matrix, single rod, unloading, and balance (the short description of used methods is resulted in paper [4]). The mean margin reactivity value for this critical assembly configuration was 4.9±0.3 β_{eff} (defined with due account for measurements errors of each method).

In order to justify the use of the matrix and single rod methods for determining the margin reactivity of critical assembly configuration 3 on critical assembly configuration 4, these methods were used to determine the efficiency of the groups of 8 control rods (8.5±0.5 β_{eff}) and compare with the results of direct measurement of this efficiency by the inverse kinetics method (8.4±0.5 β_{eff}). The obtained results coincided within measurement errors, justifying the use of such methods for margin reactivity measurement.

The experimental data are presented in Tables 1-4. Total (systematic and statistical) error of experimental results are given for the confidence probability 0,68.

Depth of immersion control rods in core, mm												Reactivity, β_{eff}
1	**2**	**3**	**4**	**5**	**6**	**7**	**8**	**9**	**10**	**11**	**12**	
0	0	0	0	0	0	0	0	0	0	0	0	0.18±0.01
0	0	0	0	0	0	0	0	0	0	0	156	0
0	0	0	0	0	0	0	0	156	0	0	0	0
0	0	0	0	0	0	0	0	400	0	0	156	-0.63±0.02
0	0	0	0	0	0	0	0	156	0	0	400	-0.63±0.02
0	400	0	0	0	0	0	0	156	0	0	0	-1.60±0.05
0	0	0	0	400	0	0	0	156	0	0	0	-1.60±0.05
0	400	0	0	400	0	0	0	156	0	0	0	-3.4±0.2
0	400	0	0	400	0	0	0	400	0	0	400	-4.4±0.2
0	400	490	0	400	490	0	0	400	0	0	400	-7.7±0.4

Tab 1. Results of measurement of reactivity of configuration 1 of critical assembly at various position control rods

Depth of immersion control rods in core, mm												Reactivity, β_{eff}
1	**2**	**3**	**4**	**5**	**6**	**7**	**8**	**9**	**10**	**11**	**12**	
0	0	0	0	0	0	0	0	0	0	0	0	0.14±0.01
0	0	0	0	0	0	0	0	0	0	0	141	0
0	0	0	0	0	0	0	0	136	0	0	0	0
0	76	0	0	0	0	0	0	0	0	0	0	0
0	0	0	0	0	0	0	0	400	0	0	141	-0.65±0.02
0	0	0	0	0	0	0	0	136	0	0	400	-0.65±0.02
0	400	0	0	0	0	0	0	136	0	0	0	-1.62±0.03
0	0	0	0	400	0	0	0	136	0	0	0	-1.61±0.03
0	0	0	400	0	0	0	0	136	0	0	0	-1.58±0.03
0	0	0	0	0	0	400	400	400	400	400	400	-4.0±0.2
400	400	490	400	400	490	0	0	0	0	0	0	-9.3±0.5
400	400	490	400	400	490	400	400	400	400	400	400	-14.0±0.7

Tab 2. Results of measurement of reactivity of configuration 2 of critical assembly at various position control rods

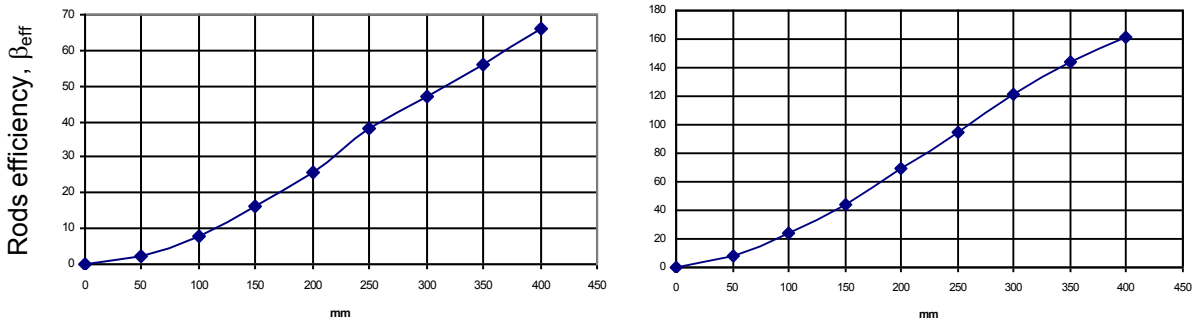

Fig 8. The dependence of the control rods efficiency on the depth of immersion for configuration 2 (on the left picture – control rod №12; on the right – control rod №5)

Depth of immersion control rods in core, mm												Reactivity, β_{eff}
1	**2**	**3**	**4**	**5**	**6**	**7**	**8**	**9**	**10**	**11**	**12**	
400	0	0	400	0	0	0	400	239	0	400	0	0
400	0	0	0	0	0	400	400	202	400	400	0	0
400	0	0	400	0	0	0	400	239	0	400	400	-0.78±0.02
400	0	0	400	400	0	0	400	239	0	400	0	-1.50±0.03
400	0	0	400	0	0	400	400	202	400	400	0	-1.69±0.03
400	400	400	400	400	400	400	400	400	400	400	400	-9.6±0.5

Tab 3. Results of measurement of reactivity of configuration 3 of critical assembly at various position control rods

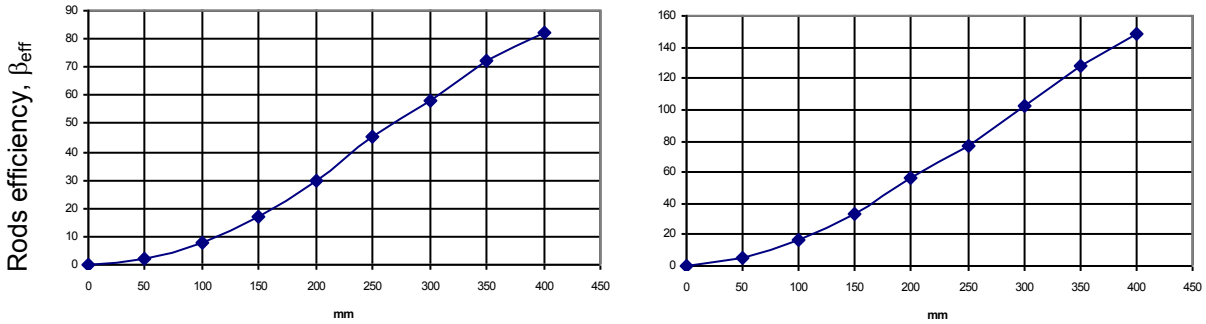

Fig 9. The dependence of the control rods efficiency on the depth of immersion for configuration 3 (on the left picture – control rod №12; on the right – control rod №5)

Depth of immersion control rods in core, mm												Reactivity, β_{eff}
1	**2**	**3**	**4**	**5**	**6**	**7**	**8**	**9**	**10**	**11**	**12**	
0	0	0	0	0	0	0	0	0	0	0	0	0.23±0.01
0	0	0	0	0	0	0	0	0	0	0	172	0
0	0	0	0	90	0	0	0	0	0	0	0	0
0	0	0	0	0	0	0	0	400	0	0	172	-0.70±0.02
0	400	0	0	0	0	0	0	0	0	0	172	-1.65±0.03
0	0	0	400	0	0	0	0	0	0	0	172	-1.64±0.03
400	0	0	400	0	0	400	400	400	400	400	400	-8.1±0.5
400	400	400	400	400	400	400	400	400	400	400	400	-14.9±0.7

Tab 4. Results of measurement of reactivity of configuration 4 of critical assembly at various position control rods

5. Conclusions

The experimental data received at the critical facility "Crystal" on non-uniform multiple zones heterogeneous uranium-zirconium hydride configurations with 21 and 36 % by enrichment on uranium-235 can be used at verification of computer codes by various libraries of the nuclear data.

6. References

[1] Polazau S.A., Sikorin S.N. "Digital reactimeter on the basis of the microcomputer and apparatus «CAMAC»", Proceedings of the Academy of Sciences of Belarus, Power engineering physical series, 1987, № 4, pp. 87-92.

[2] Buznitsky G.I., Golovach A.I., Grinevich F.A., Luk'yanets V.V., Sidoruk N.M., Sikorin S.N. "An analogous meter for measuring nuclear reactor reactivity", Proceedings of the Academy of Sciences of Belarus, Power engineering physical series, 1992, № 1, pp.22-27.

[3] Sikorin S.N., Yaroshevich O.I. "Determination of the Efficiency of Reactor-Regulating Elements by Measuring the Power Ratio in Critical States Before and After a Reactivity Perturbation", Atomic Energy, 1993, v. 74, issue 2, pp.155-157.

[4] Malykhin A.P., Sikorin S.N., Yaroshevich O.I., Levadnyi V.A. "Determination of Physical Reactor Parameters of Transportable NPP at Physical and Power Reactor Start-Up", A Symposium on Nuclear Reactor Surveillance and Diagnostics SMORN VII, 19-23 June, 1995, Avignon, France: Proceedings. Vol.2. — Paris, 1996, pp. 48-56.

THERMAL HYDRAULIC ANALYSIS OF A TYPICAL MULTI-PURPOSE RESEARCH REACTOR

S. K. MOUSAVIAN, M. H. BAHREVAR*, T. KHOSHNEVIS*
Nuclear Science & Technology Research Institute, P.O. Box. 11365-3486, Tehran, Iran
*SURENA Co., Atomic Energy Organization of Iran, Tehran, Iran

ABSTRACT

In this paper, the thermal-hydraulic analysis of a typical 30 MW Multi-Purpose Research Reactor (MPRR) has been carried out using the RELAP5/MOD3 system code to ensure that the fuel and clad temperatures are well within the acceptable limits during steady state normal operation. The PIPE FLOW EXPERT software was applied due to the primary circuit losses for obtaining the pump head and circuit components specifications. While, the core pressure drop calculations are performed using the CAUDVAP code. The thermal-hydraulic parameters such as pressure, temperature and mass flow rate through the core and primary circuit are calculated for the first core of the MPRR. The results show that the maximum fuel meat and clad temperatures of hottest Standard Fuel Element (SFE) are about 125 and 108 ℃, respectively. The clad surface temperature is well below the onset of nucleate boiling (ONB) temperature and the mass flow distribution can meet the cooling requirement of the MPRR reactor core.

1. Introduction

For more than 50 years, research reactors have played an important role in the development of nuclear science and technology. In the recent past, however, the utilization patterns of research reactors have changed remarkably. At present, new and upgraded research reactors are either facilities specialized in education, materials research and radioisotope production, or state of the art machines designed and equipped to carry out cutting edge research involving neutrons [1].

Multi-Purpose research reactors typically operate at higher than 10 MW power levels to provide the higher neutron fluxes to meet the various needs and purposes for which the reactor was planned. The MPRRs with its high neutron flux and irradiation volume will provide the appropriate platform for research and test in reactor fuels, reactor materials and increasing need of radioisotopes for application in the fields of medicine, agriculture and industry.

A typical MPRR is a 30 MW open-pool reactor with low enriched uranium (LEU) fuel assemblies consisting of U_3Si_2 powder dispersed in an aluminum matrix with a maximum uranium density of 4.8 g/cm^3. The reactor core is surrounded by an annular heavy water tank to achieve a high neutron flux and irradiation volume to maximize the number of irradiation positions available for isotope production and material irradiation. Most of the irradiation positions are accommodated in the heavy water reflector tank surrounding the core. The core grid has a 5×5 array configuration with 19 LEU fuel assemblies, 6 in-core irradiation facilities and 8 control rod plates. Reactivity control is performed by control rod plates placed in the core, constituting also the first shutdown system. A heavy water reflector tank performs a diverse and independent shutdown system by means of its drainage. The cooling of the reactor core is promoted by forced

circulation of de-mineralized water in the upward direction. Typical design parameters of the reactor core are given in Tab. 1.

Parameter	Value
Fuel material	U_3Si_2
Enrichment	19.75%
Meat Density, (g/cm^3)	6.5
Uranium density in the meat, (g/cm^3)	4.8
Fuel plate cladding and side wall material	Al-6061
Number of fuel plates	21
Meat thickness, (mm)	0.71
Cladding thickness, (mm)	0.37
Water channel thickness, (mm)	2.35
Meat width, (mm)	62.5
Meat length, (mm)	615
Water channel width, (mm)	67
Fuel Element dimensions, (mm)	80.1×760×1028
Grid plate pitch (cm)	81×77.089
Critical velocity, (m/s)	15.74
Coolant inlet temperature, (˚C)	37.8
Height of water above the top of the core, (m)	10

Tab. 1: Typical design parameters of the reactor core

In this paper, the thermal-hydraulic analysis of a typical MPRR has been carried out using the RELAP5/MOD3 computer code to ensure that the fuel and clad temperatures are well within the acceptable limits during steady state normal operation.

2. Primary cooling system characteristics

The primary cooling system of a typical MPRR is semi-closed and related to the pool water through the upper part of chimney. The primary cooling system removes core fission generated under full load by forced upward circulation of dematerialized water and transfers the heat to the secondary cooling system. The portion of the primary cooling system inside the reactor pool also removes core decay heat by natural upward circulation of the water, when the main pumps are shutdown or fail. After leaving the core in its upward flow, primary cooling system water is collected in the upper chimney and is drawn at design flow rate through a pipe towards the reactor pool boundary. A chimney rises above the core to guide the primary flow to the pump; a closure flow entering the top of the chimney prevents active particles from reaching the surface of the pool. The presence of the chimney also increases natural convection driving force improving cooling during shutdown state. This pipeline leaves the pool and goes through the concrete of the reactor block, to the decay tank. The decay tank provides a delay time to ensure that dissolved N-16 decays before the water exits the concrete shield. The main coolant line leaves the decay tank and enters the pump room area where it splits into two branches with a centrifugal pump and two heat exchangers in each branch. In the flow path of the discharge line to the reactor pool concrete there are two bypass pipelines. Figure 1 shows the schematic view of primary cooling circuit of the typical multi-purpose reactor. There are two parallel heat

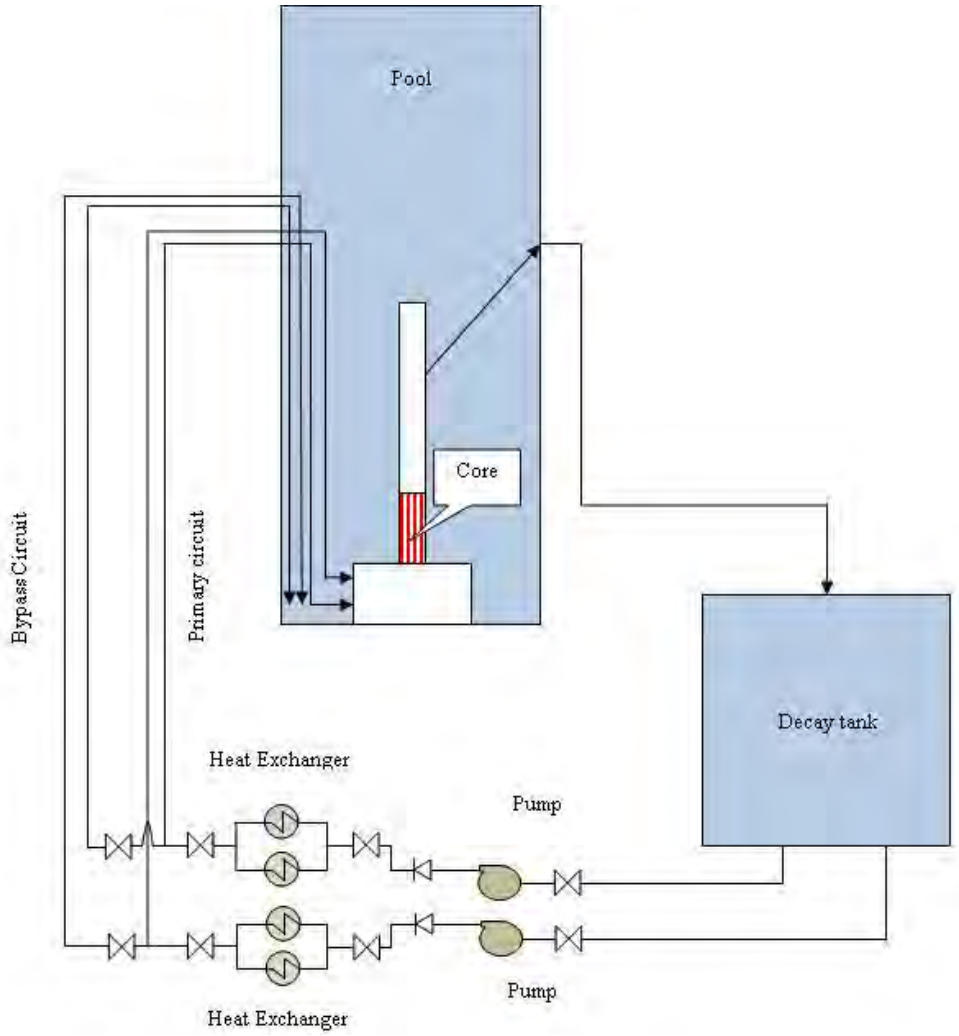
Pool
Core
Bypass Circuit
Primary circuit
Decay tank
Heat Exchanger
Pump
Pump
Heat Exchanger

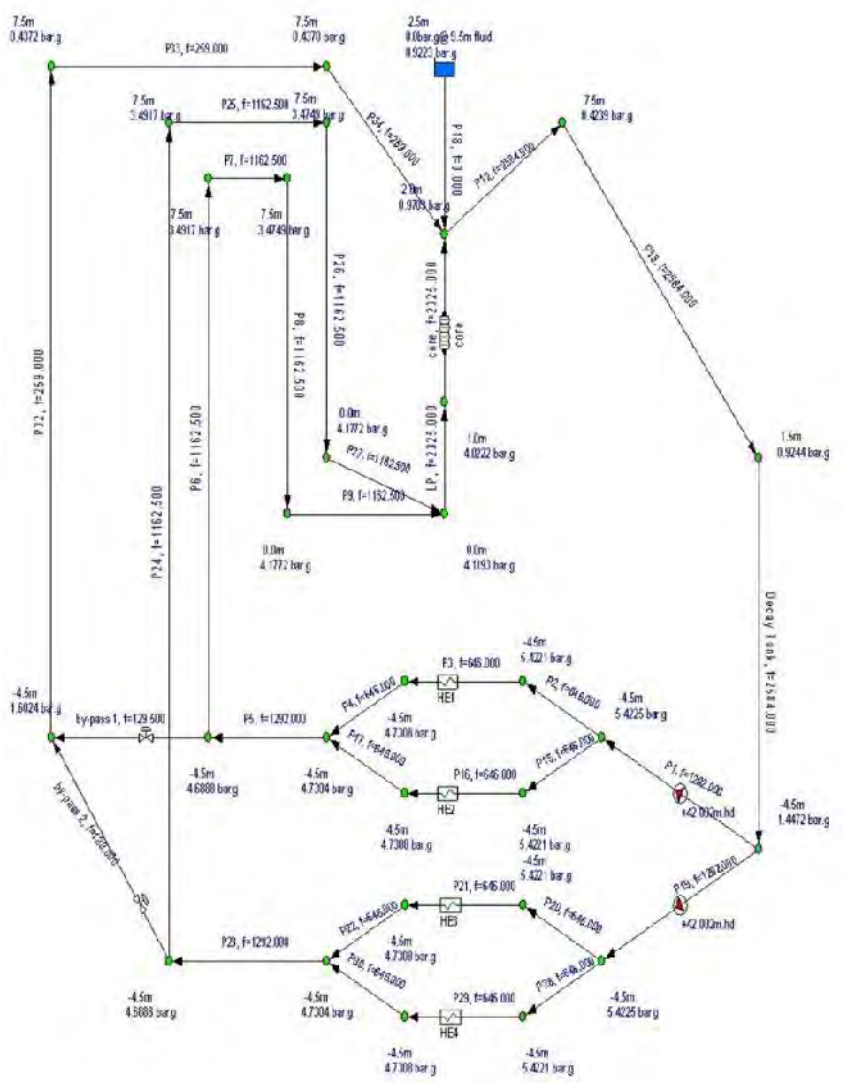

Fig. 2: Hydraulic calculations of primary cooling system

The heat exchangers are designed by Aspen software. According to the initial and boundary conditions, such as inlet and outlet temperatures of the fluid in the primary and secondary sides as well as the maximum allowable pressure drop and the maximum heat removable, the optimized heat exchanger can be determined and proposed by the Aspen. The basic specifications of the primary circuit of a typical MPRR are given in Tab. 2.

Parameter	Value
Total coolant flow rate, (m^3/hr)	2584
Core coolant flow rate, (m^3/hr)	2325
By-pass coolant flow rate, (m^3/hr)	259
Total volume of the decay tank, (m^3)	152
Pool water level, (m)	12
Water level above the core, (m)	10
Pump head (m)	42
Pump power (hp)	201.6
Moment of inertia of pumps (kg.m^2)	5.69

Tab. 2: Basic specifications of a typical MPRR

3. Thermal-hydraulic modeling using the RELAP5

Due to modeling of the primary cooling system RELAP5 computer code is used. All components of a typical multi-purpose reactor have been modeled by tube, branch, valve, pump, junction, and time-dependent volume equivalent components in RELAP5 code [3]. The RELAP5 nodalization of the reactor and primary cooling circuit is shown in Fig.3.
According to the Fig. 3, the core inlet lower plenum was modeled by a branch component (101). The reactor core area was simulated by three components 102, 103, and 104 which represent the average, hot, and core bypass channels, respectively.
The cosine shape of heat flux with a maximum total power peaking factor of 3 was considered in the hot channel (103). The average channel (102) contains 18 standard fuel elements and its power was assumed about 28.42 MW.

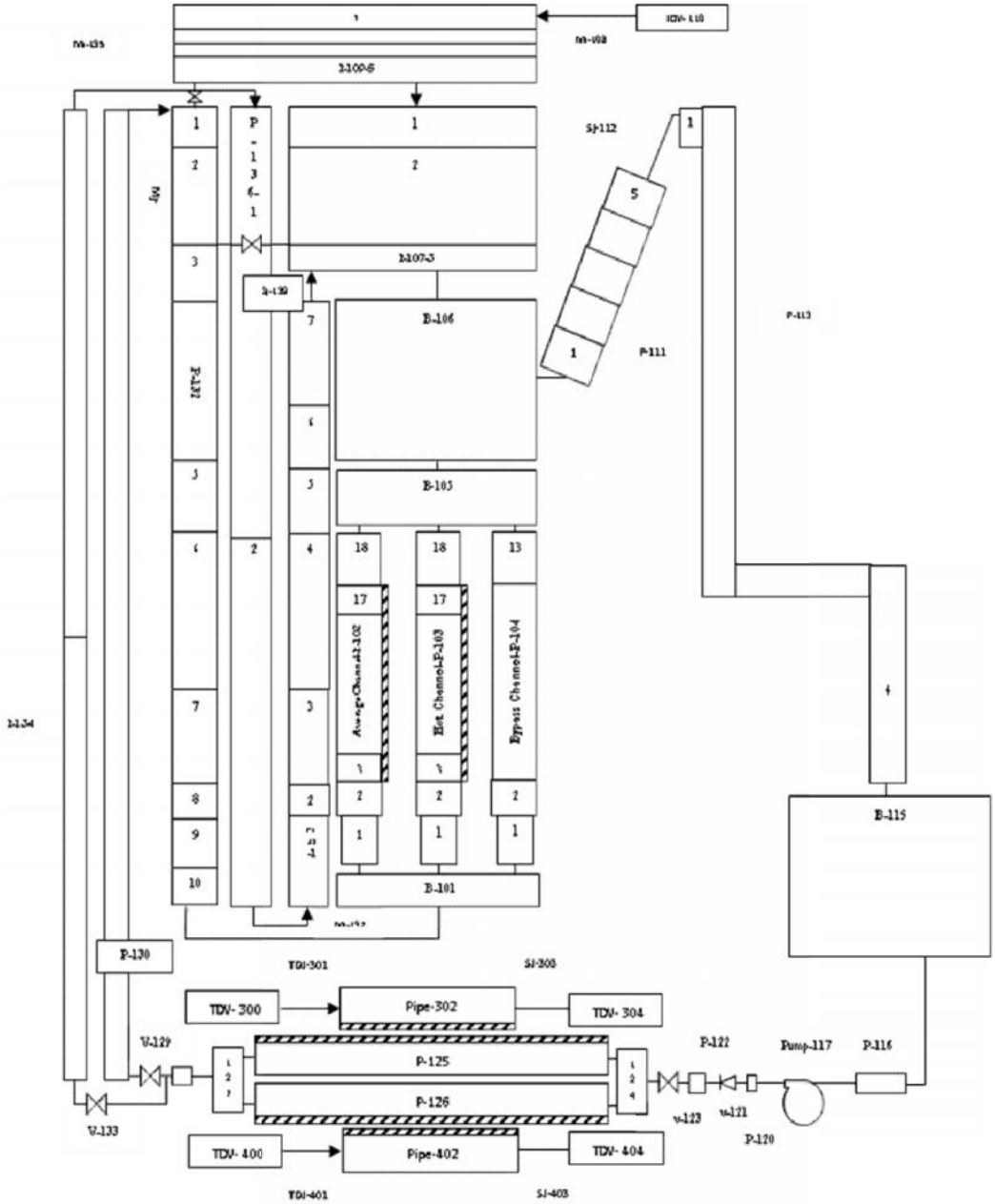

Fig. 3: RELAP5 nodalization of a typical MPRR

Branch component 105 represents the upper plenum of the reactor core, which collects the hot, average, and bypass channels mass flow rates through the core chimney (component 106). The

chimney component has two connections, first connection to the pipe component 111 (reactor nozzle outlet) and the second connection to the pool water (component 107).
The pipe component 113 is a part of the primary circuit pipeline that connects the reactor chamber to the decay tank (115). Decay tank component outlet is divided into two parallel pipelines starting from component 116 and following by primary pump component (117), main heat exchanger component (125), main primary pipeline to the core lower plenum (component 132), and bypass pipeline components (134 and 136). Moreover, pipe components (107, 109, and 138) represent the pool water. One of the connections between decay tank outlet and pool water inlet was shown in the RELAP5 nodalization.

4. Results and discussion

By gathering all of the components data and preparing the input file, RELAP5/MOD3.2 code at the following conditions was run:

- Normal operation at 30 MW,
- Taking into account 2% core bypass mass flow rate, and
- Assuming about 10% downward flow of pool water to the core chimney.

Figure 4 shows the mass flow rate distributions at different reactor core channels, chimney inlet, and total primary cooling circuit. It predicts that the mass flow rate through the average channel, hot channel, and core bypass are about 600, 33 and 13 Kg/s, respectively. Meantime, by considering the intake mass flow rate of the pool (about 72 Kg/s), by the chimney with a negative value indicates downward direction. Consequently, total primary coolant circuit mass flow rate of 718 kg/s can be obtained.
The coolant velocity distribution through the core channels and chimney is shown in Fig. 5. It describes that the fluid velocity in the channels between the fuel plates in hot and average channel is about 10 m/s.

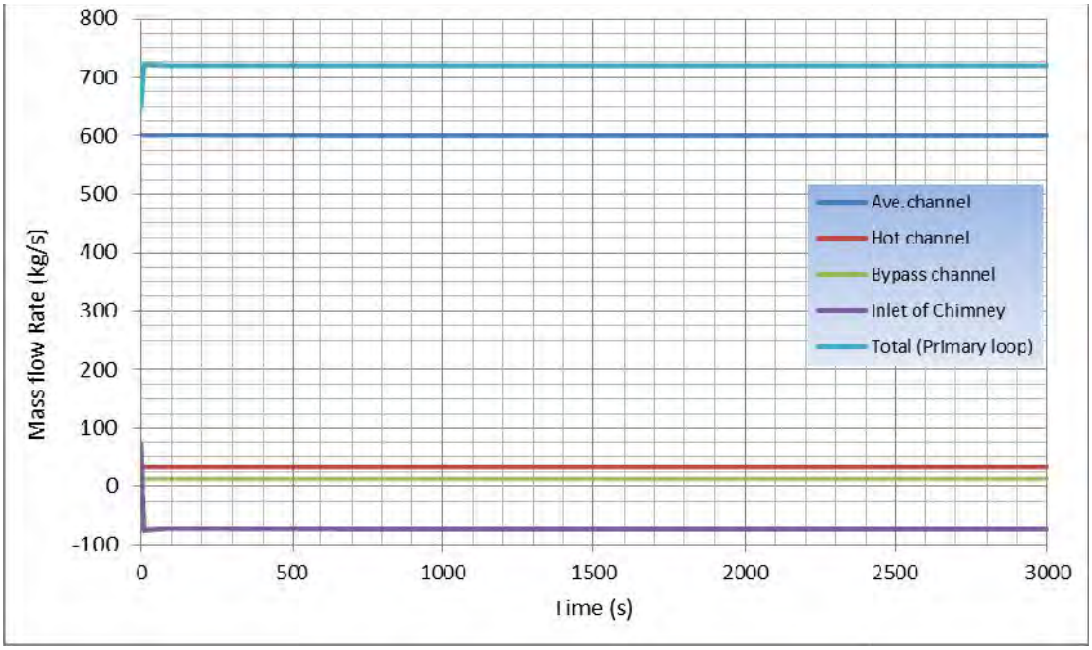

Fig. 4: Mass flow rate distribution in various components

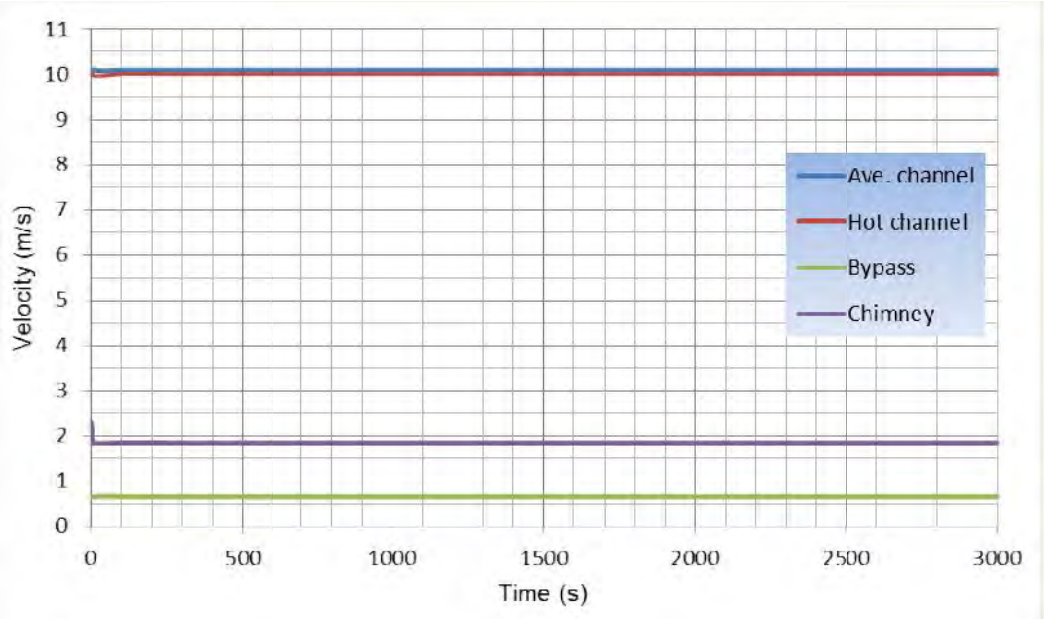

Fig. 5: Fluid velocity distribution in different parts of the MPRR

Figure 6 shows the fuel center-line, cladding surface, and coolant temperatures along the fuel height in the hot channel. According to Fig. 6, the maximum fuel meat and cladding surface temperatures reach to about 125 ^{0}C and 108 ^{0}C, respectively. Moreover, the coolant outlet temperature is about 60 ^{0}C at steady state conditions.

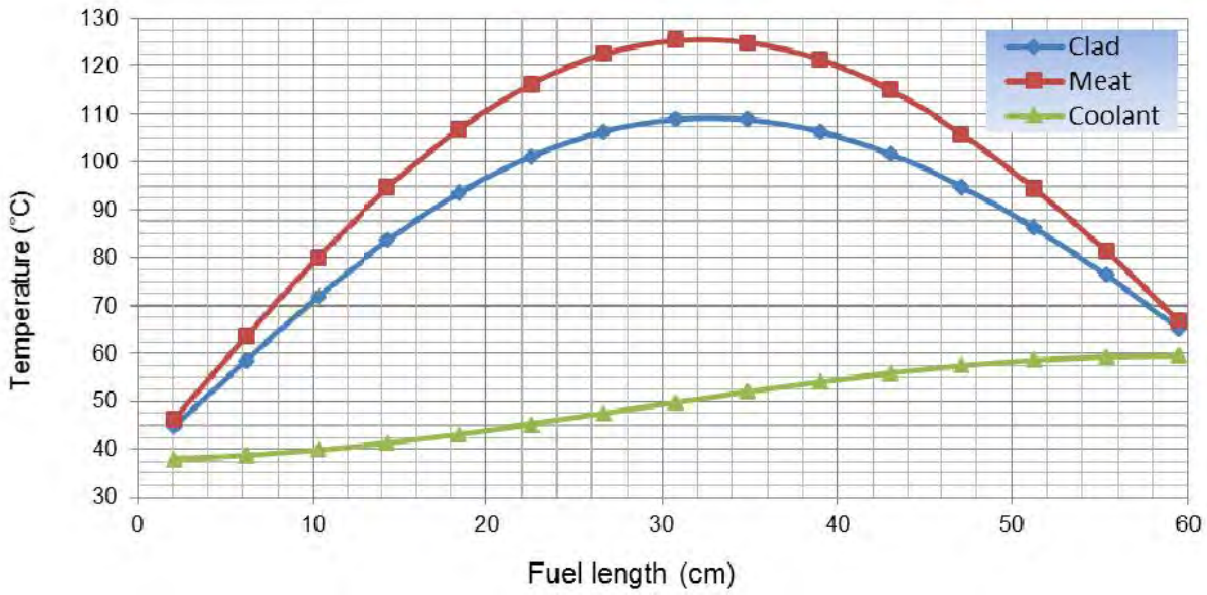

Fig. 6: Fuel center-line, cladding surface, and coolant temperatures distribution (hot channel)

The coolant pressure distribution in the reactor chamber at inlet and outlet is shown in Fig. 7. It presents that the coolant pressure at the bottom of the reactor core (lower plenum) is about 4.6 bar and its pressure at the core outlet (chimney) was reached to 1.8 bar (It is equal to the static pressure of water column above the core.). As a result, the pressure difference between core inlet and outlet is about 1.8 bar which is similar to that of CAUDVAP results.

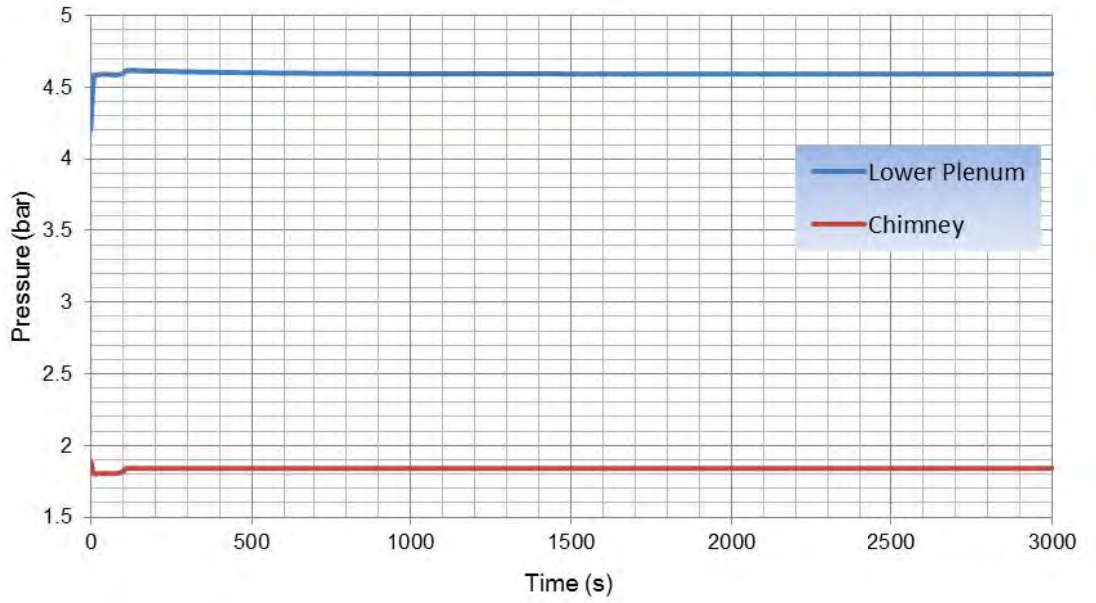

Fig. 7: Coolant pressure distribution in the reactor chamber

Figure 8 shows the pump head changes during normal operation and steady state conditions at 358.8 kg/s. It shows that the pump head after 3000 seconds was reached to the steady state conditions and its about 41 meters.

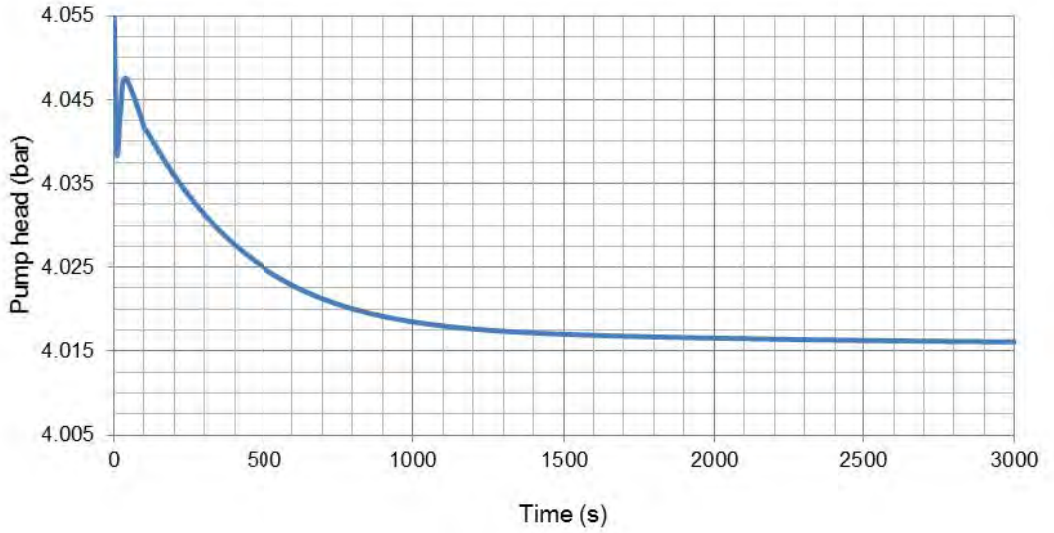

Fig. 8: Pump head

5. References

1. IAEA .(2007) .*Utilization Related Design Features of a Research Reactor,TECDOC-455* . Austria.
2. Abbate, P. (2003). *A computer program for flow distribution and pressure drop calculation in a MTR type core CAUDVAP MODE 3.60.* INVAP S. E.
3. Group, T .(1999) .*RELAP5/MOD3 Code Manual* .Idaho: SCIENTECH, Inc. Rockville, Maryland Idaho Falls.

Poster utilisation

JULES HOROWITZ REACTOR, FRANCE. DEVELOPMENT OF AN EXPERIMENTAL LOOP INTEGRATING AN OPTIMIZED IRRADIATION PROCESS.

S.GAILLOT (a), L.DIAZ (a), T.DOUSSON (b), N.WAECKEL (c), S.GAY (a), S.VITRY (a) & F.DELASSALLE (a)

(a) CEA, DEN, DTN, Nuclear Technology Department
DTN/STCP/LCIT, building 204, CEA CADARACHE
F-13108 Saint-Paul-lez-Durance, FRANCE
Stephane.gaillot@cea.fr,
Laurent.diaz@cea.fr

(b) CEA, DEN, DER, Reactor Studies Department
DER/SRJH/LEDI, building 1222, CEA CADARACHE
F-13108 Saint-Paul-lez-Durance, FRANCE
Thierry.dousson@cea.fr

(c) EDF, SEPTEN
avenue A. Dutrievoz,
69100, VILLEURBANNE, FRANCE
Nicolas.Waeckel@edf.fr

ABSTRACT

Experimental reactors enable researchers to address industry and scientific organization's needs, by providing support to the existing nuclear reactors (Gen.2), by preparing the future generations of reactors (Gen.3, Gen.4) or by supporting fusion related issues and medical applications. It is for this specific purpose that the Jules Horowitz Polyvalent Irradiation Reactor (JHR) is under construction at the CEA Cadarache Research Center (located South of France). This Material Testing Reactor (MTR type) is designed to irradiate materials or fuel samples to conduct various types of experimental tests. The reactor will also produce Mo99 radioelements that will supply 25% to 50% of current European needs.

The purpose of this paper is to describe a new fuel irradiation loop, called ADELINE[1], specifically dedicated to study fuel rod behavior under power ramp transients. The design of the instrumented loop is still ongoing but the test device will be fully operational when JHR will start. ADELINE loop is planned to perform various types of power ramps, from slow to high ramp rates, from low to very high power changes, on different types of fuel concepts such as regular fuel, PCI resistant fuel, Enhanced Accident Tolerant fuel concepts, etc…). The main feature of the test device is to provide the industry with well characterized ramps tests allowing defining reliable SCC-PCI (Stress Corrosion Cracking-Pellet Cladding Interaction) failure thresholds.

In order to increase its irradiation capacity (2 to 3 power ramps per JHR cycle), each phase of the experimental procedure has been carefully optimized: for instance, non-destructive examinations are performed before and after the test in JHR hot cells, specific loading tools have been designed to facilitate the handling phases or reliable test protocols have been qualified on a similar test device (like the one used in OSIRIS). The objective is to fulfill all the customers' needs, in a high quality experimental environment.

Key Words: ***Material Testing Reactor, Fuel irradiation loop, ADELINE, optimized irradiation process & design.***

[1] Advanced Device for Experimenting up to Limits Irradiated Nuclear fuel Elements.

1. REMINDER OF THE CONTEXT :

In the European research area, most irradiation reactors built in the 1960's are reaching their end of life (after 50 years of operation) and the question of replacing them is now under discussion. The conditions of their renewal depend on several parameters:
- needs for nuclear programs (support needed for the existing nuclear infrastructure, preparation for the future),
- needs concerning the production of radioelements for medicine (typically Mo99,…),
- needs in the field of education (maintaining the competence of specialized staff and the preparation of future generations).

The construction of a new research facility is decided by analyzing the needs that exist between different contributing countries that destined to share the tool and the investment. In the case of the JHR, the proposed facility corresponds to a material testing reactor type (MTR) designed to meet the needs of the various project partners in the best possible manner.

The JHR is an experimental platform open to the international community.

The JHR Project Consortium, created on March 19th 2007, involves the participation of several European countries and institutions including the CEA, EDF, AREVA (France), CIEMAT (Spain), the UK, VTT (Finland), Studsvik (Sweden), SCK-CEN (Belgium), UJV (Czech Republic) as well as other international representations such as DAE (India), IAEC (Israel) and JAEA (Japan).Today, the consortium is made up of 11 countries.
The contribution of the consortium members varies in nature. It may involve direct procurement of a component for the facility (circulating pumps, heat exchangers, hot cells and non-destructive examination systems) while other members contribute to the direct financing of the project. For the use of the facility, the consortium members can decide on the realization of joint experimental programs or they may carry out their own programs.

Fig.1: Overview of the JHR facility (v11.15)

2. THE JHR FACILITY:

2.1. Main performances & characteristics.

The core of the reactor consists of a compact cylindrical part (d = 60 cm, h = 60 cm) surrounded by a Beryllium annulus reflector (l = 30 cm). The core is under moderated allowing the production of high fast neutrons fluxes (typically 3.10^{14}n.cm^{-2}.s^{-1} at 100MWth). The reactor is designed for a thermal power of 100 MWth and is cooled with light water. Two operating working modes are planned, 70 & 100 MWth. Power evacuation is obtained by ascending water circulation in a closed primary circuit which is slightly pressurized (10b). The reactor is designed to handle up to 10 irradiation experiments in the core and up to 10 in the reflector in fixed position or on displacement systems permitting the adjustment of the neutron flux during the experiment (this is accomplished by moving the device either closer or farther away from the core).

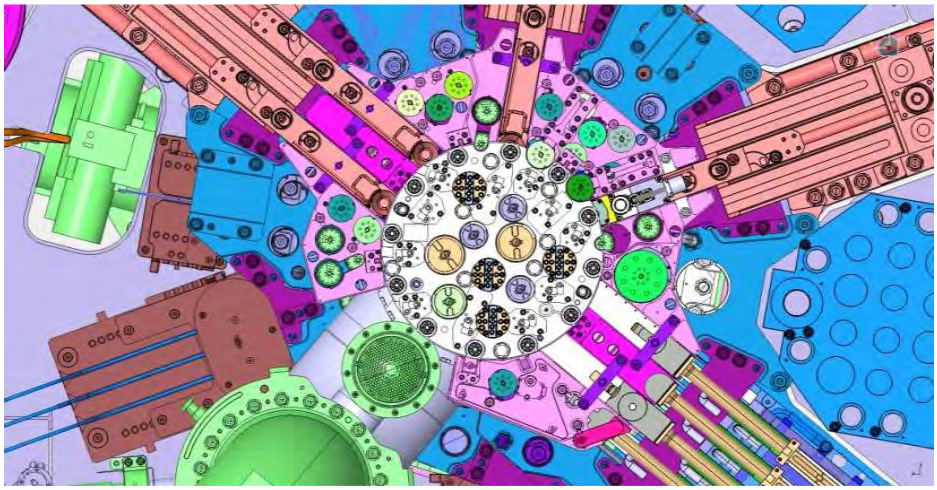

Fig.2: Upper view of the JHR core & reflector (CEA).

Main characteristics of the first core are given hereafter:

- fuel: 36 U_3SI_2 fuel assemblies, annular shape, 60 cm in length, 27 % U_5 enrichment,
- 27 neutron absorbers,
- light water moderator,
- 70 to 100 MWth thermal power,
- 25 to 30 days per cycle.

2.2. JHR allowing the integration of the entire experimental process.

The facility is made up of an infrastructure in two parts; the first being the BUR building which contains the reactor pool, the core and the area devoted to carrying out experiments. The second part of the installation concerns the BUA building which ensures the operation of all nuclear auxiliary equipment connected to the BUR. The transfers are performed by an underwater channel between the two buildings. The BUA also contains all the operational support means for irradiation processes (storage pools, hot cells, materials, fuels, radio-isotopes, the “alpha” cell, non-destructive examination cells and other utilities) [1].

2.3 . JHR schedule.

This mainly concerns the building site, equipment manufacturing, controls & start-up and divergence. The civil engineering is almost finished and should be complete by the end of this year. At the same time, the major internal equipment's are either still under study or are in the course of manufacturing. Complete installation of these equipment's in the building is in preparation.

2.4 . Startup of the JHR irradiation experiments.

After the divergence phase of the reactor, the startup phase of the experimental equipment is planned over a one trial period spanning 12 to 18 months. Once this stage is reached, the experimental loops will be operational and ready to meet the needs of future customers.

3. THE JHR IRRADIATION LOOP FOR FUEL POWER RAMPS TESTS :

3.1. Main features.

The ADELINE loop, now under study, is an experimental irradiation loop dedicated to rod irradiation functioning under LWR conditions (cf.fig.3) :
This fuel irradiation loop is composed of an in-core part located in the reactor pool and of another part located in the operation zone of the experiments (BUR, CEDE).
The in-core part includes the irradiation device equipped with a rod, the underwater lines and the fluid & electrical connections through the experimental penetrations of the pool. The other part is made up of the fluid circuit, a tight bunker and connection of the circuit with the utilities of the JHR facility. The fluid circuit is equipped with circulating pumps and pressurization systems, making it possible to obtain the circulation of water cooling towards the device and to reach the required thermal-hydraulic conditions at the bottom of the test channel (155b, 270℃, 200g/s).Th e experimental loop under study also takes into account the feedback of this kind of loop much like the ISABELLE irradiation loop which was used on the OSIRIS irradiation reactor located in SACLAY (France).

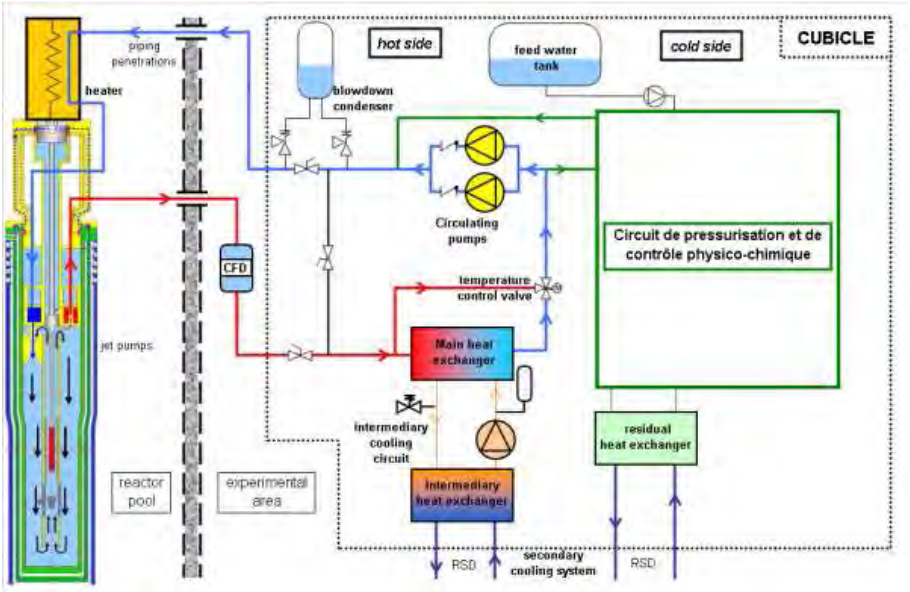

Fig.3: Simplified drawing of the ADELINE loop (CEA).

4. ANTICIPATED PERFORMANCES OF THE LOOP:

4.1 Standard TH characteristics, power levels, duration description.

The physical parameters around the rod correspond to the following PWR conditions: 155b, 320℃ with a fluid flow of 0.2kg/s and 73b, 2 80℃ for BWR conditions.
The experimental rod is composed of a UO_2 or MOx type, either irradiated or not.
The standard profile of power during the test is described hereafter:

- conditioning phase with low power (100W.cm^{-1}) ranging from a few hours to a few days,
- power ramp test with kinetics going up to 700W.cm^{-1}.min^{-1},
- power aimed at the high level of 620W.cm^{-1}+/-10W.cm^{-1} for one maximum duration of 24h,
- withdrawal of the device according to the power decrease scenario.

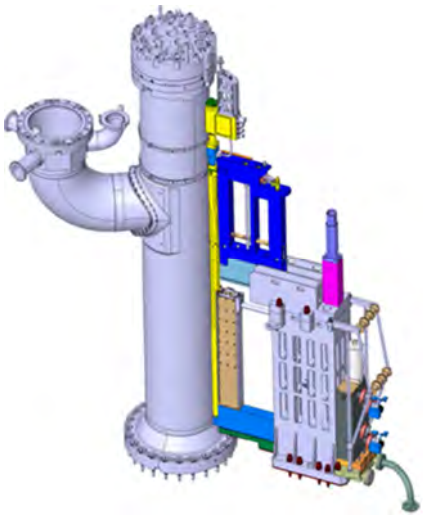

Fig.4 : JHR primary circuit & displacement system (SAD)

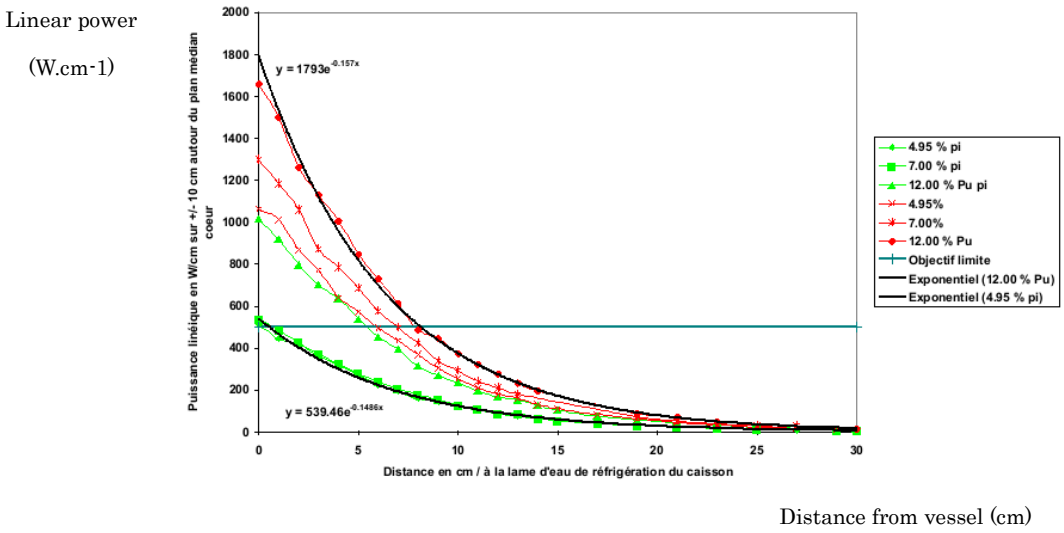

Fig.5: Example of power evolution versus SAD displacement and fuel enrichment (analytic calculations).

4.2 Two types of sample holders are planned in order to offer irradiation flexibility.

The experimental rod is fixed on a sample holder, metallic structure, which offers an axial and radial rod position during irradiation (cf. fig.6). The head of the sample holder is used as a tight closure of the device. The simplified experimental configuration permits the quick change of the rod in the underwater transfer system and makes it possible to increase the rate of the tests. For this configuration, the rod can be equipped with lengthening sensors at its ends (of LVDT type) enabling us to measure its elongation during the test. According to the objective of the test, the rod may also be more instrumented (fuel, clad temperature measurements, deformation).
This embedded instrumentation can characterize the consequences of the irradiation on the rod more precisely. Note that this instrumentation, placed on the sample holder is consumable.

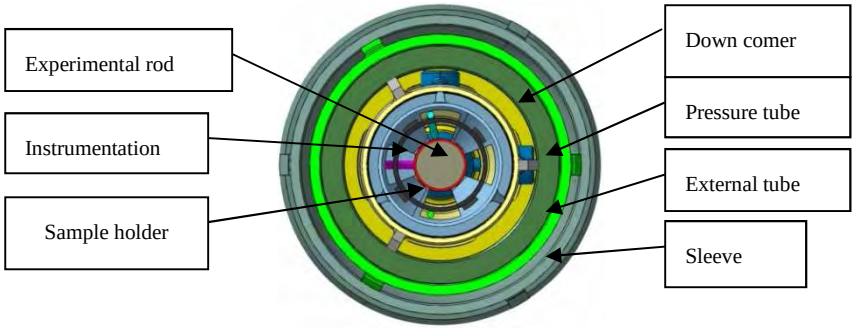

Fig. 6: Cross section view of the device with the sample holder

(CEA - preliminary design)

4.3 Device instrumentation (PI) for following the TH conditions of the device.

In order to measure the thermal hydraulic parameters of the test channel, the instrumentation holder part (PI) is equipped with various sensors (thermocouples upstream & downstream for the heat balance, flow meter (Vcone type). This instrumentation, installed on the device, is re-usable.

4.4 Pressure tube and Zy sleeve (neutron screen, probe holder and mechanical protection).

The pressure tube of the device is designed and calculated according RCC-MRX rules in order to satisfy the criteria of the different identified working conditions. The pressure tube is made of Zircaloy to optimize the thermal neutron flux on the rod.
The sleeve, surrounding the pressure tube, is designed to cool it (downward circulation of pool water between the pressure tube and the sleeve). It is also equipped with SPND[2] making it possible to measure nuclear flux during the power ramp. The sleeve has also a screen role in order to limit the gamma flux on the device. Last but not least, it also has a mechanical protection function.

[2] SPND : Self Powered Neutron Detector

5. OPTIMIZED DESIGN & INNOVATION :

5.1. Hydraulic amplification system of the in-core part: jet pumps permitting flow reduction on the cooling circuit.

In order to reduce the water flows of the ground part, an amplification flow system is implemented in the upper part of the device. Composed of an injector-conduit system, it allows entrainment of the water contained in the device by a high pressure injection of flow coming from the cooling circuit. This system can amplify the flow in the device by a factor of 4 to 5.

5.2. Adaptation of the head of the device to guarantee the tight transfer between two cycles of irradiation.

In order to accomplish an increase in the rate of tests that can be conducted through the use of the PTE (cf.fig.7), the head of the device is designed to adapt to a leak tight transfer door. To guarantee successful operation during the interface, the device and the bottom part of the PTE are both equipped with leak tight systems.

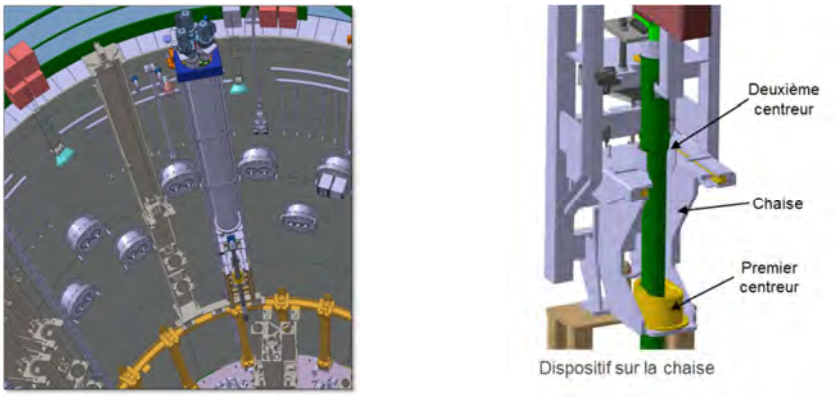

Fig. 7: Overview of the Underwater Transfer System (PTE)

5.3. On-line transmitter of clad swelling integrating a fiber optic (cf.fig.8) & [3].

During the irradiation phase, the experimental rod can be subjected to various stresses: swelling, elongation, wear. For the purpose of following these phenomena, innovating instrumentation is now being studied. One of these R&D actions involves the use of an optical-mechanics sensor permitting the on-line deformation measurement of the rod. This low-size sensor integrates an optical module, in a pressurized and deformable tight enclosure making it possible to follow rod deformation. The range of the sensor is from 0 to 1.5mm with a precision of 10 microns. The effective range of expected rod deformation during the test varies from about 0 to 0.5mm.

Fig. 8: Optical module of the sensor inserted in a body with a piston simulating the feeler piece (CEA, R&D).

6. ENGINEERING PROCESS OVERVIEW :

6.1 Introduction.

Adapted processes are applied to take into account the specific features of the device. These processes are of an iterative nature and concern various fields:
- the experimentation field characterizing the external customers' requirements which concern the neutron and thermal hydraulics performances. This input data is considered in terms of device design (capsule, loop), location in the reactor (in-core or in the reflector), pre-selection of the materials and instrumentation definition (on the device and on the loop),
- the licensing of the cell which involves defining the safety options and the requirements that the equipment must satisfy in terms of regulation,
- the operation staff defining the constraints related to the implementation and use of the equipment in the facility during the various work phases (in particular, definition of the handling tools, storage equipment),
- the engineering field where qualified personnel are in charge of the technological issues involving the equipment, the thermo-mechanical dimensioning of the components, the qualification of the critical components, the industrialization, the manufacturing controls (fabrication and assembling phases) and the start-up on site.

This process of studies, manufacturing and start-up for a new experiment requires a long time (several years) and it involves all the actors working in or around the reactor.

6.2 Safety issues.

Application of the safety report requirements for the facility and the technical guide dedicated to use of the irradiation devices:
- identification of the off-normal scenarios,
- thermal-hydraulic analyses and preliminary safety option definitions,
- identification of requirements concerning the design of the irradiation device (shells, barriers, screens,…).

According to the CEA guide, consequences analyses of various types of scenarios:
- radiological impact following the failure of the device and/or the circuit,
- mechanical impact on the core and on safety systems due to failure of the device,
- neutron effects on the core as a consequence of device removal.

The results of these analyses (based mainly on thermal hydraulics calculations (using CATHARE[3] software)) allow for the definition of a number of safety barriers and protective systems. The conclusions of these analyses define the level of mechanical calculations to be taken into account for the thermo-mechanical studies of the components which fulfill a safety function or play a role in the availability of the facility.

6.3 Regulation and Quality issues

The standards applied are French or European levels (NF, EN).
The quality process complies with the ISO9001 standard and the recent 2012-BNI Order[4] concerning the nuclear pressure containments, the French order ESP(N) is applied. The applicable codification (e.g. N2, cat IV) can result in increased controls during the manufacturing phase (e.g. volume control of the welds), hydraulic tests, periodical inspections (every 40 months) based on visual and non-destructive examinations and pressure requalification tests (every 10 years).

[3] CATHARE: Advanced Safety Code for Pressurized Water Reactors.
[4] Order of 7 February 2012 setting down the general rules pertaining to licensed nuclear facilities

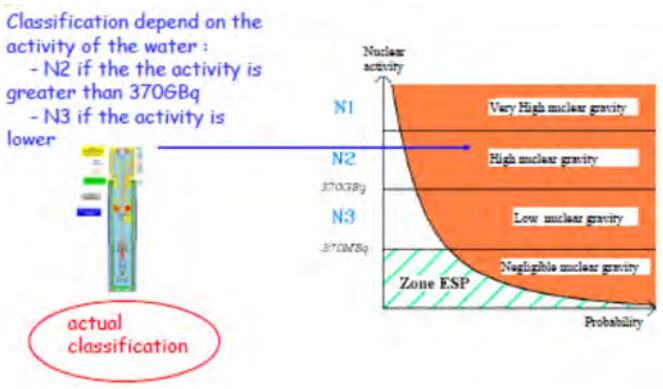

Fig. 9: ESP (N) regulation application (illustration)

6.4 Simulation (hydraulics, thermal, thermo-mechanical)

Once the preliminary data has been established, the thermo-mechanical dimensioning of the structures which have safety functions (barrier) is carried out according to the rules of the RCC-MRX(*) code (v2012) in normal and off-normal conditions. During these studies, the dimensioning criteria are checked.

(*) The RCC-MRX code consists of the technical rules applicable to the design and the construction of the mechanical equipment's on the experimental JHR reactor, its auxiliaries and its irradiation devices.

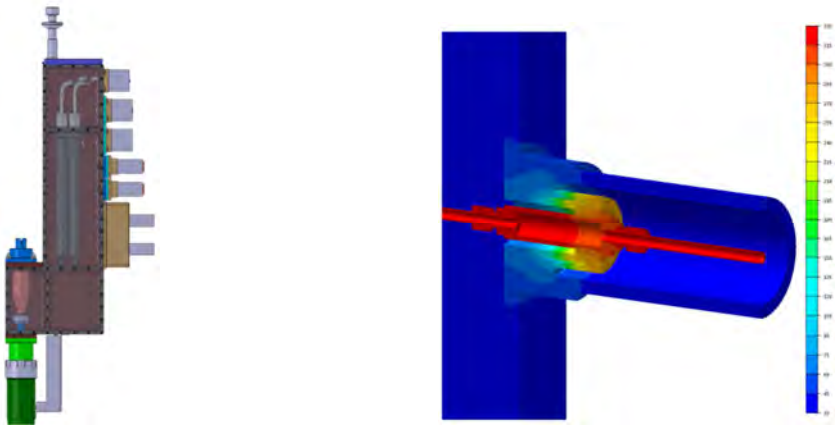

Fig.11: Engineering design & calculations (extracts)

6.5 Qualification support

Technical and technological studies are performed up to the level of a detailed design report. In parallel to this, some items may result in producing a mockup of critical components to confirm the simulation studies or to assess manufacturing issues:

Description	Out-of-pile tests	In-pile tests
Qualification of innovating components (connectors, sensors…)	X	
Behavior test of the sealing joint in normal and off-normal conditions. thermal and pressure tests.	X	
Mockup testing critical aspects of operation process. Cold checking of the kinematics of a sample holder: loading, unloading phases.	X	under water transfer system and/or in the JHR hot cell

Tab. 1: Qualification tests (illustration)

7. CONCLUSION :

The building of the JHR facility is well underway. In parallel, the studies and the manufacturing of the experimental equipment's are in progress. At the startup of the facility, a whole array of devices meeting the principal customers' requirements will be available. In particular, the loop of fuel irradiation called ADELINE functioning in LWR conditions will permit researchers to carry out power ramps tests. The experimental process of this loop has been optimized to increase the number of tests per cycle (use of a specific transfer container called PTE).
The JHR facility will integrate support equipment's (non-destructive examination systems, a storage pool, hot cells) thereby proposing a complete experimental offer to their future customers.

8. REFERENCES :

[1] C.PASCAL & Y.DEMOISY (a), S.GAILLOT, X.BRAVO & F.JAVIER (b)
Jules Horowitz Reactor Experimental Capabilities
TRTR-200-IGORR10, 12-16 Sept. 2005. Gaithersburg. MARYLAND. USA
(a) AREVA TA & NP. F-13000, Aix en Provence, France.
(b) CEA-DEN, Cadarache. F-13108 Saint-Paul-lez-Durance, France.

[2] S.GAILLOT, D.PARRAT, G.LAFFONT, C.GARNIER & C.GONNIER
The ADELINE irradiation loop in the Jules Horowitz MTR: Testing a LWR fuel rod up to the limits with a high quality level experimental process. IGORR 12, CIAE-BEIJING, P.R. CHINA, October 28-30, 2009. CEA-DEN, Cadarache, F-13108 Saint-Paul-lez-Durance, France

[3] S.GAILLOT (a), G.CHEYMOL(b)
Fuel irradiation device. Innovative instrumentation proposal for experimental phenomena real time measurement. IGORR 15 Conference. DAEJON, SOUTH KOREA, October 13-18, 2013
(a) CEA, DEN, DTN, Nuclear Technology Depart., F-13108 Saint-Paul-lez-Durance, France
(b) CEA, DEN, DANS, DPC, Physical & Chemical Depart., F-91191 Gif sur Yvette, France

[4] S.GAILLOT (a), T.DOUSSON (b), S.VITRY (a), S.GAY (a) & C.GARNIER (a)
Fuel irradiation device through Engineering Process description,
RRFM / IGORR12. PRAGUE, CZECH REPUBLIC, March 18th to 22nd, 2012
(a) CEA, DEN, DTN, Nuclear Technology Department
(b) CEA, DEN, DER, Reactors Studies Department
F-13108 Saint-Paul-lez-Durance, France

DEVELOPMENT OF IRRADIATION TARGETS FOR 99Mo PRODUCTION BY NUCLEAR FISSION

M. DURAZZO, G. CONTUBIA, J. A .B. SOUZA, E. F. URANO DE CARVALHO, H. G. RIELLA

Nuclear and Energy Research Institute IPEN-CNEN/SP
Av. Professor Lineu Prestes 2242, 05508-000, São Paulo, SP - Brazil

ABSTRACT

The use of radioisotopes in medicine is certainly one of the most important social uses of nuclear energy. The 99mTc, generated from the 99Mo nuclear decay, is the most suitable radionuclide for single photon emission computed tomography imaging technique. The 99mTc is supplied as 99Mo/99mTc generators, which provide 99mTc as the 99Mo decays. In Brazil, the generators have been imported. Currently, the world's 99Mo supplying depends on the operation of research reactors which are aged around 40 years and, therefore, are not capable of reliable operation. This situation makes the 99Mo production chain particularly vulnerable. Recent crises in the supply of 99Mo has profoundly affected the distribution of 99Mo/99mTc generators in Brazil and encouraged the starting of the RMB - Brazilian Multipurpose Reactor, which has as one of the objectives to make the country independent in the production of radioactive isotopes for medicine. The success of RMB Project will require the manufacturing technology of irradiation targets for the 99Mo production from nuclear fission. As IPEN in its history has been developing fuel for research reactors, and the manufacture of irradiation targets is based on this type of technology, IPEN began developing the technology to fabricate these targets. The manufacturing processes of two types of targets using low enriched uranium (LEU) are being studied. The first one is based on UAlx-Al dispersion targets, which is being used commercially in Argentina and Australia. The second one is based on thin foils of metallic uranium, which was developed by Indonesia with US support. This paper presents the current status of ongoing activities at IPEN-CNEN/SP related to the development of these two types of LEU irradiation targets for future production of 99Mo in RMB.

1. Introduction

Every year the world demands more than 30 million medical imaging procedures that use technetium-99m radioisotope (Tc^{99m}), which correspond to approximately 80% of all nuclear medicine diagnoses. [1] This radiopharmaceutical product derives from the radioactive decay of molybdenum-99 (99Mo), which is commercially produced in research reactors by irradiation targets that contain uranium-235. However, continuous supplying of 99Mo has decreased over the last decade, mainly due to shutdowns that have occurred in the main research reactors that produce radioisotopes [2]. To deal with this scenario, Brazil has decided to build up a multipurpose reactor which among other functions will irradiate uranium targets to produce enough 99Mo to meet domestic demand.

Because of its potential use in improvised nuclear devises, transport of fresh high enriched uranium (HEU) and storage and disposal of spent HEU from 99Mo production present a global threat.[3,4] In 2005, 95% of all 99Mo was produced by irradiation of HEU targets that are subsequently processed primarily to recover the molybdenum.[5]. Thus, there is an effort for conversion to low enriched uranium (LEU) with subsequent removal of HEU from commerce [6].

In 1981 Brazil announced the production of 99mTc with its own technology. The Brazilian demand for this radiopharmaceutical has grown significantly in Brazil, reaching today more than 320 generators per week (450 Ci), which represents 4% of the global consumption of 99 Mo [7,8]. The raw material (99 Mo) is imported.

The Brazilian strategy to face the international crises in the supply of 99Mo [9,10,11] is based on actions of short, medium and long term [7,8]. The long-term project is expected to produce 99Mo through nuclear fission of 235U using irradiation targets. This strategy depends on building a new nuclear reactor, the Brazilian Multipurpose Reactor - RMB [12], and the availability of the technology for manufacturing targets. Two different routes for 99Mo production have been studied, the conventional basic dissolution route of UAl_x-Al dispersion targets, and the Cintchem modified method [13], which employs acid dissolution of thin foils of metallic uranium targets.

There are currently two technologies available to produce LEU uranium targets. One is based on a uranium-aluminum alloy dispersed in an aluminum matrix and the other one is based on metallic uranium thin foils.

The dispersion targets are produced by the well-known technique of assembling the meat-frame-claddings ("picture-frame technique") [14,15], in which a meat containing the UAl_x and aluminum powders is produced by powder metallurgy and is encapsulated by aluminum, being isolated from the reactor environment on all sides. The value of x in the UAl_x varies depending on the target manufacturing process, with a typical value for each manufacturer. In this type of target the intermetallic UAl_2 is usually used as starting material, which will react with aluminum during the manufacture of the target, especially during hot rolling and thermal treatments, resulting in a mixture of UAl_3 and UAl_4 after manufacturing. The x in the UAl_x formula denotes a mixture of such aluminides without a defined composition, which depends on the manufacturing process.

The final form of the UAl_x-Al dispersion targets are small aluminum plates containing in its interior a dispersion meat where the UAl_x particles which will undergo fission are "embedded" in a continuous matrix of aluminum. The targets have a uranium density around 2.9 gU/cm^3 and typically contain a mass of 1.4 g of 235U. The Argentine began the development of this type of target in 2000 [16,17] and began producing 99Mo with UAl_x-Al dispersion targets in 2002. The ANSTO (Australian Nuclear Science and Technology Organization) of Australia also uses LEU UAl_x-Al dispersion targets, which are irradiated in its OPAL reactor.

Researchers from South Korea proposed an aluminum dispersion target based on uranium metal replacing UAl_x [18]. According to calculations, the reaction of uranium metal with aluminum in the dispersion during manufacturing produces the rich uranium intermetallic UAl_2 and U-Al alloy. The subsequent reaction during irradiation, which produces swelling, would be acceptable, since the irradiation time for the 99Mo production is only 7 days. The temperature at the target surface would suffer an increase of 25 °C, within the safety margins with respect to thermally induced swelling. The advantage of using this target is that the uranium density was increased from 2.9 gU/cm^3, obtained by UAl_x-Al dispersion, to 9 gU/cm^3, resulting in a substantial increase in productivity of 99Mo.

In replacement of the HEU uranium per LEU uranium in the manufacture of irradiation targets used for producing 99Mo the philosophy is not to harm the yield of the process usually adopted when the highly enriched uranium is used, as well as the quality of the final product. The only way to achieve this is not to reduce the total 235U content on the target, which means to increase 5 times the amount of low enriched uranium present. This can be achieved using targets of thin foils of metallic uranium. Such target has been developed by Argonne National Laboratory in cooperation mainly with Indonesia [19]. This type of target consists of a thin sheet of uranium metal, about 125 μm thick, which is wrapped with nickel sheets and encapsulated in an aluminum tube [20,21]. The nickel foil serves as a barrier for fission products and prevents the bonding of the uranium foil with the aluminum tube. The cylindrical design is used to ensure the structural integrity of the target, to increase heat transfer and to facilitate dismantling of the target after irradiation.

The uranium metal foil target has several important advantages compared with the UAl_x-Al dispersion target commonly used for the production of 99Mo by nuclear fission [22], due to the increased uranium loading. After irradiation, the target is disassembled in a hot cell and dissolved in nitric acid [23,24]. The targets of thin foils of LEU uranium are already being used by Indonesia [25,26].

The IAEA (International Atomic Energy Agency) encouraged the development of this type of target by creating in 2005 the "Coordinated Research Project (CRP) on Developing Techniques for Small-Scale Indigenous Production of Mo-99 using LEU or Neutron Activation", with the participation of Chile, Egypt, Indonesia, Pakistan, Poland and Romania. The experience gained by ANL and BATAN in the manufacture of LEU uranium foils targets, in its irradiation, and its subsequent chemical processing was transferred to the participant countries [27].

This paper presents the current status of ongoing activities at IPEN-CNEN/SP related to the development of these two types of LEU irradiation targets for future production of 99Mo in RMB.

2. Target Fabrication

2.2. UAl_x-Al Dispersion Targets

Figure 1 illustrates the schematic drawing of the target that was developed in this work.

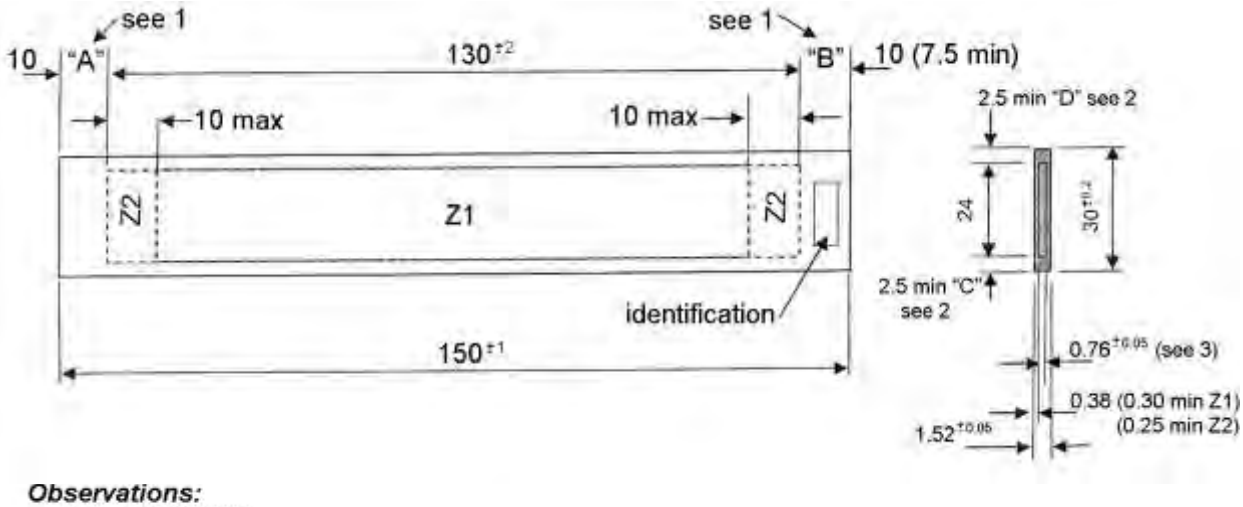

Observations:

1- "A - B" ≤ 2 mm

2- "C - D" ≤ 1 mm

3- Zone1 - medium 0.76 ± 0.05 mm
Zone 2 (*dog bone*) - maximum 1.07 mm, ensuring minimal cladding thickness in Zone 2 of 0.25 mm

Fig 1. UAl_x-Al dispersion irradiation target

The intermetallic was prepared from a mixture of metallic uranium and metallic aluminum in stoichiometric proportions to obtain UAl_2 (81.5 wt% U). The starting materials were charged into a zirconium crucible and melted using a 15 kW induction furnace. Prior the melting, the furnace was purged with argon after vacuum of 2.6×10^{-3} mbar. The UAl_x ingot was ground in a mortar under argon atmosphere.

A mixture of aluminum and UAl_x powders corresponding to 50 and 45 vol% respectively has been pressed to form the target meet, which is called briquette. It contains UAl_x particles dispersed in an aluminum matrix. The particle size distribution of the UAl_x powder in the briquette was 80 wt% of 44 to 90 μm particles and 20 wt% of particles smaller than 44 μm.

The rolling assembly consists of a picture frame, two cover plates and 15 briquettes. These components were assembled and joined by Tungsten Inert Gas (TIG) welding and then rolled to form the targets, according to the picture-frame technique [14,15]. Prior the rolling operation, the briquettes were degassed at 250 ^{o}C for 3 hours under vacuum of 0.8 x 10^{-3} mbar. Figure 2 shows the assembling operation.

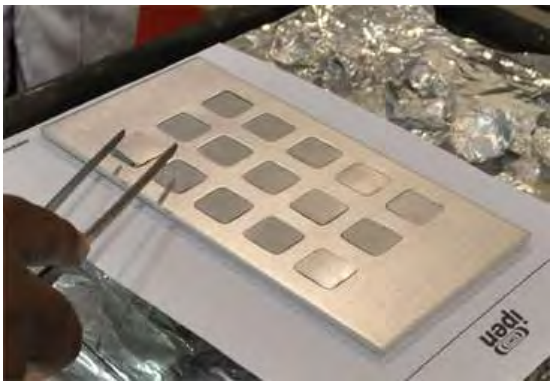

Fig 2. Photograph illustrating the assembly of multiple meats in the frame plate to be rolled for producing multiple targets

The assemblies were hot-rolled at 540 ^{o}C in six rolling passes with intermediate heating of 15 minutes between passes and an initial annealing of 1 hour. The final specified thickness for the target was reached with two cold-rolling passes. After hot rolling, the mother plate was radiographed and three targets were taken to perform heat treatment at 540 ° C for 6 hours, totaling 8.5 hours of permanence at 540 ° C. The remainder of the targets (12) was separated to complement the studies of phase transformations. After the heat treatment, the targets were cold rolled to the final specified thickness of 1.52 mm. Figure 3 shows the image obtained by radiography of the mother plate after hot rolling, which shows the positioning of the meats of the individual targets.

Fig 3. Mother plate containing multiple targets (15) after hot rolling

The pieces removed after cutting (scrap) have been extensively inspected by bending test to check the bonding. The blister test was also performed to verify the metallurgical bonding, this time with a duration of 6 hours, which was the time adopted for the heat treatment for transforming the UAl_2 to UAl_3. No problem with the quality of the bonding was observed. No bubbles were observed. Table 1 shows the main features of the three meats of the manufactured targets. All targets attended dimensional specifications for the meat.

One target was characterized by metallography. The end defects (dog-boning and fish-tail) showed the usual dimensions observed in the meats routinely produced at IPEN-CNEN/SP. The cladding thicknesses also attended to current specifications, as shown in Table 2. Figure 4 illustrates the end defects, which are typical of fuel plates fabricated by rolling.

The binary system, uranium and aluminum, forms a phase diagram which shows the existence of intermetallic compounds consisting of three phases, UAl_2, UAl_3 and UAl_4. The mixture of these phases is known in the literature as UAl_x [28]. The composition of the starting UAl_x powder prepared in the induction melting was determined by means of image

analysis and X-ray diffraction. Characterizing the phase composition in UAl_x powder used as raw material for target fabrication is important because the maximum uranium concentration depends on the phase composition presented in the starting powder. Furthermore, it is important to mention that the UAl_3 and UAl_4 are more easily dissolved in alkaline solutions than the UAl_2, which defines, ultimately, the radiochemical processing throughput after the irradiation [29]. So, the presence of UAl_2 in the UAl_x-Al dispersions target also must be quantified and minimized.

Identification	***Target Final Thickness*** *(mm)*	***Meat Dimensions (mm)***		***Specification***
		Length	***Width***	
Av13	1,49	128,10	25,00	accepted
Av14	1,49	128,42	24,67	accepted
Av15	1,49	128,67	24,92	accepted

Tab 1: Main features of meats of the targets removed from the mother plate

	Zone 1		Zone 2	
	Meat (mm) min-max	Cladding (mm) min-max	Meat (mm) min-max	Cladding (mm) min-max
Av13	0,83-0,87	0,31-0,33	0,86-0,97	0,25-0,31

Tab 2: Espessuras dos revestimentos e núcleo dos alvos fabricados

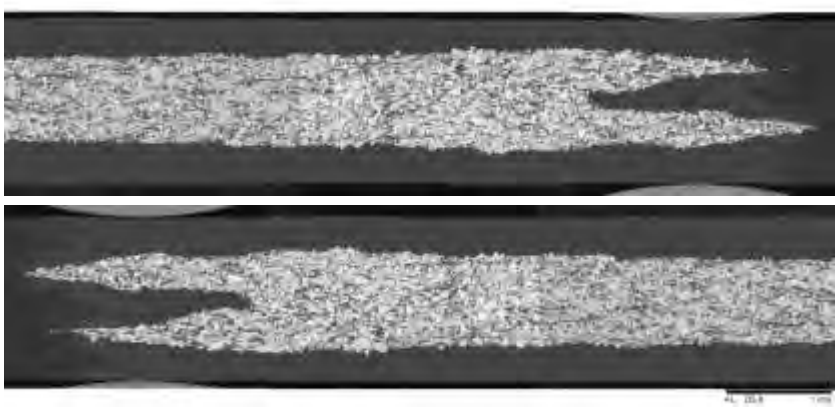

Fig. 4. Illustration of the geometry of the end defects

The phase composition was quantified by studying the microstructure of briquettes and rolled meats through scanning electron microscopy (backscattered electron image) and energy dispersive spectroscopy. X-ray diffraction data were also collected from samples of polished briquettes and rolled target meats by a Rigaku Multiflex diffractometer, operating with Cu-Kα radiation at 40 kV and 20 mA, with a scan of 0.02° and for 8 s counts. The crystalline phases were quantified using the Rietiveld method with GSAS for data refinement.

Figure 5 show a scanning electron micrograph of the cross section of a UAl_x-Al briquette. Because of the atomic number contrast obtained from the backscattered electrons, which is sensitive to the composition, it was possible to observe three shades of gray, which indicate the existence of three phases. EDS analysis were used to quantify the levels of uranium and aluminum in the three phases. Region 1 (lighter gray tone, almost white) showed a composition of 99.0 wt% U and 1.0 wt% Al. This phase was identified by X-ray diffraction as UO_2. The grayscale observed on region 2 corresponded to the concentration of

82.5 wt% uranium and 17.5 wt% aluminium, while the darker gray tone related to the region 3 showed a composition of 76.6 wt% U and 23.4 wt% Al. Based on the stoichiometric composition, the compositions of the regions 2 and 3 characterize the UAl_2 and UAl_3, respectively. The volumetric fractions of the three phases present were determined by using image analysis. Eight images were analyzed. The phase quantitation by image analysis resulted in 42.6 wt% for UAl_2, 56.26 wt% for UAl_3 and 1.2 wt% for UO_2. Chemical analysis determined the uranium content in the powder as 80.74 wt%, with a uranium loss of 0.76 wt% compared to the nominal uranium content of the starting composition of the melting charge (81.50 wt%). This loss can be attributed to the oxidation of uranium alloy during the melting process. Considering that the uranium content was determined by chemical analysis and neglecting the presence of the oxidized phase remaining in the sample, from the U-Al equilibrium diagram [28] the expected phase composition in the powder would be about 89.4 wt% for the UAl_2 and 10.6 wt% for UAl_3. The composition resulted from the image analysis shows underestimated values for the UAl_2 concentration. This is due to unavoidable errors inherent in the image obtained by scanning electron microscopy, which are discussed in greater detail in a previous work [30].

The phase composition obtained by X-ray diffraction applying the Rietveld method for the same UAl_x-Al briquette analyzed by image analysis resulted in a value of $\chi 2$ from the simulation of 66, showing a reasonable agreement between the experimental and the theoretical values. As mentioned before, the compositional analysis of the phases obtained by SEM-EDS indicated the existence of UAl_2, UAl_3 and a third phase rich in uranium (lighter gray tone, almost white, region 1 in Figure 5). This observation was confirmed by X-ray diffraction, which shows that the uranium-rich phase is UO_2. The results for the phase measurement from the Rietveld method showed 85.4 wt% for UAl_2, 12.4 wt% for UAl_3 and 2.2 wt% for UO_2. These results are very close to those expected based on the U-Al equilibrium diagram.

Due to the best results obtained with Rietiveld refinement, this method was adopted to analyze the phase composition of the fabricated targets. The phase composition of the finished target (after heat treatment) was 0.34 wt% for UAl_2, 7.94 wt% for UAl_3, 90.47 wt% for UAl_4 and 1.25 wt% for UO_2.

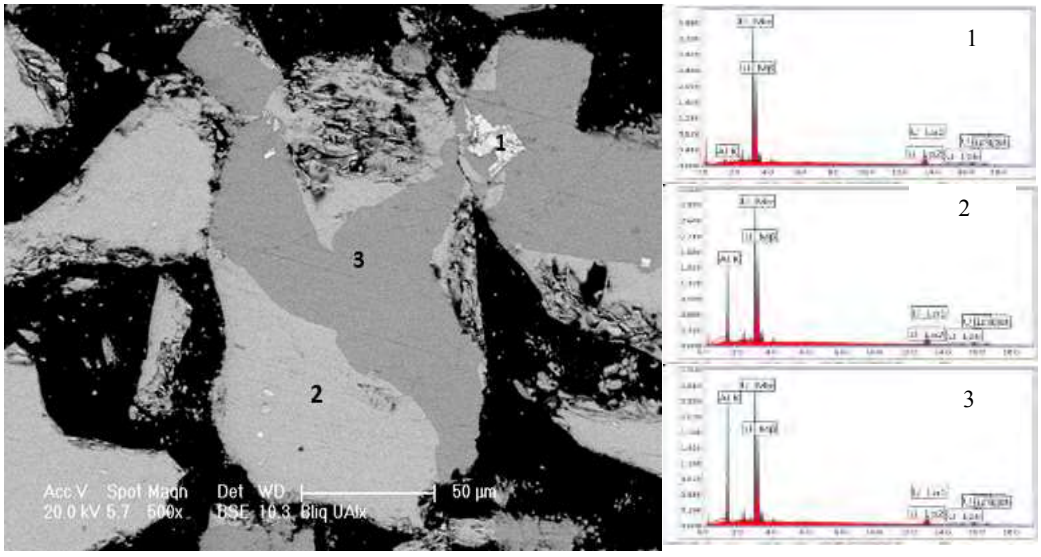

Fig 5. Scanning electron micrograph and EDS analysis of the regions designated by 1, 2 and 3. The compositions of regions 2 and 3 indicate the presence of UAl_2 and UAl_3, respectively (backscattered electrons)

2.3. Uranium Foil Targets

The IPEN-CNEN/SP is just starting its activities for the development of this type of target, which is based on Argonne-developed LEU-foil annular target [31]. In this target,

uranium foil is drawn between two Al tubes. Prior to drawing, a Ni fission-recoil barrier is wrapped around the U foil to prevent bonding of the U foil to the target walls during irradiation, so foil can be removed from the target prior to dissolution/digestion and 99Mo recovery. The work was initiated with the support of the IAEA providing an expert from Chile in this area [32], which gained large experience from the "Coordinated Research Project (CRP) on Developing Techniques for Small-Scale Indigenous Production of Mo-99 using LEU or Neutron Activation" [27].

The first step in the production of annular targets whit uranium metal foil is to manufacture the thin foil. Hot rolling and cold rolling were done to make the foil. The basic technique used in hot rolling is the picture-frame technique. For hot rolling, frame and cover from carbon steel were used to make the assembly. A metallic uranium ingot was put into the frame cavity and covered with the carbon steel cover plates.

The metallic uranium was charged into a zirconium crucible and melted using a 15 kW induction furnace. Prior the melting, the furnace was purged with argon after vacuum of 2.6×10^{-3} mbar. A graphite ingot mold is used to obtain a uranium ingot in the form of a uranium piece with 60 mm X 100 mm and 4.2 mm in thickness. From this piece, a smaller piece with 20 mm X 60 mm was cut and inserted in the cavity of the frame. The uranium ingot must be protected from oxidation during the hot rolling process. For this purpose, covers and frame of low carbon steel 4.2 mm in thickness were used as a sealing assembly. Considering that the aim is to obtain a free uranium foil after hot rolling, the steel surfaces in contact with the uranium ingot were coated with an emulsion of yttrium oxide and ethanol, and thus preventing bonding and interaction between the uranium ingot and steel. Once applied this protective coating to the surfaces, the set was assembled and sealed by TIG welding. Figure 6 illustrates this operation.

Before the hot rolling process, the assembly was annealed 1 hour at 630 °C in air. Thickness reductions of 5% were applied in the first six rolling steps and the following reductions steps were done applying 10% of reduction in each step, with intermediate annealing of 10 minutes between each reduction step. The rolling deformation achieved values between 95 % of the total reduction in the thickness of the assembly. The result of hot rolling for the assembly is shown in Figure 7. After hot rolling, the foil was annealed at 630 °C for 30 minutes.

The uranium foil resulted from hot rolling was pickled with solution of 50 vol% HNO_3 and 50 vol% water and cleaned with water and alcohol. The thickness foil resulted from hot rolling was 0.167 mm. The length was about 550 mm and the width was 60.7 mm. A piece with length of 100 mm was cut for cold rolling. Stainless steel plate was used to cover the foil during cold rolling. Stainless steel plate thickness was 1 mm with the length of 2 x 150 mm folded equally long. The width was 150 mm. Inner surfaces of the stainless steel plate were cleaned with alcohol. Cold rolling was conducted step by step with thickness reduction of about 5% in each rolling step.

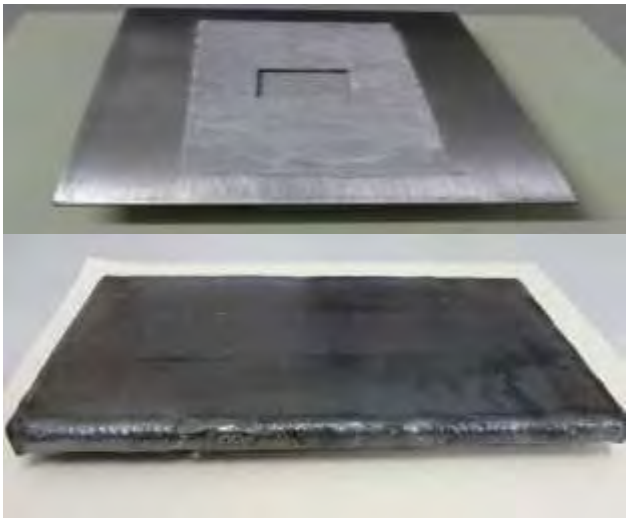

Fig 6. Frame and assembly after TIG welding

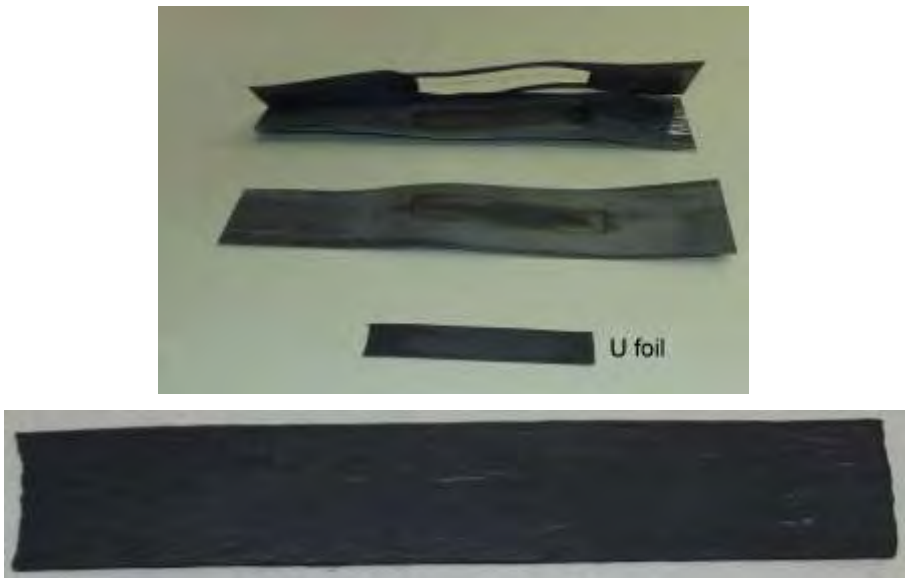

Fig 7. Assembly after hot rolling and uranium foil

The thickness of finished uranium foil was measured in eight positions. Table 3 presents the results. Figure 8 shows the finished uranium foil.

Position	Thickness (μm)
1	124
2	124
3	125
4	127
5	122
6	125
7	123
8	129

Tab 3: Thickness of the finished uranium foil

Fig 8. Finished uranium foil

3. Conclusions

The UAl_x-Al dispersion targets could be manufactured successfully. Additional work is needed to optimize the thermomechanical treatment in order to distribute the phase transformation during hot rolling process. It was possible to obtain a thin foil of uranium metal with the desired thickness with a good thickness uniformity and surface quality. Additional work will be initiated to study the assembly of the annular target.

Acknowledgments

The authors are grateful to IAEA for the technical support for this work. The authors are also grateful to FAPESP (2011/13849-9, 2015/08922-0) and CNPq (471008/2011-7, 304034/2015-0) for the research grants provided for this work.

4. References

1. "A Supply and Demand Update of the Molybdenum-99 Market-2012, 2012, https://www.oecd-nea.org/med-radio/docs/2012-supply-demand.pdf
2. "The Supply of Medical Radioisotopes: the Path to Reliability, 2011, https://www.oecd-nea.org/med-radio/reports/med-radio-reliability.pdf
3. G. F. Vandegrift, A. Bakel, A. Guelis, L. Hafenrichter, A. Hebden, J. Jerden, A. Leyva, K. Quigley, D. Stepinski, "Overview of 2007 ANL Progress for Conversion of HEU-Based Mo-99 Production as Part of the U.S. Global Threat Reduction-Conversion Program," The RERTR-2007 International Meeting on Reduced Enrichment For Research and Test Reactors, September 23-27, 2007, Prague, Czech Republic, http://www.rertr.anl.gov/RERTR29/PDF/6-2_Vandegrift.pdf
4. A. J. Kuperman, "Weaker U.S. Export Controls on Bomb-grade Uranium: Causes, Consequences, and Prospects," Proceedings of the 2005 International Meeting on Reduced Enrichment for Research and Test Reactors, November, 6-10 2005, Boston, MA, USA, http://www.rertr.anl.gov/RERTR27/Abstracts/S8-4_Kuperman.html
5. G. F. Vandegrift, "Facts and Myths Concerning "MO Production with HEU and LEU Targets" Proceedings of the International Meeting on Reduced Enrichment for Research and Test Reactors, Boston, MA, November 6-10, 2005, http://www.rertr.anl.gov/RERTR27/PDF/S8-1_VandeGrift.pdf
6. National Nuclear Security Administration, Office of Global Threat Reduction, *Strategic Plan, Reducing Nuclear and Radiological Threats Worldwide*, January 2007, http://www.nnsa.doe.gov/na-20/docs/GTRI_Strategic_Plan_2007.pdf
7. J. A. Osso Jr, J., R. Teodoro, C. R. B. R. Dias; R.R.L. Bezerra, J. L. Vilella, J. L. Correia, J. A. Perrotta, G. A. Pereira, C. L. Zapparoli Jr, J. Mengatti, "Brazilian strategies to overcome molybdenum crisis: present and future perspectives of the Multipurpose Research Reactor". RRFM 2011, March 20-24, 2011, Rome, Italy
8. J. A. Osso Jr, C.R.B.R. Dias, T. P. Brambilla, R. Teodoro, M. F. Catanoso, J. Zini, R.R.L. Bezerra, J. L. Vilella, J. L. Correia, E. Ivanov, F. M. S. Carvalho, L. Pozzo, P .L. Squair, J. Mengatti "Production of 99Mo at IPEN-CNEN/SP-Brazil". In: 2013 Topical Meeting on Molybdenum-99 Technological Development, Chicago, Illinois, April 1-4, 2013, http://mo99.ne.anl.gov/2013/pdfs/Mo99%202013%20Web%20Papers/S9-P1_Osso_Paper.pdf
9. B. Ponsard "Mo-99 supply issues: status report and lessons learned". RRFM 2010, March 21-25, 2010, Marrakech, Morocco
10. R. Cameron, A. Y. Lokhov, C. Westmacott "The supply of medical radioisotopes – an assessment of the market economics, alternative technologies and proposed policy approach to achieving sustainability". RRFM 2011, March 20-24, 2011, Rome, Italy
11. European Nuclear Society – ENS. "The medical isotope crisis", http://www.euronuclear.org/pdf/The-medical-isotope-crisis-2009-09-15.pdf
12. I. J. Obadia,; J. A. Perrotta "A sustainability analysis of the Brazilian Multipurpose Reactor project". RRFM 2010, March 21-25, 2010, Marrakech, Morocco
13. D. Wu, S. Landsberger, G. F. Vandegrift "Progress in chemical treatment of LEU targets by the modified CINTICHEM process". International RERTR Meeting. Seoul, Korea, October 7-10, 1996, http://www.rertr.anl.gov/99MO96/WU96.PDF
14. J. E. Cunninghan, E. J. Boyle "MTR-Type fuel elements". International Conference on Peaceful uses atomic energy. Geneva, August 8 to 20, 1955. V. 9: Reactor technology and chemical processing. UNITED NATIONS. New York, N.Y., 1956. p. 203-7
15. A. R. Kaufman ***Nuclear reactor fuel elements, metallurgy and fabrication***. New York, N.Y. Interscience, 1962
16. C. Kohut, M. Fuente, P. Echenique, D. Podesta, P. Adelfang "Targets development of low enrichment for production of Mo99 for fission". International RERTR Meeting. Las Vegas, Nevada, USA, October 1-6, 2000, http://www.rertr.anl.gov/Web2000/PDF/Fuente00.pdf
17. D. M. Cestau, P. R. Cristini, E. Carranza, J. Cestau, R. Bavaro, M. Bronca,; R. Centurión, A. Novello "HEU and LEU cost comparison in the production of Molybdenum-99". International RERTR Meeting. Washington, DC, USA, October 5-9, 2008

18. C. K. Kim, K. H. Kim, Y. S. Lee, H. J. Ryu, Y. M. Woo, S. J. Jang, J. M. Park, S. J. Choi “A consideration for uranium high density plate type target of uranium metal particles dispersion in aluminum matrix for 99Mo production”. RRFM 2010, March 21-25, 2010, Marrakech, Morocco
19. G. F. Vandegrift, A. J. Bakel, J. W. Thomas “Overview of 2007 ANL progress for conversion of HEU-based Mo-99 production as part of the U.S. global threat reduction conversion program”. International RERTR Meeting. Prague, Czech Republic, September 23-27, 2007, http://www.rertr.anl.gov/RERTR29/PDF/6-2_Vandegrift.pdf
20. C. Conner, I E. F. Lewandowsk, J. L. Snelgrove, M. W. Liberatore, D. E. Walker, T. C. Wiencek, D. J. McGann, G. L. Hofman, G. F. Vandegrift “Development of annular targets for 99Mo production” International RERTR Meeting. Budapest, Hungary, October 3-8, 1999, http://www.rertr.anl.gov/Web1999/Abstracts/Program.html
21. T. C. Wiencek, G. L. Hofman, E. L. Wood, C. T. Wu, J. L. Snelgrove “LEU 99Mo target fabrication and testing: Overview, status and plans”. International RERTR Meeting. Williamsburg, USA, September 18-22, 1994
22. G. L. Solbrekken, K. Turner, S. Govindarajan, P. Macarewicz, C. Allen “Development, qualification, and manufacturing of LEU-foil targetry for the production of Mo-99”. RRFM 2011, March 20-24, 2011, Rome, Italy
23. B. Briyatmoko, B. Sriyono, A. H. Gunawan, H. Lubis, A. Mutalib, A. Hambali “Experiences of HEU to LEU Mo-99 production conversion. IAEA Meeting”, http://www.iaea.org/OurWork/ST/NE/NEFW/Technical-Areas/RRS/documents/mo99/BRIYATMOKOmo99CM.pdf
24. B. Briyatmoko, Sudarmadi, A. Mutalib “Indonesia’s program for conversion of Mo-99 production to LEU fission”. In: SYMPOSIUM ON MINIMISATION OF HEU IN THE CIVILIAN SECTOR, June 17-20, 2006, Oslo, https://norwayportal.mfa.no/NR/rdonlyres/EC9F5DE51CE947AF88C060C5E1865D8A/60587/Briyatmoko_Presentation_Indonesias_Program_for_Con.pdf
25. Pacific Nortwest National Laboratory. In: WOSMIP II – Workshop on Signatures of Medical and Industrial Isotope Production. U. S. Department of Energy. November 2011. Report PNNL-21052, http://wosmip.pnnl.gov/WOSMIPII2011FinalReport.pdf
26. International Atomic Energy Agency. Production and Supply of Molybdenum-99. Annex to the Nuclear Technology Review 2010, https://www.iaea.org/About/Policy/GC/GC54/GC54InfDocuments/English/gc54inf-3-att7_en.pdf
27. International Atomic Energy Agency. CRP on Production of Mo-99 from LEU or Neutron Activation. 2005-2011. Disponível na internet no endereço: http://www.iaea.org/OurWork/ST/NE/NEFW/Technical-Areas/RRS/mo99.html
28. B. L. Bramfitt, H. P. Leighly Jr. “A Metallographic Study of Solidification and Segregation in Cast Aluminum-Uranium Alloys,” *Metallography*, **I**, pp. 165-193 (1968).
29. H. J. Cols, P. R. Cristini, A. C. Manzini, “Mo – 99 from low-enriched uranium,” Proceeding of International Meeting on Reduced Enrichment for Research and Test Reactors, Las Vegas, Nevada, October 1-6, 2000. http://www.rertr.anl.gov/Web2000/Title-Name-Abstract/Cristi00.html
30. G. Conturbia, R. H. L. Garcia, vA. M. Saliba-Silva, E. F. Urano de Carvalho, M. Durazzo “Study of Methods for Phase Characterization in Intermetallic UAlx”. RRFM 2014, March 30-April 3, 2014, Ljubljana, Slovenia
31. C. Conner, E. F. Lewandowski, J. L. Snelgrove, M. W. Liberatore, D. E. Walker, T. C. Wiencek, D. J. McGann, G. L. Hofman, G. F. Vandegrift “Development, Fabrication, and Testing of LEU Metal Foil Targets for 99Mo Production,” 22nd International Meeting on Reduced Enrichment for Research and Test Reactors (RERTR), Budapest, Hungary on October 3-8, 1999, http://www.rertr.anl.gov/Web1999/PDF/52conner99.pdf
32. J. Lisboa “Personal Communications”. Planta de Elementos Combustibles-PEC. Comisión Chilena de Energía Nuclear-CCHEN. 2015

EFFECTIVE UTILISATION OF THE REZ´S RESEARCH REACTOR LVR-15 IN BASIC, INTERDISCIPLINARY AND APPLIED RESEARCH

P. MIKULA, P. STRUNZ
Nuclear Physics Institute ASCR, v.v.i. 25068 Řež, Czech Republic

ABSTRACT

Neutron Physics Laboratory of NPI ASCR, v.v.i. operates several neutron instruments installed at the medium power reactor LVR-15 having a nominal thermal power of 10 MW and administrated by Research Centre Rez, Ltd. The following instruments are succesfully operated at the reactor: High resolution SANS diffractometer, Strain/stress scanner, Instrument for thermomechanical testing of materials, Thermal neutron depth profiling, Medium resolution powder diffractometer, Neutron optics diffractometer and Neutron activation analysis. On the dedicated instruments there are carried out research investigations on a competitive international level. Description of the most important recent research activities accompanied by several highlight results are introduced in the paper. As the reactor operates on average about 170 days per year with a pattern of operating cycles of three weeks, each followed by one week for maintenance and instrumentation development, it provides a sufficiently high number of experimental days.

1. Introduction

The present reactor LVR-15 was originally introduced in the operation in 1957 at 2 MW power. Later on, after two reconstructions the present tank type light water reactor has used the uranium fuel enriched to 36 and finally 20 percent in uranium-235 and can operate at any power up to the licensed ceiling of 10 MW. It operates on average about 170 days per year with a pattern of operating cycles of three weeks plus one week for maintenance and instrumentation development. The thermal neutron flux in the core is about $9x10^{13}$ $n.cm^{2}.s^{-1}$ (see Table 1). At present, the reactor LVR-15 belongs to the Research Centre Rez, Ltd. and is operated mainly on a commercial basis. Research and development in Research Centre Rez, Ltd. is focused on the areas of nuclear energy, nuclear reactor physics, chemistry and

Mean reactor power	10 MW
Maximum thermal neutron flux in the core	$1 \cdot 10^{18}$ $n \cdot m^{-2} \cdot s^{-1}$
Maximum fast neutrons flux in the core	$3 \cdot 10^{18}$ $n \cdot m^{-2} \cdot s^{-1}$
Maximum thermal flux in reflector (mix of Be + H_2O)	$5 \cdot 10^{17}$ $n \cdot m^{-2} \cdot s^{-1}$
Maximum thermal neutron flux in the tubes	$1 \cdot 10^{12}$ $n \cdot m^{-2} \cdot s^{-1}$
Maximum thermal flux at the exit of the tubes (100/60 mm)	$1 \cdot 10^{8}$ $n \cdot m^{-2} \cdot s^{-1}$
Irradiation channel - in fuel	$1 \cdot 10^{14}$ $n \cdot m^{-2} \cdot s^{-1}$
Irradiation channel - at core periphery	$7 \cdot 10^{13}$ $n \cdot m^{-2} \cdot s^{-1}$
Doped silicon facility	$1 \cdot 10^{13}$ $n \cdot m^{-2} \cdot s^{-1}$
High pressure water loops	$5 \cdot 10^{13}$ $n \cdot m^{-2} \cdot s^{-1}$

Tab 1: Reactor parameters

materials. The irradiation service uses the reactor namely for: Modification of Physical Characteristics of Materials, Production of Radionuclides for Radiopharmacy and Production of Radionuclide Emitters. Crucial for research and development of the reactor are technological circuits – experimental loops for modelling of experimental conditions in the reactor core and the connected reactor cooling circuits. These loops allow mechanical, thermal-hydraulic, material, corrosion and further research at parameters and under operating conditions of the reactor concept under development. By placing a loop in the experimental reactor, all the above-mentioned physical and chemical influences of reactor coolant are supplemented by radiation conditions. The results are used in services for both Czech and foreign related organizations. On the other hand, Neutron Physics Laboratory (NPL) of Nuclear Physics Institute of the Czech Academy of Sciences performs effectively neutron physics experiments when using horizontal and vertical irradiation beam channels of the reactor [1,2]. In total, NPL operates 8 instruments installed at 5 radial horizontal beam tubes (for experiments in nuclear physics, solid state physics and materials research) and two vertical irradiation channels (for neutron activation analysis) which are hired at Research Centre Rez, Ltd. High quality of the experiments carried out at the reactor in Řež is documented by the fact that NPL laboratory participates in the EU Project - ACCESS (Transnational Access to Large Facilities) in the frame of FP6- and FP7-NMI3 programme. The following instruments are used at this medium power research reactor at the competetive level (see Fig. 1): Two strain/stress scanners (HK4+HK9), Small-angle neutron scattering (SANS) diffractometer (HK8a), Neutron powder diffractometer MEREDIT (HK6), Thermal neutron depth profiling facility (HK3), Neutron Activation Analysis facility (NAA), Neutron optics diffractometer (HK8b). Effectiveness of the neutron scattering instruments is strongly supported by employment of neutron optics devices in combination with position sensitive detectors (PSD). The powder diffractometer installed at the horizontal channel HK2 is operated by the Faculty of Nuclear Sciences and Physical Engineering of the Czech Technical University in Prague.

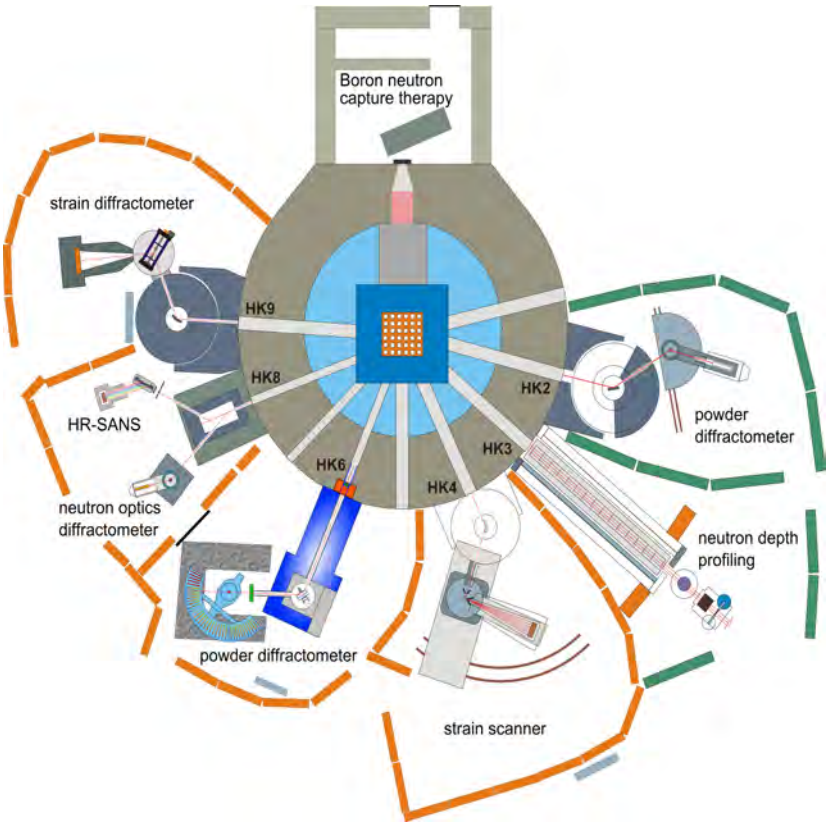

Fig. 1. Schematic sketch of neutron scattering instruments of NPI installed at LVR-15.

2. Experimental activities at the reactor LVR-15

2.1. Neutron depth profiling (NDP)

NDP is the nuclear analytical technique available to determine depth profiles of light elements in solids (i.e., ^{3}He, ^{6}Li, ^{10}B, ^{14}N, etc.). It utilizes the existence of isotopes of elements that produce prompt monoenergetic charged particles upon capture of thermal neutrons. The related multidetector spectrometer consists of a large vacuum chamber, automatic target holders and several different data acquisition systems which can be used at the same time (see Fig 2). From the energy loss spectra of emitted products the depth distributions of light elements can be reconstructed. The NDP method is an excellent tool for studies of numerous problems in solid-state physics (diffusion, sputtering), material science (corrosion), electronics, optronics, life sciences, etc. Its applicability and efficiency has steadily expanded. This method uses the following parameters of the neutron beam: cross section - the height 4 mm and the width up to 90 mm, intensity of the thermal neutron beam - 10^{7} cm^{-2}s^{-1}, Cd ratio - 10^{5}, collimation - in the verical plane ~ 1° and in the horizontal plane ~ 1°, beam homogeneity - inhomogeneous due to girland and zig-zag reflections. The list of the isotopes which can be used in the NDP method are shown in Tab. 2. Fig. 2 shows also an example of the depth profiling of Boron in CaF_2 as implanted and after an anneling [3]. In general, NDP is a non-destructive method that leaves only trace amount of residual radioactivity, and examined samples can thus be measured repeatedly. Concentrations down

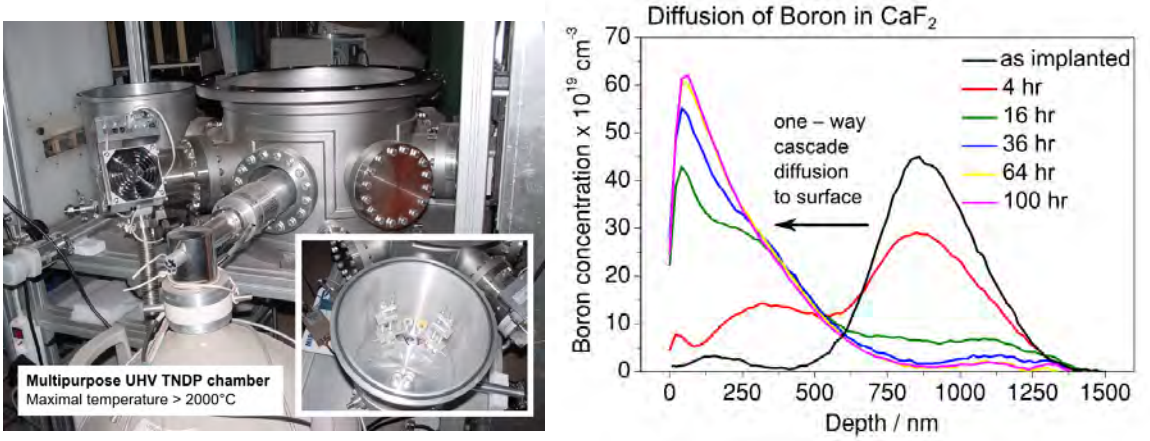

Fig. 2. Photo of the experimental chamber used for the NDP and an example of the depth profiling of Boron in CaF_2 as implanted (390 keV B, 10^{16} at. cm^{-2}) and annealed at 600ºC.

to a ppm (with a 1D mode) or even ppb (with a 2D mode) level can be determined, depending on the element and the matrix. Profiling to depths of about 15 m (e.g. Li in metals) or even 60 m (Li in polymers) can be obtained, with a depth resolution to a few nanometers only (for glancing angle geometry). The examined samples have to be solid (or liquid with very low volatility), flat with a smooth surface (with roughness of few nm only) and minimum area of at least a few mm^2. Depending on the nuclides and the used substrates the analysis takes a few tens of minutes to a few tens of hours. The NDP technique is applicable only to the elements with a relevant cross-sections and energy of reactions [4].

Nuclide	Natural abundance or activity* [at/mCi]	Nuclear reaction	Cross section [barn]	Energy of reaction products [keV]		Detection limit [at/cm^2]
^{3}He	0.13 x 10^{-3}	^{3}He(n,p)^{3}H	5326	573	191	3.1 x 10^{13}
^{6}Li	7.42	^{6}Li(n,α)^{3}H	940	2051	2734	1.8 x 10^{14}
^{7}Be*	2.5 x 10^{14}	^{7}Be(n,p)^{7}Li	48000	1438	207	3.5 x 10^{17}
^{10}B	19.6	^{10}B(n,γα)^{7}Li	3606	1471	839	4.3 x 10^{13}
^{10}B	19.6	^{10}B(n,α)^{7}Li	230	1775	1014	6.7 x 10^{14}
^{14}N	99.64	^{14}N(n,p)^{14}C	1.81	584	42	9.1 x 10^{17}
^{22}Na*	4.4 x 10^{15}	^{22}Na(n,p)^{22}Ne	31000	2247	103	4.7 x 10^{12}
^{33}S	0.76	^{33}S(n,α)^{30}Si	0.14	3091	412	1.2 x 10^{16}
^{35}Cl	75.5	^{35}Cl(n,p)^{35}S	0.49	598	17	3.4 x 10^{17}
^{59}Ni*	1.3 x 10^{20}	^{59}Ni(n,α)^{56}Fe	12.3	4757	340	1.4 x 10^{16}

List of the NDP relevant isotopes - detection limits are based on the charged particle counting rate 0.01 s^{-1}, detector→sample solid angle 0.03 Sr, and intensity of the neutron beam Φ_{th} = 10^{7} cm^{-2}s^{-1}.

Tab. 2: List of the NDP relevant isotopes

2.2. Neutron Activation Analysis (NAA)

Both short and long time irradiation for NAA can be carried out in vertical channels H1, H5, H6 and H8 of the LVR-15 reactor (see Fig. 3). Neutron fluence rates available in these channels is given in Table IV. For the short-time NAA the channel H1 is connected with the laboratory by a pneumatic system with the transport time of 3.5 s. Irradiation is carried out in a polyethylene (PE) rabbit for 10-180 s. The channels H5, H6 and H8 are used for long-time irradiation (0.5 h – several days) in 100-mm long Al-cans. In channels H5 and H8 "narrow" (inner diameter 35 mm) Al-cans are used, which accommodate up to 35 samples packed in disk shaped PE capsules, in channel H6 "broad" (inner diameter 56 mm) Al cans are used, which accommodate up to 15 quartz vials with a 8 mm outer diameter. For Epithermal Neutron Activation Analysis (ENAA) both short- and long-time irradiation are performed behind a 1-mm Cd shield allowing for selective activation with epithermal neutrons. The laboratory is equipped with several high resolution and high efficiency HPGe coaxial detectors. Both relative and k_0 - standardization can be used for quanitification of results as well as conventional -ray spectrometry. The NAA methods provide a large variety of applications: Investigations of environmental and historical materials (determination of up 40 elements in aerosol, fly ash, soil, sediment, etc., samples by a combination of Instrumental Neutron Activation Analysis (INAA) and ENAA) [5], geo- and cosmochemical samples (elemental characterization of rocks, tektites, namely moldavites, and meteorites by a combination of INAA, ENAA, and Radiochemical Neutron Activation Analysis (RNAA)), in biomedicine (determination of essential and toxic trace elements in selected human and animal tissues by a combination of INAA and RNAA to achieve the lowest element detection limits possible), in forensic science (determination of poisonous elements in selected tissues of investigated cases of contemporary and historical persons) and in chemical metrology [6] (certification of element contents in reference materials prepared by the most important producers, such as U.S. NIST, IRMM, IAEA, etc.). From the recent NAA investigations, let us introduce several of them. INAA was used to determine contents of more than 30 elements in meteorites Morávka [7] and Jesenice [8]. Environmental research was focused on the determination of ^{129}I and the ^{129}I/^{127}I ratio in biomonitors, namely, in bovine thyroid and moss, collected in the vicinity of the Temelín nuclear power plant (NPP) in south Bohemia using NAA in several modes (NAA with pre-irradiation separation followed by RNAA, and ENAA). No significant differences of ^{129}I levels and the ^{129}I/^{127}I ratios in the thyroids collected prior to the start and after several years of the NPP operation have been indicated [9]. For

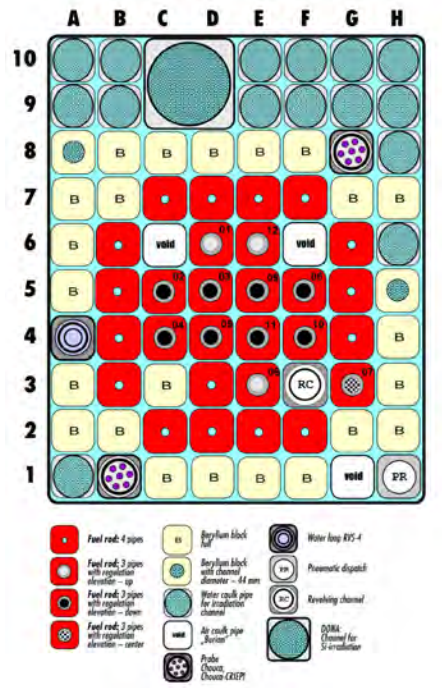

Fig. 3. LVR-15 active core layout.

Channel	H1	H5	H6	H8
Energy	Fluence rate / n.cm^{-2}.s^{-1}			
(0.0 - 0.501 eV)	3.38E+13	6.95E+13	5.98E+13	4.02E+13
(0.501 eV -10 keV)	1.49E+13	7.95E+13	6.80E+13	7.50E+12
(10 keV -0.1 MeV)	3.50E+12	2.12E+13	1.76E+13	1.81E+12
(0.1 MeV - 20 MeV)	1.08E+13	5.87E+13	7.16E+13	6.27E+12

Tab. 3: Neutron fluence rates in channels for NAA irradiation at the reactor LVR-15

agricultural and nutritional research, we used a RNAA procedure to study the Se-transfer from soil or seed to wheat plants [10] and the ability of bread and durum wheat to accumulate Se via a soil-addition procedure at sowing time [11] to increase the desired uptake of the element in the Portuguese population. Silicon is an important trace element in humans, because it reduces the absorption of aluminium in human gastrointestinal tract. The daily intake of silicon should be about 10–25 mg, and its most readily absorbable form is H_4SiO_4, which is contained in beer. Using INAA, we found that Si-concentrations in Czech lager beer(s) varied in the range of 13.7 – 44.2 mg L^{-1} [12]. Concerning the cultural heritage, in 2010, the grave of the famous astronomer Tycho Brahe was opened by a Czech–Danish research consortium and samples of his bones, hair, and teeth were procured for scientific investigation. We carried out mercury determination in segmented hair samples by RNAA. The results showed that in the last 2 months of Brahe´s life, he was not exposed to lethal (or fatal) doses of mercury, as was previously speculated [13]. Furthermore, graphene is another example of a material difficult to assay by classical analytical techniques. Therefore, elemental impurities were determined by INAA in graphene samples prepared by various oxidation procedures of graphite to graphite oxide followed by various reduction processes [14]. On the corresponding webside one can find many other NAA results usually taken in international collaboration.

2.3. Neutron Powder Diffraction

The medium resolution powder diffractometer (MEREDIT) installed at the beam channel HK6 consists basically of 3 changeable monochromators placed in a massive shielding, two large HUBER goniometer circles and a multi-detector bank which is mounted in a moulded neutron shielding made from boron carbide powder in epoxy resin. The bank contains 35 ^{3}He counters with corresponding 10' Soller collimators. The detector bank moves on air pads, which provide together with the stepping motor smooth positioning of this heavy loaded bank. Diffraction patterns can be collected in the angular range from 2° to 148° in $2\theta_S$ with the step down to 0.02° and step delay controlled by strict time or neutron flux read by a monitor. Monochromator and beam parameters are shown in Tab. 4. The diffractometer is mainly used for non destructive structure phase identification, crystalline structure determination,

Monochromator	Reflection	Wavelength Å	Minimum Δd/d (x 10^{-3})	Neutron flux n.cm^{-2}.s^{-1}	Beam size cm^2
3 bent Si single crystals	(422)	1.271	3.9 (at 56° 2θ)	~8.8 x 10^5	2 x 4
	(311)	1.877	4.4 (at 59° 2θ)	~8.6 x 10^5	2 x 4
3 mosaic Cu crystals	(220)	1.460	4.9 (at 71° 2θ)	~3.6 x 10^6	4 x 4

Tab. 4: Monochromators and beam parameters

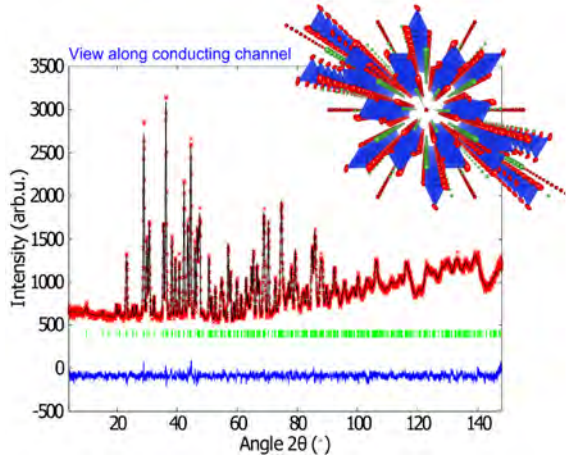

Fig. 4. Powder diffraction spectrum of $La_{9.33+x}(Si_{1-y}M_yO_4)_6O_{2+3x/2}$; M = {Fe, Al, Mg}.

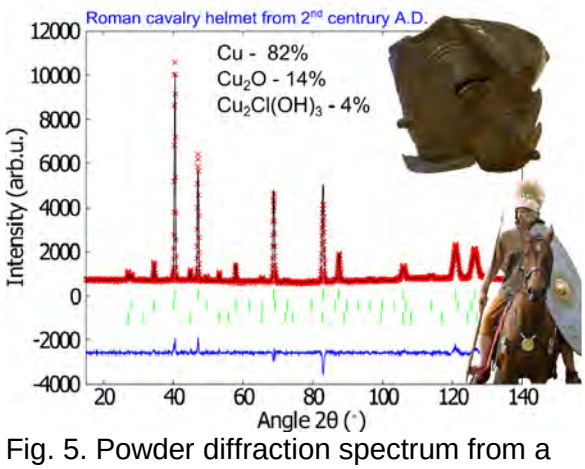

Fig. 5. Powder diffraction spectrum from a fragment of the Roman cavalry helmet.

magnetic structure determination, temperature dependent phase transition, quantitative multi-phase analysis and also for in-situ internal stress-strain evolution. The following sample environments are at a disposal: close cycle cryostat for 10 K → 300 K, vacuum furnace for 300 K → 1300 K, light furnace for 300 K → 1300 K, Euler goniometer, automatic 6 samples exchanger for RT and a deformation rig. As an application example, Fig. 4 shows diffraction spectrum serving for identification of deformation of oxygen ion conductive channels (Lanthanum silicates $La_{9.33+x}(Si_{1-y}M_yO_4)_6O_{2+3x/2}$; M = {Fe, Al, Mg} with apatite like crystal structure with space group $P6_3$ /m are interesting material due to the high oxygen ion conductivity for fuel cell applications) and Fig. 5 shows the result of the nondestructive phase analysis of the Roman cavalry helmet from 2nd century A.D., where phase analysis of the surface corrosion products and an estimation of Zn content to be of 18 wt%. in the brass material was carried out [15].

2.5. Small-Angle Neutron Scattering

Small-angle neutron scattering investigations are carried out on the double-crystal diffractometer MAUD designed for the measurements in the high momentum transfer *Q*-resolution range. In contrast to conventional double-crystal arrangements, the fully asymmetric diffraction geometry on the elastically bent Si analyzer is employed to transfer

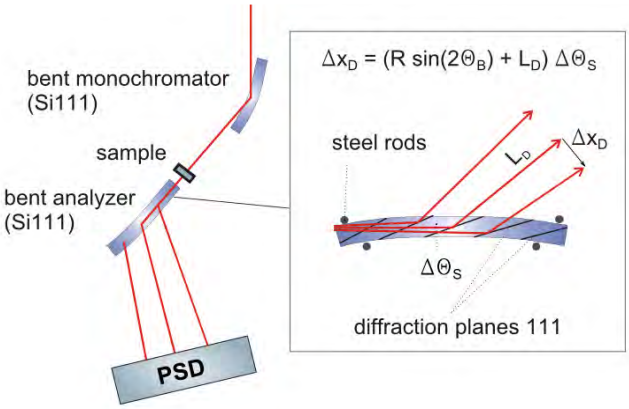

Fig. 6. Schematic sketch of the double- crystal SANS diffractometer operating in combination with PSD.

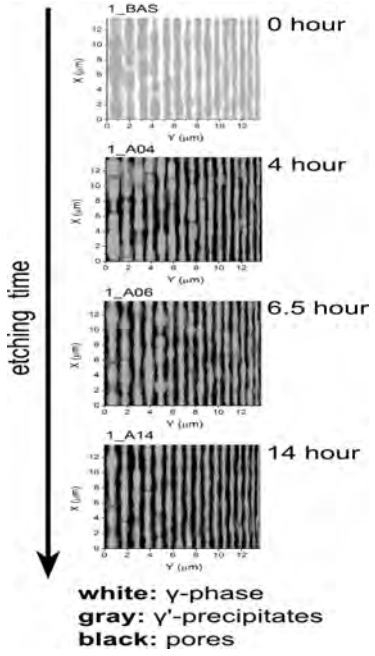

Fig. 7. Nanoporosity development in metalic membrane

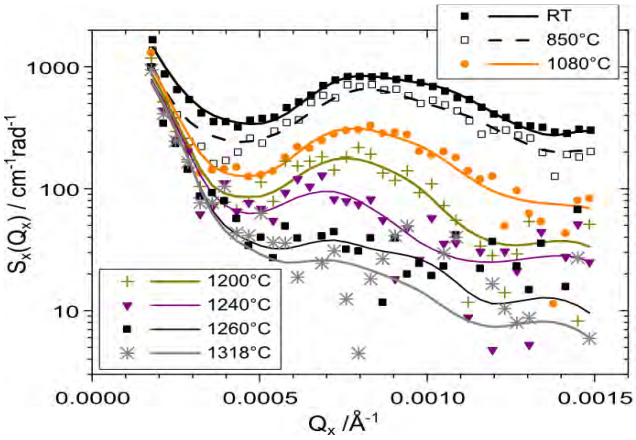

Fig. 8. Precipitate dissolution in CMSX4 single-crystal nickel-based superalloy

the angular distribution of the scattered neutrons to the spatial distribution and to analyze the whole scattering curve by a one-dimensional position sensitive detector (see Fig. 6) [16]. It reduces the exposition time per sample typically to 0.5-5 hours (depending on the *Q*-resolution and sample cross-section). The remote control of the curvatures of the monochromator and analyzer crystals makes possible to tune the instrument resolution in the ΔQ range from 10^{-4} to 10^{-3} Å^{-1}, according to the expected size of investigated inhomogeneities. An absolute calibra-tion of scattering cross-sections is possible by measuring the intensity of the direct beam (no calibration samples are required). The instrument operates in fully automatic mode, including

a sample exchanger. The SANS diffractometer is in our case mainly used for studies of inhomogeneities in the size range from 50 nm to 1000 nm i.e. large precipitates in alloys (superalloys), porous materials (superplastic ceramics, ceramic thermal barrier coatings), nano-particles in ceramic-intermetallic compounds ($MoSi_2$ with Si_3N_4 and SiC particles) and large inhomogeneities in polymers/microemulsions (dimethyl-formamide-cyclohexan domains segragated by diblock copolymer). As application examples Fig. 7 and Fig. 8 show the results of studies of the nanoporosity in metallic membrane (where the aim of the experiment was to determine a dependence of the pore depth on the etching time by using SANS) and in-situ studies of high-temperature microstructure (precipitate dissolution in CMSX4 single-crystal nickel-based superalloy was investigated), respectively [17,18].

2.6. Strain/stress scanning in polycrystalline materials

The dedicated two-axis diffractometer installed at the channel HK4 is equipped with bent Si and Ge perfect single crystal monochromators which are easily changeable according to the experimental requirements. The diffractometer is usually used for macro strain scanning of polycrystalline materials. An easy change of the instrument parameters permits one to use it also for another type of experiments, e.g. Bragg diffraction optics experiments. The diffractometer uses advantages coming from focusing both in real and momentum space and yields good resolution and luminosity, especially for samples of small dimensions [19]. The resolution properties of the device are reached in a limited range of momentum transfer for which the focusing conditions are optimized. The corresponding optimization can be done easily by using a remote control of the curvature of the monochromator. In the case of the strain scanning of the sample, the gauge volume is determined by two fixed Cd slits (2-5) mm x (3-30) mm in the incident and diffracted beams and the measurements are performed in the vicinityof the scattering angle of $2\ _S=90°$. For scanning the sample a *x-y-z* stage or ABB robot system (see Fig. 9) can be used. The instrument is controlled by PC. The diffractometer has a changeable monochromator take-off angle and can be set and operate at a suitably chosen - neutron wavelength in the thermal neutron range from 0.1 nm to 0.235 nm. In the case of -Fe and -Fe samples it usually operates at the neutron wavelength of 0.235 nm, when providing a maximum detector signal and good resolution after diffraction on -Fe(110) and/or -Fe(111) lattice planes. By recent installation of the 2D-PSD (20x20 cm^2, 2 mm spatial resolution), the acquisition of the data has been increased by a factor of 4. Depending on the sample-detector distance and the required resolution the PSD detector can cover from 10° to15° of the scattering angle $2\ _S$. The quality of the instrument are supported by the experimental results of stress measurements obtained on the welded test-sample shown in figures 10 and 11 [20]. The aim

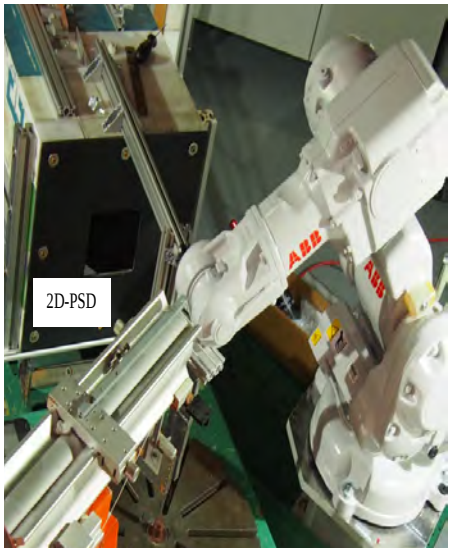

Fig. 9. Photo showing the ABB robot system and 2D-PSD detector.

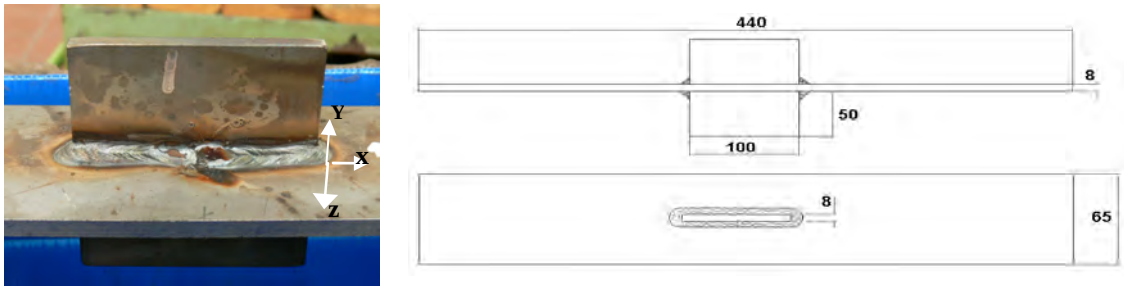

Fig. 10. Photo of the fatigue test specimen and its dimensions.

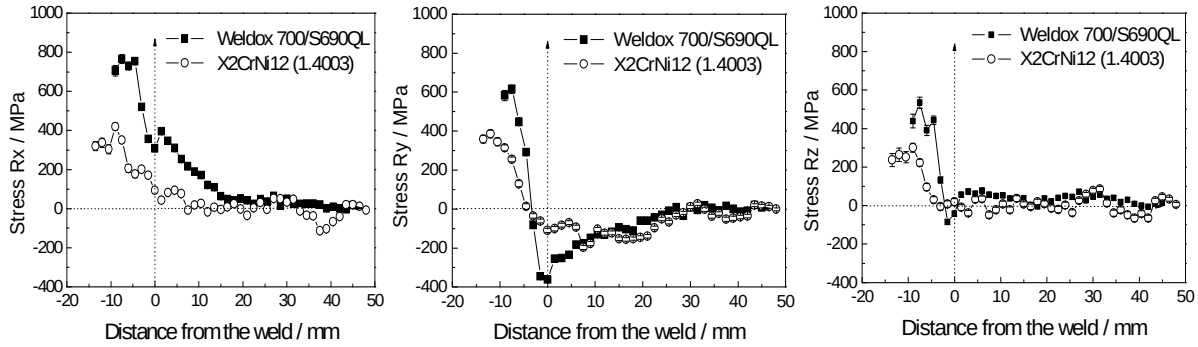

Fig. 11. Residual stress distribution in the vicinity of the welds welded by D4-6547 filler material. Parent materials: Weldox 700/S690QL and X2CrNi12 (1.4003).

of the performed residual stress studies was to find optimum composition of the additive material for electrodes in order to decrease residual stresses in the vicinity of the foot of the welding joint and consequently, to increase the fatigue strength. For samples we used parent material Weldox 700/S690QL and X2CrNi12 (1.4003) and D4-6547 filler for electrodes.

2.7. High Resolution Diffraction for Materials Research

Another high-resolution two-axis diffractometer optimized for investigation of elastic and plastic deformation studies in polycrystalline materials is installed at the channel HK9. The instrument is used especially for in-situ thermo-mechanical testing of materials, i.e. to study the deformation and transformation mechanisms of modern types of newly developed materials. Neutron diffraction performed in situ upon external loads brings a wide range of valuable structural and sub-structural parameters of the studied material which is easy to correlate with the parameters of the external load. The obtained microstructural parameters of the examined material can be directly compared with the parameters of micromechanical models. This approach brings a deeper understanding of processes ongoing in materials upon deformations, thermal treatments or phase transformations. The instrumental parameters are as follows: Horizontally and vertically focusing monochromator employing elastically bent Si single crystals, neutron wavelength - 1 Å ≤ ≤ 2.7 Å, neutron flux at the sample position - 10^5 n.cm^2.s^{-1} at =2.3 Å, angular range of scattering angles - 25°< 2 $_S$< 90° and resolution - $2 \cdot 10^{-3} \leq \Delta d/d \leq 3 \cdot 10^{-3}$. The following sample environments are at a disposal: Two deformation rigs for uni-axial loading (tension or pressure; ± 20 kN and ± 60 kN), resistance heating (T<1200°C) or hot-air heating (T< 300°C), miniature deformation machine for uni-axial loading (tension, pressure; ± 10 kN) inside an Eulerian cradle, Eulerian cradle (inner diameter of 400 mm, 0°< <160°, 0°< < 360°) and a deformation machine for cyclical bending of samples (maximum cycling frequency of 27 Hz). The neutron signal is recorded by 2D-PSD. The above described methods have been recently mainly applied to the investigation of deformation mechanisms of magnesium alloys, including the innovative application of acoustic emission method simultaneously with neutron diffraction. Complementary dataset about the loading mode dependence of twinning was obtained. Since the acoustic emission is sensitive to twin nucleation whereas diffraction to twin growth. The different behaviour of this material in tension and compression was also observed [21].

3. Summary

It has been demonstrated on sevral presented examples that high quality experiments of basic, interdisciplinary as well as applied research which could be competetive on an international level can be effectively carried out at the medium power research reactor LVR-15 in Řež. The research can cover a large scale of experimental investigations related to structure studies of new materials, structure phase transformations, chemistry, material testing, industrial product qualification, tracing of elements (e.g. in enviromental, chemical, geological and biological samples), cultural heritage, etc. Some more details about the research in NPL can be found on the web page http://neutron.ujf.cas.cz/en/npl/research.

Finally, it should be pointed out that all instruments of NPI are opened to external users and the measurements can be free when a new proposal is submitted through CANAM-ACCESS project (see http://neutron.ujf.cas.cz/en/instruments/user-access/).

Acknowledgement

The authors thank very much to colleagues from Neutron Physics Laboratory for providing related experimental results used in this paper. The experimental studies of external users on the NPI facilities are carried out in the frame of the CANAM infrastructure project LM2011019 managing by NPI ASCR Rez.

References

[1] MIKULA, P., KYSELA, J., "Řež's Medium Power Research Reactor LVR-15 Opened for External Users", Physics B, **241-243** (1998) 39.

[2] MIKULA, P., LUKÁŠ, P., STRUNZ, P., ŠAROUN, J., VRÁNA, M., DLOUHÁ, M., VRATISLAV, S., "Neutron Scattering Experiments of Materials Science at Řež's Reactor", Physica B, **241-243** (1998) 92.

[3] VACÍK, J., HNATOWICZ, V., KÖSTER, U. "Diffusion of Boron in CaF_2", American Nuckear Society Transactions **98** (2008) 422.

[4] DOWNING, R.G., et al., "Neutron Depth Profiling: Overview and Description of NIST Facilities", Journal of Research of NIST **98** (1993) 109.

[5] KUČERA, J., NOVÁK, J.K., KRANDA, K., PONCAR, J., KRAUSOVÁ, I., SOUKAL, L., CUNIN, O., LANG, M., "INAA and Petrological Study of Sandstones from the Angor Monuments", J. Radioanal Nucl. Chem. 278 (2008) 299.

[6] KUBEŠOVÁ, M., KUČERA J., "Validation of k_0 Standardization Method in Neutron Activation Analysis" (Proc. 5th Int k_0 Users Workshop, Belo Horizonte, Brazil, 2009).

[7] ŘANDA, Z. et al., "Elemental characterization of the new Czech meteorite Morávka by neutron and photon activation analysis", J. Radi. Nucl. Chem., **257** (2003) 275.

[8] BISCHOFF, A. et al., "Jesenice–A new meteorite fall from Slovenia", Meteorit. Planet. Sci. **46** (2011) 793.

[9] KRAUSOVÁ, I. et al., "Determination of ^{129}I in biomonitors collected in the vicinity of a nuclear power plant by neutron activation analysis", J. Rad. Nucl. Chem., **295** (2013) 2043.

[10] GALINHA, C. et al., "Selenium determination in cereal plants and cultivation soils by radiochemical neutron activation analysis", J. Rad. Nucl. Chem., **294** (2012) 349.

[11] GALINHA, C. et al., "Selenium in bread and durum wheats grown under a soil supplementation regime in actual field conditions, determined by cyclic and radiochemical neutron activation analysis", J. Rad. Nucl Chem., **304** (2015)139.

[12] KRAUSOVÁ, I. et al., "Impact of the brewing process on the concentration of silicon in lager beer", J. Inst. Brew., **120** (2014) 433.

[13] RASMUSSEN, K. L. et al., "Was he murdered or was he not? Part I: Analyses of mercury in the remains of Tycho Brahe**",** Archaeometry **55** (2013) 1187.

[14] WONG, C. H. A. et al., "Synthetic routes contaminate graphene materials with a whole spectrum of unanticipated metallic elements", Proc. Nat. Acad. Sci. USA, **111** (2014) 13774.

[15] SMRČOK, L., PETRÍK, I., LANGER, V., FILINCHUK, Y., BERAN, P., "X-Ray, Synchrotron, and Neutron Diffraction Analysis of Roman Cavalry Parade Helmet Fragment" Crystal Res. Technol. **45** (2010) No. 10, 1025.

[16] STRUNZ, P., ŠAROUN, J., MIKULA, P., LUKÁŠ, P., EICHHORN, F., "Double Bent Crystal SANS Setting and its Applications", J. Appl. Cryst. **30** (1997) 844.

[17] STRUNZ**.** P., MUKHERJI, D., NÄTH, O., GILLES, R., RÖSLER, J., **"**Characterization of Nanoporous Superalloy by SANS", Physica B **385–386** (2006) 626.

[18] STRUNZ, P., MUKHERJI, D., ŠAROUN, J., KEIDERLING, U., RÖSLER, J., "Pore Structure Characterization and In-Situ Diffusion Test in Nanoporous Membrane Using SANS" Journal of Physics: Conf. Series **247** (2010) 012023.

[19] MIKULA, P., VRÁNA, M., LUKÁŠ, P., ŠAROUN, J., WAGNER, V., "High-Resolution Neutron Powder Diffractometry on Samples of Small Dimensions", Materials Science Forum, **228-231** (1996) 269.
[20] MRÁZ, Ľ., KARLSSON, L., VRÁNA, M., MIKULA, P., "Residual Stress Distribution Measurement by Neutron Diffraction of the Single Pass Fillet Steel Welds", Applied Mechanics and Materials, **732** (2015) 13.
[21] ČAPEK, J., et al., "Study of the loading mode dependence of the twinning in random textured cast magnesium by acoustic emission and neutron diffraction methods", Materials Science and Engineering A - Structural materials **602** (2014) 25.

Silicon ingot thermal performance during irradiation and effects on electronic parameters

M. M. Osman*, S. A. Agamy**, M. S. Nagy**, M. Sultan

**** Nuclear Research Center, ** Alexandria University, Egypt***
mosa_osman@yahoo.com

Abstract

During the silicon ingot irradiation in a research reactor, with a high thermal neutron flux, the temperature of the silicon ingot should be less than 180 ^{0} C as a key parameter to get an electronically accepted ingot after the irradiation. It is too hard to measure the temperature of the silicon ingot during irradiation due to two main reasons, the first is that the silicon irradiation position is under water by more than ten meters while the second reason is the rotation of the silicon ingot during irradiation to achieve radial flux uniformity inside the silicon ingot (to avoid silicon self-shielding). The finite element heat transfer code (FEHT) is used to calculate the temperature distribution in the silicon ingot during irradiation. For 5 and 6 inches ingots diameter and different lengths (250mm, 400mm, 500mm) the FEHT is adopted to calculate the temperature distribution, the temperature contour, and energy rate. The calculations showed that, the modified design produced doped silicon ingot with enhanced electronic parameters than the old design with higher production capacity.

Keywords; silicon doping, heat transfer, carrier life time, resistivity

Introduction

When silicon is irradiated the objective is to produce number of phosphorus atoms in the target sample in order to obtain a given resistivity after the treatment. The resistivity of the sample is decreased by the transmutation of the silicon, by neutrons, to phosphorus. Irradiation is carried out by thermal neutrons. The basic reaction of the process:

$$Si^{30}\ (n,\gamma)\ Si^{31} \xrightarrow{t_{\frac{1}{2}}=2.6.hr} P^{31} + \beta^{-1}\ (1.47\ MeV) \qquad (1)$$

The side reaction which tends to cause the number of doped nuclei obtained by the first reaction to disappear since the capture cross section here is only 0.2 barn the amount of sulfur produced is minute in doping terms. But longer half life for decay P^{32} can impose restrictions on handling of low resistivity NTD (resistivity less than 10 ohm.cm) [1,2].

$$P^{31}\ (n,\gamma)\ P^{32} \xrightarrow{t_{\frac{1}{2}}=14.3days} S^{32} + \beta^{-1}\ (radioactivity) \qquad (2)$$

the head on collision of 1 MeV neutron with silicon atoms will knock out about 200 silicon atom from their lattice sites. Thus thermal to fast ratio in irradiating silicon is critical.
During silicon ingot irradiation, the temperature of the silicon ingot should be less than180 ^{0} C [3]. It is considered as a key parameter to get accepted ingot after irradiation. Since the silicon

Ingot temperature during irradiation control the diffusion of the impurities and defects in the silicon ingot. The charge carrier life time (electron in negative type semiconductor) affected by the diffusion of the impurities and defects which act as trapping center for the charge carrier hence, the charge carrier life time decreases. Charge carrier life time can consider the switching time for the electronic

components. It is too hard to measure the temperature of the silicon ingot during irradiation. Due to two main reasons, the first is that the silicon irradiation position is under water by more than ten meters. The second reason, that the silicon ingot is rotating during irradiation to achieve radial flux uniformity inside the silicon ingot (to avoid silicon self-shielding). The finite element heat transfer code (FEHT) [4] is used to calculate the temperature distribution in the silicon ingot during irradiation. For 5 and 6 inches ingots diameter and different lengths (250mm, 400mm, 500mm) the FEHT is adopted to calculate the temperature distribution, the temperature contour, and energy rate. The heat generation in the silicon ingot during irradiation is 20 Watt / Kg [5]. In the Temperature calculation during irradiation, two main cases have been considered:

1- fixed temperature case:

   a. inlet temperature to the ingot = outlet temperature = 40 ^{0}C

   b. inlet temperature to the ingot = 35 ^{0}C and outlet temperature = 40 ^{0}C

2- convective boundaries case (hot case, cold case)

   A- cold case (h = 128 W/Cm^2. ^{0}C, k = 0.84 W/Cm^2. ^{0}C*)*

   B- cold case (h = 159 W/Cm^2. ^{0}C, k = 0.80 W/Cm^2. ^{0}C*)*

Temperature Distribution in 500 mm ingot length and 6 inches diameter

All the boundaries are convective boundaries (cold case)

During irradiation of two silicon ingot with total length 500mm (2 ingot x 250 mm) the maximum temperature is 70.4 ^{0}C. This value is less than the safety criteria (180 ^{0}C). It is known that below 100 ^{0}C, the diffusion of impurity and defects such as swirl defect is kept to a minimum value. This gives a silicon ingot with ideal electronic parameters. Figure (1) shows the temperature distribution in 500 mm ingot length and 6 inches diameter. *All the boundaries are convective boundaries* (cold case), this is the highest temperature case. With the new design the graphite blocks are dispensed with. So this case can not be detected with new design, but the fixed temperature case is the real case.

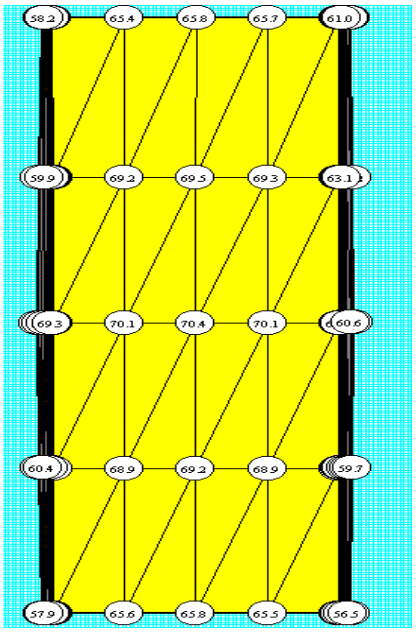

Figure (1) temp. distribution in 500 mm ingot and 6 inches diameter convective boundary

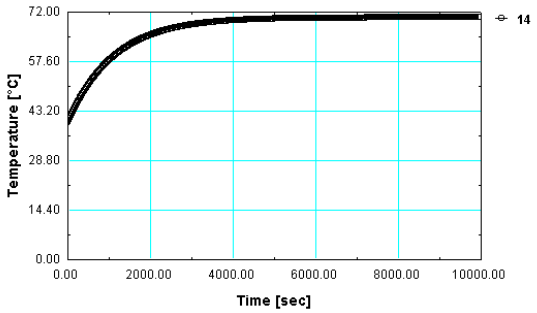

Figure (2) Maximum temperature in the 500 mm ingot and 6 inches diameter

Calculation of temperature in five inches ingot (new design)

The coolant (water) inlet temperature and outlet temperature is the same and equal to 40 ^{0}C. Coolant inlet temperature is 35 ^{0}C, and the outlet temperature is 40 ^{0}C.

Figure (3) shows the temperature distribution in 280 mm length silicon ingot, 5 inches diameter. (A) Inlet temperature = outlet temperature = 40 ^{0}C, (B) inlet temperature = 35 ^{0}C, outlet temperature = 40

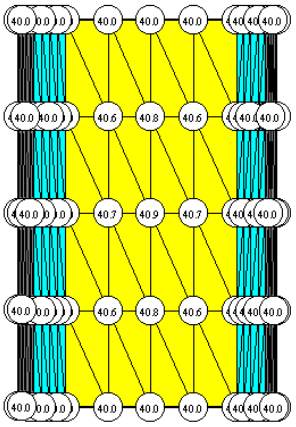

Figure (3) temperature distribution in 280 mm silicon ingot height new design T_i=T_o=40 ^{0}C

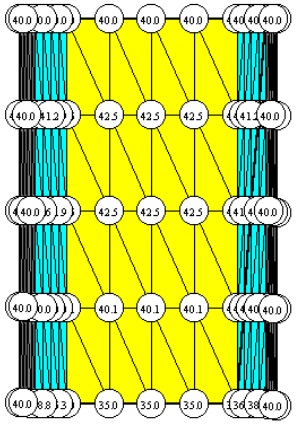

Figure (4) temp. distribution in 280 mm silicon ingot height new design T_i =35 ^{0}C, T_o=40 ^{0}C

Maximum temperature and energy rate in 280 mm ingot length and 5" diameter

Figure (5) show the maximum temperature change with the time. In case (A) the temperature saturated after very small time (120-180 Sec.) for 280 mm ingot length and 5" diameter.

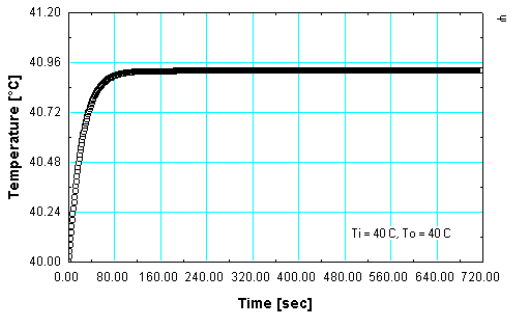

Figure (5) maximum temp. in 280 mm length silicon ingot and 5 inches diameter. (A) Inlet

Maximum energy rate in 500 mm ingot length and 5" diameter

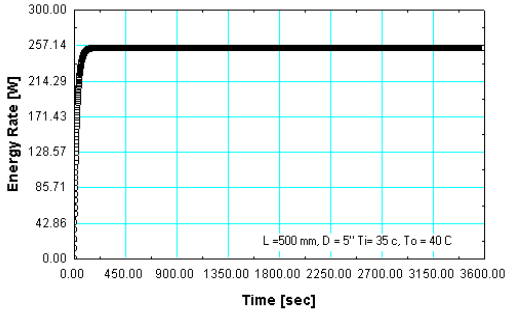

Figure (6) shows the maximum energy rate (257 W) in 500 mm ingot length and 5" diameter.

Heat generation in the silicon ingot during irradiation:

One of the input parameter to the FEHT code during calculation of temperature of the silicon ingot during irradiation. From the literature the heat generation value between 20 W/Kg to 25 W/Kg. however, the relation between the heat generation value and maximum temperature in 6-iches and 500 mm silicon ingot has been studied. At the safety limit of the maximum temperature (180 ^{0}C), the equivalent heat generation is 92 W/Kg. the safety margin in the assumed heat generation is large enough to avoid reaching the safety limit of the temperature. Figure (7) shows the relation between the heat generation in the silicon ingot during irradiation and the maximum temperature in 6-inches, 500 mm silicon ingot.

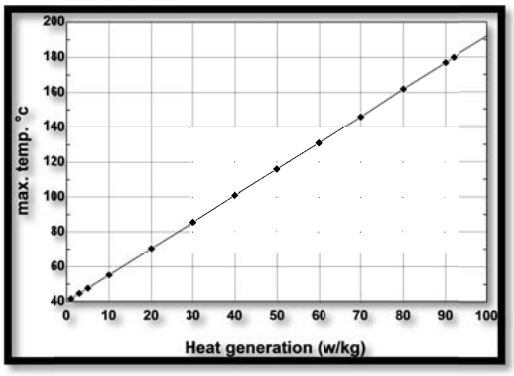

Figure (7) relation between maximum temperature and heat generation in 500 mm length and 6 -inches silicon ingot

Comparison between old and new design minority carrier life time

a- <u>Old design</u>

Figure (8) shows old design charge carrier life time (electron). A value between 4- 7.6 micro-sec has been obtained, which is a very small electron life time due to the diffusion of defects during irradiation.

Measured Life Time = 7.6 micro-sec Effective life time = 7.66 micro-sec

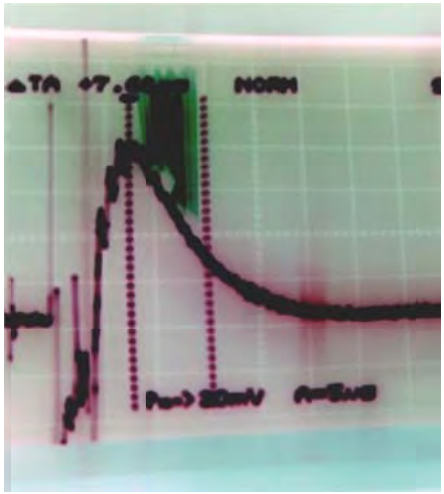

Figure (8) old design charge carrier life time

b- New design

Figure (9) shows new design charge carrier life time (electron). A value between 103- 121 micro-sec has been obtained, which is an optimum electron life time, due to the diffusion of defects kept minimum during irradiation.

Measured Life Time = 121 micro-sec

Effective life time = 138.6 micro-sec

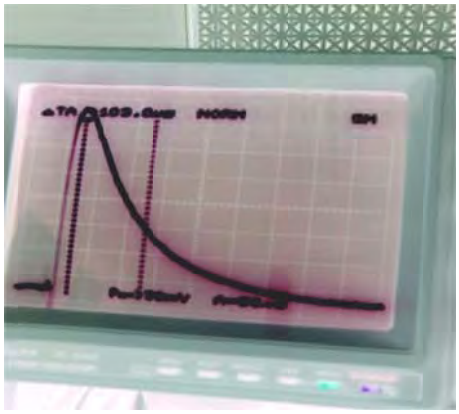

Figure (9) electron life time in silicon ingot irradiated in the new design

Conclusions

The old design (5 inches) is shown in Figure (10). The irradiation strategy and configuration in the old design has a weakness points in the design:

1- The coolant gap only 2 mm through 1200mm long (total length of the thermal column).
2- There is no direct contact between the ingot and coolant (water).
3- The ingot it self is kept in sealed aluminum container (there is a gap of air).
4- There is a graphite plugs under and above the silicon ingot with total length of the graphite of 900 mm.

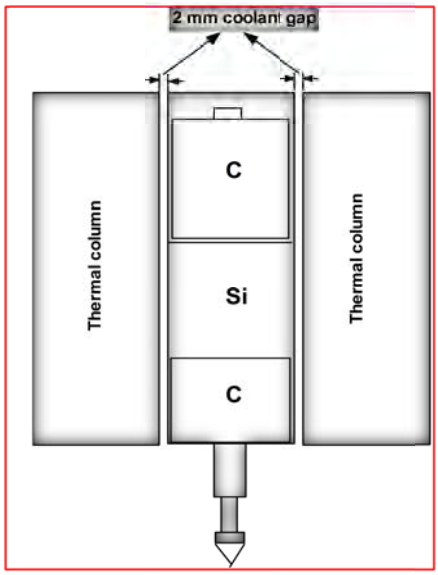

***Figure* (10) old design configuration**

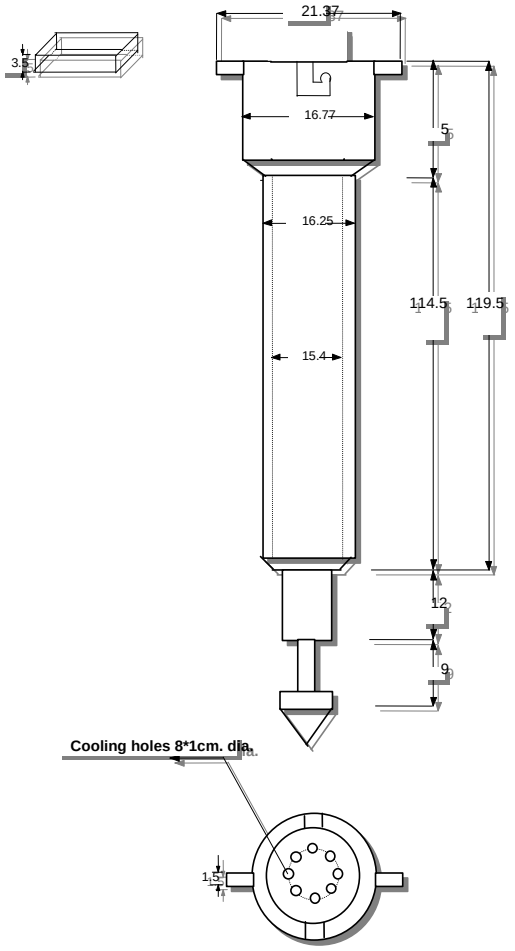

Figure (11) new design configuration

Finally never irradiate silicon ingot in sealed can. The silicon irradiation rigs design must be take into account t hree ste ps. First, is m echanical d esign w hich i ncludes a pro per m aterial. Second, is the neutronic design which includes thermal neutron to fast neutron ratio and the neutron spectrum. Third, is the t hermal design w hich ana lyzes t he tem perature d istribution ins ide the sil icon ingo t dur ing irradiation and modify the whole design if needed to produce high quality silicon ingot.

References

1. S. Mahajan, K.S. Sree Harsha "Principles of Growth and Processing of Semiconductors-international Edition" Arizona University, San jose State Univeristy. McGraw-Hill Companies. Pp. 13. 1999.
2. *2-* K.A. Jackson and W. Schroter "handbook of semiconductor technology electronic structure and properties of semiconductors " volume 2. Wiley – VCH Verlag GmbH, D69469 Weihein, Germany. PP18-20.(2000).
3. *3-* Annual book of ASTM standard Volume 10.05 electronics(II) F 81-95, PP. 95-107, (1996).
4. *4-* Finite element analysis, "FEHT", Numerical code for heat transfer analysis, 2008.
5. *5-* J.Koziel, K. Pytel and L. waltsr, " Neutron doped silicon in polish reactors", warsaw, Poland, 1988.

PERFORMANCE TEST OF SPND FOR THE DEVELOPMENT OF LLICI AT THE UCI TRIGA REACTOR

S.W. YANG, S.J. PARK, M.S. CHO
Neutron Application Technology Division, Korea Atomic Energy Research Institute
111, Daedeok-daero 989 Beongil, Yuseong-gu, Daejeon, 34057, Republic of Korea

J.T. WALLICK, G.E. MILLER
Department of Chemisty, University of California, Irvine
University of California, Irvine, Irvine, CA 92697, US

H.C. SHIN, K.H. CHA
Central Research Institute, Korea Hydro & Nuclear Power Co., Ltd
70, Yuseong-daero 1312 Beongil, Yuseong-gu, Daejeon, 34101, Republic of Korea

ABSTRACT

This test is conducted to verify the characteristics of self-powered neutron detectors (SPNDs) for the long-lived in-core instrumentation (LLICI) being developed by Korea Hydro & Nuclear Power Co., Ltd (KHNP) before a long-term irradiation test at the High flux Advanced Neutron Application Reactor (HANARO) in Korea. For this test, we search for a research reactor to meet the neutron flux level, usability, and experience. The TRIGA reactor at the University of California, Irvine (UCI) was selected because it meets the above requirements. Therefore, a performance test of SPND was conducted at the UCI TRIGA reactor. The test was carried out successfully. The test specimens are seven SPNDs and one background wire. Among the seven SPNDs, two are the same as the conventional specimens, and five are those in which the emitter material and size are changed. All SPNDs and the background wire were tied together to reduce the difference of the neutron flux and facilitate the handling, and were inserted in the central thimble. The nine reactor operations were conducted to measure the noise, sensitivity, interference, linearity, and dynamic characteristics for SPNDs. As a result of this test, we could understand the signal characteristics according to the emitter material and the size of the SPNDs and background wire. The testing method using two research reactors can be effective, and thus this case will be a good instance of cooperation. As in this study, although the power of the UCI TRIGA reactor is relatively lower that of HANARO, the signal characteristics of SPND can be confirmed under the various conditions of static and dynamic reactor operation because it is easy to change the reactor power. HANARO is more effective for a long-term irradiation test owing to the higher neutron flux. This test result in the UCI TRIGA reactor will be used as important data for the following test at HANARO.

1. Introduction

Currently, Korean nuclear power plants are using the ICI (In-Core Instrumentation) based on Rhodium-emitter SPND (Self Powered Neutron Detector). However, its lifespan is relatively short due to the rapid depletion of Rhodium. Therefore, it requires a lot of instrument replacement and waste costs. KHNP (Korea Hydro & Nuclear Power Co., Ltd) is developing LLICI (Long-Lived ICI) to overcome above disadvantages.
KHNP designed and manufactured some candidate SPNDs for the LLICI. Before the verification at a commercial nuclear power plant, the irradiation experiment for SPNDs must be conducted to verify its static and dynamic performances using a research reactor. The in-core performance test for the SPND was prepared at HANARO (High flux Advanced Neutron Application Reactor) that is a unique research reactor in Korea[1]. Although HANARO is a good research reactor for the performance test with high neutron flux, it is difficult to observe

the dynamic performance of the SPND because HANARO has the limitation of reactor power maneuver. To observe the dynamic performance of the SPND, we investigated some research reactors in other countries considering the neutron flux, possibility, facilities, cost, and experience. TRIGA reactor in the UCI (University of California, Irvine)[2] was selected for the performance test of the SPND.
In this paper, we present the performance test procedure of the SPND for the development of the LLICI at the UCI TRIGA reactor. We also focused on the international cooperation for the efficient use of research reactors.

2. Performance test for SPND
2.1 Test specimen

Table 1 shows the SPNDs for the performance test. Total seven SPNDs and one background wire were used. Among them, Rhodium-emitter SPNDs with 1.58 mm outer diameter were used as a reference that is same dimension and material with the conventional product. KHNP designed the SPNDs of LLICI using other emitter materials or changing its geometrical dimension. All SPNDs and background wire were inserted in the central thimble of UCI TRIGA reactor. During the test, minimizing the difference of neutron flux between the SPNDs is important. Also, test specimens must be easily handled during the test. Therefore, all SPNDs and background wire were tied by metal band with the aluminum foil and tube in the edge of emitter region as shown in Fig. 1.

Emitter material	Emitter length (mm)	Length (mm)	Emitter diameter (mm)/ Insulator thickness(mm)/ Outer sheath thickness(mm)	Outer diameter (mm)	Quantity (EA)
Vanadium	400	16,100	1.13 / 0.4195 / 0.43	2.829	2
Rhodium			0.46 / 0.3 / 0.26	1.58	2
Rhodium			1.13 / 0.4195 / 0.43	2.829	2
Cobalt			1.13 / 0.4195 / 0.43	2.829	1
Background wire			-	2.829	1

Table 1. The specification of SPND for the performance test

Fig. 1. The assembly of SPNDs

2.2 Test procedure

Fig. 2 shows the schematic diagram of the performance test method for the SPNDs. Assembled SPNDs and background wire were inserted into the central thimble that is dry hole for the irradiation in the center of the core. All signals of SPNDs and background wire were recorded by data acquisition system (DAS). To convert from the reactor power to the signal, the signal of compensated ionization chamber (CIC) of the UCI TRIGA reactor was connected into the DAS and recorded. The performance test has five items such as noise measurement, sensitivity, interference, linearity, and dynamic characteristics.

A. Noise measurement: The noise of each SPND was measured before the test and after the installation in central thimble to verify productivity and integrity.

B. Sensitivity: While gradually increasing the reactor power, the signal of each SPND was detected. The neutron flux of initial detecting power was compared with design value.

C. Interference: Since all SPNDs were handled in a batch, its effect must be evaluated. The test was conducted by insertion of single SPND. And we compared the signal was installation conditions between a single and a batch.

D. Linearity: We observed the linearity of the SPND signal with changing reactor power by stage.

E. Dynamic characteristics: We analyzed the signal during the power maneuver.

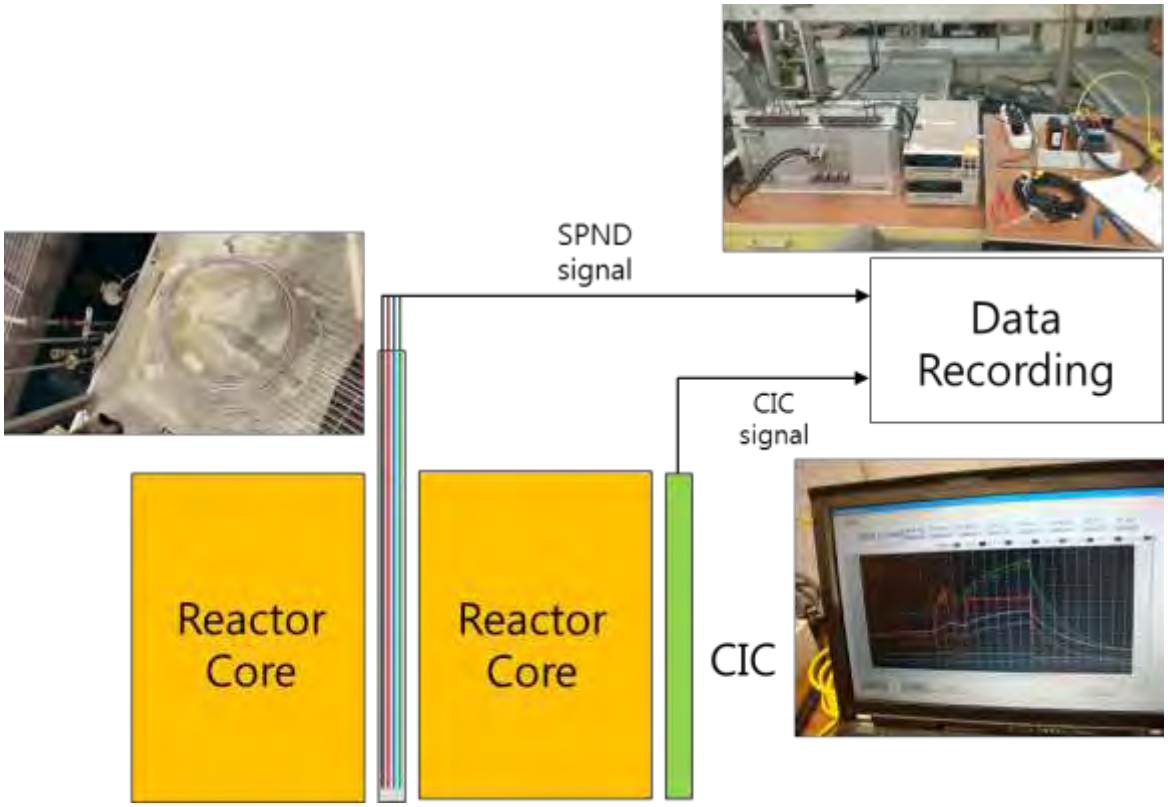

Fig. 2. The schematic diagram of the performance test method

Fig. 3 shows the typical recorded CIC raw signal of this test. The abnormal signal was found in the initial reactor operation. The reactor power was initially increased and maintained at 150 kW during 30 minute. And reactor power was changed to 200, 250, 200, 250, 225, 200 kW by stages. Total nine reactor operations were conducted for this test.

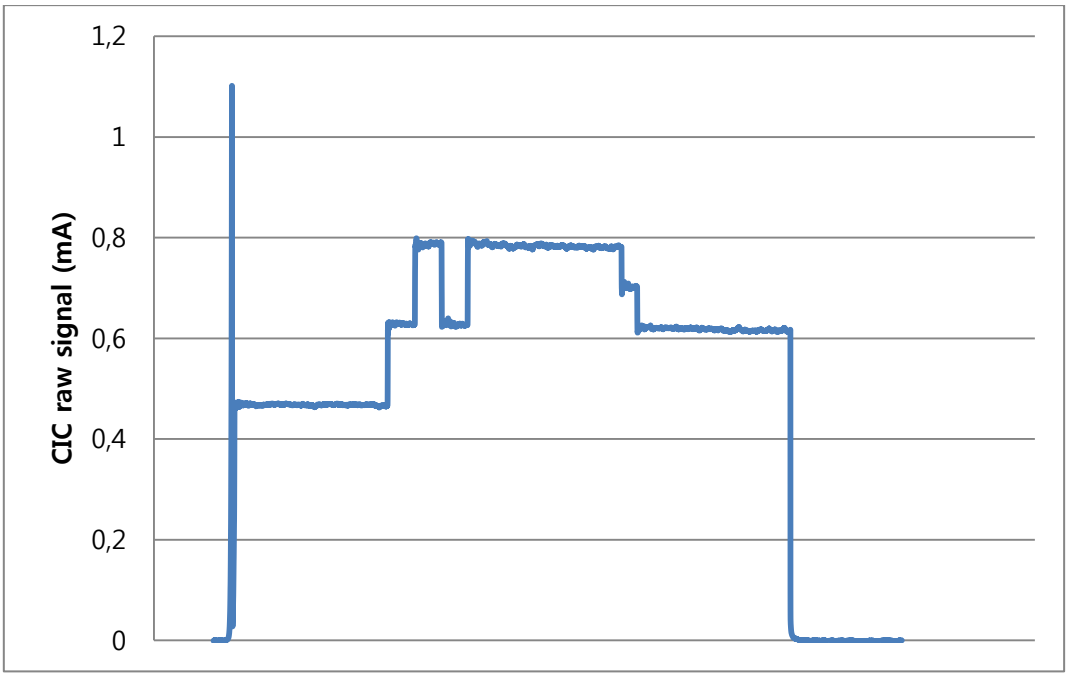

Fig. 3. The typical recorded CIC raw signal

2.3 Test results

The performance test was successfully conducted. The static and dynamic signal of SPNDs and background wire was measured and recorded by the DAS. As a result of this test, we could understand the signal characteristics according to the emitter material and the size of the SPNDs and background wire. **The measurement results are omitted in this paper due to non-disclosure agreement.**

3. International cooperation for use of research reactor

In Korea, two TRIGA reactors had been operated. However, both reactors were decommissioned. Currently, HANARO and AGN-201 are operating and KJRR is constructing. HANARO is a large-scale research reactor that is used for material irradiation test, NTD (Neutron Transmutation Doping) Silicon and radioisotope production, material research using neutron beam. AGN-201 is a small-scale reactor of 10W power. Since the operation range of the research reactors in Korea is limited, it is not appropriate to identify the characteristics of instrumentation like the SPND. Therefore, not only large-scale research reactor but also middle-scale research reactor is needed to conduct the performance test of instrumentation.
Although internationally approximately 246 research reactors are operating, large-scale research reactors are concentrated in the major industrialized countries. Therefore, it is necessary to make the international network for complementary cooperation. It has advantages of reducing construction cost of additional research reactor and efficient use of conventional research reactor. As this performance test of the SPND, the international cooperation between HANARO and the UCI TRIGA reactor will be as a good case for the development of the LLICI.

4. Conclusion and future work

Seven SPNDs and one background wire were used for this test. All specimens were tied to reduce the difference of neutron flux. This assembly was inserted in the central thimble at the UCI TRIGA reactor. We conducted the test with nine reactor operations and measured the signal of SPNDs and background wire. This test result will be used as the important data for the development of long-lived SPND and the performance test at HANARO. We are preparing the long-term static performance test at HANARO. It will be started from this year. The testing method using two research reactors can be effective, and thus this case will be a good instance of international cooperation.

Acknowledgement

This work was supported by the National Research Foundation of Korea (NRF) grant funded by the Korea government (MSIP) (No. 2013035822).

5. References

1. S. W. Yang et. al, In-pile test of self-powered neutron detectors (SPNDs) at HANARO, KAERI Report, KAERI/CR-608/2015.
2. Nuclear Analysis of the University of California – Irvine TRIGA Reactor, TRIGA Reactor Division of General Atomics, GA 39364, Rev. 0.

THE POWER CONTROL BASED SUBCRITICALITY MONITORING (PCSM) METHOD FOR ADS REACTORS

M. CARTA[1], V. FABRIZIO[1], L. FALCONI[1], A. GANDINI[2], M. G. IORIO[1], V. PELUSO[3], E. SANTORO[1], N. BURGIO[1]

[1]ENEA CR Casaccia - via Anguillarese 301 00123 Santa Maria di Galeria, Italy

[2] Dipartimento DIAEE - Università degli Studi di Roma 'La Sapienza' – Corso Vittorio Emanuele II 244 - 00186 Roma - Italy

[3]ENEA C.R. BOLOGNA - Via Martiri Monte Sole 4 - 40129 Bologna - Italy

ABSTRACT

Basing on the extension of the HGPT (Heuristical Generalized Perturbation Theory) methodology to subcritical systems [1], a procedure is proposed for the online monitoring of the subcriticality level of ADS reactors with minimal interaction with the plant normal operation. The proposed method, which shall be named with the acronym PCSM (for Power Control based Subcriticality Monitoring), consists in compensating slow, small movements of a control rod with as well slow, small alterations of the external source strength, so that the overall power is maintained constant.
The estimation of the subcriticality level requires the knowledge of a bias factor. This implies the standard precalibration of a control rod and the precalculation of the importance function associated with the reactor power control (in this case, the external neutron source strength). To this purpose a calculation procedure will be implemented into the ERANOS code so to extend its present GPT calculation modality.
An experimental verification of the proposed method on the TRIGA reactor at the ENEA Casaccia Center is been considered. The reactor would be operated at different subriticality levels corresponding to different positions of a control rod and would be driven by a suitable neutron source.

1. Introduction

A problem connected with the operation of subcritical (ADS) reactors is posed by the ability of evaluating with sufficient precision their subcriticality level. In this paper we illustrate a general approach to this problem, making use of a derivation of the zero kinetics equations relevant to these systems [1,2]. These equations have been obtained starting from the transport, or diffusion ones governing the neutron and the i'th precursor densities and resulted, in terms of the normalized power P and of the "effective" precursor density ξ_i,

$$\ell_{\text{eff}} \frac{dP}{dt} = (\rho_{\text{gen}} - \alpha\beta_{\text{eff}})P + \alpha \sum_{i=1}^{I} \lambda_i \xi_i + \zeta(1-P) + \rho_{\text{source}} \tag{1}$$

$$\frac{d\xi_i}{dt} = \beta_{i,\text{eff}} P - \lambda_i \xi_i \ , \tag{2}$$

where the coefficients represent physically significant quantities, with expressions:

$$P(t) = \frac{W(t)}{W_o(1+q)} \qquad \left(q = \frac{< \delta\boldsymbol{\Sigma}_f^T, \boldsymbol{\phi}_o >}{< \boldsymbol{\Sigma}_{f,o}^T, \boldsymbol{\phi}_o >} \right) \qquad \text{(normalized power)} \tag{3}$$

$$\xi_i = \frac{< m_{s,o}^* m_i >}{< \mathbf{n}_{s,o}^*, \bar{\chi} S_{f,o} \boldsymbol{\phi}_o >} \qquad \text{(i'th effective precursor density)} \tag{4}$$

$\bar{\chi} S_{f,o} \boldsymbol{\phi}_o$ being the fission source,

$$\ell_{\text{eff}} = \frac{< \mathbf{n}_{s,o}^*, V^{-1} \boldsymbol{\phi}_o >}{< \mathbf{n}_{s,o}^*, \bar{\chi} S_{f,o} \boldsymbol{\phi}_o >} \qquad \text{(effective prompt neutron lifetime)} \tag{5}$$

$$\rho_{gen} = \frac{< \mathbf{n}_{s,o}^*, \delta B \boldsymbol{\phi}_o > + \frac{\gamma}{W_o} < \delta \boldsymbol{\Sigma}_f, \boldsymbol{\phi}_o >}{< \mathbf{n}_{s,o}^*, \bar{\chi} S_{f,o} \boldsymbol{\phi}_o >} \ , \text{(generalized reactivity)} \tag{6}$$

with $\delta B = \delta A + \bar{\chi} \delta S_f$, δA accounting for absorption, leakage and scattering terms perturbations,

$$\rho_{\text{source}} = \frac{< \mathbf{n}_{s,o}^*, \delta \mathbf{s}_n >}{< \mathbf{n}_{s,o}^*, \bar{\chi} S_{f,o} \boldsymbol{\phi}_o >} \qquad \text{(source reactivity)} \tag{7}$$

$$\alpha = \frac{< \mathbf{n}_{s,o}^*, \chi_D S_{f,o} \boldsymbol{\phi}_o >}{< \mathbf{n}_{s,o}^*, \bar{\chi} S_{f,o} \boldsymbol{\phi}_o >} \tag{8}$$

$$\bar{\chi} \equiv (1-\beta)\chi_P + \beta \chi_D \tag{9}$$

$$\beta_{i,\text{eff}} = \frac{\sum_{g=1}^{G} \sum_{j=1}^{J} < n_{s,o,g}^* c_j \chi_{D,g}^j \beta_{i,g}^j \nu\sigma_{f,g}^j \phi_g >}{\sum_{g=1}^{G} \sum_{j=1}^{J} \sum_{i=1}^{I} < n_{s,o,g}^* c_j \chi_{D,g}^j \nu\sigma_{f,g}^j \phi_g >}, \qquad \beta_{\text{eff}} = \sum_{i=1}^{I} \beta_{i,\text{eff}} \tag{10}$$

$$\zeta = \frac{1}{< \mathbf{n}^{*}_{s,o}, \bar{\chi} S_{f,o} \boldsymbol{\phi}_o >} \equiv \frac{1 - K_{sub}}{K_{sub}} \tag{11}$$

where

$$K_{sub} = \frac{< \mathbf{n}^{*}_{s,o}, \bar{\chi} S_{f,o} \boldsymbol{\phi}_o >}{1 + < \mathbf{n}^{*}_{s,o}, \bar{\chi} S_{f,o} \boldsymbol{\phi}_o >} . \tag{12}$$

and the importance $\mathbf{n}^{*}_{s,o}$ is governed by the equation

$$B^{*}_o \mathbf{n}^{*}_{s,o} + \frac{\gamma}{W_o} \boldsymbol{\Sigma}_{f,o} = 0 \tag{13}$$

Coefficient K_{sub} merges into K_{eff} (the multiplication coefficient relevant to the fundamental eigenfunction) with the system approaching criticality.

At unperturbed, steady state conditions $P=P_o=1$ and $\xi_i = \beta_{i,\,eff}/\lambda_i$..

In the following, a method is described [2] for determining experimentally the subcriticality level basing on the above concepts. A calculation exercise will follow to demonstrate the validity of the proposed methodology and as a preliminary step to investigate on a following experimental exercise experimenting it in a subcritical version of a TRIGA reactor at the ENEA Casaccia Center driven by a Cf-252 neutron source.

2. The PCSM method

Consider a change of a (calibrated) control rod position. This would correspond to an experimental reactivity value $\left(\delta k_{eff} / k_{eff}\right)^{\mathbf{exp}}_B$. The associated value $\rho^{exp}_{gen,B}$ of the generalized reactivity could be assumed as

$$\rho^{\mathbf{exp}}_{gen,B} = \rho^{cal}_{gen,B} \; f_b \tag{14}$$

with $\rho^{cal}_{gen,B}$ given by Eq. (6) and f_b a bias factor given by the expression

$$f_b = \frac{\left(\delta k_{eff} / k_{eff}\right)^{\mathbf{exp}}_B}{\left(\delta k_{eff} / k_{eff}\right)^{calc}_B} \tag{15}$$

with $\left(\delta K_{eff} / K_{eff}\right)^{\mathbf{exp}}_B$ obtained by a standard control rod calibration and $\left(\delta K_{eff} / K_{eff}\right)^{calc}_B$ given by the expression

$$\left(\frac{\delta K_{eff}}{K_{eff}}\right)^{calc}_B = \frac{< \boldsymbol{\phi}^{*}_o, \; \delta B_B \boldsymbol{\phi}_o >}{< \boldsymbol{\phi}^{*}_o, k^{-1}_{eff} \bar{\chi} S_{f,o} \boldsymbol{\phi}_o >} \tag{16}$$

ϕ_o^* being the standard adjoint flux and δB_B the perturbation of the (diffusion, or transport) operator relevant to the control rod insertion[1].

Likewise, the source reactivity ρ_{source}^{exp}, associated with a given measured change $\delta \mathbf{s}_n^{exp}$, could be assumed as

$$\rho_{source}^{exp} = \frac{< \mathbf{n}_{s,o}^*, \delta \mathbf{s}_n^{exp} >}{< \mathbf{n}_{s,o}^*, \bar{\chi} S_{f,o} \phi_o >} . \qquad (17)$$

Recalling the definition of importance, we obtain, assuming that the perturbation of the source corresponds to a (measured) fractional change of its strength, represented by $\delta s_n^{exp}/s_n$,

$$\rho_{source}^{exp} = \frac{\delta s_n^{exp}}{s_n} \frac{1}{< \mathbf{n}_{s,o}^*, \bar{\chi} S_{f,o} \phi_o >} \equiv \frac{\delta s_n^{exp}}{s_n} \frac{1 - K_{sub}}{K_{sub}} , \qquad (18)$$

If we consider changes of the control rod and of the external source, such that the power level remains unaffected, we may write, considering Eqs.(1) and (2) at steady state conditions,

$$\rho_{gen,B}^{exp} + \rho_{source}^{exp} = 0 . \qquad (19)$$

Substituting expressions (17) and (18), we have finally

$$K_{sub} = \frac{\delta s_n^{\mathbf{exp}} / s_n}{\delta s_n^{\mathbf{exp}} / s_n - \rho_{gen,B}^{\mathbf{exp}}} , \qquad (20)$$

To note that $\Delta s_n^{\mathbf{exp}} / s_n$ and $\rho_{geB}^{\mathbf{exp}}$ have opposite signs.

So, by properly adjusting the external source strength for compensating a control rod insertion, the subcriticality index ($1-K_{sub}$) can be estimated. The adjustment could be effected gradually at steps, so that the overall power would keep practically unaltered.

3. Calculation exercise

3.1. The TRIGA reactor

RC-1 is a thermal pool reactor, based on the General Atomic TRIGA Mark II reactor design, operating at the thermal power of 1Mw [4]. The core, in the actual configuration composed of 111 standard TRIGA fuel elements, is contained in an aluminium vessel, seven meters deep, filled with demineralised water. A cylindrical graphite structure around the core is the lateral reflector of the reactor. The biological shield is provided by concrete with an average thickness of 2.2 meters. The water inside the vessel provide first biological shield, neutron moderator and cooling mean. Thermal power is removed from the core by natural convection, and exchanged with the environment through two thermohydraulic loops, coupled by two heat exchangers and two cooling

[1] The quantity $\rho_{gen,B}^{\mathbf{exp}}$ given by equation (14) could be as well, and more accurately, be obtained experimentally via a control rod calibration at subcritical conditions by measuring the multiplication coefficient k_{sub} vs. control rod insertion via pulsed source or source jerk techniques [3].

towers. The horizontal section of the core with graphite surrounding the core, a detail of the core with fuel elements, control rods and graphite dummies elements are shown in Fig 1. In Fig 2 the horizontal and vertical section of the reactor are shown, together with 3D section of the reactor with neutron channels.

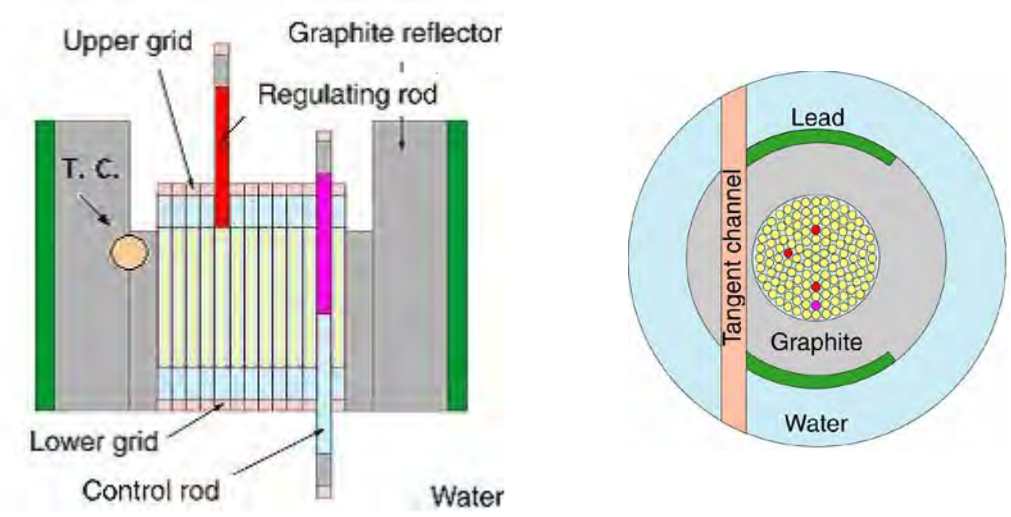

Fig 1 - Vertical section of the core and standard configuration.

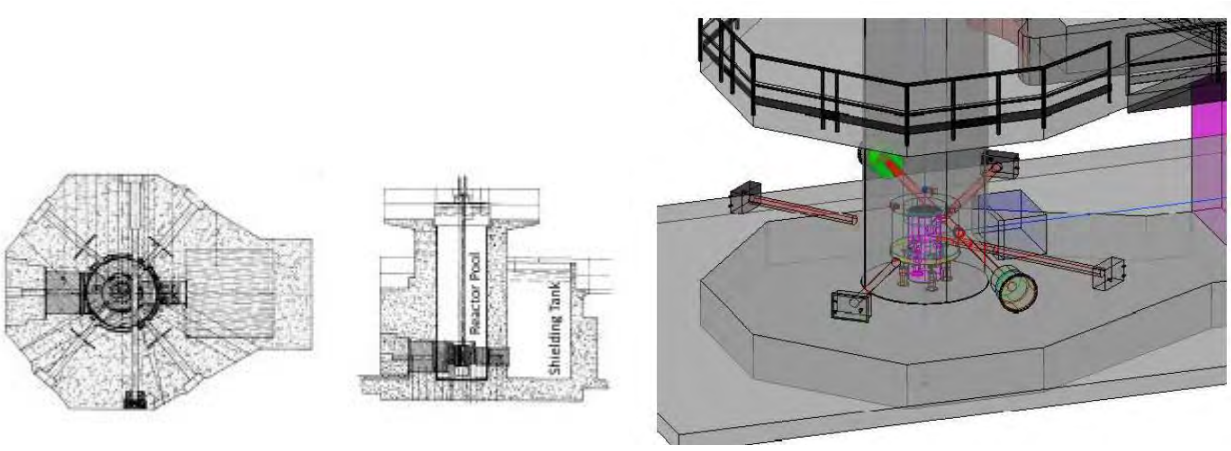

Fig 2 - Horizontal and vertical section of RC-1 research reactor and neutron channels

The reactor is controlled by four boron carbide rods: three, stainless steel cladded, are *fuel followed* type (two shims and the safety rods) whereas the last, aluminium cladded, is the regulation rod.
The reactor is monitored by a starting channel, two wide range linear channels and one safety channel. One logarithmic channel operates between 10 W and 10 MW. Three X, γ monitors , two monitors for α and β contamination, and one for gaseous contamination of the air extracted from reactor hall and radiochemical lab ensure a complete information about the radiological situation on the plant and relative laboratories.
In Fig 2 it's possible to identify the experimental channels used for neutron extraction. Other irradiation facilities are the Lazy Susan, the pneumatic transfer system and the central thimble. In Tab 1 are summarized the neutron flux available for irradiation facilities at RC-1.[4][5]

Description	Neutron flux($ncm^{-2}s^{-1}$)
Lazy Susan	$2.00\ 10^{12}$
Pneumatic transfer system(rabbit)	$1.25\ 10^{13}$
Central channel	$2.68\ 10^{13}$
Thermal column collimator	$\sim 1\ 10^{6}$
Tangential piercing channel	$\sim 1\ 10^{8}$

Tab 1 Neutron flux available at RC-1 irradiation facilities

The RC-1 core, surrounded by a graphite reflector, consists of a lattice of TRIGA stainless steel standard fuel elements, graphite dummies elements, control and regulating rods. There are 127 channels on the upper grid plate available for these core components and the grid itself is divided into seven concentric rings. One channel houses the start up source (Am-Be) while two fixed channels are available for irradiation (central channel and *rabbit*).
The TRIGA fuel elements ,cylindrical shaped and stainless steel cladded (AISI 304 - thickness 0.5 mm) consists of a ternary alloy of H-Zr-U. The Uranium is 20% enriched in ^{235}U, and represents the 8.5%wt of the total fuel weight. Two graphite cylinders at the top and the bottom of the fuel rod ensure the upper and lower neutron reflection. The fuel element is provided externally with two fittings in order to allow the remote movements and the correct placements into the grid plates. Fig 3 shows the fuel elements details. [4][5]

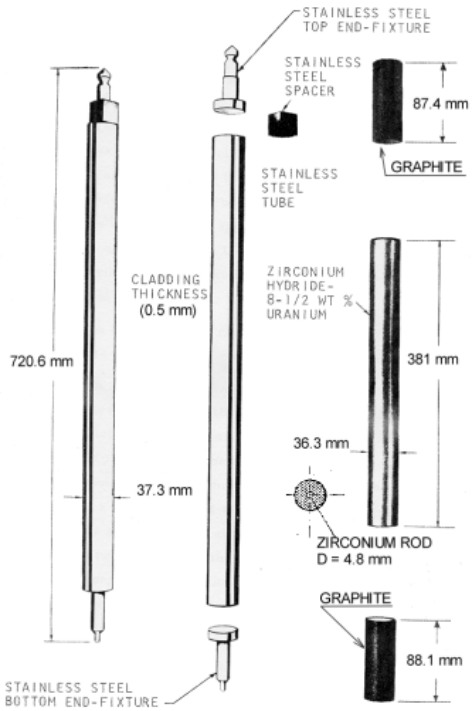

Fig 3 - Fuel element details.

The metallurgic alloy's stability is related to a variation of the total number of atoms less than 1%: The ternary mixture ensures that also in case of total burn up of ^{235}U present the total atom variation is 0.7%. Another feature regards the prescription that forces the removal of elements from the core if their burn up is higher than 35%: this is a condition linked to the U-ZR-H lattice

properties. From the point of view of the utilization, the reactor is mainly utilized for training, flux measurement and irradiation of neutron detectors.

3.2. Calculational model

The system considered, for this preliminary calculation, is a simplified TRIGA RC-1 model based on a single fuel element with its clad and inter-assemblies moderator, as shown in figure 4.
It has been considered a cylindrical pin geometry composed by four different zones, starting from the centre: metallic zirconium (grey), H-Zr-U alloy (red), stainless steel clad (pink) and water (blue).

Fig 4 – Simplified TRIGA fuel model.

The JEFF-3.1 library [6] was used for nuclear data and a simplified one energy group structure and diffusion method for flux evaluation have been used to validate this method.
Once obtained the cross sections by the ECCO cell code [7], the simplified configuration described has been made subcritical (k_{eff} = 0.95) with the control rods loading, simulated in this case by dilute boron in water. Then an external source at central middle height has been inserted to obtain the characteristically mid power of a TRIGA RC-1 fuel element (about 9 kW).
The deterministic code ERANOS [7] allows to evaluate the **n*** (see previous paragraphs), for the reference case, by the GPT (Generalized Perturbation Analysis) methodology [8], using different modules. In this model a perturbation has been applied varying the Boron density (+3.4%) into the water zone. Then the subcritical reactivity has been obtained by PCSM methodology.

3.3. Results

Considering that the average power of a fuel element in the TRIGA RC-1 reactor is about 9.089 kW, an external source with an intensity of 1.78 10^{14} ns^{-1} was loaded to reproduce the same power at about 5% subcriticality conditions.
The fission rate value corresponding to the power considered is 2.8422 10^{14} fissions/s.
The reference case has then been perturbed by a boron density variation of about +3.7%, which produced a reactivity decreases by about 1212 pcm (k_{sub} = 0.94114).
Using the HGPT methodology, the generalized reactivity was calculated (Eq. 6) obtaining the value ρ_{gen} = -1222 pcm.
The external source intensity modified in order to reestablish the initial fission rate resulted 4.278713 10^{13} ns^{-1}.

Finally, applying Eq. (20), the k_{sub} resulting in this simulation exercise was 0.95160 which compares very well with the value at initial, unperturbed subcritical conditions (see Table 2).

Case	k_{sub}
Reference	0.95200
PCSM method	0.95160
Difference	0.04%

Tab 2- Subcritical reactivity results.

4. Conclusions

The PCSM method is proposed for safely determining the subcriticality of an ADS system without significantly interfering with its normal operation. The method consists in:

- a precalibration of a control rod, for instance by source jerk techniques. The dedicated control rod should be of limited worth so that in any circumstance the system maintains well below criticality conditions. A relationship between a control rod position change and the corresponding reactivity alteration may then be established;
- during operation, a small, slow insertion of the control rod should be associated with an adjustment of the accelerator current, so that the count rate of a neutron detector in an out of core position is maintained constant, so that the same power level is maintained;
- determining the value of K_{sub}, making use of Eq. (20).

The simple numerical exercise shown above demonstrates the potentiality of the proposed methodology.
Future activity in this field are foreseen consisting:

- in a new simulation exercise on a more realistic mathematical model;
- in the preparation for an experimental campaign with the TRIGA reactor in order to validate experimentally the PCSM method.

5. References

[1] A. Gandini, *Ann. Nucl. Energy,* 28, 1193 (2001).
[2] A. Gandini, *Ann. Nucl. Energy*, 31/7, 813 (2004).
[3] M. Carta and A. D'Angelo, *Nucl. Sci. Eng*., 133, 3 (1999).
[4] L. DI PALO, RC-1 Reattore 1MW – progetto definitivo e rapporto di sicurezza , CNEN Centro Studi Nucleari Casaccia , 1966 (Italian)
[5] Dipartimento FPN, ENEA , Manuale di Operazione del reattore RC-1 1MW, C.R. Casaccia (Italian)
[6] NEA package 1745, http://www.nea.fr/abs/html/nea-1745.html, NEA-1745 ZZ-ALEPH-LIB-JEFF3.1.
[7] G. Rimpault, "Physics documentation of the ERANOS. The ECCO cell code", CEA Technical Note RT-SPRC-LEPh-97-001, 1997.
[8] A. Gandini, "Sensitivity Analysis of Source Driven Subcritical Systems by the HGPT Methodology", Proc. Intern. IAEA Techn. Committee Meet., Madrid 17-19 Sept. 1997 (IAEA-TC-903.3, p. 377), and: Annals of Nuclear Energy, 24, 1241 (1997).

NEUTRON ACTIVATION ANALYSIS IN SUPPORT OF UNDERGRADUATE RESEARCH

S.LANDSBERGER[1], D. TAMALIS[2], T. TIPPING[1], S.BIEGALSKI[1]

[1]The University of Texas at Austin, Nuclear Engineering Teaching Laboratory, 10100 Burnet Road, R-9000, Austin, Texas, USA 78758
[2] Florida Memorial University, Department of Health and Natural Sciences, Miami Gardens, Florida, USA 33054

ABSTRACT

Neutron activation analysis (NAA) is one of the best venues for experimental research training and education for undergraduate students in nuclear science and engineering. NAA covers a multitude of aspects including radiological safety, nuclear instrumentation, experimental design, data analysis, report writing and oral presentations. Over the past decade undergraduate research at the Nuclear Engineering Teaching Laboratory has remained a major focus for education and training and for graduate recruiting. The NAA facilities have been used not only by undergraduate students at The University of Texas at Austin, but also from local and foreign universities, two Historically Black College or University (HBCU) and IAEA fellows. A comprehensive overview of the projects undertaken from previous and recent projects, and the impact NAA has had on the undergraduate students for further career opportunities in industry and graduate school is described.

1. Introduction

In the past decade there have been several new academic programs in nuclear science and engineering, and nuclear chemistry in the United States and Europe. The American Chemical Society lists twenty-five universities that offer graduate degrees in nuclear and radiochemistry related fields (1) while the IAEA continues to support research reactors and fellowship programs. The World Nuclear Association recently stated that over 45 countries are actively considering embarking upon nuclear power programs that range from sophisticated economies to developing nations with the front runners being United Arab Emirates, Turkey, Vietnam, Belarus, Jordan and Poland (2). In the United States there is still a growing need to attract new researchers and staff members into national and government laboratories in the areas of nuclear nonproliferation, nuclear forensics and advanced reactor development including the nuclear fuel cycle. These positions are typically at the Ph.D. level but other opportunities exist at the BS and MS levels as well. The Department of Energy, National Laboratories, National Science Foundation, Department of Defense, etc. are all aware of the need to train the next generation of scientists and engineers for a wide variety of areas including national security. As a consequence, many different types of summer internship programs have been made available. For the last decade and beyond the Nuclear Engineering Teaching Laboratory (NETL)

has provided research opportunities in neutron activation analysis (NAA) not only to undergraduate students from The University of Texas at Austin (UT-Austin) but also to other local universities and fellows sponsored by the IAEA. These opportunities have resulted in attracting students into our own graduate program while training international students and researchers. NAA is a unique analytical method in that it provides foundational training opportunities for skillsets including gamma-ray spectroscopy, health physics, and data analysis to the students.

2. General Laboratory, Health Physics and Security Training

All the students begin with a rudimentary background check as required by UT-Austin and the U.S. Nuclear Regulatory Commission for access to the TRIGA research reactor. Each student is then required to undergo on-line training for general laboratory practices including Hazard Communication, Laboratory Safety and Hazardous Waste Management. This is followed by an on-line training of NETL radiation safety. This course provides information on how to work safely with radiation and radioactive materials at the NETL. One of the most important components of any radiological protection program is the training that is provided to facility personnel. Well-trained staff contribute significantly to the safe and efficient operation of the facility during normal and emergency situations and maintain exposures as low as reasonably achievable (ALARA). All personnel requiring unescorted access to Restricted Areas in NETL must complete radiation protection training prior to having unescorted access to Restricted Areas. Subjects covered in the training include:

- Atomic Structure and Radioactivity
- Interactions of Radiation with Matter
- Quantities and Units of Radiation
- Basic Principles of Radiation Protection
- Safe Handling of Radioactive Materials and Sources
- Radiation Detection Instruments and Surveys
- Dosimetry
- Waste Disposal
- Purchasing and Receiving Radioactive Materials
- Regulations
- Emergency Procedures
- Record Keeping

This training is presented via two online videos each about 75 minutes long. Once the videos have been viewed the student can link to access the final exam. This exam consists of multiple choice questions over topics discussed in the videos. A score of at least 70% is required to pass the exam and receive credit. After the exam each student meets with the appropriate NETL staff for security training to gain access to the building and laboratories during the day, evenings and weekends. Access to the reactor bay, which has the prompt gamma activation analysis facility, is given on a case by case basis to those students performing experiments. Each student must possess an appropriate ID badge at all times, a dosimeter when in the laboratories, and personal protective equipment as needed.

3. NAA Training

Training for the facilities and data processing is accomplished with a step by step procedure. Typically training for NAA is done by a staff/faculty member or graduate student. After a period of watching the procedures, an oversight by staff/faculty member or graduate student is done while the student is performing the NAA steps. After an initial training period the student is left to his/her own resources. A lot of emphasis is placed on ALARA radiation safety concepts, including handling of radioactive material, disposal of radioactive waste and record keeping. Utilization of detectors and analysis software is a much quicker learning process and typically students can achieve relative proficiency in a matter of one-two weeks.

4. Undergraduate Student Participants

At UT-Austin undergraduate participants originate mainly from the Department of Mechanical Engineering where the Nuclear and Radiation Engineering Program exists and from the Department of Physics which offers a Radiation Physics technical option that includes six courses in the Nuclear and Radiation Engineering program. One undergraduate student came from the Department of Biology. Southwestern University is located about 32 km north of UT-Austin and has sent two seniors to perform NAA. Florida Memorial University, a Historically Black College or University (HBCU) has been sending undergraduate students for many years who have been involved in NAA, PGAA and naturally occurring radioactivity in oil scale samples. Huston-Tillotson, a local HBCU, also sent a student who was involved for a two year period in NAA. École Nationale Supérieure d'Ingénieurs de Caen, France sent a total of four senior undergraduate students. Two undergraduate students from the Jordan University of Science and Technology and two students from Unidad Académica de Estudios Nucleares, Universidad Autónoma de Zacatecas, Mexico have performed research in NAA. Currently we have one visiting graduate student from the China University of Geosciences. We have also had two undergraduate students from the Jordan University of Science and Technology.

5. IAEA Fellowships

Through the IAEA, fellows from Instituto Tecnológico e Nuclear, Portugal; Ahmadu Bello University, Nigeria; Instituto Nacional de Investigasciones Nucleares, Mexico; Ghana Atomic Energy Commission, Ghana; Dalat Nuclear Research Center, Viet Nam; Centre National de l'Energie des Sciences et Techniques Nucléaires; Morocco; Institute of Nuclear Science and Technology, China; and the Joint Institute of Nuclear Research, Russia have visited NETL for periods of several months and performed NAA on various projects.

6. Mentoring Process and Outcomes

All university undergraduate students and IAEA fellows are closely mentored not only in research but also in career choices. Many of the UT-Austin students choose to follow graduate careers in our Nuclear and Radiation Engineering program and eventually graduate with M.S. or Ph.D. degrees and find employment staff positions at various national laboratories. Other students and IAEA fellows from other countries are also mentored particularly to attain better research skills. Students from Florida Memorial University who have performed NAA at UT-Austin have experienced research early on in their careers and have gone on to graduate school at Washington State University (1 student) and University of Nevada at Las Vegas (2 students) in radiochemistry and the Nuclear Navy as a health physicist. All of the students and IAEA fellows are required to deliver a presentation of their work and write up a report. In several instances their work has been published in peer-reviewed journals and conference proceedings. (3-11). Occasionally, when funding is available students have traveled to international

conferences in Germany, Brazil, Poland and Greece. This type of exposure has a great impact on the students' careers in choosing advanced degrees.

7. Conclusions

Our efforts in providing research opportunities in nuclear science and engineering through NAA have proven to be very successful in stimulating students to pursue advanced degrees in these areas. Our metrics have shown that many of these students have gone to rewarding careers at the BS, MS and PhD levels. Our international commitment to train students and IAEA fellows from other countries is an important cornerstone of our educational mission. While NAA is not a new analytical method it still provides the needed rigors for attaining confidence in a wide array of skillsets in nuclear science and engineering.

8. References

1. http://www.nucl-acs.org/ (Accessed February 2, 2016)
2. http://www.world-nuclear.org/information-library/country-profiles/others/emerging-nuclear-energy-countries.aspx (Accessed February 2, 2016
3. A. Michenaud-Rague, S. Robinson and S. Landsberger "Trace Elements in 11 Fruits Widely-Consumed in the USA as Determined by Neutron Activation Analysis", J. Radioanal. Nuc. Chem. 291, 237–240 (2012).
4. A. Alsabbagh, N. B. Sunbul, I. Hrahsheh, L. Zaidan and S. Landsberger, "Investigation of Jordanian Uranium Resources in Carbonate Rocks", (in press), J. Radioanal. Nucl. Chem. (2016).
5. S. Landsberger, R. Lara and D. Tamalis, "Non-Destructive Determination of ^{235}U, ^{238}U, ^{232}Th and ^{40}K Concentrations in Various Consumed Nuts and Their Implication on Radiation Dose", Levels to the Human Body", J. Radioanal. Nucl. Chem. 307, 1065-1068 (2016).
6. N. Rodriguez, M. D. Yoho and S. Landsberger, "Determination of Ag, Au, Cu and Zn in Ore Samples from Two Mexican Mines by Various Thermal and Epithermal NAA Techniques" , J. Radioanal. Nucl. Chem. 307, 955-961 (2016).
7. R. I. Palomares, K. Dayman, S. Landsberger, S.R. Biegalski, C. Z. Soderquist, A.J. Casella, M.C. Brady Raap, and J. M. Schwantes "Measuring the Noble Metal and Iodine Composition of Extracted Noble Metal Phase from Spent Nuclear Fuel Using Instrumental Neutron Activation Analysis" App. Radiat. Isotop. 98, 66-70 (2015)
8. S. Landsberger, D. Tamalis, T. Meadows and B. Clanton, "Characterization of a Uranium Contaminated Soil Site", J. Radioanal. Nucl. Chem., 296, 319-322 (2013).
9. S. Landsberger, S., D. Tamalis, T. Dudley, G. Dort, G. Kuzmin and G. George "Determination of Macroconstituents and Trace Elements in Naturally Occurring Radioactive Material in Oil Exploration Waste Products", J. Radioanal. Nucl. Chem., 298, 1717-1720 (2013).
10. Y. A. Ahmed, S. Landsberger, D.J. O'Kelly J. Braisted, H. Gabdo, I.O.B. Ewa, I.M. Umar and I.I. Funtua, "Compton Suppression Method and Epithermal NAA in the Determination of Nutrients and Heavy Metals in Nigerian Food and Beverages", App. Radiat. Isotop. 68, 1909-1914 (2010).
11. J. Z. Edwards, S. Landsberger, M.C. Freitas, Evidence of Tin and other Anthropogenic Metals in Particulate Matter in Lisbon, Portugal, J. Radioanal. Nuc. Chem., 281, 273-278, (2009).

Poster operation & maintenance

GRADED APPROACH OF COMPONENT CLASSIFICATION IN NUCLEAR RESEARCH REACTORS

YASSER E. TAWFIK

ETRR-2 Complex, Egyptian Atomic Energy Authority, P.O. Box 13759, Inshas, Cairo – EGYPT.

ABSTRACT

A graded approach is applicable in all stages of the lifetime of a research reactor (site selection, site evaluation, design, construction, commissioning, operation and decommissioning). Grading the application of management system requirements should be applied to the product, item, system, structure or components, services, activities or controls of each process. The IAEA Safety guide no. (SSG-22) presents recommendations on the graded approach to application of the safety requirements for research reactors. In these applications, a graded approach is only used in determining the scope and level of detail of the safety assessment carried out in a particular state for any particular facility or activity. In this document, the graded approach is applied for the classification of components, systems, and subsystems in ETRR-2 research reactor. Grading is applied based on many factors such as safety, reliability, design state, complexity, experience, availability, and economic factors.

1. Introduction

A graded approach is the process of ensuring that the level of analysis, documentation, and actions required by the regulatory framework to confirm the safety of a research reactor (RR) facility are commensurate with:

(1) The relative importance to safety, safeguards, and security;

(2) The magnitude of any hazard involved;

(3) The life cycle stage of a facility;

(4) The particular characteristics of a facility; and

(5) Any other relevant factors. [1]

For a system of control, a graded approach is a process or method by which the stringency (or rigor, strictness) of control measures and conditions (i.e., requirements) applied is commensurate with the likelihood and possible consequences of a loss of control. A system of control might be:

- A regulatory system applied to a research reactor;
- A management system for a research reactor operating organization;
- A control or safety system in a research reactor.

A graded approach is an application of safety requirements commensurate with the characteristics of the practice or source and the likelihood and magnitude of potential exposure. The 'graded approach' defines as follows:

1. For a system of control, such as a regulatory system or a safety system, a process or method in which the stringency of the control measures and conditions to be applied is commensurate, to the extent practicable, with the likelihood and possible consequences of, and the level of risk associated with, a loss of control.
An example of a graded approach in general would be a structured method by means of which the stringency of application of requirements is varied in accordance with the circumstances, the regulatory systems used, the management systems used, etc. For example, a method in which:
(1) The significance and complexity of a product or service, activity or controls are determined;
(2) The potential impacts of the product or service on health, safety, security, the environment, economical aspects and the achieving of quality and the organization's objectives are determined;
(3) The consequences if a product fails or if a service is carried out incorrectly are taken into account.

2. An application of safety requirements that is commensurate with the characteristics of the practice or source and with the magnitude and likelihood of the exposures.

In practical terms, a graded approach applies to management system requirements of a product, item, system, structure or component, service, activity or controls of a process commensurate with its relative importance, complexity, variability, maturity, potential impact on safety, health, environmental, security, quality and economical aspects.
By the application of a graded approach, the controls, measures, training, qualification, inspections, detail of procedures, etc. might be adapted to the level of risk or importance for safety, health, environmental, security, quality and economical aspects. In evaluating these aspects the system is to be considered holistically. [2]

The graded approach will result in an effective application of appropriate resources (time, money, staff, etc.) with regard to defined requirements. For each specific product, item, system, structure or component, service, activity or controls the graded approach will affect the type and level (extent and depth) of controls applied, for example:
- The type and level of planning and analysis;
- The type and level of verification, inspection and testing;
- The review and approval requirements of activities, documents and records;
- The detail of documentation and records;
- The type and level of evaluation of suppliers.
- The type and level of controls can change from organization to organization, with time and with the state or the life cycle stage of the facility or activity.

Risk is a fundamental consideration in determining the detailed description of procedures and the extent to which controls and measures are to be applied. A graded approach is applicable to all stages of the lifetime of a nuclear facility including sitting, design, construction, commissioning, operation and decommissioning and to all activities. During the lifetime of a facility, any grading that is performed should ensure that safety functions are preserved, that the license and the operational limits and conditions (OLC) are not challenged and there are no negative effects on the safety of the facility staff, the public, or the environment. [3]
The grading of a product, service, activity or controls of a process is based on analyses, regulatory requirements, license conditions, the OLC and engineering judgment. The grading of product, item, system, structure or components and activities will take into account the

safety function and the consequences of failure to perform their functions, in general covered by the classification of structures systems and components (SSCs), the complexity and maturity level of the technology, operating experience associated with the activities and the lifecycle stage of the facility. The management system requirements should be applied in such a way that the level of application of the requirements are commensurate with the potential risk associated with the facility or activities or with the consequences of losing knowledge (e.g., losing records or drawings, or knowledge of staff due to retirement), without adversely affecting safety.

The main benefits of grading are improvements in efficiency and effectiveness in achieving the organization's objectives through the deployment of appropriate controls and resources. An approach to grading involves:

- Identifying the product, item, system, structure or component, service, activity or controls to be graded;
- Determining the significance of and/or hazard associated with the above in relation to safety, health, environmental, security, quality and economical aspects;
- Determining the degree of the associated risk (probability and consequence) if the item, system, structure or component fails in service or if the work is incorrectly conceived or executed, that affects public, worker, or environment;
- Determining the controls required to mitigate the risk.

1.1 Objective of the graded approach

• The objective of the graded approach is to adjust application of the safety requirements for analysis, evaluation and documentation to the potential hazards associated with the reactor facilities.

• The desired effect of applying the graded approach is that resources will be used more efficiently and produce maximum benefit.

• The graded approach should be used to eliminate unproductive or unnecessary features or activities.

• All relevant requirements must be complied with. A graded approach should be used to determine the appropriate manner to comply, not to provide relief from meeting a requirement.

Application of a graded approach may include:

• Determining the significance and complexity of a product or service, the maturity of the technology involved and the experience with its application;

• Evaluation of the impacts of a product or service on health, safety, security, the environment, quality and achieving the organization's objective; and

• Assessing the consequences of failure of a product or incorrect performance of a service.[4,5]

1.2 Basis criteria for the establishment of a graded approach

The factors to be considered in establishing a basis for the application of a graded approach include but are not limited to:

(1) Reactor power;

(2) Source term;

(3) The type, amount and enrichment of special nuclear material;

(4) The type of fuel elements (properties of fuel and cladding);

(5) The type and the mass of moderator, reflector and coolant;

(6) Nuclear Design Characteristics - excess reactivity, maximum reactivity addition rate, reactivity coefficients and inherent safety features;

(7) The existence of a containment or confinement structure;

(8) The utilization of the reactor (experimental devices, fuel experiments and reactor physics experiments; and

(9) Sitting population in the emergency planning zone and proximity of the reactor to external hazards. [6,7]

2. Graded approach applications in ETRR-2 reactor

ETRR-2 is a multipurpose reactor, 22 MW, open pool type reactor with a maximum thermal neutron flux of 3.7×10^{14} n cm^{-2} s^{-1}. The reactor was designed, provided, constructed, and commissioned through the international cooperation with INVAP- Argentina [8]. There are many typical methodologies for the application of grading of management system requirements, safe transport of radioactive materials, radiation protection, classification of radioactive waste, quality assurance and quality control activities, and classification of components. The following is one of these typical applications of graded approach.

2.1 Application of grading to the classification of ETRR-2 components

The ETRR2 systems, subsystems, and components were classified according to the following entries;

Safety functions

Safety classes

Seismic classes

Quality assurance levels

Safety classes

The safety series 35-S1 “code on the safety of nuclear research reactors: design” [10] , presents specific safety functions for major safety-related components. However, it does not include a table for class assigning. Due to this reason, it has been decided to consider safety functions in the 5-SG-D1 guide [11], as the corresponding correlation between functions and safety classes.

Seismic classes

Based on the AR 3.10.1 standard “protection against earthquakes”, two types of earthquake are specified in accordance with the following definitions:

Design basis earthquakes (S1): is the most relevant earthquake among those which are expected to occur at least once during the lifetime of the installation.

Safe shutdown earthquakes (S2): is the most relevant earthquake that can reasonably be postulated for the installation emplacement on the basis of the best geological and seismological information available, so that the estimated annual occurrence probability of earthquakes greater that the postulated earthquake will not exceed 10-3.[11,12]

Based on these concepts, the following established conditions were verified for each seismic class:

Seismic Class 1: for a safe shutdown earthquake (S2), the functional condition and the condition for seismic class 2 was verified.

Seismic Class 2: for a design basis earthquake (S1), the operable condition was verified after having performed an appropriate inspection.[13]

Safety functions

Safety functions specified under the IAEA safety guide “50-SG-D1”, "safety functions and classification of components for BWR, PWR, and PTR” will be set down in order and transcribed;

a) To prevent the occurrence of transients of unacceptable reactivity.

b) To maintain the reactor in safe shutdown condition after having completed all pertinent shutdown operations.

c) To shutdown the reactor whenever necessary in order to avoid that anticipated operational occurrences may lead to accidental conditions and to shutdown the reactor in order to allay the eventual consequences of accidental conditional.

e1) To keep available sufficient quantities of reactor coolant in order to cool the core both during and after any accidental situation which does not imply a failure in the reactor coolant’s containment.

e2) To keep available sufficient quantities of reactor coolant in order to cool the core both during and after any operational situation.

f) To remove heat from the core after a coolant reactor containment failure has occurred in order to restrain or reduce fuel damage.

g) To remove decay heat during the various operational situations and accidental conditions where the reactor coolant’s containment remains intact.

h) To transfer heat derived from other safety systems to the final heat decay sink.

i) To ensure all necessary provisions such as electrical supply, compressed air, hydraulic pressure, lubrication, etc., as a support function to any of the safety systems.

j) To maintain an acceptable level of fuel cladding integrity in the reactor core.

k) To maintain the integrity of the core coolant’s containment.

m) To maintain the exposure of the public at large as well as installation personnel within acceptable limits both during and after accident conditions which may have released radioactive material from sources located outside the reactor confinement.

n) To limit discharge or release of radioactive waste or radioactive effluents in suspension in the air to levels below pre-set values during any operational situation.

o) To keep environmental conditions inside the nuclear power plant under control so that safety systems will function appropriately and to provide comfortable conditions so that personnel will carry out their major safety-related operations satisfactorily.

p) To keep control during any operational situation of radioactive releases derived from irradiated fuel being transported or stored outside the reactor coolant system though inside the reactor emplacement.

w1) Experimental devices and facilities with direct bearing on the safety of the installation.

w2) Experimental devices and facilities with some bearing on the safety of the installation.

w3) Experimental devices and facilities with no bearing on the safety of the installation.

y) To maintain radiological exposure of the installation personnel below pre-established limits during operational situations.[9]

Safety class	Characteristics	Safety functions
1	Reactor coolant pressure boundary	-
2	safety systems	k,c,e1.f.g.j
3	Safety-related systems	a,b,e2,h,l,m.o.p,q,r.n.w1.w2.y
4	Safety non-related systems	n

Tab.1; Correspondence between functions and safety classes

Description of classification table;

The table will show the code and description of the system - subsystem. Specifically, the following entries will be used for the Table heading:

Safety Function will indicate the assigned safety function

Safety Class will indicate the assigned safety class.

Seismic Class will indicate the assigned seismic class.

Quality Level will indicate the resulting quality level.

An example of classification of the ETRR-2 rector components and systems will be shown in Table 2.[16]

Sys./ Subs.	ETRR-2 Reactor System codification	Safety Function	Safety Class	Seismic Class	Quality Level
01	Reactor & Auxiliary Pool Tanks				
01-10	Reactor Tank & Welded Parts	E2, K	2	1	B
	Reactor Tank & Auxiliary Pool External Structural Parts	S	3	1	C

	Coolant Conduit Nozzle	E2,S	3	1	C
	Reactor Tank Welded or Bolted Guides & Supports	S	3	1	C
	Transfer Cell Conduit	S	3	1	C
01-20	Core Supporting Structure	A,S	3	1	C
	Ionization Chamber Tables	S	3	1	C

Tab 2: Classification of structures, systems and components

References

[1] Safety Standards Series no. NS-R-4, Safety of Research Reactors, IAEA, 2005.

[2] Safety Glossary, Terminology Used in Nuclear Safety and Radiation Protection 2007 Edition, IAEA, Vienna, 2007.

[3] The Management System for Nuclear Installations, IAEA Safety Standards Series, Safety Guide No. GS-G-3.5, IAEA, Vienna, 2009.

[4] IAEA Safety Glossary: Terminology Used in Nuclear Safety and Radiation Protection, IAEA, 2007.

[5] Safety standard no.: SSG-22S, Use of a Graded Approach in the Application of the Safety Requirements for Research Reactors, IAEA, 2012.

[6] Governmental, legal, and regulatory framework for safety, Safety Standards Series no. GSR Part 1, IAEA, 2010.

[7] The Management System for Facilities and Activities, Safety Standards Series no. GS-R-3, IAEA, 2006.

[8] ETRR-2 Safety Analysis report, Chapter 1, INVAP-EAEA, 2003.

[9] ETRR-2 Safety Analysis report, Chapter 2, INVAP-EAEA, 2003.

[10] Safety series no. : 35-S1, Code on the safety of nuclear research reactors: design, IAEA, 2005.

[11] Safety Functions and Components Classification for BWR, PWR and PTR, Safety guide no.: 50-SG-D1, IAEA, 2005.

[12] Classification of Components procedure no.: 0767-5305-3IAII-004-1E, INVAP, 2002.

[13] Seismic analysis and testing of nuclear power plants, Safety guide no.: 50-SG -S2, IAEA, 2002.

[14] Argentine Regulating Authority standard no.: AR 3.10.1, Protection against Earthquakes standard, 2001.

[15] Quality level determination procedure no. CDAD-3001-3PIGC-009-A, INVAP, 2003.

[16] Maintenance manual Doc no.: 0767-5375-3IBLI-001-1O, EAEA-INVAP, 2002.

Acknowledgments

The author is thankful for the great help and support of Dr. Mohamed A. GAHEEN-Egyptian Atomic Energy Authority (EAEA), Eng. Ashraf S. KAMOON – Egyptian Nuclear & Radiological Regulatory Authority (ENRRA), and Dr. David J.WINFIELD-Nuclear Safety Consultant- IAEA in supplying him with the needed references as well as reviewing this present document.

DEVELOPMENT OF TRANSPORTATION CONTAINER FOR THE NEUTRON STARTUP SOURCE OF HIGH TEMPERATURE ENGINEERING TEST REACTOR (HTTR)

YOSUKE SHIMAZAKI, MASATO ONO, DAISUKE TOCHIO, SHOJI TAKADA

Sector of Nuclear Science Research, Oarai Research & Development Center, Department of HTTR, HTTR Reactor Engineering Section, Japan Atomic Energy Agency
4002 Narita-cho, Oarai-machi, Higashiibaraki-gun, Ibaraki 311-1393, Japan

HIROAKI SAWAHATA, TAIKI KAWAMOTO, SHIMPEI HAMAMOTO

Sector of Nuclear Science Research, Oarai Research & Development Center, Department of HTTR, HTTR Operation Section, Japan Atomic Energy Agency
4002 Narita-cho, Oarai-machi, Higashiibaraki-gun, Ibaraki 311-1393, Japan

MASANORI SHINOHARA,

Sector of Nuclear Science Research, Oarai Research & Development Center, Department of HTTR, HTTR Project Management Section, Japan Atomic Energy Agency
4002 Narita-cho, Oarai-machi, Higashiibaraki-gun, Ibaraki 311-1393, Japan

ABSTRACT

In High Temperature Engineering Test Reactor (HTTR), three neutron startup source holders (NS holders) containing ^{252}Cf with 3.7GBq for each are loaded in the graphite blocks and loaded into the reactor core as a neutron startup source (NS) which is changed at the interval of approximately seven years. These NS holders are transported from the dealer's hot cell to HTTR using the transportation container. Loading of the NS holders to the graphite blocks is carried out using the fuel handling machine (FHM) and manipulator in the fuel handling machine maintenance pit (maintenance pit) of HTTR.

There were two technical issues for the safety handling work of the NS holders. The one is the radiation exposure caused by significant movement of the container due to an earthquake, because the conventional transportation container for NS was so large (φ1240 mm, h1855 mm) that it could not be fixed on the top floor of maintenance pit by bolts. The other is the falling of the NS holder caused by the difficult remote handling work, because the neutron startup source holder capsule (NS holder capsule) was also so long (φ155 mm, h1285 mm) that it could not be pulled into the adequate working space in the maintenance pit. Therefore, a new and low cost transportation container for NS, which can solve the issues, was developed.

To avoid the radiation exposure by neutron and gamma ray leakage, a smaller transportation

container (φ820 mm, h1150 mm), which can be fixed on the top floor of maintenance pit by bolts, was developed. In addition, to avoid the falling of the NS holder, a smaller NS holder capsule (φ75 mm, h135 mm) with simple mechanism, which can be treated easily by manipulator, was also developed.

As the result of development, the NS holder handling work was safely accomplished. Moreover, a cost reduction for manufacturing was also achieved by simplifying the mechanism and downsizing.

1. Introduction

HTTR is the first High Temperature Gas-cooled Reactor (HTGR) in Japan which was constructed in Oarai Research and Development Center of Japan Atomic Energy Agency (JAEA) to establish and upgrade the technology of the HTGRs. The first criticality of HTTR was achieved in 1998 [1]. The major specifications of HTTR are summarized in Table 1.1. The bird's-eye view of HTTR facility is shown in Fig.1.1.

^{252}Cf is employed for neutron startup source (NS) of HTTR because it has an excellent neutron yield and is stable at the service temperature of about 600 ◦C [2]. Three neutron holders (NS holders) containing ^{252}Cf are loaded into the reactor core. The NS is required to be exchanged in a proper period, because a half-life time of ^{252}Cf is about 2.6 years, as well as to keep the in-core neutron detector, Wide Range Monitor (WRM), to show a proper count to confirm the integrity of WRM, even after the reactor shut down. Exchange work of NSs was carried out two times by March 2015.

A transportation container for the NS (transportation container) is used for the procedures in the exchange work, described as follows;

(1) Transportation of NS holder capsule from the dealer's hot cell to HTTR.

(2) Putting the neutron startup source holder capsule (NS holder capsule) into the working space in the fuel handling machine (FHM) maintenance pit (maintenance pit) of HTTR by ascending and descending the NS holder capsule.

Two technical issues were recognized for the transportation container in the past two exchange works for the safety handling work of NS holder. On the other hand, it was required that an overhaul of the conventional transportation container or development of a new transportation container because the conventional transportation container was manufactured about twenty years ago. Therefore, the development of a new transportation container for NSs, which can solve these technical issues with low cost, was carried out. This paper describes the development of new transportation container of HTTR.

Table 1.1 Major specifications of HTTR

Fuel	Uranium-dioxide Coated fuel particle
U-235 enrichment	3~10 wt% (avg. 6 wt%)
Fuel type	Pin-in-block type
Moderator	Graphite
Coolant	Helium gas
Reactor power	30 MW
Reactor inlet coolant temperature	395°C
Reactor outlet coolant temperature	850°C / 950°C
Coolant pressure	4.0 MPa

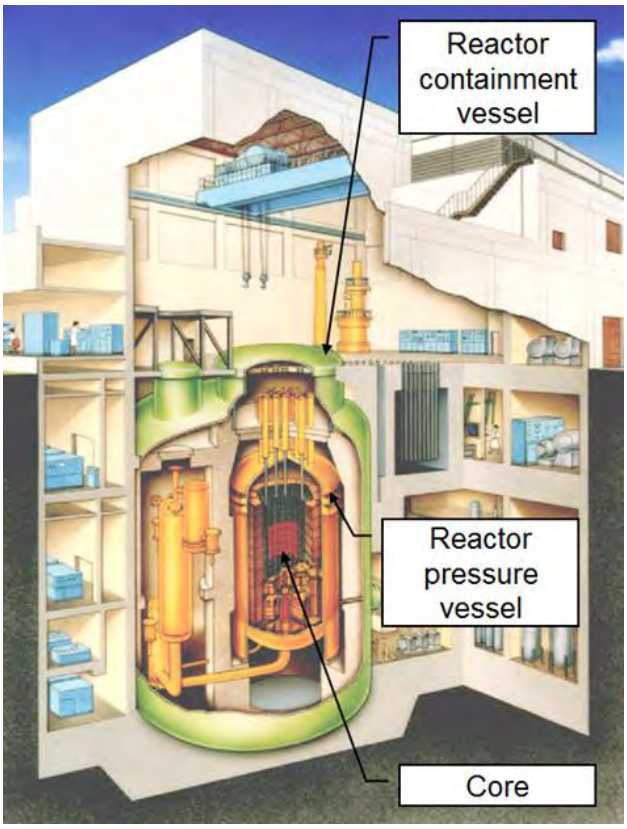

Figure 1.1 Bird's-eye view of HTTR facility

2. Neutron Start up Source of HTTR

2.1 Outline of Neutron Start up Source of HTTR

Three NS holders, which are made of SUS316L, containing ^{252}Cf, which has an excellent neutron yield and is stable at the service temperature of about 600 ◦C, with 3.7GBq for each are loaded into the reactor core. The major specifications of NS of HTTR are summarized in Table 2.1 [3].

The NS holder is a cylindrical capsule and is loaded into the control rod guide block (CR block) which is one of the core graphite components of HTTR. The arrangement of NS holder in the CR block is shown in Fig.2.1. Each CR block containing the NS holder is located at the top block in the CR block column in the core region and arranged at 120° interval. The vertical arrangement of CR block containing NS holder in the reactor core is shown in Fig.2.2.

Table 2.1 Major specifications of NS of HTTR [3]

Radio isotope	^{252}Cf
Radiation source intensity	11.1 GBq (3.7 GBq x 3)
Capsule size	φ 7.8 mm h 10 mm
Maximum allowable working temperature	800℃
Maximum allowable working pressure	4.7 MPa

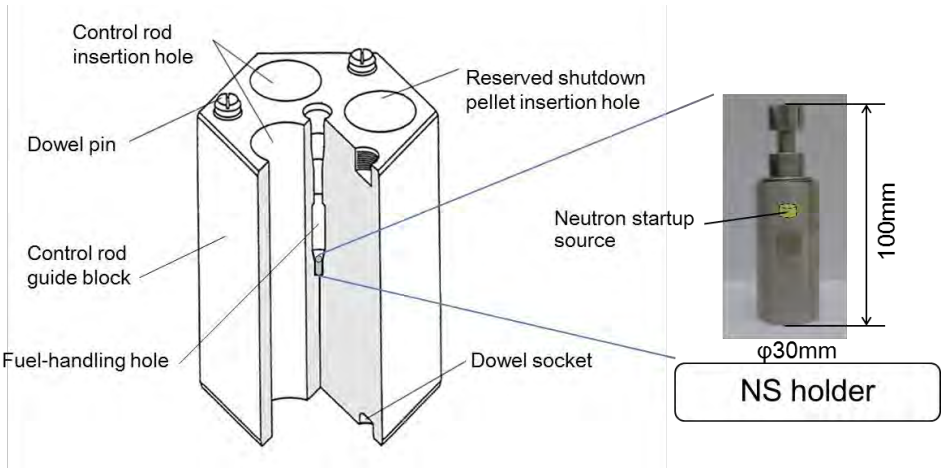

Figure 2.1 Arrangement of NS holder in CR block

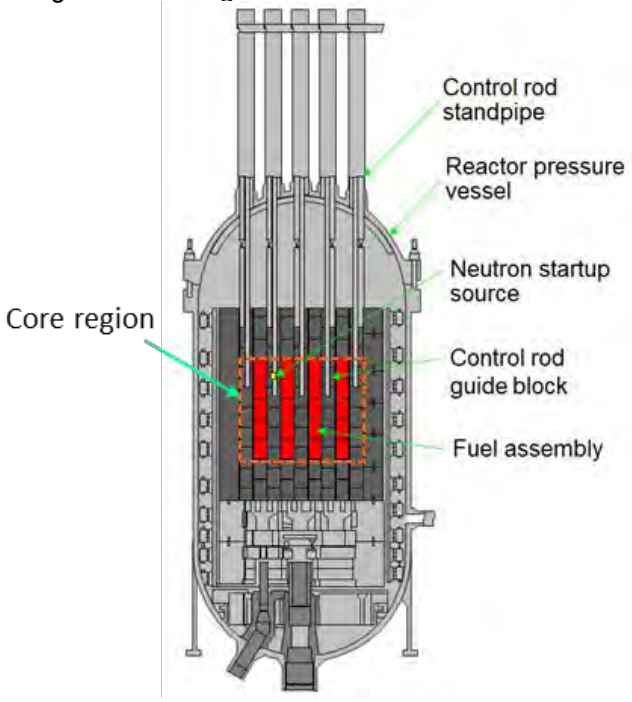

Figure 2.2 Vertical arrangement of CR block containing NS holder in reactor core

2.2 Neutron startup source exchanging procedure

Three procedures, 1) assembling of new NS holders, 2) installation of the new NS holders into the NS holder capsule and 3) loading of the NS holder capsule into the transportation container for NS are carried out in the dealer's hot cell. After that, the transportation container is transferred to HTTR.

The transportation container is put on the top floor of the maintenance pit and the new NS holder is put into the working space in the maintenance pit by descending the NS holder capsule.

One CR block containing an old NS holder and other three blocks, which are piled up in the same column, are unloaded from reactor core by the FHM and put into FHM.

The FHM is transferred to the maintenance pit by overhead crane, and the CR block containing old NS holder is put into the working space in the maintenance pit.

The old NS holder is removed from the CR block and is stored into NS storage block, which was installed beforehand, by manipulator. After that, the new NS holder is loaded into the CR block by manipulator.

The CR block containing the new NS holder and the NS storage block containing the old NS holder are lifted into the FHM.

Finally, the NS storage block is stored into the storage rack in the HTTR reactor building, and the CR block containing the new NS holder and other blocks are reloaded into the reactor core. The above-mentioned procedures are repeated three times. The schematic plan of NS exchanging procedure is shown in Fig2.3.

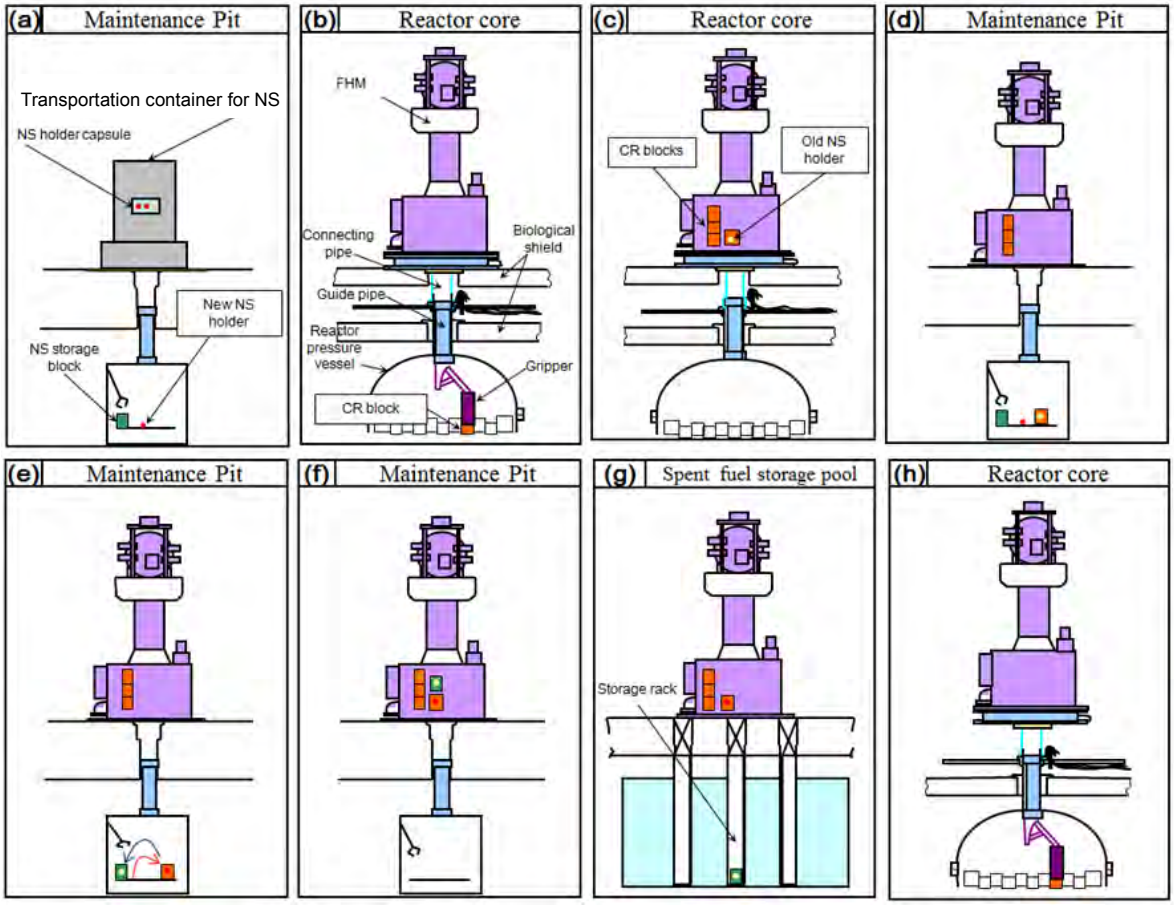

Figure 2.3 Schematic plan of NS exchanging procedure

3. Development of new transportation container for NS

Two technical issues, which are caused from the reason that the conventional transportation container was not specialized for NS of HTTR, were recognized in the past exchange work. In the past exchanging works of NS, these issues were solved by improving the working procedures. However, these issues were solved by improvement of transportation container structure in this development. This section describes the details of issues and improvement.

3.1 Prevention of neutron and gamma ray leakage

One technical issue is radiation exposure by neutron and gamma ray leakage caused by the significant movement of transportation container due to an earthquake.

The conventional transportation container was so large (φ1240 mm, h1855 mm, 6.8 ton) that it cannot be fixed on the top floor of maintenance pit by bolts as shown in Fig.3.1. Then, the conventional transportation container was fixed by belt type lashing tools on a plate, which was fixed on the top of maintenance pit by bolts [2]. Therefore, a risk for radiation exposure by neutron and gamma

ray leakage, which is accompanied by a movement of the conventional transportation container caused by a big earthquake such as Great East Japan Earthquake, was not able to be excluded.

It was found that this risk can be excluded by fixing the new transportation container on a steel plate by bolts, which can be achieved by downsizing of new transportation container while keeping the radiation shielding ability. The shielding material for neutron was changed from only paraffin to paraffin and boron carbide in order to achieve downsizing while keeping the neutron shielding ability. By fixing both the new transportation container and steel plate on the top of maintenance pit by bolts, aseismic integrity of transportation container was improved. As the result, the risk for radiation exposure by neutron and gamma ray leakage was excluded. The size and weight of the new transportation container is φ820 mm, h1150 mm, and 2 tons. The new transportation container is shown in Fig.3.2.

In addition, the safety of transportation work of transportation container by the overhead crane in the operating floor, which is the working floor of NS exchange work, was also improved due to downsizing.

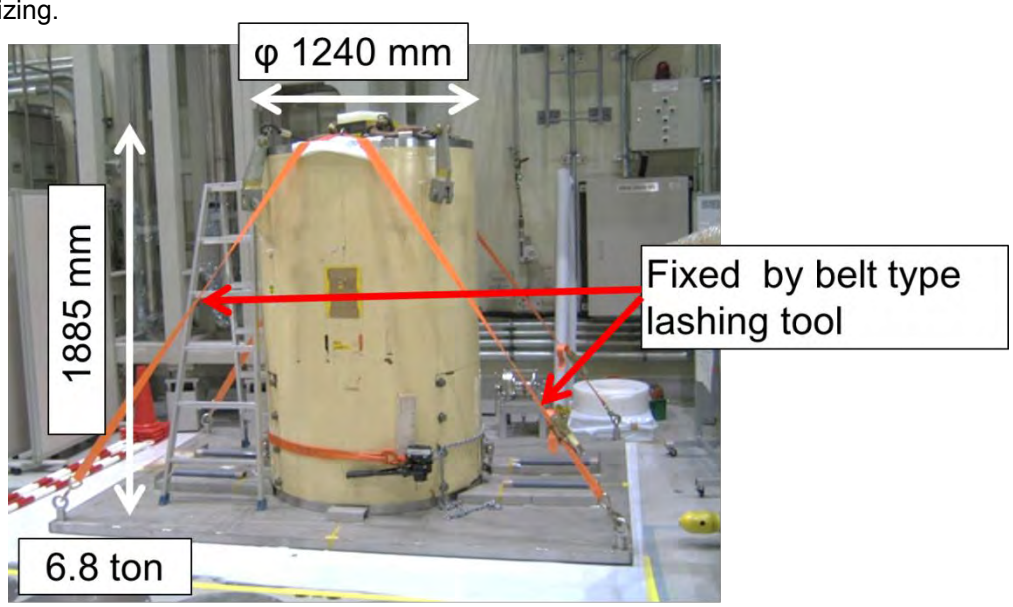

Figure 3.1 Conventional transportation container for NS

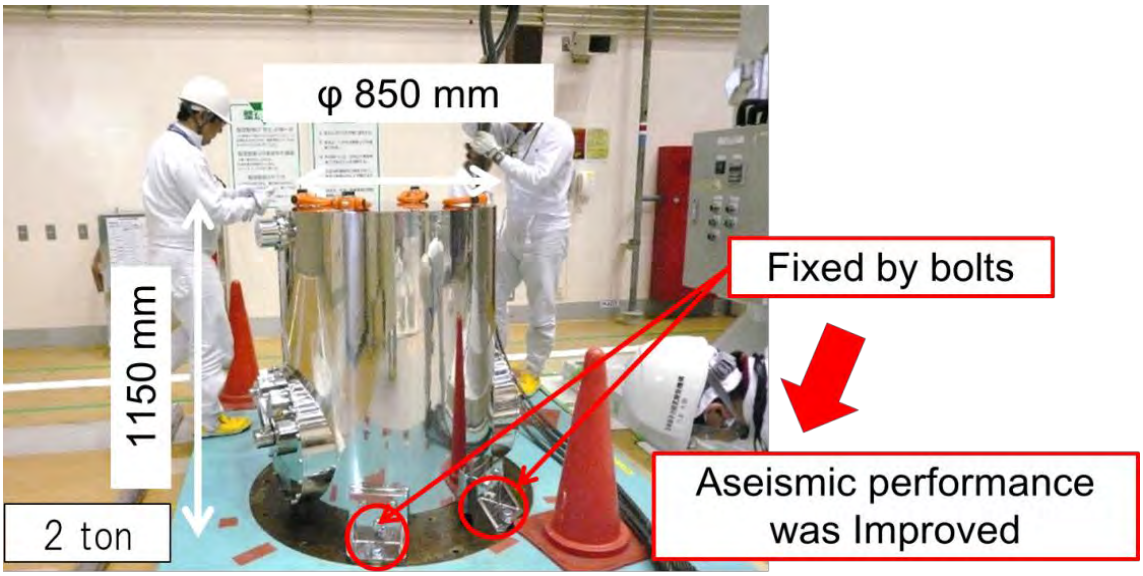

Figure 3.2 New transportation container for NS

3.2 Exclusion of falling of NS holder

The other technical issue is the falling risk of NS holder caused by the difficult remote handling.

The NS holder capsule of the conventional transportation container was so long (φ155 mm, h1285 mm) that it could not be pulled into the adequate working space in the maintenance pit. Thus, it was necessary to pull out the NS holder from the NS holder capsule at an inadequate working place far from the best position in the maintenance pit, subsequently to carry the NS holder to the best position by manipulator [2]. Therefore, the falling risk of NS holder, which is caused by handling mistake of manipulator, was not able to be excluded. The NS holder capsule of conventional transportation container is shown in Fig.3.3.

It was found that this risk can be excluded by downsizing the NS holder capsule while keeping the NS holder holding performance. Because the downsizing made it possible to pull the NS holder capsule into the adequate working space in the maintenance pit with attaching the locknut, the NS holder handling performance was improved. As the result, the falling risk of NS holder caused by the difficult remote handling was excluded. The size of new NS holder capsule is φ75 mm, h135 mm The new NS holder capsule and the improvement of neutron holder handling performance in the maintenance pit are shown in Fig.3.4 and Fig 3.5, respectively.

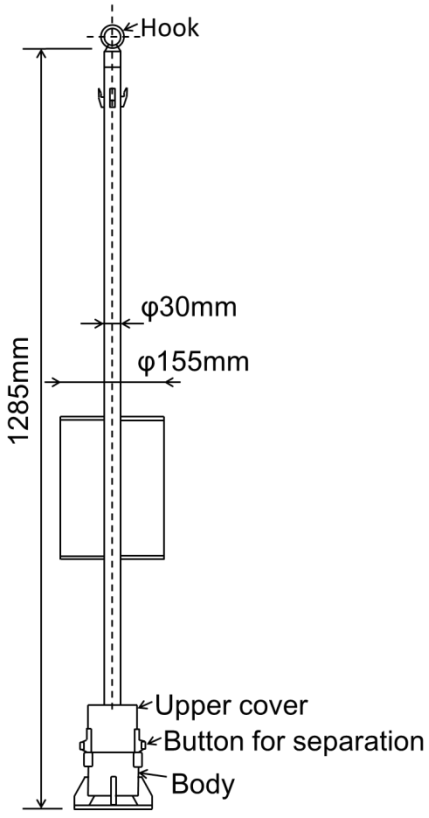

Figure 3.3 NS holder capsule of conventional transportation container [2]

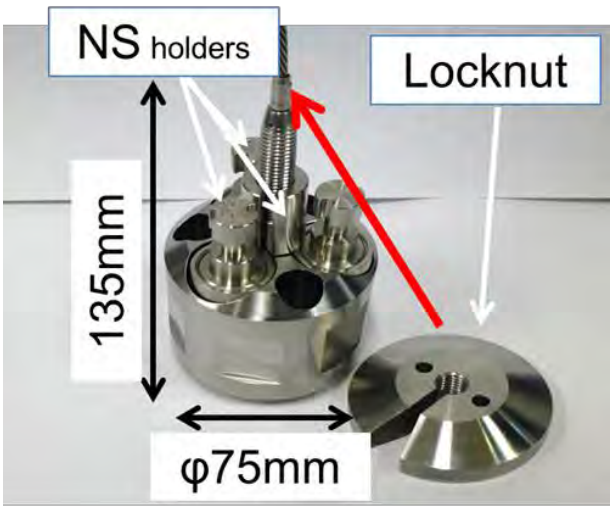

Figure 3.4 NS holder capsule of new transportation container

It was necessary to push the button for separation by manipulator and to pull up the upper cover by winch, which is set in the conventional transportation container, in order to open the conventional NS holder capsule which was a complex mechanism. On the other hand, the new NS holder capsule has simple mechanism which has screw type locking structure. Because of downsizing, simple

mechanism and so on, a cost reduction for manufacturing was also achieved. The manufacturing cost became as much as that for the overhaul of conventional transportation container.

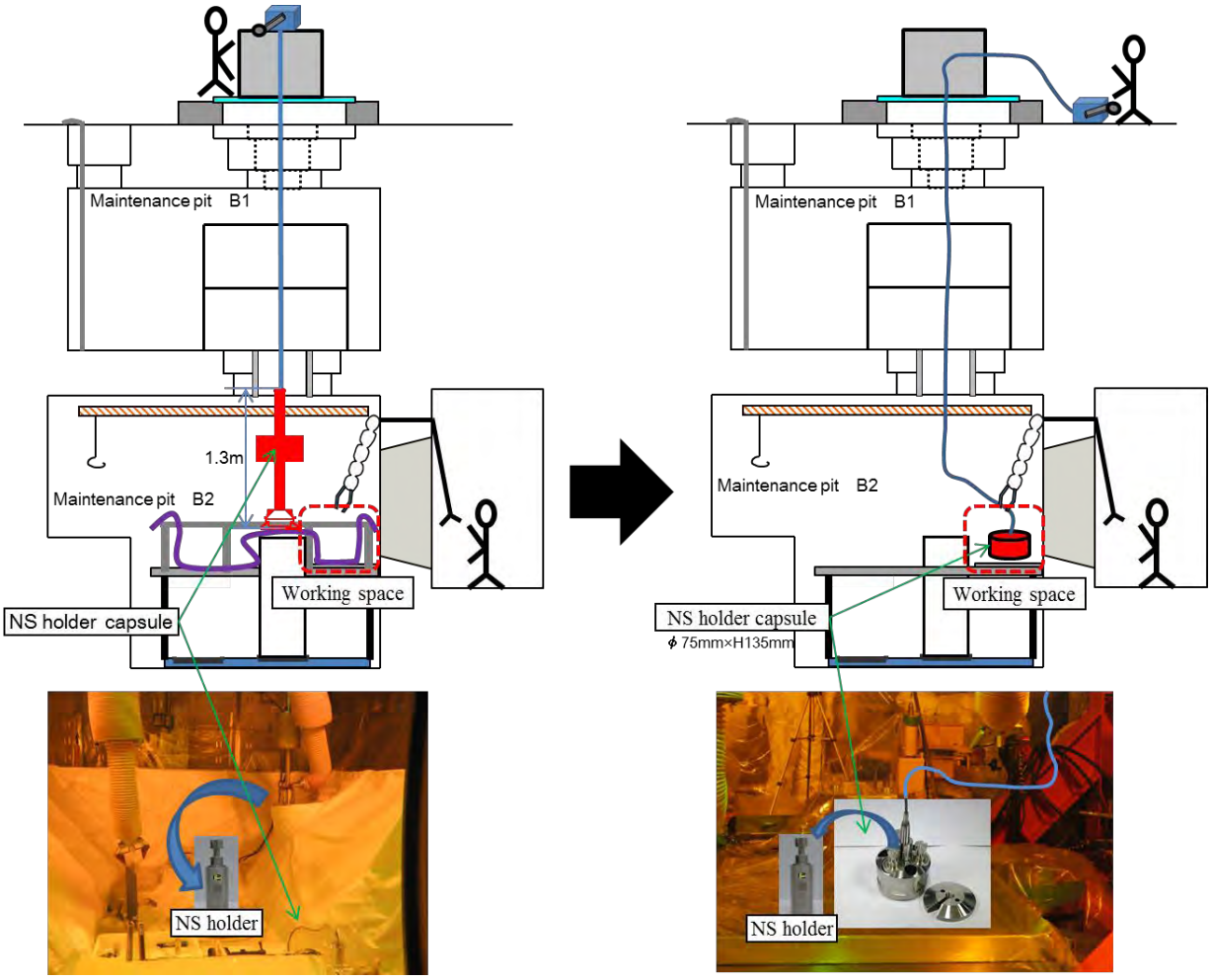

Figure 3.5 Improvement of NS holder handling performance in maintenance pit

4. Conclusion

Development of a new transportation container for NS, which can solve the technical issues recognized in the past exchange works, was carried out. The results of development are as follows;

(1) An issue for radiation exposure by neutron and gamma ray leakage was solved.

(2) An issue for falling of NS holder was solved

(3) A cost reduction for manufacturing was also achieved by simplifying the mechanism of NS holder capsule and downsizing.

In addition, NS holder handling work, which was carried out in 2015, was safely accomplished.

References

[1] Tochio, D., Watanabe, S., Motegi, T., Kawano, S., Kameyama, Y., Sekita, K., Kawasaki, K., 2007, “Operation Experience since Rise-to-power Test in High Temperature Engineering Test Reactor (HTTR)”, JAEA-Technology 2007-014.

[2] Takeda, T., Tobita, T., Mogi, H., Gomi, K., 1999, “Establishment to Handling Technique for Permanent Neutron Startup Sources of the High Temperature Engineering Test Reactor”, JAERI-Tech 99-053.
[3] Department of HTTR, 2014, “Operation, Test, Research and Development of the High Temperature Engineering Test Reactor (HTTR) (FY2013)”, JAEA-Review 2014-041.

USE OF UNICORN ANALOGUE I&C PLATFORM FOR RPS IN RESEARCH REACTOR

C. LOBRY
I&C Department, AREVA TA
1100 avenue JR Guilibert Gautier de la Lauzière, 13593 Aix en Provence - France

ABSTRACT

AREVA TA is currently developing a new safety analogue I&C Platform named UNICORN.
This Platform is basically designed to meet the requirements of a diversified safety I&C system in civil Nuclear Power Plant. The first application of UNICORN platform is a diversified non-computerized I&C system for the UK EPR Hinkley Point Project.
The UNICORN Platform can also be considered to be an alternative to computerized I&C platform to implement simple safety I&C functions, as for instance those performed by the Reactor Protection System.

The UNICORN Platform shall be understood as a set of:

- Electronic Modules – mostly based on intrinsic safety concept – which are used to implement safety and support functions in I&C system using this Platform,
- Communication Modules, computerized parts which are used to implement monitoring and maintenance functions in I&C system using this Platform,
- Cabinet / racks / accessories / wiring concepts,
- Engineering & Set Up Tools, used to design (i.e. from functional requirements to final wiring) I&C systems based on UNICORN Platform and to simulate them,
- Validation Tools for Test Bay validation activities,
- Periodic Test Tools for On Site activities.

The UNICORN Platform is suitable for the implementation of Class 1 I&C systems, according to IEC 61513 standards.

The UNICORN Platform will be fully qualified in spring 2018 in accordance with RCC-E and IEC standards (especially in terms of Electro Magnetism Compatibility, seismic and climatic environments).

The aim of the paper is to demonstrate the suitability of the UNICORN Platform to implement safety I&C functions performed by the Reactor Protection System in a Research Reactor.

In the light of typical requirements (functional requirements, safety targets…) of I&C safety functions performed by a Reactor Protection System in a Research Reactor, this paper presents:

- The UNICORN Platform, with a focus on key requirements of the platform and how these requirements are refined in terms of modules definition, modules technology, platform principles and recommended architecture,
- The suitability of UNICORN solution for such system (dispatching of the Reactor Protection System functions in UNICORN modules, safety achievement, periodic test needs, sizing…) in the case of a new installation or modernization of an existing reactor,
- The benefits, in term of cost and qualification, to use such analogue Platform in comparison with computerized technology in a Research Reactor.

1. Abbreviations

I&C	Instrumentation & Control
RPS	Reactor Protection System
RR	Research Reactor
TXS	Teleperm® XS

2. Introduction

2.1 I&C Context for Research Reactors

AREVA offers complete solutions for Research Reactors (1MW to several dozens of MW) which are intended to research organisations, with multiple application fields (technologic irradiation, fundamental research, isotopes production, education etc.).

For I&C systems, several issues are identified:

- Some installations have reached the end of their life and full new builds are needed to replace them, including new I&C,
- Some installations are getting old and some parts, as for instance I&C, and especially sub-systems such as Reactor Protection System (RPS) need to be modernized,
- Some technical evolutions (e.g. core modification, new production targets…) shall be realized on installation and the related I&C systems shall be updated and probably optimized as a whole.

In a general way, stakeholders or plants operators request I&C to be simple to operate, long-term reliable and maintainable, ensuring a high availability of the reactor and to have high performance, with a controlled cost of ownership.

According to this context and operators requirements, AREVA is proposing the following complementary technologies providing a comprehensive response for either specific requests and to meet diversity requirements in the Defence in Depth safety concept for the Plant:

- Teleperm® XS, based on a digital I&C technology, for middle power RRs,
- UNICORN, based on non-computerized modules, for low power RRs.

The Teleperm® XS also provides a non-computerized solution with some dedicated modules (FPGA based) allowing to realize some simple I&C functions.

2.2 Safety Authorities positions and standards

Design of RRs is mainly driven by NS-R-4 IAEA Safety Requirements (ref. [1]) and recently by SSG-37 IAEA Safety Standards Series (ref. [2]) dedicated to I&C systems of RRs.
According to the country and the relevant Safety Authorities, the standards rules for design and qualification is either declined in IEC, IEEE or KTA.
New safety requirements are also introduced either due to new design requirements (post Fukushima for instance) or because of local Regulation Authority requirements (Second Shutdown System for instance).

2.3 Scope

This paper is focused on UNICORN platform use for RPS of Research Reactors.
The RPS is closely linked to the reactor design and deeply associated to safety. Besides, designing such I&C system requires an organisation providing specific skills in reactor systems covering several trades.
According to SSG-37 IAEA Safety Standards Series (ref. [2]), the RPS (also including Engineering Safety Features) can be considered in the overall I&C as follows:

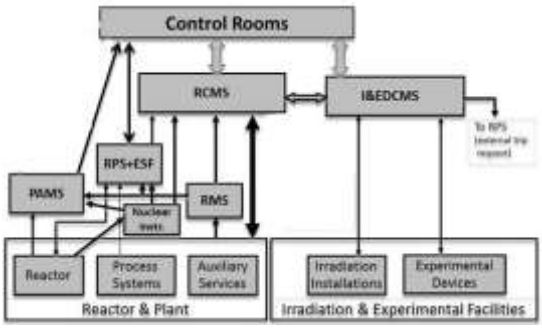

Figure 1: RPS in overall I&C

The main interfaces and scope of RPS can be represented as follows:

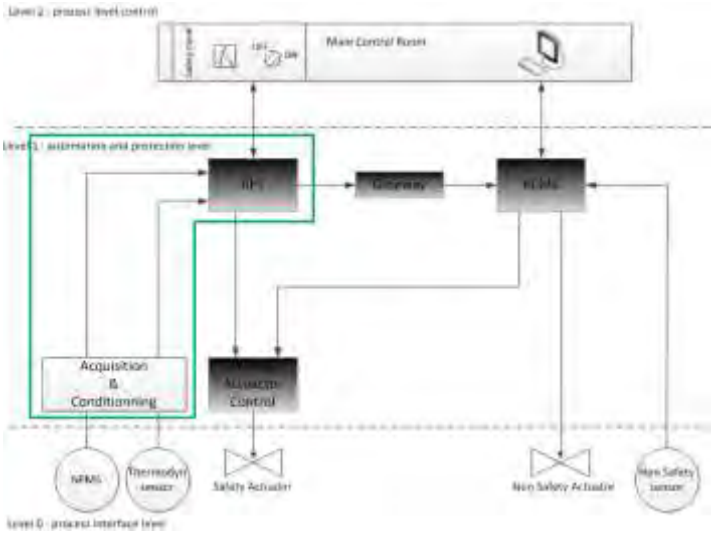

Figure 2: RPS interfaces

The UNICORN platform covers the RPS core and all its interfaces. For Acquisition and Conditioning part, UNICORN is designed to be interfaced with dedicated modules respecting its electrical features for input (i.e. acquisition of 0-24V binary signals and 4..20mA analogue signals). AREVA proposes typically Teleperm® XS acquisition and conditioning modules in interface with UNICORN solution (but other platforms can be considered).

Moreover, as the sizing of an I&C system implemented with a non-computerized technology is directly in relation with the number of I/O and functions, the UNICORN platform is dedicated to small reactors.

3. UNICORN solution

3.1 General requirements

The UNICORN platform is basically designed to meet the requirements of a diversified safety I&C system in civil Nuclear Power Plant.
It was also required to this platform to reach a satisfactory level of exhaustiveness and modularity, meaning that designed modules should be able to cope with typical safety I&C functions.

The UNICORN platform is a non-computerized platform developed to implement class 1 according to IEC 61513. As a consequence it allows to implement category A functions according to IEC 61226. This platform is currently in development (all modules have been already developed and tested) and will be available and qualified in mid of 2018.

3.2 Platform Description

3.2.1 Modules involved in safety actions

The UNICORN platform provides a set of modules for the implementation of I&C safety functions, in a full analogue signal context.
The technology of these modules is based on discrete components such as transistors or transformers. The most complex components are TTL counters and DC/DC pads.

The preferred design for these modules is based on **Magnetic Dynamic Logic** (AREVA TA proprietary technology).
This Magnetic Dynamic Logic principle is based on fail safe concept technology.
The safety of a simple logical entity (unique logical function) is guaranteed by the fact that all the possible failures of this entity are fail safe (i.e. safety action request oriented). This fail safe concept is used in the I&C system to force a "safe state" if a dangerous breakdown is detected.

These "simple" functions can thus be used alone and, as a rule, avoid failures monitoring detection. Their failures are "directed" to a safe state and it is qualitatively demonstrated, whatever is the failure mode of the used components, that no single failure leads to an undesired tolerant safety state.
The safe state is the "de-energized" on the output signal. Consequently, a power loss shall lead to the safe state.

This safe technology concept is based essentially on the following two postulates:
1. Inside a module, a static signal is converted into a dynamic signal. The transmitted signal is a dynamic signal, adapted to the final receiver of the command: any failure which leads to a state which deviates from expected characteristics (that is the totality of the possible failures, recognized by reliability handbooks) leads to the loss of the command and thus triggers the safe state.
2. Use of only discrete components, for which the failure modes are perfectly identified. It ensures that the component FMEA leads to deterministic probability of the safety (all scenarios and failures effects can be identified).

Depending on safety and availability targets for a project based on the UNICORN platform two main system architectures are possible:

- Redundant internal treatments inside a division, in order to limit the spurious activation,
- Simple internal treatment when spurious activation is not challenging (managed by simple chain or covered by the overall I&C architecture including others systems).

3.2.2 Monitoring functions

All monitored signals from safety modules are hardwire connected to concentrator modules (FPGA based) in order to send them to a recording system, called Datalogger. This recording system allows to process a large amount of data to be sent to the Gateway (see figure 2) or to be analysed offline with a dedicated tool called Datalogger Analyser (with a history of more than 3 days, depending on the system size).
The Datalogger also contributes to the realization of the Periodic Tests when connected to the Test Bench equipment. On site, all functions are testable without needing to remove modules from the cabinet.
One Datalogger shall be installed in each division and dedicated network is used to exchange data in such a way that each Datalogger has the whole configuration of the I&C system.

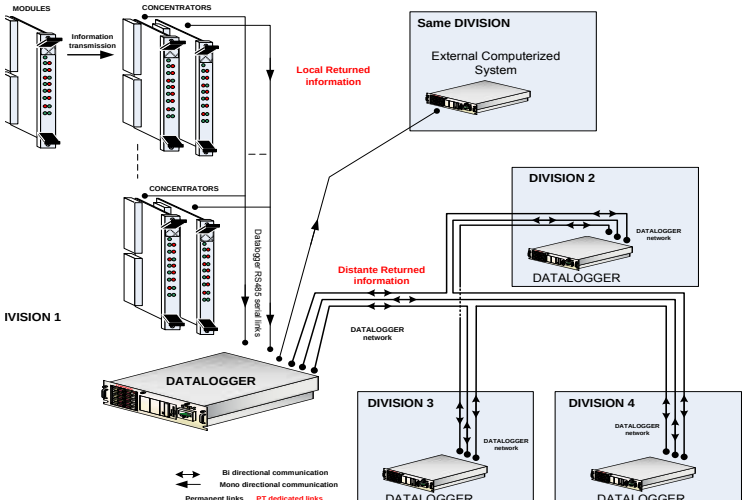

Figure 3: Monitoring network

The Datalogger does not participate to safety functions and is then class 3 classified.

3.2.3 Mechanical parts

The UNICORN platform will be qualified within a selected cabinet (w=900mm, d=400mm, h=2260mm) and its set of existing connectors (for signals from field and for tests).
All functional modules are designed in 1T/6U (160mm depth) dimensions.

3.2.4 Design and Validation Tools

A set of tools is provided in order to:

- Convert the functional needs into hardware specification using platform available parts,
- Give a data description of the signalization serial lines,
- Give cabinet and racks description,
- Generate / Provide Test Plans.
- Provide facilities for maintenance and tests.

3.3 Modules overview

Name	Classification	Main description of board
SCAT	Class 1	**S**urveillance **C**ircuit **A**nd **T**hreshold
PRD/IRD	Class 1	**P**ower **R**ange Detector & **I**ntermediate **R**ange **D**etector
LIN/QUAD	Class 1	Sensor acquisition & **LIN**ear or **QUAD**ratic transfer function
SORT	Class 1	Analogue **SORT** function and analogue exchanges between divisions
PID	Class 1	**P**roportional – **I**ntegrative - **D**erivative function
ISOLAND	Class 1	**ISOL**ATION & **AND** gate module
VOPER	Class 1	**VO**ting and **PER**missive
MEMMUX	Class 1	**MEM**orisation and de**MU**ltiple**X**er
TEMPO/PULSE	Class 1	**TEMPO**risation & **PULSE**
OR GATE	Class 1	**OR GATE**
AVACT	Class 1	**AV**ailability and **ACT**uator driver
ACT-DRV	Class 1	**ACT**uator **DRiV**er
CLAMP	Class 1	**CLAMP** - Protection of voltage overloads
LSM	Class 1	**L**ife **S**ign **M**onitoring
ALARM MGT	Class 1	**AL**arm **M**ana**G**emen**T**
CMU	Class 1	**C**abinet **M**onitoring **U**nit
CONC *	Class 1	**CONC**entrator of digital data for sending to the datalogger
ANA-CONC *	Class 1	**ANA**log **CONC**entrator of Analogue data for sending to the datalogger
DATALOGGER	Class 3	**DATALOGGER**
FUSE	Class 1	Power supply sub-distribution & **FUSE** protection
POWER RACK	Class 1	**POWER RACK** embeds two independent power sub-distributions

* CONC and ANA-CONC modules: electronic class 1, function class 3

Table 1: UNICORN modules

It has to be noted that several patterns of a given function are available on each UNICORN module (for instance, there are 6 OR gates on OR GATE module).

The figure below provides an overview of all UNICORN modules embedded in a rack.

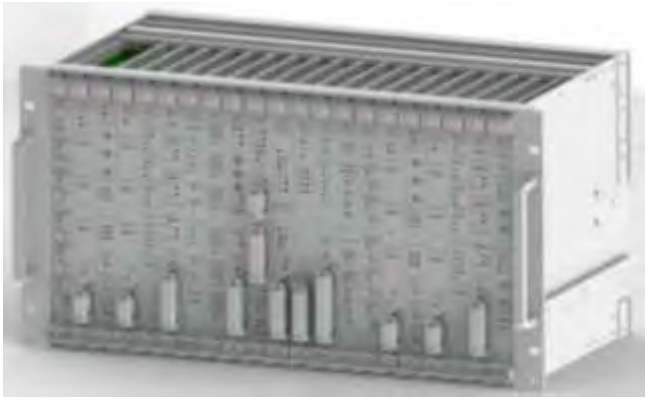

Figure 4: UNICORN modules in a rack

3.4 Typical I&C function managed by UNICORN Platform

In a typical I&C function performed by RPS, a sensor value is generally compared with a threshold value after a processing if any (e.g. for excore sensors).
In case the sensor is not working properly, a lockout, which has to be activated manually and locally, allows:

- To ignore or force it in downstream processing,
- To ignore it for external display in Main Control Room.

The result of the comparison is provided to the other divisions (1 to 3) to be used as input for the voting logic and in order to perform the actuation logic.
The following figure gives the typical scheme for such I&C function (left) and its implementation in UNICORN modules (right).

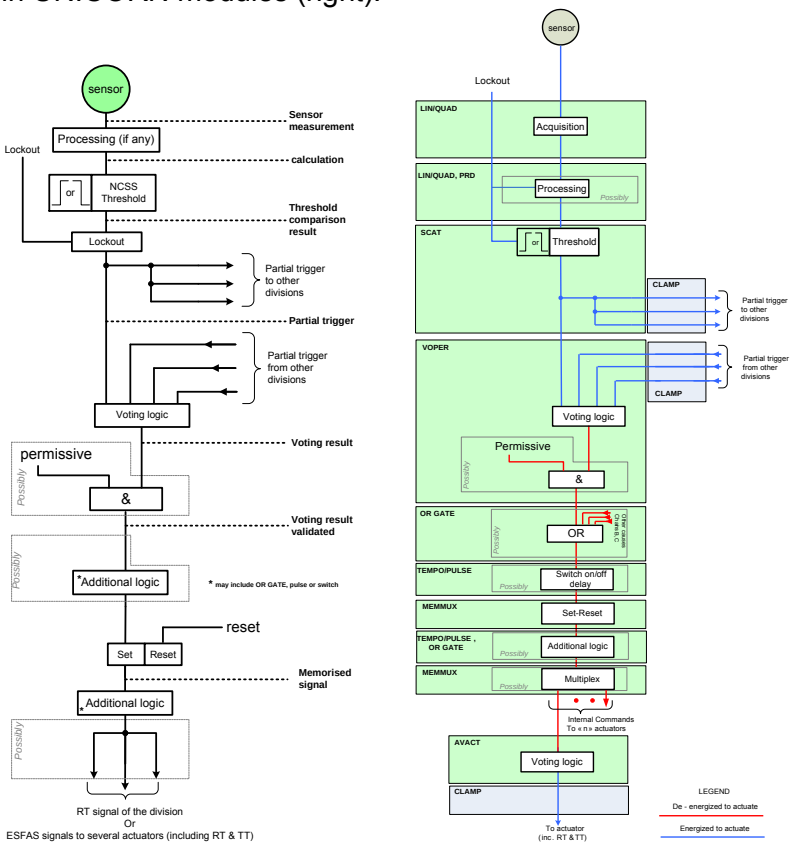

Figure 5: Typical I&C function and its implementation in UNICORN modules

Note: UNICORN platform allows to implement up to 3 internal chains inside a same division, that's why there is a final Voting Logic at the end of the function.

4. UNICORN answer to key requirements for RPS in RR

In order to realize the current analysis, **9 keys requirements** or concerns have been selected for RPS in RR:

- Functional requirements,
- Safety and availability requirements,
- Independence,
- Qualification,
- Interfaces,
- System evolution,
- IT security,
- Maintenance & Periodic Tests,
- Sizing & surface area.

4.1 Functional requirements

The first main requirement is related to the realization of the functions performed by the RPS. 2 metrics have to be considered and to be addressed:

- The amount of I&C Functions,
- The amount of I/O signals.

The feasibility of RPS functions is ensured considering that they fit to the typical scheme defined in Figure 5.

4.1.1 Amount of I&C Functions

The following table provides the list of typical RPS I&C Functions for a low power RR (based on a TRIGA type reactor).

Reactor Trip on High Flux
Reactor Trip on High Reactor Power (N16)
Reactor Trip on High Fuel Temperature
Reactor Trip on Low-low Reactor Pool Water Level
Reactor Trip on Low Primary Coolant Flow
Reactor Trip on Manual Command in Main Control Room
Reactor Trip on Magnet Power Key Switch-Off
Reactor Trip from Experiments I&C

Table 2: Typical RPS I&C Functions in Research Reactors

4.1.2 Amount of I/O signals

4.1.2.1 Inputs of the system

Typically, the types of input signals are as follows:

- excore conditioning,
- analogue signal 4-20 mA,
- conditioning for strain bridge,
- PT100,
- binary signals.

UNICORN acquisition modules allow to be interfaced with an Acquisition and Conditioning Level providing 4..20mA analogue signals and 0-24V binary signals.

According to a first sizing estimation, the following amount of inputs by division should be needed for I&C functions and monitoring functions:

- 15 Analogue signals,
- 18 Binary signals.

These figures lead approximatively to a sizing of 50 6U modules for functional needs, implying that such RPS could fit in two cabinets, including the Acquisition and Conditioning Part.

4.1.2.2 Outputs of the system

6 binary signals have to be taken into account for Reactor Trip (managed by AVACT or ACT-DRV module).
Direct signal annunciation (i.e. without alarm management and reappearance processing) to Main Control Room is already included in analogue and binary acquisition modules, so it has no impact on sizing.
Signal annunciation to RCMS is basically managed by the UNICORN platform with concentrator modules and Datalogger, so it has no impact on sizing.
The remaining signals which may impact the system are the alarms. Around 6 ALARM MNGT modules have to be provisioned.

4.2 Safety and availability requirements

The safety and availability targets are main requirements which drive the choice of an I&C architecture. The typical goals to reach are the following:

- 10^{-4} failure per demand (safety target),
- 10^{-3} spurious trip / year (availability target).

A principle of redundancy is provided by UNICORN platform to improve the reliability of I&C systems. To reach these objectives, UNICORN platform is adaptable in 1 to 4 divisions architecture.
To increase the availability of the system, 2 redundant chains can be implemented inside a same division. A third redundant chain can also be added to reach a challenging safety target on a specific function.
With an architecture based on 3 divisions, with one single redundancy inside each division, a recent analysis has proven that UNICORN is suitable for a RPS implementation in term of safety and availability requirements, according to these figures:

- $< 10^{-4}$ failure per demand (safety target),
- 10^{-4} spurious trip / year (availability target).

4.3 Independence

Independence is required between systems of different safety classes in order:

- To prevent propagation of failures from systems of lower importance of safety,
- To prevent propagation of failures from computerized I&C systems,
- To prevent propagation of failures between redundant divisions providing safety functions.

Besides, independence is also required inside RPS between modules of different safety classes in order to prevent propagation of failures between elements performing safety functions and elements performing monitoring functions within RPS.

When a postulated fault of a monitoring element is applied on a signal, the pattern behaviour of the safety function is still warranted. Components or fuses destructions are possible, but the effect shall be limited to the attacked signal.

All external outputs of the system are short-circuited and overload proven.

Non stress and non-pollution of lower classified equipment to higher classified equipment is addressed for:

- Periodic Tests & Maintenance modules (Class 3) towards Class 1 modules,
- Modules providing Signal Annunciation to RCMS (Class 3) towards Class 1 modules,

by design of the modules and by the implementation of isolation barriers and unidirectional links.

4.4 Qualification

The qualification is based on a qualitative criterion following:

- The use of this platform on other projects,
- The licensing of this platform with regards to standards and norms.

The UNICORN Platform is developed at the highest level of safety and follows the following standards and norms:

- Design : RCC-E 2012, IEC 61226, 61513, 60987, 62138 (for cat C SW parts) + 60709, 60671, 60664, 60721-3-3, 60300-x, 62380, 62340
- Qualification:
  - IEC 60780 : general qualification process,
  - IEC 60980 : seismic qualification,
  - IEC 60068-2 series : environmental qualification,
  - IEC 61000-4 series, IEC 61000-6-2 and IEC 61000-6-4 : EMC qualification,
  - IEC 60529 : IP qualification,
  - IEC 17025 : for laboratory requirements,
  - BTR : EDF document amending RCC-E and IEC levels and procedures.

4.5 Interfaces

4.5.1 With actuators

The interface with actuators is managed by:

- AVACT module in case of 2 or 3 redundant chains inside a same division,
- ACT-DRV module in case of a single chain inside a division,

A switchgear module (out of UNICORN scope) is dedicated to drive the actuator and manage the priority of orders.

AVACT and ACT-DRV modules can perform a continuity check (by injection of the current in the load) and a check-back monitoring function.

4.5.2 With other I&C

With ISOLAND module, UNICORN platform can receive binary signals from:

- Experiments I&C,
- Main Control Room.

Analogue measurement and binary status or sensors can also be sent to Main Control Room with dedicated outputs to conventional HMI on UNICORN modules.

4.5.3 With operational I&C

The Datalogger is the dedicated equipment to perform the uni-directionnal interface to the Gateway of an operational I&C. The embedded protocol is ModBus over TCP/IP, but it can be adapted depending on the project needs.

4.5.4 With NFMS

A dedicated module (PRD/IRD) allows to acquire and process Neutron Flux Measurements (Power and Intermediate Range). This module is typically interfaced with SCV1x and SCV2 neutron flux modules of the Teleperm® XS platform.
The format and the type of signals shall be checked if another NFMS supplier has to be used.

4.6 System evolution

Contrary to other non-computerized I&C platforms, the final wrapping operation is highly simplified and guided with the UNICORN Design & Validation Tools (see 3.2.4), allowing to:

- Generate the final point to point wiring list,
- Test and validate before cabling and wiring in a simulated environment.

4.7 IT Security

By design, IT Security issues are limited in UNICORN Platform. However some parts are concerned by such topic.
An IT Security analysis has been made on the platform, following ISO 27001 standard and focusing particularly on computerized based equipment (Datalogger, Test Bench), and development tools bringing some sensitive points to monitor (causeways for instance) which have been reinforced by specific security requirements (with CRC or special procedures for instance).

4.8 Maintenance & Periodic Tests

The RPS shall be designed in such a way that it can be adequately inspected, tested and maintained as appropriate, before commissioning and at regular intervals thereafter, in accordance with their safety targets.

The UNICORN Platform allows to perform Periodic Tests according to IEC 60671.
Periodic Tests shall be performed on all classified equipment (i.e. Class 1 or Class 3) embedded in the cabinets which do not perform continuous monitoring actions or for which the result can be a steady state. As a consequence Datalogger which realizes continuous operation controls is out of Periodic Tests scope.

Periodic Tests are carried out at a functional level. They concern automatic, manual and monitoring functions. The goal is to validate the overall system behaviour using its outputs, when facing a trigger condition on its external inputs. As a mean of complexity reduction and redundancies check, overlapping testing is the preferred solution.
The following figure presents the overall strategy for overlapping in a typical I&C function spread in 2 redundant chains.

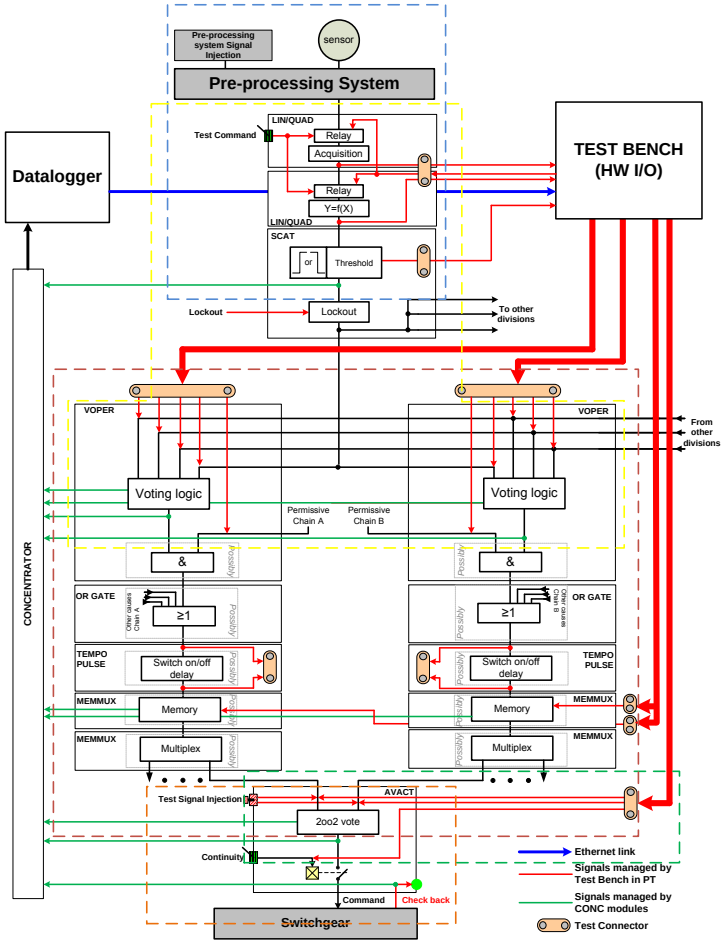

Figure 6: Periodic Tests - UNICORN overlapping principle

4.9 Sizing & surface Area

According to the sizing provided in 4.1, two cabinets per division could be sufficient, with a surface area of (w=900mm, d=400mm) each and a height of 2260mm.

5. Benefits to use such analogue Platform in RR

The following benefits have to be considered by using UNICORN Platform in RR:

- It is well suited for simple processing,
- The design of the system is faster, there is no code to develop,
- Response time is better,
- Can be considered as a diversified technology,
- It is competitive in term of costs, for a low power reactor, with a small number of I/O and I&C functions,
- IT Security demonstration is easier,
- It is compatible with the TXS integration standard, allowing to use in addition to some modules or functions available in TXS product catalogue.
- It will be a Class 1 qualified platform.

6. References

[1] INTERNATIONAL ATOMIC ENERGY AGENCY, Safety of Research Reactors, IAEA Safety Requirements No. NS-R-4, Vienna (2005).

[2] INTERNATIONAL ATOMIC ENERGY AGENCY, Instrumentation and Control Systems and Software Important to Safety for Research Reactors, IAEA Safety Standards Series No. SSG-37, Vienna (2015).

GAMMA AND NEUTRON RADIATION FIELDS ABOVE THE REACTOR POOL OF THE LVR-15 RESEARCH REACTOR

L. VIERERBL, Z. LAHODOVÁ, Z. MOJŽÍŠ, V. KLUPÁK, A. VOLJANSKIJ

Research Centre Řež, Ltd.,
Husinec-Řež 130, 25068, Czech Republic

ABSTRACT

The LVR-15 reactor is a light water research reactor, which is situated in Research Centre Rez, Husinec-Řež near Prague. The reactor operates as a multipurpose facility with maximal thermal power of 10 MW. Roughly five meters thick water layer of reactor pool is above the reactor core. About one meter above the pool surface there is the reactor head. During reactor operation, relatively high level of radiation is present in the space between the pool surface and the reactor head. This space is closed for workers during reactor operation but some objects sensitive to radiation damage (e.g. cameras, cables) can be used here and therefore it is important to know the radiation situation in this space. The radiation originates from the reactor core, radionuclides present in primary circuit water, activated parts of the reactor and from different types of secondary reactions. Main components of the radiation are gamma photons and neutrons. Neutron and gamma fields are not homogeneous in this space mainly due to the different types of the vertical channels. The measurement of fields was made in four points under the reactor head. Gamma radiation dose rate was measured with alanine detectors. Fluence rate of thermal, epithermal and fast neutrons was measured with different types of activation and track detectors. Boxes with set of detectors were fixed in their four measuring points during one reactor cycle (20 days). In the paper, description of measurement and data evaluation, and result values of gamma dose rate and neutron fluence rate are given.

1. Introduction

The LVR-15 research reactor [1], situated at the site of the Research Centre Rez near Prague, is a light water moderated and cooled tank nuclear reactor with forced cooling. The maximum reactor power is 10 MW. The fuel type is IRT-4M enriched to 19.7 % of ^{235}U and beryllium blocks are used as a reflector. Water volume in the vessel is 22 m^3. The reactor is operated in 21-day irradiation cycles with 8–10 cycles per year. The reactor operates as a multipurpose facility, mainly for material research, radionuclide production and physical experiments on horizontal neutron beams.

Above the reactor core, there is roughly five meters thick water layer of reactor pool. The reactor head is about one meter above the pool surface. With reactor shutdown, the reactor head can be open and staff can perform necessary operations above primary circuit water during limited time. Other situation is during reactor operation when reactor head is permanently closed and staff can work only on the massive head where they are sufficiently radiation protected. In the space between the pool surface and the reactor head relatively high level of radiation is present. This space is closed for workers during reactor operation but some objects sensitive to radiation damage (e.g. cameras, cables) can be used here and therefore it is important to know the radiation situation in this space. The radiation originates from the reactor core, radionuclides present in primary circuit water, activated parts of the reactor, and from different types of secondary reactions. Main components of the radiation are gamma photons and neutrons. Neutron and gamma field is not homogeneous in this space mainly due to the different types of the vertical channels, especially dry channels. The measurement of gamma and neutron fields was made in four points under the reactor head.

2. Measurement methods

2.1 Gamma radiation

Dose rate from gamma radiation was measured with alanine detectors. They have a suitable measuring range (100 Gy–100 kGy) and sufficient precision. The alanine dosimeters used [2] are composed of a mixture of alanine and polyethylene in the form of a small cylinder with a diameter and height of 4.8 mm and with a mass of 65±0.5 mg. Electron spin resonance (ESR) spectroscopy was used for evaluation of gamma doses measured by alanine dosimeters [3].

2.2 Neutron radiation

Neutron fluence rate is relatively low in the measured space. Thermal, epithermal and fast neutrons were measured with different types of activation and track detectors.

As activation detectors, five types were chosen:
1) Ni – 18 g, without Cd
2) Au – 34 mg, without Cd
3) Au – 34 mg, with Cd
4) Co – 180 mg, without Cd
5) Co – 180 mg, with Cd
In the list, typical mass and application of Cd cover are given for used elements. Induced activities of the detectors were measured with HPGe gamma spectrometry [4]. Measured radionuclides were ^{198}Au from ^{197}Au(n,γ)^{198}Au, ^{60}Co from ^{59}Co(n,γ)^{60}Co and ^{58}Co from ^{58}Ni(n,p)^{58}Co reaction. The neutron spectrum was evaluated [5] with the SAND II unfolding code using the IRDF90 dosimetry library.

As complement detectors, four types of track detectors [6] were tested for neutron detection:
1) Melinex with ^{232}Th converter,
2) CR-39 with recoiled proton detection,
3) Makrofol with recoiled nuclei detection,
4) CR-39 with ^{10}B converter.
The first three detectors are sensitive to fast neutrons, the last to thermal neutrons. Evaluation was made by etching and counting of tracks.

2.3 Detector positions and irradiation

Sets of detectors, composed of alanine, activation, and track detectors, were fixed in a glass boxes with diameter of 70 mm and height of 40 mm. Detectors were positioned in two layers, on the bottom and on the top of the box (Fig. 1).

Fig. 1. A glass box with detectors, bottom layer (left photo), top layer (right).

Schematic image of four measuring points is in Fig. 2. The points were chosen according possibility to fix the detector set (Fig. 3.) and possible camera position.

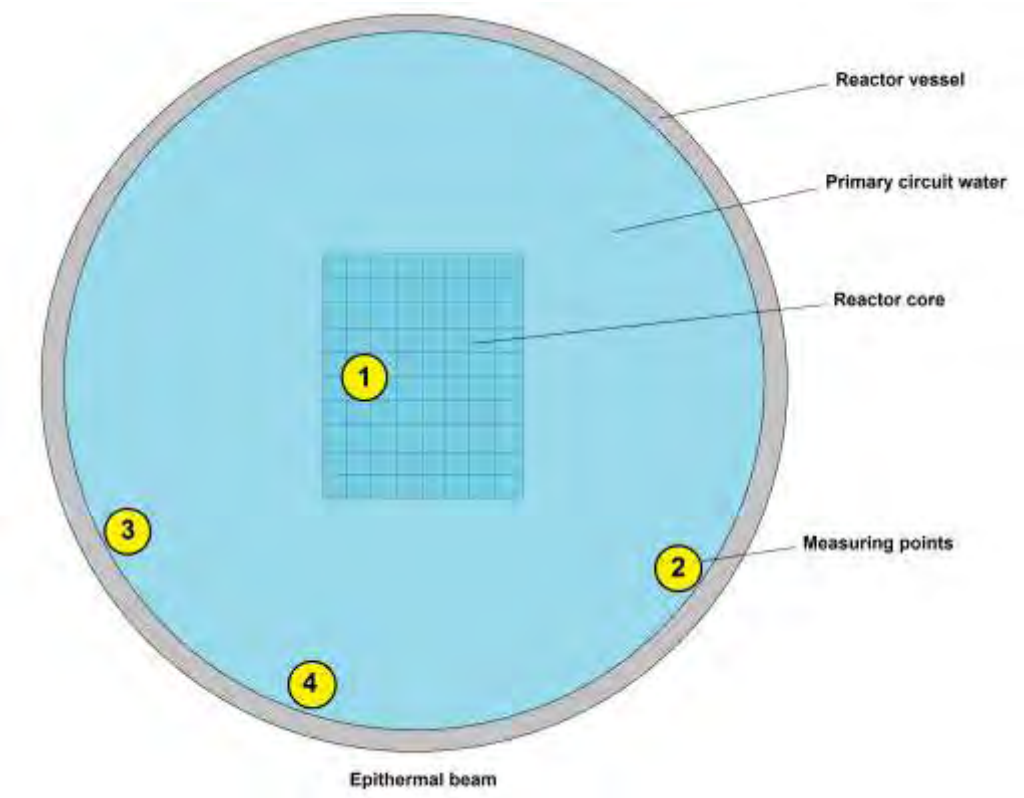

Fig. 2. Schematic top view of four measuring points - detector boxes positions.

Fig. 3. Detector box No. 4, overall view (left), detail (right).

Boxes with set of detectors were fixed in their four measuring points during one reactor cycle from 17. 4. 2015 to 20. 5. 2015. As irradiation time used for dose rate and fluence rate calculation, only reactor operation time was used (19.4.2015 to 10.5.2015 and shortly on 18.5.2015). It was 20.05 days of irradiation with 9.6 MW of average thermal reactor power. The radiation field was assumed constant in time during the irradiation. Influence of detector irradiation during reactor shutdown was neglected.

3. Results

3.1 Gamma radiation

Measured doses and dose rates for gamma radiation are in Tab. 1. Uncertainties of the values are about 10 %.

Position No.	Total dose (Gy)	Dose rate (mGy/h)
1	100	207.8
2	27	56.1
3	30	62.3
4	37	76.9

Tab. 1. Measured values of gamma radiation total dose and dose rate.

3.2 Neutron radiation

Induced activities of activation detectors were measured with HPGe detector in the LVR-15 spectrometry laboratory. Activity values of ^{198}Au for individual detectors were in range from 10 Bq to 18 Bq and for ^{60}Co from 1.3 Bq to 6 Bq. Due to low activities of ^{58}Co, all four Ni detectors were measured together with total activity result of 2.9 Bq.

Evaluated track densities for Melinex with ^{232}Th converter were from 1.6×10^4 cm^{-2} to 4.2×10^4 cm^{-2}, for CR-39 with recoiled proton detection from 9×10^5 cm^{-2} to 15×10^5 cm^{-2}, and for Makrofol with recoiled nuclei detection from 3×10^5 cm^{-2} to 5×10^5 cm^{-2}. Track density for CR-39 with ^{10}B converter was overloaded (>10^7 cm^{-2}), therefore this detector could not be evaluated.

For neutron fluence evaluation, response from Au without Cd cover, Au with Cd cover and Ni detectors were used. Values from other detectors were taken only for relative comparison due to higher uncertainties of these values. Evaluated fluence rates in four energy groups are in Tab. 2. Typical uncertainties of these values are about 30 %.

Energy groups	Fluence rate (cm^{-2}.s^{-1})			
	Position No.			
	1	2	3	4
Thermal n. (0 eV, 0.5 eV)	7.07E+03	5.49E+03	7.06E+03	4.17E+03
Epitherm. n. (0.5 eV, 10 keV)	2.11E+04	1.63E+04	2.10E+04	1.24E+04
(10 keV, 1 MeV)	7.71E+03	6.61E+03	7.64E+03	5.75E+03
Fast n. (1 MeV, 20 MeV)	4.02E+02	4.02E+02	3.93E+02	4.09E+02
Total n. (0 eV, 20 MeV)	3.62E+04	2.88E+04	3.61E+04	2.28E+04

Tab. 2. Measured values of fluence rate in four energy groups.

4. Conclusion

Description and results of gamma dose rate and neutron fluence rate measurement in four points under the LVR-15 reactor head are given. Range for gamma dose rate was evaluated as 50 mGy/h to 210 mGy/h. Fluence rate values for thermal neutrons were about 6×10^{3} $cm^{-2}.s^{-1}$ and for fast neutrons about 4×10^{2} $cm^{-2}.s^{-1}$. The measured values can serve for radiation damage estimation of materials placed under the reactor head. Due to relatively small number of measuring points and measurement only in one reactor cycle, in general cases these results can be taken only as indicative values, which depends on precise position, reactor power, irradiation channels configuration and other operation conditions.

5. Acknowledgement

This work was performed within the scope of research project R4S - NPU II.

6. References

[1] Research Centre Rez, 2013. Research Reactor LVR-15, <http://www.cvrez.cz/en/infrastructure/research-reactor-lvr-15/>

[2] D.F. Regulla, U. Deffner, Int. J. Appl. Radiat. Isot. 33 pp. 1101, (1982).

[3] W.L. McLaughlin, Radiat. Prot. Dosim. 47 (1/4) pp. 255 (1993).

[4] ASTM E181-98, 2003. Standard Test Methods for Detector Calibration and Analysis of Radionuclides.

[5] ASTM E944-08, Standard Guide for Application of Neutron Spectrum Adjustment Methods in Reactor Surveillance (2008).

[6] S.A. Durrani, R.K. Bull, in: Solid State Nuclear Track Detection, Pergamon Press, 1987.

Advances in Materials Surveillance Programme for the RA10 Research Reactor

R. VERSACI,

Subprograma de Gestión y Extensión de Vida de Centrales Nucleares de Potencia. Gerencia de Área Energía Nuclear (GAEN), Comisión Nacional de Energía Atómica (CNEA), Avda. Del Libertador 8250, (1429) Buenos Aires, Argentina.

G. BERTOLINO, A. YAWNY
División Física de Metales, Gerencia de Física CAB, Gerencia de Área Investigaciones y Aplicaciones No Nucleares, GAIyANN-CNEA, Avda Bustillo km 9500, (8400) Bariloche, Argentina.

G. ARIAS, H. BLAUMANN
Gerencia Proyecto RA10, GAEN, CNEA.
Avda Bustillo km 9500, (8400) Bariloche, Argentina.

Corresponding author: versaci@cnea.gov.ar

The RA-10 is a new multipurpose research reactor which has been decided to be built in Argentina in order to satisfy the increasing national and regional demands for radioisotopes. The RA-10 is a 30 MW thermal power open pool facility with MTR (Material Testing Reactor) type fuel assemblies.
A Surveillance Program is part of a more general Ageing Management Program and its objective is the assessment of the structural integrity of critical core materials components in order to ensure a safe and reliable long term operation. Neutron irradiation affects ductility, tensile and toughness properties of materials in general and might result in irradiation induced growth in Zirconium base structural materials. Ad-hoc surveillance programs have to be developed for research reactors considering the peculiarities of each design. In the present case, the most exposed critical components were firstly identified. Thereafter, the critical components were categorized in those that are replaceable or no replaceable along the expected life of the reactor. The materials of interest are Zircaloy-4, Zr-2.5 wt%Nb. The evaluation of the effects of irradiation is followed by periodically removing (2, 5, 10, 20, 30 and 40 years) capsules containing tensile, fracture toughness CT and small punch testing specimens representative of the different materials and thermomechanical conditions. Dosimeters are placed within the surveillance capsule and evaluated to determine the associated neutron fluence at the specific location within the vessel and time of extraction. Specimens will undergo post-irradiation testing in a hot cell facility to determine their mechanical properties (and dimensions). The obtained values will be compared with the original values and the predefined design limits to evaluate the operational margin of safety. In summary, the present paper describes the methodology of the implemented surveillance program, the test specimens, their locations and the tests to which they will be subjected.

1. Introduction

Whereas the RA10 reactor is postulated that the same should reach at the following design objectives: safe operation, high availability, nominal operating cycle 29.5 days and 2.5 days outage.

Developing a Life Management Program is critical to meet these principles in Safe, High Availability and Long Term Operation [1]. These programmes should start with the design; continue during construction, installation, commissioning, operation and decommissioning. Management of Ageing, obsolescence and economics are part of these programmes. [2] [3] [4][5].

To develop this programme we use the methodology that is shown in Figure 1.

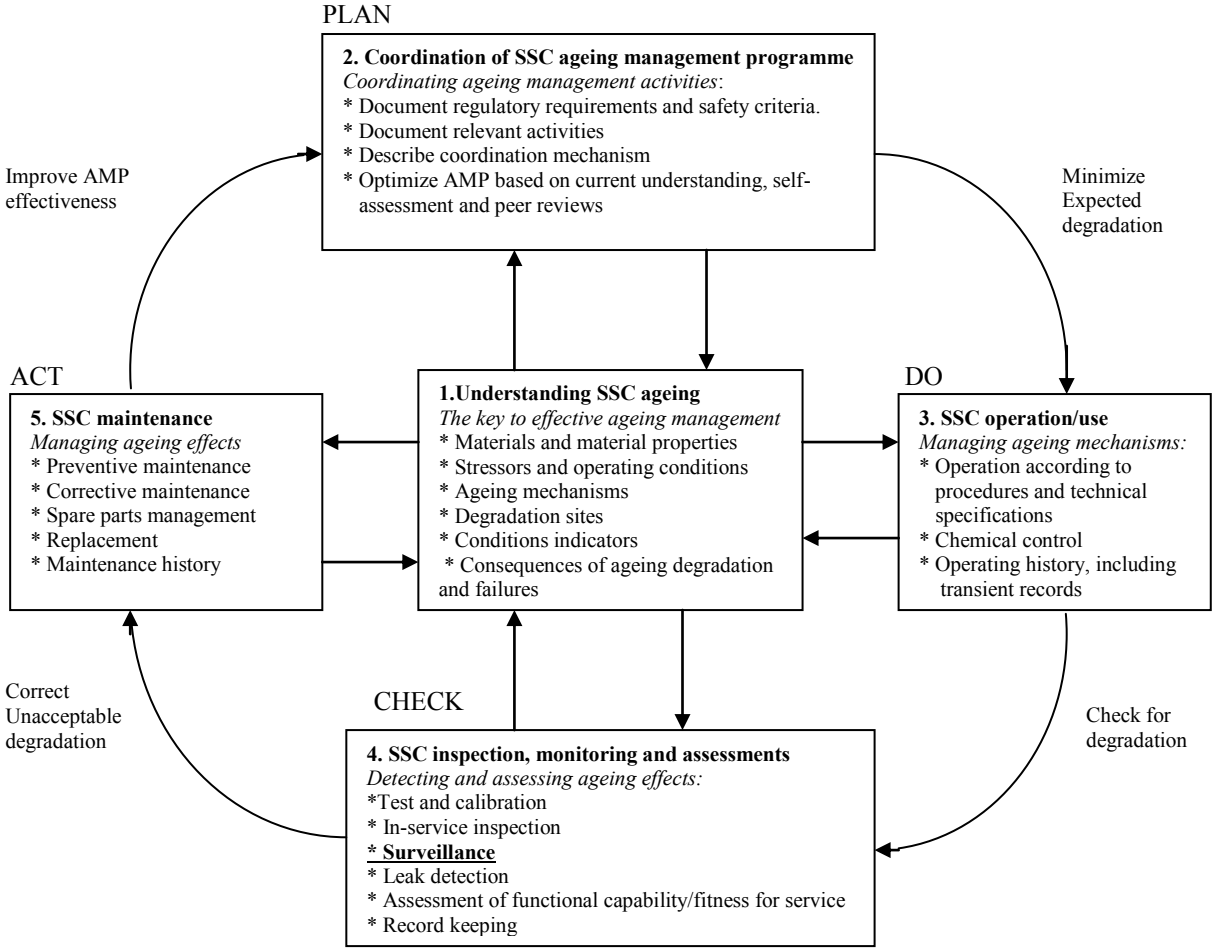

Fig 1. Ageing Management Programme Methodology

As part of this Ageing Management Programme we define a Surveillance Programme (SP). The goal of SP is to monitor changes in material properties of the essential components for safe operation of the reactor due to the effects of intense neutron radiation to which they are subjected.

These changes include: tensile properties, radiation induced growth and fracture toughness of the materials from which the critical components exposed to radiation. [6] [7][8].

The implementation of a SP requires the provision within the reactor of specimens of materials that are desired characterized in zones where the neutron flux is higher than the component they represent (with leader factor between 1 and 3). These samples will then be extracted and characterized periodically over the 40 year life contemplated in the design.

The components will be considered not replaced during the life of the reactor are: the Reflector Vessel Tank (RVT) and the Could Neutron Source Vacuum Container (CNSVC).Figure 2.

2. Components and materials

According to the information presently available, materials that will be included in the SP are "Zircaloy-4", in order to monitor the RVT, and "Zr-2.5% Nb" to monitor the CNSVC. For these alloys there is little information available on the effect of radiation at low temperature, between 40C and 60C.

The specimens chosen for the tensile tests are miniature specimens, with a minimum dimension of 30 x 8 x 2 mm, of the "dog bonne" type because they are the simplest and can be made small without seriously affecting the validity of the results. Such samples provide information on variations in the ductility and the yield stress of the material (hardening).

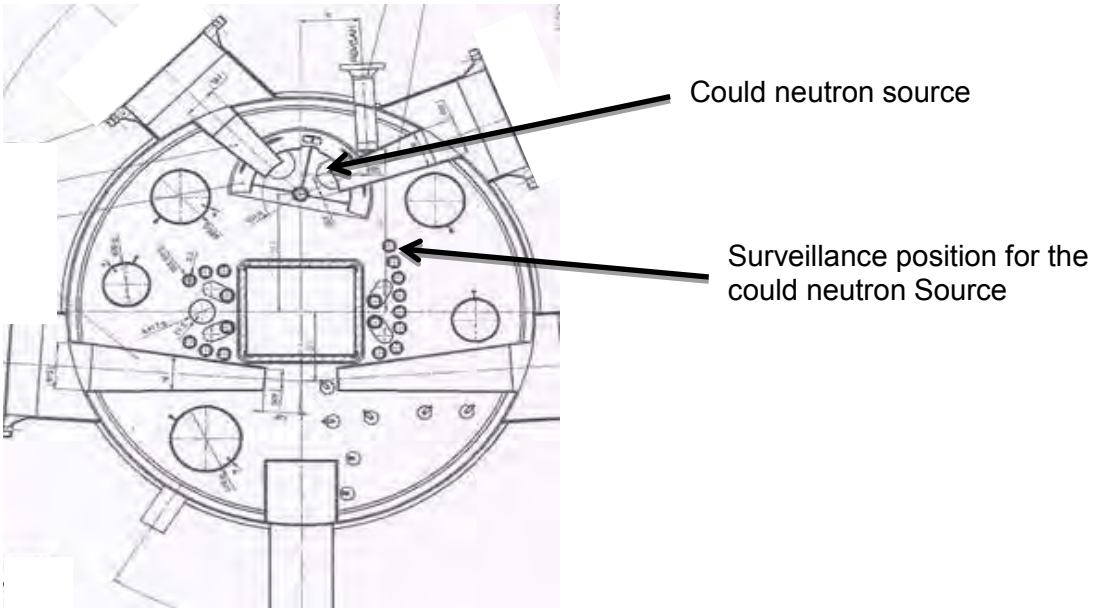

Fig 2. Reflector tank.

For the analysis of the fracture properties of the material CT (Compact Tension) dimensions to ensure the validity of results, respecting the existing rules at the time (ASTM standards). These specimens will be with pretension to analyze the effect of the incorporation of hydrogen and radiation a low temperature for the Zircaloy-4.

To evaluate the hardening and loss of ductility Small Punching Disks were used, with a minimum dimension of 10 mm diameter and 0.5 mm thick.

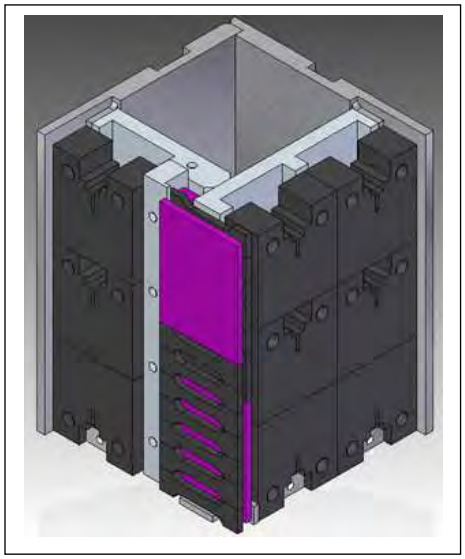

Fig.3. Coupon books for the Zircaloy-4 samples. [9]

In conclusion materials and samples must be taken into account in the design of the coupon books for the Zircaloy-4 samples (Figure 3) and also the necessary conditions, monitoring and cooling: Zircaloy-4 Base Material, welded material and heat affected zone, depending on the welding process. Another coupon book which is in the design stage will be used for Zr-2.5%Nb Base Material, welded material and heat affected zone, depending on the welding process.

2.1. Location samples

According to the distribution of fast neutron flux calculated, see Figure 4a, 4b and 4c, and due to the variation thereof with the radius and angle is required to determine more precisely that the faces of the box containers with the samples were placed.

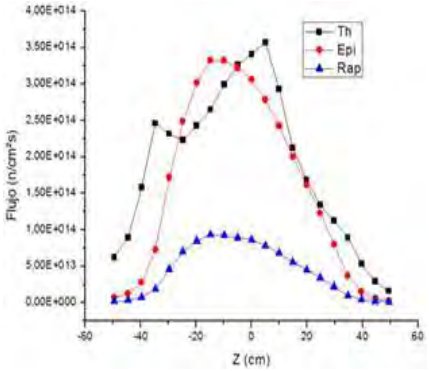

Fig. 4a. Flux at position A.[10]

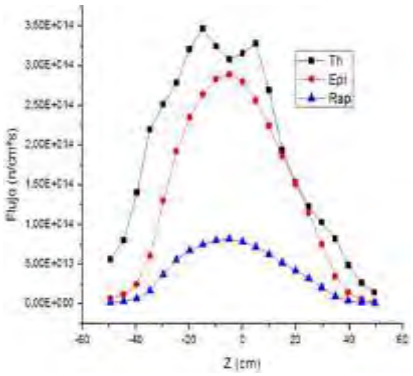

Fig. 4b. Flux at position B.[10]

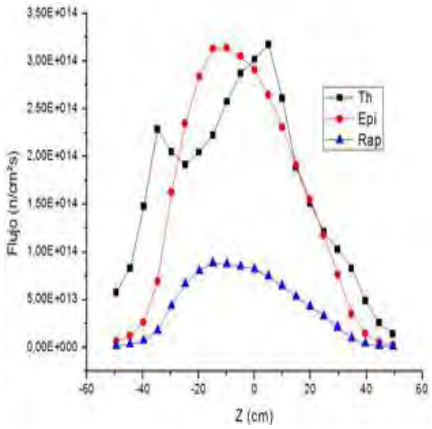

Fig. 4c. Flux at position C. [10]

Figure 5 shows surveillance in positions A, B and C determined in the inner faces, these are de positions for the Zircaloy-4 samples, 2 coupon books for each position, so there will be 6 coupon books in total.

The lifetime of Reactor used six boxes (at 2, 5, 10, 20, 30, and 40). If necessary you can add to get the coupon books 2 and 5 years.
Each coupon have the ability to accommodate the whole package of specimens that requires each instance of SP that is, not specimens with different coupon books for the same stage of tests will be taken.

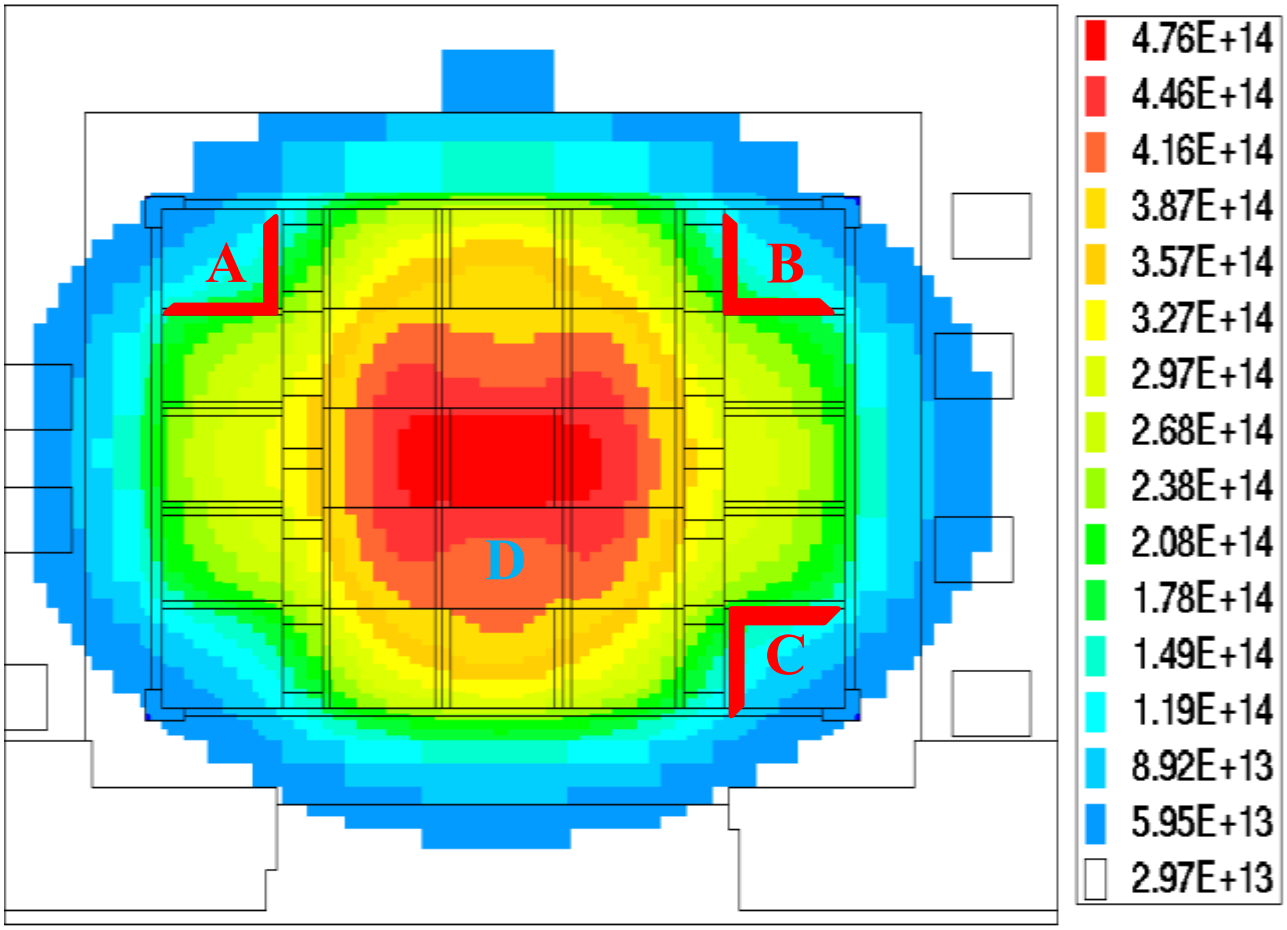

Fig. 5. Neutron flux distribution.

For programme development is of fundamental importance to have material removed during the manufacturing process of the components.
To monitor the zirconium alloy Zr-2.5 Nb, corresponding to the CNSVC, the surveillance position, inside the Reflector Tank, is shown in Figure 2 (ORI 4).

2.2. Additional information

The reactor design life of RA-10 is 40 years, however, it is estimated that a number of components will be replaced before this time. In some cases it is possible to include these components in the SP and the use of materials for the manufacture of test samples. The main components of Zircaloy-4 in this group are the control rods and the control plate structure, to be replaced after 8-10 years of operation, together with the absorber plates. From these materials we can make Charpy and CT samples and obtain additional information.

In addition we designed an experience to place samples in the area of high fast flux, position D, to analyze the effect on Zircaloy-4 at low temperature.

3. Final Remarks

As seen from Figures 4, surveillance positions receive lower flux that the tank wall in the more committed area. The surveillance specimens will receive fast flux of about 7.0E + 13 to 9.2E + 13. While the most compromised area of the tank will receive a fast flux of about 1.9E + 14.

While it does not meet the standards required for the leader factor for the surveillance programme, information that will be obtained will be useful for monitoring the tank. This will be accompanied by details of the experiences that we will be held high flux position.
The surveillance position for the Zr-2.5% Nb will have a lead factor of the order of 1.5 times.
For safe operation, high availability and long term operation is essential to have an ageing management plan of reactor critical System, Structures and Components.

4. References

[1] INTERNATIONAL ATOMIC ENERGY AGENCY, Ageing Management for Research reactors, IAEA Safety standards series N° SSG-10, (2010), 97.

[2] INTERNATIONAL ATOMIC ENERGY AGENCY, Nuclear power plant life management processes: guidelines and practices for heavy water reactors, IAEA-TECDOC-1503, (2006), 215.

[3] INTERNATIONAL ATOMIC ENERGY AGENCY, Safe long term operation on nuclear power plants, Safety reports series N°57, (2008), 194.

[4] INTERNATIONAL ATOMIC ENERGY AGENCY, Ageing management for nuclear power plants, Safety Guide, N° NS-G-2.12 (2009), 93.

[5] INTERNATIONAL ATOMIC ENERGY AGENCY, Proactive management of ageing for nuclear power plant, Safety reports series N°62, (2010), 254.

[6] INTERNATIONAL ATOMIC ENERGY AGENCY, Maintenance, periodic testing and inspection of research reactors, IAEA Safety standards series N° NS-G-4.2, (2006),143.

[7] INTERNATIONAL ATOMIC ENERGY AGENCY, Optimization of research reactor availability and reliability: recommended practices, IAEA Nuclear energy series N° NP-T-5.4, (2008), 98.

[8] INTERNATIONAL ATOMIC ENERGY AGENCY, Safety in the utilization and modification of research reactors, IAEA Safety standards series N° SSG-24, (2012), 167.

[9] CNEA-MEM--47/RA-10/0120-2-035-0

[10] CNEA- DBD-44/RA-10/7700-*2-001* Rev.: 1

QUALITY ASSURANCE AND QUALIFICATION OF NEW I&C SYSTEM AFTER REFURBISHMENT OF THE LVR-15 REACTOR

ING. JIŘÍ MATOUŠEK
I&C, dataPartner s.r.o
Senovážné nám. 241/15, 37001 České Budějovice-Czech Republic

ING. MIROSLAVA KOCHOVÁ
Project management, dataPartner s.r.o
Senovážné nám. 241/15, 37001 České Budějovice-Czech Republic

One or more instrumentation and control system (I&C) refurbishment can be expected over the research reactor lifespan due to obsolescence, ageing, reactor reconstruction, improvement of safety, maintainability or reliability issues. Nowadays obsolete analogue safety related systems are replaced by computer based systems which necessarily brings new approach to quality assurance, mainly in the SW area.

To get the approval from local regulatory body the new safety related system must demonstrate that it does not jeopardise reactor safety and all safety standards set by legislation and IAEA Safety of Research reactors – Safety Requierements document (IAEA SSS No. NS-R-4, Vienna 2005) are met.

Credibility of the whole process can be demonstrated by implementation of the quality assurance system as a part of wider extensive measures for all the activities related to systems refurbishment. The basic principle is: fault avoidance through good engineering (architecture, systems.

All the suppliers must demonstrate a safety culture system and quality assurance policy implementation. Especially for safety SW the suppliers must have qualification routines for SW based safety related systems implemented and detailed quality assurance document for managing safety related software projects (e.g. according to IEC 60880, IEC 62138) prepared. All the processes must be properly planned, proceeded, verified, approved and audited.

Functions, components and systems of the I&C must be classified based on the significance for nuclear facility safety. (IEC 61226, IEC 61513). Specific quality assurance system is applied on individual components to ensure the quality meets the classification standards during the whole project life cycle.

All the suppliers must demonstrate a safety culture system and overal quality assurance policy document , which specifies the desired quality level, resources (especially project team qualification must be taken into account), organization and management measures (coordination, communication, responsibility specification, independent 3rd person verification, auditing the proces by the customer and regulatiry body and it’s documentation.

Poster fuel cycle

A cladding thickness measurement of research reactor fuel plate using nondestructive testing method

Y.S. Lee, S.J. Park, W.J. So, Y.S. Joo

Korea Atomic Energy Research Institute, 989-111 Daedeokdaero, Yuseong, Daejeon 305-353, Republic of Korea

ABSTRACT

During fabrication of a high density fuel plate such as U-Mo dispersion fuel, quality control is very important to secure the integrity of fuel elements. To check the integrity of the fuel elements, nondestructive testing methods such as x-ray radiography, eddy current testing, and ultrasonic testing methods are applied. In KAERI, we have been developing NDT methods to check the cladding thickness and interface of the fuel plate. This paper introduces ultrasonic testing methods for the cladding thickness of the fuel plate.

We are applied an C-scan immersion ultrasonic inspection using pulse-echo technique, and the high frequency (50 MHz and 110 MHz) focus-type immersion transducers were used to measure the cladding thickness and inspect the interface between cladding and U-Mo fuel. The inspection results are checked with C-Scan images and measured the time-of-flight between the reflected signal from the fuel surface and the reflected signal from the fuel meat surface.

The results showed that the ultrasonic C-Scan inspection methods using the 50 MHz transducer and 110 MHz transducer were able to measure the fuel cladding thickness, but the inspection resolution of the 110 MHz transducer was better than that of the 50 MHz transducer because it clearly differentiated the surface signal and fuel meat signal.

STATUS UPDATE ON MINI-PLATE EXPERIMENT DESIGNS PLANNED FOR IRRADIATION IN THE ADVANCED TEST REACTOR

I. GLAGOLENKO, N. WOOLSTENHULME, M. LILLO, J. NIELSEN, D. CHOE, J. NAVARRO, C. JENSEN, D. CRAWFORD, W. JONES, S. SNOW, B. HAWKES, J. WIEST, D. KEISER JR., K. HOLDAWAY, J. SCHULTHESS, AND B. RABIN

Idaho National Laboratory,
P.O. Box 1625
Idaho Falls, ID, 83415 USA

ABSTRACT

Several mini-plate-scale fuel tests are being planned for irradiation in the Advanced Test Reactor in support of low-enriched uranium fuel development for conversion of research reactors. Three of the tests that are supported by the Office of Materials Management and Minimization, U.S. Department of Energy National Nuclear Security Administration, are currently in design phase. The first test, European Mini-Plate Irradiation Experiment (EMPIRE), is focused on developing better understanding of the factors limiting performance of the U-7Mo-based dispersion fuel, which is the prime candidate for conversion of several European research reactors (i.e., members of the HERACLES Consortium).
The other tests, Mini-Plate-1 (MP-1) and Mini-Plate-2 (MP-2), are part of the U-10Mo monolithic fuel development for conversion of U.S. research reactors. MP-1 is focused on evaluating performance of the U-10Mo monolithic fuels manufactured using different fabrication methods and MP-2 is the follow-up qualification test of the monolithic fuel downselected at the conclusion of the MP-1 test. Key design aspects of the three mini-plate irradiation tests will be discussed in this paper.

1. Introduction

Since the late 1970s, the United States, in collaboration with many countries around the world, has being working on conversion of civilian research and test reactors from highly enriched uranium to low-enriched uranium. Despite the fact that a significant number of these reactors have already been converted or decommissioned, currently, 74 reactors still remain that operate or plan to operate with highly enriched uranium fuel. For this reason, reactor conversion efforts continue to be at the forefront of the work performed by the U.S. Department of Energy National Nuclear Security Administration's Office of Material Management and Minimization. Current domestic efforts are focused on conversion of the last eight reactors in the United States, including the following five high-performance research reactors (HPRRs): Massachusetts Institute of Technology Reactor, Missouri University Research Reactor, National Bureau of Standards Reactor, High-Flux Isotope Reactor, and the Advanced Test Reactor. Conversion of these remaining reactors is challenged by the need to develop and qualify new high-density uranium fuel.
In parallel to domestic efforts, the Office of Material Management and Minimization is also engaged in collaboration with the HERACLES Consortium of the European Partners [1], regarding development and qualification of high-density uranium fuel for conversion of European HPRRs, including BR2 (Belgium), FRM 2 (Germany) and RHF and JHR (France).
The primary fuel candidates selected for conversion of HPRRs by the United States and European sides are U-10Mo monolithic and U-7Mo dispersion fuels, respectively (see Figure 1). The one exception on the European side is the German reactor FRM 2, which is also considering monolithic fuel for its conversion.

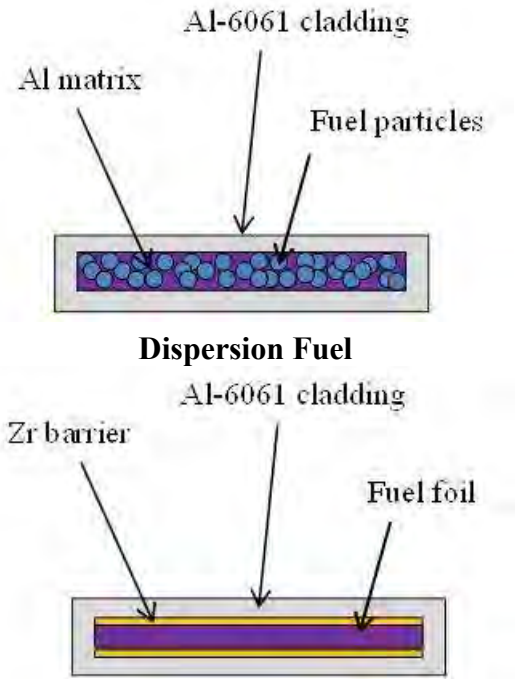

Figure 1. Schematic cross-sections of dispersion and monolithic fuels.

Development of both types of U-Mo fuels has proven to be difficult, because both the European and U.S. programs have experienced technical setbacks. On the monolithic side (i.e., United States), problems were revealed during the first attempt at full-scale fuel fabrication. Challenges with meeting fuel specifications, poor yield, high cost, and generation of U-Mo/Zr waste potentially leading to inadequate uranium resource utilization were identified as the primary areas of concern. This led to questioning the commercial viability of the existing manufacturing process, which prompted the U.S. HPRR program to reevaluate its priorities and invest significant resources into improvement of the fuel fabrication process to make it commercially viable. A subsequent irradiation testing program is planned for validating adequate fuel performance and eventually qualifying monolithic fuel.

On the dispersion side (i.e., European), fuel developers have been struggling with inadequate fuel performance at high power and high burnup conditions. Specifically, fuel plates have experienced high levels of swelling and, in some cases, plate pillowing was observed at high power/high burnup locations [2]. Several attempts were made in the past to improve fuel performance; however, it remains unclear whether U-7Mo dispersion fuel can survive the most challenging reactor operations conditions. To develop better understanding of dispersion fuel irradiation behavior and to establish factors limiting its performance, the HERACLES Consortium of European Partners launched the so-called comprehension phase within the European HPRR Fuel Development Program. During this phase, a more systematic approach has been implemented for evaluating the performance of previously irradiated fuels and for conducting special irradiation experiments that are focused on studying the effects from separate variables and establishing the true root-cause of inadequate fuel behavior.

As part of these ongoing fuel development efforts for conversion of civilian research and test reactors in the United States and Europe, three mini-plate size experiments are currently being designed at the Idaho National Laboratory for irradiation in the Advanced Test Reactor. The first test that is planned to be inserted is EMPIRE, followed by the MP-1 and MP-2 tests, respectively.

2. EMPIRE

The EMPIRE mini-plate experiment is part of the comprehension phase of the European Fuel Development Program. The purpose of this test is to prove or disprove the main hypotheses postulated by fuel development experts as potential root causes for the inadequate performance behavior of U-7Mo dispersion fuel. In addition, the test will help fill the existing gaps in understanding fuel behavior (i.e., add to comprehension) by systematically studying the effects of different parameters on fuel performance. Finally, this test will generate the first set of fuel performance data for a small number of monolithic plates with a zirconium diffusion barrier bonded by proprietary C2TWP (i.e., CERCA/CEA/TUM Welding Process). The barrier will be applied by co-rolling and physical vapor deposition techniques. Physical vapor deposition technology was developed by the Technical University of Munich in support of fuel development for conversion of the FRM 2 reactor in Germany.

Currently, two leading hypotheses are responsible for the unstable behavior of dispersion fuel. The first one, based on an interaction layer formation between U-7Mo particles and the Al matrix, is the original hypothesis proposed at the onset of problems experienced with this type of fuel at moderate irradiation conditions early in the testing program. The initial attempts to address this problem were focused on suppressing formation of the interaction layer through the silicon addition to the matrix. While fuel performance was slightly improved, the problem was not resolved completely because the plates still experienced high swelling and pillowing at high-power/high burnup tests.

This led to another more recently proposed solution that was centered on eliminating the interaction layer by coating fuel particles with about 1 to 2 microns of a ZrN diffusion barrier. It is believed that the ZrN coating should be more effective in preventing interaction between the Al matrix and U-Mo fuel when compared to the addition of silicon to the matrix. In fact, one of the primary goals of the EMPIRE test is to answer the question whether or not ZrN coating alone is sufficient in overcoming problems with fuel performance at high-power/high burnup conditions.

The second hypothesis, presented recently, is based on observation of the recrystallization process that occurs in dispersion fuels at intermediate burnup [3] and the suggested link between recrystallization and an increased level of swelling. The solution proposed for this issue is based on an attempt to delay the onset of recrystallization and high swelling by modifying the initial microstructure of the fuel through heat treatment. Because of the heat treatment, the U-7Mo alloy will become more homogeneous (i.e., decreasing the areas with low molybdenum content) and will have larger size grains. To study the effects that delaying fuel recrystallization and larger grain size have on fuel performance, both heat-treated and non-heat-treated fuel particles will be irradiated in EMPIRE.

The other aspects (i.e., remaining gaps) to be investigated in the EMPIRE experiment will include the following:

- *Effects of fission rate on fuel performance*
  - Fission rate, which is coupled with temperature, affects diffusion of the constituents
- *The influence of ZrN coating microstructure on the effectiveness of the coating in improving fuel performance*
  - A different coating microstructure is achieved through two different coating application methods: (1) atomic layer and (2) physical vapor deposition
- *Comparison of the effectiveness of the two coatings* (i.e., ZrN and ZrN/AlN) *in improving fuel performanc*e
  - The AlN layer is added to suppress diffusion of Al from the matrix to the fuel
- *Effects of fuel particle size distribution (i.e., standard and modified) on fuel performance*
- *Comparison of fuel performance between U-7Mo and U-10Mo*
  - U-Mo phases with high-Mo content show decreased swelling
- *Effects of the U-7Mo powder source on fuel performance*

- The Korean Atomic Energy Research Institute and AREVA-made powders will be compared.

Testing of the hypotheses and investigation of the variables will be accomplished using mini-plate size fuel samples (W × L × T = 2.54 × 10.16 × 0.127 cm). The size of the fuel meat zone in dispersion and monolithic fuel plates will be 1.91 × 8.26 × 0.051 cm and 1.91 × 8.26 × 0.033 cm, respectively. All dispersion fuel plates will be encapsulated in AG3NE and monolithic in AlFeNi European aluminum claddings. A total of 48 specimens are planned for irradiation. To study effects of fission rate and burnup on fuel performance, the mini-plates will be irradiated at several levels of plate power and to different levels of burnup. A number of the key specimens will be taken to the limiting operating conditions representative of the driver fuel in the BR 2 reactor: about 470-W/cm^2 peak heat flux, about 80 at.% max U-235 depletion, about 123°C plate surface temperature. These key high-power/high-burnup specimens will help answer the most critical questions regarding fuel performance and help prove or disprove postulated hypotheses.

3. MP-1

The MP-1 experiment is the first in a series of irradiation tests under the U.S. HPRR Fuel Development Program that is focused on evaluating performance of monolithic fuels manufactured using different fabrication processes.

Significant efforts in recent years were dedicated to improvement of the monolithic fuel manufacturing process. They were centered on increasing product yield, improving uranium-resource utilization, reducing cost, and making the process commercially viable. The main emphasis was placed on optimization of manufacturing steps in the existing baseline fabrication process with a co-rolled zirconium diffusion barrier, which evolved from the process developed by Idaho National Laboratory and upon demonstration of promising alternative fabrication methods. The latter mainly involve different zirconium barrier application techniques, namely plasma spraying and electroplating.

Testing of the optimized, baseline, co-rolled zirconium process and alternative plasma spray and electroplating technologies will be accomplished using mini-plate-sized fuel samples (i.e., 2.54 × 10.16 × 0.124 cm). To evaluate the effects associated with foil thickness on fuel performance, two limiting (i.e., thin and thick) U-10Mo foil geometries (i.e., 1.91 × 8.26 × 0.022 and 1.91 × 8.26 × 0.064 cm, respectively) will be irradiated. To assess the effects of limiting power and limiting burnup on fuel operation, thin foils will be tested at two target irradiation conditions: (1) medium (about 17.6 kW/cm^3) plate power to high burnup (7.6 × 10^{21} fiss/ cm^3) and (2) high (about 42.8 kW/ cm^3) power and medium (i.e., 5.5 × 10^{21} fiss/ cm^3) burnup.

Thick foils will be irradiated at low power (i.e., 7.7 kW/ cm^3) to low burnup (i.e., 4.0 × 10^{21} fiss/ cm^3). These target irradiation conditions were selected based on the limiting operating conditions of the plates (with similar fuel foil thickness) in fuel elements of the five U.S. research reactors. To achieve good statistical confidence, each sample type will have several replicates tested at each particular irradiation condition. Overall, 120 fuel specimens will be irradiated in MP-1.

Upon completion of the MP-1 test, performance of the plates manufactured using different fabrication processes will be assessed; one process will be selected for more extensive irradiation testing and qualification.

4. MP-2

The MP-2 experiment supports fuel qualification for the following three Nuclear Regulatory Commission-regulated reactors: the Massachusetts Institute of Technology Reactor, Missouri University Research Reactor, and National Bureau of Standards Reactor. The main purpose of the experiment is to demonstrate, with a high level of statistical confidence, the acceptable irradiation performance of selected fuel (and an associated fabrication process) under the range of operating conditions (i.e., fission rate and burnup) representative of these reactors. In addition, data obtained from test specimens will be used to establish appropriate fuel

performance correlations as a function of operating conditions for use in fuel qualification process and during reactor licensing and operations.

Similar to MP-1, testing will be accomplished using 2.54 × 10.16 × 0.124 cm mini-plate specimens with two limiting (i.e., thin and thick) foil geometries (i.e., 1.91 × 8.26 × 0.022 and 1.91 × 8.26 × 0.064 cm, respectively). However, the MP-2 test will also evaluate performance of the thinnest plates (i.e., 2.54 × 10.16 × 0.111 cm) with a thin foil (i.e., 1.91 × 8.26 × 0.022 cm) and thin cladding combination. Each unique plate geometry in MP-2 will be tested at several levels of fission rate and two different levels of burnup (i.e., up to the limiting) to cover the operational envelope of the reactor plate with representative geometry. The limiting operating conditions for fuel with thick foil are 8.3-kW/ cm^3 power and 3.6 × 10^{21}-fiss/ cm^3 burnup; for thin fuel with thicker cladding about 14.7-kW/ cm^3 and 7.2 × 10^{21}-fiss/ cm^3 burnup; and for thin fuel with thinner cladding about 17.3-kW/ cm^3 and 3.4 × 10^{21}-fiss/ cm^3 burnup, respectively. The goal of the experiment is to meet and exceed these conditions with some reasonable margin.

5. Hardware

All experiments will be executed using similar hardware. Two rows of fuel mini-plates will be inserted into the aluminum test capsule (Figure 2). One row of plates can contain up to four mini-plates. Up to four capsules of plates can be stacked vertically in the test train. The entire test train will be loaded in the test position in the Advanced Test Reactor (Figure 3). Depending on the experiment, large B, small I, or flux trap (i.e., south or east) positions will be utilized. Flux trap positions in the Advanced Test Reactor, because of the larger diameter, allow for up to two test trains of mini-plates inserted in the same position at the same time. All planned experimental configurations were successfully flow tested.

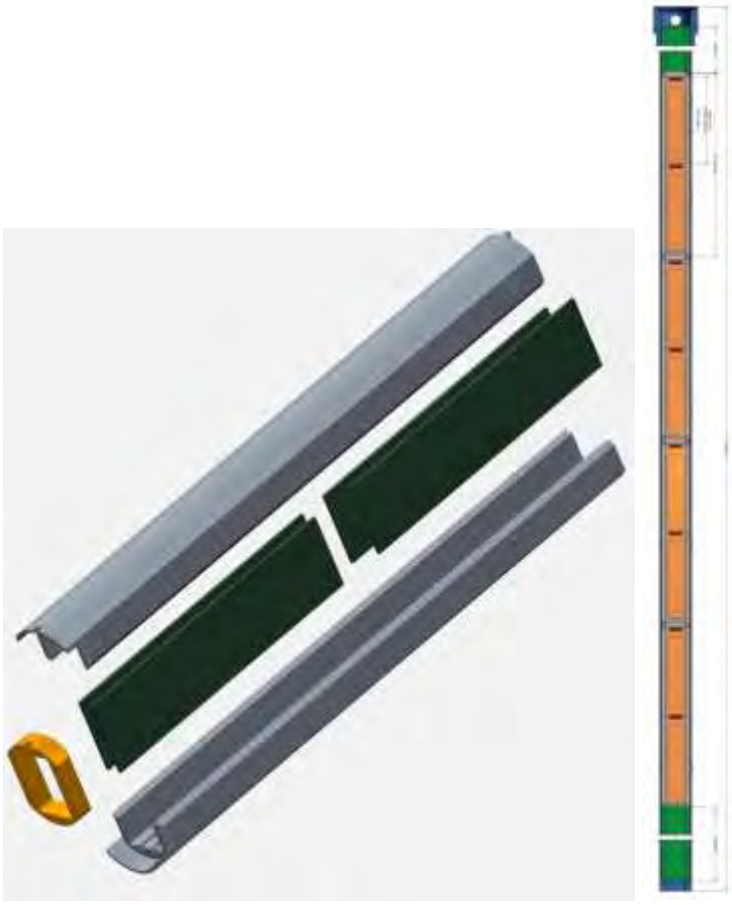

Figure 2. Test capsule assembly with two rows of fuel plates and a test train with four capsules stacked vertically.

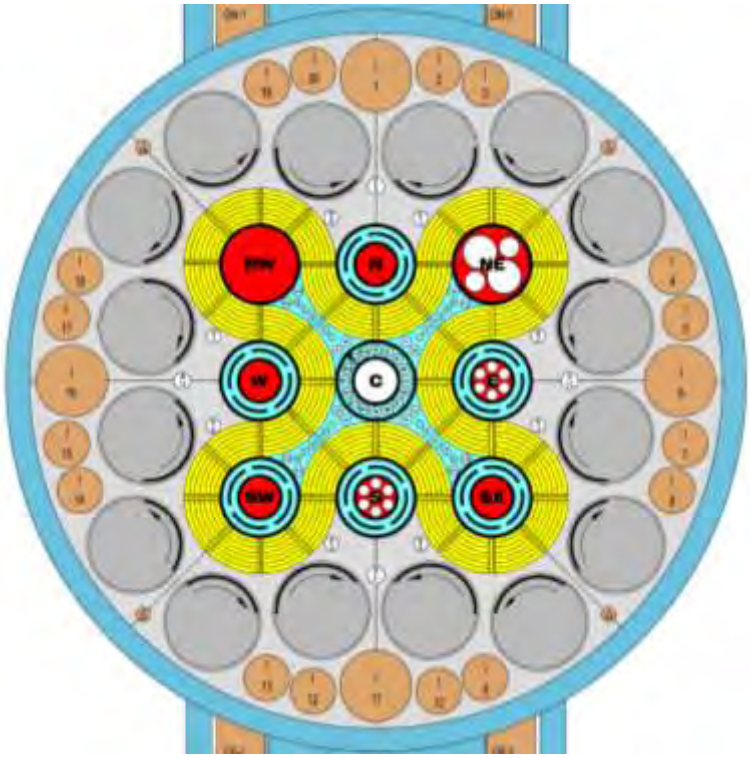

Figure 3. Cross-section of the Advanced Test Reactor core.

6. Disclaimer

Prepared for the U.S. Department of Energy/National Nuclear Security Administration
Office of Material Management and Minimization
Under DOE Idaho Operations Office
Contract DE-AC07-05ID14517

7. References

[1] http://heracles-consortium.eu/.
[2] S. Van Den Berghe and P. Lemoine, 2014, “Review of 15 years of High-Density Low-Enriched UMo Dispersion Fuel Development for Research Reactors in Europe,” *Nuclear Engineering and Technology* 46(2).
[3] A. Leenaers et al., 2015, “Fuel Swelling Interaction Layer Formation in the SELENIUM Si and ZrN Coated U(Mo) Dispersion Fuel Plates Irradiated at High Power in BR2,” *Journal of Nuclear Materials* 458: 380-393.

ION IRRADIATION AND SYNCROTRON MICRODIFFRACTION ANALYSIS OF THE UMO-AL INTERACTION LAYER

L. JAMISON, K. MO, B. YE, Y. MIAO, A. YACOUT
Nuclear Engineering Division, Argonne National Laboratory
9700 South Cass Avenue, Argonne, IL 60439 – United States

S. BHATTACHARYA
Materials Science and Engineering, Northwestern University
633 Clark Street, Evanston, IL 60208 – United States

R. XU
APS X-Ray Science Division, Argonne National Laboratory
9700 South Cass Avenue, Argonne, IL 60439 – United States

ABSTRACT

As part of the ongoing efforts to convert research and test reactors to low-enriched-uranium fuels, uranium-7wt% molybdenum alloy (U7Mo) dispersion fuels have emerged as a strong candidate for use in European high-power research reactors. One of the primary barriers to qualification of this fuel is the formation of an interaction layer between the U7Mo fuel particles and the aluminium matrix. This interaction layer can affect the swelling of the fuel plates, and can cause agglomeration of gaseous fission products into large bubbles, leading to eventual failure of the plate. Detailed understanding of the behaviour of the dispersion fuel, and the interaction layer, is necessary for fuel qualification. Experiments conducted in-pile on fuel plates are costly, time-consuming, and result in activated fuel samples, limiting the characterization that can be conducted. Instead, this study utilizes heavy-ion irradiation to induce damage in U7Mo dispersion fuel samples. 80MeV Xe ions (typical fission product and energy) were implanted into the samples at the Argonne Tandem Linac Accelerator System (ATLAS) facility at Argonne National Laboratory. Detailed characterization of the interaction layer by high-energy x-ray microdiffraction was conducted at Argonne's Advanced Photon Source (APS). This APS technique utilized a beam size of only 0.5μm x 0.5μm, enabling phase information to be determined on a much smaller scale than previously done. Upon examination of the interaction layer that formed during the heavy-ion irradiation it was determined that it is crystalline in nature, opposite to what is found during in-pile tests. It was hypothesized that this disagreement could be caused, at least in part, by the temperature difference between in-pile irradiations (~150°C) and the heavy-ion irradiation (~300°C). In order to test this hypothesis, an in-situ 1 MeV Kr ion irradiation was conducted at the Intermediate Voltage Electron Microscopy (IVEM) - Tandem facility at Argonne on a TEM foil fabricated from the interaction layer. Amorphization of the interaction layer under these conditions indicates that the irradiation temperature plays a strong role in the determination of the crystalline nature of the interaction layer in U7Mo-Al dispersion fuels. The results of both the APS microdiffraction and the IVEM-Tandem in-situ irradiation study will be discussed.

1. Introduction

Interaction layer formation in U-Mo dispersion fuel plates can negatively affect the performance of the fuel through providing the environment for swelling through gaseous fission product accumulation, leading to eventual failure of those plates. In order to study the

formation of the interaction layer, an experiment was conducted at the ATLAS facility at Argonne National Laboratory that irradiated a range of dispersion fuel samples to several doses[1]. 80MeV Xe ions were utilized to impart damage on the samples, as this is a typical fission fragment energy, where both displacement damage and gas bubble morphology can be studied with the same ion. After irradiation a selection of samples were examined with high-energy x-rays at APS, and two focused-ion-beam (FIB) prepared interaction layer samples were further irradiated at the IVEM-Tandem facility.

2. High-Energy X-ray Diffraction Analysis

Synchrotron microdiffraction was conducted at sector 34-ID-E at APS at Argonne National Laboratory. The sample for this experiment was a needle approximately 10μm × 10μm and 20μm long, fabricated with a FIB. The sample was attached to a tungsten Omniprobe tip, held in a double-walled Kapton tube. The high-energy white x-ray beam was focused down to ~0.5μm × 0.5μm beam size, which was scanned along the sample to collect phase information in a 2D array. A diffraction pattern was collected at each point in the array, an example of which is shown in Figure 1. This diffraction pattern contains a mixture of the interaction layer phase (UAl_3), α-UMo, and ɣ-UMo.

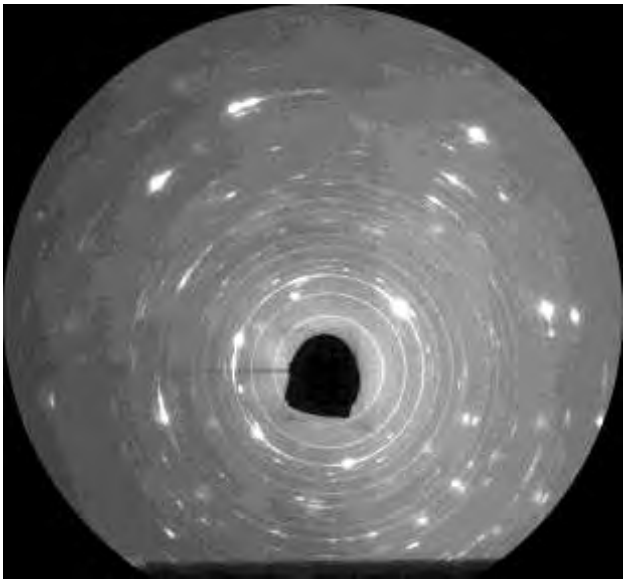

Fig 1. Example microdiffraction result from a location in the sample containing a combination of interaction layer, α-UMo, and ɣ-UMo.

In order to extract phase information from the diffraction patterns, circular integration was conducted to produce d-spacing versus intensity plots. A series of these patterns are shown in figure 2. An analysis of the integrated intensities reveals that the sample is primarily composed of UAl_3 at the surface, with an increasing amount of UMo along the ion penetration direction. The UMo is composed of a mixture of α- and ɣ- UMo, primarily ɣ-UMo near the surface and an increasing amount of α-UMo with depth into the sample. From this data, the interaction layer is observed to be entirely composed of crystalline UAl_3, consistent with another ion irradiation study of dispersion fuels conducted at a similar temperature[2]. Although these findings are in agreement with some ion-irradiation studies, they contradict what is typically observed in-pile, where the interaction layer is found to be amorphous[3, 4]. A substantial difference in experimental conditions between in-pile and this ion irradiation study is the irradiation temperature. In-pile tests typically produce a fuel temperature of approximately 150°C, substantially lower than this ion irradiation study. This temperature difference could be the reason the interaction layer is crystalline in this study, rather than amorphous. This hypothesis is supported by another ion irradiation study that was conducted at 140°C and produced an amorphous interaction layer[5]. In order to determine if the

interaction layer that developed in this experiment would be amorphous if irradiated at a lower temperature, an in-situ ion irradiation study was conducted.

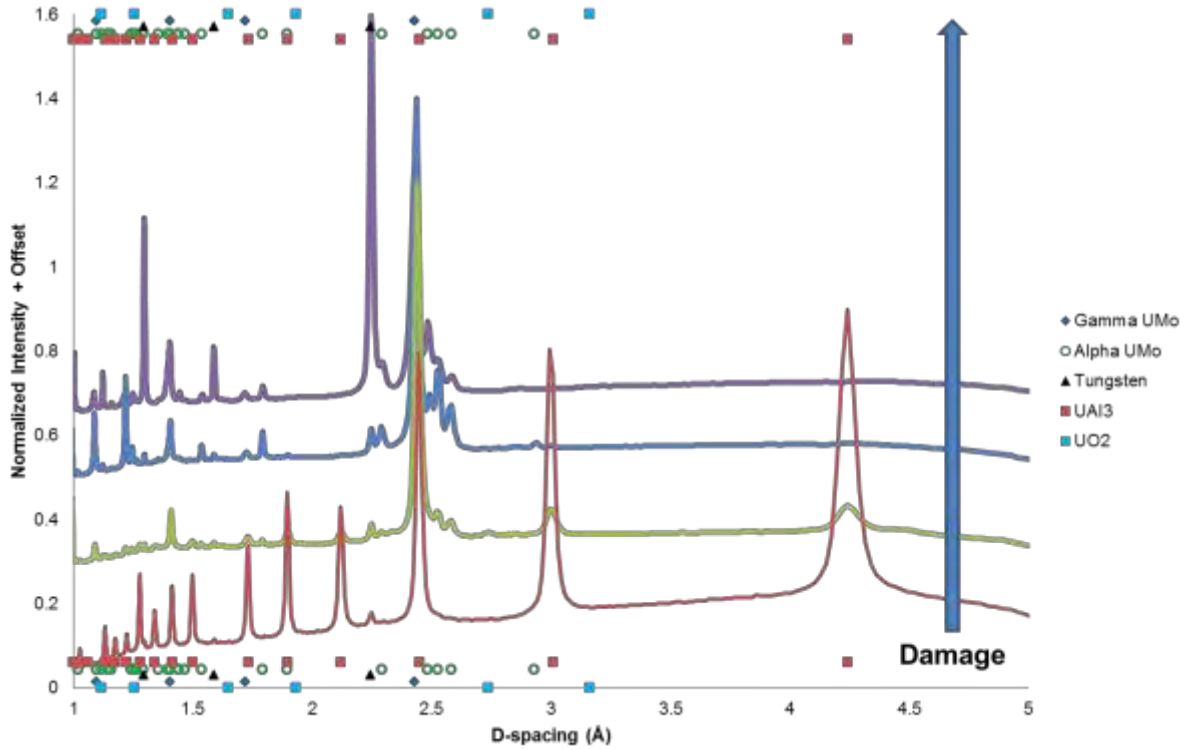

Fig 2. Series of d-spacing vs normalized intensity plots (solid lines), exhibiting the evolution of the patterns from the sample surface (mixture of α- and γ-UMo) along the ion implantation direction into an interaction layer regime (UAl_3). Standard peak locations for the phases present are identified by the markers at the top and bottom of the chart.

3. In-situ Ion Irradiation of the Nanocrystalline Interaction Layer

In-situ ion irradiation was conducted at the IVEM-Tandem facility at Argonne National Laboratory. 1.0MeV Kr ions were selected for imparting damage on the sample, as at this energy the Kr ions will be fully transmitted through the sample. Two TEM foils were prepared by FIB from the interaction layer region of the sample irradiated at ATLAS. They were irradiated at room temperature in an attempt to amorphize the interaction layer at a low dose (the dose to amorphization is a temperature-dependent phenomenon). In order to determine if the interaction layer had amorphized, the electron diffraction pattern of several regions on each sample were tracked throughout the irradiation. When a material is fully crystalline, the electron diffraction pattern consists of sharp spots. These spots evolve into a diffuse ring when the material is fully amorphous, as shown in figure 3.

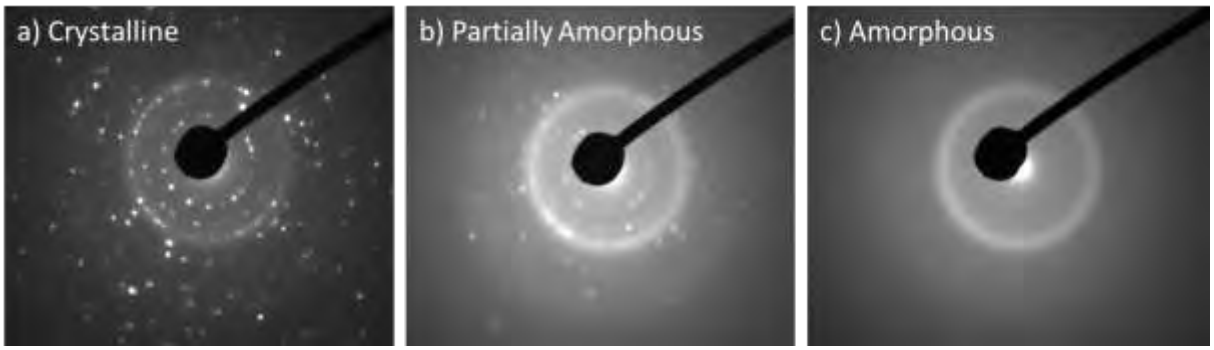

Fig 3. Evolution of the electron diffraction pattern from a) crystalline, to b) partially amorphous, and c) fully amorphous.

Two primary observations were made during the irradiation of the two interaction layer samples. The first was that the sample did amorphize at room temperature, confirming the hypothesis that the irradiation temperature plays a strong role in determining the nature of the interaction layer (crystalline vs amorphous). The second observation was that not all regions of the sample amorphized at the same damage level, including some regions that did not amorphize in the allotted experimental time. A series of diffraction patterns taken from several regions in samples 1 and 2 are shown in Figures 4 and 5, respectively, highlighting the different behaviours within the interaction layer.

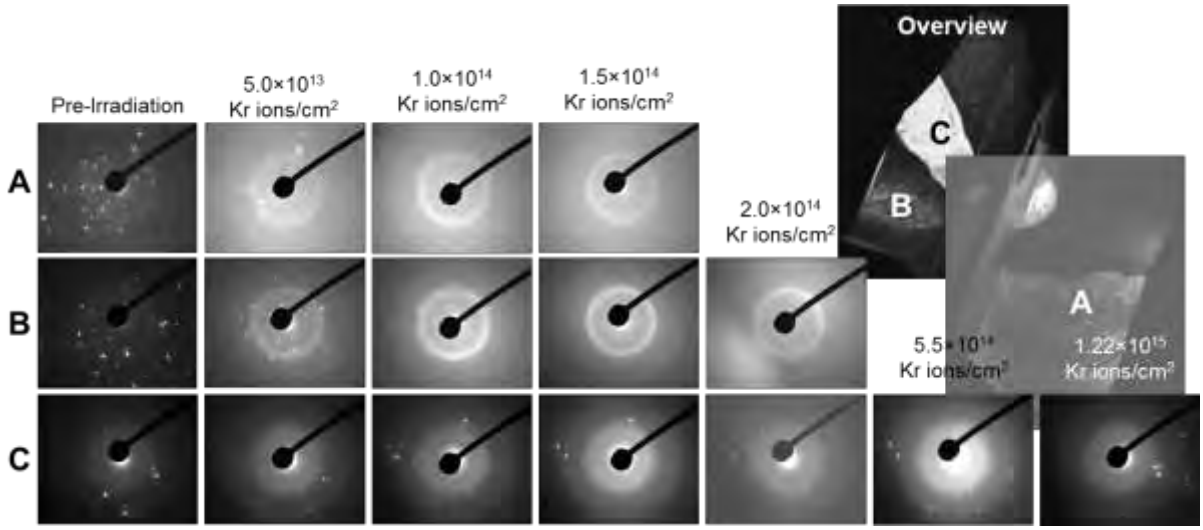

Fig 4. Evolution of the electron diffraction pattern for three regions exemplifying the range of behaviours observed. The locations tracked are marked A-C on the overview compilation image.

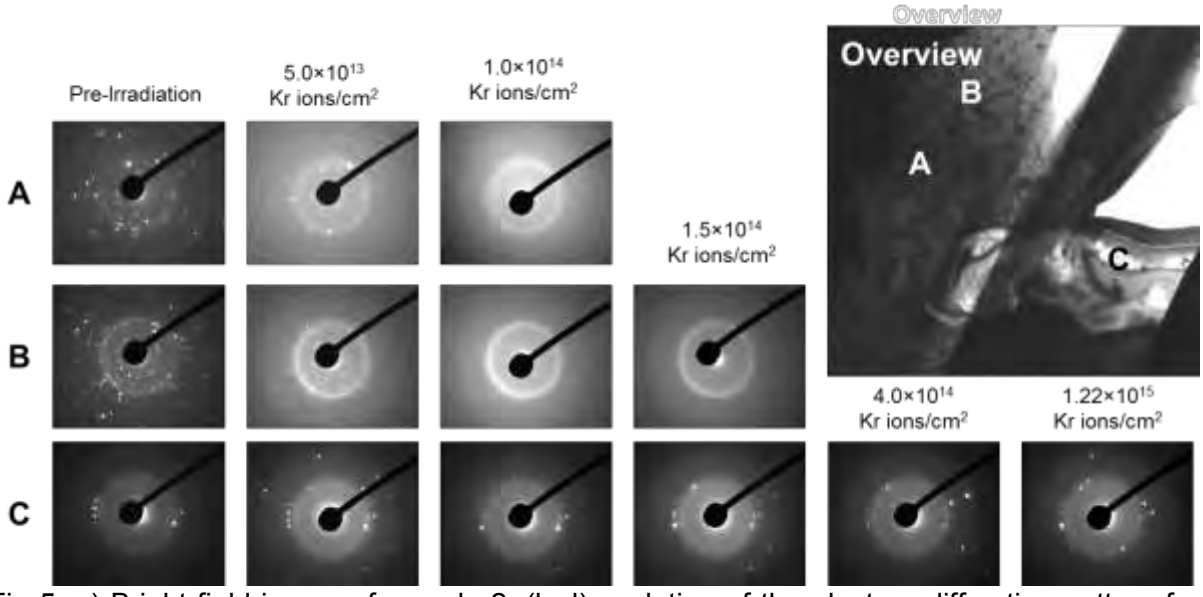

Fig 5. a) Bright field image of sample 2, (b-d) evolution of the electron diffraction pattern for three regions exemplifying the range of behaviours observed. The locations examined are marked A-C on the bright field overview image.

Irradiation studies on a range of U-Mo-Al alloys have previously been conducted, and a wide range of behaviour was observed in these samples[6, 7]. Therefore, it was hypothesized that the difference in behaviour observed in this study is due to the chemical dependence of amorphization of U-Mo-Al alloys. Z-contrast images of these samples were taken in order to compare the relative aluminium content in the regions highlighted in figure 4. These images

are shown in figure 6. In z-contrast imaging, uranium shows up as bright regions, and aluminium-rich regions are dark. By comparing the locations of the regions that amorphized or remained crystalline throughout the experiment, it can be observed that Al-rich regions are more resistant to irradiation.

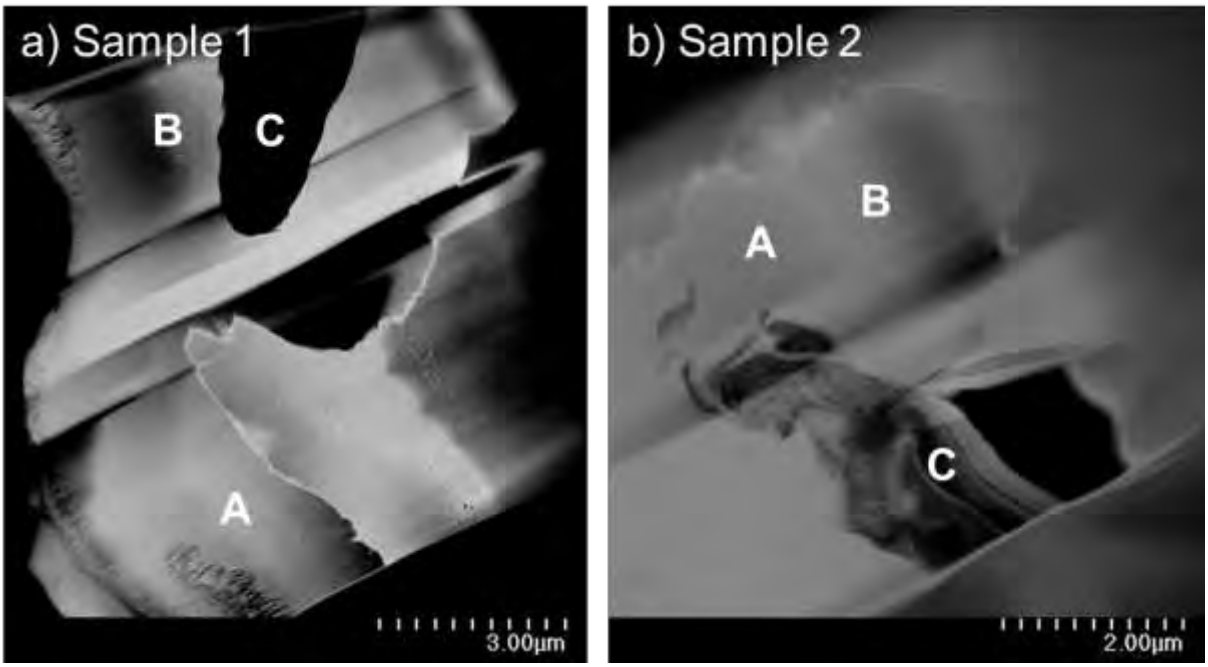

Fig 6. Z-contrast images of a) sample 1 and b) sample 2. Bright regions are uranium-rich and dark regions are aluminium-rich. Regions are designated A, B, or C to correspond to the regions marked in figures 4 and 5.

Conclusions

Interaction layer samples extracted from a UMo dispersion fuel irradiated with 80MeV Xe ions were examined by synchrotron x-ray microdiffraction and further irradiated in an in-situ ion irradiation experiment. It was determined that the interaction layer was composed primarily of crystalline UAl_3. An amorphization study was conducted at IVEM-Tandem at Argonne to determine if this phase would amorphize upon irradiation at a lower temperature, in line with the results of in-pile experiments. This study utilized 1 MeV Kr ions for in-situ irradiation to study amorphization within the sample. It was found that not only does the interaction layer amorphize, but that there is a substantial difference in dose to amorphization within the sample. From a Z-contrast TEM study, it was found that the chemical makeup of the regions within the interaction layer strongly influence the dose to amorphization. Future work will include analysis of the microdiffraction data on strains present in the developed phases, as well as a detailed chemical analysis of the sample to determine if a correlation between the aluminium-to-uranium ratio and the dose to amorphization can be established.

Acknowledgements

This work was sponsored by the U.S. Department of Energy, Office of Material Management and Minimization, National Nuclear Security Administration, under Contract No. DE-AC-02-06CH11357 between UChicago Argonne, LLC and the Department of Energy. This research used the resources of ANL's ATLAS facility and the Advanced Photon Source (operated for the DOE Office of Science by Argonne National Laboratory under Contract No. DE-AC02-06CH11357), U.S Department of Energy (DOE) Office of Science User Facilities. The electron microscopy with in situ ion irradiation was accomplished at Argonne National Laboratory at the IVEM-Tandem Facility, a U.S. Department of Energy Facility funded by the DOE Office of Nuclear Energy, operated under Contract No. DE-AC02-06CH11357 by UChicago Argonne, LLC.This work made use of the EPIC facility (NU*ANCE* Center-

Northwestern University), which has received support from the MRSEC program (NSF DMR-1121262) at the Materials Research Center; the Nanoscale Science and Engineering Center (NSF EEC-0647560) at the International Institute for Nanotechnology; and the State of Illinois, through the International Institute for Nanotechnology.

References

1. Ye, B., Bhattacharya, S., Mo, K., Yun, D., Mohamed, W., Pellin, M., Fortner, J., Kim, Y.S., Hofman, G.L., Yacout, A.M., et al. (2015). Irradiation behavior study of U–Mo/Al dispersion fuel with high energy Xe. Journal of Nuclear Materials *464*, 236-244.
2. Palancher, H., Wieschalla, N., Martin, P., Tucoulou, R., Sabathier, C., Petry, W., Berar, J.F., Valot, C., and Dubois, S. (2009). Uranium–molybdenum nuclear fuel plates behaviour under heavy ion irradiation: An X-ray diffraction analysis. Journal of Nuclear Materials *385*, 449-455.
3. Gan, J., Miller, B., Keiser Jr., D., Robinson, A., Madden, J., Medvedev, P., and Wachs, D. (2014). TEM characterization of high burn-up microstructure of U-7Mo alloy. In European Research Reactor Conference, Volume 1. (Ljubljana, Slovenia: European Nuclear Society), pp. 109-117.
4. Gan, J., Keiser Jr, D.D., Wachs, D.M., Robinson, A.B., Miller, B.D., and Allen, T.R. (2010). Transmission electron microscopy characterization of irradiated U–7Mo/Al–2Si dispersion fuel. Journal of Nuclear Materials *396*, 234-239.
5. Chiang, H.Y., Zweifel, T., Palancher, H., Bonnin, A., Beck, L., Weiser, P., Döblinger, M., Sabathier, C., Jungwirth, R., and Petry, W. (2013). Evidence of amorphous interdiffusion layer in heavy ion irradiated U–8wt%Mo/Al interfaces. Journal of Nuclear Materials *440*, 117-123.
6. Gan, J., Keiser, D.D., Miller, B.D., Kirk, M.A., Rest, J., Allen, T.R., and Wachs, D.M. (2010). Kr ion irradiation study of the depleted-uranium alloys. Journal of Nuclear Materials *407*, 48-54.
7. Gan, J., Keiser Jr, D.D., Miller, B.D., Wachs, D.M., Allen, T.R., Kirk, M., and Rest, J. (2011). Microstructure of RERTR DU-alloys irradiated with krypton ions up to 100 dpa. Journal of Nuclear Materials *411*, 174-180.

OPTIMIZATION OF A THIN U-10MO FUEL PLATE CASTING BY MODELING AND EXPERIMENT

R. M. AIKIN JR. AND D. DOMBROWSKI
Materials Science and Technology: Metallurgy, Los Alamos National Laboratory
P.O. Box 1663, Los Alamos, NM 87544

ABSTRACT

LEU U-10%Mo fuel fabrication begins with a molten metal casting process which is feedstock for fuel foil fabrication by rolling. This work describes the experiments and modeling that have been performed to optimize the casting of long thin (28 cm x 20 cm x 0.5 cm) plates of U-10%Mo using vacuum induction melting (VIM). Three casting trials where used to evaluate a preliminary design and two revised designs. The mold and casting cavity were instrumented with a number of thermocouples to determine the thermal history of the mold and casting. The resulting cast plates were analyzed for filling and solidification defects using radiography. The goal was to develop a refined mold design and casting process parameters that maximized casting yield and minimized casting defects such as porosity and Mo segregation.

1. Introduction

The production of low enriched U-10wt%Mo fuel begins by the vacuum induction melting (VIM) and casting of a rolling billet. Production options include i) casting a thicker (~2 to 3 cm) billet and then hot rolling to an intermediate thickness (0.3 cm), or ii) casting intermediate thickness billets directly. The trade off is between additional processing (rolling) versus the difficulty of casting a thin part. The mold design, casting, and process optimization of a thicker billet has previously been reported [1]. This work examines the second option with the simultaneous casting of three thin 28 cm by 20 cm by 0.5 cm billets.

2. Initial Mold Design and Casting

2.1 Casting Procedure

The initial mold design and process parameters were supplied by Y-12 [2]. This design to simultaneously cast 3 thin billets is shown in Fig. 1. The mold stack is comprised of 7 parts: a bottom and top clamp, the 4 parts of the book mold body, and a crucible on top. The 4 parts of the book mold are held together by the top and bottom mold clamps. The clamps also serve as a heat source on top and a chill on the bottom. The mold forms 3 cavities that are 28.4 cm tall by 20.3 cm wide by 0.5 cm thick. A standard 35 cm OD by 30 cm ID by 14 cm tall bottom pour crucible is used. When cast at Y-12, this crucible would be used with a knockout/rupture disk, but because of furnace differences, a stopper rod with 1.52 cm diameter pour hole was used in this study.

The mold was machined from HLM grade graphite [3]. HLM is a medium-grain extruded graphite commonly used for molds and crucibles for the casting of uranium. To prevent chemical reaction between molten uranium and the graphite mold, those parts of the mold and crucible that come in contact with the molten uranium were coated with a yittrium-oxide mold coating [4]. The mold coating was applied with an automotive style paint sprayer and allowed to dry prior to mold assembly.

Stainless steel sheathed type-K thermocouples (chromel – alumel) were inserted into holes drilled in the graphite mold. Alumina sheathed type-C thermocouples (W-5%Re – W-26%Re) with a bare-bead tip were placed in the casting cavity and cemented in place. Locations of the thermocouples are shown in Fig. 1 along with the thermocouple number. The blue dots represent the location of the type-K thermocouples in the mold, while the red dots represent the location of the type-C thermocouples in the casting cavity.

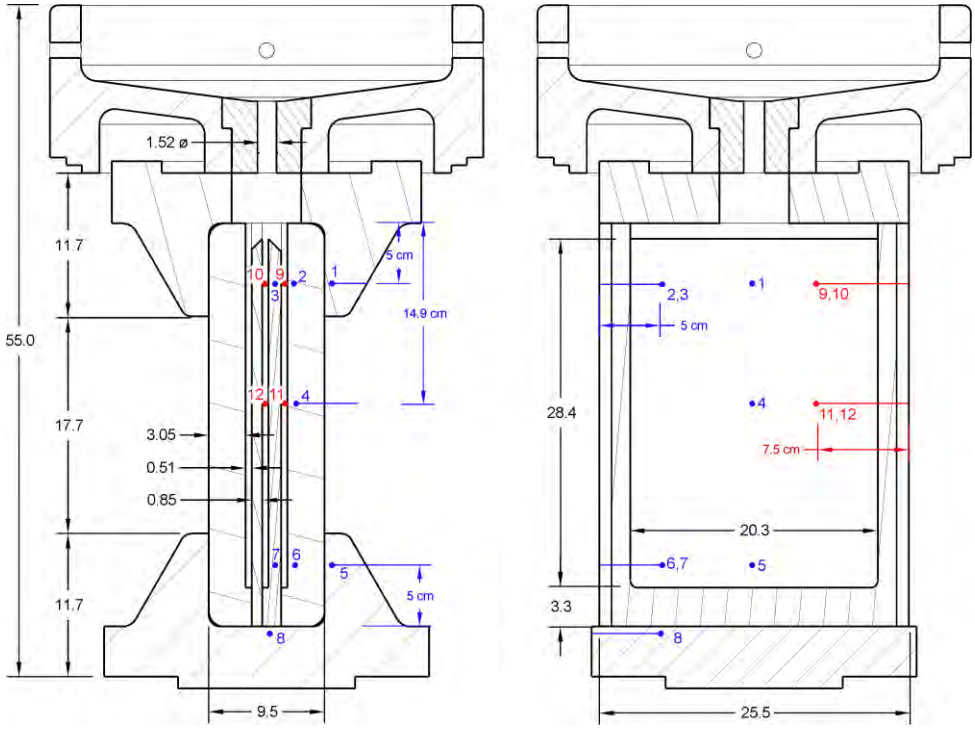

Fig. 1 Front and side views of the initial mold design. The location of thermocouples is shown with blue for thermocouples imbedded in the graphite and red for thermocouples in the casting cavity. Dimensions are in centimeters.

The crucible was charged with 17270 g of U-10Mo buttons produced by non-consumable arc-melting. The buttons were produced from high purity depleted uranium plate with approximately 65 ppm carbon and 99.95% pure molybdenum. The metal was arc-melted in a copper tundish with a tungsten electrode. Each button was melted and flipped 3 times prior to charging into the VIM crucible.

The mold stack was placed in a vacuum induction furnace. The furnace has a single induction coil 46 cm in diameter by 91 cm long. Between the mold stack and induction coil is a 4 cm thick layer of refractory insulation. The mold stack was placed with the bottom of the casting cavity at the same level as the bottom of the coil. The mold stack was supported by a 28 cm diameter graphite pedestal that was below the bottom of the coil. The coil was powered by a 100kW / 3kHz solid-state power supply. Furnace vacuum was supplied by a blower backed by a rotary-vane vacuum pump.

2.2 Casting with Initial Mold Design (1st Casting)

The initial casting followed the Y-12 recommended processing procedure. Induction power of 60 kW was applied until the metal melted and the molten metal temperature reached 1350°C. The molten metal temperature was determined by a two-color pyrometer looking in though the furnace lid and aimed on the metal surface near the stopper rod. Once the metal reached 1350°C (38 minutes), power was reduced and the metal was held at 1350°C for an additional 10 minutes. The stopper rod was removed and the molten metal was allowed to flow into the mold cavity.

The liquidus of U-10Mo is 1230°C [5-6], thus the 1350°C pouring temperature represents 120°C of superheat above the liquidus. Figure 2 shows the temperature in the mold, as a function of position, just prior to the removal of the stopper rod. The mold is quite cool at pouring time with 700°C at bottom and 1050°C at top.

Figure 3 shows the resulting cooling curves for the thermocouples in the mold and in the casting cavity. The liquidus and solidus temperatures are indicated by dotted lines. Filling time is estimated from these curves to be 15 seconds. The fact that the thermocouple traces in the casting cavity either do not reach, or barely reach the liquidus, indicates that the loss of all of

the super head and the beginning of solidification has occurred prior to the complete filling of the mold.

Comparison of thermocouples 9 and 10 and thermocouple 11 and 12 in Fig. 3(b) shows dissimilar cooling rates between the center and outer cast plates. This uneven cooling is due to the fact that the outer plates are in contact with a greater thickness (or volume) of graphite for heat to diffuse away from the casting/mold interface than the center plate. This thermal mass effect can be seen by the fact that the thermal spike is much greater in the thermocouples in the inner mold plates (TC 3 and 7) than those of the outer mold (TC 2 and 6).

The castings were joined by a very small common section connecting the three plates at the top. This connection caused the top of the plates to contract and clamp onto the inner mold sections. The inner graphite mold sections had to be broken to separate the mold and casting. The common section was then sawed off to separate the plates and allow for radiographic inspection.

The radiographic results of these 3 plates from are shown in Figure 4(a). The two dark horizontal lines in the center and right plates are the sheaths for the thermocouples imbedded in the casting cavity. The radiographs show numerous areas of "porosity" especially in lower half of castings indicated as dark bands. Also visible in Figure 4(a) is a region of non-filling on the right plate associated with a thermocouple sleeve (0.32 cm diameter sleeve vs. 0.5 cm thick cavity). This implies very marginal filling and emphasizes how cold the mold and filling conditions were.

Figure 5 shows the results of sectioning and metallographic examination of one of the dark banded region. Metallography performed on samples cut from these regions show the presence of microporsity (Fig. 5(b) and 5(c)) confirming that the dark radiographic bans are microporosity. It is likely that this microporosity was due solidification shrinkage.

3. Mold Redesign

3.1 Mold Design

As demonstrated in the initial casting, plates with a long thin nature are a challenge to cast without defects. For the purpose of this study the plate dimensions are is a design constraint that can't be altered. So the goal is to develop a mold design and corresponding process parameters that minimize or eliminates the defects for this given geometry.

The defects are principally of two kinds:
1) Filling defects - areas were liquid metal become isolated by premature freezing of the metal or areas were molten metal flows against already frozen solid.
2) Solidification shrinkage defects - areas were porosity forms because of a lack of feed metal to accommodate the contraction that occurs during solidification.

To avoid filling defects the mold needs to be filled before significant solidification can occur. To help accomplish this filling goal the following modifications were made to the original mold design -
a) Increase the mold temperature so that the hot top section of the mold is near the solidus temperature.
b) The casting cavity was rotated from being 28 cm tall by 20 cm wide to 20 cm tall and 28 cm wide. This long horizontal dimension and short vertical dimension minimizes the filling length.
c) A distributor was added to provide simultaneous and equal volume filling of all 3 plates in a controlled manner.

The distributor has an added benefit of maintaining physical separation between plates for ease of breakout.

To minimize shrinkage porosity in an alloy casting the thermal gradient should be maximized to minimize the length of the dendrites and improve flow from the hot top to the dendrite roots [7].

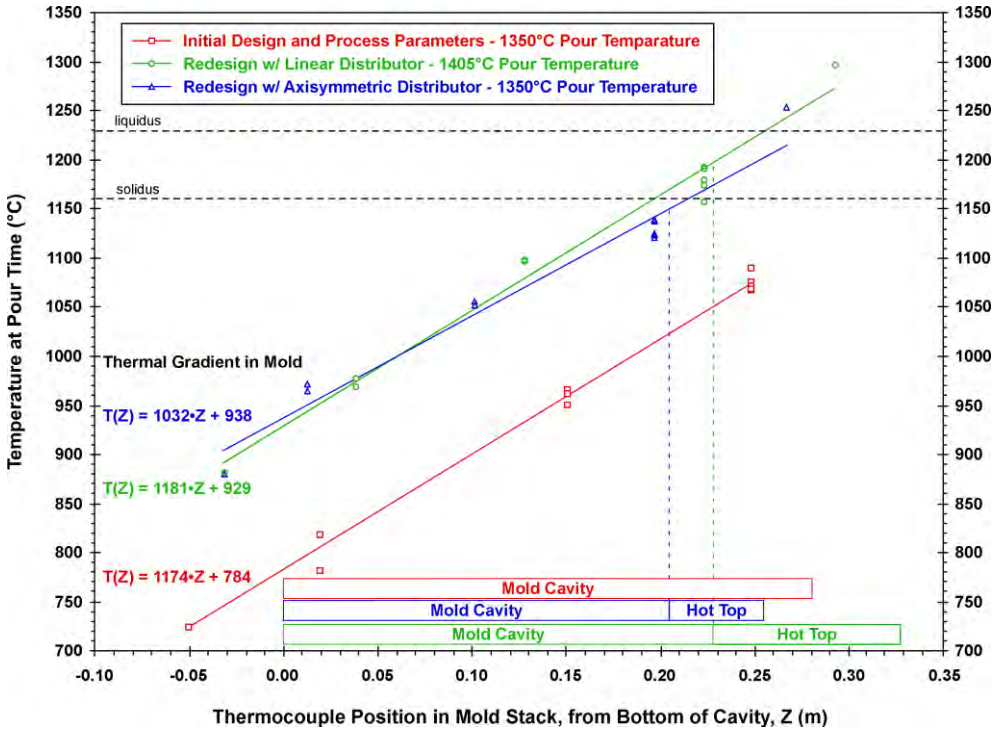

Fig. 2 Temperature as a function of position in the mold just prior to removal of the stopper rod showing initial thermal gradient in the mold for the 3 castings considered.

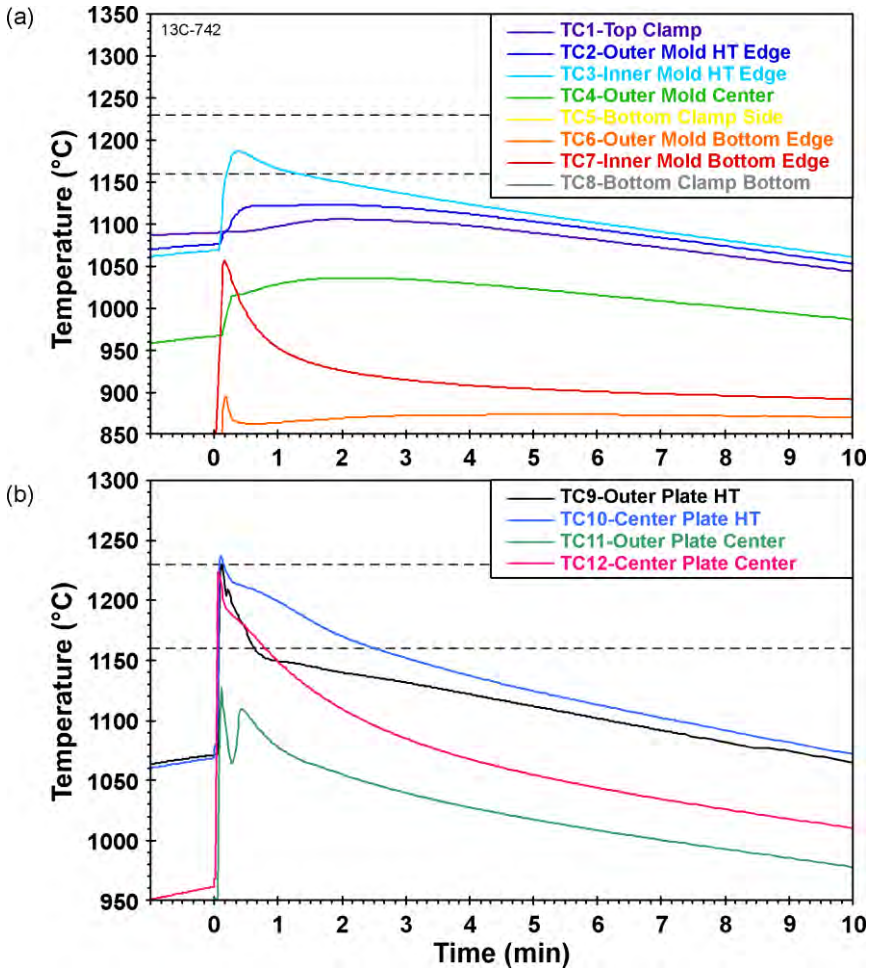

Fig. 3 Thermal history of initial mold poured at 1350°C; (a) thermocouples in mold and (b) thermocouples in casting cavity.

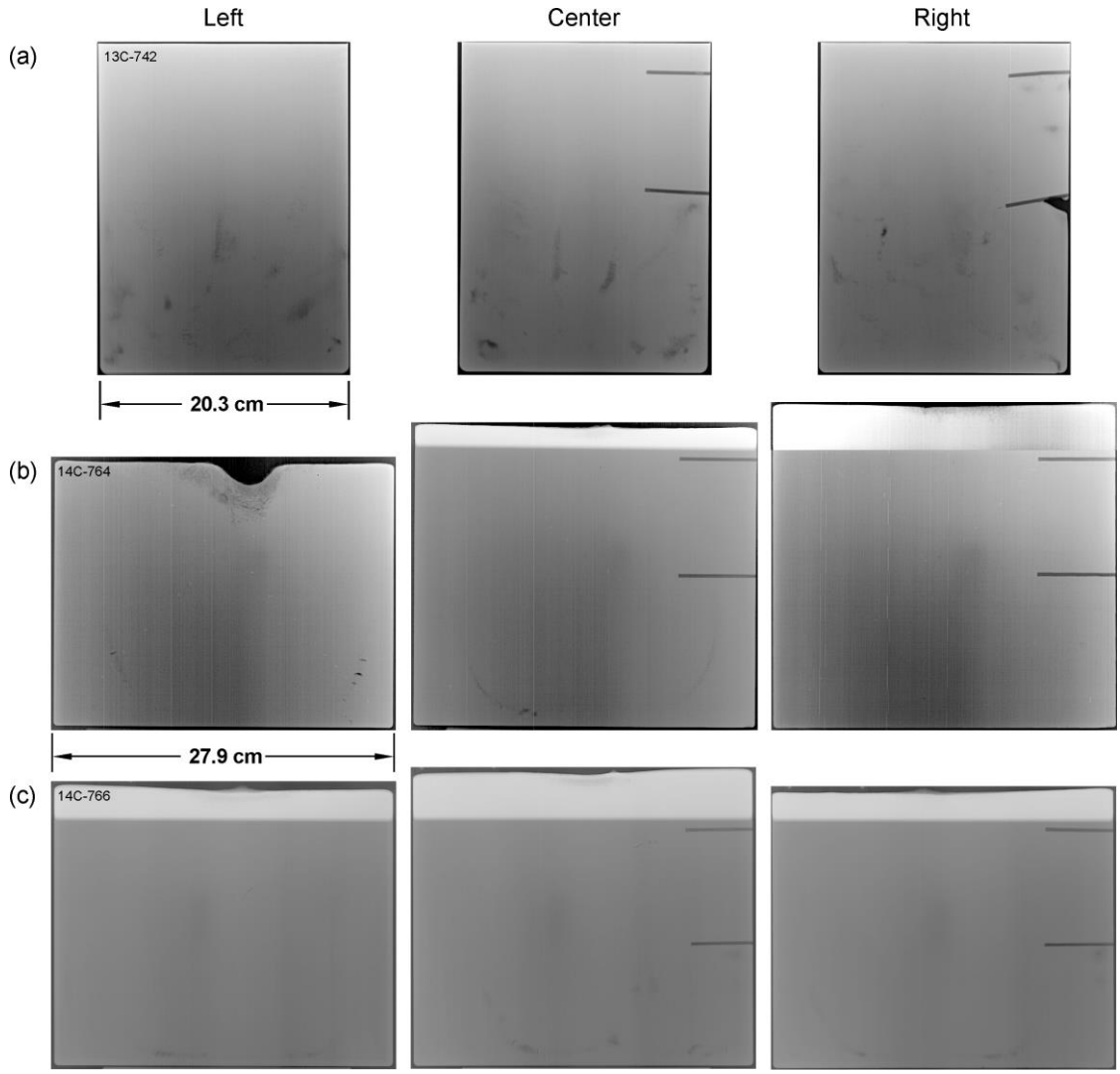

Fig. 4 Radiographic results of the three castings; (a) initial mold design, (b) redesigned mold with linear distributor, and (c) redesigned mold with axisymmetric distributor.

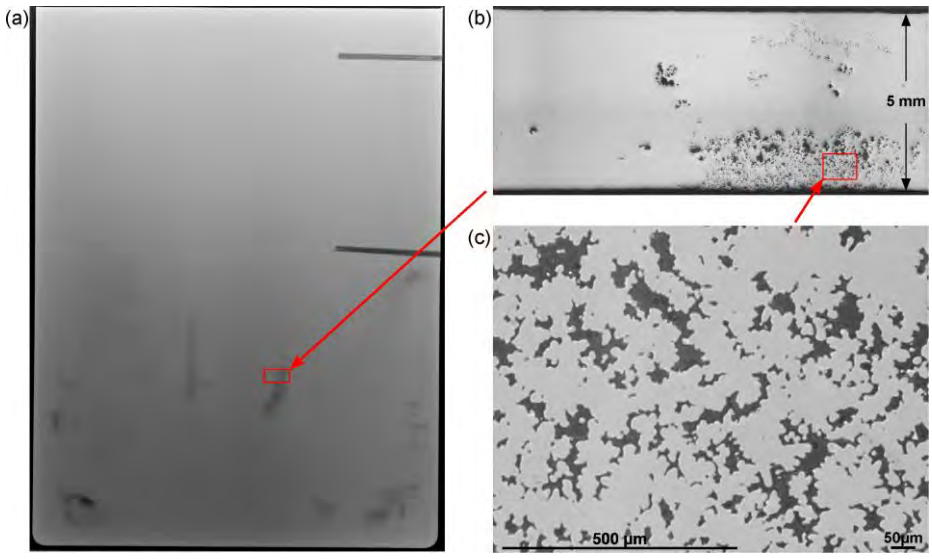

Fig. 5 Sectioning from the center plate of the 1st casting showing that radiographic indications are porosity; (a) radiograph image showing origin of metallographic section in red box, (b) through-thickness micrograph, and (c) higher magnification image of a near surface area showing shrinkage porosity.

In addition, there must be a hot top that:

- solidifies at the same time or later than the casting,
- contains sufficient liquid to compensate for the volume-contraction of the freezing metal,
- there must be a path from the hot top to allow feed metal to reach regions that need it.

Following these rules the following modifications where made to the original mold design -

d) Added a hot top with sufficient thermal mass and metal volume to feed solidification shrinkage.
e) Rotating the casting cavity was from being 28 cm tall by 20 cm wide to 20 cm tall and 28 cm wide also reduces the mold height, which can help increase the thermal gradient and decrease the molten metal feeding length from the hot top.

An additional goal is to try to ensure similar solidification time for the plates regardless of which casting cavities (center or edge) they originated from. To accomplish this, the mold thickness was "balanced" to make heat extraction rates of inner and outer plates similar by -

f) Make the outer mold wall thickness (casting to edge) to be one-half the thickness of the inner mold walls.

This revised mold design incorporating these changes is shown in Fig. 6.

3.2 Casting with Redesigned Mold with Linear Distributor (2nd Casting)

This second casting was cast quite similar to the first casting. As before, the mold was machined from HML graphite and coated with a yittrium-oxide mold coating. The type-K and type-C thermocouples were placed in the casting at locations indicated in Fig. 6. It was not discovered until casting was complete that the mold had been mistakenly machined with a 22.9 cm tall cavity, rather than the desired 20.3 cm tall cavity. This mistake was corrected in the 3rd casting and the as-built drawings are shown in Fig. 6.

The crucible was charged with 20900 g of U-10Mo buttons produced by non-consumable arc-melting. Induction power of 60 kW was applied until the metal melted and the molten metal temperature reached 1400°C. Once the metal reached 1400°C (51 minutes), power was reduced that the metal was held at 1400°C for an additional 10 minutes. The stopper rod was then removed and the molten metal allowed to flow into the mold cavity. The higher metal/crucible temperature was to try to further slow solidification and defects caused by solidification during filling.

Figure 2 shows the temperature in the mold as a function of position just prior to the removal of the stopper rod. Compared to the initial design and process parameters, the mold was significantly warmer with the hot top portion of the mold above the solidus temperature and the distributor above the liquidus temperature. This is advantageous because it minimized metal solidification and heat loss in the distributor and helped keep the metal in the hot top molten longer (while the rest of the casting solidifies).

Figure 7 shows the resulting cooling curves for the thermocouples in the mold and in the casting cavity. Thermocouple 11, in the center of the outer plate, did not return useful data. Overall, the warmer metal, mold, and mold redesign had the desired result of longer solidification times and filling was complete prior to significant solidification. Thermocouples 9 and 10 show similar solidification behavior for the center and edge plates demonstrating that balancing the mold thickness resulted in similar solidification times.

The resulting three plates had individual weights of 5153 g, 6485 g, and 7938 g for the left, center, and right plates respectively. This corresponded to no hot top, a 1.6 cm tall hot top, and a 2.5 cm tall hot top respectively. Clearly the distributor failed to deliver the same volume of metal to each of the 3 casting cavities. This is a flaw in the distributor design that needs to be corrected.

The failure of the distributor to fill the castings evenly had the unintentional consequence of providing a measure of casting soundness versus hot top size. Figure 4(b) shows the radiographs of the 3 plates. The right plate, with large (1.5" tall) hot top, appears sound with

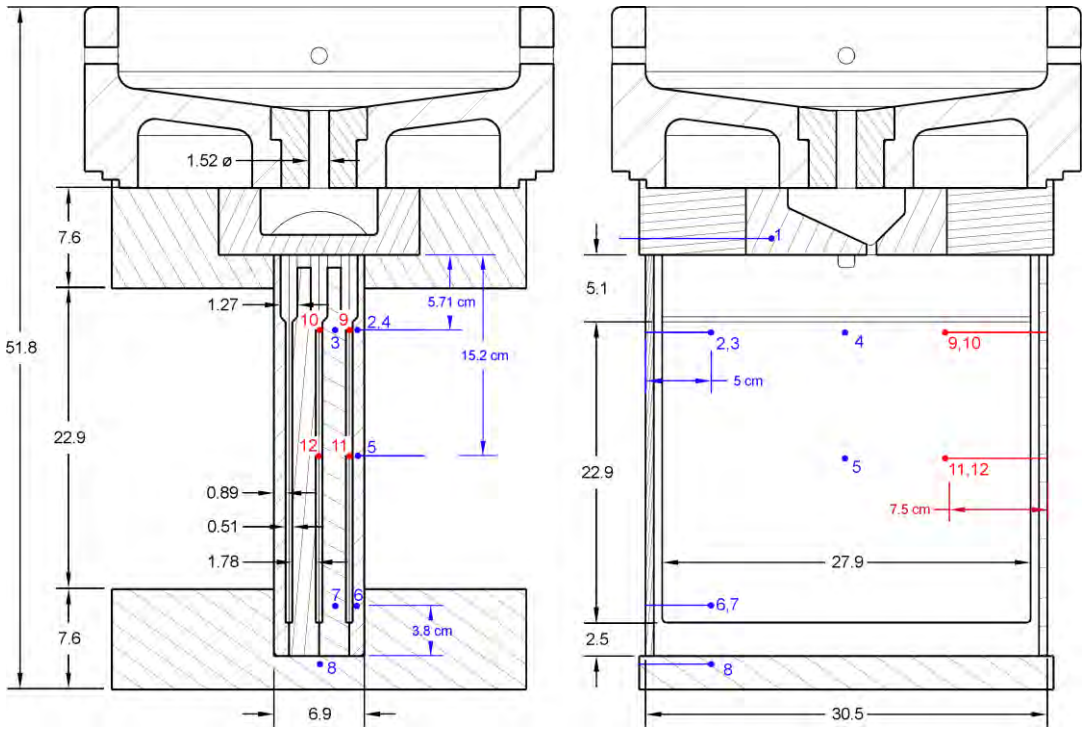

Fig. 6 Front and side views of the revised mold design with the linear distributor along with the location of thermocouples. Dimensions are in centimeters.

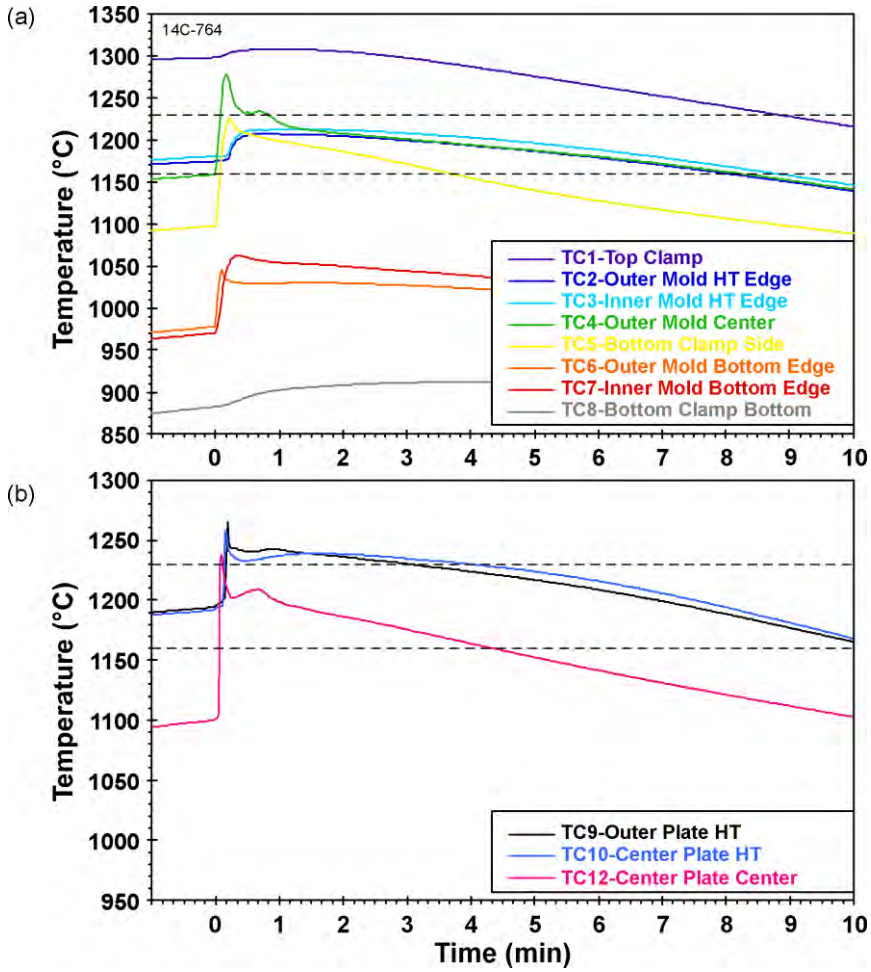

Fig. 7 Thermal history of revised mold design with the linear distributor poured at 1400°C; (a) thermocouples in mold and (b) thermocouples in casting cavity.

no defects in the plate. The center plate with medium (1.6 cm tall) hot top, and the left plate with no hot top both show a faint concave band of porosity in lower section of the casting. It is unclear if this is a filling or feeding defect. The left plate, with no hot top, has shrinkage porosity and surface shrink where top of plate subsided and fed the casting.

4. Distributor Redesign

The fact that the distributor did not evenly distribute the molten metal into the 3 cavities of the redesigned mold was unexpected and it was initially not evident why filling was unequal. To understand this unexpected filling behavior, the mold filling was simulated using the commercial computational fluid dynamics code Flow-3D [8]. FLOW-3D solves relevant time-dependent heat and fluid flow free-surface problems in three dimensions. The experimentally determined temperature of the mold at pour time was used as the initial conditions and the experimentally determined cooling curves were used to validate the code and parameters used. Only a portion of the results are presented here.

4.1 Simulation of the Linear Distributor

The details of the linear distributor used in the 2nd casting (and Fig. 6) is shown in Figure 8(a). The three holes are linear with a spacing equal to the 2.26 cm center-to-center spacing of the individual plates. The 0.76 cm diameter discharge hole was sized such that a hole of this diameter has 1/4 the cross-sectional area of the crucible's 1.52 cm diameter discharge hole. This hole is smaller than the 1/3 size that would give equal crucible to distributor sizes so that the metal backs up a bit in the distributor resulting in choked flow.

In Figure 8(b) horizontal and vertical sections though the distributor are shown at 10 seconds into the 15 second pour. The molten metal is colored by velocity magnitude (in m/s). Metal has backed up in the crucible but as shown in the horizontal section, the 3 discharge holes are not choked. The vertical section shows a stream of high velocity flow from the input stream cutting across the bottom of the distributor (below the backed up liquid). This flow causes the flow out of the 3 discharge holes to detach on the one side and results in uneven flow out of the 3 holes. The result, as shown in Fig. 8(c), is that the center plate fills to a greater extent than the two side plates. This is consistent with the observed behavior of the 2nd casting.

4.2 Simulation of an Improved Distributor Design

To avoid the unequal flow observed in the linear distributor design, 12 different distributor redesigns were considered. The redesign concepts were used to simulate the filling process. The goal was to produce even filling. For the most part the focus was on eliminating the strong flow that prevented choking of the discharge holes in the linear design of Fig. 8.

Of the dozen concepts considered the design shown in Figure 9(a) was chosen. In Figure 9(b) horizontal and vertical sections though the distributor are shown at 10 seconds into the 15 second pour. Again, the molten metal is colored by velocity magnitude (in m/s). Metal has backed up in the distributor and, as shown in the horizontal section, the 3 discharge holes are choked. The vertical section shows the there is no longer a strong sheer flow across the bottom toward the discharge holes. The result, as shown in Fig. 9(c), is that the 3 plates fill evenly in the simulation.

4.3 Casting with Redesigned Mold and Axisymmetric Distributor (3rd Casting)

This third casting was cast quite similar to the second casting. The differences were in the distributor and the height of the mold cavity. As before, the mold was machined from HML grade graphite and coated with a yittrium-oxide mold coating. The type-K and type-C thermocouples were placed in the casting at locations indicated in Fig. 10.

The crucible was charged with 21280 k of U-10Mo buttons produced by non-consumable arc-melting. In an effort to slightly reduce the solidification time of the plates, the pouring temperature of the metal was reduced from 1400 to 1350°C. Induction power of 60 kW was applied until the metal melted and the molten metal temperature reached 1350°C. Once the

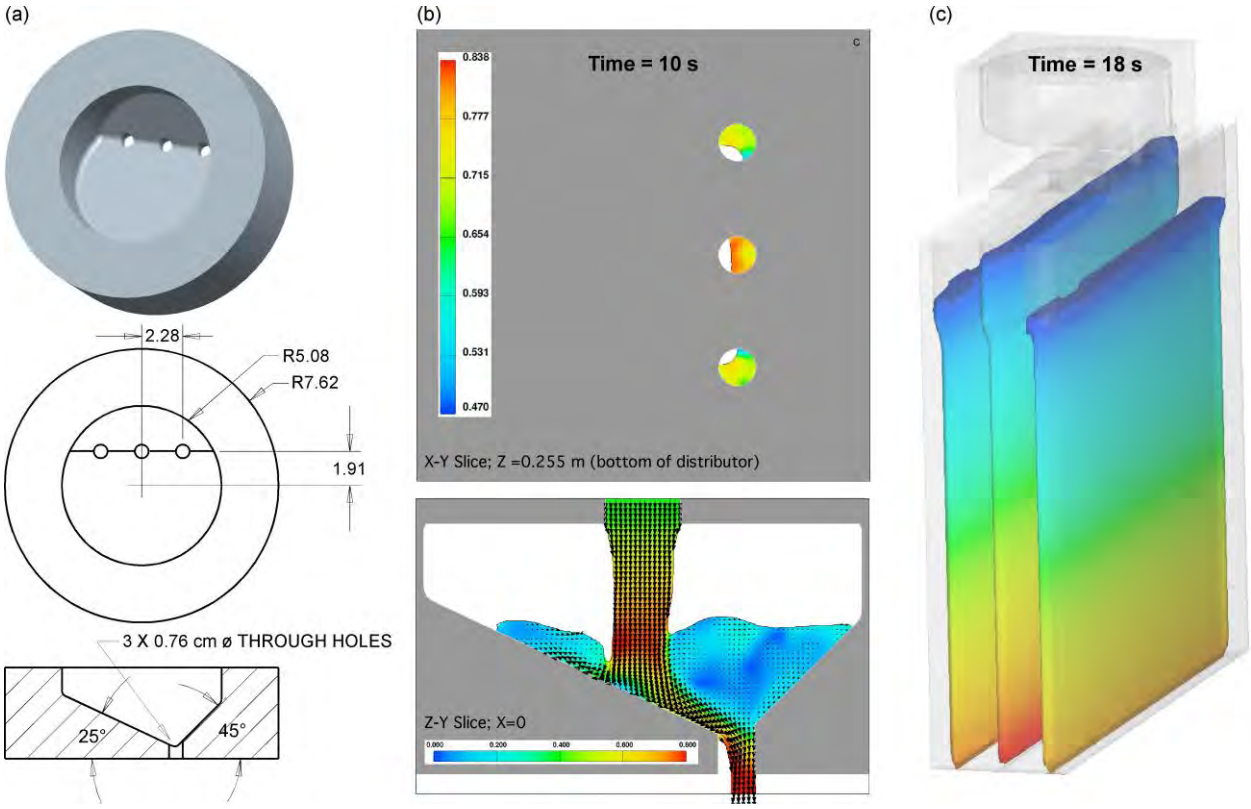

Fig. 8 Mold filling simulation of revised mold design with the linear distributor; (a) distributor geometry, (b) sections though the distributor during filling (metal colored by velocity magnitude), and (c) final unequal metal distribution in the three casting cavities.

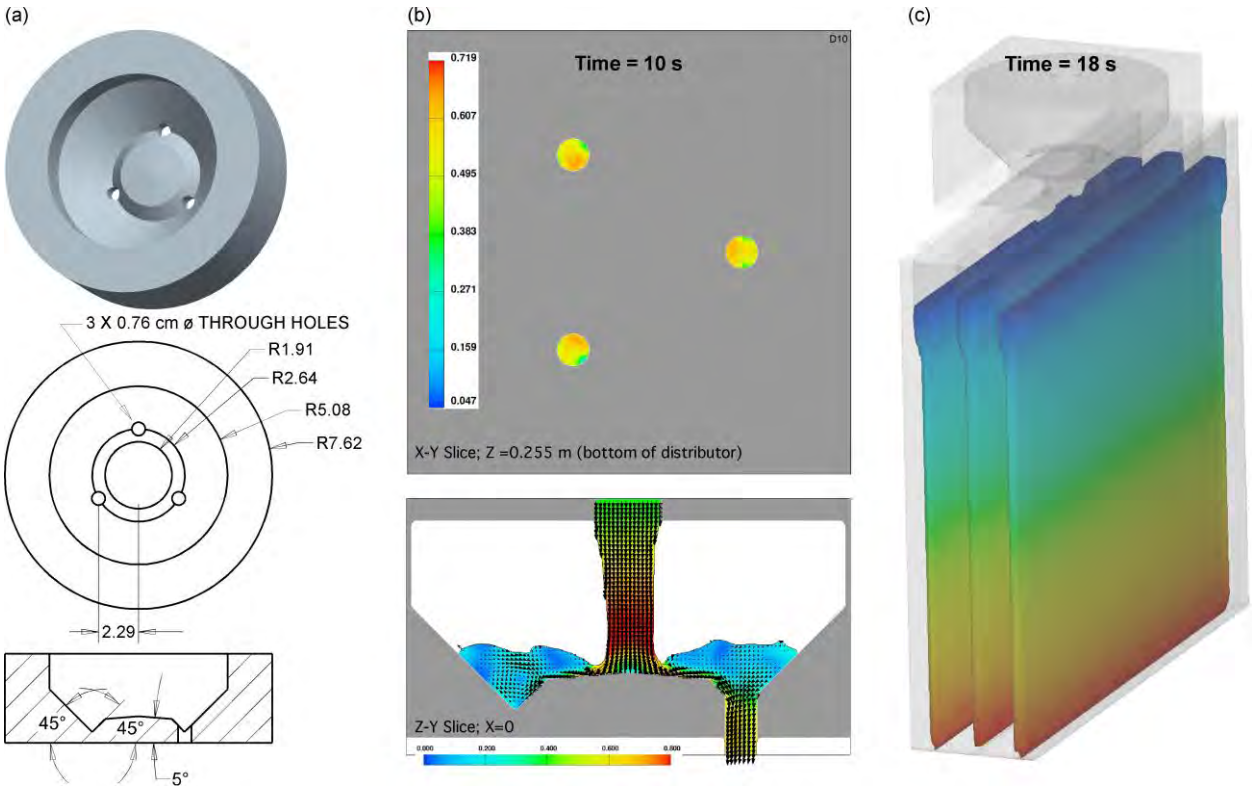

Fig. 9 Mold filling simulation of revised mold design with the axisymmetric distributor; (a) distributor geometry, (b) sections though the distributor during filling (metal colored by velocity magnitude), and (c) final nearly equal metal distribution in the three casting cavities.

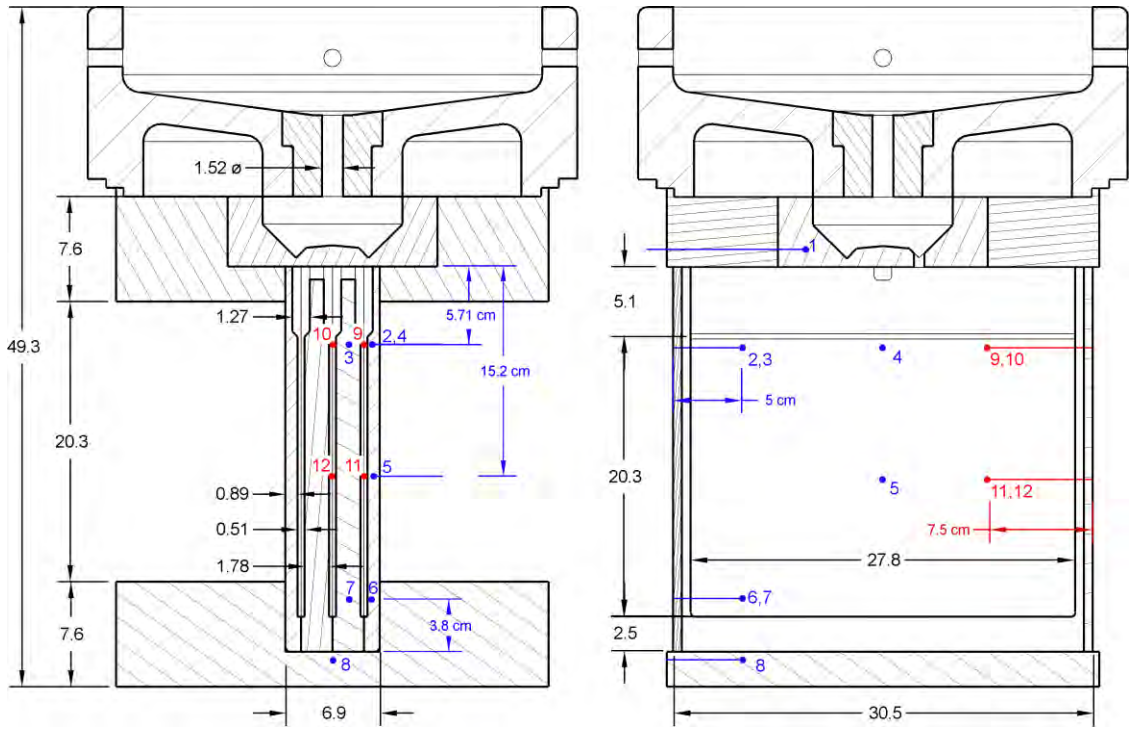

Fig. 10 Front and side views of revised mold design with the axisymmetric distributor along with the location of thermocouples. Dimensions are in centimeters.

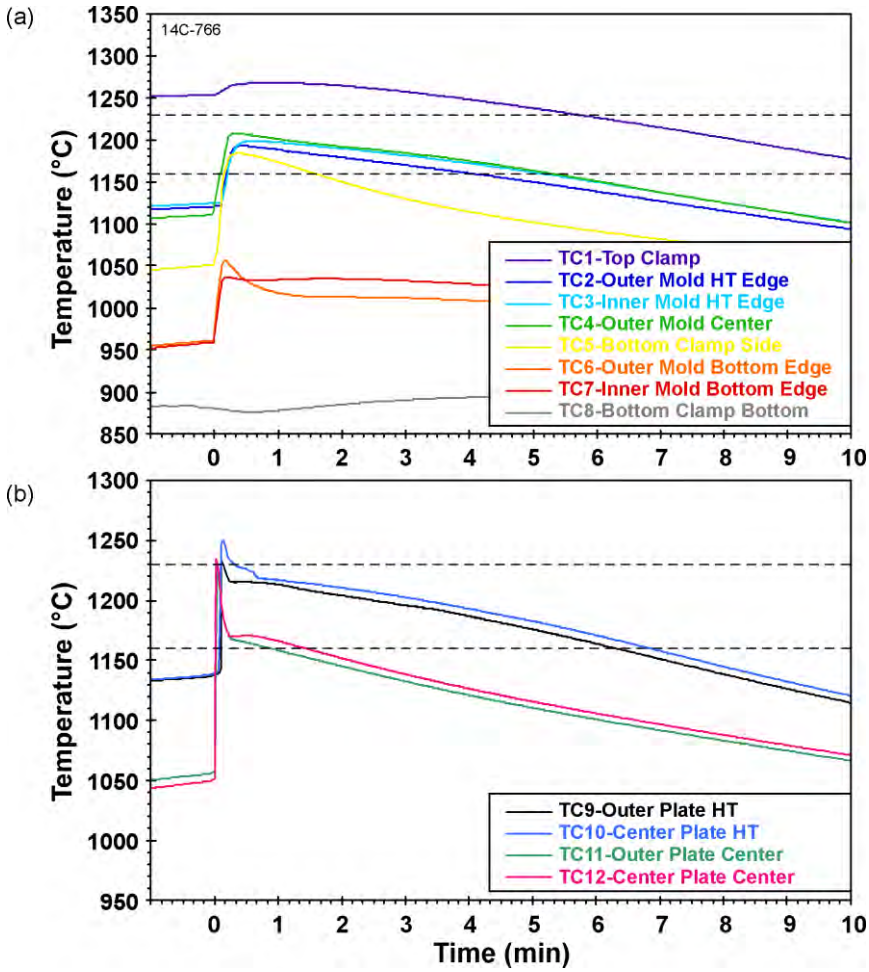

Fig. 11 Thermal history of revised mold design with the axisymmetric distributor poured at 1350°C; (a) thermocouples in mold and (b) thermocouples in casting cavity.

metal reached 1350°C (45 minutes), power was reduced that the metal was held at 1350°C for an additional 10 minutes. The stopper rod was then removed and the molten metal allowed to flow into the mold cavity.

Figure 2 shows the temperature in the mold as a function of position just prior to the removal of the stopper rod. The mold temperature is quite similar to the 2nd casting. Again hot top portion of the mold was above the solidus temperature and the distributor above the liquidus temperature.

Figure 11 shows the resulting cooling curves for the thermocouples in the mold and in the casting cavity. The solidification times are longer than the initial casting and shorter than the 2nd casting. Thermocouples 9 and 10 (and TC 11 and 12) show similar solidification behavior for the center and edge plates demonstrating that balancing the mold thickness resulted solidification times.

The resulting three plates had individual weights of 6637 g, 7179 g, and 6338 g for the left, center, and right plates respectively. The corresponding hot top heights were 2.5 cm, 3.8 cm and 2.5 cm. Although the weights were not exactly the same, this axisymmetric distributor was a significant improvement over the linear design used in the 2nd casting.

Figure 4(c) shows the radiographs of the 3 plates for the 3rd casting. Although there are a few faint concave bands of porosity in lower section of the casting, the defect content this set of 3 plates look the best of the 3 casting trials. The presence of the faint lower section defects in these castings means they are not quite as good as the best of the 2nd casting plates (the right plate with the largest hot top). It is believed that the decrease of the casting temperature from 1400 to 1350°C was a bit too much and a pouring temperature of 1400°C would be preferable for future castings.

5. Conclusions

The long (20 cm) and thin (0.5 cm) nature of the geometry of this casting makes it very difficult to cast without casting defects. Mold design and casting parameters were developed to minimize casting defects in the triple plate geometry. Care must be taken to make sure that the mold temperature is quite warm to ensure that filling can occur without significant solidification and the corresponding casting defects. Because of the very high rate of solidification, segregation of Mo during solidification is not believed to be a major concern.

Acknowledgement

The authors would like to acknowledge the financial support of the US Department of Energy Global Threat Reduction Initiative Reactor Convert program. Los Alamos National Laboratory, an affirmative action equal opportunity employer, is operated by Los Alamos National Security, LLC, for the National Nuclear Security Administration of the U.S. Department of Energy under contract DE-AC52-06NA25396.

7. References

[1] R.M. Aikin Jr. and D. Dombrowski, “Process Optimization of U-10Mo Casting by Modeling and Experiment”, European Research Reactor Conference 2014, RRFM2014-A0128 (2014).

[2] Baseline mold design and process parameters private communication H.A. Longmire, Y-12 Nat. Secruity Complex, Oak Ridge, TN, USA.

[3] HML grade graphite by SGL Carbon, LLC., St. Marys, PA USA.

[4] Type YK nonaqueous-based yttrium oxide paint by ZYP Coatings, Oak Ridge, TN USA.

[5] P.C.L. Pfeil, J. Inst. Metals, v 77, pp. 553-570 (1950).

[6] S.P. Garg and R.J. Ackermann, J Nucl. Mater., v. 64, pp. 265-274 (1977).

[7] John Campbell, Complete Casting Handbook, Butterworth, Oxford UK (2011).

[8] Flow-3D by Flow Science Inc., Santa Fe, NM USA.

CAN-LESS HIP METHOD FOR PRODUCING FUEL PLATES

T. LIENERT, M. DVORNAK, P. BURGARDT, R. FORSYTH,
R. HUDSON, B. AIKIN, AND D. DOMBROWSKI
Materials Science & Technology Division, Los Alamos National Laboratory
P O B o x 1 6 6 3 , L o s A l a m o s , N M 8 7 5 4 5 – U S A

ABSTRACT

Accomplishments in developing a new "Can-Less" HIP sample for producing fuel plates are reviewed. The proposed approach is simpler, involves fewer processing steps, provides for near net shape product, and produces less material waste relative to the legacy HIP can approach.

1. Introduction

The legacy process for fabricating fuel plates for the CONVERT program requires fabrication of stainless steel HIP "cans" that are expensive and time-consuming to fabricate. An alternate approach will lower fabrication time and costs.

Here, a "Can-Less" method for fabricating fuel plates using AA-6061 clad sheets containing a LEU-10 Mo fuel foil is introduced (Figure 1). This approach uses electron beam welding (EBW) to evacuate and seal the fuel plate assembly for HIP bonding (Figure 2). The components are held rigidly in a fixture during EBW. Welds are removed by shearing after HIP to produce the final fuel plates.

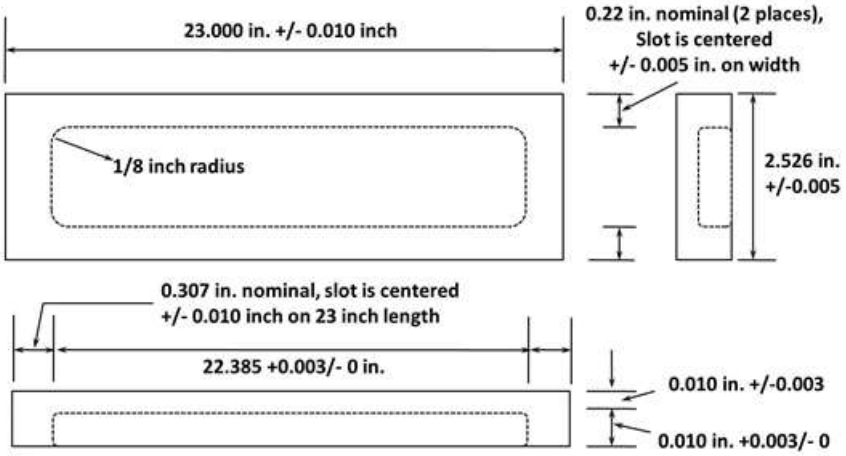

Figure 1: Schematic of bottom clad sheet for fuel plate.

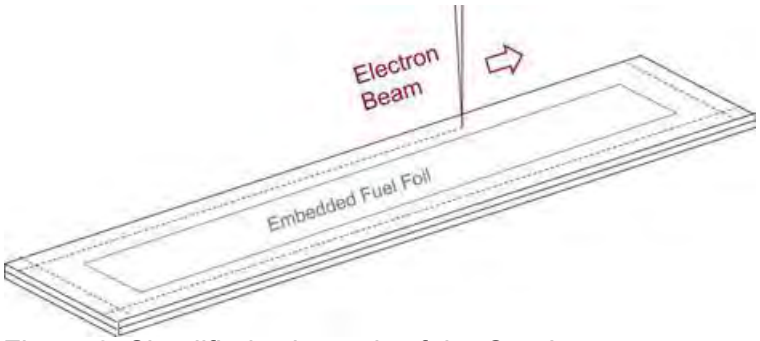

Figure 2: Simplified schematic of the Can-Less process.

2. Advantages and Challenges

The proposed approach is simpler, involves fewer processing steps, provides for near net shape product, and produces less material waste relative to the HIP can approach. The AA-6061 alloy clad sheets are susceptible to solidification cracking (Figure 3a). However, the lap weld geometry limits strain on the weld joint and aids in precluding cracking. Fixturing during EBW must prevent trapping of air between the clad sheets that may limit HIP bonding.

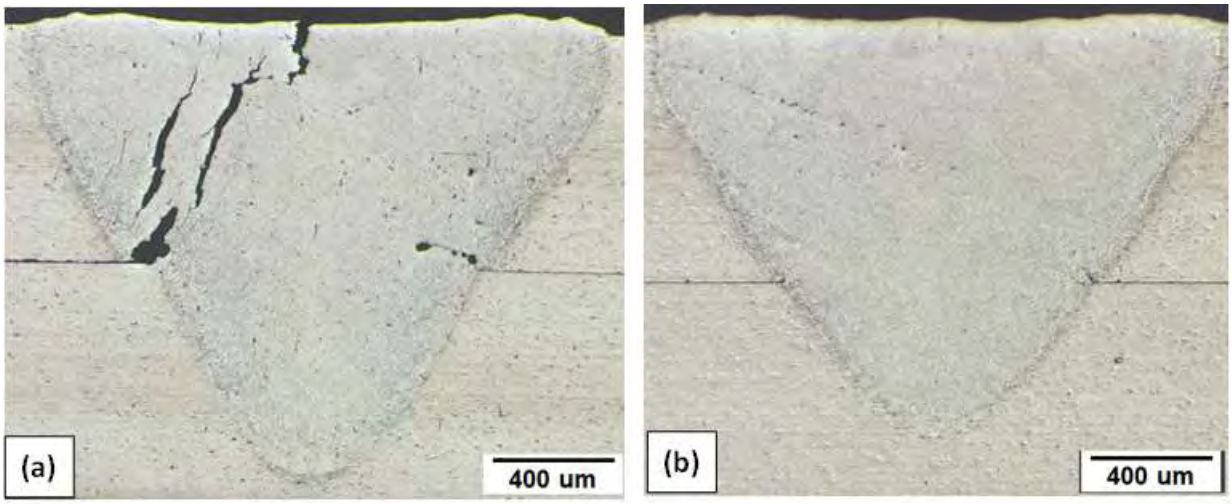

Figure 3: Solidification cracking in initial efforts (a) was eliminated by changing weld placement and parameters (b).

3. EB Welding Lessons

"Keyhole" mode EBW should be avoided to limit formation of cracks and drop-throughs. Use a defocused beam to produce a weld extending halfway into the bottom sheet (See Figure 3b), and space welds at least 3/8" from the edge of the sheets.

Clamping in the fixture must prevent formation of a local gap during welding that might promote defects and allow evacuation of air between the sheets that may produce porosity and/or prevent bonding during HIP due to oxidation.

4. HIP Fixturing

Initially, the welded fuel plates were hung in a fixture during HIP (Figure 4a). However, the plates distorted due to differences in CTE between the fuel foil and clad sheets (Figure 4b).

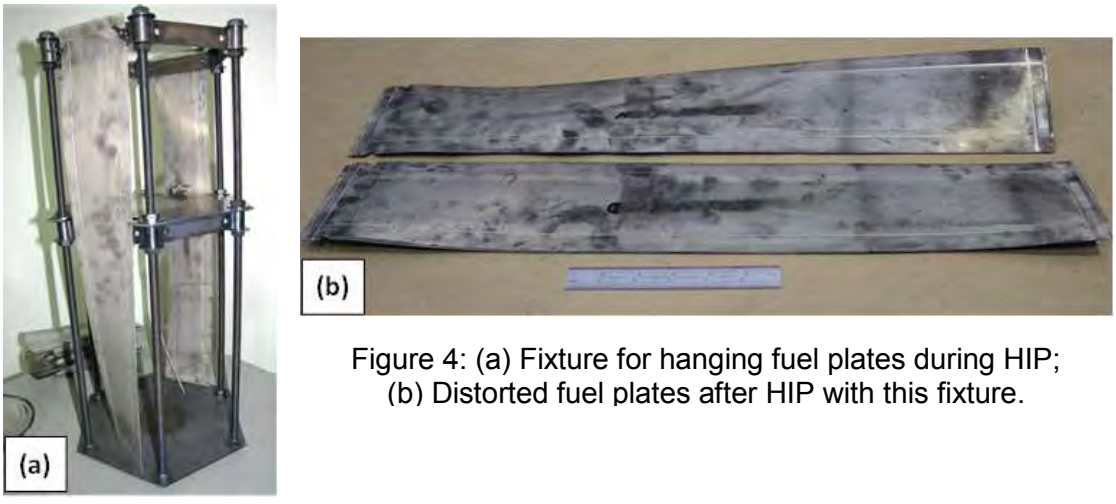

Figure 4: (a) Fixture for hanging fuel plates during HIP; (b) Distorted fuel plates after HIP with this fixture.

To address the distortion during HIP, a new HIP fixture was designed. Fuel plates were held between spring loaded plates and can also be weighted. (Figures 5 and 6).

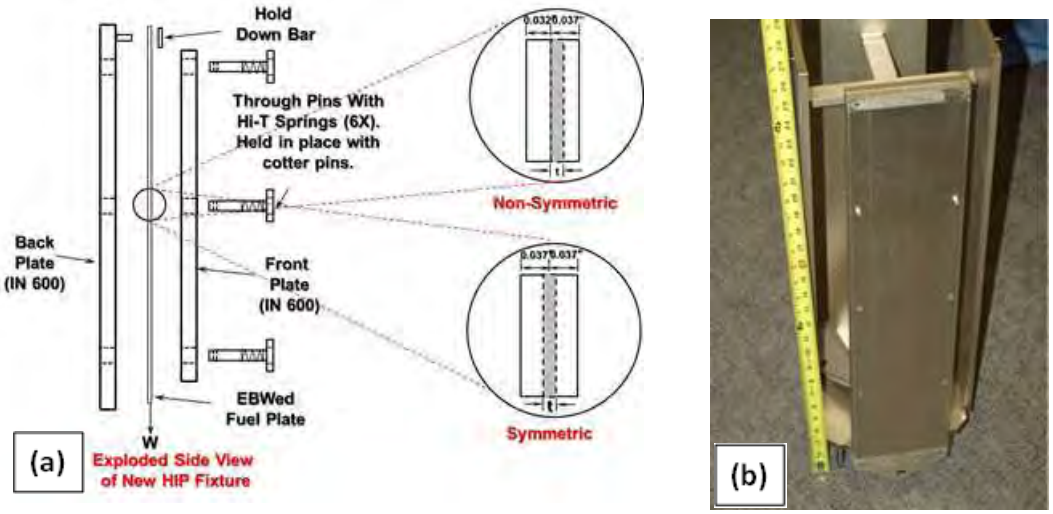

Figure 5: a) One of four sections of the spring loaded HIP fixtures; (b). Photo of spring loaded HIP fixture.

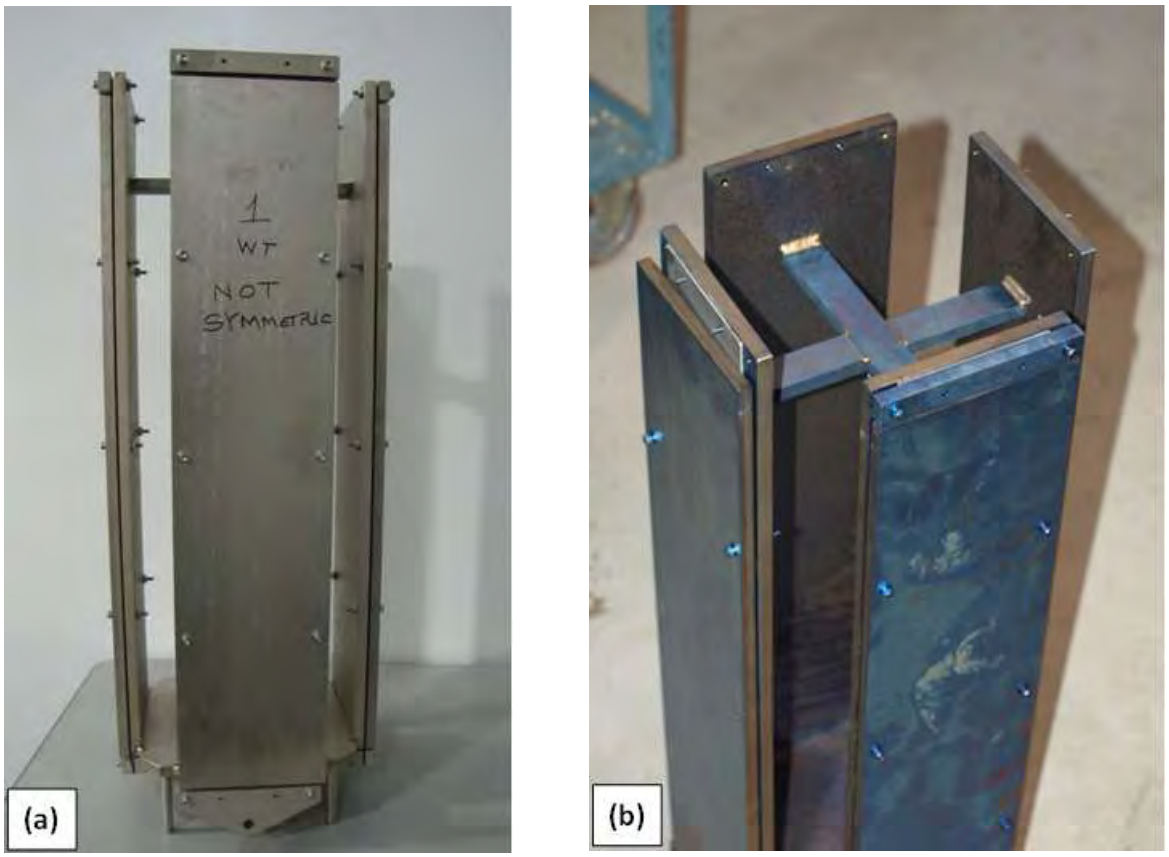

Figure 6: (a) and (b) Fuel plates in place in spring-loaded HIP.

The fuel plates after HIP using the spring-loaded fixture (Figure 7) were much flatter than with the hanging fixture.

Figure 7: Fuel plates after HIP with the spring-loaded HIP.

5. Mini-Plate 1 Experiments

In support of the Mini-Plate 1 (MP-1) experiments the clad samples and the EBW fixture were redesigned to hold four mini plate sample in the pockets (Figure 8).

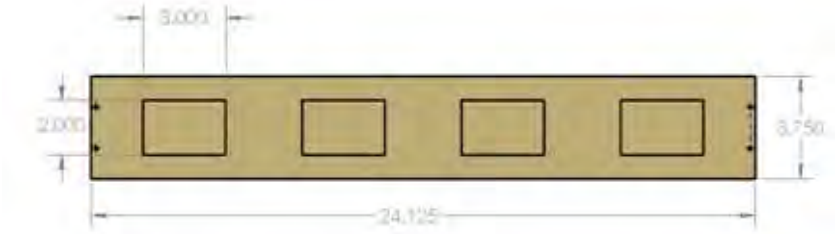

Figure 8: Drawing of bottom clad sheet for MP-1 samples.

Clad sheets are arranged in the fixture with locating holes, Figure 9 (a). Side center and corner hold-down bars are put into place and held with bolts to make the long EB welds, Figure 9(b). The center hold-down bar is removed and the toggle clamps are used to hold the fuel plates in place, Figure 9(c).

Each toggle clamp is lifted individually and replaced immediately with a cross hold-down bar, Figure 10 (a), until all cross hold-down bars are in place, Figure 10 (b). After the cross welds are made, the cross hold-down bars are removed, and the scribe fixture is inserted to allow scribing locations for accurate shearing of the mini-plate samples, Figure 10 (c).

6. Summary and Conclusions

Accomplishments in developing a new “Can-Less” HIP sample for producing fuel plates have been reviewed. The proposed approach is simpler, involves fewer processing steps, provides for near net shape product, and produces less material waste relative to the legacy HIP can approach.

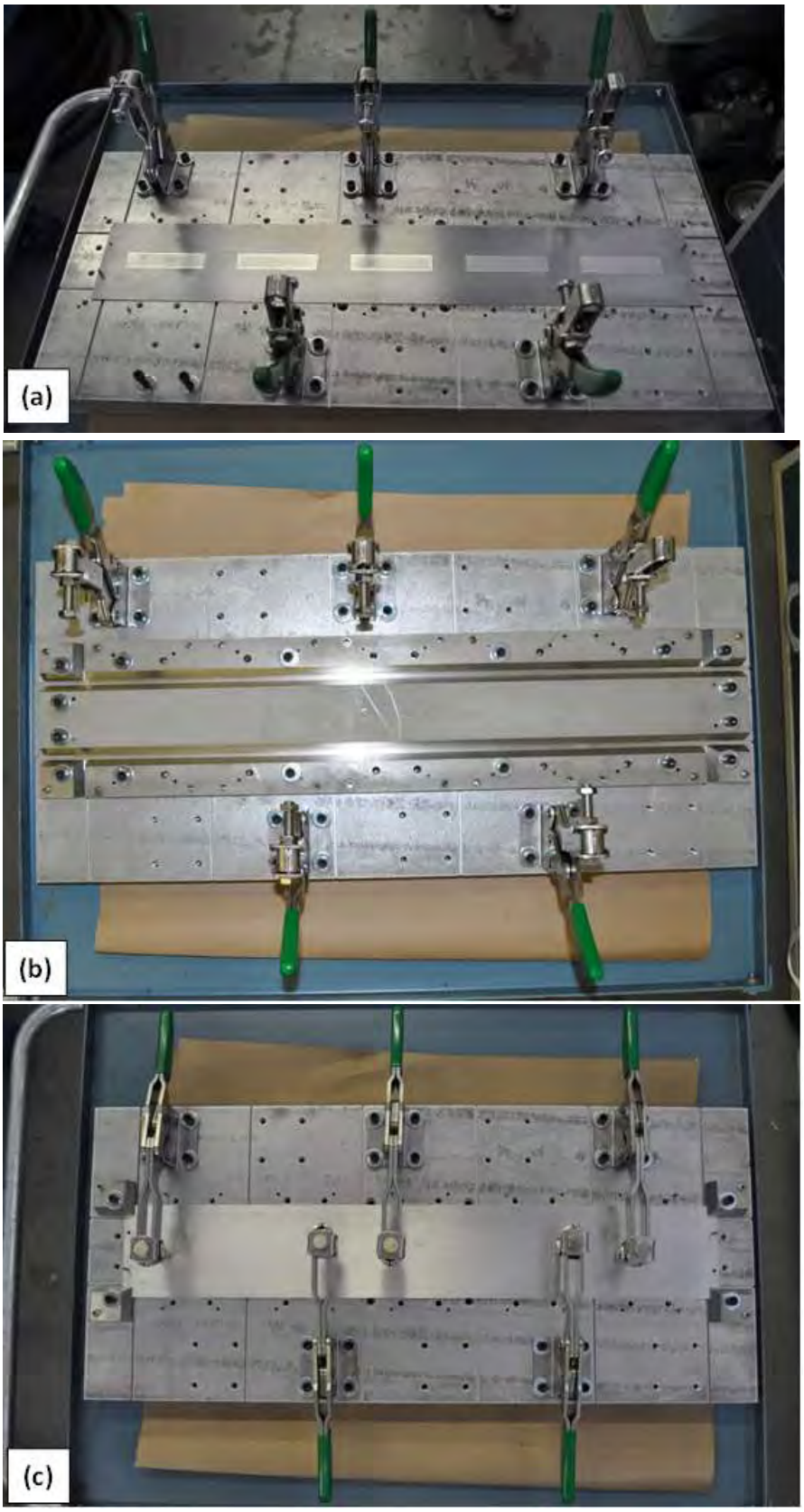

Figure 9: (a), (b) and (c): Steps in clamping sequence for producing MP-1 samples (shown outside of the EBW chamber).

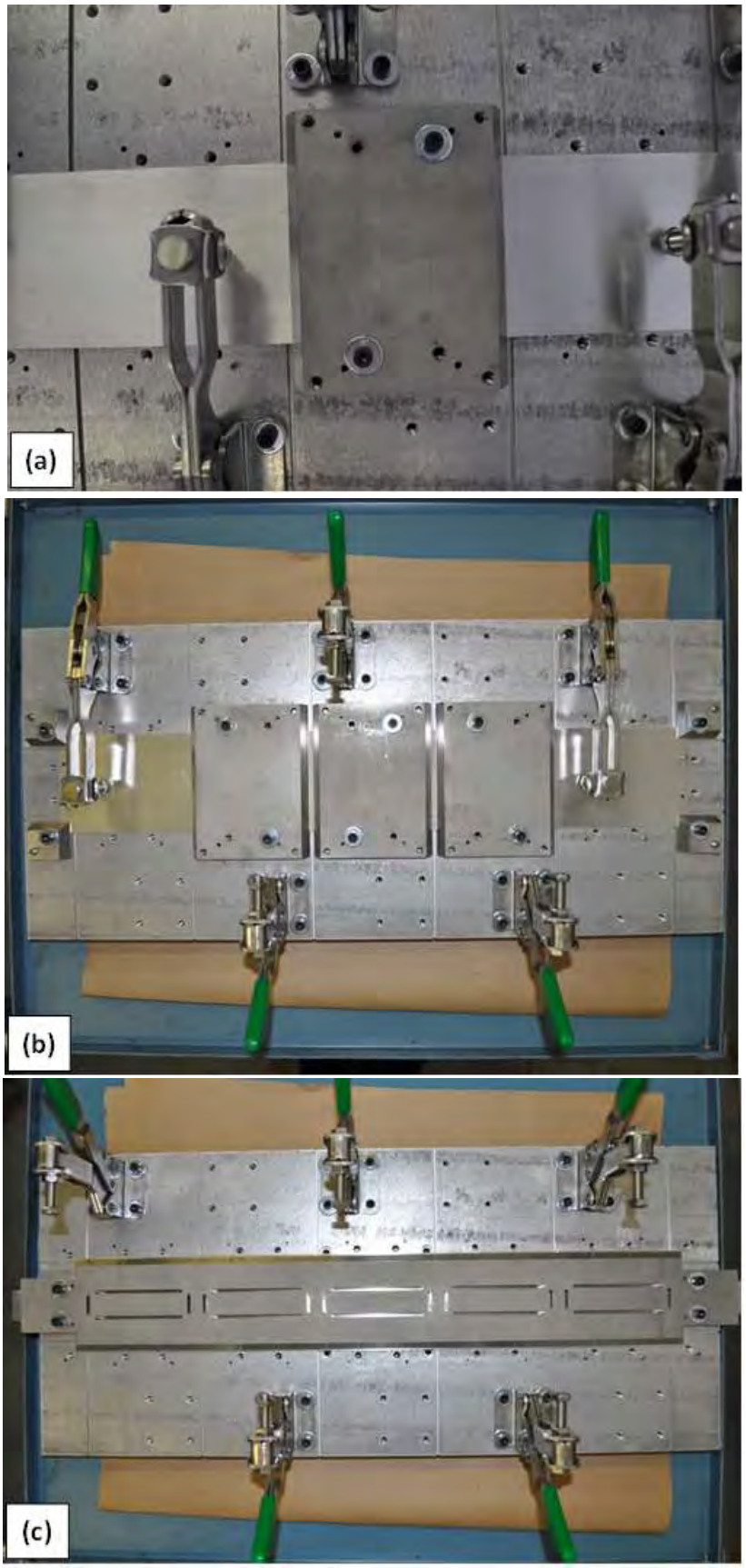

Figure 10: (a), (b) and (c): Steps in clamping sequence for producing MP-1 samples (shown outside of the EBW chamber).

ELECTROPLATING OF ZIRCONIUM ON URANIUM-MOLYBDENUM ALLOY FUEL FOR HIGH PERFORMANCE RESEARCH REACTORS.

K.D. MEINHARDT, G.W. COFFEY, C.A. LAVENDER
Pacific Northwest National Laboratory
902 Battelle Blvd, Richland WA 99354 – USA

A. SMIRNOV, A. SHCHETKOVSKIY, J.S. O'Dell
Plasma Processes
4914 Moores Mill Road Huntsville AL 35811 – USA

ABSTRACT

The Fuel Fabrication Capability (FFC) within the US High Performance Research Reactor Conversion Program, which is funded by the United States Department of Energy through NNSA NA-23 (Office of Material Management and Minimization), commissioned an investigation to determine the conceptual feasibility of using electroplating techniques to apply a coating of zirconium (Zr) onto depleted uranium/molybdenum alloy (U-10Mo). A new electroplating process for plating zirconium metal onto the U-10Mo alloy plate fuel has been developed. The plating is conducted in a proprietary molten salt mixture that does not react with the U-10Mo and produces a 25μm thick Zr layer. This approach provides an alternative method to the existing process baseline approach of roll-bonding Zr foil onto the DU-10Mo fuel foil during the fabrication of fuel elements for high performance research reactors. In order to achieve good quality plating, both the U-10Mo surface preparation and the method of residual salt removal are important. The best method for surface prep found so far, an acid wash in 8 molar nitric acid followed by an ethanol rinse, produces better results than electropolishing. The removal of the residual salt appears to have an impact on the final plating quality as well. Final washes in hot water resulted in significant amounts of plating defects that were eliminated when the salt was removed with ethanol.

1. Introduction

In support of the Fuel Fabrication Capability (FFC) within the US High Performance Research Reactor Conversion Program, which is funded through NNSA NA-23 (Office of Material Management and Minimization), Pacific Northwest National Laboratory (PNNL) has been investigating manufacturing processes for the uranium-10% molybdenum (U-10Mo) alloy plate fuel. The low-enriched U-10Mo (LEU) has been identified as the most promising alternative to the current highly-enriched uranium (HEU) used in the United States' fleet of high performance research reactors (USHPRRs). The nominal configuration of the new LEU plate fuel, shown in Figure 1, comprises a U-10Mo fuel foil enriched to slightly less than 20% U-235, a thin Zr interlayer/diffusion barrier, and a relatively thick outer cladding of 6061 aluminum. The Reactor Conversion Program is investigating several alternative approaches in order to rapidly determine the most cost-effective and robust method for manufacturing the plate fuel.

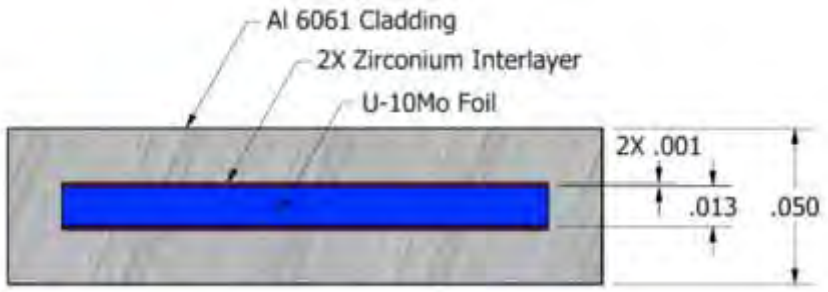

Figure 1. Nominal As-Bonded Geometry of the USHPRR U-10Mo Fuel Prior to Final Shaping (units in inches)

These alternative technologies, which include electromagnetic pulsed joining, co-extrusion, chemical vapor deposition, and physical vapor deposition, either have been, or are currently being, investigated for applying the Zr interlayer. The objective of this research was to develop a plating process that will produce a uniform zirconium metal coating nominally 25 µm in thickness onto U-10Mo foils. This process needs to be both reproducible and scalable.

2. Background

Electroplating (plating) has been used for many years as a very economical method to apply metallic coatings on metallic substrates. However, ions such as Zr, cannot be held in an aqueous electrolyte without oxidizing, so traditional aqueous plating processes will not work. Therefore, plating of Zr ions requires a different electrolyte that can retain a stable Zr ion in solution. For metals such as Zr, Mo, Ti, and U, a molten salt can be used as an electrolyte. In a molten salt electrolyte, the Zr can be retained in an ionic form without oxidizing, which enables plating to occur in a manner similar to conventional aqueous solution plating. Among the differences between salt and aqueous electrolytes are temperature, diffusion rates of the ions, and sensitivity to the surrounding environment. High temperatures are needed to keep the salt in a liquid form, and often combinations of salts are used to control the melt point. The salts are sensitive to moisture absorption, which can cause oxidation of the ions and prevent plating, so molten salt baths must be maintained in dry atmospheres, and plating must be performed under inert gas. Molten salt electrolytes that have been investigated include pure fluorides (Mellors and Senderoff 1963; Mellors and Senderoff 1966; Senderoff and Mellors 1966; Groult et al. 2011; Groult et al. 2008; Nissen and Stromatt 1968), pure chlorides (Basile et al. 1981; Flengas et al. 1968; Girginov et al. 1995; Kipouros and Flengas 1985; Lister and Flengas 1965; Malyshev et al. 2010), and mixed chlorides and fluorides (Malyshev et al. 2010; Guangsen et al. 1990; Smirnov et al. 1973; Winand 1962).

Fluoride electrolytes have advantages with respect to the simplicity of reduction reactions (Mellors and Senderoff 1966; Malyshev et al. 2010). In these fluoride salt bath studies, the cathodic processes were attributed to a reaction, which involved a single step involving a four-electron transfer (Mellors and Senderoff 1966; Mellors and Senderoff 1963; Senderoff and Mellors 1966).

In a later study, Nissen and Stromatt (1968) used molten fluoride electrolytes to deposit zirconium metal onto uranium substrates. The conditions used in this study included: a KF-LiF eutectic electrolyte containing 2 to 10 wt% ZrF_4, a Zr metal anode, a 635–675°C deposition temperature, and 20 to 40 mA/cm^2 current density. They obtained coating thicknesses to ~125 µm while maintaining fine grain sizes and few pores. The bath required continuous purification, primarily avoiding moisture, to maintain coating quality.

3. Electroplating at PNNL

A number of salt combinations were initially tested at PNNL. Most of the development work was conducted on a salt bath consisting of LiF:NaF:ZrF_4 = 26:37:37 mol%. Good plating was achieved on both copper and molybdenum substrates. However, once the substrate was changed to depleted U-10Mo (DU-10Mo), an interaction with the salt bath was discovered. It was found that UF_3, and possibly some UF_4 (here after referred to as UF_x), was produced on the foil. This was caused by the spontaneous reaction between ZrF_4 and uranium metal to form UF_x. This reaction occurred at all temperatures at which the bath was molten. There was no mention of this reaction in the literature. Two main concepts were pursued to prevent UF_x from forming: 1) increase the cathodic potential on the DU-10Mo above the free energy of formation for the UF_x, thus preventing the UF_x from forming on the foil, and 2) use alternative bath chemistries consisting of mixtures not containing ZrF_4, which would therefore not react with the uranium.

When attempting to plate with the LiF:NaF:ZrF_4 mixed salt bath, significant amounts of UF_x were formed. Three reactions between the ZrF_4 and the U metal are energetically favorable to form:

1. $U + 3ZrF_4 = 3ZrF_3 + UF_3$
2. $U + ZrF_4 = Zr + UF_4$
3. $U + 1.5\ ZrF_4 = 1.5ZrF_2 + UF_3$

The plots in Figure 2 show the formation energies of these reactions as a function of temperature and the corresponding cathodic potential needed to prevent their formation. ZrF_3 may not form due to the low formation energy, but there was evidence that Zr metal formed in the absence of a plating voltage. Figure 3 shows the results of the DU-10Mo sample inserted into the salt bath with no applied potential and then allowed to react for 10 min. There is clearly a thin layer of Zr metal on the outside of the UF_x layer. This is only possible if the U metal reduced the ZrF_4 completely.

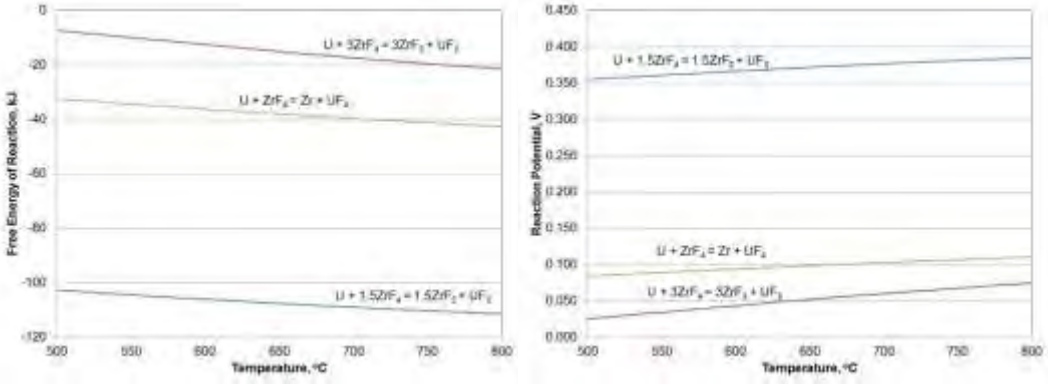

Figure 2. Calculated Free Energy of Formation and Required Cathodic Potential to Prevent Interaction of ZrF_4 and Uranium

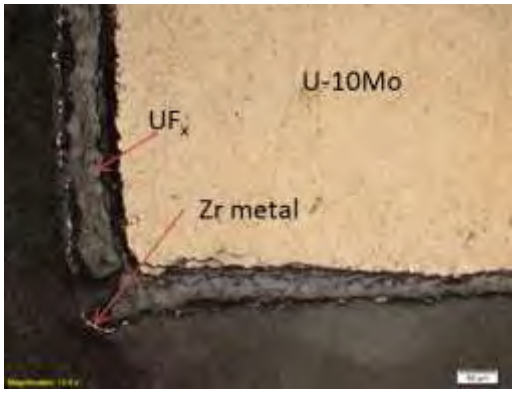

Figure 3. U-10 Mo Sample Inserted in Salt Bath with No Potential for 10 min

In an attempt to prevent the uranium from reacting with the ZrF_4, a number of tests were conducted in which the DU-10Mo was inserted into the bath with an applied potential above that needed to prevent the UF_x from forming. The insertion voltage was varied between 0.275 volts and 5 volts in an effort to mitigate this problem. The voltages were measured as a 4-point measurement taken at the sample and anode just above the salt surface. The measurements include the anode and cathode polarizations, the bath resistance, and some ohmic loss from current flow in the sample and anode. At potentials of less than one volt, the U was not protected from forming UF_x. At a 1-volt insertion potential, most of the sample was protected, but the edges still had moderate dendritic growth and some UF_x formation.

Increasing the insertion voltage to 2 volts resulted in a sample with complete encapsulation with a thickness of 15μm ±5μm. Dendritic growth was present across the sample. Figure 4 shows both edges of the cross-sectioned 2 volt sample at 100X. No UF_x was found on the sample. The DU-10Mo sample had complete wrap around coverage at the ends perpendicular to the anode, but the dendritic growth was higher than desired

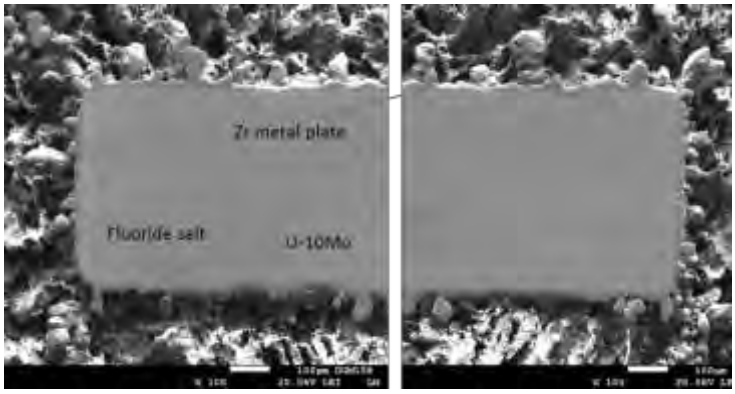

Figure 4. SEM image of the 2V, DU-10Mo sample, at 100X Magnification. No UFx is found between the Zr and the DU-10Mo, and the Zr plating completely encapsulates the DU-10Mo

The initial bath looked promising at higher voltages on small samples. However, these conditions would be difficult to scale up. Maintaining a sufficient voltage over the length of a 92 cm long sample would have been challenging due to the ohmic loss associated with the DU-10Mo resistance. This would be especially true since these voltages correspond to high current densities (>2 A/cm^2). Therefore, the new approach was to try to adopt a salt bath that did not contain any ZrF_4.

The bath tried for the next set of tests was a LiF:NaF plating bath at the eutectic molar ratio of 61 to 39 mol%. This salt bath did not contain any ZrF_4, and therefore did not react with DU to form UFx. The eutectic temperature of this bath was 652°C, which is much higher than the initial bath mixture NaF:LiF:ZrF_4 of 436°C. Realistically, the lower temperature limit on plating with the bath was around 700°C. Due to there being no ZrF_4 in the bath, the only way to get good plating on the samples was to operate in a pulse plating mode. Plating was observed on the samples, but the time to achieve the desired plating thickness was increased to around 2 hours. The combination of the higher temperature and the long plating time resulted in the approximately half of the plating reacting with the Mo in the foil, most likely to form Mo_2Zr, as shown if Figure 5. This interaction is not unexpected and should enhance the bond between the two layers, but it is excessive for the final product. Additional bath chemistries were attempted with little to no success. With programmatic milestones looming the decision was made to look outside the lab for additional help.

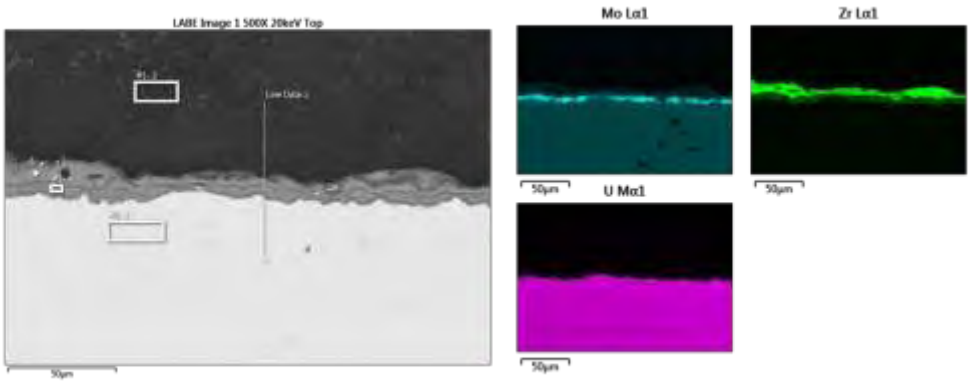

Figure 5. LiF:NaF pulsed plating sample with interaction between the Mo and Zr.

4. Electroplating at Plasma Processes

Due to the limited experience of PNNL with electroplating with molten salt, outside help was solicited. Plasma Process is one of the few companies in the world with extensive experience electroplating with molten salts. Most of their work involves plating metals such as W, Re and Ir. Within several months of starting the project they were able to come up a proprietary salt bath that could produce good electroplated DU-10Mo foils with no interaction with the DU-10Mo. An example of one of the plating tests is shown in Figure 6.

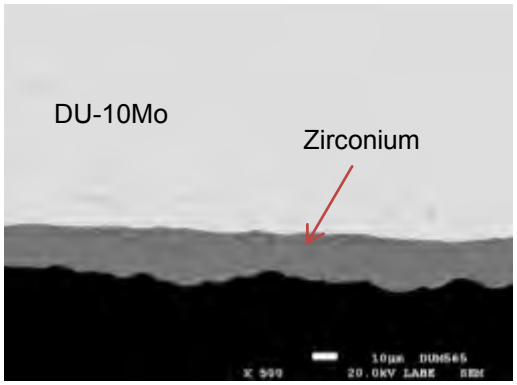

Figure 6. SEM image of the DU-10Mo sample electroplated with Zr produced at Plasma Processes.

The processing parameters are still being adjusted to improve the plating uniformity and surface finish, but the current settings are producing plated parts that would meet final specifications. No interaction with the plating bath has been observed to date. One issue that has arisen during the early testing is that the plating debonds as shown in Figure 7 upon cleaning the residual salt from the sample in hot water. The debonding was not apparent right after removal from the plating system and it is not clear if it was the result of the cleaning process or if it resulted from poor adhesion. Significant progress has been made in eliminating this failure mode. A two

pronged plan was used to address the issue consisting of a) improving the surface of the DU-10Mo foil before plating and b) changing the method to remove the residual salt from the sample.

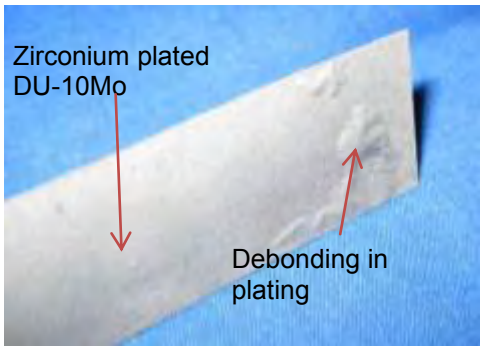

Figure 7 Photograph of a plated foil after salt removal showing poor adhesion in one section.

The samples that Plasma Processes coated were fabricated at PNNL. The samples were sheared from rolled foil and then annealed in Ar. The final cleaning step before shipping was an etch in 8 molar nitric acid for 10 minutes, rinsed first in deionized water and then in ethanol to facilitate drying. The samples appeared to be clean with very little oxidation, but after aging a few weeks the samples had a noticeable tea color to them. This small amount of oxidation does not appear to affect the plating, but it may have an impact on the adhesion of the film. To remove the oxide scale, several different techniques were tried. A paper by Gore et al. out of Los Alamos in 1957 has a section on electropolishing of uranium. They found that application of an anodic current to a sample in a bath of 75 vol.% H_2SO_4 with 15 g/L of CrO_3 kept the sample oxide free for days to weeks after electropolishing. This would be advantageous due to the time lag involved in shipping samples from PNNL to Plasma Processes, so the approach was tried. The same solution was prepared and an anodic current of 0.078 A/cm² was applied for 10 min at 30°C. The samples were extremely shiny, as shown in Figure 8, and they did not appear to oxidize for at least a week.

Figure 8 Du-10 Mo sample Electropolished for 10 min.

Samples were also prepared with only the sulfuric acid (no chromic oxide). They too appeared very shiny after cleaning, but would start to show the tea color of uranium oxide after a few days, indicating that a small amount of chrome was being left on the surface in the original bath

that retarded the oxidation of the uranium. One other set of samples were electropolished the same as the first set, but then a cathodic current was applied in an attempt to place a thin chrome strike on the surface of the DU-10Mo. Samples of electropolished DU-10Mo with chrome in solution and the samples with a chrome strike were sent to Plasma Processes for plating.

Unfortunately after plating, the electropolished samples still have some debonding in the coating after removal of the residual salt. This was also the case with the samples with the chrome strike. In fact, the samples with the chrome strike had some of the worst debonding of any of the samples plated. One of the chrome strike samples had the residual salt removed with alcohol to try and see if changing the method of removing the salt would matter, but it too showed significant debonding of the plating. It was concluded that, although the chrome may prevent oxidation of the DU-10Mo, it had a negative effect on the bond strength of the plating and was no longer pursued.

The other method used for cleaning the DU-10Mo was to reclean the samples with the same 8 molar nitric solution at Plasma Processes just before plating. The procedure was changed slightly in that Plasma Processes did not do a D.I. water rinse after the acid etch, but removed the residual acid solution with ethanol. In the initial test it appeared that water was causing the DU-10Mo foils to oxidize. Two samples were then plated with the residual salts removed with hot water. One of the samples still had debonding of the plating. The test was repeated, but this time the residual salts were removed with ethanol in an ultrasonic cleaner. This combination of acid etch before and ethanol rinse to remove the residual salt appears to has mostly eliminated the debonding of the plated foil, as shown in Figure 9. The debonding that is currently occurring does not happen right after cleaning. It may take several days to occur. It may be the result of a small amount of residual salt left on the part which is slowly reacting with the atmosphere.

Figure 9 DU-10Mo foil acid etched in 8 molar nitric; residual salt removed with ethanol.

The exact cause of the bubbling is still not known, but it may be the result of water interaction with either the zirconium plate or the DU. However the preparation of the DU-10Mo surface still has an impact since the one chrome strike sample also had the salts removed with ethanol but it still debonded.

Plasma Processes has now installed an identical system to theirs at PNNL and the production of test samples for reactor testing will begin sometime in 2016.

5. References

Basile F, E Chassaing, and G Lorthioir. 1981. Journal of Applied Electrochemistry 11, 645.

Flengas SN, JE Dutrizac, and RL Lister. 1968. Canadian Journal of Chemistry 46, 495.

Girginov A, TZ Tzvetkoff, and M Bojinov. 1995. Journal of Applied Electrochemistry 25, 993.

Groult H, A Barhoun, E Briot, F Lantelme, and CM Julien. 2011. Journal of Fluorine Chemistry 132, 1122.

Groult H, A Barhoun, H El Ghallali, S Borensztjan, and F Lantelmea. 2008. Journal of the Electrochemical Society 155, E19.

Guangsen C, M Okido, and T Oki. 1990. Journal of Applied Electrochemistry 20, 77.

Kipouros GJ and SN Flengas. 1985. Journal of the Electrochemical Society 132, 1087.

Lister RL and SN Flengas. 1965. Canadian Journal of Chemistry 43, 2947.

Malyshev V, A Gab, A Izvarina, AM Popescu, and V Constantin. 2010. Revue Roumaine De Chimie 55, 179.

Mellors GW and S Senderoff. 1963. Journal of the Electrochemical Society 110, C180.

Mellors GW and S Senderoff. 1966. Journal of the Electrochemical Society 113, 60.

Nissen DA and RW Stromatt. 1968. Zirconium Electroplating on Uranium from Molten Alkali Fluoride Salts, Battelle-Northwest.

Sakamura Y. 2004. Journal of the Electrochemical Society 151, C187.

Salannea, M, 2009, Journal of Fluorine Chemistry, 130,61-66

Senderoff S and GW Mellors. 1966. Science 153, 1475.

BURNABLE ABSORBER OPTIMIZATION IN A SUPER-FLUX RESEARCH REACTOR UTILIZING PLATE-TYPE FUEL

XUAN HA NGUYEN, PAOLO VENNERI, YONGHEE KIM*

Dept. of Nuclear and Quantum Engineering, Korea Advanced Institute of Science and Technology

291 Daehak-ro, Yuseong-Gu, 305-308 Daejeon, Korea

PHILIP BEELEY

Department of Nuclear Engineering, Khalifa University

PO Box 127788, Abu Dhabi, UAE

ABSTRACT

A novel and high performance 20-MWth plate-type pool research reactor based on coated particle fuel was successfully developed [1-2]. This research reactor has been documented to produce very high thermal and fast flux, on the order of 10^{15} and 10^{14} neutrons/cm^{2}s, respectively. Moreover, it has also improved on the inherent safety of research reactors by having a larger negative reactivity feedback due to the use of the low-enriched UO_2 coated particle fuel (CPF). The reactor is designed to operate using a 3-batch refueling cycle resulting in reduced fuel costs. However, the equilibrium core maximum excess reactivity is found to be relatively high, about 7000 pcm. In this paper, a physics study is performed to reduce the core reactivity by applying burnable absorbers (BAs) to the core. In particular, the amount and the shape of the BAs are optimized to reduce its self-shielding effect so as to minimize the burnup reactivity swing (BRS) while assuring sufficient reactivity is available for core criticality throughout the simulated irradiation cycle. A minimal BRS can help to avoid prompt core criticality, diminish control rod burden, and provide a higher reactivity margin, which thereby assures better reactor control and safer core operation. Several BAs such as Gadolinium and Cadmium are at first investigated as the potential BAs for a single-batch core and are then applied to the 2-batch cycle equilibrium core. Other major neutronics characteristics of the core such as the power profile, rod worth and temperature coefficients of reactivity are also evaluated. The neutronics analyses are completed using the Serpent 2 Monte Carlo code with the ENDF/B-VII.1 nuclear library.

1. Introduction

Research reactors have played a very important role in nuclear technology as the main neutron sources utilized in various kinds of nuclear applications such as materials activation, medical and industrial isotopes production, etc. In addition to high performance in terms of thermal and fast neutron spectrum fluxes, inherent safety features are also significant design considerations for research reactors. Moreover, by utilizing low enriched uranium in combination with a simple design and competitive capital costs can increase the proliferation resistance of the reactors and enable their implementation in developing countries. In this regard, a pool-type, super-flux, 20MWth research reactor has been successfully developed utilizing the new plate-type fuel assembly concept based on existing and well-proven CPF technology [1-2].

Another significant consideration is to pursuit efficient core reactivity management. An elegant way for such reactivity management is the use of neutron-absorbing materials in the core. By introducing the use of neutron-absorbers, the excess reactivity and reactivity swing can be minimized, therefore reducing the probability of prompt core criticality and enabling better reactor control and safer core operation.

Typically, in water-cooled reactors there are three forms of neutron-absorbing materials: control rods, burnable absorbers and chemical shims. This paper mainly focuses on the use of burnable absorbers to control the core reactivity. Generally, a burnable absorber is any nuclide which has a large neutron capture cross-section. After absorbing a neutron, the burnable absorber transmutes into a less-absorbent isotope which no longer affects the core reactivity. For water-cooled reactors, there are several potential burnable absorbers: gadolinium (Gd), cadmium (Cd), erbium (Er) and boron (B). In detail, Gd and Cd are very strong

neutron absorbers that require only small amounts in the core in order to achieve an appreciable reactivity depression. Due to their strong absorption cross section, they burn out at the beginning of cycle (BOC), making them difficult to be employed in a reactor with a long cycle. It is, however, easy to manipulate their self-shielding effects and resultantly minimize the reactivity penalty at the end of cycle (EOC). In contrast, the capture cross section of B is quite smaller than that of Gd, Cd, and Er, leading to the use of larger amounts of B to get a similar reactivity depression as other isotopes. It should be noted that the B^{10}(n, alpha)Li^{7} reaction generates gaseous helium, which should be taken into account when using boron as a burnable absorber as it can lead to the creation of voids in the material and accelerate the formation of material defects. On the other hand, Er depletes rather slowly owing to its relatively low capture cross section. However, Er has a unique thermal absorption resonance which can lead to an enhanced moderator temperature coefficient (MTC) [3]. In short, both B and Er are suitable to be employed in a reactor with long burnup cycle.

In current nuclear technology, burnable absorber design is classified into two types: integral or discrete absorbers. Integral absorbers are implemented in the fuel region through the use of poison particles [4], adding a poison coating to the fuel particle or pellet, or mixing it homogenously with the fuel matrix [5]. Obviously, it is easy to implement an integral burnable absorber since it does not require additional components. However, it may cause several adverse effects in the fuel which should be taken into account: changes in thermal-mechanical properties, gaseous buildup, and complications in fuel design. Discrete absorbers, on the other hand, are usually deployed in a non-fuel region in the fuel assembly lattice such as the guide thimble [6] or simply replacing a fuel rod [7]. The advantage of discrete absorbers is to avoid the drawbacks of integral burnable absorbers. Nevertheless, it reduces fissile inventory in the case of replacing fuel rods and the compatibility with non-fuel material should be considered.

In regards to the discussion above, an effective strategy for loading burnable absorbers into the research reactor with a single and 2-batch fuel cycle is discussed in the following sections. The neutronics analyses and design work are performed using Serpent 2 with the ENDF/B-VII.1 library. Other major neutronics characteristics of the core such as rod worth, power defect and temperature coefficients of reactivity are also evaluated.

2. Conceptual Research Reactor Design with Burnable Absorber

2.1. Innovative Fuel Design

The key innovation at the heart of the proposed reactor design is the new proposed fuel concept: plate elements with embedded Coated Particle Fuel (CPF). The innovation of this new fuel type lies in the combination of two well-known and tested fuel technologies: Aluminum matrix plate fuels and CPF [1-2].By combining these two, the new fuel is able to achieve heightened levels of safety while offering the possibility of a simple and economical fuel design.

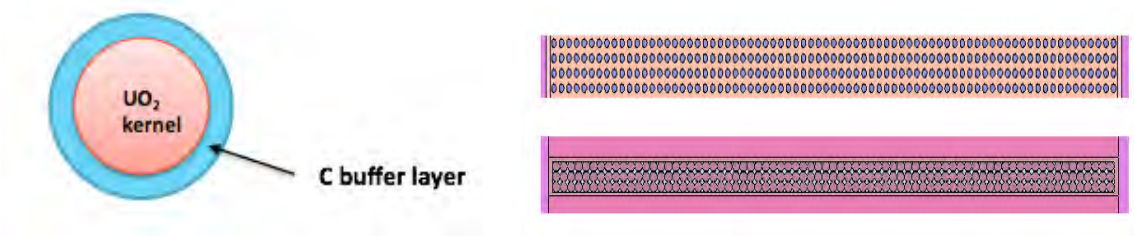

Figure 1. CPF design, axial and radial fuel plate configuration.

In contrast to previous the design in [1], the current fuel implements a regular lattice in order to prevent the occurrence of hot spots due to an uneven distribution of fuel particles in the plate [2]. A schematic of the plate and detailed parameters showing the new fuel concept are illustrated in Fig. 1 and Table 1. The objective of this is to enhance the ability of the fuel to confine fission products in case of an accident, increasing its mechanical strength and fuel loading per plate, as well as taking into account the thermal hydraulic conditions of the reactor

with the aim of maximizing the fuel temperature. This new design also allows the placing of the fuel particles such that axial layers sharing gas plenums are formed with a discrete separation, preventing a single point fuel failure. The fuel meat is then encased by the Al cladding surrounding the fuel element.

Parameter	Value
Fuel kernel radius	0.370 mm
Buffer outer radius	0.380 mm
Particle packing fraction	46.25%
Fuel parking fraction	42.70%
UO2 density	10.4 g/cc
Fuel meat thickness	2.28 mm
Cladding thickness	0.30 mm

Table 1: Fuel Configuration

2.2. Burnable Absorber Integrated with Fuel Assembly Design

One should emphasize that the objective of the proposed research reactor is to have a simple fuel design, resulting in possibly economical fuel fabrication costs. Consequently, an integral burnable absorber is not desirable as it would seriously increase the complexity of the fuel. In this regard, the discrete burnable absorber design is preferable, which means the burnable absorber is loaded in the non-fuel region. Furthermore, the loading position in the non-fuel region should satisfy following requirements:

- Avoid manipulation of coolant flow
- Achieve effective reactivity depression
- Not influence the thermal and mechanical properties of the fuel element
- Not replace any fuel element

By integrating the burnable absorber in the assembly aluminum side plate as shown in Fig. 2, all of the requirements are met. Moreover, the performance of the burnable absorber strongly depends on its self-shielding properties which can be manipulated by adjusting its geometric shape. In this paper, the poison is implemented as a long ribbon that runs the length of the side plate (70 cm long). This allows the easy manipulation of the self-shielding of the poison and uniform depletion of the absorber in the axial direction. The optimal burnable ribbon configuration was determined by varying the volume, the width-to-depth ratio (aspect ratio) and number of ribbons.

Moreover, based on the linear burnup equation, the cycle length ranges from about 1 to 2 months corresponding to 3 and single-batch fuel cycles [2], which are relatively short. Therefore, the selection of burnable absorber is limited to Gd and Cd due to their large neutron capture cross sections and resulting small reactivity penalty. Besides, Gd and Cd are compatible with the aluminum side plate since they are both metallic elements.

The loading strategy is also dependent on the number of fuel batches. In the current work, the single and 2-batch fuel cycles are considered. The fuel assembly design for both single and 2-batch fuel cycles are similar, as listed in Table 2, with the only difference being the number of ribbons integrated into the side plate, as shown in Fig. 2. For a single-batch cycle, the cycle length is set to be 60 days and the total number of ribbons is found to be 10 per assembly, consisting of two ribbon types with different aspect ratios (AR), volumes, and poisons, as illustrated in Fig. 2. Two types of ribbons enable the flat reactivity curve throughout the relatively long cycle of 60 days. For the 2-batch cycle, the equilibrium cycle length is 40 days of operation with a cooling period of 10 days. As a result of its short cycle length, the number of ribbons is 6 per assembly with only a single aspect ratio for the ribbons.

Another constraint for the loading strategy is that the excess reactivity during the cycle should never be lower than 400 pcm. This will ensure that sufficient reactivity is available for core criticality throughout the simulated irradiation cycle, except for almost zero reactivity at

EOC condition. In addition, the excess reactivity after Xenon equilibrium conditions have been reached should be around 1000 pcm to avoid prompt criticality accidents and reduce the burden on the active reactivity control system.

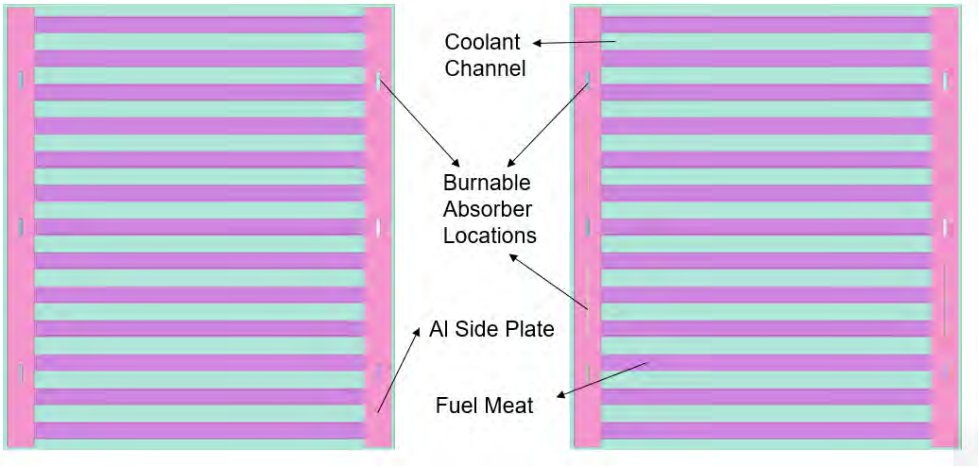

Figure 2. Plate fuel assembly designs for single- and 2-batch cycle.

Parameter	Value
FA size	75 x 65.47 mm
Number of fuel plates per FA	13
Fuel plate width (+ side clad)	56.37 mm
Fuel meat thickness	2.28 mm
Fuel meat width	55.49 mm
Clad thickness	0.30 mm
Fuel plate active height	629.52 mm
Fuel plate total height (+axial clad)	700.00 mm
Side plate thickness	4.55 mm
Volume fraction (fuel plate/coolant/side plate)	38.31% / 48.91% / 12.78%
Water channel thickness	2.889 mm
Water gap thickness between FA	0.2 mm
U mass per plate	0.312 kg
U mass per FA	4.056 kg

Table 2: Fuel Assembly Configuration

2.3. Core Design

The core presented here is a 20 MWth pool-type research reactor which implements box type fuel assemblies. Twelve fuel assemblies are arranged in a square lattice around a central flux trap inside of a beryllium box. The fuel assemblies are then surrounded by a beryllium reflector consisting of beryllium blocks measuring 80x80 mm. Distributed throughout the reflector region are two types of flux traps in addition to the central flux trap. These flux traps consist of cylinders of water in the beryllium elements of the reflector region and the central beryllium element. The flux traps are summarized in Table 3 and Fig. 3.

Irradiation Hole	Guide Tube Inner Radius	Guide Tube Outer Radius	Be Box Dimensions
1-8	37.5 mm	38.5 mm	80 mm x 80 mm
A-D	30 mm	31 mm	165 mm x 80 mm
Central	55 mm	60 mm	152 mm x 152 mm

Table 3: Irradiation hole geometries.

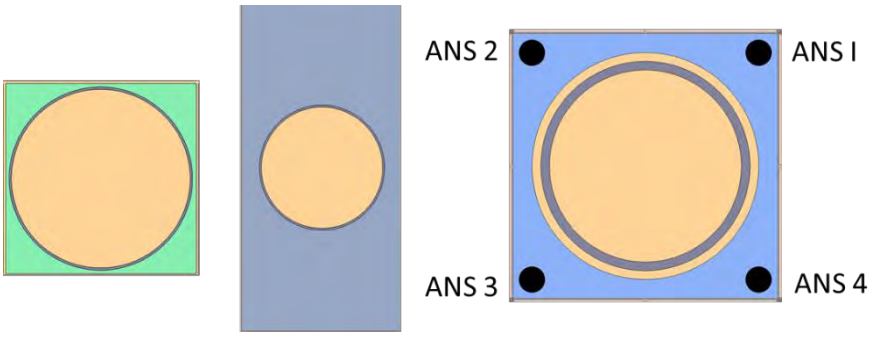

Figure 3. Geometry for 1-8, A-D, and central irradiation holes from left to right.

Among the fuel assemblies there are 4 Hafnium L-blades measuring 0.5 cm in thickness acting as the primary control mechanism. Along the inside of the central flux trap is an annular Hf absorber measuring 0.3 cm thick that is the secondary control mechanism. These are shown in Fig. 4. It is noted that in the case of normal operation, the control rod region is filled with water. The entire core then rests atop an Al grid and is suspended inside a pool of water. The various core parameters are summarized in Table 4 while the radial and axial core geometries are shown in Fig. 5.

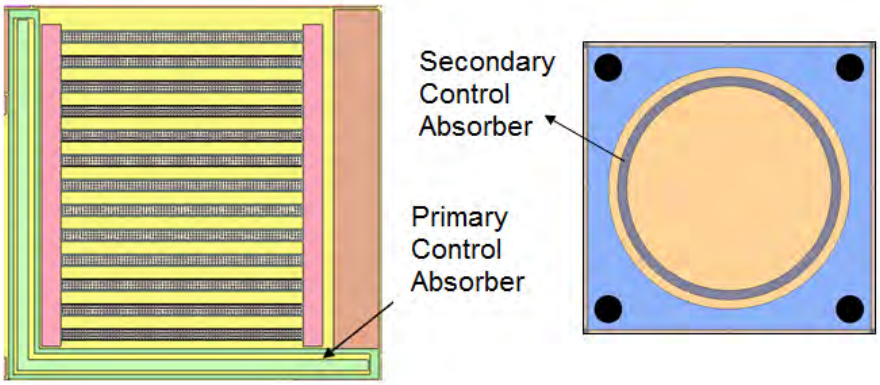

Figure 4: Primary and Secondary Control Absorber

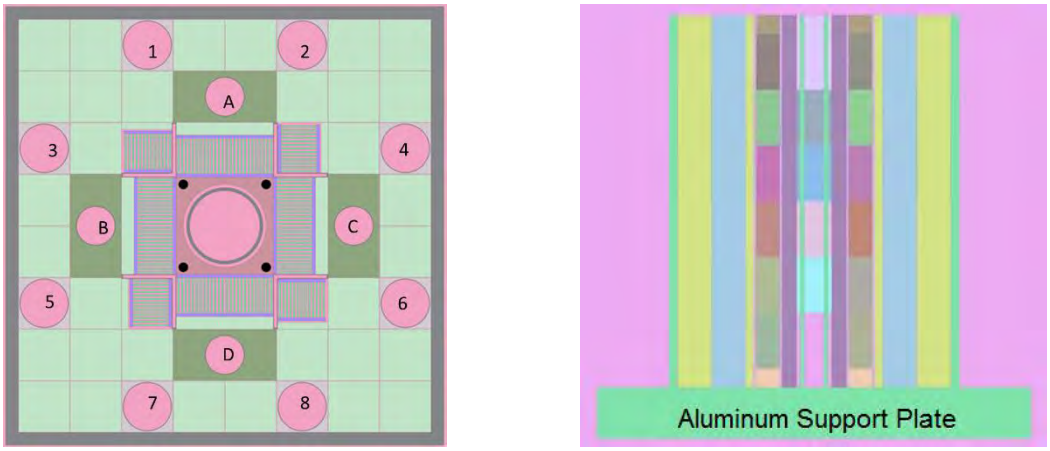

Figure 5. Radial and axial core configuration.

Parameter	Value
Thermal power	20 MW
Number of fuel assemblies	12
Number of irradiation holes	13
Uranium enrichment	19.75%
Uranium mass in the core	48.672 kg
Average coolant speed	8.42 m/s
Core inlet / outlet temperature	40.63 ^{0}C / 61.73 ^{0}C
Core pressure	1.8 bar
Al box surrounding core thickness	20 mm

Table 4: Core parameters

3. Results and Discussion.

The neutronics analyses to assess the feasibility of the application of the burnable absorber are performed using Serpent 2 [8] with the ENDF/B-VII.1 library. Other major neutronics parameters of the core such as power profile, power defect, rod worth, and temperature coefficients of reactivity are also evaluated.

3.1. Reactivity Performance

Fig. 6 depicts the multiplication factor evolution for the single-batch fuel cycle with the optimized burnable poison using natural isotopes of Cd and Gd while Table 5 summarizes important neutronic results of the simulation. Reactivity is expressed in pcm. Case 1 has 6 Gd ribbons with an aspect ratio of 5 and 6 Cd ribbons with an aspect ratio of 60. Case 2 has 6 Cd ribbons with an aspect ratio of 1 and 4 more Cd ribbons with an aspect ratio of 60. It can be seen that the k-eff behavior for both cases show a similar trend. In addition, the BOC excess reactivity is reduced from around 10500pcm to around 4900 pcm for case 2 and 4500 pcm for case 1, and the EOC reactivity penalty is rather small, around 150 pcm for both cases. The reactivity swing in case 2 is 616 pcm, which is smaller than that in case 1.

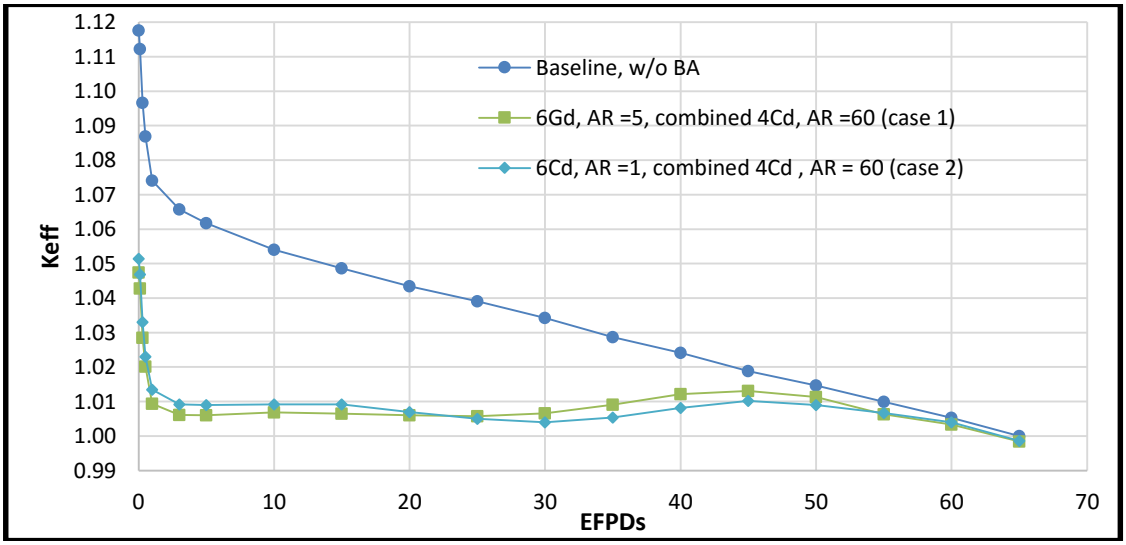

Figure 6: Multiplication factor evolution for single-batch fuel cycle

For the 2-batch cycle, a fuel shuffling scheme is simulated for the current reactor design, which is illustrated in Fig. 7. It should be noted that the fuel assembly arrangement in the 2-batch fuel cycle is asymmetric and the cycle is set to be about 40 days of operation and 10 days for cooling.

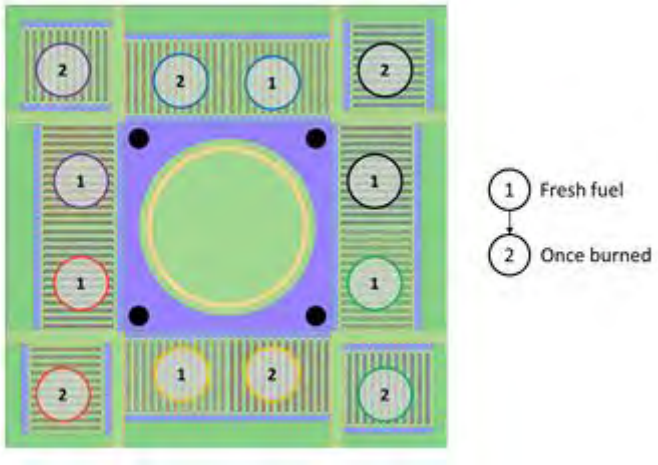

Figure 7. 2-batch fuel management scheme.

Only Cd is used as the BA in the 2-batch fuel cycle due to its better reactivity performance in the single batch compared to Gd. The volume and aspect ratio of the Cd ribbon is varied to seek the optimal case. The optimal volume of a ribbon is found to be 0.1979 cm^3. Fig. 8 and Table 5 show the k-eff value evolution and neutronic results for several aspect ratios for the equilibrium cycle.

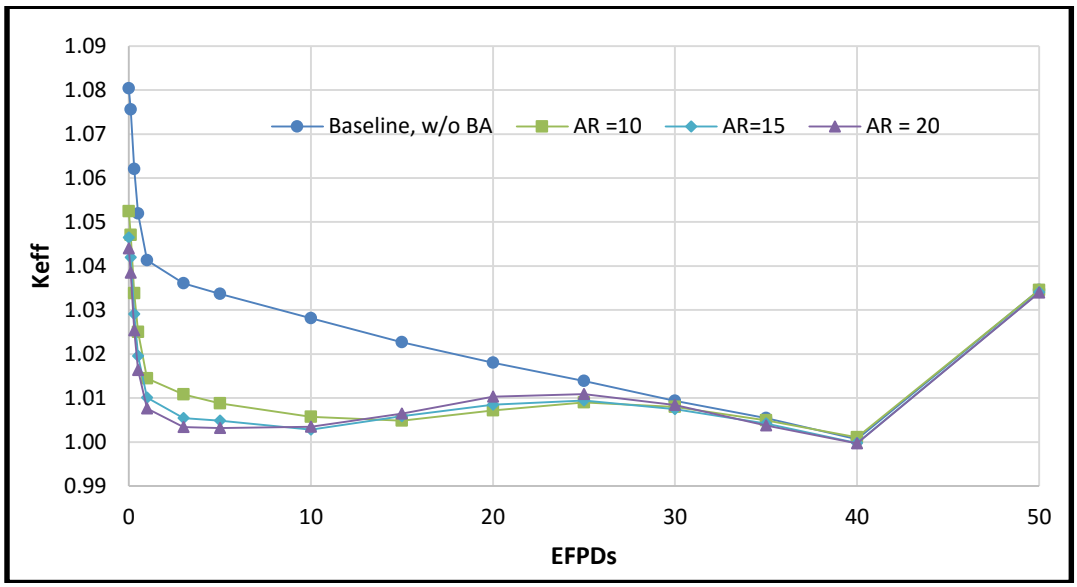

Figure 8. The keff evolution for 2-batch fuel cycle at the equilibrium cycle

	Case	Excess reactivity	EOC penalty	Lowest Reactivity	Highest Reactivity	Reactivity Swing	Std
Single-Batch	W/o BA	10519.0	0.0	-	-	-	2.3
	Case 1	4527.0	157.0	574.0	1310.0	736.0	1.4
	Case 2	4892.0	135.0	400.0	1016.0	616.0	1.5
2-Batch	W/o BA	7437.7	0.0	-	-	-	1.7
	AR = 10	4980.3	46.4	483.3	1068.9	585.6	1.6
	AR = 15	4441.0	90.1	277.0	934.6	657.6	1.4
	AR = 20	4216.9	94.6	317.2	1074.6	757.5	1.4

Table 5: Reactivity performance of single and 2-batch fuel cycle

3.2. Power Defect and Temperature Coefficient of Reactivity

Enhanced Doppler feedback is one of the chief advantages of implementing the CPF. The clearest indication of the factor can be seen in the power defect, that is the reactivity difference between hot full power (HFP) conditions and hot zero power conditions (HZP). At HFP, the entire core is at operating temperature while at HZP the core temperature is brought down to 40 °C along with a coolant density of 0.992310 g/cm3 to simulate shut down conditions. The results for the two fuel managements are summarized in Table 6. Due to the clearly negative reactivity feedback, this can be considered to be a significant enhancement to the inherent safety of the proposed research reactor.

Single-Batch	**BOC**		**EOC**	
Conditions	Reactivity (pcm)	ρ diff (HFP-HZP) (pcm)	Reactivity (pcm)	ρ diff(HFP-HZP) (pcm)
CZP	5075.07 ± 0.73		480.244 ± 0.02	
HZP	5180.05 ± 0.16	-300.73 ± 0.23	618.812 ± 0.02	-311.71 ± 0.02
HFP	4879.32 ± 0.16		307.106 ± 0.01	
2 Batch	**BOEC**		**EOEC**	
Conditions	Reactivity (pcm)	ρ diff (HFP-HZP) (pcm)	Reactivity (pcm)	ρ diff(HFP-HZP) (pcm)
CZP	4859.28 ± 0.15		181.04 ± 0.01	
HZP	4994.79 ± 0.16	-298.72 ± 0.22	314.15 ± 0.01	-309.31 ± 0.01
HFP	4696.08 ± 0.15		4.84 ± 0.00	

Table 6: Power defect for single- and 2-batch cycles at BOC and EOC

Unfortunately, the reactivity difference between HZP and cold zero power condition (CZP) is positive. That is because of large amount of water in central flux trap, which mainly governs the reactivity behavior between HZP and CZP conditions.

	Tempt. Difference(°C)	**FTC at BOC (pcm/°C)**	**FTC at EOC (pcm/°C)**
Single-Batch	20	-2.16 ± 0.37	-2.27 ± 0.36
2-Batch	20	-2.31 ± 0.24	-2.26 ± 0.24

Table 7: Fuel temperature reactivity coefficient (FTC)

In this calculation the approximate fuel and coolant temperature coefficients was calculated by the equation (1) corresponding to temperature difference from operating temperature. Table 7 and table 8 show the burnup-dependent FTC and CTC of the proposed research reactor for single and 2-batch fuel cycles. It can be seen that both FTC and CTC are clearly negative for both fuel managements at BOC and EOC.

$$FTC\ or\ CTC = \frac{\rho_{T2} - \rho_{T1}}{T_2 - T_1} \quad (1)$$

	Tempt. Difference (°C)	**CTC at BOC(pcm/°C)**	**CTC at EOC (pcm/°C)**
Single-Batch	10	-12.45 ± 0.22	-13.43 ± 0.24
2-Batch	10	-5.50 ± 0.24	-6.19 ± 0.26

Table 8: Coolant temperature reactivity coefficient (CTC)

3.3. Power Profile

The assembly-wise and plate-wise power distribution are shown on the Fig. 9 while Fig. 10 indicates the axial power distribution. The assembly-wise power distributions is uniform at BOC condition and slightly position-dependent at EOC condition. The maximum relative plate-wise power is 1.56 for the single-batch cycle and 1.59 for the 2-batch cycle at BOC condition at the outer-most plates, while the central plates in the 4 corners have the lowest relative power of 0.3 for both single and 2- batch cycles. Furthermore, the axial power is slightly bottom-skewed due to the downward coolant flow. The axial power peaking factor is about 1.3 and the lowest position witnesses the lowest axial power of 0.56.

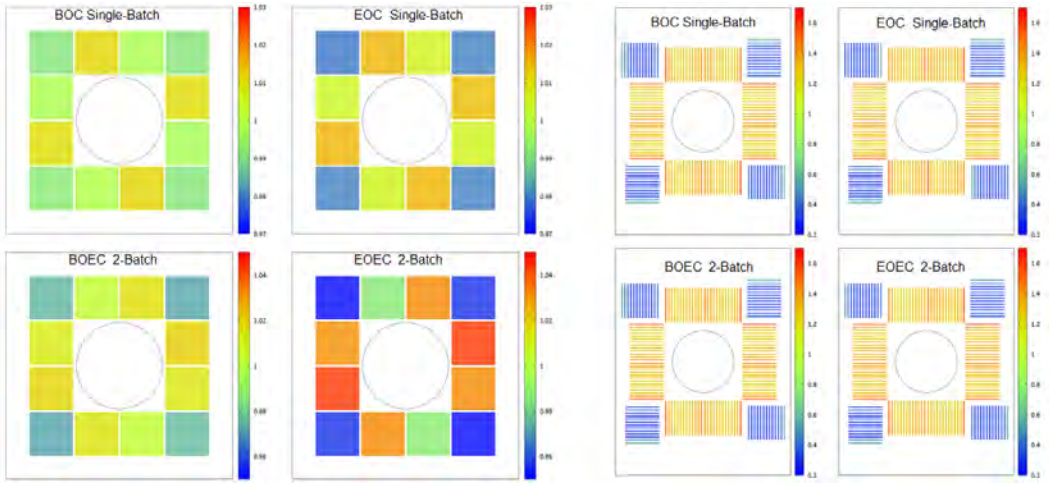

Figure 9. Assembly-wise and plate-wise power distribution

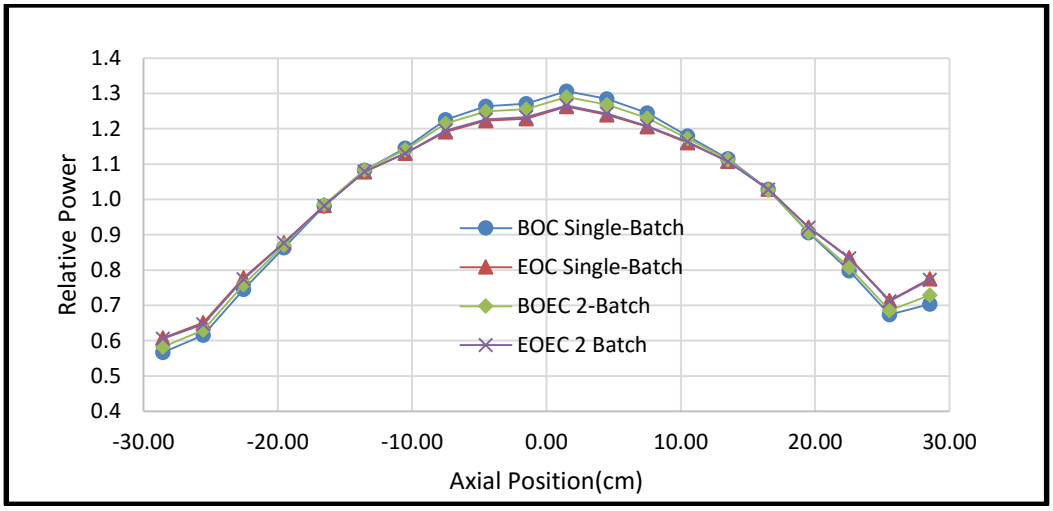

Figure 10. Axial power distribution

3.4. Shut down margin

As mentioned earlier on section 2.3, the control rods are made of metallic Hf which is compatible with the surrounding water. The primary control rod system consists of 4 L-shape metallic Hf absorbers placed in the four corners of the active core region. Meanwhile, the secondary control rod is an annular Hf absorber located inside the central flux trap. As shown in Table 9, the all rod in (ARI) worth for the primary control rod system at BOC and EOC are extremely high, greater than 20000 pcm. Meanwhile, the ARI secondary rod worth ranges from 13000 pcm to 15000 pcm.

	Single-Batch			2-Batch		
Condition	**Case**	**Worth (pcm)**	**Std. (pcm)**	**Case**	**Worth (pcm)**	**Std. (pcm)**
BOEC	ARI-Primary	21103.99	6.54	ARI-Primary	21944.27	6.59
	ARI-Secondary	12984.70	5.60	ARI-Secondary	13323.46	5.79
EOEC	ARI-Primary	23019.50	7.04	ARI-Primary	23011.45	8.16
	ARI-Secondary	14858.60	7.15	ARI-Secondary	14998.48	7.20

Table 9: Primary and secondary rod worth

4. Conclusion and Future Work

A ribbon-type burnable absorber integrated with the fuel assembly design has been successfully implemented into the proposed reactor, showing good performance in minimizing the BRS, BOC excess reactivity, and EOC reactivity penalty for both single and 2-batch fuel management. The advantage of having a minimal BRS and BOC excess reactivity is to avoid the prompt criticality and reduce dependency on active reactivity control systems, which then enhance the reactivity control of the core and reactor safety.

Additionally, among several potential burnable absorbers Cd has the best reactivity performance, which can be applied to the multi-batch fuel cycle. Also, the neutronics analyses indicate that the reactor has inherent safety features, clearly negative FTC and CTC due to utilizing the innovative plate-type fuel design.

However, one consideration that should be taken into account in future work is the positive reactivity difference between HZP and cold zero power condition (CZP).

5. Acknowledgement

This research was supported by the KUSTAR-KAIST Institute, KAIST, Korea. The authors thank Donny Hartanto for his contribution to the paper.

6. References

[1] Rully Hidayatullah, Donny Hartanto, and Yonghee Kim, "A Novel Research Reactor Concept Based on Coated Particle Fuel," Annals Nucl. Energy, vol.77 pp.477-486 (2015).

[2] Paolo Venneri, and Yonghee Kim, "Extreme Performance Multibatch Research Reactor based on Simple Plate Fuel," Trans. Am. Nucl. Soc., vol. 113, pp. 1067-1069 (2015).

[3] J.R. Secker & J.A. Brown, “Westinghouse PWR Burnable Absorber Evolution and Usage”, Winter ANS Conference, American Nuclear Society (2010)

[4] J. L. Kloosterman, “Application of Boron and Gadolinium Burnable Poison Particles in UO_2 and PuO_2 fuel in HTRs”, Annals of Nuclear Energy 30 (2003) 1087-1819

[5] S.Y. Yamanaka et al., “Thermal and Mechanical Properties of (U,Er)O2”, Journal of Nuclear Materials, volume 389, pp. 115 – 118 (2009)

[6] Mohd-Syukri Yahya, and Yonghee Kim, "Burnable absorber-integrated Guide Thimble (BigT) - II: applications to 3-D PWR core design," Journal of Nuclear Science and Technology, Available online, 2016.

[7] Chang Keun Jo, Yonghee Kim et al., “Burnable Poison for Reactivity Management in VHTR”, Annals of Nuclear Energy, 36 (2009) 298-304

[8] J.Leppänen, Serpent – A Continuous Energy Monte Carlo Reactor Physics Burnup Calculation Code, VTT Technical Research Centre of Finland, Finland (2012)

ALL-IN-ONE CHEMICAL CLEANING AND DEOXIDATION PROCESS FOR MONOLITHIC URANIUM-MOLYBDENUM FOILS

C. SCHWARZ, T. DIRKS, B. BAUMEISTER, C. STEYER, W. PETRY

Technische Universität München, Forschungs-Neutronenquelle Heinz Maier-Leibnitz (FRM II)
Lichtenbergstr. 1, 85748 Garching bei München

ABSTRACT

Monolithic uranium-molybdenum foils quickly oxidize and therefore have to be cleaned and deoxidized before further processing. This is currently mostly performed by a multi-step process including highly-concentrated nitric acid and sodium hydroxide, which require great handling care. Furthermore, the use of these chemicals is not allowed in some facilities due to their highly corrosive properties. A newly investigated acid-free cleaning process is based on an all-in-one mixed solution of proven industrial alkaline and tensidic components and a small amount of hydrogen peroxide, all of them in concentrations less hazardous than the chemicals used in current processes. Furthermore, the single-step process is less time-consuming, easier to perform and delivers higher cleaning power and surface quality, which has been confirmed by SEM and EDX analysis

1. Introduction

Researchers worldwide attempt to develop a nuclear fuel with high density based on U-Mo alloys for more than a decade [1]. The Technische Univsersität München (TUM) supports this research and aims for a conversion of the currently used disperse U_3Si_2 nuclear fuel in its high-flux neutron source Forschungs-Neutronenquelle Heinz Maier-Leibnitz (FRM II) to U-Mo fuel [2,3]. To achieve this, TUM examines conversion scenarios for FRM II [4,5] as well as U-Mo metallurgy [6] and processing of U-Mo [7]. Concerning the processing, TUMs focus for monolithic fuel plates lies on the coating with a thin Zr layer, and AlFeNi as cladding material.

An industrial manufacturing process is in current development for the monolithic U-Mo fuel plates [8,9]. The application of the Zr layer, which serves as interdiffusion barrier layer between the U-Mo and AlFeNi, is a crucial step in this process. A good bonding quality of Zr coating to the U-Mo foil is essential not only for the subsequent cladding application process, but also to ensure adequate fission heat transfer and to avoid swelling induced delamination during reactor operation of the fuel plate.

Cleanliness of the U-Mo foil surface has a major effect on the bonding quality. Surface contaminations such as impurities, dust, oxides or remaining agents from the rolling process of the foils with only weak bonding to the underlying bulk material degrade the contact area and therefore do not contribute to the adhesion. Hence, the overall bonding strength is reduced. Especially when handled in air, blank U-Mo foils are prone to the formation of brittle large-area oxide layers due to the rapid oxidation of U in contact with O_2. Thus, a proper

cleaning of the monolithic U-Mo foil is mandatory to ensure sufficient interface cleanliness right before application of the Zr coating.

A well-known cleaning method in this respect is a multi-step process of bathing the raw U-Mo fuel foil in several solutions, including a degreaser as first step, NaOH at 60 °C as second step and highly corrosive HNO_3 as deoxidation step for 6 minutes each [10]. It has already been shown that alkaline solutions like NaOH with addition of H_2O_2 provide slightly better surface quality after cleaning than pure HNO_3 [11]. To investigate this further, an industrial alkaline builder was chosen with a little H_2O_2 added and the surface quality of U-Mo foils prior and after the treatment exmined to characterize the resulting cleaning effect in comparison to the cleaning with HNO_3.

2. Materials and methods

Several foil pieces were examined with a size of about 100 mm². These have been cut from a larger foil of depleted uranium (DU) with 10 wt.% Mo still in as-fabricated state (Figure 1), but stored in air for more than a year. An optical microscope and SEM (scanning electron microscopy) were used to study the surface structure of the oxidized and cleaned foils while the elemental composition of the foil surface was analyzed via EDX (energy-dispersive X-ray spectroscopy).

Figure 1: Oxidized DU-10wt.%Mo foil. Clearly visible is the thick black U oxide layer on the foil surface.

To get an indicator for the quality of the cleaning procedures regarding surface effects and oxygen concentration, the foils were inspected before and after the chemical cleaning. However, it should be remarked that EDX measurements do actually not determine the material composition of the topmost atomic layer of the surface exclusively, but the mean composition of the upper layer up to a depth of 2-3 µm. Consequently, EDX will measure either only the oxide layer (if layer thickness of oxide is > 2-3 µm) or a mixture of oxide layer and bulk material (if layer thickness of oxide is < 2-3 µm). Furthermore, uncertainties in the EDX measurements of O due to the finite oxygen partial pressure in the SEM vacuum chamber have to be taken into consideration.

3. Surface oxide layer and impurities

The expected uranium oxides on the foil surface are UO_2, U_4O_9, U_3O_7, U_2O_5 and U_3O_8 [12], which derive from the chemical reaction [13]:

$$U + \frac{2+x}{2} O_2 \rightarrow UO_{2+x} \quad (1)$$

The non-stoichiometric UO_{2+x} will form one of the oxides mentioned above, depending on the parameter *x*, usually between 0.2 and 0.4 according to [13]. Looking at large time scales, all uranium oxides eventually form the stable U_3O_8.

Surface structure and oxygen content

The SEM measurements displayed the surface structure of the untreated DU-10wt.%Mo foils to be rough and irregular (Figure 2). Cross-section studies reveal that the oxide layer shows a thickness of 1 – 3 µm with weak adhesion to the underlying U-Mo (Figure 3). EDX analysis revealed a heterogeneous oxygen distribution on the surface on the scale of 50 µm. The averaged oxygen content was determined to be 11 wt.% O corresponding to 52 at.% over the surface.

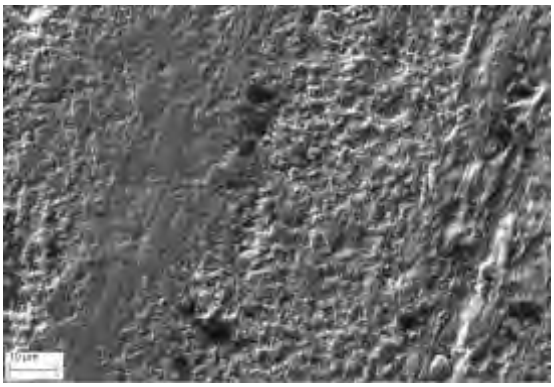

Figure 2: SEM picture of oxidized DU-10wt.%Mo foil surface. The irregularity and roughness of the surface can be seen.

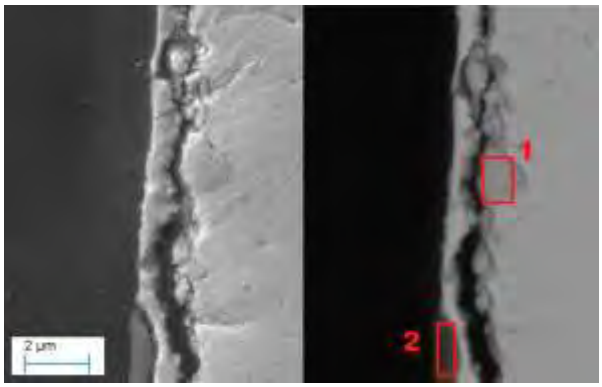

Figure 3: SEM pictures of the cross-section of an oxide layer on the surface of a DU-10wt.%Mo foil. Secondary electron image on the right and backscattered electron image for a better elemental contrast on the left. Area 1 shows high oxygen content and area 2 a typical impurity, consisting mainly of Si, Al and C.

Impurities

Impurities as seen in area 2 in Figure 3, consisting mainly of Si, Al and C, were found in various forms all over the surface, but mostly in the form of elongated grooves (Si and Al). As all grooves are oriented in the same direction, we assume that they result from the foil fabrication process, where the foils were sand-polished and lubricants were used to roll the foil.

4. Chemical cleaning methods

The deoxidation of the U-Mo foil, respectively the etching step, is highly dependent of the type of chemical agent used and its concentration. As mentioned before, aqueous solutions of HNO_3 are the most commonly used cleaning agents for U and its alloys.

The chemical reactions that describe the dissolution of UO_2 or UO_{2+x} in contact with an aqueous HNO_3 solution may be given as:

$$UO_2\,(s) + 2\,HNO_3\,(aq) + 2\,H^+\,(aq) \rightarrow UO_2^{2+}\,(aq) + 2\,NO_2\,(g) + 2\,H_2O \quad (2)$$

$$UO_2^{2+}(aq) + 3\ NO_3^-(aq) \rightarrow [UO_2(NO_3)_3]^-(aq) \quad (3)$$

For the simplicity of the equations, NO_2 is used as the evolving nitrogen oxide species. UO_2 is oxidized to the soluble UO_2^{2+} cation, which subsequently forms the well soluble $[UO_2(NO_3)_3]^-$ complex anion. Most of the evolving nitrogen oxides are getting absorbed in the water forming HNO_3 again, nevertheless some are set free and act harmful when inhaled. This adds to the high difficulty of handling, which is given by the high corrosiveness of the HNO_3 anyway.

A promising candidate for an easier to handle cleaning agent is a combination of alkaline solutions with a little H_2O_2 added, which has been investigated by [11] and is the preferred procedure considering the cleaning power. The chemical reactions responsible for the cleaning effect in this case are primarily the oxidation of UO_2 to the soluble UO_2^{2+} cation, which is given as:

$$UO_2(s) + H_2O_2(aq) \rightarrow UO_2^{2+}(aq) + 2\ OH^-(aq) \quad (4)$$

Due to the alkalinity of the solution, well soluble peroxo compounds are formed in a second reaction, consisting mainly of the $[UO_2(O_2)_3]^{4-}$ anion [14]:

$$UO_2^{2+}(aq) + 3\ O_2^{2-}(aq) \rightarrow [UO_2(O_2)_3]^{4-}(aq) \quad (5)$$

Considering this, a new cleaning procedure based on products from SurTec International GmbH was developed. The formerly used NaOH is substituted by SurTec 138, a well proven industrial alkaline builder. It consists mainly of KOH, which provides the needed alkalinity, as well as phosphates and salts of organic acids, that contribute to the cleaning. Especially for means of degreasing, SurTec 089, a non-ionic surfactant, can be added to the cleaning solution with about 0.5 vol.%. It can contribute to the removal of possibly remaining mould coating and lubricants from the fabrication process, and is designed to be used complementary to SurTec 138.

5. Experimental procedure and results

In the following experiments, cleaning procedures with several concentrations of HNO_3 and several concentrations of the combination of SurTec products and H_2O_2 were compared to each other regarding their deoxidation power and the resulting surface properties of the cleaning U-Mo foils. Further parameters like temperature and reaction time in the cleaning solutions were held constant (reaction time of 300 seconds at room temperature, if not mentioned otherwise) for better comparability. After the cleaning step, all foils were rinsed with destilled water and dried with tissues. As chemical agents aqueous solutions of HNO_3 (65 %), H_2O_2 (35 %) and SurTec 138 as well as SurTec 089 were used.

The used aqueous solutions of acid cleaning were 20, 40 and 50 vol.% of concentrated HNO_3 (65%). In the following these are refered to as the weak (w) / interdediate (i) and strong (s) HNO_3 solution.

The weak solution was insufficient regarding the removal of the oxide layer, which was clearly visible right after the treatment, as the black oxide layer only exhibited a slight brightening. The intermediate solution already had an acceptable cleaning power, but many stripes and elongate plateaus were visible in the SEM pictures (Figure 4) as relicts of the fabrication process. The foil treated with the strong solution was still a bit brighter by visual examination. The successful cleaning was confirmed by EDX analysis, which gave 2 wt.% oxygen remaining. On the other hand the SEM showed roughening of the surface and still some stripes left.

The concentrations of the alkaline cleaning solutions, again denoted as weak (w), intermediate (i) and strong (s), were in that order 4 vol.% SurTec 138 / 2 vol.% H_2O_2 (35%), 10 vol.% / 5 vol.% and 25 vol.% / 25 vol.%.

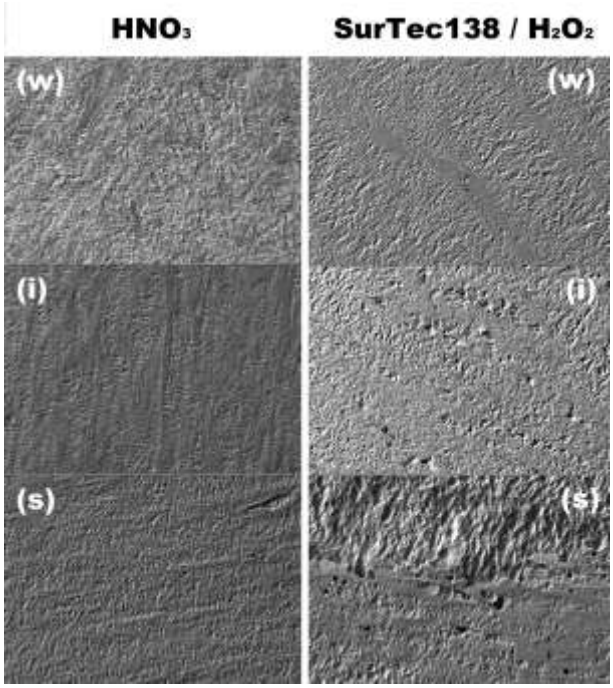

Figure 4: SEM pictures of DU-10wt.%Mo surfaces cleaned with different solutions. Comparison shows different resulting surface topologies.

The weak solution displayed already very good oxygen removal (2 – 4 wt.% O via EDX), but as with the HNO_3 cleaning procedures, there are some plateaus left as well as impurities visible (Figure 5) with the SEM as black spots of approx. 10 – 30 µm with 10 wt.% of Fe / Si and 30 wt.% of O. The surface of the foil cleaned with the intermediate solution appeared with an even brighter metallic gloss, which is confirmed by the EDX analysis, that showed 2 – 3 wt.% oxygen left. Nevertheless, some impurities like before were still found. Even though all impurities seemed to be removed by the treatment with the strong solution, the surface has been severely damaged. Cavities have been formed on a micrometer scale all over the surface and on the scale of millimeters even some peeling of upper layers was visible.

Figure 5: Optical microscope picture of a DU-10wt.%Mo surface after cleaning. The surface shows impurities in form of groups of dots consisting mainly of Fe, Si and O.

The strong HNO_3 solution and the intermediate SurTec 138 / H_2O_2 solution with 0.3 vol.% SurTec 089 added were chosen for further investigation. Figure 6 and Figure 7 show the resulting foil pieces directly after cleaning with the two procedures. The piece cleaned with HNO_3 was visibly darker than the U-Mo foil cleaned with the combination of SurTec products and H_2O_2, suggesting a higher content of remaining O in the former, which was confirmed by EDX analysis. ~ 4 wt.% O average were found on the acid cleaned surface compared to 2 – 3 wt.% O average on the U-Mo foil cleaned with the alkaline procedure. Both showed an equal amount and distribution of remaining impurities as mentioned above. Extension of reaction time of the alkaline solution with the U-Mo foil up to 15 minutes showed no further improvement neither concerning deoxidation nor removal of impurities.

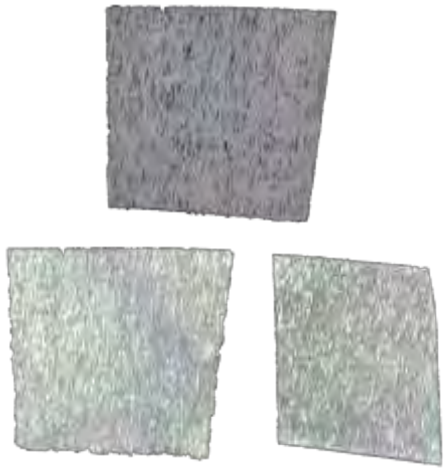

Figure 6: Optical microscope pictures of DU-10wt.%Mo foil pieces for comparison. The alkaline procedure (down left) creates a brighter foil surface than the acidic procedure (down right), which is nevertheless mainly deoxidized compared to the untreated foil piece (above).

Figure 7: DU-10wt.%Mo foil pieces cleaned with SurTec 138 / SurTec 089 / H_2O_2 (left) and HNO_3 (right). The foil piece cleaned by the alkaline procedure is brighter.

Re-oxidation behaviour

As mentioned in [11] the NaOH / H_2O_2 etching process showed a slower re-oxidation rate than the acid etching, due to possible passivation of the upper layer. Nevertheless the etching processes lead to a much rougher surface topology than untreated, oxidized foils, which will result in fast re-oxidation.

Figure 8 shows a foil, which was punctually cleaned with a solution of 10 vol.% SurTec 138 / 10 vol.% H_2O_2 resulting in a circular area of shiny metallic colour, which showed high adhesion to water compared to the surrounding oxide layer. The foil was stored under air at room temperature and investigated with SEM/EDX after 74 days. The cleaned area was visibly re-oxidized and was now of a dark brown-redish colour. The re-oxidized surface still showed the topological structure as directly after the cleaning. Whearas the oxygen concentration initially can be reduced from 12 wt.% O to 2 – 3 wt.% with the alkaline etching, the re-oxidized area yet reached 6.5 wt.% after 74 days.

The re-oxidized foil pieces (Figure 9) cleaned with the strong acidic and the intermediate alkaline solution described in the section above were again examined after 170 days storage in air. The former was visibly darker and showed 6.0 wt.% O on the surface compared to

5.6 wt.% O on the surface of the U-Mo foil cleaned with 10 vol.% SurTec138 and 5 vol.% H_2O_2.

Figure 8: DU-10wt.%Mo foil piece punctually cleaned with SurTec 138 / H_2O_2 solution directly after cleaning (left) and after several months of re-oxidation (right). Freshly re-oxidized U-Mo can be distinguished from the older oxide layer by its brown-redish colour.

Figure 9: Re-oxidized DU-10wt.%Mo foil pieces cleaned with SurTec 138 / H_2O_2 solution (left) and HNO_3 (right).

To suppress fast re-oxidation, the alkaline cleaning procedure was tested in a glove box under high-purity Ar atmosphere with a larger foil piece of about 1500 mm². After cleaning, the foil was immediately sealed in a primary aluminium bag and, together with an oxygen absorber and an oxygen indicator pill, sealed in a second aluminium bag. Figure 10 shows the foil piece unpacked from the bags after about one month. It was slightly tarnished, but exept that had no indication of significant re-oxidation by eye sight.

Figure 10: U-10wt.%Mo foil piece cleaned with SurTec 138 / SurTec 089 / H_2O_2 solution under Ar atmosphere. No significant re-oxidation visible after one month.

6. Conclusion & Outlook

It was found that polluted U-Mo foil surfaces can more effectively be cleaned by a SurTec 138 / H_2O_2 combination than with the common practice using HNO_3. It displayed a better surface quality as well as a higher cleaning power at much lower concentrations and releases no harmful oxides of nitrogen, which makes it less hazardous and therefore easier

to handle. Furthermore, including the surfactant SurTec 089, an all-in-one cleaning solution can be produced, which significantly reduces the number of process steps and is therefore less time-consuming.

7. Acknowledgements

This work was supported by a combined grant (FRM0911) from the Bundesministerium für Bildung und Forschung (BMBF) and the Bayerisches Staatsministerium für Wissenschaft, Forschung und Kunst (StMWFK).

We want to thank Y-12 National Security complex for providing the DU-10wt.%Mo foil material that was used for our experiments. We thank the radiochemistry of the TUM for providing lab space.

8. References

[1] Argonne National Lab. Homepage of the RERTR programme. 2016. http://www.rertr.anl.gov.

[2] Böning, K. et al. Conversion of the FRM II. 8th International Topical Meeting on Research Reactor Fuel Management (RRFM). München, 2004.

[3] Röhrmoser, Anton. Reduced Enrichment Program for the FRM-II, Status 2004/05. Transactions 9th International Meeting on Research Reactors Fuel Management (RRFM), 10. - 13. April 2005. Budapest, 2005. pp. 119-125.

[4] Breitkreutz, Harald. Coupled neutronics and thermal hydraulics of high density cores for FRM II. PhD thesis. Garching bei München: Technische Universität München, 2011.

[5] Röhrmoser, Anton. Reduced enrichment program for FRM II, actual status & principal study of monolithic fuel for FRM II. Proceedings on the 10th International Topical Meeting on Research Reactor Fuel Management, 30.4. - 2.5 2006. Sofia, 2006.

[6] Jungwirth, Rainer. Irradiation behavior of modified high-performance nuclear fuels. PhD thesis. Garching bei München: Technische Universität München, 2011.

[7] Schmid, Wolfgang. Construction of a sputtering reactor for the coating and processing of U-Mo nuclear fuel. PhD thesis. Garching bei München: Technische Universität München, 2011.

[8] Stepnik, B. et al. Manufacturing Progress Status of EMPIRE UMo Irradiation Experiment. RERTR-2015 International Meeting on Reduced Enrichment for Research and Test Reactors. Seoul, 2015.

[9] Steyer, C. et al. Sputter-coating of Monolithic UMo: A Status Report. RERTR-2015 International Meeting on Reduced Enrichment for Research and Test Reactors. Seoul, 2015.

[10] Hollis, H., Cummins, D. and Dombrowski, D. Optimization of Zirconium Plasma Spraying for MP-1 Fabrication. RERTR-2015 International Meeting on Reduced Enrichment for Research and Test Reactors. Seoul, 2015.

[11] Baumeister, B. et al. An alternative chemical cleaning procedure for blank monolithic U-Mo foils. RRFM - European Research Reactor Conference 2012. Prague, 2012.

[12] Ho Kang, Kweon et al. Oxidation behavior of U–10 wt% Mo alloy in air at 473–773 K. Journal of Nuclear Materials. 2002, Vol. 304, 2-3, pp. 242-245.

[13] Ritchie, A. G. A Review of the rates of reaction of Uranium with Oxygen and Water vapour at temperatures up to 300°C. Journal of Nuclear Materials. 1981, Vol. 102, 1-2, pp. 170-182.

[14] Jander, Blasius. Lehrbuch der analytischen und präparativen anorganischen Chemie, 16. Auflage. Stuttgart: S. Hirzel Verlag, 2006.

DESIGN, FABRICATION AND CALIBRATION OF THE SLOWPOKE-2 LEU COMMISSIONING ROD ASSEMBLY

C. KOCLAS, A. MUFTUOGLU, A. TEYSSEDOU, C. CHILIAN
Department of Engineering Physics, Polytechnique Montreal
Québec, Canada

C. GRANT
International Centre for Environmental and Nuclear Sciences, Mona Campus
University of the West Indies, Kingston, Jamaica

ABSTRACT

Within the framework of Material Management and Minimization Conversion Program of the U.S. Department of Energy National Nuclear Security Administration, the Argonne National Laboratory approved the manufacturing by Polytechnique Montreal of a Jamaica's SLOWPOKE-2 reactor (JM-1) mock-up, including reactor removal tools and commissioning rods. This mock-up reactor was then used to practice dry runs of the JM-1 irradiated core removal and fresh core loading operations of the conversion of the JM-1 to LEU fuel. One of the most critical elements in the commissioning of a new reactor core is the commissioning rod assembly. Hence, this paper presents the design, the fabrication, the dry runs performed at Polytechnique Montreal, as well as the calibration of a complete commissioning rod assembly (including commissioning rod) carried out at Jamaica's International Centre for Environmental and Nuclear Sciences.

1 Introduction

In 1984, Atomic Energy Canada Ltd. (AECL) commissioned its last HEU (High Enriched Uranium) fueled SLOWPOKE-2 reactor, named JM-1 [1], in operation at the International Center for Environmental and Nuclear Sciences (ICENS) at the University of the West Indies in Kingston, Jamaica. In 2009, with support from the International Atomic Energy Agency (IAEA), Jamaica submitted a formal request to both the Global Threat Reduction Initiative (GTRI) and the Reduced Enrichment for Research and Test Reactor (RERTR) programs for the conversion of the JM-1 reactor from HEU to LEU (Low Enriched Uranium). Since the inception of RERTR, Argonne National Laboratory (ANL) provided technical coordination and support for the Conversion Program, including Jamaica's research reactor. In April 2015, ANL selected the personnel of the SLOWPOKE Reactor Laboratory at Polytechnique Montreal to provide the environment and the expertise for tooling, testing and rehearsing JM-1 conversion activities.

Amongst the nine HEU SLOWPOKE reactors commissioned by AECL between 1970 and 1984, only one was converted to LEU, in 1997 at Polytechnique Montreal [2,3,4]. In 1985, the first LEU fueled SLOWPOKE-2 reactor was commissioned at the Royal Military College of Canada (RMC) in Kingston, Ontario. Between 1971 and 1997, AECL utilized the same commissioning rod assembly for commissioning eleven SLOWPOKE reactors. This assembly was not available for the JM-1 conversion. The technical information for this assembly was very shortly described in the *Ecole Polytechnique SLOWPOKE-2 Reactor Physics Commissioning Manual* [5]. In this context, the objectives of the present work are to design, manufacture and test a commissioning rod assembly suitable for the safe commissioning of the Jamaican reactor with LEU. The proposed system must meet and surpass the technical requirements of the old commissioning rod assembly used in 1997 during the conversion of the Polytechnique Montreal LEU SLOWPOKE-2 reactor. Hence, this paper presents the design, some fabrication features, the results of dry runs performed at Polytechnique Montreal, as well as calibrations of the complete commission-

ing rod assembly set-up carried out using the JM-1 reactor operating with HEU at ICENS in Jamaica.

2 Overall Design Criteria

The commissioning rod required by JM-1 reactor must satisfy eight inches of vertical displacement at a speed of 0.5 inches/second. The movement must be performed using an appropriate and reliable electrical motor operated from a user-friendly interface (i.e. a command console). The positions of this rod must be clearly provided to the operator and visual safety lights must indicate when it reaches the bottom or top limits of the span displacement. Moreover, the rod should be able to maintain accurately a stationary position when no actions are taken. Furthermore, the operator should be able to move the rod to a desired position with high precision. This requirement constitutes a weakness of the system previously designed by AECL [5]. In fact, it proved to be difficult to obtain a fine control of rod's location, leading to overshooting the desired position when approaching it and thus, requiring several small correction attempts to reach the desired value. This drawback was mainly due to a lack of fine motion control in their system. Therefore, we proposed a new design which corrected this weakness. As shown schematically in Figure 1, we proposed a strategy based on the use of a stepper motor due to its compatibility with digital command interfaces and its capability of reaching a given position with high repeatability and accuracy. The coupling between the motor and the rod displacement mechanism was achieved by means of an axial planetary reducer gearhead. As shown in the figure, a rotary encoder was used to recover the angular position of the motor, which was then converted into the vertical position of the rod. To this purpose, the use of a closed-loop feedback configuration, instead of counting motor steps, permitted the position of the rod to be determined with high reliability. In addition, the proposed design allows the user to monitor the position of the rod even though the motor is disengaged, which is obviously impossible with open-loop systems. In particular, the use of the encoder also permits the stationary position of the rod to be determined. This is a great advantage compared with the use of an open loop (i.e. due to possible motor slips). The displacement of the rod is driven by a pulley without slip, via an inextensible stainless steel cable. The pulley is designed to permit the required rod travel range to be achieved in less than a full rotation. To satisfy angular accuracy, a gearhead couples the pulley to the stepper motor. The vertical position of the rod with respect to a predetermined reference is numerically and graphically shown on a liquid crystal display (LCD). A microcontroller simultaneously manages the motor via a driver circuit, monitors the angular reading of the encoder, its reference signal within a position window generated by a micro switch, converts these readings into a vertical displacement, detects the status of pushbuttons and handles all display functions. The complete commissioning rod set-up includes the following items: i) two commissioning rods; ii) a command console which houses the electronics, the power supply, the display, indicator lights, pushbuttons and fuses, and iii) a drive unit which contains the stepper motor with all necessary mechanical assemblies, as well

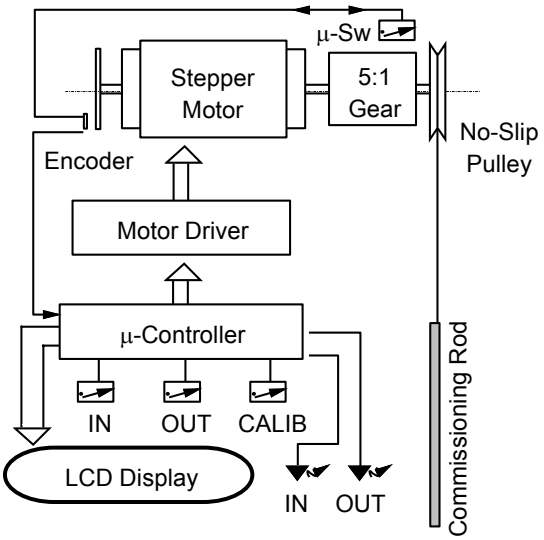

Fig.1 Schematic of the proposed closed-

as the rotary encoder mounted on a robust aluminium support. These items are described with more details in the following sections.

3 The Hardware

This section provides information about the technique used to manufacture the commissioning control rods. Furthermore, details concerning the design of other components such as the control system console ergonomics, the motor driver and the circuitry are also discussed.

3.1 Commissioning Rods

Two commissioning rods were manufactured; in both cases the absorber was made of 7.5" long x 0.95" external diameter Cd tubes. The Cd tubes were fabricated by rolling 0.032" thick Cd sheet (ESPI Metals, USA). In one of the rods (rod 1) the core inside the Cd tube consists of a 0.875" diameter aluminium solid rod that extends 2.93" above the external Cd tube sheet. Within this extra length, the diameter of the aluminium rod is increased to 0.95"; it contains a 1/4"-20 threated hole on the top surface to attach the supporting stainless-steel cable. The water-tight housing was made of 10.56" long x 1.020" diameter aluminium tube having an inner diameter of 0.958". Before inserting the absorber, the bottom end of housing was hermetically closed by initially welding a 1/16" thick aluminium disk. The top was afterwards closed by welding the housing tube to the outside of the top end of the aluminium rod. The second rod (rod 2) was similar to rod 1 except that the inner core inside the Cd tube was 7.0" long x 0.875" diameter polyethylene rod. The polyethylene rod extended up to the bottom end of the Cd tube, nevertheless a 0.5" thick air gap between the top of the polyethylene rod and the bottom of the 2.93" long upper aluminium rod was necessary to avoid the melting of polyethylene rod during the welding process. After manufacturing the commissioning rods, the following information was obtained: i) mass of Cd in rod 1= 99.025 g, total mass rod 1 = 450 g; ii) mass of Cd in rod 2 = 99.135 g, total mass rod 2 = 287 g. These two designs were modelled by ANL with the MCNP JM-1 reactor model. Hence, they calculated the difference between the fully inserted and fully extracted position for each of the previous commissioning rod configurations. The MCNP estimated reactivity value for the rod 1 was - 4.97 ± 0.04 mk (i.e. negative reactivity). For the commissioning rod 2 (i.e. with polyethylene), this value decreased to -5.37 ± 0.06 mk. According to the MCNP calculations, the reactivity of the commissioning rod 2 was very close to the -5.3 mk as reported for the old commissioning rod previously used for SLOWPOKE-2 reactors [5]. Therefore, the rod 2 was selected for commissioning of JM-1 reactor from HEU to LEU.

3.2 The Control Console Ergonomics

The design must satisfy both safe and intuitive operation; therefore, some efforts were initially devoted to determine appropriate console ergonomics. Hence, the console was manufactured around a 5.25" x 17" x 9" metal box. These dimensions where selected so it fits on a standard instrument mounting rack such as the one used at ICENS. The front panel of this unit features a 20 characters per line, 2 lines liquid crystal display (LCD) with a white backlight that permits good readability under most indoor lighting conditions. Two round white pushbuttons (22 mm diameter) with a good tactile feel were installed one above the other close to the left side of the LCD. The upper pushbutton is used to command the rod “OUT” action, while the lower one moves the rod “IN” (see the Figure 2). On the right side of each of these pushbuttons, bright 3 mm red LEDs are used to indicate when the rod travel limits are reached (i.e. according to their respective IN or OUT directions). It was decided to use external LEDs rather than using buttons with built-in indicators to bring a greater visibility to the operator while depressing a pushbutton. In the upper right part of the panel, a blue pushbutton of the same size as the other two serves to set a chosen rod position to be considered as a “Zero” (i.e. the lower limit of the rod displacement after its initial calibration), from which the rod position is determined. Note that the total rod movement is constrained to 8" above the “Zero”. If it is necessary to reassign the

"Zero" to another location, this blue pushbutton can also be used to clear its value. Since safety constituted a major criterion of the design, accidental pushbutton operation is prevented by two keylock switches. One of these switches is placed just below the "Zero" setting pushbutton to prevent inadvertent action. The second keylock switch that locks the three pushbutton actions, is installed on the bottom left part of the front panel. These switches are ON (i.e. closed contacts) only when their respective keys are inserted and rotated clockwise past the engagement point. Also, these keys can be removed only when their contacts are opened; consequently a key in a vertical position or removed from the switch indicates that the pushbuttons are deactivated. Figure 2 shows a front view of the command console that illustrates the general description given above. This layout of front panel components provided an intuitive and user-friendly interaction between the operator and the control unit. The back of the console contains the terminal blocks for the connection to the encoder and the motor driver. Herewith, we have also located the proper switch as well as independent fuse holders for the power supply, the motor driver circuit board and the digital circuit board.

Fig.2 Front-view of the control console

3.3 The Commissioning Rod Drive Unit

This system consists of a hybrid stepper motor with a dual-ended shaft. As shown in Figure 1, one end is coupled to the encoder and the other one is coupled to a planetary 5:1 reducer gearhead. This gearhead drives the pulley-cable system that moves the rod. The stepper motor selected for this purpose (NMB Technologies, Model 23KM-K762-99V) has a resolution of 200 steps per revolution. The console electronics drives it in 400 half steps per revolution, hence combined with the reducer ratio the pulley is moved with a resolution of 1/2000 turn. The pulley with the 0.063" diameter stainless steel cable has an effective diameter of 4.309" and can move the commissioning rod with a precision of +/- 0.007". It is important to mention that this value exceeds the +/-0.01" resolution of the AECL system [5]. As shown in Figure 1, a rotary encoder (Yumo, Model E6B2-CWZ3E) is installed at the back side of the motor rather than in front of the rod pulley-cable system; consequently, this design eliminates the presence of mechanical components hanging in front of the pulley. This topology permits the space in front of the pulley-cable assembly to be unencumbered from any obstacle. This feature provides additional space for reactor core removal and insertion operations which obviously increases safety. The rotary encoder has two quadrature channels which generate 1024 pulses each for determining both the direction and the angle of rotation. The electronics is able to detect the rising and falling edges of these pulses and thus, provides a resolution of 2048 bits per revolution. In addition, this incremental encoder has an independent channel that produces a single pulse per revolution which is used as a reference signal. Since the encoder is coupled directly to the motor, it rotates five time for a single rotation of the pulley. Hence, along a complete pulley rotation, the encoder generates five reference signals. Therefore, in order to obtain a single reliable reference, a micro-switch is activated by a small brass cam installed on the back surface of the pulley (see the Figure 1). To use one of the five encoder signals per revolution to obtain a unique reference, the reference signal is sent to the microcontroller via a micro switch. Furthermore, the encoder is accurately set in such a way that the reference signal is received (micro-switch triggered ON) when the cam is at the midpoint of the short travel zone. Once the cable is properly installed on the pulley, the reference signal is generated when the rod is at slightly lower position than the envisioned "Zero" location, for instance at the bottom of the commissioning rod tube. Consequently, in order to search the reference, the commissioning rod must be inserted below "Zero"; thus, it should not be raised during the search of the reference procedure.

When the operator sets the “Zero”, its distance from the encoder reference is stored in the microcontroller’s non-volatile memory (more details about the logic of this process is given in Section 4). In the event of a loss of electrical power, this particular feature allows the “Zero” to be easily recovered, which increases both the reliability and safe operation of the commissioning rod control system. Prior to setting the “Zero”, the system displays the distance from the reference signal (it has a total travel range of 12"). Once the “Zero” is set, the rod position is measured with respect to this point and then the travel distance is established to the design range of 8". Since the encoder is directly coupled to the motor and the pulley to the gear box, any backlash that could be introduced by this mechanism must be smaller than the resolution of the encoder. This condition was largely satisfied with the gearhead selected for this purpose (Parker, Model PS60-005-L2, 5:1 ratio, low backlash option). The mechanical components of the commissioning rod driver are installed on a support frame bolted to the reactor suspension structure in such a way that the cable passes through the axis of the commissioning rod guide installed in the reactor mock-up. Furthermore, to guarantee full compatibility and easy implementation on both, mock-up of Polytechnique Montreal and Jamaica’s reactor, the holes for the commissioning rod driver support in the suspension frame of the mock-up were drilled at the same location as those existing in the suspension frame of JM-1 reactor.

3.4 The Electronics

The control console unit contains two circuit boards: one that handles logic operations and a second one that contains the circuitry that controls and drives the stepper motor. The logic circuit is implemented around an 8-bit microcontroller that features three input/output ports. A six bit port is used to read the status of the three pushbuttons as well as the three channels of the rotary encoder. A four bit port is used to control the stepper motor driver. An eight bit port is used for sending the commands and the data to the LCD, as well to turn ON-OFF the two LED indicator. The motor driver is a simple dual H-bridge constant voltage circuit. These bridges allow the motor to work in bi-polar mode, i.e. to use the entire windings instead of half of them as is the case in unipolar configurations; thus, the centre tap of the windings are not used. Furthermore, the use of full windings increases the motor torque and reduces electrical current requirements. Nevertheless, the higher inductance of this arrangement is not necessarily a problem because the rotational speed is relatively low (i.e. about 11 rpm for moving the commissioning rod at 0.5"/s). In addition, the topology of the implemented H-bridges allows both side of each bridges to be controlled individually and prevents the two power transistors of each branches from conducting at the same time. This arrangement permits one or the two motor windings to be deactivated and avoids short-circuiting the bridges in case of driver command errors. A network of low power transistors is used as an interface between the microcontroller and the power transistors. Even though the selected power transistors have built-in protection diodes, as an extra precaution, external additional fly back diodes were installed on each pair of emitters and collectors.

4 Firmware

The embedded firmware is stored and executed by an 8 bit RISC microcontroller. The program is coded in assembly language; it operates by satisfying real-time constraints. Figure 3 shows a flow sheet diagram of the whole control process. The required vertical displacement speed of the commissioning rod is obtained by reading the pushbutton switches in an interrupt service routine triggered by the overflow of a built-in timer module. When this interrupt occurs, the timer registers are reloaded with the needed value; hence, another overflow happens again 13.538 ms later. If a pushbutton is depressed requesting a motion in the “IN” or “OUT” direction and the travel limit is not reached in that particular direction, the stepper motor is instructed to perform a half step. To offer fine motion control, when a pushbutton is first depressed, only one step is executed and for the next 36 timer overflow interrupts, no step command are sent. Thus, depress-

ing a pushbutton by less than 0.5 second moves the commissioning rod 0.007". Nevertheless, holding the button pushed longer than 0.5 seconds will displace the rod at the design speed. The position of the commissioning rod is determined from the number of encoder pulses that are counted from its reference signal or from the “Zero” setting set by the operator. Since missed pulses in incremental encoder generate cumulative errors, particular precautions are taken to avoid or reduce this potential flaw. To this aim, a change on the level of the channel “A” of the encoder, which indicates that a rotation has occurred, is treated with the highest priority with respect to all other tasks. To this end, when such an event is detected, an interrupt is triggered, the registers containing the position are updated and tests are performed to check whether or not the travel limits are met or exceeded before returning from the interrupt service routine. Furthermore, this interrupt source is always serviced before the timer overflow interrupt, should the interrupt flags of both sources of interrupts be set when the program reaches the interrupt service routine. This strategy prevents further step commands to be sent to the stepper motor while encoder pulses are still received by the micro-controller. It must be pointed out that we have not observed that this self-moderating behaviour has any significant effect on the rod travel speed. In addition, to further reduce the chances of missing encoder pulses, the microcontroller’s clock speed is increased during the interrupt service routine; thus, the program is able to complete the treatment of the interrupt faster and it becomes much sooner ready for handling the next one. It is obvious that the timer prescaler is consequently adjusted to compensate for the change of clock frequency and thus, maintain the proper timing. Upon powering the system up, the LCD turns ON all its pixels during a lapse of three seconds to confirm its proper operation. The limit LED indicators are also turned ON during this sequence; afterwards, the version number of the firmware is displayed on the LCD. After the LCD initialization, the unit indicates whether or not a “Zero” has been set and asks the operator to find the reference. If a “Zero” is already set, the operator will be asked to retrieve it after having found the reference. The reference is thus found by inserting the rod by depressing the “IN” pushbutton. If the “Zero” is not set, once the reference is found, the rod travel span is then limited between 0 to 12" above this reference. Provisions were made to bound this displacement to 12", preventing the pulley to perform a complete rotation and thus, avoiding the cable to be winding on itself. Nevertheless, it is important to mention that the system operates in this mode as long as the operator is unable to set a “Zero”. Since during the commissioning, the core reactivity must be determined for different rod elevations, the upper limit of a desired rod travel should be specified. Afterwards, the operator must insert the commissioning rod 8.000" below the aforementioned upper limit and depress the calibration button, with both keylock switches at the ON position. However, the “Zero” must be above the encoder reference but less than 4.010" above it to be accepted by the system. Then, the upper line of

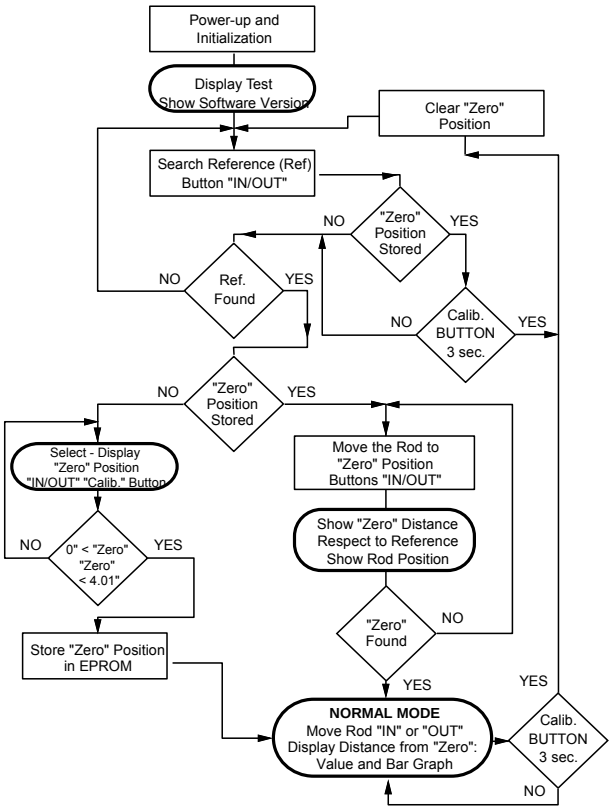

Fig.3 Firmware flow sheet diagram

the display indicates the rod travel from the “Zero” and the lower line presents graphically the rod position; the total rod displacement span is now bounded between 0 to 8.000" with respect to the “Zero”. If the unit is powered up when a “Zero” was already stored in the EPROM, after the operator finds the reference, the display will indicate the distance of the stored “Zero” with respect to the reference. Similarly to the former case, the second LCD line will indicate the current rod travel starting from the reference. When the location of the “Zero” is reached, the system will automatically resume to normal operation (see Figure 3); it will indicate the rod travel from the “Zero” providing a numerical and a graphical representation of the commissioning rod position. As indicated in Figure 3, a stored value of “Zero” can be erased by holding the calibration button for more than three seconds. Nevertheless, for safety reasons this operation requires the two keylock switches to be in their ON positions. This operation cannot be performed during the system initialization (i.e. display test and firmware version indication) and if the reference is found but the former “Zero” is not yet reached.

5 Dry Runs: Commissioning Rod and Motor Drive Test on the Mock-up

During dry runs tests, it was seen that the commissioning rod motor drive successfully raised and lowered the commissioning rod in the guide tube that was installed in the mock-up of Polytechnique Montreal. The two rods described in Section 3.1 were installed and tested. It was determined that their weights were appropriate to keep the driving cable taut enough within the water-filled guide tube.

5.1 Test of Commissioning Rod Position Readout

During the initial setup, with the readout indicating 0.000 inches, the rod was moved down to touch the bottom of the irradiation site #5; with the cable taut, the upper end of the cable was attached to the pulley. The readout then indicates the position relative to the encoder reference and relative to the bottom of the irradiation site #5. During the first test of the commissioning rod position readout, when the commissioning rod position readout indicated a displacement of 8.000", the actual displacement of the cable was measured by a digital calliper to be 7.860". The readout software was modified to correct this 1.7% error. Further tests confirmed that the readout corresponds to the actual displacement of the rod (i.e. 8.00"). The speed of 0.5”/s was validated by repeating the tests and measuring the lapsed times with a stopwatch.

5.2 Installation and Manipulation of the Commissioning Rods

The lower end of the commissioning rod guide tube was installed in the irradiation site #5 of the annular reflector of the mock-up. The guide tube was fixed to the top end using the commissioning rod guide tube cover plate. After that, to avoid any jamming risk, the commissioning rod guide tube should not be inserted too far into the annular reflector. The procedure used to place the tube at the proper height was demonstrated and validated during the dry runs as follows: The tube was first placed on top of the core top plate, which is 3/4” above the top of the annular reflector. The cover plate was inserted along the tube until it touched the top plate; a hairline mark was traced on the tube at the top of the cover plate level and another line made 5.5" higher. Afterwards, based on the last indication mark, the tube was inserted 5.5". Once the guide tube was installed, the commissioning rod drive unit was firmly bolted to the mock-up top plate.

The commissioning rod with polyethylene core was manually inserted to point of touching the bottom of the guiding tube. Subsequently, the pulley was turned just until the reference signal from the encoder was reached. Then, with the rod just barely touching the bottom of the irradiation site #5, the cable was fastened to the pulley. Once these operations were completed, the drive unit was tested several times, i.e. by inserting and removing the rod. These tests validated that the use of the IN and OUT pushbuttons permitted to move the commissioning rod according

to design specifications within a 12" range from the bottom of the hole, at correct speed. In addition, it was observed that the weight of the rod 2 in water was sufficient to guarantee the correct tautness of the stainless steel cable. During these tests, the precision of the rod positioning was validated as +/-0.007". Finally, with the rod positioned at 1" above bottom of irradiation site #5, the “Zero” was set to limit the rod movement within a span of 0 - 8" relative to this point.

6 Calibration

The JM-1 reactor was under operation using HEU fuel and a single control rod installed at the centre of the core. The value of reactivity introduced by the control rod was estimated at -5.3 mk. Even though the commissioning rod should provide a similar value, it has been considered that the range of -4.5 mk to -6.0 mk was acceptable. To increase the safety margins, the polyethylene commissioning rod 2 was selected for calibration and further LEU fuel loading activities. The commissioning rod was calibrated in the JM-1 reactor during the final days of operation with HEU fuel. After removing the irradiation tube #5 which introduced -0.52 mk of reactivity, the commissioning rod guide tube was installed in that location in the Be reflector. This calibration was used to estimate the reactivity introduced by this rod when LEU fuel is used. To this aim, it must be pointed out that similar measurements carried out in other SLOWPOKE reactors with HEU and LEU fuels have indicated that the reactivity values are similar.

A complete measurement of the worth of the commissioning rod as a function of position required sub-critical measurements of neutron multiplication factor with constant photoneutrons source produced in the Be reflector by gamma-rays from decaying fission products. In order to ensure that this source was sufficiently constant during the period of the measurements, the reactor was shut down (control rod fully inserted) before the measurements for a period of 9 days so that short-lived fission products that can produce photoneutrons had decayed to levels where their contribution to the source is negligible.

The calibration measurements were made with an ion chamber (LND, Model 50460) and a BF3 detector (LND, Model 2025). The BF3 detector provides the most accurate sub-critical neutron flux measurements because part of the ion chamber is due to fission product gamma-rays. The ion chamber was used for supercritical period measurements and critical balance measurements and it was also useful to observe the approach to stability of the neutron flux during the sub-critical measurements.

The commissioning rod was initially installed to the bottom of the irradiation site #5, the fully inserted position, and was subsequently raised and lowered using the drive system described above. The commissioning rod was withdrawn in successive steps and the steady state count rate of the BF3 at each position was recorded until it was clear that the rod has passed the point at which the reactivity it is holding down had been reduced to a negligible level. The rough initial calculation of the commissioning rod worth was -6.42 mk. A soft re“Zero” was performed at 0.850" from the reference equivalent to -5.42 mk reactivity insertion. During the actual LEU commissioning the 8" range extended from a “Zero” position (0.850" from the reference) to the position at which the rod just has zero worth.

With the reactor under manual control, the control rod was withdrawn to make the reactor critical, the flux was measured by the ion chamber to a level at which a good critical balance can be achieved. The control rod position was measured at this balance point. The known calibration of the control rod and the just measured critical position were then used to find the degree of subcriticality with the control rod fully inserted. This value was used to calculate the effective source strength, and further the worth of the commissioning rod at the points were flux levels were measured. After this pre-calibration, an improved initial calibration was performed starting with the commissioning rod fully withdrawn and the reactor critical on the control rod. The commis-

sioning rod was inserted to a new fixed position and criticality was maintained by withdrawal of the control rod. The difference between the old and new critical positions of the control rod and the known calibration of the control rod were used to calculate the reactivity worth equivalent to the movement of the commissioning rod. This procedure was repeated several times at different positions of the commissioning rod. This improved initial calibration indicated a worth of -5.80 mk for the commissioning rod.

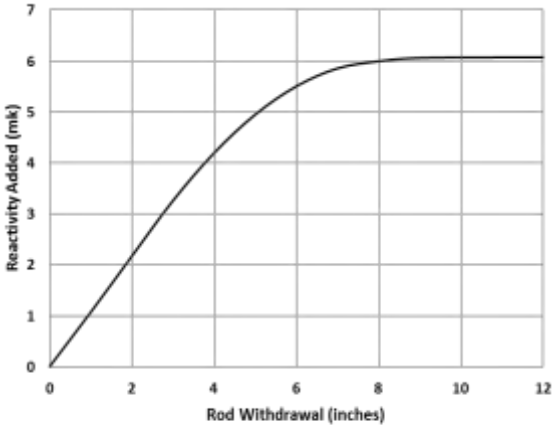

Fig. 4 Commissioning rod reactivity function of the vertical position

Finally, starting with the control rod fully withdrawn and the reactor critical on the commissioning rod, the commissioning rod was withdrawn to initiate an exponential increase in flux. The doubling time of this transient was used to calculate the reactivity insertion corresponding to the movement of the commissioning rod. The procedure was repeated for a few more successively larger commissioning rod withdrawals, culminating in complete withdrawal of the rod for measuring the excess reactivity of the reactor. These data were used to provide the final calibration of the commissioning rod over the range from critical to fully withdrawn. The final commissioning rod's worth was determined to be -6.03 mk. Since the accepted reactivity scale of the reactor is based on the worth of the delayed neutron fraction used in the conversion of doubling time to reactivity these final measurements provided the best calibration of the rod. Figure 4 shows the reactivity introduced by the commissioning rod as a function of its vertical positions, once its calibration procedures were completed.

7 Conclusion

A new commissioning rod assembly for the SLOWPOKE-2 reactor was developed for the JM-1 reactor conversion. Practicing on a full-scale mock-up demonstrated that the assembly was suitable for the designed purpose and provided the conversion team with the necessary insight into LEU commissioning activities. The ability to carry out the calibration of the commissioning rod ahead time lead to the successful commissioning of the Jamaican JM-1 LEU reactor at the beginning of October 2015.

8 References

[1] J. Preston, C. Grant. *The Status of HEU to LEU Core Conversion Activities at the Jamaica Slowpoke*. CNL Nuclear Review, 2014, 51-55.

[2] C.N. Grant, J. Preston, C. Chilian, G. Kennedy. *SLOWPOKE-2 Refuelling – Past Experience and New Challenges*. Transactions of the RRFM, St. Petersburg, Russia, 2013.

[3] G. Kennedy and J. St. Pierre, L.G.I. Bennett and K.S. Nielsen, *LEU-Fuelled SLOWPOKE-2 Research Reactors: Operational Experience and Utilisation*, Transactions of the International Meeting on RERTR, San Carlos de Bariloche, Argentina, 2002.

[4] G. Kennedy, G. Marleau. *Refuelling the SLOWPOKE-2 reactor at Ecole Polytechnique: Procedure and proposed experiments*. Proceedings of the Canadian Nuclear Society Conference, Ottawa, Canada, 1997.

[5] G. Edwards, R.T. Jones. *Ecole Polytechnique SLOWPOKE-2 Reactor Physics Commissioning Manual*, *AECL*, April 1997.

HOT ISOSTATIC PRESS BONDING OF ALUMINUM CLADDING TO MONOLITHINC FUEL FOILS

K.D. CLARKE, L.A. TUCKER, S.D. IMHOFF, M.J. DVORNAK, B. AIKIN, V.D. VARGAS, J.D. MONTALVO, R. HUDSON, M.E. MAURO, D.J. ALEXANDER, AND D.E. DOMBROWSKI

Materials Science & Technology: Metallurgy (MST-6), Los Alamos National Laboratory
PO Box 1663, Mail Stop G770, Los Alamos, New Mexico, 87545, USA

C. LIU, M. LOVATO

Materials Science & Technology: Materials Science in Radiation and Dynamics Extremes (MST-8), Los Alamos National Laboratory
PO Box 1663, Mail Stop G770, Los Alamos, New Mexico, 87545, USA

ABSTRACT

Hot Isostatic Pressing (HIP) has been selected as a manufacturing process to bond 6061-aluminum alloy cladding to monolithic fuel foils for high-powered research and test reactors. This manuscript describes work to optimize the manufacturing path toward an efficient and robust production process. A formed-can HIP approach has improved quality, and minimized material usage, eliminated machining, reduced the amount of welding required, and substantially improved dimensional stability of the hip can and final fuel plate. This work supports the U.S. Department of Energy National Nuclear Security Administration (DOE/NNSA) Office of Material Management and Minimization (M^3) Reactor Conversion Program, which aims to reduce or eliminate the use of highly enriched uranium (HEU) dispersion fuels in high-powered research reactors in the United States by replacement with low enriched uranium (LEU) alloy monolithic fuel plates.

1. Introduction

1.1 Background

The evolution of the HIP process has included many participants at, primarily, Idaho National Laboratory and Los Alamos National Laboratory, and developments and updates have been regularly published in the literature [1-14], and have shown that the HIP process can achieve high-quality bonding of cladding around the monolithic fuel foil [15-23].

1.2 Objective

The ongoing optimization work is an effort to modify the baseline HIP processing path to enable high-volume manufacturing with improved efficiency. The production-optimized HIP can design goals were determined by LANL and Babcock & Wilcox (B&W) to include maintaining or improving the quality of the fuel plates produced with the baseline scaled-up mini can design, while simultaneously minimizing material usage, improving dimensional stability, easing assembly and disassembly, eliminating machining, and significantly reducing welding.

2. Results and Discussion

2.1 Formed-can HIP approach and design

The concept employed is to evolve from a successful six-piece HIP can design [1-8] to a formed-can design [9-14] to improve repeatability and quality of the final product and reduce manufacturing effort, both in direct costs and labor.

Through a series of sub-scale and full-scale experiments [9-14], an optimized, full-size, and scalable design has been developed, Fig. 1.

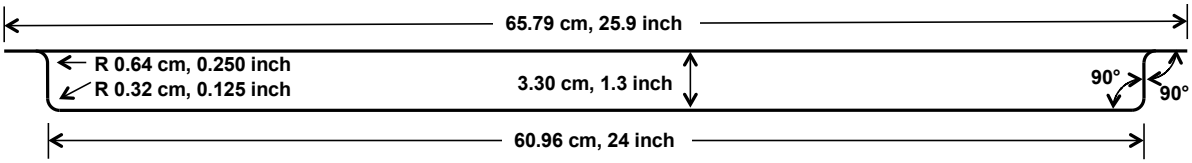

(a)

(b)

Fig. 1 (a) Drawing and (b) image of the finalized HIP can design, incorporating tight punch and flange radii, vertical walls, and a flat flange to facilitate welding. Width of can is 12.70 cm (5.0 inches), and the radii of the corner of the can are 2.54 cm (1.0 inch).

The can design incorporates several characteristics that simplify or reduce cost in the manufacturing process, including utilizing 1.25 mm (0.050 inch) thick mild steel, a right-angle flange, vertical side walls, a substantial depth, a tight punch radius, and a tight flange radius. The mild steel can is economically favorable over the previous can design (stainless steel) and limits the mass of can material that must be disposed of after processing by 75% (2.3 vs. 9.1 kg, or 5 vs. 20 lbs). The right-angle flange facilitates flexibility in welding processes, allowing either electron-beam welding (EBW) or tungsten inert gas (TIG) manual welding processes to be used to seal the can prior to HIP processing. Vertical side walls simplify the assembly process since all components in the internal stack up are the same size, and further means that most strongbacks are interchangeable (except the bottom strongback, which will require some machined radius to fit the can) and can be recycled readily. The depth of 3.3 cm permits efficiency and flexibility in stackup design, allowing for 6 or more plates per can, but flexibility to reduce that number as needed for manufacturing efficiency. The amount of machining required for the bottom strongback to fit tightly into the can is minimized by the tight punch radius, and follows the contour of the bottom of the can, promoting excellent stress distribution throughout the can. The tight flange radius minimizes the empty space in the can, reducing the movement on any internal stackup components and ensuring low stresses in the can material after the can has collapsed onto the stackup during the HIP process.

Using a thin-walled can also results in substantial improvement in stress distribution on the internal stackup, as shown in Fig. 2. The images in Fig. 2a and 2b depict the vertical stresses normal to the fuel plates as they are stacked in the HIP can. The consistent stress distribution throughout the cross-section in the formed sheet metal HIP can reduces the stress shadowing near the walls in the six-sided can design. This stress shadowing has also been seen experimentally, as shown in Fig. 2c.

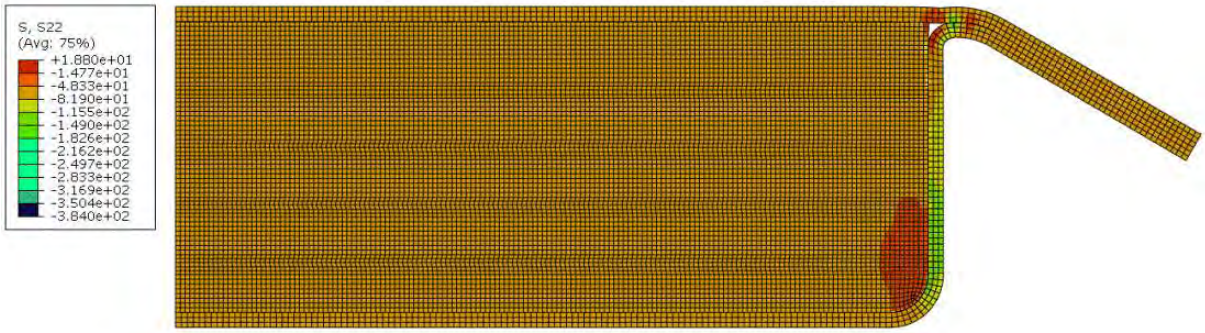

(a)

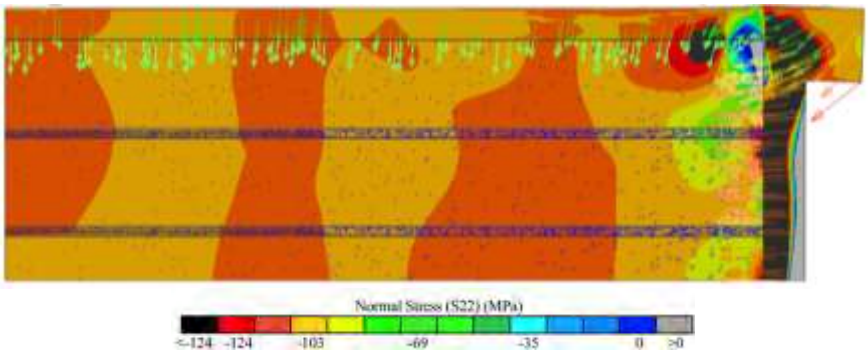

(b)

(c)

Fig. 2 (a) Fully coupled thermal-mechanical model of the final formed HIP can design, showing excellent vertical (S22) stress distribution throughout the can, and (b) simple deformation model showing S22 stress distribution in the previous, 6-sided, HIP can design, showing stress shadowing near the walls of the can. Quarter cross-section models showing stress distribution at maximum pressure and temperature of HIP cycle (560°C, 104 MPa or 15 ksi). (c) Opened six-sided HIP can showing top of top strongback, with a “racetrack” of undeformed strongback material around the edges of the can, indicating significant stress-shadowing near the can walls.

The formed can design can also be easily scaled up or down to accommodate longer or wider fuel plates as necessary, including the 121.9 cm (48-inch) long fuel plates for the Advanced Test Reactor (ATR) at INL, or small-scale samples for reactor qualification experiments.

2.2 HIP process details

The HIP process has been specified in a processing summary document, which includes details of each step in the procedure and guidance on execution of each step [24]. The primary steps are cleaning, application of parting agent, assembly, seal-welding, evacuation and bakeout, HIP processing, and de-canning. Of particular importance to the process is ensuring the parting agent does not outgas during the HIP process, resulting in internal resistance which counteracts the HIP pressure and reduces the effective pressure. Several differential scanning calorimetry studies have been performed on various parting agents, and MoS_2 aerosol spray and brush-applied Neolube No. 1 and No. 2 would satisfy the requirements. Figure 3 shows results from simulated HIP thermal cycles for each of these parting agents, and suggests the bakeout of 315°C for 60 minutes under vacuum, followed by exposure to ambient air for 12 hours or more results in varying non-water mass loss during a simulated HIP cycle, with the MoS_2 showing the least and the Neolube No. 2 showing the most. It may be beneficial to increase the bakeout temperature to 350°C for 60 minutes to minimize this post-bakeout mass loss, as suggested in [14].

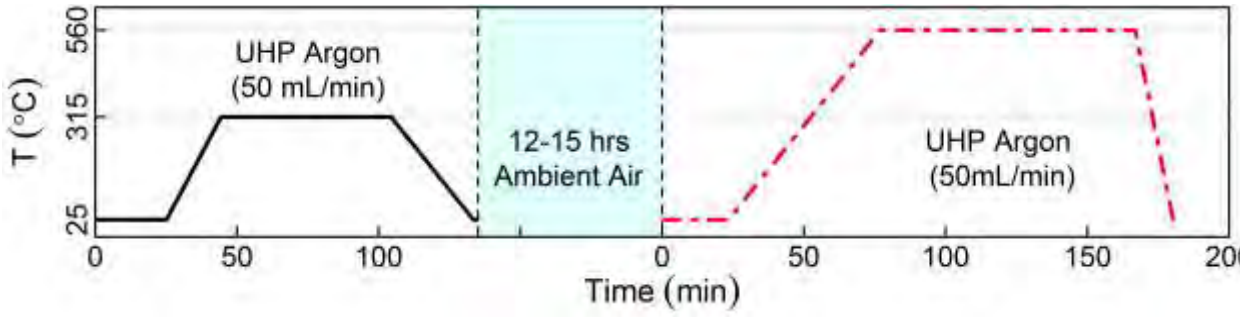

(a)

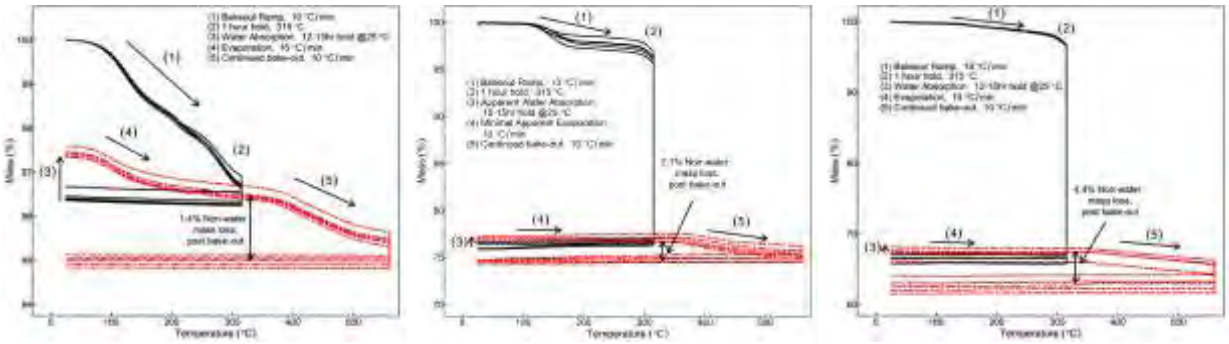

(b) (c) (d)

Fig. 6 (a) Experimental TGA cycle used to evaluate mass loss for (b) MoS_2, (c) Neolube No. 1, and (d) Neolube No. 2. The cycle is intended to simulate a 315°C bakeout, ambient air hold, and standard HIP cycle.

3. Summary

A formed HIP can approach has been developed and tested, resulting in a viable and efficient processing path for the cladding of aluminum to monolithic fuel foils to facilitate the conversion of high powered research reactors to LEU from HEU fuels. The formed can design has been optimized to result in high-quality fuel plates, while lowering materials and labor cost and reducing the waste material produced in the process. Technology transfer is

underway to transfer the process to the manufacturing facility intended to produce fuel plates to supply to research reactors.

4. References

[1] D.E. Burkes, D.D. Keiser, D.M. Wachs, J.S. Larson, M.D. Chapple, “Characterization of Monolithic Fuel Foil Properties and Bond Strength”, RRFM 2007, Lyon, France, March 11-15, 2007.

[2] G.A. Moore, F.J. Rice, N.E. Woolstenhulme, W.D. Swank, D.C. Haggard, J. Jue, B.H. Park, S.E. Steffler, N.P. Hallinan, M.D. Chapple, and D.E. Burkes, “Monolithic Fuel Fabrication Process Development at the Idaho National Laboratory”, RERTR, Washington, D.C., October 5-9, 2008.

[3] G.A. Moore, F.J. Rice, N.E. Woolstenhulme, J-F. Jue, B.H. Park, S.E. Steffler, N.P. Hallinan, M.D. Chapple, M.C. Marshall, B.I. Mackowiak, C.R. Clark, and B.H. Rabin, “Monolithic Fuel Fabrication Process Development at the Idaho National Laboratory”, RERTR, Beijing, China, Nov. 1-5, 2009.

[4] J-F. Jue, B.H. Park, C.R. Clark, G.A. Moore, and D.D. Keiser Jr., “Fabrication of Monolithic RERTR Fuels by Hot Isostatic Pressing”, Nuclear Technology, Vol. 172, Nov. 2010, pp. 204-210.

[5] J. Katz, K. Clarke, B. Mihaila, J. Crapps, B. Aikin, V. Vargas, R. Weinberg, A. Duffield, and D. Dombrowski, “Scale-up of the HIP Bonding Process for Aluminum Clad LEU Reactor Fuel”, RERTR 2011, Santiago, Chile, October 23-27, 2011.

[6] J. Crapps, K.D. Clarke, J. Katz, J.D. Alexander, B. Aikin, V. Vargas, J. Montalvo, D.E. Dombrowski, B. Mihaila, “Hot Isostatic Press Manufacturing Process Development for Fabrication of RERTR Monolithic Fuel Plates”, Powdermet 2012, Nashville, TN June 10-13 2012.

[7] K.D. Clarke, C.E. Cross, R.E. Hackenberg, R.J. McCabe, J.D. Montalvo, M.J. Dvornak, R.L. Edwards, J.M. Crapps, R.R. Trujillo, B. Aikin, V.D. Vargas, K.J. Hollis, T.J. Lienert, B. Mihaila, D.L. Hammon, R.W. Hudson, T.J. Tucker, J.E. Scott, A.N. Duffield, R.Y. Weinberg, and D.E. Dombrowski, “Development of Aluminum-Clad Fuel Plate Processing Through Canned and Canless Hot Isostatic Pressing (HIP), and Studies of Aluminum Cladding Grain Growth during HIP”, RERTR 2012, Warsaw, Poland, October 14-17, 2012.

[8] J. Crapps, K. Clarke, J. Katz, D.J. Alexander, B. Aikin, V.D. Vargas, J.D. Montalvo, D.E. Dombrowski, B. Mihaila, “Development of the hot isostatic press process for monolithic nuclear fuel”, Nuclear Engineering and Design, Vol. 254, January 2013, pp. 43-52.

[9] K.D. Clarke, J.D. Katz, M.J. Dvornak, J.M. Crapps, B. Aikin, B. Mihaila, J.E. Scott, and D.E. Dombrowski, “Full-Scale Baseline and Formed-Can Approaches to Hot Isostatic Press Processing of Monolithic Fuel Plates”, Powdermet 2013, Chicago, IL, June 24-27, 2013.

[10] K.D. Clarke, J. Crapps, J. Scott, B. Aikin, V. Vargas, M. Dvornak, A. Duffield, R. Weinberg, D. Alexander, J. Montalvo, R. Hudson, B. Mihaila, C. Liu, M. Lovato, D. Dombrowski, “Hot Isostatic Press Can Optimization for Aluminum Cladding of U-10Mo Reactor Fuel Plates: FY12 Final Report and FY 13 Update”, August 2013, Los Alamos National Laboratory LA-UR-13-26706.

[11] K.D. Clarke, L.A. Tucker, J.E. Scott, B. Aikin, V.D. Vargas, M.J. Dvornak, R.W. Hudson, D.E. Dombrowski, “Monolithic Fuel Plate Development: HIP Can Optimization”, European Research Reactor Conference: RRFM 2014, March 30 to April 3, 2014.

[12] K.D. Clarke, L.A. Tucker, M.J. Dvornak, B. Aikin, V.D. Vargas, R.W. Hudson, J.E. Scott, M.E. Mauro, D.E. Dombrowski, “A Formed-Can Approach to Hot Isostatic Press Manufacturing of LEU-10 wt. pct. Molybdenum Monolithic Fuel Plates” Powdermet 2014, May 18-22, 2014, Orlando, FL.

[13] D.E. Dombrowski, R.M. Aikin, K.D. Clarke, T. Lienert, P.O. Dickerson, L.A. Tucker, D.A. Summa, D.J. Alexander, M. Hill, “LANL Progress on U-Mo Fuel Fabrication

Process Development", Reduced Enrichment for Research and Test Reactors (RERTR), Vienna, Austria, Oct. 12-16, 2014.
[14] K.D. Clarke, L.A. Tucker, S.D. Imhoff, M.J. Dvornak, B. Aikin, V.D. Vargas, J.D. Montalvo, R. Hudson, M.E. Mauro, and D.E. Dombrowski, "Hot Isostatic Press Manufacturing of LEU-10 wt. pct. Molybdenum Monolithic Fuel Plates", Powdermet 2015, May 17-20, 2015, San Diego, CA.
[15] C. Liu, M.L. Lovato, K.D. Clarke, D.J. Alexander, W.R. Blumenthal, "Miniature Bulge Test and Energy Release Rate in HIPed Aluminum/Aluminum Interfacial Fracture", LANL publication LA-UR-14-20640.
[16] C. Liu, M.L. Lovato, K.D. Clarke, D.J. Alexander, W.R. Blumenthal, "Miniature bulge test and energy release rate in HIPed aluminum/aluminum interfacial fracture", submitted to J. of the Mechanics and Physics of Solids, Oct. 2014.
[17] N.A. Mara, J. Crapps, T. Wynn, K. Clarke, P. Dickerson, D.E. Dombrowski, B. Mihaila, and A. Antoniu, "Nanomechanical Behavior of U-10Mo/Zr/Al Fuel Assemblies", RERTR 2011, Santiago, Chile, October 23-27, 2011.
[18] Nathan A. Mara, Justin Crapps, Thomas A. Wynn, Kester D. Clarke, Antonia Antoniou, Patricia O. Dickerson, David E. Dombrowski, Bogdan Mihaila (2013): Microcantilever bend testing and finite element simulations of HIP-ed interface-free bulk Al and Al–Al HIP bonded interfaces, Philosophical Magazine, DOI: 10.1080/14786435.2013.786192N. Vol. 93, Iss. 21, April 2013, pp. 2749-2758.
[19] D. Dombrowski, C. Liu, M.L. Lovato, D.J. Alexander, K.D. Clarke, N.A. Mara, M.B. Prime, D.W. Brown, B. Clausen, "Experimental Investigation of Bonding Strength and Residual Stresses in HIP Clad Fuel Plates", Powdermet 2013, Chicago, IL, June 24-27, 2013.
[20] C. Liu, N.A. Mara, M.L. Lovato, D.J. Alexander, K.D. Clarke, K.J. Hollis, D.E. Dombrowski, W.M. Mook, "Bonding Toughness Measurements in LEU Fuel Plates", Reduced Enrichment for Research and Test Reactors (RERTR) 2014, Vienna, Austria, Oct. 12-16, 2014.
[21] C. Liu, M.L. Lovato, D.J. Alexander, K.D. Clarke, N.A. Mara, W.M. Mook, M.B. Prime, D.W. Brown, - "Experimental Investigation of Bonding Strength and Residual Stresses in LEU Fuel Plates", RERTR 2012, Warsaw, Poland, October 14-17, 2012.
[22] N.A. Mara, J. Crapps, T. Wynn, K. Clarke, P. Dickerson, D.E. Dombrowski, B. Mihaila A. Antoniou, "Nanomechanical Behavior of U-10Mo/Zr/Al Fuel Assemblies", RERTR 2011, October 23-27, 2011, Santiago, Chile.
[23] C. Liu, M. Lovato, W. Blumenthal, K. Clarke, D. Alexander, "Interfacial Tensile Strength of Al/Al and Al/Zr/DU-10wt.%Mo", RERTR 2010, October 10-14, 2010, Lisbon, Portugal.
[24] K.D. Clarke, "Formed HIP Can Processing", LANL report LA-UR-15-25831, July 2015.

IMPLEMENTATION OF REACTOR CORE CONVERSION FOR GHARR-1

H. C. ODOI, I. J. K. ABOH
National Nuclear Research Institute
Ghana Atomic Energy Commission, Atomic Road, Kwabenya, Accra – Ghana

J. A. MORMAN
Nuclear Engineering Division, Argonne National Laboratory
9700 South Cass Avenue, Bldg. 201 Argonne, IL 60439

ABSTRACT

The Ghana Research Reactor-1 (GHARR-1) is one of Chinese's Miniature Neutron Source Reactor (MNSR) which was purchased under a tripartite agreement between Ghana, China and the IAEA. The reactor was installed in 1994 and has since been in operation without any incident. It has been used chiefly for Neutron Activation Analysis (NAA) and Training of students in the field of Nuclear Engineering. The GHARR-1 has been earmarked for the Conversion of Core from HEU to LEU which is in accordance with the then GTRI program and other related and/or associated programs. Over the past few years the National Nuclear Research Institute (NNRI), the Operating Organization of the Research Reactor for the Ghana Atomic Energy Commission (GAEC), has undertaken various tasks in order to implement the replacement of the reactor core. These include Neutronics and Thermal Hydraulics computations to ascertain the feasibility of changing the reactor core from HEU to LEU. The computations were done in collaboration with Argonne National Laboratory (ANL), International Atomic Energy Agency (IAEA) and other MNSR operating countries including China. Recently, a Project Management Team has been established to plan and execute necessary activities in order to successfully complete the Reactor Core Conversion to the latter; this is under the auspices of Idaho National Laboratory (INL). Various tasks that have been accomplished lately and others which are line up for the near future are presented in this paper.

1. Introduction

The Ghana Research Reactor-1 (GHARR-1) has nominal power 30 kW and employs 90.2 % highly enriched uranium (HEU) as fuel, light water as moderator, coolant and shield, and beryllium as reflector. The reactor is cooled by natural convection. GHARR-1 is a commercial type of the Miniature Neutron Source Reactor (MNSR) designed, manufactured and constructed by China Institute of Atomic Energy (CIAE), Beijing, China. It is designed for use in universities, hospitals and research institutes mainly for neutron activation analysis, production of short-lived radioisotopes, education and manpower development. The reactor is located at the National Nuclear Research Institute (NNRI) of Ghana Atomic Energy Commission (GAEC) [1].

Other features include: the fuel elements are all enriched uranium-aluminium (U-Al) alloy extrusion clad with aluminium. They are arranged in 10 multi-concentric circle layers at a pitch distance of 10.95 mm. The element cage consists of 2 grid plates, 4 tie

rods and a guide tube for the control rod. Screws connect the 2 grid plates and 4 tie rods. The total number of lattice positions is 354 and the number of fuel elements is 344. The remaining positions are occupied with 6 dummy aluminium elements.

In 2006, the IAEA put together all the MNSR Operating Countries to undertake a Coordinated Research Project (CRP) that will ascertain the feasibility of replacing the HEU fuel of Reactor with LEU. This CRP was successfully completed in March 2012 after various meetings were held to discuss results and prepare the way forward. Subsequently, a Working Group was established to monitor the progress of the various MNSRs Conversion Activities and to share lessons learnt with the fraternity [2].

The NNRI is in support of the conversion of fuel from HEU to LEU and has undertaken various steps to achieve this. There has been a number on Expert and Consultancy Meetings over the last two or three years to

The proposed LEU fuel is basically expected to come with:

1. A change in fuel material from UAl_4 to UO_2 [3].
2. The enrichment of fuel to be changed from 90.2 % to 13.0 %. The enrichment proposed earlier was 12.5 % and was changed to make room for manufacturer's inbuilt features.
3. Number of fuel pins may change from 344 to 339. This was expected to be 348 for the 12.5 % enrichment proposed earlier; it does not give enough room for additional fuel pins which may be needed due to error in manufacturing of the 12.5 % fuel. (Maximum number of fuel pins that may be placed in the reactor core is 350)
4. The fuel pin clad will change from Al to Zrc-4.
5. The radius of Control rod will be slightly increased.

2. Tasks

Neutronics and Thermal Hydraulics computations were done with the 12.5% enriched LEU and subsequently with a 13.0 % to ensure the not more than 350 fuel pins would be need for normal operation of the Core.
Table 1 shows the some criticality results of the computed

Table 1 Comparison of Excess Reactivity Computed for various Cores

Fuel Material	Enrichment %	No. of Fuel Pins	Excess Reactivity, mk
UAl_4	90.2	344	4.00
UO_2	12.5	348	3.76
UO_2	13.0	348	> 4.5
UO_2	13.0	339	4.32

In other developments, computations to estimate the reactivity for various core layouts inside the reactor vessel and transfer cask will be done. These will be calculated and analyzed to support the GHARR-1 fuel cage removal operations. It is imperative that sub-criticality must be guaranteed with substantial margin, i.e., **k-effective +3σ < 0.95**

[4] for the most reactive configurations conceivable during normal operations or accident scenarios.

The spent fuel inventory will be calculated for the whole core of 344 pins. The depletion will cover the whole GHARR1 operational history **from 17 December, 1994 through 25 June, 2016**. Bounding operational conditions are assumed as follows: reactor operated at 15 kW power level, 6 hours per day, 5 days per week, 4 weeks per month, and 12 months per year.

Fuel composition at the End-of-Life (EOL) plus 30-day cooling will be taken from the ORIGEN-S output. Only the actinides and 2 fission products Pm-149 and Sm-149 which are important to reactivity are expected to be kept separately in MCNP5 models. Most of I-135 and Xe-135 will have decayed away after 30-day cooling.

3. Project Management Plan Tasks [5]

A group of staff from the NNRI have been put together to form the project management team. The team is to ensure successful planning and execution of the Reactor Core Conversion Activities. Major tasks and various subtasks have been identified and currently form the basis of activities that are ongoing. The major tasks and subtasks are enumerated below:

i. Project Leadership
   a. Project Management
   b. Project Travel

ii. Transport Package and Licensing
   a. Type B Cask Licensing
   b. Type C Cask Licensing
   c. Interim Transfer Cask

iii. GHARR-1 Reactor Building Preparations and Modifications
   a. Facility Preparations
   b. Core Removal Preparation
   c. Building / Site Security
   d. Outside Loading Area (Layout) and Site Roads
   e. Personnel Training/Certification

iv. Ghana Shipment Preparation/Approval
   a. Transport Approval and Export License
   b. Facility Operations Safety Analysis
   c. Ghana Shipping License
   d. Nuclear Data Documents
   e. Transport and Customs Documents.

4. The Regulator

The Radiation Protection Board (RPB) has been notified of the Core Conversion Program and they are preparing for the task ahead in terms of Licensing and Approvals. There have been numerous of interactions between the Operators and the Regulators on activities and expectations. One of imminent activities, a Training Program for Regulatory body and Operating Organization on licensing and documentation

procedures, is scheduled for second week in November, 2015 [6].

The RPB has already approved the Specification of 13 % LEU fuel to be fabricated and shipped to Ghana for the replacement of the HEU fuel. This was approved on the condition that some of the criticality and kinetic parameters computed for the 12.5% would be redone for the 13 % fuel [7].

5. Tools

The Core Conversion activities will require different types of specific tools and other supporting apparatus. These will be used either directly or indirectly for the reactor core removal whiles others may be for storage. The list of such equipment that has been identified at the time of writing this paper is given in Table 2. Potential organizations have been contacted for the supply of the equipment. Some agreements and/or contracts have been finalized in most cases to ensure timely supply of these resources.

Table 2: List of Main Equipment for the Core Conversion Activity

No.	Equipment	Remarks
i.	Interim Transfer cask with dolly and pathway	Housing the irradiated core upon removal from the vessel for interim storage
ii.	SKODA MNSR Cast (Type B) with He leak testing equipment	Contains a basket which will accommodate the irradiated core directly
iii.	TUK-145/C-MNSR-(Type Cask)	For air shipment
iv.	Radiation Tolerant Underwater Camera Systems	For inspection of Reactor Components and observing activities in vessel water
v.	Cranes	Lifting Core and Casks
vi.	Electric Generator	Source of Electrical Power for Core Conversion Activities
vii.	Lead Shield	Shielding against gamma rays
viii.	Stainless Steel Container	For storage of components which will be removed from the reactor vessel and not re-used
ix.	CCTV	For monitoring activities remotely in Reactor Hall
x.	Laser Level	Positioning of components

There is also the need for the renovation of instrumentation and control with replacement of few components to improve the measurements of parameters necessary for the core replacement. There have been level of discussion with the CIAE and there

are readily available components for this purpose based on contracts to be reached.

6. Challenges

This is the first time a decision is been made to change the fuel of the Ghana Research Reactor-1. Most of the activities will to be done for the first time in the country and hence not much of experience had been acquired in this area. This has the potential of spending more time in executing tasks which would otherwise take a relatively shorter time. For this reason much training and dry runs would to undertaken to ensure all tasks are done in a professional manner as possible to achieve the successful core conversion with little or no difficulties.

Another factor is the power situation in the country now and for that matter a generator will be employed during the conversion period. Initially the electrical generator was proposed to be a backup but with the crises deepening without any clear solution, it has become necessary to engage the generator fully for the project. This gives rise to an additional fuel cost for running the generator.

7. Conclusion

The regulatory body has given approval for the fabrication of the 13.0 % LEU fuel. Detailed computations were completed under the IAEA CRP but with the increment in the enrichment from 12.5 % to 13.0 % there is the need to re-calculate most of the parameters, especially the reactivity, shutdown margin, etc. and the effects of the increment of thermal hydraulics. Various organizations have been contracted for the supply of most of the equipments listed.

8. Acknowledge

We wish to acknowledge – with gratitude – the DOE, IAEA, INL and ANL for the goals put up to minimize or eliminate the use of HEU in Civil Organizations around the world. Our appreciation also goes to the CIAE for their efforts to support the conversion of MNSR’s.

9. References

[1] E. H. K. Akaho et al; Safety Analysis Report - Ghana Research Reactor-1. GAEC-NNRI-RT-90. March, 1995.

[2] Minutes - International Atomic Energy Agency, Coordinated Research Project (CRP) on "Conversion of Miniature Neutron Source Reactors (MNSR) from Highly Enriched Uranium Core to Low Enriched Uranium Core” Third Research Coordination Meeting Vienna International Centre, Room A0531. 13-14 March, 2012.

[3] H. C. Odoi et al; Core Conversion Safety Analysis Report for GHARR-1 (draft) - 2012.

[4] Jay Liaw, (Private Communication) Nuclear Engineering Division – Argonne National Laboratory, USA. August 2015.

[5] Statement of Work; Project Management – Ghana MNSR Shipment. January 2015

[6] MINUTES of the Consultancy Meeting to review the implementation status of the Ghanaian HEU MNSR core removal project Beijing, China; 27-28 August, 2015.

[7] Letter of Approval for the Fuel – Radiation Protection Institute of Ghana Atomic Energy Commission, Ref. No. RPI/RT-30A/Vol. II/43, 4 May, 2015.

European Nuclear Society
Avenue des Arts 56
1000 Brussels, Belgium
Telephone: +32 2 505 30 50 - FAX: +32 2 502 39 02
rrfm2016@euronuclear.org
www.rrfm2016.org